Tectonics of the Western Mediterranean and North Africa

Edited by
G. Moratti and A. Chalouan

Geological Society
Special Publication 262

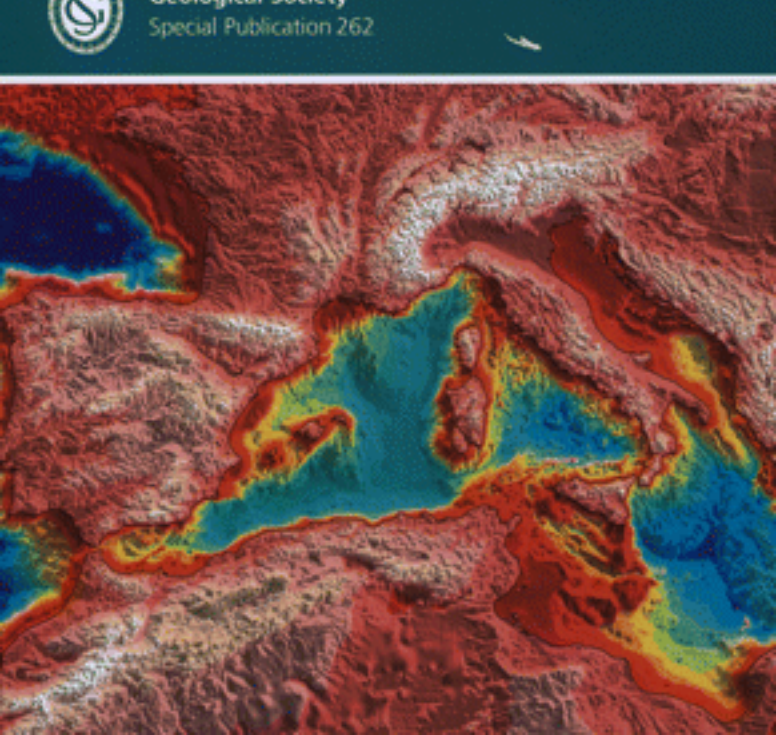

Tectonics of the Western Mediterranean and North Africa

Edited by
G. Moratti and A. Chalouan

Geological Society
Special Publication 262

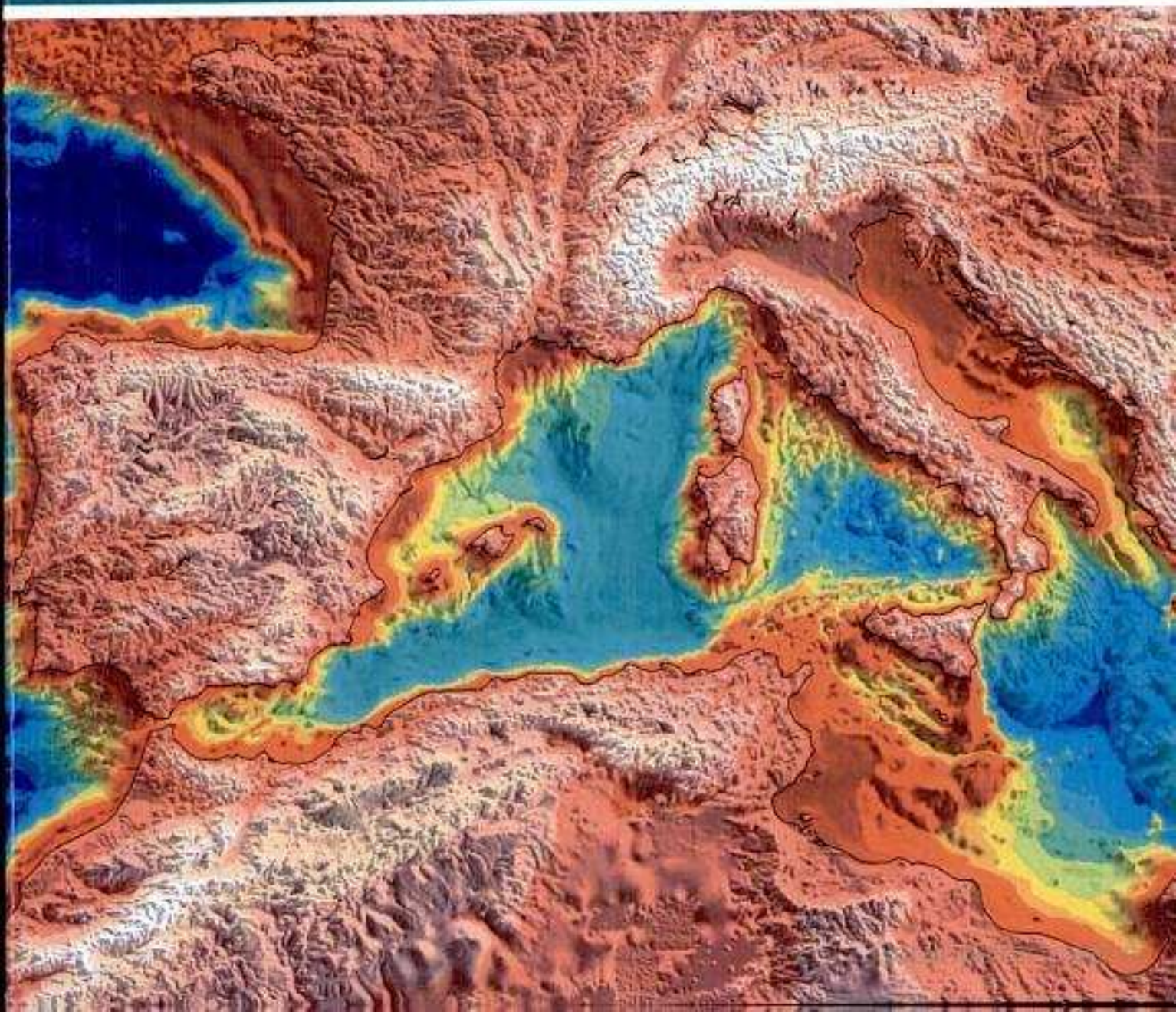

Tectonics of the Western Mediterranean and North Africa

Geological Society books refereeing procedures

The Society makes every effort to ensure that the scientific and production quality of its books matches that of its journals. Since 1997, all book proposals have been refereed by specialist reviewers as well as by the Society's Books Editorial Committee. If the referees identify weaknesses in the proposal, these must be addressed before the proposal is accepted.

Once the book is accepted, the Society Book Editors ensure that the volume editors follow strict guidelines on refereeing and quality control. We insist that individual papers can only be accepted after satisfactory review by two independent referees. The questions on the review forms are similar to those for *Journal of the Geological Society*. The referees' forms and comments must be available to the Society's Book Editors on request.

Although many of the books result from meetings, the editors are expected to commission papers that were not presented at the meeting to ensure that the book provides a balanced coverage of the subject. Being accepted for presentation at the meeting does not guarantee inclusion in the book.

More information about submitting a proposal and producing a book for the Society can be found on its web site: www.geolsoc.org.uk.

It is recommended that reference to all or part of this book should be made in one of the following ways:

MORATTI, G. & CHALOUAN, A. (eds) 2006. *Tectonics of the Western Mediterranean and North Africa.* Geological Society, London, Special Publications, **262.**

PIANGIAMORE, G. L., FAGGIONI, O. & BARBANO, M. S. 2006. Crustal magnetism of the southern Tyrrhenian Sea from aeromagnetic surveys. *In*: MORATTI, G. & CHALOUAN, A. (eds) *Tectonics of the Western Mediterranean and North Africa.* Geological Society, London, Special Publications, **262,** 337–348.

GEOLOGICAL SOCIETY SPECIAL PUBLICATION NO. 262

Tectonics of the Western Mediterranean and North Africa

EDITED BY

G. MORATTI

CNR-Institute of Geosciences and Earth Resources, Italy

and

A. CHALOUAN

University of Mohammed V Agdal, Rabat, Morocco

2006
Published by
The Geological Society
London

THE GEOLOGICAL SOCIETY

The Geological Society of London (GSL) was founded in 1807. It is the oldest national geological society in the world and the largest in Europe. It was incorporated under Royal Charter in 1825 and is Registered Charity 210161.

The Society is the UK national learned and professional society for geology with a worldwide Fellowship (FGS) of 9000. The Society has the power to confer Chartered status on suitably qualified Fellows, and about 2000 of the Fellowship carry the title (CGeol). Chartered Geologists may also obtain the equivalent European title, European Geologist (EurGeol). One fifth of the Society's fellowship resides outside the UK. To find out more about the Society, log on to www.geolsoc.org.uk.

The Geological Society Publishing House (Bath, UK) produces the Society's international journals and books, and acts as European distributor for selected publications of the American Association of Petroleum Geologists (AAPG), the American Geological Institute (AGI), the Indonesian Petroleum Association (IPA), the Geological Society of America (GSA), the Society for Sedimentary Geology (SEPM) and the Geologists' Association (GA). Joint marketing agreements ensure that GSL Fellows may purchase these societies' publications at a discount. The Society's online bookshop (accessible from www.geolsoc.org.uk) offers secure book purchasing with your credit or debit card.

To find out about joining the Society and benefiting from substantial discounts on publications of GSL and other societies worldwide, consult www.geolsoc.org.uk, or contact the Fellowship Department at: The Geological Society, Burlington House, Piccadilly, London W1J 0BG: Tel. +44 (0)20 7434 9944; Fax +44 (0)20 7439 8975; E-mail: enquiries@geolsoc.org.uk.

For information about the Society's meetings, consult *Events* on www.geolsoc.org.uk. To find out more about the Society's Corporate Affiliates Scheme, write to enquiries@geolsoc.org.uk.

Published by The Geological Society from:
The Geological Society Publishing House
Unit 7, Brassmill Enterprise Centre
Brassmill Lane
Bath BA1 3JN, UK

Orders: Tel. +44 (0)1225 445046
Fax +44 (0)1225 442836
Online bookshop: www.geolsoc.org.uk/bookshop

British Library Cataloguing in Publication Data
A catalogue record for this book is available from the British Library.

ISBN-10: 1-86239-202-1
ISBN-13: 978-1-86239-202-1

Typeset by Techset Composition, Salisbury, UK
Printed by MPG Books, Bodmin UK.

Distributors

USA
AAPG Bookstore
PO Box 979
Tulsa
OK 74101-0979
USA
Orders: Tel.+1 918 584-2555
Fax +1 918 560-2652
E-mail bookstore@aapg.org

India
Affiliated East-West Press Private Ltd
Marketing Division
G-1/16 Ansari Road, Darya Ganj
New Delhi 110 002
India
Orders: Tel. +91 11 2327-9113/2326-4180
Fax +91 11 2326-0538
E-mail affiliat@vsnl.com

Japan
Kanda Book Trading Company
Cityhouse Tama 204
Tsurumaki 1-3-10
Tama-shi, Tokyo 206-0034
Japan
Orders: Tel. +81 (0)423 57-7650
Fax +81 (0)423 57-7651
Email geokanda@ma.kcom.ne.jp

Contents

Preface

The Western Mediterranean Alpine chains, resulting from the convergence between the Eurasian and African plates, surround this sea describing three of the most tightly arcuate orogenic belts in the world.

The Alps show a northward convexity and a complex structure, which began to develop during the early Cretaceous when the Apulian plate collided with the Eurasian plate, and continued during the Eocene and into the early Neogene.

The other two oroclines, the Gibraltar arc, connecting the Betics to the Kabylides through the Rif, and the Calabrian arc, connecting the Apennines to the Maghrebides, form the western and eastern ends of the western peri-Mediterranean chains. The southern branches of these two oroclines join one another along the Maghrebian chain, whereas their northern branches fade away both in the Alps and into the Algerian–Provençal basin. Although they have opposite convexity and are about 2000 km distant from one another, their geological histories are comparable.

The main goal of this book is to contribute to a better knowledge of these two oroclines, and to improve our understanding of their genesis and tectonic evolution. To this purpose, the papers presented in this book discuss in detail: (1) new palaeogeographical reconstructions of the evolution and geodynamic significance of the 'Verrucano' and 'Pseudoverrucano' in the central–western Mediterranean Alpine chains (**Perrone *et al.***) and of the Upper Cretaceous–Eocene carbonate turbidites of the Northern Apennines (**Argnani *et al.***); (2) relationships between sedimentology and tectonics in the internal zones of both oroclines through marine (**Piangiamore *et al.***; **Gamberi & Marani**) and field geology studies (**El Kadiri *et al.***; **Chaabani & Razgallah; Oujidi *et al.***; **El Kadiri *et al.***; **Chalouan *et al.***; **El Kadiri *et al.***; **Mattioni *et al.***); (3) the northern and southern fronts of the Gibraltar arc (**Ruano *et al.***; **Chalouan *et al.***; **El Kadiri *et al.***; **Pedrera *et al.***); (4) basin development in the Iberian foreland (**Segura *et al.***); (5) recent deformations at the northern border of the Adriatic indenter (**Massironi *et al.***); (6) eustatic versus tectonic-controlled basin development during the Plio-Pleistocene in the Southern Apennines (**Benvenuti *et al.***; **Capraro *et al.***); (7) seismicity and seismotectonics both in Sicily (**Tondi *et al.***) and in Morocco (**Ait Brahim *et al.***); (8) relationships between fluid geochemistry and active tectonics in Morocco (**Tassi *et al.***).

The majority of these papers were presented at the 'Geology of the Mediterranean Area' session of the 32nd IGC held in Florence on 20–28 August 2004. The Editors wish to thank the following reviewers, who contributed to improve the final quality of this book:

Fabrizio Agosta, Stanford University, Stanford, CA, USA
Djilali Benouar, Bab Ezzouar University, Algiers, Algeria
Albert Casas, Barcelona University, Barcelona, Spain
Giuseppe Cassinis, Pavia University, Pavia, Italy
Giuseppe Cello, Camerino University, Camerino, Italy
Rosa Cidu, Cagliari University, Cagliari, Italy
Ana Crespo-Blanc, Granada University, Granada, Spain
Paolo Dattilo, Total E&P, Borneo BV
Agata Di Stefano, Catania University, Catania, Italy
Kalil El Kadiri, Abdelmalek Essaidi University, Tetuan, Morocco
Frank Ethridge, Colorado State University, Ft Collins, CO, USA
Dan Faulkner, Liverpool University, Liverpool, UK
Franco Fonnesu, ENI, S. Donato Milanese, Italy
Jesus Galindo Zaldivar, Granada University, Granada, Spain
Francesco Guerrera, Urbino University, Urbino, Italy
Reinhard Hesse, McGill University, Montreal, Que., Canada
Christian Hoeppfner, Mohammed V-Agdal University, Rabat, Morocco
Layachi Imlahi, Abdelmalek Essaidi University, Tetuan, Morocco
John Jones, University College, London, UK
Ian Sverre Laberg, Tromsø University, Tromsø, Norway
Angel Carlos Lopez-Garrido, CSIC-Géologia Mediterranea, Granada, Spain
Michaela Lukesch, Bern University, Bern, Switzerland
Stefano Mazzoli, 'Federico II' University, Napoli, Italy
Fida Medina, Mohammed V-Agdal University, Rabat, Morocco
André Michard, Ecole Normale Supérieure, Paris, France
Federico Oloriz, Granada University, Granada, Spain

Vincenzo Perrone, Urbino University, Urbino, Italy
Tullio Pescatore, Sannio University, Benevento, Italy
Thomas Pletsch, Federal Institute for Geosciences and Mineral Resources, Hannover, Germany
Giacomo Prosser, Basilicata University, Potenza, Italy
Mohamed Ramdani, Mohammed V-Agdal University, Rabat, Morocco
Federico Sani, Florence University, Florence, Italy
Carlos Sanz de Galdeano, CSIC-Géologia Mediterranea, Granada, Spain
Rodolfo Sprovieri, Palermo University, Palermo, Italy
Charles Turner, The Open University, Milton Keynes, UK
Walter Wildi, Geneva, Switzerland
Wilfried Winkler, ETHZ, Zürich, Switzerland
Slavcho Yanev, Bulgarian Academy of Sciences, Sofia, Bulgaria

Two authors of this Special Publication, Francesco Antonio Decandia and Giuseppe Cello, died suddenly just before this book went to press. With great sorrow, Giovanna Moratti would like to dedicate this book to Tonino and Peppe, who were great geologists, but above all very good friends.

Giovanna Moratti
Ahmed Chalouan

'Verrucano' and 'Pseudoverrucano' in the Central–Western Mediterranean Alpine Chains: palaeogeographical evolution and geodynamic significance

V. PERRONE[1], A. MARTÍN-ALGARRA[2], S. CRITELLI[3], F. A. DECANDIA[4], M. D'ERRICO[5], A. ESTEVEZ[6], A. IANNACE[5], A. LAZZAROTTO[4], M. MARTÍN-MARTÍN[6], I. MARTÍN-ROJAS[6], S. MAZZOLI[5], A. MESSINA[7], G. MONGELLI[8], S. VITALE[5] & M. N. ZAGHLOUL[9]

[1]*Istituto di Geologia dell'Università 'Carlo Bo' di Urbino, Campus Scientifico Località Crocicchia, 61029 Urbino, Italy (e-mail: perrone@uniurb.it.)*

[2]*Departamento de Estratigrafía y Palaeontología de la Universidad de Granada, Campus de Fuentenueva, 18071 Granada, Spain*

[3]*Dipartimento di Scienze della Terra dell'Università della Calabria, Via P. Bucci, 87030 Arcavacata di Rende, Italy*

[4]*Dipartimento di Scienze della Terra dell'Università di Siena, Via Laterina 8, 53100 Siena, Italy*

[5]*Dipartimento di Scienze della Terra dell'Università 'Federico II' di Napoli, Largo San Marcellino 10, 80138 Napoli, Italy*

[6]*Departamento de Ciencias de la Tierra y del Medio Ambiente de la Universidad de Alicante, Campus de San Vicente, Apdo. Correos 99, 03080 Alicante, Spain*

[7]*Dipartimento di Scienze della Terra dell'Università di Messina, Salita Sperone 31, 98166 Messina, Italy*

[8]*Dipartimento di Scienze Geologiche dell'Università della Basilicata, 85100 Potenza, Italy*

[9]*Département de Sciences de la Terre et d'Océanologie de l'Université 'Abdel Maleek Essâadi' de Tanger, Tangier, Morocco*

Abstract: The Anisian–Carnian Verrucano Group of the Tuscan Metamorphic Units and the Triassic–Hettangian Pseudoverrucano Formation of the homonymous unit are mainly continental redbeds occurring in Tuscany at the base of the Alpine orogenic cycle. A study carried out throughout the Apennine, Maghrebian and Betic Chains emphasized the presence in all these orogenic belts of deposits more or less coeval and similar both to the metamorphic Verrucano and to the unmetamorphosed Pseudoverrucano. Thus, the distinction of Verrucano and Pseudoverrucano successions has a palaeogeographical and geodynamic importance at the scale of the Western Mediterranean. Both successions developed during the continental rift stage of Pangaea, which led to later break-up at the edges of a future microplate, interposed between the Europe, Africa and Adria–Apulia plates, but they are characterized by different tectonometamorphic evolution. Pseudoverrucano-like deposits, devoid of Alpine metamorphism, characterize the highest tectonic units of the nappe stack and they overthrust units bearing Verrucano-like deposits. These latter show an Alpine tectonometamorphic history marked during the Miocene by intense deformation and HP/LT metamorphism (at pressures in the range of 0.8–2 GPa), followed by a retrograde phase associated with decompression, suggesting subduction and subsequent exhumation of continental crust. Intriguing palaeogeographical problems arise from the analysis of Verrucano-bearing units, because the same evolution seems to characterize both units considered to belong to a realm similar to that of the north-verging Austroalpine nappe system and some units referred to the south-verging fold–thrust belt derived from the Adria–Apulia palaeomargin.

From: MORATTI, G. & CHALOUAN, A. (eds) 2006. *Tectonics of the Western Mediterranean and North Africa.* Geological Society, London, Special Publications, **262**, 1–43.
0305-8719/06/$15.00

The stratigraphic base of the Alpine Sedimentary Cycle in the Alpine Chains of the western and central Mediterranean is frequently formed by continental redbeds that are known as 'Verrucano', a term used for the first time by Savi (1832) for metamorphosed continental clastic rocks underlying Mesozoic successions in Tuscany, particularly well exposed in the Monte Pisano (Monte della Verruca) area. Everywhere, these facies are dominantly made of continental, reddish, purple and yellow–greenish sandstones, conglomerates and mudrocks, with subordinate shallow marine evaporites and carbonates. They rest unconformably on Palaeozoic sedimentary, metasedimentary and plutonic rocks deformed during the Variscan Orogenic Cycle, and are covered by marine carbonate and clastic Mesozoic and Cenozoic strata, which may be as young as Aquitanian.

In the last century, however, the term Verrucano was used in all the chains of the Western Mediterranean, from the Alps to the Gibraltar Arc, as a common term to identify lithostratigraphic units resulting from the erosion of the Hercynian Chain and its subsequent volcanoes (Trumpy, cited by Trevisan 1966). Thus, the term was generally employed for sedimentary rocks of Permian and Triassic age, deposited as continental redbeds in different geodynamic contexts (see Rutten 1969; Lemoine 1978; Cassinis *et al.* 1979, and references therein) and also for sediments representing late Hercynian molasses, such as the well-known Verrucano of the Glarus Alps (Fisch & Ryf 1966).

In contrast, we agree with researchers who used the term Verrucano exclusively for prevailingly continental deposits, unconformably overlying the Hercynian basement and representing the onset of the Alpine Cycle (see Cassinis *et al.* 1979). The Verrucano clastic deposits are best interpreted as a tectofacies testifying to the onset, in the first phases of Alpine history, of early continental rifting in a wide area of western Pangaea (Cassinis *et al.* 1979). This rifting aborted before oceanization (Cassinis *et al.* 1979; Kligfield 1979; Passeri 1985; Rau *et al.* 1985; Martini *et al.* 1986), because Jurassic–Cretaceous rifting, and subsequent break-off and spreading, generally did not follow previous structural strikes but independent neoformed fractures.

The frequent inaccurate use of the term Verrucano can be explained taking into account two main reasons.

(1) The age of the early intracontinental rifting, coeval with the deposition of Verrucano redbeds, is debated and difficult to define clearly in many areas, because of the scarcity of fossils. Moreover, a diachronism is generally evident from place to place.

(2) Large amounts of Verrucano-like redbeds were deposited, during the Permian and Triassic, in the Western Pangaea areas. In addition, rocks representative both of late Hercynian molasses and of the base of the Alpine Cycle sometimes occur in the same region and nappes (for a critical review, see Cassinis *et al.* 1979).

In the Alps, Verrucano facies of Permian and Early Triassic age are particularly well developed in the strongly deformed Internal Domains (Penninic, in particular Briançonnian, and Austroalpine nappes), although they are also known in some external units, such as the Helvetic nappes of the Glarus Alps (Rutten 1969). Similarly to the time- and facies-equivalent Permian Rotliegende deposits of the Germanic Alpine foreland (Henningsen & Katzung 1998), the continental redbeds known as Permian Verrucano Alpino (especially in the Southern Alps, where they are also named Verrucano Lombardo, or Val Gardena Sandstones: Bosellini *et al.* 1996), locally reach enormous thickness and are associated with huge amounts of acidic to intermediate volcanic rocks.

The undeformed Permian redbeds and vulcanites of the extra-Alpine Röt deposits are usually covered by thick Upper Permian salt deposits (Zechstein), which underlie a new sedimentary cycle of Triassic continental redbeds, which forms the lower unit of the Germanic Triassic facies belt, the Buntsandstein facies (Henningsen & Katzung 1998). Southwards, towards the Alps, these deposits change laterally to progressively more open marine carbonates, which constitute the Alpine Triassic facies belt (Lemoine 1978).

In the Central–Western Mediterranean Chains, from the Betic Cordillera to the Northern Apennines and from the Rif to Calabria, redbeds considered as Verrucano facies are usually Triassic, but they can exceptionally reach the earliest Jurassic (Calabrian–Peloritanian Arc), and a Permian age for the base cannot be excluded in the Betic Cordillera and Rif. In addition, these deposits are vertically and laterally related to Triassic marine carbonates with Alpine facies and are systematically found within tectonic units belonging to the Internal Domains of all these chains. Nevertheless, with the exception of the Apenninic and Sicilian External Domains, whose Triassic deposits are marine with Alpine facies, redbeds in the Betic–Maghrebian External Domains and in their Iberian and African forelands belong to the Germanic and Germano-Andalusian Triassic facies belts. In Spain, very thick continental redbeds are widely present both below and above Middle Triassic marine Muschelkalk carbonates, and are included either in Buntsandstein or in Keuper facies (Sopeña *et al.* 1988; Pérez-López 1998).

However, in Tuscany, Lotti (1891) introduced the term 'Pseudoverrucano' to indicate a clastic deposit, lithologically similar to the Tuscan Verrucano *sensu stricto*, but not affected by Alpine

metamorphism. The Pseudoverrucano was considered by Lotti to be younger, probably Cretaceous in age, because it was interpreted to be stratigraphically interposed between Liassic and Eocene levels of the Tuscan successions. Today, these deposits are interpreted as representing the Upper Triassic stratigraphic base of an independent allochthonous tectonic unit named the Pseudoverrucano Unit. This unit is considered to be the uppermost tectonic unit that originated from the Tuscan Domain (Decandia *et al.* 1980). The term Pseudoverrucano has never been used for redbeds cropping out in other chains of the Western Mediterranean.

Studies on the North Apenninic Lower Mesozoic clastic successions, therefore, permit as to distinguish two Triassic stratigraphic sequences, which have marked differences in their post-Triassic tectonosedimentary evolution.

(1) the Verrucano Group successions (Rau & Tongiorgi 1974; Cassinis *et al.* 1979) are exclusive of the Tuscan Metamorphic Units (Massa, Apuane and Monticiano–Roccastrada Units) and are Anisian– Carnian in age. They consist mainly of continental clastic deposits, grading upwards to evaporitic–carbonatic deposits during the late Carnian–Norian. These rocks are followed by younger basinal sediments and experienced a Neogene metamorphism.

(2) The unmetamorphosed Pseudoverrucano successions, characterizing the Pseudoverrucano tectonic unit, consist of Triassic–lowermost Jurassic reddish conglomerates and sandstones, in which thin levels of Rhaetian marine sandy limestones occur (Costantini *et al.* 1980*a*). The clastic deposits are followed by Liassic carbonate platform and basin deposits (Costantini *et al.* 1980*a*,*b*; Decandia & Lazzarotto 1980).

A re-examination of the successions for which the term Verrucano has been used in the Western Mediterranean Alpine Chains, from the Betic Cordillera to the Apennines, has never been carried out. In our opinion, such re-examination is necessary to better define the palaeogeographical evolution and the geodynamic significance of rock successions that were given this name and to verify if their history is concordant with that of the Verrucano in its type area of the Tuscan Northern Apennines.

In this synthesis therefore, we re-examine the Alpine tectonosedimentary evolution of all units containing Triassic redbeds and their metamorphic equivalents, from the Northern Apennines to the Betic Cordillera (Fig. 1). The aims of this study are to verify whether: (1) Verrucano- and Pseudoverrucano-like successions are also distinguishable in other orogenic sectors of the Western Mediterranean chains; (2) these deposits have a Triassic and post-Triassic tectonosedimentary

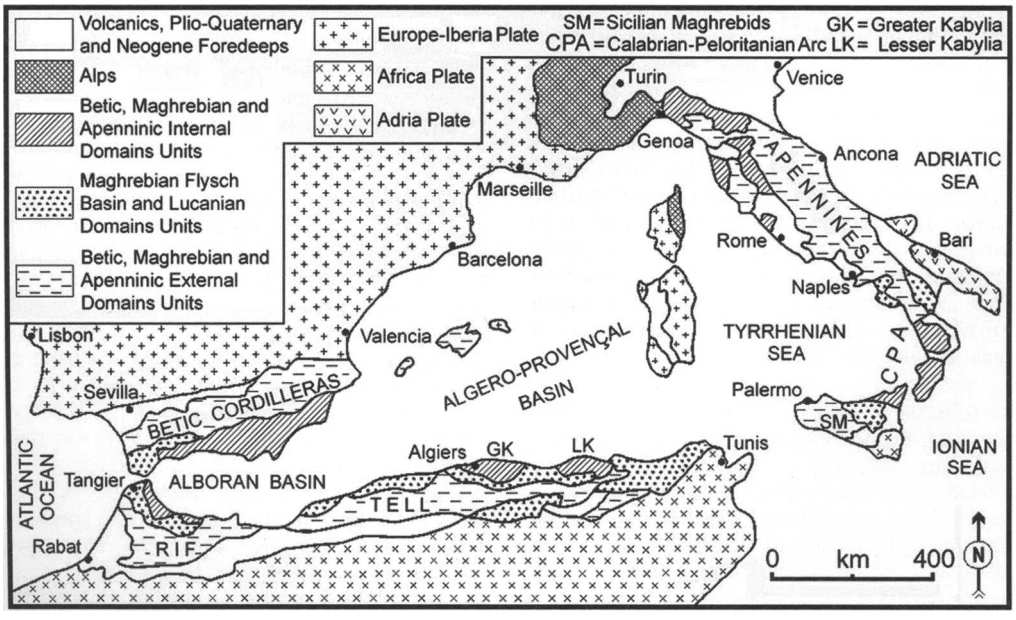

Fig. 1. Geological sketch map of the Alpine Chains in the Central–Western Mediterranean region.

evolution similar to those of the Tuscan Verrucano and Pseudoverrucano.

In our opinion, the available data allow us to hypothesize a common history for all the units containing Verrucano–Pseudoverrucano-like redbeds in the Western Mediterranean Alpine belts. It is suggested that these units are representative of one palaeogeographical domain, formed in the Mid-Triassic or earlier, which underwent a similar post-Triassic evolution up to the onset of convergence-related tectonics, which led to the accretion of the sedimentary successions to the developing chains. During the Cenozoic compressional tectonics, however, Verrucano- and Pseudoverrucano-bearing successions experienced a different deformation history; this has resulted in the formation of two different Verrucano and Pseudoverrucano subdomains. The results of the present research may provide important constraints on palaeogeographical and palaeotectonic reconstructions of the evolution of the Alpine circum-Mediterranean orogen.

Pseudoverrucano-type successions

Northern Apennines

Pseudoverrucano deposits (Triassic). The Pseudoverrucano Unit crops out exclusively in small and scattered areas of southern Tuscany (Fig. 2) and this does not allow us to carry out a detailed reconstruction of its evolution. Its stratigraphic or tectonic substratum is unknown. Stratigraphic successions and a palaeogeographical scheme are reported in Figure 3. The successions start with continental alluvial and braided deposits, made up mainly of reddish conglomerates and sandstones with minor and thin violet or yellowish pelitic beds. The outcrop thickness reaches 30 m. Conglomerate clasts consist of white or pink quartz, subordinate quartzite, and red or black chert. The redbed succession is azoic, but in its upper part thin levels of limestones bearing *Triasina hantkeni* are locally intercalated within the clastic rocks (Costantini *et al.* 1980*b*). Consequently, the age of the clastic basal formation (Pseudoverrucano Formation *sensu stricto*) is essentially Triassic, although an earliest Liassic age of the uppermost levels cannot be ruled out.

Post-Triassic succession (Lower Jurassic–Upper Jurassic). Redbed successions of the Pseudoverrucano Unit are followed by grey to pink thick-bedded oolitic limestones (Montebrandoli locality) and by dark grey marls and cherty limestones with ammonites (Punta delle Rocchette locality). These rocks are Liassic in age and Domerian levels have been recognized with certainty. The upper part of the Montebrandoli oolitic limestone is cut by thin neptunian dykes and shows karstic cavities filled by pink limestone with Toarcian *Ammonitico Rosso* facies (Costantini *et al.* 1980*b*). In the Collecchio locality, the Montebrandoli limestone is disconformably overlain by mainly calcareous heterometric megabreccias (Poggio Morcone breccias), fed by the underlying formations, with a marly–calcareous red or pink matrix bearing *Posidonomya* and rare ammonites of Mid-Jurassic age, capped by few beds of red or grey–green Upper Jurassic radiolarites (Costantini *et al.* 1980*b*).

Palaeogeographical evolution. The tectonosedimentary evolution suggests the existence of a continental area up to earliest Jurassic time, in which some marine episodes are indicated by rare thin levels of Rhaetian *Triasina* limestones. From the Early Jurassic, the onset of extensional tectonics, related to the opening of the Tethyan Ocean, resulted in complex palaeoenvironmental conditions. Synsedimentary tectonics produced the development of morpho-structural highs and lows in the basin floor and, consequently, of sudden vertical and lateral changes, from neritic to pelagic environments, as indicated by the deposition of Pliensbachian–Toarcian platform carbonates, pelagic marly and cherty limestones.

During the Mid-Jurassic, enhanced extensional tectonics was responsible for the sedimentation of coarse calcareous breccias, followed by radiolarites in the Late Jurassic. The lack of younger terrains referable to the Pseudoverrucano Unit with certainty does not allow one to unravel its post-Jurassic evolution and to constrain its deformation age. However, it can be seen that the Pseudoverrucano Unit represents in the Northern Apennines the highest Tuscan tectonic unit.

Southern Apennines–Sicilian Maghrebids

Pseudoverrucano-like deposits. Unmetamorphosed continental redbeds, which show lithological successions and tectonosedimentary evolution comparable with that of the Tuscan Pseudoverrucano Unit, occur in some nappes of the Calabrian–Peloritanian Arc (Fig. 4). Nappes characterizing this orogenic sector, made up of Palaeozoic basements and Meso-Cenozoic cover, have been considered as the most internal units of both the Southern Apennines and Sicilian Maghrebids (Durand Delga & Fontboté 1980; Bouillin *et al.* 1986; Guerrera *et al.* 1993).

Middle?–Upper Triassic continental deposits occur at the base of the Meso-Cenozoic covers of the Sila, Stilo, Piraino and Longi–Taormina Units (Fig. 4). Their stratigraphic successions (Fig. 5) are characterized by typical redbeds, unconformable on Hercynian phyllites and metarenites, intruded by late Hercynian granitoids. The redbed

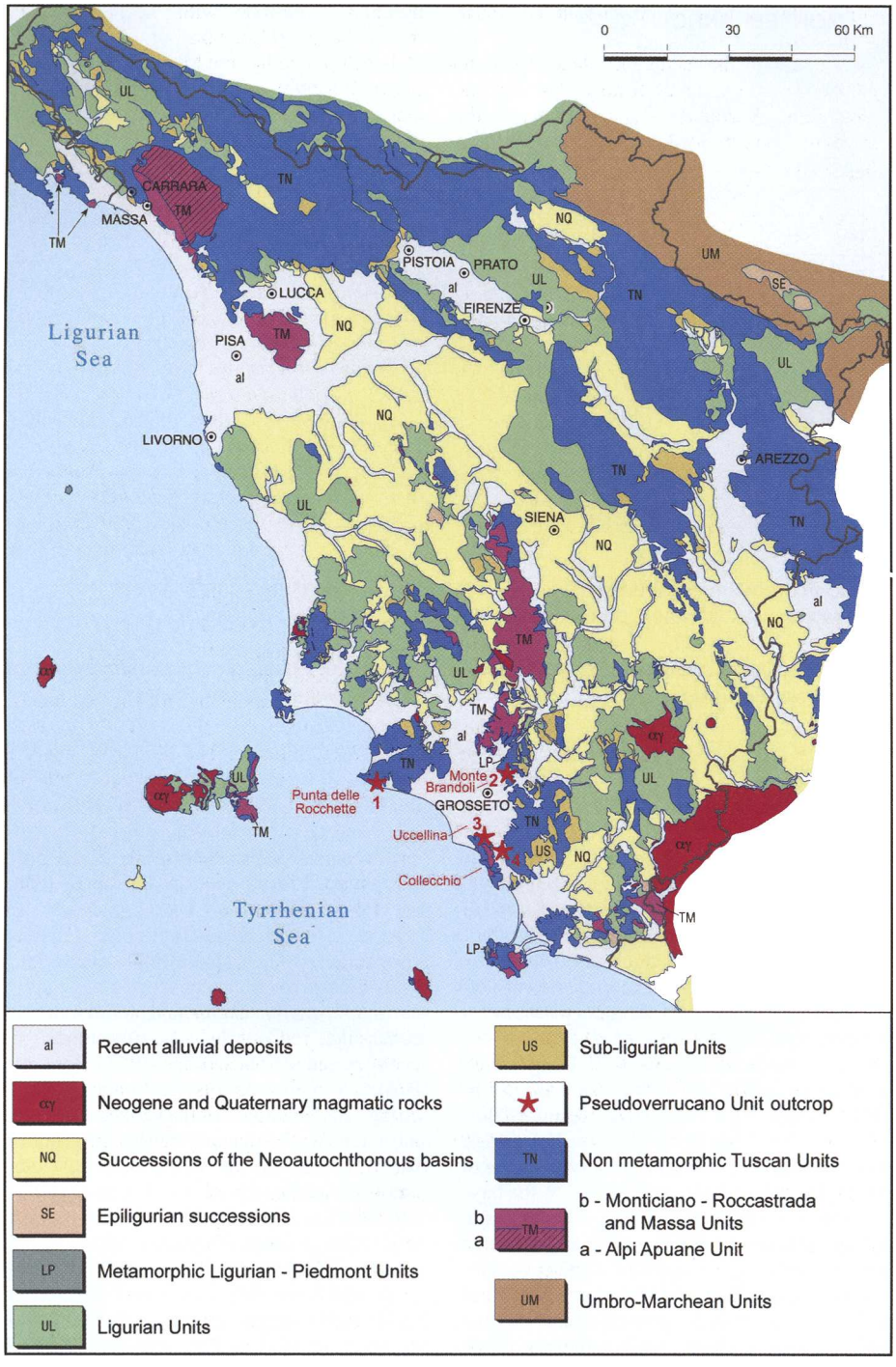

Fig. 2. Schematic geological map of Tuscany. The TM-b Unit to the NW of the Livorno–Firenze alignment corresponds to the Massa Unit; the TM-b Unit to SE of this alignment corresponds to the Monticiano–Roccastrada Unit.

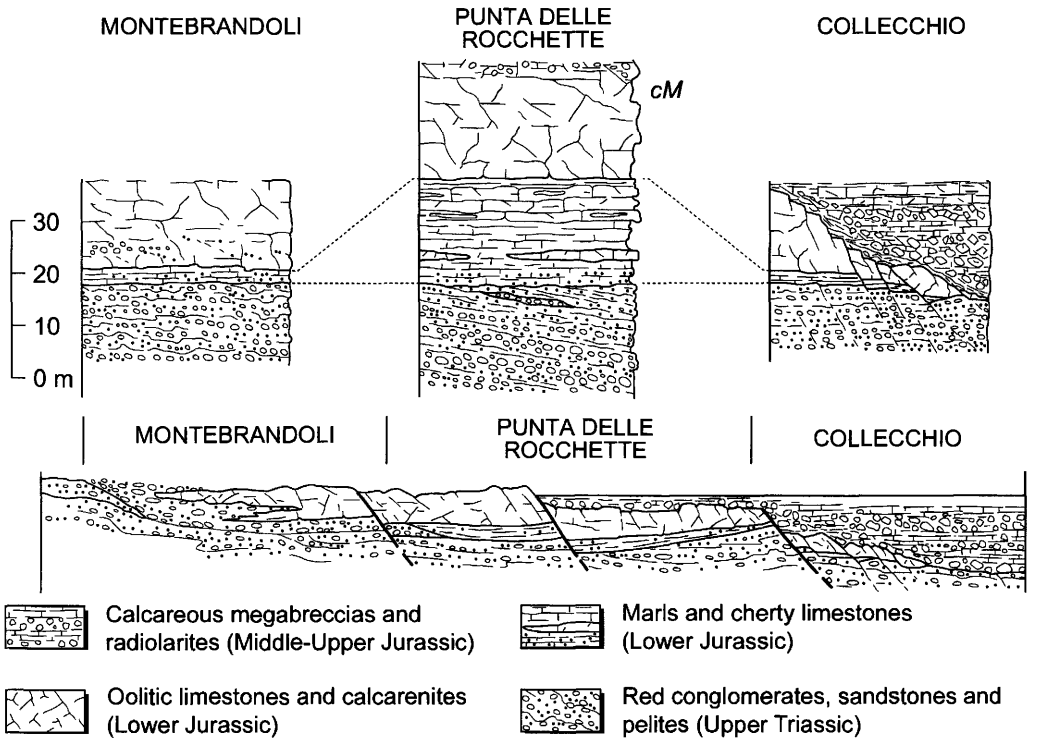

Fig. 3. Stratigraphic columns and Jurassic palaeogeographical schematic section of the Pseudoverrucano Unit in Southern Tuscany. Modified from Costantini *et al.* (1980*a*).

successions are exclusively made up of clastic rocks (red quartzarenites and minor quartzose conglomerates and red–purple mudrocks). The most complete succession occurs in the Longi–Taormina Unit, where redbeds, up to 300 m thick, are topped by *c.* 20 m of greyish sandstones, silty clays and yellowish dolostones, in which Hettangian palinofloras have been recognized (Baudelot *et al.* 1988). In the Sila Unit, redbeds occur in the Longobucco Sequence (Young *et al.* 1986; Santantonio & Teale 1987): they lie on Palaeozoic metamorphites and granitoids and are followed by Hettangian brown pelites, yellowish sandstones, conglomerates and black pelites (Baudelot *et al.* 1988). At the base of the Mesozoic succession of the Stilo Unit, clastic deposits are lacking or are reduced to a few metres of thin palaeosoils and/or sandstones and pelites. In the Tiriolo area, where the thickest succession occurs, continental redbeds, probably Late Triassic in age, follow shallow-water sands and clays of few metres in thickness (Critelli & Ferrini 1988). In the Piraino Unit, which is made of several small tectonic slices (Cecca *et al.* 2002), typical purple conglomerates and sandstones, 20 m thick, characterize the lowest slice.

Post-Pseudoverrucano successions (Lower Jurassic–Aquitanian). Clastic deposits on top of redbeds in the Longi–Taormina Unit gradually change upwards to neritic black limestones (Hettangian–Sinemurian). The succession continues with Upper Liassic to Oligocene slope and pelagic deposits (marls; marly, cherty and nodular limestones; scaglia-like red marls and limestones, rich in neritic re-sediments; Lentini 1975; Bonardi *et al.* 1976). A network of neptunian dykes, also cutting across the Palaeozoic basement, suggests that extensional tectonics clearly acted during and after Toarcian time. The succession ends with Aquitanian siliciclastic turbidites (de Capoa *et al.* 1997).

In the Sila Unit, the Longobucco redbeds pass upwards to Sinemurian neritic sandy limestones, rapidly grading to Pliensbachian–Toarcian slope marls and turbiditic sediments (Magri *et al.* 1965). Deposits younger than Early Jurassic are recognizable in the Caloveto Sequence, where redbeds are lacking and Sinemurian carbonate platform rocks directly lie on the Palaeozoic basement. In the Caloveto Sequence, neritic carbonates are followed by Pliensbachian–Toarcian slope sediments and by Middle Jurassic–lowermost

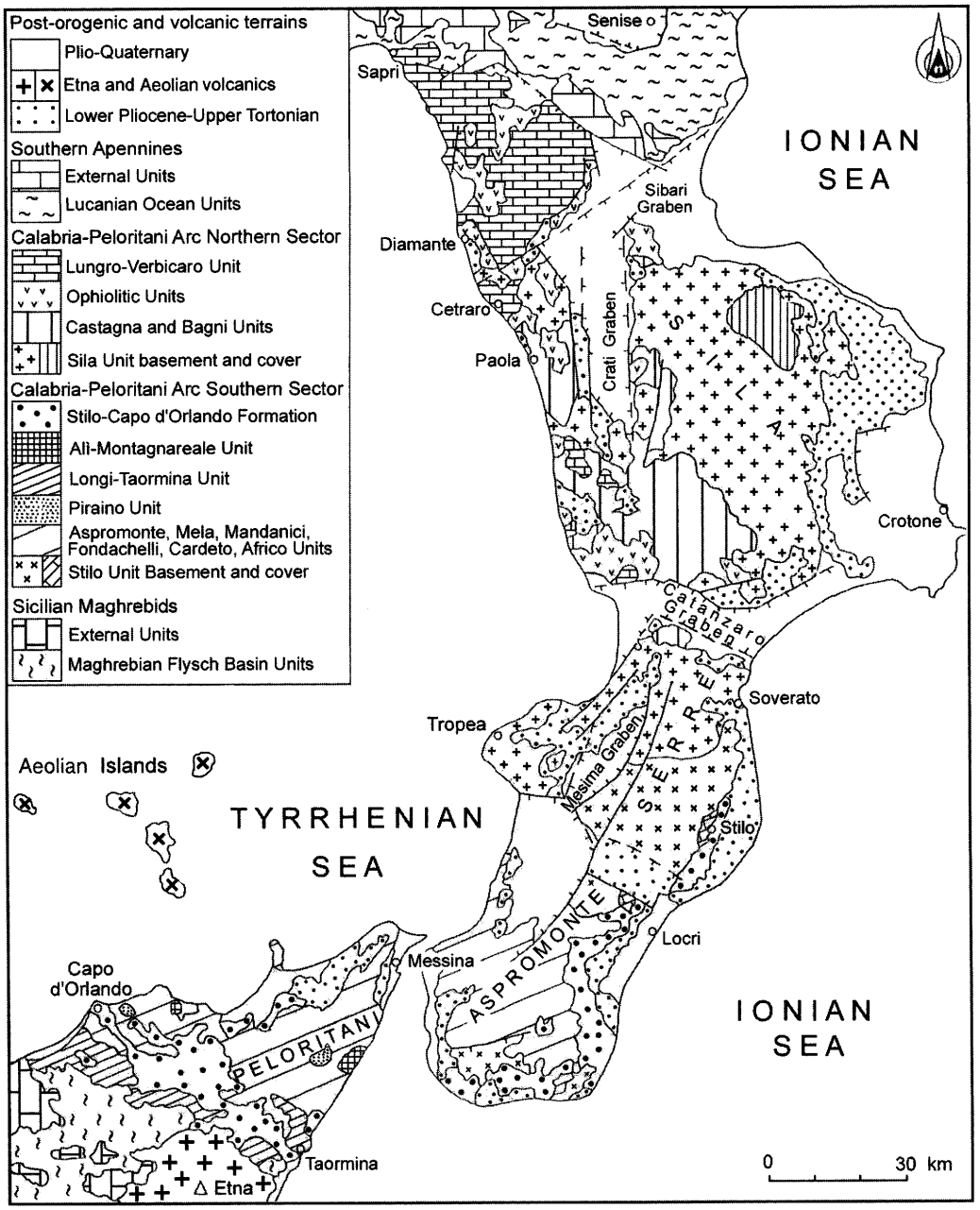

Fig. 4. Schematic geological map of the Calabrian–Peloritanian Arc. Verrucano-like deposits are present in the Lungro–Verbicaro, Bagni and Alì–Montagnareale Units; Pseudoverrucano-like deposits occur in the Sila, Stilo, Longi–Taormina and Piraino Units.

Cretaceous pelagic deposits (marls, sandstones, cherty limestones, nodular limestones, radiolarites and *Calpionella* limestones; Santantonio & Teale 1987). A prominent network of neptunian dykes, related to the strong extensional tectonics associated with the Tethys opening, cuts across both Mesozoic and Palaeozoic terrains (Bouillin & Bellomo 1990).

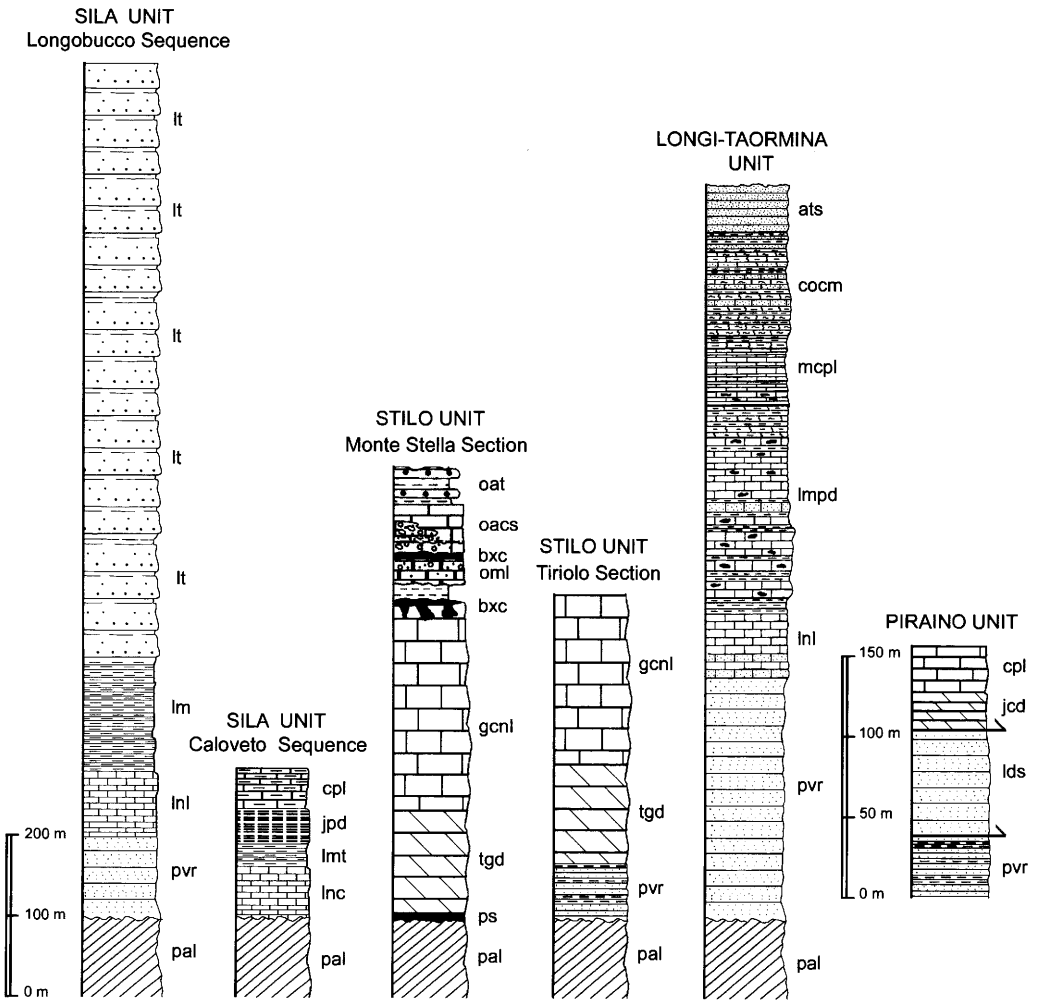

Fig. 5. Stratigraphic columns of the Pseudoverrucano-bearing units of the Calabrian–Peloritanian Arc (Longi–Taormina, Sila, Stilo and Piraino). pal, Palaeozoic epimetamorphites and granitoids; pvr, Upper Triassic redbeds; lnl, Hettangian–Sinemurian neritic limestones; lm, Pliensbachian slope marls; lt, Domerian–Toarcian turbidites; lnc, Sinemurian neritic limestones; lmt, Pliensbachian–Toarcian slope marls and turbidites; jpd, Middle–Upper Jurassic pelagic sediments; cpl, Lower Cretaceous pelagic limestones; ps, palaeosoil; tgd, Upper Triassic–Lowermost Jurassic dolostones; gcnl, Jurassic–Cretaceous neritic limestones; bxc, bauxitic clays; oml, lower Oligocene marls and limestones; oacs, upper Oligocene–Aquitanian calcarenites and conglomerates; oat, Aquitanian turbiditic marls and sandstones; lmpd, Carixian–Upper Jurassic pelagic sediments; mcpl, Tithonian–Albian maiolica-like pelagic limestones; cocm, Cenomanian–Oligocene scaglia-like limestones and marls; ats, Aquitanian turbiditic sandstones; lds, Toarcian–Aalenian sandstones; jcd, Jurassic?–Cretaceous? dolostones.

The post-Triassic succession of the Stilo Unit is the only one in the Calabrian–Peloritanian Arc made up of shelf and ramp carbonates. It is characterized by Mesozoic dolostones, limestones and calcareous breccias, and by Oligocene marsh marls, calcareous conglomerates and calcarenites, sometimes rich in metamorphic and plutonic rock débris, shows repeated hiatuses, marked by hardground, karst and bauxitic clay, and is topped by Aquitanian siliciclastic turbidites and marls (Bonardi *et al.* 2002, 2003).

In the Piraino Unit, finally, the lowest slice forming the unit, made up of redbeds, is followed by another slice where a siliciclastic formation with upper Pliensbachian–middle Aalenian ammonites, whereas Jurassic?–Cretaceous? crystalline

dolostones and Cretaceous nodular, crinoidal and cherty limestones constitute the uppermost slice of the unit (Cecca *et al.* 2002).

Palaeogeographical evolution. As regards the Mid-Triassic–Jurassic interval, the tectonosedimentary evolution in the Longi–Taormina, Sila and Piraino successions is similar to that of the Tuscan Pseudoverrucano Unit. It can be summarized as follows: (1) deposition, during Mid-Late Triassic times, of continental redbeds on a Variscan basement, whose uppermost levels are represented by mid-Carboniferous clastic deposits of Culm facies (Bouillin *et al.* 1987; Spalletta & Vai 1989); (2) development of a carbonate platform during the Hettangian–Sinemurian transgression; (3) platform deepening and development of slope and basinal facies in the Pliensbachian; (4) development of breccias and neptunian dykes associated with extensional tectonics (Toarcian–Late Jurassic). In the Longi–Taormina Unit, pelagic sedimentation persisted until the development of Aquitanian foredeep sediments predating the deformation (de Capoa *et al.* 1997). In the Stilo Unit the sedimentary evolution was different; the succession here consists of neritic and paralic sediments and is marked by repeated hiatuses, hard-grounds and bauxitic clays. However, its foredeep deposits and subsequent deformation are coeval with those of the Longi–Taormina Unit (Bonardi *et al.* 2003).

Tellian Maghrebids

In the Tellian sector of the Maghrebian Chain our own observations are sparse. Data from the literature indicate that Triassic redbeds occur in the Internal Units of the Lesser and Greater Kabylias and in the Babors Units, these latter related to the External Tellian Units.

Pseudoverrucano-like deposits. In Kabylias, Middle–Upper Triassic redbeds (Raoult 1974; Wildi 1983; Tefiani *et al.* 1991; Kotanski *et al.* 2004), resting on Palaeozoic phyllites and metarenites (Ordovician–Carboniferous), characterize the base of the Meso-Cenozoic covers of the Dorsale Calcaire Units, which constitute the structural lowest units of the Kabylide Complexes.

The redbeds are mainly made up of red–violet conglomerates, including quartz, quartzite and black radiolarite clasts, sandstones and pelites. In some sections, thin Middle Triassic carbonate beds testify to a local marine environment. Upwards, the succession grades into red and greenish pelites, followed by whitish, pink and yellow quartzarenites.

Post-Pseudoverrucano successions (Lower Jurassic–Oligocene?) and palaeogeographical evolution. The appearance of beds of dolostones alternating with green and red pelites precedes the deposition of Rhaetian–Lowermost Jurassic neritic carbonates, represented by dark grey crystalline dolostones, dolomitic limestones and whitish massive limestones. Neritic sediments are replaced by pelagic deposits (marly, nodular and cherty limestones; marls) in the Pliensbachian, which persist up to the Palaeogene. Neptunian dykes mark Jurassic extension (Bouillin & Naak 1989). In many units (Kef Sebargoud, Rhedir, Tengout; Raoult 1974), Jurassic and Cretaceous successions are characterized by hiatuses, mainly in the Upper Cretaceous sequences. In these instances, Palaeogene sedimentation starts with calcareous breccias and massive limestones containing algae and larger foraminifers (Raoult 1974). The most recent strata are represented by sandstones (Nummulitique II; Raoult 1974) of Oligocene or possibly younger age (Guerrera *et al.* 1993).

Alpine metamorphism is lacking and the successions display a lithological and stratigraphic evolution comparable with that of the units containing Pseudoverrucano-type deposits. Coutelle (1987) and Coutelle & Delteil (1989) showed similarities between the stratigraphic successions of some Kabylian Units and those of the Calabrian–Peloritanian Arc and Tuscan Nappe. Those workers placed all these groups of units, passing one into the other, in the same palaeogeographical belt, named the Intermediate Continental Domain and considered as the western part of the Adria–Apulia Plate.

Rifian Maghrebids

Pseudoverrucano-like deposits (Saladilla Formation, Triassic). In the Rifian Maghrebids (Fig. 6) Middle–Upper Triassic redbeds, which show Pseudoverrucano-like facies, occur at the base of the Meso-Cenozoic cover of both Ghomaride and Internal Dorsale Calcaire Units (Nold *et al.* 1981; Wildi 1983; Fig. 7) and, as their equivalent formations of the Betic Cordillera, have been grouped in the Saladilla Formation (Martín-Algarra *et al.* 1995; Maate 1996). This formation (Fig. 7) rests on a Hercynian basement, whose uppermost strata are represented by middle Carboniferous clastic deposits of Culm facies. The Internal Dorsale Calcaire units are generally detached from their basement, similar to the Triassic redbeds, which are completely unknown in the outermost Internal Dorsale Calcaire units (Hafa Ferkennix Nappe); however, they are widely present at the base of the innermost Internal Dorsale Calcaire units (El Babat Nappe) with a lithostratigraphy similar to the cover of Ghomarides *sensu stricto*, but usually with finer-grained, more distal facies and thickness up to 125 m. In few localities (south

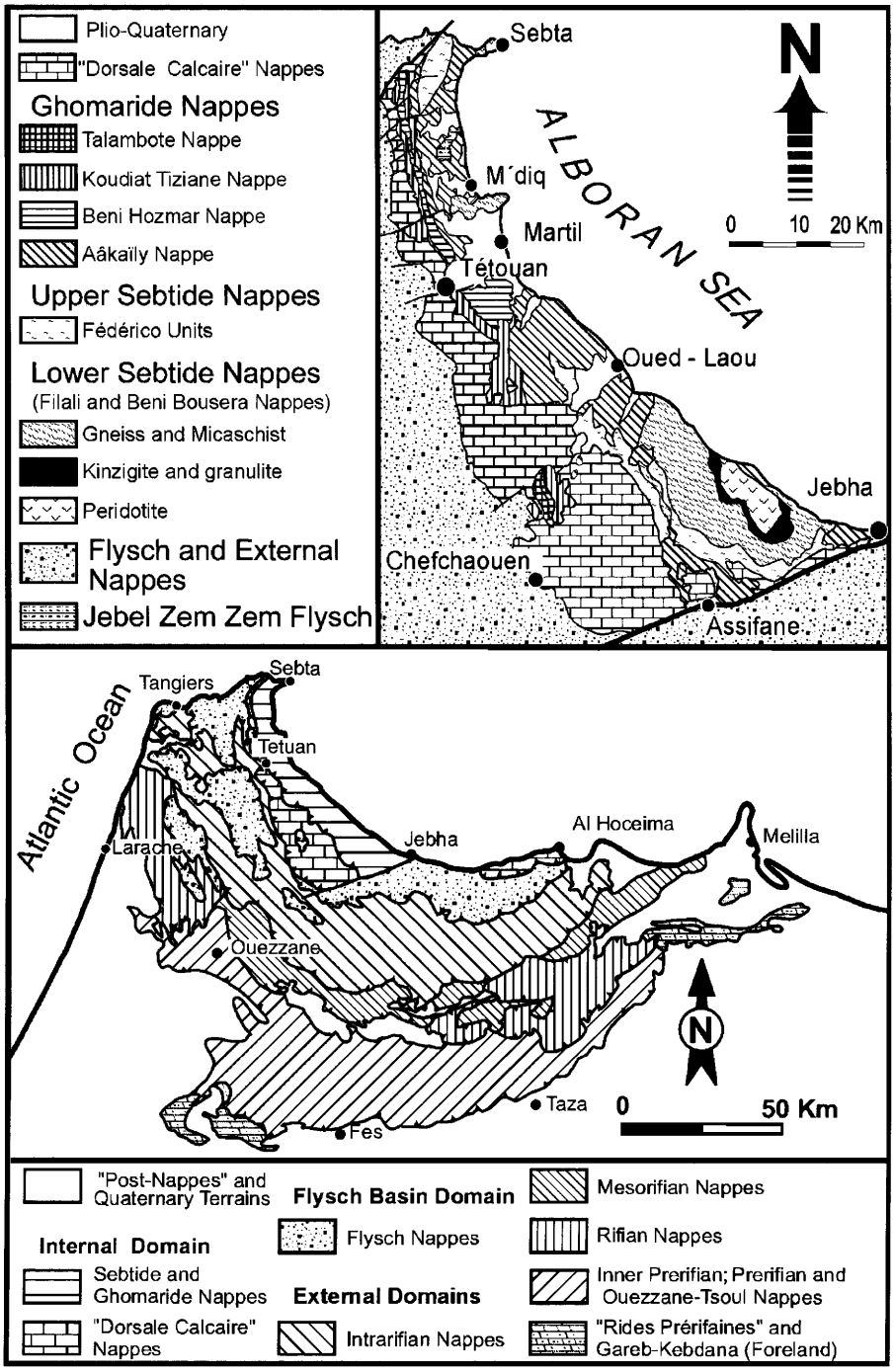

Fig. 6. Schematic geological map of the Rifian sector of the Maghrebian Chain and of the Internal Units of the Rifian Maghrebids. Modified from Suter (1980). Pseudoverrucano-like deposits occur in the Ghomaride and 'Dorsale Calcaire' Nappes; Verrucano-like deposits are present in the Upper Sebtide Units. The External Nappes are characterized by redbeds of Germano-Andalusian facies.

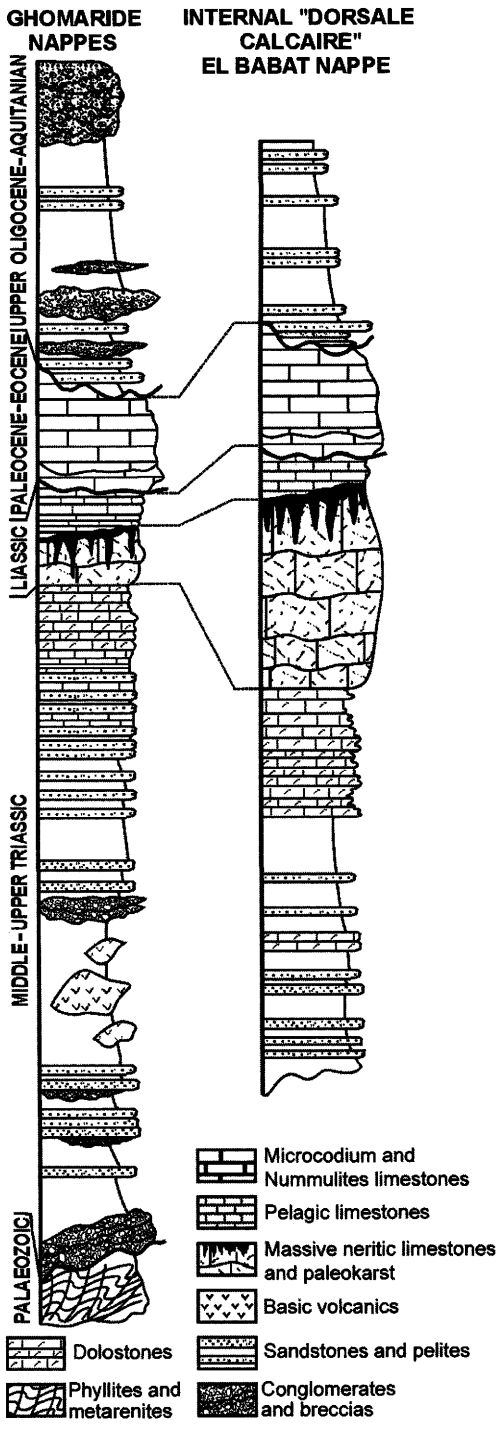

Fig. 7. Stratigraphic columns of the Rifian Ghomaride cover and Internal 'Dorsale Calcaire' Nappes (not to scale).

of Tetouan), El Babat Triassic redbeds lie unconformably on Palaeozoic rocks of the Koudiat Tiziane Ghomaride Nappe, forming a single tectonic unit (Maate *et al.* 1993*b*; Martín-Algarra *et al.* 1995; Maate 1996).

The stratigraphic succession of the Saladilla Fm, up to 400 m thick (Fig. 7), starts with coarse quartzose conglomerates and/or coarse-grained red sandstones, and continues with red quartzarenites and mudrocks including channelized conglomerates and sometimes basic volcanic flows (Chalouan 1986). Although a Permian age was proposed for the lower part of this succession (Milliard 1959) it has not been confirmed by more recent studies, and late Anisian–early Ladinian pollen was found near the top of red sandstones of the lower half of the succession (Baudelot *et al.* 1984; Martín-Algarra *et al.* 1995). The succession is followed by yellowish, white and pink sandstones alternating with red clays in which a 5–20 m thick interval of marls and sandy dolostones is locally present. The upper part of the succession is formed by yellowish quartz-rich conglomerates with rounded dolostone clasts alternating with, and changing upwards to, red, yellow and greenish sandstones and pelites, palynologically dated as late Carnian, with some dolostone and gypsum beds (Maate *et al.* 1993*b*; Martín-Algarra *et al.* 1995; Maate 1996).

The Saladilla Formation deposits are organized in two transgressive, thinning and fining upward megasequences of Mid-Triassic and Late Triassic age, respectively. The lower megasequence shows an evolution from alluvial and fluvial deposits to shallow marine carbonates upwards. Palaeocurrents indicate river flow towards the west and SW, and provenance of clastic deposits from erosion areas located towards the east (Maate 1996). The Late Triassic megasequence started after a regression followed by erosion and redeposition of Mid-Triassic carbonate clasts in high-energy, sandy conglomeratic (beach) environments and, since the late Carnian, was followed by deposition in a wide pelitic coastal plain (mudflat) with some carbonate and evaporite episodes.

Post-Pseudoverrucano successions (Lower Jurassic–Aquitanian). The presence on top of the Saladilla Fm of undated dolostones, followed by shallow marine white massive limestones suggests transgression and development of an Early Jurassic shallow carbonate platform dated as Sinemurian in the Ghomaride cover *sensu stricto*, where this succession is only few tens of metres thick. In the Internal Dorsale Nappes the dolostones are much thicker (up to 200 m) and, in their lower part, include isolated cross-bedded conglomerate

intervals with well-rounded white quartz clasts and oolitic–bioclastic limestones bearing the Rhaetian foraminifer *Triasina hantkeni*; they are followed by thick (up to 300 m) Hettangian–Sinemurian white massive neritic limestones (Maate 1996).

This shallow marine platform underwent break-off, tilting and local development of palaeokarst surfaces during the Pliensbachian (Maate *et al.* 1991; Maate 1996). This event was followed either in the Ghomaride cover *sensu stricto* or in the El Babat Nappe by deposition of condensed upper Pliensbachian–Toarcian silty and fine sandy cherty limestones and marls, and nodular limestones, but no younger Mesozoic deposits are present (Maate *et al.* 1991; Maate & Martín-Algarra 1992, 1993; Maate 1996). However, the succession of the Hafa Ferkennix Nappe is thicker and less condensed: it includes Pliensbachian–Toarcian cherty limestones, marls and nodular limestones, Middle–Upper Jurassic radiolarites, Tithonian–Neocomian greenish calcilutites, Lower Cretaceous calcareous breccias, and uppermost Cretaceous–Eocene pink and green marls (Maate *et al.* 1993*a*; Maate 1996).

In the Ghomaride cover *sensu stricto* and in some Internal Dorsale Units Palaeocene-Eocene *Microcodium*, *Alveolina* and *Nummulites* limestones lie directly on Jurassic–Cretaceous rocks and laterally evolve to pelagic scaglia-like marls (Maate *et al.* 1991, 2000; Maate 1996). Upper Oligocene–Aquitanian synorogenic siliciclastic sandstones and conglomerates were deposited during deformation of the Ghomaride realm and before the final emplacement of the El Babat and Hafa Ferkennix Nappes (Maate 1996). In the latter the conglomerates are associated with upper Oligocene marls and calcareous sandstones reaching more than 200 m in thickness. The stratigraphic successions are capped by massive, clast-supported, heterometric, Aquitanian conglomerates and breccias rich in clasts of prealpine (and subordinately alpinized) plutonic and metamorphic rocks (Martín-Algarra *et al.* 2000).

Betic Cordillera

Pseudoverrucano-like deposits (Saladilla Formation, Triassic). Triassic redbeds with Pseudoverrucano-like facies and associated marine sediments occur in the highest tectonic units of the Betic Internal Domain, the Malaguide Complex (Fig. 8). They are included in the Saladilla Formation, which was defined only in the Malaguide Units (Roep 1972). The Malaguide Meso-Cenozoic stratigraphic successions are similar to those of the Rifian Ghomarides, thus testifying to an equivalent tectonosedimentary history and deformational evolution (Martín-Algarra 1987, 2004; Maate 1996). However, they are frequently thicker and stratigraphically more complete than the Ghomaride

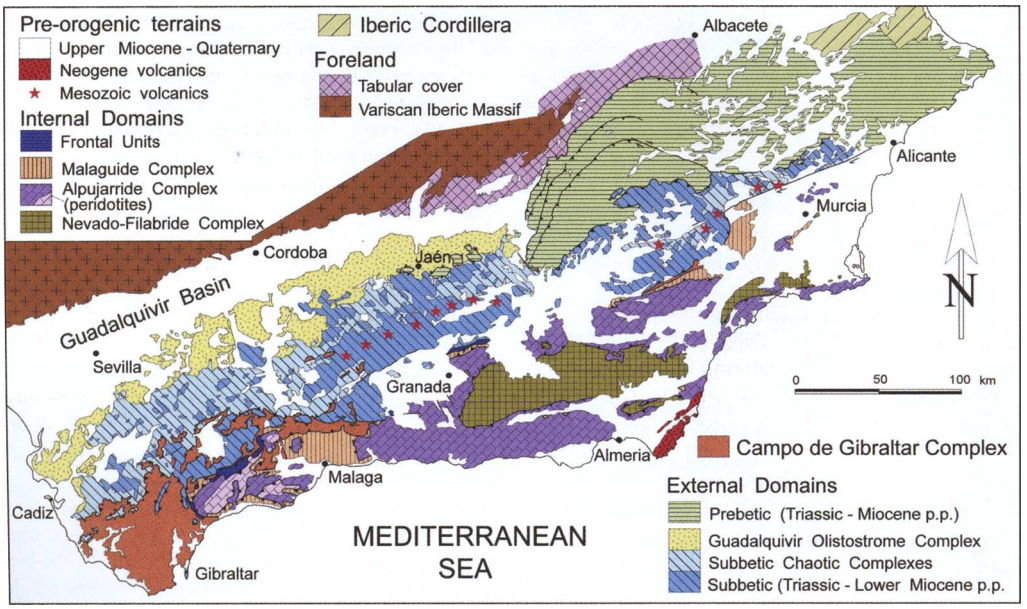

Fig. 8. Schematic geological map of the Betic Cordilleras. Modified from Vera (2004). Verrucano-like deposits occur in the Alpujarride Complex; Pseudoverrucano-like deposits characterize the Malaguide Complex. The External Domains (Subbetic and Prebetic Units) are characterized by redbeds of Germano-Andalusian facies.

successions, especially in the Morrón de Totana Unit of Sierra Espuña, in SE Spain (Martín-Martín 1996; Sanz de Galdeano *et al.* 2000; Martín-Martín *et al.* 2003; Caracuel *et al.* 2006).

Usually two transgressive megasequences (three in Sierra Espuña) can be distinguished in the Malaguide Triassic redbeds successions (Fig. 9). The first megasequence starts with red pelites with intercalated sandstones and quartz-rich polygenic conglomerates in which coarse-grained and thicker-bedded intervals frequently (but not always) concentrate in the stratigraphically lower part, forming thinning and fining upwards sequences, deposited in alluvial–fluvial environments with more distal (floodplain) facies toward the top of the succession (Roep 1972; Martín-Algarra *et al.* 1995). Scarce palynological data indicate a Mid-Triassic (early Anisian) age for this part of the succession (Simon & Kozur 1977; Mäkel & Rondeel 1979). Available palaeocurrent measurements from cross-bedded sandstones obtained in various Malaguide outcrops indicate provenances from an erosional area located to the south and SE (locally SW: Sierra Espuña), of the present-day Saladilla Fm outcrops (Mäkel 1982, 1988; Mäkel *et al.* 1984). Marine transgression is indicated by massive to well-stratified dolostones (up to 160 m thick in Sierra Espuña) with shallow marine facies and Ladinian–early Carnian fossils (Mäkel 1985) on top of continental redbeds.

Ladinian–Carnian dolostones were partially eroded (or totally in many outcrops) during regression related to the beginning of the second transgressive megasequence. This starts with mudflat varicoloured, mainly reddish, pelites and sandstones with intercalated conglomerates bearing carbonate pebbles (up to 100 m thick in Sierra Espuña; Sanz de Galdeano *et al.* 2000), associated with yellow cross-bedded sandstones with rounded dolostone clasts deposited in beach environments (Roep 1972). These coastal plain facies associations are covered by upper Carnian shallow marine marls, marly limestones, limestones and dolostones, above which Lower Jurassic platform carbonates are usually found (Martín-Algarra *et al.* 1995). In Sierra Espuña these dolostones contain chert nodules and ribbons (Mäkel 1985) and are followed by cross-bedded sandstones and polygenic conglomerates, which represent the base of the third sequence, and by uppermost Triassic grey clays with gypsum beds (25 m thick) changing progressively to the Jurassic succession (Sanz de Galdeano *et al.* 2000).

Post-Pseudoverrucano successions (Lower Jurassic–Aquitanian). The Malaguide Jurassic (Martín-Algarra 2004; Caracuel *et al.* 2006) starts with shallow marine dolostones (Hettangian?) followed by Sinemurian white, oolitic–oncolitic, biomicritic, crinoidal and *Lithiotis* limestones. After an unconformity on top of platform limestones, Domerian–Toarcian cephalopod-rich yellowish nodular limestones with ferruginous oolites were deposited. These condensed pelagic sediments are followed by Middle Jurassic micritic, crinoidal and cherty limestones topped by two hardgrounds of early Bajocian and early Callovian age, respectively. The Upper Jurassic rocks are represented by middle Oxfordian marls and marly limestones evolving to limestones, by lower Kimmeridgian massive and nodular limestones and, finally, by upper Tithonian marls with crinoids and calpionellids, which are covered by limestones and marly limestones of early Berriasian age. A palaeokarst surface separates these Cretaceous rocks from glauconitic–phosphatic calcareous green sands, breccias and marls (Albian–Turonian) while a further unconformity occurs at the base of Upper Cretaceous white and pink, scaglia-like marls and marly limestones (Martín-Algarra 2004).

Following a further unconformity at the top of the Mesozoic succession, Palaeocene deposits include *Microcodium*-rich shallow marine limestones and continental marls and conglomerates with garumnian facies (Martín-Martín *et al.* 1998), whereas Eocene and lower Oligocene rocks are represented by different shallow marine formations rich in larger foraminifera (Martín-Martín *et al.* 1997*a*,*b*). The succession (Fig. 9) is unconformably capped by upper Oligocene to Aquitanian mainly clastic deposits (Ciudad Granada Group; Guerrera *et al.* 1993), which, in Sierra Espuña, rest on a first generation of Malaguide cover tectonic units (Martín-Martín 1996; Martín-Martín & Martín-Algarra 2002), fan delta calcareous conglomerates, sandstones, limestones and marls (Bosque Fm) and siliciclastic deep marine turbidites (immature sandstones, pelites and polygenic conglomerates; Río Pliego Fm). As their equivalent Ghomaride deposits, these conglomerates contain clasts of plutonic and metamorphic rocks identical to those widely cropping out in the pre-Alpine basements of the Calabrian–Peloritanian and Kabylian Units, a fact pointing towards a close proximity between all these domains up to, at least, the end of the Aquitanian (Martín-Algarra *et al.* 2000; Careri *et al.* 2004).

Petrology and sandstone detrital modes

Triassic–Lowermost Jurassic continental redbeds of Pseudoverrucano facies have been analysed to determine the sedimentary evolution, provenance and burial history of this facies.

The studies have been carried out both in the Internal Domains of the Mediterranean Chains

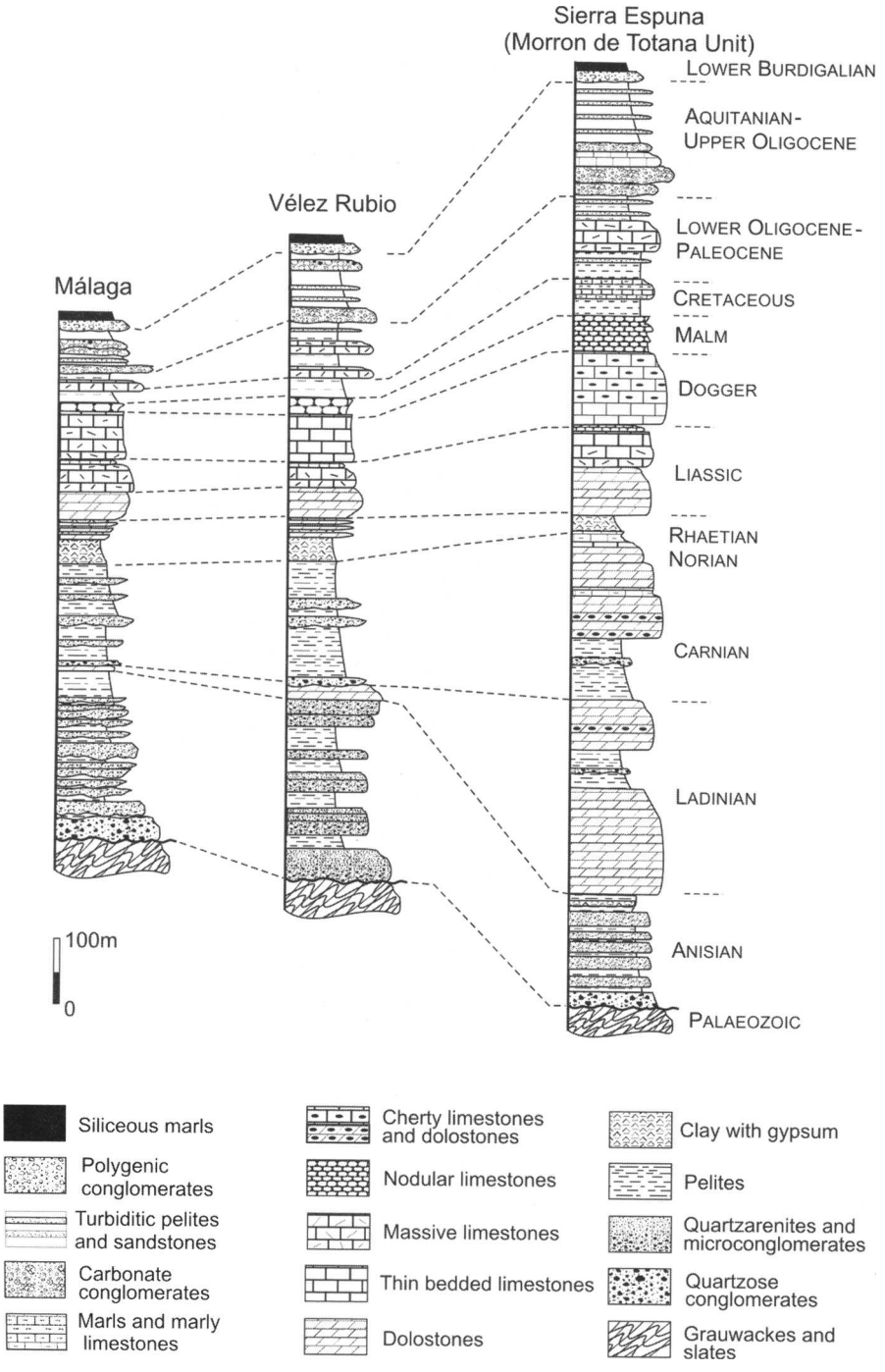

Fig. 9. Synthetic stratigraphic columns of the Betic Malaguide Nappes. The Tertiary succession in Sierra Espuña corresponds to areas of reduced thickness.

from the Gibraltar Arc to the Calabrian–Peloritanian Arc and in the Tuscan Pseudoverrucano Unit. A significant number of sandstone and mudrock specimens, sampled in three to five stratigraphic sections in all these orogenic sectors, have been considered.

Pseudoverrucano sandstones range from prevailingly quartzarenite to quartzolithic (Fig. 10), containing abundant monocrystalline and polycrystalline quartz; feldspar is subordinate. Lithic fragments include slate, radiolarian chert, argillaceous chert and minor felsic volcanic rocks. Conglomerate clasts consist mainly of quartz and include the same lithologies as the lithic fragments in sandstones.

The nature of the clastic deposits, both in sandstone and conglomerate strata, suggests a provenance dominantly from sedimentary and metasedimentary rocks of the Palaeozoic basements of the redbeds, which include mainly Cambrian to

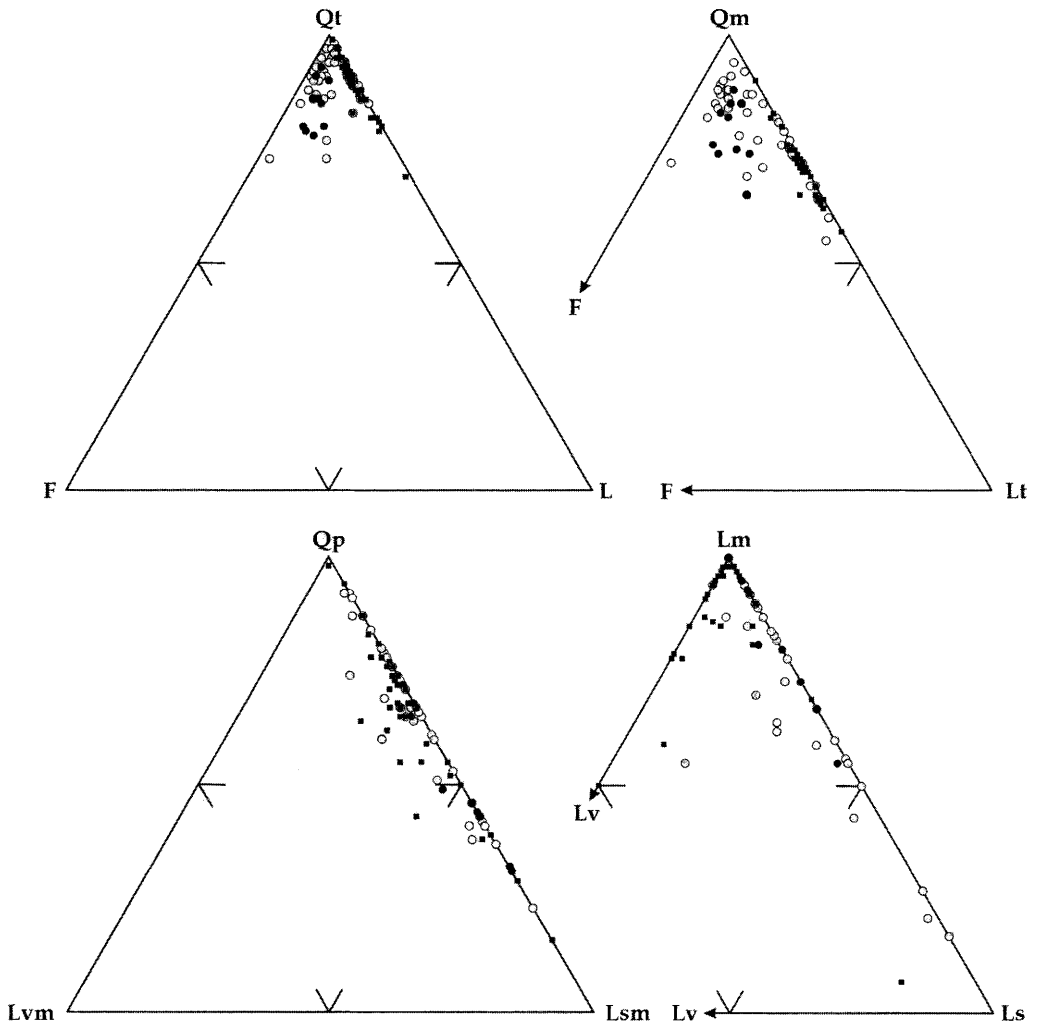

Fig. 10. Qt–F–L, Qm–F–Lt, Qp–Lvm–Lsm and Lm–Lv–Ls triangular plots for redbed sandstones of the Betic Malaguide (○), Rifain Ghomaride–'Dorsale Calcaire' (•), Tuscany and Calabrian–Peloritanian Arc (▪) Nappes. Qt, total (monocrystalline + polycrystalline) quartz including cherts; Qm, monocrystalline quartz; Qp, polycrystalline quartz including chert; F, feldspars; L, aphanitic lithic fragments (L = Lv + Lm + Ls); Lt, aphanitic lithic fragments + polycrystalline quartz; Lm, metamorphic lithic fragments; Lv, volcanic lithic fragments; Ls, sedimentary lithic fragments; Lvm, volcanic and metavolcanic lithic fragments; Lsm, sedimentary and metasedimentary lithic fragments.

mid-Carboniferous successions of clastic rocks (dominantly metarenites and metapelites), subordinate carbonates and radiolarian cherts.

In these basements, Ordovician to Permian mafic to felsic volcanic, subvolcanic and volcaniclastic rocks are scarce, whereas late Variscan, or older, plutonites and high-grade metamorphic rocks are known only in Calabria and Kabylias, which contribute only subordinately as source terrains for the redbeds. Two alternative hypotheses could be put forward to explain the scarcity or absence of plutonic and/or high-grade metamorphic rock fragments in both sandstones and conglomerates, cropping out in regions where plutonic rocks are at present widely exposed (such as the Calabrian–Peloritanian Arc): (1) the plutonic bodies were not exposed at the time of deposition; or (2) strong chemical weathering conditions mask the provenance signal. Strong chemical weathering of plutonic rocks in a hot, episodically humid climate with a prolonged dry season would produce illitization of silicate minerals, oxidation of iron and concentration of quartz in thick soil profiles, which, later denuded by fluvial erosion, would produce relatively mature quartz-rich red deposits. Geochemistry of mudrock beds present in the sandstone successions confirms these weathering processes and the provenance from quartzose metasedimentary sources.

Redbed quartzose sandstones from all the studied successions have been extensively modified by deep burial from diagenetic to anchimetamorphic zones. The related processes include compaction, pressure solution, precipitation of authigenic minerals, dissolution of framework grains, and substantial reduction of porosity. Most detrital grains show three or more contacts with neighbouring grains, indicative of mechanically consolidated sandstones. Many mica grains and soft lithic grains (shale, slate and phyllite) and rip-up clasts have undergone ductile deformation to form pseudomatrix.

Sandstones display heterogeneous distribution of authigenic quartz, kaolinite, illite and feldspar, with minor carbonate cementation. Authigenic quartz formed as zoned syntaxial overgrowths on detrital quartz is the principal cement of these sandstones. However, the occurrence of quartz cement varies in the studied samples depending on the presence of continuous clay coats that may retard quartz cementation. Extensive dissolution and kaolinization of detrital feldspar, mica and clay pseudomatrix occurred probably under an eodiagenetic meteoric regime. K-feldspar overgrowth, feldspar albitization and minor albite overgrowth occur where pore-filling kaolinite is also abundant.

The tectonic setting of the redbeds basins during the Triassic to earliest Jurassic implies that sandstone composition from nearly all regions should reflect provenances within a continental block (Fig. 10). A majority of the suites in all studied regions, in fact, show quartzose framework modes reflecting derivation from stable parts of the continent. Only some suites in each region display slightly more feldspathic framework modes, characteristic of the transitional group derived from continental blocks. Continental block-derived sandstones are particularly evident in the Rifian and Betic redbed sandstones. Source areas for these latter suites were probably characterized by somewhat greater relief with respect to the cratonic provenance areas. In the Calabrian–Peloritanian Arc, quartz-rich sandstones of cratonic and transitional origin occur not only during Triassic continental rift-valley sedimentation but also during following Early–Mid-Jurassic passive margin turbiditic deposition (Zuffa *et al.* 1980; Cecca *et al.* 2002). In all regions, a few sandstone suites show frameworks containing enough lithic fragments (quartzolithic *sensu stricto*) to plot within the provenance field for derivation from recycled orogens on either a QtFL or a QmFLt plot (Fig. 10; see the caption for explanation of recalculated parameters). In these cases, the lithic fragments were derived from sedimentary and metasedimentary rocks of the Variscan and pre-Variscan orogenies, and local volcanic fields related to both Permian and Triassic rifting events or to older Palaeozoic metavolcanic and volcanic suites.

Mineralogy and geochemistry of mudrocks

Chemical data from redbed mudrocks provide informations about source-area composition, palaeoweathering, sorting and recycling. Mudrocks were collected on Rif and Betic Chains and from Calabrian–Peloritanian Arc (Longi–Taormina and Sila Units).

Source-area weathering. Weathering processes that occurred in source rocks have been detected using the Chemical Index of Alteration (CIA; Nesbitt & Young 1982), the Chemical Index of Weathering (CIW; Harnois 1988) and the Plagioclase Index of Alteration (PIA; Fedo *et al.* 1995). The CIA values for redbeds are very low (66–73, average = 69.9 $\pm$ 1.7) and they plot in the A–K side of the A–CN–K diagram, close to the muscovite field (Fig. 11a), suggesting a K enrichment during burial history. Redbeds have a uniform CIW (95–98, average = 97.1 $\pm$ 0.65) close to the A apex in the A–C–N plot (Fig. 11b), testifying to intense weathering in steady-state conditions, in which material removal rate matches the production of mineralogically uniform weathering products generated in the upper zone of the soil profile. Unweathered plagioclase have a PIA value of 50

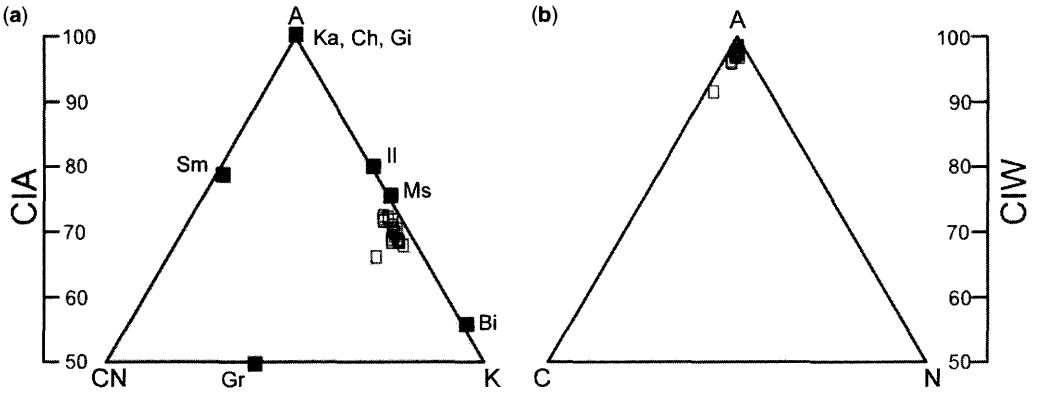

Fig. 11. (**a**) Ternary A–CN–K plot (A is Al_2O_3; CN, CaO + Na_2O; K, K_2O). The samples fall close to the A–K join along a trend indicating K addition during diagenesis. Gr, granite; Bi, biotite; Ms, muscovite; Il, illite; Ka, kaolinite; Ch, chlorite; Gi, gibbsite; S, smectite. (**b**) Ternary A–C–N plot (A is Al_2O_3; C, CaO; N, Na_2O). The samples fall close to the A apex, suggesting intense weathering at the source.

whereas the Post-Archaean Australian Shales (PAAS) have a PIA value of 79. Redbeds have very high PIA values (93–97, average = 95.3 ± 1.08), suggesting that most of the plagioclase has been converted to clay minerals. Results from the CIW and PIA, therefore, confirm intense weathering at the source area.

Recycling and provenance. Ancient sediments may undergo recycling and the Zr/Sc v. Th/Sc diagram (Fig. 12a) is a useful tool to assess the recycling processes (McLennan *et al.* 1993). It can be observed that the redbeds are not clustered along the primary compositional trend but fall along a trend involving zircon addition and thus sediment recycling. This is also consistent with changes in the Al_2O_3–TiO_2–Zr diagram (Fig. 12b).

As for the provenance, the Eu anomaly, which is retained as the more conservative proxy of parental affinity (McLennan *et al.* 1993; Mongelli *et al.* 1998; Cullers 2000), is slightly higher (average $Eu/Eu^* = 0.73 \pm 0.04$) than the PAAS value ($Eu/Eu^* = 0.66$). Thus, the average Eu/Eu^* of redbeds could monitor an important supply of low Eu/Eu^* mafic detritus that compensates for the recycling effect by reducing Eu/Eu^*. In our case, however, the recycling effect on the Eu anomaly was minor and, in turn, the low Eu/Eu^* mafic detritus supply was also minor although not negligible. The limited importance of a mafic supply is

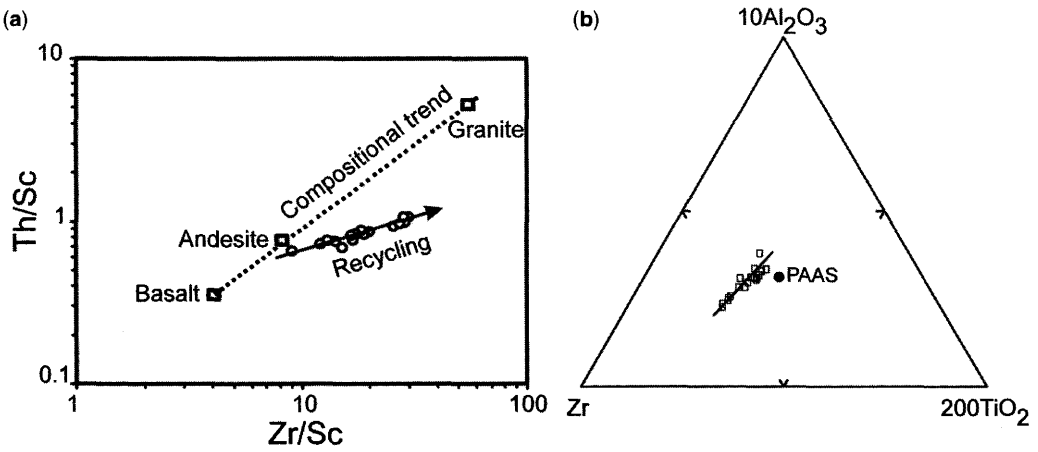

Fig. 12. Th/Sc v. Zr/Sc (**a**) and ternary $10Al_2O_3$–Zr–200 TiO_2 (**b**) plots. PAAS, Post-Archaean Australian Shales. The samples depart from the compositional trend, indicating zircon addition suggestive of a recycling effect.

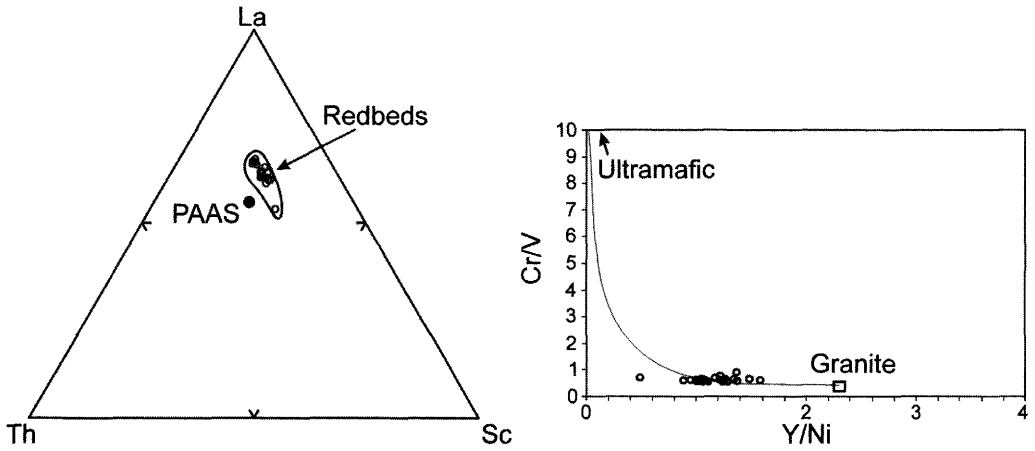

Fig. 13. Ternary La–Th–Sc (**a**) and Cr/V v. Y/Ni plots (**b**). PAAS, Post-Archaean Australian Shales. Both plots rule out a significant mafic–ultramafic supply.

also confirmed by other provenance proxies including the La–Th–Sc plot and the Cr/V and Y/Ni ratios. In the La–Th–Sc ternary diagram (Fig. 13a), which discriminates felsic sources from more mafic sources (e.g. Bhatia & Crook 1986; Cullers 1994), the redbeds fall in a region, close to the PAAS point, that clearly rules out a predominantly mafic source. Finally, a significant mafic–ultramafic supply is ruled out also on the basis of the mixing curve between granite and a mafic–ultramafic end-member in the Y/Ni v. Cr/V diagram (Fig. 13b).

To determine the degree of post-sedimentary processes possibly affecting the samples analysed in the present study and the range of temperature they experienced, the X-ray diffraction (XRD)-based illite 'crystallinity' technique (Merriman & Peacor 1999) was used. The illite crystallinity index (IC) and the percentage of illite in the illite–smectite (I/S) mixed layers were measured on the <2 μm size fraction XRD patterns from oriented mounts for the clay-rich levels from the continental redbeds. The percentage of illitic layers in I/S mixed layers, estimated following Moore & Reynolds (1997), is in the range of 70–90% ($R = 1$ and 3 ordering, Reickeweite number). In all the studied successions, the Kübler index values range between 0.65° and 0.28° $\Delta 2\theta$ (average = 0.45° ± 0.1° $\Delta 2\theta$). These values indicate conditions ranging from the diagenetic zone (0.45–0.65° $\Delta 2\theta$) to the anchizone (0.30–0.40° $\Delta 2\theta$).

In conclusion, detrital modes and geochemistry of the Triassic to lowermost Jurassic continental redbeds suggest a provenance dominantly from Palaeozoic sedimentary and metasedimentary rocks similar to those forming the pre-Alpine basements underlying redbeds. Petrography and mineralogy of redbeds testify to a complex burial history. The estimated temperature experienced by the Triassic to lowermost Jurassic redbeds, obtained by coupling data on the percentage of illitic layers in I/S mixed layers with the values of the Kübler index, is in the range of 100–180 °C. Starting from the temperature estimates obtained by geothermometers based on clay minerals, the diagenetic–tectonic evolution should correspond to a lithostatic–tectonic loading of about 5–6 km.

The sedimentary evolution of Middle-Triassic–Lowermost Jurassic quartzose redbeds is homogeneous in all outcrops of the studied orogenic sectors, suggesting a common palaeogeographical and palaeotectonic evolution since break-up of Pangaea. They can be considered as a regional petrofacies that outlines the onset of the continental rift valley stage of the Mesozoic taphrogenesis in Western Pangaea, which allowed the opening of the Western Neo-Tethys Ocean. Therefore, these redbeds could represent a key stratigraphic marker to distinguish a particular continental block within the Western Mediterranean Domains.

Verrucano-type successions

Northern Apennines

Stratigraphy of the Verrucano Group. The Verrucano Group deposits occur in all the Tuscan Metamorphic Units, particularly in the Massa and Monticiano–Roccastrada Units (Fig. 2). In all these units the Verrucano deposits unconformably overlie a pre-Alpine basement, represented mainly by Palaeozoic phyllites and metarenites with some intercalated layers of metavolcanic rocks and metadolo-stones and, locally, post-Hercynian continental or marine deposits of Late Carboniferous–Permian

age. In the Monticiano–Roccastrada Unit, the metamorphic Monte Argentario Sandstone Formation (Upper Permian–Lower Triassic) is interposed between the Palaeozoic basement and the Verrucano Group deposits (Cirilli *et al.* 2002; Lazzarotto *et al.* 2003).

The Verrucano Group mainly consists of detrital continental formations, deposited in an oxidizing environment. Rau & Tongiorgi (1974) considered that the violet colour characteristic of some of these deposits results from the metamorphic overprint at the expense of Buntsandstein-type, originally reddish sediments.

In the most complete succession of the Northern Apennines (Massa Unit), two sedimentary cycles, separated by a disconformity surface, have been distinguished (Passeri 1985; Rau *et al.* 1985; Martíni *et al.* 1986). The lower cycle, Anisian–Ladinian in age, is characterized by frequent marine strata and by alkaline metabasalts (Punta Bianca; Monte Brugiana). The upper cycle (Verrucano Group *sensu stricto*) starts with upper Ladinian continental sediments, evolving in the late Carnian to carbonate–evaporitic deposits. The Verrucano Group is followed by Norian–Liassic platform carbonates grading, in the Middle Liassic, into basinal pelagic deposits.

In the Apuane Unit (Giannini & Lazzarotto 1975; Fig. 14), the continental deposits are lacking or limited to a few metres of Middle Triassic–Carnian violet quartz-bearing metaconglomerates, rare quartzites and phyllites alternating with grey–reddish carbonate quartzites, microcrystalline dolostones, grey and greenish phyllites (Carnian; Vinca Fm), followed by Norian hypersaline platform dolostones (Grezzoni Fm; Ciarapica & Passeri 1978).

The Verrucano of the Massa Unit was described in detail by Rau & Tongiorgi (1974) and Tongiorgi *et al.* (1977) in the Monti Pisani, but the most complete succession crops out at Punta Bianca promontory.

In the Monti Pisani area, Rau & Tongiorgi (1974) distinguished in the Verrucano Group the continental Middle Triassic Verruca Formation and the Carnian Quarziti di Monte Serra Formation, in which marine sedimentary facies are present (Fig. 14). The Verruca Formation, unconformable on Palaeozoic phyllites and metarenites, includes three members, from bottom to top: (1) Anageniti Grossolane Member, made up of reddish coarse conglomerates, 40–100 m thick, with a quartz–micaceous sandy matrix; centimetre-sized clasts are mainly of quartz and minor quartzites and rhyolites; (2) Scisti Violetti Member, formed by violet phyllites and quartzose phyllites, 180–200 m thick, with some intercalated beds or lenses of sandstones and conglomerates; (3) Anageniti Minute Member, formed by 100–170 m of well-bedded whitish quartzites, associated with light quartzose phyllites and violet or greenish phyllites. The lithological and sedimentological features of the Verruca Fm indicate continental environments evolving from alluvial fan to alluvial plain crossed by braided seasonal streams in a semi-arid climate. In the overlying Quarziti di Monte Serra Formation, between 280 and 480 m thick, made up mainly of micaceous quartzites, quartzose phyllites and phyllites, it is possible to recognize four members indicating different transitional or marine environments. From the bottom to top, one can recognize the Scisti Verdi, Quarziti Verdi, Quarziti Bianco-rosa and Quarziti Viola Zonate Members, indicating lagoon–marine, sandy shore, deltaic platform and coastal pond environments, respectively. The last member of the Quarziti di Monte Serra Formation is followed by the Norian dolostones of the Grezzoni Formation.

The Verruca and Quarziti di Monte Serra Formations are usually correlated with the upper Ladinian(?)–Carnian upper cycle of the Punta Bianca promontory (see below). In the Monte Pisano area, therefore, Anisian–Ladinian rocks of the Verrucano Group should not be deposited.

Two sedimentary cycles, as noted above, are recognizable in the succession of the Punta Bianca area (Passeri 1985; Rau *et al.* 1985; Martíni *et al.* 1986). Both cycles show a progressive evolution from continental to marine environment. The Anisian–Ladinian lower cycle (Fig. 14) starts with alluvial fan conglomerates, unconformable on Palaeozoic phyllites, fed by the underlying basement, which grade to a coastal plain sandy–silty sequence followed by clayey limestones and well-bedded limestones rich in dasycladacean algae, indicating the progressive development of a restricted platform marine environment. Sedimentation abruptly passes to turbiditic calcarenites and sandstones and to clast-supported heterometric coarse white calcareous breccias, with interbedded calcarenites and calcareous mudstones. Clasts prevailingly consist of *Diplopora* and crinoid limestones. The sequence continues with frequent calcarenite beds, associated with lenticular conglomerates, sandstones, violet or grey–greenish siltstones and claystones, calcareous breccias, followed by a volcanic interval, made up by basaltic lavas, locally with pillows, and volcaniclastic rocks, capped by thin beds of red cherts. The last phase of the lower cycle is represented by a new level of calcareous breccias, 15 m thick, whose upper beds show palaeokarst structures indicating an abrupt emersion.

The upper cycle (upper Ladinian?–Carnian) is almost exclusively made up of fluvial terrigenous sediments with, in the upper part, littoral and tidal sediments; that is, from bottom to top, violet siltites

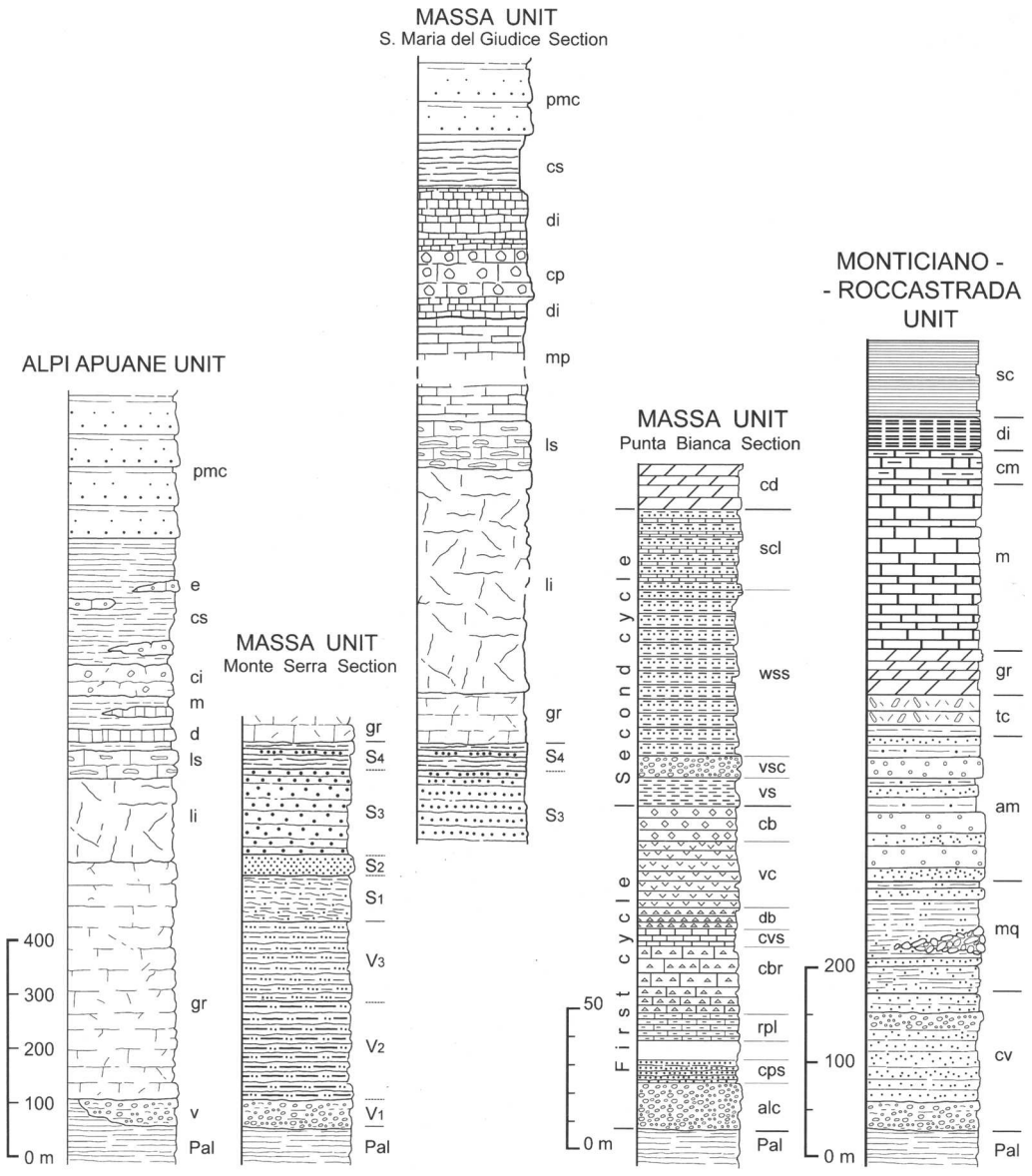

Fig. 14. Stratigraphic columns of Metamorphic Tuscan Units. Alpi Apuane Unit: Pal, Palaeozoic metamorphites; v, Middle–Upper Triassic Verrucano redbeds; gr, Norian dolostones; li, Hettangian–Sinemurian dolomitic and calcareous marbles; ls, Pliensbachian–Toarcian cherty metalimestones; m and d, Middle and Upper Jurassic calc-schists and radiolarites; ci, Lower Cretaceous crinoidal cherty metalimestones; cs and e, Upper Cretaceous–lower Oligocene calc-schists and calcarenites with nummulites; pmc, upper Oligocene–Aquitanian turbidite metasandstones. Massa Unit (Monte Serra Section): Pal, Palaeozoic metamorphites; Mid Triassic Verruca Formation: V_1, coarse conglomerates (Anageniti Grossolane Member); V_2, phyllites and sandstones (Scisti Violetti Member); V_3, quartzites and phyllites (Anageniti Minute Member); Carnian Quarziti di Monte Serra Formation: S_1, phyllites and micaceous quartzites (Scisti Verdi Member); S_2, green quartzites (Quarziti Verdi Member); S_3, light quartzites and phyllites (Quarziti Bianco-rosa Member); S_4, hematitic micaceous quartzites (Quarziti Viola Zonate Member); gr, Norian dolostones. Massa Unit (Santa Maria del Giudice Section): Carnian Quarziti di Monte Serra Formation: S_3, light quartzites and phyllites (Quarziti Bianco-rosa Member); S_4, hematitic micaceous quartzites (Quarziti Viola Zonate Member); gr, Upper Carnian–Rhaetian dolostones; li, Hettangian–Sinemurian dolomitic and calcareous marbles; ls, Pliensbachian–Toarcian cherty metalimestones; mp, Middle Jurassic *Posidonomya* Marls; di and cp, Upper Jurassic

and claystones, passing to red–purple and violet sandstones and quartz clast-rich conglomerates, repeated alternations of quartzose sandstones, siltstones and slates, with some thin carbonate beds in the uppermost levels. The sequence ends with phyllites, fine-grained quartzose sandstones, carbonate phyllites and yellowish carbonates and evaporites.

Within the Monticiano–Roccastrada Unit, the Verrucano Group (Costantini *et al.* 1987; Fig. 14) consists of four formations, including the Tocchi Formation in the upper part. Below the Tocchi Formation, three silicidastic formations, varying from conglomerates to pelites, occur.

The stratigraphic succession starts with the Civitella Marittima Formation, made up of 200 m of thin-bedded green to light grey fine- to coarse-grained metasandstones, intercalated with lenses of metaconglomerates and minor grey or violet metasiltstones. Metaconglomerates, up to 60 m thick, show white abundant quartz clasts, up to 15 cm in size, in a quartzose sandy matrix. This formation has been considered Mid-Triassic in age and correlated (Lazzarotto *et al.* 2003) with the lower cycle of Punta Bianca.

The overlying Monte Quoio Formation, up to 200 m thick, consists of purple metasandstones and metasiltstones intercalated with lenticular beds of polygenic metaconglomerates. These latter are characterized by centimetre–decimetre-sized clasts of white and pink quartz, white, violet and green quartzites, and minor black siltites, violet phyllites and pink or red limestones with Anisian neritic fossils. The Monte Quoio Fm grades into the Anageniti Minute Formation, consisting of yellowish or whitish-pink quartzites and metaconglomerates intercalated with purple and minor grey–green metasiltstones and phyllites, followed by the Tocchi Formation, made up of breccias with clasts of grey–greenish and violet phyllites in a yellowish carbonate matrix, alternating with evaporitic limestones, metalimestones, quartzites and phyllites.

The Monte Quoio and the Anageniti Minute Formations have been correlelated (Lazzarotto *et al.* 2003) with the Verruca Fm of Monte Pisano and with the lower part of the upper cycle of Punta Bianca and considered to be Ladinian in age, whereas the Tocchi Fm is considered to be Carnian in age, on the basis of microfossils in some of the carbonate beds.

The Triassic stratigraphic succession of the Monticiano–Roccastrada Unit ends with Norian–Rhaetian grey dolostones and dolomitic limestones (Grezzoni Fm).

Post-Verrucano successions (Norian–Aquitanian). As noted above, in all the Tuscan Metamorphic Units the oldest post-Verrucano rocks are represented by Norian–Rhaetian dolostones. The post-Triassic succession of the Apuane Unit (Giannini & Lazzarotto 1975; Carmignani *et al.* 1987; Conti *et al.* 2004) continues with Hettangian–Sinemurian dolomitic marbles and calcareous marbles (the 'Carrara Marbles'), followed by cherty metalimestones and calc-schists ('Cipollini'; middle Lower to middle Middle Jurassic), radiolarites ('Diaspri'; Callovian–Tithonian), and cherty metalimestones bearing crinoids (Lower Cretaceous). This prevailingly carbonate sequence passes to Lower Cretaceous–lower Oligocene sericitic schists and calc-schists and it is closed by metasandstones of turbidite Pseudomacigno Formation (upper Oligocene–lower Miocene).

In the Massa Unit, the successive sedimentary evolution of the Verrucano Group can be seen in the northwestern side of Monte Pisano, in the Santa Maria del Giudice sequence (Rau & Tongiorgi 1974). The Quarziti di Monte Serra Fm (Fig. 14) is followed by upper Carnian rauhwackes, Norian–Rhaetian dark grey dolostones (Grezzoni Fm) and metalimestones, lowermost Jurassic marbles (Calcari Ceroidi) and cherty limestones, Middle Jurassic *Posidonomya* marls, Upper Jurassic radiolarites and multicoloured sericitic schists (Cretaceous–lower Oligocene). The succession is capped by the turbidite sandstones of the Pseudomacigno Fm (upper Oligocene–lower Miocene).

---

radiolarites and cherty metalimestones; cs, Cretaceous–lower Oligocene multicoloured sericitic schists; pmc, upper Oligocene–Aquitanian turbidite metasandstones. Massa Unit (Punta Bianca Section; according to Rau *et al.* 1985): Pal, Palaeozoic metamorphites; Anisian–Ladinian lower cycle: alc, alluvial fan conglomerates; cps, coastal plain sandstones and siltstones; rpl, restricted platform metalimestones; cbr, calcareous breccias and calcarenites; cvs, calcarenites, carbonatic shales, conglomerates and siltstones; db, calcareous breccias with diplopores; vc, basalts and volcanoclastic rocks; cb, carbonatic breccias; upper Ladinian?–Carnian upper cycle: vs, violet siltstones; vsc, violet quartzose sandstones and conglomerates; wss, white and violet quartzose sandstones and silstones; scl, sandstones and siltstones with thin carbonatic levels; cd, calcareous–dolomitic evaporite deposits. Monticiano–Roccastrada Unit: Pal, Palaeozoic metamorphites; cv, Middle Triassic metasandstones with metaconglomerate lenses; mq, Ladinian metasandstones and metasiltstones; am, Ladinian quartzites and violet phyllites; tc, Carnian breccias and evaporite carbonates; gr, Norian dolostones; m, lowermost Jurassic marbles; cm, di and sc, Lower Cretaceous cherty marbles, siliceous metapelites and varicoloured sericite schists.

The post-Triassic stratigraphic succession of the Monticiano–Roccastrada Unit above the Grezzoni Fm continues with lowermost Jurassic massive yellow, pinkish and white marbles (Marmi Fm), followed by some disconformable Upper Cretaceous heteropic formations consisting of well-bedded cherty marbles, siliceous metapelites and metaradiolarites, and varicoloured sericite schists and metamarls (Costantini *et al.* 1987).

Tectonosedimentary evolution of the Tuscan Verrucano and comparison with that of the Tuscan Pseudoverrucano. The tectonosedimentary evolution of the Tuscan Metamorphic Units is certainly more complex than that of the Pseudoverrucano Unit. As regards the Triassic terrains, two sedimentary cycles have been identified in the Punta Bianca section (Fig. 14) of the Massa Unit and in the Monticiano–Roccastrada Unit, whereas in the Apuane Unit and in the Monte Pisano area only terrains referable to the upper cycle occur. The first marine beds, represented by neritic limestones, appear in the Anisian of the Punta Bianca section, and Anisian limestone clasts are also present in the Ladinian Monte Quoio Fm of the Monticiano–Roccastrada Unit. In the Punta Bianca section, the Ladinian is almost entirely characterized by calcareous neritic deposits and calcareous breccias, testifying to the rapid evolution and tectonic fragmentation and resedimentation of carbonate platforms as a result of a peak of tectonic activity which, during the late Ladinian, produces basin uplifting and the disconformable deposition of siliciclastic continental sediments of the upper cycle. Extensional tectonic activity is also marked by the occurrence of basic alkaline volcanic rocks.

After the late Ladinian?–Carnian, clastic deposits of the second cycle were covered by evaporitic–carbonatic sediments, starting with deposition of Carnian evaporites, followed by Norian dolostones and by Rhaetian–lowermost Jurassic neritic limestones. From the Pliensbachian onwards, sedimentation becomes pelagic and is characterized by nodular, cherty and marly limestones and, eventually, by radiolarites. Marly–calcareous pelagic and turbidite sediments persist until the late Oligocene–early Miocene, when siliciclastic turbidite sediments, deposited within the Apennine foreland basin system, testify to the onset of compressional deformation and the incorporation of the Tuscan Metamorphic Units within the orogenic edifice.

Deformation and metamorphism of the Verrucano Group. Miocene deformation was accompanied by metamorphism. Recent petrological studies allow us to completely rewrite the metamorphic history of the Tuscan Metamorphic Units. In the eastern part of Monte Argentario, the lower part of the Verrucano succession of the Monticiano–Roccastrada Unit includes psammitic and pelitic metasediments characterized by quartz, muscovite, hematite, chloritoid, sudoite, pyrophyllite, rare chlorite, kaolinite and dolomite, and by quartz segregations with quartz, calcite, chlorite, cookeite, white mica, kaolinite and localized Mg- or Fe-carpholite (Theye *et al.* 1997). The upper levels are characterized by a quartz–muscovite–hematite assemblage with subordinate chlorite, paragonite, pyrophyllite and localized carpholite in quartz segregations.

The reconstructed polystage metamorphic evolution (Fig. 15) indicates a P–T path characterized by a first stage showing peak conditions at $P > 0.8$ GPa and $T = 300$–400 °C (Mg-carpholite, chlorite, quartz assemblage in the pyrophyllite stability field) in the lower levels, and at $P > 0.7$ GPa and $T = 300$–350 °C (carpholite and pyrophyllite assemblage) in the upper levels. The second stage (exhumation path) is marked by isothermal decompression at $P < 0.5$ GPa (sudoite–pyrophyllite assemblage) and subsequent cooling at low T (<300 °C) and P (late kaolinite).

A similar evolution has been also reconstructed in the Mid-Tuscan Dorsal region (Monticiano–Monte Leoni area; Giorgetti *et al.* 1998). Verrucano metasediments consist of phyllites and Al-rich quartzites including newly formed muscovite, chlorite, chloritoid, pyrophyllite, sudoite, paragonite and kaolinite. Mg-carpholite is also present in synfolial quartz–calcite veins.

Different stages in the P–T path have been delineated. Peak conditions took place at $P = 0.8$–1.0 GPa and $T = 400$–420 °C, in the lower levels, and comparable or slightly lower P and $T = 350$–360 °C in the upper levels (chlorite, phengite, chloritoid, pyrophyllite, Mg-carpholite; syn- to post-kinematic assemblage). A retrograde isothermal path was followed during decompression at $P < 0.5$–0.6 GPa (sudoite and pyrophyllite assemblage; late kaolinite).

In the Apuane Unit, peak metamorphic conditions were attained during the first deformation phase and the occurrence of pyrophyllite + quartz assemblages indicates P of 0.5–0.6 GPa and T between 300 and 450 °C (Di Pisa *et al.* 1985; Franceschelli *et al.* 1986, 1997; Schultz 1996; Molli *et al.* 2000*b*) or 0.6–0.8 GPa (Jolivet *et al.* 1998). During the second deformation phase, $T = 380$ °C in the eastern area and 340 °C in the western area were reached (Molli *et al.* 2000*a*).

Metapelites of the Verrucano Formation in the Massa Unit (Molli *et al.* 2000*b*) result from two deformation phases. The D_1 phase was responsible

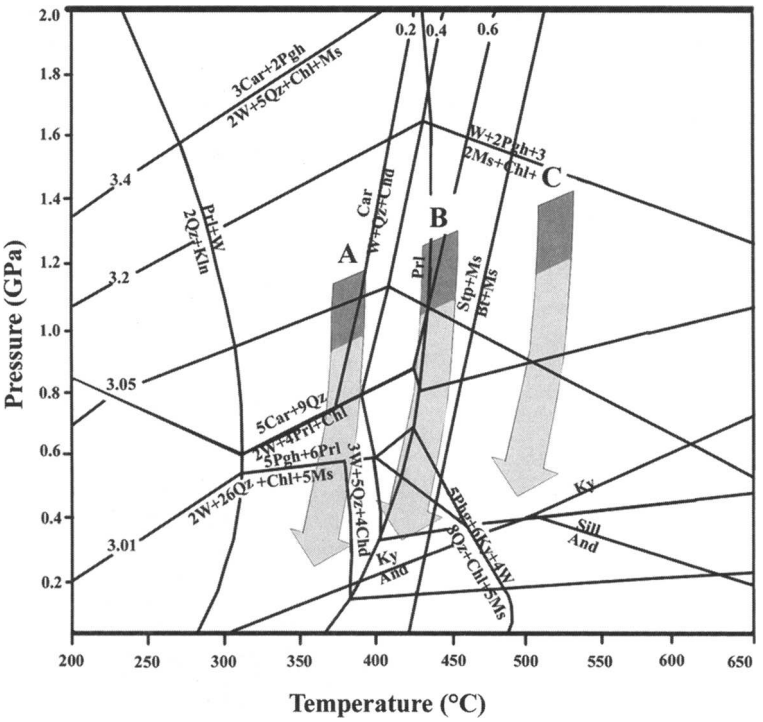

Fig. 15. *P–T* paths of the Tuscan Metamorphic Units: dark shaded arrow indicates syncollisional peak stage; light shaded arrow indicates exhumation decompression stage. A, Monticiano–Roccastrada Unit; B, Alpi Apuane Unit; C, Massa Unit. Minerals of the metamorphic reactions: Qz, quartz; Kln, kaolinite; Prl, pyrophyllite; W, water; Car, carpholite; Phg, phengite; Chl, chlorite; Ms, muscovite; Chd, chloritoid; Ky, kyanite; And, andalusite; Stp, stilpnomelane; Bt, biotite, Sill, sillimanite. Petrogenetic grid is modified after Oberhänsli *et al.* (1995).

for the development of the main foliation defined by quartz, white micas (muscovite ± paragonite), chlorite, and chloritoid ± kyanite. The same minerals developed up to post-D_1. The D_2 phase was responsible for the development of a crenulation cleavage marked by phyllosilicates. The reconstructed thermobaric conditions indicate that the metamorphic peak occurred at $P > 0.8$ GPa and $T = 400–500$ °C (within the kyanite stability field). The retrograde path involved a decrease of P and T with continued chloritoid development (within the pyrophyllite stability field).

These data indicate that during Neogene deformation in the Northern Apennines significant crustal thickening occurred and the Tuscan continental crust was underthrust to depths characterized by pressures of 0.5–0.6 to 1.0 GPa.

This tectonometamorphic evolution, when it is considered within the general framework outlined in this paper and compared with the other study areas, may put into question the generally accepted location of the Tuscan Metamorphic Units on the Adria–Apulia continental margin. In any case, with respect to the convergent tectonic stages, the Tuscan Metamorphic Units seem to have been located in a more external position than the Pseudoverrucano Sub-domain.

Southern Apennines–Sicilian Maghrebids

Verrucano-like successions. In the internal units of these orogenic sectors, cropping out in the Calabrian–Peloritanian Arc, terrains comparable with the Verrucano of the Tuscan Metamorphic Units are recognizable only in the Bagni and Alì–Montagnareale Unit. Terrains correlatable to the Verrucano are present also in the San Donato and Verbicaro Units (Amodio Morelli *et al.* 1976), recently redefined as the Lungro–Verbicaro Unit (Iannace *et al.* 2004*b*, 2005). This latter unit has been traditionally attributed to the Adria–Apulia margin and, therefore, considered as an external Apenninic unit. This attribution has been only recently discussed (Perrone 1996).

The Bagni Unit (Amodio Morelli *et al.* 1976) shows features similar to those of the

Verrucano-bearing units, because its succession (Fig. 16) is affected by Alpine metamorphism and shows an early evolution to a marine environment (Upper Triassic dolostones; Scandone 1970). The basement, widely cropping out in the Calabrian Coastal Chain and in the Sila Massif (Fig. 4), is formed by Palaeozoic phyllites and metarenites, with abundant porphyroid levels, on which a few and scattered thin strips of Mesozoic cover occur. The basal layers of this cover (Dietrich 1976) are represented by a few metres of red–purple metasandstones and metaconglomerates with violet metasiltites, the latter forming the most frequent lithology.

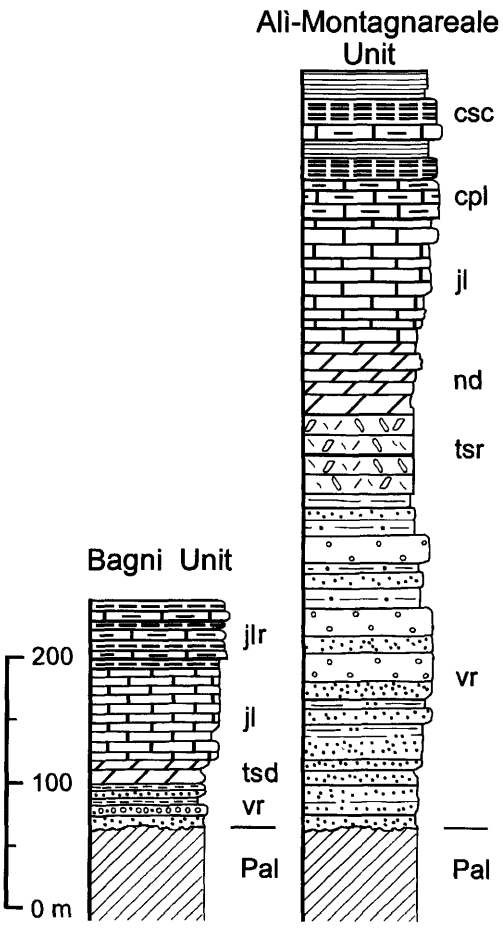

Fig. 16. Stratigraphic column of the Bagni and Alì–Montagnareale Unit. Bagni Unit: Pal, Palaeozoic phyllites and metarenites; vr, Upper Triassic reddish metapelites, metarenites and metaconglomerates; tsd, metadolostones; jl, Jurassic metalimestones and cherty metalimestones; jlr, Upper Jurassic–Lower Cretaceous? cherty metalimestones and metaradiolarites. Alì–Montagnareale Unit: Pal, Palaeozoic phyllites and metarenites; vr, Middle Triassic reddish metapelites, metarenites and metaconglomerates; tsr, Carnian calcareous–dolomitic evaporites; nd, Norian–lowermost Jurassic metadolostones and black metalimestones; jl, Jurassic marly and cherty metalimestones; cpl, Cretaceous pelagic metalimestones; csc, Cretaceous variegated siliceous metaclaystones.

The Alì–Montagnareale Unit, cropping out in two small areas in the Peloritani Mountains (Fig. 4), also shows characteristics close to those of the Verrucano, its succession being (Fig. 16) affected by metamorphism and showing an early evolution to a marine environment (Carnian evaporites and Norian dolostones). The basement is made up of Lower Devonian–Carboniferous dark graphite phyllites, metarenites and metaconglomerates with plant remains. The metamorphic Alpine cover starts with alternating reddish metapelites, metarenites and metaconglomerates (200–250 m thick), passing to 60 m of pinkish to yellowish rauhwackes (Carnian) and Norian metadolostones.

The Lungro–Verbicaro Unit (Iannace *et al.* 2004*b*, 2005) is widely exposed in northern Calabria (Fig. 4). The lowest levels of the stratigraphic succession crop out in the Monte Caramolo area (Fig. 17), where they consist of a thick succession (at least 400 m) of grey, silvery and bluish phyllites, and minor metarenites, in which lenses of metalimestones furnished Anisian–lower Ladinian algae (Bousquet & Dubois 1967; Iannace *et al.* 1995). Phyllites pass to a thick formation of grey to black, sometimes nodular, marbles, which in the upper part of the formation grade laterally to a Ladinian–Carnian reef complex, consisting of boundstones with sponges and biogenic crusts, as well as fore-reef breccias. The grey–black marbles are followed by upper Carnian–lower Norian metadolostones and laminated dolomitic metalimestones, deposited in a shallow open shelf and in a subtidal restricted environment, respectively. The sequence continues with typical Norian Hauptdolomit facies. Megabreccias and neptunian dykes testify to a strong synsedimentary tectonics in both the Ladinian and early Norian. Towards the south, in the Sant'Agata area, phyllites, calcschists, metarenites and metalimestones are interbedded with the upper Carnian dolostones (Fig. 17) and these lithologies become dominant southwards, in the Coastal Chain Cetraro tectonic window (Fig. 17). In both the Sant'Agata and Cetraro areas the succession evolves to vacuolar brecciated dolostones passing to bedded evaporites, followed by Norian Hauptdolomit and Rhaetian–lowermost Jurassic metalimestones with frequent slumps, slump breccias and reddish metapelites.

Iannace *et al.* (2004*a*, 2005) have pointed out the huge thickness (over 1200 m) of Ladinian–Norian carbonates in the Lungro–Verbicaro Unit. Within

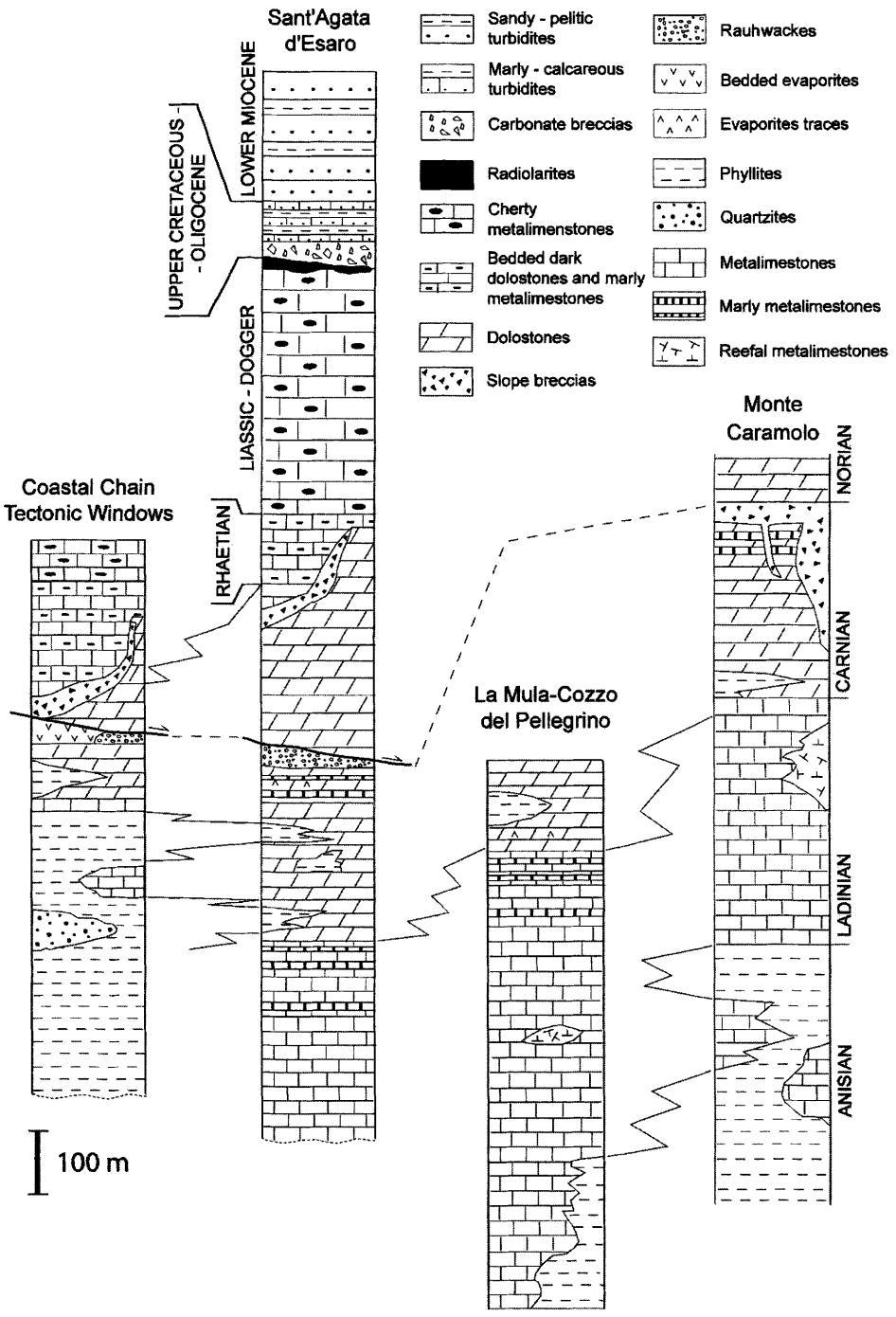

Fig. 17. Stratigraphic columns of the Lungro–Verbicaro Unit. Verrucano-like successions cover the Anisian–Carnian time span.

the Western Mediterranean, successions showing equivalent facies and thickness for the same interval occur only in the Alpujarride Units of the Betic Cordillera.

Post-Verrucano successions (Norian–Aquitanian). The post-Verrucano succession of the Bagni Unit (Dietrich 1976) starts with some metres of probably Upper Triassic grey and blackish, sometimes brecciated, saccharoid metadolostones. The dolostones are followed by thin-bedded grey to light-coloured metalimestones and cherty metalimestones with some beds of quartzose–calcareous microbreccias, grading upwards into alternations of grey and white cherty metalimestones and red, green and black metaradiolarites, with thin layers of dark metapelites and some beds of microbreccias. The calcareous succession, clearly turbiditic and up to 120 m thick, is barren and a Jurassic to Early Cretaceous age has been suggested on the basis of the lithology and stratigraphic position.

Above the Carnian rauhwackes, the stratigraphic succession of the Alí-Montagnareale Unit continues with 100 m of grey to yellowish metadolostones and black metalimestones (Norian–lowermost Jurassic), followed by 100 m of pelagic grey to bluish marly and cherty metalimestones, metamarls with intercalations of silicified metacalcarenites and microbreccias, and variegated siliceous metaclaystones (Fig. 16). In these pelagic sequences, Domerian to Lower Cretaceous levels have been recognized (Somma *et al.* 2005).

In the Lungro–Verbicaro Unit (Fig. 17), the Jurassic succession, lying above the Verrucano-like rocks and the already described Upper Triassic carbonates, continues with cherty metalimestones and some metres of red and green radiolarites. A stratigraphic gap and a disconformity separate the Jurassic rocks from Upper Cretaceous–Oligocene coarse carbonate breccias, calcareous and marly–calcareous turbidites and, finally, lower Miocene metapelites and metarenites. Basic lavas cross both Triassic and Jurassic layers. Successions characterized by similar stratigraphic development and referable to the Lungro–Verbicaro Unit have been recognized in tectonic windows of the Calabrian Coastal Chain, up to the Catanzaro graben (Fig. 4).

Tectonometamorphic evolution. The deformation and metamorphic evolution of the Bagni Unit require new and detailed analyses, because no studies have been carried out after those of Bonardi *et al.* (1974), Dietrich (1976) and Colonna & Simone (1978). From a critical review of these papers, however, it seems possible to recognize HP Alpine metamorphic recrystallizations (presence of blue amphibole, phengitic white mica, etc.).

The Alì–Montagnareale Unit displays ductile structures that developed during three Alpine deformation phases (Somma *et al.* 2005). Petrological data on metapelites indicate the occurrence of a polystage metamorphism: the first stage developed under P around 0.4 GPa and T between 300 and 360 °C (phengitic white mica (3.3–3.25 Si contents p.f.u.) + paragonite + chlorite + quartz + hematite + graphite ± pyrophyllite assemblage). The second stage took place at lower P and T conditions compared with the first stage.

The rocks of the Lungro–Verbicaro Unit were strongly deformed and affected by HP/LT metamorphism during Miocene tectonic phases (Fig. 18). Their tectonometamorphic evolution is characterized by four deformation phases (D_1 to D_4), three of them accompanied by metamorphism. Metamorphic index minerals of the FeO–MgO–Al_2O_3–SiO_2–H_2O (FMASH) system occur (Iannace *et al.* 2004*b*; Messina *et al.* 2004). These deformation phases are constrained between the early Burdigalian age of the youngest levels of the Lungro–Verbicaro Unit and the late Tortonian age of the clastic deposits unconformable above it.

In the upper levels of the unit these minerals are present in: (1) synfolial quartz veins, with ferro- ($X_{Mg} = 0.36–0.49$) to Mg-carpholite ($X_{Mg} = 0.51–0.57$) + chlorite + phengite + carbonate + quartz assemblage; (2) phyllites associated with quartz–carpholite veins, with chlorite + phengite + calcite + dolomite + quartz assemblage. In the quartz–carpholite veins, different carpholite structural sites have been recognized: syn- to post-D_1 prismatic crystals, syn-D_2 subgranular crystals and syn-D_2 to syn-D_3 needle-like crystals. The replacement of carpholite in chlorite + phengitic white mica starts in late D_3 and continues to D_4.

In the lower levels of the Lungro-Verbicaro Unit, metamorphic index minerals occur in quartz ± chlorite + chloritoid + phengitic white mica phyllites.

The first foliation, defined by phengitic white mica, chloritoid and chlorite, is preserved in microlithons, wrapped by the main foliation, S_2, defined by rotated chloritoid and recrystallized quartz, muscovite and chlorite.

The P–T path of the metamorphic history of the Lungro–Verbicaro Unit is typical of a polystage HP/LT event (Fig. 18). The first stage, related to syn-collisional peak conditions, took place during D_1, at P between 1.6 and 1.4 GPa and T around 350 °C (within the pyrophyllite stability field) in the upper levels of the unit, and it is defined by the quartz + phengite (Si = 3.30–3.25 p.f.u.) + Fe–Mg-carpholite assemblage in quartz veins, and by the phengite + chlorite assemblage in surrounding phyllites. In the lower levels of the unit, the first stage was reached at P between 1.8 and 1.6 GPa and T around 420 °C (within the kyanite stability field) and it is marked by the phengite + chloritoid ± chlorite assemblage in phyllites. The second stage involves several steps

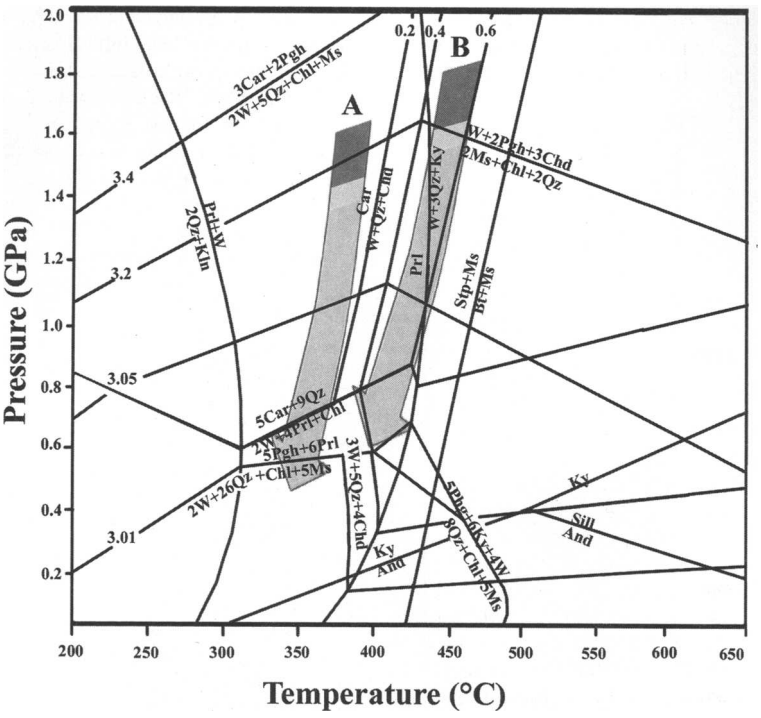

Fig. 18. *P–T* path of the Lungro–Verbicaro Unit: dark shaded arrow indicates syncollisional peak stage; light shaded arrow indicates exhumation decompression stage. A, upper levels of the unit; B, lower levels of the unit. Minerals of the metamorphic reactions are as in Figure 15. Petrogenetic grid is modified after Oberhänsli *et al.* (1995).

of the exhumation path, which begins, during the D_2 (first step), with a weak decompression, indicated by the decrease of celadonitic content in muscovite and by the absence of chloritoid and the presence of biotite in phyllites of the lower levels. It continues in the late D_2 and in syn-D_3 (second step), with an isothermal decompression, starting in the upper levels at $P < 0.6$ GPa (within the pyrophyllite field), with the growth of chlorite + less phengitic white mica as the alteration products of carpholite, and in the lower levels at $P < 0.8$ GPa (within the kyanite stability field), with the development of chlorite + muscovite + opaque minerals after chloritoid. Therefore, subduction to considerable depths and subsequent exhumation appears to have taken place for the rocks of the Lungro–Verbicaro Zone during Miocene tectonism.

As for the Tuscan Metamorphic Units, the tectonometamorphic evolution outlined above may pose questions on the traditional attribution of the Lungro–Verbicaro and Coastal Chain Carbonate tectonic windows successions to the Adria–Apulia continental margin and the consequent interpretation of these units as External South-Appennine Units. According to Perrone (1996), the terrains now attributed to the Lungro–Verbicaro Unit have to be referred to the Calabrian–Peloritanian Arc. Therefore, like the other continental units of the arc, they would represent South-Apennine Internal Units, originating from a continental block (Mesomediterranean Microplate; Guerrera *et al.* 1993) that separated different realms of the Tethys Ocean since the Jurassic.

Tellian Maghrebids

Verrucano-like Triassic metamorphic successions are up to now unknown in the Tellian Maghrebids. However, we consider that the Babors Units, considered as Tellian External Units back-thrust over the Maghrebian Flysch Basin Units, have some features that are worthy of analysis. The occurrence of (1) Triassic redbeds different from the typical Germano-Andalusian facies of the Tellian External Units (Bourmouche *et al.* 1996), (2) Alpine metamorphism, and (3) a stratigraphic succession characterized by thick Carnian evaporites and Norian dolostones, Jurassic neritic and pelagic limestones could put into question the attribution of the Babors Units to the External Tellian

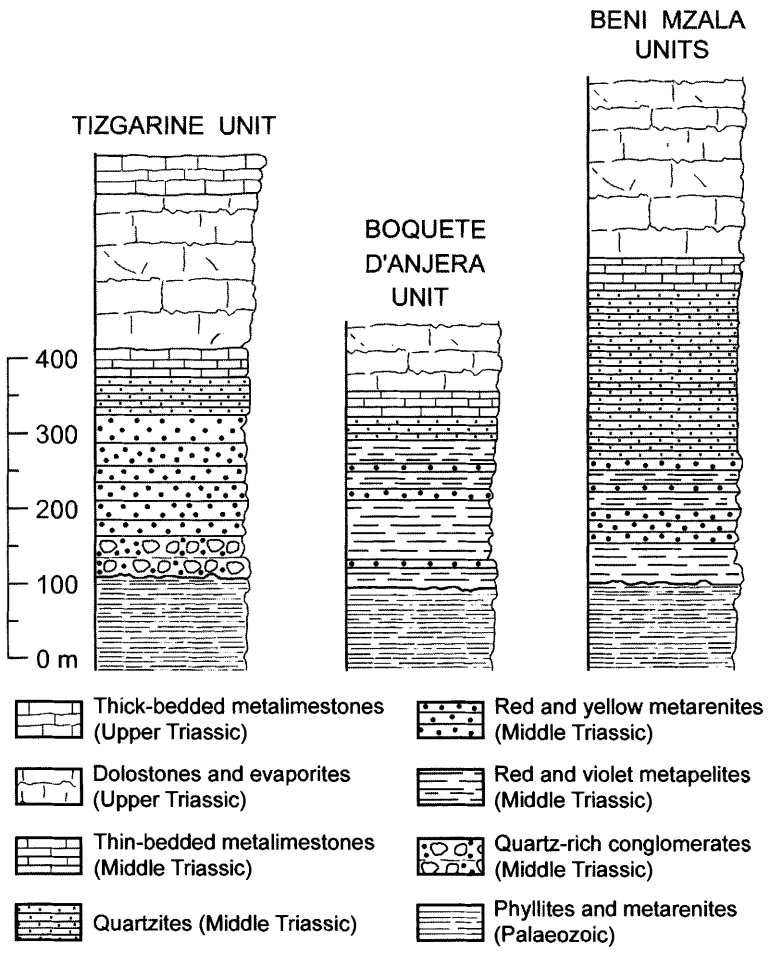

Fig. 19. Stratigraphic columns of the Rifian Upper Sebtide Units (Federico Slices).

Units. Finally, according to Coutelle & Delteil (1989), the stratigraphic succession of the Internal Babors shows strong similarities to the Tuscan successions.

Rifian Maghrebids

In the Internal Rif, metamorphic successions similar to the Tuscan Verrucano are present in the Upper Sebtide Units, known as Federico Slices. These units, underlying the Ghomaride and Dorsale Calcaire Nappes, crop out in two areas of the Northern Rif, west of Sebta (Beni Mzala window) and in a narrow belt parallel to the coastline between Assifane and Oued Laou (Fig. 6).

The successions of the Upper Sebtide Units, which show similar lithostratigraphical sequences, are shown in Figure 19 (Zaghloul 1994). Their main features can be summarized as follows: (1) the successions consist of only Middle–Upper Triassic strata, unconformably lying on Middle(?) Carboniferous metasedimentary rocks; (2) they start with some metres of coarse quartz-rich conglomerates and are characterized mainly by violet, greenish, yellowish and silvery metapelites and metarenites with some conglomerate layers, followed by quartzites and thin-bedded metalimestones containing Middle-Triassic dasycladacean algae, Upper Triassic(?) evaporites and massive dolostones, and eventually thick-bedded metalimestones; (3) as in many Verrucano-type Apennic and Betic successions, no rocks younger than Triassic have been recognized; (4) the rocks have undergone HP/LT metamorphism, characterized by increasing pressure and temperature, from the upper to the lower tectonic unit, with each unit

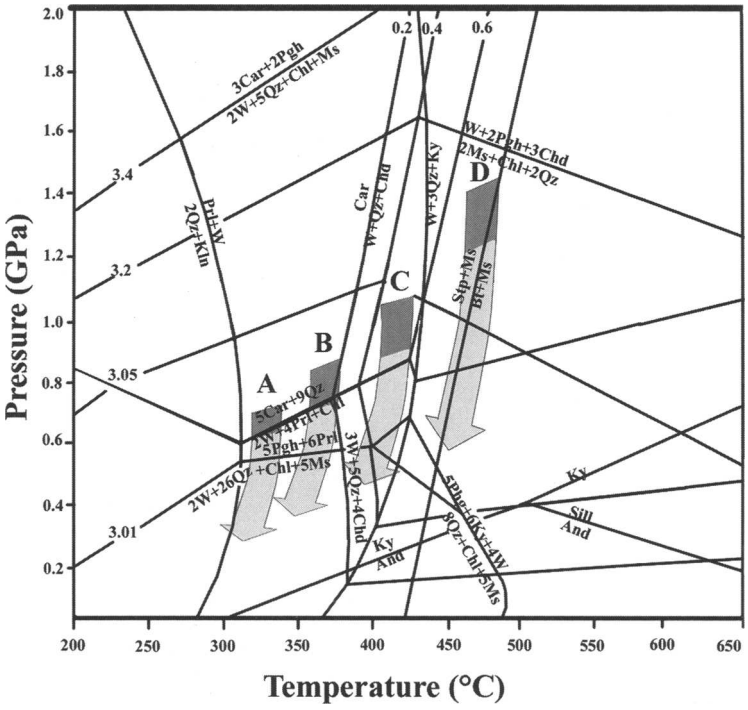

Fig. 20. *P–T* path of the Rifian Upper Sebtide Units (Federico Slices): dark shaded arrow indicates syncollisional peak stage; light shaded arrow indicates exhumation decompression stage. A, Tizgarine Unit; B, Boquete de Anjera; C, Upper Beni Mzala Unit (lower levels); D, Lower Beni Mzala Unit (lower levels). Minerals of the metamorphic reactions are as in Figure 15. Petrogenetic grid is modified after Oberhänsli *et al.* (1995).

being characterized by its own peak pressure–temperature conditions (Bouybaouène 1993; Bouybaouène *et al.* 1995; Goffé *et al.* 1996).

In particular, as regards the metamorphic evolution of the Federico Slices (Fig. 20), in the Tizgarine Unit, cookeite–pyrophyllite–phengite mineral assemblages indicate $P = 0.1–0.5$ GPa and $T = 300$ °C. In the Boquete de Anjera Unit, the occurrence of sudoite + Mg-chlorite + phengite in the quartz veins, with chloritoid in the surrounding schists, suggests P close to 0.7 GPa and $T = 300–350$ °C. In the Upper Beni Mzala Unit, Mg-carpholite relics in chloritoid–quartz or kyanite–quartz veins are typical of blueschist-facies conditions evolving from $P = 0.8–1.0$ GPa and $T = 380–420$ °C to $P = 1.2–1.5$ GPa and $T = 430–450$ °C. In the Lower Beni Mzala Unit, Mg-carpholite relics in Mg-chloritoid + quartz veins, and talc + phengite assemblages in quartz + kyanite segregations point to eclogite-facies conditions, extending from $P = 1.2–1.5$ GPa and $T = 430–480$ °C to P about 2.0 GPa and $T = 550$ °C. The retrograde $P–T$ path is constrained only for the Beni Mzala Units. The occurrence of tremolite + talc + phlogopite + chlorite assemblage in the Lower Beni Mzala Unit indicates an early exhumation to 0.8 GPa, either isothermal or at slightly increasing T. Further unloading with decreasing T corresponds to the crystallization of late paragonite, muscovite, chlorite, kaolinite and cookeite in both the Lower Beni Mzala Unit and the Upper Beni Mzala Unit.

The HP–LT metamorphism indicates an Alpine subduction event and subsequent exhumation of these units (Bouybaouène *et al.* 1995; Goffé *et al.* 1996).

Betic Cordillera

In the Betic Cordillera (Fig. 8), successions showing lithological features, age, tectonosedimentary evolution and metamorphism similar to those of the Apenninic Verrucano are widely present in the units of the Alpujarride Complex, which underlies the Malaguide Complex (Delgado *et al.* 1981). These successions are especially well developed in the Lower Alpujarride Units, but also in some Intermediate Alpujarride Units (Felix Unit from Sierra de Gádor, SE Spain; Martín-Rojas 2004) and in the Higher Alpujarride Units located close

to the outer border of the Internal Zones, from the Gibraltar Arc (Casares Slices, strictly equivalent to the Rifian Federico Slices) to the eastern Betic Cordillera (Sierra Espuña area), which show lithostratigraphic and metamorphic features transitional to those of the Malaguide Pseudoverrucano-like Triassic deposits (Sanz de Galdeano *et al.* 2000, 2001).

Verrucano-like successions. Representative stratigraphic successions of the Alpujarride Units are reported in Figure 21. Alpujarride Verrucano-like successions lie on black schists attributed to the Palaeozoic and start with muscovite-rich light-coloured (from silvery grey to grey–green to blue–violet), fine-grained micaschists, phyllites and quartzites, with abundant quartz veins stretched along the main Alpine foliation. They include gypsum- and carbonate-bearing horizons dated as Early–Mid-Triassic as well as basic subvolcanic and volcanic rocks, which are also present in the overlying Triassic carbonate successions (Delgado *et al.* 1981; Simon & Visscher 1983; Kozur *et al.* 1985; Sanz de Galdeano 1997; Garcia-Tortosa 2002; Martín-Rojas 2004). The metapelitic and quartzitic succession grades progressively upwards, and laterally, to thick carbonate sequences, the ensemble being more or less intensely recrystallized as a result of the Alpine metamorphism.

The carbonate successions can be very thick in several units (more than 2 km), especially in the Lower and Intermediate Alpujarrides, and always show mainly shallow marine Alpine Triassic facies and fossils. They are organized in two main transgressive–regressive cycles. The lower cycle is transitional with the underlying phyllites and quartzites and is formed by Anisian massive to bedded, mainly shallow marine and sometimes reefal (Braga & Martín 1987*a*) dolostones and limestones, lower Ladinian hemipelagic marls and cherty limestones, followed by a thick succession of Ladinian bedded limestones with subordinate lenticular decametric dolostone horizons, frequently with zebra structures, which, toward the upper part of the cycle (Ladinian–Carnian transition), contain important F–Pb–Zn (Ag) ore deposits. A regression on top of the mineralized interval is marked by the presence of Carnian marls, clays and fine-grained sands with some dolostone and gypsum beds, followed by a thick succeession (>1 km thick in many sites) of well-bedded to massive shallow marine to reefal dolostones with Hauptdolomit facies and abundant fossils (benthic Foraminifera and dasycladacean algae; e.g. Delgado *et al.* 1981; Braga & Martín 1987*b*; Martín & Braga 1987) that allow them to be dated as latest Carnian–Norian. No post-Triassic sediments are usually described in the Alpujarride Complex but, in some northern Lower Alpujarride Units, condensed pelagic sediments of Jurassic, Cretaceous and Tertiary age, up to the early Miocene, are also present above dated shallow marine Rhaetian massive limestones (see Martín-Algarra 2004, for a recent revision).

Tectonometamorphic evolution. Many petrological studies, carried out on various units of the Alpujárride Complex, showed HP/LT assemblages (Goffé *et al.* 1989, 1996; Azañón *et al.* 1992, 1995, 1997, 1998; Azañón 1994; Azañón & Goffé 1997; Booth-Rea *et al.* 2002). Our new data, concerning in particular the Adra and Felix Units (Martín Rojas 2004), enhance the previous knowledge.

In the Salobreña Unit (Fig. 22) a prograde blueschist-facies metamorphic evolution has been reconstructed (Azañón & Goffé 1997). It is marked by three assemblages: (1) Mg-carpholite + chlorite + chloritoid + quartz ± kyanite; (2) Mg-carpholite + chlorite + kyanite + quartz; (3) kyanite + chloritoid + chlorite. Sudoite occurs as an alteration of Mg-carpholite in assemblages (1) and (2), whereas phengite and paragonite are both main phases in the schists and late alteration products of carpholite and kyanite, in addition to chlorite, pyrophyllite or cookeite. Margarite replaces chloritoid and very late kaolinite develops around kyanite and cookeite. The reconstructed P–T conditions show that metamorphism evolves from 0.8 to 1.2 GPa and from 400 to 480 °C.

In The Adra Unit (Fig. 22), which, according to Azañón *et al.* (1997) consists of a Palaeozoic basement and a Permian and/or Triassic cover, the HP/LT D_1 phase, related to thickening and continental subduction, developed at $P = 0.8$ GPa and $T = 430$ °C in the Fe–Mg-carpholite-bearing Permo-Triassic schists and at $P > 1.0$ GPa and $T = 570$ °C in the kyanite–garnet schists of the Palaeozoic basement. An almost isothermal pressure decrease followed during the thinning and associated vertical shortening (D_2 phase). It was responsible for the S_2 main foliation, marked by a prograde zoning from Permo-Triassic schists (biotite + chloritoid) to garnet schists (biotite + garnet + staurolite) and sillimanite schists (biotite + garnet + sillimanite) of the Palaeozoic basement. D_2 metamorphism occurred at $P < 0.65$ GPa in the whole unit and at $T = 420$ °C in the upper levels, and from 510 °C (garnet schists) to 700 °C (sillimanite schists) in the lower levels. A second thickening phase (D_3 phase) was responsible for the S_3 pressure-solution cleavage in the upper levels and for a crenulation cleavage in the lower levels. D_3 phase occurred at lower P–T conditions ($P = 0.3$ GPa; T from 500 to 600 °C).

An Alpine metamorphic evolution similar to that recognized in the Salobreña and Adra Units occurs

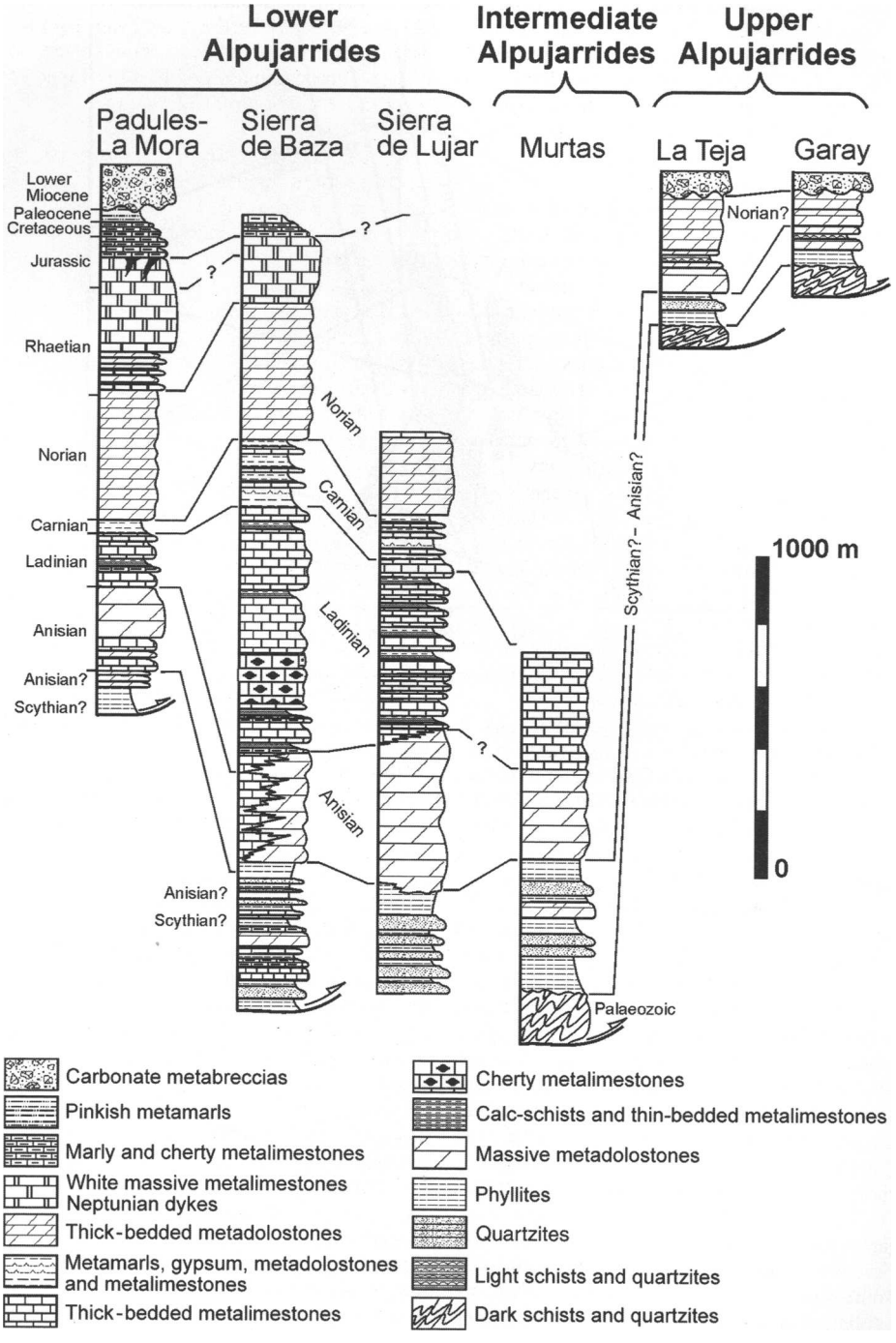

Fig. 21. Stratigraphic columns for some Betic Alpujarride Units.

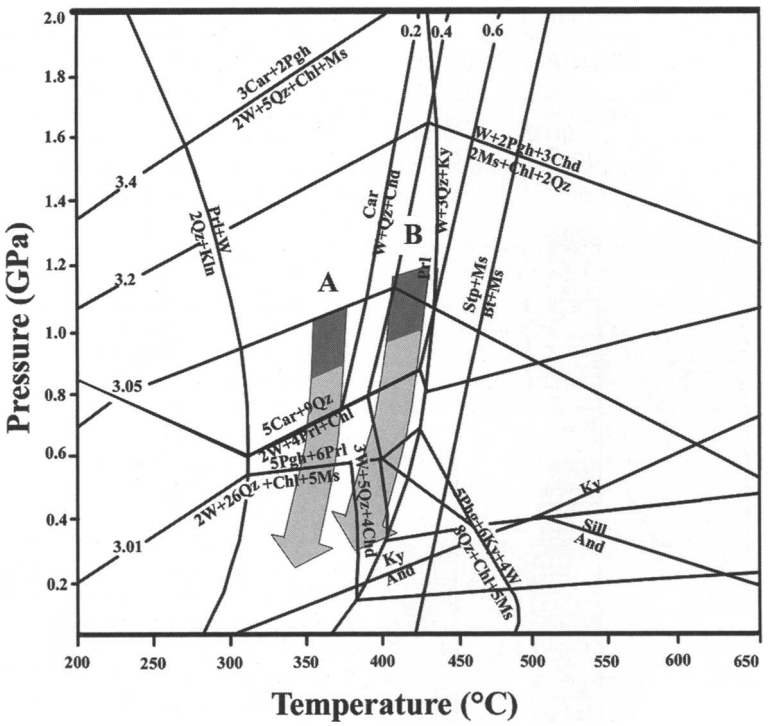

Fig. 22. *P–T* path of the Betic Alpujarride Units: dark shaded arrow indicates syncollisional peak stage; light shaded arrow indicates exhumation decompression stage. A, Felix Unit Triassic upper levels; B, Felix Unit Triassic lower levels, Adra and Salobreña Units upper levels. Minerals of the metamorphic reactions are as in Figure 15. Petrogenetic grid is modified after Oberhänsli *et al.* (1995).

also in the Felix Unit (Fig. 22), which consists of a Triassic cover and a Palaeozoic basement, the latter lacking the lowest levels (sillimanite-bearing schists) occurring in the Adra Unit (Martín Rojas 2004). The reconstructed metamorphic history testifies to a prograde zoning increasing towards the base of the sequence. A first HP/LT stage, related to D_1 thickening phase, occurred at P between 0.8 and 1.0 GPa. T reached values <360 °C in the highest levels of the Triassic phyllites (phengite + chlorite + carpholite? assemblage), between 360 and 420 °C in the lowest phyllite levels (phengite + chlorite + chloritoid+ stilpnomelane or biotite) and 480–500 °C (phengite + chloritoid + biotite + garnet) in the garnet schists of the Palaeozoic basement.

A second stage, related to the D_2 isothermal decompression phase, was responsible for the S_2 main foliation and developed at $P < 0.8$ GPa both throughout the Triassic phyllites (less phengitic white mica, stilpnomelane and chloritoid destabilization) and in the Palaeozoic schists. A second thickening D_3 phase was responsible for the S_3 cleavage, occurred at lower P–T conditions than S_2 (according to zoning, white mica ± chlorite ± biotite). It is related to the end of the decompression path and caused a continuous development of andalusite in the Palaeozoic basement.

Polystage HP/LT metamorphism has been recognized also in other units of the Alpujarride Complex, such as the Trevenque Unit (peak conditions at $P > 0.7$–0.8 GPa and T 300–330 °C, marked by Fe-carpholite + chloritoid + chlorite + aragonite assemblage; Goffé *et al.* 1989), the Alcazar (= Escalate) Unit ($P > 0.7$–0.8 GPa, T around 450–500 °C, Mg-rich chloritoid + chlorite + kyanite + calcite assemblage; Goffé *et al.* 1989), the Escalate Unit (P between 0.7 and 0.9 GPa and T between 330 and 430 °C; Azañón & Goffé 1997), and the Jubrique and Benarrabà Units (P around 0.8 GPa and maximum T of 400 °C in the upper levels and $P > 0.8$ GPa and $T < 450$ °C in the lower ones; Azañón *et al.* 1995).

The Alpine geodynamic evolution of Alpujarride Verrucano-like facies can be summarized as follows (Fig. 22): the HP/LT metamorphism occurred at P between 0.7 and 1.2 GPa and T between 300–350° and 420–480 °C (first stage),

MLP/LT metamorphism developed at P between 0.6 and 0.2 GPa and T between 300 and 480 °C (second stage), and LP/LT metamorphism took place at $P < 0.2$ GPa and $T < 350$ °C. In the Intermediate Alpujarride Complex, the HP/LT stage has been dated as latest Oligocene (25 Ma), whereas the second stage has been dated as latest Aquitanian–earliest Burdigalian (19 Ma, Monié *et al.* 1991).

In conclusion, the Alpujarride Complex shows a sedimentary and tectonometamorphic evolution similar to that of the Verrucano-like successions in other Central–Western Mediterranean orogenic sectors, in particular to that of the Lungro–Verbicaro Unit of the Calabrian–Peloritanian Arc, including (1) deposition of very thick Anisian–Ladinian platform carbonates, (2) latest Oligocene–early Miocene underthrusting to very great depths, (3) HP/LT metamorphism and (4) subsequent exhumation.

Discussion

The Triassic (Pseudo-)Verrucano Domain: a palaeogeographical definition

The comparative analysis and correlation of successions marking the base of the Alpine cycle in the Western Mediterranean chains indicate that both Pseudoverrucano-type deposits and its Verrucano metamorphic equivalent are not exclusive to the Northern Apennines: they are also recognizable in the tectonic units that originated from the Internal Domains of the South Apennine, Maghrebian and Betic Chains, and also in some units up to now attributed to the External Domains. It must be emphasized that the term Verrucano has been frequently (and loosely) applied in these areas (in particular, in the Betic Cordillera) to non-metamorphic Pseudoverrucano lithofacies in the same way as the term is applied to Permian redbeds in the Alps, whereas the metamorphic lithologies have been usually named 'Permo-Werfenian', using an older Austroalpine-derived terminology (see Fallot 1948, among many others).

All the studied units can be joined together to form a single Triassic palaeogeographical domain, if the following aspects are considered: (1) there are strong similarities between all the studied Triassic rock successions; (2) the Western Tethyan oceanic basins opened after the end of the Triassic; (3) the Late Cretaceous–Palaeogene–Early Neogene geodynamic evolution was very complex but equivalent in all the studied areas, with different phases of subduction, exhumation, thrusting and subsequent orogenesis that affected all the Internal Domains; (4) finally, during the Miocene, the orogenic belt deriving from the deformation of the Internal Domains was fragmented and the fragments were dispersed around the Western Mediterranean to form, today, independent and isolated elements. The Triassic domain was characterized by the deposition both of Pseudoverrucano lithofacies and of sedimentary precursors of the metamorphic Verrucano successions. However, the Verrucano successions are characterized not only by their original depositional features (similar to those of Pseudoverrucano Triassic continental redbeds) but also by their post-Triassic metamorphic evolution. This, being equivalent in the studied successions around the Western Mediterranean, demonstrates their proximity to areas affected by Tertiary subduction and Alpine orogenesis. The latter were responsible for transforming Triassic continental redbeds into carpholite-bearing, high-pressure–low-temperature metamorphic rocks. In short, it is necessary to clearly distinguish between the features associated with the post-depositional, Triassic and younger tectonic evolution, and the original depositional–palaeogeographical features of these rocks that formed during the Triassic and subordinately during the early Jurassic. The latter permit us to define a Triassic Verrucano–Pseudoverrucano palaeogeographical domain, termed hereafter the (Pseudo-)Verrucano Domain.

Triassic continental redbeds were also widely present in the European Germanic Triassic, and in the Iberian and North African Germano-Andalusian Triassic facies belts, which were located close to large continental areas (from which the terrigenous clastic supply was derived). These, during later Tertiary orogenesis, constituted the forelands to the Western Mediterranean Alpine belts. In contrast, the Triassic (Pseudo-)Verrucano Domain was palaeogeographically and palaeotectonically different from, and independent of, these European–Iberian–African Germanic and Germano-Andalusian Triassic facies belts, from which it was completely isolated. Verrucano–Pseudoverrucano successions, in fact, characterize a comparatively small area, which later formed the hinterland to the Western Mediterranean Alpine Belts. This hinterland, which since Mid-Jurassic time was completely separated from the Europe–Iberia, Africa and Adria–Apulia Plates to form a microcontinent in the Western Tethys (Mesomediterranean Microplate; Guerrera *et al.* 1993; Bonardi *et al.* 2001; Michard *et al.* 2002), was completely destroyed during Alpine tectonic phases, forming the Internal Units of the Western Mediterranean Alpine Belts.

Therefore, the (Pseudo-)Verrucano Domain was located around a small mountain area, from which alluvial depositional systems provided siliciclastic supply to neighbouring nascent continental

sedimentary basins formed during Triassic rifting. Petrographically, these clastic sediments were similar in the various studied areas. They reveal the erosion of metamorphosed Palaeozoic successions extensively intruded by felsic (tonalite, granodiorite to granite) plutonic rocks; that is, rock associations very similar to those that crop out widely in the Calabrian–Peloritanian Arc and in the Kabylias. Strong chemical weathering of such rocks under tropical, hot and episodically humid climate with a prolonged dry season (BSh climate according to the Köppen–Geiger classification) resulted in oxidation of iron and rubefaction of soils and sediments (reddening), and caused illitization of silicate minerals and concentration of quartz in thick soil profiles. These soils were later denuded by fluvial erosion, producing relatively mature, quartz-rich red deposits. Further details can be added to this picture in the Betic Cordillera and Rifian Maghrebids, where stratigraphic correlation reveals that Triassic Alpujarride and Sebtide deposits of Verrucano-type metamorphic lithofacies were sedimentologically more distal and closer to marine realms than Malaguide and Ghomaride Pseudoverrucano-type deposits (Martín-Algarra *et al.* 1995). Moreover, palaeocurrent analysis clearly indicates that the terrigenous clastic deposits were derived from rapid erosion of regions of high relief to the south and SE, and to the east and NE of the present-day outcrops of the Malaguide and Ghomaride Realms, respectively, whereas in the other realms (Kabylias and Calabrian–Peloritanian Arc) they were derived form the north, NW and west.

The (Pseudo-)Verrucano Domain was already defined in Mid-Triassic times. Its differentiation probably started in the Late Palaeozoic because, as pointed out by M. Durand Delga (in Baudelot *et al.* 1984), Upper Carboniferous–Permian clastic and volcanic successions, which are well developed in the neighbouring regions, are lacking in the domain characterized by the studied redbeds. This observation still can be accepted, although in Tuscany recent studies pointed out the occurrence of Lower Triassic clastic deposits, which constitute a sedimentary cycle interposed between Palaeozoic terrains and the Middle Triassic Verrucano lithofacies (Cirilli *et al.* 2002; Lazzarotto *et al.* 2003). Locally, the (Pseudo-)Verrucano continental redbeds changed progressively laterally and upwards to thick, Middle to Upper Triassic marine carbonate deposits with typical Alpine lithofacies. These were deposited from at least the early Anisian and, outwards of the future Alpine belt, laterally passed into Germano-Andalusian facies belts. Such thick Alpine marine lithofacies are widely present in the Austroalpine Units of the Alps, in the Alpujarride Units of the Betic Cordillera and in the External Domains of the Southern Apennines and Sicily, as well as in the Betic Rondaide and Rifian External Dorsale Calcaire Units, whose lowest levels are late Carnian in age. These latter have been also interpreted as a part of the Sebtide–Alpujarride successions, detached in correspondence to Carnian evaporites and emplaced as 'frontal units' (Martín-Algarra 2004). In many places, all the above units are also associated with synsedimentary basaltic volcanism, owing to the development of strongly subsiding rift basins. Therefore, during the Mid-Triassic and, especially, the Late Triassic transgressions, most continental areas of the (Pseudo-)Verrucano Domain were invaded by the Alpine sea and transformed to coastal to shallow-marine, carbonate to evaporitic environments.

In short, during the progressive development of the Triassic rift basins, emerged areas persisted in the central part of the continental block that was otherwise covered by shallow-marine carbonate platforms with Alpine facies. In the emerged areas, crystalline rocks were eroded and provided terrigenous clastic deposits to surrounding continental rift basins of the (Pseudo-)Verrucano Domain. In our opinion, the same areas of high relief that provided terrigenous supply to the Betic–Rifian Verrucano–Pseudoverrucano basins (or contiguous mountain areas located towards the south and east of the former) also provided siliciclastic sediments towards the south, SE and east, to feed the Pseudoverrucano-type deposits of the Kabylias and of the Calabrian–Peloritanian Arc and, finally, towards the north and NE to form the Northern Apenninic Verrucano *sensu stricto* and Pseudoverrucano *sensu stricto* deposits. If the Permian–Triassic plate configuration is considered (see, e.g. Ziegler 1988, 1993), it is clear that to the south and east of the Kabylian-Calabrian-Peloritanian Psudoverrucano facies belt more distal, transitional and marine areas, characterized by carbonate sedimentation, were widely present (Fig. 23*a*–*c*).

Post-Triassic stratigraphic and geodynamic evolution

The palaeogeographically contiguous Verrucano and Pseudoverrucano facies belts, already well characterized in the Mid-Triassic, show a similar tectonosedimentary evolution from the Pliensbachian onwards, during the opening of the Neo-Tethys Ocean. This opening transformed large continental crust areas, characterized by carbonate platform sedimentation, into pelagic basins within the complex, fault-controlled peri-Tethyan margins. During the Cenozoic collisional events, in contrast, both facies belts underwent

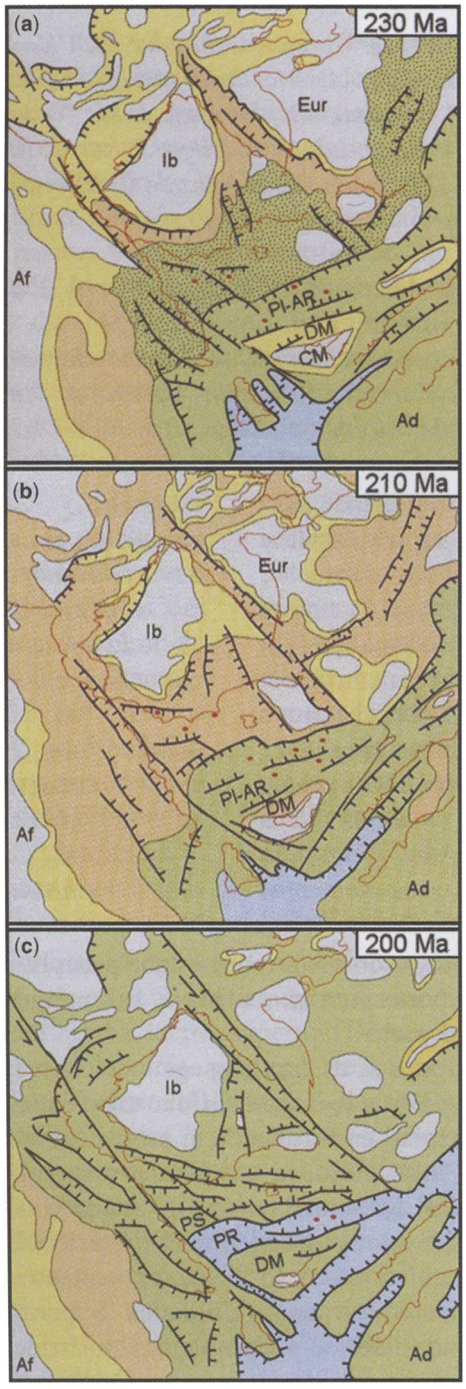

Fig. 23. Ladinian (**a**), Norian (**b**) and Early Liassic (**c**) palaeogeographical sketches of the westernmost Tethys area (modified from Vera 2004). Grey: continents, erosion areas. Yellow: continental basins (including Pseudoverrucano-type environments). Orange: siliciclastic and evaporitic coastal plains (also continental basins in (b) and (c). Green: shallow-marine environments of Germanic (shadowed) and Alpine facies. Light blue: pelagic environments on continental crust (intraplatform basins and continental margins). Red: volcanism. Eur, Europa Plate; Ib, Iberia Plate; Ad, Adria–Apulia Plate; Af, Africa Plate; CM, Mesomediterranean Continent; DM, Malaguide Domain; Pl–AR, Alpujarride–Rondaide Platform; PS, South Iberian Palaeomargin; PR, Rondaide Palaeomargin.

different deformation history, which makes it necessary to distinguish between post-Triassic Verrucano and Pseudoverrucano sub-domains.

Pseudoverrucano Sub-domain. The oldest dated sediments recognized in the Pseudoverrucano Sub-domain are Mid-Triassic continental (fluvial and alluvial) redbeds dated with pollen in the Betic Cordillera and in the Rif (Simon & Kozur 1977; Mäkel & Rondeel 1979; Baudelot *et al.* 1984; Martín-Algarra *et al.* 1995). Continental environments locally persisted until the Hettangian (Calabrian–Peloritanian Arc). Carbonate platform sedimentation covered these continental areas in the Sinemurian, but these shallow-marine deposits abruptly changed everywhere, from the Pliensbachian to the Toarcian, into pelagic or turbidite sediments. Siliciclastic deposits testify to the presence of emerged lands up to the Aalenian (Piraino Unit; Cecca *et al.* 2002), whereas mainly carbonate breccias and neptunian dykes Mid–Late Jurassic in age may be related to extensional tectonics associated with the opening of the Western Tethys Ocean. Pliensbachian to early Miocene facies zonation in the Betic–Rifian Malaguide–Ghomaride belt reveals opening of the sedimentary environments towards areas located outwards of the internal domains; that is, towards the north and NW in the Betic Cordillera and towards the west and SW in the Rif. In the Kabylias and in the Calabrian–Peloritanian Arc the facies zonation also indicates more distal and deeper environments outwards of the internal domains, which, in this case, are located towards the south, SE and east.

In Tuscany and the Calabrian–Peloritanian Arc, several stratigraphic successions end with Cretaceous strata and, in Calabria, this evolution has been interpreted as an effect of Eo-Alpine tectonics (Bonardi *et al.* 2001). In contrast, other successions reach the late Oligocene–early Miocene, when they underwent deformation. In any case, the units containing the Pseudoverrucano lithofacies underwent deformation at shallow crustal levels and therefore they were not affected by Alpine metamorphism.

Verrucano Sub-domain. As mentioned above, the Verrucano Sub-domain displays a more complex Triassic tectonosedimentary evolution, characterized by the development of locally thick Mid-Triassic carbonate platforms, calcareous breccias and basaltic volcanism, testifying to the onset of an important early rift phase not only in continental but also in marine environments. This event is particularly clear in Tuscany, where an intra-late Ladinian disconformity and subsequent Carnian continental deposits mark the end of this early rifting phase before later Jurassic rifting and subsequent break-up. Shallow-marine carbonate sedimentation occurs again during Carnian to Early Jurassic times with the deposition of evaporites followed by platform dolomitic and calcareous deposits. Sedimentation continued with pelagic marly, carbonate and siliceous sediments, and locally turbidites, with small changes to latest Oligocene–early Miocene time, when the Verrucano Sub-domain was involved in continental collision and thick synorogenic siliciclastic turbidite successions started to accumulate within the Apennine foreland basin system and in the Maghrebian and Betic Flysch Troughs.

During the Palaeogene to Miocene convergence and collisional events, the units originating from the Verrucano Sub-domain underwent polyphase deformation and metamorphism, indicating underthrusting at significant depths (involving continental subduction in most of the cases) and later exhumation. The metamorphic evolution of Verrucano-like facies is marked by several steps in the P–T path. For units such as the Upper Beni Mzala (Upper Sebtides, Morocco), Escalate, Salobreña, Adra, Felix (Alpujarride Spain), Monticiano–Roccastrada (Northern Apennine), Lungro-Verbicaro (Calabrian–Peloritanian Arc), syn-convergence high-pressure peak conditions (first stage) reached P between 0.8 and 1.8 GPa with T between 300 and 430 °C, within the pyrophyllite or kyanite stability field (carpholite + chlorite + pyrophyllite + chloritoid assemblage) typical of blueschist-facies metamorphism. Otherwise the metamorphic peak reached $T > 430$ °C (within the Mg-chloritoid + kyanite stability field), as in the Massa Unit (Northern Apennines), and maximum pressures reached values in the range of 1.5–2.0 Gpa, with T between 380 and 450 °C (within the chloritoid + kyanite stability field; after Mg-carpholite development), typical of eclogite-facies metamorphism, as in the Lower Beni Mzala Unit (Upper Sebtides, Morocco).

Locally, peak conditions were lower, such as in the Tizgarine (Upper Sebtide, Morocco) and Alì–Montagnareale Units (Calabrian–Peloritanian Arc), where $P < 0.5$ GPa and $T = 300$–360 °C (pyrophyllite–phengite + chlorite–cookeite assemblage) are recorded.

The exhumation-related second stage is marked by a retrograde greenschist- to sub-greenschist-facies metamorphism at $P < 0.6$ GPa and, in most instances, roughly constant T (isothermal decompression), mostly within the pyrophyllite field. Rarely, decompression ends with cooling (third stage) to $T < 300$ °C in the kaolinite stability field.

In synthesis, the reconstructed metamorphic path indicates a geodynamic evolution marked by a high-pressure phase, implying subduction or collision-related thickening of continental crust and underthrusting of Verrucano deposits to depths locally in excess of 50 km, followed by a retrograde isothermal greenschist-facies metamorphism associated with decompression. Occasionally, a late cooling phase records the final emplacement and exhumation of the studied units.

An almost generalized décollement along the Upper Triassic evaporites allowed the overlying Upper Triassic–lower Miocene successions to detach from their substrata. As a result, many units deriving from the Verrucano Sub-domain are formed only by Triassic and older strata.

Concluding remarks

The distinction between Verrucano and Pseudoverrucano successions, first evidenced in the Triassic successions of the Northern Apennines, has a regional importance at the scale of the Western Mediterranean, because successions similar to the Verrucano and Pseudoverrucano are recognizable in all the Internal Domains of the Betic, Maghrebian and Apenninic Chains. A different palaeogeographical and geodynamic evolution is documented for Verrucano- and Pseudoverrucano-bearing successions from the Triassic to the beginning of the deformation leading to the building of the orogens. The differences were enhanced during the Cenozoic compressional tectonics, when Verrucano- and Pseudoverrucano-bearing successions experienced different deformation histories.

However, the terms Verrucano and Pseudoverrucano can be correctly used to indicate the Triassic redbeds of the Internal Domains of the Western Mediterranean Chains, because these redbeds have the same age and meaning as those of the Tuscan area where the terms were first defined.

The similar sedimentary and tectonic evolution, unravelled for the units bearing Verrucano- and Pseudoverrucano-like successions in all the Alpine Chains of the Western Mediterranean orogen, suggests a single Mesozoic palaeogeographical domain for their original location, before the onset of convergence-related deformation. The basement

of this domain was a block of pre-Late Carboniferous–Permian? continental crust that started to be detached from Pangaea after having been deformed during the Variscan Orogeny. This Mesomediterranean Block was the Triassic precursor of the Jurassic–early Miocene Mesomediterranean Microplate, which, owing to the Jurassic–Cretaceous opening of Neo-Tethys, separated the northern Piemontese–Ligurian–Nevadofilabride Ocean from the eastern and southern (Lucanian–Maghrebian) oceanic branch of Tethys (Martín-Algarra 1987; Guerrera *et al.* 1993; Perrone 1996; Bonardi *et al.* 2001; de Capoa *et al.* 2002; Michard *et al.* 2002).

The Triassic Mesomediterranean Block had a central erosional mountain area (Mesomediterranean Microcontinent), which provided terrigenous sediments to surrounding intracontinental rift basins that formed the (Pseudo-)Verrucano Domain. These continental basins with redbeds laterally evolved to deeper zones in which marine sediments were deposited from at least Mid-Triassic time. After having been deeply eroded during the Triassic, the former mountain areas were transformed in a peneplaned continental area of low relief, whereas the formerly continental (inner) and marine (outer) sedimentation areas respectively evolved, from the beginning of the Jurassic, to proximal and distal, outward deepening continental margins dominated by carbonate neritic to hemipelagic sedimentation. From the Late Cretaceous to the early Miocene, the Mesomediterranean Microplate acted as the hinterland of the Western Mediterranean Alpine Belts, forming the overriding plate above subduction zones. This hinterland was completely destroyed during the Alpine tectogenetic phases, forming the Internal Units of the Western Mediterranean orogenic belt. Finally, during late and post-orogenic extensional tectonics after Miocene subduction, the formerly unique orogenic belt was disintegrated owing to the Neogene opening of the Algerian–Balearic–Provençal and Tyrrhenian Basins of the Western Mediterranean (Guerrera *et al.* 1993).

In the light of the proposed model, intriguing palaeogeographical problems arise, because a similar tectonosedimentary evolution seems to characterize both (1) units considered to belong to the Austroalpine nappe system (the Betic–Rifian units derived from the Verrucano Sub-domain; Wildi 1983; Martín-Algarra 1987; Chalouan & Michard 1990, 2004; Michard *et al.* 2002), and (2) units referred to the Adria–Apulia fold–thrust belt (Tuscan Metamorphic Units in the Northern Apennines and Lungro–Verbicaro Unit in the Calabrian–Peloritanian Arc).

As regards the Tuscan Metamorphic and Lungro–Verbicaro Units, it may be difficult to envisage subduction to depths developing pressures of 0.8–1.6 GPa for units referable to the Adria–Apulia fold–thrust belt. A viable alternative is represented by the possibility that originally these units also were located on the same palaeogeographical element as the Sebtide and Alpujarride Units of the Gibraltar Arc; that is, the Mesomediterranean Microplate (Guerrera *et al.* 1993). Palaeogeographical sketches are shown in Figure 23a–c. Finally, if the Verrucano- and Pseudoverrucano-bearing successions are characteristic of the Mesomediterranean Microplate, some questions arise also for the Alps as regards the palaeogeographical location of the Verrucano-bearing Pennidic and Austroalpine units for which the term Verrucano is correctly used.

In conclusion, Verrucano and Pseudoverrucano successions developed during the continental rifting stage that led to the complete break-up and disintegration of Pangaea. They were probably located along the margins of a minor continental block interposed between the Europe, Africa and Adria–Apulia Plates, which later, in Jurassic time, formed the Mesomediterranean Microplate. Remnants of this microplate occur exclusively in the internal tectonostratigraphic units of the Western Mediterranean orogenic system. They have been interpreted as originating from deformation and collision of the microplate with the Iberian, African and Adriatic–Apulian foreland regions.

Based on the available data, it can be envisaged that the post-Triassic Mesomediterranean Microplate started to differentiate as a continental crust block tectonically detached from the neighbouring domains (Sardinia–Corsica Block, Iberia, Africa, Adria–Apulia) from the Mid-Triassic, because its boundaries seem to coincide with those of the basins in which Verrucano and Pseudoverrucano successions were deposited. The beginning of the differentiation of the continental crust block that was the precursor of the Mesomediterranean Microplate and its detachment from Pangaea was probably even earlier than the Mid-Triassic, as all the domains located on it (excluding the Tuscan Domain) are characterized by the absence of Upper Carboniferous–Permian sedimentary and volcanic terrains. These latter terrains, however, are well developed in the Moroccan Atlas, Iberia, Pyrenees, Languedoc, Provence, Sardinia and Corsica: all these areas were external to the Mesomediterranean Microplate and only subordinately implicated in the Alpine sedimentary evolution and the subsequent orogenesis.

This research has been carried out within the MIUR-COFIN Project 2001.04.5835 'Età e caratteri dei depositi tipo Verrucano dall'Appennino Settentrionale alle Cordigliere Betiche: implicazioni per l'evoluzione

paleogeografica e strutturale delle Catene Alpine del Mediterraneo Centro-occidentale'(support to V. Perrone, University of Urbino). Financial support from MIUR-COFIN Project 2002 (to F. A. Decandia, University of Siena) and DGI-MEC Research project CGL 2005-03887 and from Research Group no. 164 (4089) to A. Martín-Algarra is also acknowledged. The authors are indebted to G. Cassinis and S. Yanev for their constructive reviews, useful comments and suggestions.

References

AMODIO MORELLI, L., BONARDI, G., COLONNA, V., *ET AL.* 1976. L'arco calabro-peloritano nell'orogene appenninico-maghrebide. *Memorie della Società Geologica Italiana*, **16**, 1–60.

AZAÑÓN, J. M. 1994. *Metamorfismo de alta presión/baja temperatura, baja presión/alta temperatura y tectónica del complejo Alpujárride (cordilleras Bético-Rifeñas).* PhD thesis, Granada University.

AZAÑÓN, J. M. & GOFFÉ, B. 1997. Ferro- and magnesiocarpholite assemblages as record of high-*P*, low-*T* metamorphism in the Central Alpujarrides, Betic Cordillera (SE Spain). *European Journal of Mineralogy*, **9**, 1035–1051.

AZAÑÓN, J. M., GARCIA-DUEÑAS, V. & GOFFÉ, B. 1992. High pressure mineral assemblages in the Trevenque Unit (Central Alpujárrides, Andalucía). *Geogaceta*, **11**, 81–84.

AZAÑÓN, J. M., BALANYÁ, J. C. & GARCÍA-DUEÑAS, V. 1995. Registro metamórfico de alta presión–baja temperatura en la unidad de Jubrique e imbricaciones de Benarrabá (Cordillera Bético-Rifeña). *Geogaceta*, **17**, 133–134.

AZAÑÓN, J. M., CRESPO-BLANC, A. & GARCÍA-DUEÑAS, V. 1997. Continental collision, crustal thinning and nappe-forming during the Pre-Miocene evolution of the Alpujarride Complex (Alboran Domain, Betics). *Journal of Structural Geology*, **19**, 1055–1071.

AZAÑÓN, J. M., GARCÍA-DUEÑAS, V. & GOFFÉ, B. 1998. Exhumation of high-pressure metapelites and coeval crustal extension in the Alpujarride complex (Betic Cordillera). *Tectonophysics*, **285**, 231–252.

BAUDELOT, S., BOUHDADI, S. & DURAND DELGA, M. 1984. Datation palynologique du Trias moyen au sein des Grès rouges 'Permo-triasiques' des environs de Tétouan (Rif septentrional, Maroc). *Comptes Rendus de l'Académie des Sciences*, **299**, 1061–1068.

BAUDELOT, S., BOUILLIN, J. P., DURAND-DELGA, M., GIUNTA, G. & OLIVIER, P. 1988. Datazioni palinologiche dell'Hettangiano alla base della trasgressione mesozoica sul 'Verrucano' della Sila (Calabria) e dei Monti Peloritani (Sicilia). *Bollettino della Società Geologica Italiana*, **95**, 49–74.

BHATIA, M. R. & CROOK, K. A. W. 1986. Trace element characteristics of graywackes and tectonic setting discrimination of sedimentary basins. *Contributions to Mineralogy and Petrology*, **92**, 181–193.

BONARDI, G., PERRONE, V. & ZUPPETTA, A. 1974. I rapporti tra 'filladi', 'metabasiti' e 'scisti micacei' nell'area tra Paola e Rose (Calabria). *Bollettino della Società Geologica Italiana*, **93**, 245–276.

BONARDI, G., GIUNTA, G., LIGUORI, V., PERRONE, V., RUSSO, M. & ZUPPETTA, A. 1976. Schema geologico dei Monti Peloritani. *Bollettino della Società Geologica Italiana*, **95**, 49–74.

BONARDI, G., CAVAZZA, W., PERRONE, V. & ROSSI, S. 2001. Calabria–Peloritani Terrane and Northern Ionian Sea. *In*: VAI, G. B. & MARTINI, I. P. (eds) *Anatomy of an Orogen: the Apennines and Adjacent Mediterranean Basins*. Kluwer Academic, Dordrecht, 287–306.

BONARDI, G., DE CAPOA, P., DI STASO, A., MARTÍN-MARTÍN, M., MARTÍN-ROJAS, I., PERRONE, V. & TENT-MANCLÚS, J. E. 2002. New constraints to the geodynamic evolution of the southern sector of the Calabria–Peloritani Arc (Italy). *Comptes Rendus, Geosciences*, **334**, 423–430.

BONARDI, G., DE CAPOA, P., DI STASO, A., *ET AL.* 2003. Oligocene to Lower Miocene deposits of the Calabria–Peloritani Arc southern subterrane (Italy) and geodynamic correlations with the Spain Betics and Morocco Rif. *Geodinamica Acta*, **16**, 149–169.

BOOTH-REA, G., AZAÑÓN, J. M., GOFFÉ, B., VIDAL, O. & MARTÍNEZ-MARTÍNEZ, J. M. 2002. High-pressure, low temperature metamorphism in the Alpujarride Units of southeastern Betics (Spain). *Comptes Rendus, Geosciences*, **334**, 857–865.

BOSELLINI, A., NERI, C. & STEFANI, M. 1996. *Introduzione alla Geologia delle Dolomiti.* Società Geologica Italiana, 78ª Riunione Estiva San Cassiano (BZ), 9–62.

BOUILLIN, J. P. & BELLOMO, D. 1990. Les filons sédimentaires jurassiques de Longobucco/Caloveto (Calabre, Italie); application à l'étude des paléostructures d'une marge téthysienne. *Geodinamica Acta*, **4**, 111–120.

BOUILLIN, J. P. & NAAK, M. 1989. Découverte de filons sédimentaires carectérisant une tectonique distensive jurassique dans le Djurdjura (Dorsale calcaire maghrébine, Algérie). *Comptes Rendus de l'Académie des Sciences*, **309**, 1371–1376.

BOUILLIN, J. P., DURAND DELGA, M. & OLIVIER, P. 1986. Betic–Rifian and Tyrrhenian Arcs: distinctive features, genesis and development stages. *In*: WEZEL, F. C. (ed.) *The Origin of Arcs*. Elsevier, Amsterdam, 321–338.

BOUILLIN, J. P., MAJESTÉ-MENJOULAS, C., BAUDELOT, S., CYGAN, C. & FOURNIER-VINAS, C. 1987. Les formations paléozoïques de l'Arc Calabro-Péloritain dans leur cadre structural. *Bollettino della Società Geologica Italiana*, **106**, 683–689.

BOURMOUCHE, R., DURAND DELGA, M., LACHKAR, G. & VILA, J. M. 1996. Découverte de palynoflores du Trias supérieur (Carnien moyen–supérieur) dans les grès rouges du Djebel Mchid Aïcha (zone tellienne, Algérie nord-orientale). *Comptes Rendus de l'Académie des Sciences*, **322**, 765–772.

BOUSQUET, J. C. & DUBOIS, R. 1967. Découverte de niveaux anisiens et caractères du métamorphisme alpin dans la région de Lungro (Calabre). *Comptes Rendus de l'Académie des Sciences*, **264**, 204–207.

BOUYBAOUÈNE, M. L. 1993. *Etude pétrologique des métapelites des Sebtides supérieures, Rif interne, Maroc: une évolution métamorphique de haute pression*. PhD thesis, Rabat University.

BOUYBAOUÈNE, M., GOFFÉ, B. & MICHARD, A. 1995. High-pressure, low-temperature metamorphism in the Sebtide nappes, northern Rif, Morocco. *Geogaceta*, **17**, 117–119.

BRAGA, J. C & MARTÍN, J. M. 1987*a*. Sedimentación cíclica lagunar y bioconstrucciones asociadas en el Trías Superior alpujárride. *Cuadernos de Geología Ibérica*, **11**, 459–473.

BRAGA, J. C & MARTÍN, J. M. 1987*b*. Distribución de algas dasycladáceas en el Trías alpujárride. *Cuadernos de Geología Ibérica*, **11**, 475–489.

CARACUEL, J. E., SANDOVAL, J., MARTÍN-MARTÍN, M., ESTÉVEZ, A. & MARTÍN-ROJAS, I. 2006. Jurassic biostratigraphy and palaeoenvironmental evolution of the Malaguide Complex from Sierra Espuña (Internal Betic Zone, SE Spain). *Geobios*, **39**, 25–42.

CARERI, G., GUERRERA, F., MARTÍN-ALGARRA, A., MARTÍN-MARTÍN, M., MESSINA, A. & PERRONE, V. 2004. Petrography and geochemistry of granitoid pebbles from the Oligocene–Miocene deposits of the Internal Rifian chain (Morocco): a possible new hypothesis of provenance and palaeogeographical implications—Discussion. *Geologica Carpathica*, **55**, 341–348.

CARMIGNANI, L., GATTIGLIO, M., KALIN, O. & MECCHERI, M. 1987. *Guida all'escursione sul Complesso metamorfico delle Alpi Apuane*. Tipografia Editrice Pisana, Pisa.

CASSINIS, G., ELTER, G., RAU, A. & TONGIORGI, M. 1979. Verrucano: a tectofacies of the Alpine–Mediterranean Southern Europe. *Memorie della Società Geologica Italiana*, **20**, 135–149.

CECCA, F., CRITELLI, S., DE CAPOA, P., DI STASO, A., GIARDINO, S., MESSINA, A. & PERRONE, V. 2002. Nouvelle datation et interprétation de la succession sédimentaire de Sant'Angelo di Brolo (Monts Péloritains; Italie méridionale): conséquences pour la paléogéographie mésozoïque de la region Thétydée de la Méditerranée centrale. *Bulletin de la Societé Géologique de France*, **173**, 171–184.

CHALOUAN, A. 1986. *Les Nappes Ghomarides (Rif septentrional, Maroc): un terrain varisque dans la chaîne alpine*. PhD thesis, Strasbourg University.

CHALOUAN, A. & MICHARD, A. 1990. The Ghomarides Nappes, Rif Coastal Range, Morocco: a Variscan chip in the Alpine belt. *Tectonics*, **9**, 165–183.

CHALOUAN, A. & MICHARD, A., 2004. The Alpine Rif Belt (Morocco): a case of mountain building in a subduction–subduction–transform fault triple junction. *Pure and Applied Geophysics*, **161**, 489–519.

CIARAPICA, G. & PASSERI, L. 1978. I Grezzoni del Nucleo Apuano. Nascita, sviluppo e morte di una piattaforma carbonatica iperalina. *Bollettino della Società Geologica Italiana*, **97**, 527–564.

CIRILLI, S., DECANDIA, F. A., LAZZAROTTO, A., PANDELI, E., RETTORI, R., SANDRELLI, F. & SPINA, A. 2002. Stratigraphy and depositional environment of the Mt. Argentario sandstone Fm. (southern Tuscany, Italy). *Bollettino della Società Geologica Italiana, volume speciale 1*, 489–498.

COLONNA, V. & SIMONE, A. (1978). Gli 'scisti del Fiume Savuto': un contributo alla conoscenza dell'Unità del Fiume Bagni nella Calabria Centrale. *Bollettino della Società Geologica Italiana*, **97**, 699–709.

CONTI, P., CARMIGNANI, L., GIGLIA, G., MECCHERI, M. & FANTOZZI, P. L. 2004. Evolution of geological interpretations in the Alpi Apuane Metamorphic Complex, and their relevance for the geology of the Northern Apennines. *In*: *Geology of Tuscany*. Geological Survey of Tuscan Region, Florence, 241–262.

COSTANTINI, A., DECANDIA, F. A., GANDIN, A., GIANNINI, E., LAZZAROTTO, A. & SANDRELLI, F. 1980*a*. Lo Pseudoverrucano nella Toscana meridionale. *Memorie della Società Geologica Italiana*, **21**, 395–401.

COSTANTINI, A., GANDIN, A. & SANDRELLI, F. 1980*b*. L'Unità dello Pseudoverrucano nell'area di Collecchio (Toscana meridionale). *Memorie della Società Geologica Italiana*, **21**, 413–425.

COSTANTINI, A., DECANDIA, F. A., LAZZAROTTO, A. & SANDRELLI, F. 1987. L'Unità di Monticiano–Roccastrada fra la Montagnola Senese e il Monte Leoni (Toscana meridionale). *Atti Ticinensi di Scienze della Terra*, **31**, 382–420.

COUTELLE, A. 1987. Les avant-fosses miocènes de l'orogène berebeère. *Memorie della Società Geologica Italiana*, **38**, 317–328.

COUTELLE, A. & DELTEIL, J. 1989. La suture alpine en Méditerranée occidentale. Remarques sur une synthèse et rappel d'une autre conception. *Bulletin de la Societé Géologique de France*, **8**(V), 859–863.

CRITELLI, S. & FERRINI, G. 1988. Litostratigrafia e Petrografia delle areniti di Monte Tiriolo (Trias Superiore), Calabria Centrale. *Memorie della Società Geologica Italiana*, **41**, 717–731.

CULLERS, R. L. 1994. The controls on the major and trace element variation of shales, siltstones, and sandstones of Pennsylvanian–Permian age from uplifted continental blocks in Colorado to platform sediments in Kansas, USA. *Geochimica et Cosmochimica Acta*, **58**, 4955–4972.

CULLERS, R. L. 2000. The geochemistry of shales, siltstones and sandstones of Pennsylvanian–Permian age, Colorado, USA: implications for provenance and metamorphic studies. *Lithos*, **51**, 181–203.

DECANDIA, F. A. & LAZZAROTTO, A. 1980. L'Unità dello Pseudoverrucano negli affioramenti di Punta delle Rocchette, dei Monti dell'Uccellina e di Montebrandoli (Toscana meridionale). *Memorie della Società Geologica Italiana*, **21**, 403–412.

DECANDIA, F. A., GIANNINI, E. & LAZZAROTTO, A. 1980. Evoluzione palaeogeografia del margine appenninico nella Toscana a Sud dell'Arno.

Memorie della Società Geologica Italiana, **21**, 375–383.

DE CAPOA, P., GUERRERA, F., PERRONE, V. & SERRANO, F. 1997. New biostratigraphic data on the Frazzanò Formation (Longi–Taormina Unit): consequences on defining the deformation age of the Calabria–Peloritanian Arc southern sector. *Rivista Italiana di Palaeontologia e Stratigrafia*, **103**, 343–356.

DE CAPOA, P., DI STASO, A., GUERRERA, F., PERRONE, V. & TRAMONTANA, M. 2002. The extension of the Maghrebian Flysch Basin in the Apenninic Chain; palaeogeographic and palaeotectonic implications. *Travaux de l'Institut Scientifique de Rabat*, **21**, 77–92.

DELGADO, F., ESTEVEZ, A., MARTÍN, J. M. & MARTÍN-ALGARRA, A. 1981. Observaciones sobre la estratigrafía de la formation carbonatada de los mantos alpujárrides (Cordillera Bética). *Estudios Geológicos*, **37**, 45–57.

DIETRICH, D. 1976. La geologia della Catena Costiera Calabra tra Cetraro e Guardia Piemontese. *Memorie della Società Geologica Italiana*, **16**, 61–121.

DI PISA, A., FRANCESCHELLI, M., LEONI, I. & MECCHERI, M. 1985. Regional variation of the metamorphic temperatures across the Tuscanid I Unit and its implications on the Alpine metamorphism (Apuan Alps, N-Tuscany). *Neues Jahrbuch für Mineralogie, Abbandlungen*, **151**, 197–211.

DURAND DELGA, M. & FONTBOTÉ, J. M. 1980. Le cadre structural de la Méditerranée occidentale. *Mémoires du Bureau de Recherches Géologiques et Minières*, **115**, 67–85.

FALLOT, P. 1948. Les Cordillères Bétiques. *Estudios Geológicos*, **8**, 83–172.

FEDO, C. M., NESBITT, H. W. & YOUNG, G. M. 1995. Unraveling the effect of potassium metasomatism in sedimentary rocks and palaeosols, with implications for palaeoweathering conditions and provenance. *Geology*, **23**, 921–924.

FISCH, W. & RYF, W. 1966. Der Verrucano in den Glarner Alpen. *Atti del Symposium sul Verrucano, Pisa 1965*. Società Toscana di Scienze Naturali, Arti Grafiche Pacini Mariotti, Pisa, 233–244.

FRANCESCHELLI, M., LEONI, I., MEMMI, I. & PUXEDDU, M. 1986. Regional distribution of Al-silicates and metamorphic zonation in the low-grade Verrucano metasediments from the northern Apennines, Italy. *Journal of Metamorphic Geology*, **4**, 309–321.

FRANCESCHELLI, M., MEMMI, I., CARANGIU, G. & GIANELLI, G. 1997. Prograde and retrograde chloritoid zoning in low temperature metamorphism, Alpi Apuane, Italy. *Schweizerische Mineralogische und Petrographische Mitteilungen*, **77**, 41–50.

GARCÍA-TORTOSA, F. J. 2002. *Los complejos tectónicos Alpujárride y Maláguide en el sector oriental de la Zona Interna Bética. Estratigrafía, relaciones tectónicas y evolución palaeogeográfica durante el Triásico*. PhD thesis, Granada University.

GIANNINI, E. & LAZZAROTTO, A. 1975. Tectonic evolution of the Northern Apennines. *In*: SQUYRES, C. (ed.) *Geology of Italy*. The Earth Sciences Society of the Libyan Arab Republic, Tripoli, 237–287.

GIORGETTI, G., GOFFÉ, B., MEMMI, I. & NIETO, F. 1998. Metamorphic evolution of Verrucano metasediments in northern Apennines: new petrologicalal constraints. *European Journal of Mineralogy*, **10**, 1295–1308.

GOFFÉ, B., MICHARD, A., GARCÍA-DUEÑAS, V., *ET AL.* 1989. First evidence of high-pressure, low-temperature metamorphism in the Alpujarride nappes, Betic Cordilleras (S.E. Spain). *European Journal of Mineralogy*, **1**, 139–142.

GOFFÉ, B., AZAÑON, J. M., BOUYBAOUÈNE, M. & JULLIEN, M. 1996. Metamorphic cookeite in Alpine metapelites from Rif, northern Morocco, and the Betic Chain, southern Spain. *European Journal of Mineralogy*, **8**, 335–348.

GUERRERA, F., MARTÍN-ALGARRA, A. & PERRONE, V. 1993. Late Oligocene–Miocene syn-/late-orogenic successions in Western and Central Mediterranean Chains from the Betic Cordillera to the Southern Apennines. *Terra Nova*, **5**, 525–544.

HARNOIS, L., 1988. The C.I.W. index: a new chemical index of weathering. *Sedimentary Geology*, **55**, 319–322.

HENNINGSEN, D. & KATZUNG, G. 1998. *Einführung in die Geologie Deutchlands*, 5th edn. Enke, Stuttgart.

IANNACE, A., BONI, M. & ZAMPARELLI, V. 1995. The Middle–Upper Triassic of the San Donato Unit Auct. (northern Calabria): stratigraphy, palaeogeography and tectonic implications. *Rivista Italiana di Palaeontologia e Stratigrafia*, **101**, 301–324.

IANNACE, A., GARCÍA-TORTOSA, F. J. & VITALE, S. 2004*a*. The Triassic metasedimentary successions across the boundary between Southern Apennines and Calabrian Arc (Northern Calabria, Italy). *Geological Journal*, **40**, 155–171.

IANNACE, A., VITALE, S, BONARDI, G., *ET AL.* 2004*b*. Miocene deformation and exhumation of HP/LT rocks at the Internal–External Zone boundary of the southern Apennines, Italy. *32nd International Gelogical Congress, Florence, Italy, 20–28 August 2004, Session G*, 209.10.

IANNACE, A., BONARDI, G., D'ERRICO, M., MAZZOLI, S., PERRONE, V. & VITALE, S. 2005. Structural setting and tectonic evolution of the Apennine Units of Northern Calabria. *Comptes Rendus, Geosciences*, **337**, 1541–1550.

JOLIVET, L., FACCENNA, C., GOFFÉ, B., *ET AL.* 1998. Midcrustal shear zones in postorogenic extension: example from the northern Tyrrhenian Sea. *Journal of Geophysical Research*, **103**, 12123–12160.

KLIGFIELD, R. 1979. The Northern Apennines as a collisional orogen. *American Journal of Science*, **279**, 676–691.

KOTANSKI, Z., GIERLINSKI, G. & PTASZYNSKI, T. 2004. Reptile tracks (*Rotodactylus*) from the Middle Triassic of the Djurdjura Mountains in Algeria. *Geological Quarterly*, **48**, 89–96.

KOZUR, H., MULDER-BLANKEN, C. W. & SIMON, O. 1985. On the Triassic of the Betic Cordilleras (Southern Spain), with special emphasis on holothurian sclerites. *Proceedings Koninklijke*

Nederlandse Akademie van Wetenschappen, **B 88**, 83–110.

LAZZAROTTO, A., ALDINUCCI, M., CIRILLI, S., *ET AL.* 2003. Stratigraphic correlation of the Upper Palaeozoic–Triassic successions in southern Tuscany, Italy. *Bollettino della Società Geologica Italiana, volume speciale 2*, 25–35.

LEMOINE, M. 1978. *Geological Atlas of Alpine Europe and Adjoining Alpine Areas*. Elsevier, Amsterdam.

LENTINI, F. 1975. Le successioni mesozoico-terziarie dell'Unità di Longi (complesso Calabride) nei Peloritani occidentali (Sicilia). *Bollettino della Società Geologica Italiana*, **94**, 1477–1503.

LOTTI, B. 1891. Note descrittive sul rilevamento geologico delle Tavolette d'Orbetello, Talamone e Grosseto nella Maremma toscana. *Bollettino del Regio Comitato Geologico Italiano*, **22**, 10–32.

MAATE, A. 1996. *Estratigrafía y evolución palaeogeográfica alpina del Dominio Gomáride (Rif Interno, Marruecos)*. PhD thesis, Granada University.

MAATE, A. & MARTÍN-ALGARRA, A. 1992. Evolution paléogéographique liasique de la Dorsale calcaire du Haouz et de la couverture des Ghomarides entre El Onsar et El Kouf (Rif septentrional, Maroc). *Comptes Rendus de l'Académie des Sciences*, **314**, 1485–1491.

MAATE, A. & MARTÍN-ALGARRA, A. 1993. Nuevos datos sobre la estratigrafía de las escamas de la Hafa El Banat y de Fahs Dohor (Hauz interno, Rif septentrional, Marruecos). *Geogaceta*, **13**, 72–75.

MAATE, A., MARTÍN-ALGARRA, A. & OUAZZANI-TOUHAMI, A. 1991. Les paléokarsts de l'unité de Buluazen (Chaîne calcaire du Haouz, Rif Interne, Maroc). Conséquences paléogéographiques. *Comptes Rendus de l'Académie des Sciences*, **313**, 1059–1064.

MAATE, A., MARTÍN-ALGARRA, A., O' DOGHERTY, L., SANDOVAL, J. & BAUMGARTNER, P. O. 1993*a*. Découverte du Dogger dans la Dorsale calcaire interne au Sud de Tétouan (Rif septentrional, Maroc). Conséquences paléogéographiques. *Comptes Rendus de l'Académie des Sciences de Paris*, **317**, 227–233.

MAATE, A., SOLÉ DE PORTA, N. & MARTÍN-ALGARRA, A. 1993*b*. Données paléontologiques nouvelles sur le Carnien des séries rouges des Maghrébides (Ghomarides et Dorsale calcaire du Rif septentrional, Maroc). *Comptes Rendus de l'Académie des Sciences*, **316**, 137–143.

MAATE, A., MARTÍN-ALGARRA, A., MARTÍN-MARTÍN, M. & SERRA-KIEL, J. 2000. Nouvelles données sur le Paléocène–Éocène des zones internes bético-rifaines. *Geobios*, **33**, 409–418.

MAGRI, G., SIDOTI, G. & SPADA, A. 1965. Rilevamento geologico sul versante settentrionale della Sila (Calabria). *Memorie e Note dell'Istituto di Geologia Applicata dell'Università di Napoli*, **9**, 5–59.

MÄKEL, G. H. 1982. Statistical analysis of palaeocurrent directions in the Malaguide Complex in the zone from Chirivel to the Sierra Espuña (Betic Cordillera, Spain). *Proceedings Koninklijke Nederlandse Akademie van Wetenschappen*, **85**, 241–248.

MÄKEL, G. H. 1985. The geology of the Malaguide Complex and its bearing on the geodynamic evolution of the Betic–Rif orogen (southern Spain and Northern Morocco). *GUA Papers of Geology*, **22**, 1–263.

MÄKEL, G. H. 1988. The geology of the Late Palaeozoic sequences of the Betic–Rif and Tell Orogens; implications for the palaeogeography of the Western Mediterranean. *Proceedings Koninklijke Nederlandse Akademie van Wetenschappen*, **92**, 251–276.

MÄKEL, G. H. & RONDEEL, H. E. 1979. Differences in stratigraphy and metamorphism between superposed Malaguide and Alpujarride units in the Espuña area (Betic cordilleras, SE Spain). *Estudios Geologicos*, **35**, 109–117.

MÄKEL, G. H., RONDEEL, H. E. & VANDENBERG, J. 1984. Triassic palaeomagnetic data from the Subbetic and the Malaguide Complex of the Betic Cordilleras (Southeast Spain). *Tectonophysics*, **101**, 131–141.

MARTÍN, J. M & BRAGA, J. C. 1987. Bioconstrucciones del Anisiense–Ladiniense en el Trías alpujárride. *Cuadernos de Geología Ibérica*, **11**, 421–444.

MARTÍN-ALGARRA, A. 1987. *Evolución geológica alpina del contacto entre las Zonas Internas y las Zonas Externas de la Cordillera Bética*. PhD thesis, Granada University.

MARTÍN-ALGARRA, A. (coord.) 2004. Zonas Internas Béticas. *In*: VERA, J. A. (ed.) *Geología de España*, SGE–IGME, Madrid, 395–437.

MARTÍN-ALGARRA, A., SOLÉ DE PORTA, N. & MAATE, A. 1995. El Triásico del Maláguide–Gomáride (Formación Saladilla, Cordillera Bética Occidental y Rif Septentrional). Nuevos datos sobre su edad y significado palaeogeográfico. *Cuadernos de Geología Ibérica*, **19**, 249–278.

MARTÍN-ALGARRA, A., MESSINA, A., PERRONE, V., RUSSO, S., MAATE, A. & MARTÍN-MARTÍN, M. 2000. A lost realm in the Internal Domains of the Betic–Rifian Orogen (Spain and Morocco): evidence from Oligo-Aquitanian conglomerates and consequences for Alpine geodynamic evolution. *Journal of Geology*, **108**, 447–467.

MARTINI, I. P., RAU, A. & TONGIORGI, M. 1986. Syntectonic sedimentation in a Middle Triassic rift, Northern Apennines, Italy. *Sedimentary Geology*, **47**, 121–219.

MARTÍN-MARTÍN, M. 1996. *El Terciario del Dominio Maláguide en Sierra Espuña (Cordillera Bética oriental, SE España): estratigrafía y evolución Palaeogeográfica*. PhD, thesis, Granada University.

MARTÍN-MARTÍN, M. & MARTÍN-ALGARRA, A. 2002. Thrust sequence and syntectonic sedimentation in a piggy-back basin (Mula–Pliego Basin, Oligo-Aquitanian: Internal Betic Zone, SE Spain). *Comptes Rendus, Geosciences*, **334**, 363–370.

MARTÍN-MARTÍN, M., EL MAMOUNE, B., MARTÍN-PÉREZ, J. A., SERRA-KIEL, J. & MARTÍN-ALGARRA, A. 1997*a*. Timing of deformation in

the Malaguide of the Sierra Espuña (Southeastern Spain). Geodynamic evolution of the Betic Internal Zone. *Geologie en Mijnbouw*, **75**, 309–316.

MARTÍN-MARTÍN, M., EL MAMOUNE, B., MARTÍN-ALGARRA, A. & SERRA-KIEL, J. 1997*b*. La Formation As, datée de l'Oligocène, est impliquée dans les charriages des unités malaguides supérieures de la Sierra Espuña (zones internes bétiques, prov. de Murcie, Espagne). *Comptes Rendus de l'Académie des Sciences*, **325**, 861–868.

MARTÍN-MARTÍN, M., SERRA-KIEL, J., EL MAMOUNE, B., MARTÍN-ALGARRA, A. & SERRANO, F. 1998. Le Paléocène des Malaguides orientales (Cordillères bétiques, Espagne): stratigraphie et paléogéographie. *Comptes Rendus de l'Académie des Sciences*, **326**, 35–41.

MARTÍN-MARTÍN, M., MARTÍN-ALGARRA, A. & SERRA-KIEL, J. 2003. El Terciario del área de Sierra Espuña. *In*: FERNÁNDEZ, J., GARCÍA, F., SORIA, J. M. & VISERAS, C. (eds) *Itinerarios geológicos por el Terciario de la Cordillera Bética (V Congreso del Grupo Español del Terciario)*, Departamento de Estratigrafia y Palaeontología, Universidad de Granada, 27–49.

MARTÍN-ROJAS, I. 2004. *Las unidades internas del sector de la Sierra de Gador: estructura y evolución geodinámica*. PhD thesis, Alicante University.

MCLENNAN, S. M., HEMMING, D. K. & HANSON, G. N. 1993. Geochemical approaches to sedimentation, provenance and tectonics. *In*: BASU, A. & JOHNSON, M. J. (eds) *Processes Controlling the Composition of Clastic Sediments*. Geological Society of America Special Papers, **284**, 21–40.

MERRIMAN, R. J. & PEACOR, D. R. 1999. Very low grade metapelites: mineralogy, microfabric and measuring reaction progress. *In*: FREY, M. & ROBINSON, D. (eds) *Low-grade Metamorphism*. Blackwell Science, Oxford, 10–58.

MESSINA, A., BONARDI, G., COMPAGNONI, R., FERRANDO, S., MACAIONE, E. & PERRONE, V. 2004. High pressure metamorphism in Middle Triassic to Miocene metasediments of Catena Costiera (Northern Calabria, Italy). *32nd International Geological Congress, Florence, 20–28 August 2004, General Symposium* G, 20.10.

MICHARD, A., CHALOUAN, A., FEINBERG, H., GOFFÉ, B. & MONTIGNY, R. 2002. How does the Alpine belt end between Spain and Morocco? *Bulletin de la Societé Géologique de France*, **173**, 3–15.

MILLIARD, Y. 1959. Sur l'existence du Permien dans le massif paléozique interne du Rif. *Comptes Rendus de l'Académie des Sciences*, **249**, 1051–1052.

MOLLI, G., CONTI, P., GIORGETTI, G., MECCHERI, M. & OESTERLING, N. 2000*a*. Microfabric study on the deformational and thermal history of the Alpi Apuane marbles (Carrara marbles), Italy. *Journal of Structural Geology*, **22**, 1809–1825.

MOLLI, G., GIORGETTI, G. & MECCHERI, M. 2000*b*. Structural and petrologicalal constraints on the tectono-metamorphic evolution of the Massa Unit (Alpi Apuane, NW Tuscany, Italy). *Geological Journal*, **35**, 251–264.

MONGELLI, G., CULLERS, R., DINELLI, E. & ROTTURA, A. 1998. Elemental mobility during the weathering of exposed lower crust: the kinzigitic paragneisses from the Serre, Calabria, Southern Italy. *Terra Nova*, **10**, 190–195.

MONIÉ, P., GALINDO-ZALDÍVAR, J., GONZÁLEZ-LODEIRO, F., GOFFÉ, B. & JABALOY, A. 1991. $^{39}Ar/^{40}Ar$ geochronology of Alpine tectonism in the Betic Cordilleras. *Journal of the Geological Society, London*, **148**, 289–297.

MOORE, D. M. & REYNOLDS, R. C. 1997. *X-ray Diffraction and Identification and Analysis of Clay Minerals*. Oxford University Press, Oxford.

NESBITT, H. W. & YOUNG, G. M. 1982. Early Proterozoic climates and plate motions inferred from major element chemistry of lutites. *Nature*, **299**, 715–717.

NOLD, M., UTTINGER, J. & WILDI, W. 1981. Géologie de la Dorsale calcaire entre Tétouan et Assifane (Rif interne, Maroc). *Notes et Mémoires du Service Géologique du Maroc*, **300**, 1–233.

OBERHÄNSLI, R., GOFFÉ, B. & BOUSQUET, R. 1995. Record of a HP–LT metamorphic evolution in the Valais zone: geodynamic implications. Bollettino del Museo Regionale di Scienze Naturali di Torino, **13**, 13–22.

PASSERI, L. 1985. Il Trias dell'Unità di Punta Bianca. *Memorie della Società Geologica Italiana*, **30**, 105–114.

PÉREZ-LÓPEZ, A. D. 1998. Epicontinental Triassic of the Southern Iberian Continental Margin (Betic Cordillera, Spain). *Zentralblatt für Geologie und Paläontologie*, **9–10**, 1009–1031.

PERRONE, V. 1996. Une nouvelle hypothèse sur la position paléogéographique et l'évolution tectonique des Unités de Verbicaro et de San Donato (région calabro-lucanienne; Italie): implications sur la limite Alpes–Apennin en Calabre. *Comptes Rendus de l'Académie des Sciences*, **322**, 877–884.

RAOULT, J. F. 1974. Géologie du centre de la Chaîne Numidique (Nord du Constantinois, Algérie). *Mémoires de la Societé Géologique de France*, **121**, 1–162.

RAU, A. & TONGIORGI, M. 1974. Geologia dei Monti Pisani a SE della Valle del Guappero. *Memorie della Società Geologica Italiana*, **13**, 227–408.

RAU, A., TONGIORGI, M. & MARTINI, I. P. 1985. La successione di Punta Bianca: un esempio di rift 'abortivo' nel Trias Medio del Dominio Toscano. *Memorie della Società Geologica Italiana*, **30**, 115–125.

ROEP, T. B. 1972. Stratigraphy of the 'Permo-Triassic' Saladilla formation and its tectonic setting in the Betic of Malaga (Vélez Rubio region, SE Spain). *Proceedings Koninklijke Nederlandse Akademie van Wetenschappen*, **75**, 223–247.

RUTTEN, M. G. 1969. *The Geology of Western Europe*. Elsevier, Amsterdam.

SANTANTONIO, M. & TEALE, T. 1987. An example of the use of detrital episodes in elucidating complex basin histories: the Caloveto and Longobucco Groups of N.E. Calabria, S. Italy. *In*: LEGGETT, J. K. & ZUFFA, G. G. (eds) *Marine Clastic Sedimentology*. Graham & Trotman, London, 62–74.

SANZ DE GALDEANO, C. 1997. *La Zona Interna Bético–Rifeña*. Monografica Tierras del Sur, **18**, Granada University.

SANZ DE GALDEANO, C., MARTÍN-MARTÍN, M. & ESTÉVEZ, A. 2000. Unidades tectónicas y estructura del sector meridional de Sierra Espuña (Cordillera Bética, Murcia). *Estudios Geológicos*, **56**, 269–278.

SANZ DE GALDEANO, C., ANDREO, B., GARCÍA-TORTOSA, F. J. & LÓPEZ-GARRIDO, A. C. 2001. The Triassic palaeogeographic transition between the Alpujarride and Malaguide complexes, Betic–Rif Internal Zone (S Spain, N Morocco). *Palaeogeography, Palaeoclimatology, Palaeoecology*, **167**, 157–173.

SAVI, P. 1832. Lettera al Signore Girolamo Guidoni di Massa concernente osservazioni geognostiche sui terreni antichi toscani, concernenti specialmente i Monti Pisani, le Alpi Apuane e la Lunigiana. *Nuovo Giornale dei Letterati*, **24**, 202–217.

SCANDONE, P. 1970. Mesozoico trasgressivo nella Catena Costiera della Calabria. *Atti Accademia Pontaniana in Napoli*, **20**, 387–396.

SCHULTZ, H. 1996. Analyse der variszisch-apenninischen Deformations-geschichte des paläozoischen Basements der Apuaner Alpen (Toskana, Italien). *Berliner Geowissenschaftiche Abhandlungen, Reihe A: Geologie und Paläontologie*, **188**, 108–118.

SIMON, O. & KOZUR, H. 1977. New data on the (Permo)-Triassic of the Betic Zone (southern Spain). *Cuadernos de Geología Ibérica*, **4**, 307–322.

SIMON, O. & VISSCHER, H. 1983. El Pérmico de las Cordilleras Béticas. *In*: MARTÍNEZ-DÍAZ, C. (coord.) *Carbonífero y Pérmico de España. Actas X Congreso International Carbonífero*, IGME, Madrid, 453–499.

SOMMA, R., MESSINA, A. & MAZZOLI, S. 2005. Synorogenic extension in the Peloritani Alpine Thrust Belt (NE Sicily, Italy): evidence from the Alì Unit. *Comptes Rendus, Géoscience*, **337**, 861–871.

SOPEÑA, A., LÓPEZ, J., ARCHE, A., PÉREZ-ARLUCEA, M., RAMOS, A., VIRGILI, C. & HERNANDO, S. 1988. Permian and Triassic Rift Basins of the Iberian Peninsula. *In*: MANSPEIZER, W. (ed.) *Triassic-Jurassic Rifting*. Developments in Geotectonics, **22B**, 757–786.

SPALLETTA, C. & VAI, G. B. 1989. Stratigraphic correlation forms of the Calabrian–Peloritan Arc (Southern Italy). *Rendiconti della Società Geologica Italiana*, **12**, 411–416.

SUTER, G. 1980. *Carte géologique de la Chaîne rifaine au 1/500 000*. Notes et Mémoires du Service Géologique du Maroc, **245a-b**, 1–60.

TEFIANI, M., BAUDELOT, S. & BOURMOUCHE, R. 1991. Datations palynologiques du Trias du Djurdjura (Algérie). Implications géodynamiques. *Comptes Rendus de l'Académie des Sciences*, **313**, 451–456.

THEYE, T., REINHARDT, J., GOFFÉ, B., JOLIVET, L. & BRUNET, C. 1997. Ferro- and magnesiocarpholite from the Monte Argentario (Italy): first evidence for high-pressure metamorphism of the metasedimentary Verrucano sequence, and significance for P–T path reconstruction. *European Journal of Mineralogy*, **9**, 859–873.

TONGIORGI, M., RAU, A. & MARTINI, I. P. 1977. Sedimentology of Early Alpine, fluvio-marine, clastic deposits (Verrucano–Triassic) in the Monti Pisani (Italy). *Sedimentary Geology*, **17**, 311–332.

TREVISAN, L. 1966. Considerazioni sui Verrucani. *Atti del Symposium sul Verrucano, Pisa 1965*. Società Toscana di Scienze Naturali Arti Grafiche Pacini Mariotti, Pisa, 393–401.

VERA, J. A. (ed.) 2004. *Geologia de España*. SGE–IGME, Madrid.

WILDI, W. 1983. La chaîne tello-rifaine (Algérie, Maroc, Tunisie): structure, stratigraphie et évolution du Trias au Miocène. *Revue de Géographie Physique et Géologie Dynamique*, **24**, 201–297.

YOUNG, J. R., TEALE, C. T. & BOWN, P. R. 1986. Revision of the stratigraphy of the Longobucco Group (Liassic, southern Italy) based on new data from nannofossils and ammonites. *Eclogae Geologicae Helvetiae*, **79**, 117–135.

ZIEGLER, P. A. 1988. Post-Hercynian plate reorganization in the Tethys and Arctic–North Atlantic Domains. *In*: MANSPEIZER, W. (ed.) *Triassic–Jurassic Rifting*. Developments in Geotectonics, **22B**, 711–755.

ZAGHLOUL, 1994. *Les unités Federico septentrionales (Rif interne, Maroc) Inventaire des déformations et leur contexte géodynamique dans la chaîne Bético-rifaine*.Third cycle thesis, Rabat University.

ZIEGLER, P. A. 1993. Late Palaeozoic–Early Mesozoic plate reorganization: evolution and demise of the Variscan fold belt. *In*: RAUMER, J. F. & NEUBAUER, F. (eds) *Pre-Mesozoic Geology in the Alps*. Springer, Berlín, 203–216.

ZUFFA, G. G., GAUDIO, W. & ROVITO, S. 1980. Detrital mode evolution of the rifted continental margin Longobucco Sequence (Jurassic) Calabrian Arc. *Journal of Sedimentary Petrology*, **50**, 51–61.

'Transgressive washing' concept: a sequence stratigraphic approach for calci- and siliciclastic turbidites

KH. EL KADIRI[1], A. CHALOUAN[2], A. BAHMAD[3], F. SALHI[4] & H. LIEMLAHI[1]

[1]*Université Abdelmalik Essaadi, Faculté des Sciences, BP 2121, Dép. Géologie, M'Hannech II, 93003 Tetuan, Morocco (e-mail: khkadiri@fst.ac.ma)*

[2]*Université Mohammed V-Agdal, Faculté des Sciences, Av. Ibn Batouta, BP 1014, Dép. Géologie, Agdal, 10000 Rabat, Morocco*

[3]*Société Nationale d'Etudes du Détroit de Gibraltar (SNED), 31, r. Al Alaouyine, Rabat, Morocco*

[4]*Université Chouaib Doukali, Faculté des Sciences, Dép. Géologie, El Jadida, Morocco*

Abstract: Carbonate breccias, calciturbidites and sandstone flysch sediments are typically assigned to the lowstand regime, based on the double assumption that these thick sedimentary packages necessitate (1) emergence phases for the production of their terrigenous material, and (2) a relatively lower position of the shoreline, which did not lie too far from the shelf-break line. In strictly regarding these conditions, we can run the risk of neglecting the role played by the transgression-related currents in reworking and exporting basinward bioclastic and siliciclastic sands from shelves. The 'transgressive washing' concept proposed here accounts for the latter mechanism, particularly in the case when the stratigraphic record shows that the onset of both the calci- and siliciclastic material was contemporaneous with newly marine-encroached continental source areas. Four examples from the Rifian internal (source) and external zones (basin) are presented to illustrate this phenomenon.

Tectonic control of turbidite successions is well documented in the Alpine Realm, during both the compressive (e.g. Auboin 1964; Guerrera *et al.* 1993, among the numerous studies dealing with the western Mediterranean flysch deposits) and the extensional phases (e.g. Eberli 1987, 1988, 1991). In contrast, the possible eustatic control on these successions is regarded differently by researchers, depending upon the aim of their research.

(1) In certain Exxon group models (e.g. Posamentier & Vail 1988; Posamentier *et al.* 1988), an increase in turbidite activity has been classically ascribed to lowstand conditions, during which the receptacle-effect exerted by the platform is attenuated. Turbidite systems I, II and III (Mutti 1985, 1992; Mutti & Normark 1987, 1991; Kolla & Macurda 1988) and their diagnostic sedimentary features remain the main comparison models when analysing and interpreting siliciclastic turbidites in outcrop.

(2) In other models dealing with carbonate platforms, turbidite activity is often linked to highstand phases (the highstand shedding concept: Mullins 1983; Droxler & Schlager 1985; Eberli 1988; Eberli & Ginsburg 1989; Glaser & Droxler 1991; Handford & Loucks 1993), particularly when the carbonate factory 'keeps up' with the rising sea level (Kendall & Schlager 1981; Sarg 1988). Carbonate production may be reduced when sea level falls and drastically diminishes the inundated productive area, or inversely, when a too rapid sea-level rise leads the platform to 'give up' below the euphotic zone (e.g. Neumann & Macintyre 1985; El Kadiri 2002*a*,*b*). Both conditions may result in a sediment starvation in the adjacent depths. Thus, carbonate and siliciclastic turbidites are often known to display opposite behaviours with respect to sea-level changes (e.g. Tucker & Wright 1990; Handford & Loucks 1993).

(3) Workers who described in detail the turbidite facies (carbonate as well as siliciclastic ones) and the hydrodynamic processes involved during their transport and deposition, have taken the sequence stratigraphic interpretation with caution, to such a point that some of them have questioned the above-mentioned models. Thus, both complexity and diversity of turbidite accumulations appear to them too wide to be accounted for by these models (see, e.g. the synthesis by Mutti (1992) and Shanmugam (2000)). These sedimentary packages may be related in some way to sequence stratigraphy via sedimentation-rate changes, which controlled their time–space stacking in a given slope–basin setting.

(4) Workers who described trace fossil assemblages have presented reliable information about

From: MORATTI, G. & CHALOUAN, A. (eds) 2006. *Tectonics of the Western Mediterranean and North Africa.* Geological Society, London, Special Publications, **262**, 45–53.
0305-8719/06/$15.00

the time–space turbidite occurrence (e.g. presence of multi-layer v. single-layer colonizers, softground or firmground colonization suite) and the palaeo-environmental changes (e.g. oxygen supply, organic matter input, substrate consistency, bottom-current intensity, etc.), which allow us to take promising steps towards the sequence stratigraphic interpretation of turbidite successions (e.g. MacEachern *et al.* 1992, 1999; Pemberton & MacEachern 1995; Savrda 1995; Uchman 1995, 1999; Bromley 1996; MacEachern & Burton 2000; Savrda *et al.* 2001*a*,*b*). Trace fossils are a common feature in deep-water deposits and we can no longer miss the opportunity to collect some useful ichnofabric data when studying these deep-water packages.

In the present work, it seems relevant to us to highlight a fifth complementary approach, through which a causal link may be established between the episodic calciturbidite breccias (i.e. clean grain flows) and the relative sea-level changes; namely, the triggering mechanisms responsible for the export of the turbidite material (we exclude here seismicity-induced large-scale collapses from tectonically oversteepened margins; e.g. Payros *et al.* 1999). Regarding the discussion by Spence & Tucker (1997), Haas (1999) and Payros *et al.* (1999), the processes involved in this issue still require a deeper understanding.

Stratigraphy

The stratigraphic examples were selected from (1) from the late Cretaceous and/or Palaeogene transgressive cover of the Ghomaride domain and its bordering calcareous chain (the so-called Dorsale Calcaire), both representing source areas, and (2) coeval sedimentary packages intercalated within flysch successions belonging to the Maureta-nian and Numidian nappes. The latter units are well known to derive from the 'Flysch Trough' (e.g. Durand-Delga 1972), which bordered the internal zones (Fig. 1).

Early Campanian breccias

Early Campanian basal breccias transgressively cover a conspicuous palaeokarst surface in the internal Dorsale units (palaeokarst 3, El Kadiri *et al.* 1989), and mark the sudden return to the marine regime after a long-lasting emergence–karstification history (Valanginian–Santonian). This surface independently affects early Liassic white massive limestones and Tithonian–Berriasian *Calpionella*-rich mudstones (Fig. 2, columns 2A). Thin *Globotruncana*-rich mudstones make up their matrix.

Detailed stratigraphic data from late Cretaceous calciturbidites (see El Kadiri *et al.* 2006) of the Béni Ider area, interestingly, show that this event is roughly correlatable with the onset of thick-bedded, early Campanian chaotic breccias onto early Senonian green pelites. Regionally, these breccias develop as key reference strata (e.g. Rar Aghroud and Beni Laïth basinal successions) and show a sharp ravinement surface at their base. Many of their clasts have palaeokarst features and strongly suggest that they have a causal link with the palaeo-karst-sealing breccias in the internal Dorsale.

Early Eocene sandstones

Nummulite-bearing, early Eocene, white sand-stones (10–20 m thick) mark the onset of the marine cycle in the Ghomaride terranes after their long emergence history from mid-Jurassic to Palaeocene times (Maaté 1984; El Kadiri 1991; El Kadiri *et al.* 1992; Hlila 2005). In El Onzar, Dradia and Talembote sections (Fig. 2, columns 2B) these white sandstones transgressively seal a similar palaeokarst surface overlying early Liassic white massive limestones.

Interestingly, identical, white sandstones of early Eocene age suddenly ravine late Palaeocene calci-turbidites in all Palaeogene basinal successions known in the Béni Ider area (external domain). Whatever the interpretation one makes about the sudden input of this siliciclastic material within a carbonate-dominated deposition, these key sand-stones should be considered in the same tectonic/and or eustatic context as coeval Nummulite-bearing white sandstones that transgressively rest on the Ghomaride Liassic cover.

Latest Eocene–early Oligocene breccias ('Breccias Nummuliticas')

The latest Eocene–early Oligocene, Nummulite-rich breccias (the so-called 'Breccias Nummuliticas', Nold *et al.* 1981) are by far the most ubiquitous car-bonate chaotic breccias in almost all the Dorsale calcaire units (e.g. data compiled by Hlila 2005). They transgressively cover Triassic dolomites and early Liassic massive limestones, and mark the return of the marine regime after the Barthonian emergence (Hlila 2005). In the case of the Hafat Srir unit (Internal Dorsale), located 5 km south of the city of Tetuan, the Breccias Nummuliticas seal a rust-coloured, palaeosoil-originated surface (Fig. 2, columns 2C). In thin sections, almost all the soil-altered carbonate clasts proved to derive from such a palaeosoil (see discussion below).

It is also noteworthy that Fe-coated hardground surfaces lie on top of the majority of breccia beds. The successive ferruginization processes increase upwards before the whole breccia interval (20–40 m in thickness) was covered by a thick marly

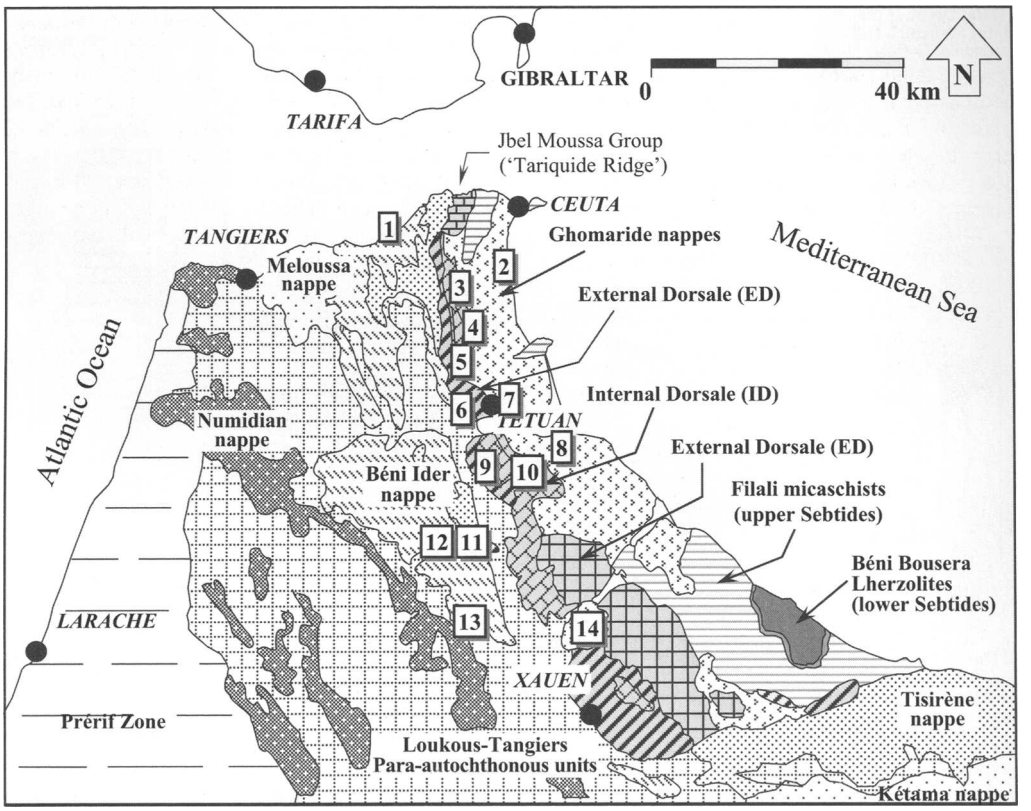

Fig. 1. Location map of the studied sections, most of which are located to either side of the internal–external front (see also stratigraphic columns in Fig. 2). 1, Sidi Zahara; 2, Fnidek; 3, Dradia; 4, Hafat Uestia II (Internal Dorsale); 5, El Onzar; 6, Béni Imrane; 7, Kellalyine; 8, Béni Maaden; 9, Hafat Ferkenich (Internal Dorsale); 10, Hafat Srir; 11, Oued El Kébir; 12, Rar Aghroud; 13, Béni Laïth; 14, Talembote.

succession. Obviously, the maximum ferruginization levels point to the transgressive-peak condition (compare a condensed section) just after the Breccias Nummiliticas-related event (e.g. data compiled by El Kadiri 2002*a*).

In the Béni Ider basinal successions (Oued El Kébir, Béni Imrane, Béni Laïth), latest Eocene–early Oligocene, coarse-grained, carbonate breccias sharply ravine late Eocene, lime-poor, red shales and develop in the R1/R2 grain-flow facies (Lowe 1982, i.e. Facies F3 of Mutti 1992). Generally, these breccias display both thinning- and fining-upward trends before being covered by red to varicoloured marls ('scaglia' facies).

Latest Oligocene–Aquitanian holoquartzose sandstones

Conglomerates and sandstones of the Ciudad Granada–Fnidek formation are chiefly made up of Filonian white quartz and have a very low content of schist and granite pebbles. This formation is one of the well-documented transgressive formations sealing the Ghomaride and Malaguide terranes (Fig. 2, columns 2D) in the internal zones of the Gibraltar arc (Martin-Algarra 1987; Feinberg *et al.* 1990; El Kadiri *et al.* 2001; Hlila 2005). The origin of its strikingly near-pure siliciclastic material has long been debated. On the assumption that this material requires a prolonged alteration history, many workers have suggested Calabrian, Sardinian or even African sources (see data compiled by Hoyez 1989).

Field evidence from quartz pebble-rich palaeosoils that occur over the Rifian upper Sebtide units (Cabo Negro Massif) shows that this 'apparently' mature material could easily come from a very friable micaschist of the basement rock, where the numerous quartz dykes are the only competent source levels. This means that the 'strong lithological selection' commonly suggested for this holoquartzose material was originally determined merely by the lithological

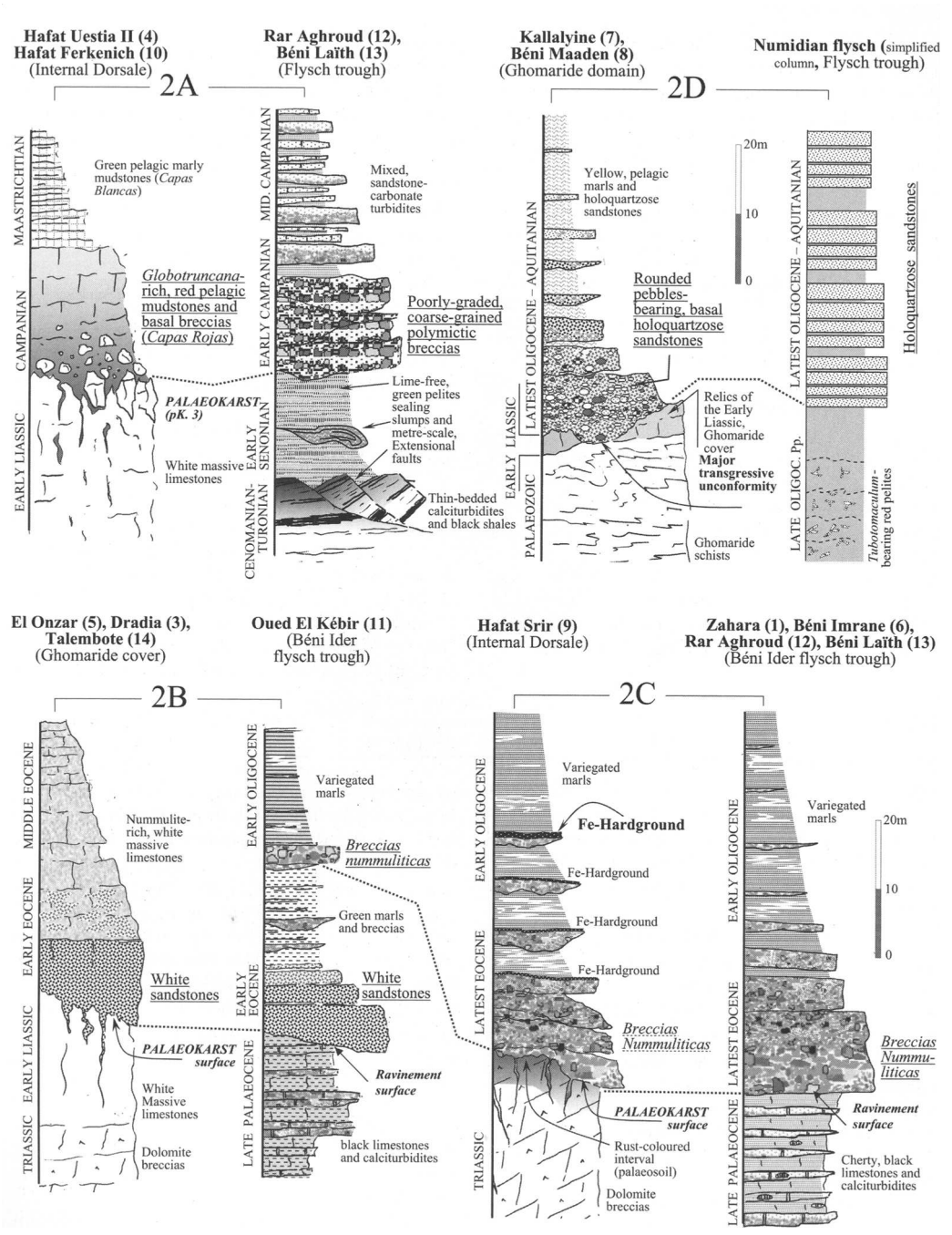

Fig. 2. Correlation of selected late Cretaceous–early Miocene key sections, showing transgressive strata on palaeokarst and palaeosoil surfaces (Ghomarides, Internal Dorsale Calcaire), with their coeval, depth-equivalent turbidite deposits in the Flysch Trough (Rar Aghroud and Béni Laïth successions, mainly). Columns 2B and 2C are placed together for convenience (i.e. better appraisal of 'Breccias Nummuliticas' key horizons). Section numbers refer to the location map in Figure 1.

nature of the rock source itself, not by extensive alteration–transportation processes. Sedimentological evidence supports such a suggestion in that (1) the highly resistant quartzitic sandstone pebbles deriving from Ghomaride–Malaguide sources, and the granitic pebbles (of unknown origin) occur only in a very low proportion; (2) the basal levels of the Ciudad Granada–Fnidek formation generally display coarse-grained structureless conglomerates of the R1/R2 facies of Lowe (1982), which testify to rock-fall or base-of-slope proximal deposits.

In the basinal area, late Oligocene–Aquitanian holoquartzose sandstones make up the majority of the Peri-Mediterranean Numidian flysch deposits. The onset of this huge siliciclastic regime onto the pelagic, Tubotomaculum-bearing red shales (the so-called infra-Numidian shales) also occurred as mass transport from a source where the initial stock of holoquartzose material was already prepared. Logically, the timing and the triggering mechanism behind the export of this continental material towards the basin should be regarded in the same way as the coeval, and synformational, transgressive holoquartzose puddingstones and sandstones of the Ciudad Granada Formation.

Discussion

The four examples described above raise the question of the context in which calciturbidites and clean holoquartzose sands moved from their primary continental sources (tectonically induced large-scale gravity flows from submarine slopes are not considered here). Attention should be paid to the following facts.

(1) The first step through which the continent-produced, carbonate clastic material reaches the flooded platform will theoretically be ascribed to river transport. However, breccia and coarse sands are known to be mostly trapped in river beds because river currents are fluid gravity flows (Shanmugam 2000). In contrast, submarine currents are sediment gravity flows that are known to be very low in suspended sediments (Shanmugam 2000, p. 299). Thus, muds and silts (<0.1 mm in diameter) would dominate the river-exported load. This agrees with the fact that mud- and silt-dominated successions generally characterize late highstand- and early lowstand-related regressive phases (e.g. Vail *et al.* 1991; Savrda *et al.* 2001*a*). Furthermore, outside the oversteepened slopes, displacement of pure coarse material in subaerial conditions is difficult or even inconceivable because of its high shear strength (e.g. Spence & Tucker 1997). Introduction of water pressure inside a subaerial clastic material is required to facilitate shear stress. In emerged parts of isolated platforms, this may be accomplished during subsequent transgressive pulses.

(2) Storms and hurricanes exert a washing effect on the sea floor lying above the storm wave base. In fact, storm- and hurricane-related washing processes result in great amounts of sands (≥ 0.1 mm in diameter) and coarse-grained clastic material being carried seawards to the outer platform (winnowing processes, Einsele 1992; polishing processes, Stow & Mayall 2000; Viana & Stow 2000). Subsequent export towards the adjacent slope and basin by a spillover mechanism (Stow & Mayall 2000; Viana & Stow 2000) is now thought to be the triggering factor of major gravity-flow events. Modern analogue examples have been documented off the western Atlantic platform margins (Doyle *et al.* 1979; Hill & Bowen 1983; Pietrafesa 1983; Stanley *et al.* 1984). One can easily deduce that this phenomenon can be more efficient in directly exporting clastic material to a basin from shallow-water isolated platforms, as an abrupt shelf-break and steep slopes commonly border them. Modern examples of this are well documented around the Bahamas islands, where flat-topped margins (Glaser & Droxler 1991; Handford & Loucks 1993) export shallow-water-produced carbonate muds to adjacent lows.

(3) A sediment-destabilizing effect is caused by fluid-pressure release when the sea-level drop results in diminishing the trapping effect caused by water-column pressure (e.g. Evans *et al.* 1996; Spence & Tucker 1997; Stow & Mayall 2000). Such a phenomenon, which can favour mobilization of large gravity flows even onto gentle slopes, generally occurs beneath upwelling zones producing a sufficient amount of organic matter. It requires a high sedimentation rate to constantly bury organic matter (see the description of the balance between preservation and oxidation of organic matter by Wetzel & Uchman (1998)). However, large-scale gravity flows may intermittently be destabilized from oversupplied delta fronts.

The first two points above are complementary and may provide an important clue in making a link between relative sea-level changes and turbidite events. They allow us to reconstruct the four-step scenario presented in Figure 3. It is referred to here as a 'Transgressive washing' process. Two facts support the scenario proposed, as follows.

(1) Ubiquitous palaeosoil-altered clasts together with bioclasts represent a typical component of calciturbidites and breccias. They show that this carbonate clastic material was, in many cases, directly sourced from submerging palaeokarst areas and did not necessarily originate from

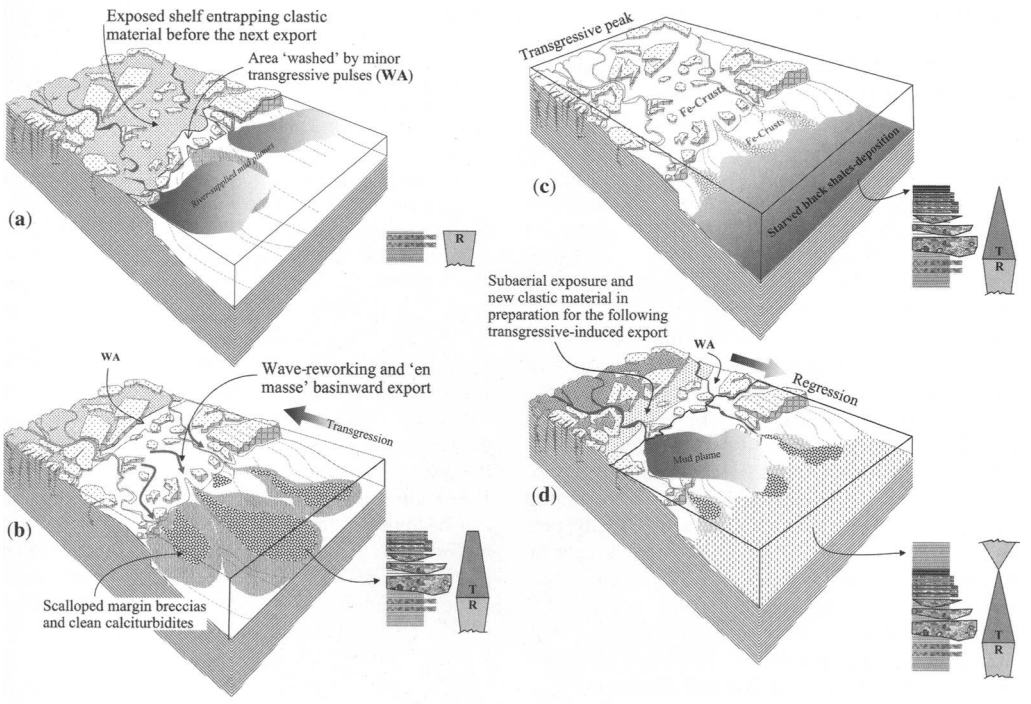

Fig. 3. Presentation of the 'transgressive washing' concept, proposed here to explain the timing of the clean turbidites (calciturbidites and holoquartzose turbidites) with respect to the relative sea-level changes. (**a**) Both the topographic entrapment of clastic material on land and karstic areas and the high shear strength in subaerial conditions do not seem to favour delivery of major clastic material during lowstand conditions. (**b**) Hydrodynamics forced by transgressive pulses is here envisaged to be the main factor triggering the export of platform material. (**c**) Emplacement of the main carbonate breccias is more likely to be linked to the major transgressive events, as they are generally followed by starved black-shale deposits, omission surfaces and/or Fe-crusts recording flooding episodes. (**d**) Lowstand regime may indirectly result in minor calciturbidites phases, as an emerged area favours the production of clastic material that is often punctuated by minor transgressive pulses.

submarine fracturing processes (e.g. hydraulic breccias, fault breccias).

(2) A second component is represented by the occurrence of shallow-water benthic organisms (Foraminifera, encrusting algae, bivalves, reef debris). Their presence, together with reworked glaucony grains, indicates a source from a shallow carbonate platform, which underwent both relative starvation and bottom-current activity. Such platform conditions are known to develop during transgressive phases (e.g. Baum & Vail 1988; Loutit *et al.* 1988; Galloway 1989; Hesselbo & Huggett 2001; Savrda *et al.* 2001*b*).

On the whole, both the production and export of the clean calciturbidite material would result from two successive complementary phases: (1) subaerial exposure making available clastic material for potential export; (2) transgressive washing as a result of storm-induced bottom currents, which commonly accompany the onset of transgressions (firmground and Fe-hardground surfaces are a common feature in the resulting sediment packages). Additional outer-shelf to basin export (over gentle ramps) may be induced by polishing–spillover processes such as those described by Viana & Stow (2000). Concomitance of these ravinement processes with transgressive phases has also been well documented by Swift (1968, 1975), Nummedal & Swift (1987), MacEachern *et al.* (1992) and Savrda *et al.* (2001*a*).

Conclusion

The 'transgressive washing' concept is proposed here to include in a single scenario the subaerial exposure phase and the subsequent transgressive washing phase. It means that shallow-water- and/or lithoclast-dominated turbidite flows may point to major transgressive pulses, which characterize the onset of transgressions (i.e. just after platform emergence), as well as to minor transgressive

pulses, which commonly interrupt the regressive trend. However, the occurrence of breccias and major calciturbidite packages in the stratigraphic record has suggested lowstand conditions to many workers (e.g. Spence & Tucker 1997). This may be true in cases where the production of such material requires the supply areas to emerge and to be closely juxtaposed to the shelf-break. However, the fundamental question remains of how the trapped clastic material in these subaerial sources can be released. The transgressive washing scenario proposed here accounts for the timing of subsequent shelf to basin export.

The authors acknowledge financial support from the 'Société Nationale d'Etude du Détroit', SNED, Rabat, Morocco. They express their sincere thanks to A. Lopez-Garrido and F. Oloriz-Saez (University of Granada) for their thorough reviews and constructive criticisms.

References

AUBOIN, J. 1964. Reflexions sur le faciès 'ammonitico-rosso'. *Bulletin de la Société Géologique de France*, **6**, 475–501.

BAUM, G. R. & VAIL, P. R. 1988. Sequence stratigraphy concepts applied to Palaeogene outcrops, Gulf and Atlantic basins. *In*: WILGUS, C. K., HASTINGS, B. S., KENDALL, C. G. S. C., POSAMENTIER, H. W., ROSS, C. A. & VAN WAGONER, J. C. (eds) *Sea Level Changes—an Integrated Approach.* Society of Economic Paleontologists and Mineralogists, Society for Sedimentary Geology, Special Publications, **42**, 309–327.

BROMLEY, R. G. 1996. *Trace Fossils. Biology, Taphonomy and Applications*, 2nd edn. Chapman & Hall, London.

DOYLE, L. J., PILKEY, O. H. & WOO, C. C. 1979. Sedimentation on the eastern United States continental slope. *In*: DOYLE, L. J. & PILKEY, O. H. (eds) *Geology of Continental Slopes.* Society of Economic Paleontologists and Mineralogists, Society for Sedimentary Geology, Special Publications, **27**, 119–129.

DROXLER, A. W. & SCHLAGER, W. 1985. Glacial versus interglacial sedimentation rates and turbidites frequency in the Bahamas. *Geology*, **13**, 799–802.

DURAND-DELGA, M. 1972. La courbure de Gibraltar, extrémité occidentale des chaînes alpines, unit l'Europe et l'Afrique. *Eclogae Geologicae Helveticae*, **65**, 267–278.

EBERLI, G. 1987. Carbonate turbidite sequence deposited in rift-basin of the Jurassic Tethys Ocean (eastern Alps, Switzerland). *Sedimentology*, **34**, 363–388.

EBERLI, G. 1988. The evolution of the southern continental margin of the Jurassic Tethys Ocean as recorded in the Allgäu Formation of the austroalpine nappes of Graubünden (Switzerland). *Eclogae Geologicae Helveticae*, **81**, 175–214.

EBERLI, G. P. 1991. Calcareous turbidites and their relationship to sea-level fluctuations and tectonism. *In*: EINSELE, G., RICKEN, W. & SEILACHER, A. (eds) *Cycles and Events in Stratigraphy.* Springer, Berlin, 340–359.

EBERLI, G. & GINSBURG, R. N. 1989. Cainozoic progradation of north-western Great Bahama Bank, a record of lateral platform growth and sea level fluctuations. *In*: CREVELLO, P. D., WILSON, J. L., SARG, J. F. & READ, J. F. (eds) *Controls on Carbonate Platform and Basin Development.* Society of Economic Paleontologists and Mineralogists, Society for Sedimentary Geology, Special Publications, **44**, 339–351.

EINSELE, G. 1992. *Sedimentary Basins. Evolution, Facies, and Sediment Budget.* Springer, Berlin.

EL KADIRI, KH. 1991. *La Dorsale Calcaire (Rif interne, Maroc): stratigraphie, sédimentologie et évolution géodynamique d'une marge alpine durant le Mésozoïque. Mise en évidence d'un modèle.* Doctorat d'Etat Thesis, University of Tetuan.

EL KADIRI, KH. 2002*a*. 'Tectono-eustatic sequences' of the Jurassic successions from the Dorsale Calcaire (internal Rif, Morocco): evidence from a eustatic and tectonic scenario. *Geologica Romana*, **36**, 71–104.

EL KADIRI, KH. 2002*b*. Jurassic ferruginous hardgrounds of the 'Dorsale Calcaire' and the Jbel Moussa Group (internal Rif, Morocco): stratigraphical context and paleoceanographic consequences of mineralization processes. *Geologica Romana*, **36**, 33–70.

EL KADIRI, KH., LINARES, A. & OLORIZ, F. 1989 La Dorsale calcaire interne entre les Accidents de l'Oued Martil et de l'Oued Laou (Rif septentrional, Maroc): évolutions stratigraphique et géodynamique au cours du Jurassique–Crétacé. *Communicações Serviços Geológicos de Portugal*, **75**, 39–65.

EL KADIRI, KH., LINARES, A. & OLORIZ, F. 1992. La Dorsale Calcaire rifaine (Maroc septentrional): évolution stratigraphique et géodynamique durant le Jurassique–Crétacé. *Notes et Mémoires du Service Géologique du Maroc*, **366**, 217–265.

EL KADIRI, KH., CHALOUAN, A., EL MRIHI, A., *ET AL.* 2001. Les formations sédimentaires olistolitiques de l'Oligocène supérieur–Miocène inférieur dans l'unité ghomaride des Béni Hozmar (secteur de Talembote, Rif septentrional, Maroc). *Eclogae Geologicae Helveticae*, **94**, 313–320.

EL KADIRI, KH., EL KADIRI, K., CHALOUAN, A., BAHAMD, A., SALHI, F. & LIEMLAHI, H. 2006. Transgressive–regressive facies cycles in late Cretaceous calciturbidites from the Mauretanian Series, Béni Ider thrust sheet, northwestern External Rif, Morocco: an application of the 'facies tract–facies sequence' concept. *In*: MORATTI, G. & CHALOUAN, A. (eds) *Tectonics of the Western Mediterranean and North Africa.* Geological Society, London, Special Publications, **262**, 177–192.

EVANS, D., KING, E. L., KENYON, N. H., BRETT, C. & WALLIS, D. 1996. Evidence for long-term

instability in the Storegga Slides region off western Norway. *Marine Geology*, **130**, 281–292.

FEINBERG, H., MAATÉ, A., BOUHDADI, S., DURAND DELGA, M., MAGNÉ, J. & OLIVIER, PH. 1990. Signification des dépôts de l'Oligocène supérieur–Miocène inférieur du Rif interne (Maroc) dans l'évolution géodynamique de l'arc de Gibraltar. *Comptes Rendus de l'Académie des Sciences*, **310**, 1487–1495.

GALLOWAY, W. E. 1989. Genetic stratigraphic sequences in basin analysis I: architecture and genesis of flooding-surface bounded depositional units. *AAPG Bulletin*, **73**, 125–142.

GLASER, K. S. & DROXLER, A. W. 1991. High production and highstand shedding from deeply submerged carbonate banks, northern Nicaragua Rise. *Journal of Sedimentary Petrology*, **61**, 128–142.

GUERRERA, F., MARTIN-ALGARRA, A. & PERRONE, V. 1993. Late Oligocene–Miocene syn/late orogenic successions in Western and Central Mediterranean chains from the Betic Cordillera to the Southern Apennines. *Terra Nova*, **5**, 525–544.

HAAS, J. 1999. Genesis of late Cretaceous toe-of-slope breccias in the Bakony Mts, Hungary. *Sedimentary Geology*, **128**, 51–66.

HANDFORD, C. R. & LOUCKS, R. G. 1993. Carbonate depositional sequences and systems tracts—responses of carbonate platforms to relative sea-level changes. *In*: LOUCKS, R. G. & SARG, J. F. (eds) *Carbonate Sequence Stratigraphy: Recent Developments and Applications.* American Association of Petroleum Geologists, Memoirs, **57**, 3–41.

HESSELBO, S. P. & HUGGETT, J. M. 2001. Glaucony in ocean-margin sequence stratigraphy (Oligocene–Pliocene, offshore New Jersey, U.S.A., ODP leg 174a). *Journal of Sedimentary Research*, **71**, 599–607.

HILL, P. R. & BOWEN, A. J. 1983. Modern sediment dynamics at the shelf–slope boundary off Nova Scotia. *In*: STANLEY, D. J. & MOORE, G. T. (eds) *The Shelfbreak: a Critical Interface on Continental Margins.* Society of Economic Paleontologists and Mineralogists, Society for Sedimentary Geology, Special Publications, **33**, 265–276.

HLILA, R. 2005. *Evolution tectono-sédimentaire tertiaire au front ouest du domaine d'Alboran (Ghomarides et Dorsale calcaire, Rif septentrional, Maroc).* Diplôme d'Etudes Supérieures Thesis, University of Tétouan.

HOYEZ, B. 1989. *Le Numidien et les flyschs oligo-miocènes de la bordure sud de la Méditerranée occidentale.* Doctorat d'Etat Thesis, University of Lille.

KENDALL, C. G. & SCHLAGER, W. 1981. Carbonates and relative changes in sea-level. *Marine Geology*, **44**, 181–212.

KOLLA, V. & MACURDA, D. B., JR 1988. Sea-level changes and timing of turbidity-current events in deep-sea fan systems. *In*: WILGUS, C. K., HASTINGS, B. S., KENDALL, C. G. S. C., POSAMENTIER, H. W., ROSS, C. A. & VAN WAGONER, J. C. (eds) *Sea Level Changes—an Integrated Approach.* Society of Economic Paleontologists and Mineralogists, Society for Sedimentary Geology, Special Publications, **42**, 381–393.

LOUTIT, T. S., HARDENBOL, J. & VAIL, P. R. 1988. Condensed sections: the key to age determination and correlation of continental margin sequences. *In*: WILGUS, C. K., HASTINGS, B. S., KENDALL, C. G. S. C., POSAMENTIER, H. W., ROSS, C. A. & VAN WAGONER, J. C. (eds) *Sea Level Changes—an Integrated Approach.* Society of Economic Paleontologists and Mineralogists, Society for Sedimentary Geology, Special Publications, **42**, 183–213.

LOWE, D. R. 1982. Sediment gravity flows: II. Depositional models with special reference to the deposits of high-density turbidity currents. *Journal of Sedimentary Petrology*, **52**, 279–297.

MAATÉ, A. 1984. *Etude géologique de la couverture mésozoïque et cénozoïque des unités ghomarides au nord de Tétouan (Rif interne, Maroc).* Thesis, University of Toulouse.

MACEACHERN, J. A. & BURTON, J. A. 2000. Firmground Zoophycos in the Lower Cretaceous Viking Formation, Alberta: a distal expression of the Glossifungites Ichnofacies. *Palaios*, **15**, 387–398.

MACEACHERN, J. A., BECHTEL, D. J. & PEMBERTON, S. G. 1992. Ichnology and sedimentology of transgressive deposits, transgressively-related deposits and transgressive systems tracts in the Viking Formation of Alberta. *In*: PEMBERTON, S. G. (ed.) *Application of Ichnology to Petroleum Exploration.* Society of Economic Paleontologists and Mineralogists, Society for Sedimentary Geology, Special Publications, **17**, 252–290.

MACEACHERN, J. A., STELCK, S. R. & PEMBERTON, S. G. 1999. Marine and marginal marine mudstone deposition: paleoenvironmental interpretation based on the integration of ichnology, palynology and foraminiferal paleoecology. Society of Economic Paleontologists and Mineralogists, Society for Sedimentary Geology, Special Publications, **64**, 205–225.

MARTIN-ALGARRA, A. 1987. *Evolución geológica alpina del contacto entre las zonas internas y las zonas externas de la Cordillera Betica (Sector central y occidental).* Doctoral Thesis, University of Granada.

MULLINS, H. T. 1983. Comment on: 'Eustatic control of turbidites and winnowed turbidites'. *Geology*, **11**, 57–58.

MUTTI, E. 1985. Turbidite systems and their relation to depositional sequences. *In*: ZUFFA, G. G. (ed.) *Provenance in Arenites.* Reidel, Dordrecht, 65–93.

MUTTI, E. 1992. *Turbidite Sandstones.* Agip, Special Publication, Milano Instituto di Geologia.

MUTTI, E. & NORMARK, W. R. 1987. Comparing examples of modern and ancient turbidite systems: problems and concepts. *In*: LEGGETT, J. K. & ZUFFA, G. G. (eds) *Marine Clastic Sedimentology: Concepts and Case Studies.* Graham & Trotman, London, 1–38.

MUTTI, E. & NORMARK, W. R. 1991. An integrated approach to the study of turbidite systems. *In*:

WEIMER, P. & LINK, H. (eds) *Seismic Facies and Sedimentary Processes of Submarine Fans and Turbidite Systems*. Springer, Berlin, 75–106.

NEUMANN, A. C. & MACINTYRE, I. 1985. Reef response to sea level rise: keep-up, catch-up or give-up. (Réponse d'un récif à la remontée du niveau de la mer: la suivre, le rattraper, ou y renoncer.) *Proceeding of the Fifth International Coral Reef Congress, Tahiti*, **3**, 105–110.

NOLD, M., UTTINGER, J. & WILDI, W. 1981. *Géologie de la Dorsale calcaire entre Tétouan et Assifane (Rif interne, Maroc)*. Notes et Mémoires du Service Géologique du Maroc, **300**, 1–233.

NUMMEDAL, D. & SWIFT, D. J. P. 1987. Transgressive stratigraphy at sequence-bounding unconformities: some principles derived from Holocene and Cretaceous examples. *In*: PILEY, D. & HOWARDS, J. D. (eds) *Sea-Level Fluctuations and Coastal Evolution*. Society of Economic Paleontologists and Mineralogists, Society for Sedimentary Geology, Special Publications, **41**, 241–260.

PAYROS, A., PUJALTE, V. & ORUE-ETXEBARRIA, X. 1999. The South Pyrenean Eocene carbonate megabreccias revisited: new interpretation based on evidence from the Pamplona Basin. *Sedimentary Geology*, **125**, 165–194.

PEMBERTON, S. G. & MCEACHERN, J. A. 1995. The sequence stratigraphy significance of trace fossils: examples from the Cretaceous foreland Basin of Alberta, Canada. *In*: VAN WAGONER, J. C. & BERTRAM, G. T. (eds) *Sequence Stratigraphy of Foreland Basin Deposits—Outcrop and Subsurface Examples from the Cretaceous of North America*. American Association of Petroleum Geologists, Memoirs, **64**, 429–475.

PIETRAFESA, L. J. 1983. Shelfbreak circulation, front and physical oceanography: east and west coast perspectives. *In*: STANLEY, D. J. & MOORE, G. T. (eds) *The Shelfbreak: a Critical Interface on Continental Margins*. Society of Economic Paleontologists and Mineralogists, Society for Sedimentary Geology, Special Publications, **33**, 233–250.

POSAMENTIER, H. W. & VAIL, P. R. 1988. Eustatic controls on clastic deposition II—sequence and systems tracts models. *In*: WILGUS, C. K., HASTINGS, B. S., KENDALL, C. G. S. C., POSAMENTIER, H. W., ROSS, C. A. & VAN WAGONER, J. C. (eds) *Sea Level Changes—an Integrated Approach*. Society of Economic Paleontologists and Mineralogists, Society for Sedimentary Geology, Special Publications, **42**, 125–154.

POSAMENTIER, H. W., JERVEY, M. T. & VAIL, P. R. 1988. Eustatic controls on clastic deposition I—Conceptual framework. *In*: WILGUS, C. K., HASTINGS, B. S., KENDALL, C. G. S. C., POSAMENTIER, H. W., ROSS, C. A. & VAN WAGONER, J. C. (eds) *Sea Level Changes—an Integrated Approach*. Society of Economic Paleontologists and Mineralogists, Society for Sedimentary Geology, Special Publications, **42**, 109–124.

SARG, J. F. 1988. Carbonate sequence stratigraphy. *In*: WILGUS, C. K., HASTINGS, B. S., KENDALL, C. G. S. C., POSAMENTIER, H. W., ROSS, C. A. & VAN WAGONER, J. C. (eds) *Sea Level Changes—an Integrated Approach*. Society of Economic, Paleontologists and Mineralogists, Society for Sedimentary Geology, Special Publications, **42**, 155–181.

SAVRDA, C. E. 1995. Ichnologic applications in paleoceanographic, paleoclimatic, and sea-level studies. *Palaios*, **10**, 565–577.

SAVRDA, C. E., KRAWINKEL, H., MCCARTHY, M. G., MCHUGH, C. M. G., OLSON, H. C. & MOUNTAIN, G. 2001*a*. Ichnofabrics of a Pleistocene slope succession, New Jersey margin: relations to climate and sea-level dynamics. *Palaeogeography, Palaeoclimatology, Palaeoecology*, **171**, 41–61.

SAVRDA, C. E., BROWNING, J. V., KRAWINKEL, H. & HESSELBO, S. P. 2001*b*. Firmground ichnofabrics in deep-water sequence stratigraphy, Tertiary cliniform-toe deposits, New Jersey Slope. *Palaios*, **16**, 294–305.

SHANMUGAM, G. 2000. 50 years of the turbidite paradigm (1950s–1990s): deep-water processes and facies models—a critical perspective. *Marine and Petroleum Geology*, **17**, 285–342.

SPENCE, G. H. & TUCKER, M. E. 1997. Genesis of limestone megabreccias and their significance in carbonate sequence stratigraphic models: a review. *Sedimentary Geology*, **112**, 163–193.

STANLEY, D. J., NELSEN, T. A. & STUCKENRATH, R. 1984. Recent sedimentation on the New Jersey slope and rise. *Science*, **226**, 125–133.

STOW, D. A. V. & MAYALL, M. 2000. Deep-water sedimentary systems: new models for the 21st century. *Marine and Petroleum Geology*, **17**, 125–135.

SWIFT, D. J. P. 1968. Coastal erosion and transgressive stratigraphy. *Journal of Geology*, **76**, 444–456.

SWIFT, D. J. P. 1975. Tidal sand ridges and shoal retreat massifs. *Marine Geology*, **18**, 105–134.

TUCKER, M. E. & WRIGHT, V. P. 1990. *Carbonate Sedimentology*. Blackwell Scientific, Oxford.

UCHMAN, A. 1995. Taxonomy and palaeocology of flysch trace fossils: the Marnoso-arenacea Formation and associated facies (Miocene, Northern Apennines, Italy). *Beringeria*, **15**, 3–315.

UCHMAN, A. 1999. Ichnology of the Rhenodanubian Flysch (Lower Cretaceous–Eocene) in Austria and Germany. *Beringeria*, **25**, 67–173.

VAIL, P. R., AUDEMARD, F., BOWMAN, S. A., EISNER, P. N. & PEREZ-CRUZ, C. 1991. The stratigraphic signatures of tectonics, eustasy and sedimentology—an overview. *In*: EINSELE, G., RICKEN, W. & SEILACHER, A. (eds) *Cycles and Events in Stratigraphy*. Springer, Berlin, 617–659.

VIANA, A. & STOW, D. A. V. 2000. Seafloor polishing and sand spillover at the outer shelf to upper slope boundary. *In*: STOW, D. A. V. (ed.) *Contourite Watch*. International Geological Correlation Programme 432, Newsletter, **4**, 7–8.

WETZEL, A. & UCHMAN, A. 1998. Deep-sea benthic food content recorded by ichnofacies: a conceptual model based on observations from Palaeogene flysch, Carpathians, Poland. *Palaios*, **13**, 533–546.

Aptian sedimentation: an example of interaction between tectonics and eustatics in Central Tunisia

FREDJ CHAABANI[1] & SALWA RAZGALLAH[2]

[1]*Université de Tunis El Manar, Faculté des Sciences de Tunis, Département de Géologie, Laboratoire des Ressources Minérales et Environnement, 1060 Tunis, Tunisia (e-mail: fredjchaabani@yahoo.com)*

[2]*Université de Tunis El Manar, Faculté des Sciences de Tunis, Département de Géologie, Laboratoire de Biostratigraphie, 1060 Tunis, Tunisia*

Abstract: To reconstruct the sequence evolution and distribution of deposits during the Aptian in the Central Tunisian platform, the present study was mainly based on a sedimentological approach. The palaeogeographical reconstruction shows an inner and an external platform separated by the highs of the Central Tunisian islands. These are characterized by carbonate-dominated deposits evolving towards the north into a pelagic marl-dominated sedimentation. The NW–SE- to east–west-directed faults show an important sedimentary control. In fact, a system of tilted blocks located towards the SW characterizes a large part of the platform. The subsidence evolution during the Aptian was marked by a recovery of extensional tectonics. Finally, some halokinetic vertical movements were responsible for several highs during the latest Barremian. The Central Tunisian platform evolution was controlled by drift of the African platform during the opening of the Atlantic Ocean.

The Lower Cretaceous sedimentation in Central Tunisia (Central and Southern Atlas) occurred in a relatively stable domain delimited to the south by the Saharan Platform and to the north by the Tunisia trough (Sillon Tunisien). This study area is outlined by the South Atlas Flexure, which represents the main tectonic feature separating the Saharan Platform from the North African Atlas (Fig. 1).

The area includes a wide continental platform composed of two main tilted blocks bounded by the major NW–SE- to east–west-trending faults (i.e. Gafsa fault, Kasserine fault, Sbiba fault) (Fig. 2). The northern block corresponds to an outer shelf that passes gradually northward into an open marine basin. The southern block consists of an inner shelf grading southward into a supratidal to continental domain. From at least the Jurassic, the Central Tunisian platform was limited to the east by a north–south-trending high zone, known as the North–South Axis ('Nord–Sud Axis', Burollet 1956). During the Cretaceous this structure behaved as a palaeogeographical barrier separating the Central Tunisian platform from the eastern Tunisian open sea. To the west of this barrier, the Central Tunisian platform also displays a westward stepped series of blocks limited by north–south-trending major faults (e.g. Sidi Ali Ben Aoun fault).

During the Aptian, Central Tunisia was characterized mainly by shallow-marine carbonate sedimentation. To the north, the Tunisian trough, considered as a subsiding zone from Jurassic time, is characterized by a pelagic facies (Fig. 3).

To the south of the Saharan Platform, the Aptian is characterized by a facies of mixed sediments, carbonate, silt, clay and evaporite.

Many studies have been published on the stratigraphy of the Aptian interval (Pervinquière 1903; Arnould Saget 1952; Barnaba 1965; Busson 1966; Bismuth *et al.* 1981; Ben Youssef *et al.* 1985*a*, *b*; Ben Youssef & Peybernes 1986; Abdallah 1987; Kessibi & Kharbachi 1990; Chaabani *et al.* 1992; Chaabani 1995). The main tectonic features have been outlined by Castany (1951), Zargouni (1985) Zargouni *et al.* (1985), Bédir (1995), Boukadi & Bédir (1996) and Zouari *et al.* (1999). The deposional sequences of the Cretaceous deposits were first studied by M'Rabet (1987) and Ben Youssef (1999). The palaeogeographical aspect has been approached by Busson (1966), Boltenhagen (1981), Marie *et al.* (1984) and Ben Ferjani *et al.* (1999).

Methods

During the Aptian a continuous marine sedimentation occurred in many areas of Central Tunisia. Some of the best exposures are located in the southern part of the southern Tunisian Atlas.

Our work is based on a lithostratigrahic analysis aiming to establish the lithostratigraphic units of the

From: MORATTI, G. & CHALOUAN, A. (eds) 2006. *Tectonics of the Western Mediterranean and North Africa.* Geological Society, London, Special Publications, **262**, 55–74.
0305-8719/06/$15.00

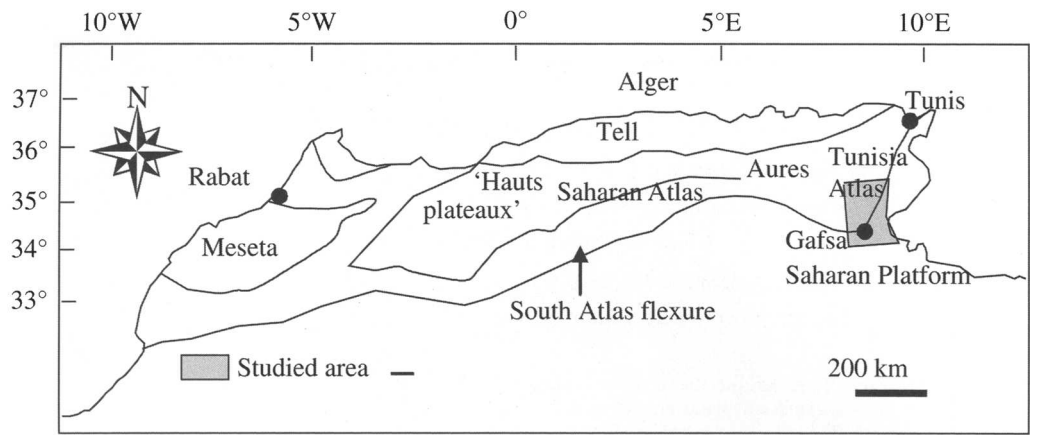

Fig. 1. Geography and geology of Central Tunisia and the Aures Basin.

main Aptian outcrops of Central Tunisia. This is completed by a biostratigraphical and sedimentological study and the well-dated units are integrated in a sequence-stratigraphic study. The sequence boundary corresponds generally to an unconformity, which can be represented by a hard-ground as defined by Bromley (1975), or by a superposition of contrasted facies suggesting a sharp change in the depositional environment across the surface, inferring a reasonable break (Clari *et al.* 1995). The established sequences allow us to make correlations in Central Tunisia and to establish an isochron map of the Aptian sequence within this area. We propose finally a block diagram synthesizing the relationships between sedimentary filling, tectonics and sea-level changes.

Lithostratigraphy

In the Aptian succession in Tunisia, the so-called Orbata Formation passes laterally into the Serj Formation. The two formations mainly consist of carbonate deposits. The first name is used to describe the Aptian succession in Central Tunisia; the second is used to describe the basinal facies of northern Tunisia during the same interval. In the study area, the Orbata Formation rests on the Sidi Aïch Formation, which is mainly represented by fine-grained sand and siltstone. This formation, attributed to the Barremian by Chekma *et al.* (1991), was deposited in a shallow-marine environment.

Gafsa area

The Orbata outcrop (reference section). In Central Tunisia, Burollet (1956) defined the Orbata Formation in the type locality Jebel Orbata (Fig. 2), which corresponds to a wide anticline affected to the west and south by the Gafsa fault, a major structural feature of the region. Although M'Rabet (1987) redefined this formation including the Lower Albian, in this study we prefer to preserve the original description of Burollet (1956).

The type section is located about 10 km west of Gafsa. In this locality, the Orbata Formation overlies a well-developed siliciclastic series, ending with the Sidi Aïch Formation sand (Unit 0), which is Barremian in age (Fig. 4). The measured section in this locality (Jebel Orbata) shows five lithological units (Fig. 5a).

The Orbata Formation starts with a carbonate interval (Unit 1), traditionally referred to as the Aptian bar ('la barre aptienne', Busson 1966) (Fig. 4). This unit is 50 m thick and is composed of various dolomitic massive facies including many bioturbated levels dominated by large-scale massive and laminated dolostone beds. It consists of dolosparite alternating with dolomicrosparite (Fig. 5b) containing locally bioclasts and intraclasts. The contact of this unit with the silt and the sand of the Sidi Aïch Formation is transitional (Fig. 5c). The presence of marine bioclasts, bivalves, gastropods, benthic foraminifers and intense bioturbation indicates a subtidal environment (Collinson & Thompson 1982). As observed throughout Central and Southern Tunisia, the 'Aptian bar' or the 'Saharan bar' is a regional marker horizon. Based both on its stratigraphic position and the faunistic assemblage of Unit 2, its age ranges from the Latest Barremian to Early Aptian (Ben Youssef *et al.* 1985*a*, *b*; Chaabani *et al.* 1992).

Unit 2, which is 70 m thick, conformably rests on the Unit 1 (barre aptienne) and is formed, from base to top, of shales alternating with subordinate laminated mudstone followed by alternation of green oyster marls and massive to laminated carbonates.

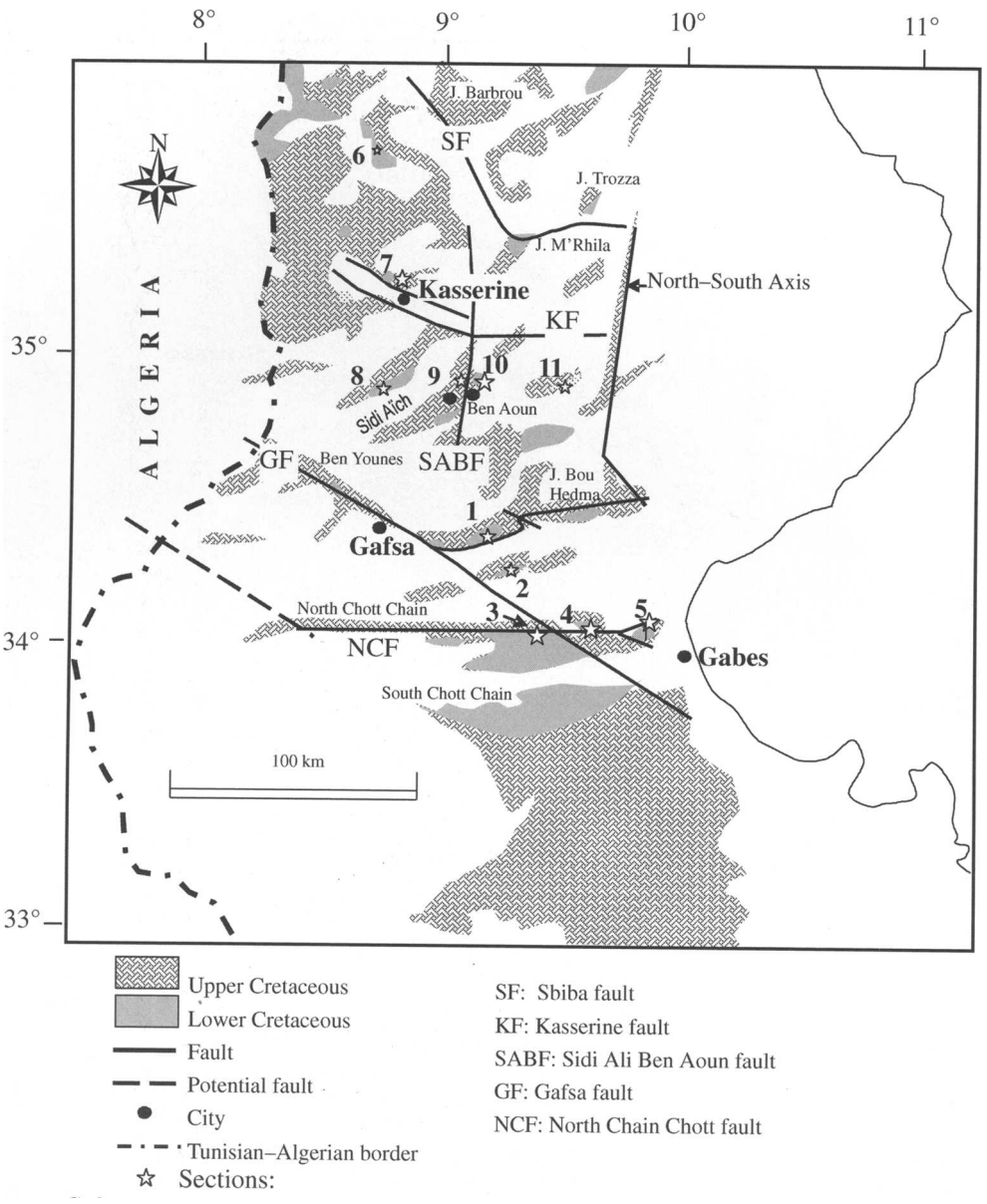

- **Gafsa area** : 1- J.Orbata (9°4';34°24'); 2- J.Chemsi (9°20; 34°15); 3- J. Bir Oum Ali (9°12'; 34°8'); 4- J.Naïmia. (20°20'; 34°8'); 5.- J.Fatnassa (9°50'; 34°6')
- **Kasserine area** : 6- J.Boulahneche (8°55'; 34°40'); 7- J.Semmama (7°50'; 35°15'); 8- J.Ouaddada (7°45'; 34°54') ; 9-J.Zitoun (9°5'; 34°56); 10- J.El Hafey (9°12'; 34°56); 11- J.Kebar (9°28';34°56);

Fig. 2. Exposed and cited localities in Central Tunisia and simplified structural map (extract from geological map of Tunisia at 1/500 000 (Office National des Mines de Tunisie).

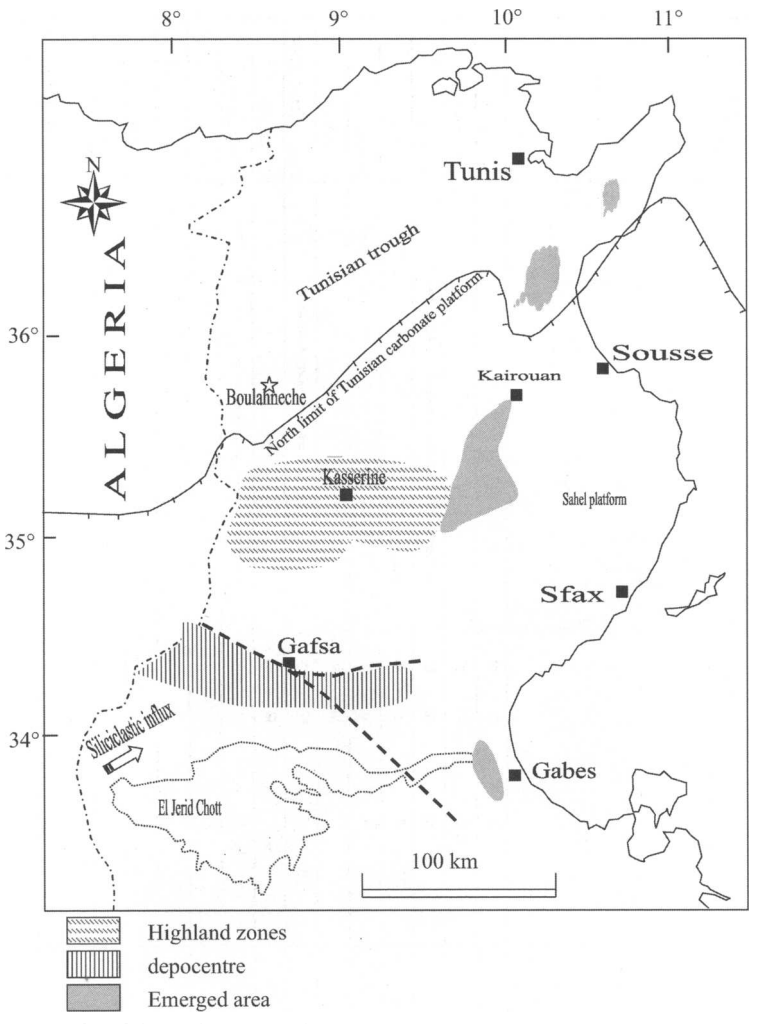

Fig. 3. Palaeogeography of the Aptian in Tunisia (modified from Tlatli 1980; M'Rabet 1987).

The carbonate units consist of mudstone to wackestone surmounted by very fine-grained cross-bedded bioclastic packstone to grainstone with pellets, ooliths, echinoderms, bivalves, *Palorbitolina lenticularis* (Blumer) and *Choffatella decipiens* (Schlumberger) and other benthic Foraminifera. This assemblage indicates an open marine but shallow-water deposit where ooliths developed under strong wave action or tidal influence (Fig. 5d).

The presence of *Palorbitolina lenticularis* (Blumer) and *Choffatella decipiens* (Schlumberger) yields an early Aptian age (Bedoulian) for this unit. Unit 2 shows an arrangement of progradational parasequences, representing a highstand system tract (HST). The first occurrence of the oolitic facies suggests the onset of a regressive tendency, which finishes with the top of Unit 3. The maximum flooding surface (MFS) would correspond to the top of Unit 1.

Unit 2 is overlain by evaporites and minor carbonates (Unit 3) (Fig. 4). These deposits are 90 m thick and display a lenticular geometry at the southern flank of the Orbata anticline. Thin carbonates and marl beds occur locally interfingered with gypsum. This evaporite episode corresponds to a lagoonal environment and reflects the regressive part of the HST.

Unit 3 is abruptly overlain by fine-grained sandstones and marls (Unit 4) (Fig. 4). The contact

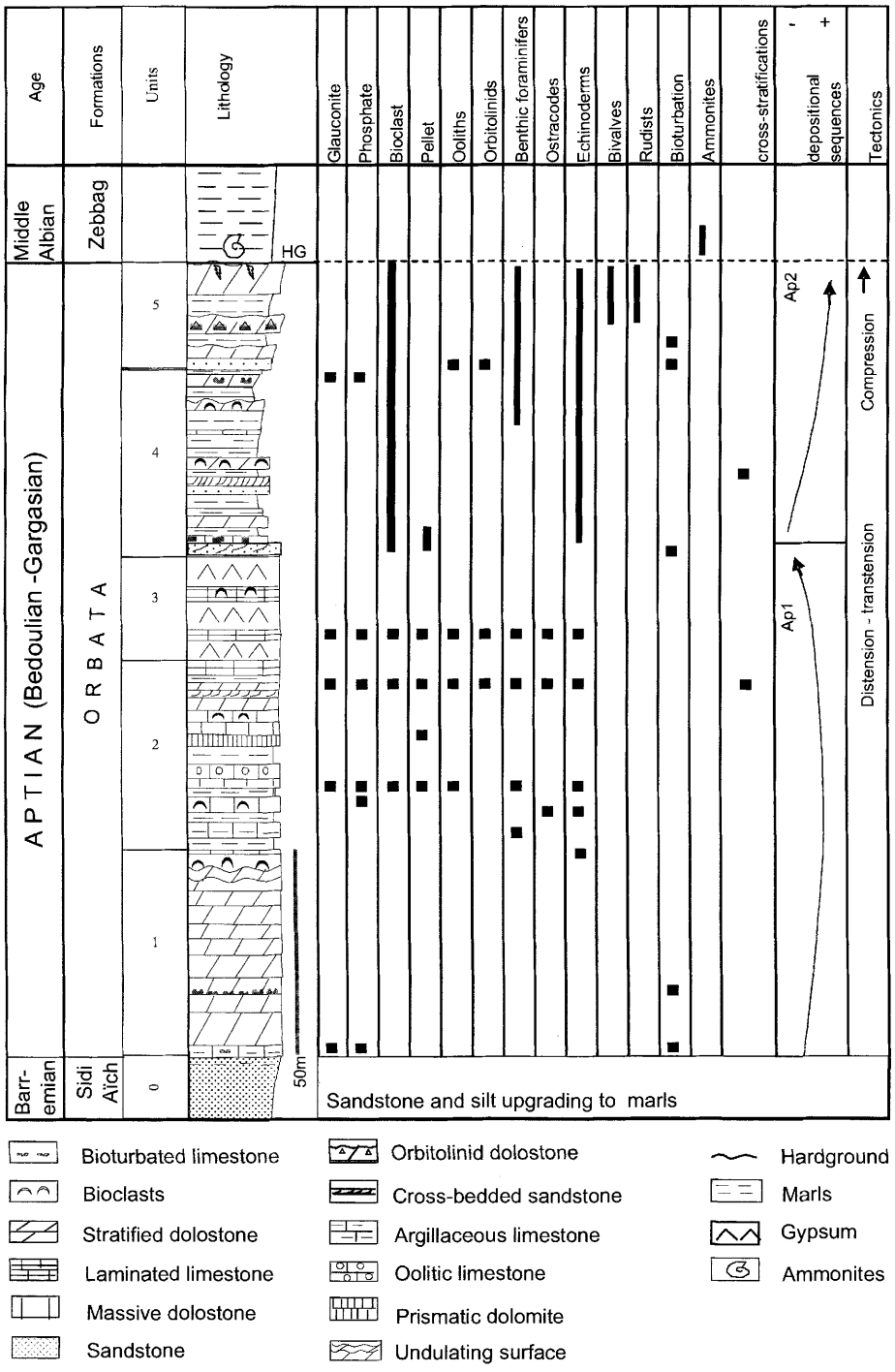

Fig. 4. Lithostratigraphical log of the Upper Barremian–Aptian succession of the Orbata section (reference section).

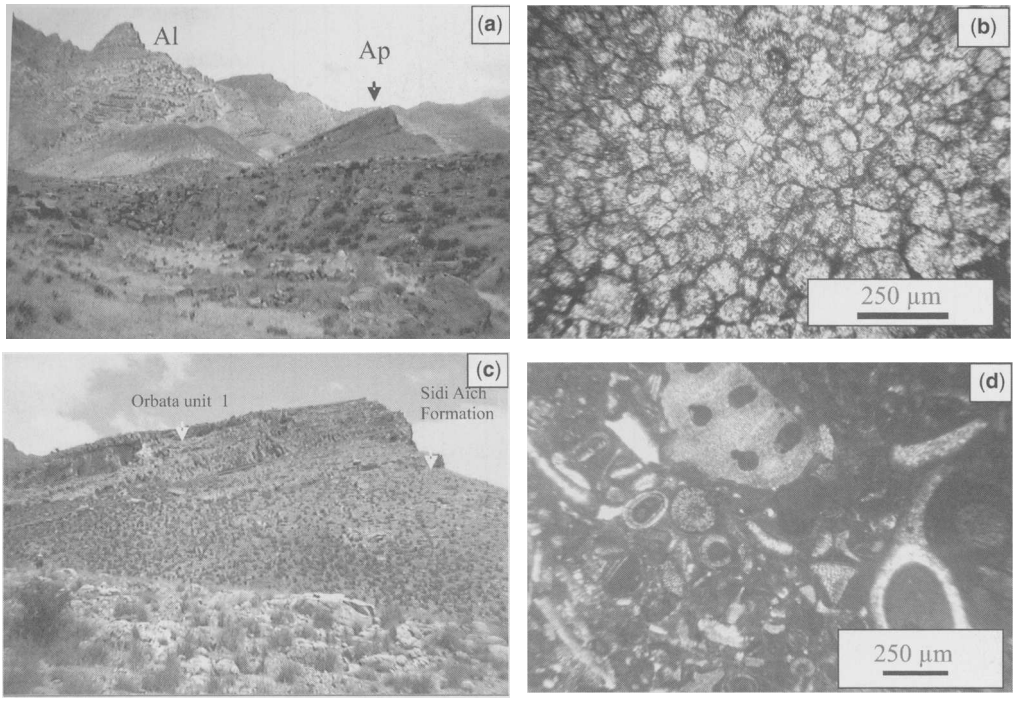

Fig. 5. Orbata Formation in the reference section. (**a**) General view showing the Aptian succession (Ap), which starts with a dolomitic cliff (right) and the well-developed carbonate cliff of the Upper Albian (Al) (left). (**b**) In thin section, the dolostone of Unit 1 corresponds mainly to a dolosparite facies. (**c**) The sandstone of Sidi Aïch Formation covered by the cliff of the Orbata Unit 1 composed of massive dolomite. (**d**) In thin section, some levels of Unit 2 show packstone rich in apatite, ooliths, and bioclasts.

between Units 1 and 3 is a sequence boundary represented by a coplanar surface indicating a sharp change in the depositional environment across the contact surface. In the analysed section, Unit 4 is *c.* 28 m thick. The lower interval of Unit 4 in the Orbata area starts with thin to medium cross-bedded sand with marl and silt intercalations grading up to alternations of marly siltstone and carbonate. These consist of dark grey limestone to dolostone composed of oolitic and pellitic packstone to grainstone. These alternations grade up to marl and bioclastic carbonates characterized, locally, by cross-stratification and including bivalves, echinoderms, bryozoans and ostracodes. The uppermost part consists of fossiliferous and glauconitic marl alternating with medium to thick beds of sand to sandy limestone. The carbonates are mainly packstone to grainstone containing bivalves, gastropods, miliolids, pellets and ooliths. The presence of many taxa of benthic Foraminifera indicates a shallow-marine environment.

Unit 4 passes upward gradually to Unit 5, which is characterized by a decrease of the siliciclastic flux and the dominance of the carbonate facies. This unit corresponds to five parasequences, characterized by a dominance of carbonate deposits (Fig. 6a).

(1) The first one (6.7 m) consists of glauconitic silty marl, sand and sandy dolomites grading up to massive clastic dolomite containing a rich marine fauna including orbitolinids (Fig. 6b) bivalves and gastropods.

(2) The second one is composed from bottom to top of marl, sandy dolomite and massive burrowed dolomite containing a rich fauna of bivalves (Fig. 6c) and gastropods.

(3) The third one consists of fossiliferous green marl grading up to bioclastic sandy dolomite and ending with massive dolomite rich in rudists topped by local bored and ferruginous hardground.

(4) The fourth one consists of alternations of marl and thinly bedded bioclastic limestone grading up to orbitolinids-rich (Fig. 6d) and massive dolomite.

(5) The uppermost deposit is similar to the fourth parasequence but it is particularly rich in rudists (Fig. 6e and f). It also contains bryozoans and algal debris.

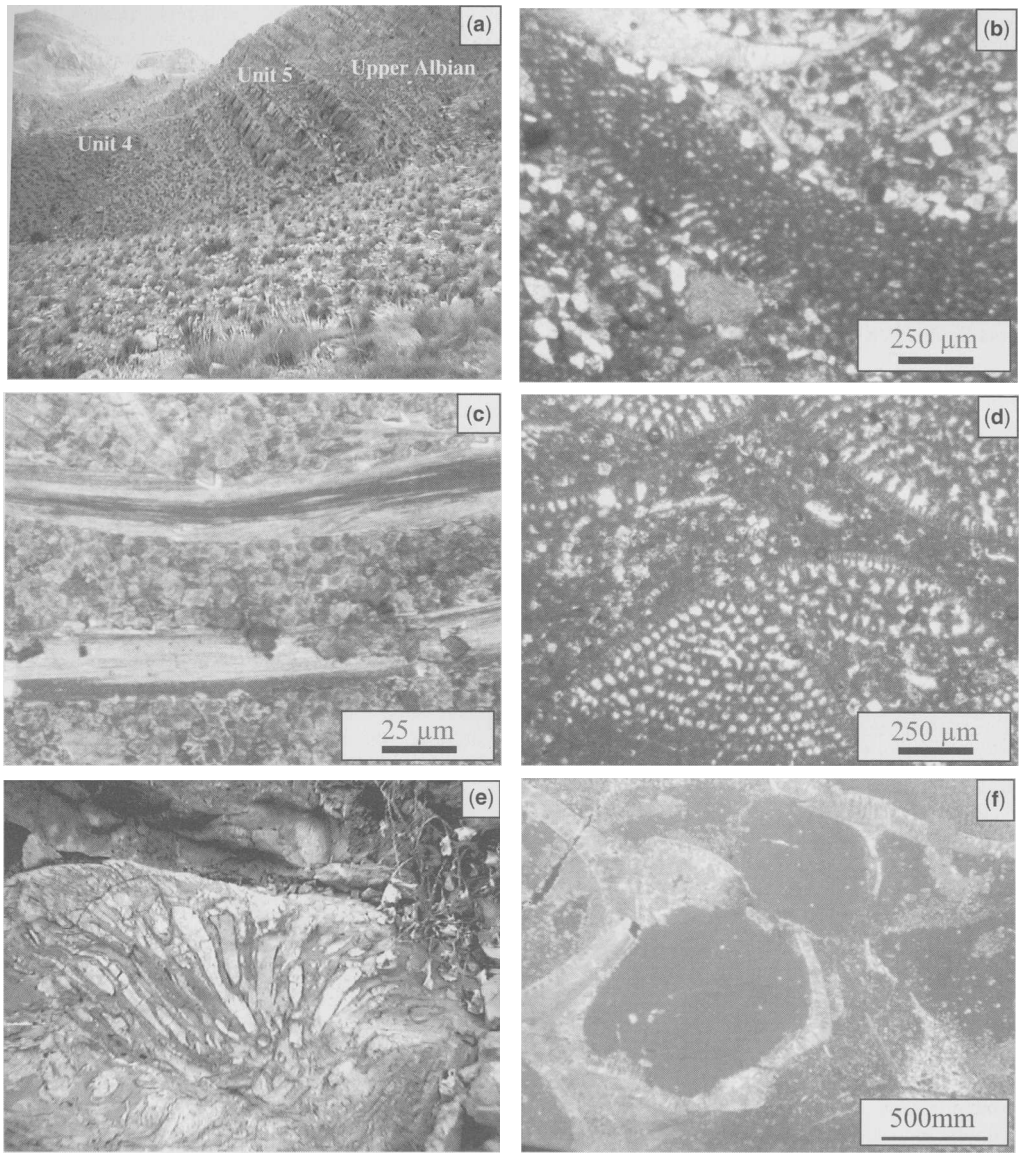

Fig. 6. Orbata Formation of Jebel Orbata (reference section). (**a**) The photograph shows the succession of Units 4 and 5 of the Orbata Formation. (**b**) Orbitolinid facies of the sandy carbonate phases of the first parasequence of Unit 5. (**c**) Partially dolomitized bivalve sections in the carbonate phase of the second parasequence of Unit 5. (**d**) In thin section, the lowermost part of the fourth carbonate phases of Unit 5 is usually rich in orbitolinids. (**e**) Rudist colonies are well developed in the upper part of some carbonate phases of the fourth and the fifth parasequences of Unit 5. (**f**) In thin section, the rudists are filled with micrite (the top of Unit 5).

This Upper Aptian sequence is well dated by *Orbitolina* (Mesorbitolina) *texana* (Roemer) and *Eoradiolites* (rudists), identified by Chihi (pers. comm.), and contains a rich marine fauna including rudists, oysters, nerineids, gastropods and orbitolinids, which are common throughout the study area.

The continuity of this unit, which drapes the underlying Unit 4 throughout Central Tunisia, is remarkable. However, the reference outcrop is very rich in rudist-rich colonies. Oolitic and pellitic deposits, representing an increasing energy, are well developed in the intertidal margin of the

inner platform (Gafsa Basin). The top of this unit is marked by an unconformable surface corresponding to a sedimentary hiatus covering the Clansayesian–Lower Albian interval.

The Chemsi outcrop. This outcrop is exposed 25 km to the south of Jebel Orbata (Fig. 2) and has been analysed by Chaabani *et al.* (1992), who reported a 350 m thick interval stratigraphically coincident with the previously discussed section; Unit 1 of the Orbata Formation crops out only partially. This unit is composed of massive dolomite containing cherty levels in the upper part (Fig. 7).

Unit 2 (Fig. 7) contains a rich benthic fauna composed of *Orbitolina (Mesorbitolina) lotzei*, *Palorbitolina lenticularis*, *Choffatella decipiens*, *Nezzazatinella* cf. *picardi*, *Lenticulina* sp., *Textularia* sp. and the ostracodes *Cythereis btaterensis btaterensis*, *Cythereis* sp., *Paracytheropteron* sp. and *Cytherella* sp. (Fig. 8).

Unit 3 is mainly composed of thick series of gypsum alternating with very thin carbonate and marly beds (Figs 7 and 9a).

Unit 4 (Fig. 9b) is thicker and richer in sand, which is laterally covered and contains a rich benthic fauna: *Orbitolina (Mesorbitolina) subconcava*, *Nezzazatinella* cf. *picardi*, *Lenticulina* sp., *Textularia* sp., and the ostracodes *Cythereis btaterensis btaterensis*, *Cythereis btaterensis immunicostata*, *Cythereis* sp., *Paracytheropteron* sp. and *Cytherella* sp., as well as some ammonite debris.

Unit 5 (Fig. 9b and c), which is mainly composed of massive dolomite, exhibits many similarities of facies evolution to the reference section and contains a rich fauna mainly represented by *Orbitolina (Mesorbitolina) texana* and *Eoradilites* rudists. This unit is covered with alternations of marls and dominant carbonates (Fig. 9c), which are attributed to the Late Albian (Arnould Saget 1952).

Jebel Naïmia (North Chott Chain). Jebel Naïmia, located south of Gafsa (about 50 km) in the southern part of the study area (North Chott Chain), shows a similar succession to the reference section. It has been previously noted by Abdallah (1987) that in Jebel Naïmia, the lower unit (Unit 1) is not exposed. The succession starts with alternations of marl and carbonates (Unit 2) grading upto a mixed facies of marls, carbonates and gypsum (Unit 3). The carbonates are represented by mudstone, packstone and locally grainstone containing echinoderms, orbitolinids, green algae, ooliths and lithoclasts deposited in a subtidal to intertidal environment. In the uppermost part, the gypsum indicates a lagoonal environment.

The upper part of the series is 50 m thick and is characterized by a mixed facies composed of marly carbonates, sandstones and sands. It contains a marine fauna and some wood debris (Unit 4) indicating an infralittoral (prodelta) environment. The carbonates are mainly packstone to grainstone rich in bivalves, orbitolinids, glauconitic and phosphate particles. The uppermost part of the series shows massive orbitolinid dolomite (equivalent to Unit 5) probably indicating subtidal environment. The Middle to Upper Albian deposit rests unconformably of an erosional surface over the Aptian series (Gargasian).

Bir Oum Ali. Laterally, at Bir Oum Ali, situated about 10 km to the west of Jebel Naïmia, Unit 1 of the Orbata Formation described by Ben Youssef *et al.* (1985*a*, *b*) is 120 m thick and conformably overlies the sand of the Sidi Aïch Formation. It is composed of five units.

Unit 1, which is about 30 m thick, corresponds to a massive bioclastic dolomite with echinoderms, rudists and benthic Foraminifera.

Unit 2 (35 m thick) is composed of alternations of marls and bioclastic carbonate containing in the upper part bioclastic carbonate with cross-bedded stratification. This succession is covered by a succession of thin-bedded grey limestone.

Unit 3 (30 m) corresponds to alternations of bioclastic limestone with oysters, dolomite and clay. Laterally, this unit contains many intercalations of gypsum beds.

Unit 4, 30 m thick, is composed of a sand and sandstone alternation with cross-bedded stratification containing bioclastic carbonate with oysters.

Unit 5, reduced to 2 m in thickness, is made up of bioclastic dolostone containing rudists and nerineid gastropods and could be the equivalent of Unit 5 of the reference section. This unit ends with an erosional surface (Ben Youssef *et al.* 1985*a*, *b*). This formation is overlain by the pelagic Albian marls, well dated with ammonites.

The Fatnassa outcrop. This section, located 100 km south of Gafsa, is probably made of Units 1 and 2. Unit 1 is composed of 20 m of massive dolomite surmounting the palaeosoil of the Sidi Aïch Formation (Fig. 10a). The contact between these two formations is sharp. In this locality, the Aptian bar is capped by the development of a thick bio-eroded ferruginous crust (hardground). Unit 2 is very thin (1 m). It consists of marls and dolostone alternations, ending with complex hardground surfaces composed of two or more red and ferruginous bored surfaces (Fig. 10b) separated by 1 m thick deposits. The lithification of these hardgrounds is indicated by the presence of borings probably corresponding to bivalve activity. Their cross-section is circular with an average diameter of 1.5 cm. No fauna have been observed in this

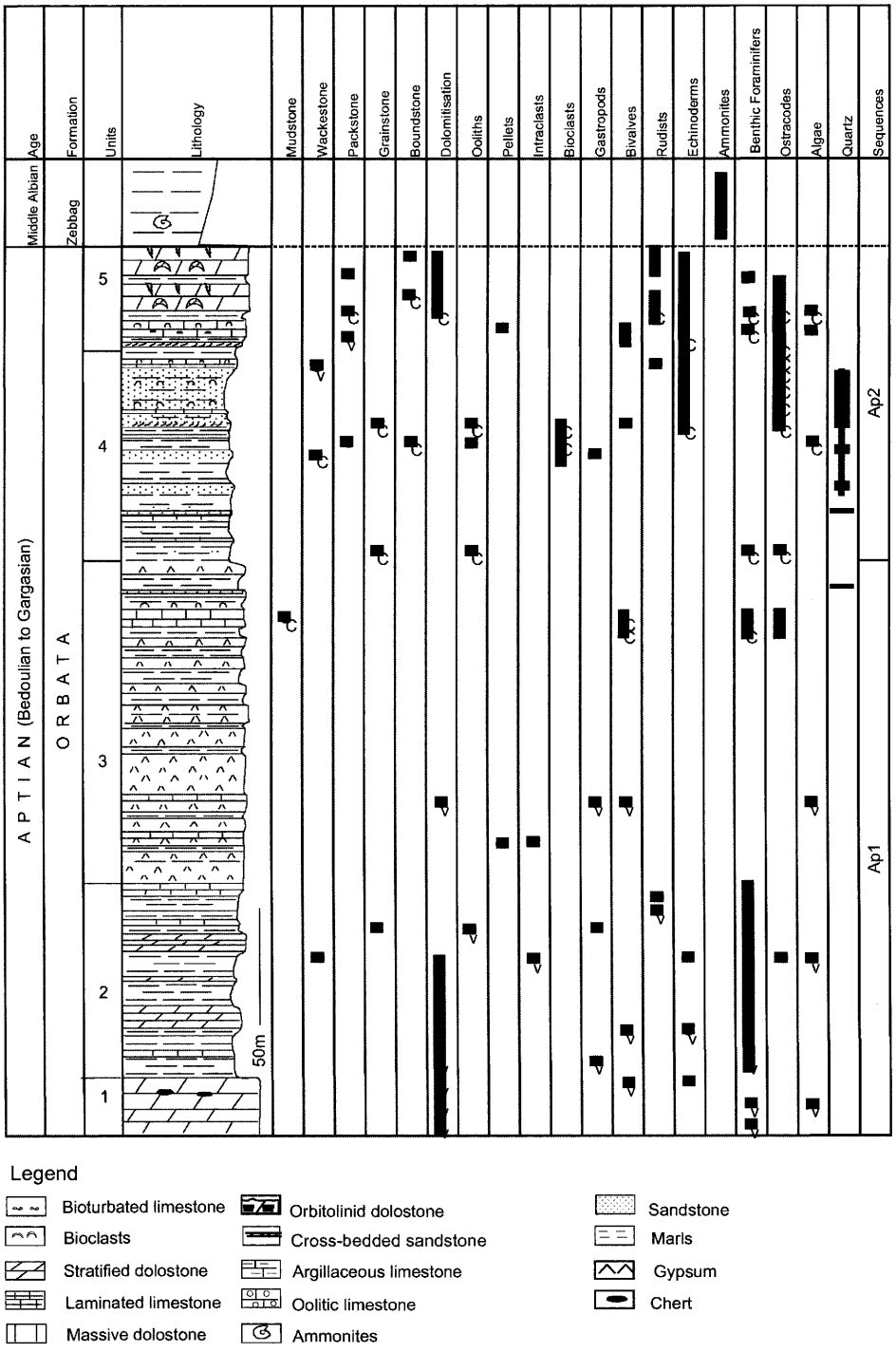

Fig. 7. Lithostratigraphical log of the Upper Barremian–Aptian succession of the Orbata section in Jebel Chemsi.

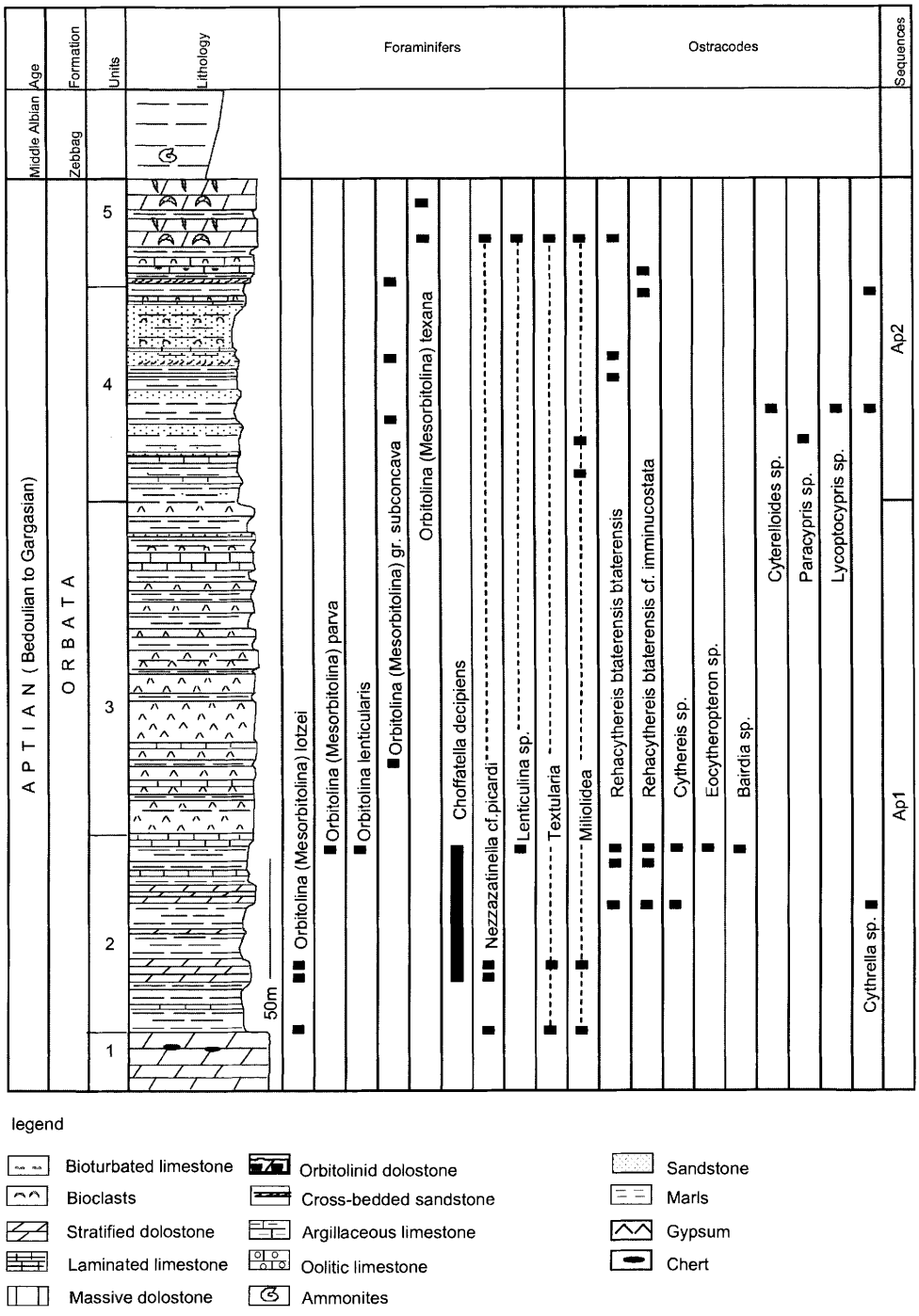

Fig. 8. Stratigraphical log of the Upper Barremian–Aptian succession of the Orbata section in Jebel Chemsi.

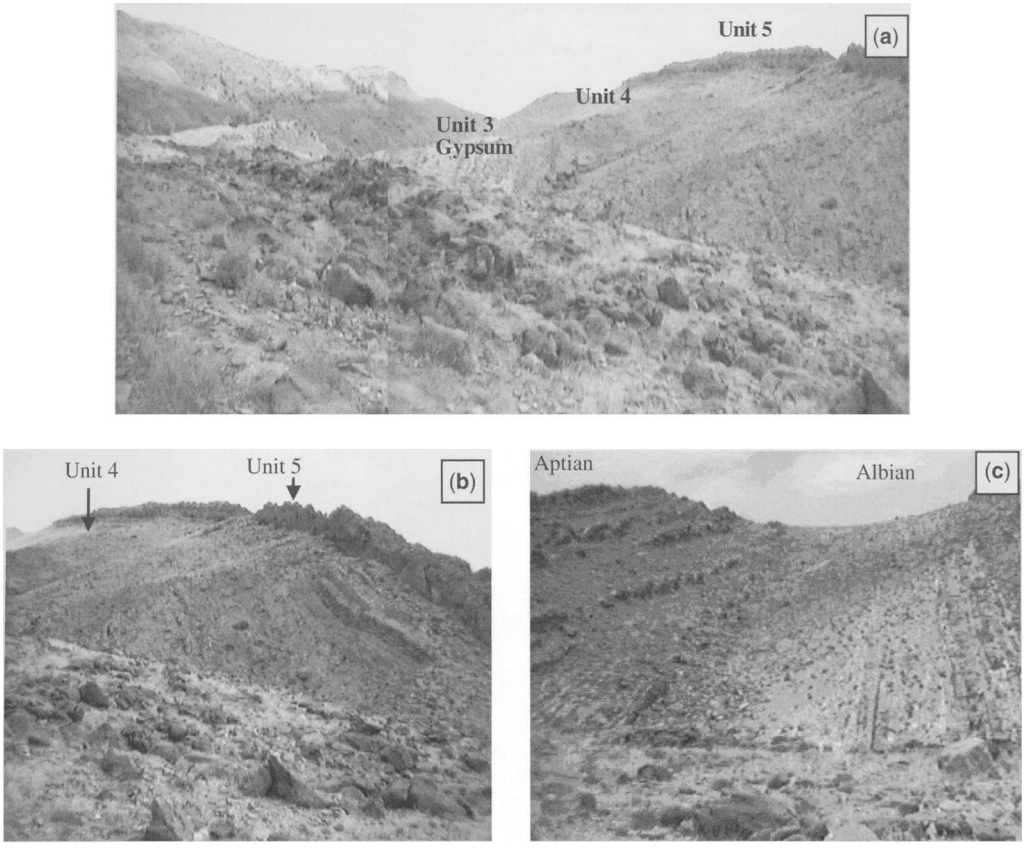

Fig. 9. Orbata Formation in Jebel Chemsi. (**a**) General view of Orbata Formation showing the Aptian succession from the base (left) to the top (right). (**b**) The upper part of the Orbata Formation showing the alternation of silt, sand and marls of Unit 4 and the dolomitic cliff of Unit 5. (**c**) The Aptian–Albian boundary: the upper Albian alternation rests unconformably on the Gargasian cliff.

dolomitized microfacies. However, the borings are filled with fine-grained silt and marls.

Laterally, in the southeastern part of Fatnassa, Unit 1 is capped by an eroded surface characterized by the presence of micro-karsts (about 1 cm wide) filled with sparitic calcite (Fig. 10c). This succession is covered by an alternation of marls and bioclastic limestone attributed to the Coniacian. Towards the west (about 1 km), the Orbata Formation is absent and the Coniacian conglomerates overlie the bored hardground of Unit 1 or even directly the Barremian sand of the Sidi Aïch Formation (Fig. 10d). The conglomerate pebbles correspond to reworked Aptian elements.

Kesserine area

The Orbata Formation crops out in many mountains: jebels Chaambi, Semmama, Ouaddada, Selloum, Sidi Aïch, El Hefay, Kebar, etc. Representative sections only are described below.

Ouaddada. In this locality, situated north of the study area (Fig. 2), M'Rabet (1987) defined three members in the Aptian series, which can be summarized as follows.

(1) The lower member (70 m) starts with a dolomitic massive bar, which is a wackestone facies containing rudist debris, miliolids and ooliths (Unit 1). The middle part is formed by alternations of marl and dolosparites containing bivalves, echinoderms and benthic Foraminifera (*Trochammina vocantiana*, *Trochammina* sp., *Choffatella decipiens*, *Ammobaculites* aff. *subcretaceous*, *Ammobaculites* sp. and orbitolinids (Unit 2). This member is surmounted by laminated dolomite (Unit 3 probably).

(2) The middle member, 65 m thick, is subdivided into three entities. The first one is a marly dolostone containing some ooliths, rudists and nerineid gastropods. The second one is composed of marly limestone. In thin section, the limestone is represented by wackestone to packstone containing

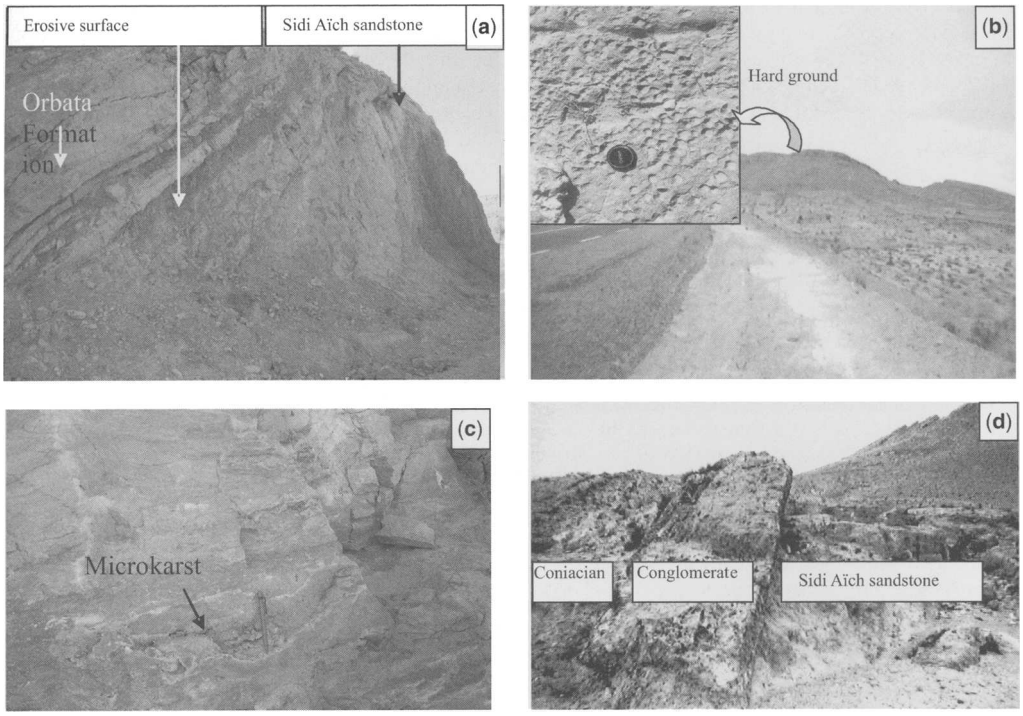

Fig. 10. Fatnassa section. (**a**) Aptian lateral variation showing a reduced Unit 1 overlying the Barremian palaeosols of the Sidi Aïch Formation. (**b**) General view and the hardground ending the Aptian. (**c**) Microkarst partially filled with sparite, observed in Unit 1 of the Jebel Fatnassa south flank. (**d**) A gap in the Aptian sequence; the Barremian sandstone is directly covered by the Coniacian conglomerate.

nerineid gastropods, echinoderm debris and rare bryozoans, orbitolinids, miliolids, ostracodes and locally abundant ooliths. The third one is represented by dolomitic sandstones and dolostones with rare ooliths, and phosphatic and glauconitic grains. This member, which is the equivalent of the Unit 4 of the reference section, seems to be widespread in the Aptian platform of Central Tunisia.

(3) The upper member is mainly dolomitic and is 25 m thick. It contains rudists and nerineid gastropods, and should be the equivalent of Unit 5 of the reference section.

In this section we outline the presence of a sedimentary hiatus covering the Late Aptian–Early Albian interval.

At Jebel Zitoun, situated 30 km east of Jebel Ouddada (Fig. 2), the Aptian is represented by the lower part of the Orbata Formation. It is formed mainly of marls and bioclastic dolomite ending with laminated dolomite containing birds' eyes and mudcracks. Laterally, at Jebel El Hafey, situated 5 km to the east of Jebel Zitoun, the same formation is reduced to 10 m thickness, and consists of laminated dolomite with birds' eyes and mudcracks (Fig. 2). The same series is represented by about 30 m of massive dolostone at Jebel Kebar, situated 25 km to the east of Jebel El Hefay (Fig. 2). It consists of dolosparite to dolomicrosparite with traces of dissolution of orbitolinids and oysters. The top of this facies is eroded and is unconformably overlain by paludous limestone with characea attributed by Khessibi (1978) to the Aptian–Albian *pro parte* interval.

Jebel Semmama. Jebel Semmama is located 60 km north of Gafsa. The Aptian outcrop is 47 m thick and has the same lithological characteristics as those of the Orbata section. Unit 1 is composed of massive sandy dolomite overlain by massive dolomite, characterized by bioturbations, and containing echinoderm debris and gastropods. The series continues with alternations of marly dolostones and sandstones (Unit 2). This unit is surmounted by massive and laminated dolostone (Unit 3). The upper part consists of alternations of marl, sand and sandy dolomite followed by 10 m of massive dolomite, which is generally non-fossiliferous except for rare orbitolinids (Unit 5). The top of this unit is marked by a bored surface.

The borings are related to bivalve activity and are filled with vadose micrite sediments containing fine quartz grains and suggesting an intertidal origin (M'Rabet 1987). In this locality the Upper Albian deposits rest unconformably on the Aptian succession.

Biostratigraphic data

The biostratigraphic interpretation of the mainly shallow-marine lower Aptian deposits is based on benthic taxa (Fig. 8). For the Orbata Formation, the most important Foraminifera (orbitolinids) and ostracodes are *Orbitolina* (*Mesorbitolina*) *lotzei* and *Choffatella decipiens.*

Based on its stratigraphic position, the age of Unit 1 ranges from the latest Barremian to the Early Aptian. A Gargasian age for Units 2–5 is confirmed by the assemblage of *Orbitolina* (*M.*) *parva*, *O.* (*M.*) *subconcava* and *O.* (*M.*) texana (identified by Schroder). The ostracode assemblage is characterized by the presence of *Rehacythereis btaterensis* cf. *immunicostata*, *Paracypris* sp., *Cytherelloidea* sp. and *Cytherella* sp.

The presence of *Knemiceras* in the succession overlying the Orbata Formation allows us to attribute this succession to the Late Albian. Therefore the interval from the latest Aptian to the Early Albian is not represented in the Central Tunisian platform.

Sequence-stratigraphic interpretation

The Orbata platform and its equivalent have a large north to south extent in Tunisia, suggesting a transgressive system tract (TST) recording the general transgression that marked the Late Barremian–Early Aptian (Bedoulian). The Aptian succession and its palaeoenvironmental context allow to recognize two depositional sequences, Ap1 and Ap2.

Sequence Ap1

This sequence corresponds to Units 1, 2 and 3. The transgressive tidal shoreline and shallow-marine shelf deposition occurring during a high sea level (TST) correspond to the upper Sidi Aïch Formation, extending from north to south and eventually throughout the Gafsa Basin shelf. The maximum flooding surface (MFS), recording the transition to highstand conditions, occurred during the deposition of the uppermost part of Unit 1. It is marked by a ferruginous hardground, which is locally bioeroded. The HST corresponds to Units 2 and 3. Above the flooding surface, the facies of Unit 2 is characterized by ooliths, pellets, bivalves, echinoderms, miliolid packstone and bioclastic grainstone. This sedimentation suggests a high-energy environment. Unit 2 consists of a marly parasequence, which progrades southward over the entire Gafsa Basin. The evaporitic phase of this unit represents the regressive part of the HST of the third-order Aptian sequence (Ap1). The sequence boundary corresponds to a sharp change in the depositional environment across the surface, and a prolonged break in sedimentation may reasonably be inferred (Clari *et al.* 1995).

The evolution of sequence Ap1 is summarized in Figure 11, which shows that during the Late Barremian–Early Aptian, a first carbonate platform existed, characterized by a shallow-marine environment. This has a wide geographical extent and is relatively reduced on some highlands towards the south, indicating vertical halokinetic movements, particularly in Jebel Fatnassa (Ben Ferjani *et al.* 1990) and Jebel Kebar (Hlaîem 1998) (Fig. 12). After a widespread regression, the Central Tunisian platform attained a flat-topped morphology at the end of Unit 1 deposition. Tectonic activity initiated subsidence and local uplift during the HST. Unit 1 is locally marked by a ferruginous surface that corresponds to the MFS, which is characterized by the presence of bioturbation and the accumulation of bioclasts and dolomite intraclasts. This surface is covered by the HST, formed by aggradational parasequences composed of high-energy facies corresponding to the first stage of the drowned platform filling.

Sequence Ap2

The sequence Ap2 overlies Unit 3, and corresponds to Units 4 and 5. The sedimentation is dominated by siliciclastic deposits at the base and carbonate facies in the upper part (Fig. 13). The benthic fauna is mainly represented by orbitolinids, oysters, rudists and echinoderms. The dominant sand and silt sediments were mainly transported from a SSW source (M'Rabet 1987). This tidal deltaic facies is interpreted as the transgressive phase of this sequence, which reaches its maximum with the deposition of the reefal facies. The carbonate-dominated parasequences correspond to the upper part of the TST of the second-order Aptian sequence (Ap2). The TST interval therefore shows the development of a carbonate platform, with rudist colonies being developed over some relative highs.

The uppermost part of the sequence Ap2 is marked by an unconformity. The Upper Aptian to Lower–Middle Albian interval is absent. This gap extends to the Saharan Platform, in South and Central Tunisia (Barnaba 1965; Busson 1966; Ben Youssef *et al.* 1985*a*, *b*; Chaabani *et al.* 1992; Chaabani 1995).

Locally, in the highlands of Central Tunisia at Jebel Kebar, this interval is represented by a continental series, composed of silt and red marls containing characea and palaeosoils (Khessibi 1978; M'Rabet 1987).

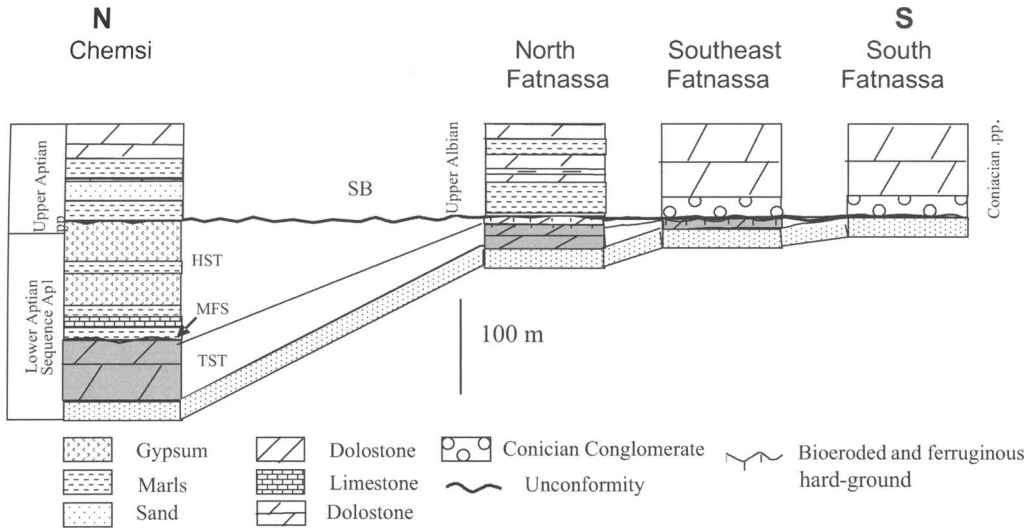

Fig. 11. Evolution of the Ap1 sequence toward the south of the inner platform (Gafsa Basin). SB, Sequence boundary; MFS, maximum flooding surface; TST, transgressive system tract; HST, highstand system tract.

Correlation profiles and geodynamic context

The correlation established between seven Aptian sections covering an area from the Fatnassa uplift to Jebel Boulahneche situated north of Kasserine (Fig. 2) allows us to illustrate the depositional distribution of the Aptian succession. Figure 14 is a north–south profile showing a rapid decrease in thickness of the Aptian succession towards the north and the south to Jebel Bouahneche and the Fatnassa anticline, respectively. This variation affects all the lithological units. Only Unit 1 is present in the southern flank of the Fatnassa anticline

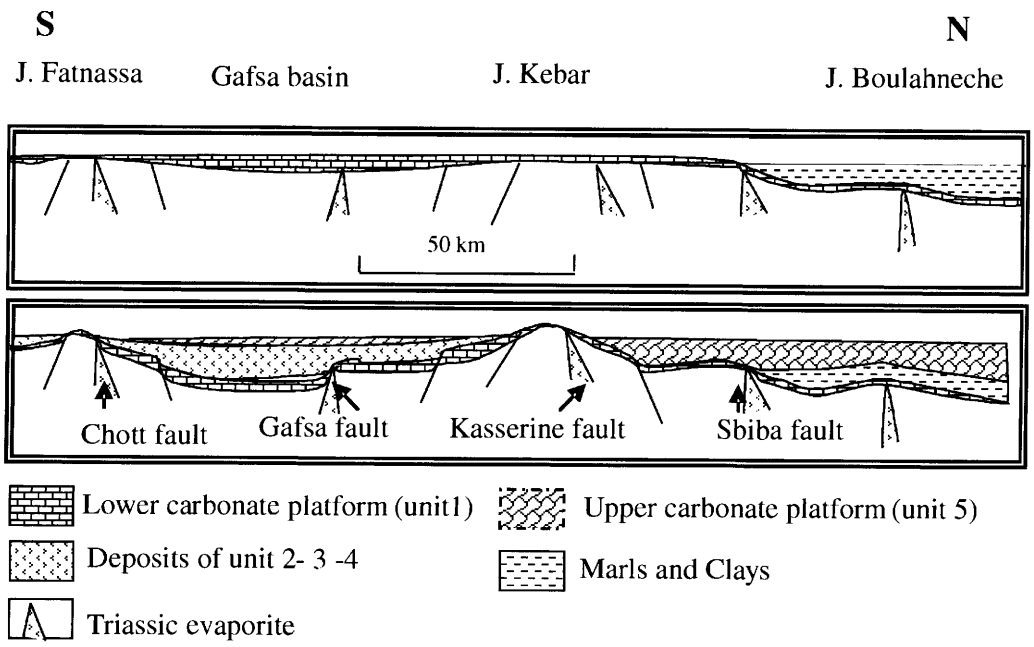

Fig. 12. Geodynamic context and model of Aptian deposits in Central Tunisia.

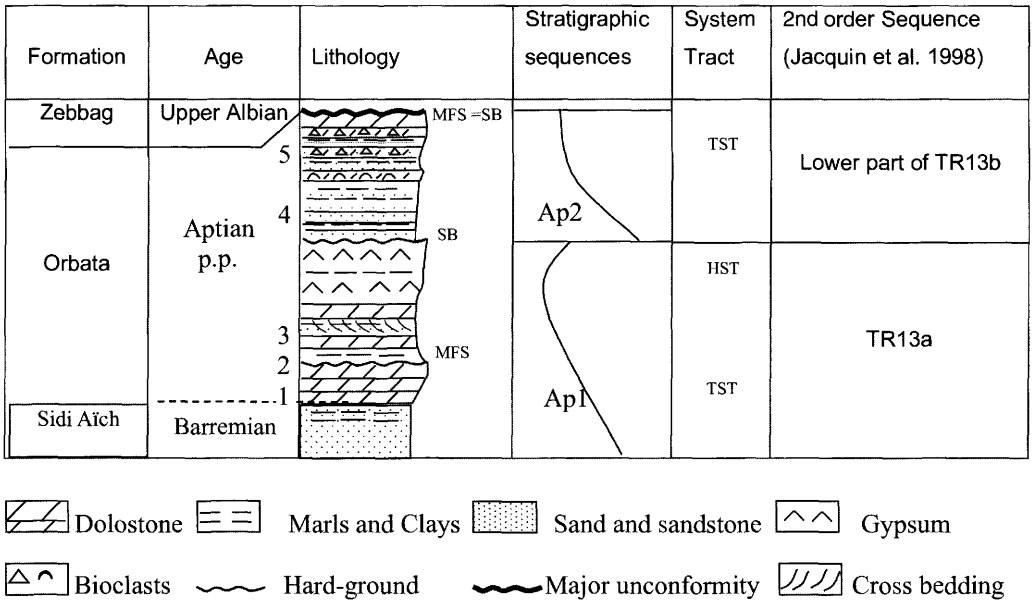

Fig. 13. Comparison of the Aptian stratigraphic sequences of Central Tunisia with the second-order cycle in the North Atlantic and Western Europe. TST, Transgressive system tract; HST, highstand system tract; MFS, maximum flooding surface; SB, sequence boundary.

and at Jebel Kebar (Fig. 12). On the other hand, the Boulahneche section is believed to have been deposited on a halokinetically induced high (Marie *et al.* 1984). The great thickness of the Aptian succession at Jebel Chemsi indicates a subsiding zone situated between the Chemsi and the Orbata faults (Fig. 12).

The east–west profile (Fig. 15) shows lesser thicknesses at Jebel Kebar and Jebel El Hafey, which can be explained by the presence of palaeohighs grading laterally to a basinal area located in the western part of Central Tunisia, where deposition of thick series occurred. This variation is controlled by the north–south-trending Sidi Ali Ben Aoun fault and by the flexural subsidence of the Sidi Aïch area (Chekma 1996).

Also, the isopach map (Fig. 16) shows three blocks characterized by varying subsidence gradients: from south to north, we can distinguish the following.

(1) The block of Fatnassa (North Chott Chain) forms a high zone, slightly tilted towards the west. This block is limited to the north by an east–west fault of the North Chott Chain and to the west (Jebel Fatnassa) by a NW–SE fault. This resistant block was affected during the Jurassic by diapirism of the Triassic salt (Zargouni 1985).

(2) The Gafsa area corresponds to a relatively subsiding zone centred in the Gafsa Basin, where we can distinguish a depocentre located at the Chemsi sector, resulting from a synsedimentary extensional movement of the Gafsa fault (Chaabani *et al.* 1992). This fault, characterized by a NW–SE trend in the western part and an east–west trend in the eastern part of the study area, limits the Gafsa Basin to the north.

(3) The Kasserine area can be subdivided into two sub-blocks. The eastern sub-block corresponds to Jebel Kebar and Jebel El Hafey. The Aptian is represented only by the first unit (Early Aptian). The maximum recorded thickness is about 50 m at Jebel Kebar and the minimum is recorded in the eastern part of Jebel Kebar (0 m). It is limited to the west by the north–south-trending Sidi Ali Ben Aoun fault, to the east by the 'North–South Axis fault' and to the north by the east–west Kasserine fault. In the western sub-block, the Aptian series increases progressively from the eastern to the western part of the area (Fig. 15); this variation suggests a system of tilted blocks trending SW. This phenomenon may be explained by the presence of the Sidi Ali Ben Aoun fault and the flexure of Sidi Aïch. The proposed model is slightly different from that of Bismuth *et al.* (1981), which was adapted by Chekma (1996), and Ben Youssef (1998) and suggests a slope towards the south. Moreover, the same model has been hypothesized by Herket (2004) in eastern Algeria, the structure of which forms the continuation of Central Tunisia.

Towards the north, the Orbata Formation carbonate passes laterally into the Serj facies (Tandia 2000) characterized by the presence of bioherms,

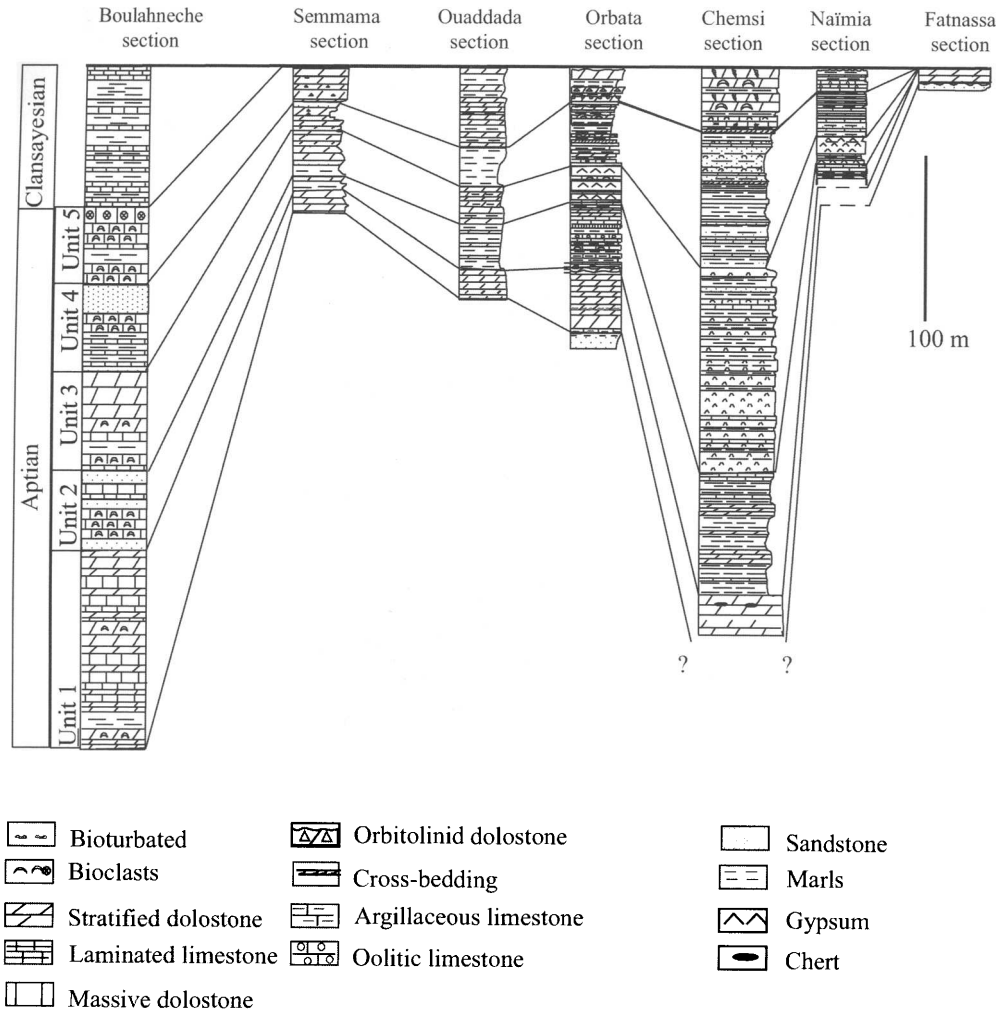

Fig. 14. North–south correlation and sedimentological interpretation of the Orbata Formation of Central Tunisia.

which developed on isolated highlands, possibly as a result of Triassic salt vertical movements (Marie *et al.* 1984).

An Aptian interpretative configuration of Central Tunisia is shown in Figure 17, to explain the observed north–south variation.

Conclusions

Our sedimentological and palaeontological studies of the Orbata Formation of Central Tunisia lead us to define two transgressive–regressive sequences. These depositional sequences can be identified, mapped and correlated throughout the region. They are interpreted as resulting from a combination of extensional tectonics, variations in siliciclastic sediment supply and dispersed systems, and eustatics. These depositional sequences, integrated with biostratigraphical data, have the potential to be correlated throughout Central Tunisia and provide a framework for a regional and possible global correlation of the Aptian series.

The thickness variations and the main tectonic elements support the interpretation that the Aptian sedimentation was controlled by north–south, NW–SW and east–west faults (similar to the Jurassic inherited 'tilted blocks') (Zargouni 1985), as well as by eustatic events.

Based on the above sequence descriptions, a depositional model history for the Orbata Formation

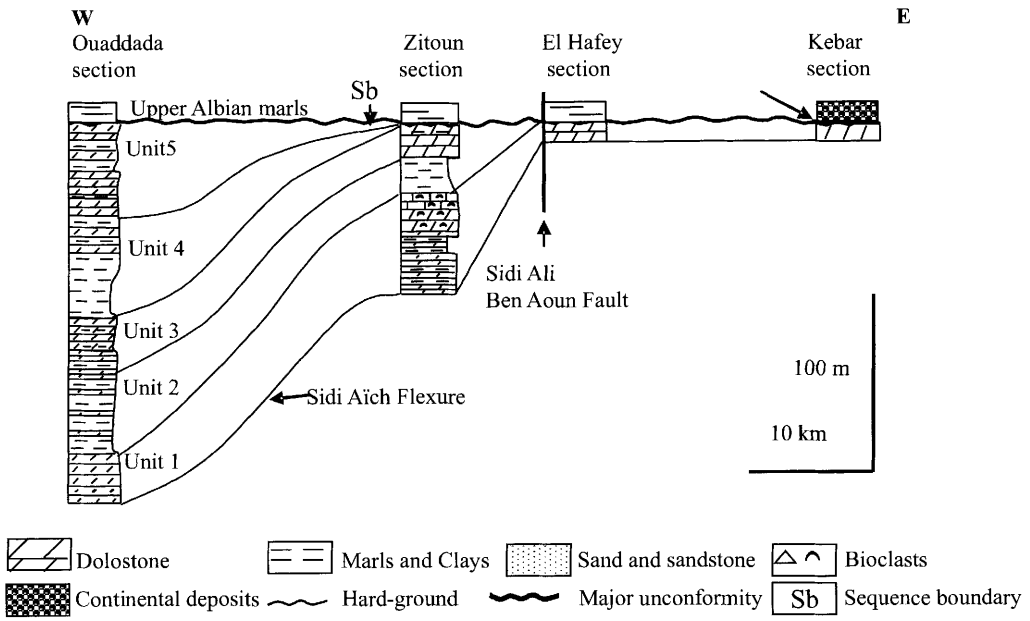

Fig. 15. East–west correlation profile of the Aptian series in the northern sub-block of Central Tunisia.

of Central Tunisia is proposed (Fig. 17). This model permits us to summarize the Aptian platform history as follows.

Tectonic activity initiated differential subsidence or local uplift during a high sea level, which led to partial platform exposure (Jebel Fatnassa, Jebel Kebar, etc.). This highly structured Central Tunisian platform was marked by isolated barrier islands. These latter were drowned by a major transgression that occurred in many areas of the Tethyan region, particularly in the Sahara Platform, in west

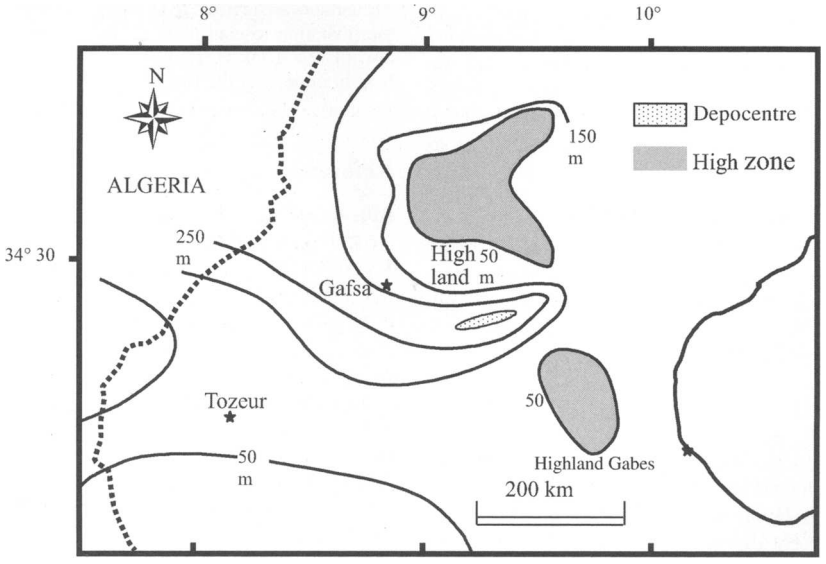

Fig. 16. Isopach map of Central Tunisian Aptian sedimentation.

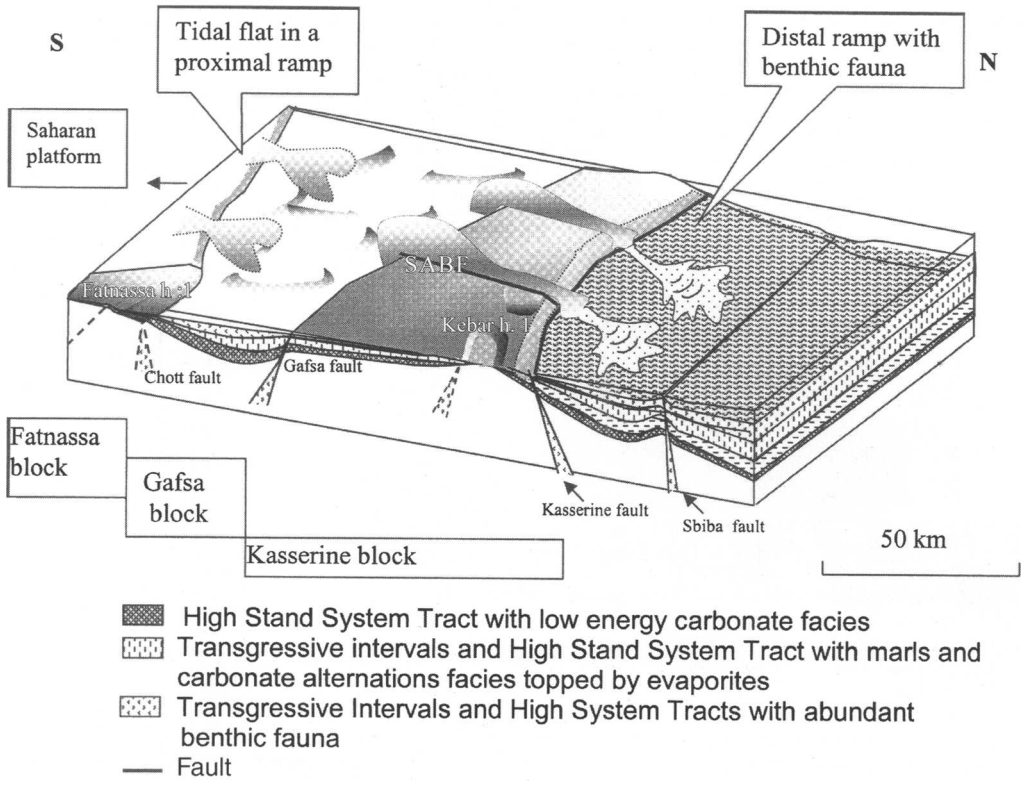

Fig. 17. Block diagram representing a sedimentary model of the Central Tunisian platform during the Aptian. h.l., highland; SABF, Sidi Ali Ben Aoun fault.

Africa (Tarfaya) (Choubert *et al.* 1971; Burollet & Busson 1980), in the Arabian peninsula and in many other areas of the Peritethys carbonate platform (Jacquin & de Graciansky 1998; Jacquin *et al.* 1998).

Basin filling occurred by aggradational paraseq-uences and the development of a lagoonal environment. The boundary of this sequence is not a major erosional unconformity. It corresponds to a sharp change in the environment.

A new rise of sea level was probably associated with a climatic change, creating a new detritic flux.

As a reponse to the arid climate, the detrital input gradually disappeared and was progressively replaced by predominantly high-energy carbonates.

A sedimentary break corresponding to a rapid sea-level fall followed. A hardground occurs at the top of sequence Ap2, where it presents a marked stratigraphic gap extending from the Aptian to the Middle Albian.

A new sea-level rise, more marked than the Aptian one, finally corresponds to the development of the Late Albian (Vraconian) carbonate platform, which covered a wide region in Central Tunisia.

The authors are grateful to G. Moratti and A. Chalouan for the invitation to contribute to this volume. They would also like to thank H. Hemissi and A. Mabrouk for their help in improving the English.

References

ABDALLAH, H. 1987. *Le Crétacé supérieur de la chaîne nord des Chotts (Sud tunisien)*. Thèse Doctorat ès-Sciences Géologique, Université de Bourgogne.

ARNOULD SAGET, S. 1952. Sur l'existence de couches à *Knemiceras* en Tunisie méridionale. *XIX Congrès de Géologie International, Alger*, **XXI**, 269–275.

BARNABA, P. F. 1965. Studio stratigrafico sul Cretaceo della Tunisia Meridionale. *Rivista Italiana di Paleontologia e Statigrafia*, **71**(3), 883–912.

BÉDIR, M. 1995. *Mécanismes géophysiques des bassins associés aux couloirs de coulissement de la marge atlasique de la Tunisie*. Thèse d'Etat, Université Tunis II.

BEN FERJANI, A., BUROLLET, P. F. & MEJRI, F. (eds) 1990. *Petroleum Geology of Tunisia*. Entreprise Tunisienne d'Activités Pétrolières, Tunis.

BEN YOUSSEF, M. 1999. *Stratigraphie génétique du Crétacé de Tunisie. Micropaléontologie, stratigraphie séquentielle et géodynamique des bassins de la marge sud et péritéthysienne*. Thèse Doctorat d'Etat, Université de Tunis El Manar.

BEN YOUSSEF, M. & PEYBERNES, B. 1986. Données micropaléontologiques et biostratigraphiqes nouvelles sur le Crétacé inférieur marin du Sud tunisien. *Journal of Earth Sciences*, **5**(3), 217–231.

BEN YOUSSEF, M., BIELY, A., KAMOUN, Y. & ZOUARI, H. 1985*a*. L'Albien moyen et supérieur à *Knemiceras* forme la base de la grande transgression crétacée au Tébaga de Médenine. *Comptes Rendus Sommaire, Académie des Sciences*, **300**(II), 19.

BEN YOUSSEF, M., BIELY, A. & MEMMI, L. 1985*b*. La formation Orbata (Aptien) en Tunisie méridionale, précisions biostratigraphiques nouvelles. *Notes du Service Géologique de Tunisie*, **51**, 16.

BISMUTH, H., BOLTENHAGEN, C., DONZE, P., LE FEVRE, J. & SAINT MARC, P. 1981. Le Crétacé moyen et supérieur du jebel Semmama (Tunisie du centre–nord); micropaléontologie et évolution sédimentologique. *Bulletin des Centres de Recherches Exploration–Production Elf–Aquitaine*, **5**, 193–267.

BOLTENHAGEN, C. 1981. Paléogéographie du Crétacé moyen de la Tunisie centrale. *Actes du 1er Congrès National des Sciences de la Terre, Tunis*, **II**, 97–114.

BOUKADI, N. & BÉDIR, M. 1996. L'halocinèse en Tunisie. Contexte tectonique et chronologique des évènements. *Comptes Rendus de l'Académie des Sciences*, **322**(IIa), 587–594.

BROMLEY, R. G. 1975. Trace fossils and omission surfaces. *In*: FREY, R. W. (ed.) *The Study of Trace Fossils*. Springer, New York, 399–428.

BUROLLET, P. F. 1956. Contribution à l'étude stratigraphique de la Tunisie centrale. *Annale Mine Géologie, Tunis*, **18**, 345.

BUROLLET, P. F. & BUSSON, G. 1980. Plateforme saharienne et mésogée au cours du Crétacé. *Notes et Mémoires, Total Compagnie Française de Pétrole*, **18**, 17–26.

BUSSON, G., DUFAURE, P. & FOURY, G. 1966. Nouvelles observations sur l'âge de la transgression crétacée du Tébaga de Médenine et du Sahara tunisien. *Comptes Rendus Sommaire, Séances de la Société Géologique de France*, **3**, 135–136.

CASTANY, G. 1951. Etude géologique de l'Atlas tunisien oriental. *Annales des Mines et de la Géologie, Tunisie*, **8**, 595.

CHAABANI, F. 1995. *Dynamique de la partie orientale du bassin de Gafsa au Crétacé et au Paléogène: étude minéralogique et géochimique de la série phosphatée éocène (Tunisie méridionale)*. Thèse d'Etat, Université de Tunis el Manar.

CHAABANI, F., GARGOURI RAZGALLAH, S. & TURKI, M. M. 1992. L'Aptien de l'est du sillon de Gafsa (Tunisie-centro-méridionale). Etude biostratigraphique et sédimentologique. *Notes du Service Géologique de Tunisie*, **59**, 43–57.

CHEKMA, H. 1996. *Etude stratigraphique, sédimentologique et tectonique de la région de Bir El Hafey–Sidi Ali Ben Aoun (Tunisie centrale)*. Thèse (Doctoral), Université de Tunis El Manar.

CHEKMA, H., GARGOURI-RAZGALLAH, H., DONZE, P. & MEMMI, L. 1991. Le Crétacé inférieur de la région de Bir El Hafey: précision chronostratigraphique sur les formations Bouheddma, Sidi Aïch, Orbata et Zebbag. *Notes du Service Géologique de Tunisie*, **56**.

CHOUBERT, G., FORE-MURET, A. & HOTTINGER, L. 1971. La série stratigraphique de Tarfaya (Maroc méridional) et le problème de la naissance de l'Océan Atlantique. *Notes du Service Géologique de Maroc*, **31**(237), 29–40.

CLARI, P. A., DELA PIERRE, F. & MARTIRE, L. 1995. Discontinuities in carbonate successions: identification, interpretation and classification of some Italian examples. *Sedimentary Geology*, **100**, 97–121.

COLLINSON, J. D. & THOMPSON, D. B. (eds) 1982. *Sedimentary Structures*. George Allen & Unwin, London.

HERKET, M. 2004. Contrôle eustatique et paléogéographique de la sédimentation du Crétacé supérieur du Bassin des Aurès (Algérie). *Bulletin de la Société Géologique de France*, **1756**(3), 273–288.

HLAIEM, A. 1998. *Etude géophysique et géologique des bassins et des chaînes de Tunisie centrale et méridionale durant le Mésozoïque et le Cénozoïque. Evolution structurale, modélisation géothermie et implications pétrolières*. Thèse Doctorat Université. Pierre & Marie Curie Paris VI.

JACQUIN, T. & DE GRACIANSKY, P. C. 1998. Major transgressive/regressive cycles. The stratigraphic signature of European Basins. *In*: DE GRACIANSKY, P. C., HARDENBOL, J., JACQUIN, T. & VAIL, P. R. (eds) *Mesozoic and Cenozoic Sequence Stratigraphy of European Basins*. SEPM Special Publications, **60**, 15–29.

JACQUIN, T., RUSCIADELLI, G., AMEDRO, F., DE GRACIANSKY, P. C. & MAGNIEZ-JANNIN, F. 1998. The North Atlantic cycles: an overview of second order transgressive–regressive cycles in the Lower Cretaceous of Western Europe. *In*: DE GRACIANSKY, P. C., HARDENBOL, J., JACQUIN, T. & VAIL, P. R. (eds) *Mesozoic and Cenozoic Sequence Stratigraphy of European Basins*. SEPM Special Publications, **60**, 397–409.

KHESSIBI, M. 1978. Observations géologiques dans le jebel Kebar (mouvements tectoniques antécénomaniens). *Notes du Service Géologique de Tunisie*, **42**, 21–27.

KHESSIBI, M. & KHARBACHI, S. 1990. Etude comparative des grès 'Albo-Aptien' de Foum El Argoub, de Bir Oum Ali et de Chenini (abstract) *2ème Congrés Nationale des Sciences de la Terre de Tunisie*. Société des Sciences de la Terre de Tunisie.

MARIE, J., TROUVE, P., DESFORGES, G. & DUFAURE, P. 1984. Nouveaux éléments de paléogéographie du Crétacé de Tunis. *Notes et Mémoires TOTAL-CFP, Paris*, **19**, 37.

M'RABET, A. 1987. Stratigraphie, sédimentation et diagenèse carbonatée des séries du Crétacé inférieur de Tunisie. *Annales des Mines et de la Géologie, Tunisie*, **30**, 412.

PERVINQUIÈRE, L. 1903. *Etude géologique de la Tunisie centrale*. Thèse Doctorat és Sciences Naturelles, Université de Paris.

TANDIA, S. 2000. *Etude lithostratigraphique et sédimentologique des séries du Crétacé inférieur (Barrémien–Albien) de la Tunisie centro-septentrionale (régions du Krib et de Tajerouine)*. Thèse (Doctoral), Université de Tunis El Manar.

TLATLI, M. 1980. *Etudes des calcaires de l'Albo-Aptien des Djebels Serdj et Bellouta (Tunisie Centrale)*. Thèse 3ème cycle. Université de Provence, Marseille.

ZARGOUNI, F. 1985. *Tectonique de l'Atlas méridional de Tunisie, évolution géodynamique et cinématique des structures de cisaillement*. Thèse Doctorat ès Sciences, Université Louis Pasteur, Institut de Géologie, Strasbourg.

ZARGOUNI, F., RABIA, M. Ch. & ABBÈS, Ch. 1985. Rôle des couloirs de cisaillement de Gafsa et de Négrine–Tozeur dans la structuration du faisceau des plis des chotts, éléments de l'accident sud-atlasique. *Comptes Rendus de l'Academie des Sciences, Série II* **301**(11), 831–834.

ZOUARI, H., TURKI, M. M., DELTEI, J. & STEPHAN, J. F. 1999. Tectonique transtensive de la paléomarge tunisienne au cours de l'Aptian–Campanian. *Bulletin de la Société Géologique de France*, **170**, 295–301.

Synsedimentary tectonics of the Triassic Carbonate Formation of the Oujda Mountains (Eastern Meseta, Morocco): geodynamic implications

M. OUJIDI[1], O. AZZOUZ[1] & S. ELMI[2]

[1]*Faculty of Sciences, Laboratory of Geodynamics, LGVBS Oujda, Morocco (e-mail: oujidi@yahoo.com)*

[2]*CNRS UMR 5125, Université de Lyon 1, France*

Abstract: The Ladinian–Carnian tectonic instability is well recorded within the Carbonate Formation of the Oujda Mountains (Eastern Meseta, Morocco). It was induced by a bidirectional extensional palaeo-state of stress (ENE–WSW and NNW–SSE) resulting in the development of the Oujda Mountains Triassic basins that open towards the Western Tethyan domain. This extensional event correlates with an early episode of Tethyan rifting, which is coeval with the Ladinian–Carnian extensional episode of the Alpine domain. The structural development of these basins was controlled by an extensional reactivation of Hercynian faults, with N70°E and N160°E fault trends predominating over the N35°E and N120°E ones. Therefore, the Ladinian–Carnian palaeo-state of stress of the Oujda Mountains is fundamentally different from that of the Triassic–Liassic basins to the west, in Central Morocco and the Atlas belts, where the N45°E-trending, sinistral fault trend predominates over the N70°E and N90°E fault trends.

The aim of this paper is to understand the dynamic processes of the initial Mesozoic dislocation of the northwestern side of Gondwana and the first stage of continental rifting of the Central Atlantic. Following the Variscan orogeny, the break-up of Gondwana occurred in the Late Carboniferous (Stampfli *et al.* 1991). Along the northern African–Arabian plate margin, several rift basins were active during Permian and Triassic time (Fig. 1); this rifting propagated westwards from the NE Arabian margin to Morocco (Guiraud 1998).

The Triassic succession of the Oujda Mountains, cropping out in the NE extremity of the Moroccan autochthonous domain, because of its palaeogeographical location in the SW margin of the Maghrebian Tethys (Salvan 1984; Marcoux *et al.* 1993), is of great significance for studying the geodynamic control of the Triassic rifting and the transition to Liassic structuring.

The Oujda Mountains (Fig. 2a and d) form a narrow relief trending ENE–WSW (Fig. 2a and b). They are bounded to the north by the Angad plain and the Béni Snassen Mountains, and southwards by the High Plateaux. Eastwards, they extend into Algeria, through the mountains of Rhar Roubane and Tlemcen (Lucas 1942; Elmi 1973, 1983).

The Triassic series lie unconformably over the deformed Palaeozoic basement, which is composed mainly of Ordovician–Silurian sandstones and schist, and weathered Visean granodiorites. According to Rakus (1979), the complete Triassic stratigraphic succession includes (Fig. 2c): (1) Lower Red Beds; (2) Lower Dolerites; (3) Middle Carbonate Formation; (4) Upper Dolerites; (5) Upper Red Beds. A silicified stromatholitic level locally marks the base of the Upper Red Beds (Oujidi & Elmi 1992). The Middle Carbonate Formation represents a stratigraphic reference level on a regional scale, and was slightly affected by the Alpine orogeny. From >3 to 13 m in thickness, this formation is made up of dolomite and limestone beds alternating with marly levels and dolomitic micro-beds (Oujidi 1994). These levels are often well laminated and bedded, which allows delineation of sedimentary and tectonic phenomena, particularly slumps and lateral changes in facies and thickness. Sedimentological analysis shows that, depending on the area, the whole of this formation is composed of two or three coastal shallowing-upward sequences (Oujidi 1994, 2000).

The Carbonate Formation has strong palaeogeographical implications, as it records the first Tethyan marine onlap of the northeastern margin of Morocco during the late Ladinian–early Carnian (Crasquin-Soleau *et al.* 1997). Moreover, it shows many synsedimentary deformations that allow us to understand the synsedimentary tectonics associated with the evolution of the Triassic basins, and consequently the tectonic pattern related to this Ladinian–Carnian rifting episode (Oujidi & Elmi 2000).

A previous study (Oujidi & Elmi 2000) based on the analysis of isopach maps of the Triassic

From: MORATTI, G. & CHALOUAN, A. (eds) 2006. *Tectonics of the Western Mediterranean and North Africa.* Geological Society, London, Special Publications, **262**, 75–85.
0305-8719/06/$15.00

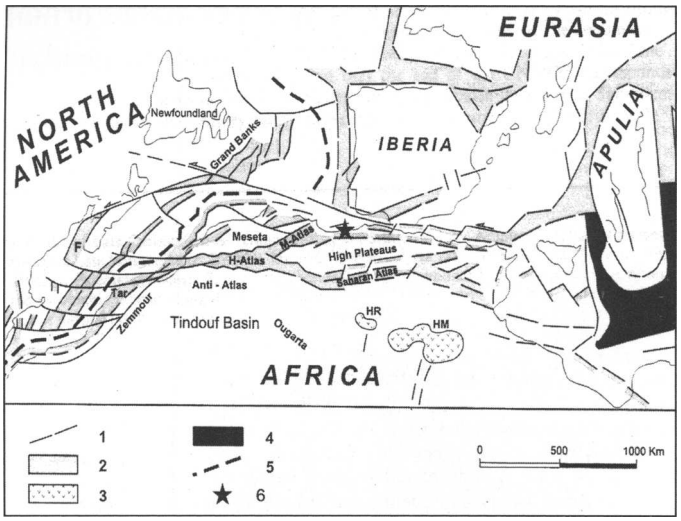

Fig. 1. Schematic map of Triassic rifting along the northwestern African margin and adjacent areas, for Late Norian time (*c.* 212 Ma). Modified from Marcoux *et al.* (1993) and Guiraud (1998). 1, Major fault; 2, rift; 3, northern Algerian Sahara effusive province (trachybasalts, andesites); 4, thinned continental crust, possibly locally oceanized (East Mediterranean Basin); 5, future plate limit; 6, palaeogeographic location of the study area; F, Fundy Basin; HM, Hassi Messaoud; HR, Hassi R'Mel; Tar, Tarfaya Basin.

successions of the Oujda Mountains, pointed out the importance of the N70°E and N160°E regional structures during the structural partitioning of this region into small horsts and grabens accompanied by tholeiitic basalt flows. This structuring is in accordance with an extensional tectonic event similar to that described in the external Dorsale (the Carnian–Hettangian sequences of the Moroccan Internal Rif Domain, El Kadiri & Faouzi 1996), the Alpine area (Mégard-Galli & Faure 1988; Tricart *et al.* 1988; Lemoine *et al.* 1989) for the Ladinian–Carnian, and in the Atlas belts (Laville 1981; Laville & Piqué 1993; Piqué & Laville 1993; Piqué *et al.* 1998; Oujidi *et al.* 2000).

To contribute to understanding of the Triassic tectonic framework, we re-examine the Carbonate Formation in this study, using a new approach based on both the microtectonic analysis of the synsedimentary faults and the description of the induced deformation structures. Three key sites were selected on the basis of the isopach map of the Carbonate Formation (Oujidi & Elmi 2000). They are located in distinct geological settings related to the main N70°E and N160°E regional faults (Fig. 3): the Oum Lahsene site is located at the junction between two palaeogeographical borders oriented N160°E and N70°E; the Guenfouda site is located in the central part of the Oujda Triassic sub-basins, where a horst exists, controlled by subequatorial faults; the Jbel El Hamra site is located in the northern border of the Oujda Mountains, where Triassic basins are oriented N70°E.

We attempt to determine for each site the pattern of the deformations and the related stress field, and compare the regional pattern with other examples of extensional synrift structures described in the Western Mediterranean Alpine domain and intramontane basins of the Atlas belt.

Synsedimentary structures

The Carbonate Formation exhibits an abundance of breccias, slumps, normal faults and major thickness changes. These gravity-induced deformations are often coupled with extensional normal faults sealed at different levels of the formation, and appear in partially lithified layers. They reveal significant tectonic instability related to an extension–rotation pattern dynamic field associated with the development of the Triassic basins.

Gliding phenomena

The tectonic instability in the Carbonate Formation is associated with the development of gravity-induced deformations such as decimetre- to metre-scale gliding phenomena, which may affect the whole Carbonate Formation. In the majority of cases, slump structures occur in the vicinity of low-dip normal faults, generally corresponding to an exaggeration of listric faults (Fig. 4a). These phenomena occur even on gentle slopes and were preferentially triggered along soft and plastic argillaceous layers. The

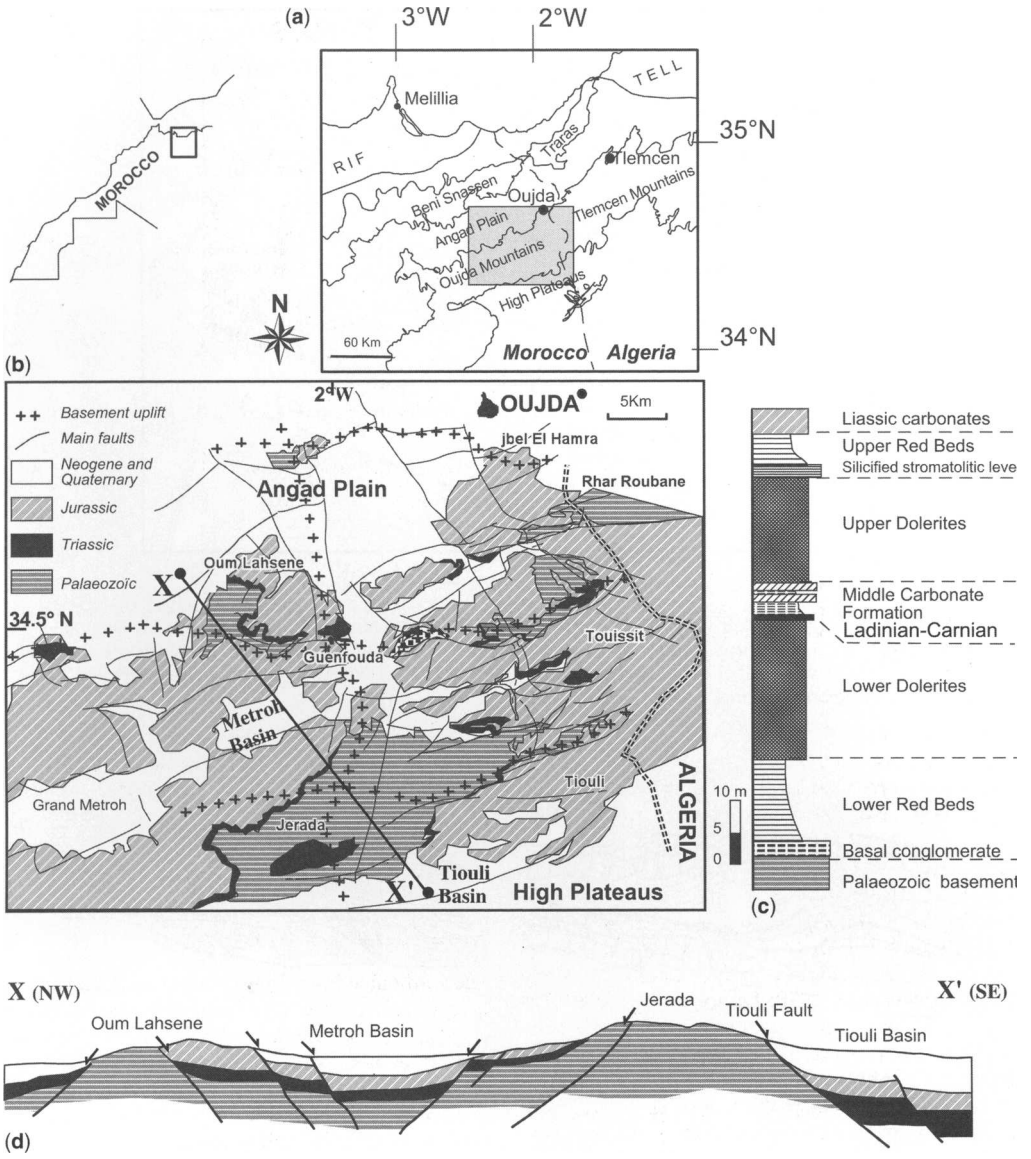

Fig. 2. (**a**) Location of the study area. (**b**) Structural sketch of the Oujda Mountains (after Valin & Rakus 1979). (**c**) Stratigraphic position of the Middle Carbonate Formation in the Triassic and early Liassic series of the Oujda Mountains. (**d**) Schematic structural section across the Oujda Mountains.

stratigraphic analysis illustrates several generations of gliding structures, which are confined to the relatively soft levels (clayey and marly beds), where they are often accompanied by breccias, slumps, microfolds and reverse faults.

Breccias

Breccias are mainly known in the lower levels of the Carbonate Formation. They are usually monogenic and cemented by an abundant beige to chocolate brown matrix of crystallized dolomite. The breccias are made of centimetre- to decimetre-sized fragments and are structureless. They result from a differential diagenetic lithification of the carbonate layer. At the water–sediment interface, carbonate stromatolitic facies were indurated by earliest dolomitization (Purser 1980). The relatively competent strata have undergone complex fracturing, generating joint patterns (Tricart *et al.* 1986).

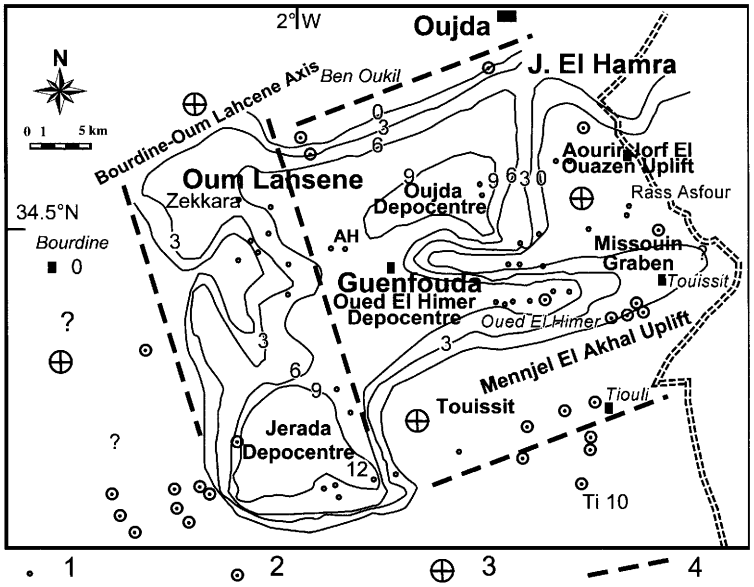

Fig. 3. Isopach map of the Middle Carbonate Formation (modified from Oujidi & Elmi 2000). Key: 1, outcrop sections; 2, boreholes; 3, Palaeozoic basement permanently emerged; 4, main structural axis. The three key sites are: Jbel El Hamra; AH, Genfouda (Jbel Ahaifoune), and Oum Lahsene. Ti 10, Tiouli 10 borehole; contours labelled 3, 6, 9 and 12 indicate thickness in metres.

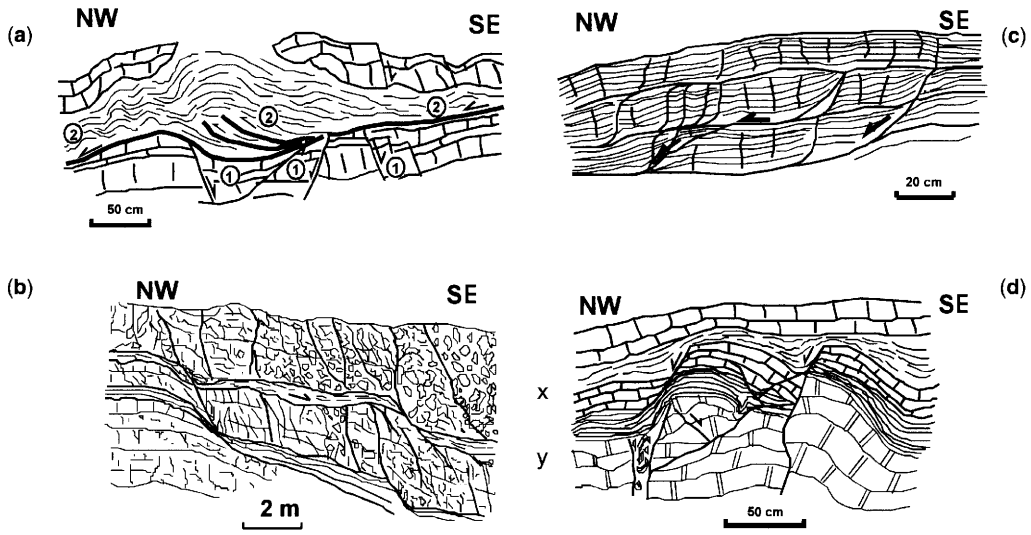

Fig. 4. Examples of instability associated with synsedimentary normal faults (Oum Lahsene site). (**a**) Flat differential slip locally shown by some micro-slumps. (1) First generation set of faults, allowing vertical dislocation; (2) second generation set of faults, allowing gliding and horizontal displacement. (**b**) Example of open extension joints in stromatolitic beds engendering an incipient brecciation. (**c**) Differential brecciation affecting a set of beds (X). It is associated with normal listric faults and bed-on-bed slips triggered along marly levels (Y). (**d**) Synsedimentary torsion of the layers and the fault planes by the subsequent slip effects.

Differential gliding of the hardened stromatolitic strata over the marly interbeds produced a joint network that evolved progressively into open faults, subsequently filled by non-lithified carbonate muds (Fig. 4b); the isolated prisms are more or less wrapped within an abundant dolomicritic matrix, resulting in intraformational breccias (Fig. 4c) that are sealed by the overlying deposits.

Slump structures and reverse faults

Centimetre- to metre-sized slump structures are slightly developed and limited to simple open undulations, rarely showing overturned limbs. They are mainly related to the lithological and rheological features of the beds, which are coherent enough to form slumps. In addition, these structures are always progressively sealed by the overlying levels of the Carbonate Formation (Fig. 4d).

The induced compressive structures consist of reverse faults often accompanied by open undulations and disharmonic folds (Fig. 4a) and always sealed by the overlying levels. A detailed analysis of these structures shows that they are only local disturbances, which could also be related to the extensional tectonic regime. Cascade gravitational gliding occurs, often along irregular surfaces that can form obstacles, which stop the downwards mass displacement (Fig. 4a and d). Under gravity effects, compressive structures can be developed locally.

These gliding phenomena develop also at a regional scale, where they affect the whole formation. Indeed, tectonic analysis shows that the basal levels of the Carbonate Formation are often reactivated as normal faults, allowing slip and horizontal displacement of the whole formation. Furthermore, there is a good coincidence between the tectonics of the Carbonate Formation and that of the two sets of normal faults previously described (N70°E and N160°E).

Synsedimentary normal faults

At the bed scale, lateral thickness changes are a very common feature, and are triggered by synsedimentary normal faults and related strata tilting. The deposits sealing these deformations may gradually fill the topographic irregularities created by the tilting of the fault blocks as shown in Figure 4d. Some thickness changes are abrupt and frequently occur together with intraformational breccias (Fig. 4c).

Thickness changes also appear at the outcrop scale, where successive cross-sections illustrate thickening or disappearance of some levels of the Carbonate Formation (Oujidi 1994). This phenomenon can also be detected at the regional scale, as clearly illustrated in the isopach map of the Carbonate Formation (Fig. 2). This phenomenon reveals the unstable conditions that have controlled the sedimentary regime within the Triassic basins, which often developed as discontinuous, shallow-water depocentres.

The synsedimentary normal faults are often listric and are expressed in three dimensions by relaying planes. Depending on the heterogeneity and the mechanical anisotropy of the carbonate material, the fault planes bend and preferentially follow the plastic argillaceous and marly interbeds. They are generally accompanied by rotation of the downthrown blocks (Fig. 5b) or by antithetic faults (Fig. 5c). The fault sets are radial or conjugate, dipping mainly to the north (ranging from NE to NW), and resulting in horst and graben structures of several metres to a decametre in size. (Fig. 5a).

Tectonic analysis allows us to describe several sets of normal faults of variable throw that extend from one area to another, probably related to the main regional faults that controlled the opening of the Triassic basins (Oujidi 1994; Oujidi & Elmi 2000). The main results obtained from the three selected sites are presented below.

Oum Lahsene site

NE–SW (N40–55°E) and WNW–ESE (N110–125°E) fault systems are recognizable at this site. However, these faults appear to be coeval, as they are interrupted in a criss-cross geometry (Fig. 5d) and are sealed by the upper levels of the same formation. Detailed observation of slickensides on some fault planes displays a feeble sinistral and dextral strike-slip component for the NE–SW and WNW–ESE faults, respectively (pitch 70°–90°, Fig. 6a1). Furthermore, a minor third NNW–SSE (N160°E)- directed fault set shows centimetre- to decimetre-scale normal displacements associated with abundant fracture joints parallel to the main fault strike.

Guenfouda site

As at the Oum Lahsene site, we have observed normal fault systems trending NE–SW (N35–55°E) and WNW–ESE (N110–120°E). They display respectively sinistral and dextral components. Furthermore, the stereogram plot (Fig. 6b1) shows another fault set with a NNW–SSE (N160°E) trend. These faults are often listric and associated with other synthetic faults with throws of decimetres to several metres, similar to those observed at the Oum Lahsene site.

Jbel El Hamra site

In contrast to the other sites, the Jbel El Hamra site gives evidence that the extensional tectonics was

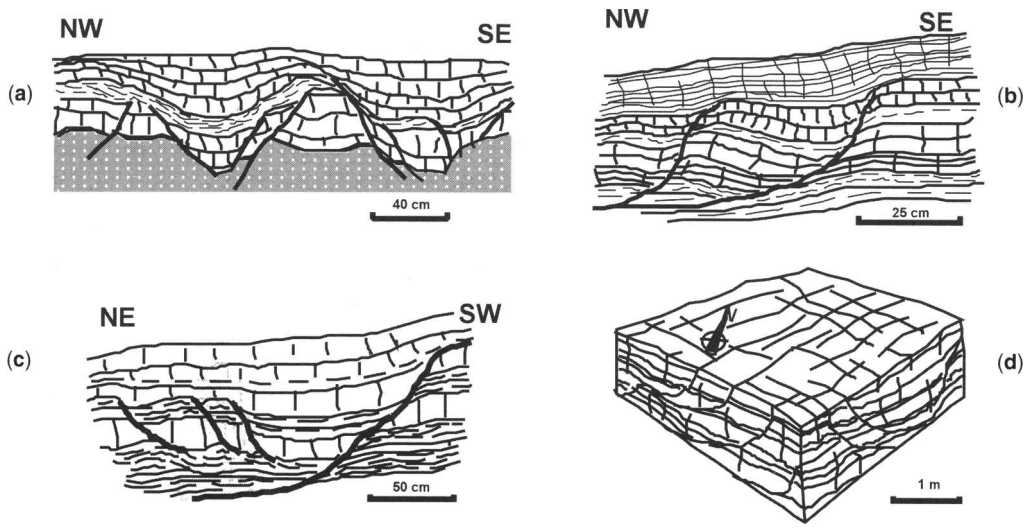

Fig. 5. Examples of synsedimentary normal faults in the Middle Carbonate Formation: (**a**) Jbel Hamra site; (**b**)–(**d**) Guenfouda site. (a) Conjugate faults. (b) Rotation against slope associated with listric step faults. (c) Synthetic and antithetic listric faults. (d) Two families of listric subperpendicular faults, which cross-cut each other within the same bed.

mainly dominated by the ENE–WSW (N70°E)-trending normal faults (Fig. 6c1), which display minor sinistral or dextral components. These faults often have a throw of decimetres to several metres, with the fault plane facing north. Also, relatively rare N20°E and N120°E normal faults with low throw are present (Fig. 6c1). Together, these faults have resulted in a complex structure of asymmetric horsts and grabens, testifying to a general northward downthrow of the basin.

Tectonic analysis

At the Oum Lahsene and Guenfouda sites, the analytical computation (using the software of Allmendinger *et al.* 1989–1994) shows that these normal fault sets are related to an extensional state of stress where σ_3 is oriented ENE–WSW with an extensional component, σ_2, oriented NNW–SSE (Fig. 6a2 and b2). At Jbel El Hamra the analytical computation shows that the faults are related to an extensional state of stress in which σ_3 is oriented NNW–SSE, with a minor extensional component σ_2 trending ENE–WSW (Fig. 6c2).

This difference is due to the location of the study sites relative to the regional N160°E and N70°E faults, which control the geometry of the Triassic basins as shown in the Carbonate Formation isopach map (Fig. 3, Oujidi & Elmi 2000). Thus, at the Guenfouda and Oum Lahsene sites, the tectonic instability is mainly controlled by the N160°E faults whereas at Jbel El Hamra, located on the northern edge of the Oujda Mountains, it is controlled by the N70°E faults.

The minor faults of Oum Lahsene and Guenfouda are preferentially oriented with N35–55°E and N100–120°E trends that do not correspond to the trends of faults determining the basins' depocentres (N70°E and N160°E, Oujidi & Elmi 2000). Some of the minor studied faults with listric geometry do not seem to continue at depth, and therefore may be related to the upper part of landslides, as proposed in Figure 8, below. Hancock (1985) showed good examples of the development of orthogonal tensional joint sets by local stress changes in a general stress field. These models, although relating to joints and not to faults, may be considered for the study area. In fact, at the same place and time it is not possible to have two simultaneous trends of extension, but they may change with time and be different in neighbouring regions.

Discussion

The Carbonate Formation constitutes a useful lithostratigraphic key stratum, as it corresponds to a competent bar, interlayered between two friable basaltic and clayey formations. Consequently, this formation recorded several Triassic minor tectonic features. The synsedimentary tectonic structures in the Carbonate Formation testify to an important instability induced by an early episode of Tethyan rifting during Ladinian–Carnian time (Oujidi & Elmi 2000).

The tectonic analysis reveals several sets of synsedimentary faults, whose importance varies from one site to another. Their activations are related to

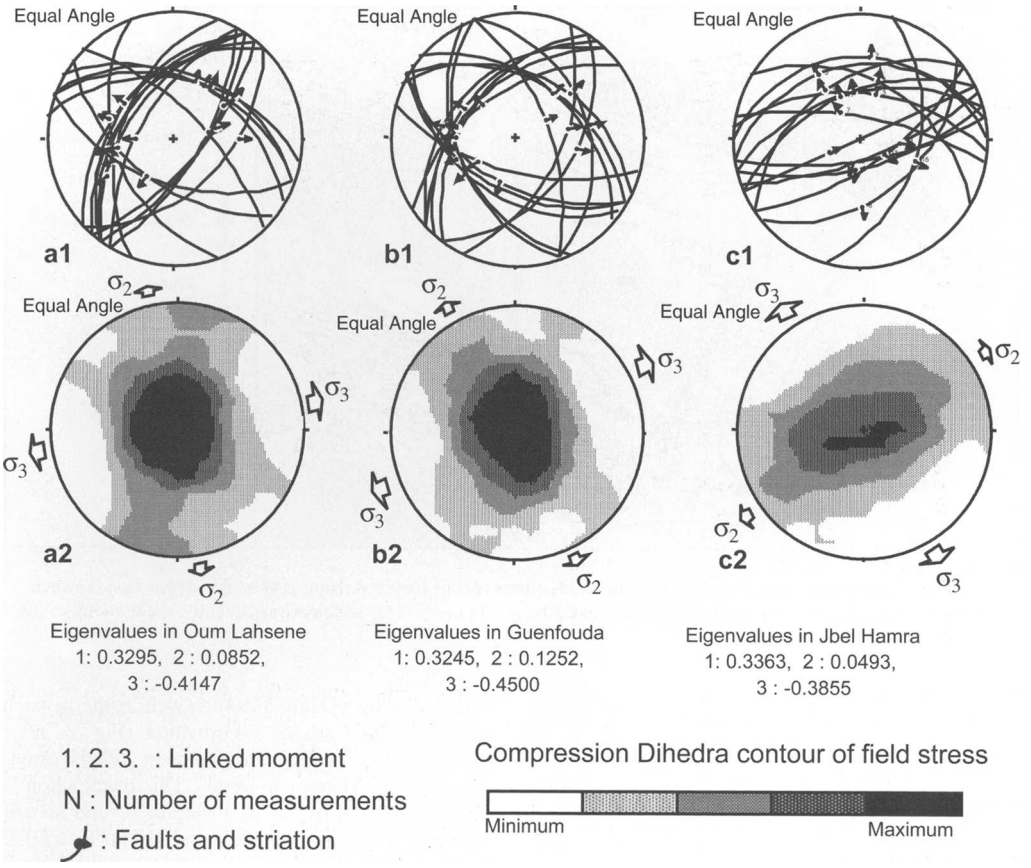

Fig. 6. Lower hemisphere stereographic representation of the attitudes of the synsedimentary faults (**a1**), (**b1**) and (**c1**), and of the distribution of the extensional stress fields (**a2**), (**b2**) and (**c2**) at the Oum Lahsene, Guenfouda and Jbel El Hamra sites, respectively. (Drawn using the Faultkin 3.7 software, Allmendinger *et al.* 1989–1994).

a bidirectional extensional tectonic regime acting alternatively in different places in two sub-orthogonal directions. At the Oum Lahsene and Guenfouda sites, we notice a predominance of the ENE–WSW extensional trend, whereas the Jbel El Hamra site shows a predominance of the NNW–SSE extensional trend. In this bidirectional extensional regime, the differentiation of the Mid–Late Triassic basins is mainly accommodated by the action of faults of regional importance (N160°E and N70°E trends) that show a strong normal component. Other sets of normal faults, trending N35–55°E and N100–120°E, are of lesser importance and their strike-slip component is often feeble.

This bidirectional extensional tectonic regime was also found within the Lower Dolerite Formation, where the structuring occurs conformably with the Carbonate Formation. Indeed, it was controlled by normal fault sets of the same attitude. Nevertheless, these structures are notably of large scale and show decametre-sized throws. They produce on the surface of the Lower Dolerites Formation horsts and grabens with a chequerboard structure. This fact has been also confirmed by the isopach map of the Lower Dolerite Formation of the Oujda Mountains (Oujidi & Elmi 2000) (Fig. 7). Subsequently, the Carbonate Formation corresponds to the detached cover, which moulds the underlying unstable chequer board structure, defined at the top of the Lower Dolerites (Fig. 7). When the dip directions of slopes formed by faults below the Carbonate Formation are diverging, the bar is affected by open faults (Fig. 8a), as in the case of the Oum Lahsene site. The voids thus created were filled by blocks and breccias, which derive from the destruction of the Carbonate Formation itself. Alternatively, at the Guenfouda

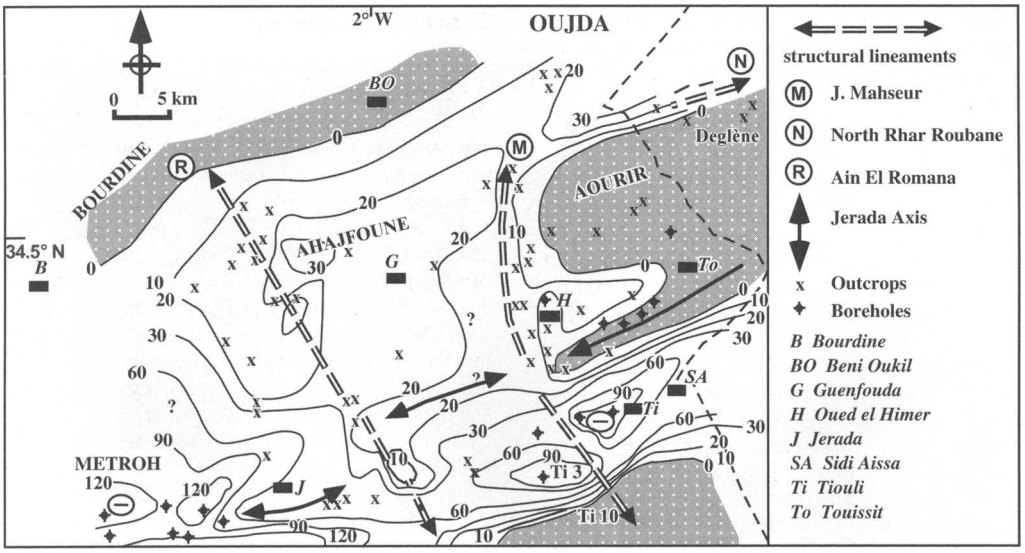

Fig. 7. Lower Dolerites isopach map of the Oujda Mountains (after Oujidi & Elmi 2000). The distinction between Upper and Lower Dolerites is impossible where the Carbonate Formation is missing. Consequently, the drawing of the Tiouli depression is hypothetical.

site, where the dip directions of the formation converge, we have noticed sets of reverse faults allowing a partial superposition of the two segments of the formation (Fig. 8b).

The orientation of the fault sets coincides with those of the main Hercynian and late Hercynian faults described in Palaeozoic formations of the region (Valin & Rakus 1979 (Fig. 1b); Hoepffner 1987; Houari 1987; Oujidi 1994; Torbi 1996). Consequently, the geometry of the Triassic basins has been controlled by the extensional reactivation and heritage of the former faults. Indeed, the borders of the Triassic basins (Oujidi 1994) as well as the isopach trends of the Carbonate Formation (Fig. 3, after Oujidi & Elmi 2000) are in agreement with the orientations of the Hercynian trends. This reactivation is also emphasized by the existence of several sets of dykes of different size and trend (N160°E, N50°E and N120°E) (Oujidi 1994) that cross the Lower Dolerites Formation and are all sealed by the lower levels of the Carbonate Formation. Nevertheless, the faults trending N50°E, N120°E and N160°E are prolonged across the Carbonate Formation. This phenomenon corroborates the model of Laville &

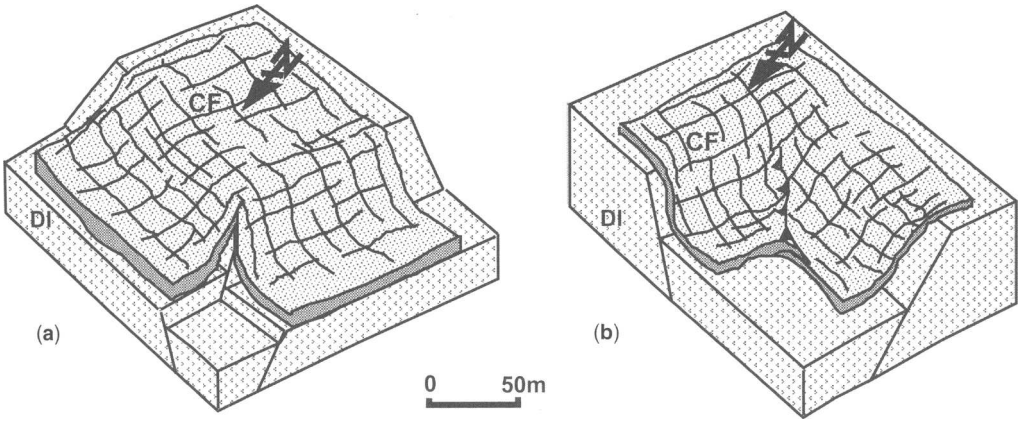

Fig. 8. Diagram illustrating the slip processes of the Middle Carbonate Formation over the chequer-work structure of the Lower Dolerites. (**a**) Tear of the bar by open faults. (**b**) Superposition of two segments of the Carbonate Formation by opposite faults. Dl, Lower Dolerites; CF, Carbonate Formation.

Piqué (1993), according to which the opening of the Triassic basins resulted from the reactivation of Hercynian crustal discontinuities, along normal-oblique faults.

In the present study, the tectonic and structural analyses have been carried out primarily on surface features limited to the Carbonate Formation and the Lower Dolerites Formation. Consequently, it is not sufficient to decide which of the two extensional stress orientations was dominant, or to determine the attitudes of the underlying structures that have controlled the opening of the studied Triassic basins.

The co-occurrence of the major fault system N160°E and N70°E and the minor fault system N50°E and N120°E is tied to the perpendicular disposition of the respective attitudes of the first ones with respect to the two maximal extensional axes (ENE–WSW and NNW–SSE) of this bidirectional system. The N70°E and N160°E fault sets define, in the Oujda Mountains, an L-shaped structural model similar to that described by Dardeau (1984) and Lemoine *et al.* (1989) in the Western Mediterranean, where it is of Late Triassic age. In the Western Alps, this "L" pattern was also explained by a reactivation of Hercynian faults during Tethyan rifting, in a NW–SE extensional system. The NE–SW faults will engender the opening of the Ligurian Tethys during early Jurassic time, whereas the NW–SE faults will act as transfer faults (Lemoine *et al.* 1989). This structural model was partly transposed by Piqué & Laville (1993) for the Moroccan Atlas rifting. However, transfer faults should be strike-slip faults, but no strike-slip faults were detected at the three sites studied (Fig. 6).

The Ladinian–Carnian palaeo-states of stress, in the Oujda Mountains, are different from those of the Triassic–early Liassic transition. Indeed, the isopach map of the Upper Red Beds Formation (Oujidi & Elmi 2000) shows a well-marked predominance of the NE–SW trend in relation to the main direction of fracturing observed on the Carbonate Formation isopach map (Fig. 3). The same observations were also made in the western Mediterranean by Mégard-Galli & Faure (1988), who emphasized a change in orientation of the Briançonnais domain between the extensional palaeo-state of stress of the Ladinian–Carnian (σ_3 N60°E) and that of the Jurassic (σ_3 N140°E). In the Triassic–Liassic basins of the High and Middle Atlas and Central Morocco, the main extensional axis is practically the same, oriented NW–SE (Piqué & Laville 1993; Piqué *et al.* 1998; Ait Brahim *et al.* 2002). These basins of Atlantic influence are indeed controlled by NE–SW, mainly normal faults, accompanied by N70°E- and N90°E-trending sinistral transtensional faults (Oujidi *et al.* 2000).

Concluding remarks

The synsedimentary tectonic instability recorded in the Carbonate Formation of the Oujda Mountains and the associated volcanic activity testify to an early episode of Tethyan rifting during Ladinian–Carnian time, in accordance with the so-called 'Aborted Carnian Rifting'(Mégard-Galli & Faure 1988; Oujidi & Elmi 2000). Stratigraphic and structural analyses give evidence that differentiation into sub-basins during the Ladinian–Carnian was defined by a bidirectional extensional model of ENE–WSW and NNW–SSE trends. This structuring has been adjusted by the reactivation of the principal Hercynian and Late Hercynian tectonic discontinuities, with a dominant role of the N160°E and N70°E faults compared with the N35°E and N120°E ones. The two former subperpendicular fault sets indicate an L-shaped structural model, previously described in the Western Mediterranean (Dardeau 1984; Mégard-Galli & Faure 1988) and the Atlas belt (Laville & Piqué 1993). These results are in accordance with the Tethyan-influenced structuring (Guiraud 1998; Courel *et al.* 2000; Oujidi *et al.* 2000).

On the other hand, it is necessary to underline that palaeo-stress fields of the Ladinian–Carnian Carbonate Formation are different from those of the Triassic–Liassic transition (Oujidi 1994; Oujidi *et al.* 2000). This phenomenon testifies to a stress field discrepancy between the two successive periods. Indeed, during the late Triassic and early Liassic, the NW extensional trend, controlled by N45°E-trending normal faults, is predominant in the Oujda Mountains (Oujidi 1994), in the Western Mediterranean (Dardeau 1984; Mégard-Galli & Faure 1988) and in the Atlas belt (Laville & Piqué 1993). These palaeo-states of stress are in accordance with the Atlantic structuring (Laville & Piqué 1993; Guiraud 1998; Courel *et al.* 2000; Oujidi *et al.* 2000).

The authors are grateful to reviewers K. El Kadiri, C. Sanz de Galdeano, C. Hoepffner, J. Galindo-Zaldivar and V. Perrone, whose objective comments and suggestions improved this paper considerably. This research has been supported by the Oujda Geological Survey Centre and financed by Holcim-Maroc.

References

AIT BRAHIM, L., CHOTIN, P., HINAJ, S., *ET AL.* 2002. Paleostress evolution in the Moroccan African margin from Triassic to Present. *Tectonophysics*, **357**, 187–205.

ALLMENDINGER, R., MARRETT, R. A. & CLADOUHOS, T. 1989–1994. Fault kinematics version 3.8a, a program for analyzing fault slip data. Unpublished document.

COUREL, L., AÏT SALEM, BEN ISMAIL, H., *ET AL.* 2000. An overview of epicontinental Triassic series of Maghreb. *In*: LERCHE, I. & BACHMANN, G. H. Proceeding of Epicontinental Triassic International Symposium, Halle, Germany. *Zentrablatt Für Geologie and Paläontologie, Teil I*, **9–10**, 1145–1166.

CRASQUIN-SOLEAU, S., RAKUS, M., OUJIDI, M., ET-TOUHAMI, M. & BENAOUISS, N. 1997. Découverte d'une faune d'ostracodes dans le Trias des monts d'Oujda (Maroc) Relation entre les plateformes nord et sud de la Téthys. *Comptes Rendus de l'Académie des Sciences, Série IIa*, **324**, 111–118.

DARDEAU, G. 1984. Préfiguration de l'arc alpin dès le rifting téthysien, en bordure du domaine dauphinois (domaine externe des Alpes occidentales françaises). *Bulletin de la Société Géologique de France*, **7**(26), 1319–1324.

EL KADIRI, K. & FAOUZI, M. 1996. Les formations carbonatées massives de la Dorsale calcaire externe (Rif interne, Maroc), un exemple de plateforme tidale sous contrôle géodynamique durant le Trias moyen–Lias inférieur. *Mines, Géologie et & Energie*, **55**, 79–92.

ELMI, S. 1973. Décrochements et mouvements atlasiques dans la région frontalière algéro-marocaine. *Comptes Rendus de l'Académie des Sciences*, **276**(D), 1521–1524.

ELMI, S. 1983. L'évolution des monts de Rhar Roubane (Algérie occidentale) au début du Jurassique. *In*: LANG, J. (ed.) *Livre Jubilaire Gabriel Lucas; Géologie Sédimentaire*. Mémoires Géologiques de l'Université de Dijon, **7**, 401–412.

GUIRAUD, R. 1998. Mesozoic rifting and basin inversion along the northern African Tethyan margin: an overview. *In*: MACGREGOR, D. S., MOODY, R. T. J. & CLARK-LOWES, D. D. (eds) *Petroleum Geology of North Africa*. Geological Society, London, Special Publications **132**, 217–229.

HANCOCK, P. L. 1985. Brittle microtectonics: principles and practice. *Journal of Structural Geology*, **7**(3–4), 437–457.

HOEPFFNER, C. 1987. *La tectonique hercynienne dans l'Est du Maroc*. Thèse Doctorat és Sciences Université Louis Pasteur, Strasbourg.

HOUARI, M. R. 1987. *Etude géologique de la boutonnière paléozoïque des Zekkara (Maroc oriental); sa place dans le contexte de la chaîne hercynienne*. Thèse de 3ème cycle, Ecole Normale Supérieure Souissi, Rabat.

LAVILLE, E. 1981. Rôle des décrochements dans le mécanisme de formation des bassins d'effondrement du Haut Atlas marocain au cours des temps triasiques et liasiques. *Bulletin de la Société Géologique de France*, **XXIII**(3), 303–312.

LAVILLE, E. & PIQUÉ, A. 1993. La distension crustale atlantique et atlasique au Maroc au début du Mésozoïque: le rejeu de structures hercyniennes. *Bulletin de la Société Géologique de France*, **162**(6), 1161–1171.

LEMOINE, M., DARDEAU, G., DELPECH, P. Y., *ET AL.* 1989. Extension synrift et failles transformantes jurassiques dans les Alpes occidentales (1988). *Comptes Rendus de l'Académie des Sciences, Série II*, **309**, 1711–1716.

LUCAS, G. 1942. *Description géologique et pétrographique des Monts du Rhar Roubane et Sidi El Abed (frontière algéro-marocaine)*. Mémoires de la Service Carte Géologique d'Algérie, **2**(16).

MARCOUX, J., BAUD, A., RICOU, L. E., *ET AL.* 1993. Late Norian (215 to 212 Ma). *In*: DERCOURT, J., RICOU, L. E. & VRIELYNCK, B. (eds) *Atlas Tethys Paleoenvironmental Maps*. BEICIP-FRANLAB, Rueil-Malmaison.

MÉGARD-GALLI, J. & FAURE, J. L. 1988. Tectonique distensive et sédimentation au Ladinien supérieur–Carnien dans la zone briançonnaise. *Bulletin de la Société Géologique de France*, (8), **IV**(5), 705–715.

OUJIDI, M. 1994. *Le complexe volcano-sédimentaire rouge du Trias et de la base du Lias du Pays des Horsts (Maroc Oriental). Géodynamique des bassins, dynamique sédimentaire et phénomènes de silicification*. Thèse Doctorat es Sciences, Université. Mohammed 1 Oujda.

OUJIDI, M. 2000. Triassic marine onlap in the southwestern peritethyan domain, example of Oujda Mountains (Eastern Morocco). *In*: LERCHE, I. & BACHMANN, G. H. *Proceeding of Epicontinental Triassic International Symposium, Halle, Germany*. Zentralblatt für Geologie und Paläontologie, Teil I, Heft 9–10, 1243–1268.

OUJIDI, M. & ELMI, S. 1992. Silicification des horizons carbonatés du complexe volcano-sédimentaire du Maroc oriental (Trias–base Lias). *In*: SCHMITT, J. M & GALL, Q. (eds) *Minéralogical and Geochimical Records of Paleoweathering*. Mémoire des Sciences de la Terre, **18**, 97–113.

OUJIDI, M. & ELMI, S. 2000. Evolution de l'architecture des Monts d'Oujda (Maroc oriental) pendant le Trias et au début du Jurassique. Séance spécialisée GFC–SGF–SGA: Les marges téthysiennes d'Afrique du Nord, Paris 1997. *Bulletin de la Société Géologique de France*, **171**(2), 169–179.

OUJIDI, M., BENAOUISS, N., COUREL, L., *ET AL.* 2000. Triassic series of Morocco: stratigraphy, paleogeography, and structuring of southern Peri-Tethyan platform. An overview. *In*: CRASQUIN-SOLEAU, S. & BARRIER, E. (eds) *Peri-Tethys Memoir 5. New Data on Peri-Tethyan Sedimentary Basins*. Mémoires du Muséum National d'Histoire Naturelle, **182**, 23–38.

PIQUÉ, A. & LAVILLE, E. 1993. L'ouverture de l'Atlantique central: un rejeu en extension des structures paléozoïques? *Comptes Rendus de l'Académie des Sciences, Série II*, **317**, 1325–1332.

PIQUÉ, A., AÏT BRAHIM, L., AÏT OUALI, R., *ET AL.* 1998. Évolution structurale des domaines atlasiques du Maghreb au Méso-Cénozoïque; le rôle des structures héritées dans la déformation du domaine atlasique de l'Afrique du Nord. *Bulletin de la Société Géologique de France*, **169**(6), 797–810.

PURSER, B. H. 1980. Les paléosebkhas du Miocène inférieur dans le sud-est de l'Iran. *Bulletin des Centres de Recherche, d'Exploration et de Production Elf–Aquitaine*, **4**(1), 235–244.

RAKUS, M. 1979. Evolution et position paléogéographique des Monts d'Oujda au cours du Mésozoïque. *Mines, Géologie et Energie*, **46**, 75–78.

SALVAN, H. M. 1984. Les formations évaporitiques du Trias marocain. Problèmes stratigraphiques, paléogéographiques et paléoclimatologiques. Quelques réflexions. *Revue de Géographie physique et de Géologie Dynamique*, **25**(3), 187–203.

STAMPFLI, G. M., MARCOUX, J. & BAUD, A. 1991. Tethyan margin in space and time. *Palaeogeography, Palaeoclimatology, Palaeoecology*, **87**, 373–409.

TORBI, A. 1996. Stratigraphie et évolution structurale paléozoïque d'un segment de la meseta orientale marocaine (Monts de Sud-Est d'Oujda): rôle des décrochements dans la formation de l'olistostrome intraviséen et le plutonisme tardihercynien. *Journal of African Earth Sciences*, **22**(4), 549–563.

TRICART, P., BLONDEL, T. & BOUAZIZ, S. 1986. Quelques exemples de diaclases précoces en domaine de plate-forme (Tunisie): leur utilité pour dépister une extension structurale. *Comptes Rendus de l'Académie des Sciences, Série II*, **303**, 975–980.

TRICART, P., BOURBON, M., CHENET, P. Y., *ET AL.* 1988. Tectonique synsédimentaire triasico-jurassique et rifting téthysien dans la nappe briançonnaise de Peyre-Haute (Alpes occidentales). *Bulletin de la Société Géologique de France*, (8), **IV**(4), 669–680.

VALIN, F. & RAKUS, M. 1979. *Etude géologique du Paléozoïque et de la couverture mésozoïque des Monts d'Oujda (Maroc oriental)*. Rapport, Service Régional de la Géologie Oujda, Maroc, **60**.

Recent palaeostresses from striated pebbles related to fold development in a mountain front: the Prerif Ridges (Rif Cordillera, Morocco)

P. RUANO[1], K. BARGACH[2], J. GALINDO-ZALDÍVAR[3], A. CHALOUAN[2] & M. AHMAMOU[2]

[1]*Departament de Geodinàmica i Geofísica, Facultat de Geologia, Universitat de Barcelona, Martí i Franquès s/n, 08028 Barcelona, Spain*

[2]*Département des Sciences de la Terre, Faculté des Sciences, Université Mohammed V-Agdal, BP 1014, Rabat, Morocco*

[3]*Departamento de Geodinámica, Universidad de Granada, 18071, Granada, Spain (e-mail: jgalindo@ugr.es)*

Abstract: The southern mountain front of the Rif Cordillera (Morocco) provides impressive geological evidence of the most recent deformations related to the activity of the Eurasian–African plate boundary in the Western Mediterranean. In this region, striated and pitted pebbles are analysed from Pliocene–Quaternary rocks located in the southern front of the Prerif Ridges, which have been deformed by south-vergent folds of decametre to hectometre sizes. Striated and pitted pebbles represent a tectonic deformation structure which, although very scarce in nature, is revealed as one of the most complete for determining palaeostresses. In Jbel Trhat and Jbel Zerhoun of the Rif mountain front, north–south to NNW–SSE prolate compression stress ellipsoids are related to an initial stage of south-vergent fold development during the progressive tilting of conglomerate layers. Finally, oblate stress ellipsoids indicate extension parallel to the fold axes. The north–south trend of the determined compression is compatible with a tectonic setting where the NW–SE convergence of the Eurasian and African plates is modified by the westward motion of large crustal blocks such as the Alboran Domain or the southwestward motion of blocks in the Rif Cordillera.

The building of mountain ranges is a consequence of the relative motion of tectonic plates. However, the relationships between plate motions and the observed mesoscopic deformation structures are not always easy to elucidate. The presence of wide stripes of deformation related to plate boundaries that may include different mobile tectonic blocks, and the heterogeneity of previously deformed rocks, gives rise to the local perturbation of stresses and, at larger scale and among other factors, the development of arched orogens (Jackson & McKenzie 1988) such as the Betic–Rif Cordilleras in the Western Mediterranean (Fig. 1).

The interest of mountain fronts lies in the fact that they provide evidence of the deformations related to recent plate motions because young sedimentary sequences record the recent tectonic phases. Also, sedimentary rocks of these areas generally display a more homogeneous behaviour at large scale than the deformed metamorphic rocks belonging to the internal zones of the chains. The classical deformation pattern in compressional orogenic wedges is the 'piggy-back' thrust sequence (Butler 1982), where the active structures are located precisely at the mountain fronts, with a progressive propagation towards the foreland basins. The mountain fronts are determined mainly by the cropping out of reverse faults that join a basal thrust, or by vergent folds that may be associated with reverse blind faults (Boyer & Elliott 1982; Vann *et al.* 1986).

The determination of palaeostresses from brittle structures sheds light on the tectonic processes responsible for the development of geological structures in the mountain ranges at different scales. Although the geometry of folds and faults at map scale may provide information on the main regional stresses active in a region, a more precise determination of the palaeostress ellipsoids would result from the study of fault orientations at outcrop scale, with the help of statistical–graphical (e.g. right dihedra diagrams, Angelier 1977; Angelier & Mechler 1977) or numerical methods (e.g. Carey & Brunier 1974; Etchecopar *et al.* 1981; Galindo-Zaldívar & González-Lodeiro 1988; Angelier 1990). Most of these methods require the measurement of the orientation of a large number of

From: MORATTI, G. & CHALOUAN, A. (eds) 2006. *Tectonics of the Western Mediterranean and North Africa.* Geological Society, London, Special Publications, **262**, 87–99.
0305-8719/06/$15.00

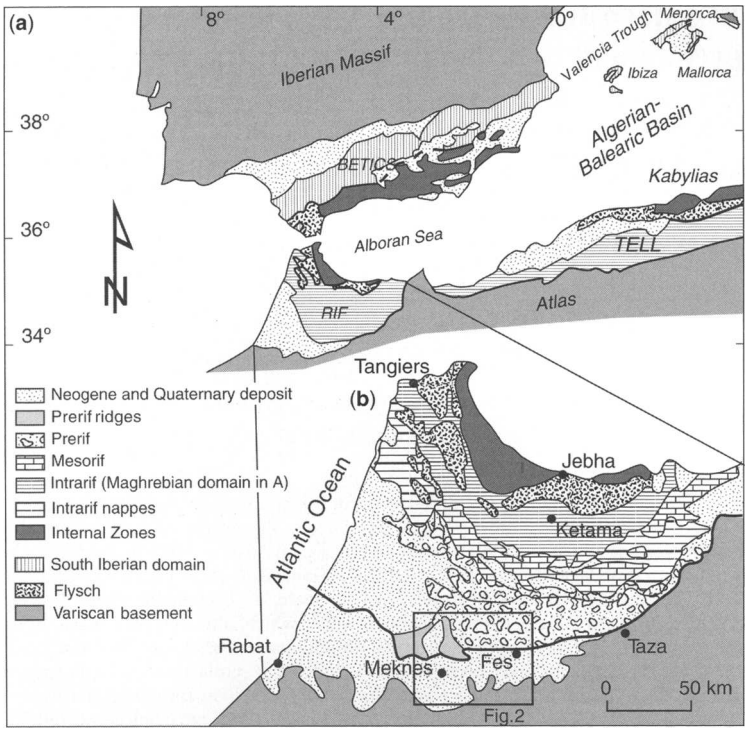

Fig. 1. Map of the Western Mediterranean (**a**), showing the geological setting of the Rif Cordillera (**b**).

microfaults (usually more than 15), in outcrops that tend to be several tens of metres long. The consistency of the palaeostress ellipsoids determined by microfault analysis is checked against the orientation of other brittle structures such as stylolites or tension joints.

Striated and pitted pebbles, with homogeneous character at outcrop scale, represent one of the most useful structures that help in determining palaeostress orientations (Sanz de Galdeano & Estévez 1981; Schrader 1988; Taboada 1992; Ruano & Galindo-Zaldívar 2004). Even in a small rock volume, it is possible to measure over one hundred striae on the surface of a pebble; and when solution pits develop, they provide independent evidence of the trend of compression. Although striated and pitted pebbles are uncommon in nature, some have been found in the frontal section of the Rif Cordillera (Bargach *et al.* 2004).

This study focuses on the stresses that were active in the frontal part of the Rif Cordillera during tilting of Plio-Quaternary conglomerate layers related to the development of folds, as shown by striated pebbles located in Jbel Trhat and Jbel Zerhoun. We will then discuss the palaeostresses at the mountain front in the frame of the recent motion of this area of the Eurasian–African plate boundary.

Regional setting

The Betic and Rif Cordilleras, which join westward at the Gibraltar Strait, are formed by an Alpine arched orogen that developed in the Western Mediterranean (Fig. 1). The relative recent convergence at a rate of 4.9 mm a^{-1} of the major Eurasian and African plates (DeMets *et al.* 1994) together with the westward displacement of the Alboran Domain (García-Dueñas & Balanyá 1986; formerly the 'Alboran microplate' of Andrieux *et al.* 1971) as an independent tectonic element, has created a tectonically unstable region with overprinted deformations. The Eurasian–African NW–SE convergent plate boundary in the Western Mediterranean is associated with a broad zone of deformation, more than 300 km wide, where a complex set of active compressional structures located in the outer regions and extensional structures in the inner regions affects the previously deformed rocks of the Betic–Rif Cordilleras (Galindo-Zaldívar *et al.* 1993).

The Rif can be subdivided into three domains: the Internal Rif (or Internal Domain), which derives from the Alboran microplate, a Flysch Domain, of probable oceanic origin, and the External Rif (External Domain) (Suter 1980). The Internal Rif

is made up of metamorphic complexes that include Palaeozoic rocks cropping out in the NE part of the cordillera and extending below the Alboran Sea. However, the External Rif is mainly formed by carbonate and siliciclastic sedimentary rocks of Triassic and younger ages, belonging to the African margin. On the basis of their sedimentary sequences, the External Zones are divided into Intrarif, Mesorif and Prerif (Fig. 1).

The frontal part of the cordillera is formed by a thrust-and-fold belt, with a large thrust sheet of Cretaceous to Miocene marls (the Prerif thrust sheet), separated from the Saïss and Gharb foreland basins by the large Prerif Ridge folds (Fig. 2). The Prerif Ridges ('Rides Prerifaines') form the frontal part of the Rif mountains, and are grouped into two great ensembles separated by the Volubilis depression. The western group, comprising jbels Bou Draa, Outita, Moulay Yakoub Hamma, Nouillat, Ari, Koudiat Bou Azouf, Kheloua and Kefs, is arched in a horseshoe shape, convex towards the west. The eastern group (the ridges of Tselfat, Bou Kannfoud, Fert-el-Bir, Dehar-en-Sour, Zerhoun, Nesrani and Kannoufa) forms a more open arc than the western group. To the east, Jbel Trhat and Jbel Zalarh are two tiny insulated ridges cropping out on either side of Fes.

The Prerif Ridges are elongated crests associated with folds and reverse faults developed by the southward propagation of the Alpine deformation affecting the Rif Chain. The development of this type of structure requires a detachment level, which, in the Prerif thrust sheets, is generally located at the Triassic–Palaeozoic basement boundary (El Mourabet 1996; Zizi 1996; El Haddaoui 2000). Present-day seismicity confirms the activity of the tectonic structures. Jbel Trhat and Jbel Zerhoun are two main ridges of the Prerif Ridges where striated conglomerates crop out in slightly different tectonic settings, illustrating the variability of the Rif front.

Jbel Trhat (Fig. 3), located in the eastern part of the tectonic arc, represents a south-vergent fold, with an approximately N80°E axis, that deforms all the sedimentary sequence, including a layer of subvertical or even reversed Pliocene–Quaternary conglomerates. Hectometre to kilometre size folds affect the conglomerate layers. This ridge shows no evidence of south-vergent reverse faults. Conglomerates are generally clast-supported and are formed by metre-thick layers of very rounded carbonate pebbles of variable sphericity that may reach decimetre diameters. Pebbles of conglomerate layers are generally affected by solution pits and striations. Thus, these conglomerates may indicate the stresses active at the mountain front.

Jbel Zerhoun (Fig. 4), located in the central western part of the mountain front, is a south-vergent fold formed mainly by Jurassic limestones and deformed in its southern limb by reverse faults. These faults affect rocks up to the

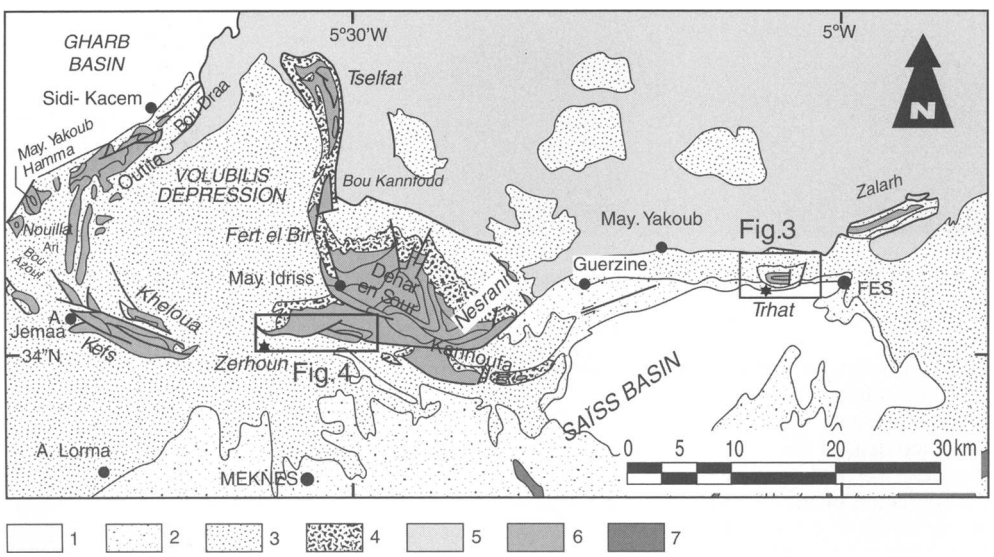

Fig. 2. The mountain front of the Rif Cordillera. Detailed geological map of the Prerif Ridges and Saïss Basin. 1, Quaternary sediments; 2, Pliocene sediments; 3, Upper Miocene rocks; 4, Lower Miocene rocks; 5, Nappe Prerifaine; 6, Prerif Ridges; 7, Middle Atlas. Stars indicate the position of the studied outcrops.

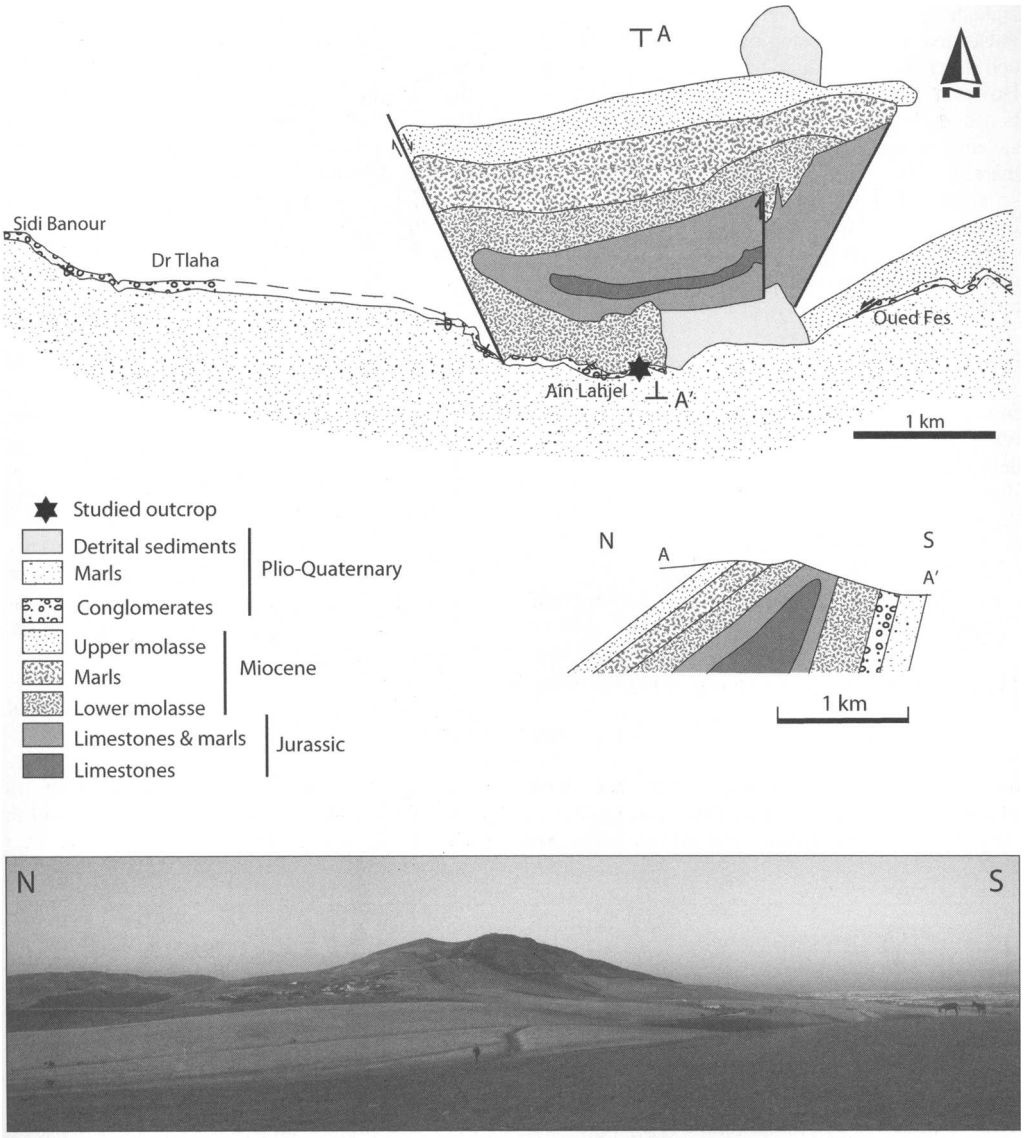

Fig. 3. Jbel Trhat. Geological map, cross-section and field view.

Pliocene–Quaternary units of the foreland Saïss Basin. The outcrop of conglomerates with striated pebbles is located south of Jbel Zerhoun and in the northern half of the Saïss Basin. Pliocene conglomerates are subhorizontal and may represent the deformation of the foreland basin in a region near the mountain front. The Saïss Basin is filled by late Miocene to Quaternary sedimentary rocks that lie unconformably at its southern border on the Variscan basement represented by the Moroccan Meseta.

Palaeostress from striated and pitted pebbles

Palaeostress ellipsoids are generally determined using the orientation of brittle structures, such as faults, joints and pressure-solution structures (Hancock 1985). The orientation of neoformed faults in an isotropic non-fractured rock following the Anderson (1951) or Reches (1978, 1983) conjugate fault model gives a direct indication of the orientation of the main stresses. On other hand,

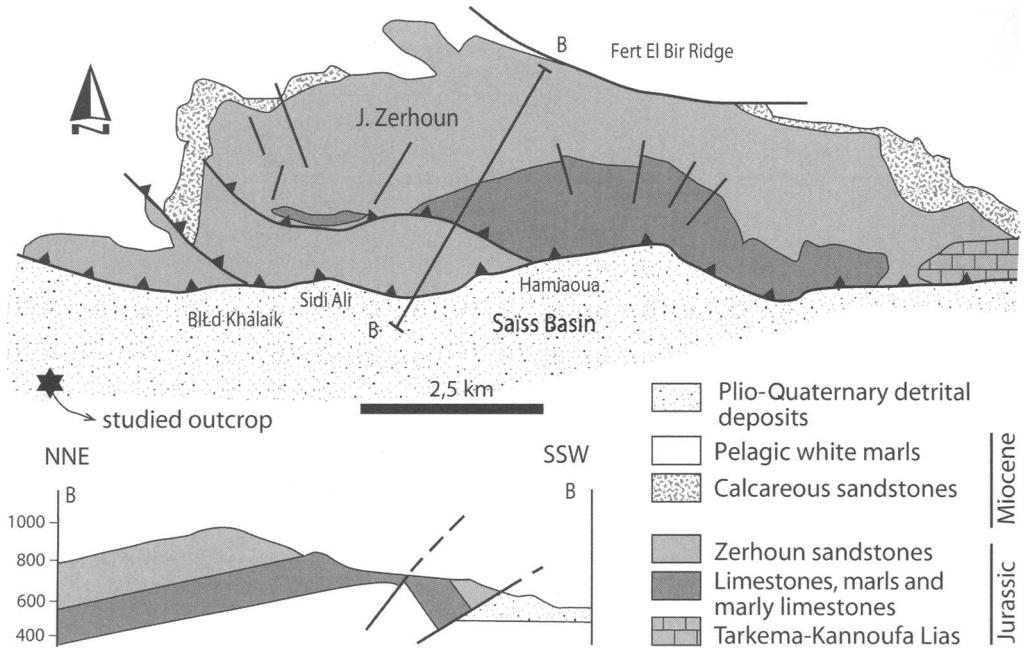

Fig. 4. Jbel Zerhoun. Geological map and cross-section.

analysis of striae on reactivated fault surfaces of different orientations adds new constraints to palaeostress determination and allows us to pin down the axial ratio of stress ellipsoids (Carey 1979) or even to distinguish overprinted faulting stages (Etchecopar *et al.* 1981; Galindo-Zaldívar & González-Lodeiro 1988; Angelier 1990). The statistical methods assume that the stresses are approximately homogeneous at the outcrop scale, and although theoretically only four data are required to calculate a palaeostress ellipsoid, commonly at least 15 data of striae orientation are needed to provide reliable results. Taking such measurements in the field usually involves studying outcrops of tens to hundreds of metres.

Striations and pitted pebbles represent relevant structures for palaeostress determination because they provide two independent sources of information in a small rock volume. These structures are developed by the interaction between pebbles and the rock matrix, when the rocks undergo small tectonic deformations that favour internal sliding. Solution pits develop when insoluble elements of the matrix, such as quartz sand grains, come in contact with the surface of a soluble, generally calcareous, pebble. The progressive incisions of siliciclastic particles on the pebble surface produce asymmetric prod marks (Fig. 5) that indicate the sense of motion of the microfaults.

The applied stress determines the orientation of striae developed on the surface of a striated pebble. Each pebble can allow us to measure over a hundred striae with different orientations, as well as showing the orientation of pressure solution marks. Sanz de Galdeano & Estévez (1981) described the striation on pebbles in intramontane basins of the Betic Cordillera, pointing out that the trend of compression coincides with the trend of the solution pits or the trend of the pole of divergence of striations. Schrader (1988) and Taboada (1992) modelled the pattern of striae orientation that would develop theoretically on spherical pebbles that have undergone different types of single deformations.

To determine palaeostresses in each studied outcrop of the Prerif Ridges (Figs 3 and 4), several striated pebbles of the same outcrop were sampled, and the field orientation was marked on each pebble. In the laboratory, each pebble was cleaned and reoriented on plasticine to the same position as in the field to measure the upper face; then, the pebble was inverted to measure the lower face (Ruano & Galindo-Zaldívar 2004). Each pebble is considered as an independent palaeostress measurement station and all the measurements are integrated in a common orientation diagram (e.g. Fig. 6), that includes the orientation of microfaults and solution marks. The single

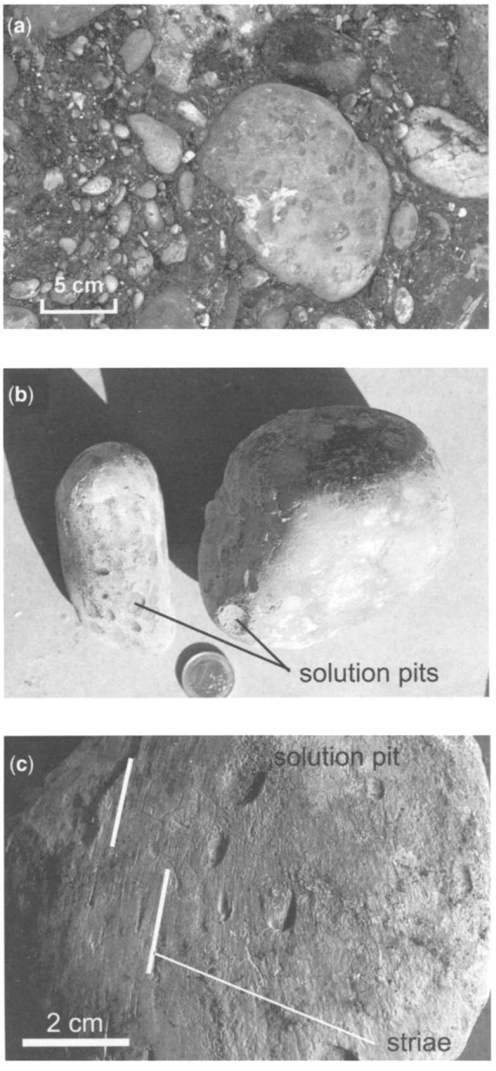

Fig. 5. Structures on striated pebbles. (**a**) Field appearance of clast-supported conglomerates with striated pebbles. (**b**) Solution pits. (**c**) Striae on pebble surface. (Note the presence of asymmetric striations indicating the sense of motion.)

deformation striae pattern on spherical pebbles (Schrader 1988; Taboada 1992) cannot be directly applied to real field data that are the result of overprinted stages.

The palaeostress determination from striae on pebble surfaces was carried out with the search grid method (Galindo-Zaldívar & González-Lodeiro 1988), the validity of which has been previously demonstrated (Ruano & Galindo-Zaldívar 2004). This method allows us to establish overprinted stress ellipsoids, and to combine measures of striae orientations of known and unknown regimes. Moreover, there is no substantial influence from the size or irregularities in shape of the pebbles when determining the palaeostresses. For these reasons, striated and pitted pebbles in a small rock volume combine the advantages of other brittle structures, including faults and solution marks, to signal the evolution of palaeostresses. Solution pits develop on surfaces orthogonal to the maximum compressive stress, and should be considered as stylolite structures (Hancock 1985). Figure 6 shows an example of the results from a single pebble, and allows a comparison of the results obtained from striae and solution pits.

Palaeostress determinations from striae on pebbles have the same strengths and weaknesses as field measurements along quarry outcrops. The study of several pebbles from conglomerates of the same outcrop makes it possible to compare the results and to check them for consistency, which may support palaeostress homogeneity at outcrop scale.

Jbel Trhat

We analysed eight pebbles from the vertical conglomerate layers of Jbel Trhat (Fig. 3). The solution marks seen in some of the pebbles are basically located at the two opposite pebble poles along subvertical to SSW-plunging lines. In one pebble, solution pits show different inclinations along a subvertical plane of NE–SW orientation. These data point to the presence of a subvertical to steeply SSW-inclined compression.

The different trends of striae observed on the same pebble surface indicate overprinted deformations with different palaeostress ellipsoids. This is confirmed in the palaeostress analysis carried out using the microfaults of each pebble (Table 1), which led us to obtain two or three different overprinted faulting stages. In interpreting the significance of palaeostress ellipsoids, the order of the ellipsoid determination is not significant because it depends only on the abundance of striae corresponding to each phase of faulting. It is necessary to select the odd axis of each ellipsoid, which represents the axis that is most different from the intermediate stress axis: σ_1 in prolate ellipsoids and σ_3 in oblate ellipsoids (italic entries in Table 1). The odd axes allow us to compare the results of different pebbles. In fact, in pure prolate ellipsoids, σ_2 has a value near σ_3 and there is a well-defined trend of compression and a poorly defined trend of extension. Likewise, in oblate ellipsoids σ_2 has a value near σ_1, and the trend of extension is well determined but the trend of compression is poorly constrained. In the cases of intermediate axial ratios, it is necessary to consider both σ_1 and σ_3 axis orientations.

Axial ratios $((\sigma_2 - \sigma_3)/(\sigma_1 - \sigma_3))$ of palaeostress ellipsoids of Jbel Trhat indicate the presence of both prolate and oblate shapes. All the significant

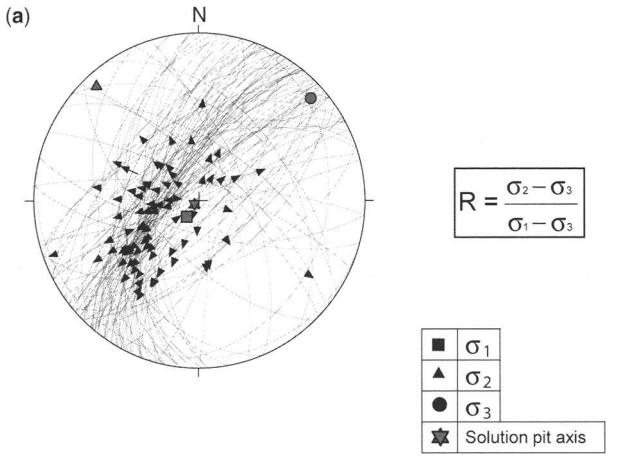

(c)

PHASE	Fit	R	σ_1	σ_2	σ_3		Data (N)	Total measured striae
1	Fair	0,2	N217°E/80°	N318°E/02°	N48°E/10°		65 (23)	101
2	Fair	0,06	N226°E/56°	N134°E/02°	N43°E/34°		37 (7)	

N: non-assigned data

Fig. 6. Example of palaeostress determination from a pebble (M4, Jbel Trhat). Solution pit axis (star) and tangent planes to pebble surface with striae are represented by displacement vectors (arrows): (**a**) great circle; (**b**) poles. Short lines are undetermined movements. (**c**) Stress ellipsoid axes determined on the studied pebble. Equal area projection, lower hemisphere.

stress axes obtained from all the pebbles of Jbel Trhat may be represented together (Fig. 7), indicating that, in general, prolate stress ellipsoids are more abundant than oblate ones. The σ_1 odd axes indicate a subvertical and southward-plunging trend of compression that is in agreement with the trends obtained from solution pits. The intermediate to oblate stress ellipsoids point, in general, to an ENE trend of extension, roughly similar to the trend of the fold axis.

Jbel Zerhoun

The conglomerates with striated pebbles located in the southern part of the mountain front represented by Jbel Zerhoun and in the northern side of the foreland Saïss Basin (Fig. 4) are found in a subhorizontal layer with scarce evidence of mesoscopic tectonic deformation, yet they are affected by consistent striations. As in Jbel Trhat, pebbles are mainly calcareous and are surrounded by a matrix including insoluble siliciclastic particles. The four pebbles selected from this layer show evidence of a polyphase deformation including two or three stress ellipsoids (Table 2). This outcrop has a general predominance of oblate to intermediate stress ellipsoids, indicating an east–west–oriented extension (Fig. 8). There is also evidence of radial extension, with two ellipsoids characterized by subvertical σ_1 axes, and of intermediate stresses characterized by steeply plunging σ_1 and a gently eastward-plunging σ_3. In addition, one of the well-defined stress ellipsoids combines north–south compression with east–west extension.

Table 1. *Palaeostresses determined in pebbles of Jbel Trhat*

Pebble	Number of measured striae	Phase	Fit	R	σ_1		σ_2		σ_3	
					Direction	Dip (deg)	Direction	Dip (deg)	Direction	Dip (deg)
F1	59	1	Fair	0.18	*N192°E*	*30*	N315°E	43	N81°E	32
		2	Fair	0.42	*N210°E*	*30*	N333°E	43	*N99°E*	*32*
		3	Good	0.35	*N164°E*	*78*	N344°E	12	*N74°E*	*0*
F2	68	1	Fair	0.65	N222°E	52	N33°E	38	*N126°E*	*5*
		2	Fair	0.17	*N179°E*	*21*	N327°E	65	N84°E	12
		3	Fair	0.28	*N338°E*	*39*	N134°E	49	N238°E	12
F3	79	1	Good	0.56	*N320°E*	*63*	N214°E	8	*N120°E*	*26*
		2	Good	0.25	*N131°E*	*87*	N266°E	2	N356°E	2
		3	Fair	0.69	N143°E	54	N327°E	36	*N236°E*	*2*
F4	42	1	Good	0.05	*N170°E*	*82*	N66°E	2	N336°E	8
		2	Fair	0.01	*N86°E*	*58*	N303°E	27	N204°E	16
F6	107	1	Fair	0.87	N342°E	26	N224°E	44	*N92°E*	*35*
		2	Fair	0.70	N223°E	82	N357°E	6	*N888°E*	*6*
F8	61	1	Fair	0.07	*N257°E*	*64*	N354°E	4	N86°E	26
		2	Fair	0.18	*N289°E*	*70*	N188°E	4	N97°E	20
F9	43	1	Good	0.41	*N186°E*	*37*	N297°E	26	*N53°E*	*42*
		2	Fair	0.64	*N160°E*	*25*	N46°E	40	*N273°E*	*39*
F11	63	1	Fair	0.28	*N183°E*	*33*	N277°E	7	N17°E	56
		2	Fair	0.10	*N254°E*	*61*	N39°E	24	N135°E	15
M4	101	1	Fair	0.20	*N217°E*	*80*	N318°E	2	N48°E	10
		2	Fair	0.06	*N226°E*	*56*	N134°E	2	N43°E	34

Entries in italics indicate the odd axes, which are significant for comparing results.
$R = (\sigma_2 - \sigma_3)/(\sigma_1 - \sigma_3)$. Prolate: $0 \leq R \leq 0.33$; oblate: $0.66 \leq R \leq 1$.

These complex overprinted stresses are supported by the overall compatibility of the theoretical and observed striae from pebble palaeostress calculation (Table 2).

Discussion

The southern front of the Rif Cordillera is characterized by the presence of a typical fold-and-thrust belt. In this region south-vergent folds develop, as in Jbel Trhat, which may be affected by reverse faults as in Jbel Zerhoun (Figs 2–4), pointing to a roughly north–south compressional stress (Bargach *et al.* 2004). This stress field is in agreement with the trend of compression determined in regional studies of the Rif Cordillera (Ahmamou & Chalouan 1988; Aït Brahim & Chotin 1989; Morel 1989). These deformations develop above a detachment level located at depth and are related to the propagation of the deformations of the Eurasian–African plate convergence towards the Rif mountain front, separating the sedimentary cover from a metamorphic basement formed by the Moroccan Meseta and the Middle Atlas. The presence of conglomerates with striated pebbles provides an excellent opportunity to advance our knowledge of the stress features in a mountain front and in its foreland.

In general studies, the analysis of striae is largely centred on homogeneous rocks such as limestones or sandstones. The fractures in conglomerate layers, however, can be considered good markers for reconstructing the deformation history of sedimentary sequences, because in general they do not show great perturbations of stresses around each pebble (Petit *et al.* 1985). The trend of compression obtained from striae orientation and well-developed solution pits in pebbles of Jbel Trhat are in agreement, supporting both approaches for palaeostress determination in pebbles.

All the pebbles of the studied outcrops show evidence of polyphase deformations, pointing to a complex overprinting of palaeostresses. However, when the odd axes of all the palaeostress ellipsoids of the bulk of pebbles from each outcrop are considered, predominant stresses that are representative of the tectonic evolution can be inferred.

The two analysed outcrops are located in the same general tectonic setting, but in different parts of the structure. The Plio-Quaternary conglomerates of the southern limb of Jbel Trhat lie vertically (Oued Fez), or may be reversed (Ain Lahjel, Sidi Banour). Considering the present-day position of the pebbles in subvertical ENE–WSW-oriented layers, palaeostress determinations

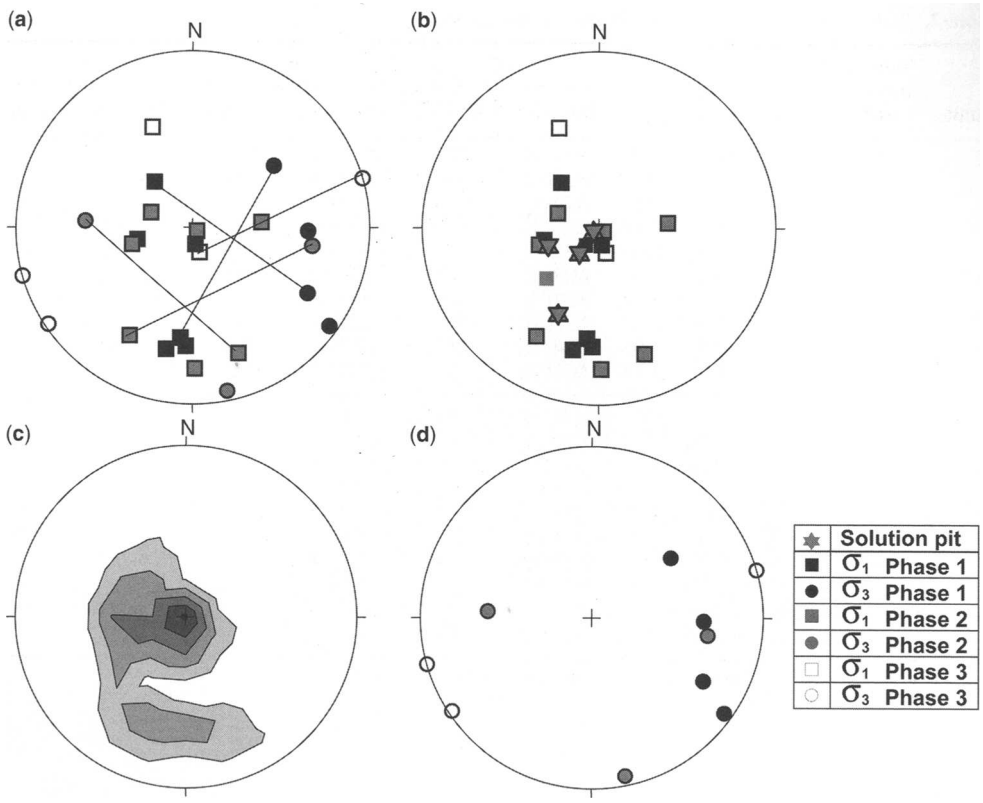

Fig. 7. Palaeostress determinations from striated and pitted pebbles of Jbel Trhat. Lower hemisphere, equal area projection. (**a**) Odd axes of stress ellipsoids. The lines join σ_1 and σ_3 axes of intermediate stress ellipsoids. (**b**) Poles of σ_1 odd axes in prolate and intermediate stress ellipsoids and solution pits orientations. (**c**) Density contour diagram of σ_1 odd axes in (b). (**d**) Poles of σ_3 odd axes of oblate and intermediate stress ellipsoids.

(Table 1) indicate the presence of a progressive deformation simultaneous to tilting (Fig. 9). The subvertical compression axes of the prolate stress ellipsoids may be restored to the horizontal, indicating a NNW–SSE compression. The prolate to intermediate palaeostresses with compressional stress axes plunging south may represent the palaeostresses developed during tilting of the layers (Fig. 9). All these palaeostresses indicate a well-defined initial NNW–SSE trend of compression that is recorded during different stages of tilting, and is in agreement with the development of ENE–WSW-oriented folds. Palaeostress ellipsoids corresponding to the last stages of tilting are less abundant, however. Oblate stress ellipsoids are scarce, and when considered in conjunction with the intermediate ones, indicate a trend of minimum stress axes roughly subparallel to the fold axes (Figs 3 and 7). No clear chronology can be established between the two types of stresses. At any rate, during the compression, when the NNW–SSE stresses increase, the vertical stresses may approach the horizontal ones and the minimum stress axis may become subparallel to the fold axes, and probably in this case the oblate ellipsoids are more recent.

Petit *et al.* (1985) studied the brittle deformation of conglomerate layers of the High Atlas and underlined evidence of the different stages of fold development. The striated pebbles of Jbel Trhat outcrop, as analysed here, would likewise indicate that during fold development a well-directed prolate stress ellipsoid was active, in addition to subordinate extension subparallel to the fold axis.

Jbel Zerhoun outcrop, with subhorizontal conglomerate layers located south of the mountain front, provides evidence for the palaeostresses of the foreland basin. The analysis of conglomerate pebbles (Table 2) shows a stress field more variable than in Jbel Trhat, with predominant oblate to intermediate ellipsoids generally characterized by east–west trends of minimum stresses. One

Table 2. *Palaeostresses determined in pebbles of Jbel Zerhoun*

Pebble	Number of measured striae	Phase	Fit	R	σ_1		σ_2		σ_3	
					Direction	Dip (deg)	Direction	Dip (deg)	Direction	Dip (deg)
G1	60	1	Good	0.14	*N64°E*	*72*	*N211°E*	15	N304°E	9
		2	Good	0.67	N170°E	80	*N350°E*	10	*N80°E*	*0*
		3	Fair	0.83	N238°E	8	*N339°E*	53	*N142°E*	*36*
G3	30	1	Fair	0.95	N197°E	18	*N334°E*	66	*N102°E*	*15*
		2	Fair	0.59	*N321°E*	*46*	*N179°E*	37	*N73°E*	*37*
G5	51	1	Fair	0.34	*N186°E*	*11*	*N55°E*	74	*N279°E*	*12*
		2	Fair	0.34	*N220°E*	*60*	*N16°E*	28	*N111°E*	*11*
		3	Fair	0.70	N274°E	83	*N150°E*	4	*N60°E*	*6*
G6	32	1	Fair	0.66	N348°E	14	*N205°E*	73	*N80°E*	*10*
		2	Fair	0.12	*N39°E*	*72*	*N221°E*	18	N130°E	1

Entries in italics indicate the odd axes, which are significant for comparing results.
$R = (\sigma_2 - \sigma_3)/(\sigma_1 - \sigma_3)$. Prolate: $0 \leq R \leq 0.33$; oblate: $0.66 \leq R \leq 1$.

ellipsoid of intermediate shape combines north–south compression and east–west extension (Fig. 8). Furthermore, the prolate stress ellipsoids indicate radial extension. Hence, the foreland basin may be generally subject to extension in a low stress field as a consequence of the arching of the basement below the load of the Rif Cordillera. The propagation of the mountain front would therefore produce north–south compression resulting in an oblate stress ellipsoid with a minimum stress roughly parallel to the mountain front (Fig. 9).

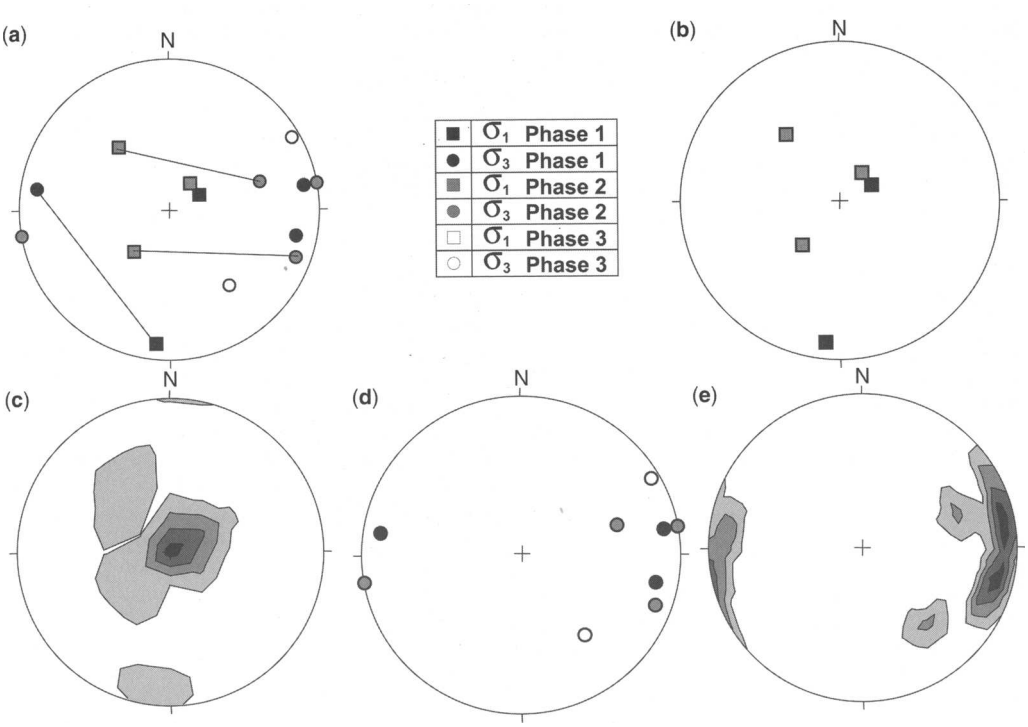

Fig. 8. Palaeostress determinations from striated and pitted pebbles south of Jbel Zerhoun. Lower hemisphere, equal area projection. (**a**) Odd axes of stress ellipsoids. The lines join σ_1 and σ_3 axes of intermediate stress ellipsoids. (**b**) Poles of σ_1 odd axes in prolate and intermediate stress ellipsoids. (**c**) Density contour diagram of σ_1 odd axes in (b). (**d**) Poles of σ_3 odd axes of oblate and intermediate stress ellipsoids. (**e**) Density contour diagram of σ_3 odd axes in (d).

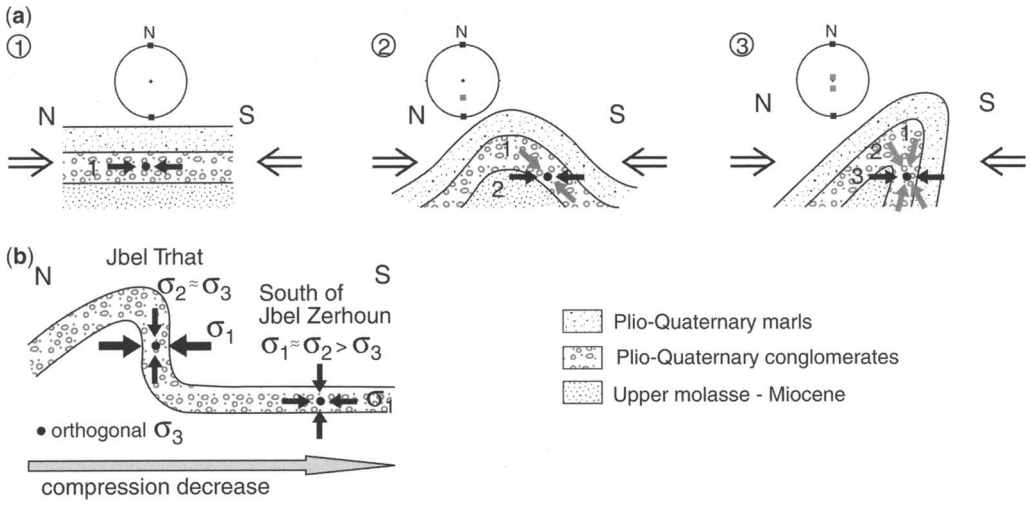

Fig. 9. Sketch of fold development and stresses in the mountain front.

The present-day deformations related to the Eurasian–African plate boundary are identified better in the mountain front because it forms a border of the deformation area, and they affect rocks that were not largely deformed previously and that show less heterogeneity. A deformed sedimentary sequence extending to the Plio-Quaternary further supports the recent age of the tectonic structures. Although the main aim of this study is to determinate palaeostresses in relation to fold development and only two outcrops are shown in detail, the north–south to NNW–SSE compressional stresses that develop the south-vergent folds are in agreement with the NW–SE present-day convergence between the Eurasian and African plates; yet the trend of compression shows a slight deviation to north–south with respect to the trend of plate convergence. This fact may indicate a possible interaction with the local thrusts and fault in the region.

Conclusions

Striated and pitted pebbles, although very scarce in nature, give more reliable insights into palaeostresses than other brittle structures of larger sizes, because they provide two independent data from within a very small rock volume and the results can be confirmed by the study of different pebbles of the same outcrop. The methods for determining palaeostresses from fault striae (e.g. the search grid method) have been proven to be adequate for the analysis of the striated surfaces of pebbles. Moreover, striated and pitted pebbles allow us to record small deformation intensities at shallow crustal levels, as is shown in this study.

The Prerif Ridges represent a fold-and-thrust belt characterized by south-vergent folds with reverse limbs (e.g. Jbel Trhat), in some cases affected by reverse faults (Jbel Zerhoun), bounded to the south by the Saïss foreland basin. Analysis of the striations on pebbles of conglomerates belonging to the frontal part of the Prerif Ridges in Jbel Trhat outcrop shows that, in the present position, the main deformation is related to prolate stress ellipsoids, with subvertical or southward-inclined compression axes. The development of the pebble striations may be related to the same deformation that produced ENE–WSW-oriented folds. Therefore, if the folds are restored, the pebble data suggest that after Pliocene time the area was subject to a prolate, constant and well-defined NNW–SSE-directed horizontal compression that produced folds with southward vergences and progressively tilted the conglomerate layers.

Comparing the results of the two outcrops, the mountain front appears as a boundary from which horizontal compression decreases progressively towards the foreland, and prolate NNW–SSE horizontal compressional stresses orthogonal to the mountain front decrease and occur in transition to oblate stresses with a minimum stress axis subparallel to the front. Meanwhile, the foreland basin is under the influence of variable stresses ranging from more intense NNW–SSE compression to radial extension.

The study of tectonic deformations in this region indicates NNW–SSE trends of recent shortening and compression in the Rif mountain front that are directly related to the present-day and recent NW–SE convergence of the European and African plates, probably modified by a late tendency of westward motion of the Alboran Domain.

The comments of C. Hoepffner and F. Medina have improved the quality of this paper. Research has been financed by collaborative Spanish–Moroccan projects of the Junta de Andalucía, the AECI and CICYT project BTE2003-01699.

References

AHMAMOU, M. & CHALOUAN, A. 1988. Distension synsédimentaire plio-quaternaire et rotation antihoraire des contraintes au Quaternaire ancien sur la bordure nord du bassin du Saïss (Maroc). *Bulletin de l'Institut Scientifique, Rabat*, **12**, 19–26.

AÏT BRAHIM, L. & CHOTIN, P. 1989. Genèse et déformation des bassins néogènes du Rif central (Maroc) au cours du rapprochement Europe–Afrique. *Geodinamica Acta*, **3**(4), 295–304.

ANDERSON, E. M. 1951. *The Dynamics of Faulting*. Oliver & Boyd, Edinburgh.

ANDRIEUX, J., FONTBOTÉ, J. M. & MATTAUER, M. 1971. Sur un modèle explicatif de l'Arc de Gibraltar. *Earth and Planetary Science Letters*, **12**, 191–198.

ANGELIER, J. 1977. La reconstitution dynamique et géométrique de la tectonique de failles á partir de mesures locales (plans de failles, stries, sens de jeu, rejets): quelques précisions. *Comptes Rendus de l'Académie des Sciences*, **285**, 1309–1318.

ANGELIER, J. 1990. Inversion of field data in fault tectonics to obtain the regional stresses. III. A new rapid direct inversion method by analytical means. *Geophysical Journal International*, **103**, 363–376.

ANGELIER, J. & MECHLER, P. 1977. Sur une méthode graphique de recherche des contraintes principales également utilisable en tectonique et en séismologie: la méthode des dièdres droits. *Bulletin de la Société Géologique de France*, 7, **XIX**(6), 1309–1318.

BARGACH, K., RUANO, P., CHABLI, A., *ET AL.* 2004. Recent tectonic deformations and stresses in the frontal part of the Rif Cordillera and the Saïss Basin (Fes and Rabat regions, Morocco). *Pure and Applied Geophysics*, **161**, 521–540.

BOYER, S. E. & ELLIOTT, D. 1982. Thrust systems. *AAPG Bulletin*, **66**(9), 1196–1230.

BUTLER, R. W. H. 1982. The terminology of structures in thrust belts. *Journal of Structural Geology*, **4**(3), 239–245.

CAREY, E. 1979. Recherche des directions principales de contraintes associées au jeu d'une population de failles. *Revue de Géographie Physique et Géologie Dynamique*, **21**(1), 57–66.

CAREY, E. & BRUNIER, B. 1974. Analyse théorique et numérique d'un modèle mécanique élémentaire appliqué á l'étude d'une population de failles. *Comptes Rendus de l'Académie des Sciences*, **279**, 891–894.

DEMETS, C., GORDON, R. G., ARGUS, D. F. & STEIN, S. 1994. Effect of recent revisions to the geomagnetic reversal time scale on estimate of current plate motions. *Geophysical Research Letters*, **21**(20), 2191–2194.

EL HADDAOUI, Z. 2000. *Influence de la géométrie d'un bassin jurassique sur la propagation des chevauchements néogènes: geodynamique meso-cenozoïque des Rides Sud-rifaines (Maroc). Modélisation géométrique et numérique*. Thèse de 3ème cycle, Université Mohammed V, Rabat.

EL MOURABET, M. 1996. *Evolution structurale du Prérif occidental et des bassins de Saïss et du Gharb du Trias au Néogène basée sur les données de subsurface (sismique réflexion et gravimétrie)*. Thèse de 3ème cycle, Universitè Mohammed V, Rabat.

ETCHECOPAR, A., VASSEUR, G. & DAIGNIERES, M. 1981. An inverse problem in microtectonics for the determination of stress tensors from fault striation analysis. *Journal of Structural Geology*, **3**(1), 51–65.

GALINDO-ZALDÍVAR, J. & GONZÁLEZ-LODEIRO, F. 1988. Faulting phase differentiation by means of computer search on a grid pattern. *Annales Tectonicae*, **2**, 90–97.

GALINDO-ZALDÍVAR, J., GONZÁLEZ-LODEIRO, F. & JABALOY, A. 1993. Stress and paleostress in the Betic–Rif Cordilleras (Miocene to present-day). *Tectonophysics*, **227**, 105–126.

GARCÍA-DUEÑAS, V. & BALANYÁ, J. C. 1986. Estructura y naturaleza del arco de Gibraltar. *Maleo, Boletim Informativo da Sociedade Geológica de Lisboa*, **2**, 23.

HANCOCK, P. L. 1985. Brittle microtectonics: principles and practice. *Journal of Structural Geology*, **7**(3–4), 437–457.

JACKSON, J. & MCKENZIE, D. 1988. The relationship between plate motions and seismic moment tensors, and the rates of active deformation in the Mediterranean and Middle East. *Geophysical Journal of the Royal Astronomical Society*, **93**, 45–73.

MOREL, J. L. 1989. Etats de contraintes et cinématique de la chaîne rifaine (Maroc) du Tortonien à l'actuel. *Geodinamica Acta*, **3**(4), 283–294.

PETIT, J. P., RAYNAUD, S. & CAUTRU, J. P. 1985. Microtectonique cassante lors du plissement d'un conglomérat (Mio-Pliocéne du Haut Atlas–Maroc). *Bulletin de la Société Géologique de France*, **8**(3), 415–421.

RECHES, Z. 1978. Analysis of faulting in three-dimensional strain field. *Tectonophysics*, **47**, 109–129.

RECHES, Z. 1983. Faulting of rocks in three-dimensional strain fields. II Theoretical analysis. *Tectonophysics*, **95**, 133–156.

RUANO, P. & GALINDO-ZALDÍVAR, J. 2004. Striated and pitted pebbles as paleostress markers: an example from the central transect of the Betic Cordillera (SE Spain). *Tectonophysics*, **379**, 183–198.

SANZ DE GALDEANO, C. & ESTÉVEZ, A. 1981. Estriaciones tectónicas en cantos de conglomerados. Su estudio en las Depresiones de Granada y Guadix-Baza. *Estudios Geologicos*, **37**, 227–232.

SCHRADER, F. 1988. Symmetry of pebble-deformation involving solution pits and slip-lineations in the northern Alpine Molasse Basin. *Journal of Structural Geology*, **10**(1), 41–52.

SUTER, G. 1980. *Carte géologique de la chaîne rifaine à 1/500 000.* Notes et Mémoires du Service Géologique du Maroc, **245a**.

TABOADA, A. 1992. *Modélisation numérique en tectonique*. PhD thesis, University of Montpellier II.

VANN, R. I., GRAHAM, R. H. & HAYWARD, A. B. 1986. The structure of mountain front. *Journal of Structural Geology*, **8**(3–4), 215–227.

ZIZI, M. 1996. *Triassic–Jurassic extensional systems and their Neogene reactivation in north-eastern Morocco (the prerifaines ridges and Guercif basins)*. PhD thesis, Rice University, Houston, TX.

Tectonic wedge escape in the southwestern front of the Rif Cordillera (Morocco)

A. CHALOUAN[1], J. GALINDO-ZALDÍVAR[2], M. AKIL[1], C. MARÍN[3], A. CHABLI[1], P. RUANO[4], K. BARGACH[1], C. SANZ DE GALDEANO[5], M. BENMAKHLOUF [2,6], M. AHMAMOU[1] & L. GOURARI[7]

[1]*Département des Sciences de la Terre, Faculté des Sciences, Université Mohammed V-Agdal, BP 1014, Rabat, Morocco (e-mail: chalouan@fsr.ac.ma)*

[2]*Departamento de Geodinámica, Universidad de Granada, 18071, Granada, Spain*

[3]*Instituto Geológico y Minero de España, Río Rosas 23, 28003 Madrid, Spain*

[4]*Institute for Crustal Studies, University of California, Santa Barbara, CA 93106-1100, USA*

[5]*Instituto Andaluz de Ciencias de la Tierra, CSIC-Universidad de Granada, 18071, Granada, Spain*

[6]*Département de Géologie, Faculté des Sciences de Tétouan, Université Abdelmalek Essaadi, Tétouan, Morocco*

[7]*Département de Géologie, Faculté des Sciences Dhar el-Mashraz, Université Sidi Mohamed Ben Abdellah, Fès, Morocco*

Abstract: The Rif Cordillera is a part of the Alpine orogenic arc in the Western Mediterranean, which was developed by the interaction of the westward motion of the Alboran Domain between the converging Eurasian and African plates. The Prerif Ridges, located along the southwestern front of the Rif, are south-vergent folds that are in places associated with faults affecting Jurassic to Quaternary sedimentary rocks and slope breccias that evidence the deformations that were active over the Neogene–Quaternary period. The different southward or southwestward displacement of each Prerif Ridge is related to the development of frontal and lateral ramps, which may or may not reach the surface. Oblique shortening may be explained by southwestward escape of large tectonic wedges, bounded by large strike-slip faults: the North–Middle Atlas fault which extends northward into the Alboran Sea, the Fez–Tissa–Taïneste fault, the Bou Draa–Sidi Fili fault, the Jebha fault and the Fahies fault. The relative displacement of these tectonic wedges toward the SW may explain the NNE–SSW to ENE–WSW compression observed in the Rif front and in the northern part of its Meseta–Atlas foreland.

The Betic–Rif Cordilleras developed in the Western Mediterranean as a consequence of the relative motion of the African and Eurasian plates, with a recent NW–SE convergence of 4 mm a^{-1} (De Mets *et al.* 1990). The western part of these cordilleras forms an arc produced by the westward motion of the relatively rigid Alboran Domain, located in the internal part of the tectonic arc, between the two plates (Fig. 1). The Alboran Domain (García-Dueñas & Balanyá 1986) is an independent tectonic element formely known as the 'Alboran microplate' (Andrieux *et al.* 1971), which at present is undergoing internal deformation. Changes of the relative motion of the three main tectonic plates are reflected by overprinted deformations, well recorded in the Rif Cordillera, and in particular in its frontal part (Frizon de Lamotte *et al.* 2000; Chalouan *et al.* 2001) and by the development of the arcuate belt (Platt *et al.* 2003).

The front of the Rif Cordillera includes the External Prerif (the 'Nappe Prérifaine') and the overthrusting Rif thrust sheets, which crop out towards the inner part of the Cordillera (Fig. 2). The age of the main deformations responsible for the thrust sheet emplacement in this region is younger towards the front, starting from the Late Miocene (Tortonian–Messinian), with the displacement of the Rif over its Meseta–Atlas foreland, and the development of thrusts in the frontal part of the Prerif Ridges. In addition, the Prerif Ridges have undergone a late deformation (Miocene–present) that affected the sediments of the Neogene–Quaternary basins, between the Rif and the foreland (Feinberg 1986;

From: MORATTI, G. & CHALOUAN, A. (eds) 2006. *Tectonics of the Western Mediterranean and North Africa.* Geological Society, London, Special Publications, **262**, 101–118.
0305-8719/06/$15.00

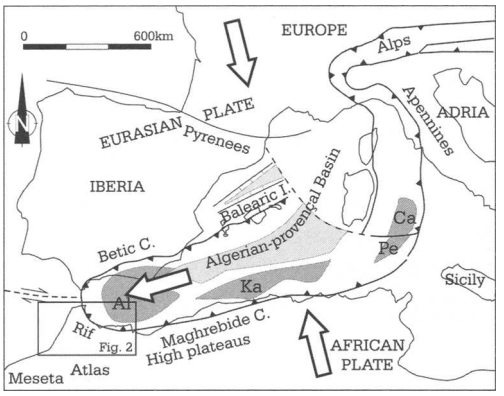

Fig. 1. Main tectonic elements in the Western Mediterranean since the Early Miocene. Dark grey, Alkapeca derived terranes: Al, Alboran; Ka, Kabylias; Pe, Peloritani; Ca, Calabria. Light grey, deep basins.

Samaka *et al.* 1997). These regional deformations are associated with an anticlockwise rotation of the trend of compression (Morel 1988; Aït Brahim 1991). Whereas the Tortonian deformations are related to a NE–SW-oriented compression, the Messinian ones are related to a north–south-trending compression, which, during the Pliocene and the Quaternary, rotated to NNW–SSE, in agreement with the trend of the recent convergence between the African and Eurasian plates.

In this framework, the lateral escape tectonics may be a process of great importance during the development of the cordillera. According to Royden (1993), escape tectonics may occur in a direction oblique or orthogonal to the plate convergence in zones of relatively thin continental crust. In this framework, escape tectonics may develop from an initial stage involving subduction with trench retreat (rollback subduction).

The aim of this paper is to analyse the compressional and extensional deformations of the southwestern part of the Rif mountain front (External Prerif) represented by the Prerif Ridges' folds and thrusts, the Plio-Quaternary sediments deposited in the foreland basin (Saïss Basin) and the foreland basement formed by the northern Meseta and Middle Atlas. The recent tectonic structures that affect rocks of Pliocene to Quaternary age show evidence of variable trends of compression (NNW–SSE, north–south and NE–SW) related to the activity of major crustal faults. These data lead us to propose the southwestward lateral escape of tectonic wedges bounded by crustal transcurrent and thrust faults in the Rif Cordillera. The deformation of its frontal part in a skin tectonic model is a consequence of the interaction of the minor blocks located between the Eurasian and African plates.

Geological and tectonic setting

The development of the Rif Cordillera is the consequence of the overprinting of several Alpine deformations, sometimes on Variscan structures, affecting its Internal and external zones to a different extent. Whereas the internal zone of the Rif Cordillera is formed by Palaeozoic and Mesozoic sequences that are partially affected by Alpine metamorphism, the external zone is made up of Mesozoic and Cenozoic sedimentary rocks including calcareous and marly series. From the inner to the outer parts of the External Rif, three tectonic areas are differentiated: the Intrarif, the Mesorif and the Prerif zones (Fig. 2). Between the internal and external zones, flysch nappes overthrusting the Neogene metamorphic rocks of the Ketama unit crop out.

The internal zone, comprising the Sebtide and Ghomaride metamorphic complexes, underwent the main Alpine deformation during the Eocene–Late Oligocene (Kornprobst 1974; Chalouan *et al.* 2000, 2001, 2003; Chalouan & Michard 2004). The ductile and brittle deformations that developed during this stage mainly consist of folds and thrusts, with main north–south to NNW–SSE trends and a west to SW vergence. In the Sebtide units, the metamorphism related to these deformations reaches blueschist and eclogite facies (Goffé *et al.* 1997; Bouybaouene *et al.* 1998), confirming that HP/LT metamorphic conditions were attained in a subduction zone (Chalouan *et al.* 2001, 2003).

The external zone, located south of the Jebha fault zone (Fig. 2), underwent main Alpine deformations mostly during the Late Tortonian. These deformations developed east–west-oriented structures including folds, thrusts and foliation. However, these structures locally show a north–south preferred orientation: (1) along the western Mesorif, where Ben Yaïch (1991) described west-vergent folds and thrusts that deform the Mesorif and Intrarif units of Loukkos and external Tangier; (2) in the Ouezzane thrust sheets, located north, west and south of Ouezzane (Fig. 2), where Tejera de León (1993, 1997) described thrusts and folds that deform Eocene to middle Miocene rocks; (3) along the Habt thrust sheet and the Intrarif in the region of Ksar El Kebir–Arbaoua; this region was studied by Zakir (2004) and Zakir *et al.* (2004), who noted the presence of ramps and accommodation folds.

The foreland cover involved in the Rif frontal thrust deformations, and that constitutes the Prerif Ridges, is affected by thrusts and fold-related faults of east–west (Zarhoun, Trhatt and Zalagh), NW–SE (Kefs and Kannoufa), north–south (Tselfat and Outita) and NE–SW (Bou Draa) orientations, forming two large arched structures (Fig. 3).

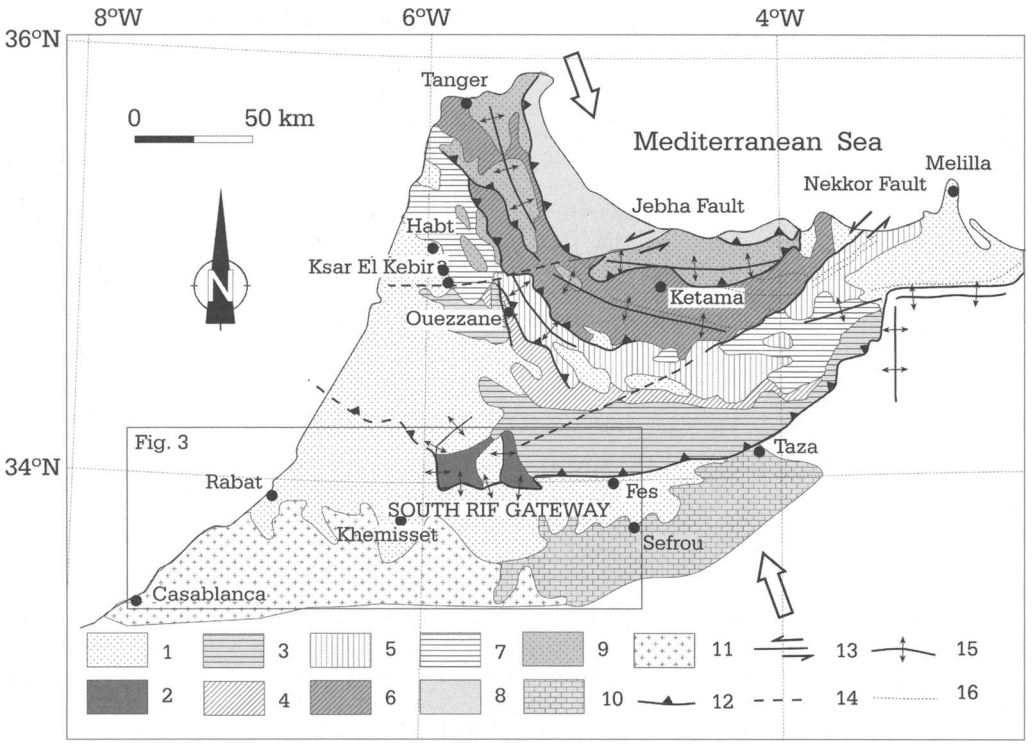

Fig. 2. Main Alpine structures of the Rif Cordillera. 1, Saïss–Gharb–Maamoura Neogene foreland basins; 2, Prerif Ridges; 3, External Prerif (Prerif Nappe and Rifian Ouezzane thrust sheets); 4, Internal Prerif; 5, Mesorif; 6, Intrarif (Ketama metamorphic unit and Tangiers–Loukkos unit); 7, Rifian thrust sheets; 8, internal zones; 9, flysch nappes; 10, Middle Atlas; 11, Meseta; 12, thrust; 13, strike-slip fault; 14, supposed fault; 15, large antiform; 16, fold trace orientation.

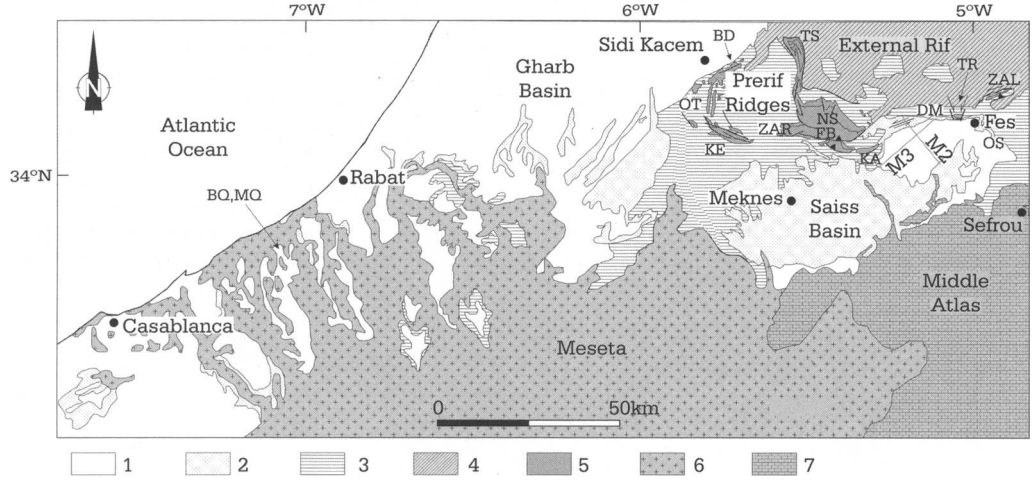

Fig. 3. Geological sketch of the southwestern Rif front and its Meseta–Atlas foreland. 1, Quaternary sediments; 2, Pliocene marine and lacustrine sediments of Saïss Basin; 3, Upper Miocene rocks; 4, External Prerif (Prerif Nappe and Rifian Ouezzane thrust sheets); 5, Prerif ridges; 6, Meseta foreland; 7, Middle Atlas foreland. BD, Bou Draa ridge; BQ, Brahma quarry; DM, Draa el Merga; FB, Fert el Bir ridge; KA, Kannoufa ridge; KE, Kefs ridge; MQ, Mjeddba quarry; NS, Dehar en Nsour ridge; OS, Oued Sebou; OT, Outita ridge; TR, Trhatt ridge; TS, Tselfat ridge; ZAL, Zalagh ridge; ZAR, Zarhoun ridge.

Recent compressional deformations in the Rif front and in its Meseta–Middle Atlas foreland

The analysed sectors are located along: the front of the Prerif (External Prerif or Prerif Nappe) (Figs 2 and 3); the Prerif Ridges, and particularly their southern and western fronts; the northern border of the South Rif gateway, in particular the Saïss Basin; the Atlas foreland in the Sefrou region; and the Mesetian foreland in the Casablanca region (Fig. 3). The determination of palaeostresses has been done taking into account the major and minor faults measured along large distances. Detailed analyses were possible only in some selected outcrops, such as the Jbel Trhatt or the Plio-Quaternary quarries between Casablanca and Rabat.

Rif front and Prerif Ridges

Jbel Zalagh, located NE of Fez (Fig. 4), is an ENE–WSW-trending narrow elongated Prerif ridge, formed by Jurassic and Tertiary rocks cropping out along an antiform. The Jurassic formations consist, from bottom to top, of 200–300 m of Lower Liassic crystalline, massive dolostones (Faugères 1978), Middle Liassic well-stratified limestones (60–100 m) overlain by marly limestones with chert (15 m), and finally marls with intercalations of limestone (60 m) of Late Liassic–Dogger age. The Tertiary formations are, from bottom to top, molasse formed by marly sands and conglomerate, white marls unconformably overlying the molasse and locally lying on the Jurassic rocks, the complex Prerif Nappe, Messinian marls that appear locally on the southern side close to Aïn Laaleg (Wernli 1988), and finally a Plio-Quaternary conglomeratic formation on top that is sometimes unconformable on the Jurassic Zalagh limestones.

Faugères (1978) considered Jbel Zalagh to be a southward very steeply dipping monoclinal structure, bounded to the south and to the north by two almost vertical N70°E-oriented faults. The northern

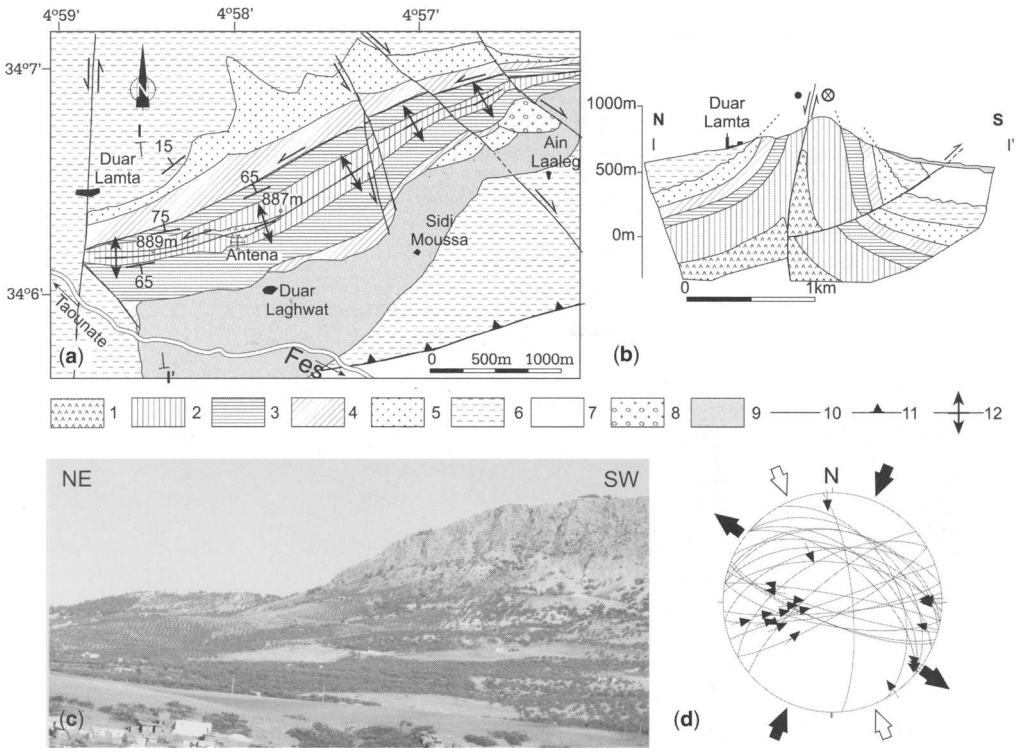

Fig. 4. Jbel Zalagh. Geological map (**a**) and cross-section (**b**). 1, Triassic rocks; 2, lower Liassic dolostones; 3, middle Liassic limestones; 4, upper Liassic–Bajocian marls and limestones; 5, upper Miocene molasse; 6, upper Miocene marls; 7, upper Miocene Prerif Nappe; 8, Quaternary slope breccias; 9, Quaternary sediments; 10, fault; 11, thrust; 12, anticline. (**c**) View of fault scarp in the northern limb of Zalagh ridge. (**d**) Stresses and measured microfaults, equal area projection, lower hemisphere. Black arrows, oldest stresses; white arrows, youngest stresses.

fault has been considered by Moratti *et al.* (2003) as an active fault related to a NNE–SSW compression that produced a sharp scarp (Fig. 4c), affecting recent deposits, and responsible for the seismic activity of the region. Structural analysis of this sector shows that Jbel Zalagh is, rather, a close to tight and faulted fold (Fig. 4). The southern limb of the fold occupies the whole southern side of the crest, and partially its summit. The hinge of the fold appears only toward the summit. The northern limb of the fold appears in the central and eastern part of the northern side of the crest. On the other hand, this limb is partially absent in the western region as a result of the N70°E-fault located along the fold (Fig. 4). In addition, the Jbel Zalagh anticline is affected by ENE–WSW south-verging reverse faults and by NW–SE dextral faults, mainly in the eastern extremity. The reverse faults could be interpreted as frontal ramps that formed simultaneously with the main fold in a NNW–SSE compressional deformation.

The two main fault sets recognized in the region show evidence of recent activity. The N70°E fault of the northern side has a high dip (70°–80° north or south) and a main horizontal sinistral slip with a minor vertical component that downthrows the northern block. This fault is of Quaternary age (Moratti *et al.* 2003), and has been active after the development of the fold. The N170°E–N30°E sinistral and N135°E–150°E dextral faults are even more recent, as they affect the N70°E fault and show Quaternary slope deposits on the southern side of Jbel Zalagh. Microtectonic analysis of these faults suggests that the trend of the maximum compressional axis (σ_1) responsible for the oldest N70°E fault was NNE–SSW, whereas the second stage, responsible for the strike-slip transversal faults, was a NW–SE-oriented compression (Fig. 4).

Jbel Trhatt, located west of Fez, is an east–west-trending anticline resulting from a recent north–south shortening, affecting Jurassic and Miocene series (Fig. 5). Its structure has similarities to that of Jbel Zalagh, but without outcrops of the lower–Middle Liassic series, which are known only from boreholes (Faugères 1978). In the

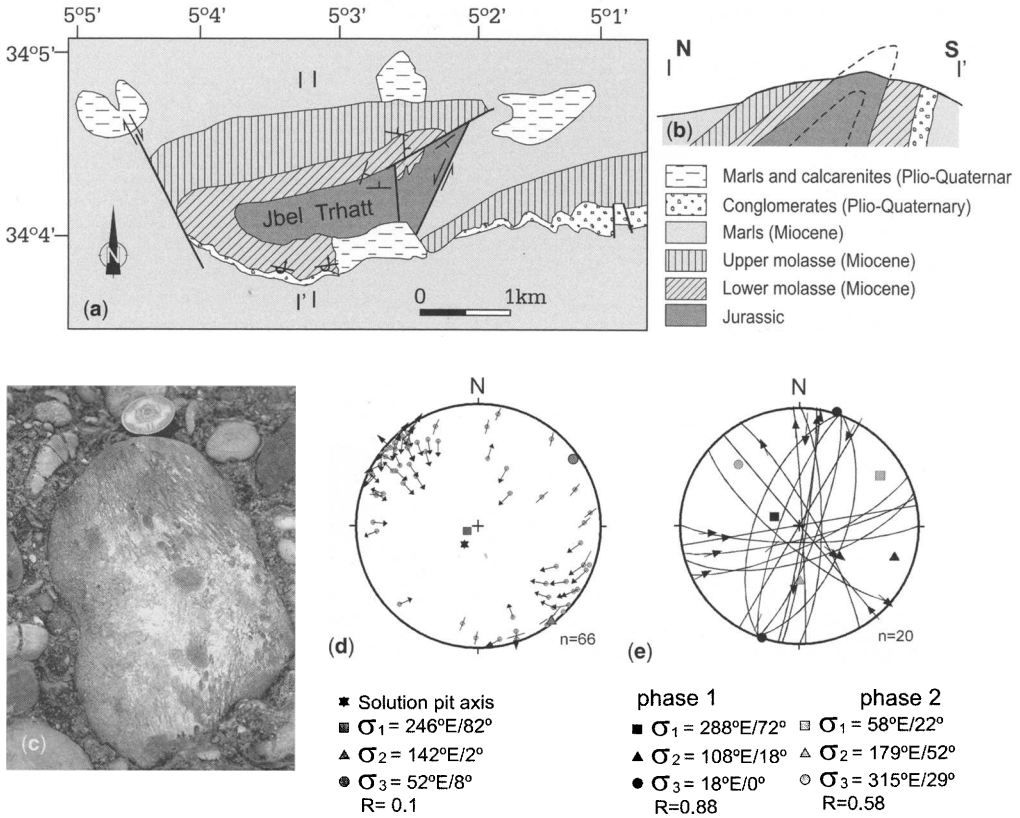

Fig. 5. Jbel Trhatt. Geological map (**a**) and cross-section (**b**). (**c**) Field view of striated pebbles. (**d**) Palaeostress determination from striated pebbles. (**e**) Palaeostress determination from microfaults, lower hemisphere, equal area projection. *n*, number of data; *R* (axial ratio) = $[(\sigma_2 - \sigma_3)/(\sigma_1 - \sigma_3)]$.

southern limb of this south-verging anticline, almost vertical or overturned Plio-Quaternary conglomerates, marls and limestones overlie the previous series with a low-angle unconformity. The conglomerate mainly consists of rounded calcareous pebbles. Analysis of striations and solution pits in pebbles from the southern part of Jbel Trhatt reveals, for each studied pebble, two or three palaeo-states of stress, with a main subvertical compressional axis (Fig. 5) (Bargach *et al.* 2004; Ruano *et al.* 2006), or northward-inclined axes, which, when folding is restored, point to a north–south-trending shortening. The Jbel Trhatt anticline is bounded to the west by a NW–SE dextral fault, and, to the east, by a NNE–SSW sinistral fault (Fig. 5). This pattern indicates a Quaternary push of this hill southward. The N30°E sinistral fault displaces Jbel Trhatt from Jbel Zalagh by 5 km. These faults also appear to be related to a north–south compression.

Jbel Kannoufa is formed by a monocline of Jurassic rocks gently dipping northward (Fig. 6a). However, it shows locally, in its southern front, parts of an anticlinal hinge and its steeply dipping southern limb. The Jurassic series of Jbel Kannoufa consists of thick Lower Liassic massive dolostones and limestones, and middle Liassic bioclastic and oolitic limestones (Faugères 1978; Bargach *et al.* 2004). Jbel Kannoufa is an inclined anticline clearly associated with longitudinal reverse faults (Bargach *et al.* 2004). This ridge has an east–west to ESE–WNW elongation and shows very high asymmetry, with a southward vergence. The southern limb is cut by WNW–ESE reverse faults (Fig. 6c) and longitudinal sinistral strike-slip faults (Fig. 6d) that affect the Miocene marls and

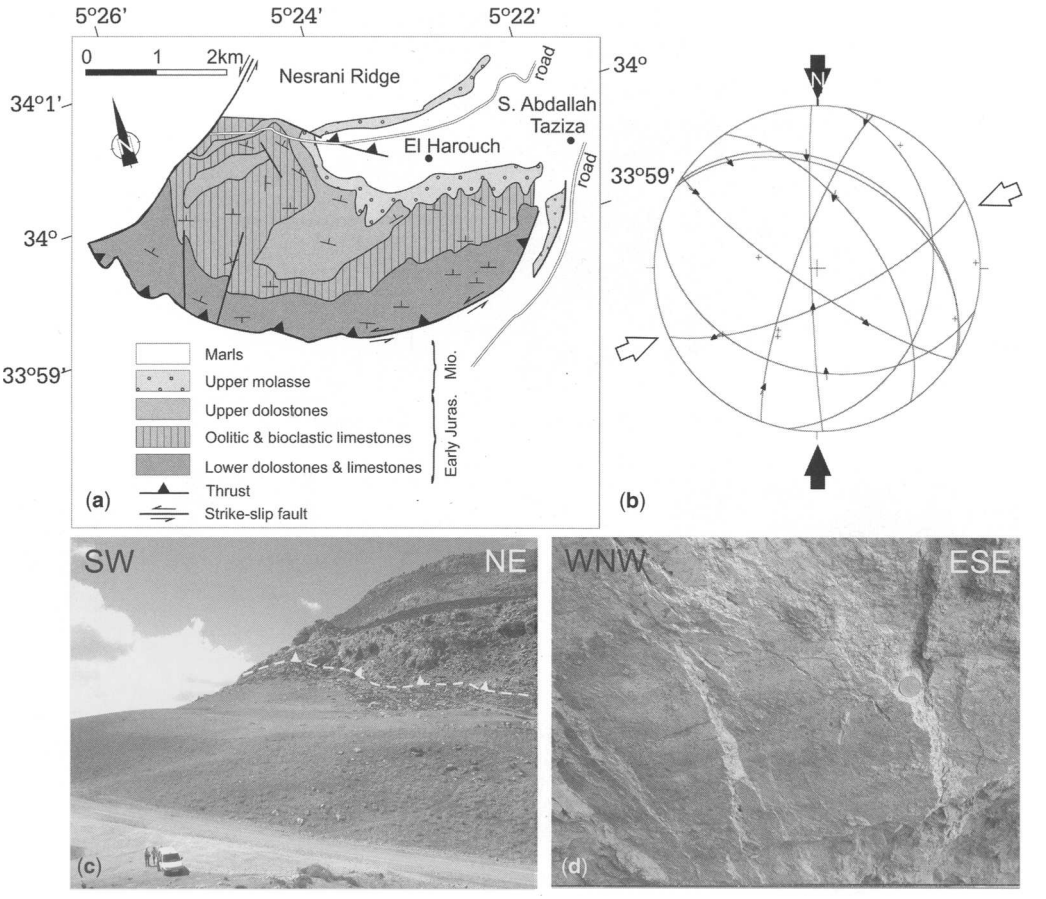

Fig. 6. Jbel Kannoufa. Geological map (**a**), stresses and measured microfaults (**b**), equal area projection, lower hemisphere. Black arrows, probable oldest compression; white arrows, probable youngest compression. (**c**) Field view of the frontal thrust. (**d**) Detailed view of a sinistral fault observed in the frontal part of the ridge.

molasse, the Saïss Plio-Quaternary lacustrine formations and, locally, even late Quaternary terraces. The microstructures show north–south as well as east–west to ENE–WSW-oriented main compressions (Fig. 6b).

Jbel Zarhoun forms an important east–west-oriented relief dominating the Meknes flat region. It is a faulted east–west elongated anticline, with a large northern low-dipping limb and a reduced southern flank, where frontal longitudinal faults are well developed (Fig. 7a). The Jurassic series consist of Lower and Middle Liassic limestones and dolostones, Toarcian–Aalenian marls and limestones, and Bajocian grey marls and coarse sandstones. The Jurassic series is covered by middle Miocene molasses and Upper Miocene white marls. Jbel Zarhoun is overthrust to the north by the thrust sheets forming the Jbels Dhar Nsour and Fert El Bir, which are also formed by Jurassic to Miocene Prerif Ridge rocks. Longitudinal frontal faults from the southern boundary of the Jbel Zarhoun Ridge, and displace the Jurassic formations onto the Upper Miocene marls and the lacustrine Plio-Quaternary rocks of the Saïss Basin. The east–west longitudinal faults are south-verging reverse faults, sometimes cross-cut by high-angle sinistral strike-slip faults (Fig. 7). The main compressional stresses deduced from sinistral motions have an ENE–WSW trend.

The Bou Draa and Outita ridges are situated SE of Sidi Kacem, in the northwestern extremity of the Prerif Ridges, delimited by N50–70°E-oriented faults from the Neogene Gharb basin (Fig. 3). They are NE–SW NW-verging anticlines. The Jurassic series cropping out in these ridges consists of Toarcian–Aalenian marls, limestones and sands, overlain by Bajocian sandstones, clays and dolostones. This series is unconformably covered by Upper Miocene molasse and white marls (Faugères 1978). The N50–70°E faults that form the northwestern

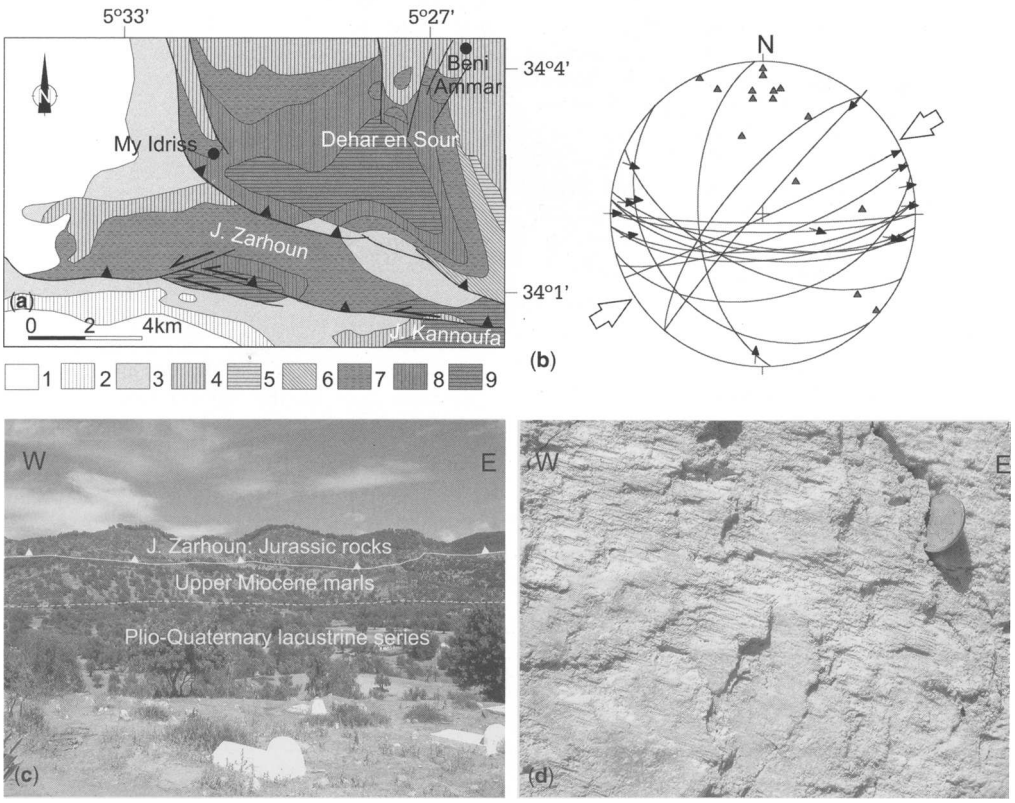

Fig. 7. Jbel Zarhoun. (**a**) Geological map. 1, Quaternary sediments; 2, Plio-Quaternary lacustrine sediments; 3, upper Miocene marls and conglomerates; 4, middle Miocene molasse; 5, Eocene marls; 6, Cretaceous marls; 7, Bajocian Zarhoun sandstones; 8, upper Liassic marls and limestones; 9, lower and middle Liassic limestones. (**b**) Stresses and measured microfaults, equal area projection, lower hemisphere. (**c**) Field view of the frontal thrust. (**d**) Detailed view of a sinistral fault observed in the frontal part of the ridge.

boundary of the ridges affect the Jurassic and Miocene rocks, and locally the Plio-Quaternary lacustrine formations (conglomerates and limestones) of the Saïss Basin. These are dextral strike-slip faults with a normal component when dipping NW, and a reverse component when dipping SE. This zone of shearing could be responsible for the rise and southward emplacement of the Prerif Ridges and for the 2000 m downthrow of the Gharb Basin. In seismic sections (Zizi 1996; Kenafi 2002), the fault zone of Bou Draa clearly appears as a system of very steep faults, Which first created a graben in which the Jurassic sediments deposited, and then underwent a tectonic inversion that produced the ridges. The Gharb Basin appears as a collapsed zone, its rear being compressed near the contact with the ridges of Bou Draa-Outita, and its centre and frontal part in extension (Flinch 1993; Flinch 1996). The microtectonic measurements taken along this zone point to two deformation stages: an ENE–WSW-oriented compression and a NNW–SSE-oriented extension (Fig. 8), which could be contemporaneous.

Along the South Rif gateway (Fig. 2), and especially in the northern border of the Saïss Basin, two outcrops have been studied: the Tensiftian conglomerates of Oued Sebou, and the lacustrine limestones of Draâ El Merga, respectively located 12 km to the ESE and 20 km WSW of Fez (Fig. 3). On the southern side of Oued Sebou (UTM, $x = 555.3$ km; $y = 381.6$ km) a fluvial conglomeratic formation of Quaternary (Tensiftian) age crops out (Gourari 2001), overthrust by middle Miocene grey marls of the Saïss Basin. The reverse fault shows an east–west-oriented surface of several hundreds of metres, dipping 50° north, and yielding striae oriented N150–160°E with a dextral component. The vertical displacement of this fault cannot be determined precisely, as the base of the Quaternary formation is not visible, but it is at least 20 m. This reverse fault indicates a NNW–SSE shortening.

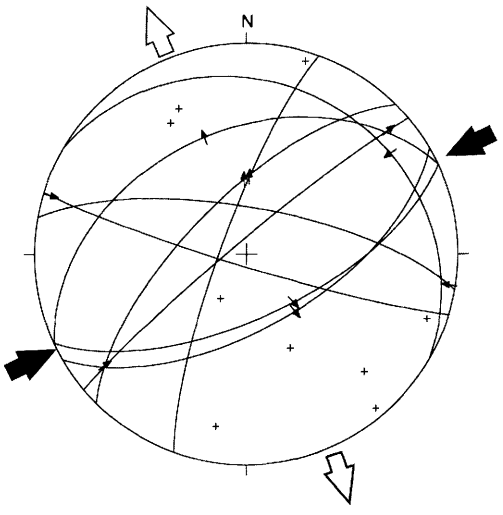

Fig. 8. Measured microfaults and stresses in Bou Draâ–Outita ridges, equal area projection, lower hemisphere. Black and white arrows indicate two stress phases.

The region of Draâ El Merga is characterized by N70–90°E-oriented areas of high relief where the Plio-Quaternary limestones of the Saïss lacustrine formation crop out. Ahmamou & Chalouan (1988) described N120–150°E kilometre sized en echelon folds, which are located in a N70–90°E narrow strip associated with sinistral faults and were reactivated during the Quaternary by a NNE–SSW regional shortening. This fault zone is also indicated by the seismic profiles (Fig. 9) that cross this region (Zizi 1996), which show two subparallel fault planes delimiting a shear zone in which the shallowest formations (Plio-Quaternary lacustrine rocks) appear in a very open anticline. In its NE extremity, this fault seems to affect shallower levels up to the Tertiary cover.

Meseta–Middle Atlas foreland

The recent Plio-Quaternary compressive deformations have also been studied in the foreland, along the Middle Atlas and the Meseta. Sefrou (Fig. 3) is located in the northern extremity of the tabular Middle Atlas, where the subhorizontal Lower Liassic dolostones and limestones are covered by unconformable Plio-Quaternary lacustrine formations of the Saïss Basin or by the Quaternary fluvial or travertine formations (Charrière 1990; Gourari 2001; Ahmamou 2002; Hinaje 2004). The conglomerates and the lacustrine limestones of the Saïss Basin that crop out north of Sefrou, along the main road to Fez, are affected by east–west to NW–SE very open folds, indicating a north–south to NE–SW regional shortening.

In the Moroccan Meseta, near Casablanca, the Palaeozoic series is covered by Quaternary marine terraces and aeolian deposits. Six Quaternary marine terraces (Akil 1990; Chabli *et al.* 2003) and several aeolain deposits crop out in the quarries of Brahma and Mjeddba (Figs 3 and 10). These deposits, of early Quaternary (Messaoudien) and mid-Quaternary (Maarifien and Anfatien) ages, are affected by N90–110°E sinistral and north–south dextral strike-slip faults. The states of stress calculated from these faults indicate NNE–SSW, NE–SW and east–west compressive deformations (Fig. 10).

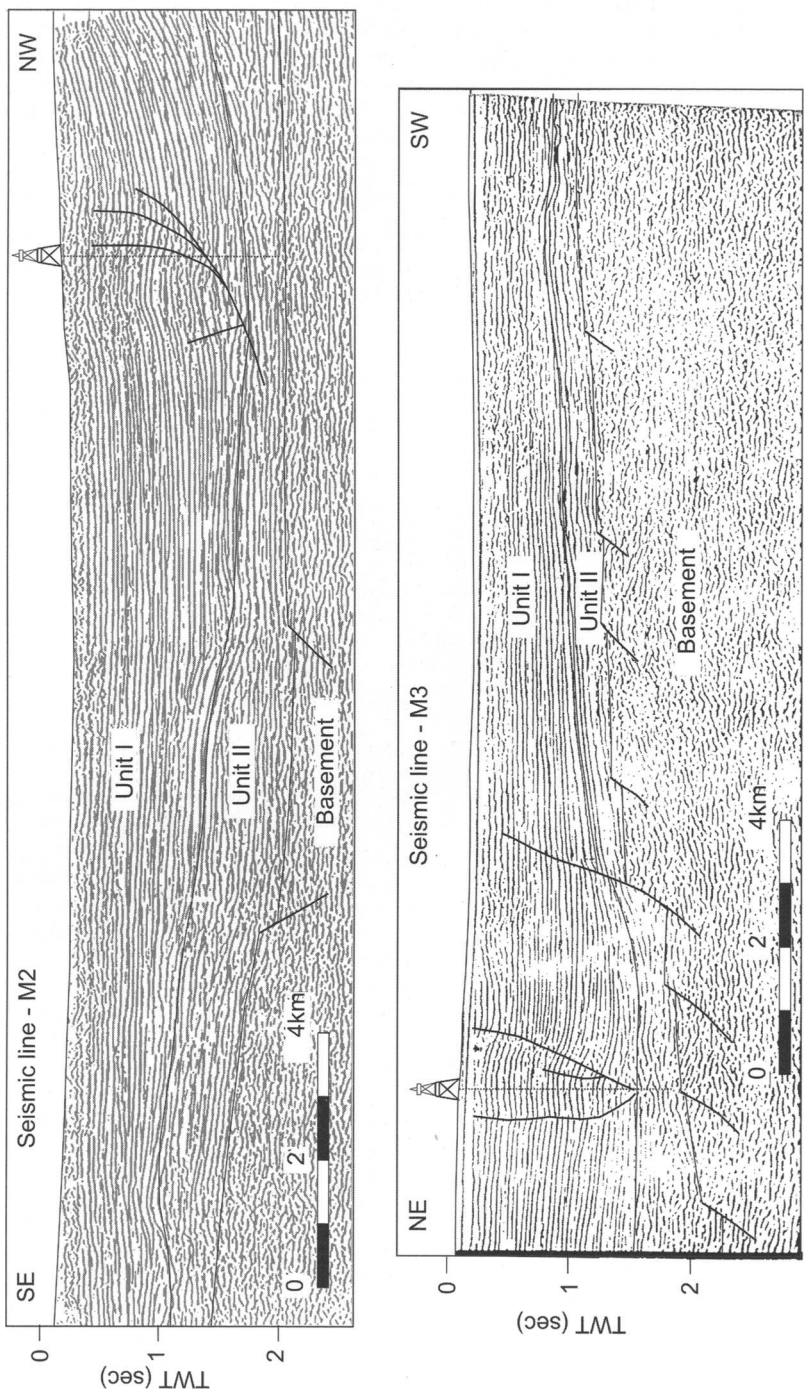

Fig. 9. Multichannel seismic profiles M2 and M3 in the eastern part of the Saïss Basin. Location shown in Figure 3. Unit I, Miocene, Pliocene and Quaternary rocks; Unit II, Mesozoic rocks. TWT, two-way travel time.

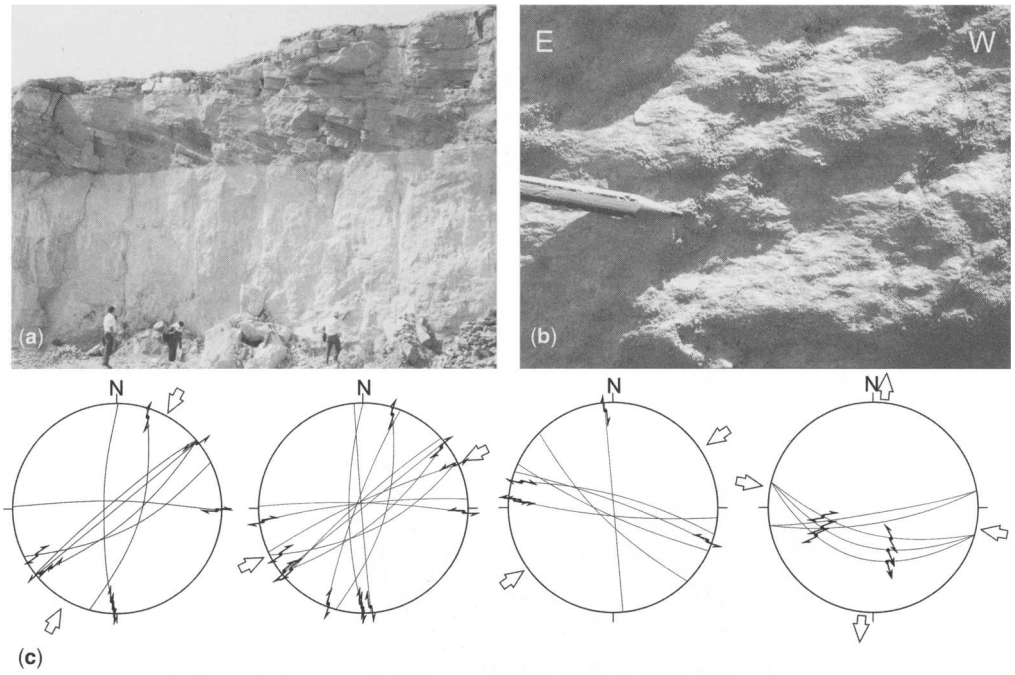

Fig. 10. Recent deformations in the Casablanca region. (**a**) Field view of the Quaternary marine and aeolian deposits affected by brittle deformations. (**b**) Detailed view of a sinistral fault. (**c**) Stresses and measured microfaults, equal area projection, lower hemisphere in different sectors of the Brahma and Mjeddba quarries in the lower and middle Quaternary sediments.

Main faults in the Rif Cordillera

The Rif mountain front can be regarded as a key area for understanding the evolution of the recent deformations related to the relative motion of the Eurasian, African and Alboran Domains. The results of our study indicate that this boundary zone, formed by the External Rif, the Prerif Ridges and the northern part of Meseta and Middle Atlas forelands, has undergone either simultaneous or successive north–south; NE–SW- and even east–west-trending shortenings (Fig. 11). The deformations of this boundary zone certainly resulted from a push of the Rif not only towards the south, but also towards the SW or even the west. These data cannot be considered in a single regional stress field, and for their adequate interpretation it

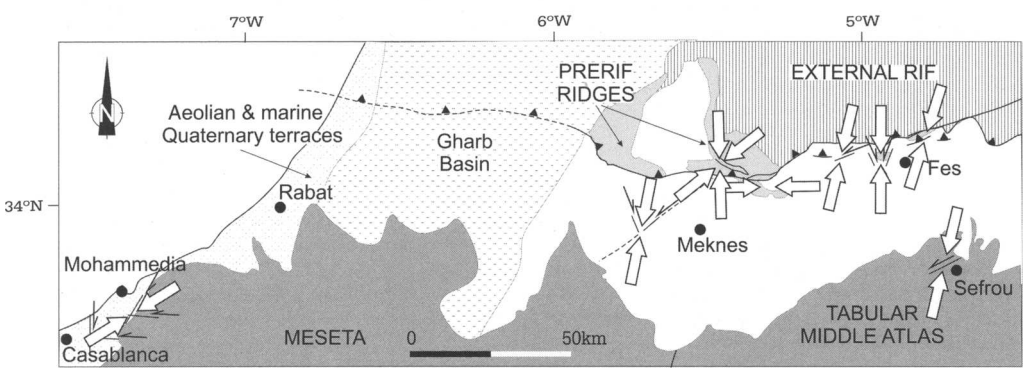

Fig. 11. Orientation of compressional stresses determined from the study of Quaternary structures in the Rif front and its Meseta–Middle Atlas foreland.

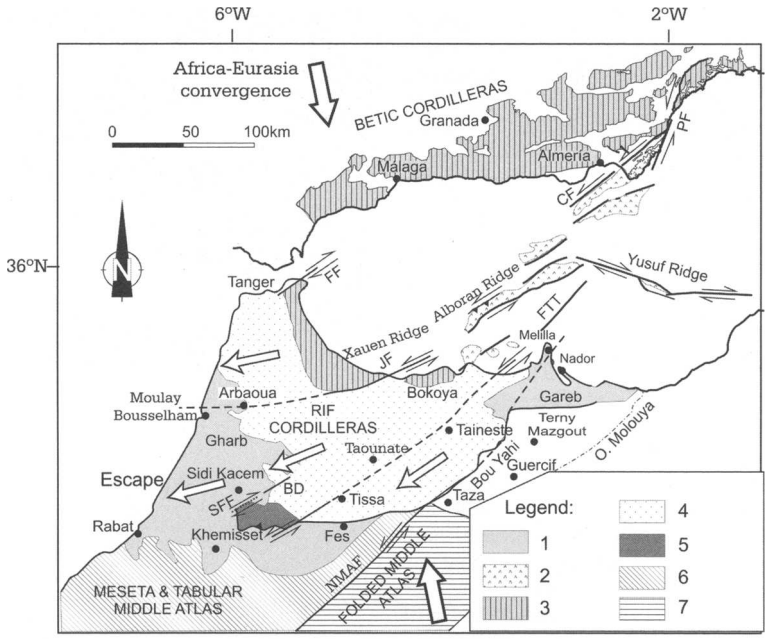

Fig. 12. Tectonic model of wedge escape in the Rif Cordillera. 1, Neogene and Quaternary basins; 2, Neogene volcanic rocks; 3, internal zones. 4, flysch nappes and External Rif; 5, Prerif ridges; 6, Meseta and Tabular Middle Atlas; 7, folded Middle Atlas. BD, Bou Draa fault; CF, Carboneras fault; FF, Fahies fault; FTT, Fez–Tissa–Taineste fault; JF, Jebha fault; NMAF, North–Middle Atlas fault; PF, Palomares fault; SFF, Sidi Fili–Bou Draa fault.

is necessary to take into account the features of the main crustal faults: those crossing the Rif chain and the Meseta–Middle Atlas Forelands (Fig. 12).

The North–Middle Atlas fault zone

The NE–SW-oriented North–Middle Atlas fault (NMAF) was defined by Colo (1961) as a major fault zone separating two different palaeogeographical domains: the tabular and the folded Middle Atlas (Figs 2 and 12). This fault zone, about 200 km long, develops between Taza to the north and the High Moulouya to the south. It is an old fault, which was active during the Liassic Atlas rifting and inherited from Variscan NE–SW structures (Laville & Piqué 1991). This fault shows a sinistral transpressional activity during the pre-Miocene structuring of the Middle Atlas (Robillard 1978, 1979; Charrière 1990). It was also active up to the Plio-Quaternary, as it deforms and tilts the Pliocene and Villafranchian formations (Martin 1981) and determines and deforms the volcanic Quaternary lava flows (Thomas & Fedan 1988), as also shown by palaeomagnetic studies (El Azzab & El Wartiti 1988). Harmand & Moukadiri (1986) suggested a model involving a sinistral motion of the NMAF during the Quaternary, related to the volcanic eruptions that exploited N170° E-oriented tension cracks. This fault has been described by some workers as a very important basement fault, continuing to Agadir in the south (Jacobshagen 1992), and it could be the source of the geothermal anomaly observed along this direction (Bahi *et al.* 1983). Bernini *et al.* (2000) associated this fault with a lineament that bounds and advances the Prerif with respect to the Middle Atlas in the Guercif Neogene basin and, according to Piqué *et al.* (1998), this fault zone behaved during the Neogene–Pleistocene period like a lithospheric mega-shear zone. In the Rif 1:500 000 geological map, the eastern boundary of the Rif, north of Taza, seems to coincide perfectly with the prolongation of the NMAF, which would therefore represent a sinistral lateral ramp of the Rif. The sinistral shift of the Rif front may be a consequence of the activity of this fault. Moreover, in the Terni–Mazgout area, the continuation of the Middle Atlas to the north of the Guercif Basin, as well as in the Gareb Massif, situated south of Nador, Hervouët (1985) pointed out north–south (N170–20°E)- and NE–SW (N40°E)-oriented sinistral faults that affect the Plio-Quaternary lacustrine formations (Hamel 1971) and the Quaternary basalts aged 1.7–1.5 Ma, according to Cantagrel & Harmand (1984) and Harmand & Cantagrel (1984). The continuation

of this fault into the Alboran Sea north of Melilla is not well constrained, although Andeweg & Cloetingh (2001) proposed that it continues towards the Carboneras and Palomares faults in the east of the Betic Cordilleras, and forms the trans-Alboran Fault. However, the Alboran and Yussuf ridges, oriented N60°E and N100°E, interrupt its continuity (Fig. 12). This fault zone may also be considered as an active fault, as recent earthquakes in Nador in November and December 2004 reached magnitudes near five.

The Fez–Tissa–Taïneste fault zone

The Fez–Tissa–Taïneste fault zone (FTT) crops out between Fez and Taïneste, along the Fez–Tissa–Taounate road, and may extend as far as the Nekkor fault. This fault is emphasized by slices and tectonic horses of Triassic salts and gypsum, develops steep N50–70°E-oriented fault planes, and shows sinistral and dip-slip kinematic indicators. Fault planes are observed in Late Miocene formations (Tortonian marls of the Prerif Nappe and the middle Pliocene sands of Redom). The fault could be responsible for the 15 km sinistral displacement of the Prerif front west of Fez, of the overlying Ouezzane thrust sheet, and of the northern limit of the south Rif corridor (Fig. 12). This fault is offset by about 5 km in the northern prolongation of the N20–40°E probable sinistral fault zone that displaces Jbel Zalagh and Jbel Trhatt (Fig. 3). The FTT fault could be relayed southward by other sinistral faults of parallel direction, which appear in the Saïss Basin or are hidden under the lacustrine formations. Among these, the Draa El Marga fault, oriented N70°E (Fig. 9), which passes between Jbel Trhatt and Moulay Yakoub, has been described by Ahmamou & Chalouan (1988).

Morel (1988) extended this fault zone toward the SW as far as Meknes and toward the NE to the Oued Kert (the Meknès–Fez–Kert fault), with its end located west of Nador. According to Morel, the fault bounds the eastern metamorphic Mesorif (Temsamane unit) to the east.

The Bou Draa–Sidi Fili fault zone

The Sidi Fili fault is buried under the Neogene and Quaternary sediments of the Saïss–Gharb Basins, but can be observed on the seismic sections or inferred from boreholes (Feinberg 1986). This fault zone is oriented NE–SW, with a SE dip, and was active as a normal fault during the Triassic–Jurassic rifting. During the Tertiary compression, it was reactivated as a reverse fault, contributing to the development of the Prerif Ridges, mainly the western ridges of Bou Draa–Outita (Zizi 1996; Kenafi 2002).

The NE–SW dextral Bou Draa fault zone (BD), located a few kilometres east of Sidi Kacem and delimiting the western border of the Bou Draa ridge, is in continuity with the Sidi Fili fault zone (Fig. 12), which has led some researchers to relate them. These faults were active together, as a dextral lateral ramp, during the Tortonian–Messinian southwestward emplacement of the western Prerif Ridges. The most recent rocks affected by these faults are of Messinian age, but a dextral Plio-Quaternary reactivation is feasible, as the Plio-Quaternary lacustrine formations are tilted or overthrust at the front of the western ridges (Kefs, Kannoufa and Zarhoun jbels).

The Jebha fault zone

The N70°E-oriented Jebha fault zone (JF) forms the southern border of the northwestern internal Rifian Domain (Figs 2 and 12). It has a sinistral component and may represent a lateral ramp during the westward progression of the internal domain after the early Burdigalian (Olivier 1981). The structures of the Internal Rif (Ghomarides, Sebtides and Dorsal complexes) are interrupted and deformed along this fault zone. The minimum sinistral displacement of the fault zone is estimated at 50 km, taking into account the displacement of the Bokoya massif (Fig. 12). Seismic reflection profiles indicate an eastern continuation of this fault zone in the Alboran Sea, with the same orientation. It bounds the ridges of Xauen and Alboran, was reactivated as reverse (Bourgois *et al.* 1992; Comas *et al.* 1992, 1999) and sinistral faults with reverse vertical components (Chalouan *et al.* 1997), and affects Pliocene and even Quaternary formations (Chalouan *et al.* 1997).

The continuation of the Jebha fault toward the west is not very obvious. Several workers have assigned an important palaeogeographical role to this fault in the External Rif (Morley 1987, 1992; Tejera de León 1993, 1997), whereas others have pointed out deformations of the Tertiary outcrops of the External Rif (Morel 1988; Ben Yaïch 1991; Zakir 2004). Morel (1988) mapped east–west folds affecting the Early Pliocene formations in the westernmost prolongation of this fault, in the area of Moulay Bousselham (Fig. 12). On the other hand, in the region of Arbaoua, we observed N110–160°E reverse faults affecting the Villafranchian continental conglomerates that may be related to the prologation of the Jebha fault (Figs 2 and 12). The gravimetric map likewise suggests the continuity of this fault in the External Rif (Morley 1987). This fault zone was probably active as sinistral, but the Palaeozoic, Mesozoic and Cenozoic

(Eocene to early Miocene) formations of the Ghomarides–Sebtides are also affected by N70–90°E dextral wrench faults (Benmakhlouf *et al.* 2005).

The Fahiès fault zone

This fault zone, first described by Kornprobst (1974), is a NE–SW to ENE–WSW fault that extends 15 km, bounding the Internal Rif to the north (Fig. 12). It has a main dextral displacement and crosscuts the north–south-oriented structures of the Internal Rif, producing their clockwise rotation from N170°E to N20–30°E. The Predorsalian thrust sheet and the other flysch deposits (Tisirène and Beni Ider) are also truncated by this fault. According to Ben Yaïch (1981), the dextral slip of this fault zone was active after the flysch emplacement. In the Internal Rif, Kornprobst (1974) and Zaghloul (1994) have indicated that this dextral fault affected the already emplaced Ghomarides and Dorsal complexes, and the Sebtide units, which show an Aquitanian–Burdigalian (19–25 Ma) metamorphism.

Discussion

The new data presented in this paper mainly contribute to highlight the Plio-Quaternary evolution of the frontal part of the Rif and its foreland. These data are integrated into the evolution of the whole Rif Cordillera (Chalouan *et al.* 2001, 2003; Michard *et al.* 2002; Chalouan & Michard 2004).

East–west to NE–SW major sinistral fault zones, well developed in the central and eastern regions, deform the Rif Cordillera, and in some cases reach the frontal part. These faults have been active at least from the Early Miocene (Jebha fault) to the Messinian–Pliocene (Olivier 1981; Ahmamou & Chalouan 1987; Morel 1988; Bargach *et al.* 2004). Moderate activity of several faults has continued to the Plio-Quaternary (Jebha fault, Morel 1988; Chalouan *et al.* 1997), and other new fault zones have developed, such as the Fez–Tissa–Taïneste and Sidi Fili–Bou Draâ fault zones. Seismic data indicate that the latter two also affect the basement (Fig. 9; Zizi 1996). These crustal faults determined the southwestward displacement of the Prerif Ridges. The Fez–Tissa–Taïneste fault could also be a crustal fault, characterized by horses and thrust sheets of deformed Triassic marly and evaporitic rocks. Its southwestern part is recognized in seismic profiles (Benmakhlouf 2001). This fault may be responsible for the development of the N120°E en echelon folds observed in the sedimentary cover in the Draâ El Merga area (Fig. 3, Ahmamou & Chalouan 1988).

The major fault zones affecting the Rif Cordillera have orientations between N45°E and N70°E. The NE–SW fault zones are located in the eastern Rif, whereas the ENE–WSW ones are mainly located in the northern and western regions, with a progressive change in trend between these two extreme orientations. The fault zones recognized in the Rif Cordillera (e.g. Sidi Fili fault, Morel 1988; Zizi 1996) extend southwestward beneath the Saïss Basin and the western Meseta. Other parallel faults can be interpreted from the seismic reflection profiles in the northern front of the Prerif Ridges and in the Gharb Basin (Flinch 1993; Zouhri *et al.* 2002), possibly representing deep faults formed during the Variscan orogenesis.

The eastern boundary of the Rif Cordillera is a N40°E-trending contact with the foreland (represented by the Neogene Guercif Basin, and the front of Jurassic and Palaeozoic rocks of BouYahi–Terni–Mazgout and Gareb massif; Fig. 12). This limit is located in the continuation of the North–Middle Atlas fault zone. The mainly sinistral transcurrent regime of these major fault zones during the Quaternary is supported by several studies (Charrière 1990; Charroud 1990; Andeweg & Cloetingh 2001); Andeweg & Cloetingh proposed that the North–Middle Atlas fault zone extends into the Rif foreland Bou Yahi fault zone and to the sinistral faults in the Betic Cordillera. Those workers indicated that during the Plio-Quaternary, the central and western Betic Cordilleras, the Alboran Sea, the Rif (Fig. 1), the Moroccan Meseta and the Middle Atlas (Fig. 2) were all displaced southwestward with respect to the surrounding Atlas, high plateaux, eastern Alboran Sea and eastern Betic Cordilleras (Sanz de Galdeano 1990*a*,*b*; Jacobshagen 1992).

Taking into account the field data presented in this paper and the previous studies on the region, it is considered that the transcurrent and thrust-related displacements along large fault zones determined the tectonic evolution of the Rif Cordillera during the Miocene and the Quaternary. The main fault zones, oriented ENE–WSW (e.g. Jebha) in the northwestern Rif, and NE–SW in the SE (e.g. Fez–Tissa–Taïneste, and North–Middle Atlas), generally have a sinistral strike-slip motion, leading to the southwestward displacement of the tectonic units. Whereas towards the internal zone, in the northern part of the Rif, these major faults probably affect the whole crust, towards the mountain front, most of the faults affect only the detached cover on a Variscan basement and are related to a thin-skin tectonics. In most cases, there are not enough geophysical data to study in detail the prolongation at depth of the faults.

However, some of the main fault zones may affect the whole Rif Cordillera and foreland crust.

The Jebha fault has been interpreted as a lateral ramp (Andrieux *et al.* 1971) of the Internal Rif, but geological and gravimetric (Morley 1987) studies suggest that this fault continues towards the WSW into the External Rif and the foreland, and may be considered a Variscan–Atlas crustal fault (Menvielle & Le Mouël 1985). This fault separates a northern block with a relatively thin continental crust from the continental crust with normal thickness of the African margin (Van Den Bosch 1981; Morley 1987; Tejera de León 1997; Chalouan *et al.* 2001). On the Atlantic margin, this fault coincides with a zone of transition between oceanic crust to the north and continental crust to the south. Several workers (Morley 1987; Ben Yaïch 1991; Tejera de León 1997; Zakir *et al.* 2004) have suggested that this fault affects the crust and would have both influenced sedimentation and provoked deformations from the late Mesozoic to the Miocene, or even later, during the Alpine deformations of the Rif. Morel (1988) related the Plio-Quaternary deformations affecting the region of Moulay Bousselham and Arbaoua (Fig. 12) to this fault. The North–Middle Atlas fault extends southward to the Moroccan Atlantic coast and is considered to be a Variscan crustal fault (Bahi *et al.* 1983; Charrière 1990; Jacobshagen 1992; Bernini *et al.* 2000) reactivated during the Mesozoic rifting and the Tertiary–Quaternary north–south compressions. These two trans-Rif crustal faults extend also northeastward to the Alboran Sea and are associated with the main deformations in the Alboran Ridge, where Plio-Quaternary sediments are affected by folds and east–west thrust faults (Tesson *et al.* 1987; Maldonado *et al.* 1992; Chalouan *et al.* 1997, 2001; Comas *et al.* 1999).

The shortening caused by the Eurasia–Africa convergence was accommodated by deformation in the Alboran Sea and in the External Rif, represented by transfer and reverse faults in the Mesozoic and Cenozoic cover detached along the Triassic evaporite and clay levels (Zizi 1996; Samaka *et al.* 1997), and by the southwestward displacement of thick crustal wedges along deep faults (such as the Jebha fault and NMAF) affecting the central–eastern Rif and Moroccan Meseta.

According to Platt *et al.* (2003), the Alpine late Miocene folds and thrusts of the External Rif were initially N150°E-oriented in the central and eastern Rif, and became east–west-oriented after undergoing an anti-clockwise rotation of up to 55°, which is more intense near the Jebha fault. This could be due to the southwestward displacement of the thick crustal wedge bounded by the Jebha fault and NMAF.

The first stages of wedge escape probably occurred in the Rif Cordillera between the early Miocene and the Pliocene, as a result of the activity of the Jebha and Nekor faults. The activity of these structures allowed the development of the central Rif arc, located in the Mesorif and also in the post-thrust basins of Taounate, with a preferred NW–SE orientation, but with curved fold axes (Morel 1988; Samaka *et al.* 1997; Samaka 1999). During the final stages of this southwestward escape, the sinistral faults of Sidi Fili–Bou Draâ, Fez–Tissa–Taïneste, and probably the North–Middle Atlas–Melilla fault zone (Jacobshagen 1992; Bernini *et al.* 2000; Sani *et al.* 2000; Andeweg & Cloetingh 2001), would have been the most active ones, relaying the previous faults. This period produced the southwestward expulsion of the Prerif Ridges, related to the development of the two tectonic arcs, the displacement of the Prerif Nappe and its emplacement in the Gharb–Maamoura Basin. The southwestward expulsion of the Rif is partially accommodated by the thrusts located at the front of several Prerif Ridges (Jbels Kannoufa and Zarhoun), or by blind thrusts related to south-vergent folds (e.g. Jbel Trhatt). In front of these ridges, north–south, NE–SW and even ENE–WSW compressional stresses have been determined from mesostructural sites of measurement.

The few N70–90°E dextral fault planes observed along the Jebha fault zone are an indication supporting that this large fault zone was not only active with a sinistral regime, as a result of the fault position in the centre of the Rif. As a sinistral fault, it allows the escape of the northern Rif (north of the fault trace), and as a dextral fault it permits the escape of the central–eastern Rif (the zone located between the Jebha fault and the North–Middle Atlas fault).

These deformations affect recent sedimentary rocks (of early to mid-Quaternary age: Tansiftian to Maarifian), located mainly in the Rif front and in its western part, indicating that these areas continue to be tectonically active. In addition, this region shows seismic activity, with earthquake focal mechanisms showing variable trends (NW–SE, north–south and even NE–SW) of the horizontal pressure axes (Medina & Cherkaoui 1992; Medina 1995).

This region also shows a positive heat flow anomaly, mainly along the Prerif Ridges (Rimi *et al.* 1998), which is most intense along the Nekor fault zone and the Prerif front. An alignment of thermal sources (Benmakhlouf 2001; Winckel 2002; Winckel *et al.* 2002) is observed along the Bou Draa fault. This setting is typical of regions with deep evaporitic diapirs or Variscan granite basement (Rimi *et al.* 1998), or with recent tectonic activity that has resulted in brecciated fault zones (Bahi *et al.* 1983; Ahmamou & Chalouan 1988; Benmakhlouf 2001; Winckel *et al.* 2002).

The development of the Rif mountain front is probably a consequence of the interaction of two distinct main tectonic processes: (1) the opening of the Algerian–Provençal basin in the Western Mediterranean, which contributed to the westward motion of the Alboran Domain (e.g. Boillot *et al.* 1984; Sanz de Galdeano 1990*a*,*b*) between the Eurasian and African plates; (2) the development of the first stages of the Betic–Rif Cordilleras tectonic arc. In addition, the recent NW–SE convergence between the Eurasian and African plates (De Mets *et al.* 1990) allows the southwestward escape of the Rif–Meseta tectonic wedge located between major crustal fault zones of the Rif Cordillera: the Jebha fault (N70°E), and the Fez–Tissa–Taïneste (N50°E) and North–Middle Atlas fault zones (N50°E). Along with the major blocks, other tectonic wedges of smaller size were expelled southwestward in the same way. In the frontal part of the Rif Cordillera, this expulsion is favoured by the presence of the subsiding Gharb Basin, open towards the Atlantic, which continues to undergo compressional deformations in its eastern sector (Flinch 1993; Litto *et al.* 2001) and extension in the western areas.

This changing tectonic scenario supports an anticlockwise rotation of the trend of maximum compression. Whereas the development of the first structures related to the southwestward tectonic wedge expulsion is in agreement with the NE–SW trend of maximum compression, a progressive transition has finally allowed the predominance of the NNW–SSE compression related to the present-day plate convergence.

Conclusions

The Rif mountain front, and in particular the Prerif Ridges front, is characterized by recent and active south-vergent tectonic structures such as thrusts, reverse and strike-slip faults, and folds, which produce tilting and even overturning of the sedimentary sequences, sometimes to those of Pliocene and Quaternaryage. These structures allow us to determine NW–SE and north–south main trends, and local NE–SW and even east–west trends of compression. The compressional structures deform, locally, sequences up to the Middle Atlas and Quaternary sedimentary rocks of the Moroccan coastal Meseta.

In addition, the Rif Cordillera and the Saïss and Gharb Basins are deformed by N40°E–N70°E transcurrent crustal fault zones that deform the basement. These major faults, which have been identified in outcrops and on seismic profiles, bound large crustal blocks and generally have a sinistral strike-slip component. Two major fault zones with trends of N70°E (in the NW) and N40°E (in the SE) have resulted in a large wedge-shaped block in the southwestern Rif Cordillera that may have escaped southwestward. This displacement of tectonic blocks may be the consequence of the combined activity of the NW–SE convergence of the Eurasian and African plates, and oceanic expansion in the Western Mediterranean during the development of the Algerian–Provençal Basin.

The lateral southwestward escape of the orogenic wedges bounded by transcurrent and thrust faults along the Rif front involved thin-skin tectonics, also indicated by the deformation in the borders of the Saïss and Gharb–Maamoura Basins surrounding the Rif front, the latter being open to the Atlantic. The westward motion continued to recent times, favoured by the activity of the crustal fault zone located between the Rif and the Atlas, and emphasized by the presence of thermal sources, high heat flow and seismic activity.

Although in some areas the NE–SW compressional palaeostresses related to the southwestward tectonic wedge expulsion predominate, in other regions (and in a transitional way) where the activity of this tectonic process is more moderate, the NNW–SSE compression related to the convergence of the Eurasian and African plates predominates. The frontal part of the Rif Cordillera is a key area for studying the variability of the deformations related to the NW–SE convergent Eurasian–African plate boundary, modified by the interaction of a complex set of tectonic elements between the major plates.

The comments of A. Michard and F. Medina have greatly improved the quality of this contribution. The research has been financed by collaborative Spanish–Moroccan projects of the Junta de Andalucía, the AECI and CICYT project BTE2003-01699.

References

AHMAMOU, A. 2002. *Evolution et dynamique sédimentaire des carbonates fluvio-lacustres plio-quaternaires dans le Saïss de Fès (Maroc).* Thèse d'Etat, Université Mohammed V, Rabat.

AHMAMOU, A. & CHALOUAN, A. 1988. Distension synsédimentaire plio-quaternaire et rotation antihoraire des contraintes au Quaternaire ancien sur la bordure nord du bassin du Saïss (Maroc). *Bulletin de l'Institut Scientifique, Rabat*, **12**, 19–26.

AÏT BRAHIM, L. 1991. *Tectonique cassante et états de contraintes récents au Nord du Maroc. Contribution à l'étude du risque sismotectonique.* Thèse Doctorat d'Etat, Université Mohammed V, Rabat.

AKIL, M. 1990. *Les dépôts quaternaires littoraux entre Casablanca et Cap Beddouza (Meseta côtière marocaine): études géomorphologiques et*

sédimentologiques. Thèse Doctorat d'Etat, Université Mohammed V, Rabat.

ANDEWEG, B. & CLOETINGH, S. 2001. Evidence for an active sinistral shear zone in the western Alboran region. *Terra Nova*, **13**, 44–50.

ANDRIEUX, J., FONTBOTÉ, J. M. & MATTAUER, M. 1971. Sur un modèle explicatif de l'Arc de Gibraltar. *Earth and Planetary Science Letters*, **12**, 191–198.

BAHI, L., EL YAMINE, N. & RISLER, J. J. 1983. Linéaments géothermiques au Maroc. *Comptes Rendus de l'Académie des Sciences, Série II*, **296**, 1087–1092.

BARGACH, K., RUANO, P., CHABLI, A., *ET AL.* 2004. Recent tectonic deformations and stresses in the frontal part of the Rif Cordillera and the Saïss Basin (Fez and Rabat regions, Morocco). *Pure and Applied Geophysics*, **161**, 521–540.

BENMAKHLOUF, M. 2001. *Les sources thermales du Maroc septentrional: relation entre le thermalisme et la tectonique.* Thèse Doctorat d'Etat, Université Mohammed V, Rabat.

BENMAKHLOUF, M., GALINDO-ZALDÍVAR, J., CHALOUAN, A., SANZ DE GALDEANO, C., AHMAMOU, M. & LÓPEZ-GARRIDO, A. C. 2005. Cinemática y paleoesfuerzos en la zona de falla transcurrente de Jebha–Chrafate (Rif septentrional, Marruecos). *Geogaceta*, **38**, 71–74.

BEN YAÏCH, A. 1981. *Etude géologique de la Dorsale calcaire entre Tlata Taghramt et Ben Youens (Haouz Rif, Maroc).* Diplôme Etudes Supérieures Thèse, Université Mohammed V, Rabat.

BEN YAÏCH, A. 1991. *Evolution tectono-sédimentaire du Rif externe centro-occidental (région de M'Sila et Ouezzane, Maroc): la marge africaine du jurassique au Crétacé; les bassins néogènes d'avant fosse.* Thèse d'Etat, Université de Pau et des Pays de l'Adour.

BERNINI, M., BOCCALETTI, M., MORATTI, G. & PAPANI, G. 2000. Structural development of the Taza–Guercif Basin as a constraint for the Middle Atlas Shear Zone tectonic evolution. *Marine and Petroleum Geology*, **18**, 391–408.

BOILLOT, G., MONTADERT, L., LEMOINE, M. & BIJU-DUVAL, B. 1984. *Les Marges continentales actuelles et fossiles autour de la France.* Masson, Paris.

BOURGOIS, J., MAUFFRET, A., AMMAR, A. & DEMNATI, A. 1992. Multichannel seismic data imaging of inversion tectonics of the Alboran ridge (Western Mediterranean Sea). *Geo-Marine Letters*, **12**, 165–172.

BOUYBAOUENE, M. L., GOFFÉ, B. & MICHARD, A. 1998. High-pressure granulites on top of the Beni Bousera Peridotite, Rif Belt Morocco: a record of an ancient thickened crust in the Alboran domain. *Bulletin de la Société Géologique de France*, **169**, 153–162.

CANTAGREL, J. M. & HARMAND, C. 1984. Le volcanisme récent du Moyen-Atlas (Maroc): chronologie K/Ar et cadre géodynamique. *10ème Réunion Annuelle des Sciences de la Terre, Bordeaux*, 115.

CHABLI, A., GALINDO-ZALDÍVAR, J., AKIL, M., *ET AL.* 2003. *Nouvelles observations sédimentologiques, stratigraphiques et néotectoniques sur les formations plio-quaternaires de la région de Témara.* Notes et Mémoires du Service Géologique du Maroc, **452**, 293–300.

CHALOUAN, A. & MICHARD, A. 2004. The Alpine Rif Belt (Morocco): a case of mountain building in a subduction–subduction–transform fault triple junction. *Pure and Applied Geophysics*, **161**, 489–519.

CHALOUAN, A., SAJI, R., MICHARD, A. & BALLY, A.W. 1997. Neogene tectonic evolution of the southwestern Alboran basin as inferred from seismic data of Morocco. *AAPG Bulletin*, **81**, 1161–1184.

CHALOUAN, A., GALINDO-ZALDÍVAR, J., BARGACH, K., *ET AL.* 2000. Deformaciones recientes en el frente de la Cordillera Rifeña (Prerif, Marruecos). *Geogaceta*, **29**, 43–46.

CHALOUAN, A., MICHARD, A., FEINBERG, H., MONTIGNY, R. & SADDIQI, O. 2001. The Rif mountains building (Morocco): a new tectonic scenario. *Bulletin de la société Geologique de France*, **172**(5), 603–616.

CHALOUAN, A., MICHARD, A., FEINBERG, H., MONTIGNY, R. & SADDIQI, O. 2003. *L'édification de la chaîne du Rif (Maroc) dans le cadre tectonique méditerranéen.* Notes et Mémoires du Service géologique du Maroc, **447**, 69–98.

CHARRIÈRE, A. 1990. *Héritage hercynien et évolution géodynamique alpine d'une chaîne intracontinentale: le Moyen-Atlas au SE de Fès (Maroc).* Thèse Doctorat d'Etat, Université de Toulouse.

CHARROUD, M. 1990. *Evolution géodynamique de la partie sud-ouest du Moyen-Atlas durant le passage Jurassique–Crétacé, le Crétacé et le Paléogène: un exemple d'évolution intraplaque.* Diplôme Etudes Supérieures Thèse, Université Mohammed V, Rabat.

COLO, G. 1961. *Contribution à l'étude du Jurassique du Moyen Atlas septentrional (Maroc).* Notes et Mémoires du Service Géologique du Maroc, **139**.

COMAS, M. C., GARCIA-DUEÑAS, V & JURADO, J. 1992. Neogene tectonic evolution of the Alboran Sea from MCS data. *Geo-Marine Letters*, **12**, 157–164.

COMAS, M. C., PLATT, J. P., SOTO, J. I. & WATTS, A. B. 1999. The origin and tectonic history of the Alboran basin: insights from ODP leg 161 results. *In*: ZAHN, R., COMAS, M. C. & KLAUS, A. (eds) *Proceeding of the Ocean Drilling Program, Scientific Results, 161.* Ocean Drilling Program, College station, TX, 555–580.

DE METS, C., GORDON, G. G., ARGUS, D. F. & STEIN, S. 1990. Current plate motions. *Geophysical Journal International*, **101**, 425–478.

EL AZZAB, D. & EL WARTITI, M. 1988. Paleomagnetism of Middle Atlas lavas (Morocco): recent rotations. *Comptes Rendus de l'Académie des Sciences, Série IIA*, **327**(8), 509–512.

FAUGÈRES, J. C. 1978. *Les Rides sud rifaines; évolution sédimentaire et structurale d'un bassin atlantico-mésogène de la marge africaine.* Thèse Doctorat d'Etat, Université de Bordeaux I.

FEINBERG, H. 1986. *Les séries tertiaires des zones externes du rif (Maroc); biostratigraphie, paléoécologie et aperçue tectonique.* Notes et Mémoires du Service Géologique du Maroc, **315**.

FLINCH, F. J. 1993. *Tectonic evolution of the Gibraltar arc.* PhD thesis, Rice University, Houston, TX.

FLINCH, F. J. 1996. Accretion and extensional collapse of the external western Rif (Northern Morocco). *Mémoires du Muséum National de l' Histoire Naturelle de Paris*, **170**, 61–85.

FRIZON DE LAMOTTE, D., SAINT BEZAR, B., BRACÈNE, R. & MERCIER, E. 2000. The two main steps of the Atlas building and geodynamics of the western Mediterranean. *Tectonics*, **19**, 740–761.

GARCÍA-DUEÑAS, V. & BALANYÁ, J. C. 1986. Estructura y naturaleza del Arco de Gibraltar. *Maleo Boletim Informativo da Sociedade Geológica de Portugal*, **2**, 23.

GOFFÉ, B., AZAÑÓN, J. M., BOUYBAOUEN, M. L. & JULLIEN, M. 1997. Métamorphic cookeite in Alpine metapilites from Rif (northern Morocco) and Betic Chains (southern Spain). *European Journal of Mineralogy*, **6**, 897–911.

GOURARI, L. 2001. *Etude hydrochimique, morphologique, lithostratigraphique, sédimentologique et pétrographique des dépôts travertino-détritiques actuels et plio-quaternaires du bassin karstique de l'Oued Aggay (Causse de Sefrou, Maroc).* Thèse Doctorat d'Etat, Université de Fès.

HAMEL, CH. 1971. *Carte géologique au 1/100 000 de Tistoutine.* Notes et Mémoires du Service Géologique du Maroc, **167**.

HARMAND, C. & CANTAGREL, J. M. 1984. Le volcanisme alcalin tertiaire et quaternaire du Moyen-Atlas (Maroc): chronologie K/Ar et cadre géodynamique. *Journal of African Earth Sciences*, **2**(1), 51–55.

HARMAND, C. & MOUKADIRI, A. 1986. Synchronisme entre tectonique compressive et volcanisme alcalin: exemple de la province quaternaire du Moyen-Atlas (Maroc). *Bulletin de la Société Géologique de France, Série II*, **8**(4), 595–603.

HERVOUËT, Y. 1985. *Géodynamique alpine (Trias–actuel) de la marge septentrional de l'Afrique du Nord du bassin de Guercif (Maroc oriental).* Thèse d'Etat, Université de Pau et des Pays de l'Adour.

HINAJE, S. 2004. *Tectonique cassante et paléochamps de contraintes dans le Moyen Atlas et le Haut Atlas central (Midelt-Errachidia) depuis le Trias jusqu'à l'Actuel.* Thèse Doctorat d'Etat, Université Mohammed V, Rabat.

JACOBSHAGEN, V. 1992. Major fracture zones of Morocco: the South Atlas and the Transalboran fault systems. *Geologische Rundschau*, **81**, 185–197.

KENAFI, J. 2002. *Evolution structurale méso-cénozoïque des Rides périfaines (Maroc): halocinèse, géométrie et reconstitution géodynamique. Apport de données de sismique réflexion et de forages pétroliers.* Thèse de Doctorat, Université de Kénitra.

KORNPROBST, J. 1974. *Contribution à l'étude pétrographique et structurale de la zone interne du Rif (Maroc septentrional).* Notes et Mémoires du Service Géologique du Maroc, **251**.

LAVILLE, E. & PIQUÉ, A. 1991. La distension crustale atlantique et atlasique du Maroc au début du Mésozoïque: le rejeu des structures hercyniennes. *Bulletin de la Société Géologique de France*. **162**, 1161–1171.

LITTO, W., JAAÏDI, E., MEDINA, F. & DAKKI, M. 2001. Seismic study of the structure of the northern margin of the Gharb basin (Morocco)—evidence for a late Miocene distension. *Eclogae Geologicae Helvetica*, **94**, 63–74.

MALDONADO, A., CAMPILLO, A. C., MAUFFRET, A., ALONSO, B., WOODSIDE, J. & CAMPOS, J. 1992. Alboran Sea late Cenozoic tectonic and stratigraphic evolution. *Geo-Marine Letters*, **12**, 179–186.

MARTIN, J. 1981. *Le Moyen Atlas central, étude géomorphologique.* Notes et Mémoires du Service Géologique du Maroc, Rabat, **258** and **258bis**.

MEDINA, F. 1995. Present-day state of stress in Northern Morocco from focal mechanism analysis. *Journal of Structural Geology*, **17**(7), 1035–1046.

MEDINA, F. & CHERKAOUI, T. E. 1992. Mécanismes au foyer des séismes du Maroc et des régions voisines (1959–1986). *Journal of Structural Geology*, **17**, 1035–1046.

MENVIELLE, M. & LE MOUËL, J.-L. 1985. Existence d'une anomalie de conductivité dans le Haut-Atlas marocain et concentration des courants telluriques à l'échelle régionale. *Bulletin de la Société Geéologique de France*, **8**(1), 553–558.

MICHARD, A., CHALOUAN, A., FEINBERG, H., GOFFÉ, B. & MONTIGNY, R. 2002. How does the Alpine belt end between Spain and Morocco? *Bulletin de la Société Géologique de France*, **173**, 3–15.

MORATTI, G., PICCARDI, L., VANNUCCI, G., BELARDINELLI, M. E., DAHMANI, M., BENDKIK, A. & CHENAKEB, M. 2003. The 1755 'Meknes' earthquake (Morocco): field data and geodynamic implications. *Journal of Geodynamics*, **36**, 305–322.

MOREL, J. L. 1988. Evolution récente de l'orogène rifain et de son avant-pays depuis la fin de la mise en place des nappes (Rif–Maroc). *Geodiffusion Memoire*, **4**, Paris.

MORLEY, K. 1987. Origin of major cross element zone: Morocco Rif. *Geology*, **15**, 761–764.

MORLEY, C. K. 1992. Notes on Neogene basin history of the Western Alboran Sea and its implications for the tectonic evolution of the Rif–Betic orogenic belt. *Journal of African Earth Sciences*, **14**, 57–65.

OLIVIER, PH. 1981. L'Accident de Jebha–Chrafate (Rif, Maroc). *Revue de Géologie Dynamique et Géographie Physique*, **22**, 201–212.

PIQUÉ, A., AIT BRAHIM, L., EL AZZOUZI, E., MAURY, R. C., BELLON, H., SEMROUD, B. & LAVILLE, E. 1998. Le poinçon maghrébin: contraintes structurales et géochimiques. *Comptes Rendus de l'Académie des Sciences*, **326**, 575–581.

PLATT, J. P., ALLERTON, S., KIRKER, A., MANDEVILLE, C., MAYFIELD, A., PLATZMAN, E. S. & RIMI, A. 2003. The ultimate arc: differential displacement, oroclinal bending, and vertical

axis rotation in the External Betic–Rif arc. *Tectonics*, **22**, 1017, doi: 10.1029/2001TC001321.

RIMI, A, CHALOUAN, A. & BAHI, L. 1998. Heat flow in the westernmost part of the Alpine Mediterranean system (the Rif, Morocco). *Tectonophysics*, **285**, 135–146.

ROBILLARD, D. 1978. *Etude structurale du Moyen Atlas septentrional au sud de Taza (Maroc).* Thèse Doctorat 3ème cycle, Université de Lille.

ROBILLARD, D. 1979. Tectonique synsédimentaire du Moyen Atlas septentrional au sud de Taza (Maroc). *Bulletin de la Société Géologique de France*, **7**(4), 441–447.

ROYDEN, L. H. 1993. Evolution of retreating subduction boundaries formed during continental collision. *Tectonics*, **12**, 629–638.

RUANO, P., BARGACH, K., GALINDO-ZALDÍVAR, J., CHALOUAN, A. & AHMAMOU, M. 2006. Recent palaeostresses from striated pebbles related to fold development in a mountain front: the Prerif Ridges (Rif Cordillera, Morocco). *In*: MORATTI, G. & CHALOUAN, A. (eds) *Tectonics of the Western Mediterranean and North Africa.* Geological Society, London, Special Publications, **262**, 87–99.

SAMAKA, F. 1999. *Apport de la géophysique (sismique réflexion) à l'étude de l'évolution sédimentologique, structurale et paléogéographique des bassins supra-nappes du Rif central.* Thèse de Doctorat, Université Mohammed V, Rabat.

SAMAKA, F., BENYAICH, A., DAKKI, M., HÇAINE, M. & BALLY, A. W. 1997. Origine et inversion des bassins miocènes supra-nappes du Rif central (Maroc). Etude de surfaces et de subsurface. Exemple des bassins de Taounate et de Tafrant. *Geodinamica Acta*, **10**, 30–40.

SANI, F., ZIZI, M. & BALLY, A. W. 2000. The Neogene–Quaternary evolution of the Guercif Basin (Morocco) reconstructed from seismic line interpretation. *Marine and Petroleum Geology*, **17**, 343–357.

SANZ DE GALDEANO, C. 1990*a*. Geologic evolution of the Betic Cordilleras in the Western Mediterranean, Miocene to the present. *Tectonophysics*, **172**, 107–119.

SANZ DE GALDEANO, C. 1990*b*. La prolongación hacia el sur de las fosas y desgarres del Norte y Centro de Europa: una propuesta de interpretación. *Revista de la Sociedad Geologica de España*, **3**, 231–241.

TEJERA DE LEÓN, J. 1993. *Les bassins néogènes d'avant-pays du Rif externe occidental liés à la transformante Jebha–Arbaoua (Maroc).* Thèse Doctorat d'Etat, Université de Pau et des Pays de l'Adour.

TEJERA DE LEÓN, J. 1997. Signification de la limite Jebha–Arbaoua (Maroc nord-occidental): une rampe latérale au dessus d'une discontinuité crustale héritée de la période de rifting. *Journal of African Earth Sciences*, **24**, 455–472.

TESSON, M., GENSOUS, B. & LABRAÏMI, M. 1987. Seismic analysis of the southern margin of the Alboran Sea. *Journal of African Earth Sciences*, **6**, 813–821.

THOMAS, G. & FEDAN, B. 1988. Activité de l'accident nord–moyen-atlasique au nord de Boulemane (Maroc). Au cours du Mio-Pliocène. *12ème Réunion Annuelle des Sciences de la Terre, Lille*, 125.

VAN DEN BOSCH, J. W. H. 1981. *Mémoire explicatif de la carte gravimétrique du Maroc (provinces du Nord) au 1/500 000.* Notes et Mémoires du Service Géologique, no. 234, 219.

WERNLI, R. 1988. *Micropaléontologie du Néogène post nappes du Maroc septentrional et description systématique des foraminifères planctoniques.* Notes et Mémoires du Service Géologique du Maroc, **331**.

WINCKEL, A. 2002. *Essai d'établissement d'une typologie de sources thermales par une approche hydrochimique, isotopique et tectonique. Exemple du Maroc.* Thèse de Doctorat, Université Paris XI d'Orsay.

WINCKEL, A., MARLIN, C., DEVER, L., MOREL, J. L., EL MORABITI, K., BEN MAKHLOUF, M. & CHALOUAN, A. 2002. Apport des isotopes stables dans l'estimation des altitudes de recharge de sources thermales du Maroc septentrional et oriental. *Comptes Rendus Geosciences*, **334**, 469–474.

ZAGHLOUL, M. N. 1994. *Les unités Federico septentrionales (Rif interne, Maroc) inventaire des déformations et contexte géodynamique.* Thèse, Diplôme Etudes Supérieures, Université Mohammed V, Rabat.

ZAKIR, A. 2004. *Les bassins tertiaires d'avant-fosse du Rif externe nord-occidental: approche sédimentologique et structurale des séries turbiditiques de la région d'El Ksar El Kebir.* Thèse de Doctorat, Université Mohammed V, Rabat.

ZAKIR, A. CHALOUAN, A. & FEINBERG, H. 2004. Plis de propagation et conséquences de leur rupture en domaine d'avant-chaîne, Rif nord-occidental, Maroc. *Bulletin de la Société Géologique de France*, **173**, 3–15.

ZIZI, M. 1996. *Triassic–Jurassic extensional systems and their Neogene reactivation in northeastern Morocco (the Prerifaines Ridges and Guercif basin).* PhD thesis, Rice University, Houston, TX.

ZOUHRI, L., LAMOUROUX, C. & BURET, C. 2002. La Mamora, charnière entre la Meseta et le Rif: son importance dans l'évolution géodynamique post-paléozoique du Maroc. *Geodinamica Acta*, **14**, 361–372.

Geophysical and geological interpretation of discrepancies in site residuals in northern Morocco: a simple qualitative approach

L. AIT BRAHIM[1], I. MOUAYN[1], A. ABDELOUAFI[1], M. BENHALIMA[1] & B. TADILI[2]

[1]*Université Mohammed V, Faculté des Sciences, Avenue Ibn Battouta, Laboratoire des Risque Géologiques, BP 1014 Rabat-Agdal, Morocco (e-mail: aitbrahi@fsr.ac.ma)*

[2]*Université Mohammed V, Institut Scientifique, Département de Physique de Globe, Rabat, Morocco*

Abstract: Surface geology, gravimetric, and heat flow data are used to explain discrepancies between M_D site residuals, using the average magnitude site residuals ($AMSR_j$) which are opposite of the station corrections ($cSta_j$) calculated for the 25 selected short-period seismic stations of the Moroccan seismological network. M_D site residuals range from -0.29 to $+0.32$, and appear to be the result of the complex interaction of the predominant near-station geophysical and geological parameters. With this simple qualitative approach, we found that high negative residuals are obtained for older well-consolidated Precambrian crystalline rocks with low surface heat flow, and high positive residuals are attributed to recent unconsolidated sediments with high heat flow. The explanation for the intermediate residual values remains more complex and requires more accuracy and better quality data, and may not be fully justified in this study.

Calibration of the northern Morocco seismic stations (newly installed, from 1989 to 1994) allowed us to set a relationship for duration magnitude in the form

$$M_{Dij} = -0.14 + 1.63 \log_{10}(\tau_{ij}) + 0.031(\Delta_{ij} + cSta_j)$$

where τ_{ij} and Δ_{ij} represent respectively the duration and epicentral distance for the ith event at the jth station. $cSta_j$ is the station correction term derived from the M_D formula given by Mouayn *et al.* (2004). Previously, duration magnitude formulae were determined in Morocco by Frogneux (1980) and Cherkaoui (1991) for stations installed from 1937 to 1989 (portable instruments were also used).

In the present study, $cSta_j$ is introduced to reduce the tendency of stations to either overestimate or underestimate calculated magnitudes. This tendency may be caused conjointly by instrument and site conditions. Therefore, separating instrument and site effects requires a delicate approach, which involves the installation of all the seismometers at the same site and the recording of sufficient data to calibrate the stations. The instrument corrections can then easily be deduced and subtracted from the original $cSta_j$ to obtain the best site correction. Thus, only instruments with similar response curves were selected (1 Hz natural frequency, vertical-component SS-1 Kinemetriks Ranger seismometers). Sensitivity (36 ± 6 dB) and class component consequently did not introduce significant errors in $cSta_j$. Amplification or attenuation is practically constant for the stations of this study. We attribute $cSta_j$ entirely to compensate the effect of the station site quantified by the scalar; $-cSta_j$ is assumed to represent the site residual in the following.

$cSta_j$ is introduced to reduce the particular effect of geological and geophysical heterogeneity at the station sites, and therefore can be viewed as the resulting error in the prediction of the coda length assuming a simple quantification of the physical parameters of a seismic event. Here, site corrections (station corrections) $cSta_j$ are those obtained by Mouayn *et al.* (2004) in the range -0.29 to 0.32 magnitude unit (see Table 1).

In an attempt to check for the eventual correlation between these corrections and the geological and geophysical properties in the vicinity of the stations, we prefer to use the site residual, which is the average magnitude site residual ($AMSR_j$), the opposite of the $cSta_j$ algebraic value (Table 1).

In this simple qualitative approach, we shall not attempt to isolate effects of the seismic wave propagation from those resulting from the station site's geological and geophysical conditions. We assume that physical attenuation properties in the immediate vicinity of the stations exert a significant influence on the seismic wave. Characteristics of recorded signals (amplitude, duration and frequencies) appear to be a direct consequence of the impact of geological and geophysical factors such as structural domain, local tectonics, age and degree of consolidation of rocks, and local surface heat flow density.

From: MORATTI, G. & CHALOUAN, A. (eds) 2006. *Tectonics of the Western Mediterranean and North Africa.* Geological Society, London, Special Publications, **262**, 119–129.
0305-8719/06/$15.00

Table 1. *Station corrections ($cSta_j$)*

No.	Code	Name	Sub-network	Coordinates		$cSta_j$	$AMSR_j$	Data
				Lat. (N)	Long. (W)			
1	TIO	Tiouine	Non-Telemetered	30.550	−7.150	0.29	−0.29	77
2	OUK	Oukaimden	Chichaoua	31.209	−7.868	0.24	−0.24	24
3	TZK	Tazeka	Ifrane	34.089	−4.184	0.17	−0.17	151
4	TAF	Tafouralt	Non-Telemetered	34.480	−2.240	0.16	−0.16	101
5	MIF	Mishlifen	Ifrane	33.409	−5.229	0.16	−0.16	48
6	ZAI	Zaio	Zaio	34.803	−2.746	0.15	−0.15	114
7	ZFT	Ezzeft	Midelt	32.034	−4.352	0.15	−0.15	29
8	KIB	El Ksiba	Beni Mellal	32.576	−6.039	0.13	−0.13	81
9	IFR	Ifrane	Non-Telemetered	33.310	−5.070	0.12	−0.12	125
10	CZD	Col de Zad	Midelt	33.033	−5.043	0.08	−0.08	127
11	TNF	Tounfite	Midelt	32.530	−5.319	0.07	−0.07	26
12	TZC	Tazercounte	Beni Mellal	32.148	−6.490	0.06	−0.06	50
13	PAL	Palemas	Zaio	35.225	−3.942	−0.04	0.04	109
14	JBB	Jbel Babet	Zaio	35.013	−4.198	−0.06	0.06	49
15	DKH	Dar Kharkour	Tanger	35.490	−5.360	−0.08	0.08	51
16	TOU	Touzarine	Zaio	34.962	−3.754	−0.08	0.08	122
17	CPS	Cap Spartel	Tanger	35.791	−5.910	−0.11	0.11	87
18	TGT	Taghat	Ifrane	34.070	−5.055	−0.11	0.11	95
19	RSA	Sarsar	Tanger	34.877	−5.828	−0.12	0.12	74
20	BIT	Ibn Batouta	Tanger	35.648	−5.729	−0.13	0.13	63
21	TSY	Inine Sidi l'Yamani	Tanger	35.373	−5.970	−0.14	0.14	97
22	JHA	Jbel Lahdid	Chichaoua	31.736	−9.454	−0.23	0.23	23
23	CIA	Chichaoua	Chichaoua	31.565	−8.759	−0.25	0.25	58
24	RTC	Rabat Centre	Centre	33.990	−6.858	−0.32	0.32	44
25	AVE	Averoes	Non-Telemetered	33.170	−7.240	−0.32	0.32	109

Magnitude formula used: $M_{Dij} = -0.14 + 1.63\log_{10}(\tau_{ij}) + 0.031(\Delta_{ij}) + cSta_j$.
$AMSR_j$ = average magnitude station residual = $-cSta_j$.

Geological setting

Morocco has a wide range of structural units as a result of the major geological events that occurred principally during the Mesozoic and the Cenozoic (Fig. 1). The Anti-Atlas is the southernmost domain. It is composed of Precambrian formations of the West African basement, which were deformed and granitized at the time of the Eburnean and Pan-African events (Leblanc & Lancelot 1980; Piqué 1994). The Mesetas (Western and Eastern) are two Palaeozoic folded formations (Lagarde 1985; Piqué & Michard 1989), with a Meso-Cenozoic tabular cover. The Middle and the High Atlas are two intra-continental belts principally composed of Mesozoic formations that are slightly deformed, with boundaries marked by fault zones (Laville 1985; Fedan 1988). The general trend of the chain is ENE–WSW, but becomes east–west for the eastern High Atlas. The Rif Domain in the north is characterized by complex Alpine thrusting tectonics. In its internal zone, Palaeozoic nappes with a Mesozoic cover predominate (Chalouan *et al.* 2001). In the external zone we note the presence of Mesozoic and Cenozoic nappes. The major tectonic features in the Rif are two left-lateral faults (Leblanc & Olivier 1984): the Jebha (ENE–WSW) and Nekor (NE–SW) faults.

Methods

Derivation of the M_D equation

To adjust M_D against our data (*independent set*; Mouayn *et al.* 2004), we use a two-stage iterative procedure. In the first stage we solve for the constants c_{01}, c_{11} and c_{21} by regressing initially τ and Δ against mb^{IGN} with the station corrections $cSta_j$ being reset to zero. The quantities c_{01}, c_{11} and c_{21} are the resultant coefficients of the first iteration of the regression. In the second stage the c_{i1} were substituted into the equation obtained and $cSta_{j1}$ was estimated. The first station corrections $cSta_{j1}$ are included in the next iteration of the regression, and the process is repeated until the variance and standard errors converge to a stable minimum, with station corrections being updated between iterations. The adopted coefficients c_0, c_1 and c_2 are those obtained from the last iteration of the regression as $c_{0k} = c_0$, $c_{1k} = c_1$ and $c_{2k} = c_2$, and $cSta_j = \sum cSta_{jk}$, where k is the number of iterations. The resultant magnitude estimate formulation is

$$M_{Dij} = -0.14 + 1.63\log_{10}(\tau_{ij}) + 0.031(\Delta_{ij}) + cSta_j$$

where $c_0 = -0.14$, $c_1 = 1.63$ and $c_2 = 0.031$. The values of $cSta_j$ are listed in Table 1. The magnitude

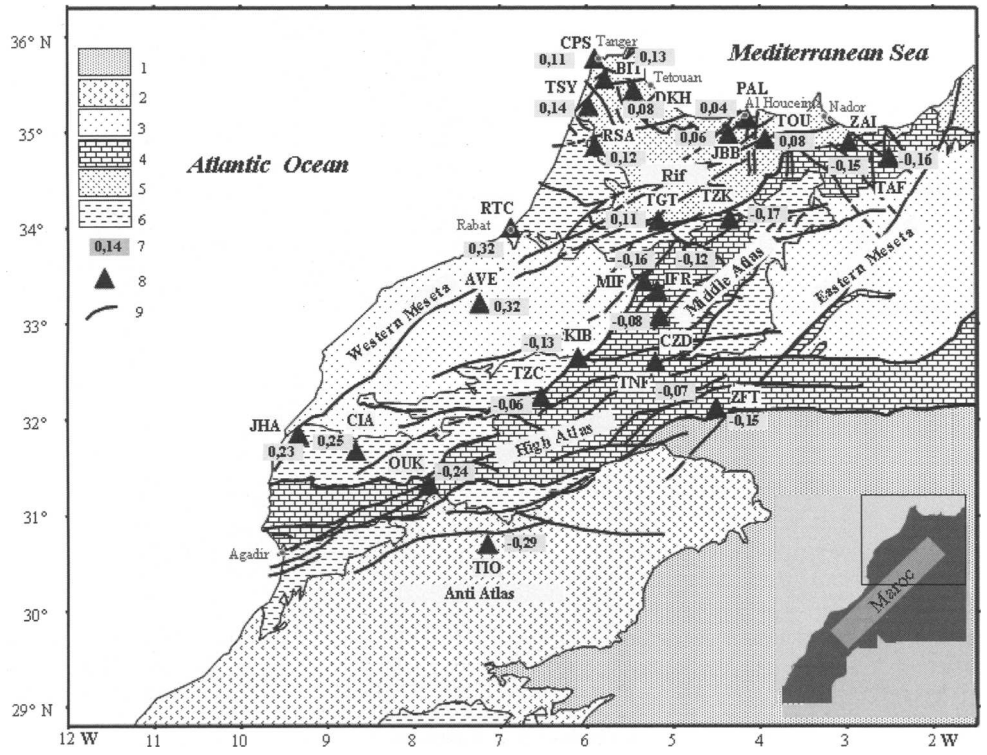

Fig. 1. Structural sketch of northern Morocco. 1, African Domain; 2, Anti-Atlas Domain; 3, Hercynian Meseta Domain; 4, Atlas Domain; 5, Rif Domain; 6, Neogene and Quaternary basins; 7, average station magnitude residual (sample); 8, short-period seismic station; 9, fault.

of the *i*th event is the mean of individual station estimates M_{Dij}, and M_D uncertainty is the standard deviation of the mean.

Surface geology, geophysical factors and their influence on site residuals

To understand the influence of the interaction of geological and geophysical factors (such as surface geology and heat flow) on durations recorded at the 25 stations of this study, and consequently their influence on the site residuals obtained (Table 1), we have plotted contour lines corresponding to these residuals at the station locations (Fig. 1), and superimposed the isolines on a simplified geological map of Morocco. Our stations fall into six distinct groups of residual values.

Results

Station Group 1 (SG-1)

This group includes stations TIO and OUK, with the highest site residual values of −0.29 and −0.24, respectively. TIO is situated on Precambrian formations of the Anti-Atlas chain, which is composed of West African basement rocks, deformed and granitized at the time of the Eburnean and Panafrican events and stable since then (Piqué 1994). Station OUK is located in the Precambrian massif of Marrakech (High Atlas chain). Both stations are sited on similar rocks (Fig. 2). The negative values of the residuals show clearly that the essentially crystalline and metamorphic sites have a tendency to shorten considerably the durations of recorded signals. Moreover, this domain is characterized by a low surface heat flow density ranging between 40 and 65 mW m^{-2} (Fig. 3).

Station Group 2 (SG-2)

This second group consists of seven stations: ZAI (−0.15), TAF (−0.16), TZK (−0.17), MIF (−0.16), IFR (−0.12), KIB (−0.13) and ZFT (−0.15). For these stations the residuals have intermediate negative values. Excepting ZFT, which does not have any evident geographical or geological link with the other stations, the majority of these

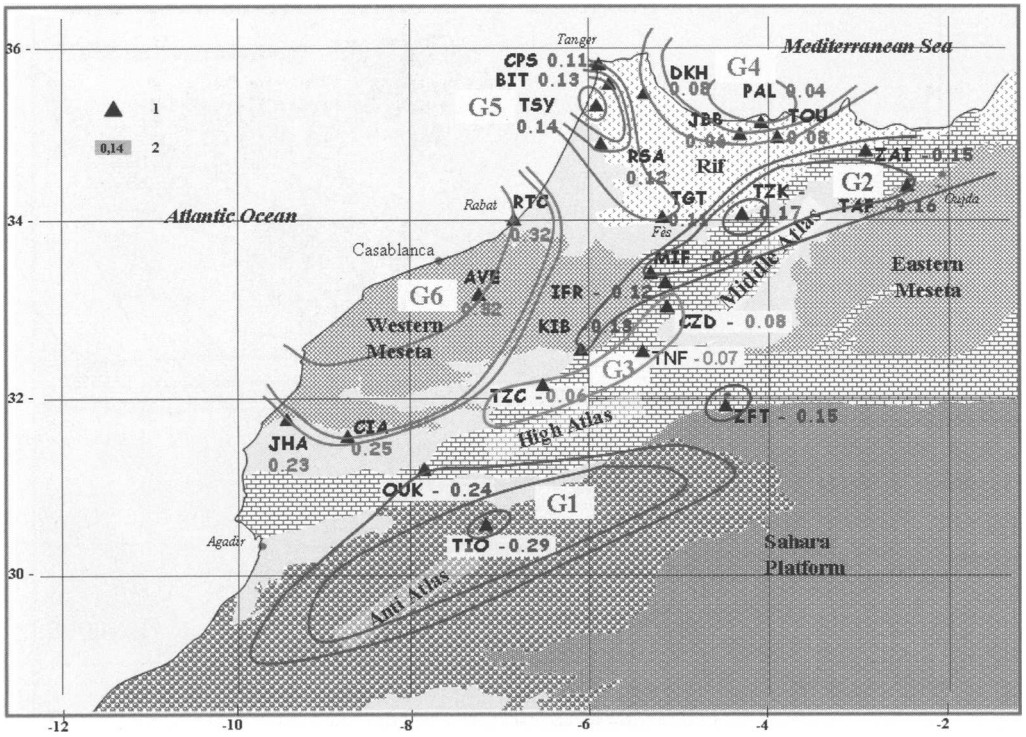

Fig. 2. Geological sketch of northern Morocco with isolines delimiting six groups of residual site values (G1, G2, G3, G4, G5 and G6). 1, Short period seismic station; 2, M_D site residual per station (sample).

stations are located in the Middle Atlas Domain, characterized by emergence of reduced Palaeozoic formations, and by a Meso-Cenozoic, Neogene and Quaternary cover (folded or tabular). These stations are arranged within a NE–SW band, from Zaio-Oujda to Khénifra-Ksiba. This corridor is also characterized by important Quaternary volcanic rocks (Michard 1976; Piqué 1994; El Azouzi 2000). This NE–SW direction corresponds to regions of lithospheric discontinuity that controlled the emplacement of the late Palaeozoic granitic bodies (Piqué 1994) (Fig. 2). Surface heat flow density for the region ranges between 70 and 100 mW m^{-2} (Rimi 1999) (Fig. 3). Residuals for this group are also negative. Therefore these sites tend to shorten significantly recorded signals.

Stations Group 3 (SG-3)

In this group, stations CZD (−0.08), TNF (−0.07) and TZC (−0.06) have slight negative residuals. They are situated in the southern part of the Middle Atlas, particularly along the major fault zones that mark the transition between the Middle Atlas and neighbouring structural domains (SW extremity of the Eastern Meseta, formed by the Midelt Palaeozoic formation, and the High Atlas): the Ait Oufela fault zone, and the High Atlas northern limit faults (Fig. 2). Moreover, this geographical domain is characterized by the lowest heat flow density (Rimi 1999) (Fig. 3) and has a deep crustal root (Seber 1995).

Station Groups 4 and 5 (SG-4 and SG-5)

Generally, stations of these groups belong to the Rif Domain (Fig. 1). For this reason we will describe their common properties before discussing their individual characteristics. Overall, the Rif Domain is characterized by its complex geology, intense fracturing (Chalouan *et al.* 1997; Ait Brahim *et al.* 2002; Ait Brahim 2003), the presence of small Neogene coastal basins and a relatively high geothermal gradient (Rimi 2001). The dense fracture network favours fluid circulation that generates convection (Rimi 2001). A decrease in recorded signal amplitude is noted. Moreover, the stations of SG-4 (except for DKH) are located in the zone of the Rif characterized by a minimum heat flow density (Fig. 3), whereas SG-5 is situated in the western part of the Rif Domain, with high heat flow (Fig. 3).

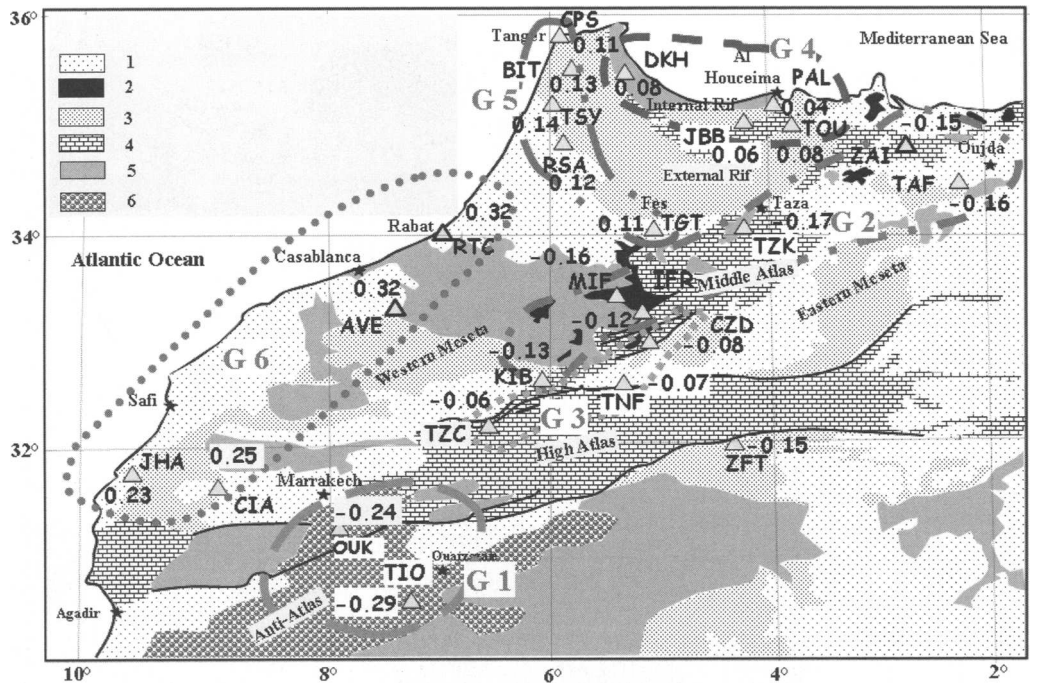

Fig. 3. Location and distribution of the six groups of stations with values of site residuals; their location and distribution is according to the substratum. 1, Neogene and Quaternary cover; 2, Neogene and Quaternary volcanism; 3, undifferentiated Meso-Cenozoic cover; 4, Triassic–Jurassic cover; 5, Palaeozoic emergence; 6, Precambrian formations.

Station Group 4 (SG-4)

The stations of this group are DKH (0.08), JBB (0.06), TOU (0.08) and PAL (0.04). They belong to the Internal Rif Domain (Fig. 2), which was deformed and metamorphosed as result of the Africa–Iberia collision (Michard *et al.* 2002). This domain involves Palaeozoic rigid formations, volcanic masses (Chalouan *et al.* 2001), and small Neogene coastal sedimentary basins. The positive residuals of this group are very small.

Station Group 5 (SG-5)

Stations CPS (0.11), BIT (0.13), TSY (0.14), RSA (0.12) and TGT (0.11), make up the group, located in the External Rif Domain (Fig. 2), which is composed of Mesozoic and Cenozoic formations of the folded and transported African margin. The sites of these stations, which have intermediate positive residuals, are characterized by their high surface heat flow density (Fig. 3), caused by hot fluid circulations that follow the fracture network in the region (Rimi 1999). This region coincides also with a low gravity anomaly (−150 mGal) (Fig. 4). This important anomaly is related to a deep crustal root, resulting in the replacement of lithospheric material by asthenospheric material in the External Rif (Seber *et al.* 1996; Vidal 1977).

Station Group 6 (SG-6)

The stations of this group are RTC (0.32), AVE (0.32), CIA (0.25) and JHA (0.23). They belong to the Western Meseta Domain, characterized by widely exposed Palaeozoic formations (Fig. 2). In the western part of this domain, we note the presence of Neogene coastal basins. These stations have the highest positive residuals. A considerable lengthening of recorded duration is expected here.

Discussion

In this section we shall attempt to give an explanation for the differences observed in the values obtained for each group of stations in terms of surface geology and geothermal structure at sites of stations.

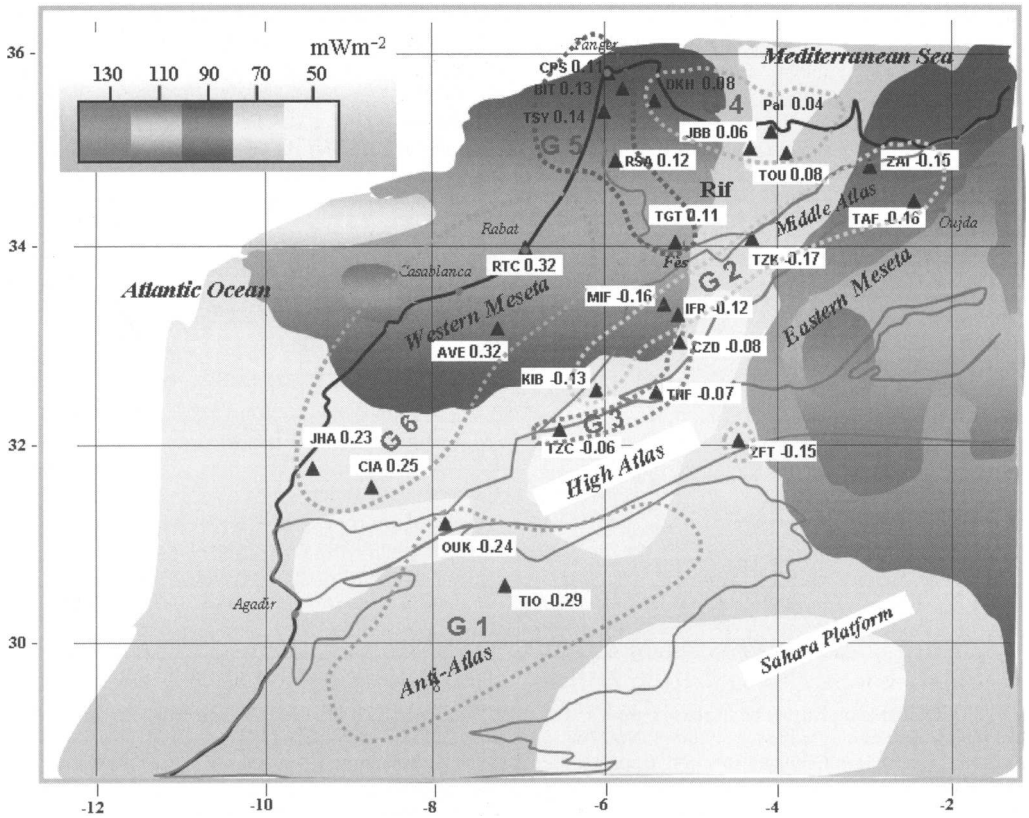

Fig. 4. Site residual values superimposed on a simplified map of surface heat flow density in northern Morocco.

SG-1, with the highest negative residuals, is situated on an old crystalline basement, which forms, from a geophysical point of view, a medium with 'simple' geology. Such rocks present few scatterers of seismic waves and consequently, may generate short signals (Guttenberg & Richter 1956; Borcherdt & Glassmoyer 1992; Eaton 1992; Su *et al.* 1992). Compaction of such old rocks contributes significantly to the normal transmission of seismic energy between the rock particles. The high impedance of these media seems to dissipate a great part of the seismic energy. Moreover, this domain is characterized by a low surface heat flow density ranging between 40 and 65 mW m^{-2} (Rimi 1999) (Fig. 3). It is known that there is a dependence between surface heat flow and the velocity of high-frequency compressional waves, especially the P phase (Kubik 1988; Sharma *et al.* 1991; Rimi 1999). This relationship indicates that V_p increases significantly in areas with low heat flow. For instance, in the Rif area (Fig. 1), low-density shallow asthenospheric material (Seber 1996), coincides with very low Pn velocity group (Hatzfeld & Bensari 1977).

To summarize the results for SG-1, we can consider that the high negative residual values (average: −0.26) may be attributed to the combination of at least two factors: the geological nature of the old compact crystalline formations, and the low surface heat flow in the region.

SG-2 is located on (or in the immediate vicinity of) Palaeozoic rigid formations, which generally favour attenuation of seismic waves (Guttenberg & Richter 1956; Borcherdt & Glassmoyer 1992; Eaton 1992; Su *et al.* 1992). In contrast, the high heat flow density in the area is responsible for perturbations that generate long signals (low crustal wave velocities) (Kubic 1988; Sharma *et al.* 1991; Rimi 1999). In this case, values for these residuals (average: −0.15) may be considered as the combined result of: (1) their location on rigid and relatively old rocks characterized by high impedance; (2) the high heat flow as a consequence of recent volcanism in the region, which may exert an opposite influence.

Geographically, SG-3 is situated between SG-1 and SG-2, which are both considered as sited on

attenuating media. Relatively short durations were expected here. We assume that the major fault zones in this area contribute to the lengthening of durations because of belated arrivals of trapped phases. These major fault zones form a guide supporting the waves and the complicated sequence of their internal reverberations, which progressively inject energy into the neighbouring rocks (Kang & McMechan 1993). The attenuating effect of this medium (rigid and competent rock), which shortens durations, is compensated by the late liberation of the energy trapped in the fault zones, which lengthens durations, resulting finally in near-zero residuals values (about −0.07).

For SG-4, geophysical and geological conditions can be summarized as follows: metamorphosed compacted rocks and Palaeozoic rigid formations imply systematic shortening of recorded durations and consequently negative residuals (Guttenberg & Richter 1956; Borcherdt & Glassmoyer 1992; Eaton 1992; Su *et al.* 1992). On the other hand, the intensely fractured medium favours longer durations (Kang & McMechan 1993), and the influence of recent sedimentary basins is also known to generate longer durations for the P and S phases (Guttenberg & Richter 1956; Borcherdt & Glassmoyer 1992; Eaton 1992; Su *et al.* 1992; Kang & McMechan 1993). Positive residuals are expected in this case. The complex geophysical and geological conditions in this domain seem to have opposing effects on wave propagation, resulting in very small residual values for the group (average 0.07).

In SG-5, the greater heat flow (Rimi 1999) and the existence of asthenospheric material may be correlated with the increase in V_p. These two parameters (high surface heat flow density and high negative gravity anomaly) can explain the values of the residuals obtained in an attenuating domain (Seber *et al.* 1996). The example of a digital seismogram (vertical-component, pass band 2–10 Hz) for a seismic event occurring in the Rif tectonic boundary (Fig. 5a) shows significant attenuation of the shear waves (S phase). Stations BIT and MIF are located at equal distances from the epicentre, but with opposite azimuths. Seismic waves crossing the Rif lose their entire shear wave energy. No Sg arrival was identified on the BIT record. In contrast, waves propagating towards the south (MIF) clearly show the arrival of high-frequency S phase. As the distance covered is short (126 km), this indicates that the energy loss that seismic waves undergo while crossing the Rif Domain is caused by geometrical attenuation. Thus, we attribute it to frequency-dependent anelastic attenuation.

A second seismogram example also shows the absence of an S phase (Fig. 5b). This event was located in the eastern part of the Rif (Seber 1995). Both epicentres selected to show this attenuation effect are situated in the Rif Domain. A third example, for an epicentre outside the Rif, clearly shows the recording of this shear-wave S phase by stations RSA and CPS (Fig. 5c). Attenuation is accentuated significantly when both station and epicentre are in the Rif.

For this group of stations we take into account the existence of a major morphological structure along the continental margin to the Gibraltar Strait. This structure is responsible for focusing seismic waves towards these stations (Seber *et al.* 1993). The influence of this structure is reflected in a notable increase in recorded durations, and consequently may justify the positive values of residuals of these stations (average 0.12). Residuals obtained for stations of SG-4 and SG-5 located in the Rif Domain may not be accurately explained without considering the simultaneous interaction of several geological and geophysical factors.

To explain residual values for SG-6, we note the following: (1) the location of these stations on Neogene basins or in their immediate vicinity; (2) the existence of zones with a focusing effect, which can influence seismic signals before they reach these stations (Seber 1995); (3) a high surface heat flow density ranging between 100 and 130 mW m^{-2} (Rimi 1999) (Fig. 3).

(1) In younger unconsolidated sediments, reverberations in the surface layers lead to lengthening of the signal duration. Moreover, low impedance of these formations is responsible for the amplification (by resonance) observed in such conditions. High-frequency phases respond well to the theoretical ray law for a given heterogeneity. According to this law, and from Su *et al.* (1992), the site amplification factor (and consequently, the site residual, as they are linearly correlated) is proportional to the square root of the impedance. Site residual has its highest positive value for younger, less consolidated sediments (Guttenberg & Richter 1956; Borcherdt & Glassmoyer 1992; Eaton 1992; Su *et al.* 1992). This value decreases with the age and state of consolidation of the geological formation for all frequencies ranging between 1.5 and 12 Hz. Furthermore, Menerould & Bard (1987) have shown that the seismic signal is significantly modified in step with the mechanical behaviour of rocks.

(2) In a study of the propagation of high-frequency waves generated by Atlantic seismic events recorded by Moroccan stations, Seber *et al.* (1993) noted a common characteristic in the records; an S phase arrival with a large amplitude is obtained on the majority of the records, but its velocity is too slow for it to be considered as a 'simple' Sn phase. Another late seismic wave phase recorded is also observed, and the travel time duration of this

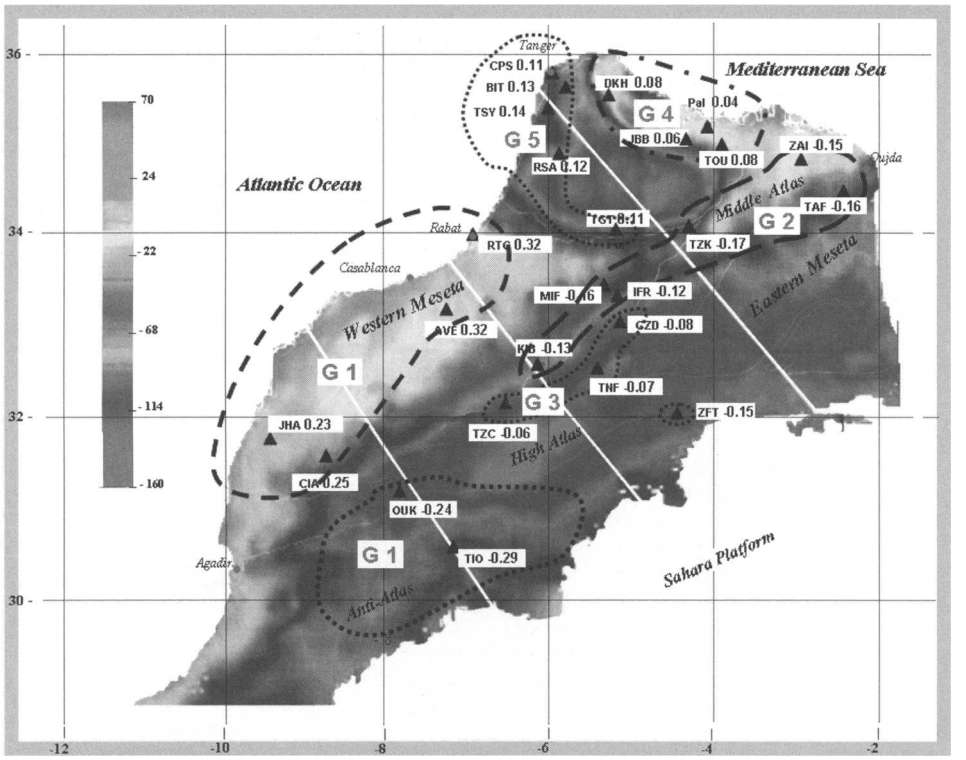

Fig. 5. Site residual values superimposed on a Bouguer gravity anomaly map of northern Morocco.

phase corresponds to the travel time of the Sn phase. The large-amplitude, low-velocity, S phase is interpreted as the result of the Sn to Sg conversion (Seber *et al.* 1993). This conversion is attributed to the thickness of the crust along the continental margin and the coastal zones (Seber *et al.* 1993). Two conversion zones are thus observed, and are considered as a caustic zone, because a sudden increase of the Moho discontinuity depth is noted. This focusing effect is responsible for the recorded large amplitudes for the converted S phases (Seber *et al.* 1993).

(3) The high surface heat flow density (100–130 mW m^{-2}) in the northern part of the Western Meseta (Fig. 3) becomes suddenly less important towards the south (70–90 mW m^{-2}). This observation provides an additional explanation for the relative decrease of the residuals from the north (0.32 at AVE and 0.32 at RTC) to the south (0.25 at CIA and 0.23 at JHA). This is because of the relationship between heat flow and high-frequency phase velocities (Kubic 1988; Sharma *et al.* 1991; Rimi 1999).

Conclusion

A simple qualitative method to explain the discrepancies of the site residual values of 25 seismic stations consists in the use of all the available geological and geophysical data, integrated and combined according to their prevalence in a given region.

Six groups of residual values are thus differentiated. SG-1 (TIO and OUK) is characterized by high negative residuals (−0.29 and −0.24), which indicate the tendency of these stations to record considerably shortened durations. The residual values are attributed to the combined effect of at least three parameters: (1) the nature of the geological formations, which are old, well compacted and crystallized; (2) the low surface heat flow in the region; (3) the attenuation caused by the geometrical propagation resulting from the long distances from the source to the station. SG-2 group, ZAI (−0.15), TAF (−0.16), TZK (−0.17), MIF (−0.16), IFR (−0.12), KIB (−0.13) and ZFT (−0.15), with intermediate negative residuals, records relatively short durations. These residuals seem to be the combined effect of: (1) the location of the stations on rigid geological formations characterized by their high impedance, which results in the loss of a great part of the seismic signal; (2) the high heat flow in the region, which may exert an opposed influence by lengthening durations. SG-3, consisting of CZD (−0.08), TNF (−0.07) and TZC (−0.06), has slight negative

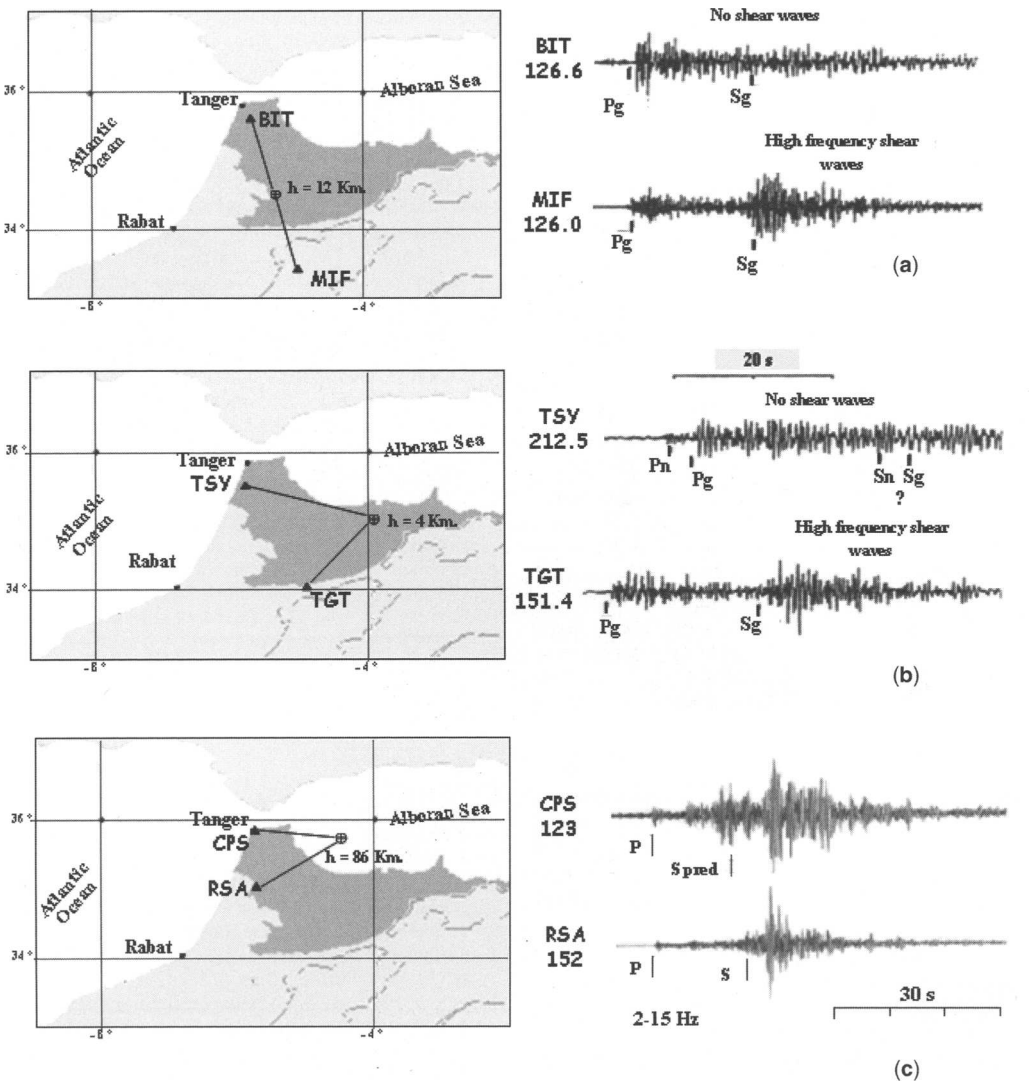

Fig. 6. (**a**, **b**) Examples of seismograms showing the high attenuation of shear waves for stations located in the Rif in the case of seismic events occurring in the Rif (modified from Seber 1995). (**c**) Examples of seismograms showing the efficiency of shear waves for the Rif stations in the case of a seismic event occuring outside the Rif (modified from Calvert *et al.* 2000).

residuals, resulting from the following effects: (1) the stations are situated in the zone between two attenuating regions (SG-1 and SG-2); (2) the major faults marking this zone significantly increase the recorded durations as a result of the energy of the late phase arrivals being trapped in faulted areas; (3) in contrast to SG-2, a low heat flow density is observed here, and therefore we can exclude perturbations that can generate an increase recorded durations. The attenuating effect of the rigid geological formations is compensated by the late liberation of the seismic wave energy trapped in the faulted zones. SG-4, consisting of DKH (0.08), JBB (−0.06), TOU (−0.08) and PAL (−0.04), is located in the metamorphosed and deformed (by African–Iberian collision) Internal Rif Domain. Residuals here are the result of the following factors: (1) the rocks of this region are compact Palaeozoic geological formations, which are considered as an attenuating medium (Seber *et al.* 1996); (2) the intense faulting in the region (Ait Brahim 2003), and the short source–station distances in this zone result in lengthened durations, and consequently,

compensate for the attenuation expected in this zone, resulting in very small residual values. SG-5, consisting of CPS (0.11), BIT (0.13), TSY (0.14), RSA (0.12) and TGT (0.11), is composed of stations also belonging to the Rif Domain in a zone characterized by: (1) the presence of a deep crustal root responsible for the replacement of lithospheric by asthenospheric low-velocity material in the External Rif (with a low Bougeur anomaly of −150 mGal); (2) the high heat flow density in this zone. These two parameters may cause a considerable increase in recorded durations in a domain known for its attenuation (Seber *et al.* 1996). SG-6, consisting of RTC (0.32), AVE (0.32), CIA (0.25) and JHA (0.23), shows high positive residuals. These sites record considerably increased durations. We attribute this to at least three principal factors: (1) the stations are located on recent unconsolidated Neogene and Quaternary sediments of the coastal Meseta Domain, which is known for its amplification (as a result of low impedance) (Su *et al.* 1992); (2) the high heat flow density recorded in this area may lengthen durations; (3) the existence of focusing zones along the continental Moroccan margin is also responsible for increasing the recorded signals' durations, and for the considerable amplification of recorded Atlantic seismic events.

This work was carried out within the framework of UNESCO–IUGS–IGCP project 457 'Natural Environmental and Technological Disasters', Seismic Hazard and Risk Assessment in North Africa, and project Ictp-n et.40, of the North African Seismological Group (NASG).

References

AIT BRAHIM, L. 2003. Cinématique des principales failles de la chaîne rifaine, cadre sismotectonique et risque sismique. *Travaux de l'Institut Scientifique, Rabat*, **21**, 141–150.

AIT BRAHIM, L., CHOTIN, P., HINAJ, S., *ET AL.* 2002. Paleostress evolution in the Moroccan African margin from Triassic to Present. *Tectonophysics*, **357**, 187–205.

AZZOUZI, M., GRIFFITHS, B., *ET AL.* 1999. Evolution des sources du volcanisme marocain au cours du Néogène. *Comptes Rendus Academie de Science, Paris*, **329**, 95–102.

BORCHERDT, R. D. & GLASSMOYER, G. 1992. On the characteristics of local geology and their influence on ground motions generated by the Loma Prieta earthquake in the San Fransisco Bay region, California. *Bulletin of the Seismological Society of America*, **82**, 603–641.

CALVERT, A., SANDVOL, E., DOGAN, S., BARAZANGI, M., VIDAL, F., ALGUACIL, G. & JABOUR, N. 2000. Propagation of regional seismic phases (Lg and Sn) and Pn velocity structure along the Africa-Iberia plate boundary zone: tectonic implications. *Journal of Geophysical Research*, **142**, 384–408.

CHALOUAN, A., SAJI, R., MICHARD, A. & BALLY, A. W. 1997. Neogene tectonic evolution of the southwestern Alboran basin as inferred from seismic data of Morocco. *AAPG Bulletin*, **817**, 1161–1184.

CHALOUAN, A., MICHARD, A., FEINBERG, H., MONTIGNY, R. & SADDIQI, O. 2001. The Rif mountain building (Morocco): a new tectonic scenario. *Bulletin de la Société Géologique de France, 7*, **172**(5), 603–616.

CHERKAOUI, T. E. 1991. *Contribution à l'étude de l'aléa sismique au Maroc*. Thèse 3ème cycle, Université Joseph Fourier, Grenoble.

EATON, J. P. 1992. Determination of amplitude and duration magnitude and site residuals from short-period seismographs in northern California. *Bulletin of the Seismological Society of America*, **82**(2), 533–579.

FEDAN, B. 1988. *Evolution géodynamique d'un bassin intraplaque sur décrochements: le Moyen Atlas (Maroc) durant le Méso-Cénozoïque*. Thèse d'Etat, Université. Mohamed V, Rabat.

FROGNEUX, M. 1980. *La sismicité marocaine de 1972 à 1978. Etude des paramètres à la source des séismes proches*. Thèse 3ème cycle, Université de Grenoble.

GUTTENBERG, B. & RICHTER, C. F. 1956. Magnitude and energy of earthquakes. *Annales Geophysicae*, **9**, 1–15.

HATZFELD, D. & BENSARI, D. 1977. Grands profils sismiques dans la région de l'Arc de Gibraltar. *Bulletin de la Société Géologique de France, 7*, **XIX**(4), 749–756.

KANG, I. K. & MCMECHAN, G. A. 1993. Effect of viscoelasticity on seismic wave propagation in fault zones, near surface sediments, and inclusions. *Bulletin of the Seismological Society of America*, **83**(3), 890–906.

KUBIC, J. 1988. Relation between the field of surface heat flow and the distribution of Pn-wave velocities for continents. *Studia Geophysica et Geodaetica*, **32**, 287–299.

LAGARDE, J. L. 1985. Cisaillements ductiles et plutons granitiques contemporains de la déformation hercynienne post-viséenne de la Meseta marocaine. *Hercynica*, **1**, 29–37.

LAVILLE, E. 1985. *Evolution sédimentaire, tectonique et magmatique du bassin jurassique du Haut Atlas (Maroc): modèle en relais multiples de décrochements*. Thèse de Doctorat d'Etat, Université de Montpellier.

LEBLANC, M. & LANCELOT, J. R. 1980. Interprétation géodynamique du domaine panafricain de l'Anti Atlas (Maroc) à partir de données géologiques et géochronologiques. *Journal Canadien des Sciences de la Terre*, **17**, 173–174.

LEBLANC, D. & OLIVIER, P. 1984. Role of strike-slip faults in the Betic–Rifian orogeny. *Tectonophysics*, **101**, 345–355.

MÉNEROUD, J. P. & BARD, P. Y. 1987. Modification du signal sismique par la topographie. Cas de la vallée

de la Roya (Alpes-Maritimes). *Bulletin Liaison Laboratoires des Ponts et Chaussées*, **151**, 140–151.

MICHARD, A. 1976. Eléments de géologie marocaine. *Notes et Mémoires du Service Géologique du Maroc*, **252**, 1–408.

MICHARD, A., CHALOUAN, A., FEINBERG, H., GOFFE, B. & MONTIGNY, R. 2002. How does the Alpine belt end between Spain and Morocco? *Bulletin de la Société Géologique de France*, **173**(1), 3–15.

MOUAYN, I., TADILI, B., AIT BRAHIM, L., RAMDANI, M., LIMOURI, M. & JABOUR, N. 2004. Duration magnitude scale and site residuals for Northern Morocco. *Pure and Applied Geophysics*, **161**, 1060–1081.

PIQUÉ, A. 1994. *Géologie du Maroc. Les domaines régionaux et leur évolution structurale*. Pumag, Marrakech.

PIQUÉ, A. & MICHARD, A. 1989. Moroccan Hercynides: a synopsis. The Palaeozoic sedimentary and tectonic evolution at the northern margin of West Africa. *American Journal of Science*, **289**, 286–330.

RIMI, A. 1999. Mantle heat flow and geotherms for the main geologic domains in Morocco. *Geologishe Rundschau*, **88**, 458–766

RIMI, A. 2001. *Carte de densité du flux de chaleur et du gradient géothermique dans le Nord du Maroc*. Special Publication of Symposium: La Chaîne Rifaine dans son Cadre Méditerranéen Occidental, Rabat, 29–30 October, 2001.

SEBER, D. 1995. *Lithospheric and upper mantle structure beneath northern Morocco and central Syria*. PhD thesis, Cornell University, Ithaca, NY.

SEBER, D., BARAZANGI, M., TADILI, B., RAMDANI, M., BENBRAHIM, A., BENSARI, D. & El ALAMI, S. O. 1993. Sn to Sg conversion and focusing along the Atlantic margin, Morocco: implications for earthquake hazard evaluation. *Geophysical Research Letters*, **20**(14), 1503–1506.

SEBER, D., BARAZANGI, M., Tadili B., RAMDANI, M., BENBRAHIM, A. & BENSARI, D. 1996. Three-dimensional upper mantle structure beneath the intraplate Atlas and interplate Rif mountains of Morocco. *Journal of Geophysical Research*, **101**(B2), 3125–3138.

SHARMA, S. R., SUNDAR, A., RAO, V. K. & RAMANA, D. V. 1991. Surface heat flow and Pn velocity distribution in peninsular India. *Journal of Geodynamics*, **13**, 67–76.

SU, F., AKI, K., TENG, T. & ZENG, Y. 1992. The relation between site amplification factor and surficial geology in central California. *Bulletin of the Seismological Society of America*, **82**(2), 580–602.

VIDAL, J. C. 1977. Structure actuelle et évolution depuis le Miocéne de la chaine rifaine (partie Sud de l'Arc de Gibraltar). *Bulletin de la Societé Géologique de France*, 7, **XIX**, 389–396.

Fluid geochemistry versus tectonic setting: the case study of Morocco

F. TASSI[1], O. VASELLI[1,2], G. MORATTI[2], L. PICCARDI[2], A. MINISSALE[2], R. POREDA[3], A. DELGADO HUERTAS[4], A. BENDKIK[5], M. CHENAKEB[5] & D. TEDESCO[6]

[1]*Department of Earth Sciences, University of Florence, Via G. La Pira, 4, 50121 Florence, Italy*

[2]*CNR-Institute of Geosciences and Earth Resources, Via G. La Pira, 4, 50121 Florence, Italy (e-mail: gmoratti@geo.unifi.it)*

[3]*Department of Earth and Environmental Sciences, University of Rochester, 227 Hutchinson Hall, Rochester, NY 14627, USA*

[4]*Estacion Experimental de Zaidin (CSIC), Prof. Albareda 1, 18008 Granada, Spain*

[5]*Ministère de l'Energie et des Mines, Direction du Devéloppement Minier, BP 6208, Rabat-Institut, Morocco*

[6]*Department of Environmental Sciences, 2nd University of Napoli, Via Vivaldi 43, 81100 Caserta, Italy*

Abstract: This paper presents the results of an extensive chemical and isotopic investigation on natural thermal and cold fluids (spring waters and associated gases) discharging throughout the main geological domains of Morocco. The chemical features of the thermal springs are mainly dependent on rock dissolution involving Triassic evaporite formations, producing either Na–Cl or Ca–SO_4 composition, although mixing with shallower connate high-saline waters in Neogene post-orogenic sedimentary layers cannot be ruled out. Only in the Moroccan Meseta and Anti-Atlas domains have spring discharges probably undergone equilibration as a result of water–rock interaction in granites. Of the chemical and isotopic features of the gas seeps, $^3He/^4He$ ratios and $\delta^{13}C-CO_2$ values indicate the occurrence of a significant contribution of mantle-derived gas, especially at Oulmès (Moroccan Meseta) and Tinejdad-Erfoud (Anti-Atlas), where associated waters are found to equilibrate at relatively high temperatures (*c.* 130 °C). These areas are also characterized by the presence of Pliocene to Quaternary basaltic volcanic rocks. Thermal discharges located along the Rif front and related to the NE–SW-oriented main strike-slip faults are associated with a CH_4- and/or N_2-rich gas phase, derived respectively from a crustal or an atmospheric source. Some of them have significant contents of ^3He that could indicate the rising of mantle fluids. Such a striking isotopic signature, which is not related to any recent volcanism visible at surface, is likely to be associated with cooling magma at depth related to transpressive fault systems. Similarly, in the northeastern area, the small, although significant, enrichment of ^3He in the gas discharges seeping out along the Nekor seismic active fault and related to Pliocene–Quaternary basalts also suggests a deep-seated (magmatic) contribution. The distribution of thermal discharges is strongly related to the main active tectonic structures of Morocco. Moreover, this study indicates the presence of deep active tectonic structures in areas until now considered as stable. In particular, the NE–SW-trending Nekor fault may be part of a major system that extends to the Moroccan Meseta and into the Smaala–Oulmès fault system, thus emerging as a deep structure with crustal significance.

The geochemical features of natural fluid discharges, such as cold and thermal springs and associated gas phases, have an important role in comprehending physico-chemical processes acting at depth (i.e. water–rock interaction, mixing) and in retrieving clues of deep-seated inputs (hydrothermal, metamorphic and magmatic). Fluid circulation in the shallow crust is particularly active at plate boundaries as a result of: (1) rugged morphology; (2) perturbations of the thermal vertical profiles induced by subduction slabs and the rise of mantle material, which favour convection of fluids (e.g. Oliver 1986, 1992; Sverjensky & Garven 1992); (3) active tectonics. Active faults provide open pathways for the circulation of such fluids (Barnes *et al.* 1978). When deep-sourced fluids pass through the shallow

From: MORATTI, G. & CHALOUAN, A. (eds) 2006. *Tectonics of the Western Mediterranean and North Africa.* Geological Society, London, Special Publications, **262**, 131–145.
0305-8719/06/$15.00

crust, they may undergo, while rising to the surface, phase separation, mixing with meteoric-dominated aquifers and chemical re-equilibration. As a consequence, on a regional scale, their resulting chemical and isotopic composition at the surface is highly variable (e.g. Vaselli *et al.* 2002; Minissale 2004).

A detailed study of the chemical characteristics of fluid discharges is worth while in Morocco, whose tectonic setting reflects a long-lived and complex evolution. Three Alpine chains (the Rif, the NE–SW-trending Middle Atlas and the east–west-oriented High Atlas) develop north of the Anti-Atlas Domain, which represents the northern limit of the African Shield, and are superimposed on the Hercynian belt, which largely crops out in the Moroccan Meseta (Fig. 1). The entire orogenic system is strongly affected by inherited structures, some of which are still active. In particular, field evidence supports the fact that the Middle Atlas Shear Zone is a complex active boundary (Bernini *et al.* 2000), as is also suggested by the many Pliocene–Quaternary basaltic outcrops, scattered from the Anti-Atlas to the Mediterranean coast (e.g. Maury *et al.* 2000).

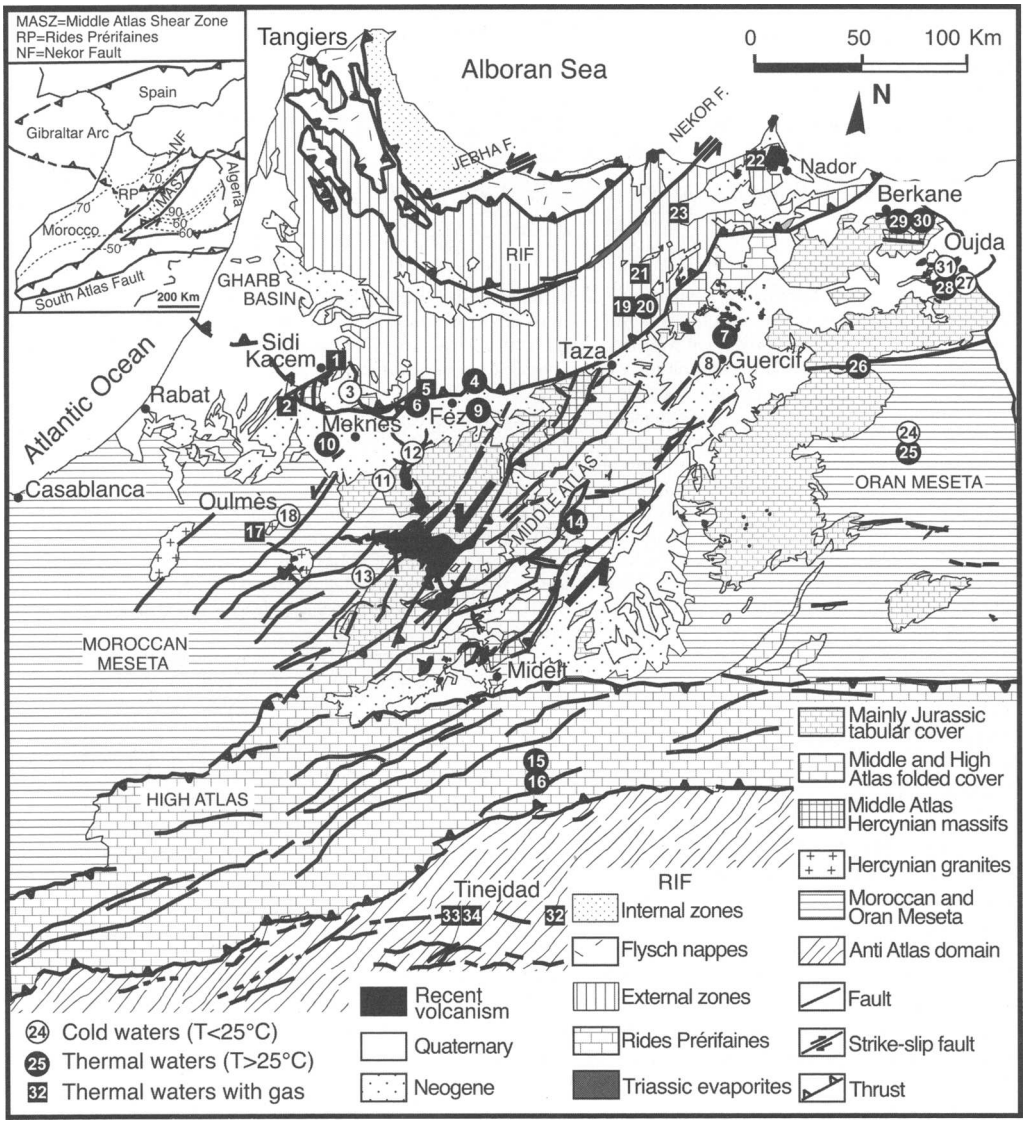

Fig. 1. Schematic geological map of Morocco (data from Carte Géologique du Maroc 1975, 1985, 1988, 1991; Suter 1980*a*,*b*; Baudin *et al.* 2001*b*; Bendkik 2004; Chenakeb 2004) and location of the water and gas sampling sites. In the inset, dotted isolines suggest the rough trend of heat flow density (Rimi & Lucazeau 1987).

In this paper we try to: (1) use the composition and location of natural thermal and gas discharges throughout the main domains to relate the present deep fluid circulation to the most relevant tectonic structures; (2) detect connections with active tectonics; (3) eventually, recognize the presence of shallow active hydrothermal systems.

Geological setting

From a geological point of view, Morocco is one of the most fascinating regions in the Mediterranean area, reflecting a long-lived history that started in the Precambrian and is still active. As a consequence of this evolution, in central–northern Morocco several structural domains (Fig. 1) can be distinguished, as follows.

(1) The Anti-Atlas, to the south, consists of Precambrian rocks of the Pan-African Belt, overlain by a gently folded Palaeozoic cover (e.g. Choubert 1963; Michard 1976).

(2) The Mesetas, in Central and Eastern Morocco, are composed of metamorphic and granitic Palaeozoic rocks of the Hercynian Belt, covered by a tabular Mesozoic–Cenozoic succession (e.g. Piqué 2001); the Palaeozoic rocks mostly crop out in the Moroccan Meseta, to the west, where Hercynian granitic bodies are present, whereas in the Oran Meseta large Pliocene–Quaternary continental basins developed (e.g. Carte Géologique du Maroc 1985; Baudin *et al.* 2001*a*,*b*).

(3) The Middle and High Atlas are relatively narrow mountain belts mainly consisting of Mesozoic carbonates and terrigenous Cenozoic successions (e.g. Choubert & Faure-Muret 1960–1962; du Dresnay 1988). This realm developed on a series of pre-existing structural weak zones that dissected the Hercynian Belt and controlled the Permian–Triassic opening of the Atlas basins. During the Alpine orogeny, inversion of these structures led to the closure of the basins and the formation of the intracontinental Atlas chains (e.g. Michard 1976; Mattauer *et al.* 1977; Laville & Piqué 1991).

(4) The Rif, to the north, is a thrust-and-fold belt belonging to the Mediterranean Alpine chains that underwent polyphase deformation from Late Eocene to Quaternary time, with the deformational front migrating southwards, towards the external zones (e.g. Wildi 1983; Chalouan *et al.* 2001). The frontal thrust of the Rif bounds to the south the onshore southern branch of the Gibraltar Arc, creating a large foreland basin, which is dissected along roughly NE–SW-trending faults into the Gharb, Meknes and Guercif Basins (Fig. 1).

All the structural domains of Morocco are strongly affected by inherited structures that were reactivated during the Hercynian and Alpine orogeneses (e.g. Piqué *et al.* 1987). These structures, marking the limits of the Permian–Triassic basins at the onset of the Alpine cycle, controlled the distribution of sedimentation, in particular of the Triassic–early Jurassic evaporites that can be found widely distributed in both the Rif and Atlas domains and, subordinately, in the Mesetas (Salvan 1974).

The three Alpine belts, superimposed and accreted onto the older chains, are limited by east–west- and NE–SW-trending main structures, whose present-day activity as a result of the roughly north–south-directed Africa–Eurasia convergence is demonstrated by a diffuse seismicity (Hatzfeld & Frogneux 1981; Medina & Cherkaoui 1992; Hatzfeld *et al.* 1993). Both the northern and southern borders of the High Atlas are east–west-trending active thrusts (Dutour & Ferrandini 1985; Froitzheim *et al.* 1988; Jacobshagen *et al.* 1988; Zouine *et al.* 1996; Piccardi *et al.* 2001). Also active are the east–west-trending 'Rides Prérifaines', which are the expression of the frontal thrust of the Rif in the Meknes–Fez area (Moratti *et al.* 2003; Piccardi *et al.* 2004). The NE–SW-trending faults, limiting the Middle Atlas, underwent, and still are subject to, sinistral transpression under the same compression (e.g. Jacobshagen *et al.* 1988; Fedan *et al.* 1989; Boccaletti *et al.* 1990; Bernini *et al.* 1996, 1999, 2000; Gomez *et al.* 1996).

Inherited structures with the same orientation are also developed within the main structural domains. Major sinistral transpressive faults, the Jebha and Nekor faults, and the northern extension of the Middle Atlas Shear Zone affect the Rif and constitute lateral ramps of the major thrust fronts (Olivier 1981–1982; Leblanc & Olivier 1984; Hernandez *et al.* 1987; Bernini *et al.* 1996, 1999, 2000; Tejera de Leon 1997). The Nekor fault, in particular, is one of the most important seismic structures of Morocco (Medina 1995; Calvert *et al.* 1997). The Nekor fault is usually indicated only as the lateral ramp of one of the main internal thrusts of the Rif (Fig. 1). Segments prolonging this structure to the south under the thick Rifian cover and joining with the frontal thrust of the Rif have been suggested by Meghraoui *et al.* (1996). The entire Middle and High Atlas are internally affected by NE–SW- and ENE–WSW-oriented mainly sinistral transpressive faults. NE–SW- and east–west-trending fault systems are also developed in the Mesetas and in the Anti-Atlas domains, respectively (Fig. 1).

Sampling procedures and analytical methods

Water and associated gases from most thermal springs of Morocco and from some cold springs and rivers for reference were collected during three sampling campaigns, carried out in October 2002, September 2003 and July 2004 in the framework

of the scientific co-operation between Morocco and Italy.

Thermal spring water discharges are distributed over a wide area, from the Alboran Sea coast to the north towards the Anti-Atlas Domain (samples 32, 33 and 34) to the south, and from the Oran Meseta (samples 24, 25 and 26) to the Moroccan Meseta (samples 13, 17 and 18) in the east–west direction, including the Rif, Middle Atlas and High Atlas domains (Fig. 1).

Temperature and pH of water discharges were measured in the field. Alkalinity (titration with 0.01 N HCl), B (Azometina-H method; Bencini 1985), NH_4 (molecular spectrophotometry), the main anions (SO_4, Cl, Br, F and NO_3 with a Dionex DX100 ionic chromatograph) and cations (Ca, Mg, Na, K and Li with a Perkin–Elmer AAnalyst 100) were determined in the Geochemistry Laboratories of CNR-IGG and the Department of Earth Sciences of Florence.

$^{18}O/^{16}O$ and $^{2}H/H$ isotopic ratios (expressed as $\delta^{18}O$ and δD ‰V-SMOW) in water samples were determined using a Finnigan Delta Plus XL mass spectrometer at CSIC Laboratories in Granada. Oxygen isotopes were analysed using the CO_2–H_2O equilibration method of Epstein & Mayeda (1953). The hydrogen isotopic measurements were carried out on H_2 obtained after the reaction of 10 μl of water with metallic zinc at 500 °C according to the analytical procedure described by Coleman *et al.* (1982). The experimental error was ±0.1‰ and ±1‰ for $\delta^{18}O$ and δD values, respectively, using EEZ-3 and EEZ-4 as internal standards, which were previously calibrated against V-SMOW and SLAP reference standards.

Gases were collected by using a plastic funnel positioned upside-down in the bubbling gas, to which preweighed and pre-evacuated 50 ml Thorion-tapped glass tubes, partially filled with 20 ml of a 0.15M $Cd(OH)_2$ and 4M NaOH solution, were connected. Gas sampling lasted until the vacuum head-space pressure reached that of the discharging vent. Acidic gases (CO_2 and H_2S) were trapped in the alkaline solution, and residual non-condensable gases (N_2, O_2, CO, H_2, He, Ar, Ne, CH_4 and light hydrocarbons) accumulated in the head-space. During sampling, H_2S reacts with Cd^{2+} in solution to form poorly soluble CdS (Montegrossi *et al.* 2001).

In the laboratory, inorganic gas compounds (N_2, H_2, He, O_2, Ar and Ne) were analysed using a gas chromatograph (Shimadzu 15a) equipped with a thermal conductivity detector (TCD), by using a long molecular sieve column (9 m at a temperature of 30 °C) to obtain a satisfactory separation between H_2, He and Ne peaks. To split Ar from O_2 the temperature was lowered to 0 °C by using cryogenic equipment (Shimadzu CRG-15) fed by liquid CO_2. Light hydrocarbons (C_2–C_6 compounds) were analysed by gas chromatography using a flame ionization detector (FID) and by using a column packed with Chromosorb 80/100 mesh coated with 23% SP 1700 (Tassi *et al.* 2004).

After the chromatographic analysis, the solution and the solid precipitates were centrifuged to separate the two phases. CdS in the solid phase was dissolved and oxidized with H_2O_2 and then analysed for H_2S by ion chromatography as SO_4^{2-}, whereas CO_2 in the caustic solution was analysed by titration with 0.5N HCl (Montegrossi *et al.* 2001). Precision is generally <1% for major gas components and <5% for minor and trace compounds.

The $^{13}C/^{12}C$ isotopic ratio of CO_2 (expressed as $\delta^{13}C$ ‰ V-PDB) was determined with a Finnigan Delta S mass spectrometer in Florence after extraction and purification of the gas mixture by standard procedures (Evans *et al.* 1998). Internal (Carrara and San Vincenzo marbles) and international (NBS18 and NBS19) standards were used for estimation of external precision. Analytical error is ±0.05‰. The reproducibility of δ values for C is ±0.1‰.

$^{3}He/^{4}He$ and $^{40}Ar/^{36}Ar$ ratios were determined using a noble gas mass spectrometer (VG5400) at the Department of Earth and Environmental Sciences, University of Rochester (NY). The mass spectrometer adequately measures ^{3}He without interference from HD and H_3. The gas samples were processed on a stainless steel and Corning-1724 glass high-vacuum line. Water vapour and CO_2 were removed at −90 °C and −195 °C, respectively, and N_2 and O_2 reacted with Zr–Al alloy (SAES-ST707). Ar and Ne were adsorbed on activated charcoal at −195 K and at −230 K, respectively. SAES-ST-101 getters (one in the inlet line and two in the mass spectrometer) reduce the HD^+ background to *c.* 1000 ions/s^{-1}. $^{3}He/^{4}He$ ratios were analysed by a Faraday cup (resolution of 200) and a Johnston electron multiplier (resolution of 600) for sequential analyses of the ^{4}He (Faraday cup) and ^{3}He (multiplier) beams. On the axial collector (resolution of 600) $^{3}He^+$ is completely separated from HD^+ with a baseline separation of <2% of the HD^+ peak. The contribution of HD^+ to the ^{3}He peak is <0.1 ion/s^{-1} at 1000 ions/s^{-1} of HD^+. The analytical error for the $^{3}He/^{4}He$ ratio estimation is about 0.3%. After completion of the helium analysis, $^{40}Ar/^{36}Ar$ ratios are measured on a split of the purified argon. Sensitivity for argon is about 4×10^{-4} AT^{-1} and precision is about 0.2%.

Results and discussion

Chemical composition of waters

Outlet temperatures, pH values, contents of major and minor components and total dissolved solids (TDS) values of water discharges are reported in Table 1.

Table 1. *Outlet temperatures, pH and TDS values, chemical composition and $\delta^{18}O$ and $\delta^{2}H$ values (expressed as ‰ V-SMOW) of the water discharges from Morocco*

Sample	Location	T (°C)	pH	HCO_3	SO_4	Cl	Na	K	Ca	Mg	NH_4	B	NO_3	F	Br	Li	TDS	$\delta^{18}O$	$\delta^{2}H$
1	Moulay Yacoub de Bab Tiouka	19.0	6.28	662	78	18750	10100	127	952	455	n.d.	20	5.9	12.50	37.50	4.60	31204	−4.52	−28.9
2	Moulay Yacoub Hamma	40.0	6.45	293	1075	2250	1562	34	359	121	n.d.	1.9	0.6	4.50	0.45	0.54	5701	−5.21	−28.9
3	Volubilis	20.2	7.60	319	7	23	9	1	77	23	n.d.	0.07	27.5	0.45	0.30	0.00	488	−5.30	−28.5
4	Hammam Zalag	34.0	6.84	256	150	2140	1275	26	139	45.1	n.d.	0.32	0.4	1.00	2.75	1.07	4036	−6.27	−35.3
5	Moulay Yacoub	53.2	6.14	270	15	16000	8400	265	1065	333	n.d.	5.5	1.1	2.65	35.00	12.00	26404	−4.68	−38.0
6	Skounate	33.0	7.45	336	29	230	148	2	68	28.9	n.d.	0.06	6.9	0.11	0.25	0.04	849	−4.23	−33.1
7	Gue Titir	43.2	6.63	204	2500	4375	2130	26	950	280	n.d.	0.22	1.3	0.80	21.50	0.67	10489	−8.43	−54.3
8	Guercif	24.3	n.d.	427	138	135	79	5	125	42	n.d.	0.00	35.0	0.38	0.23	0.03	986	−5.95	−52.5
9	Sidi Harazem	31.0	n.d.	342	13	350	159	4	81	46	n.d.	0.00	0.2	2.50	0.38	0.14	997	−7.56	−42.4
11	El Hajeb	18.0	8.80	331	7	4	8	0.9	52	36	n.d.	0.00	25.0	0.15	0.05	0.00	464	−7.25	−40.2
12	Ain Bitit	16.8	8.40	366	3	10	7	1	79	21	n.d.	0.00	7.8	0.10	0.09	0.00	494	−7.76	−44.5
13	Ain Leuh	14.0	6.86	457	23	15	2	0.9	87	43	n.d.	0.00	6.8	0.40	0.11	0.00	635	−8.75	−49.3
14	Imouzer des Marmoucha	36.2	6.84	433	70	227	150	1	98.5	33	n.d.	0.00	1.6	0.45	0.21	0.02	1014	−9.08	−55.4
15	Rich 1	32.0	8.11	259	75	588	349	3	78.5	26	n.d.	0.04	8.8	2.13	0.48	0.03	1389	−8.31	−50.7
16	Rich 2 (Oued Ziz)	43.5	7.04	262	1275	2700	1663	19	474	80	n.d.	0.17	0.8	1.75	3.55	0.11	6479	−8.74	−58.6
17	Haya (Oulmès)	42.0	6.31	1037	13	225	244	24	124	57	n.d.	0.64	0.7	3.00	1.25	4.80	1733	−5.93	−38.0
18	Haya 2 (cold)	22.0	8.88	146	7	12	26	6	21	9.2	n.d.	0.00	1.1	0.38	0.09	0.00	229	−6.20	−36.3
19	Hajra Safra	23.0	6.62	518	3500	6750	5525	10	970	105	2.70	6.1	0.4	3.20	5.50	0.16	17396	−3.60	−42.3
20	Hajra Safra 2	20.0	7.66	1238	775	2450	2350	11	48	105	33	2.5	0.3	4.70	2.70	0.14	7020	−2.50	−34.6
21	Al Hamra	24.5	6.36	1513	575	24	265	7	341	78	0.58	0.28	0.6	0.95	0.03	0.16	2806	−6.55	−39.2
22	Haddou Ou Amar	28.5	6.57	396	710	1950	1175	48	324	77	0.76	0.86	2.8	1.25	2.30	0.60	4689	−0.02	−25.9
23	Chifa	29.0	6.52	1342	350	240	353	7	268	80	0.65	0.43	0.2	2.50	0.50	0.33	2644	−2.76	−34.1
24	Oued Chareft	19.0	8.34	229	110	39	32	3	63	38	0.05	0.14	0.6	1.65	0.05	0.02	516	−0.94	−40.9
25	Beni Mathar	25.5	7.59	220	425	430	188	6	170	87	0.06	0.17	1.2	0.95	1.10	0.04	1529	−7.10	−60.5
26	Gufait	26.0	7.37	305	225	280	107	3	146	71	0.06	0.14	0.3	1.88	0.60	0.03	1140	−8.46	−58.2
27	Oujda South	23.0	7.55	414	43	53	23	1	78	50	0.08	0.06	2.1	0.50	0.08	0.00	664	−3.71	−44.8
28	Ben Kachour	50.0	6.98	367	237	1065	840	10	92	40	0.06	0.11	0.6	0.80	1.20	0.10	2654	−6.40	−47.3
29	Kiss 1	27.0	7.15	305	125	400	218	4	129	49	0.05	0.10	6.5	0.25	1.00	0.03	1237	−5.25	−41.7
30	Fezouane	38.0	7.00	342	27	16	15	0.8	66	33	0.08	0.05	3.8	6.00	0.15	0.02	510	−2.48	−37.3
31	Oujda West	25.0	8.00	267	55	270	119	13	68	65	0.09	0.10	3.2	0.45	0.60	0.02	861	−3.16	−36.8
32	Tassamounte	28.5	7.10	1726	43	125	294	26	189	155	0.06	0.38	1.3	3.25	0.45	0.49	2563	−5.41	−40.6
33	Lalla Mimouna	25.5	6.50	2300	250	460	699	94	42	194	0.11	0.92	1.6	0.55	1.25	1.45	4045	−3.24	−50.1
34	Lalla Mimouna Bir	26.0	7.54	327	87	55	52	0.4	115	16	0.08	0.18	19.8	0.45	0.15	0.05	673	−7.71	−54.5

Ion contents are in mg l^{-1}; n.d., not determined.

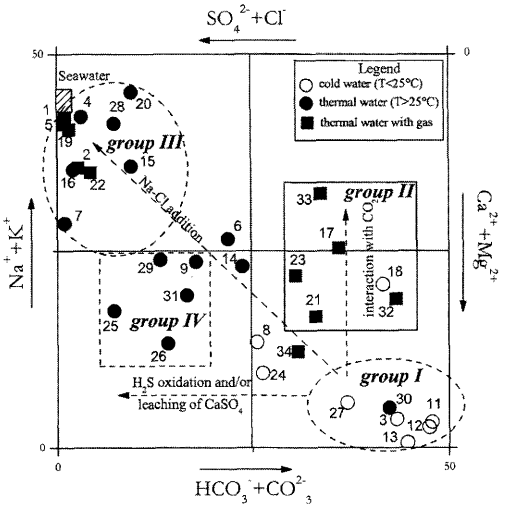

Fig. 2. Langelier–Ludwig (Langelier & Ludwig 1942) diagram for the water samples from Morocco.

The geochemical classification based on the distribution of water samples on the Langelier–Ludwig diagram (Langelier & Ludwig 1942) (Fig. 2) shows that the cold ($T < 25$ °C) waters are relatively diluted (TDS < 1000 mg l^{-1}) and have a Ca–HCO_3 composition (group I), typical of worldwide running water and groundwaters. Setting aside sample 30 (Fezouane), Ca–HCO_3 waters with >25 °C outlet temperatures are generally characterized by a higher salinity (TDS up to 2800 mg l^{-1}; Table 1) (group II; Fig. 2). As shown in Figure 3, samples 17 (Haya-Oulmès), 21 (Al Hamra 2), 23 (Chifa), 32 (Tassamounte) and 33 (Lalla Mimouna) show relatively high HCO_3 (up to 2300 mg l^{-1}) and, at a minor extent, Na (up to 699 mg l^{-1}) contents, probably related to both the presence of CO_2 (all these thermal springs are associated with a CO_2-rich gas phase) that changes to HCO_3 at pH > 4.3, and Ca–Na ion-exchange between circulating water and clay-bearing sedimentary formations (Drever 1997). This is particularly true for samples 17 and 33, whose composition is characterized by a Na–HCO_3 facies (Fig. 2).

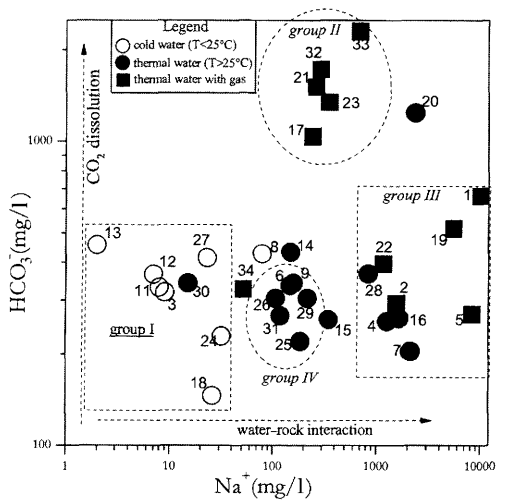

Fig. 3. Na v. HCO_3 binary diagram for water samples from Morocco.

The third group (group III; Fig. 2) includes the majority of the water discharges roughly aligned in an east–west direction between the Rif and the Middle Atlas domains (samples 1, 2, 4, 5, 7, 19, 20, 22 and 28; Fig. 1), as well as those of the High Atlas Domain (samples 15 and 16; Fig. 1). They show a Na–Cl composition with a wide range of outlet temperatures (between 19 and 53 °C; Table 1) and medium to high salinity (some of them have TDS values up to 31 g l^{-1}: Moulay Yacoub de Bab Tiouka, sample 1 in Table 1). Such compositional characteristics may be ascribed to the interaction with NaCl-rich Triassic evaporitic formations, waters from which may mix, to differing degrees, with shallower and much less saline aquifers while rising to the surface. A fourth group (group IV; Fig. 2) can be distinguished and includes the thermal springs of the Oujda province (samples 25, 26, 29 and 31; Table 1), in the Oran Meseta, and Sidi Harazem water (sample 9) located close to the town of Fez (Fig. 1). This group has a Ca–SO_4 composition, relatively low salinity (TDS is between 860 and 1500 mg l^{-1}) and outlet temperatures ranging between 25 and 36 °C (Table 1). With the exception of sample 9, the high proportions of SO_4 with respect to the other anions may reflect the oxidation of a H_2S-rich gas phase, produced by either the decomposition of organic material at shallow depths in the Neogene sedimentary formations and/or the leaching of sulphates from evaporitic layers.

The chemistry of water samples characterized by compositions intermediate between the four recognized groups (Fig. 2), such as Guercif, Oued Chareft (samples 8 and 24), Skounate, Imouzer des Marmoucha and Lalla Mimouna Bir (samples 6, 14 and 34), seems to be deriving by the mixing, to varying degrees, of the different compositional end-members described so far.

The relative abundances of F, Br and Li provide further insights into the main processes controlling the chemistry of the Moroccan water discharges. As shown in Figure 4, all the (Na–Ca)–HCO_3 (samples 17, 21, 23, 32 and 33) and a few Na–Cl (samples 2, 4, 5, 6 and 22) thermal waters have

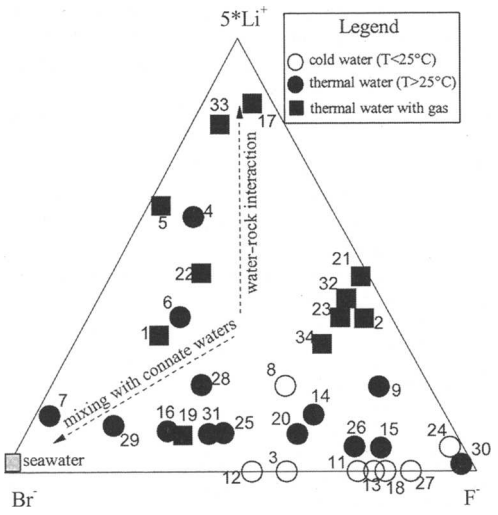

Fig. 4. F–Li × 5–Br ternary diagram for water samples from Morocco.

significant Li enrichment as a result of prolonged water–rock interaction in silicate formations and possibly favoured by the presence of a CO_2-rich gas phase that characterizes the (Na–Ca)–HCO_3 waters. In contrast, the chemistry of thermal waters that are enriched in Br and have relatively high TDS values (samples 1, 7, 16, 19, 25, 28 and 29) seems to be mainly related to the mixing to varying degrees with connate saline waters.

Isotopic composition of waters

Analytical data for $\delta^{18}O$ and δD values of water discharges range from −9.1 to −0.02‰ and from −60.5 to −28.5‰ (V-SMOW), respectively (Table 1). The $\delta^{18}O$–δD diagram in Figure 5 shows that the majority of cold waters and several thermal waters of the Rif, Middle and High Atlas domains (samples 2, 4, 7, 11, 14, 15 and 16) are aligned between the Global Meteoric Water Line (GMWL; Craig 1961) and the Mediterranean Meteoric Water Line (MMWL; Gatt & Carmi 1970). In contrast, the remaining thermal waters and three cold springs (samples 8, 24 and 27), whose chemical composition is slightly different from that of the other cold discharges in their higher SO_4 and Ca contents (Table 1), show a positive ^{18}O shift, which is possibly due to isotopic exchanges during water–rock interactions of meteoric water that permeated underground at different altitudes. Alternatively, the distribution of $\delta^{18}O$ and $\delta^{2}H$ ratios in water samples may be explained in terms of the contribution of isotopically heavy connate waters and/or the effect of evaporation (Fig. 5).

Chemical composition of gases

Chemical and isotopic (carbon in CO_2, argon and helium) compositions of the 11 gas phases associated with the thermal springs are listed in Table 2.

On the basis of their main components four groups can be distinguished: (1) CO_2-rich gases (samples 17, 21 32 and 33), associated with the Ca(Na)–HCO_3 and Na–HCO_3 water samples; (2) N_2-rich gases (samples 2 and 15), related to Na–Cl waters of medium salinity (Table 1); (3) CH_4-rich gases (samples 1 and 5), seeping out with high-saline Na–Cl waters discharging in the Rif Domain; (4) CO_2–N_2-rich gases (samples 19, 22 and 23), related to medium to high-salinity Na–Cl and Ca–HCO_3 waters whose origin can be regarded as a mixing process between rising CO_2-rich and descending N_2-rich meteoric-derived end-members.

As shown in the O_2–Ar–Ne ternary diagram (Fig. 6), Ar/Ne ratios in the Moroccan gases range between those of air-saturated water (ASW) at 20 °C (Ar/Ne = 1700) and 80 °C (Ar/Ne = 940), for pure water, respectively. This indicates that argon and neon have mainly originated from the atmosphere and, at the same time, their ratios exclude any air contamination during sampling ($Ar/Ne_{air} \approx 525$). Moreover, O_2 appears to be strongly depleted, particularly for the N_2-rich gases, possibly as a result of bacterial activity-induced oxidation processes, redox reactions among gas species and water–rock interaction.

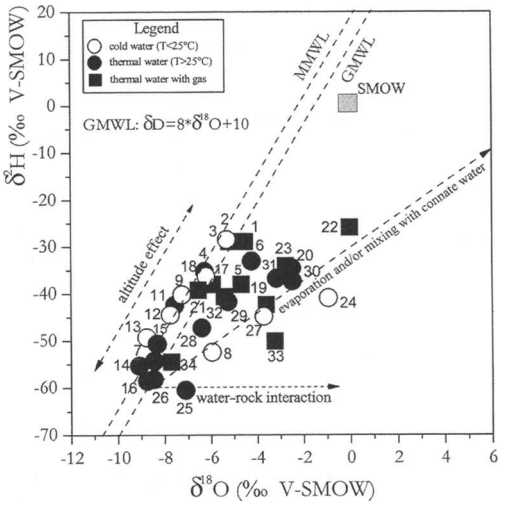

Fig. 5. $\delta^{18}O$ v. δD binary diagram for water samples from Morocco. GMWL, Global Meteoric Water Line; MMWL, Mediterranean Meteoric Water Line.

Table 2. *Chemical composition, $\delta^{13}C$ in CO_2 (PDB) and R/R_a values of the gas samples from Morocco*

Sample	Location	CO_2	H_2S	N_2	Ar	O_2	CH_4	Ne	He	H_2	C_2H_6	C_3H_8	i-C_4H_{10}	R/R_a	He/Ne	$^{40}Ar/^{36}Ar$	$\delta^{13}C$
1	Moulay Yacoub de Bab Tiouka	18.521	<0.001	38.861	0.677	0.057	39.89	0.00051	0.3582	0.0002	0.72095	0.32471	0.00023	1.558	703	296	n.d.
2	Moulay Yacoub Hamma	0.846	<0.001	97.262	1.501	0.104	0.2463	0.0012	0.0371	0.0011	0.00121	0.00008	0.00003	n.d.	31	n.d.	n.d.
5	Moulay Yacoub	0.553	0.125	1.590	0.038	0.003	97.10	0.00003	0.0132	0.0061	0.51830	0.05660	0.00015	1.253	443	294	n.d.
15	Rich	0.987	<0.001	92.957	2.066	3.724	0.2463	0.00128	0.0182	0.0005	0.00097	0.00005	0.00002	0.453	14	336	n.d.
17	Oulmès	98.629	<0.001	0.8774	0.021	0.256	0.0320	0.00001	0.1854	<0.0001	<0.00001	<0.00001	<0.00001	3.864	18570	298	−4.25
19	Hayra Safra	20.840	<0.001	71.226	1.656	6.121	0.1550	0.0012	<0.0001	<0.0001	<0.00001	<0.00001	<0.00001	0.311	299	348	−19.30
21	Al Hamra	93.665	<0.001	6.183	0.092	0.039	0.0009	0.00006	0.0195	0.0004	<0.00001	<0.00001	<0.00001	0.203	325	506	−12.60
22	Haddou ou Amar	23.617	<0.001	75.210	0.725	0.292	0.0059	0.00053	0.1445	0.0058	<0.00001	<0.00001	<0.00001	0.507	273	321	−9.09
23	Chifa	55.515	<0.001	42.520	0.655	1.253	0.0015	0.00051	0.0557	<0.0001	<0.00001	<0.00001	<0.00001	0.224	109	298	−11.19
32	Tassamounte	97.538	<0.001	1.8747	0.046	0.517	0.0051	0.00003	0.0157	0.0035	<0.00001	<0.00001	<0.00001	1.737	523	296	−5.03
33	Lalla Mimouna	97.319	<0.001	1.541	0.035	0.502	0.0018	0.00003	0.6009	0.0015	<0.00001	<0.00001	<0.00001	2.822	20127	301	−4.90

Gas contents are in μmol mol^{-1}. $^3He/^4He$ ratio is expressed as R/R_a where R is the $^3He/^4He$ ratio in the sample and Ra is that of the air (1.39×10^{-6}) (Mamyrin & Tolstikhin 1984). n.d., not determined.

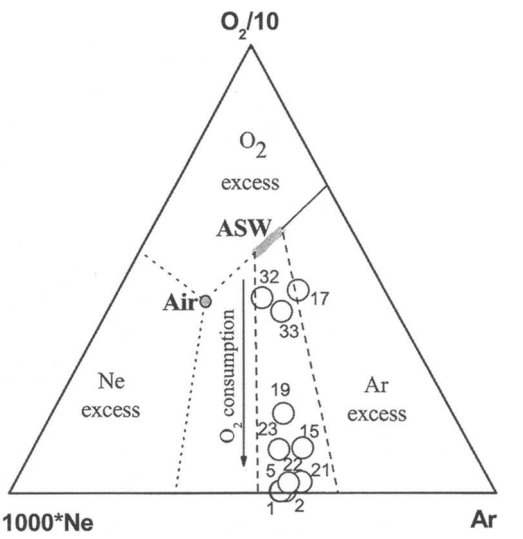

Fig. 6. Ar–O_2/10–Ne × 1000 ternary diagram for gas samples from Morocco. Air and air-saturated water (ASW) compositions are reported.

The $N_2/100 \times He-10-Ar$ diagram (Fig. 7), in which the compositions of potential sources of gases deriving from air, ASW, crust and mantle (Giggenbach *et al.* 1983) are reported, shows that N_2/Ar ratios (between 41 and 104) are slightly above those of ASW, suggesting a limited but detectable N_2 input from non-atmospheric sources. Moreover, many gas samples are enriched in He with respect to air and ASW, because of the addition of radiogenic ^4He from the crust (Xu *et al.* 1997). Concerning the organic gas fraction, the C_2-C_6 hydrocarbon gas compounds are generally below the analytical detection limit (0.00001 vol. %; Table 2), with the exception of the CO_2-poor gases of the Rif and the High Atlas domains (samples 1, 2, 5 and 15). The latter have significant amounts of ethane, propane and iso-butane (up to 0.721, 0.324 and 0.00023 vol. %, respectively). Such a distribution of hydrocarbon compounds is commonly found to originate from bacterial activity at low temperature (e.g. Capaccioni *et al.* 1993; Mango 2000), although the relatively low values of the $CH_4/(C_2H_6 + C_3H_8)$ ratio (ranging between 38 and 240) seem to suggest some contribution of thermogenic organic gas species produced in a hydrothermal environment (Whiticar 1990; Darling 1998).

Isotopic composition of gases

The $\delta^{13}C-CO_2$ values of the three mixed CO_2-N_2 (samples 19, 22 and 23) and the Al Hamra

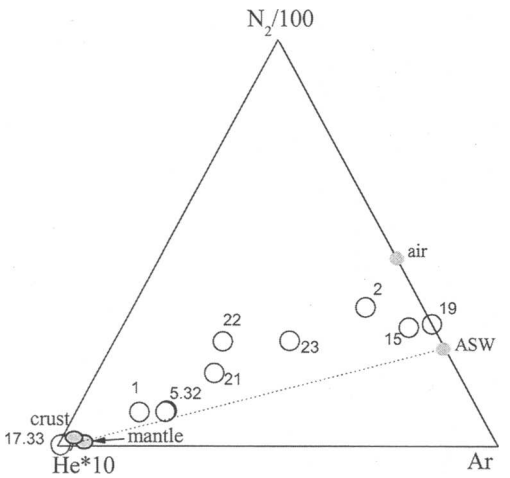

Fig. 7. Ar–N_2/100–He × 10 ternary diagram for gas samples from Morocco. Air and air-saturated water (ASW) compositions are reported. Crust and mantle fields are also reported (Giggenbach *et al.* 1983).

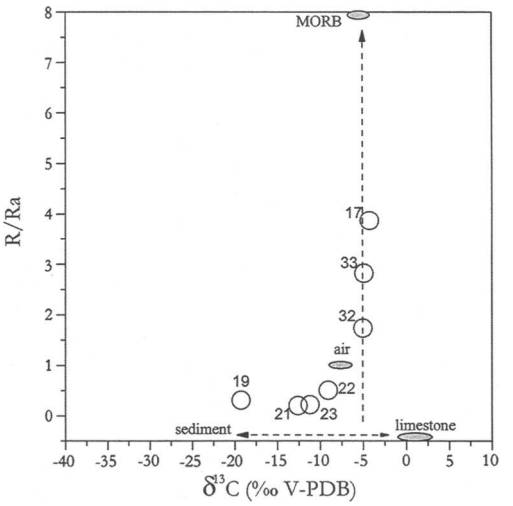

Fig. 8. R/R_a v. $\delta^{13}C$ binary diagram for gas samples from Morocco.

CO_2-dominated (sample 21) gases vary between −9.1 and −19.3‰ (V-PDB), the ^{12}C enrichment probably being related to the degradation of organic matter (soil-CO_2) (Talma & Netterberg 1983; Cerling 1984, 1991; Salomons & Mook 1986; Reyes *et al.* 1998). It is noteworthy that the relatively low $\delta^{13}C$ value of sample 19 (−19.3‰) can be ascribed to the fact that this gas was extracted *in situ* from the liquid phase by using a tested stripping method. This procedure would cause a carbon fractionation during sampling (Tassi *et al.* 2004).

The $^3He/^4He$ ratios of these samples range from 0.2 to 0.5 R/R_a, indicating a certain, but small (between 2.5 and 6%), contribution of mantle-derived ^3He (Marty *et al.* 1992), whereas the $^{40}Ar/^{36}Ar$ ratios are similar to that of air (298). In contrast, the high $^{40}Ar/^{36}Ar$ ratio (up to 506) measured in Al Hamra gas sample (sample 21) indicates a significant enrichment in crustal ^{40}Ar. Thus, the underground circulation of the fluids feeding these discharges seems to be mainly limited to relatively shallow systems, as is also supported by the low outlet temperatures (below 29 °C; Table 1).

The Oulmès, Lalla Mimouna and Tassamounte CO_2-rich gases (samples 17, 32 and 33) are characterized by higher $\delta^{13}C$ (between −4.2 and −5.0‰) and fall in the typical range of mantle-sourced CO_2 (e.g. Hoefs 1973; Rollinson 1993). This is consistent with the R/R_a values (1.74 and 3.86), which indicate a significant (up to 48%) contribution of mantle ^3He (Fig. 8). On the other hand, Ar seems to be completely atmospheric ($^{40}Ar/^{36}Ar$ ratios for samples 17 and 32 are 298 and 301, respectively). On this basis, the thermal springs discharging the CO_2-rich gases are intimately related to the deep-seated systems, and are affected by the shallow environment only to a very limited extent.

The $^3He/^4He$ ratio of the CH_4-rich gases (1.25 and 1.56 R/R_a for samples 1 and 5, respectively; Table 2) suggests a lower ^3He mantle contribution, although it is relevant when compared with that of the CO_2-rich gases. This finding is apparently in contrast to the compositional features of these gases, whose high CH_4 and N_2 contents (up to 97.0 and 38.9 vol. %, respectively; Table 2) must be referred to a shallow source. This anomalous feature can be explained by considering the $CO_2/^3He$ ratio, which can be regarded as a useful tracer to estimate the possible sources of the collected fluids. The low $CO_2/^3He$ ratios of both the CO_2-rich and the CH_4-rich samples (10^7–10^8), even lower than those found in mid-ocean ridge basalt (MORB)-related gases (10^9), can only be produced by a mixing between a deep (mantle) and a shallow CO_2-poor gas component, a process that is not able to significantly affect the $CO_2/^3He$ ratio.

Geothermometry

The distribution of heat flow in northern and central Morocco was evaluated by bottom-hole thermal gradient profiles carried out in a large number of deep oil exploration wells (e.g. Rimi & Lucazeau 1987; Rimi 1999; Zarhoule 1999; Zarhoule *et al.* 2001).

The thermal profiles show a general increase of heat flow rate from south to north. The Anti-Atlas shows the lowest subsurface temperatures (the

geothermal gradient is about 14 °C km^{-1}), similar to that of the West African shield (Brigaud *et al.* 1985), whereas the Moroccan Meseta and the High Atlas are characterized by temperature–depth profiles typical of normal continental crust (about 30 °C km^{-1}). Conversely, the Rif, the Middle Atlas and the Oran Meseta, located between the High Atlas and the Alboran Sea, have the highest heat flow (Fig. 1). In these areas the geothermal gradient ranges from 40 to 62 °C km^{-1}, possibly in relation to the presence of extensive Pliocene–Quaternary basaltic volcanism (Carte Géologique du Maroc 1985; Hernandez & Bellon 1985; Hernandez *et al.* 1987; Rachdi 1995).

The more interesting zone of Morocco for geothermal investigation seems to be located in its NE sector (Cermak 1982). The relatively high number of thermal discharges is probably caused by the higher thermal gradient, to which more than 100 thermal springs in the Rif region (Benmakhlouf 2001; Winckel 2002; Winckel *et al.* 2002) are coupled.

The analytical data for the fluid discharges presented in this study may be used to acquire further insights into the temperature path with depth that may be expected in Morocco. Concerning the evaluation of deep temperature by some of the most common geothermometers, such as Na–K (Fournier 1979), Na–K–Ca (Fournier & Truesdell 1973) and Na–Li (Fouillac & Michard 1981), it should be noted that, in most cases, these techniques cannot be reliable. As previously mentioned, water samples belonging to group III (high-saline Na–Cl) appear to be strongly affected by dilution with shallow aquifers waters, the latter being characterized by a Ca–HCO_3 (group I) composition. On the other hand, Ca(Na)–HCO_3 and Ca–SO_4 thermal waters are generally too immature for the application of these geothermometric techniques.

Both aspects can be observed in the K/10–Na/1000–$Mg^{1/2}$ ternary diagram of Figure 9 (Giggenbach 1988) where most samples group close the 'low-temperature' Mg corner, or in the partial equilibrium–dilution sector. Furthermore, chalcedony and quartz geothermometers (Arnosson *et al.* 1983) give low equilibrium temperatures (<100 °C), often below the outlet temperatures, for most Moroccan thermal waters (data for SiO_2 contents are from Cidu & Bahaj (1998, 2000) and Mimi *et al.* 1998), as a result of silica precipitation during fluid rise and/or dilution with shallow aquifers. The only exception is represented by sample 17 (Oulmès), which has 153 mg l^{-1} of SiO_2, corresponding to an equilibrium temperature (chalcedony geothermometer) of about 135 °C, whereas Na–K and Na–K–Ca geothermometers produce unusually high temperatures (>150 °C).

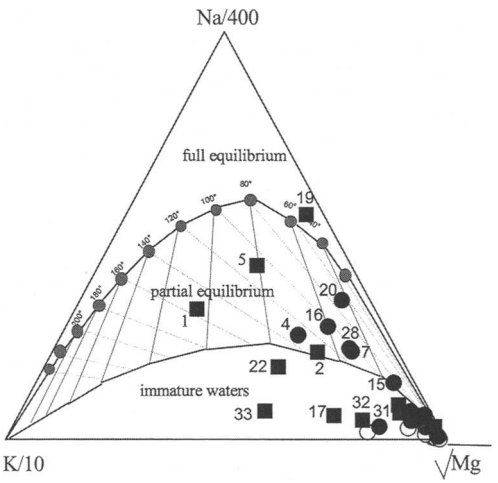

Fig. 9. $Mg^{1/2}$–Na/400–K/10 ternary diagram for water samples from Morocco.

Similarly to what is observed for the application of liquid-phase geothermometers, gas-based geothermometry does not produce satisfactory deep temperatures. The addition of biogenic CH_4 and/or of dissolved atmospheric phases (i.e. N_2, Ar and Ne) to the thermal paths at shallow depth in the crust jeopardizes any geothermometric calculation of the Moroccan gases. These secondary processes can produce gas compositions that lead to the estimation of unrealistic low equilibration temperatures (Giggenbach 1991).

For the CO_2-rich gases of Lalla Mimouna and Tassamounte, which are less diluted by organic and atmospheric components (Ar and CH_4 are <0.05 and <0.005 vol. %, respectively), the application of gas geothermometry techniques seems to be more reliable. One of the most suitable gas geothermometers for the assessment of equilibrium temperatures in hydrothermal reservoirs is that based on the H_2/Ar ratio (Giggenbach 1991). By assuming that (1) the redox conditions are controlled by a generic FeO–$FeO_{1.5}$ rock buffer system ('GT' system; Giggenbach 1987, 1993), regarded as the most appropriate one for <300 °C hydrothermal fluids, and (2) Ar is constrained by air saturation in a saline brine (Chiodini *et al.* 2001), the H_2/Ar geothermometer provides equilibrium temperatures in the range of 120–130 °C, consistent with that calculated for the Oulmès sample (number 17) by liquid-phase geothermometry.

Conclusions

Similarly to many countries located along the suture zone of the former Tethys Ocean (Italy, Greece,

Turkey, etc.), Morocco has a very complex circulation of fluids at depth. Meteoric-sourced waters are driven by rugged topography from high towards lower lands and mix with counter-flow thermal waters and associated gas phase rising along the main fault systems.

Thermal springs of Morocco show large compositional and isotopic differences, ranging from typical groundwater and running water (group I) to more saline Ca(Na)–HCO_3 (group II), Na–Cl (group III) and Ca–SO_4 (group IV) waters. These chemical features are mainly produced by water–rock interaction and rock dissolution processes, which mainly affect the Triassic evaporitic formations that are rich in high-soluble NaCl and $MgCl_2$ salts (Salvan 1974). Thermal waters in the Oujda area have a Ca–SO_4 composition, indicating that gypsum is the main evaporitic phase.

As shown in Figure 1, thermal discharges are clearly aligned along, or located close to, the main regional tectonic structures and active faults, allowing the rapid rise of the hot fluids circulating at depth. Helium isotopic ratios suggest that a significant mantle contribution occurs not only at the thermal discharges of the Moroccan Meseta and the Anti-Atlas domains, marked by a CO_2-rich deep-sourced gas phase (samples 17, 32 and 33), but also at two springs (samples 1 and 5) emerging along the Rif thrust front (Fig. 1), associated with a $CH_4(N_2)$-rich gas phase that is clearly produced in a shallow environment. High contents of CH_4–N_2 coupled with the presence of significant amounts of mantle ^3He are typical of gases discharging in active transpressive structures, such as the San Andreas fault (Kennedy *et al.* 1997), without the presence of shallow active hydrothermal systems. In the Meknes area two main fault systems intersect: (1) the active east–west-trending thrusts of the Rides Prérifaines (Moratti *et al.* 2003; Piccardi

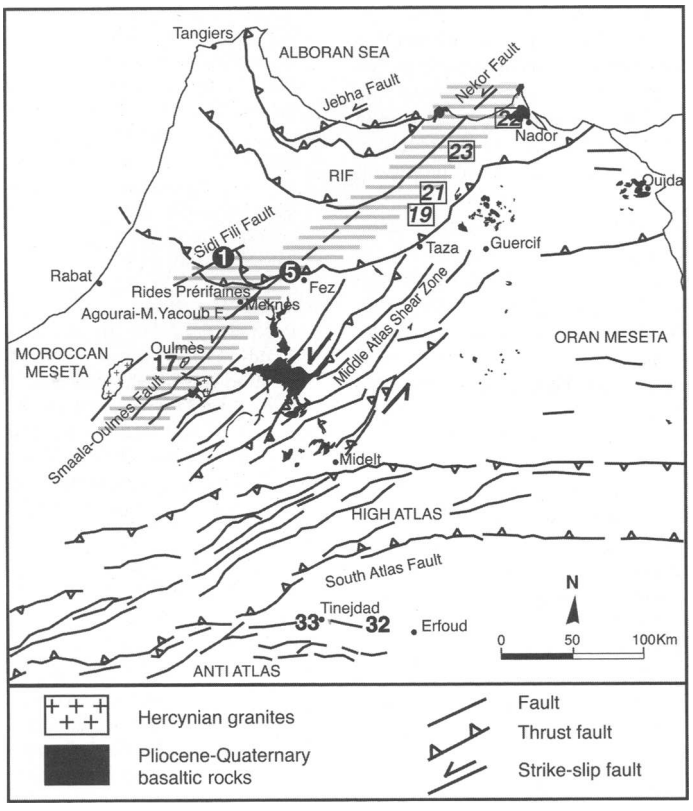

Fig. 10. Schematic structural map of Morocco indicating the NE–SW-trending continuous active crustal structure developing from Oulmès to the Mediterranean coast (shaded with grey lines). Bold black numbers refer to samples located in the Moroccan Meseta and Anti-Atlas, characterized by high helium isotopic ratios and a CO_2-rich deep-sourced gas phase. White numbers in black circles refer to samples located along the Rides Prérifaines, characterized by significant mantle ^3He associated with $CH_4(N_2)$-rich gases. Numbers in squares refer to gas samples located in the Rif along the Nekor fault, characterized by a small mantle signature of helium isotopes.

et al. 2004) and (2) the NE–SW-trending mainly sinistral transpressive structures represented in outcrop by the Sidi Fili fault and the Agourai-Moulay Yacoub fault, along which Triassic evaporites crop out (Fig. 10). This surface pattern, together with the presence of many thermal sources and active travertine deposits, argues for a connection at depth between the NE–SW-trending fault system and the east–west-trending active thrusts of the Rides Prérifaines, and may account for the distribution of ^{3}He anomalies over a wide area along the frontal thrust of the Rif in the Meknes area (Fig. 10). The contemporary presence of ^{3}He anomalies and minor outcrops of active basaltic volcanism at Oulmès, in the Moroccan Meseta Domain and at Lalla Mimouna and Tassamounte, in the Anti-Atlas Domain, could be explained by mantle-related magmas residing in the crust. The 'magmatic' carbon isotopic signature of these CO_2-rich discharges, together with ^{3}He anomalies, clearly indicates that CO_2, probably from mantle degassing or deep hydrothermal systems, is able to rise through deep faults (Fig. 10).

The only other area where the mantle signature of helium isotopes, although small, is detectable in the thermal discharges is the eastern Rif Domain, between Nador and Taza (samples 19, 21, 22 and 23, labelled in Fig. 10), related to the main tectonic structures of Nekor and the eastern termination of the Rif thrust front.

In conclusion, the geochemical and isotopic data indicate a contribution for a mantle source along a NE–SW direction, corresponding to major surface transpressive structures (Nekor fault, Sidi Fili fault, Agourai–Moulay Yacoub fault system, Smaala–Oulmès fault system, Fig. 10), which may point to the presence of an active continuous crustal structure at depth.

Research carried out in the framework of the joint project 'Structural analysis, active tectonics and fluids geochemistry in the Rif–Middle Atlas–High Atlas System of Morocco' (Italian Scientific Responsible: G. Moratti; Moroccan Scientific Responsible: A. Bendkik) funded by the bilateral agreement between CNR (Italy) and CNRST (Morocco). We wish to express our thanks to R. Cidu and A. Michard for their useful suggestions and comments, which contributed to improve the manuscript.

References

ARNOSSON, S., GUNNLAUGSSON, E. & SVAVARSSON, H. 1983. The elements of geothermal waters in Iceland. III. Chemical geothermometry in geothermal investigations. *Geochimica et Cosmochimica Acta*, **47**, 567–577.

BARNES, I., EVANS, W. C. & WHITE, L. D. 1978. *Global distribution of CO_2 and major zone of seismicity*. US Geological Survey Open-File Report, **78–39**.

BAUDIN, T., CHÈVREMONT, P., RAZIN, P., *ET AL.* 2001*a*. *Carte Géologique du Maroc au 1/50 000, Feuille d'Oulmès, Mémoire explicatif*. Notes et Mémoires du Service Géologique du Maroc, **410bis**.

BAUDIN, T., ROGER, J., CHÈVREMONT, P., *ET AL.* 2001*b*. *Carte Géologique du Maroc (1/50 000), Feuille Oulmès*. Notes et Mémoires du Service Géologique du Maroc, **410**.

BENCINI, A. 1985. Applicabilità del metodo dell'Azometina-H alla determinazione del Boro nelle acque naturali. *Rendiconti della Società Italiana di Mineralogia e Petrologia*, **40**, 311–316.

BENDKIK, A. 2004. *Carte Géologique du Maroc, Sidi Kacem, Echelle 1/50 000*. Notes et Mémoires du Service Géologique du Maroc, **431**.

BENMAKHLOUF, M. 2001. *Les sources thermales du Maroc septentrional: relation entre la tectonique et le thermalisme*. PhD thesis, Université Mohammed V, Rabat.

BERNINI, M., BOCCALETTI, M., EL MOKHTARI, J., GELATI, R., MORATTI, G. & PAPANI, G. 1996. *Neogene sedimentary and tectonic evolution of the Taza–Guercif Basin. Its significance in the Rif–Middle Atlas orogenic system*. Notes et Mémoires du Service Géologique du Maroc, **387**, 85–96.

BERNINI, M., BOCCALETTI, M., GELATI, R., MORATTI, G., PAPANI, G. & EL MOKHTARI, J. 1999. Tectonics and sedimentation in the Taza–Guercif Basin, northern Morocco: implications for the Neogene evolution of the Rif–Middle Atlas orogenic system. *Journal of Petroleum Geology*, **22**, 114–128.

BERNINI, M., BOCCALETTI, M., MORATTI, G. & PAPANI, G. 2000. Structural development of the Taza–Guercif Basin as a constraint for the Middle Atlas Shear Zone tectonic evolution. *Marine and Petroleum Geology*, **17**(3), 391–408.

BOCCALETTI, M., GELATI, R., PAPANI, G., BERNINI, M., EL MOKHTARI, J. & MORATTI, G. 1990. The Gibraltar Arc: an example of neoalpine arcuate deformation connected with ensialic shear zones. *Memorie della Società Geologica Italiana*, **45**, 409–423.

BRIGAUD, F., LUCAZEAU, F., LY, S. & SAUVAGE, J. F. 1985. Heat flow from the West African shields. *Geophysical Research Letters*, **12**(9), 549–552.

CALVERT, A., GOMEZ, F., SEBER, D., BARAZANGI, M., JABOUR, N., IBENBRAHIM, A. & DEMNATI, A. 1997. An integrated geophysical investigation of recent seismicity in the Al-Hoceima region of north Morocco. *Bulletin of the Seismological Society of America*, **87**(3), 637–651.

CAPACCIONI, B., MARTINI, M., MANGANI, F., GIANNINI, G., NAPPI, G. & PRATI, F. 1993. Light hydrocarbons in gas-emissions from volcanic areas and geothermal fields. *Geochemical Journal*, **27**, 7–17.

CARTE GÉOLOGIQUE DU MAROC 1975. *Carte Géologique du Maroc, Echelle 1/200 000 'Jbel*

Saghro–Dadès'. Notes et Mémoires du Service Géologique du Maroc, **161**.

CARTE GÉOLOGIQUE DU MAROC 1985. *Carte Géologique du Maroc, Echelle 1/1.000.000*. Publication du Service Géologique du Maroc, **260**.

CARTE GÉOLOGIQUE DU MAROC 1988. *Carte Géologique du Maroc, Echelle 1/200 000 'Todrha–Ma'der'*. Notes et Mémoires du Service Géologique du Maroc, **243**.

CARTE GÉOLOGIQUE DU MAROC 1991. *Carte Géologique du Maroc, Echelle 1/100 000 'Ain Bni Mathar'*. Notes et Mémoires du Service Géologique du Maroc, **361**.

CERLING, T. E. 1984. The stable isotopic composition of modern soil carbonate and its relationship to climate. *Earth and Planetary Science Letters*, **71**, 229–240.

CERLING, T. E. 1991. Carbon dioxide in the atmosphere: evidence from Cenozoic and Mesozoic paleosoils. *American Journal of Science*, **291**, 377–400.

CERMAK, V. 1982. Crustal temperature and mantle heat flow in Europe. *Tectonophysics*, **83**, 123–142.

CHALOUAN, A., MICHARD, A., FEINBERG, H., MONTIGNY, R. & SADDIQI, O. 2001. The Rif mountain building (Morocco): a new tectonic scenario. *Bulletin de la Société Géologique de France*, **172**(5), 603–616.

CHENAKEB, M. 2004. *Carte Géologique du Maroc, Beni Ammar, Echelle 1/50 000*. Notes et Mémoires du Service Géologique du Maroc, **428**.

CHIODINI, G., MARINI, L. & RUSSO, M. 2001. Geochemical evidence for the existence of high-temperature hydrothermal brines at Vesuvio Volcano, Italy. *Geochimica et Cosmochimica Acta*, **65**, 2129–2147.

CHOUBERT, G. 1963. *Histoire géologique du Précambrien de l'Anti-Atlas. Tome 1*. Notes et Mémoires du Service Géologique du Maroc, **162**.

CHOUBERT, G. & FAURE-MURET, A. 1960–1962. *Evolution du domaine atlasique marocain depuis les temps paléozoïques. Livre à la Mémoire de P. Fallot, Société Géologique de France, Mémoire hors-série*, **1**, 447–527.

CIDU, R. & BAHAJ, S. 1998. Geochemistry of thermal waters from northern Morocco: preliminary results. *Mines, Géologie et Energie*, **57**, 203–212.

CIDU, R. & BAHAJ, S. 2000. Geochemistry of thermal waters from Morocco. *Geothermics*, **29**, 407–430.

COLEMAN, M. L., SHEPHERD, T. J., ROUSE, J. E. & MOORE, G. R. 1982. Reduction of water with zinc for hydrogen isotope analysis. *Analytical Chemistry*, **54**, 993–995.

CRAIG, H. 1961. Isotopic variations in meteoric water. *Science*, **133**, 1702–1703.

DARLING, W. G. 1998. Hydrothermal hydrocarbon gases: 1, Genesis and geothermometry. *Applied Geochemistry*, **13**, 815–824.

DREVER, J. 1997. *The Geochemistry of Natural Waters. Surface and Groudwater Environment*. Prentice–Hall, Upper Saddle River, NJ.

DU DRESNAY, R. 1988. Recent data on the geology of the Middle Atlas (Morocco). *In*: JACOBSHAGEN, V. H. (ed.) *The Atlas System of Morocco*. Springer, Berlin, 293–320.

DUTOUR, A. & FERRANDINI, J. 1985. Nouvelles observations néotectoniques dans le Haut Atlas de Marrakech et le Haouz central (Maroc). Apports sur l'évolution récente d'un segment du bâti atlasique. *Revue de Géologie Dynamique et Géographie Physique*, **26**(5), 285–297.

EPSTEIN, S. & MAYEDA, T. K. 1953. Variation of the $^{18}O/^{16}O$ ratio in natural waters. *Geochimica et Cosmochimica Acta*, **4**, 213–224.

EVANS, W. C., WHITE, L. D. & RAPP, J. B. 1998. Geochemistry of some gases in hydrothermal fluids from the southern Juan de Fuca ridge. *Journal of Geophysical Research*, **15**, 305–313.

FEDAN, B., LAVILLE, E. & EL MEZGUELDI, A. 1989. Le bassin jurassique du Moyen Atlas (Maroc): exemple de bassin sur relais de décrochements. *Bulletin de la Société Géologique de France, Série VIII*, **5**, 1123–1236.

FOUILLAC, C. & MICHARD, G. 1981. Sodium/lithium ratio in water applied to the geothermometry of geothermal reservoirs. *Geothermics*, **10**, 55–70.

FOURNIER, R. O. 1979. A revised equation for the Na/K geothermometer. *Geothermal Resources Council Transactions*, **3**, 221–224.

FOURNIER, R. O. & TRUESDELL, A. H. 1973. An empirical Na–K–Ca geothermometer for natural waters. *Geochimica et Cosmochimica Acta*, **37**, 1255–1275.

FROITZHEIM, N., STETS, J. & WURSTER, P. 1988. Aspects of western High Atlas tectonics. *In*: JACOBSHAGEN, V. H. (ed.) *The Atlas System of Morocco*. Springer, Berlin, 219–244.

GATT, J. R. & CARMI, I. 1970. Evolution of the isotopic composition of atmospheric waters in the Mediterranean Sea area. *Journal of Geophysical Research*, **75**, 3032–3048.

GIGGENBACH, W. F. 1987. Redox processes governing the chemistry of fumarolic gas discharges from White Island, New Zealand. *Applied Geochemistry*, **2**, 143–161.

GIGGENBACH, W. F. 1988. Geothermal solute equilibria. Derivation of Na–K–Mg–Ca geoindicators. *Geochimica et Cosmochimica Acta*, **52**, 2749–2765.

GIGGENBACH, W. F. 1991. Chemical techniques in geothermal exploration. *In*: D'AMORE, F. (ed.) *Application of Geochemistry in Geothermal Reservoir Development*. UNITAR/UNDP, Rome, 119–144.

GIGGENBACH, W. F. 1993. Redox control of gas composition in Philippine volcanic–hydrothermal systems. *Geothermics*, **22**, 575–587.

GIGGENBACH, W. F., GONFIANTINI, R., JANGI, B. L. & TRUESDELL, A. H. 1983. Isotopic and chemical composition of Parbati valley geothermal discharges, NW Himalaya. *Geothermics*, **22**, 575–587.

GOMEZ, F., BARAZANGI, M. & BENSAID, M. 1996. Active tectonism in the intracontinental Middle Atlas Mountains of Morocco: synchronous crustal shortening and extension. *Journal of the Geological Society, London*, **153**, 389–402.

HATZFELD, D. & FROGNEUX, M. 1981. Intermediate depth seismicity in the western Mediterranean

unrelated to subduction of oceanic lithosphere. *Nature*, **292**, 443–445.

HATZFELD, D., CAILLOT, V., CHERKAOUI, T. E., JEBLI, H. & MEDINA, F. 1993. Microearthquake seismicity and fault plane solutions around the Nékor strike-slip fault, Morocco. *Earth and Planetary Science Letters*, **120**, 31–41.

HERNANDEZ, J. & BELLON, H. 1985. Chronologie K–Ar du volcanisme miocène du Rif oriental (Maroc): implications tectoniques et magmatologiques. *Revue de Géologie Dynamique et Géographie Physique*, **26**(2), 85–94.

HERNANDEZ, J., DE LAROUZIÈRE, F. D., BOLZE, J. & BORDET, P. 1987. Le magmatisme néogène bético-rifain et le couloir de décrochement trans-Alboran. *Bulletin de la Société Géologique de France, Série. VIII*, **3**, 257–267.

HOEFS, J. 1973. *Stable Isotope Geochemistry*. Springer, Berlin.

JACOBSHAGEN, V. H., GORLER, K. & GIESE, P. 1988. Geodynamic evolution of the Atlas System (Morocco). *In*: JACOBSHAGEN, V. H. (ed.) *The Atlas System of Morocco*. Springer, Berlin, 481–499.

KENNEDY, B. M., KHARAKA, Y. K., EVANS, W. C., *ET AL.* 1997. Mantle fluids in the San Andreas fault system, California. *Science*, **278**, 1278–1281.

LANGELIER, W. F. & LUDWIG, H. F. 1942. Graphical method for indicating the mineral character of natural waters. *Journal of the American Waterworks Association*, **34**, 335–352.

LAVILLE, E. & PIQUÉ, A. 1991. La distension crustale atlantique et atlasique au Maroc au début du Mésozoïque: le rejeu des structures hercyniennes. *Bulletin de la Société Géologique de France*, **162**, 1161–1171.

LEBLANC, D. & OLIVIER, P. 1984. Role of strike-slip faults in the Betic–Rifean orogeny. *Tectonophysics*, **101**, 345–355.

MAMYRIN, B. A. & TOLSTIKHIN, I. N. 1984. *Helium Isotopes in Nature*. Elsevier, Amsterdam.

MANGO, F. D. 2000. The origin of light hydrocarbons. *Geochimica et Cosmochimica Acta*, **64**, 1265–1277.

MARTY, B., O'NIONS, R. K., OXBURGH, E. R., MARTEL, D. & LOMBARDI, S. 1992. Helium isotopes in Alpine region. *Tectonophysics*, **206**, 71–78.

MATTAUER, M., TAPPONNIER, P. & PROUST, F. 1977. Sur les mécanismes de formation des chaînes intracontinentales. L'exemple des chaînes atlasiques du Maroc. *Bulletin de la Société Géologique de France, Série VII*, **19**, 521–526.

MAURY, R. C., FOURCADEB, S., COULONC, C., *ET AL.* 2000. Post-collisional Neogene magmatism of the Mediterranean Maghreb margin: a consequence of slab breakoff. *Comptes Rendus de l'Académie des Sciences, Série IIA*, **331**(3), 159–173.

MEDINA, F. 1995. Present-day state of stress in northern Morocco from focal mechanism analysis. *Journal of Structural Geology*, **17**(7), 1035–1046.

MEDINA, F. & CHERKAOUI, T. E. 1992. Mécanismes au foyer des séismes du Maroc et des régions voisines (1959–1986). Conséquences tectoniques. *Eclogae Geologicae Helvetiae*, **85**(2), 433–457.

MEGHRAOUI, M., MOREL, J.-L., ANDRIEUX, J. & DAHMANI, M. 1996. Tectonique plio-quaternaire de la chaîne tello-rifaine et de la mer d'Alboran. Une zone complexe de convergence continent–continent. *Bulletin de la Société Géologique de France*, **167**(1), 141–157.

MICHARD, A. 1976. *Elements de Géologie Marocaine*. Notes et Mémoires du Service Géologique du Maroc, **252**.

MIMI, A. L., BEN DHIA, A., BOURI, S., LAHRACH, A., BEN ABITATE, L. & BOUCHAREB-HAOUCHIM, F. Z. 1998. Application of chemical geothermometer to thermal springs of the Maghreb, North Africa. *Geothermics*, **27**, 211–233.

MINISSALE, A. 2004. Origin, transport and discharge of CO_2 in central Italy. *Earth-Science Reviews*, **66**, 89–141.

MONTEGROSSI, G., TASSI, F., VASELLI, O., BUCCIANTI, A. & GAROFALO, K. 2001. Sulfur species in volcanic gases. *Analytical Chemistry*, **73**, 3709–3715.

MORATTI, G., PICCARDI, L., VANNUCCI, G., BELARDINELLI, M. E., DAHMANI, M., BENDKIK, A. & CHENAKEB, M. 2003. The 1755 'Meknes' Earthquake (Morocco): field data and geodynamic implications. *Journal of Geodynamics*, **36**(1–2), 305–322.

OLIVER, J. 1986. Fluids expelled tectonically from orogenic belts: their role in hydrocarbon migration and other geological phenomena. *Geology*, **14**, 99–102.

OLIVER, J. 1992. The spots and stains of plate tectonics. *Earth-Science Reviews*, **32**, 77–106.

OLIVIER, P. 1981–1982. L'accident de Jebha-Chrafate (Rif, Maroc). *Revue de Géologie Dynamique et Géographie Physique*, **23**(2), 97–106.

PICCARDI, L., MORATTI, G., DAHMANI, M., BENDKIK, A. & CHENAKEB, M. 2001. Neotectonic evolution and seismotectonics in the Rif–Atlas system (Morocco): preliminary data. *Programmes with Abstracts Volume of the GSA–GSL Global Meeting 'Earth System Processes', Edinburgh, Scotland, 24–28 June 2001*, 51.

PICCARDI, L., MORATTI, G., VANNUCCI, G., BENDKIK, A. & CHENAKEB, M. 2004. Seismotectonics of the 1755 Meknes Earthquake (Morocco). *Studi Geologici Camerti, Special Issue*, 123–127.

PIQUÉ, A. 2001. *Geology of Northwest Africa*. Borntraeger, Stuttgart.

PIQUÉ, A., DAHMANI, M., JEANNETTE, D. & BAHI, L. 1987. Permanence of structural lines in Morocco from Precambrian to Present. *Journal of African Earth Sciences*, **6**(3), 247–256.

RACHDI, H. 1995. *Etude du volcanisme plio-quaternaire du Maroc central: pétrographie, géochimie et minéralogie. Comparaison avec des laves types du Moyen Atlas et du Rekkam*. Notes et Mémoires du Service Géologique du Maroc, **381**.

REYES, E., PEREZ DEL VILLAR, L., DELGADO, A., CORTEZZI, G., NÚÑEZ, R., PELAYO, M. & COZAR,

J. S. 1998. Carbonation processes at the El Berrocal natural analogue granitic system (Spain): inferences from mineralogical and stable isotope studies. *Chemical Geology*, **150**, 293–315.

RIMI, A. 1999. Mantle heat flow and geotherms for the main geologic domains in Morocco. *International Journal of Earth Sciences*, **88**, 458–466.

RIMI, A. & LUCAZEAU, F. 1987. Heat flow density measurement in northern Morocco. *Journal of African Earth Sciences*, **6**(6), 835–843.

ROLLINSON, H. 1993. *Using Geochemical Data*. Longman, Harlow.

SALOMONS, W. & MOOK, W. G. 1986. Isotope geochemistry of carbonate in the weathering zone. *In*: FRITZ, P. & FONTES, J. C. (ed.) *Handbook of Environmental Isotope Geochemistry 2, The Terrestrial Environment*. Elsevier, Amsterdam, 239–268.

SALVAN, H. M. 1974. Les séries salifères triasiques du Maroc. Comparaison avec les séries homologues d'Algérie et de Tunisie. Nouvelles possibilités d'interprétation. *Notes du Service Géologique du Maroc*, **35**(225), 7–25.

SUTER, G. 1980*a*. *Carte géologique de la Chaîne Rifaine, échelle 1:500.000*. Notes et Mémoires du Service Géologique du Maroc, **245a**.

SUTER, G. 1980*b*. *Carte structurale du Maroc, échelle 1:500.000*. Notes et Mémoires du Service Géologique du Maroc, **245b**.

SVERJENSKY, G. H. & GARVEN, G. 1992. Tracing great fluid migrations. *Nature*, **365**, 481–482.

TALMA, A. S. & NETTERBERG, F. 1983. Stable isotope abundances in calcretes. *In*: WILSON, D. (ed.) *Residual Deposits: Surface Related Weathering Processes and Materials*. Blackwell, Oxford, 221–233.

TASSI, F., MONTEGROSSI, G. & VASELLI, O. 2004. *Metodologie di campionamento ed analisi di fasi gassose*. CNR-IGG, Florence, Internal Report **1/2003**.

TEJERA DE LEON, J. 1997. Signification de la limite Jebha–Arbaoua (Maroc nord-occidental): une rampe latérale au-dessus d'une discontinuité crustale héritée de la période de 'rifting'. *Journal of African Earth Sciences*, **24**(4), 455–472.

VASELLI, O., MINISSALE, A., TASSI, F., MAGRO, G., SEGHEDI, I., IOANE, M. & SZAKACS, A. 2002. A geochemical traverse across the Eastern Carpathians (Carpatho-Pannonian Region, Romania): constraints on the origin and evolution of the mineral water and gas discharges. *Chemical Geology*, **182**, 637–654.

WHITICAR, M. J. 1990. Hydrothermal hydrocarbon gases in the sediments of the King George Basin, Bransfield Strait, Antarctica. *Applied Geochemistry*, **5**, 135–147.

WILDI, W. 1983. La chaîne tello-rifaine (Algérie, Maroc, Tunisie): structure, stratigraphie et évolution du Trias au Miocène. *Revue de Géologie Dynamique et Géographie Physique*, **24**, 201–297.

WINCKEL, A. 2002. *Establissment d'une typologie des eaux thermals par une approche hydrochimique, isotopique et tectonique. Example du Maroc*. PhD thesis, Université. de Paris-Sud.

WINCKEL, A., MARLIN, C., DEVER, L., MOREL, J. L., MORABITI, K., MAKHLOUF, M. B. & CHALOUAN, A. 2002. Apport des isotopes stables dans l'estimation des altitudes de recharge de sources thermales du Maroc. *Comptes Rendus, Geoscience*, **334**, 469–474.

XU, S., NAKAI, S., WAKITA, H., WANG, X. & FENG, X. 1997. Effects of hydrothermal processes in the chemical and isotopic composition of mantle-derived gases in SE China. *Geothermics*, **26**, 179–192.

ZARHOULE, Y. 1999. *Potentialités géothermiques du Maroc: approche intégrée par les temperatures profondes et indices de surface*. PhD thesis, University of Science, Oujda.

ZARHOULE, Y., LAHRACHE, A., BEN ABIDATE, L., KHATTACH, D., BOURI, S., BOUKDIR, A. & BEN DHIA, H. 2001. La prospection géothermique de surface au Maroc: hydrodynamisme, anomalies géothermiques et indices de surface. *Journal of African Earth Sciences*, **32**(4), 851–867.

ZOUINE, E. M., MOREL, J. L., ANDRIEUX, J., DAHMANI, M. & FAURE-MURET, A. 1996. *Modalité et calendrier des déformations cénozoïques dans le Haut Atlas (Maroc)*. Notes et Mémoires du Service Géologique du Maroc, **387**, 11–20.

Factorial correspondence analysis: a useful tool in palaeogeographical reconstructions; example from late Cretaceous calciturbidites of the northwestern External Rif (Morocco)

KH. EL KADIRI[1], K. EL KADIRI[2], A. CHALOUAN[3], A. BAHMAD[4], F. SALHI[5], & H. LIEMLAHI[1]

[1]*Université Abdelmalek Essaadi, Faculté des Sciences, BP 2121, Dép. Géologie, M'Hannech II, 93003 Tetuan, Morocco (e-mail: khkadiri@fst.ac.ma)*

[2]*Université Abdelmalek Essaadi, Faculté des Sciences, BP 2121, Dép. Mathématiques, M'Hannech II, 93003 Tetuan, Morocco*

[3]*Université Mohammed V-Agdal, Faculté des Sciences, Av. Ibn Batouta, BP 1014, Dép. Géologie, Agdal, 10000 Rabat, Morocco*

[4]*Société Nationale d'Etudes du Détroit de Gibraltar (SNED), 31 r. Al Alaouyine, Rabat, Morocco*

[5]*Université Chouaib Doukali, Faculté des Sciences, Dép. Géologie, El Jadida, Morocco*

Abstract: Factorial correspondence analysis proved to be a useful statistical tool when comparing the clastic input of distinct deposits and searching for their source area. Here we analyse and compare the reworked carbonate clastic material in the late Cretaceous calciturbidites of the Béni Ider area (Rifian External Domain) and the Internal Dorsale Calcaire (Internal Domain). The main result is that the source area for the Béni Ider calciturbidites was a neighbouring, isolated, shallow carbonate platform, the basement of which consists of a Jurassic succession of the Internal Dorsale Calcaire type. However, statistical comparison with the coeval pelagic deposits of to the latter domain leads us to exclude the Dorsale Calcaire as a possible origin of these Béni Ider calciturbidites. The source area was probably a lost carbonate platform, which should be located in the open External Domain. This result appears to be consistent with the Tariquide Ridge hypothesis and gives new insights into the palaeogeographical scheme of the flysch trough.

Along the Internide–Externide front of the Moroccan Rif mountains, two contrasting structural domains are juxtaposed: (1) the Dorsale Calcaire, mainly composed of Jurassic–Cretaceous carbonate-dominated materials, indicating a carbonate platform bordering westwards the Internal Zones (e.g. El Kadiri 1984, 1991; Olivier 1984; El Hatimi 1991); (2) the flysch domain, which has long been considered as deriving from a flysch trough lying between the Internal Zones-related palaeomargin and the African one (e.g. Bouillin *et al.* 1970, 1986; Durand-Delga 1972, 1980; Didon *et al.* 1973; Raoult 1974; Bourgois 1978). Based on late Jurassic and earliest Cretaceous pelagic successions (radiolarites and 'complexe à Aptychus', respectively), the Mauretanian series was located on the northern side of the flysch trough, i.e. close to the Dorsale Calcaire-related carbonate platform (Didon *et al.* 1973). However, these two facies were widespread over the Tethyan Realm and the extent to which the Dorsale Calcaire could have acted as the source area for the flysch trough during early Cretaceous–Miocene times remains an unsettled issue, especially for the case of the late Cretaceous–Eocene calciturbidite successions.

It may be possible to shed new light on this broad palaeogeographical scheme through a study based on the statistical analysis of the reworked carbonate clasts in the late Cretaceous calciturbidite successions lying on both sides of the Externide–Internide front, i.e. the Dorsale Calcaire and the neighbouring Béni Ider flysch successions.

Successions studied and origin of the samples analysed

The material studied was sampled from coeval, late Cretaceous strata belonging to the principal Internal Dorsale unit (Internal Domain) and the well-developed, late Cretaceous calciturbidites of the Béni Ider flysch series (External Domain, Fig. 1). These two areas were selected because the reworked

From: MORATTI, G. & CHALOUAN, A. (eds) 2006. *Tectonics of the Western Mediterranean and North Africa.* Geological Society, London, Special Publications, **262**, 147–160.
0305-8719/06/$15.00

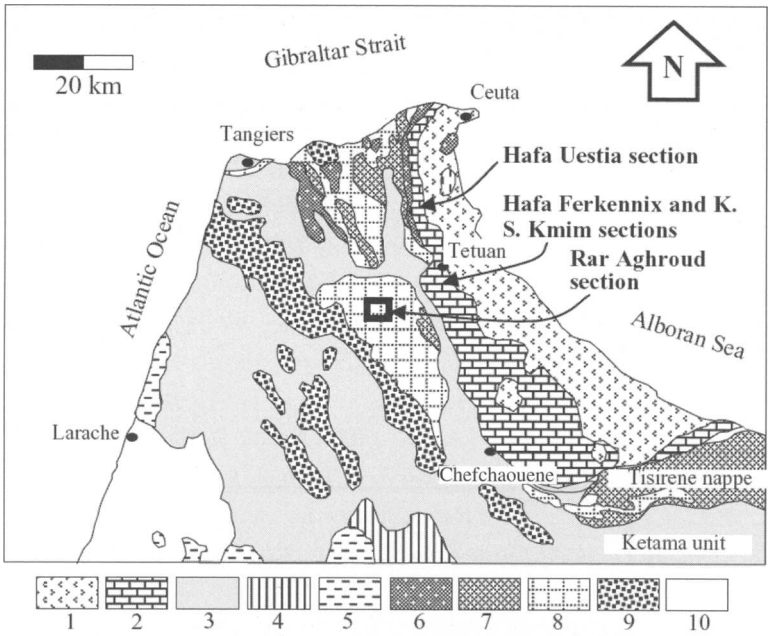

Fig. 1. A. Simplified geological map of the northwestern Rif belt and location of the studied sections. 1,2, Internal Rif Domain; 3–10, external Rif Domain. 1, Palaeozoic nappes and metamorphic units; 2, Calcareous Chain (Dorsale Calcaire, mainly Triassic and Jurassic); 3, Intrarif zone with the Tangier–Ketama parautochthonous units (late Cretaceous); 4, Mesorif zone; 5, Prerif zone; 6, Massylian sandstone flysch (mainly Albian–Aptian); 7, Tisirène sandstone flysch (mainly Albian–Aptian); 8, Béni Ider series (late Cretaceous–early Burdigalian); 9, Numidian sandstone flysch (mainly Aquitanian); 10, Post-nappe Miocene and Quaternary.

carbonate clastic material proved to be, in thin sections, of the same nature. This material strongly recalls the Liassic and Tithonian–Berriasian facies that is well known in the Hafat Ferkenich and Hafat Uestia units of the Internal Dorsale (e.g. El Kadiri *et al.* 1989). From the base upwards these facies are: dolomite breccias (of Triassic age); white, massive limestones (of earliest Hettangian–Sinemurian age); *Posidonia*-rich mudstones (the so-called 'calcaires à filaments'; Toarcian); *Saccocoma*-rich mudstones (latest Kimmeridgian–early Tithonian); *Calpionella*-rich mudstones (late Tithonian–Berriasian).

In the Hafat Ferkenich and Hafat Uestia units, coarse-grained breccias and calciturbidites transgressively rest upon a conspicuous, polyphase palaeokarst surface that developed independently on these five facies (El Kadiri *et al.* 1989, 1992), and from which they logically sourced their carbonate clastic material. However, the presence of the same clastic material also in the palaeogeographically distant Béni Ider area, in a proximal turbidite facies, remains hard to understand, especially if we consider that the large external Dorsale units lie between these areas.

The statistical analysis, presented below, was undertaken because these five facies proved to be ubiquitous in all the late Cretaceous Béni Ider turbidites we have analysed in the northwestern External Rif.

Table 1 gives the percentage values resulting from the systematic counting of the reworked lithoclasts, bioclasts and quartz grains in 76 selected samples. These values are obtained through point counting of several hundreds (300–1000) of clasts per sample. The majority of the samples come from distinct stratigraphic levels (of late Cretaceous age) throughout the Rar Aghroud section (Béni Ider area, Fig. 1). The counting also included coeval calciturbidite levels from the Oued El Kébir section (located near Rar Aghroud locality) as well as from the Internal Dorsale: the Hafat Ferkenich and Kobat Sidi Kmim sections, both located 3 km south of the city of Tetuan.

Conceptual framework and method

Two facts make the statistical assessment significant: (1) the base-of-slope gravity-flow discharges

Table 1. *Calculated percentages of different clasts from the Rar Aghroud section (samples B11–B65) and the Oued El Kébir section (samples EK11–EK25)*

Samples	SOUB	DOL	CB	CF	CALP	RAD	COR	BEN	FB	FP	SPE	QE	QF	Rcl
FS.6														
B65	0.00	12.70	45.04	2.09	2.26	0.00	0.00	2.78	0.87	0.52	0.00	0.00	33.74	25.00
B64	0.00	3.24	73.93	2.21	1.62	0.00	0.00	3.24	0.59	0.44	0.00	0.00	14.73	30.00
B63	0.00	20.31	56.48	3.24	5.12	0.00	0.00	1.19	0.00	0.00	0.00	0.00	13.65	15.00
B62	0.45	27.93	39.19	2.25	0.00	0.00	0.00	0.90	0.45	0.00	0.00	0.00	28.83	25.00
B61	0.00	32.14	36.90	1.19	0.00	0.00	0.00	0.00	0.00	0.40	0.00	0.00	29.37	20.00
FS.5														
B57	0.43	1.56	5.70	0.00	0.00	0.00	11.26	6.24	15.24	1.33	0.00	0.00	58.26	5.00
B56	0.35	1.33	2.63	0.00	0.00	0.00	6.24	3.27	23.27	0.63	0.00	0.00	62.28	5.00
B55	0.24	2.37	7.33	0.00	0.00	0.00	9.24	9.33	25.13	0.33	0.00	0.00	46.05	5.00
B54	0.30	1.21	2.33	0.00	0.00	0.00	10.24	4.96	9.11	0.61	0.00	0.00	71.24	5.00
B53	0.62	2.89	9.09	0.00	0.00	0.00	20.37	5.17	14.79	0.83	0.00	0.00	46.24	5.00
B52	0.35	3.11	16.96	0.00	0.00	0.00	3.27	4.33	17.30	1.21	0.00	0.00	53.48	5.00
B51	0.00	1.06	4.24	0.00	0.00	0.00	7.33	2.12	14.93	1.06	0.00	0.00	69.27	5.00
FS.4														
B46	0.00	0.00	10.63	0.00	0.00	0.00	0.00	12.64	2.70	70.70	0.00	9.24	0.00	2.00
B45	0.00	0.00	7.33	0.00	0.00	0.00	0.00	9.53	3.13	56.96	0.00	23.06	0.00	2.00
B44	0.00	0.00	9.27	0.00	0.00	0.00	0.00	7.96	8.40	65.92	0.00	8.46	0.00	2.00
B43	0.00	0.00	8.93	0.00	0.00	0.00	0.00	8.93	3.57	71.43	0.00	7.14	0.00	2.00
B42	0.00	0.00	9.73	0.00	0.00	0.00	0.00	10.96	6.44	49.50	0.00	23.37	0.00	2.00
B41	0.00	0.00	8.23	0.00	0.00	0.00	0.00	1.59	4.58	82.32	0.00	3.27	0.00	2.00
FS.3														
B312	0.00	0.00	87.90	0.00	0.00	0.00	3.24	3.85	1.28	1.56	0.00	2.18	0.00	5.00
B311	0.00	0.00	78.19	0.00	0.00	0.00	2.37	5.53	2.70	0.71	0.00	10.51	0.00	5.00
B310	0.00	0.00	82.41	0.00	0.00	0.00	1.24	5.52	3.35	1.28	0.00	6.19	0.00	10.00
B39	0.00	0.00	86.04	0.00	0.00	0.00	4.33	3.36	2.35	1.12	0.00	2.80	0.00	5.00
B38	0.00	0.00	86.99	0.00	0.00	0.00	0.37	3.83	3.20	0.80	0.00	4.80	0.00	5.00
B37	0.00	0.77	84.17	0.00	0.00	0.00	4.32	4.45	3.23	0.60	0.00	2.46	0.00	2.00
B36	0.69	0.69	89.50	0.00	0.00	0.00	1.02	2.59	2.07	1.38	0.00	2.07	0.00	5.00
B35	0.00	0.00	84.84	0.00	0.13	0.00	0.63	3.32	1.95	0.98	0.00	8.14	0.00	5.00
B34	1.10	0.63	83.18	0.00	0.00	0.00	0.84	5.66	3.46	3.14	0.00	1.99	0.00	2.00
B33	0.97	6.99	66.40	0.00	0.00	0.00	1.37	2.72	0.97	1.17	0.00	19.42	0.00	10.00
B32	0.00	2.45	46.35	0.16	0.16	0.00	3.97	1.31	19.61	11.29	0.00	14.71	0.00	2.00
B31	1.08	2.15	70.25	0.36	0.00	0.00	2.40	6.09	0.72	1.43	0.00	15.52	0.00	5.00
FS.2														
B28	1.66	2.38	69.42	0.00	0.87	0.00	1.33	10.40	5.62	2.37	0.00	5.97	0.00	15.00
B27	0.65	0.12	68.99	2.37	0.96	0.00	0.00	15.24	0.97	8.33	0.00	2.37	0.00	15.00
B26	1.99	1.97	57.40	0.00	2.37	0.00	0.12	26.40	2.40	7.24	0.00	0.13	0.00	20.00
B25	3.25	2.97	61.69	3.65	0.24	0.00	0.14	19.37	7.17	1.40	0.00	0.14	0.00	5.00

(*continued*)

Table 1. *Continued*

Samples	SOUB	DOL	CB	CF	CALP	RAD	COR	BEN	FB	FP	SPE	QE	QF	Rcl
B24	1.39	2.08	77.64	0.42	0.28	0.00	0.00	6.81	3.19	6.81	0.00	1.39	0.00	10.00
B23	0.94	3.52	60.07	0.23	1.41	0.00	2.37	15.49	7.75	4.23	0.00	3.99	0.00	20.00
B22	0.40	4.11	73.87	0.13	0.27	0.00	0.00	8.36	1.86	9.02	0.00	1.99	0.00	20.00
B21	1.20	2.52	81.73	0.22	0.44	0.00	0.00	7.22	3.39	2.19	0.00	1.09	0.00	20.00
FS.1														
B19	5.92	3.83	76.66	0.00	6.62	0.00	0.00	0.00	0.35	4.18	0.00	0.00	2.44	25.00
B18	1.24	0.89	91.21	0.36	3.37	0.00	0.00	0.53	0.36	1.24	0.00	0.00	0.80	25.00
B17	1.63	2.39	83.29	0.00	4.90	0.00	0.00	0.50	3.77	3.14	0.00	0.00	0.38	20.00
B16	3.77	4.09	68.55	0.94	12.26	0.00	0.00	3.46	2.83	4.09	0.00	0.00	0.00	30.00
B15	1.70	5.97	68.32	0.71	2.41	0.00	0.00	3.41	0.14	0.00	17.05	0.00	0.28	30.00
B14	2.80	4.09	65.09	0.22	3.45	0.00	0.00	1.51	0.00	0.00	22.63	0.00	0.22	25.00
B13	1.15	4.90	59.37	1.44	3.46	0.00	0.00	0.86	0.00	0.00	28.24	0.00	0.58	25.00
B12	0.83	7.01	79.95	0.58	2.64	0.00	0.00	6.93	0.50	1.07	0.00	0.00	0.50	25.00
B11	2.36	9.74	75.80	1.53	3.76	0.00	0.00	3.34	0.70	2.09	0.00	0.00	0.70	25.00
Oued El Kébir														
EK25	4.06	3.19	80.87	0.00	2.90	0.00	0.00	1.16	0.00	3.48	0.00	3.77	0.58	5.00
EK24	3.30	2.06	71.75	0.00	2.27	0.00	0.00	0.82	0.21	3.71	0.00	15.67	0.21	5.00
EK23	0.00	5.29	34.41	0.00	1.76	0.00	0.00	0.00	0.00	0.00	55.59	2.94	0.00	15.00
EK22	0.00	0.64	6.99	0.00	0.32	0.00	0.00	0.64	0.00	0.00	89.51	1.91	0.00	15.00
EK21	0.00	1.47	11.44	0.00	0.88	0.00	0.00	0.88	0.00	0.00	83.58	1.76	0.00	15.00
EK14	0.00	1.04	91.82	0.12	0.98	0.00	0.00	2.93	0.67	1.22	0.00	0.92	0.31	25.00
EK13	0.62	1.18	80.05	0.50	1.06	0.00	0.00	2.49	1.12	10.25	0.00	1.49	1.24	25.00
EK12	0.55	2.90	76.78	0.35	2.00	0.00	0.00	1.90	2.60	7.04	0.00	4.84	1.05	25.00
EK11	0.77	1.55	85.71	0.18	0.95	0.00	0.00	1.13	1.07	5.18	0.00	1.49	1.96	25.00
Internal Dorsale														
T25	0.00	0.00	92.73	1.21	2.42	1.82	0.00	1.82	0.00	0.00	0.00	0.00	0.00	2.00
T24	0.00	2.87	90.80	0.57	5.17	0.57	0.00	0.00	0.00	0.00	0.00	0.00	0.00	2.00
T23	0.00	0.00	87.62	0.00	1.98	3.47	0.00	5.45	1.49	0.00	0.00	0.00	0.00	2.00
T22	0.00	0.00	85.60	4.00	1.60	0.80	0.00	6.40	1.60	0.00	0.00	0.00	0.00	0.00
T21	0.00	0.00	50.00	3.15	0.39	0.79	0.00	0.00	0.00	45.67	0.00	0.00	0.00	0.00
T15	0.00	0.63	48.24	2.70	3.30	0.00	0.00	3.97	0.24	2.97	0.00	37.97	0.00	2.00
T14	0.13	0.23	36.26	3.14	4.97	0.00	0.00	2.33	1.93	3.70	0.00	43.95	3.37	0.00
T13	0.00	0.00	53.22	1.33	1.37	0.00	0.00	5.37	0.24	1.33	0.00	35.83	1.33	2.00
T12	0.27	0.18	42.65	0.36	2.63	0.00	0.00	4.99	0.82	0.73	0.00	46.28	1.09	0.00
T11	0.00	0.17	45.70	1.32	1.66	0.00	0.00	9.27	1.16	2.81	0.00	37.25	0.66	0.00

Two other sections from the Internal *Dorsale* (samples T11–T15 from Hafat Ferkenich section and samples T21–T25 from Kobat Sidi Kmim section) are included in the statistical analysis for comparison with the Béni Ider calciturbidites. Two main types of clasts are distinguished. (1) Clasts supplied from the platform substratum: SOUB, older basement (schists, gneiss, quartzites, etc.); DOL, massive dolomites; CB, white massive limestones; CF, 'calcaires à filaments'; CALP, Calpionellid- and/or *Saccocoma*-rich limestones; RAD, red radiolarites; RCL, diverse rust–yellow altered clasts. (2) Clasts derived from penecontemporaneous biogenic material; BEN, diverse macrobenthos (bivalves, gastropods, algae, etc.); FB, benthic Foraminifera; PF, planktonic Foraminifera; SPE, sponge spicules and fragments. Additional elements, which may be independent of these sources, are represented by QE ('quartz en écharde') of pedological origin and QF (vein-derived, crystalline quartz; the so-called quartz filonien) reworked from old metamorphic rocks and/or old conglomerates of unknown origin.

commonly carry great volumes of clastic material so that the latter should be satisfactorily representative of the material produced in the source area; (2) the mixing processes within turbulent flows may be high enough to homogenize their clastic content. In addition, clean calciturbidite flows generally stop via frictional freezing, so the clast content at the sample scale may reflect the initial composition of their parent flows (in the sense of Mutti (1992) and El Kadiri *et al.* (2006)).

The statistical method used here is factorial correspondence analysis (FCA, Benzecri 1973; Diday *et al.* 1983; Saporta 1990), which has proved to be useful in many sedimentological and biostratigraphical studies (Rey *et al.* 1994; Bonnet *et al.* 1999; Lezin *et al.* 2000). From a pure statistical point of view, this method provides a comprehensive view for a set **I** of elements described by a set **J** of properties. FCA generally results in a geometrical 2D scheme displaying the main relationships between the components of sets **I** and **J**, taken together or separately, or even between the elements of a specified set **I** or **J** considered independently. Numerical data form the primary basis of this analysis in a rectangular **I**–**J** crossing-table, or in a square $\mathbf{I} \times \mathbf{I}$ or $\mathbf{J} \times \mathbf{J}$ table. Treating these (by means of computer software: Statistica VF5, in the present study) consists in projecting all the elements of a set **I** in the space $\mathbf{IR}^j$, which results in a cloud of points, whose dispersal pattern reveals the relationships between them. Such a visual-based assessment may best be accomplished through repeating and comparing the projection in distinct planes. In these, each of the two axes is defined by an outlying element (i.e. the element showing the highest value on the considered axes). Usually, the main axes D1 and D2 often provide at least 50% of the whole statistical information.

Geologically, elements of set **I** correspond to samples, which are collected from distinct stratigraphic intervals and outcrops, so this set may in turn be subdivided into distinct sample sets (i.e. facies sequence). Comparison of these is possible when projecting the samples in the factorial plane. Properties of set **J** correspond to the various components of a given sample, namely the lithoclasts, bioclasts and quartz. Factorial behaviour of these in a given projection plane may be interpreted separately or in conjunction with that of samples in the same plane.

It is noteworthy that the main plane D1–D2 does not necessarily provide the most important result, because the axes D1 and D2 are generally defined by the ubiquitous and most abundant clasts. Indeed, some key clasts of great significance may be represented by the axis D3 or D4 if they are confined to specific levels and/or are poorly represented in the treated samples because of their original scarcity in the source area. Then, a wide spectrum of plane projections (for axis pairs D1–D2, D1–D3, D1–D4, D2–D3, D2–D4, D3–D4) is needed to compare and select the most significant results.

The application of factorial correspondence analysis to Table 1 consists of three steps that complement each other.

Stage I: clasts taken as variables. Their distribution over the factorial space reflects their relative proportions and abundance throughout the samples treated. The grouping of some of the clasts as small cloud(s) means that they have similar behaviour relative to the remaining clasts, especially relative to the two distinct clasts whose highest values define the two factorial-space axes. It is possible to see them separated by changing the projection factorial-plane (there are six possible planes defined by the four axes D1–D4, see above).

Stage II: samples taken as variables. The samples display behaviour over the factorial space depending upon their relative clast input. It is noteworthy that the grouping of many samples as dense cloud(s) may be interpreted not only as the clasts having similar behaviour relative to the remaining samples, but also as a consequence of one or more ubiquitous clasts, which quantitatively dominate the reworked material. For example the CB-type clasts (derived from the regionally well-known white massive limestones, i.e. the so-called 'Calcaires Blancs', CB) may be represented by as many as 1000 elements within a single sample, whereas CALP-type clasts (derived from the reduced *Calpionella*-rich mudstones) may be scarce or represented by < 100 elements. Such relative proportions are pre-determined by the overall composition of the source materials and not by selective transportation processes. Significant, statistical sample behaviour would be brought out by changing the projection-plane axes, or by the elimination of the most ubiquitous clast(s) from the statistical analysis. In contrast, an isolated sample, clearly separated from the principal sample cloud, indicates a clast or several clasts whose occurrence is exceptional in the overall succession (e.g. bioclasts SPE corresponding to the sponge spicules and fragments). Unfortunately, it is such a clast type that determines certain factorial axes. Additional projections are then tentatively obtained by removing these exceptional clasts.

Stage III: sections taken together or separately in the statistical analysis. Both clast- and sample-type projections should not be carried out in treating the studied samples together, regardless of their

Table 2. *Factorial planes selected (A1–H2) for the factorial correspondence analysis*

Variables	The six planes	All the variables	RA + EK + ID		RA + EK	RA + ID			RA
			CB excepted	Lithoclasts only	All data	SPE excepted	Lithoclasts + Qz	Lithoclasts only	SPE excepted
Clasts	D1–D2						F1		
	D1–D3	A1		C1					H1
	D1–D4								
	D2–D3								
	D2–D4					E1			
	D3–D4		B1		D1			G1	
Samples	D1–D2						F2		
	D1–D3	A2		C2					H2
	D1–D4								
	D2–D3								
	D2–D4					E2			
	D3–D4		B2		D2			G2	

The planes selected do not necessarily correspond to the main axes D1 and D2 because the information given by these mainly concerns variables displaying extreme behaviours (i.e. very abundant and ubiquitous clasts, such as variable CB) or that are strictly confined to some stratigraphic levels (e.g. variable SPE). It was necessary to remove them from some projections to show the relative behaviour of the remaining clasts. This operation is tentatively repeated for the studied sections taken together or separately.

origin. Significant difference in behaviour of variables may hypothetically be possible between distinct sections. Thus, for the Rar Aghroud facies sequences, the best results are obtained below in eliminating the samples coming from other sections.

Altogether, 96 distinct planes have been analysed (Table 2), among which 16 are selected (Fig. 2 planes A1 and A2 to H1 and H2) to provide better evidence of the statistical behaviour of the reworked carbonate material. The selected planes do not necessarily correspond to those defined by the major axes D1 and D2. This graphical result provides a valuable basis for comparison of the vertically stacked facies sequences of the studied Béni Ider succession, and the regionally patched, late Cretaceous calciturbidites (e.g. internal Dorsale).

Statistical analysis of the reworked carbonate clasts in the Béni Ider and 'Dorsale calcaire' calciturbidites

The results we obtained are presented according to the diagrams shown in Figure 2. The information they provide often outpaces our interpretative capabilities, although it has clear sedimentological significance, such as to oppose the bioclast to the lithoclasts in the factorial space, or the pedological quartz (QE, 'quartz en écharde', Meyer 1987) to the metamorphic rock-derived quartz (QF, the so-called 'quartz filonien').

We will emphasize, below, the cases in which the dispersal pattern of variables allows us to distinguish the previously defined facies sequences from each other (FS.1–FS.6), on one hand, and the Béni Ider calciturbidites from the Internal Dorsale ones, on the other.

Diagrams A1 and A2: all the samples and clasts are treated in factorial correspondence analysis

Diagram A1 shows planktonic Foraminifera (FP) and sponge spicules (SPE) clearly separated from the major cloud, because these variables are occasionally present in some levels within the Rar Aghroud and Oued El Kébir sections. The major clast cloud is split into three clusters depending upon the relative abundance of the clasts within the following facies sequences: FS.5 (cluster with QF, FB, COR), FS.3 (cluster with FB, QE) and FS.1–FS.3–FS.6, which are taken together with the internal Dorsale (the remainder clasts). At the same time, the FCA clearly separated the clasts reworked from the material produced by the platform itself (by both its inundated and emerged parts: mixture of bioclasts plus quartz) from that derived from its Triassic–Jurassic substratum.

Diagram **A2** brings out the main samples responsible for the preceding clast distribution. Nearly all the samples from FS.4 and FS.5, as well as some samples from FS.1 and the Oued El Kébir section (EK, which is the lateral equivalent of FS.1 of Rar Aghroud section) diverge from the major cloud according to a pattern with three trends.

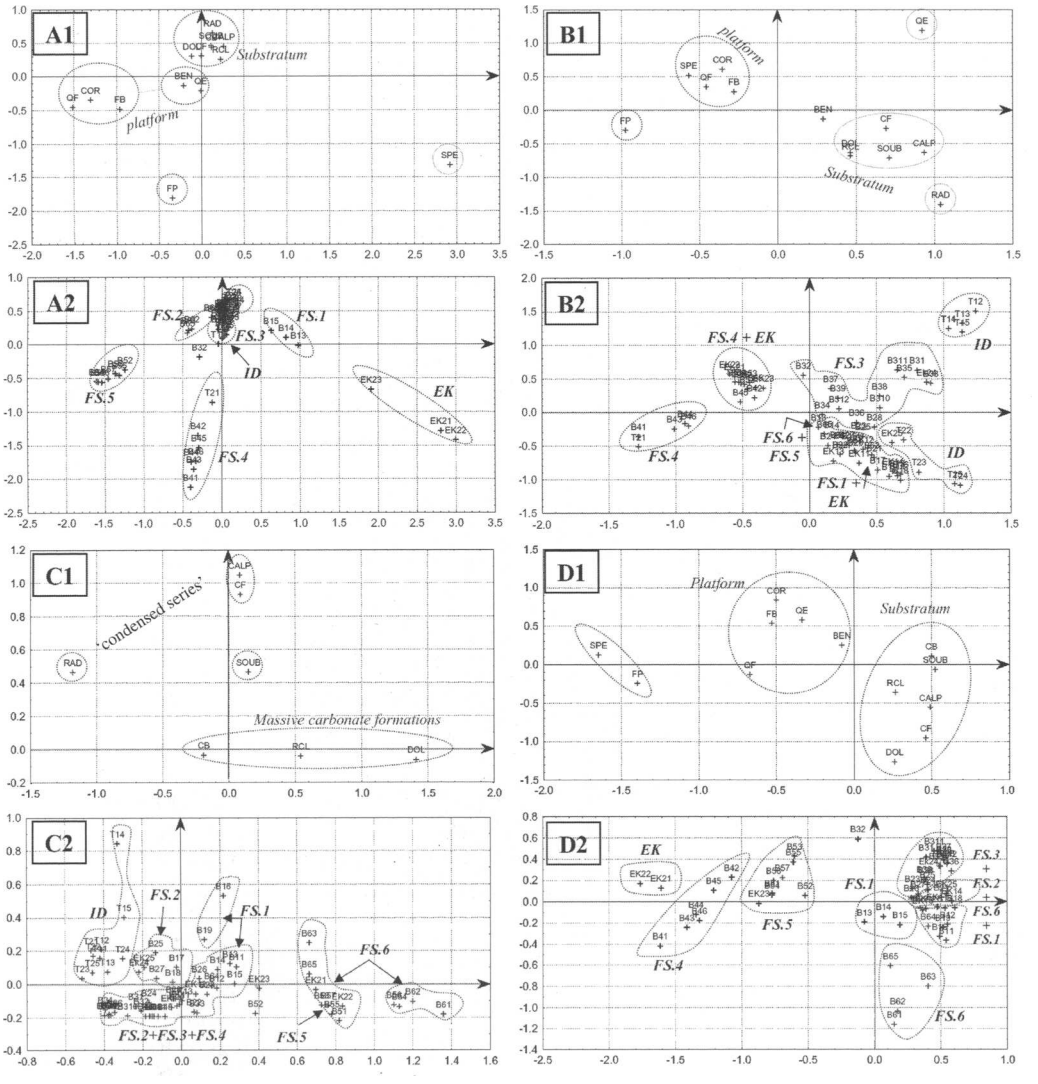

Fig. 2. The planes in which the clasts are taken as variables (A1 and A2 to H1 and H2) clearly show differentiation into two groups depending on the clast origin; namely, from the platform substratum or from the material of the inundated platform itself. Within each of these groups, when taken separately, the distinction is clearly made between clasts supplied from the massive carbonate formations (Triassic–early Jurassic in age) and those supplied from the 'condensed series'-type (late Liassic and latest Jurassic), or those derived from a terrigenous source (see text for details).

Diagrams B1 and B2: all data are treated, except the variable CB (clasts derived from the white massive limestones)

Diagram B1 is obtained by excluding the over-abundant variable CB from the statistical analysis, which allows the clast cloud to be dissociated into a lithoclasts-dominated group (positive values along the axis 3) and a group dominated by the elements characterizing FS.5 (namely, COR, QF and FB). Variables QE, FP and RAD (radiolarite-derived clasts) are clearly separated from these clouds and show extreme values as a result of their abundance in specific levels. It is noteworthy that the variables RCL (rust–yellow clasts that have undergone rubefaction) and DOL show near-identical behaviour, which agrees with the common observation in thin section that the majority of the RCL clasts correspond to altered dolomites.

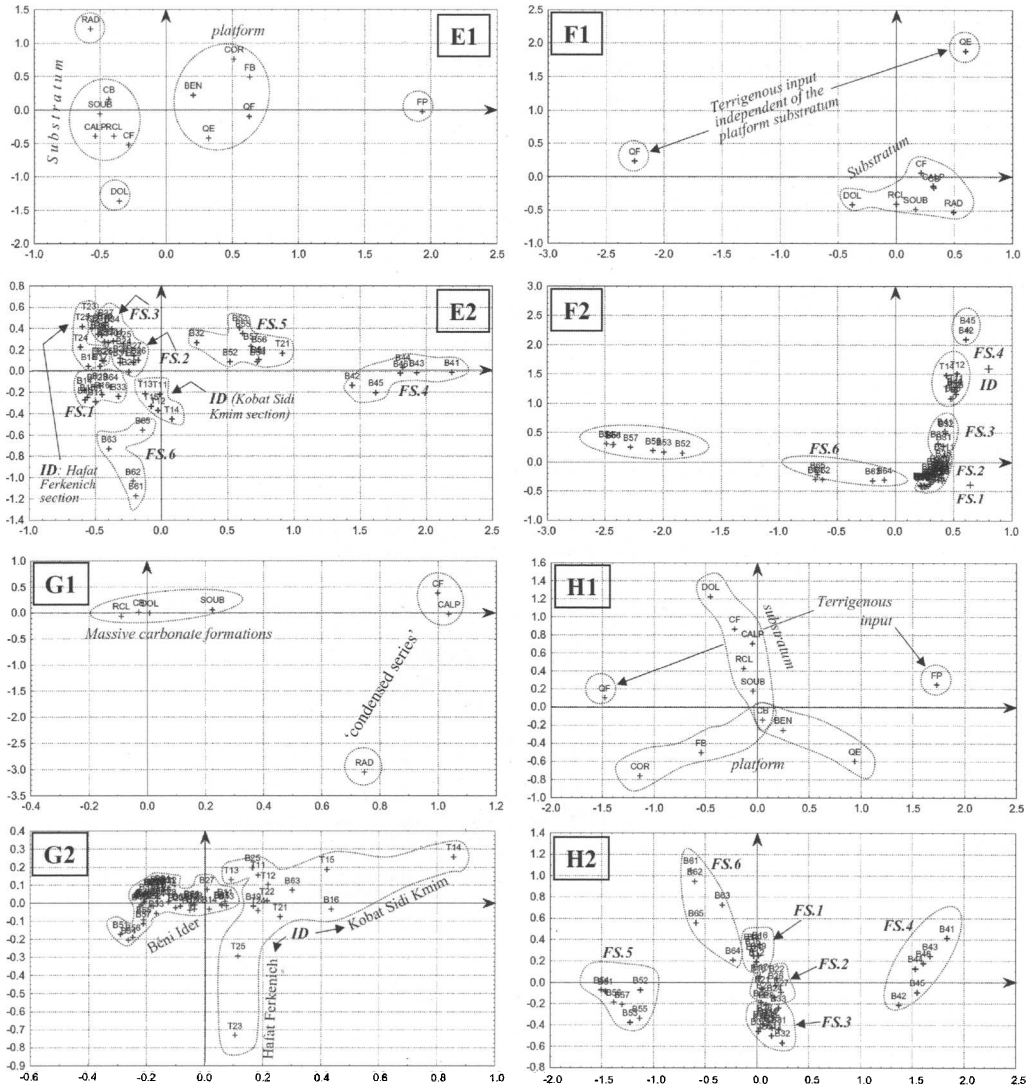

Fig. 2. (*Continued*)

In diagram B2, this clast behaviour results in the samples of the Internal Dorsale and almost all those of FS.3 being separated from other clouds, which consist of a mixture of samples pertaining to the remaining facies sequences. The axis 3 puts the two sections selected in the Internal Dorsale, Hafat Ferkenich and Kobat Sidi Kmim sections, against the other, as a result of the presence of radiolarite clasts (RAD) in the former and the QE in the second. Equivalent contrary behaviour is shown by FS.3 and FS.1 + EK because of the presence of bioclasts (BEN) together with the QE in the former and the predominance of the lithoclasts derived from dolomites (DOL + RCL) and from the older basement (SOUB) in the second group.

Diagrams C1 and C2: lithoclasts only

In diagram C1 the axis D3 separates the variables CF and CALP derived from the reduced series (the late Liassic filament-rich and Tithonian–Berriasian *Calpionella*-rich mudstones, respectively) from those derived from the massive carbonate formations (Triassic–earliest Jurassic, DOL, RCL and CB). The clasts RAD derived from radiolarites are separated from these clouds because of their occasional

presence in the Hafat Ferkenich section. A noteworthy feature is the factorial position of the clasts CALP and CF relative to the clasts SOUB derived from the older basement of the platform (mainly schist and gneiss clasts). If we take into account that the erosion of an undeformed series acts through time *per descensum*, and results in successive exhumation of the vertically stacked strata, it should be expected, instead, that these clasts derived from Jurassic pelagic strata would have a closer relationship with the clasts sourced from the immediately underlying late Triassic–early Liassic massive carbonate formations (CB and DOL, mainly). The factorial affinity of the variables CALP and CF with the variable SOUB may indicate that the 'condensed series' were, in the source area, deposited discordantly on the older basement. This fact has never been observed in the Internal Dorsale successions.

In diagram C2, the majority of the samples show low values with respect to the axis D3, as a result of the overabundance of the clasts CB, DOL and RCL, whereas many samples from ID and FS.1 present the highest values because of the abundance, at the same time, of the clasts CALP and CF (this result may be obtained through comparison with diagram C1). The samples from the Internal Dorsale calciturbidites may be arranged in a distinct cloud because of the presence of clasts RAD sourced from the radiolarites. This criterion allows them to be fundamentally distinguished from the Béni Ider samples.

Diagrams D1 and D2: Béni Ider calciturbidites only

In diagram D1, the lithoclasts derived from the older basement and the Jurassic substratum of the source platform (SOUB, DOL, RCL, CB, CF and CALP) are clearly separated from the benthic material of the latter (FB, benthic Foraminifera; COR, reef debris; BEN, diverse benthos including bivalves, gastropods, algae, echinoid spines and rudist fragments), and from the quartz grains (QE, QF) that typically invade shallow bioclastic sands. Such a fundamental discrimination, although hard to determine without the statistical analysis, shows that the supplying parent flows may originate independently from the platform material or from its basement. We will suggest below a possible interpretation for this based on a newly defined concept: 'transgressive washing'. It should be noted how both the planktonic Foraminifera (FP) and the sponge spicules (SPE) are clearly separated from the bioclast cloud, which is consistent with the difference between the palaeoenvironmental conditions, that are favourable to them.

Diagram D2 shows which facies-sequence distribution results from the preceding discrimination. The group FS.1 + FS.2 + FS.3 + FS.6 consists of high lithoclast proportions, with its facies sequences being distinguished based upon the dominant lithoclasts, whereas the group FS.4 + FS.5 + EK primarily consists of bioclasts, with its facies sequences being separated depending upon the planktonic or benthic signature.

Diagrams E1 and E2: comparison between the sections from Rar Aghroud and from the Internal Dorsale, based upon the main elements

Variable SPE is excluded here because its occurrence characterizes only some levels within the Cenomanian–Turonian interval (FS. 1).

In diagram E1 we can recognize the preceding discrimination between the lithoclasts and the bioclasts, with their respective values being opposed along the axis D2. The variables DOL and RAD are drawn apart from the lithoclast cloud and are opposed along the axis D4. Variables RAD and COR display the highest values along this axis, but are opposed along the axis D2. The variable FP is drawn apart from the main cloud formed by the bioclasts and their associated quartz, and displays the highest value along the axis D2.

Considered together, these clast behaviours allow, in diagram E2, a better discrimination to be made between the two sections from the Internal Dorsale, on one hand, and between the Rar Aghroud facies sequences, on the other.

Diagrams F1 and F2: comparison Internal Dorsale–Béni Ider, based upon the lithoclasts and quartz

Diagram F1 clearly separates the two types of quartz (QF: 'filonien' quartz, derived from quartzite and metamorphic rocks; QE: 'quartz en écharde' of pedological origin) from each other and from the lithoclast cloud, derived from the massive carbonate formations and the older basement of the source platform. This behaviour may easily be explained for QE, which is of pedological origin (Meyer 1987). In contrast, QF may also be sourced from the older basement, so its isolation in the factorial space seems less easy to understand. However, the fact that the factorial plane D1–D2 brings together the clasts derived from a same stratigraphic column strongly suggests that QF was derived from a denuded basement or originated in any other area independent of the platform carbonate substratum. Its sudden occurrence in the base of

FS.5 (early Maastrichtian) pinpoints a key event, which must be related to environmental and/or eustatic changes.

In diagram F2, the facies sequences are discriminated and arranged between the three preceding opposite poles. The samples from the Internal Dorsale are brought close to the QE pole together with the samples from FS.4. The remaining facies sequences are clearly separated from the Internal Dorsale.

Diagrams G1 and G2: comparison internal Dorsale–Béni Ider, based upon the lithoclasts only

Diagram G1 shows that the variables CALP and CF are clearly separated from the main lithoclast cloud. They acquire the highest values along the axis D3, whereas the variable RAD is isolated by the axis D4, along which it acquires an extreme negative value. Isolation of this variable may be regarded (in the same way as for QF in diagram F1) as a consequence of a distinct source (i.e. a radiolarite-intercalated succession), which supplied the Hafat Ferkenich section, relative to that from which the coeval Kobat–Sidi-Kmim calciturbidites were derived (radiolarite-devoid succession). Along the axis D3, the high and near-equal values of the variables CALP and CF may be interpreted by the fact that these clasts were sourced from juxtaposed levels in the source area. This is consistent with the field observation made regionally in the Internal Dorsale, that the *Calpionella*-rich mudstones discordantly overlie the filament-rich ones (with a significant gap between them; El Kadiri *et al.* 1989). However, this deduction does not necessarily mean that the Internal *Dorsale* acted as source area for the Béni-Ider calciturbidites.

In diagram G2, the preceding discrimination between the variables CALP-CF/RAD and the other allows us to clearly distinguish the whole of the Béni Ider calciturbidites from that of the Internal Dorsale.

Diagrams H1 and H2: Rar-Aghroud section solely

Diagrams H1 and H2 recall diagrams D1 and D2 in excluding the Internal Dorsale. Here the Oued El Kébir section is also excluded because it may be assumed that a distinct position with respect to the source area, within the same palaeogeographical setting (i.e. the Béni Ider trough), may result in significant differences in the clast content. This precaution is mentioned to better evidence the actual behaviour of the pre-defined, Rar Aghroud facies sequences. An additional precaution is taken by excluding the variable SPE, whose overabundance in specific levels of FS.1 seems to us partly related to turbidite grain segregation.

In diagram H1, the ubiquitous variable CB acts as an intersection point of three major, elongated clast clouds, which obliquely diverge from each other (at angles near 120°). The variables FP and QF are opposed, along the axis D1, a fact that is consistent with the tendency of the pelagic signature and the terrigenous input to be mutually exclusive.

Diagram H2 shows the factorial scheme that results from the preceding clast behaviour, when the samples are taken as variables. A noteworthy feature is the arrangement of the samples according to their respective facies sequences. Among these, FS.1, FS.2 and FS.3 are juxtaposed according to their chronological order along the axis D3, as a result of the progressive depletion with time of the clasts CALP and CF, compared with the enrichment in clasts BEN and in QE. FS.6, at the top of the Rar Aghroud section (latest Maastrichtian), strikingly involves again the clasts CALP and CF, which explains why its factorial position is close to that of FS.1. The opposite factorial positions of FS.4 and FS.5 along the axis D1 result from the contrasting behaviour of the pelagic signature of the former and the terrigenous character of the latter.

On the whole, the factorial arrangement of these facies sequences gives evidence that each of them was supplied by a generation of parent flows that involved distinct clast populations. This result may have an important bearing on the sequence stratigraphy interpretation (see below).

Discussion

The lithological description presented above was first prompted by the common occurrence within the Béni Ider, late Cretaceous calciturbidites of clasts derived from the following two key facies: the Liassic filament-bearing mudstones and the Tithonian–Berriasian *Calpionella*- or *Saccocoma*-rich mudstones (at the Cenomanian–Turonian and latest Maastrichtian levels). These facies are well known in the Jurassic–earliest Cretaceous successions of the Internal Dorsale, so they give the first impression that the Béni Ider calciturbidites would have been sourced from the carbonate successions of the Rifian Internal Domain (i.e. Dorsale Calcaire). A similar conclusion was previously drawn by Maghrebian researchers, who noted the presence of pebbles derived from crystalline rocks within the late Oligocene–Aquitanian strata of the Béni Ider flysch. Recently, such an assumption was questioned by Puglisi *et al.* (2001) and Zaghloul *et al.* (2002), who showed through statistical analysis that the Béni Ider material was not sourced directly from the metamorphic Ghomarides' terranes known at present but from a lost continental crust segment.

The statistical analysis of the stratigraphically underlying late Cretaceous calciturbidites presented

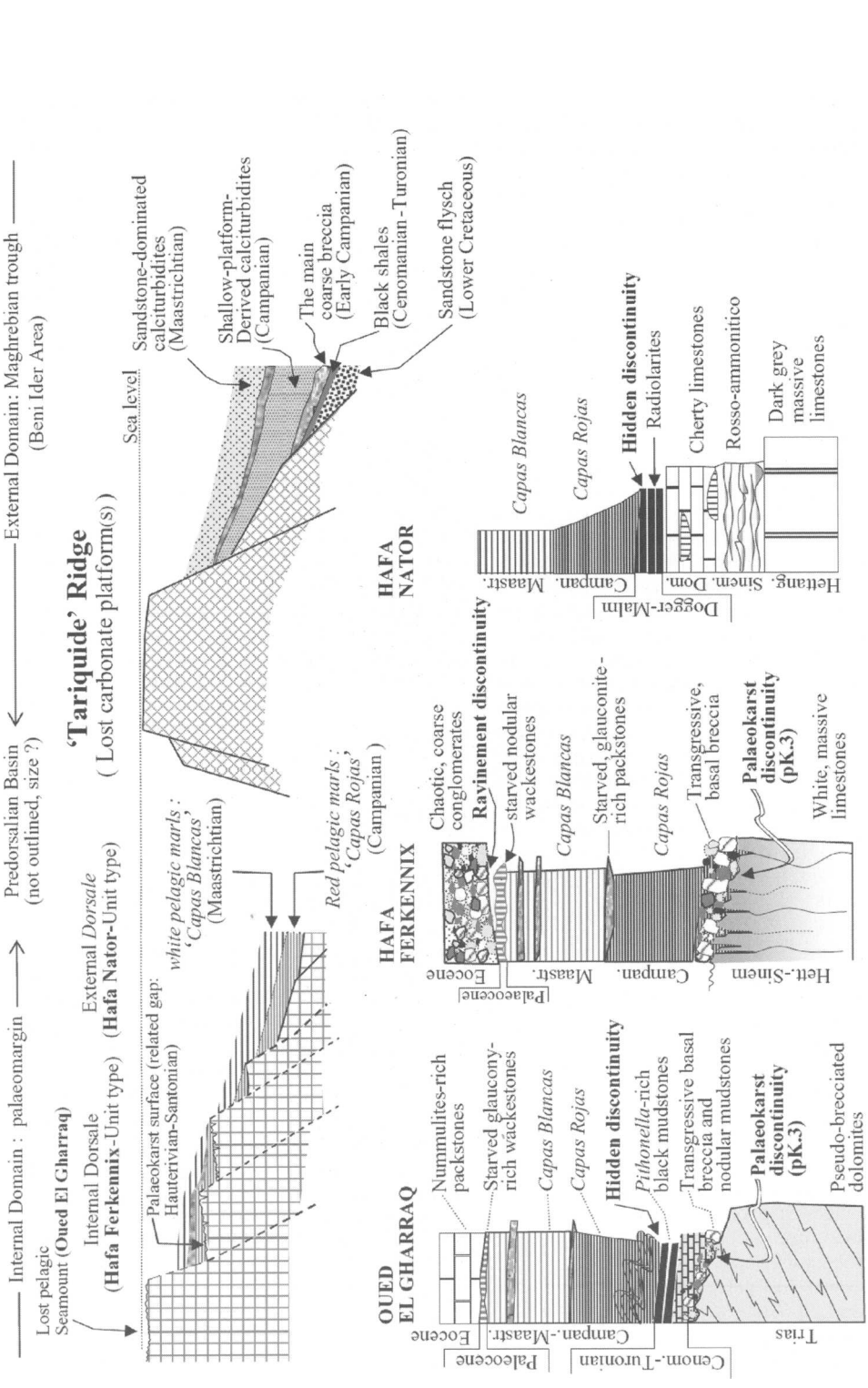

Fig. 3. Palaeogeographical reconstruction envisaged for a lost, 'Tariquide Ridge'-type isolated platform lying between the external Dorsale–Predorsalian domain and the proximal margin of the Maghrebian Trough (Béni Ider area) as postulated by Durand Delga (1972). Stratigraphic differences between age-equivalent strata in the Internal Domain (Oued El Gharraq, Hafa Ferkennix and Hafa Nator units) and the External Domain (Béni Ider area), and the statistical analysis of reworked clasts in both cases, clearly exclude the Internal Domain as a possible source for the Béni Ider calciturbidite material.

above appears consistent with this result, as it equally (1) leads us to question the first impression given by their carbonate lithoclasts that they would have originated from the tectonically juxtaposed Dorsale Calcaire and (2) provides evidence that their source was a lost carbonate platform, which should be reconstructed in the external domain itself. Overall, the petrographical analysis undertaken in the Internal Dorsale and the Béni Ider area, in conjunction with the stratigraphic comparison between these distinct domains, allows the following two conclusions to be drawn.

(1) A land-disconnected source may be suggested for the Béni Ider calciturbidites (Fig. 3). A notable feature is the proximal, clean breccia flows interbedded within them (i.e. grain-flows of Lowe 1982; facies F3 of Mutti 1992). Their thinner division, if not detached from the corresponding parent flow, reveals that they sometimes involve a mixture of shallow-water skeletal grains (reef debris, encrusting algae, benthic Foraminifera; mainly FS.3b and FS.5), sometimes planktonic muds, namely the radiolarian-rich mudstones during Cenomanian–Turonian times and the planktonic Foraminifera during the Campanian (mainly FS.1 and FS.4). The sheet-like geometry of most of these calciturbidites and the small-scale channelling (on outcrop scale) of the breccia flows strongly suggest deposition at the base of a steep slope (i.e. close to a shallow-water, shedding system). This depositional setting is inconsistent with one receiving the oversupplied, terrigenous-mud-rich, turbidity systems I–III (Mutti 1985; Mutti & Normark 1987, 1991), and should best be classified as an isolated carbonate platform (Cook & Taylor 1977; Cook & Egbert 1981; Cook & Mullins 1983; Sarg 1988; Handford & Loucks 1993). It is possible that it has a wide, shoal-water, flat-topped component landwards, and a distally steepened ramp seawards. Such a physiography seems to satisfactorily account for the stratal pattern, the petrographical composition and the regional extent of the Béni Ider calciturbidites (see also the similar discussion by Yose & Heller (1989)). Measurements of palaeocurrent directions based on flute-casts indicate currents travelling from a direction N15–N45, mainly N20–30 (see El Kadiri *et al.* 2006), which provides supporting evidence that they were supplied from a distinct source with respect to the neighbouring Dorsale Calcaire.

(2) A second, lost pelagic seamount could also be reconstructed along the eastern side of the palaeogeographical area corresponding to the Internal Dorsale. It shed into the latter, during Campanian and Maastrichtian times, small carbonate mudflows rich in pelagic Foraminifera, which resulted in the so-called 'Capas Rojas', and 'Capas Blancas', respectively (El Kadiri *et al.* 1989). These key facies are extend regionally throughout the Gibraltar arc and clearly differ from the coeval Béni Ider calciturbidites (Fig. 3).

Conclusion

The quantitative study of the reworked material, using factorial correspondence analysis, has primarily ledus to clearly distinguish the clastic content of the late Cretaceous calciturbidites of the Béni Ider unit (External Domain) from that of coeval carbonate material belonging to the neighbouring Internal Dorsale Calcaire units. Furthermore, several stratigraphic intervals have been characterized depending on the distinct clast populations successively delivered by the source area mainly (quartz, lithoclasts and bioclasts). Thus, this statistical method may have an important bearing on palaeogeographical reconstructions.

The authors are grateful to the Société Nationale d'Etude du Détroit, SNED, Rabat, Morocco, for financial support. They express their sincere thanks to L. Imlahi (Department of Mathematics, Tetuan) and A. Lopez-Guarrido (Department of Stratigraphy, Granada) for their fruitful remarks.

References

BENZECRI, J. P. 1973. *L'analyse des données. Tone II: l'analyse des correspondances*. Dunod, Paris.

BONNET, L., ANDREU, B., REY, J., CUBAYNES, R., RUGET, C., N'ZABA MAKA, O. & BRUNEL, F. 1999. Fluctuations of environmental factors as seen by means of statistical analyses in micropaleontological assemblages from Liassic series. *Micropaleontology*, **45**, 4–14.

BOUILLIN, J. P., DURAND-DELGA, M., GÉLARD, J. P., *ET AL.* 1970. Définition d'un flysch Massylien et d'un flysch Maurétanien au sein des flyschs allochtones de l'Algérie. *Comptes Rendus de l'Académie des Sciences*, **270**, 2249–2252.

BOUILLIN, J. P., DURAND-DELGA, M. & OLIVIER, P. 1986. Betic-Rifian and Tyrrhenian arcs: distinctive features, genesis and development stages. *In*: WEZEL, F. C. (ed.) *The Origin of the Arcs*. Elsevier, Amsterdam, 281–304.

BOURGOIS, J. 1978. *La transversale de Ronda, Cordillères bétiques, Espagne. Données géologiques pour un modèle d'évolution de l'Arc de Gibraltar*. Thesis, University of Besançon.

COOK, H. E. & EGBERT, R. M. 1981. Carbonate submarine fans along a Palaeozoic prograding continental margin, western United States (abstract). *AAPG Bulletin*, **65**, 913.

COOK, H. & MULLINS, H. T. 1983. Basin margin environment. *In*: SCHOLLE, P. A., BEBOUT, D. G. & MOORE, C. H. (eds) *Carbonate Depositional Environments*. American Association of Petroleum Geologists, Memoirs, **33**, 539–617.

COOK, H. E. & TAYLOR, M. E. 1977. Comparison of continental slope and shelf environments in the Upper Cambrian and Lowest Ordovician of Nevada. *In*: COOK, H. E. & ENOS, P. (eds) *Deep-Water Carbonate Environments*. Society of Economic Paleontologists and Mineralogists, Society for Sedimentary Geology, Special Publications, **25**, 51–82.

DIDAY, E., LEMAIRE, J., POUGET, P. & TESTUT, F. 1983. *Eléments d'analyse des données*. Dunod, Paris.

DIDON, J., DURAND-DELGA, M. & KORNPROBST, J. 1973. Homologies géologiques entre les deux rives du détroit de Gibraltar. *Bulletin de la Société Géologique de France*, **15**, 77–105.

DURAND-DELGA, M. 1972. La courbure de Gibraltar, extrémité occidentale des chaînes alpines, unit l'Europe et l'Afrique. *Eclogae Geologicae Helveticae*, **65**, 267–278.

DURAND-DELGA, M. 1980. Considérations sur les flyschs du Crétacé inférieur dans les chaînes alpines d'Europe. *Bulletin de la Société Géologique de France*, **22**, 15–30.

EL HATIMI, N. 1991. *Rifting mésozoïque sur la bordure occidentale du Rif interne (Maroc). Evolution géodynamique d'un secteur de la marge ouest-téthysienne. Exemples du Haouz et du Groupe du J. Moussa*. Diplôme d'Etudes Supérieures Thesis, University of Pau.

EL KADIRI, KH. 1984. *Les radiolarites jurassiques des klippes de Chrafate (Rif septentrional, Maroc): stratigraphie, taxonomie*. Doctorat de 3ème Cycle Thesis, University of Pau, France.

EL KADIRI, KH. 1991. *La Dorsale Calcaire (Rif interne, Maroc): stratigraphie, sédimentologie et évolution géodynamique d'une marge alpine durant le Mésozoïque. Mise en évidence d'un modèle*. Doctorat d'Etat Thesis, University of Tetuan.

EL KADIRI, KH., LINARES, A. & OLORIZ, F. 1989. La Dorsale calcaire interne entre les Accidents de l'Oued Martil et de l'Oued Laou (Rif septentrional, Maroc): évolutions stratigraphique et géodynamique au cours du Jurassique–Crétacé. *Communicações Serviços Geológicos de Portugal*, **75**, 39–65.

EL KADIRI, KH., LINARES, A. & OLORIZ, F. 1992. La Dorsale Calcaire rifaine (Maroc septentrional): évolution stratigraphique et géodynamique durant le Jurassique–Crétacé. Notes et Mémoires du Service Géologique du Maroc, **336**, 217–265.

EL KADIRI, KH., EL KADIRI, K., CHALOUAN, A., BAHAMD, A., SALHI, F., LIEMLAHI, H. & HLILA, R. (2006). Transgressive–regressive facies cycles in late Cretaceous calciturbidites from the Mauretanian Series (Béni Ider thrust sheet, northwestern external Rif, Morocco): an application of the 'facies tract–facies sequence' concept. *In*: MORATTI, G. & CHALOUAN, A. (eds) *Tectonics of the Western Mediterranean and North Africa*. Geological Society, London, Special Publications, **262**, 45–53.

HANDFORD, C. R. & LOUCKS, R. G. 1993. Carbonate depositional sequences and systems tracts — responses of carbonate platforms to relative sea-level changes. *In*: LOUCKS, R. G & SARG, J. F. (eds) *Carbonate Sequence Stratigraphy; Recent Developments and Applications*, American Association of Petroleum Geologists, Memoirs, **57**, 3–41.

LEZIN, C., BONNET, L., REY, J., CUBAYNES, R. & PELISSIE, T. 2000. Contribution de l'analyse quantitative des faciès aux corrélations stratigraphiques, exemple du Toarcien supérieur–Aalénien dans le Quercy, SW France. *Bulletin de la Société Géologique de France*, **171**(1), 91–102.

LOWE, D. R. 1982. Sediment gravity flows: II. Depositional models with special reference to the deposits of high-density turbidity currents. *Journal of Sedimentary Petrology*, **52**, 279–297.

MEYER, R. 1987. *Paléolatérites et paléosols, l'empreinte du continent dans les séries sédimentaires*. Bureau de Recherches Géologiques et Minières, Manuel et Méthodes, **13**.

MUTTI, E. 1985. Turbidite systems and their relation to depositional sequences. *In*: ZUFFA, G. G. (ed.) *Provenance in Arenites*. Reidel, Dordrecht, 65–93.

MUTTI, E. 1992. *Turbidite Sandstones*. Agip, Special Publications, Instituto di Geologia, Milan.

MUTTI, E. & NORMARK, W. R. 1987. Comparing examples of modern and ancient turbidite systems: problems and concepts. *In*: LEGGETT, J. K. & ZUFFA, G. G. (eds), *Marine Clastic Sedimentology: Concepts and Case Studies*. Graham Trotman, London, 1–38.

MUTTI, E. & NORMARK, W. R. 1991. An integrated approach to the study of turbidite systems. *In*: WEIMER, P. & LINK, H. (eds) Seismic Facies and Sedimentary Processes of Submarine Fans and Turbidite Systems. Springer, Berlin, E75–106.

OLIVIER, P. 1984. *Evolution de la limite entre les Zones internes et les Zones externes dans l'Arc de Gibraltar (Maroc Espagne)*. Doctoral d'Etat Thesis, University Paul Sabatier, Toulouse.

PUGLISI, D., ZAGHLOUL, M. N. & MAATÉ, A. 2001. Evidence of sedimentary supply from plutonic sources in the Oligocene–Miocene flyschs of the Rifian Chain (Morocco): provenance and palaeogeographic implications. *Bollettino della Società Geologica Italiana*, **120**, 55–68.

RAOULT, J. F. 1974. *Géologie du centre de la Chaîne Numidique (nord du Constantinois, Algérie)*. Mémoires de la Société Géologique de France, **121**.

REY, J., BONNET, L., CUBAYNES, R., QAJOUN, A. & RUGET, C. 1994. Sequence stratigraphy and biological signals: statistical studies of benthic Foraminifera from Liassic series. *Palaeogeography, Palaeoclimatology, Palaeoecology*, **111**, 149–171.

SAPORTA, G. 1990. *Probabilities, Analyse des Données et Statistique*. Technip, Paris.

SARG, J. F. 1988. Carbonate sequence stratigraphy. *In*: WILGUS, C. K., HASTINGS, B. S., KENDALL, C. G. ST. C., POSAMENTIER, H. W., ROSS, C. A. & VAN WAGONER, J. C. (eds) *Sea Level Changes—An Integrated Approach*. Society of Economic Palaeontologists and Mineralogists, Society for Sedimentary Geology, Special Publications, **42**, 155–181.

YOSE, L. A. & HELLER, P. L. 1989. Sea-level control of mixed-carbonate–siliciclastic, gravity-flow deposition: lower part of the Keeler Canyon Formation (Pennsylvanian), south-eastern California. *Geological Society of America Bulletin*, **101**, 427–439.

ZAGHLOUL, M. N., GUERRERA, F., LOIACONO, F., MAIORANO, P. & PUGLISI, D. 2002. Stratigraphy and petrography of the Béni Ider flysch in the Tétouan area (Rif Chain, Morocco). *Bollettino della Società Geologica Italiana*, **121**, 69–85.

Mauretanian flysch nappe in the northwestern Rif Cordillera (Morocco): deformation chronology and evidence for a complex nappe emplacement

A. CHALOUAN[1], A. EL MRIHI[2], KH. EL KADIRI[2], A. BAHMAD[3], F. SALHI[4] & R. HLILA[2]

[1]*Université Mohammed V-Agdal, Faculté des Sciences, Dep. Geology, BP 1014, Rabat, Morocco (e-mail: chalouan@fsr.ac.ma)*

[2]*Université Abdelmalek Essaadi, Faculté des Sciences, Dep. Geology, BP 2121, 93003 Tetuan, Morocco*

[3]*Société Nationale d'Etudes du Détroit, (SNED), 31 r. Al Alaouyine, Rabat, Morocco*

[4]*Université Chouaib Doukali, Faculté des Sciences, El Jadida, Morocco*

Abstract: This study deals with the Mauretanian flysch nappe in the southern side of the Gibraltar Strait, NW of the Rif belt (Morocco), where it is possible to better appraise the stacking pattern of its two structural components (the Tisirene and Béni Ider nappes), and to decipher the chronology of deformation and its structural relationships with the overlying (Predorsalian and Numidian nappes) and the underlying nappes (Melloussa and Intrarif units). It is found that the main deformations were produced by an intermittent compressional regime, during which north–south- to NW–SE-directed compressional phases alternated with ENE–WSW to east–west-directed compressional ones. Whereas the former were generated by the Africa–Iberia convergence and resulted in small-scale thrusts and a brittle deformation style, the latter were driven by the west-drifting Alboran plate and resulted in paroxysmal fold–thrust deformations. Field evidence shows that the emplacement of the Mauretanian nappe over the Massylian one and the Intrarif units operated by interrelated compressional and gravitational processes, by virtue of which the majority of nappes stacked in an out-of-sequence regime. The precise age of the paroxysmal phases remains uncertain because of paucity or absence of direct stratigraphical data. However, this structural evolution is likely to have started as early as the mid-Burdigalian, when sedimentation synchronously ceased in the flysch trough. Its final phases may be placed precisely between the Langhian (N8) age of the most recent formations overlapped by these nappes and the late Tortonian age of the oldest formations transgressively covering them.

The Rif belt represents the westernmost part of the Maghrebian Alpine chain, which crops out along the Mediterranean coast of North Africa, from the Calabrian to the Gibraltar arc (Fig. 1a). Three structural domains form the Rif (Fig. 1a):

(1) the internal domain, which consists of a triple nappe complex, the Dorsale–Ghomarides–Sebtides, which are respectively made up of Mesozoic carbonate rocks, Variscan-derived Palaeozoic terranes and high-grade metamorphic and mantle rocks (e.g. Kornprobst 1974; Chalouan 1986).

(2) The Flysch domain, which resulted from deformation of the 'Flysch Trough' formations (Durand-Delga 1972) into complex nappe piles. This domain is mostly confined along elongated areas that now form the outline of the Gibraltar arc (Fig. 1a and b). Depending upon their position within the initial basin and their stratigraphic relationships, the siliciclastic flysch units can be grouped into two main stratigraphic successions (Bouillin *et al.* 1970; Raoult 1974): (a) the Mauretanian series, which is generally located close to the northern margin of the Flysch Trough and consists of the Tisirene flysch, of late Jurassic–early Cretaceous age, and the Béni Ider flysch, of Palaeogene–Mid-Burdigalian age; (b) the Massylian series, which is located close to its southern palaeomargin and consists of the early Cretaceous Massylian flysch (*sensu stricto*) and the Numidian flysch, of Palaeogene to early Burdigalian age.

(3) The external domain, basically consisting of (a) late Cretaceous, pelite-dominated parautochthonous terranes (Tangiers–Loukous units) and (b) Triassic to Tertiary, carbonate and siliciclastic parautochthonous to autochthonous terranes (Mesorif–Prerif).

The external domain derived from the African palaeomargin of the Maghrebian–Apenninic chain, whereas the Internal Domain was a part of

From: MORATTI, G. & CHALOUAN, A. (eds) 2006. *Tectonics of the Western Mediterranean and North Africa.* Geological Society, London, Special Publications, **262**, 161–175.
0305-8719/06/$15.00

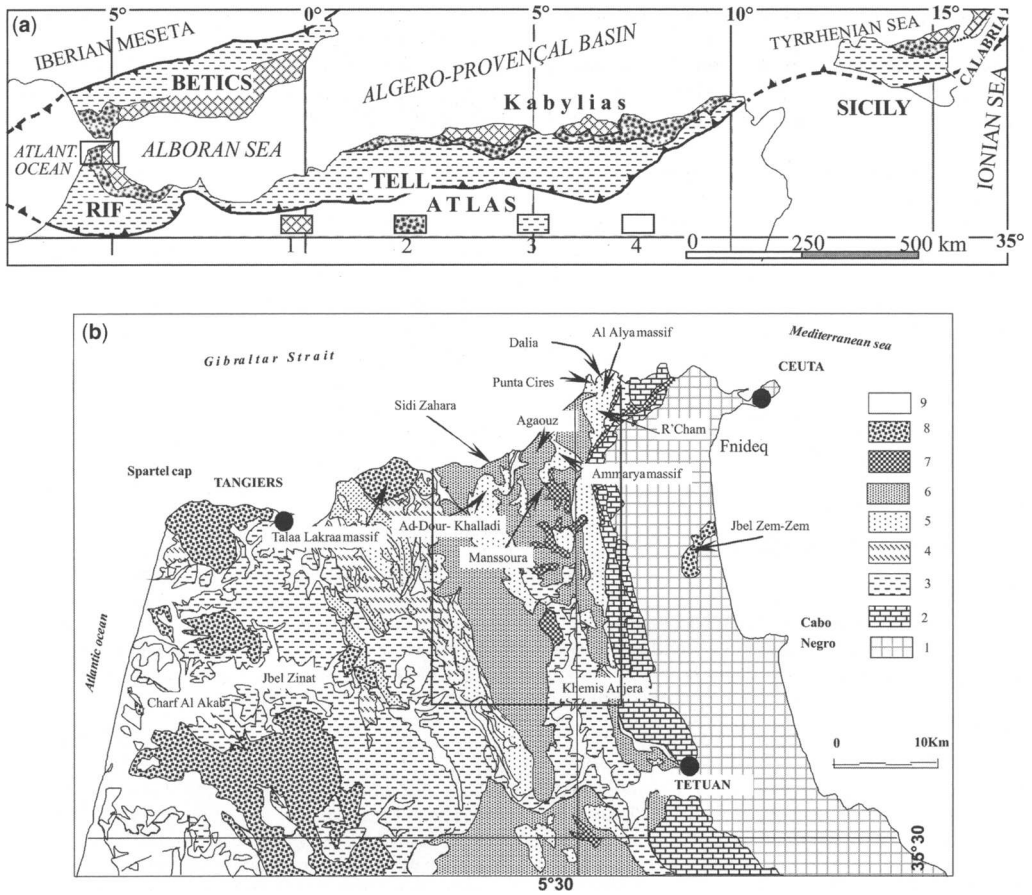

Fig. 1. Flysch nappes in the Western Mediterranean realm. (**a**) 1, Internal zones; 2, flysch nappes; 3, external zones; 4, foreland. Rectangle indicates location of northwestern Rif. (**b**) Structural map of the northwestern Rif chain. 1, Sebtide and Ghmaride units; 2, Calcareous chain; 3, Tangiers unit; 4, Massylian Melloussa nappe; 5, Mauretanian Tisirene nappe; 6, Mauretanian Béni Ider nappe; 7, Predorsalian unit; 8, Numidian nappe; 9, post-nappe formations. Outline indicates location of study area.

the AlKaPeCa microplate (Bouillin *et al.* 1986) located between Africa and Eurasia during the pre-paroxysmal history. The Flysch Trough, which extended between Sicily and the Gibraltar area, represented the deepest part of this palaeogeographical setting and could have an oceanic to transitional crust (Durand-Delga *et al.* 2000). Indeed, at the base of the flysch series, ophiolitic rocks may locally form the basement of late Jurassic–early Cretaceous pelagic strata (Michard *et al.* 1992; Durand-Delga *et al.* 2000), or may be embedded within preflysch units (Andrieux 1971; Durand-Delga *et al.* 2000).

At the scale of the Mediterranean area, although there is acceptance that the structure of the Betic–Maghrebian chain resulted from the Eurasia–AlKaPeCa–Africa triple convergence, the geodynamic mechanism still remains a matter of debate. It may have involved: (1) collision without subduction (Platt & Vissers 1989; Vissers *et al.* 1995; Turner *et al.* 1999); (2) collision with a single north-dipping subduction (Zeck 1996, 1997; Lonergan & White 1997); (3) collision with two successive subductions, namely a late Cretaceous–mid-Oligocene, south-dipping subduction (Alpine–Betic subduction) followed by a late Oligocene–early Miocene, north-dipping subduction (Apenninic–Maghrebian subduction; Chalouan *et al.* 2001; Chalouan & Michard 2004).

In this context, the siliciclastic flysch successions play a palaeogeographical and structural key role, as they bear the record of an oceanic domain that has entirely disappeared, and form the frontal part of an 'accretionary prism' that subsequently thrust the African and locally the Betic margins.

Recently, several sedimentological and stratigraphical studies have focused on the siliciclastic flysch successions, but the outcrop conditions and the complex nappe deformations allowed only scarce detailed structural analyses; for example, by Andrieux (1971) and Besson (1984) in the Moroccan central Rif, and by Lújan *et al.* (1999, 2000) Crespo-Blanc & Campos (2001) and Crespo-Blanc & Lújan (2002) in the Spanish 'Campo de Gibraltar'.

The main aim of this paper is to describe and decipher the deformation style, kinematics and timing of the Mauretanian nappe emplacement, in a structural key area of the central part of the Gibraltar arc (Fig. 1a). New insights are expected to be made into the Gibraltar arc genesis and the kinematics of the three plates involved during the paroxysmal history.

Geological setting of the Mauretanian nappe

Regionally, the Tisirene and Béni Ider nappes extend throughout the Betic–Maghrebian–Calabrian chain. The Tisirene nappe corresponds to the 'Flysch de Los Nogales' in the Spanish Campo de Gibraltar, the 'Flysch de Guerrouch' in the Algerian Kabylies, and the Sicilian 'Flysch del Monte Sorro' (Bouillin *et al.* 1970).

Stratigraphically, the late Jurassic–early Cretaceous Tisirene series and the Palaeogene–mid-Burdigalian Béni Ider series were grouped by Bouillin *et al.* (1970) and Raoult (1974) in a single stratigraphic column, based on field data from the Algerian Little Kabylia. In the Rif, the best field evidence for late Cretaceous transitional strata between the last Tisirene sandstone beds and the first Béni Ider Palaeogene turbidites comes from well-exposed coastal outcrops in the study area (Fig. 2). These strata consist of incompetent thin-bedded calciturbidites and red shales (similar strata were described by El Kadiri *et al.* (2003) in the Béni Ider area). They act as the large-scale detachment level that resulted in differentiating the Tisirene and the Béni Ider nappes. Other pelite-dominated incompetent strata occur in the Berriasian–Valanginian interval (the so-called 'preflysch'), just below the Hauterivian–Albian thick-bedded sandstones (sandstones A, Fig. 2) (see more detailed age data of Durand-Delga *et al.* 1999). In a similar way, they caused the general detachment of these sandstones from their Jurassic basement. In the study area, no Jurassic series are known, probably because they were completely buried below the nappe piles.

The Punta Cires massif, located in the easternmost part of the study area (Fig. 1b), displays the most complete Mauretanian series. Here, the Tisirene flysch shows its principal sandstone interval (*c.* 300–400 m, of late Aptian–mid-Albian age, Fig. 2b) preceded by the thin-bedded 'preflysch' episode (*c.* 100–150 m, Fig. 2a). Below the latter is a decametre-scale, sandstone–shale alternation (*c.* 200–300 m, of Barremian–Aptian *pro parte* age). We shall see below that these additional shaly intervals were responsible for second-order structures within the Tisirene slices and thrust–folds (Fig. 2).

Late Cretaceous calciturbidites overlying the last thick sandstone beds crop out along the R'Mel River and immediately west of the Nfihihya massif (southern prolongation of Punta Cires). They grade upwards to Palaeocene–early Oligocene, nummulite-rich calciturbidites (Fig. 2c), which are covered by mid-Oligocene–early Burdigalian, thick-bedded micaceous sandstones (Béni Ider Flysch *sensu stricto*, Fig. 2d). The latter consist of a near-homogeneous, marl–sandstone alternation that forms large friable terranes along the southern side of the Gibraltar Strait, between Oued R'Mel Playa, to the east, and the first Tangiers Numidian massifs to the west. Such a large-scale incompetent rheology strongly contrasts with that of the Tisirene sandstones in the high superstructural nappes.

South and west of this coastal band, emerge the Massylian quartzites (Melloussa nappe) and the Tangier pelites (Tangiers parautochthonous unit), respectively (Fig. 1b). The latter are overthrust by the Numidian-like Tala–Lakraa massif (i.e. the Spanish Bolonia Flysch) and by diverse true Numidian massifs (e.g. Tangiers, Dar Zhirou massifs).

South and east of the study area (Fig. 3) occurs a 15 km long, dextral strike-slip fault system (the so-called 'accident de Fahies', Kornprobst 1974; Zagloul 1994; El Fahssi 1999; El Mrihi 1995, 2005) that abruptly severs the kilometre-scale Béni Mzala anticline (involving Ghomaride and upper Sebtide units) and twists the northern end of the calcareous Haouz Chain. With respect to this latter point, the Mauretanian flysch nappe (Al Alya massif) underwent back-thrusting and a dextral lateral displacement along the Fahies fault of about 4 km (see below).

To decipher the main tectonic phases, we will focus on the internal deformation recorded within the principal Tisirene and Béni Ider allochthonous terranes. Their stacking pattern and relation to the surrounding orogenic nappe edifice is outlined.

Deformation chronology

The Mauretanian flysch successions commonly bear the record of a polyphase tectonic history. Cross-cutting relationships allow us to reconstruct six

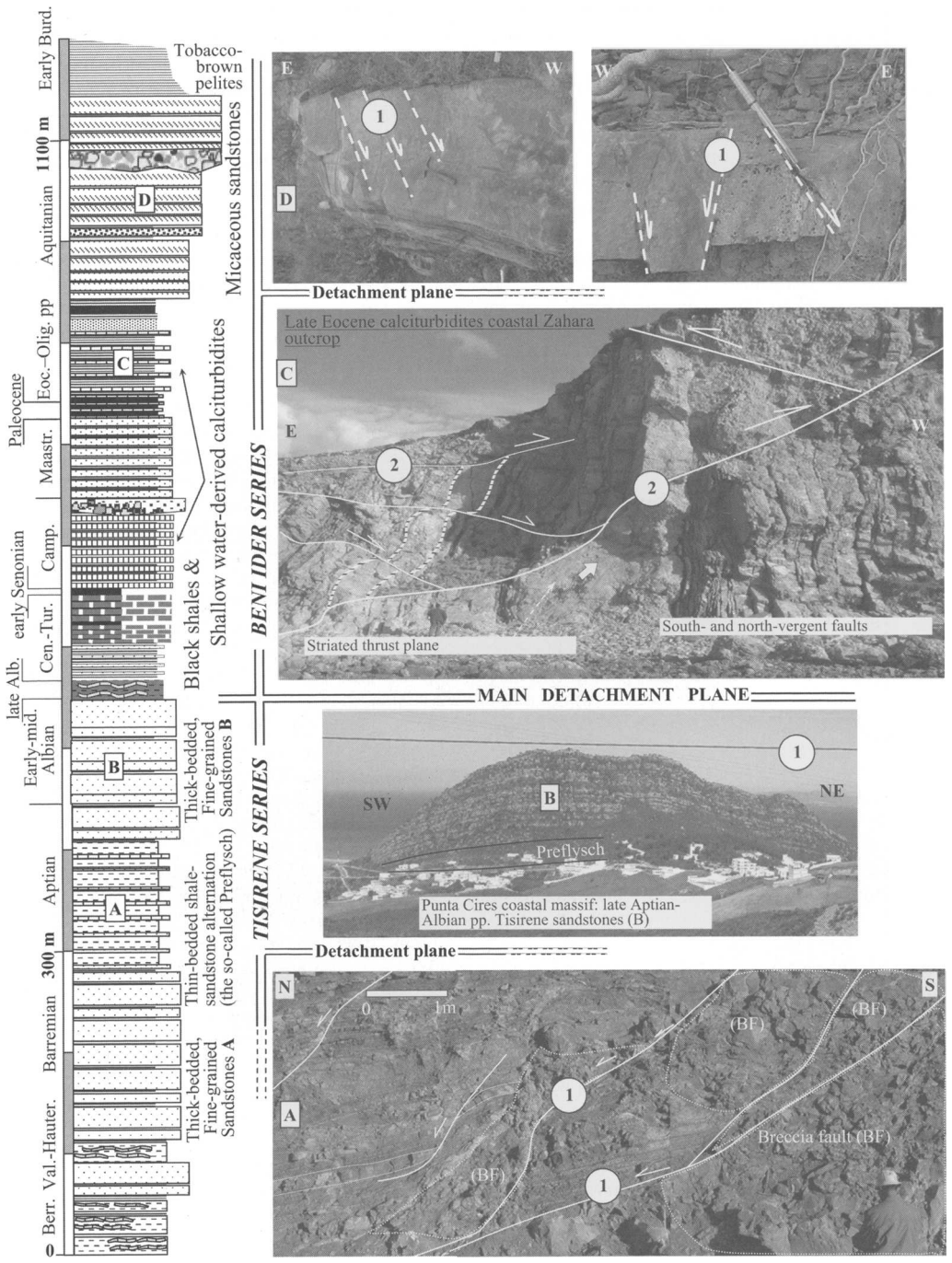

Fig. 2. Stratigraphic column of the Mauretanian series, i.e. the lower Cretaceous Tisirene succession and upper Cretaceous–Palaeogene Béni Ider succession. 1, Synsedimentary normal faults; 2, south-vergent thrust–faults. pp., *pro parte*.

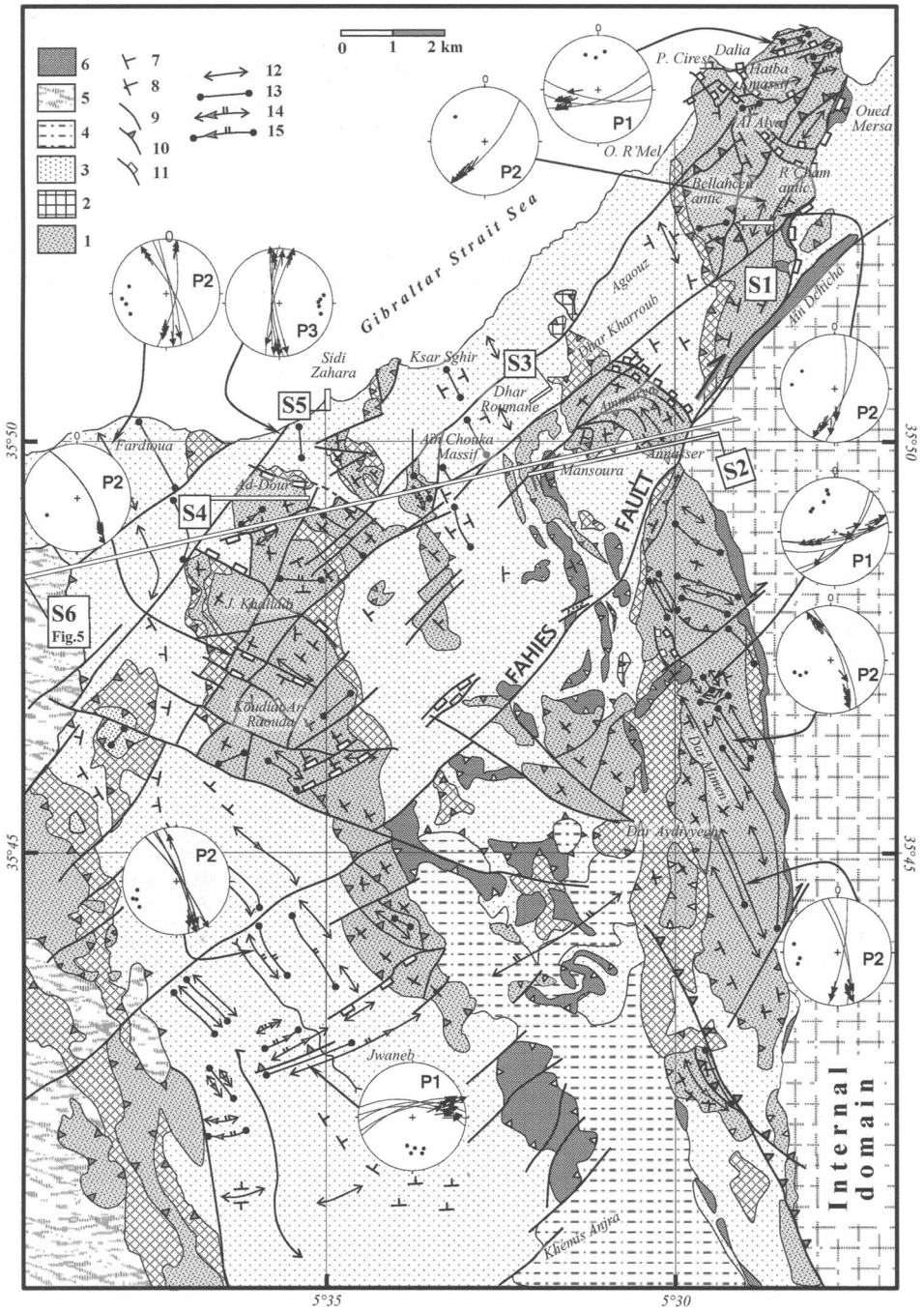

Fig. 3. Structural map of the studied Mauretanian nappes and stereogram projections of the main deformation phase-related folds (P1, south-vergent folds; P2, west-vergent folds; P3, east-vergent folds). 1, Tisirene nappe (early Cretaceous, fine-grained sandstone flysch); 2, basal slices of the Tisirene nappe (late Cretaceous calciturbidites); 3, Béni Ider nappe (late Oligocene–Aquitanian micaceous sandstones); 4, Tangiers Intrarif unit (late Cretaceous pelites); 5, Massylian nappe (Albian to late Cretaceous sandstones and shales); 6, Predorsalian nappe (late Oligocene–Aquitanian sandstones); 7, strike and dip of normal series; 8, strike and dip of overturned series; 9, strike-slip fault; 10, overthrust; 11, normal fault; 12, anticline; 13, syncline; 14, 15, west-plunging axis and/or north-vergent overfolds.

main phases, with the first being related to the pre-orogenic, synsedimentary evolution of the flysch basin, during early Cretaceous–Palaeogene times. The other phases occurred during the Miocene synorogenic history, and some of them appear to be directly linked to the nappe emplacement.

Synsedimentary tectonics

Synsedimentary tectonic features developed during the deposition of the Tisirene and the Béni Ider Flysch successions. They are centimetre- to decametre-scale normal faults, slump structures, structureless debris flows and olistostromes. From the stratigraphic base upward these structures occur as follows.

(1) Normal faults and slump structures occur with a high density in the first sandstone episode (Hauterivian–Barremian, Durand-Delga *et al.* 1999) of the Tisirene series (the most conspicuous examples can be found along the road crossing the northern flank of the Tisirene Hatba massif, in the eastern part of the study area, Fig. 2a).

(2) Centimetre- to metre-scale normal faults and mixed siliciclastic and carbonate debris flows occur near-systematically in the Cenomanian–Turonian calciturbidite and phthanitic strata. Decametre-scale faults generally cross the whole of these structures before being sealed by early Senonian pelites. Good examples are found in the Béni Mejmel Tisirene massif, west of the study area, and many others occur in the Béni Ider area along the Oued El Kebir River (El Kadiri *et al.* 2003).

(3) Olistostromes at various scales frequently occur in the early Senonian pelites. Metre- to decametre-scale boulders inherited from the underlying strata, including the Tisirene sandstones, are embedded within monotonous, lime-free green pelites.

(4) Large-scale olistostromes involving decametre- to hectometre-scale sedimentary klippes are the most common features of the latest Eocene–early Oligocene levels. They occurred just before the onset of the first siliciclastic deposits that suddenly interrupted the preceding long-lasting late Cretaceous–Eocene carbonate regime. Examples occur in the coastal Sidi Zahara outcrop (close to the village of Ksar Sghir) and further south in the Tamezzakht area (El Kadiri *et al.* 2004).

(5) Normal faults at various scales and coarse-grained debris flows are also common features in certain levels within the micaceous sandstone packages (Fig. 2c and d). In Aïn Chouka massif (overhanging Ksar Sghir village), debris flows rework boulders derived from the oldest chaotic breccias, as well as a mixture of magmatic, metamorphic and carbonate pebbles inherited from unknown basements (i.e. lost palaeogeographical domains).

These five successive synsedimentary stages denote tectonic events at the regional scale. They may be linked to either pure extensional phases or contraction-related gravitational collapses.

North-verging compressional phase

Tisirene nappe. Evidence for the first north–south-directed compressional tectonics preceding the paroxysmal phase comes from one of the two main Tisirene thrust sheets of the study area, the Alya-Dar Mimen massif, which is a north–south-oriented Tisirene band, 2–3 km wide and 20 km long. It bounds the Calcareous chain and extends from the Punta Cires–El Alya coastal massifs to the north, to Dar Mimen mount to the south (Fig. 3). The whole of this thrust sheet corresponds to a single normal series that, according to Durand-Delga *et al.* (1999), could stratigraphically pass up into Tertiary micaceous sandstones (Béni Ider nappe; see above). Evidence for a north-vergent compressional phase comes from two localities.

(1) In the northern part of Al Alya thrust sheet, well-exposed coastal outcrops between Dalia and Oued Marsa beaches display thick-bedded yellow sandstones and clayey intervals belonging to the sandy phase I of the Tisirene series (Hauterivian–Barremian *pro parte*). These strata show directions ranging from N60°E to 100°E, and are affected by decametre- to hectometre-scale folds, whose axis is N80°E to N100°E. North-vergent minor folds occur only close to the basal thrust plane. These structures are associated with reverse, south-dipping, N75°E–90°E-directed faults, and s–c structures indicating a north-vergent tectonic transport.

(2) In the Dar Mimen massif, detailed structural analysis reveals successive folds of metre- to decametre-scale. They are asymmetrical and directed east–west, and sometimes show a pronounced north-vergent overfolding. They are refolded by kilometre-scale NW–SE-directed west-vergent folds.

The second Tisirene sheet corresponds to small-scale klippes that occupy various structural positions, and may be formed of normal or reverse series. Generally, they are thrust over the Béni Ider nappe or locally, the Meloussa nappe, and display a complex internal deformation that prevents us from assessing the effect of this first north-vergent compressional phase.

Béni Ider nappe. The Béni Ider nappe crops out, in the northwestern Rif, as a large thrust sheet of about 20 km in width and 40 km in length. It is dominated by a normal series that may over thrust both the

Meloussa nappe and the Tangiers unit. The north–south compressional phase is here expressed by metre- to hectometre-scale east–west-directed folds that are generally upright or isoclinal. They are locally sheared, and may be overturned towards the south or the north. Good examples occur in several localities, particularly in Jwaneb village, west of Khemis Anjera. Here, well-delineated, decametre- to kilometre-scale transverse folds are visible both in the field and on the aerial photographs. They affect the Tertiary Béni Ider flysch, the thick sandstone body of which forms the NE and SW limbs of kilometre-scale, longitudinal folds. The latter structures are directed N120–150 and may be ascribed to a west-vergent phase (see below). The plunge axis of the transverse folds may have distinct directions (N10 to N100) and dip (0–60°, towards the NE or the SW) depending upon the position of these folds with respect to the longitudinal folds. Thus, the plunge of the axis of the transverse folds may be horizontal along the hinge line, whereas in the limbs it may dip steeply in various directions. In addition, the axial plane may dip steeply towards the south or SE, and even the north. This complex structure is due to the effect of longitudinal folds that subsequently refolded the transverse folds. The north-verging compressional phase seems to have a relatively moderate intensity and generated smaller folds and thrust structures, particularly along narrow shear bands.

*West-vergent compressional phase and Mauretanian nappe diverticulation**

The east–west compressional phase produced by far the most intense syncollisional deformations, which are responsible for the main architectural lines of the Rif belt. Submeridian longitudinal folds, thrusting and back-thrusting structures represent its principal signatures.

To illustrate this phase we describe the structure at three localities in the Tisirene nappe and one in the Béni Ider nappe.

Al Alya–Dar-Mimen massif. The common deformations here are decametre- to hectometre-scale upright, north–south and NW–SE folds with a more or less west-vergent overturning. They were probably formed during an incipient detachment stage of the whole of this Tisirene sheet.

Figure 4a, section S1 is a cross-section of two major decametre-scale anticlines located close to the road between Ain Dchicha and Oued R'Mel beach. The R'Cham anticline is a submeridian, N165°E-trending, decametre-scale knee fold, inclined towards the west. Asymmetric folds develop in its short limb, associated with west-vergent thrust planes. The Koudiet Belahcen anticline is a N30°E-directed, overturned west-vergent decametre-scale fold (Fig. 5f). It involves a pelite-dominated interval and exhibits, in its long and short limbs, west-vergent thrust planes with ESE–WNW-directed striae. This is an out-of-sequence thrust by virtue of which the internal R'Cham anticline is thrust onto the external Balahcen anticline. These west-vergent folds and thrust structures are disrupted by east-vergent reverse faults, and secondarily by late low-angle normal faults.

Dhar Kharroub–Ammarya massif. This entirely consists of reverse successions made up of the second sandstone body described by Durand-Delga *et al.* (1999, Barremian *pro parte*–Albian *pro parte*). These units are deformed in folds and in a package of hectometre- to kilometre-scale thrust sheets stacking in a superstructural position above the Béni Ider nappe (Fig. 4b, section S2 and Fig. 5e). In contrast, the latter shows a normal series affected by tight hectometre-scale folds with a submeridian axis. The mechanical contact between these two contrasting thrust sheets sharply truncates their respective structures. An additional illustration of this truncation is given in Fig. 4c, section S3 at a smaller scale.

Ad-Dour–Khalladi massif. This extends over a band 3–4 km wide and about 10 km long. Its steeply NE-dipping, thick-bedded Tisirene sandstones form conspicuous chevron lines that make this nappe the most attractive one in the study area. Field analyses reveal an unusual double structure both in the northern (Ad-Dour mount, Fig. 3 and Fig. 4d, section S4) and southern part (Koudiat Ar Raouda, Fig. 3) of this great massif. It results from the package of two unequal sheets: (1) an eastern higher, west-vergent sheet made up of an inverted series corresponding to the first sandstone body (Durand-Delga *et al.* 1999); (2) a less voluminous lower sheet, forming a N20°E syncline structure, also made up of an inverted series of the same sandstone facies (Fig. 4d, section S4 and Fig. 5a and c). This double structure lies above a sharp truncation contact upon both the Béni Ider and the Massylian nappes.

Béni Ider nappe. In the Béni Ider nappe, the west-vergent compressional phase is characterized by north–south-trending, upright or westward

*We follow the original definition of the '*diverticulation*' process as initially presented by Lugeon (1943) and subsequently emended by Foucault & Raoult (1995): '*Phenomenon through which a succession of sedimentary strata split up, along stratification planes, into two or several independent units that may secondarily stack in a nappe pile, resulting with the youngest strata in the lowermost position and the oldest strata uppermost*'.

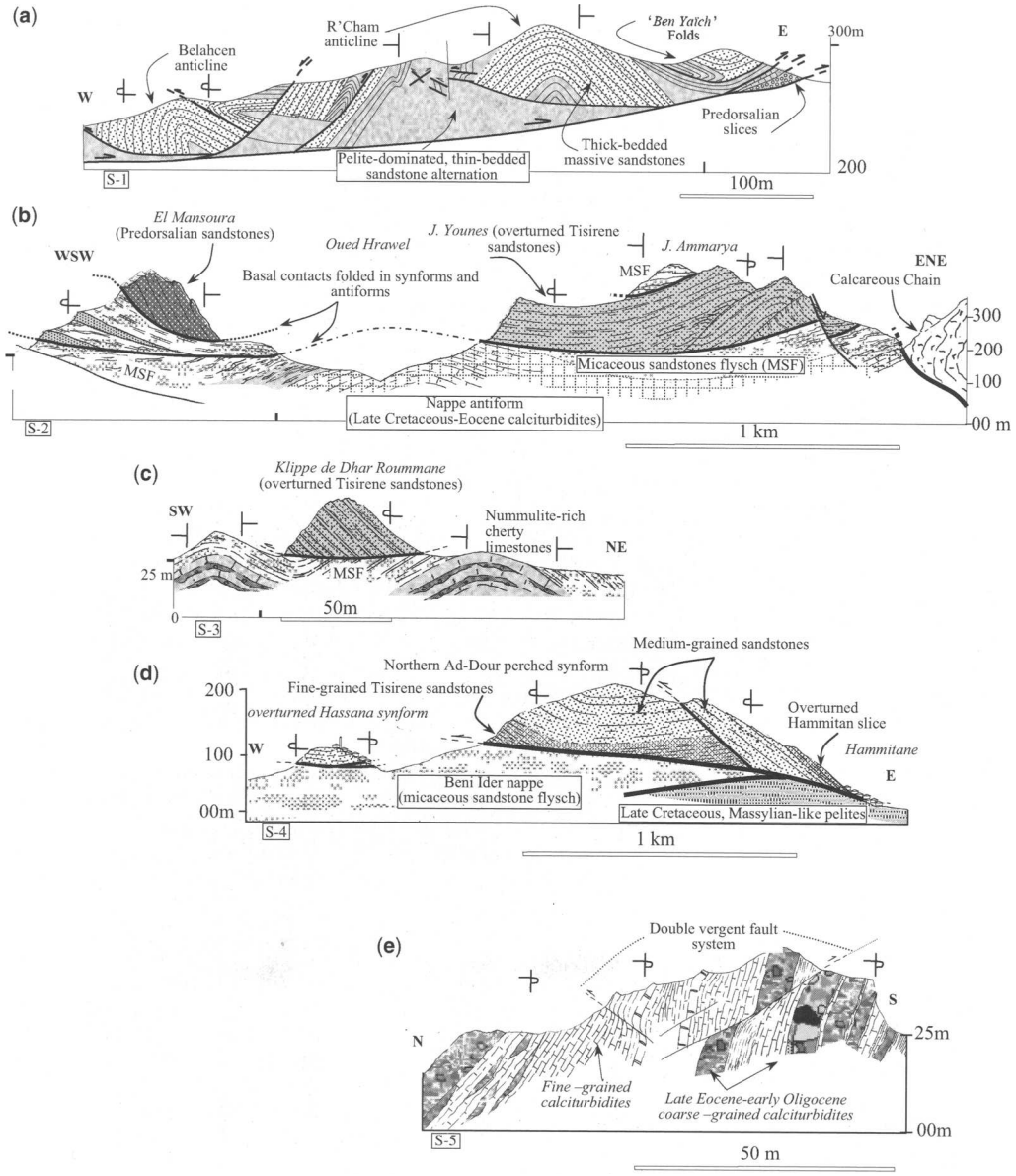

Fig. 4. Serial cross-sections S1–S5 taken at various scales from Tisirne and Béni Ider massifs. (**a**) Section S1: R'cham and Belahcen west-vergent folds, subsequently affected by east-vergent thrusts and late normal faults. (**b**) Section S2: overturned and refolded Tisirene slices, which were subsequently overthrust by Béni Ider nappe (J. Ammarya) and the Predorsalian (El Mansoura), and then affected by late normal faults. (**c**) Section S3: overturned Tisirene klippe (Dhar Roummane) overlapping the Béni Ider nappe through a sharp truncating basal contact. (**d**) Section S4: overturned and refolded Tisirene nappe, which has been overthrust by late Cretaceous and Tertiary Béni Ider nappes. (**e**) Section S5: Eocene–late Oligocene breccia and calciturbidites, which are overturned and affected by late south-vergent thrusts. The symbols indicate strike and dip of normal and overturned series.

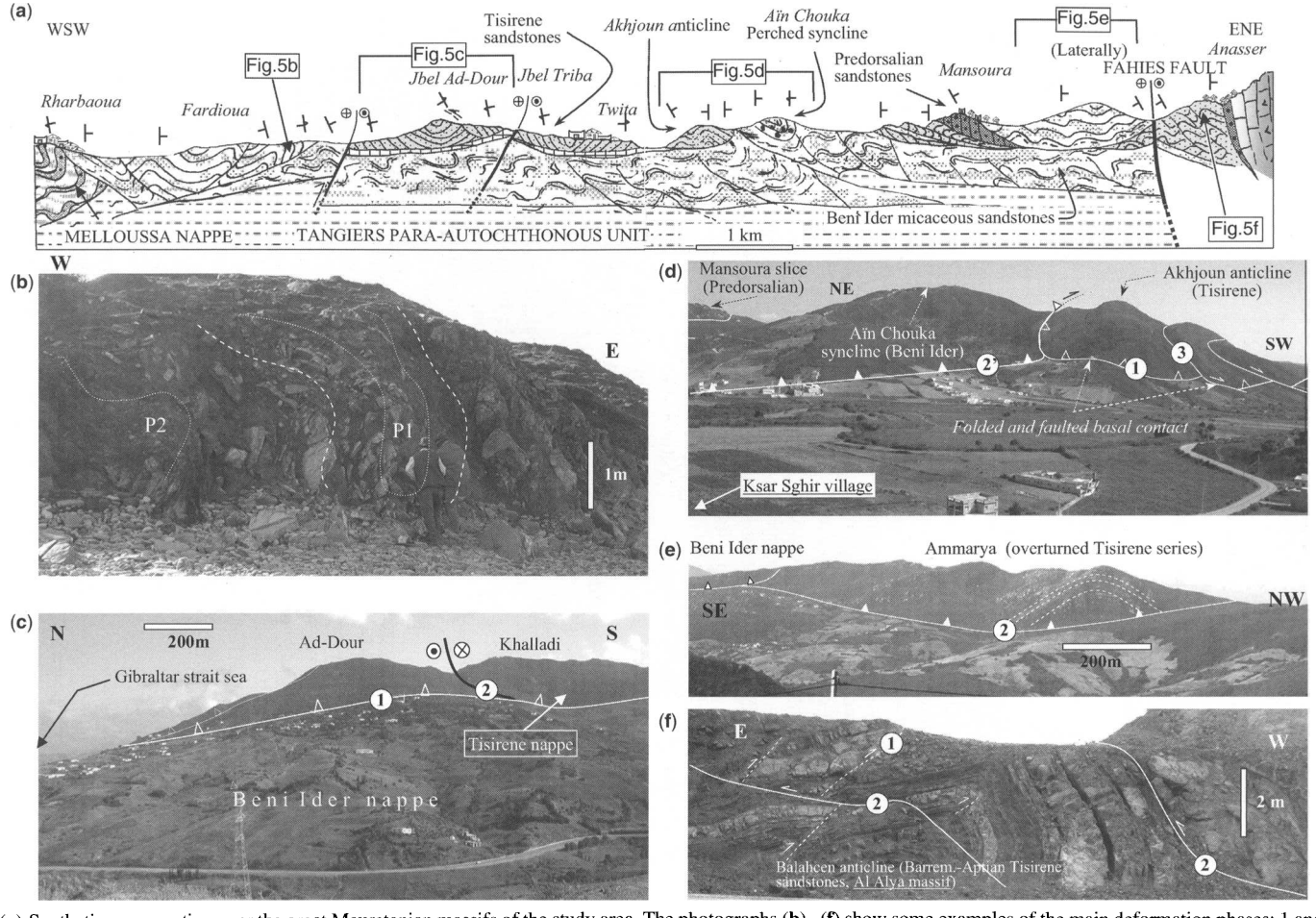

Fig. 5. (**a**) Synthetic cross-section over the great Mauretanian massifs of the study area. The photographs (**b**)–(**f**) show some examples of the main deformation phases: 1 and 2, west-vergent and east-vergent folds and thrusts, respectively; 2′, conjugate thrusts; 3, late normal faults.

overturned folds, refolding, in many places, former compressional north–south structures. These folds are of metre to kilometre scales (Fig. 5).

Between Ksar-es-Srhir and Oued R'Mel the structure consists of a great westward-inclined synclinorium with its subhorizontal axis directed N160–170°E (the Aïn Chouka syncline, Fig. 5a and d). In the limbs of this synclinorium there are hectometre-scale, west-vergent anticlines associated with east-dipping thrust planes. Thus, a fault-propagation–fold system can be deduced.

This deformation induced west-vergent folds and ramps before evolving into a general detachment of the Mauretanian Tertiary series (Fig. 5a).

The Tertiary Béni Ider nappe, made up of marls and incompetent micaceous sandstone successions, generally consists of north–south-overturned folds, which are associated with west-vergent reverse faults. It was subsequently thrust over the Massylian nappe (Melloussa nappe) and the Tangiers unit, which are dominated by early Cretaceous and late Cretaceous pelitic successions, respectively. These two units in turn form overturned folds with west-vergent thrusts. A sharp truncation contact separates them from the overriding Béni Ider nappe.

Such a structural setting strongly suggests that the whole Béni Ider sheet originated by a gravitationally driven large-scale detachment from its early Cretaceous Tisirene sandstone basement.

East-vergent compressional phase and the back-thrust processes

The preceding west-vergent thrusting was followed by a back-thrusting stage characterized by both an eastern vergence and a markedly increasing intensity towards the east (El Fahssi 1999; El Mrihi 2005). Thus, good examples of the latter phase may be seen in the easternmost part of the studied area, in the eastern flank of the Al Alya–Al Hatba massif (Fig. 3). In contrast to the external vergence of its western flank, its eastern one is made up of the east-vergent Tisirene–Predorsalian–Numidian nappe pile. The Predorsalian nappe may be trapped beneath the frontal contact of the internal zones, whereas the Numidian nappe dominantly occupies, more to the exterior, a superstructural position.

Field expressions of this back-thrusting phase are, among others: (1) fault planes of various size associated in some places with the east-oriented overlapping structures (Fig. 5a and b); they may be flat or slightly dipping towards the external domain, and striae along these faults are directed N70–120°E; (2) metre-scale reverse faults decapitating the hinges of the north–south anticlines, such as that clearly visible in the Belahcen anticline (Fig. 5b).

Generally, field evidence shows that the back-thrust movements in this sector were closely related to the dextral Fahies strike-slip fault, the effects of which extend southwards into the J. Mimen massif where the originally NW–SE-directed fold axis shifts from NNW–SSE to north–south.

South-vergent compressional phase

Various overturned folds associated with reverse north-dipping faults were observed in many places in the study area. The Sidi Zahara coastal outcrop (Fig. 2c and Fig. 4c, section S5) provides one of the clearest examples. It shows the extent to which a late south-vergent compressional phase can sometimes intensely rework pre-existing compressional structures. Signatures of this phase seem to have a patchy distribution in the study area, which makes it difficult to appraise its exact intensity.

Late orogenic deformations

Field evidence shows that an important part of the architectural features of the studied area was formed by late orogenic gravitational collapses, indicating a huge extensional phase. These collapses were likely to have started just after the piling up of the nappe edifice (i.e. the Tisirene–Béni Ider–Melloussa–Tangiers units) reached its culmination.

Also, this extensional phase seems to have a close relationship with the rifting phase of the Alboran Sea. It generated two types of normal faults.

(1) Large-scale, low-angle normal faults, which were responsible for gravitational slipping of tectonic scraps along planes slightly tilted towards the east. In the internal zones, the Intrarif-derived J. Zem Zem Numidian klippe and the Predorsalian-derived Fnidek sheet (both located between the cities of Tetuan and Ceuta, Fig. 1b) would be ascribed to this category (Chalouan *et al.* 1995).

(2) Longitudinal and transverse high-angle normal faults. The basin of Charf Al Akab, filled with post-nappe marine deposits of Tortonian–Messinian age (Medioni & Wernli 1978), would have opened as a consequence of these faults.

In the study area, these faults affected almost all the flanks of the enormous Tisirene–Béni Ider nappe piles. They were responsible for the majority of small-scale Tisirene klippes in low positions. In contrast to the Tisirene massifs, which are still preserved in their superstructural position, these klippes commonly show a dense normal-fault network.

Similar high- and low-angle faults were shown in seismic sections crossing the Alboran Sea (Chalouan *et al.* 1997). These may affect, at a large scale, the middle Miocene (Serravallian) and

Tortonian series, and could be coeval with those observed in the flysch nappes.

Deformation ages

In the Intrarif flysch domain, precise dating of the paroxysmal phases responsible for the emplacement of the Mauretanian nappes still remains a hard task, as marine sediments of the extended (Chalouan *et al.* 2001) mid-Miocene–Tortonian *pro parte* time interval are lacking. However, interesting approaches may be made based on some clues from regional data, particularly those from the Numidian nappe, which may be associated with datable structures.

(1) The marine regime almost synchronously ceased in the early mid-Burdigalian for all the flysch successions known in the Intrarif domain, a fact that strongly suggests compressional phases regionally starting as early as this age.

(2) Two interesting depocentres came into being in the external part of the Intrarif domain: the Béni Issef (western Rif, Feinberg 1986) and the J. Binet (eastern Rif, Wernli 1987) extensional satellite basins. Both are filled with siliciclastic and marly pelagic sequences of earliest Langhian (or even latest Burdigalian?)–Serravallian *pro parte* age (Leblanc 1975; Leblanc & Feinberg 1982; Feinberg 1986; Wernli 1987). Interestingly, the transgressive, coarse-grained conglomerates lying at the base of the Béni Issef sequence are dominated by Numidian-derived pebbles, which clearly denote that the Numidian nappe, and consequently the other flysch nappes, derived from the Flysch Trough, were already formed at the Burdigalian–Langhian transition. Likewise, these conglomerates seal the major thrust contacts between the overriding Tangiers units and the underlying parautochthonous Loukous unit. This give additional support for a mid- to late Burdigalian construction phase.

(3) More externally, in the northwesternmost part of the Rif, the Numidian nappe reaches its maximal extent and overthrusts the Habt unit (i.e. the detached Tertiary cover of the Intrarifian Tangiers unit), the stratigraphical top of which has been dated as Langhian (zone N8) by many workers (Ben Yaich 1991; Tejera de Leon 1993; Abdelkhalilki 1997).

These data show that the construction of the flysch nappe edifice began as early as the mid-Burdigalian and reached its orogenic culmination by the Serravallian (i.e. before the collapse of early Langhian satellite basins). Subsequently, the whole nappe edifice was the subject of large-scale tangential displacements that led to its frontal zone (the western Numidian nappes and the parautochthonous Tangiers unit) being emplaced over the most external part of the Intrarifian domain (after the Langhian, zone N8).

Discussion and scenario of nappe emplacement

Detailed examination of the tectonic deformation along the southern side of the Gibraltar Strait, mainly focused on Mauretanian material, has allowed us to reconstruct the chronology of the deformation that affected these series during both the pre- and synorogenic histories; that is, from the opening of an oceanic deep basin until its closure, and even during its existence as a chain of mountains.

From the palaeogeographical point of view, the flysch series of these nappes were deposited as early as the late Jurassic, partly upon an oceanic-type crust (Michard *et al.* 1992; Durand-Delga *et al.* 2000) in a deep and narrow basin, the so-called 'Flysch Trough'. The latter was produced during the well-documented palaeomargin-related Jurassic extensional phases (e.g. El Kadiri 1984, 1991; El Hatimi 1991; El Kadiri *et al.* 1992). During the early Cretaceous, this narrow basin was bounded by the two crustal transform faults that intermittently induced the drifting of the AlKaPeCa microplate with respect to the North African margin (Chalouan *et al.* 2001; Michard *et al.* 2002). Thus, the tectonic synsedimentary signatures recorded in the early Cretaceous Tisirene flysch may tentatively be assigned to this early drifting phase. As far as the tectonic instability phases during Cenomanian–Turonian, early Senonian and early Oligocene times are concerned, they may be regarded as indirect reverberations of the coeval global-scale plate-tectonic movements. Some of their direct regional causes have been deciphered and described by El Kadiri *et al.* (2003, 2004) and El Kadiri *et al.* (2006) as involving external isolated carbonate platforms. These platforms entirely disappeared, either through normal fracturing (late Cretaceous–Eocene) or drowning beneath the mid-Oligocene–Burdigalian thick siliciclastic packages.

The synorogenic history of the Mauretanian nappe formation occurred in four major compressional phases. The first, found in this area, was related to a submeridian shortening and generated a local north-vergent overlapping. The second compressional phase had an almost equatorial direction (east–west to ENE–WSW) and gave rise to overturned folds associated with overlapping and ramp structures of a pronounced western vergence. Evidence of these structures can be seen both in the flysch nappes and in the parautochthonous Tangiers unit, which represents the northern margin of the

African plate. This phase evolved into another compressional phase with the same orientation but that induced two causally linked processes: the dextral movement of the strike-slip faults of the Fahies system, and the related ENE-vergent back-thrust structures. The latest compressional phase was oriented NNW–SSE and resulted in south-vergent structures, mainly confined within narrow shear bands.

Two alternative interpretations may be proposed to explain the two near-perpendicular structures (ENE and NNW) recorded in the Mauretanian nappes: (1) a general tectonic compression, the structures of which locally experienced rotations, as emphasized by Crespo-Blanc & Campos (2001) and Platt *et al.* (2003) in the Betic Cordillera. In the Rif, this solution implies two rotation episodes, successively related to the north-vergent and the south-vergent compressional phases; (2) two real perpendicular compressions, one NNW–ESE and the other ENE–WSW.

Supporting the first alternative are palaeomagnetic data collected by many researchers that provide evidence of structure rotations occurring during the Neogene throughout the Gibraltar arc. The values of these rotations vary significantly across the internal and external zones. Thus, the internal Rif underwent an anticlockwise block rotation of 55° (Platzmann *et al.* 1993) to 76° (Feinberg *et al.* 1996), whereas the internal Betic counterparts underwent clockwise rotations of 20° (Platzmann *et al.* 1993) to 45° (Feinberg *et al.* 1996). In the external Rif, palaeomagnetic results by Platt *et al.* (2003) indicate rotations of at least 60°, particularly in its central and eastern parts. Platt *et al.* assumed that the first structures (folds and accretionary prism thrusts) were primarily generated during the Alboran–African plate convergence, and were directed N328, so that the N60–80 structures known east of the Jebha fault should be ascribed to the rotation processes.

In the study area, the dominantly N330-directed structures exclude rotation processes, which supports the second alternative mentioned above. Furthermore, the plate kinematics data from the Western Mediterranean realm give additional support to a twofold, north–south and east–west contractional regime: Dewey *et al.* (1989) and Platt *et al.* (2003) showed that: (1) the Iberian and African plates converged by 200–250 km in an overall NNW direction; the resulting shortening was chiefly accommodated by the Betic–Rif structures, and to a lesser extent by the Atlas chains (*c.* 30 km, Gomez *et al.* 2000); (2) the Alboran plate moved towards the WSW between Iberia and Africa by 250–300 km, a process that initially resulted in structures directed N328.

On the whole, the structural data described in this study lead us to propose the following scenario.

(1) The east–west compressional phase generated west-vergent folds and thrusts within the Flysch Trough and the Intrarif Tangiers and Ketama units (Andrieux 1971; Besson 1984). These three domains would have already been translated over the African margin as a consequence of the north-dipping Maghrebian subduction (Chalouan *et al.* 2001; Michard *et al.* 2002; Chalouan & Michard 2004) that acted between Africa and the Alboran plate from the late Oligocene in more eastern regions.

(2) This compression subsequently resulted in diverticulation processes within the Mauretanian nappes, precisely located within incompetent levels (see above). One of the main results is the high relief produced by the accretionary prism in the frontal zone between Africa and the Alboran plate. The diverticulation processes would have first used the late Cretaceous incompetent levels to almost completely detach the Béni Ider micaceous sandy interval as huge gravitational bodies. Later, the shortening produced west-vergent, overturned or recumbent folds, and led the preceding relief to culminate to the point where it triggered the gravitational expulsion of the freshly formed Tisirene piles. The best illustration of these events remains the basal truncation that sharply separates, as a general rule, two contrasting edifices: the superstructural, strongly deformed Tisirene massive sandstones from the underlying less deformed Béni Ider relatively incompetent sandstones.

(3) In the internal domain, a similar scenario may be envisaged for the 'Dorsale Calcaire'. Thus, early Burdigalian olistostromes progressively increased in scale during the early–mid-Burdigalian (El Kadiri *et al.* 2001; Hlila 2005), a phenomenon that culminated in stacking epiglyptic large-scale, massive carbonate slices. At the end of this paroxysmal, compressional east–west phase, the whole pre-structured 'Dorsale Calcaire' overlapped (in an out-of-sequence thrust regime) the flysch nappes and their parautochthonous units, through a basal truncation contact. The latter feature strongly recalls the preceding truncation separating the Tisirene and Béni Ider nappes.

(4) It seems that this tectonic reconstruction strongly recalls the out-of-sequence emplacement as stressed by Morley (1988) for the whole Rif belt. Nevertheless, at the scale of the whole Rif, a piggy-back thrust regime occurred, if we take into account that: (a) the nappe emplacement in the internal zones generally occurred during the late Oligocene (e.g. Ghomaride nappes, Chalouan, 1986) and the late Aquitanian (Sebtide emplacement,

Hlila, 2005); (b) the paroxysmal phase of the Flysch Trough occurred during the Mid-Burdigalian–Langhian *pro parte*; (c) the evolution of the Meso- and Pre-Rif domains lasted until the late Miocene (Wildi 1983; Feinberg 1986; Wernli 1987).

As a complement of these three successive events, it is noteworthy that the east–west back-thrusting phase, well marked in the study area, disappears further south in the Rif. In the Betic Cordillera, it develops only in the northern margin of the Gibraltar Strait. Therefore this phase appears to be primarily confined to the central part of the Betic–Rif arcuate segment.

Conclusions

The Rif flysch nappes, along the southern side of the Gibraltar Strait, have recorded a polyphase structural history, during which north–south and east–west shortening processes coexisted. These were respectively related to the Africa–Iberia and the Alboran plate–Africa convergences, respectively. The Africa–Iberia convergence appears to be mainly responsible for north- to NW-vergent thrusts in the Spanish 'Campo de Gibraltar' and the concomitant overthrusting of some Maghrebian Flysch nappes over the South Iberian margin (the so-called 'Flysch Hispanisation', Bourgois, 1978), whereas the Alboran drifting generated the west-vergent paroxysmal structures and large-scale diverticulations in the Rif segment of the Gibraltar arc. In the latter case, if an out-of-sequence structural stacking may be proposed for the emplacement of the Flysch Trough-derived nappes (intra-Rif domain), a piggy-back regime may also satisfactorily be invoked for the entire evolution of the Mesorif and Prerif domains.

Available age data, compiled from syn- and post-orogenic depocentre sequences, allow the paroxysmal phase responsible for the flysch nappe emplacement to be located within the Mid-Burdigalian–Langhian *pro parte* time interval.

The authors are grateful to reviewers A. Crespo-Blanc (University of Granada), F. Medina (University of Rabat) and C. Sanz de Galdeano (University of Granada) for their helpful remarks and suggestions. The authors are also indebted to SNED Office (Société Nationale d'Etudes du Détroit, Rabat) for providing financial support during the field trips.

References

ABDELKHALILKI, L. 1997. *Evolution tectono-sédimentaire des dépôts gravitaires dans le Prérif interne et l'unité du Habt (Rif externe occidental, Maroc): mise en place dans les bassins néogènes d'avant-fosse*. Diplôme Etudes Supérieures Thesis, Université. Mohammed V, Rabat.

ANDRIEUX, J. 1971. *La structure du Rif central. Etude des relations entre la tectonique de compression et les nappes de glissement dans un tronçon de la chaîne alpine*. Notes et Mémoires du Service Géologique du Maroc, **235**.

BEN YAÏCH, A. 1991. *Evolution tectono-sédimentaire du Rif externe centro-occidental (régions de M'Sila et Ouezzane, Maroc)*. Doctorat d'Etat Thesis, Université de Pau, France.

BESSON, F. 1984. *Etude géologique et structurale des nappes de flyschs et des zones externes dans la région de l'Oued Rhiss (Rif central)*. Doctorat d'Etat Thesis, Université de Paris.

BOUILLIN, J. P., DURAND-DELGA, M., GÉLARD, J. P., *ET AL.* 1970. Définition d'un flysch Massylien et d'un flysch Maurétanien au sein des flyschs allochtones de l'Algérie. *Comptes Rendus de l'Académie des Sciences*, **270**, 2249–2252.

BOUILLIN, J. P., DURAND-DELGA, M. & OLIVIER, PH. 1986. Betic–Rifian and Tyrrhenian arcs: distinctive features, genesis and development stages. *In*: WEZEL, F.-C. (ed.) *The Origin of the Arcs*. Elsevier, Amsterdam, 281–304.

BOURGOIS, J. 1978. *La transversale de Ronda. Cordillères Bétiques, Espagne. Données géologiques pour un modèle d'évolution de l'arc de Gibraltar*. Doctorat d'Etat Thesis, Université de Besançon.

CHALOUAN, A. 1986. *Les nappes Ghomarides (Rif septentrional, Maroc), un terrain varisque dans la chaîne Alpine*. Doctorat d'Etat Thesis, Université Louis Pasteur, Strasbourg.

CHALOUAN, A. & MICHARD, A. 2004. The Alpine Rif Belt (Morocco): a case of mountain building in a subduction–subduction–transform fault triple junction. *Pure and Applied Geophysics*, **161**, 489–519.

CHALOUAN, A., OUAZANI-TOUHAMI, A., MOUHIR, L., SAJI, R. & BENMAKHLOUF, M. 1995. Les failles normales à faible pendage du Rif interne (Maroc) et leur effet sur l'amincissement crustal du domaine d'Alboran. *Geogaceta*, **17**, 107–109.

CHALOUAN, A., SAJI, R., MICHARD, A. & BALLY, A. W. 1997. Neogene tectonic evolution of the southwestern Alboran basin as inferred from seismic data of Morocco. *AAPG Bulletin*, **81**, 1161–1184.

CHALOUAN, A., MICHARD, A., FEINBERG, H., MONTIGNY, R. & SADDIQI, O. 2001. The Rif mountains building (Morocco): a new tectonic scenario. *Bulletin de la Société Géologique de France*, **172**(5), 603–616.

CRESPO-BLANC, A. & CAMPOS, J. S. 2001. Structure and kinematics of the south Iberian paleomargin and its relationship with the Flysch Trough units: extensional tectonics within the Gibraltar arc fold-and-thrust belt (western Betics). *Journal of Structural Geology*, **23**, 10.

CRESPO-BLANC, A. & LÚJAN, M. 2002. Some considerations about the geometry of the boundaries between units of the south Iberian and Flysch Trough domains from commercial seismic profiles

and wells. *Revista de la Sociedad Geologica de España*, **15**(3–4), 193–200.

DEWEY, J. F., HELMAN, M. L., TURCO, E., HUTTON, D. W. H. & KNOTT, S. D. 1989. Kinematics of the western Mediterranean. *In*: COWARD, M. P., DIETRICH, D. & PARK, R. G. (eds) *Alpine Tectonics*. Geological Society, London, Special Publications, **45**, 265–284.

DURAND-DELGA, M. 1972. La courbure de Gibraltar, extrémité occidentale des chaînes alpines, unit l'Europe et l'Afrique. *Eclogae Geologicae Helveticae*, **65**, 267–278.

DURAND-DELGA, M., GARDIN, S. & OLIVIER, PH. 1999. Datation des Flyschs éocrétacés maurétaniens des Maghrébides: la formation du Jbel Tisirène. *Comptes Rendus de l'Académie des Sciences*, **328**, 701–709.

DURAND-DELGA, M., ROSSI, P., OLIVIER, P. & PUGLISI, D. 2000. Situation structurale et nature ophiolitique de roches basiques jurassiques associées aux flyschs maghrébins du Rif (Maroc) et de Sicile (Italie). *Comptes Rendus de l'Académie des Sciences*, **331**, 29–38.

EL FAHSSI, A. 1999. *Tectonique alpine, néotectonique et etude des formations marines quaternaires de la rive sud du détroit de Gibraltar entre Tanger et Sebta (Rif, Maroc)*. Thesis Diplôme Etudes Supérieures, Université Mohammed V, Rabat.

EL HATIMI, N. 1991. *Rifting mésozoïque sur la bordure occidentale du Rif interne (Maroc). Evolution géodynamique d'un secteur de la marge ouest-téthysienne. Exemples du Haouz et du Groupe du J. Moussa*. Doctorat d'Etat Thesis, Université de Pau.

EL KADIRI, KH. 1984. *Les radiolarites jurassiques des klippes de Chrafate (Rif septentrional, Maroc): stratigraphie, taxonomie*. Doctorat de 3ème cycle Thèse, Université de Pau.

EL KADIRI, KH. 1991. *La Dorsale Calcaire (Rif interne, Maroc): stratigraphie, sédimentologie et évolution géodynamique d'une marge alpine durant le Mésozoïque. Mise en évidence d'un modèle*. Doctorat d'Etat Thesis, Université de Tetuan.

EL KADIRI, KH., LINARES, A. & OLORIZ, F. 1992. *La Dorsale Calcaire rifaine (Maroc septentrional): évolution stratigraphique et géodynamique durant le Jurassique–Crétacé*. Notes et Mémoires du Service Géologique du Maroc, **336**, 217–265.

EL KADIRI, K., CHALOUAN, A., EL MRIHI, A., *ET AL.* 2001. Les formations sédimentaires olistolitiques de l'Oligocène supérieur–Miocène inférieur dans l'unité ghomaride des Béni Hozmar (secteur de Talembote, Rif septentrional, Maroc). *Eclogae Geologicae Helviticae*, **94**, 313–320.

EL KADIRI, KH., EL KADIRI, K. & RAHOUTI, A. 2003. Sédimentologie et ichnologie des calciturbidites du Crétacé supérieur–Oligocène inférieur de la série Maurétanienne (nappe des Béni Ider, Rif septentrional, Maroc): implications paléogéographiques. *Bulletin de l'Institut Scientifique de Rabat*, **25**, 73–91.

EL KADIRI, KH., SERRANO, F., HLILA, R., *ET AL.* 2004. Lithostratigraphy and sedimentology of the Latest Cretaceous–Early Burdigalian Tamezzakht Succession (Northern Rif, Morocco): consequences for its sequence stratigraphic interpretation. *Facies*, **25**, 477–503.

EL MRIHI, A. 1995. Structures alphines des zones extemes et des nappes de flysch à l'ouest de la chaîne du Haouz (Rif septentrional, Maroc). Theis Diplôme Etudes Supérieures, Université Mohammed V, Rabat.

EL MRIHI, A. 2005. *Structure et cinématique de mise en place des nappes de flyschs maurétaniens (Rif externe nord occidental): elaboration d'un modèle*. Doctorat d'Etat Thesis, Université de Tetuan.

FEINBERG, H. 1986. *Les séries tertiaires du Rif externe*. Notes et Mémoires du Service Géologique du Maroc, **315**.

FEINBERG, H., SADDIQI, O. & MICHARD, A. 1996. New constraints on the bending of the Gibraltar Arc from paleomagnetism of the Ronda peridotite (Betic Cordilleras, Spain). *In*: MORRIS, A. & TARLING, D. H. (eds). *Palaeomagnetism and Tectonics of the Mediterranean Region*. Geological Society of London, Special Publications, **105**, 43–52.

FOUCAULT, A. & RAOULT, J.-F. 1995. *Dictionnaire de Gíologie*. Dunod Paris.

GOMEZ, F., BEAUCHAMP, W. & BARAZANGI, M. 2000. Role of the Atlas mountains (northwest Africa) within the African–Eurasian plate-boundary zone. *Geology*, **28**, 775–778.

HLILA, R. 2005. *Evolution tectono-sédimentaire tertiare au front ouest du domaine d'Alboran (Ghomarides et Dorsale calcaire, Rif septentrional, Maroc)*. Doctorat d'Etat Thesis, Université de Tetuan.

KORNPROBST, J. 1974. *Contribution à l'étude pétrographique et structurale de la zone interne du Rif (Maroc septentrional)*. Notes et Mémoires du Service Géologique du Maroc, **251**.

LEBLANC, D. 1975. *Etude géologique dans le Rif oriental au Nord de Taza (Maroc)*. Doctorat d'Etat Thesis, Université de Toulouse, France.

LEBLANC, D. & FEINBERG, H. 1982. Nouvelles données stratigraphiques et structurales sur le Numidien du Rif oriental (Maroc). Implications géodinamiques. *Bulletin de la Société Géologique de France*, **24**(4), 861–865.

LONERGAN, L. & WHITE, N. 1997. Origin of the Betic–Rif mountain belt. *Tectonics*, **16**(3), 504–522.

LUGEON, M. 1943. Une nouvelle hypothèse tectonique: la diverticulation. *Bulletin de la Société Vaudoise des Sciences Naturelles*, **62**, 301–303.

LÚJAN, M., CRESPO-BLANC, A. & BALANYA, J. C. 1999. Structure and kinematics of the Aljibe unit, north of Cadiz Province (Flysch Trough complex, Betics). *Geogaceta*, **26**, 47–50.

LÚJAN, M. BALANYA, J. C. & CRESPO-BLANC, A. 2000. Contractional and extensional tectonics in flysch and Peribetic units (Gibraltar arc, SW Spain): new constraints on emplacement mechanisms. *Comptes Rendus de l'Académie des Sciences*, **330**, 631–638.

MEDIONI, R. & WERNLI, R. 1978. *Etude géologique du bassin post nappe Miopliocéne du Charf El Akab (Province de Tanger, Maroc)*. Notes et Mémoires du Service Géologique du Maroc, **40**(275), 107–133.

MICHARD, A., FEINBERG, H., EL-AZZAB, D., BOUYBAOUÈNE, M. & SADDIQI, O. 1992. A serpentinite ridge in a collisional paleomargin setting: the Beni-Malek massif, External Rif, Morocco. *Earth and Planetary Science Letters*, **113**, 435–442.

MICHARD, A., CHALOUAN, A., FEINBERG, H., GOFFÉ, B. & MONTIGNY, R. 2002. How does the alpine belt end between Spain and Morocco? *Bulletin de la Société Géologique de France*, **173**(1), 3–15.

MORLEY, C. K. 1988. The tectonic evolution of the Zoumi Sandstones, western Moroccan Rif. *Journal of the Geological Society, London*, **145**, 55–63.

PLATT, J. P. & VISSERS, R. L. M. 1989. Extensional collapse of thickened continental lithosphere: a working hypothesis for the Alboran sea and Gibraltar arc. *Geology*, **17**, 540–543.

PLATT, J. P., ALLERTON, S., KIRKER, C., MANDEVILLE, C., MAYFIELD, A., PLATZMAN, E. S. & RIMI, A. 2003. The ultimate arc: differential displacement, oroclinal bending, and vertical axis rotation in the External Betic–Rif arc. *Tectonics*, **22**(3), 1017.

PLATZMANN, E. S., PLATT, J. P. & OLIVIER, P. 1993. Paleomagnetic rotations and fault kinematics in the Rif Arc of Morocco. *Journal of the Geological Society, London*, **150**, 707–718.

RAOULT, J. F. 1974. *Géologie du centre de la Chaîne Numidique (nord du Constantinois, Algérie)*. Mémoires de la Société Géologique de France, **121**, 1–162.

TEJERA DE LEON, J. 1993. *Les bassins néogènes d'avant-pays du Rif externe occidental liés a la transformante Jebha–Arbaoua (Maroc)*. Doctorat d'Etat Thesis, Université Mohammed V, Rabat.

TURNER, S. P., PLATT J. P., GEORGE, R. M. M., KELLEY, S. P., PEARSON, D. G. & NOWELL, G. M. 1999. Magmatism associated with orogenic collapse of the Betic–Alboran Domain, SE Spain. *Journal of Petrology*, **40**, 1011–1036.

VISSERS, R. L. M., PLATT, J. P. & VAN DER VAL, D. 1995. Late orogenic extension of the Betic Cordillera and the Alboran Domain: a lithospheric view. *Tectonics*, **14**, 786–803.

WERNLI, R. 1987. *Micropaléontologie du Néogène post-nappes du Maroc septentrional et description systématique des foraminifères planctoniques*. Notes et Mémoires du Service Géologique du Maroc, **331**.

WILDI, W. 1983. La chaîne tello-rifaine (Algérie, Maroc, Tunisie): structure, stratigraphie et évolution du Trias au Miocène. *Revue de Géologie Dynamique et de Géographie Physique*, **24**(3), 201–297.

ZAGHLOUL, M. N. 1994. *Les unités Federico septentrionales (Rif interne, Maroc): inventaire des déformations et contexte géodynamique*. Thesis Diplôme Etudes Supérieures, Université Mohammed V, Rabat.

ZECK, H. P. 1996. Betic–Rif orogeny: subduction of Mesozoic Tethys lithosphere under eastward drifting Iberia, slab detachment shortly before 22 Ma and subsequent uplift and extensional tectonics. *Tectonophysics*, **254**, 1–116.

ZECK, H. P. 1997. Mantle peridotites outlining the Gibraltar arc-centrifugal extensional allochthons derived from the earlier Alpine, westward subducted nappe pile. *Tectonophysics*, **281**, 195–207.

Transgressive–regressive facies cycles in late Cretaceous calciturbidites from the Mauretanian Series, Béni Ider thrust sheet, northwestern External Rif, Morocco: application of the 'facies tract–facies sequence' concept

KH. EL KADIRI[1], K. EL KADIRI[2], A. CHALOUAN[3], A. BAHMAD[4], F. SALHI[5], H. LIEMLAHI[1] & R. HLILA[1]

[1]*Université Abdelmalik Essaadi, Faculté des Sciences, BP 2121, Dép. Géologie, M'Hannech II, 93003 Tetuan, Morocco (e-mail: khkadiri@fst.ac.ma)*

[2]*Université Abdelmalek Essaadi, Faculté des Sciences, BP 2121, Dép. Mathématiques, M'Hannech II, 93003 Tetuan, Morocco*

[3]*Université Mohammed V-Agdal, Faculté des Sciences, Av. Ibn Batouta, BP 1014, Dép. Géologie, Agdal, 10000 Rabat, Morocco*

[4]*Société Nationale d'Etudes du Détroit de Gibraltar (SNED), 31, r. Al Alaouyines, Rabat, Morocco*

[5]*Université Chouaib Doukali, Faculté des Sciences, Dép. Géologie, El Jadida, Morocco*

Abstract: Late Cretaceous mixed carbonate–siliciclastic, thin-bedded turbidites occur between the two great sandstone packages of the Mauretanian Series (the Tisirène and the Béni Ider sandstone flyschs, of early Cretaceous and late Oligocene–early Burdigalian age, respectively). The application of the facies tract–facies sequence model allows subdivision of the studied calciturbidites into five distinct facies sequences (FS.1–5), which equal five transgressive–regressive facies cycles. These cycles mainly consist of thinning upward calciturbidites, which almost all start with coarse-grained carbonate breccias, and passing upward into a shale-dominated interval. Fe-stained discontinuities, together with sedimentological and ichnological evidence, lead us to assign these two lithological components to a transgressive and a regressive trend, respectively. This result provides new insights into the sequence-stratigraphic interpretation of turbiditic successions.

Shallow-water-derived calciturbidites, which fringe carbonate platforms and pelagic seamounts, may record tectonic, eustatic and/or climatic events that occurred in the neighbouring source areas. In the Alpine and pre-Alpine realms where carbonate shelves and seamounts are often strongly deformed or have completely disappeared, calciturbidites have been used in palaeogeographical reconstructions for distinct periods, such as the Palaeozoic (Cook & Mullins 1983; Yose & Heller 1989), the Triassic (e.g. Masetti *et al.* 1989; Burchell *et al.* 1990), the Jurassic (Eberli 1987, 1988, 1991; El Kadiri 1991) and the Cretaceous (Haas 1999).

In the flysch domain (the so-called Intrarif), late Cretaceous–Eocene calciturbidites commonly occur as basal slices beneath the Béni Ider nappe. They were first studied by Thurow (1987), who presented a detailed stratigraphic description.

Following this interesting work, and taking into account the recent progress in understanding of turbidite depositional environments and their possible interpretation in terms of sequence stratigraphy (e.g. recent synthesis by Mutti 1992; Shanmugam 2000; Stow & Mayall 2000), it is relevant to characterize successive turbidite intervals according to the parent flow–facies tract scheme of Mutti (1992), and to indicate their possible sequence-stratigraphic significance (see Fig. 1).

Conceptual basis

Three main criteria were used by Mutti (1992) to define turbidite systems (TSs): (1) mappable sedimentary packages (depositional component), which may be ranked within the fourth–fifth or even within the second–third time-orders depending upon the sedimentation rate (according to the hierarchical classification of turbidites by Mutti & Normark (1987) and Mutti (1992)); (2) the same source of turbidite material (erosional component); (3) intercalation of shaly intervals, which punctuate

From: MORATTI, G. & CHALOUAN, A. (eds) 2006. *Tectonics of the Western Mediterranean and North Africa.* Geological Society, London, Special Publications, **262**, 177–192.
0305-8719/06/$15.00

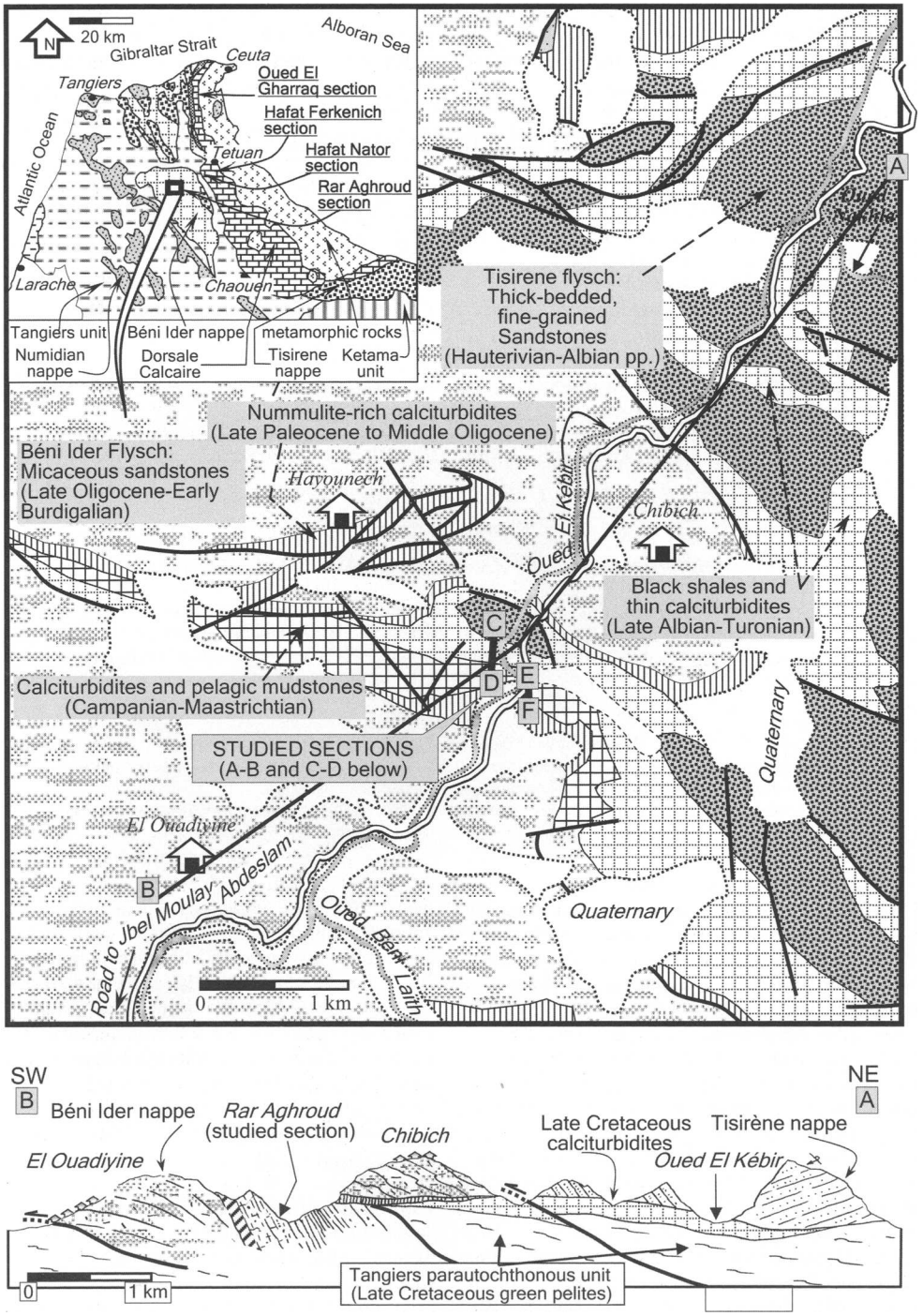

Fig. 1. Location map and structural setting of the studied Rar Aghroud section (map slightly modified from Didon 2006). It should be noted that almost all the Late Cretaceous–Eocene calciturbidite strata are involved as tectonic slices below the Tisirène nappe, which caused their intense deformation. The Rar Agroud sequence is here preserved at the stratigraphic base of the Béni Ider unit and was less strongly deformed than that unit. pp. *pro parte*.

the main turbidite events. Internally, a TS may show hierarchical stratal clustering, that is, turbidite stages (TSGs) that resemble the stratigraphic architecture of the TS at a smaller scale, as well as turbidite substages (TSSGs) showing a high-frequency turbidite structure throughout a TSG. The lateral expression of genetically related TSSGs corresponds to the classical 'turbidite facies association' of Mutti & Ricci Lucchi (1975), whereas the vertical expression of the latter is termed the facies sequence (Mutti 1992).

Both TSs and TSGs, may be found within studied successions. They exhibit several mappable gravity-flow packages averaging 20–40 m in thickness and separated by 3–5 m thick, shale-dominated intervals. Furthermore, these packages have distinct petrographical compositions and most of them contain coarse breccias at their base (see below). Moreover, the latter seem to pinpoint changes affecting the source area.

The petrographical changes across the main breccia level(s) (see statistical analysis, El Kadiri *et al.* 2006*a*, *b*) allow comparison of this stacking pattern with the schemes proposed by Mutti & Normark (1987, 1991) and Mutti (1992) based upon downslope grain-segregation processes within a parent flow, which results in the differentiation of facies tracts. These facies tracts may be detached or attached depending upon the extent to which detachment levels are activated between significant grain divisions (Fig. 2).

In the case studied here, detached facies tracts made up of basal divisions (highly efficient flows, Amy *et al.* 2000) and/or attached facies tracts are preserved in the lower part of each gravity-flow package distinguished in the Rar Aghroud section (Figs 3 and 4; the latter shows a direct image of the textural composition of the pre-detached parent flow). In contrast, facies tracts with the basal division missing characterize its upper part (poorly efficient flows, Amy *et al.* 2000).

However, the sedimentation rate seems to us too low to allow subdivision of the section studied into several decametre-scale, fining-upward FSs. For convenience, we consider here an FS as resulting from a special type of parent flow (i.e. of the same textural composition as the successive facies tracts) regardless of the number of backstepping, fining-upward, successive facies tracts (Fig. 2). This simplification is supported by the fact that the backstepping–thinning-upward trend occurs only once throughout each main gravity-flow package bounded by two pelitic intervals. For this reason, FSs of Figures 3 and 4 are elevated to the TSG level according to the hierarchical classification of the turbidite packages by Mutti & Normark (1987). Thus redefined, an FS may account for the change in textural composition of the material delivered from the source area in response to eustatic and/or tectonic controls.

Five main types of attached facies tracts are recognized throughout the late Cretaceous Rar Aghroud succession (Figs 3 and 4). We shall see below that they may be correlated with the second-order (3–50 Ma) transgressive–regressive facies cycles defined by Vail *et al.* (1991) and Jacquin & de Graciansky (1998).

Description of the transgressive–regressive facies cycles of the Béni Ider calciturbidites

To focus the final discussion on the sequence-stratigraphic interpretation, we will advance some well-documented sedimentological interpretations together with facies description. Five main transgressive–regressive facies cycles (referred to as T/RFC.1 to 5, according to Jacquin & de Graciansky 1998) can be distinguished throughout the Cenomanian–Maastrichtian interval (Figs 3 and 4). They are preceded by a late Albian cycle, which should be ascribed to the underlying Tisirène turbidite complex (in the sense of Mutti & Normark 1987, 1991; cycle not considered below).

T/RFC.1 (=facies sequence FS.1, Cenomanian–early Senonian; 20 m)

This cycle starts with the first true calciturbidites overlying the latest Albian pelagic mudstone–shale alternation (breccias Br.1, Fig. 3). The majority of beds display attached facies tracts (Fig. 5, FS.1). In the basal breccias, ubiquitous glaucony (rounded grains) and pyrite aggregates are noteworthy. The latter may independently occur as inner filling or coating within algae, bivalves, echinoderms, large Foraminifera and debris of siliceous-sponge reefs, which indicates iron redistribution during early diagenesis under anoxic conditions. Glaucony is well known to originate on shallow-water shelves before being reworked together with bioclastic sands (Baum & Vail 1988; Loutit *et al.* 1988; Hesselbo & Huggett 2001; Savrda *et al.* 2001*b*). In many cases the basal breccia division passes upward into a biosiliceous division exclusively made up of spicule- and bone-like sponge fragments, which in turn grades upward into a radiolarian-rich division. In both siliceous divisions, a mudstone matrix is generally present, but if not, biosiliceous material becomes contiguous and transforms into structureless quartzite, i.e. the so-called cherty limestones in field geology.

The major components of these facies tracts originated in distinct parts of the source area. Siliceous sponges are known to develop on

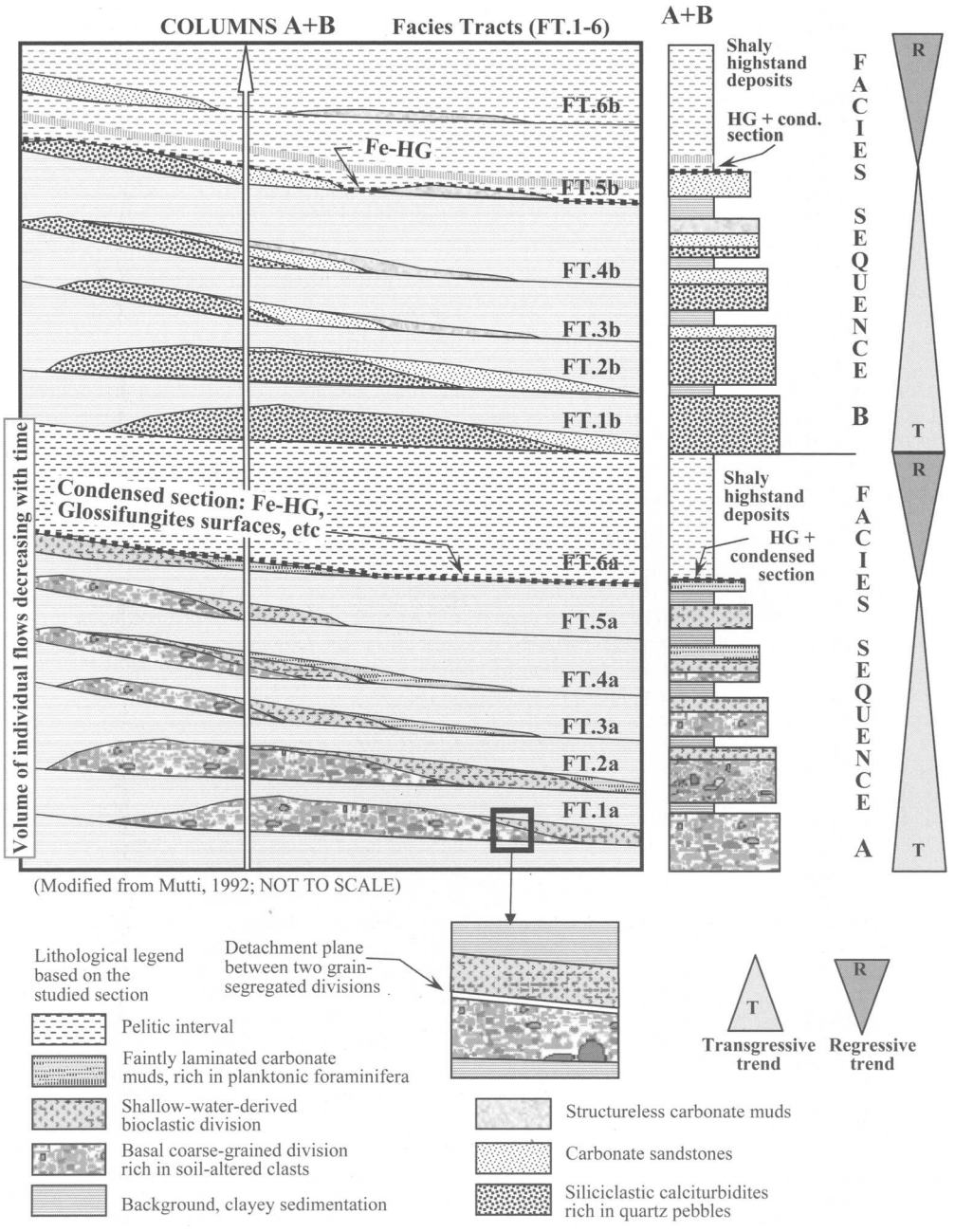

Fig. 2. Idealized model of the facies tract–facies sequence concept (modified from Mutti 1992) showing vertical stacking of two backstepping calciturbidite packages (column A + B). It should be noted that: (1) each of the latter packages ends with a simple or composite Fe-stained hardground or firmground surface (e.g. *Glossifungites* surfaces) representing the condensed section; (2) highstand deposits develop generally as mud-dominated intervals. Detachment of a facies tract (FT) may occur when the distance travelled favours downslope grain-segregation processes to 'mature' original parent flows in the form of vertically stacked grain divisions. Maturation (and subsequent detachment) also depends on the initial volume of parent flows delivered from source areas, which in turn is controlled by eustasy and/or tectonics.

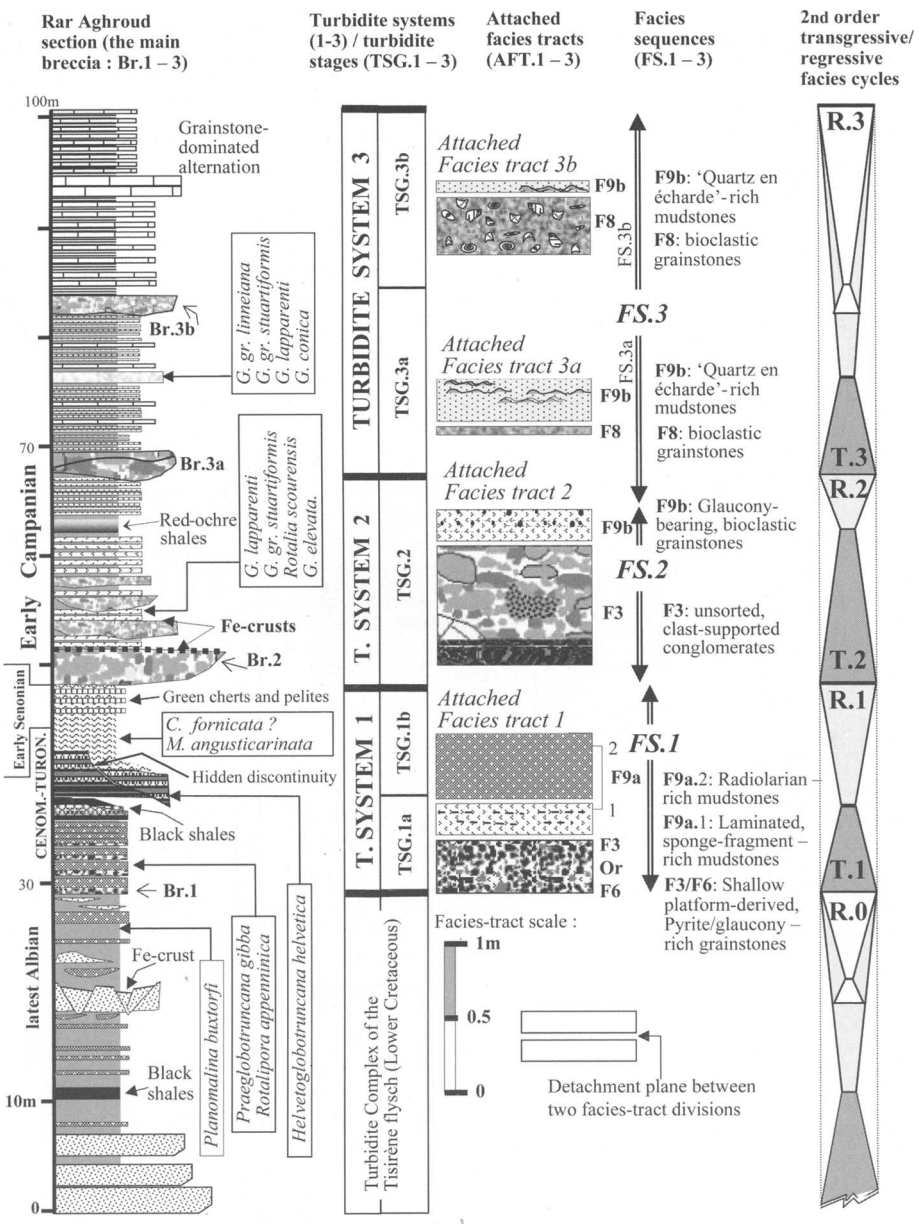

Fig. 3. Facies and sequence-stratigraphic interpretation of the Rar Aghroud section. Successive parent-flow-derived facies tracts relate to stratigraphic intervals that may correspond to both a transgressive–regressive facies cycle and a turbidite system. Because of the relatively small thickness of sedimentation, the time-order of turbidite system, turbidite stage (TSG) and facies sequence units does not correspond to that proposed by Mutti (1992) for the thick turbidite successions (details in text).

relatively hard substrates, in shallow waters between the fair-weather wave base and the storm wave base (Clarkson 1993), to 200–250 m depth (e.g. Whitney *et al.* 2005), whereas radiolarian oozes commonly accumulate up slope below the upwelling zones. Despite the spicules and radiolarians being mixed in the parent turbidite flow, downslope grain-interaction processes forced separation of these bioclast-types through differential hydrodynamic behaviour during the late stage of transport. The resulting detachment

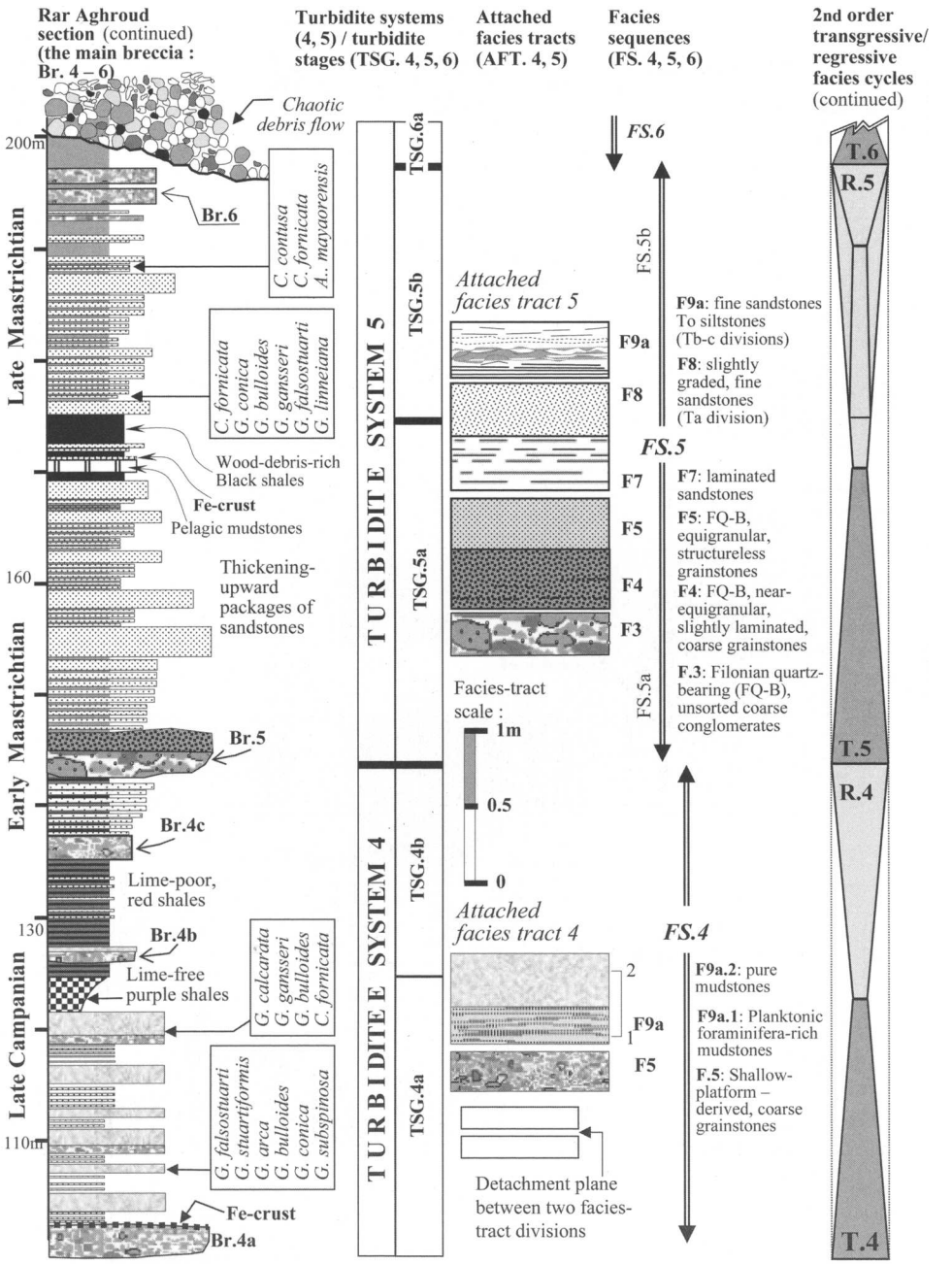

planes, and hence beds, may give a false stratigraphic appearance of distinct episodes of deposition independently involving bioclastic grainstones, spiculites and cherty horizons. In Campanian T/RF cycles, turbidite flows show similar mixtures, although with foraminiferans instead of radiolarians (see below).

A conspicuous black shale interval could represent the transgressive peak of this cycle (*c.* 80–150 cm, Cenomanian–Turonian transition in age, Fig. 5). It consists of centimetre- to decimetre-scale, structureless black mudstones and shales. The former may be accompanied by the basal bioclastic

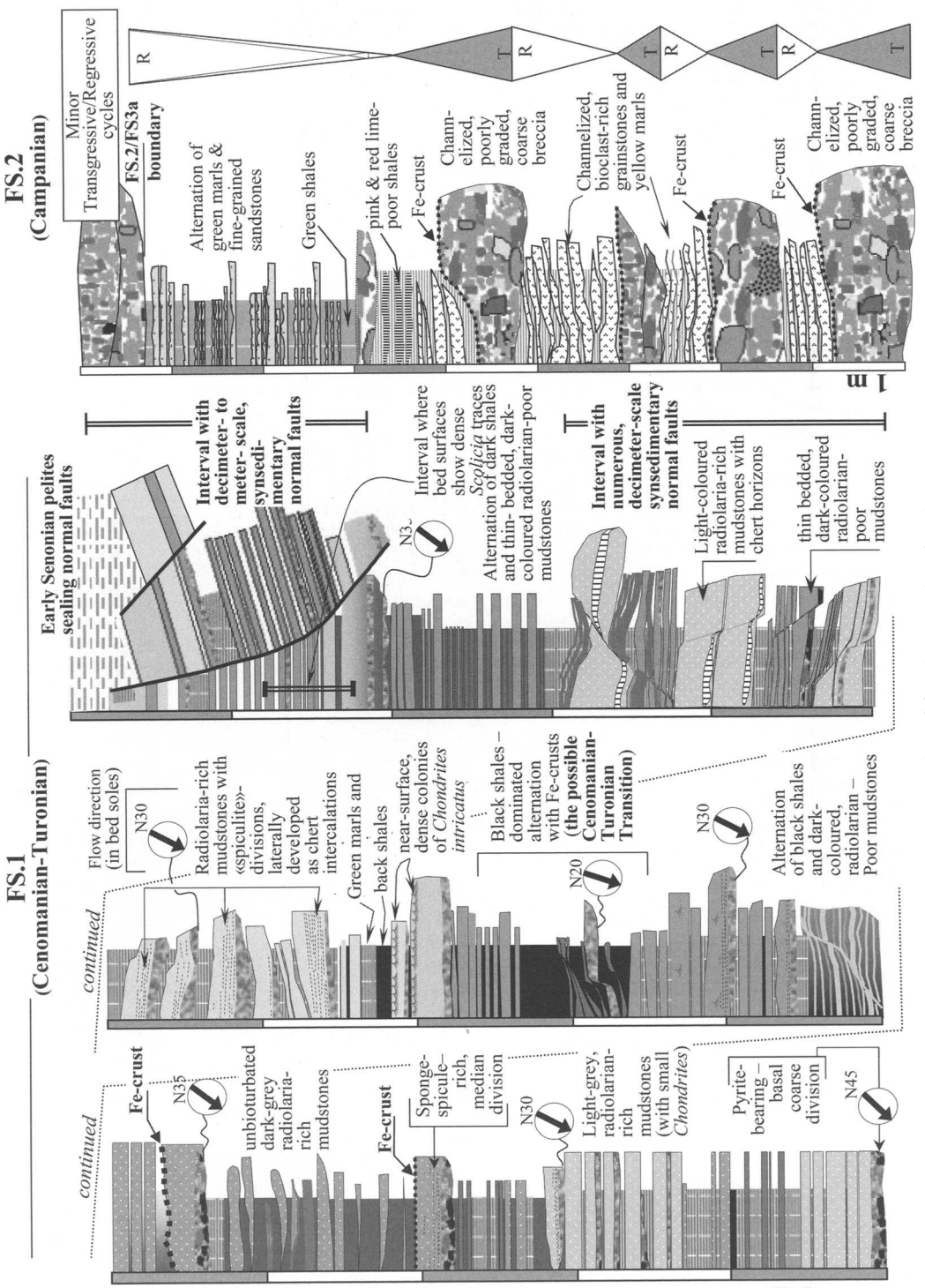

Fig. 5. Selected bed-by-bed lithological columns for facies sequences FS.1–FS.2 in the Rar Aghroud section. Facies are plotted as in Figure 3 (further details are shown in Fig. 7).

grainstones, but the preceding sponge-fragment and radiolarian-rich divisions are replaced by carbonate muds of unknown origin. The temporary disappearance of the biosiliceous signal may be a consequence of environmental stresses (i.e. platform drowning and sluggish ocean circulation), which commonly accompany large flooding episodes (e.g. Hallam & Wignall 1999). This interval displays successive omission surfaces and iron-stained hardgrounds, which could be the expression of superimposed condensed sections (Jacquin & de Graciansky 1998, p. 35). The regressive trend starts with recurrence of grey biosiliceous flows together with persisting dark-coloured carbonate muds over a 50 cm thick interval. Some successive top beds (2–5) of the grey biosiliceous flow contain numerous *Scolicia* (Fig. 6c) and dense colonies of *Chondrites intricatus* in near-surface position (Fig. 6b) as well as small *Zoophycos*. However, no *Ichnia* is observed in the black mudstones. This ichnological signature strongly suggests oxygen-related cyclicity that is likely to have a relationship with relative eustatic changes (compiled data by El Kadiri 2002*a*; El Kadiri *et al.* 2005). However, the cyclicity pattern seems to us too complex to be interpreted in terms of minor T/R cycles.

Lime-poor green pelites, which are often intercalated between mudstone beds, suddenly become dominant over a 4 m thick interval (early Senonian, Fig. 3). Thin, pyrite-bearing sandstone beds are intercalated throughout the lower 2 m, and they are replaced by thin-bedded green cherts in the upper half. Overall, this pelite-dominated interval typically points to a regressive trend, which is known to force widespread fine clastic input from continental mud plumes (e.g. Eschard 2001; Savrda *et al.* 2001*a*). Short transgressive pulses resulting in clean grainstones–sands couplets punctuate it.

T/RFC.2 (= facies sequence FS.2, early Campanian; 20 m)

This cycle starts with thick-bedded coarse grain flows (Br.2 in Fig. 3) corresponding to the facies F3 of Mutti (1992). They erode the underlying early Senonian cherty green pelites, from which they rip up numerous green-chert clasts. Of particular interest are decimetre-scale yellow sandstones blocks reworked from the underlying early Cretaceous Tisirene strata. Both elements will not reappear in breccia flows of overlying cycles.

Almost all calciturbidite flows of this cycle are discontinuous and thinning upwards (Fig. 5, column FS.2). They are capped with bioclastic, glauconybearing grainstones. Such a bioclast–glaucony mixture typically points to a transgressive trend (Baum & Vail 1988; Loutit *et al.* 1988; Galloway 1989; Vail *et al.* 1991; Ghibaudo *et al.* 1996; Robaszynski *et al.* 1998; Hesselbo & Huggett 2001; Savrda *et al.* 2001*b*). The top of the grainstone-capping breccia beds displays patches of ferruginous coating (Type I crusts of Nieto Albert 1996) that recalls the polygenic omission surfaces (POS) defined by Clari *et al.* (1995). The absence of Fe-coating on top of the pure grain-supported breccias (grainstone division–detached breccias) may be explained in terms of the existing relationship between Fe-encrusting processes and lithology of the host rock (El Kadiri 2002*a*). Simple omission surfaces (SOS; i.e. not reaching the Fe-coating stage described above) are rather common on grainstone beds. When the upper part of these grainstones displays a mudstone division, large *Chondrites* delineated by glaucony coating and spaced galleries of *Arenicolites* occur in epichnial position (Fig. 6a), whereas small *Zoophycos* may be present in endichnial position (Fig. 6h). All these bed surfaces recall flooding-related omission surfaces of various orders that are common in the condensed section and could, otherwise, bound smaller-scale parasequences (van Wagoner *et al.* 1988).

Lime-free pink to ochre–red shales (*c.* 0.5 m) overlie these breccia-dominated flows. They indicate the transgressive peak, which commonly results in shallowing of the calcite compensation depth (CCD), and relative sediment starvation through diminishing carbonate productivity of both benthic and planktonic groups (Haq 1991, 1993; El Kadiri 2002*a*).

These considerations seem to us consistent with the facies change observed in the middle part of FS.2 (Fig. 5). The colour change from pink or ochre–red shales to green ones is paired with both abrupt increase in quartz input and strong decrease in bioclasts, which may result from narrowing shelves forcing lower shallow-water productivity. This facies change clearly indicates an important regressive trend following the transgressive peak (i.e. lime-free ochre–red shale).

T/RFC.3 (= facies sequence FS.3, Campanian pro parte*, 30 m)*

This cycle starts with two 50–60 cm thick, discontinuous breccias (Br.3a). Beds resulting from attached facies tracts consist of two main divisions; namely, the bioclast-bearing grainstones (i.e. Mutti's F8 facies) followed by quartz-rich mudstones (i.e. F9b facies). This cycle comprises two sub-facies sequences with the first one (10 m) being dominated by thin-bedded sandstones, and the second (20 m) by normally graded grainstones (Fig. 7; both of these are shown in column FS.3). An intercalated, 60 cm thick, coarse-grained breccia (Br.3b) between these sequences supports their distinction.

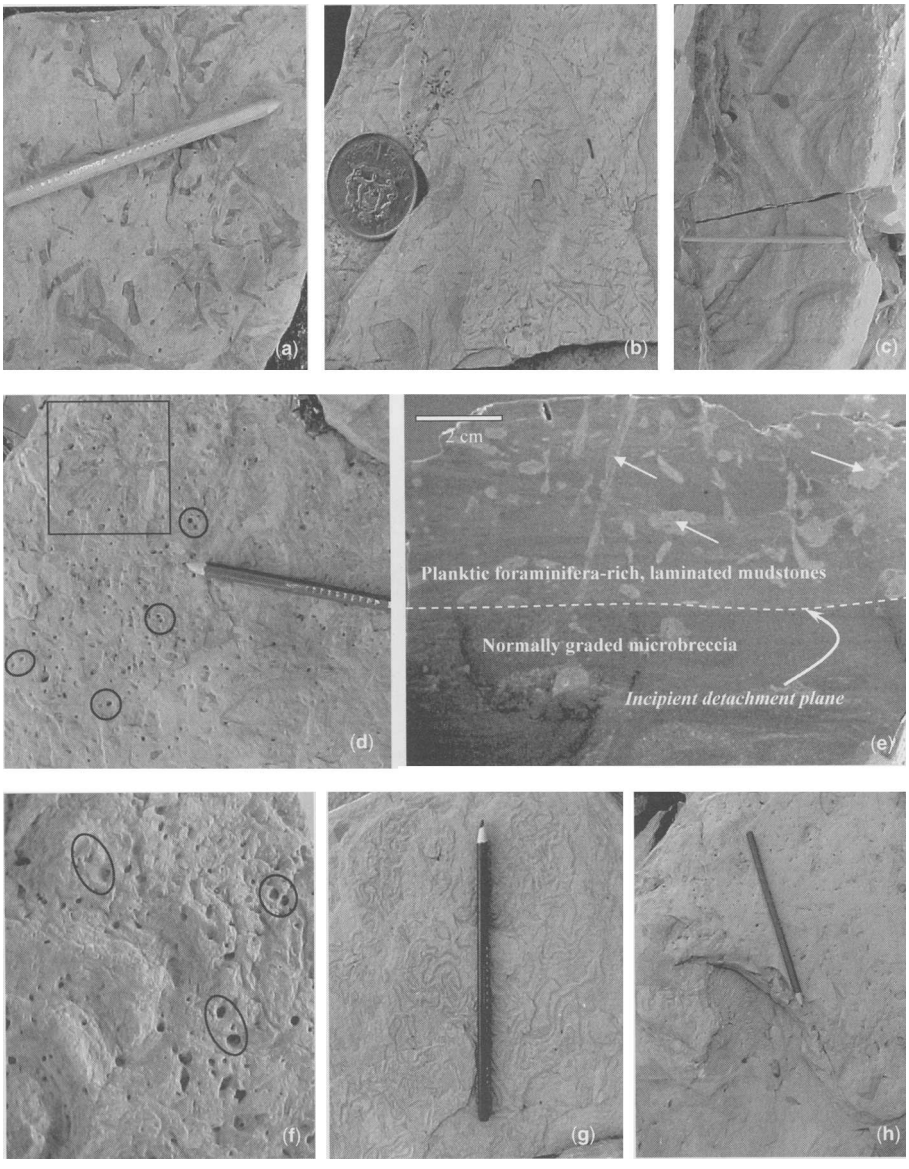

Fig. 6. (**a**) Firmground surface of a mudstone bed from FS.1. It shows large *Chondrites* cross-cut by galleries of *Arenicolites*(?), which indicate two distinct stages of colonization. The contrasting dark colour of these traces, with respect to the host rock, is due to a green, authigenic glauconitic staining. (**b**) *Chondrites intricatus* (Brongniart) densely spaced in the upper part of a 20 cm thick mudstone bed intercalated with black shales of FS.1. (**c**) Densely spaced *Scolicia* traces on a 15 cm thick radiolarian-rich mudstone bed of FS.1. This stage of colonization is often followed by a perforating *Arenicolites*(?) one. (**d**) Firmground surface (FS.4) with dense 'micro-holes' of *Arenicolites*(?) and/or *Diplocraterion* (circles). This stage of colonization was preceded by atypical traces and by a *Lorenzinia*-like trace (square). (**e**) Vertical polished section prepared from the bed shown in (d), showing the diverse geometry of the depth prolongations of the 'micro-holes'. All are filled with green, authigenic glaucony. (**f**) Firmground to hardground surface on a 3 cm thick bed of FS.3, showing a good example of a *Scolicia* trace that is clearly cross-cut by very dense 'micro-holes' of *Arenicolites*(?) and/or *Diplocraterion* (circles). Rust-coloured Fe-coating may independently cover all these traces. (**g**) *Nereites irregularis* (Schafhäutl) in the upper silty laminae of a sandstone bed of FS.3. In contrast to other pascichnia traces (e.g. *Scolicia*), *N. irregularis* have never been observed to be cross-cut by the firmground-perforating domichnia. (**h**) *Zoophycos* in endichnial position within a mudstone bed of FS.2. It is cross-cut by spaced domichnia traces (*Arenicolites*(?) and/or *Diplocraterion*).

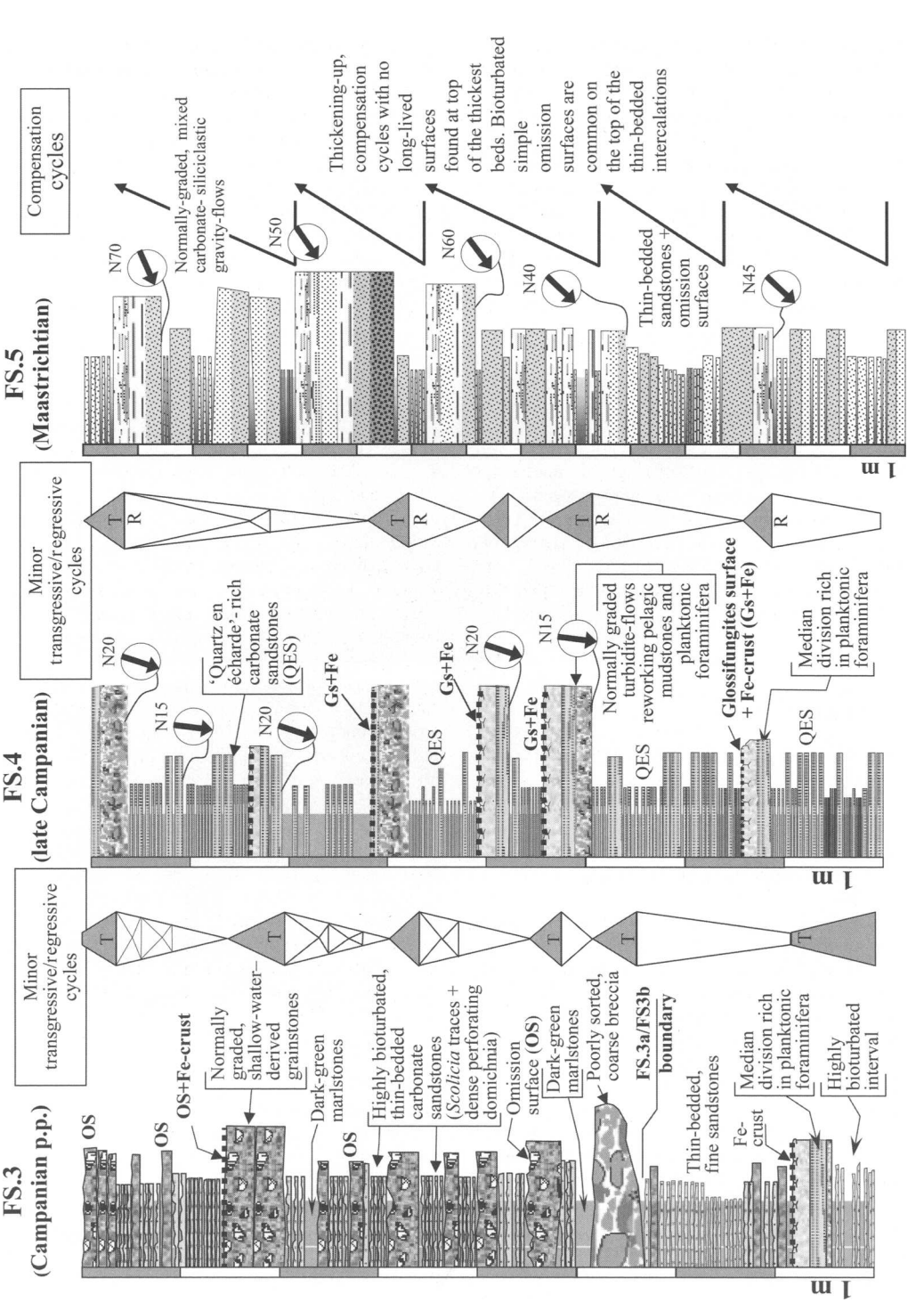

Fig. 7. Selected bed-by-bed lithological columns for facies sequences FS.3–FS.5 in the Rar Aghroud section. The difference in lithological composition between FS.2–FS.3-type and FS.1–FS.4-type small-scale cycles should be noted. In the former, transgressive-induced gravity flows involve shallow-water-derived bioclasts, whereas the latter mainly involve planktonic muds. Fe-coating is common on top of the major breccia and turbidite beds, and may be regarded as minor flooding surfaces following transgressive pulses. In the FS.4 column, many of these omission surfaces have ichnological signatures indicating the *Glossifungites* Ichnofacies.

In this case, the transgressive peak interval is recognized on the basis of both ichnological features and lithofacies. Throughout the upper third of FS.3a, almost all thin sandstone beds show: (1) dense *Arenicolites* at the top, which suggests available bottom-level nutrients, firmground conditions and a relatively low sedimentary rate (Fig. 6f); (2) dense pre-depositional *Graphoglyptids* at the sole, which point to starved deep-water settings experiencing no bottom current and zero or very low benthic food input during the sedimentation of the shaly interbeds (Wetzel 1991; Uchman 1995; Bromley 1996). Within this highly bioturbated interval a single planktonic bed is intercalated. Accordingly, this interval indicates the condensed section.

The overlying grainstone-dominated calciturbidites could represent the subsequent regressive trend. They consist of a rhythmic alternation of shallow-water-derived, bioclastic grainstones, thin-bedded sandstones and dark green marlstones. Spaced intercalations of glauconitic breccias (20–30 cm) may be linked to minor transgressive pulses that typically interrupt the overall regressive regime (Fig. 7). From the ichnological point of view, the preceding *Arenicolites*-rich ichnofabrics was replaced by a *Nereites irregularis* (Schafhäutl) one (Fig. 6g).

T/RFC.4 (= facies sequence FS.4, late Campanian, 40 m)

This cycle starts with an unsorted, grain-supported coarse breccia (*c.* 1 m, Br.4a). Its upper surface displays a conspicuous Fe-coating (POS), which indicates protracted omission following the transgressive pulse responsible for the breccia flow. The whole cycle may be split into two facies sequences, FS.4a and FS.4b.

FS.4a (*c.* 25 m) consists of a rhythmic alternation of well-graded pelagic-mud-dominated flows (10–100 cm) and decimetre-scale terrigenous horizons, which in turn consist of a centimetre-scale carbonate sandstones–green shales alternation. Almost all quartz grains from the carbonate sandstones correspond to the 'Quartz en écharde'-type of pedological origin (Meyer 1987). Bed-by-bed analysis of facies tracts (Fig. 7) shows that both sandstone and pelagic-mud-dominated beds never resulted from grain segregation and then detachment of these two grain types from the same parent flow. Thus, this rhythmic alternation involves two distinct parent flows, and reflects a high-frequency fluctuation in environmental conditions at the source area. The pelagic-mud-bearing attached facies tracts strongly recall the 'calcilutites' described in detail by Stow *et al.* (1984) from the Senonian Scaglia Rossa, which is well known in the Umbro-Marchean Apennines. In both cases the main flows consist of the following grain divisions: (1) graded grainstones (Mutti's F5 facies); (2) cross-stratified packstones–wackestones rich in planktonic Foraminifera; (3) structureless pure mudstones, which are known to have originated from coccolith oozes (e.g. Farinacci 1964, 1969; Busson *et al.* 1997). The last two divisions develop in Mutti's F9a facies.

A bed-by-bed survey reveals that the decimetre-scale beds (40–70 cm) consist of attached facies tracts. Detached facies tracts (5–30 cm) result from truncation of the basal division. The upper surface of almost all limestone beds records polyphase omission history during which: (1) the softground–early firmground stage was inhabited by fodinichnia (in the sense of Seilacher 1964; Bromley 1996), namely *Zoophycos* and large *Chondrites* (*Ch. targionii*, e.g. Uchman 1998, 1999); (2) the firmground stage was dominated by burrowing domichnia represented by abundant *Arenicolites*, *Skolithos* and *Diplocraterion*, all of which may be superimposed on the preceding fodinichnia burrows. Polished and thin sections reveal that almost all the galleries were filled up with authigenic glaucony grains (Fig. 6d and e). These are known to have derived from *in situ* faecal pellet mineralization in starved deep-water settings (Hesselbo & Huggett 2001). It is noteworthy that the contact between the green glauconitic filling and the rust-coloured host rock is sharp. This observation is one of the main criteria used to indicate firmground conditions (Savrda *et al.* 2001*a*). Pemberton & MacEachern (1995) and Gingras *et al.* (2001) documented omission surfaces with a very similar ichnofabric, which indicates the *Glossifungites* ichnofacies (in the sense of Seilacher 1967).

A further stage is marked by variable degrees of substrate ferruginization on several omission surfaces. It is a *per descensum* mineralization, which acted over several centimetres depth into the host rock via epigenesis. El Kadiri (2002*a*) documented near-identical examples in Liassic marly limestones from the 'Dorsale Calcaire' and showed the microbial origin of this phenomenon, which occurs in oxygen-poor, inhospitable environments (similar results have also been given by Mamet *et al.* 1997; Préat *et al.* 2000).

Many workers have emphasized the sequence-stratigraphic significance of *Glossifungites* surfaces (MacEachern *et al.* 1992, 1999; Pemberton & MacEachern 1995; Savrda 1995; Bromley 1996; MacEachern & Burton 2000; Savrda *et al.* 2001*a*,*b*). Depending on the cycle order considered, they are now thought to mark minor to major transgressive pulses; that is, parasequence-bounding minor flooding surfaces (van Wagoner *et al.* 1988) or omission surface(s) within the condensed section (e.g. Loutit *et al.* 1988). Then, depending on the scale at which

we consider these surfaces, the two following results become established: (1) their common occurrence on the top of turbidite beds derived from breccia-bearing facies tracts indicates breccia flows originating from transgressive pulses; (2) the vertical distribution of the *Glossifungites* surfaces over the FS.4a interval (bed-by-bed analysis, Fig. 7) clearly indicates a transgressive trend, the peak of which is confined, just above the last planktonic-mud-bearing flow, in lime-free purple pelites (1 m thick, Fig. 3). These facts point to depths below the CCD, in accordance with the 'erosive–corrosive cycles' concept (Haq 1991, 1993).

Ochre–red, carbonate-poor shales dominate the upper half of the cycle (FS.4b, 15 m in thickness). Thin, decimetre- to metre-spaced planktonic intercalations persist over a 5 m thick interval before being replaced by carbonate sandstones over an interval of equal thickness. A graded breccia (B4.b, 40–60 cm) is intercalated between them. This red-shale-dominated sedimentary package is in turn punctuated by a conspicuous, unsorted coarse-grained breccia (B4.c, 70–100 cm), which results in a third distinct interval. This displays thickening-upward sandstones developed in facies F9b of Mutti (Tc–Td divisions of Bouma 1962). The topmost surface in these two breccias being silty and undergoing dense bioturbation again indicates an omission history. Overall, the sandstone enrichment and the thickening-up ward trend could be the expression of a regressive trend, with the intercalated breccias being the product of breaking transgressive pulses (third–fourth orders). Lending support to this regressive trend is the sea-level fall that occurred as early as the late Campanian (Floquet 1998) and the concomitant cooling event that is indicated by the positive $\delta^{18}O‰$ values (Abreu *et al.* 1998).

T/RFC.5 (= facies sequence FS.5, Maastrichtian; 60 m)

As recognized for the preceding cycles, an important gravity-flow event underlined the onset of this cycle (Br.5). It resulted in a conspicuous attached facies tract in which the six main divisions (F3 to F9b) defined by Mutti (1992) are maintained together in an unattached bed. This bed, among others, allows us to define a new type of facies tract (attached facies tract 5, Fig. 2). Mutti's facies F6 is generally missing, because of its discontinuous character, as expected. However, the main change identified in this study is the sudden input of the filonian-type quartz (Fig. 4). Vertically, the thickening-upward trend recalls the compensation cycles of Mutti & Sonnino (1981), which are well documented in lobe deposits. Tabular mud-draped scours (Mutti & Normark 1987, 1991; Mutti 1992) and mudstone rip-up clasts are frequent over the whole cycle, indicating proximal to median lobe deposits (Fig. 7, column FS.5).

Comparing the preceding cycles, both greater thickness and lobe construction clearly testify to a sudden increase in the efficiency of the turbidite flows as a result of the increased energy and parent-flow volume. In addition to the newly arriving filonian quartz, statistical analysis (El Kadiri *et al.* 2006*b*) shows that carbonates also delivered a great amount of shallow-water benthic material (e.g. reef and rudist debris, orbitoids, algae) at the same time.

The T/RF cycle 5 also differs from the preceding T/RF cycle 4 by the occurrence of black shale interstratifications, which are rich in wood debris indicating terrestrial origin. This feature strongly recalls dark shale intercalations within the so-called 'gréso-micacé' sandstone flysch of late Oligocene–early Burdigalian. Thus, Maastrichtian black shales differ from the Cenomanian–Turonian ones (T/RF cycle 1) in the planktonic origin of the latter, which is well known at the global scale (e.g. Arthur *et al.* 1984, 1987; Kuhnt *et al.* 1986; Stow *et al.* 2001). In following the interpretation of wood debris as a common feature in the transgressive interval (Posamentier & Vail 1988; Vail *et al.* 1991; Savrda 1991; Savrda *et al.* 1993), the black shale interval lying in the middle part of this cycle may correspond to its transgressive peak.

Discussion

Sedimentological, ichnological and lithological data show that the relative sea-level changes closely controlled the timing of the studied calciturbidites. Three additional remarks can be made.

(1) The modest thickness of the Rar Aghroud section (Vraconian–Maastrichtian, 200 m) does not allow us to distinguish depositional cycles of the third order (0.5–3 Ma, e.g. Duval *et al.* 1998), particularly in the Cenomanian–early Senonian interval, for which only one second-order cycle is recognized. The choice of the second-order cycle interpretation is favoured to account not only for their time duration, but also for the existence of thickest late Campanian–Maastrichtian successions (300–500 m) belonging to the Mauretanian series and the Tangiers units. In these, similar tens of metres thick, calciturbidite package–muddy interval couplets may develop in a higher time-order. The four cycles differentiated in the Campanian–Maastrichtian at the Aghroud section are considered to have an average duration of 4.6 Ma and may be ranked within the second-order cycles, following the hierarchy of the stratigraphic cycles defined by Duval *et al.* (1998). They

can be correlated with the four second-order Campanian–Maastrichtian cycles found in the Boreal domain and North America by Hardenbol *et al.* (1998).

(2) This reduced sedimentation results in cycles made up of backstepping-type sequences (in the sense of Jacquin & de Graciansky 1998). These in turn consist only of the transgressive interval–highstand couplets (Jacquin & de Graciansky 1998, p. 35) with the bioclastic grainstone–terrigenous mud couplets being their common expression.

(3) Béni Ider calciturbidites show that such a stacking pattern dominated by backstepping sequences remains unchanged at the regional scale and throughout late Cretaceous–Eocene times. We can therefore relate it to a specific palaeogeographical setting rather than a specific stage during the whole sequence-stratigraphic evolution (backstepping stage of Jacquin & de Graciansky 1998). Isolated carbonate platform(s), more or less disconnected from the continent, seem to us the likeliest palaeogeographical source of these bioclastic-grainstone-dominated turbiditic sequences, with the terrigenous mud supply remaining constantly reduced.

Conclusion

An integrated study including lithological, ichnological and facies tract–facies sequence description constitutes the first attempt to make a sequence-stratigraphic interpretation (via the lithological prediction method, Posamentier & James 1993) of the Cretaceous calciturbidites in the flysch Intrarif Domain. It is applied to the well-differentiated Rar Aghroud section, to provide a working hypothesis for the understanding of the rest of the Cretaceous–Palaeogene calciturbidites, which are widespread in the External Rif Domain.

The authors are indebted to the Société Nationale d'Etude du Détroit, SNED, Rabat, Morocco for their financial support. They express their sincere thanks to F. Oloriz-Saez (University of Granada) and W. Wildi (University of Zürich) for their constructive reviews and criticisms.

References

ABREU, V. S., HARDENBOL, J., HADDAD, G. A., BAUM, G. R., DROXLER, A. W. & VAIL, P. R. 1998. Oxygen isotope synthesis: a Cretaceous ice-house? *In*: DE GRACIANSKY, P. C., HARDENBOL, J., JACQUIN, T. & VAIL, P. R. (eds) *Mesozoic and Cenozoic Sequence Stratigraphy of European Basins*. Society of Economic Paleontologists and Mineralogists, Society for Sedimentary Geology, Special Publications, **60**, 75–80.

AMY, L., KNELLER, B. & MCCAFFREY, W. (eds) 2000. *Evaluating the Links between Turbidite Characteristics and Gross System Architecture: Upscaling Insight from the Turbidite-Sheet System of Peïra Cava, SE France*. Society of Economic Paleontologists and Mineralogists, Society for Sedimentary Geology, Special Publications, **20**.

ARTHUR, M. A., DEAN, W. E. & STOW, D. A. V. 1984. Models for the deposition of Mesozoic–Cenozoic fine-grained organic-carbon-rich sediment in the deep sea. *In*: STOW, D. A. V. & PIPER, D. J. W. (eds) *Fine-grained Sediments: Deep Water Processes and Facies*. Geological Society, London, Special Publications, **15**, 527–560.

ARTHUR, M. A., SCHLANGER, S. O. & JENKYNS, H. C. 1987. The Cenomanian–Turonian oceanic anoxic event II. Palaeoceanographic controls on organic-matter production. *In*: BROOKS, J. & FLEET, A. J. (eds) *Marine Petroleum Source Rocks*. Geological Society, London, Special Publications, **26**, 401–420.

BAUM, G. R. & VAIL, P. R. 1988. Sequence stratigraphy concepts applied to Palaeogene outcrops, Gulf and Atlantic basins. *In*: WILGUS, C. K., HASTINGS, B. S., KENDALL, C. G. ST. C., POSAMENTIER, H. W., ROSS, C. A. & VAN WAGONER, J. C. (eds) *Sea Level Changes—An Integrated Approach*. Society of Economic Paleontologists and Mineralogists, Society for Sedimentary Geology, Special Publications, **42**, 309–327.

BOUMA, A. 1962. *Sedimentology of Some Flysch Deposits, a Graphic Approach to Facies Interpretation*. Elsevier, Amsterdam.

BROMLEY, R. G. 1996. *Trace Fossils. Biology, Taphonomy and Applications*, 2nd edn. Chapman & Hall, London.

BURCHELL, M. T., STEFANI, M. & MASETTI, D. 1990. Cyclic sedimentation in the southern alpine Rhaetic: the importance of climate and eustasy in controlling platform–basin interactions. *Sedimentology*, **37**, 795–815.

BUSSON, G., NOËL, D. & CORNÉE, A. 1997. Les coccolithophoridées, contributeurs essentiels de la fraction calcaire des sédiments marins du Jurassique moyen–supérieur: contraste entre les populations des calcaires et des marnes. *Bulletin de la Société Géologique de France*, **5**, 601–609.

CLARI, P. A., DE LA PIERRE, F. & MARTIRE, L. 1995. Discontinuities in carbonate successions: identification, interpretation and classification of some Italian examples. *Sedimentary Geology*, **100**, 97–121.

CLARKSON, E. N. K. 1993. *Invertebrate Palaeontology and Evolution. Sponges*. Readers in Palaeontology, **3**. Chapman & Hall, London, 81–96.

COOK, H. & MULLINS, H. T. 1983. Basin margin environment. *In*: SCHOLLE, P. A., BEBOUT, D. G. & MOORE, C. H. (eds) *Carbonate Depositional Environments*. American Association of Petroleum Geologists Memoirs, **33**, 539–617.

DIDON, J. 2006. *Carte Géologique 1/50.000. Feuille Souk Larba Béni Hassane*. Notes et Mémoires du Service Géologique du Maroc (in press).

DURAND-DELGA, M. 1972. La courbure de Gibraltar, extrémité occidentale des chaînes alpines, unit l'Europe et l'Afrique. *Eclogae Geologicae Helvetiae*, **65**, 267–278.

DUVAL, B. C., CRAMEZ, C. & VAIL, P. R. 1998. Stratigraphic cycles and major marine source rocks. *In*: DE GRACIANSKY, P. C., HARDENBOL, J., JACQUIN, T. & VAIL, P. R. (eds) *Mesozoic and Cenozoic Sequence Stratigraphy of European Basins*. Society of Economic Paleontologists and Mineralogists, Society for Sedimentary Geology, Special Publications, **60**, 43–51.

EBERLI, G. 1987. Carbonate turbidite sequence deposited in rift-basin of the Jurassic Tethys Ocean (eastern Alps, Switzerland). *Sedimentology*, **34**, 363–388.

EBERLI, G. 1988. The evolution of the southern continental margin of the Jurassic Tethys Ocean as recorded in the Allgäu Formation of the austroalpine nappes of Graubünden (Switzerland). *Eclogae Geologicae Helvetiae*, **81**, 175–214.

EBERLI, G. P. 1991. Calcareous turbidites and their relationship to sea-level fluctuations and tectonism. *In*: EINSELE, G., RICKEN, W. & SEILACHER, A. (eds) *Cycles and Events in Stratigraphy*. Springer, Berlin, 340–359.

EL KADIRI, KH. 1991. *La Dorsale Calcaire (Rif interne, Maroc): stratigraphie, sédimentologie et évolution géodynamique d'une marge alpine durant le Mésozoïque. Mise en évidence d'un modèle*. Doctorat d'Etat Thesis, University Tetuan.

EL KADIRI, KH. 2002*a*. 'Tectono-eustatic sequences' of the Jurassic successions from the *Dorsale Calcaire* (internal Rif, Morocco): evidence from a eustatic and tectonic scenario. *Geologica Romana*, **36**, 71–104.

EL KADIRI, KH. 2002*b*. Jurassic ferruginous hardgrounds of the 'Dorsale Calcaire' and the Jbel Moussa Group (internal Rif, Morocco): stratigraphical context and palaeoceanographic consequences of mineralization processes. *Geologica Romana*, **36**, 33–70.

EL KADIRI, KH., SERRANO, F., HLILA, R., *ET AL.* 2005. Lithostratigraphy and sedimentology of the latest Cretaceous–early Burdigalian Tamezzakht Succession (Northern Rif, Morocco): consequences for its sequence stratigraphic interpretation. *Facies*, **50**, 477–503.

EL KADIRI, KH., CHALOUAN, A., BAHMAD, A., SALHI, F. & LIEMLAHI, H. 2006*a*. 'Transgressive washing' concept: a sequence stratigraphic approach for calci- and siliciclastic turbidites. *In*: MORATTI, G. & CHALOUAN, A. (eds) *Tectonics of the Western Mediterranean and North Africa*. Geological Society, London, Special Publications, **262**, 45–53.

EL KADIRI, KH., EL KADIRI, K., CHALOUAN, A., BAHMAD, A., SALHI, F. & LIEMLAHI, H. 2006*b*. Factorial correspondence analysis: a useful tool in palaeogeographical reconstructions; example from late Cretaceous calciturbidites of the northwestern External Rif (Morocco). *In*: MORATTI, G. & CHALOUAN, A. (eds) *Tectonics of the Western Mediterranean and North Africa*. Geological Society, London, Special Publications, **262**, 147–160.

ESCHARD, R. 2001. Geological factors controlling sediment transport from platform to deep basin: a review. *Marine and Petroleum Geology*, **18**, 487–490.

FARINACCI, A. 1964. Microrganismi dei calcari 'Maiolica' e 'Scaglia' osservati al microscopio elettronico (nannoconi e coccolithophoridi). *Bollettino della Società Paleontologica Italiana*, **3**, 2–11.

FARINACCI, A. 1969. Characteristics of micrite grains in the Apennines. *Geologica Romana*, **8**, 47–69.

FLOQUET, M. 1998. Outcrop cycle stratigraphy of shallow ramp deposits: the late Cretaceous series on the Castilian ramp (northern Spain). *In*: DE GRACIANSKY, P. C., HARDENBOL, J., JACQUIN, T. & VAIL, P. R. (eds) *Mesozoic and Cenozoic Sequence Stratigraphy of European Basins*. Society of Economic Paleontologists and Mineralogists, Society for Sedimentary Geology, Special Publications, **60**, 343–361.

GALLOWAY, W. E. 1989. Genetic stratigraphic sequences in basin analysis I: architecture and genesis of flooding-surface bounded depositional units. *AAPG Bulletin*, **73**, 125–142.

GHIBAUDO, G., GRANDESSO, P., MASSARI, F. & UCHMAN, A. 1996. Use of trace fossils in delineating sequence stratigraphic surfaces (Tertiary Venetian Basin, northeastern Italy). *Palaeogeography, Palaeoclimatology, Palaeoecology*, **120**, 261–279.

GINGRAS, K. M., PEMBERTON, S. G. & SAUNDERS, T. 2001. Bathymetry, sediment texture, and substrate cohesiveness; their impact on modern Glossifungites trace assemblages at Willapa Bay, Washington. *Palaeogeography, Palaeoclimatology, Palaeoecology*, **169**, 1–21.

HAAS, J. 1999. Genesis of late Cretaceous toe-of-slope breccias in the Bakony Mts, Hungary. *Sedimentary Geology*, **128**, 51–66.

HALLAM, A. & WIGNALL, P. B. 1999. Mass extinctions and sea-level changes. *Earth-Science Reviews*, **48**, 217–250.

HAQ, B. U. 1991. Sequence stratigraphy, sea-level change, and significance for the deep sea. *In*: MACDONALDS, D. I. M. (eds) *Sedimentation, Tectonics and Eustasy. Sea-Level Changes at Active Margins*. Inernational Association of Sedimentologists, Special Publications, **12**, 3–39.

HAQ, B. U. 1993. Deep-sea response to eustatic change and significance of gas hydrates for continental margin stratigraphy. *In*: POSAMENTIER, H. W., SUMMERHAYES, C. P., HAQ, B. U. & ALLEN, G. P. (eds) *Sequence Stratigraphy and Facies Associations*. International Association of Sedimentologists, Special Publications, **18**, 93–106.

HARDENBOL, J., THIERRY, J., FARLEY, M. B., JACQUIN, T., DE GRACIANSKY, P. C. & VAIL, P. R. 1998. Mesozoic and Cenozoic sequence chronostratigraphic framework of European basins. *In*: DE GRACIANSKY, P. C., HARDENBOL, J., JACQUIN, T. & VAIL, P. R. (eds) *Mesozoic and Cenozoic Sequence Stratigraphy of European Basins*. Society of Economic Paleontologists and Mineralogists, Society for Sedimentary Geology, Special Publications, **60**, 3–13.

HESSELBO, S. P. & HUGGETT, J. M. 2001. Glaucony in ocean-margin sequence stratigraphy (Oligocene–Pliocene, offshore New Jersey, U.S.A., ODP leg 174a). *Journal of Sedimentary Research*, **71**, 599–607.

JACQUIN, T. & DE GRACIANSKY, P. C. 1998. Transgressive/regressive (second order) facies cycles: the effect of tectono-eustasy. *In*: DE GRACIANSKY, P. C., HARDENBOL, J., JACQUIN, T. & VAIL, P. R. (eds) *Mesozoic and Cenozoic Sequence Stratigraphy of European Basins*. Society of Economic Paleontologists and Mineralogists, Society for Sedimentary Geology, Special Publications, **60**, 31–42.

KUHNT, W., THUROW, J., WIEDMANN, J. & HERBIN, J. P. 1986. Oceanic anoxic conditions around the Cenomanian–Turonian boundary and the response of the biota. *Mitteilung–Geologie und Paläontologie Institut, Universitat Tübingen*, **60**, 205–246.

LOUTIT, T. S., HARDENBOL, J. & VAIL, P. R. 1988. Condensed sections: the key to age determination and correlation of continental margin sequences. *In*: WILGUS, C. K., HASTINGS, B. S., KENDALL, C. G. ST. C., POSAMENTIER, H. W., ROSS, C. A. & VAN WAGONER, J. C. (eds) *Sea Level Changes—An Integrated Approach*. Society of Economic Paleontologists and Mineralogists, Society for Sedimentary Geology, Special Publications, **42**, 183–213.

MACEACHERN, J. A. & BURTON, J. A. 2000. Firmground *Zoophycos* in the Lower Cretaceous Viking Formation, Alberta: a distal expression of the Glossifungites Ichnofacies. *Palaios*, **15**, 387–398.

MACEACHERN, J. A., BECHTEL, D. J. & PEMBERTON, S. G. 1992. Ichnology and sedimentology of transgressive deposits, transgressively-related deposits and transgressive systems tracts in the Viking Formation of Alberta. *In*: PEMBERTON, S. G. (ed.) *Application of Ichnology to Petroleum Exploration*. Society of Economic Paleontologists and Mineralogists, Society for Sedimentary Geology, Special Publications, **17**, 252–290.

MACEACHERN, J. A., STELCK, S. R. & PEMBERTON, S. G. 1999. Marine and marginal marine mudstone deposition: palaeoenvironmental interpretation based on the integration of ichnology, palynology and foraminiferal palaeoecology. *In*: BERGMAN, K. M. & SNEDDEN, J. W. (eds) *Isolated Marine Sand Bodies: Sequence Stratigraphic Analysis and Sedimentological Interpretation*. Society of Economic Paleontologists and Mineralogists, Society for Sedimentary Geology, Special Publications, **64**, 205–225.

MAMET, B., PRÉAT, A. & DE RIDDER, C. 1997. Bacterial origin of the red pigmentation in the Devonian Slivenec Limestone, Czech Republic. *Facies*, **76**, 173–188.

MASETTI, D., STEFANI, M. & BURCHELL, M. 1989. Asymmetric cycles in the Rhaetic facies of the Southern Alps: platform–basin interactions governed by eustatic and climatic oscillations. *Rivista Italiana di Paleontologia e Stratigrafia*, **94**, 401–423.

MEYER, R. 1987. *Paléolatérites et paléosols, l'empreinte du continent dans les séries sédimentaires*. Bureau de Recherches Géologiques et Minières, Manuel et Méthodes, **13**.

MUTTI, E. 1992. Turbidite Sandstones. Agip, Special Publication. Instituto di Geologia, Milano.

MUTTI, E. & NORMARK, W. R. 1987. Comparing examples of modern and ancient turbidite systems: problems and concepts. *In*: LEGGETT, J. K. & ZUFFA, G. G. (eds) *Marine Clastic Sedimentology: Concepts and Case Studies*. Graham & Trotman, London, 1–38.

MUTTI, E. & NORMARK, W. R. 1991. An integrated approach to the study of turbidite systems. *In*: WEIMER, P. & LINK, H. (eds) *Seismic Facies and Sedimentary Processes of Submarine Fans and Turbidite Systems*. Springer, Berlin, 75–106.

MUTTI, E. & RICCI LUCCHI, F. 1975. Turbidite facies and facies associations. *In*: MUTTI, E., PAREA, G. C., RICCI LUCCHI, F. *ET AL.* (eds) *Examples of Turbidite Facies from Selected Formation of the Northern Apennines, Field Trip Guidebook*. International Congress of Sedimentologists, Nice, France, 21–36.

MUTTI, E. & SONNINO, M. 1981. Compensation cycles: a diagnostic feature of turbidite sandstone lobes. International Association of Sedimentologists 2nd European Regional Meeting (abstracts), Bologna, Italy, 120–123.

NIETO ALBERT, L. M. 1996. *La cuenca subbetica mesozoica en el sector oriental de las Cordilleras Beticas*. Tesis Doctoral, University of Granada.

PEMBERTON, S. G. & MCEACHERN, J. A. 1995. The sequence stratigraphy significance of trace fossils in examples from the Cretaceous of Alberta. *In*: VAN WAGONER, J. A. & BERTRAM, G. T. (eds) *Sequence Stratigraphy of Foreland Basin Deposits–Outcrop and Subsurface Examples from the Cretaceous of North America*. American Association of Petroleum Geologists, Memoirs, **64**, 429–475.

POSAMENTIER, H. W. & JAMES, D. P. 1993. An overview of sequence-stratigraphic concepts: uses and abuses. *In*: POSAMENTIER, H. W., SUMMERHAYES, C. P., HAQ, B. U. & ALLEN, G. P. (eds) *Sequence Stratigraphy and Facies Associations*. International Association of Sedimentologists, Special Publications, **18**, 3–18.

POSAMENTIER, H. W. & VAIL, P. R. 1988. Eustatic controls on clastic deposition II—sequence and systems tracts models. *In*: WILGUS, C. K., HASTINGS, B. S., KENDALL, C. G. ST. C., POSAMENTIER, H. W., ROSS, C. A. & VAN WAGONER, J. C. (eds) *Sea Level Changes—An Integrated Approach*. Society of Economic Paleontologists and Mineralogists, Society for Sedimentary Geology, Special Publications, **42**, 125–154.

PRÉAT, A., MAMET, B., DE RIDDER, C., BOULVAIN, F. & GILLAN, D. 2000. Iron bacterial and fungal mats, Bajocian stratotype (Mid-Jurassic, northern Normandy, France). *Sedimentary Geology*, **137**, 107–126.

ROBASZYNSKI, F., GALE, A., JUIGNET, P., AMÉDRO, F. & HARDENBOL, J. 1998. Sequence stratigraphy in the upper Cretaceous series of the Anglo-Paris Basin: exemplified by the Cenomanian stage. *In*: DE GRACIANSKY, P. C., HARDENBOL, J., JACQUIN, T. & VAIL, P. R. (eds) *Mesozoic and Cenozoic Sequence Stratigraphy of European Basins*. Society of Economic Paleontologists and Mineralogists, Society for Sedimentary Geology, Special Publications, **60**, 363–386.

SAVRDA, C. E. 1991. Ichnology in sequence stratigraphic studies: an example from the Lower Palaeocene of Alabama. *Palaios*, **6**, 39–53.

SAVRDA, C. E. 1995. Ichnologic applications in palaeoceanographic, palaeoclimatic, and sea-level studies. *Palaios*, **10**, 565–577.

SAVRDA, C. E., OZALAS, K., DEMKO, T. H., HUCHISON, R. A. & SCHEIWE, TH. D. 1993. Log-grounds and the ichnofossil Teredolites in transgressive deposits of the Clayton Formation (Lower Palaeocene), Western Alabama. *Palaios*, **8**, 311–324.

SAVRDA, C. E., KRAWINKEL, H., MCCARTHY, M. G., MCHUGH, C. M. G., OLSON, H. C. & MOUNTAIN, G. 2001*a*. Ichnofabrics of a Pleistocene slope succession, New Jersey margin: relations to climate and sea-level dynamics. *Palaeogeography, Palaeoclimatology, Palaeoecology*, **171**, 41–61.

SAVRDA, C. E., BROWNING, J. V., KRAWINKEL, H. & HESSELBO, S. P. 2001*b*. Firmground ichnofabrics in deep-water sequence stratigraphy, Tertiary cliniform-toe deposits, New Jersey Slope. *Palaios*, **16**, 294–305.

SEILACHER, A. 1964. Biogenic sedimentary structures. *In*: IMBRIE, J. & NEWELL, N. (eds) *Approaches to Palaeocology*. Wiley, New York, 296–316.

SEILACHER, A. 1967. Bathymetry of trace fossils. *Marine Geology*, **5**, 413–428.

SHANMUGAM, G. 2000. 50 years of the turbidite paradigm (1950s–1990s): deep-water processes and facies models—a critical perspective. *Marine and Petroleum Geology*, **17**, 285–342.

STOW, D. A. V. & MAYALL, M. 2000. Deep-water sedimentary systems: new models for the 21st century. *Marine and Petroleum Geology*, **17**, 125–135.

STOW, D. A. V., WEZEL, F. C., SAVELLI, D., RAINEY, S. C. R. & ANGELL, G. 1984. Depositional model for calcilutites: Scaglia Rossa limestones, Umbro-Marchean Apennines. *In*: STOW, D. A. V. & PIPER, D. J. W. (eds) *Fine-Grained Sediments: Deep Water Processes and Facies*. Geological Society, London, Special Publications, **15**, 223–241.

STOW, D. A. V., HUC, A.-Y. & BERTRAND, P. 2001. Depositional processes of black shales in deep water. *Marine and Petroleum Geology*, **18**, 491–498.

THUROW, J. 1987. *Die Kretazischen Turbiditserien im Gibraltarbogen: Bindeglied zwischen Atlantischer und Tethyaler Entwicklung*. PhD Thesis, University of Tübingen.

UCHMAN, A. 1995. Taxonomy and palaeocology of flysch trace fossils: the Marnoso-arenacea Formation and associated facies (Miocene, Northern Apennines, Italy). *Beringeria*, **15**, 3–315.

UCHMAN, A. 1998. Taxonomy and ethology of flysch trace fossils: revision of the Marian Ksiazkiewocz collection and studies of complementary material. *Annales Societatis Geologorum Poloniae*, **68**, 105–218.

UCHMAN, A. 1999. Ichnology of the Rhenodanubian Flysch (Lower Cretaceous–Eocene) in Austria and Germany. *Beringeria*, **25**, 67–173.

VAIL, P. R., AUDEMARD, F., BOWMAN, S. A., EISNER, P. N. & PEREZ-CRUZ, C. 1991. The stratigraphic signatures of tectonics, eustasy and sedimentology—an overview. *In*: EINSELE, G., RICKEN, W. & SEILACHER, A. (eds) *Cycles and Events in Stratigraphy*. Springer, Berlin, 617–659.

VAN WAGONER, J. C., POSAMENTIER, H. W., MITCHUM, R. M., VAIL, P. R., SARG, J. F., LOUTIT, T. S. & HARDENBOL, J. 1988. An overview of the fundamentals of sequence stratigraphy and key definitions. *In*: WILGUS, C. K., HASTINGS, B. S., KENDALL, C. G. ST. C., POSAMENTIER, H. W., ROSS, C. A. & VAN WAGONER, J. C. (eds) *Sea Level Changes—An Integrated Approach*. Society of Economic Paleontologists and Mineralogists, Society for Sedimentary Geology, Special Publications, **42**, 39–45.

WETZEL, A. 1991. Ecologic interpretation of deep-sea trace fossil communities. *Palaeogeography, Palaeoclimatology, Palaeoecology*, **85**, 47–69.

WHITNEY, F., CONWAY, K. W., THOMSON, R. E., BARRIE, J. V., KRAUTTER, M. & MUNGOV, G. 2005. Oceanographic habitat of sponge reefs of the western Canadian continental shelf. *Continental Shelf Research*, **25**(2), 211–226.

YOSE, L. A. & HELLER, P. L. 1989. Sea-level control of mixed-carbonate–siliciclastic, gravity-flow deposition: lower part of the Keeler Canyon Formation (Pennsylvanian), southeastern California. *Geological Society of America Bulletin*, **101**, 427–439.

Regional correlations across the Internides–Externides front (northwestern Rif Belt, Morocco) during the Late Cretaceous–Early Burdigalian times: palaeogeographical and palaeotectonic implications

KH. EL KADIRI[1], R. HLILA[1], C. SANZ DE GALDEANO[2], A. C. LÓPEZ-GARRIDO[2], A. CHALOUAN[3], F. SERRANO[4], A. BAHMAD[5], A. GUERRA-MERCHÁN[4] & H. LIEMLAHI[1]

[1]*Université Abdelmalek Essaadi, Faculté des Sciences, Dep. Geology, BP 2121, 93003 Tetuan, Morocco (e-mail: khkadiri@fst.ac.ma)*

[2]*University of Granada, Facultad de Ciencias, Dep. Geodinamica, Av. Fuente Nueva, 18002 Granada, Spain*

[3]*Université Mohammed V-Agdal, Faculté des Sciences, Dep. Geology, BP 1014, 10000 Rabat, Morocco*

[4]*University of Malaga, Dep. Ecologia & Geologia, Teatinos, Malaga, Spain*

[5]*Société Nationale d'Etudes du Détroit de Gibraltar (SNED), 31 r. Al Alaouyines, Rabat, Morocco*

Abstract: New insights into the palaeogeographical evolution of the Rifian Internides and their external surroundings are inferred from six key stratigraphic successions selected across the Internides–Externides front. These successions span a time interval ranging from the late Cretaceous to the early Burdigalian. The main results are: (1) important lost palaeogeographical domains should be located during the late Cretaceous–Eocene between the present-day Ghomarides and the Dorsale Calcaire, on one hand, and between the Predorsalian units and the Flysch Trough as isolated carbonate platforms, on the other hand; (2) during the late Eocene–early Oligocene an extensional tectonic event, well marked in the Dorsale Calcaire, caused the collapse of these platforms and resulted in olistostromes and coarse-grained breccias in both the Predorsalian and the Béni Ider areas; (3) by the beginning of mid-Oligocene, an overturning contractional event in the Ghomarides resulted in the regional onset of the siliciclastic depositional regime throughtout these palaeogeographical areas; (4) during the Aquitanian–early Burdigalian, the stepwise return of pelagic deposition in the Ghomarides indicates extensional phases, whereas the homogenization of the same pelagic facies over the Dorsale Calcaire and its external surroundings may indicate that the previously distant palaeogeographical areas were brought nearer (i.e. just before large-scale thrusting).

The Gibraltar arc consists of two juxtaposed structural domains: (1) the Internal Domain, (Internides) where the orogenic contractions started from Oligocene time and generally resulted in high-grade metamorphism, particularly in its innermost part; (2) the External Domain (Externides), where the outward migrating orogenic contractions during Miocene time progressively produced piggy-back–foredeep basins and ramp-anticline structures. The culmination of these phenomena during the paroxysmal phase resulted in a high accretionary prism and successive large-scale gravitational processes (Chalouan *et al.* 2006).

The Tertiary sedimentary filling within and/or close to these forming basins was differently interpreted in both domains. Whereas there is acceptance that the filling of the main flysch depocentres in the External Domain occurred shortly before the paroxysmal nappe emplacement, or even as syntectonic deposits, competing hypotheses were presented for the equivalent strata in the Internal domain. Some workers attempted to link them to post-orogenic deposits transgressively sealing the paroxysmal structures (e.g. Durand-Delga *et al.* 1993), whereas others considered them as recording a near-continuous marine regime entirely predating the main orogenic events (e.g. Maaté 1996). Recently, detailed stratigraphic studies of the Oligo-Miocene cover were carried out in the Malaguides (Guerrera *et al.* 1993; Martin-Martin *et al.* 1997) and the Ghomarides (Feinberg *et al.* 1990; El Kadiri *et al.* 2000, 2001). They showed that the

From: MORATTI, G. & CHALOUAN, A. (eds) 2006. *Tectonics of the Western Mediterranean and North Africa.* Geological Society, London, Special Publications, **262**, 193–215.
0305-8719/06/$15.00

Oligo-Miocene sedimentary cycles were episodically induced by extension-related marine encroachments punctuating contractional events during a polyphase tectonic scenario (Comas *et al.* 1992; Garcia-Dueñas *et al.* 1992; Chalouan *et al.* 1997).

The aim of this paper is to extend this approach to time-equivalent depositional series belonging to both sides of the Internide–Externide front (i.e. the Dorsale Calcaire, Predorsalian and Béni Ider series). Some of the studied series are newly dated and/or described herein. Good examples are provided by: (1) the Dradia–El Onzar and Talembote sections in the Ghomaride Domain; (2) the Hafat Srir section in the Dorsale Calcaire; (3) the well-exposed Tamezzakht succession (located in the Predorsalian zone) that belongs to this frontal zone, to which special attention will be paid here. Its extended time-range (from the late Cretaceous the early Burdigalian), gravity-flow events, and well-delineated discontinuities are used to monitor regional-scale correlations across the Internal–External Domains (see El Kadiri *et al.* 2005, for detailed sedimentological data).

The general interest of this approach is to promote the correlation between the internal and the external zones in deciphering the tectonic and/or eustatic significance of their coeval deposits. Thus, these two domains can no longer be taken as two independent geological realms when reconstructing the tectonosedimentary evolution of the Gibraltar arc evolution.

Geological background

The Rifian Internal zones (Fig. 1) consist of a complex nappe pile resulting from the westward-vergent stacking of three distinct units: the Sebtides, Ghomarides and the Dorsale Calcaire.

The Sebtides consist of varied metamorphic nappes, including a granulitic–mantle ultramafic unit, which is underlain (Sebta massif) and overlain (Béni Bousera massif) by gneiss and schists of upper-crustal affinities. These in turn are overthrust or are overlapped by detached high-pressure–low-temperature metapelitic strata, mainly of late Palaeozoic–Triassic age (Federico units; Bouybaouène *et al.* 1995), a fact that supports the attribution of the Sebtide nappe emplacement to the Alpine orogeny. The ultramafic rocks of Béni Bousera essentially consist of spinel-bearing

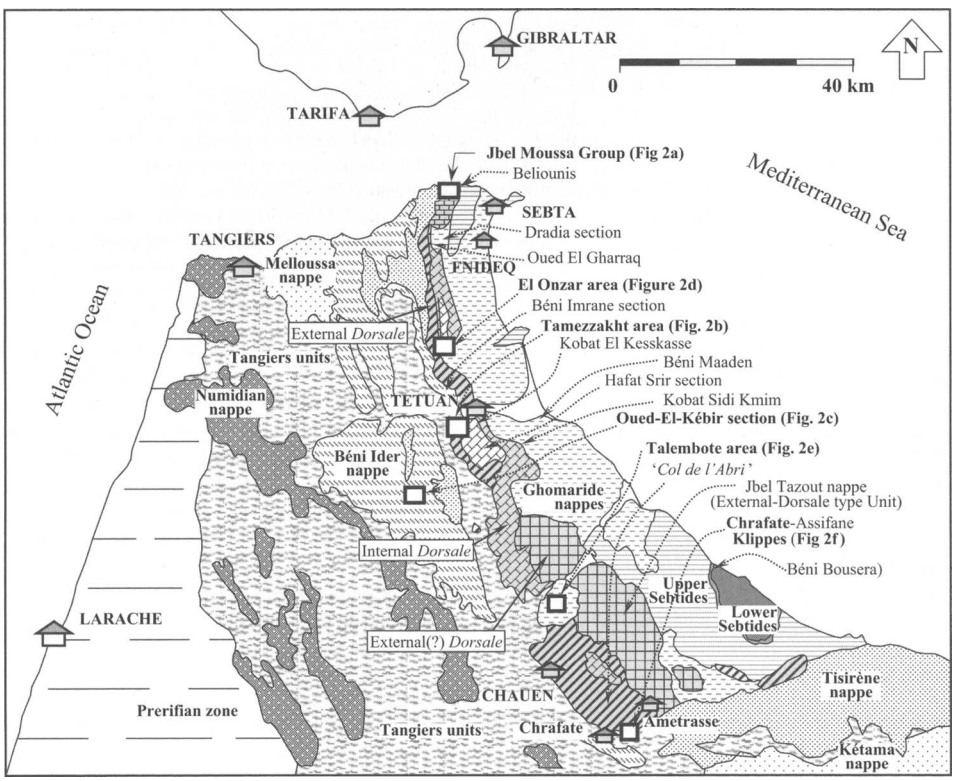

Fig. 1. Geological map of the northwestern Rif belt and location of the study areas (see Fig. 2 for details).

lherzolites. They were interpreted as a hot asthenospheric dome (Loomis 1975; Platt & Vissers 1989) or conversely as pre-Alpine slivers uprooted from Precambrian infracrustal levels and emplaced in the upper crust (Kornprobst 1974). Integrated approaches including detailed structural field-survey (Reubert *et al.* 1982; Saddiqi *et al.* 1988) and geochronological analyses (Sanchez-Rodriguez & Gebauer 2000) showed that the lower Sebtide lherzolites were initially derived from a lithospheric mantle, and were subsequently emplaced as tectonic slivers within upper crustal levels. This scenario occurred in two main stages, during Tethyan rifting at about 183–131 Ma, and during Palaeogene subduction–collision (Chalouan *et al.* 2001; Michard *et al.* 2002). Geochemical data (Targuisti 1994), and even the stratigraphic record (El Kadiri *et al.* 1992, 1995), support the idea that the Béni Bousera–Ronda peridotites derived from an asthenospheric dome, the ascent of which started as early as Mesozoic time (Sanchez-Rodriguez & Gebauer 2000). The conditions and kinematics of their final exhumation as well as of that of the surrounding metamorphic rocks are still a matter of debate (see, for example, the discussion by Balanya & Garcia-Dueñas 1987; Lonergan & White 1997; Azañon *et al.* 1998; Morales *et al.* 1999; Azañon & Crespo-Blanc 2000; Calvert *et al.* 2000).

The Ghomaride nappes (Kornprobst 1974; Chalouan 1986) generally thrust the Sebtides. They mainly consist of Palaeozoic schists, which compositionally resemble their Hercynian homologues known at present in the eastern Moroccan Meseta (Chalouan 1986), a fact that supports a palaeogeographical reconstruction in which they originally derived from an eastern domain, where they formed the westernmost part of the 'AlKaPeCa' palaeoplate (Bouillin *et al.* 1986; Chalouan & Michard 1990; Guerrera *et al.* 1993). Lithofacies, metamorphism and the position within the nappe pile allow four main nappes to be distinguished (Chalouan 1986; Chalouan & Michard 1990).

The Dorsale Calcaire was first interpreted as corresponding to the Alpine Ghomaride cover (Durand Delga *et al.* 1962; Kornprobst 1974) detached from its Palaeozoic basement during Tertiary thrusting. However, characterization of an independent Mesozoic Ghomaride cover with respect to the carbonate Jurassic strata of the Dorsale Calcaire, on one hand (Maaté 1984, 1996; El Kadiri 1991; El Kadiri *et al.* 1992), and detailed stratigraphic analyses of the entire Mesozoic successions of both the Internal and the External Dorsale, on the other hand (Nold *et al.* 1981; El Kadiri 1984, 1991; Olivier 1984; El Hatimi 1991; Maaté 1996), led to the two latter being assigned to the palaeomargin bordering westwards and/or southwards the Rif 'Internal zones'. This result appears in accordance with the concept of a 'Predorsalian zone' (Didon *et al.* 1973) that palaeogeographically corresponded to the deepest part of this palaeomargin (e.g. Chrafate Klippes units, Assifane units, El Hatimi 1982; El Kadiri 1984; El Hatimi *et al.* 1988; Ben Yaïch *et al.* 1988). Triassic–earliest Jurassic, thick-bedded, shallow-water carbonate limestones make up the main massifs of the Dorsale Calcaire. They may be topped with polyphase palaeokarst surfaces in the Internal Dorsale (El Kadiri 1991; Maaté 1996) and with Fe-encrusted hardgrounds in the External Dorsale (El Kadiri 2002*a*,*b*).

In the Internal Dorsale, reduced pelagic series may diachronously onlap the massive carbonate formations. The most noteworthy of these are developed in rosso-ammonitico facies during the Domerian–Toarcian, and in *Saccocoma*- and/or *Calpionella*-rich mudstones during the Tithonian–Berriasian. A long-lasting palaeokarst history occurred in the intervening time span (El Kadiri 1991; El Kadiri *et al.* 1992), a feature that recalls the Mid–Late Jurassic 'Main Gap' found by Farinacci (1996, 2002) and Farinacci *et al.* (1997) in the Central Mediterranean Apennine areas. The most distinctive features of the External Dorsale are: (1) the rosso-ammonitico facies and cherty limestones, which can start as early as the Sinemurian (e.g. *Arnioceras*-rich strata, Fallot 1937; Griffon 1966); (2) the red and/or green radiolarites, the onset of which occurred as early as the Liassic–Dogger transition (El Kadiri 1984, 1991). For this reason, they were considered as being amongst the earliest continental-margin-related Jurassic, biosiliceous deposits in the Tethyan realm (De Wever *et al.* 1985). They continued until early Tithonian time (El Kadiri 1991).

In both Dorsale units, Cretaceous successions recorded important hiatuses during the Hauterivian–Albian *pro parte* and the early Senonian, the best characterized ones being the Campanian and Maastrichtian *Globotruncana*-rich marly mudstones referred to as 'Capas Rojas' and 'Capas Blancas', respectively (El Kadiri 1991). Palaeogene successions consist of: (1) thin nodular black shales of Paleocene age; (2) variegated marl–nummulitic sand alternations of Eocene–mid-Oligocene age (Griffon 1966; Raoult 1966; Nold *et al.* 1981; Maaté *et al.* 1993; Hlila 1994, 2005; Maaté 1996); (3) micaceous rust-coloured sandstones, during the late Oligocene–(?)early Aquitanian.

Tectonically, the fact that the latter deposits are considered as being the youngest strata trapped between different slices (Nold *et al.* 1981) suggested a first phase of thrusting during the Aquitanian. Later, characterization of early Burdigalian marine strata involved in both the internal and external fronts of the Dorsale Calcaire (Feinberg & Olivier 1983; Ben Yaïch *et al.* 1986; Feinberg

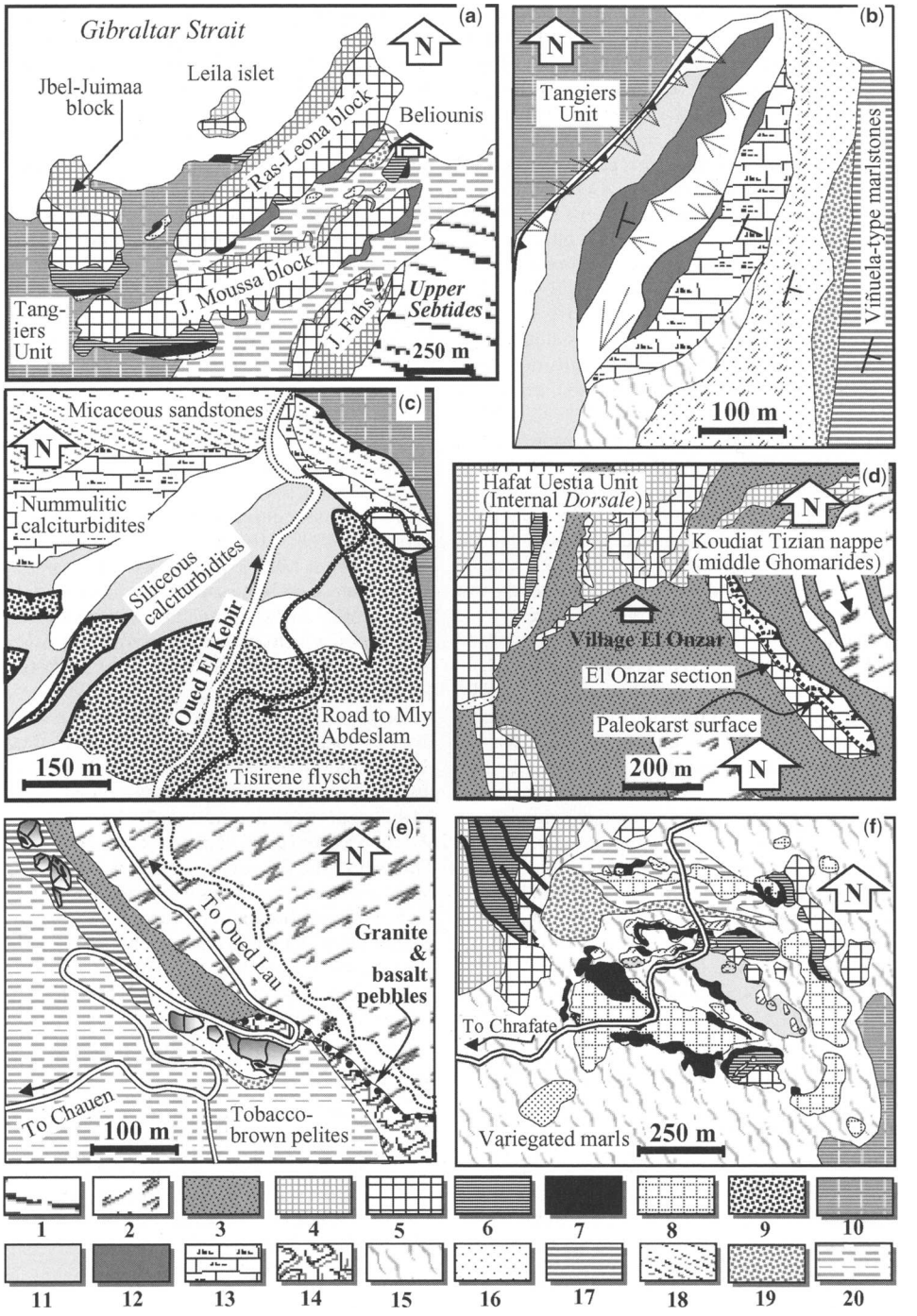

Fig. 2. Geological–structural setting of the areas including the investigated successions. (**a**) Jbel Moussa Group (modified from Kornprobst & Durand Delga 1985); (**b**) northern part of the Tamezzakht sector (this work); (**c**) main lithological components of the Mauretanian series cropping out the vicinity of the Oued-El-Kébir in the Béni Ider area (simplified from Didon 2006); (**d**) example of a residue of the karstified Ghomaride carbonate cover close to the Internal Dorsale (El Onzar succession, simplified from Raoult 1966); (**e**) Ghomaride siliciclastic cover in the Talembote area (simplified from El Kadiri *et al.* 2001), (**f**) western Chrafate Klippes, a good example of the Predorsalian olistostromes

et al. 1990; El Kadiri *et al.* 2001) led researchers to envisage a second phase, during which the whole Dorsale nappe pile underwent large-scale thrusting before being trapped between the Ghomaride terranes and the flysch–nappe domain. In some segments (Haouz chain), the latter event resulted in a double 'encapuchonnement' process (e.g. Raoult 1966; Hlila 1994, 2005), a kinematic scenario that explains the backthrusting and related fan-shaped structures.

The northern part of the Rif calcareous chain (Dorsale Calcaire) is occupied by the Jbel Moussa Group, which is dominated by four kilometre-scale juxtaposed tilted blocks (J. Moussa, J. Juimaa and Ras Leona and Leila) of a Jurassic continental passive palaeomargin (El Kadiri *et al.* 1990; El Hatimi 1991). All these blocks exhibit Triassic–early Cretaceous successions that strongly recall the Spanish Penibetics (Fallot 1937; El Hatimi 1991), the Gibraltar and Los Pastores massifs (Durand Delga & Villiaumey 1963), and/or the Southern Middle Subbetics (El Kadiri *et al.* 1990). The fact that the J. Moussa Group is thrust directly over the Tangiers units and its Spanish equivalents (Gibraltar and Pastores, both occurring in the external Campo de Gibraltar area), led Durand-Delga (1972, p. 274) to assign all these calcareous blocks to an external 'Cretaceous cordillera' separating the Mauretanian and the Massylian basins. This palaeogeographical setting proved to be identical to that proposed by Raoult (1974) for the Algerian 'Prekabyle basement'. Concurrently, Didon *et al.* (1973) defined the Predorsalian units as corresponding to a narrow basin externally bordering the Dorsale Calcaire units. It is noteworthy that the Predorsalian zone was characterized by the Aquitanian Numidian-like sandstones (the so-called 'Beliounis sandstones'), which were fundamentally defined in the J. Moussa Group itself. Thus, this Group implicitly bears the double definition of a Predorsalian zone and an external ridge. The 'Tariquide Ridge' is herein used in the strict sense of a high palaeogeographical zone delivering shallow-water carbonate material (calciturbidites) to both the Predorsalian and the Mauretanian trough during the late Cretaceous–early Oligocene.

The External zones are dominated by large-scale 'parautochthonous' terranes (the Tangiers, Ketama and Loukous units, mainly), and their overriding sandstone–flysch nappes. These in turn may thrust each other along well-delineated parallel structures, which act as the topographical lines of the Gibraltar arc. Although palaeogeographical reconstructions of the External zones still remain a subject of debate, especially for the Mesozoic, there is agreement that their tectonosedimentary evolution during the Tertiary was primarily conditioned by piggy-back basins and ramp-anticline structures, both generated by deep detachment planes (e.g. Morley 1987, 1988, 1992; Ben Yaïch 1991).

Close to the internal border, the External Domain (the so-called Intrarif) was strongly deformed so that its parautochthonous units locally show schistosity (Andrieux 1971; Frizon de Lamotte 1985) and the flysch successions were totally uprooted. The deformation style is predominantly characterized by duplex structures and imbricate slices.

Stratigraphic reconstructions carried out mainly by Durand-Delga (1972) and Durand Delga & Didon (1984*a*,*b*) led researchers to recognize the two main flysch successions previously defined in the Kabylian domains (Bouillin *et al.* 1970): (1) the Mauretanian series, which includes in its lower half the Tisirène early Cretaceous calciturbidites and holoquartzous sandstones, and in its upper half the Béni Ider late Cretaceous–Aquitanian calciturbidites and micaceous sandstones; (2) the Massylian series, which may encompass in a single stratigraphic column the Barremian–Albian olive–green sandstone flysch (Massylian *sensu*

Fig. 2. *Continued.* (simplified from El Kadiri 1984). 1, low-grade-metamorphosed Triassic strata (Federico units, upper Sebtides); 2, Palaeozoic schists; 3, Verrucano-type Triassic red sandstones; 4, late Triassic dolomites; 5, earliest Liassic massive limestones; 6, mid- to late Liassic pelagic successions (cherty limestones and/or rosso-ammonitico facies); 7, mid- to late Jurassic red radiolarites; 8, latest Tithonian–Berriasian *Aptychus*-bearing calciturbidites; 9, Aptian–Albian, thick-bedded, fine-grained sandstones (Tisirene flysch); 10, carbonate-poor, green pelites (Tangiers units, Campanian–Maastrichtian mainly); 11, Campanian–Maastrichtian (mainly) calciturbidites of the Mauretanian series and the Chrafate Klippes; 12, *Microcodium*-bearing Paleocene calcarenites; 13, Nummulite-rich, white massive grainstones (El Onzar succession, (d)) and calciturbidites (Tamezzakht and Oued-El-Kébir areas; (b) and (c), respectively); 14; late Oligocene chaotic mixture of the Talembote area, reworking Triassic strata, with a basal coarse-grained conglomerate rich in granite and basalt pebbles; 15, latest Eocene–mid-Oligocene variegated marls with large-scale olistoliths, particularly in the Predorsalian zone; 16, late Oligocene–Aquitanian yellow soft marls with large-scale olistoliths inherited from Triassic and Eocene massive carbonates (Tamezzakht and Talembote successions, (b) and (e), respectively); 17, early Burdigalian Viñuela-type green pelagic marlstones with similar large-scale olistoliths (in Tamezzakht and Talembote areas); 18, late Oligocene–early Burdigalian micaceous sandstones (the so-called 'Béni Ider' Flysch); 19, late Oligocene–Aquitanian holoquartzose yellow sandstones (the so-called 'Beliounis' sandstones); 20, early Burdigalian, carbonate-poor, tobacco brown pelites and holoquartzose tobacco brown channelized sandstones (Talembote and Chrafate Klippes).

stricto) and the late Oligocene–Aquitanian Numidian sandstones. However, in the latter case upper Cretaceous transitional strata are not yet clearly characterized.

On the whole, these flysch series were used to define the Maghrebian 'Flysch Trough' (Didon *et al.* 1973; Bourgois 1978; Durand-Delga 1980; Martin-Algarra 1987), along which the Mauretanian flyschs were located, close to the AlKaPeCa palaeomargin (Bouillin *et al.* 1986). In contrast, the Massylian flyschs were located close to the African palaeomargin (e.g. Raoult 1974). In the Rif domain the latter palaeomargin is represented by the Jurassic terrigenous series (mainly 'Ferrysch' successions, Wildi 1981) known in the Mésorif and Prérif zones (e.g. compiled data of Ben Yaïch 1991; Benzaggagh 1996).

On the basis of the stratigraphic data given below, we shall see that the Flysch Trough can no longer be considered to be formed by a single, large-scale homogeneous basin, as the existence of external isolated platform(s) subdivided it into at least two elementary basins (see also El Kadiri *et al.* 2003).

Stratigraphic framework of the selected successions

Six study areas (Fig. 2) have been selected from the principal domains known in the Internal zones and the surrounding External ones, namely the Ghomarides, the Dorsale Calcaire, the 'Tariquide Ridge' and the Flysch Trough. Their stratigraphic successions are thoroughly reassessed (Fig. 3) and their possible juxtaposition during the early Burdigalian is outlined to better assess the sources of the carbonate clastic material. The Tamezzakht succession appears to be the most complete, as it spans a wide time-interval ranging from the latest Cretaceous to the early Burdigalian. Thus, it provides a rare opportunity to appraise a long-term tectonosedimentary evolution through a single stratigraphic column.

In the Ghomaride domain

The El Onzar and Dradia successions (Figs 2d and 3) crop out close to the Ghomaride–Dorsale boundary in the northernmost part of the Ghomaride domain, north of the city of Tetuan. They provide some of the best evidence known for the Ghomaride Eocene cover. In addition to the lithostratigraphic description and dating controls given by several workers (e.g. Raoult 1966; El Kadiri *et al.* 1992; Maaté 1996) and completed herein, we have found two complex discontinuity surfaces in these successions, at the very base of the Eocene strata and at their top.

In both outcrops, white nummulitic sandstones and Nummulite-rich massive grainstones rest on early Liassic white massive limestones after a conspicuous palaeokarst discontinuity (palaeokarst surface 1, Figs 2 and 3). This may indicate that the Ghomaride terranes experienced a protracted emersion history during the Mesozoic–Paleocene, resulting in the near-complete removal of their carbonate cover.

The stratigraphic top of the nummulitic white limestone bar (10–30 m) in turn shows an important palaeokarst surface (palaeokarst surface 2, Fig. 3). In some cases (El Onzar succession), karstic relief (small-scale kamenitzas and palaeosinkholes) is filled with red to brown sandstones made up of the 'en-echarde'-type quartz, which originated from pedological processes (Meyer 1987). An algal–*Discocyclina*-rich grainstone bed (0.10–1 m) transgressively rests on the palaeokarst surface. It is generally capped with a remarkable Fe-crust (Fe-HG, Fig. 3), from which bacteria-produced Fe-epigenesis processes (e.g. Préat *et al.* 2000; El Kadiri 2002*a*) may extend several decametres downwards into the host rock, which becomes rust coloured. Outcrop survey shows that this Fe-crust also may directly cap the underlying nummulitic bar when the transgressive *Discocyclina*-rich deposition is laterally lacking, as occurs in many transgressive deposits (e.g. lag gravel of Plint (1988), transgressive lag deposit of Fürsich *et al.* (1991), transgressive lags of Burkhalter (1995) and hiatal shell concentrations of Rivas *et al.* (1997), among others). Thus, the double discontinuity (palaeokarst + HG) at the top of the nummulitic bar may best be classified as a rock-ground surface in the sense of Clari *et al.* (1995).

Dating controls based on benthic Foraminifera lead us to assign the stratigraphic top of the nummulitic bar to the late Lutetian (e.g. Raoult 1974; see also Table 1, sample ONZ 5).

Yellow to rust-coloured marls (20–30 m) sharply overlie the Fe-hardground surface. In their upper half they contain fine-grained sandstone intercalations, which progressively dominate the depositional regime (see the possible interpretation below). They yield planktonic Foraminifera indicating a latest Lutetian–Early Bartonianage (Table 1, sample ONZ 10)

In the Talembote area (Fig. 2e) located 40 km south of the city of Tetuan close to the Internide–Externide front, decametre-scale sedimentary klippes are embedded within an Aquitanian–early Burdigalian siliciclastic matrix (Fig. 3). They exhibit an identical Liassic–Eocene stratigraphic succession with the same discontinuities and lithological components, and their presence here may have an important bearing on the palaeogeographical reconstructions (see below).

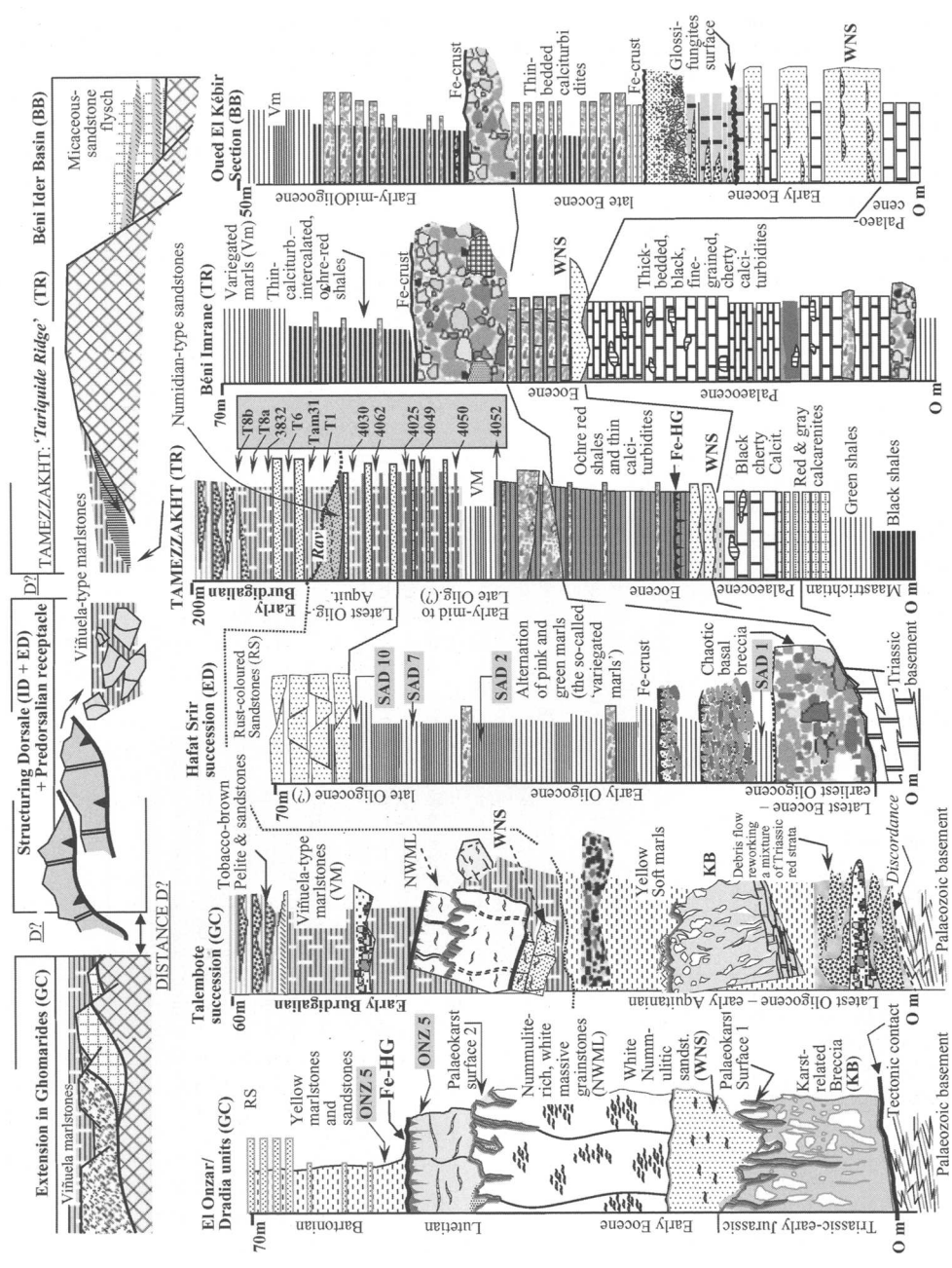

Fig. 3. Stratigraphic correlation of the studied successions, selected from distinct domains of the northwestern Rif belt: the Ghomaride domain (Dradia–El Onzar units, Talembote succession), the (Calcareous) Dorsale Calcaire (Hafat Srir succession) of the Internal zones; the Predorsalian fringe (Béni Imrane succession), and the Béni Ider area (Oued-El-Kébir section) of the External zones (see text for details). The upper part of the figure tentatively proposes a possible reconstruction of this scenario during the early Burdigalian, i.e. just before the orogenic paroxysm (the shortening distance D? remains uncertain). Grey shading indicates the sampling levels from which new biostratigraphic dates are given in Tables 1 and 2.

Table 1. *Foraminifera assemblages found in the El Onzar succession (Ghomaride Eocene cover) and the latest Eocene–mid-Oligocene Hafat Srir succession (Internal Dorsale south of the city of Tetuan)*

Sections samples and levels	Planktonic and benthic Foraminifera	Age
Hafat srir section (Internal Dorsale)		
SAD 10 (topmost level of the marly succession)	*Globigerina galavisi* Bermúdez, *G. tripartita* Koch, *G. ampliapertura* Bolli, *G. increbescens* Bandy, *G. venezuelana* Hedberg, *G. euapertura* Jenkins, *G. eocaena* Gumbel, *G. corpulenta* Subbotina, *G. praebulloides* Blow, *Globigerina ouachitaensis* H. & Wall, *G. ciperoensis* Bolli, *Neogloboquadrina opima* Bolli (?), *N. nana* Bolli, *Globorotaloides suteri* Bolli, *Catapsydrax unicavus* B. Loeb. & Tap., *C. dissimilis* Cush. & Berm	Late mid-Oligocene
SAD 7 (upper part of the marly succession)	*Globigerina galavisi* Bermúdez, *G. tripartita* Koch, *G. venezuelana* Hedberg, *G. euapertura* Jenkins, *G. ampliapertura* Bolli, *G. increbescens* Bandy, *G. angiporoides* Hornibrook, *G. eocaena* Gumbel, *G. corpulenta* Subbotina, *G. praebulloides* Blow, *G. ouachitaensis* H. & Wall, *G. ciperoensis* Bolli, *Neogloboquadrina nana* Bolli, *Globorotaloides suteri* Bolli, *Catapsydrax unicavus* Loeb. & Tap, *C. dissimilis* Cush. & Berm	Late early Oligocene
SAD 2 (middle part of the marly succession)	*Globigerina galavisi* Bermúdez, *G. venezuelana* Hedberg, *G. euapertura* Jenkins, *G. ampliapertura* Bolli, *G. increbescens* Bandy, *G. angiporoides* Hornibrook, *G. eocaena* Gumbel, *G. corpulenta* Subbotina, *G. ouachitaensis* H. & Wall, *G. praebulloides* Blow, *Neogloboquadrina nana* Bolli, *Globorotalia gemma* Jenkins, *Globorotaloides suteri* Bolli, *Catapsydrax unicavus* B. Loeb. & Tap, *C. dissimilis* Cush. & Berm, *Psuedohastigerina micra* (Cole)	Early Oligocene
SAD 1 (yellow-marl-intercalated basal breccias)	*Globigerina galavisi* Bermúdez, *G. tripartita* Koch, *G. venezuelana* Hedberg, *G. increbescens* Bandy, *G. eocaena* Gumbel, *G. corpulenta* Subbotina, *Globigerina praebulloides* Blow, *Globigerinatheka subconglobata* (Shut.), *Globigerinatheka index* (Finlay), *Globigerinatheka semiinvoluta* (Keijzer), *Turborotalia cerroazulensis* Cole, *T. cocaensis* Cushman, *Globorotaloides suteri* Bolli	Latest Eocene
El onzar section (Ghomaride cover)		
ONZ 10 (lower part of the marl–sandstone alternation)	*Subbotina linaperta* (Finlay), *S. frontosa* (Subbotina), *S. inaequispira* (Subbotina), *Muricoglobigerina senni* (Beckman), *Acarinina primitiva* (Finlay), *A. broedemanni anapates* (Cus & ber.), *A. bullbrooki* (Bolli), *A. spinuloinflata* (Bandy), *A. cuneicamerta* (Blow), *Morozovella spinulosa* (Cushman), *M. lehneri* (Cush. & Jarvis), *Trucarotaloides topilensis* (Cushman), *T. pseudodubia* (Bandy), *Clavigerinella eocanica* (Nuttall), *Globigerinatheka subconglobata* (Shut.) *Globigerinatheka kugleri* (Bolli, Loeb. & Tapp.), *Globigerinatheka index* (Finlay), *Turborotalia pessagnoensis* (Tou. & Bol.), *Neogloboquadrina griffinae* Blow, *N. wilsoni* (Cole), *Globigerinella subangulata* Eugeno	Latest Lutetian to early Bartonian
ONZ 5* (stratigraphic top of the nummulitic bar)	*Discocyclina* sp., *Nummulites millecaput* (Boubee), *N. maximus* D'Archiac, *Assilina* sp., *Asterigerina* sp.	Late Lutetian

*Benthic Foraminifera.

The most noteworthy feature of the Talembote Tertiary succession is the facies contrast, which is well marked in the field, between its four sedimentary formations ranging from the late Oligocene to the early Burdigalian (El Kadiri *et al.* 2001, and Fig. 2e). For regional correlation, it is relevant to note the sharp facies change from the yellow soft marls of the second formation (latest Oligocene–Aquitanian *pro parte*) to the green pelagic marlstones of the overlying third formation (earliest Burdigalian). The former facies is particularly rich in planktonic Foraminifera (El Kadiri *et al.* 2001) and contains in its upper half spaced intercalations of yellow Alozaina-type sandstones, a facies widespread in the Aquitanian Malaguide cover and that of the northern part of the Ghomaride terranes. The second contains siliceous horizons and strongly recalls the Viñuela-type pelagic deposition (El Kadiri *et al.* 2001).

Various coarse-grained breccia flows are intercalated within the Talembote pelagic successions. All exhibit the same mixture of carbonate and metamorphic clastic material, with the ubiquitous Nummulite-rich and reefal boundstone blocks derived from a lost Palaeogene carbonate platform. Also ubiquitous are granitic and alkaline-basalt pebbles. The former were discovered *in situ* within the Carboniferous Marbella conglomerates, from which they are presumed to have been derived. In contrast, the origin of the alkaline basalts still remains unclear.

In the Internal zones of the Betic Cordillera, the coeval early Burdigalian Las Millanas–Viñuela Formation contains a basal conglomerate exhibiting the same clastic mixture. This may indicate that the source of supply was the same and had a wide palaeogeographical extent. Otherwise, it is relevant to note the presence, within the Spanish early Burdigalian conglomerates, of almost unaltered blocks and pebbles of the usual Alpujarride–Sebtide facies, namely peridotites and garnet gneiss. Such pebbles have not yet been discovered in the Ghomaride cover.

In the Dorsale Calcaire

In the Dorsale Calcaire the most pronounced discontinuity is delineated by the widespread late Eocene–early Oligocene Breccias Nummuliticas (Nold *et al.* 1981) that independently rest on normal-fault-denuded Triassic or Jurassic strata, which pinpoint a regional extensional event. The Hafat Srir section, cropping out in the northern part of the Internal Dorsale (south of the city of Tetuan), provides a good example of this: it starts with a 5 m thick, ungraded, coarse-grained nummulitic breccia bed (facies R1 of Lowe 1982; facies F3 of Mutti 1992) that directly reworks pedologically pre-altered, rust-coloured Triassic dolomites. This basal breccia passes up into a thinning-upward alternation (*c.* 150 m thick) of pelagic marls and graded breccias. Well-developed Fe-crusts carpet near all the basal breccia beds. Yellowish pelagic marls, between them, yield planktonic Foraminifera indicating a latest Eocene age (Table 1, sample SAD 1). The overlying marly succession, which spans the early to mid-Oligocene interval (Maaté *et al.* 1993; Table 1, samples SAD 2, 7 and 10), comprises a rhythmic metre-scale alternation of carbonate-rich green marls and carbonate-poor pink marls, a fact that may be ascribed to cycles related to the calcite compensation depth (CCD) fluctuation, redox and/or productivity (Eicher & Diner 1991; Einsele & Ricken 1991). The Hafat Srir marly alternation may satisfactorily be used to interpret the origin of the widespread early to mid-Oligocene 'variegated marls' as the result of reworking and mixing by slope processes of the same kind of cyclic deposits.

These marly deposits are sharply overlain, after an erosive surface, by micaceous, wood-debris-bearing, rust-coloured sandstones, probably of late Oligocene–Aquitanian age (Hlila 2005). The onset of this siliciclastic depositional regime may be ascribed to a second extensional event, as shown by numerous synsedimentary normal faults. In thin section the rust colour is proved to be due to the presence of a large amount of pre-rubefaction, palaeosoil-derived carbonate clasts together with white and black quartz grains.

In the Predorsalian zone

The most representative successions of the Predorsalian zone crop out in the well-studied Chrafate klippe area (Didon *et al.* 1973; Lespinasse 1975; Nold *et al.* 1981; El Kadiri 1984, 1991; Olivier 1984; Ben Yaïch *et al.* 1988) where the early Oligocene 'variegated marls' (Fig. 2f) form decametre- to hectometre-scale sedimentary klippes, inherited from Dorsale-type lost units, and pass upward into late Oligocene–Aquitanian Numidian-like sandstones (i.e. Beliounis sandstones, Didon *et al.* 1973). These two stratigraphic components (olistostromes and sandstones) are separately known in the Internal domain and the External one, respectively. As part of this peculiar zone we would like to consider the Tamezzakht stratigraphic succession (Figs 1, 2b and 3), which also combines features separately known in the Internal domain and the External one. This succession displays in its lower half a late Cretaceous–early Oligocene calciturbidite–shale alternation, similar to that of the external Béni Ider series. In contrast, its upper half is chiefly made up of early to mid-Oligocene variegated pelagic marls and rust-coloured

sandstones. The latter are developed in the same Dorsale-type facies (see Table 2 for dating controls). They pass upward into late Oligocene–early Burdigalian pelagic deposits made up of yellow marls–green marlstone couplets identical to those previously described in the early Miocene Ghomaride cover. In addition, the intercalation within the late Oligocene–Aquitanian levels of the Beliounis-type sandstone facies supports the attribution of the Tamezzakht succession to the Predorsalian zone.

In thin section, the calciturbidite flows commonly reveal the presence of carbonate clasts, whose facies strongly recalls the Internal Dorsale Jurassic series, namely the shallow-water white massive grainstones (earliest Liassic) and the *Calpionella–Saccocoma*-rich mudstones (Tithonian–Berriasian). However, the interposition of the External Dorsale between the Internal one and the Predorsalian zone, on the one hand, and the proximal character of the calciturbidite discharges, on the other, lead us to suggest a distinct carbonate source with respect to the Internal domain. Palaeocurrent directions that we have measured on the bed surfaces of the calciturbidite interval are N70°–N80°, with the current flowing towards the internal zones (from WSW to ENE, i.e. from an external source). In the overlying siliciclastic interval the current direction is N20°–N60°, mainly N30°–N40°, flowing from SW to NE. Thus, the clastic material of the Tamezzakht succession could be sourced from an external lost terrane, a result that fits well with the 'Tariquide Ridge' hypothesis (Durand-Delga 1972) and recalls the Penibetic and/or Ultra-Internal Subbetic seamounts of the southern Betic Cordillera.

The most noteworthy feature of the Tamezzakht pelagic marly deposits (late Oligocene–early Burdigalian) is the rhythmic alternation of yellow soft marls and green marlstones. In the Ghomaride cover, both facies are strictly limited to the latest Oligocene–Aquitanian and the early Burdigalian, respectively.

Surrounding External Domain

Two Paleocene–mid-Oligocene successions with stratigraphic features similar to those previously described can be selected from the surrounding External Domain: the Béni Imrane succession, which crops out north of the city of Tetuan between the Predorsalian zone and the Tangiers unit, and the Oued-El-Kebir succession cropping out along the main river crossing the Béni Ider area, 25–30 km SW of the city of Tetuan (Fig. 2c).

Black, thick-bedded cherty mudstones rich in small planktonic Foraminifera (*Subbotina pseudobulloides* (Plummer) and *Planorotalites compressa* (Plummer)) of Paleocene age make up the lower half of the Béni Imrane succession (*c.* 30 m). They can be accompanied by a channelized, coarse-grained basal division, which reveals that the black mudstones came from up-slope pelagic muds. They are sharply overlain by *c.* 5 m thick, thin-bedded calciturbidites with the sandy fraction being rich in penecontemporaneous Nummulites of Eocene age. Hence, there has been an important environmental change affecting the source area across the Paleocene–Eocene boundary, from exporting plankton-dominated muds into producing and shedding shallow-water-rich bioclastic sands together with an important lithoclastic fraction deriving from its carbonate substratum. A channelized white, Nummulite-bearing sandstone bed (WNS, Fig. 3) occurs in the intervening the stratigraphic levels. The latter facies also appears at the very base of both the Eocene deep-sea calciturbidites of the Tamezzakht succession and the Eocene shallow-water, limestone bar of the Ghomaride cover, a result that suggests key strata of regional correlation potential (WNS, Figs 3 and 4).

A 3–5 m thick, coarse-grained, poorly graded conglomerate bed sharply overlies the calciturbidite interval. It is covered with an Fe-crust and probably pinpoints the same extensional event that resulted in the latest Eocene–early Oligocene chaotic breccias in the Internal Dorsale and the Tamezzakht succession. The Béni Imrane Palaeogene series ends with a shaly interval (most probably of early to mid-Oligocene age, by comparison with dating controls obtained from Tamezzakht similar levels), made up in its lower half of ochre–red, lime-poor shales with thin intercalations of calciturbidites, and in its upper half of variegated marls.

The Oued-El-Kébir section exhibits the same lithostratigraphical features, particularly: (1) the WNS key strata; (2) the Fe-crust-capped, chaotic breccia overlying the Eocene calciturbidites; (3) the early to mid-Oligocene ochre–red shales, a facies well known in the remainder of the external Béni Ider area (the so-called 'flysch coloré').

Regardless of the relative palaeogeographical position of the Oued-El-Kébir section, the entire Palaeogene stratigraphic evolution outlined in the Internal domain and close to its border seems to have been strongly influenced by a neighbouring carbonate platform. By the beginning of the late Oligocene, the total disappearance of the clastic carbonate material was combined with the onset of the siliciclastic depositional regime. Thus, at that time, the supplying carbonate platform(s) was (were) probably destroyed and/or drowned under the siliciclastic accumulations. In both cases, the sharp contact between the early–mid-Oligocene calciturbidite-intercalated red shales and the late Oligocene sandstone-intercalated yellow marls may be regarded as a depth-equivalent of the

Table 2. *Foraminifera assemblages found in the upper half of the Tamezzakht succession (Predorsalian zone)*

Main facies and samples	Planktonic Foraminifera and Calcareous nannoplankton	Age
Viñuela-type marlstone-dominated alternation		Late early-Burdigalian
T 8b*	*Helicosphaera carteri, H. kamptneri, Sphenolithus gr. abies/neoabies, Cyclicargolithus floridanus, C. abisectus, Reticulofenestra pseudoumbilica*	
T 8a*	*Helicosphaera carteri, H. kamptneri, Sphenolithus gr. abies/neoabies, Cyclicargolithus floridanus, C. abisectus, Reticulofenestra cf. pseudoumbilica*	
3832 and 3822	*Globigerina venezuelana* Hedberg, *G. praebulloides* Blow, *G. woodi* Jenkins, *Globigerinoides altiaperturus* Bolli, *Neogloboquadrina nana* (Bolli), *N. siakensis* (LeRoy), *Globoquadrina baroemoenensis* (LeRoy), *Globorotaloides suteri* Bolli, *Catapsydrax unicavus* Bolli, Loeblich & Tappan, *C. dissimilis* (Cushman & Bermùdez)	Early Burdigalian
T 6*	*Helicosphaera ampliapertura, H. scissura, Sphenolithus gr. abies/neoabies*	
Tam 31*	*Helicosphaera ampliapertura* (small variety), *H. carteri, H. kamptneri, Sphenolithus gr. abies/neoabies, Cyclicargolithus floridanus, C. abisectus*	
T 1*	*Helicosphaera ampliaperta* (small variety), *Discoaster druggii, D. deflandrii, Cyclicargolithus floridanus, C. abisectus, E. formosa*	
Beliounis-type sandstones		
4030	Planktonic Foraminifera as in sample 4049, but with *N. siakensis* (LeRoy)	Aquitanian (?) to Late Olig.
Yellow-marl-dominated alternation		
4062	Planktonic Foraminifera as in sample 4049, but with *N. siakensis* (LeRoy)	Late mid-Oligocene
4025	Planktonic Foraminifera as in sample 4049	
4049	*Globigerina galavisi* Bermùdez, *G. tripartita* Koch, *G. venezuelana* Hedberg, *G. euapertura* Jenkins, *G. ampliapertura* Bolli, *G. increbescens* Bandy, *G. eocaena* Gumbel, *G. corpulenta* Subbotina, *Neogloboquadrina opima* (Bolli), *N. nana* (Bolli), *Globorotaloides suteri* Bolli, *Catapsydrax unicavus* Bolli, Loeblich & Tappan, *C. dissimilis* (Cushman & Bermùdez)	
4050	*Globigerina galavisi* Bermùdez, *G. corpulenta* Subbotina	
Nummulitic sand-intercalated red shales		
4052	*Globigerina galavisi* Bermùdez, *G. venezuelana* Hedberg, *G. euapertura* Jenkins, *G. ampliapertura* Bolli, *G. prebulloides* Blow	Early to mid-Oligocene

*Calcareous nannoplankton.

drowning–suffocation discontinuity in the sense of Schlager (1989, p. 7).

Petrographical evidence from the very base of the graded sandstone beds shows a mixture of basement-derived detrital fragments, namely, filonian-type quartz, schist, feldspar and micas. They are probably sourced from a tectonically raised, new source area(s). Regional correlations with both the External domain and the Internal one support such an assumption (see below).

Discussion: regional correlations

Figure 4 summarizes the facies contents of the palaeogeographical domains outlined in Figure 3, and highlights the recognized discontinuities (erosional, palaeokarstic and Fe-hardground-type surfaces) and the main calciturbidite and tectono-sedimentary events. It should be noted that the Tamezzakht succession appears to be the most complete, with its facies being more clearly contrasted in the field (El Kadiri *et al.* 2005). Its position in a transitional area between the Internal domain and the External one makes it a useful starting point for regional correlations. From the latest Cretaceous onwards the main lines of comparison are described below (see also Fig. 3).

The latest Maastrichtian–early Paleocene pelagic-dominated strata (black shales and reduced ochre–red shales, facies 5 and 6, respectively, Fig. 4) at the base of the Tamezzakht succession strongly recall their time-equivalent strata known in (1) the Dorsale Calcaire as Capas Blancas (facies 3, Fig. 4), made up of dark-coloured marl–limestone alternations (of Maastrichtian–(?)Paleocene *pro parte* age, Griffon 1966; El Kadiri 1991); (2) the Jbel Moussa Group in the facies of ochre–red and black, lime-poor shales of lower Paleocene age (facies 6b, Ras Leona and Taoura sections, El Kadiri *et al.* 1990); (3) the southernmost External Dorsale ('Col de l'Abri' section, Nold *et al.* 1981; El Kadiri 1984) in the facies of variegated to ochre–red lime-poor shales of Maastrichtian–(?)Paleocene *pro parte* age (facies 4). In contrast, the Maastrichtian–Paleocene strata in the Béni Ider area are represented by thick packages of mixed carbonate–siliciclastic turbidites (facies 7, El Kadiri *et al.* 2003), but within which intercalations of ochre–red lime-poor shales are a very common component.

The thick-bedded late Paleocene dark-coloured calciturbidites (facies 11) present a striking lithofacies analogue in the Béni Imrane area located 5 km NW of Tetuan, which may correspond to a lateral equivalent of the Tamezzakht succession. In the southern Dorsale Calcaire units Paleocene strata are generally poorly characterized and in most cases dating controls do not allow us to distinguish them from the underlying condensed late Cretaceous pelagic deposits or the overlying Eocene marly strata (Nold *et al.* 1981, p. 134). In its northern part, near the Kobat Sidi Kmim slice, a coarse-grained chaotic breccia (*c.* 15–20 m thick, facies 9) unconformably overlies a Campanian–Maastrichtian Capas Rojas–Capas Blancas pelagic series (facies 1 and 3). Dark-coloured marls intercalated between the basal breccia flows contain planktonic Foraminifera of late Paleocene age (El Kadiri *et al.* 2003). The most conspicuous example of Paleocene gravity-flow events was found in the J. Moussa Group: as noted by El Hatimi (1991) and El Kadiri (1991), its largest elements, of up 1 km in length (Ras Leona and J. Moussa Blocks), are partly embedded within ochre–red and black shales of Late Maastrichtian–Paleocene age (facies 12). All these Paleocene chaotic breccia were probably linked to regional tectonic pulses, as they form also a widespread key stratum in the Kabylian domain (e.g. Raoult 1974). In many places throughout the northern Dorsale Calcaire (Haouz Belt), Raoult (1966) noted a Paleocene age for the *Microcodium*-bearing calcareous sandstones (facies 10, Fig. 4), which transgressively overlie the massive carbonate formations. Ben Yaïch *et al.* (1986) and Hlila (2005) described and dated in the Oued El Gharraq section an interesting dark-coloured glaucony-rich, bioclastic level (*c.* 30 cm, facies 8), which transgressively erodes late Cretaceous 'Capas Blancas'-type strata, and lies at the very base of the white massive Nummulite-rich grainstones (facies 14b). Similarly, *Microcodium*-bearing calciturbidites characterize the late Paleocene calciturbidites in the Flysch Trough (facies 13).

Petrographical evidence from the Maastrichtian–Eocene Tamezzakht calciturbidites (facies 6–11) and from the Béni Ider Flysch Trough (facies 2, 7 and 13), show that the reworked lithoclasts were inherited from Triassic–early Jurassic, massive carbonate formations, mainly dolomites and white massive limestones, as well as from latest Jurassic–earliest Cretaceous pelagic series, namely *Calpionella*- and/or *Saccocoma*-rich mudstones. Complementary results have been obtained from equivalent late Cretaceous–early Oligocene calciturbidite strata of the Béni Ider area by Blumenthal *et al.* (1958), and recently by El Kadiri *et al.* (2003, 2006). Interestingly, such facies make up precisely the successions known in the Internal Dorsale units (e.g. Griffon 1966; Raoult 1966; Nold *et al.* 1981; El Kadiri *et al.* 1989; Maaté 1996) and the Jbel Moussa Group (El Kadiri *et al.* 1990). In contrast, lithoclasts derived from key facies of the External Dorsale (red radiolarites, *Aptychus*-rich mudstones) are lacking despite the fact that the

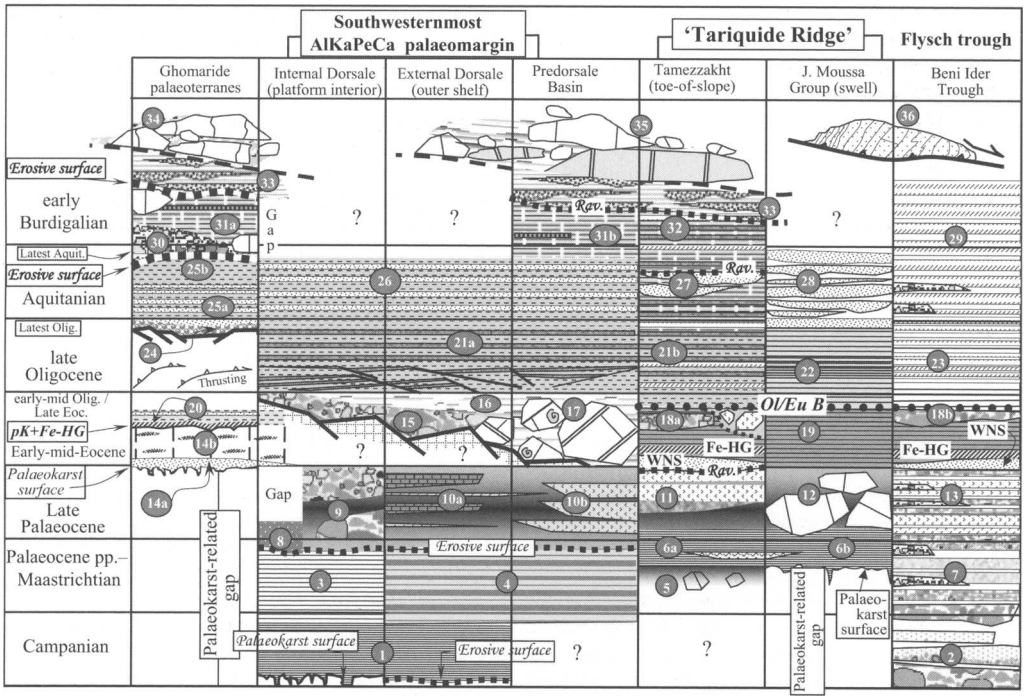

Fig. 4. Facies correlation and the tectonosedimentary events in the southwesternmost AlKaPeCa palaeomargin, the Tariquide Ridge and the Flysch Trough, based on selected data from: the Talembote area (Ghomaride terranes), Oued El Gharraq and Hafat Srir sections (Internal Dorsale), J. Lakraa, Hafat Nator, Saaden and Ametrasse–Bettara units (External Dorsale), Chrafate Klippes (Predorsalian domain), Beliounis and Ras Leona Klippes of the eastern part of the J. Moussa Group (Tariquide Ridge) and the Oued-El-Kébir successions (Béni Ider trough). 1, 'Capas Rojas'-type marlstones; 2, thick-bedded calciturbidites; 3, 'Capas Blancas'-type marlstones; 4, variegated marls (scaglia rossa facies); 5, black shales and resedimented blocks; 6, ochre–red marlstones and slope calcarenites in Tamezzakht (6a) and the eastern J. Moussa Group (6b); 7, calciturbidite–black shale alternation; 8, glaucony-rich bioclastic wackestones of the Oued El Gharraq section); 9, chaotic megabreccias and black shales (Kobat Sidi Kmim section); 10, black-shale pelagic limestone alternation (10a) and *Microcodium*-bearing turbidites and pelagic mudstone (10b); 11, *Microcodium*-rich, thick-bedded calciturbidites; 12, hectometre-scale olistoliths, i.e. eastern elements of the J. Moussa Group; 13, medium- to thick-bedded *Microcodium*-rich calciturbidites (late Paleocene); 14a, early Eocene, Nummulite-bearing white sandstones; 14b, Nummulite-rich massive white limestones; 15, latest Eocene–earliest Oligocene coarse-grained conglomerates (the so-called Breccias Nummuliticas); 16, variegated marls; 17, large-scale olistoliths embedded within the latest Eocene–early Oligocene variegated marls (i.e. Chrafate Klippes, Assifane blocks, etc.); 18a, 18b, coarse-grained calciturbidites and olistoliths; 19, ochre–red lime-poor shales (RSF); 20, yellow soft marls with thin intercalations of sandstones (Bartonian); 21a, micaceous, wood-debris-bearing, carbonate sandstones, i.e. the so-called 'Grès Roux' (late Oligocene–(?)early Aquitanian); 21b, 'Grès Roux'–micaceous sandstones alternation and yellow soft pelagic marls (mid- to late Oligocene); 22, green and yellow pelagic marls underlying the Beliounis sandstones; 23, thin-bedded micaceous sandstones and yellow marls; 24, holoquartzose puddingstones, with scarce granite pebbles (basal conglomerate of the Alozaina-type formation): latest Oligocene–early Aquitanian; 25a, yellow sandstone–marl alternation; 25b, yellow soft pelagic marls (late Aquitanian *pro paste*); 26, fine-grained yellow sandstones (Aquitanian); 27, channelized Beliounis-type sandstones (late Oligocene–Aquitanian); 28, Aquitanian Beliounis sandstones (cropping out in the village of Beliounis); 29, thick-bedded micaceous sandstones; 30, chaotic basal breccias and olistoliths containing a mixture of carbonate clasts as well as granite and basalt pebbles; 31, early Burdigalian Viñuela-type marlstones with thin chert levels, cropping out in the Talembote area (31a) and in the Predorsalian Chrafate Klippe zone (31b); 32, 'Grès Roux'–micaceous sandstones alternation and Viñuela-type marlstones (early Burdigalian); 33, tobacco brown pelites and Numidian-type sandstones (early to mid-Burdigalian) with resedimented blocks inherited from lost Ghomaride terranes; 34, chaotic complex reworking a mixture of blocks inherited from the Internal Dorsale and the Ghomaride cover; 35, chaotic complex reworking blocks from both the Internal and the External Dorsale; 36, nappe emplacement, probably triggered from late Burdigalian time.

latter domain was palaeogeographically placed between the Internal Dorsale and the Tamezzakht area. Thus, calciturbidites of the Tamezzakht succession (and those of the Béni Ider succession) are likely to have been derived from an external shallow-water high area and not from the neighbouring Dorsale Calcaire. Support is given to this assumption by the following three criteria. (1) Both the Internal Dorsale and the external Dorsale during this time interval were completely drowned, as is clearly shown by the three ubiquitous pelagic facies: 'Capas Rojas' (Campanian), 'Capas Blancas' (Maastrichtian) and black shales (mainly of late Paleocene age). In contrast, the petrographical evidence shows the abundance of rust-coloured, palaeo-altered clasts in the Béni Ider and Tamezzakht Paleocene calciturbidites, which indicates that this clastic material was reworked from an adjacent emerged area. (2) The east-moving slump structures in the late Cretaceous–Paleocene calcarenites point to east-dipping (towards the internal zone) palaeoslopes. (3) The palaeocurrent directions indicate currents flowing towards the internal domain and directed N70°E–N85°E, mainly N80°E.

In contrast to the late Paleocene black shales and *Microcodium*-bearing pelagic black mudstones of the Dorsale Calcaire (facies 9 and 10a) the coeval thick-bedded black calciturbidites of the Predorsalian (facies 10b), Tamezzakht (facies 11) and Béni Ider series (facies 13) are almost exclusively made up of *Microcodium* crystal grains. The *Microcodium* colonies (originally defined by Glück 1912) are known to correspond to microbial mats 'decaying' limestones on palaeosoils (Freytet 1970; Bodergat 1974) and palaeokarst surfaces (Meyer 1987; El Kadiri *et al.* 1992). Thus, the latter *Microcodium*-rich calciturbidites were sourced from large-scale emerged karstic areas, which cannot be envisaged in the Dorsale Calcaire, as the latter was totally drowned during Campanian–Paleocene times (El Kadiri *et al.* 1989, 1992). It is noteworthy that the basinward export of the greatest volume of *Microcodium* material was mostly triggered during the late Paleocene transgressive regime (compare the. 'transgressive washing' process described by El Kadiri *et al.* 2006).

These important results are in accordance with the 'Tariquide Ridge' hypothesis of Durand-Delga (1972), which postulates that an isolated pelagic platform should be reconstructed in the northernmost part of the External zones (i.e. Jbel Moussa Group). The above-mentioned petrographical data strongly suggest that the 'Tariquide Ridge' would have had an important southward prolongation in the external zones and therefore would have separated the Predorsalian zone from the Mauretanian Flysch Trough during Jurassic–early Oligocene times. Thus, the Predorsalian zone significantly differs from the initial Predorsalian scheme of Didon *et al.* (1973) and Olivier (1984) who reconstructed the Predorsalian as a narrow transitory palaeogeographical zone directly connected to the external Flysch Trough. The scheme proposed here may explain why the Predorsalian zone did not receive the widespread early Cretaceous sandstone flysch (i.e. Tisirene flysch). Interestingly, the fact that the Predorsalian series received intercalations of Numidian-like sandstone flysch during latest Oligocene–Aquitanian times may indicate that an important tectonic event occurred during the mid- to late Oligocene and resulted in the disappearance of the so-called 'Tariquide Ridge'. We shall see below that this turning event: (1) was immediately preceded by large-scale resedimentation phenomena (latest Eocene–early Oligocene), partly reworking the material of the above-mentioned ridge itself; (2) was coeval with the onset of the widespread micaceous sandstone flysch (i.e. Béni Ider flysch), which indicates a tectonically raised new clastic source.

At present, late Cretaceous–Paleocene marine strata are unknown in the Ghomaride domain (Maaté 1984, 1996; El Kadiri 1991). In almost all the patched outcrops of the carbonate cover, discovered in this domain, white Nummulite-bearing carbonate sandstones (WNS, Fig. 3) of earliest Eocene (Illerdian) age (facies 14a, Fig. 4) directly fill the karstic cavities developed in the Liassic carbonate successions (e.g. El Onzar unit, El Kadiri *et al.* 1992). It is noteworthy that all the early Eocene transgressive shallow-water limestones at present known in the Ghomaride domain are never found directly discordant on the Palaeozoic schists. The fact that they are fundamentally linked to early Jurassic strata (e.g. El Onzar and Talembote sections, Fig. 3) and frequently occur as olistolithes within the Alozaina- and Viñuela-type Tertiary formations (e.g. Talembote section, Fig. 3), strongly suggests that these fragments of the assumed early Eocene 'Ghomaride cover' were originally derived from Ghomaride-like lost terranes and not from the at present defined Ghomaride units. A similar conclusion may be inferred from the basal conglomerates of these two Tertiary formations (El Kadiri *et al.* 2001; Hlila 2005) and from coeval conglomerates overtopping the Tertiary Ametrasse unit (southern external Dorsale, Nold *et al.* 1981; Hlila 2005), which are, in both cases, rich in granite, basalt pebbles and reefal blocks of unknown origin. The fact that these conglomerates preferentially occur close to the Ghomaride–Dorsale contact (e.g. Talembote, Béni Maaden) and within the Dorsale Calcaire itself, strongly suggests that their source was located between the Ghomaride terranes and the Dorsale Calcaire.

Regarding the successive transgressive peaks shown in the long- and short-term eustatic curves by Haq *et al.* (1987) and Hardenbol *et al.* (1998, charts 1 and 2), the late Cretaceous–Paleocene transgressive peaks were markedly higher than those of Eocene times. This leads us to suggest that: (1) the Ghomaride realm (*sensu lato*) experienced a long-term Mesozoic karstic regime (El Kadiri *et al.* 1992); (2) the onset of the Tertiary marine regime from the beginning of the Eocene was driven by a regional-scale tectonic collapse. Interestingly, equivalent transgressive Nummulite-bearing sandstones that developed in a strikingly identical lithofacies make up a metre-scale interval at the base of the Eocene calciturbidites in many sections throughout the Béni Ider area (Fig. 3). They can serve as key strata not only because of their high correlation potential, but also as they allow the onset of a transgressive regime to be delineated even within near-homogenous base-of-slope calciturbidite packages. In the Oued-El-Kébir section (Fig. 3) a conspicuous *Thallassinoides*-burrowed firmground surface (i.e. *Glossifungites*-type surface; e.g. Savrda 1995; MacEachern & Burton 2000; Savrda *et al.* 2001*a*,*b*) immediately follows the WNS facies, and probably marks the related transgressive peak.

Importantly, the same light-coloured carbonate sandstones exist in the Tamezzakht section. They clearly erode the lime-free siliceous green shales of the underlying facies (facies 11), upon which they unconformably rest along a low-angle hidden discontinuity (in the sense of Clari *et al.* 1995). Two Fe-encrusted surfaces cap the immediately overlying beds and may be regarded, in the same way, as corresponding to the consequent transgressive peak. Hence, the following thin-calciturbidite-intercalated ochre–red shales could normally correspond to the late highstand–lowstand regime, during which terrigenous-mud-dominated packages are the most common components (e.g. Savrda *et al.* 2001*a*).

Within the Tamezzakht succession, conspicuous grain-flow events occur in the upper part of the ochre–red shales of Eocene–early Oligocene age (facies 18a), probably close to the Eocene–Oligocene boundary. They laterally evolve into a discontinuous olistostrome-like formation, which can rest uncomfortably on the underlying strata of late Cretaceous–Paleocene age (facies 5 and 6). This collapse event may correlate with the regional-scale onset of chaotic breccias in both the Dorsale Calcaire (facies 15, Breccias Nummuliticas, Nold *et al.* 1981) and the Flysch Trough. In the former (e.g. Hafat Srir section, Fig. 3) they unconformably rest on the Triassic–Liassic massive carbonate formations and seal large-scale extensional structures (see also the geological maps of Kornprobst *et al.* 1975, 1979). In the second, chaotic breccias cap the Eocene calciturbidites before being buried under an ochre–red shale-dominated succession (facies 18b). In addition, El Kadiri (1984), De Wever *et al.* (1985) and Ben Yaïch *et al.* (1988) showed that the sedimentary Chrafate Klippes (facies 17), which represent the southernmost part of the Predorsalian domain, were embedded within variegated marls of latest Eocene–early Oligocene age (facies 16). Concurrently, the absence of coeval marine strata in the Ghomaride domain is noteworthy. Marine sedimentation seems not have returned before the onset of the widespread latest Oligocene transgressive holoquartzose puddingstones (facies 24), which lie at the base of the Aquitanian yellow marl–sandstone alternation (facies 25, i.e. Ciudad-Granada–Fnideq Formation).

In the northernmost part of the Ghomaride domain, the Fnideq sandstones commonly seal normal faults at different scales, which points to a regional extensional event. In the Dorsale–Predorsalian couplet, the rust-coloured sandstones (facies 21a) that start shortly before, during the late Oligocene, also seal normal faults at different scales. A more comprehensive assessment of the regional-scale tectonic controls that might be proposed for the whole late Oligocene history needs to account for other time-equivalent events known throughout the whole Betic–Rif Internal zones, which is beyond the scope of this paper. It should be noted, for instance, that this extensional event in both the Ghomarides and Dorsale Calcaire occurred just after the mid- to late Oligocene paroxysmal phase that is well documented in the Ghomaride units (e.g. Chalouan 1986; Durand-Delga *et al.* 1993).

The abrupt facies change that is well delineated in the field between the 'oligotrophic' ochre–red shales (facies 19 in the Tamezzakht, J. Moussa and Béni Ider areas) and the 'eutrophic' green pelagic marls (oligotrophy–eutrophy boundary, Ol/Eu B, Fig. 4) is seemingly linked to the well-documented global-scale climatic change that occurred close to the Eocene–Oligocene boundary. It is evidenced by the turnover of planktonic Foraminifera (see examples by Molina *et al.* 1986, 1988, 1996, amongst others) as a result of a sudden global cooling event paired with enhanced ocean circulation (e.g. Pomerol 1985; Marty *et al.* 1988; Zachos *et al.* 1993, 1995; Diester-Haass & Zahn 1996; Barnes 1999). These climatic events were essentially induced by the immediately preceding tectonic collapses, which resulted in the opening and/or rearrangement of intercontinental seaways (e.g. between Antarctica and South America, Pomerol 1985; Wilson *et al.* 1998). Thus, the successions selected in this study provide an interesting record of such a twofold tectonic and climatic event: the coarse-grained

conglomerates (facies 15, 17 and 18) and olistostromes (facies 17) fit well with this scenario.

We would like to compare this Oligocene scenario with two strikingly near-identical events, which occurred close to the Jurassic–Cretaceous boundary and at the Turonian–early Senonian boundary, respectively. The former was recorded similarly by an abrupt facies change between the 'oligotrophic' ochre–red radiolaritic shales (late Jurassic) and the coccolith-formed yellow hemipelagic marls (late Tithonian–early Cretaceous). This is the Kuenen event (Roth 1989), which is known throughout the Tethyan realm to be similarly induced by a tectonic-mediated ocean-circulation intensification (De Wever *et al.* 1986; El Kadiri 2002*b*). In the latter case the early Senonian eutrophic green pelites sharply seal normal faults affecting the immediately underlying ochre–red Turonian shales and calciturbidites (El Kadiri *et al.* 2003). These examples support the causal link proposed above between tectonics and abrupt facies change. In the case of the onset of the early to mid-Oligocene eutrophic shales (Dorsale calcaire; Tamezzakht, Béni Ider), the related tectonic event may obviously be linked to the Ghomaride paroxysmal phase.

The rust-coloured sandstones (the so-called 'Grès Roux'; Fallot 1937; Griffon 1966) typify the late Oligocene siliclastic regime in all the stratigraphic series known in the Dorsale Calcaire (facies 21a) and last until the early Burdigalian in the Tamezzakht succession (facies 21b and 32). Petrographical evidence shows that this regime reworks a mixture of metamorphic-rock-derived, immature lithoclasts that do not seem to be sourced from the Rifian Sebtide–Ghomaride terranes or from their Betic counterparts. Their petrographical features seem to us similar to those described by Puglisi *et al.* (2001) in both the Tertiary Ghomaride cover and the time-equivalent strata in the Béni Ider flysch successions. About 10 palaeocurrent directions measured on the sole of the sandstone beds indicate currents directed N20°–N60°, mainly N30°–N40°, and flowing from the SW to the NE (i.e. towards the internal domain from an external source). Thus, like the underlying calciturbidites, these sandstone flows could be sourced from (an) external lost terrane(s). Seemingly, the same may be true for the Dorsale-Calcaire 'Grès Roux', the sole of which gives evidence of north-flowing currents (our measurements were taken in the Tamezzakht area, i.e. in the Hafat Srir section along the road to the television mast). In the latter domain the current directions were probably modified by a near north–south-directed half-graben physiography. However, reconstruction of the late Oligocene–Aquitanian sandstone source(s) remains a hard task and requires more dating controls and careful regional-scale correlations (partly involving sedimentological and environmental data as a comparison tool) throughout both the Internal and External zones. For instance, it is noteworthy that: (1) a tectonic event (i.e. the mid- to late Oligocene paroxysmal phase in the Ghomaride domain) could be responsible for the emplacement (and/or emergence) of new supplying terranes close to or partly on the previous nummulitic carbonate source, which resulted in its complete and irreversible drowning under the siliciclastic accumulations; (2) the whole palaeogeographical setting was likely to undergo significant modifications (i.e. in placing together previously distant areas). Concurrently with the rust-coloured sandstones, this result may additionally be supported by the interlayered metre-scale micaceous sandstones, which undoubtedly reflect the rise of another juxtaposed terrigenous source.

In the Ghomaride domain, the chaotic, coarse-grained conglomerate lying at the very base of the early Burdigalian marlstones (i.e. Viñuela Formation) is well documented in the Betic Internal zones as transgressively onlapping the Palaeozoic terranes (Sanz de Galdeano *et al.* 1993; Serrano *et al.* 1995; López-Garrido & Sanz de Galdeano 1999). These rocks erode the Aquitanian yellow pelagic marls of the underlying formation (Alozaina Formation) and could indicate a tectonically controlled collapse. This large-scale event resulted in the generalization of the siliceous marlstones of hemipelagic signature throughout the Betic–Rif Internal zones. The fact that this facies of high correlation potential makes up decametre-thick intervals in the upper third of the Tamezzakht succession (facies 32) and the Predorsalian units (facies 31b) leads us to the conclusion that the palaeogeographical setting of the latter external units became relatively close to the structuring of the Internal zones during the late Aquitanian–early Burdigalian.

With regard to the pelagic sedimentation regime, it seems possible that there are three lines of comparison between the Tamezzakht succession and that of the Talembote area recently described by El Kadiri *et al.* (2001) close to the Internide–Externide front (Fig. 3). (1) In the Tamezzakht area, the entire mid-Oligocene–early Burdigalian pelagic marly deposition develops in a rhythmic alternation of centimetre to decimetre intervals of yellow marls and 'early' Viñuela-type green marlstones, with the latter cyclic component being dominant in early Burdigalian time. In the Talembote area, these two facies are clearly separated in time as two contrasted lithological intervals, with an erosional discontinuity between them close to the Aquitanian–Burdigalian transition (see Fig. 3). Thus, the difference between the Tamezzakht pelagic deposition (i.e. close to the

External Domain) and the Talembote one (Internal Domain) may basically be related to the diachronism of the Viñuela-type marlstones. (2) Lithofacies and biostratigraphic dating allow us to distinguish in the Predorsalian domain two types of early Miocene holoquartzose sandstones: the first corresponds to the classical Numidian-like, yellow to rust-coloured sandstones (facies 27 and 28, Fig. 4) defined by Durand–Delga (1972) and Didon *et al.* (1973) in the village of Beliounis (J. Moussa Group) as characterizing the depositional regime of the Predorsalian zone during the late Oligocene–Aquitanian, (i.e. synchronously with the external Numidian flysch deposition). This facies, sometimes poorly consolidated, is generally poorly graded and all the quartz grains are rounded and may be white, red or black. Very similar yellow sandstones coevally spread over the Ghomaride–Malaguide domains (Fnideq and Alozaina Formations, respectively, facies 25a, Fig. 4). We have found identical facies within the late Oligocene–Aquitanian levels of the Tamezzakht succession, a result that lends additional support to ascribing the Tamezzakht area to the Predorsalian zone. The second type of sandstone facies corresponds to tobacco brown holoquartzose sandstones, in which the quartz grains may be rounded or not and are predominantly glass-green coloured. Individual beds may show graded bedding into fine pelites. This second sandstone facies strictly occurs within the tobacco brown pelites of early to mid-Burdigalianage (El Hatimi 1982; El Kadiri *et al.* 2001; Hlila 2005) and its distinction fits well with the early 'Neonumidian'-sandstone concept defined by Bourgois (1978) in the Internal zones of the Betic Cordilleras.

The upper levels of early Burdigalian tobacco brown pelites receive increasing gravity-flow discharges that evolve into huge olistostrome complexes carrying large olistoliths. These derived from either the Ghomaride–Internal Dorsale couplet (facies 34, example in the Talembote area) or the External Dorsale (facies 35; for the examples occur in Tamezzakht, Chrafate Klippes and Kobat El Kesskasse olistostrome) with Palaeogene variegated marly strata being trapped between them. The immediately superimposed Dorsale nappe pile may tentatively be considered as resulting from the culmination of the same phenomenon.

Conclusion

The aim of this paper was to provide a basis for synthesizing the more significant facies, discontinuities and gravity-flow discharges from the Rif Internal Domain and its surroundings. It seems that almost all the data point to tectonic events of regional or global scale. The above interpretation provides the three following results.

(1) Apart from certain widespread facies of high correlation potential, the late Cretaceous–early Oligocene strata studied above exhibit important differences, so that their respective depocentres should be located in distant palaeogeographical areas. We can retain the possibility that: (a) important Ghomaride-like lost terranes could be located between the present-day defined Ghomaride units and the Internal Dorsale; (b) symmetrically, one or several isolated carbonate platforms could be located within the external zones, i.e. 'Tariquide'-like ridge(s), which have played a major role as the source delivering, at a large scale, calciturbidites to the Predorsalian and Flysch basins.

(2) The relationship between the internal and the external zone, which has long been considered as being marked by a narrow transitional zone (the classical Predorsale concept), was likely to have involved more than a simple palaeogeographical area, as shown by the Chrafate klippes and the J. Moussa Group, which are remains of a wider and more complex area. The latter probably underwent successive palaeogeographical modifications with time. For instance, it should be noted that during late Cretaceous–Eocene times, the Predorsalian zone(s) were separated from the Flysch Trough by the above-mentioned 'Tariquide'-like ridge(s). The collapse and final disappearance of the latter occurred during the latest Eocene–early Oligocene, i.e. concurrently with (a) the disappearance of the external prolongation of the external Dorsale units (i.e. Chrafate Klippe olistostromes), (b) the onset of the Dorsale calcaire megabreccias (Breccias Nummuliticas) and (c) other large-scale gravity events (e.g. Talembote olistostromes).

(3) The major discontinuities, coarse-grained discharges and facies changes (e.g. newly raised sources) may be ascribed to distal reverberations of the contractional phases that occurred in the old Ghomaride realm during the early to mid-Oligocene–early Burdigalian time interval. The progressive homogenization of some key facies (rust-coloured sandstones, Beliounis and Neo-Numidian ones as well as the Viñuela-type marlstones) to previously distant palaeogeographical zones during Aquitanian–early Burdigalian times may be paralleled by the shortening processes that resulted in a new palaeogeographical setting.

However, reconstructing a reliable tectonosedimentary evolution requires new insights into the following issues.

(1) What was the triggering mechanism(s) of the chaotic, coarse-grained gravity flows? Despite these commonly occuring as deposits that transgressively

overlie previous emerged areas, their intercalation within and/or at the top of pelagic marly successions leads us to raise the question of contractional (nappe front) versus extensional (normal fault) tectonic controls. A eustatic signature cannot be excluded, as megabreccias are generally ascribed to lowstand phases (e.g. Haas 1999; Ineson & Surlyk 2000).

(2) What is the significance of the four Palaeogene–early Miocene formations (with discontinuities between them), well documented in the Malaguide–Ghomaride domain, in terms of eustatic controls (i.e. Exxon sequence) versus a tectonic one?

(3) What is the extent of the entirely disappeared palaeogeographical zones? Indeed, the clastic mixture reworked in the Alozaina and Viñuela formations (Betic Cordillera) and in their Rif counterparts, points to very extensive lost source areas. This leads us to question how far we can still maintain the classical scheme that immediately juxtaposes the Sebtides, Ghomarides, Dorsale, Predorsale and Mauretanian flysch?

(4) Was the kinematics of nappe emplacement determined by tectonic driving forces (subduction phases, Lonergan & White 1997; Chalouan *et al.* 2001) or by gravitational ones (Weijermars 1987; Doblas & Oyarzun 1989; El Kadiri *et al.* 1995)? A possible continuum process and/or causal link between them may tentatively be suggested in the case of the large-scale gravity flows proved to immediately precede the nappe-pile emplacement.

Integrated approaches involving sedimentology, sequence-stratigraphic interpretation, comprehensive inventory of sedimentary discontinuities, close biostratigraphic dating and detailed mapping, as well as more extended regional correlations, are expected to shed additional light on these issues, and are in progress.

The authors express their sincere thanks to A. Michard (University of Paris) and W. Wildi (University of Zürich) for their thorough reviews and constructive remarks. This work was financially supported by both the Société Nationale d'Etude du Détroit, SNED, Rabat, Morocco and the 'Junta de Andalucia' Project A49/02 (M): 'Las Formaciones cenozicas de la zona Interna...' (Spain).

References

ANDRIEUX, J. 1971. *La structure du Rif central. Etude des relations entre la tectonique de compression et les nappes de glissement dans un tronçon de la chaîne alpine.* Notes et Mémoires du Service Géologique du Maroc, **235**, 1–155.

AZAÑON, J. M. & CRESPO-BLANC, A. 2000. Exhumation during a continental collision inferred from the tectonometamorphic evolution of the Alpujarride Complex in the central Betics (Alboran domain, SE Spain). *Tectonics*, **19**, 549–565.

AZANON, J. M., GARCIA-DUENAS, V. & GOFFÉ, B. 1998. Exhumation of high-pressure metapelites and coeval crustal extension in the Alpujarride complex (Betic Cordillera). *Tectonophysics*, **285**, 231–252.

BALANYA, J. C. & GARCIA-DUENAS, V. 1987. Les directions structurales dans le domaine d'Alboran de part et d'autre du Détroit de Gibraltar. *Comptes Rendus de l'Académie des Sciences, Série II*, **304**(15), 929–932.

BARNES, C. R. 1999. Palaeoceanography and palaeoclimatology: an Earth system perspective. *Chemical Geology*, **161**, 17–35.

BEN YAÏCH, A. 1991. *Evolution tectono-sédimentaire du Rif externe centre occidental (régions de M'Sila et Ouezzane, Maroc).* Doctorat d'Etat Thesis, University of Pau, France.

BEN YAÏCH, A., MAATÉ, A., FEINBERG, H., MAGNÉ, J. & DURAND-DELGA, M. 1986. Implications de niveaux du Miocène inférieur dans les retrochevauchements de la Dorsale calcaire rifaine (Maroc): signification à l'échelle de l'Arc de Gibraltar. *Comptes Rendus de l'Académie des Sciences, Série II*, **302**(8), 587–592.

BEN YAÏCH, A., DUÉE, G., EL HATIMI, N. & EL KADIRI, KH. 1988. *La formation à klippes sédimentaires d'âge oligo-burdigalien du Rif septentrional (Maroc): signification géodynamique.* Notes et Mémoires du Service Géologique du Maroc, **334**, 99–126.

BENZAGGAGH, M. 1996. *Le Malm supérieur et le Berriasien dans le Prérif interne et le Mésorif (Rif, Maroc): stratigraphie, sédimentologie, paléogéographie et évolution tectono-sédimentaire.* Doctorat d'Etat Thesis, University of Rabat.

BLUMENTHAL, M., DURAND DELGA, M. & FALLOT, P. 1958. *Données nouvelles sur le Tithonique, le Crétacé et l'Eocène de la zone marno-schisteuse du Rif septentrional (Maroc).* Notes et Mémoires du Service Géologique du Maroc, **16**(143), 35–58.

BODERGAT, A. M. 1974. *Les* Microcodium, *milieux et modes de développement.* Documents du Laboratoire de Géologie de la Faculté des Sciences de Lyon, **62**, 137–235.

BOUILLIN, J. P., DURAND-DELGA, M., GÉLARD, J. P., *ET AL.* 1970. Définition d'un flysch Massylien et d'un flysch Maurétanien au sein des flyschs allochtones de l'Algérie. *Comptes Rendus de l'Académie des Sciences*, **270**, 2249–2252.

BOUILLIN, J. P., DURAND-DELGA, M. & OLIVIER, PH. 1986. Betic–Rifian and Tyrrhenian arcs: distinctive features, genesis and development stages. *In:* WETZEL, F.-C. (ed.), *The Origin of the Arcs.* Elsevier, Amsterdam, 281–304.

BOURGOIS, J. 1978. *La transversale de Ronda. Cordillères Bétiques, Espagne. Données géologiques pour un modèle d'évolution de l'arc de Gibraltar.* Doctorat d'Etat Thesis, University of Besançon.

BOUYBAOUÈNE, M. L., GOFFÉ, B. & MICHARD, A. 1995. High-pressure, low-temperature metamorphism in the Sebtides nappes, northern Rif, Morocco. *Geogaceta*, **17**, 117–119.

BURKHALTER, R. M. 1995. Ooidal ironstones and ferruginous microbialites: origin and relation to

sequence stratigraphy (Aalenian and Bajocian, Swiss Jura Mountains). *Sedimentology*, **42**, 57–74.

CALVERT, A., SANDVOL, E., SEBER, D., *ET AL.* 2000. Geodynamic evolution of the lithosphere and upper mantle beneath the Alboran region of the western Mediterranean: constraints from travel time tomography. *Journal of Geophysical Research*, **105**, 10871–10898.

CHALOUAN, A. 1986. *Les nappes Ghomarides (Rif septentrional, Maroc), un terrain varisque dans la chaîne Alpine*. Doctorat d'Etat Thesis, University Louis Pasteur, Strasbourg.

CHALOUAN, A. & MICHARD, A. 1990. The Ghomaride nappes, Rif, coastal Range, Morocco: a Variscan chip in the Alpine belt. *Tectonics*, **15**, 187–200.

CHALOUAN, A., SAJI, R., MICHARD, A. & BALLY, A. W. 1997. Neogene tectonic evolution of the south-western Alboran basin as inferred from seismic data of Morocco. *AAPG Bulletin*, **81**, 1161–1184.

CHALOUAN, A., MICHARD, A., FEINBERG, H., MONTIGNY, R. & SADDIQI, O. 2001. The Rif mountains building (Morocco): a new tectonic scenario. *Bulletin de la Société Géologique de France*, **172**(5), 603–616.

CHALOUAN, A., EL MRIHI, A., EL KADIRI, KH., BAHMAD, A., SALHI, F. & HLILA, R. 2006. Mauretanian flysch nappe in the northwestern Rif Cordillera (Morocco): deformation chronology and evidence for a complex nappe emplacement. *In*: MORATTI, G. & CHALOUAN, A. (eds) *Tectonics of the Western Mediterranean and North Africa*, Geological Society, London, Special Publications, **262**, 161–175.

CLARI, P. A., DELA PIERRE, F. & MARTIRE, L. 1995. Discontinuities in carbonate successions: identification, interpretation and classification of some Italian examples. *Sedimentary Geology*, **100**, 97–121.

COMAS, M. C., GARCIA-DUEÑAS, V. & JURADO, V. 1992. Neogene tectonic evolution of the Alboran Sea from MCS data. *Geomarine Letters*, **12**(2–3), 157–164.

DE WEVER, P., DUÉE, G. & EL KADIRI, KH. 1985. Les séries stratigraphiques des klippes de Chrafate (Rif septentrional, Maroc): témoins d'une marge continentale subsidente au cours du Jurassique–Crétacé. *Bulletin de la Société Géologique de France*, 8th series, **I**(3), 363–379.

DE WEVER, P., RICOU, L. E. & FOURCADE, E. 1986. La fin brutale de l'optimum radiolaritique au Jurassique terminal: l'effet de la circulation océanique. *Comptes Rendus de l'Académie des Sciences, Série II*, **302**(9), 665–670.

DIDON, J. 2006. *Carte géologique du Rif, feuille de Khémis Béni—Arouss, 1/50 000*. Notes et Mémoires du Service Géologique du Maroc.

DIDON, J., DURAND-DELGA, M. & KORNPROBST, J. 1973. Homologies géologiques entre les deux rives du détroit de Gibraltar. *Bulletin de la Société Géologique de France*, **15**, 77–105.

DIESTER-HAASS, L. & ZAHN, R. 1996. Eocene–Oligocene transition in the Southern Ocean: history of water mass circulation and biological productivity. *Geology*, **24**, 163–166.

DOBLAS, M. & OYARZUN, R. 1989. Neogene extensional collapse in the Mediterranean (Betic–Rif Alpine orogenic belt): implications for the genesis of the Gibraltar Arc and magmatic activity. *Geology*, **17**, 430–433.

DURAND-DELGA, M. 1972. La courbure de Gibraltar, extrémité occidentale des chaînes alpines, unit l'Europe et l'Afrique. *Eclogae Geologicae Helveticae*, **65**, 267–278.

DURAND-DELGA, M. 1980. La Méditerranée occidentale: étapes de sa genèse et problèmes structuraux liés à celle-ci. *Livre Jubiliaire de la Société Géologique de France à la Mémoire de P. Lucas*. Mémoire hors série, **10**, 1830–1980.

DURAND-DELGA, M. & DIDON, J. 1984*a*. *Carte géologique du Rif, Feuille de Ksar Es-Srhir, 1/50 000*. Notes et Mémoires du Service Géologique du Maroc, **295**.

DURAND-DELGA, M. & DIDON, J. 1984*b*. *Carte géologique du Rif, Feuille de Melloussa, 1/50 000*. Notes et Mémoires du Service Géologique du Maroc, **296**.

DURAND-DELGA, M. & VILLIAUMEY, M. 1963. Sur la stratigraphie et la tectonique du Jebel Moussa. *Bulletin de la Société Géologique de France*, 7th series, **5**(1), 70–79.

DURAND-DELGA, M., HOTTINGER, L., MARÇAIS, J., MATTAUER, M., MILLIARD, Y. & SUTER, G. 1962. Données actuelles sur la structure du Rif. *Livre à la Mémoire de Paul Fallot, Société Géologique de France*. Mémoire hors série, **1**, 399–422.

DURAND-DELGA, M., FEINBERG, H., MAGNÉ, J., OLIVIER, PH. & ANGLADA, R. 1993. Les formations oligo-miocènes discordantes sur les Malaguides et les Alpujarrides et leurs implications dans l'évolution géodynamique des cordillères Bétiques (Espagne) et de la Méditerranée d'Alboran. *Comptes Rendus de l'Académie des Sciences, Série II*, **317**, 679–687.

EICHER, D. L. & DINER, R. 1991. Environmental factors controlling Cretaceous limestone–marlstone rhythms. *In*: EINSELE, G., RICKEN, W. & SEILAKHER, A. (eds) *Cycles and Events in Stratigraphy*, Springer, Berlin, 79–93.

EINSELE, G. & RICKEN, W. 1991. Limestone–marl alternations—an overview. *In*: EINSELE, G., Diplôme d'Etudes RICKEN, W. & SEILACHER, A. (eds) *Cycles and Events in Stratigraphy*. Springer, Berlin, 23–47.

EL HATIMI, N. 1982. *Contribution à l'étude géologique et structurale de la région d'Assifane (Rif, Maroc)*. Diplôme d'Etudes Thesis, University of Rabat.

EL HATIMI, N. 1991. *Rifting mésozoïque sur la bordure occidentale du Rif interne (Maroc). Evolution géodynamique d'un secteur de la marge ouest-téthysienne. Exemples du Haouz et du Groupe du J. Moussa*. Doctorat d'Etat Thesis, University of Pau.

EL HATIMI, N., BEN YAICH, A. & EL KADIRI, KH. 1988. Evolution méso-cénozoïque à la limite Zones Internes–Zones Externes dans la chaîne

rifaine. *Bulletin de l'Institut Scientifique de Rabat*, **12**, 9–18.

EL KADIRI, KH. 1984. *Les radiolarites jurassiques des klippes de Chrafate (Rif septentrional, Maroc): stratigraphie, taxonomie*. Doctorat du 3ème cycle Thèse, University of Pau.

EL KADIRI, KH. 1991. *La Dorsale Calcaire (Rif interne, Maroc): Stratigraphie, sédimentologie et évolution géodynamique d'une marge alpine durant le Mésozoïque. Mise en évidence d'un modèle*. Doctorat d'Etat Thesis, University of Tetuan.

EL KADIRI, KH. 2002*a*. Jurassic ferruginous hardgrounds of the 'Dorsale Calcaire' and the Jbel Moussa Group (internal Rif, Morocco): stratigraphical context and palaeoceanographic consequences of mineralization processes. *Geologica Romana*, **36**, 33–70.

EL KADIRI, KH. 2002*b*. 'Tectono-eustatic sequences' of the Jurassic successions from the Dorsale Calcaire (internal Rif, Morocco): evidence from a eustatic and tectonic scenario. *Geologica Romana*, **36**, 71–104.

EL KADIRI, KH., LINARES, A. & OLORIZ, F. 1989. La Dorsale calcaire interne entre les Accidents de l'Oued Martil et de l'Oued Laou (Rif septentrional, Maroc): évolutions stratigraphique et géodynamique au cours du Jurassique–Crétacé. *Comunicações Serviços Geológicos de Portugal*, **75**, 39–65.

EL KADIRI, KH., LINARES, A. & OLORIZ, F. 1990. Les éléments du Groupe du Jbel Moussa (Chaîne Calcaire, Rif, Maroc): évolutions stratigraphique et géodynamique au cours du Jurassique–Crétacé. *Comunicações Serviços Geológicos de Portugal*, **76**, 141–161.

EL KADIRI, KH., LINARES, A. & OLORIZ, F. 1992. *La Dorsale Calcaire rifaine (Maroc septentrional): évolution stratigraphique et géodynamique durant le Jurassique–Crétacé*. Notes et Mémoires du Service Géologique du Maroc, **336**, 217–265.

EL KADIRI, KH., OLORIZ, F. & LINARES, A. 1995. Evolution tectono-sédimentaire alpine autour de l'Arc de Gibraltar et mise en évidence de la cinématique de remontée d'un dôme de l'asténosphère depuis le Jurassique jusqu'au Néogène. *Geogaceta*, **17**, 104–106.

EL KADIRI, KH., CHALOUAN, A., EL MRIHI, A., HLILA, R., LOPEZ-GARRIDO, A. C., SANZ DE GALDEANO, C. & SERRANO, F. 2000. Descubrimiento del Burdigaliense (Formación Viñuela) en la cobertera ghomáride de Ceuta (Rif Septentrional). *Geogaceta*, **28**, 43–46.

EL KADIRI, K., CHALOUAN, A., EL MRIHI, A., *ET AL.* 2001. Les formations sédimentaires olistolitiques de l'Oligocène supérieur–Miocène inférieur dans l'unité ghomaride des Béni Hozmar (secteur de Talembote, Rif septentrional, Maroc). *Eclogae Geologicae Helveticae*, **94**, 313–320.

EL KADIRI, KH., EL KADIRI, K. & RAHOUTI, A. 2003. Sédimentologie et ichnologie des calciturbidites du Crétacé supérieur–Oligocène inférieur de la série Maurétanienne (nappe des Béni Ider, Rif septentrional, Maroc): implications paléogéographiques. *Bulletin de l'Institut Scientifique de Rabat*, **25**, 73–91.

EL KADIRI, KH., SERRANO, F., HLILA, R., *ET AL.* 2005. Lithostratigraphy and sedimentology of the latest Cretaceous–searly Burdigalian Tamezzakht Succession (Northern Rif, Morocco): consequences for its sequence stratigraphic interpretation. *Facies*, **50**, 477–503.

EL KADIRI, KH., CHALOUAN, A., BAHMAD, A., SALHI, F. & LIEMLAHI, H. (2006). 'Transgressive washing' concept: a sequence stratigraphic approach for calci- and siliciclastic turbidites. *In*: MORATTI, G. & CHALOUAN, A. (eds) *Tectonics of the Western Mediterranean and North Africa*. Geological Society, London, Special Publications, **262**, 45–53.

FALLOT, P. 1937. *Essai sur la géologie du Rif septentrional*. Notes et Mémoires du Service Géologique du Maroc, **4**, 1–553.

FARINACCI, A. 1996. Depositional discontinuity and biosequence concept. Examples from Mesozoic western Tethys. *Palaeopelagos*, **6**, 211–227.

FARINACCI, A. 2002. Palaeosol in Apennine carbonate platform connected with Jurassic 'Main Gap' discontinuity. Vallepiert Palaeosol. *Geologica Romana*, **36**, 163–167.

FARINACCI, A., BÖLÜKBAI, S. & RIDOLFI, V. 1997. The Tethyan Jurassic 'main gap' in the Tinaz Tepe section of the Barla Dag area, Western Taurus, Turkey. *Palaeopelagos*, **7**, 7–26.

FEINBERG, H. & OLIVIER, PH. 1983. Datation des termes aquitaniens et burdigaliens dans la zone prédorsalienne bético-rifaine et ses conséquences. *Comptes Rendus de l'Académie des Sciences, Série II*, **296**, 473–476.

FEINBERG, H., MAATÉ, A., BOUHDADI, S., DURAND-DELGA, M., MAATE, M., MAGNÉ, J. & OLIVIER, PH. 1990. Signification des dépôts de l'Oligocène supérieur–Miocène inférieur du Rif interne (Maroc), dans l'évolution géodynamique de l'Arc de Gibraltar. *Comptes Rendus de l'Académie des Sciences, Série II*, **310**, 1487–1495.

FREYTET, P. 1970. *Les dépôts continentaux et marins du Crétacé supérieur et des couches de passage à l'Eocène en Languedoc*. Doctorat d'Etat Thesis, Université Orsay-Paris-Sud.

FRIZON DE LAMOTTE, D. 1985. *La structure du Rif oriental (Maroc). Rôle de la tectonique longitudinale et importance des fluides*. Doctorat d'Etat Thesis, University Pierre et Marie Curie, Paris.

FÜRSICH, F. T., OSCHMANN, W., JAITLY, A. K. & SINGH, I. B. 1991. Faunal response to transgressive–regressive cycles: example from the Jurassic of western India. *Palaeogeography, Palaeoclimatology, Palaeoecology*, 85, 149–159.

GARCIA-DUEÑAS, V., BALANYA, J. C. & MARTINEZ MARTINEZ, J. M. 1992. Miocene extensional detachments in the outcropping basement of the northern Alboran basin (Betics) and their implications. *Geo-Marine Letters*, **12**(2–3), 88–95.

GLÜCK, H. 1912. Eine neue gesteinbildende Siphonee (Codiacée) aus dem marinen Tertiar von Suddeutschland. *Mitteilungen der Badische Geologischen Landesanstalt*, **7**, 3–24.

GRIFFON, J. C. 1966. *La Dorsale calcaire au sud de Tétouan*. Notes et Mémoires du Service Géologique du Maroc, **184**, 149–223.

GUERRERA, J., MARTIN-ALGARRA, A. & PERRONE, V. 1993. Late Oligocene–Miocene syn-/late-

orogenic successions in western and central Mediterranean chains from the Betic Cordillera to the southern Apennines. *Terra Nova*, **5**, 525–544.

HAAS, J. 1999. Genesis of late Cretaceous toe-of-slope breccias in the Bakony Mts, Hungary. *Sedimentary Geology*, **128**, 51–66.

HAQ, B. U., HARDENBOL, J. & VAIL, P. R. 1987. Chronology of fluctuating sea-levels since the Triassic. *Science*, **235**, 1156–1167.

HARDENBOL, J., THIERRY, J., FARLEY, M. B., JACQUIN, T., DE GRACIANSKY, P. C. & VAIL, P. R. 1998. *Mesozoic and Cenozoic sequence chronostratigraphic framework of European Basins. In*: DE GRACIANSKY, P. C., HARDENBOL, J. JACQUIN, T. & VAIL, P. R. (eds) *Mesozoic and Cenozoic Sequence Stratigraphy of European basins.* Society of Economic, Paleontologists and Mineralogists, Society for Sedimentary Geology, Special Publications, **60**, 3–13.

HLILA, R. 1994. *Etude des déformations miocènes dans la chaîne calcaire du Haouz (entre Tétouan et le col du Drauy).* Diplôme d'Etudes Supérieures Thesis, University of Tetuan.

HLILA, R. 2005. *Evolution tectono-sédimentaire tertiaire au front ouest du domaine d'Alboran (Ghomarides et Dorsale calcaire, Rif septentrional, Maroc).* Doctorat d'Etat Thesis, University of Tetuan.

INESON, J. R. & SURLYK, F. 2000. Carbonate megabreccias in a sequence stratigraphic context; evidence from the Cambrian of Greenland. *In*: HUNT, D. & GAWTHORPE, R. L. (eds). *Sedimentary Responses to Forced Regressions.* Geological Society, London, Special Publications, **172**, 47–68.

KORNPROBST, J. 1974. *Contribution à l'étude pétrographique et structurale de la zone interne du Rif (Maroc septentrional).* Notes et Mémoires du Service Géologique du Maroc, **251**, 1–260.

KORNPROBST, J. & DURAND-DELGA, M. 1985. *Carte géologique du Rif, Feuille Sebta, 1 : 50 000.* Notes et Mémoires Service géologique du Maroc, **291**.

KORNPROBST, J., WILDI, W., NOLD, M., GUTNIC, M. & LESPINASSE, P. 1975. *Carte Géologique du Rif, feuille de Bab Taza, 1/50.000.* Notes et Mémoires du Service Géologique du Maroc, **288**.

KORNPROBST, J., NOLD, M. & WILDI, W. 1979. *Carte Géologique du Rif, feuille de Talembote, 1/50.000.* Notes et Mémoires du Service Géologique du Maroc, **290**.

LESPINASSE, P. 1975. *Géologie des zone externes et des flyschs entre Chaouen et Zoumi (Centre de la chaîne rifaine du Maroc.* Doctorat d'Etat Thesis, Université Paul Sabatier, Toulouse.

LONERGAN, L. & WHITE, N. 1997. Origin of the Betic–Rif mountain belt. *Tectonics*, **16**, 504–522.

LOOMIS, T. P. 1975. Tertiary mantle diapirism, orogeny, and plate tectonics east of Strait of Gibraltar. *American Journal of Science*, **275**, 1–30.

LÓPEZ-GARRIDO, A. C. & SANZ DE GALDEANO, C. 1999. Neogene sedimentation and tectonic–eustatic control of the Malaga Basin, south Spain. *Journal of Petroleum Geology*, **22**, 81–96.

LOWE, D. R. 1982. Sediment gravity flows: II. Depositional models with special reference to the deposits of high-density turbidity currents. *Journal of Sedimentary Petrology*, **52**, 279–297.

MAATÉ, A. 1984. *Etude géologique de la couverture mésozoïque et cénozoïque des unités ghomarides au nord de Tétouan (Rif interne, Maroc).* Doctorat de 3ème Cycle Thesis, University of Toulouse.

MAATÉ, A. 1996. *Estratigrafia y evolucion palaeogeografica alpina del dominio Gomaride (Rif interno, Marruecos).* Doctoral Thesis, University of Granada.

MAATÉ, A., MARTIN-ALGARRA, A. & SERRANO, F. 1993. El Terciario de la unidad de Saaden (Dorsal externa, Rif Septentrional, Marruecos. *Geogaceta*, **14**, 91–93.

MACEACHERN, J. A. & BURTON, J. A. 2000. Firmground Zoophycos in the Lower Cretaceous Viking Formation, Alberta: a distal expression of the Glossifungites Ichnofacies. *Palaios*, **15**, 387–398.

MARTIN-ALGARRA, A. 1987. *Evolucion geologica alpina del contacto entre la zonas internas y las zonas externas de la Cordillera Betica.* Doctoral Thesis, University of Granada.

MARTIN-MARTIN, M., MARTIN-ALGARRA, A. & SERRAKIEL, J. 1997. El Terciario del Dominio Malaguide en Sierra Espuña (provincia de Murcia, SE España). *Revista de la Sociedad Geologica de España*, **10**, 265–280.

MARTY, R., DUNBAR, R., MARTIN, J. B. & BAKER, P. 1988. Late Eocene diatomite from the Peruvian coastal desert, coastal upwelling in the eastern Pacific, and Pacific circulation before the terminal Eocene event. *Geology*, **16**, 818–822.

MEYER, R. 1987. *Paléolatérites et paléosols, l'empreinte du continent dans les séries sédimentaires.* Bureau de Recherches Géologiques et Minières, Manuel et Méthodes, **13**.

MICHARD, A., CHALOUAN, A., FEINBERG, H., GOFFÉ, B. & MONTIGNY, R. 2002. How does the alpine belt end between Spain and Morocco? *Bulletin de la Société Géologique de France*, **173**(1), 3–15.

MOLINA, E., MONACO, P., NOCCHI, M. & PARISI, G. 1986. Biostratigraphic correlation between the Central Subbetic (Spain) and Umbro-Marchean (Italy) pelagic sequences at the Eocene/Oligocene boundary using Foraminifera. *Developments in Palaeontology and Stratigraphy*, **9**, 75–85.

MOLINA, E., KELLER, G. & MADILL, M. 1988. Late Eocene to Oligocene events: Molino de Cobo, Betic Cordillera, Spain. *Revista Española de Micropaleontologia*, **20**, 491–514.

MOLINA, E., ARENILLAS, I., ARZ, J. A., CANUDO, J. I., GONZALVO, C., ORTIZ, N. & PARDO, A. 1996. Síntesis bioestratigráfica y eventos Palaeoceanográficos del Cretácico (Maastrichtiense) al Mioceno (Langhiense) basada en Foraminíferos. *Revista Española de Paleontologia, (Numero Extra)*, 195–203.

MORALES, J., SERRANO, F., JABALOY, A., *ET AL.* 1999. Active continental subduction beneath the Betic Cordillera and the Alboran Sea. *Geology*, **27**, 735–738.

MORLEY, C. K. 1987. Origin of a major cross-element zone: Moroccan Rif. *Geology*, **15**, 761–764.

MORLEY, C. K. 1988. The tectonic evolution of the Zoumi Sandstones, western Moroccan Rif. *Journal of the Geological Society, London*, **145**, 55–63.

MORLEY, C. K. 1992. Tectonic and sedimentary evidence for synchronous and out-of-sequence thrusting, Larache–Asilah area, Western Moroccan Rif. *Journal of the Geological Society, London*, **149**, 39–49.

MUTTI, E. 1992. *Turbidite sandstones*. Agip, Special Publication, Instituto di Geologia, Milan, 1–275.

NOLD, M., UTTINGER, J. & WILDI, W. 1981. *Géologie de la Dorsale Calcaire ente Tétouan et Assifane (Rif Interne, Maroc)*. Notes et Mémoires du Service Géologique du Maroc, **300**, 1–233.

OLIVIER, PH. 1984. *Evolution de la limite entre les Zones internes et les Zones externes dans l'Arc de Gibraltar (Maroc, Espagne)*. Doctorat d'Etat Thesis, Université Paul Sabatier, Toulouse.

PLATT, J. P. & VISSERS, R. L. M. 1989. A working hypothesis for the Alboran Sea and Gibraltar arc. *Geology*, **17**, 540–543.

PLINT, A. G. 1988. Sharp-based shoreface sequences and 'offshore bars' in the Cardium Formation of Alberta: their relationship to relative changes in sea level. *In*: WILGUS, C. K., HASTINGS, B. S., KENDALL, C. G. ST. C., POSAMENTIER, H. W., ROSS, C. A. & VAN WAGONER, J. C. *Sea Level Changes—An Integrated Approach*. Society of Economic, Palaeontologists and Mineralogists, Society for Sedimentary Geology, Special Publications, **42**, 357–370.

POMEROL, CH. 1985. La transition Eocène–Oligocène est-elle un phénomène progressif ou brutal. *Bulletin de la Société Géologique de France*, 8th series, **I**(2), 263–367.

PRÉAT, A., MAMET, B., DE RIDDER, C., BOULVAIN, F. & GILLAN, D. 2000. Iron bacterial and fungal mats, Bajocian stratotype (Mid-Jurassic, northern Normandy, France). *Sedimentary Geology*, **137**, 107–126.

PUGLISI, D., ZAGHLOUL, M. N. & MAATÉ, A. 2001. Evidence of sedimentary supply from plutonic sources in the Oligocene–Miocene flyschs of the Rifian Chain (Morocco): provenance and palaeogeographic implications. *Bollettino della Società Geologica Italiana*, **120**, 55–68.

RAOULT, F. 1966. *La chaîne du Haouz du Col d'Azlu d'Arabia au Bab Aonzar*. Notes et Mémoires du Service Géologique du Maroc, **184**, 61–146.

RAOULT, J. F. 1974. *Géologie du centre de la Chaîne Numidique (nord du Constantinois, Algérie)*. Mémoires de la Société Géologique de France, **121**, 1–162.

REUBERT, I., MICHARD, A., CHALOUAN, A., JUTEAU, TH. & JERMOUMI, B. 1982. Structure and emplacement of the Alpine-type peridotites from Béni-Bousera, Rif, Morocco: a polyphase tectonic interpretation. *Tectonophysics*, **82**, 231–251.

RIVAS, P., AGUIRRE, J. & BRAGA, J. 1997. Entolium beds: hiatal shell concentrations in starved pelagic settings (middle Liassic, SE Spain). *Eclogae Geologicae Helvetiae*, **90**, 293–301.

ROTH, P. H. 1989. Ocean circulation and calcareous nannoplankton evolution during the Jurassic and Cretaceous. *Palaeogeography, Palaeoclimatology, Palaeoecology*, **74**, 11–126.

SADDIQI, O., REUBERT, I. & MICHARD, A. 1988. Sur la tectonique de dénudation du manteau infracontinental dans les Béni Bousera, Rif septentrional, Maroc. *Comptes Rendus de l'Académie des Sciences, Série II*, **307**, 657–662.

SANCHEZ-RODRIGUEZ, L. & GEBAUER, D. 2000. Mesozoic formation of pyroxenites and gabbros in the Ronda area (southern Spain), followed by early Miocene subduction metamorphism and emplacement into the middle crust: U–Pb sensitive high-resolution microprobe dating of zircon. *Tectonophysics*, **316**, 19–44.

SANZ DE GALDEANO, C., SERRANO, F., LOPEZ GARRIDO, A. C. & MARTIN PEREZ, J. A. 1993. Palaeogeography of the Late Aquitanian-Early Burdigalian Basin in the western Betic Internal zone. *Geobios*, **26**(1), 43–55.

SAVRDA, C. E. 1995. Ichnologic applications in palaeoceanographic, palaeoclimatic, and sea-level studies. *Palaios*, **10**, 565–577.

SAVRDA, C. E., BROWNING, J. V., KRAWINKEL, H. & HESSELBO, S. P. 2001*a*. Firmground ichnofabrics in deep-water sequence stratigraphy, Tertiary cliniform-toe deposits, New Jersey Slope. *Palaios*, **16**, 294–305.

SAVRDA, C. E., KRAWINKEL, H., MCCARTHY, M. G., MCHUGH, C. M. G., OLSON, H. C. & MOUNTAIN, G. 2001*b*. Ichnofabrics of a Pleistocene slope succession, New Jersey margin: relations to climate and sea-level dynamics. *Palaeogeography, Palaeoclimatology, Palaeoecology*, **171**, 41–61.

SCHLAGER, W. 1989. Drowning unconformities on carbonate platforms. *In*: CREVELLO, P. D., WILSON, J. L., SARG, J. F. & READ, J. F. *Controls on Carbonate Platform and Basin Development*. Society of Economic, Palaeontologists and Mineralogists, Society for Sedimentary Geology, Special Publications, **44**, 15–25.

SERRANO, F., SANZ DE GALDEANO, C., DELGADO, F., LÓPEZ-GARRIDO, A. C. & MARTÍN-ALGARRA, A. 1995. The Mesozoic and Cenozoic Complex in the Malaga area: a Palaeogene olistostrome-type chaotic complex (Betic Cordillera, Spain). *Geologie en Mijnbouw*, **74**, 105–116.

TARGUISTI, K. 1994. *Petrologia y geoquimica de los macizos ultramaficos de Ojen (Andalucia) y de Béni Bousera (Rif septentrional, Marruecos)*. Doctoral Thesis, University of Granada.

WEIJERMARS, R. 1987. The Palaeomares brittle–ductile shear zone of southern Spain. *Journal of Structural Geology*, **9**, 139–157.

WILDI, W. 1981. Le Ferrysch: cône de sédimentation détritique en eau profonde à la bordure nord-ouest de l'Afrique au Jurassique moyen à supérieur (Rif externe, Maroc). *Eclogae Geologicae Helveticae*, **74**, 481–527.

WILSON, G. S., ROBERTS, A. P., VEROSUB, K. L., FLORINDO, F. & SAGNOTTI, L. 1998. Magnetostratigraphic chronology of the Eocene–Oligocene transition in the CIROS-1 core, Victoria Land margin, Antarctica: implications for Antarctic

glacial history. *Geological Society of America Bulletin*, **110**, 35–47.

ZACHOS, J. C., LOHMANN, K. C., WALKER, J. C. G. & WISE, S. W. 1993. Abrupt climate change and transient climates during the Palaeogene: a marine perspective. *Journal of Geology*, **101**, 191–213.

ZACHOS, J., SALAMY, K., QUINN, T. M. & DIESTER-HAASS, L. 1995. The late Eocene–early Oligocene deep-sea sediment record of continental glaciations, ocean productivity and deep water circulation and chemistry. American Geophysical Union, Spring Meeting Abstracts, 187.

Fault and fold interaction during the development of the Neogene–Quaternary Almería–Níjar basin (SE Betic Cordilleras)

ANTONIO PEDRERA[1], CARLOS MARÍN-LECHADO[2], JESÚS GALINDO-ZALDÍVAR[1], LUIS ROBERTO RODRÍGUEZ-FERNÁNDEZ[2] & ANA RUIZ-CONSTÁN[1]

[1]*Departamento de Geodinámica, Universidad de Granada, 18071 Granada, Spain (e-mail: jgalindo@ugr.es)*

[2]*Instituto Geológico y Minero de España, Urb. Alcázar del Genil, Edificio Zulema, no. 4 Bajo, 18006 Granada, Spain*

Abstract: The Neogene–Quaternary Almería–Níjar basin includes the Carboneras Fault, which constitutes a major left-lateral feature of the Betic Cordilleras. New gravity data help to determine the geometry of the sedimentary infill. The region underwent NE–SW extension during the Tortonian and local NW–SE compression during the first stages of Sierra Alhamilla uplift. During the Messinian, the sinistral strike-slip motion along the Carboneras Fault Zone, the dextral strike-slip motion along NW–SE-oriented faults, and the development of large folds such as the Sierra Alhamilla antiform, suggest clockwise rotation (towards the north) of the maximum stress axis (σ_1). During the Pliocene, a NNW–SSE-oriented compression also contributes to fold development. Finally, during the Quaternary, an ENE–WSW-directed extension controls the development of NW–SE-oriented normal oblique faults. The most recent local normal activity of the Carboneras Fault is related to this extension, whereas its behaviour as a left-lateral strike-slip fault may be a consequence of the accommodation of NW–SE normal fault displacements. Basic rock bodies, recognized by means of a detailed study of the magnetic anomalies, are related to the volcanic activity known to have occurred in the area in Late Miocene times.

The oblique convergence between the African and Eurasian plates, in the Western Mediterranean, is responsible for the development of the Betic and Rif Cordilleras on the wide band of deformation related to the plate boundary. These cordilleras constitute the western end of the European Alpine Chain and are separated by the Alboran Sea. The kinematics of the plate boundary (at present, convergence at $4\ mm\ a^{-1}$ in a NW–SE direction; DeMets *et al.* 1990) result in a regional NW–SE-trending compressive stress field with an associated NE–SW extension, which is most intense towards the internal parts of the cordilleras, although the stress field is highly variable in detail and includes areas of radial extension (Galindo-Zaldívar *et al.* 1993).

Taking into account both the lithological and the tectonic units of the Betic and Rif Cordilleras, the region may be subdivided into External and Internal Zones, which are separated by Flysch units (Fig. 1). The External Zones of the Betic and Rif Cordilleras are composed of sedimentary Mesozoic and Cenozoic rocks deposited on the European and African Variscan margins. The Internal Zones are formed by several metamorphic complexes that include Palaeozoic rocks. The main complexes in the Betic Cordilleras are, from bottom to top, the Nevado–Filábride, the Alpujárride and the Maláguide (Egeler 1963; Egeler & Simon 1969).

The main relief of the Internal Zones of the Betic Cordilleras is related to tectonic structures active since the Late Miocene. The antiforms correspond to east–west elongated mountains (Sierra Nevada, Sierra de los Filabres, Sierra de Gádor and Sierra Alhamilla) and the synforms correspond to elongated depressions between these mountain ranges (Weijermars *et al.* 1985; Galindo-Zaldívar *et al.* 2003; Sanz de Galdeano & Alfaro 2004). Whereas in the central Betic Cordilleras folds developed simultaneously to normal faults located along the borders of the mountain ranges (Galindo-Zaldívar *et al.* 2003), the eastern part of the Betic Cordilleras is affected by a fault system formed by large transcurrent sinistral faults (the Palomares and Carboneras faults) (Bousquet & Philip 1976; Bousquet 1979; Sanz de Galdeano 1983; Ott d'Estevou & Montenant 1985; Rutter *et al.* 1986; Montenat *et al.* 1987; Weijermars 1987; Montenant & Ott d'Estevou 1990; Silva *et al.* 1993), that probably continue into the Alboran Sea and into the northern Rif Cordilleras and constitute the Trans-Alboran Shear Zone (Larouzière *et al.* 1988).

From: MORATTI, G. & CHALOUAN, A. (eds) 2006. *Tectonics of the Western Mediterranean and North Africa.* Geological Society, London, Special Publications, **262**, 217–230.
0305-8719/06/$15.00

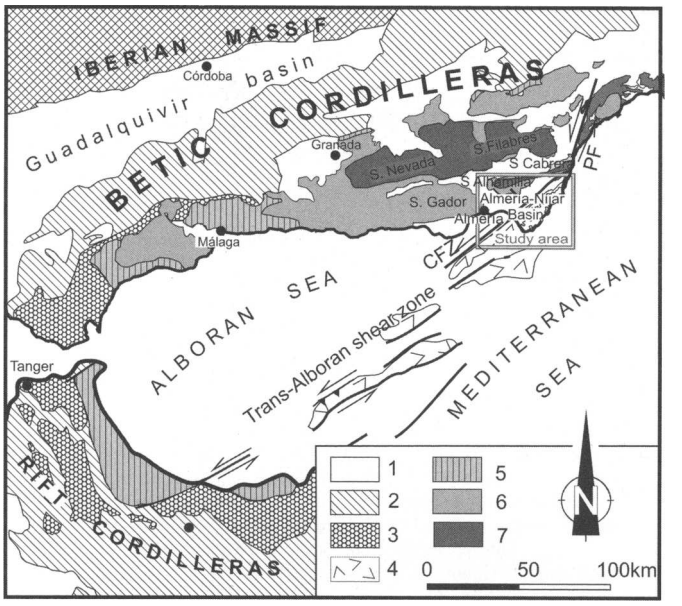

Fig. 1. Geological sketch of the Betic–Rif Cordillera. 1, Neogene and Quaternary sediments; 2, External Zones; 3, Flysch Units; 4, Neogene volcanic rocks; 5, Maláguide and Ghomáride complex and Predorsal and Dorsal complexes; 6, Alpujárride and Sébtide Complex; 7, Nevado–Filábride Complex; CFZ, Carboneras Fault Zone; PF, Palomares Fault.

The Almería–Níjar basin is located in the southeastern Betic Cordilleras, and is connected southwestwards with the Alboran Sea (Figs 1 and 2). The Neogene sediments were deposited on a basement that is variable in nature. The basement of the northwestern part of the Almería–Níjar basin is formed by Alpujárride and locally by Nevado–Filábride metapelites and marbles of Palaeozoic and Triassic ages. This region is affected by low- and high-angle normal faults (Martínez-Martínez & Azañón 1997). Tortonian to Early Messinian volcanic rocks crop out mainly along the southeastern basin margin, and although they generally represent the substratum of the sedimentary sequence filling the basin, sometimes volcanic rocks are also intercalated with the sediments (Bellon *et al.* 1983; Turner *et al.* 1999; Scotney *et al.* 2000). The sedimentary sequence of the Almería–Níjar basin starts with poorly represented middle Miocene rocks followed by Tortonian calcarenites and by Messinian marls with interlayered gypsum (Völk & Rondeel 1964; Addicot *et al.* 1979; Ott d'Estevou 1980; Baena & Voermans 1983; Van de Poel 1991; Martín *et al.* 1993). The Pliocene is represented by marls, sands and calcarenites. The top of the sequence consists of Quaternary detrital alluvial sedimentary deposits, and beach sediments occurring mostly in the southwestern sector.

The Carboneras Fault, which subdivides the Almería–Níjar basin, is formed by several subvertical and subparallel surfaces with a NE–SW trend (Faulkner *et al.* 2003) and has had a sinistral strike-slip kinematics since the Miocene and probably to the Pliocene (Ott d'Estevou & Montenant 1985). During the Late Pleistocene and Holocene, the fault kinematics changes to normal (Bell *et al.* 1997). Available studies from the northeastern sector of the Almería–Níjar basin (Montenant & Ott d'Estevou 1990; Huigbregtse *et al.* 1998) and the Sorbas basin (Stapel *et al.* 1996; Huigbregtse *et al.* 1998), located to the north of Sierra Alhamilla, indicate two main regional stress fields: a NW–SE compression from Tortonian to Early Messinian time, and a north–south compression from late Early Messinian to Quaternary time. The Plio-Quaternary deformations in the area have been analysed by Marín-Lechado *et al.* (2005), who have described a regional NE–SW extension with a subvertical maximum compressive stress in the upper crust, although local stresses indicating NW–SE compression have also been recognized. Near the Carboneras Fault, there is a great variability in the palaeostresses determined, including the occurrence of a NNE–SSW-oriented maximum compressive axis that is compatible with sinistral strike-slip tectonics.

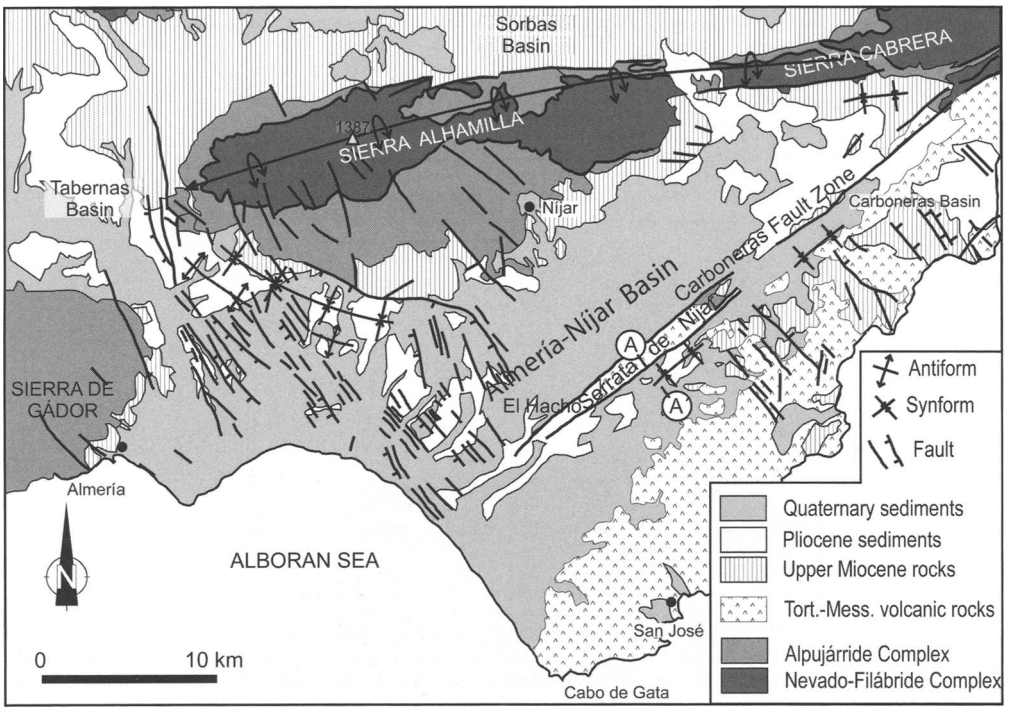

Fig. 2. Tectonic sketch of the Almería–Níjar basin and the surrounding areas. The position of the cross-section of Figure 5d is marked (A–A′).

In contrast to the considerable number of available geological studies (e.g. Montenat & Ott d'Estevou 1990, and references herein; Boorsma 1993), there are no detailed geophysical studies in this region that would help to determine the deep structure of the Neogene–Quaternary basin. In addition, the relationships between the activity of the various faults, large folds, volcanism and sedimentation remain controversial.

The aim of this paper is to analyse the interaction between extensional and transcurrent faults and folds that determine the spatial distribution and characteristics of the Neogene sedimentary filling of the Almería–Níjar basin. This study also focuses on the activity of the Carboneras Fault, which shows variable kinematics in the frame of a changing regional stress field. To this purpose, we performed a detailed analysis of the brittle deformation structures exposed in the area. Finally, the results of our study contribute to establishing the extent and nature of the Neogene volcanism in this area, and to determining the thickness of the Almería–Níjar basin infill and the nature of its bedrock units. New gravity and magnetic data have been interpreted in light of the available geological information.

Gravity and magnetic data acquisition and processing

Gravity data were acquired by means of a Worden Master gravity-meter, with a maximum accuracy of 0.01 mGal. The relative positioning of the gravity stations was done with a global positioning system (GPS) receiver and the heights of the stations were determined with a barometric altimeter with an accuracy of 0.5 m. Gravity measurement stations are located along six profiles (Fig. 3). Two profiles (5 and 6, Fig. 3) strike NE–SW, approximately parallel to the basin boundaries, and are located along the two blocks separated by the Carboneras Fault. The four remaining profiles (1–4, Fig. 3) strike NW–SE, orthogonal to the fault, and provide complete sections of the basins, from the metamorphic rocks of Sierra Alhamilla to the volcanic rocks of Cabo de Gata. The average distance between stations along the profiles was about 300 m.

The gravity values were established with reference to the Almería gravimetric base (Instituto Geográfico Nacional), which allows us to determine the absolute gravity values along all the profiles. The Bouguer anomaly was obtained considering a

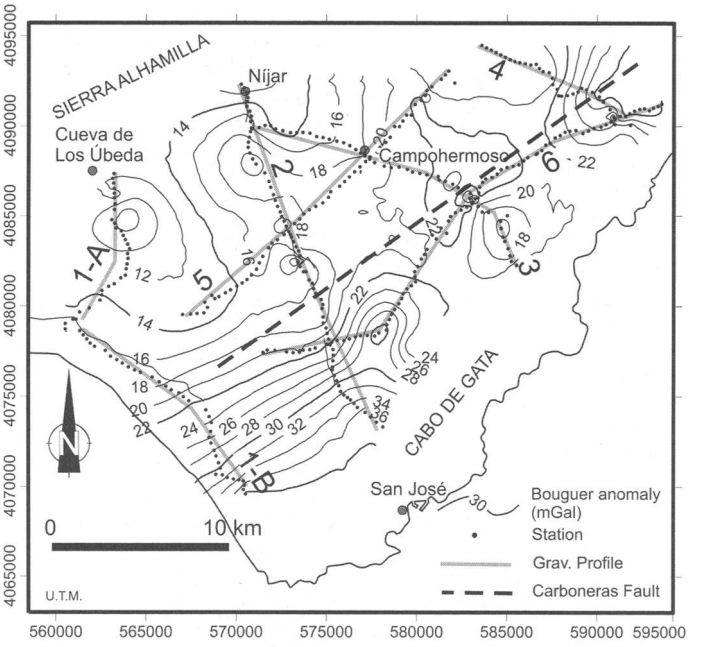

Fig. 3. Bouguer anomaly map, showing the position of the geophysical sites and the profile traces. Reference density is 2.67 g cm^{-3}.

reference density of 2.67 g cm^{-3} and applying the topographic correction to a radius of 10 km calculated from a digital elevation model with a grid of 100 m. The results obtained along the profiles were interpolated to determine the Bouguer anomaly map of the region (Fig. 3). The regional anomaly was established taking into account the acquired data and the Spanish 1:1 000 000 gravimetric map (Instituto Geográfico Nacional 1976). The residual anomaly map (Fig. 4) aims to show the anomalies related to a change in thickness and lithological nature of the sedimentary infill, and related to the presence of interlayered volcanic rocks.

The total intensity of the magnetic field was determined simultaneously to the gravity measurements, using a GSM 8 proton precession magnetometer with a maximum accuracy of 1 nT. The magnetic anomaly was calculated considering the IGRF 2000 value (IAGA 2000). The spikes were eliminated and the diurnal variations were corrected taking into account drift through the measurement cycles. Metallic constructions interfered with the magnetic anomalies obtained in some profiles. To obtain direct susceptibility values from rock outcrops, field magnetic susceptibility measurements were made using a portable Exploranium kappameter KT-9 susceptometer.

Residual gravity and magnetic 2D models, developed with GRAVMAG v. 1.7 software (Pedley *et al.* 1993), are proposed along the measured profiles. These models contribute to establishing the deep structure of the region. Whereas the gravity data mainly determine the variability of sedimentary infill thickness, the magnetic data allow us to establish the nature of the basin basement and the distribution of volcanic rocks.

Main tectonic structures in the Almería–Níjar basin

The Almería–Níjar basin is filled by Neogene and Quaternary sediments deposited between the southern limb of the Sierra Alhamilla antiform and the range represented by the volcanic edifices of the Cabo de Gata. The basin is deformed by folds and transcurrent and normal faults.

Folds

The Sierra Alhamilla antiform (Figs 2 and 5) is the largest fold in the study area. It is an ENE–WSW, north-vergent fold, with a subvertical or even reverse northern flank, a south-dipping axial surface and a westward periclinal end (Weijermars *et al.* 1985). Its maximum width is 12 km and the

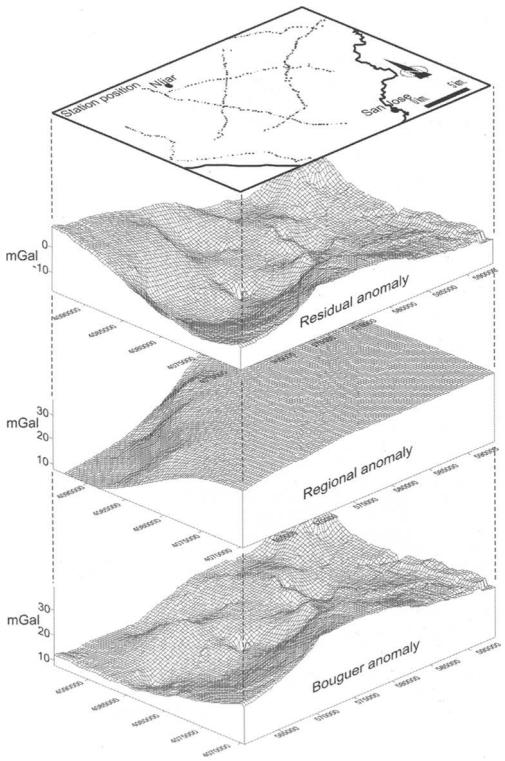

Fig. 4. Three-dimensional Bouguer, regional and residual anomaly maps. Reference density is 2.67 g cm^{-3}. The surface that represented the residual anomaly has a close relationship to the sedimentary rock thickness of the Almería–Níjar basin filling.

highest peak is 1387 m above sea level (a.s.l.). Braga *et al.* (2003) estimated an uplift average rate for the entire antiform from the upper Tortonian rocks of 180 m Ma^{-1}. The fold affects the basement rocks and the basin margin Tortonian and Messinian sediments.

The Neogene sediments that fill the Almería–Níjar sedimentary basin are also deformed by a set of minor folds (Figs 2 and 5). In the southeastern border of Sierra Alhamilla, near the Carboneras Fault, Huibregtse *et al.* (1998) recognized folds with N70°E-oriented axes that affect Pliocene sediments, and related them to the transpressive deformation associated with the sinistral movement of the Carboneras Fault. Along the southwestern end of Sierra Alhamilla, folds have wavelengths of several hundreds of metres and are open to gentle. The minor fold axes, fitting the western periclinal end of the large antiform of Sierra Alhamilla, show a WNW–ESE predominant orientation (Fig. 2) and deform rocks as young as Pliocene sediments (Fig. 5a).

In addition to the open folds, in the southeastern block, near the Carboneras Fault Zone, a closed synform (Fig. 5d) with very high-angle dipping bedding is observed in Neogene sediments (Montenant & Ott d'Estevou 1990; Scotney *et al.* 2000). Montenant & Ott d'Estevou (1990) interpreted the vertical bedding in this area as a consequence of the development of a syncline during the transpressive stage of the Carboneras Fault in Messinian times. The bedding surfaces show vertical striations (Fig. 5c). Kinematic analysis of the fault surfaces indicates that the downthrown block is the northwestern one, where, however, the uplifted Serrata de Níjar is located, as a consequence of the flexural slip deformation.

The presence of Late Tortonian–Early Messinian folded sediments below Messinian less folded sediments would indicate that the minor folds and the Sierra Alhamilla larger open fold started to develop from Messinian time (Weijermars *et al.* 1985; Braga *et al.* 2003; Sanz de Galdeano & Alfaro 2004).

Brittle structures

The Almería-Níjar basin faults have been studied in detail since the earliest papers produced by the Groupe de Recherche Néotectonique de l'Arc de Gibraltar (1977) and up to recent times (Faulkner *et al.* 2003), owing to the good quality of the outcrops and intense tectonic activity. Although large transcurrent faults have been studied in detail, research on the recent normal faulting of this region is scarce, yet indicates a relevant tectonic activity (Marín-Lechado *et al.* 2005).

The Carboneras Fault Zone (CFZ) crosses the Níjar basin in a N40°E direction, and divides the area into two main blocks, the northwestern and southeastern ones. It comprises several lower-rank features recording a sinistral slip component (Bousquet & Montenant 1974). The Miocene sediments, together with metamorphic and volcanic basement rocks, crop out along a highly deformed zone (Van de Poel 1991; Faulkner *et al.* 2003), where different fault surfaces extending hundreds of metres are associated with fault rocks a few metres thick (Rutter *et al.* 1986). Fault surfaces bound an elongated ridge corresponding to La Serrata de Níjar. Montenant & Ott d'Estevou (1990) considered the activity of the fault to be simultaneous with Late Miocene deep-water sedimentation and volcanic rock eruption, whereas Keller *et al.* (1995) and Scotney *et al.* (2000) suggested an initial movement during the mid-Miocene (11 Ma), as unconformable Tortonian volcanic rocks and even Tortonian sediments lie over fault rocks developed in the metamorphic basement (Ott d'Estevou & Montenant 1985). The sinistral strike-slip movement from Late Tortonian time was estimated at 18 km by

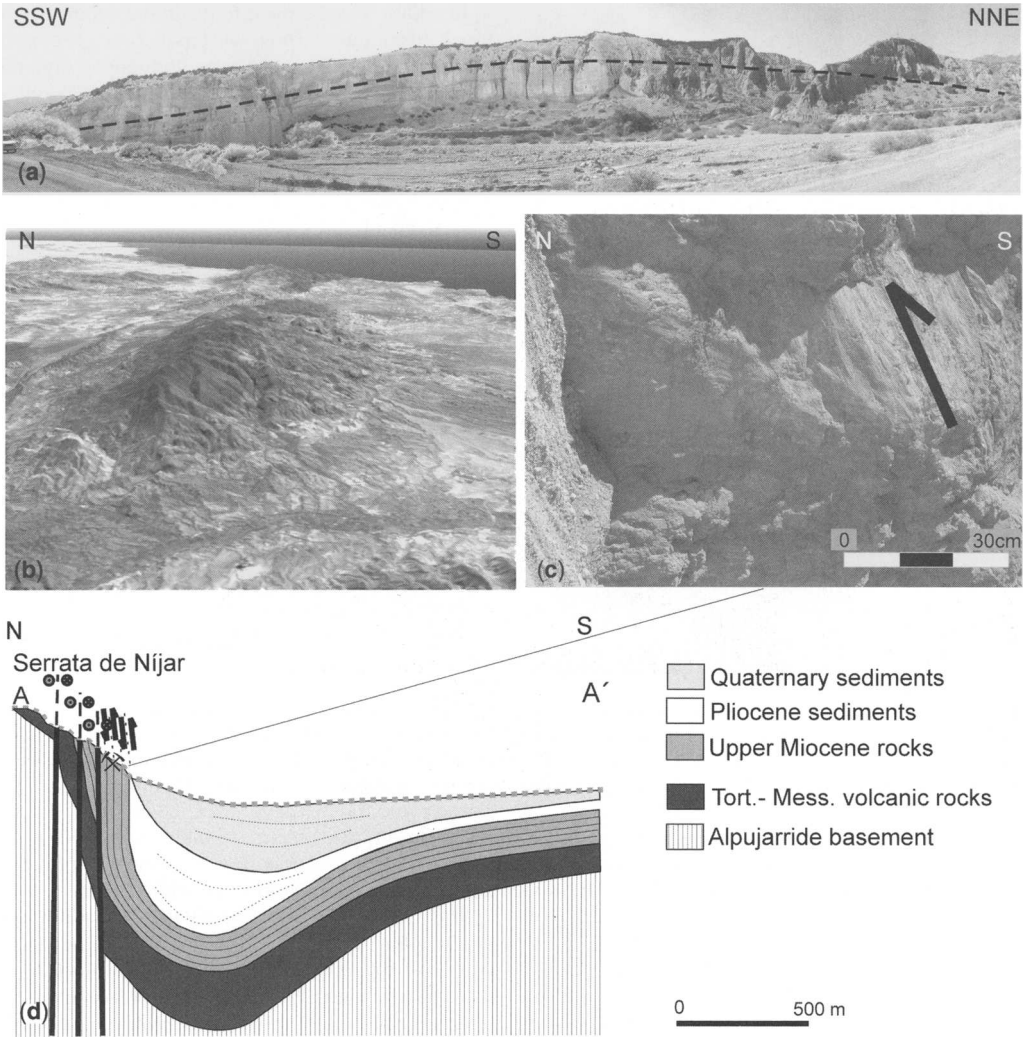

Fig. 5. Example of folds developed in the Almería–Níjar basin. (**a**) WNW–ESE Pliocene open fold located in the western periclinal end of Sierra Alhamilla. (**b**) Aerial image restored from the topography and satellite data of the Sierra Alhamilla antiform. (**c**) Vertical striations observed in a very high-angle dipping strata surface. The viewer is situated in the upthrown block. (**d**) Cross-section located south of the Carboneras Fault Zone of an asymmetrical synclinel with a northern vertical flank (position shown in Fig. 2).

Montenant & Ott d'Estevou (1990). However, other workers have estimated a horizontal movement from the mid-Messinian of 30–40 km on the basis of the displacement of volcanic rocks and sediment position (Rutter *et al.* 1986; Weijermars 1987). During the Holocene, the marine terrace dislocation indicates a normal displacement of the CFZ (Bell *et al.* 1997).

Field observations of the Plio-Quaternary sediments point to little recent activity of the CFZ, as shown by undisturbed sediment covering the central sector (Fig. 2). The recent tectonic activity is observed only locally, for instance in the SW sector, where N30°–45°E subvertical sinistral strike-slip faults with minor displacement deform Pleistocene sediments (e.g. alluvial fan conglomerates, El Hacho zone, *x*: 572.500, *y*: 4.079.500, Figs 2 and 6a). In this locality, a metre-thick fault gouge separates the Pleistocene conglomerates from the Pliocene grey–yellow sands and modifies the drainage network, exhibiting a left-lateral slip component.

The Níjar–Almería basin is also deformed by other normal and transcurrent faults. In the western end of Sierra Alhamilla, a set of NW–SE normal faults, generally dipping to the SW,

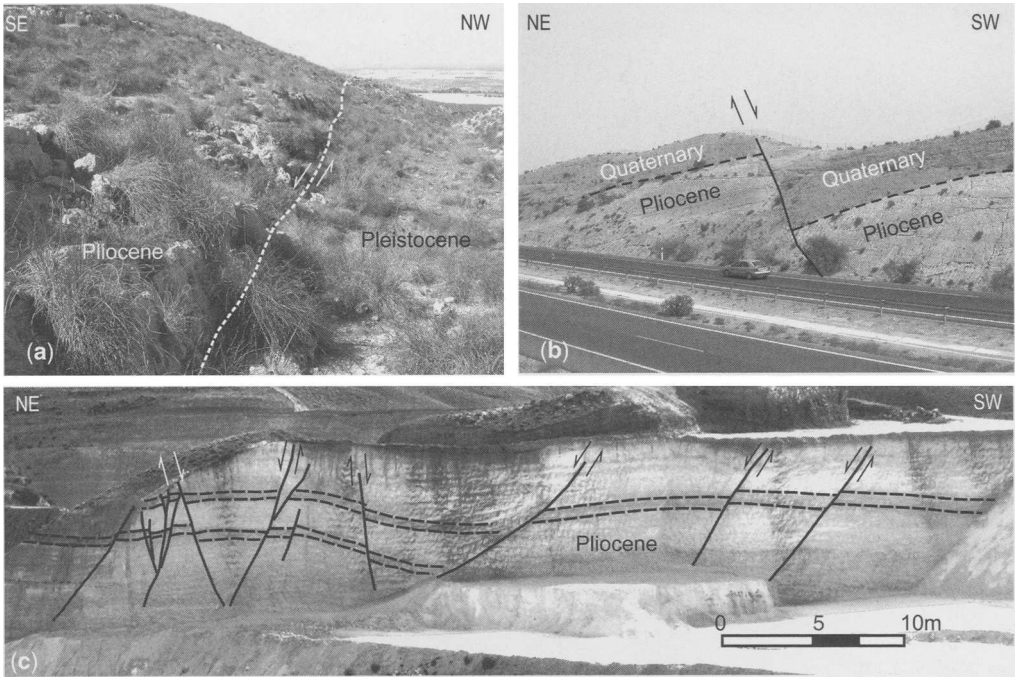

Fig. 6. Field examples of faults developed in the Almería–Níjar and Carboneras basins. (**a**) Sinistral strike-slip fault with a NE–SW orientation that deforms Pleistocene and Pliocene rocks in El Hacho. (**b**) Recent synsedimentary NW–SE normal fault situated NW of El Hacho, in the northern block of the CFZ. (**c**) Pliocene rocks situated in the eastern part of the region (Carboneras basin) and deformed by NW–SE-oriented normal faults dipping NE.

deforms the Late Tortonian sediments and generates a half-graben between Sierra Alhamilla and Sierra de Gádor (Montenant & Ott d'Estevou 1990). The Tortonian conglomerates of the southern border of Sierra Alhamilla are also affected by N150°–160°E normal faults, occasionally covered by undisturbed Messinian sediment (Montenant & Ott d'Estevou 1990). These faults show striae that indicate initially normal kinematics overprinted by dextral strike-slip kinematics, but the Tortonian age of the rocks only indicates the maximum age of faulting. In the northern sector of the Almería–Níjar basin, subvertical NE–SW-oriented sinistral strike-slip faults affect the Messinian sediments. Nevertheless, NW–SE-oriented dextral faults are well developed and occasionally affect rocks to earliest Pliocene sediments. Pliocene and Quaternary rocks of the Almería–Níjar basin are deformed by NW–SE-oriented normal faults, generally dipping 60° to the SW in the western part of the basin, that sometimes show evidence of synsedimentary activity, such as the development of small asymmetric wedge infill (Fig. 6b). Moreover, normal synsedimentary Pliocene normal faults, mainly dipping northeastwards, have been recognized in the small Carboneras basin (Figs 2 and 6c).

The Neogene and Quaternary rocks are generally affected by variable-sized joints distributed in one or two sets (Fig. 7d). The Quaternary sediments are deformed by NW–SE-oriented tension joints (Fig. 7d) that are also observed in older deposits (e.g. Messinian and Pliocene, Fig. 7a and 7c), indicating a NE–SW orientation of the σ_3 axis. A set of hybrid joints that deforms Pliocene rocks (Fig. 7b) also indicates a NW–SE orientation of the σ_1 axis, probably active locally at shallow crustal levels, before the Quaternary.

Geophysical data and deep structure

The new acquired gravity and magnetic data allow us to illustrate the deep structure of the basin. In addition, available borehole data are used to constrain the structure at shallow levels.

The Bouguer anomaly values decrease regionally towards the NW (Figs 3 and 4), indicating an increase in crustal thickness towards the Betic Cordillera, as modelled with regional gravity data by Torné & Banda (1992). The negative residual anomaly (Fig. 4) shows that the thickness of the sedimentary infill increases generally towards the

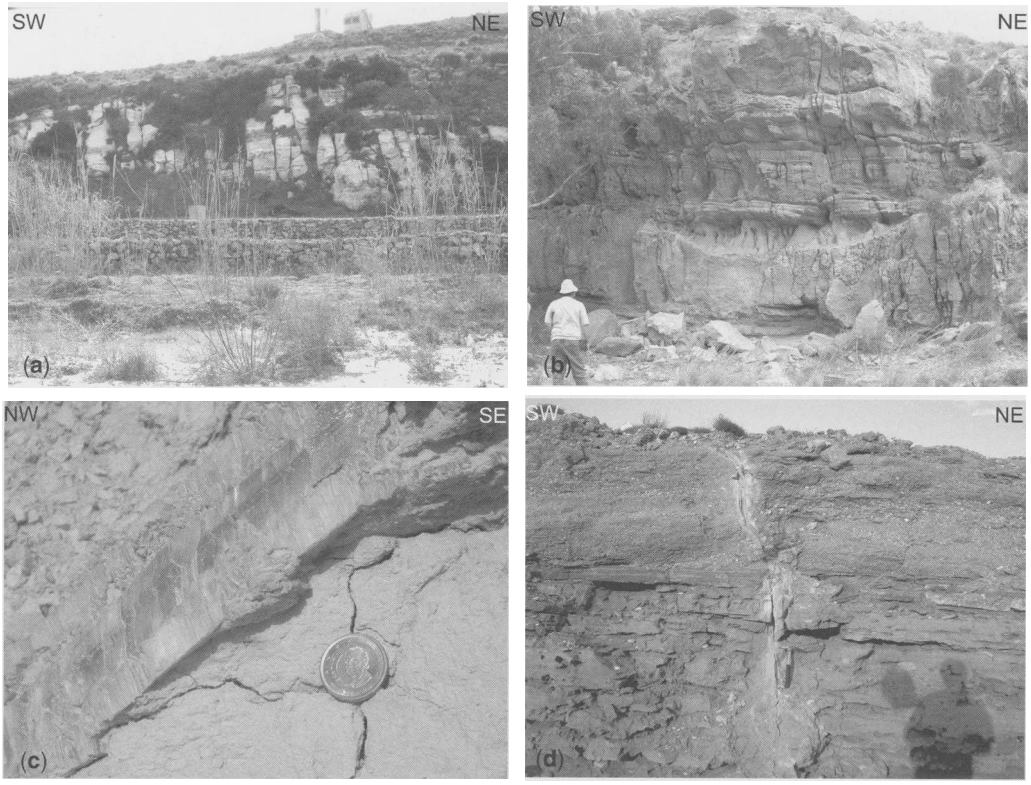

Fig. 7. Field examples of joints developed in the Almería–Níjar basin. (**a**) NW–SE tension joints affecting Messinian sediments and located in the easternmost sector of the basin. (**b**) Hybrid joints fracturing Pliocene calcarenites. (**c**) Detail of gypsum fibres filling an open tensional joint developed in Pliocene sands. (**d**) Tensional joint developed in alluvial sediments of Quaternary age.

SW. The maximum values of residual anomalies are reached near the basin boundaries that correspond to outcrops of the metamorphic rocks of Sierra Alhamilla, to the NW, and to the volcanic rocks of Sierra de Gata, to the SE. The anomalies related to the CFZ are better developed towards the NE end of the basin.

Residual gravity and magnetic anomalies were considered together in 2D models (Figs 8 and 9) to determine the deep structure of the basin, taking into account the main geological bodies whose boundaries can be clearly recognized in borehole data (borehole database of the Instituto Geológico y Minero de España) and in surface observations. For gravity modelling, an average density was considered for each unit in view of their predominant lithology and the standard values (Robinson & Çoruh 1988; Telford *et al.* 1990). Above the metamorphic and volcanic basement rocks (2.67 g cm^{-3}), three main units of sedimentary infill were distinguished. The lowest unit consists of Late Miocene marls and gypsums (2.2 g cm^{-3}) overlain unconformably by Pliocene marls and calcarenites (2.35 g cm^{-3}). The top of the basin infill is represented by Quaternary detrital poorly consolidated continental sediments (2 g cm^{-3}). In addition, some volcanic bodies interlayered with the Late Miocene sediments were modelled with a density (2.7–2.8 g cm^{-3}) that varies in the different profiles, to attain the best fit between measured and theoretical anomalies.

An irregular basement is observed in the gravity model profiles in two directions: both parallel to and orthogonal to the basin borders, crossing the CFZ. The deformation and the displacement of the basin substratum by the CFZ is variable along strike, and in profiles 3 and 4 an along-basement elevation associated with a sharp elongated depression coincides clearly with the CFZ.

Magnetic modelling allows us to specify the distribution of volcanic rocks and the geometry of the basement in the southern part of the basin. Magnetic susceptibility was measured in some volcanic rocks cropping out in the area, giving values between

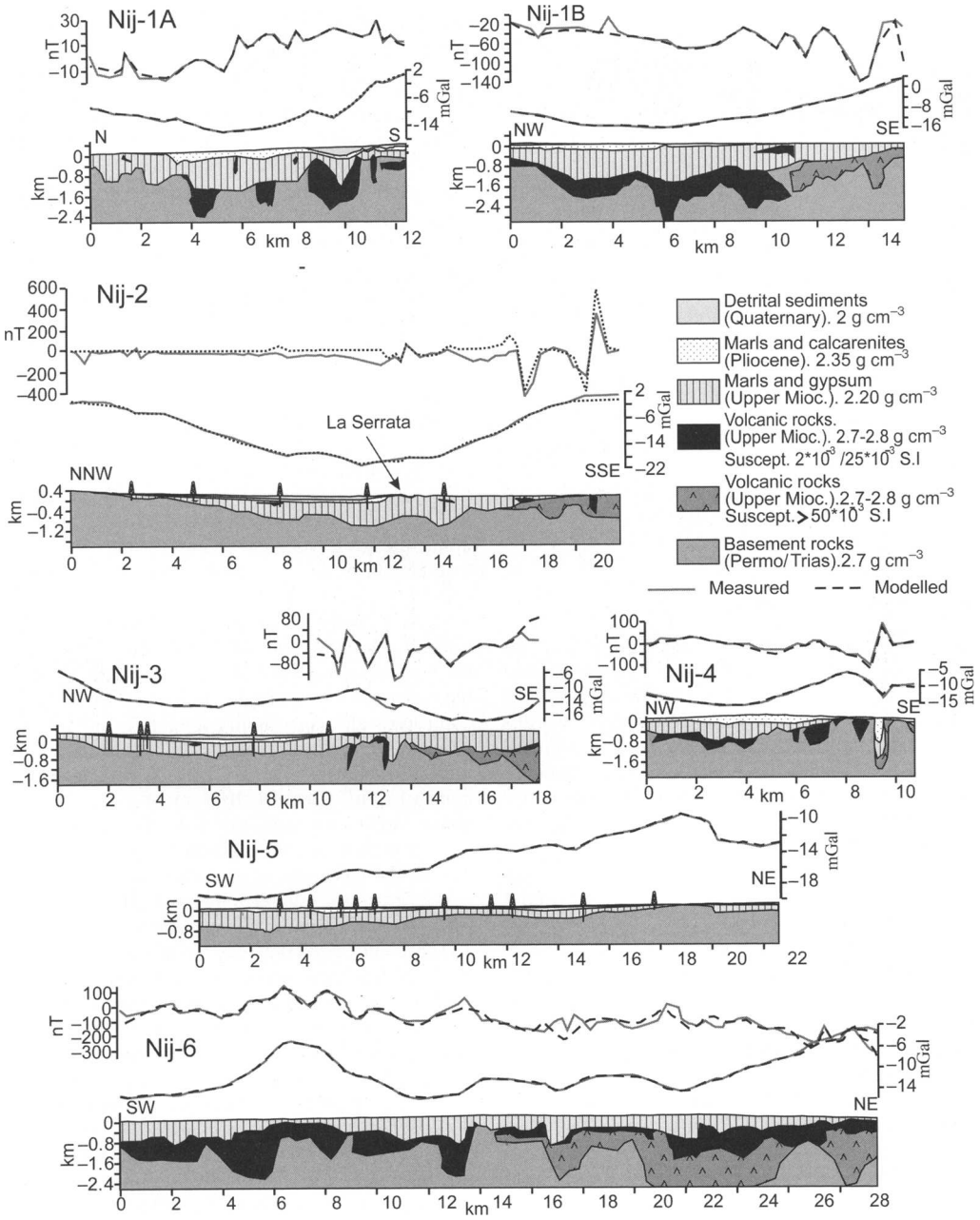

Fig. 8. Two-dimensional gravity and magnetic models. The position of the profiles is marked in Figure 3.

0.2×10^{-3} and 18×10^{-3} SI units. The dipoles observed in the region, with maxima to the north and minima to the south, suggest either that the magnetic anomalies are only a consequence of contrast in susceptibility values, or that the remanent magnetization is parallel to the induced one. The best fit of measured and theoretical magnetic anomalies during modelling is achieved when a susceptibility greater than field measurements (2×10^{-3} to 60×10^{-3} SI) is considered. This fact may indicate the existence of a remanent magnetism component in the rocks subparallel to the induced susceptibility.

The palaeomagnetic studies in the area (Calvo *et al.* 1994) confirm that the volcanic rocks have not undergone large rotations. In the models we can distinguish two groups of volcanic rock with susceptibility values between 2×10^{-3} and 25×10^{-3} SI, and greater than 50×10^{-3} SI, respectively. Taking into account the rocks cropping out in the Cabo de Gata and the susceptibility ranges (Telford *et al.* 1990), these two units may correspond to intermediate to basic volcanic rocks.

The magnetic modelling shows that volcanic rocks are irregularly distributed in the basin, although they are more abundant near the southeastern sector, near Sierra de Gata. The rocks with susceptibility values ranging between 2×10^{-3} and 25×10^{-3} SI units are interlayered with the sedimentary infill or constitute the basin basement. The volcanic rocks with susceptibility values greater than 50×10^{-3} SI units have an irregular distribution, and are found only in the basement of the southeastern block of the CFZ.

Discussion

The Almería–Níjar basin is an excellent area for analysing the interactions between extensional and transcurrent faults and folds related to the development of the relief in the southeastern Betic Cordilleras from the Tortonian to the present (Fig. 2). The above structures determine the crustal thickening from the Alboran Sea towards the major elevations of the Cordilleras, as shown by the progressive decrease to the NW of the Bouguer anomaly, whereas the occurrence of Neogene and Quaternary rocks provides evidence on the timing of the recent deformations.

The major structures in the Almería–Níjar basin are: (1) the Sierra Alhamilla antiform, to the north, which started to form from Late Tortonian–Messinian time (Weijermars *et al.* 1985); (2) the volcanic edifices of the Cabo de Gata, to the SE, which were emplaced during Tortonian to Early Messinian time (Bellon *et al.* 1983; Turner *et al.* 1999) (Fig. 2); (3) the sinistral CFZ (Rutter *et al.* 1986; Weijermars *et al.* 1987; Montenant & Ott d'Estevou 1990), which separates the basin into main two blocks.

The variability of the basin infill thickness and the morphostructural characteristics of the substratum were established by analysing the results of a new gravity survey and the available borehole data. Gravity models (Figs 8 and 9) clearly indicate the irregular geometry of the high-density basement top that corresponds to the Alpujárride rocks cropping out in Sierra Alhamilla, or to the volcanic edifices that constitute the Cabo de Gata. In general, where the basin basement is deeper, the basin infill is thicker (as in the southwestern sector, where it is connected to the Alboran Sea), and vice versa. The basin basement geometry is very irregular in sections parallel or orthogonal to the basin borders. The northwestern part of the basin shows depocentres and morphostructural highs related mainly to the activity of the NW–SE normal faults, some of them extending along the basin borders and continuing to the Sierra Alhamilla. The geometry of the basement, in the southeastern part, is determined by the complex palaeorelief of the volcanic edifices of the Cabo de Gata.

According to some workers (Bernini *et al.* 1990; Montenat & Ott d'Estevou 1990), the CFZ was interpreted to be active since the Late Miocene; however, there is no clear evidence of its recent activity, and in some sectors, it is characterized by a Quaternary normal kinematics (Bell *et al.* 1997) or by sinistral strike-slip motion (El Hacho zone, Figs 2 and 6a). The CFZ has a variable expression along the gravity profiles (Figs 8 and 9). In the central–northeastern region there is a sharp feature related to a basement high, to the NW, and a marked depression, to the SE, forming a closed fold in Messinian rocks. However, to the SW there is no appreciable difference in the depth of the basement when the two blocks of the CFZ are compared, although in the field it is possible to observe the continuity of the fault zone along the linear Serrata de Níjar (Fig. 2). This setting may point to a differential behaviour of the fault zone along strike: towards the SW the transcurrent motion is more regular and does not substantially disturb the basement depth, whereas in the northeastern region it may develop vertical relative displacement of fault blocks producing small basin and basement highs that may be interpreted as transtensional and transpressional structures.

The analysis of the magnetic anomaly data helped to determine the distribution of the volcanic rocks, either in the basin substratum or in interlayers within the sedimentary infill. The magnetic and borehole data show that in the basement of the NW block, volcanic rocks are well represented, though less abundant than in the SE block, and sometimes are also interlayered within sedimentary rocks (Fig. 9). These data suggest that the strike-slip component of the CFZ is not necessarily tens of kilometres, because rock outcrops are not good markers for determining the strike displacement. A smaller strike-slip displacement is more compatible with the activity of the CFZ and the obliquely oriented Palomares Fault Zone (Fig. 1) during the Late Miocene.

A well-developed set of NW–SE-oriented normal faults offers good evidence of very recent tectonic activity, as recorded by the presence of

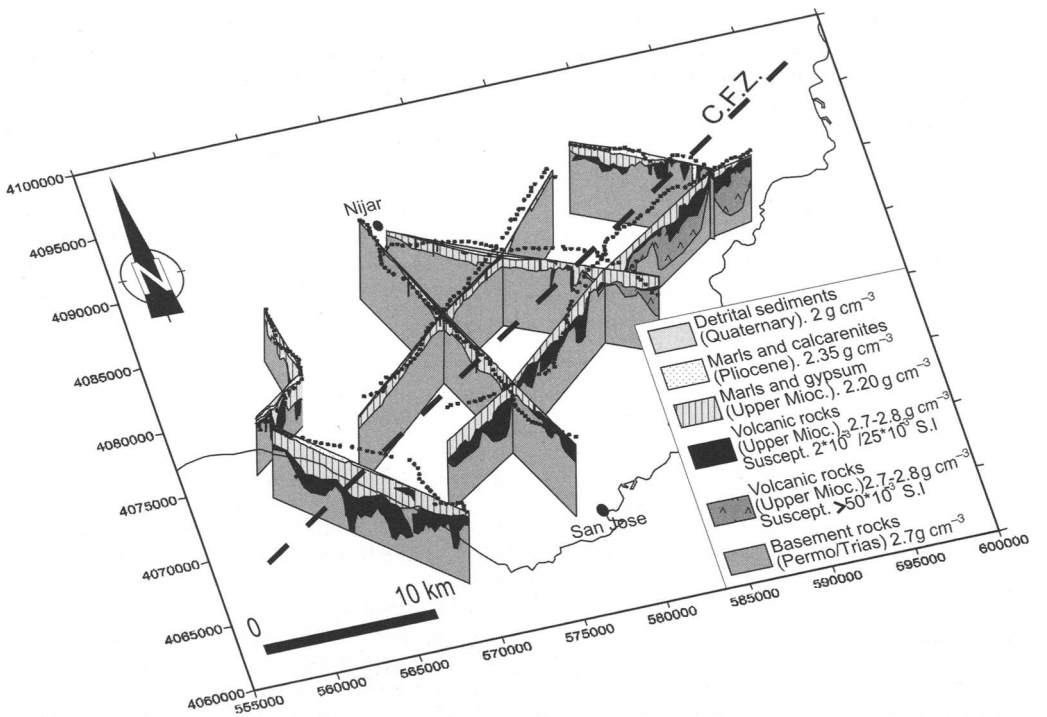

Fig. 9. Location of the geophysical models and relation with the CFZ position. It should be noted that the volcanism is located in both fault blocks and the main depocentre of the Níjar–Almería basin is situated in the southwestern part of the basin, north of the CFZ.

wedge-shaped sedimentary infill (Figs 8 and 9) and by the occurrence of fresh-looking topographic scarps (Fig. 6). These are mainly located in the western part of the basin, between the Sierra Alhamilla antiform and the CFZ, and in the eastern sector, in the Carboneras basin. This fault set is roughly orthogonal to the CFZ (Fig. 2).

As concerns folding, the region is deformed by open to closed folds (Figs 2 and 5). Some of them, like those located in the northwestern part of the basin, may be related to the large Sierra Alhamilla antiform. Additional closed folds are located near the CFZ, and are characterized by subvertical or even reverse flanks (Fig. 5); these may be associated with transcurrent fault activity (Montenat & Ott d'Estevou 1990). These closed folds accommodate the transpressive movement of the CFZ by means of a flexural slip mechanism that develops subvertical striation on the bedding surfaces.

The analysis of microfaults in rocks of different ages (Stapel *et al.* 1996; Huibregtse *et al.* 1998) points to a clockwise rotation of the stresses from a NW–SE-oriented maximum compression, during the Tortonian, to a north–south compression since the Messinian (in the NE sector of the Almería–Níjar basin). This result is compatible with the sinistral character of the CFZ. Marín-Lechado *et al.* (2005) studied microfaults and joints that indicate the occurrence, during the Pliocene, of a NW–SE-oriented maximum compression (σ_1) simultaneous with a NE–SW extension (σ_3). During the Quaternary, although the uplift of the region would suggest regional compression, palaeostress determinations (Marín-Lechado *et al.* 2005), the occurrence of NW–SE normal faults (Figs 2 and 6b), and the local normal kinematics of the CFZ (Bell *et al.* 1997) all indicate that the maximum stress is subvertical. It is suggested therefore that the NW–SE to north–south compression induced by the convergence between the European and African plates is probably active at deep crustal levels, hence producing the relief uplift, whereas the development of extensional structures is confined within the upper crustal levels (Galindo-Zaldívar *et al.* 2003). The development of NE–SW normal faults may also produce local strike-slip reactivation of the CFZ (Fig. 6a). Thus, in general, the Neogene–Quaternary evolution of the area is determined by a variable trend of the σ_3 axis, generally oriented from NE–SW to east–west, and by a σ_1 axis that is either subvertical or subhorizontal, but with NW–SE to north–south orientation.

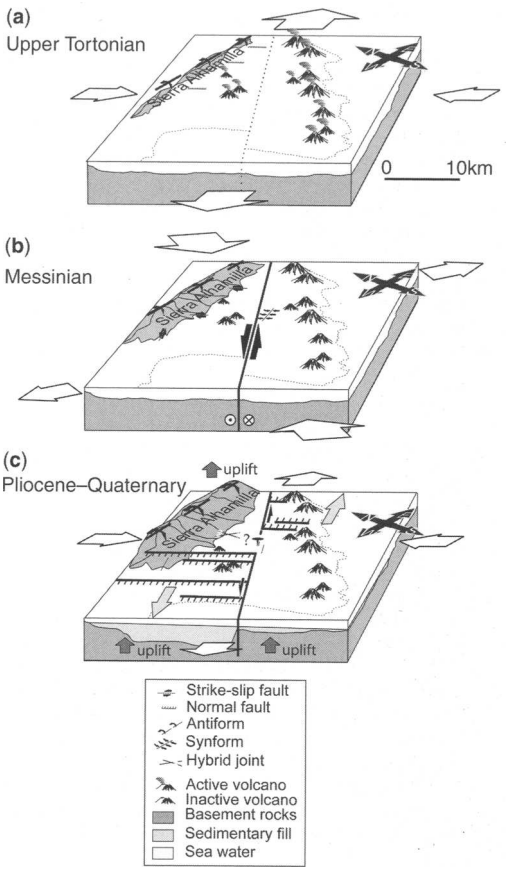

Fig. 10. Block diagrams representing the evolution of the main structures and the regional stress field in the Almería–Níjar basin. The changing stress field is analysed in three stages, showing the interaction of the extensional and transcurrent faults and folds during Late Tortonian, Messinian and Pliocene–Quaternary times.

Conclusions

The results of this study allow us to characterize the main features of the evolution of the Almería–Níjar basin since the Tortonian. The Almería–Níjar basin infill thickness increases generally towards the SW, but it shows an irregular geometry as a consequence of the depocentre location and topography, which are related to fault activity and to the Neogene volcanism in the area.

The available geological data on Tortonian deformations indicate that the region has possibly undergone a NW–SE compression and orthogonal extension, which is incompatible with the activity of the NE–SW-oriented CFZ (Fig. 10a). In this stage, the Sierra Alhamilla antiform starts to develop (Latest Tortonian–Earliest Messinian) and there is volcanic activity mainly concentrated in the Cabo de Gata region. The presence, after Earliest Messinian, of north–south to NNE–SSW compression may have activated the CFZ (Fig. 10b) in a variable setting. Transpressional and transtensional structures develop in the NE part of the CFZ, producing an irregular geometry of the basin basement and the inversion of small basins by closed folds. Towards the SW, a pure strike-slip motion, with no related steps in the basement, takes place. The slip on the fault may be moderate, taking into account that the volcanism is located in both fault blocks, and there are no clear displaced markers. During the Pliocene, the region is affected by a NW–SE compression and an orthogonal extension, which contribute to the development of open folds and faults with related depocentres. The progressive switching to an extensional setting in the upper crust, simultaneous to the uplift related to compression in lower crustal levels as a result of plate convergence, activates NW–SE-striking normal faults orthogonal to the CFZ. At present (Fig. 10c) the CFZ may have moderate activity and may constitute a left-lateral fault that accommodates the slip related to the most active NW–SE normal faults, although local normal kinematics (Bell *et al.* 1997) may also accommodate the extension of the upper crust.

This study was supported by CICYT project BTE2003-01699. The comments of F. Sani and G. Cello have greatly improved the quality of this contribution.

References

ADDICOTT, W. O., SNAVELY, P. D., POORE, R. Z. & BUKRY, D. 1979. La secuencia neógena marina de los Campos de Dalías y de Níjar (Almería). *Estudios Geológicos*, **35**, 609–631.

BAENA, J. & VOERMANS, F. 1983. *Mapa y memoria explicativa de la Hoja 1.045 (Almería).* IGME Map 1045, scale 1:50 000.

BELL, J. W., AMELUNG, F. & KING, G. 1997. Preliminary late Quaternary slip history of the Carboneras fault, southeastern Spain. *Journal of Geodynamics*, **24**, 51–66.

BELLON, H., BORDET, P. & MONTENAT, C. 1983. Chronologie du magmatisme néogène des Cordillères Bétiques (Espagne meridionale). *Bulletin de la Société Géologique de France*, **25**(2), 205–217.

BERNINI, M., BOCCALETTI, M., GELATI, R., MORATTI, G., PAPANI, G. & TORTORICI, L. 1990. The role of E–W transpressive movements in the evolution of the Neogene basins of the Betic Cordillera. *Annales Tectonicae*, **4**(2), 81–95.

BOORSMA, L. J. 1993. *Syn-tectonic sedimentation in a Neogene strike-slip basin (Serrata area, SE Spain).* PhD thesis, Free University, Amsterdam.

BOUSQUET, J. C. 1979. Strike-slip faults in southeastern Spain. *Tectonophysics*, **52**, 277–286.

BOUSQUET, J. C. & MONTENANT, C. 1974. Présence de décrochement Nord-Est, Sud-Ouest plioquaternaires dans les Cordillères bétiques orientales (Espagne). Extension et signification générale. *Comptes Rendus de l'Académie des Sciences*, **278**, 2617–2620.

BOUSQUET, J. C. & PHILIP, H. 1976. Observations microtectoniques sur la compression Nord–Sud quaternaire des Cordillères bétiques orientales (Espagne méridionale, Arc de Gibraltar). *Bulletin de la Société Géologique de France*, **18**(3), 711–734.

BRAGA, J. C., MARTÍN, J. M. & QUESADA, C. 2003. Patterns and average rates of late Neogene–Recent uplift of the Betic Cordillera, SE Spain. *Geomorphology*, **50**, 3–26.

CALVO, M., OSETE, M. L. & VEGAS, R. 1994. Palaeomagnetic rotations in opposite senses in southeastern Spain. *Geophysical Research Letters*, **21**(9), 761–764.

DEMETS, C., GORDON, R. G., ARGUS D. F. & STEIN, S. 1990. Current plate motions. *Geophysical Journal International*, **101**, 425–478.

EGELER, C. G. 1963. On the tectonics of the eastern Betic Cordilleras (SE Spain). *Geologische Rundschau*, **52**, 260–269.

EGELER, C. G. & SIMON, O. J. 1969. Orogenic evolution of the Betic Zone (Betic Cordilleras, Spain), with emphasis on the nappe structures. *Geologie en Mijnbouw*, **48**, 296–305.

FAULKNER, D. R., LEWIS, A. C. & RUTTER, E. H. 2003. On the internal structure and mechanics of large strike-slip fault zones; field observations of the Carboneras Fault in southeastern Spain. *Tectonophysics*, **367**, 235–251.

GALINDO-ZALDÍVAR, J., GONZÁLEZ-LODEIRO, F. & JABALOY, A. 1993. Stress and paleostress in Betic–Rif cordilleras (Miocene to present-day). *Tectonophysics*, **227**, 105–126.

GALINDO-ZALDÍVAR, J., GIL, A. J., BORQUE, M. J., *ET AL.* 2003. Active faulting in the Internal Zones of the central Betic Cordilleras (SE Spain). *Journal of Geodynamics*, **36**, 239–250.

GROUPE DE RECHERCHE NÉOTECTONIQUE DE L'ARC DE GIBRALTAR 1977. L'histoire tectonique récente (Tortonien à Quaternaire) de l'Arc de Gibraltar et des bordures de la mer d'Alboran. *Bulletin de la Société Géologique de France*, **19**, 575–614.

HUIBREGTSE, P., ALEBEEK, H. V., ZAAL, M. & BIERMANN, C. 1998. Paleostress analysis of the northern Níjar and southern Vera basins: constraints for the Neogene displacement history of major strike-slip faults in the Betic Cordilleras, SE Spain. *Tectonophysics*, **300**, 79–101.

IAGA 2000. International Geomagnetic Reference Field 2000. *Geophysical Journal International*, **141**, 259–262.

INSTITUTO GEOGRÁFICO NACIONAL (IGN) 1976. *Mapa gravimétrico de España 1:1.000.000.*

KELLER, J. V. A., HALL, S. H., DART, C. J. & MCCLAY, K. R. 1995. The geometry and evolution of a transpressional strike-slip system: the Carboneras fault, SE Spain. *Journal of the Geological Society, London*, **152**, 339–351.

LAROUZIÈRE, F. D., DE BOLZE, J., BORDET, P., HERNANDEZ, J., MONTENAT, C. & OTT D'ESTEVOU, P. 1988. The Betic segment of the lithospheric Trans-Alboran shear zone during the Late Miocene. *Tectonophysics*, **152**, 41–52.

MARÍN-LECHADO, C., GALINDO-ZALDIVAR, J., RODRÍGUEZ-FERNÁNDEZ, L. R., SERRANO, I. & PEDRERA, A. 2005. Active faults, seismicity and stresses in an internal boundary of a tectonic arc (Campo de Dalías and Níjar, southeastern Betic Cordilleras, Spain). *Tectonophysics*, **396**, 81–96.

MARTIN, J. M., BRAGA, J. C., FRANSEEN, E. K. & MANKIEWICZ, C. 1993. Depositional sequences and correlation of middle(?) to late Miocene carbonate complexes, Las Negras and Níjar areas, south-eastern Spain; discussion and reply. *Sedimentology*, **40**(2), 351–356.

MARTÍNEZ-MARTINEZ, J. M. & AZAÑÓN, J. M. 1997. Mode of extensional tectonics in the southeastern Betics (SE Spain): implications for the tectonic evolution of the peri-Alborán orogenic system. *Tectonics*, **16**(2), 205–225.

MONTENAT, C. & OTT D'ESTEVOU, P. 1990. *Les bassins néogènes du domaine bétique oriental (Espagne).* Documents et Travaux de l'IGAL, Paris, **12**.

MONTENAT, C., OTT D'ESTEVOU, P. & MASSE, P. 1987. Tectonic–sedimentary characters of the Betic Neogene basins evolving in a crustal transcurrent shear zone (SE Spain). *Bulletin des Centres de Recherche Exploration–Production, Elf-Aquitaine*, **11**, 1–22.

OTT D'ESTEVOU, P. 1980. *Evolution dynamique du basin Néogene de Sorbas (Cordillères Bétiques orientales, Espagne).* PhD thesis, University of Paris.

OTT D'ESTEVOU, P. & MONTENANT, C. 1985. Evolution structurale de la zone bétique orientale (Espagne) du Tortonien à l'Holocene. *Comptes Rendus de l'Académie des Sciences*, **300**, 363–368.

PEDLEY, R. C., BUSBY, J. P. & DABEK, Z. K. 1993. *GRAVMAG.* British Geological Survey, Technical Report **WK/93/26/R**.

ROBINSON, E. S. & ÇORUH, C. 1988. *Basic Exploration Geophysics.* Wiley, Chichester.

RUTTER, E. H., MADDOCK, R. H., HALL, S. H. & WHITE, S. H. 1986. Comparative microstructures of natural and experimentally produced clay-bearing fault gouges. *Pure and Applied Geophysics*, **124**, 3–30.

SANZ DE GALDEANO, C. 1983. Los accidentes y fracturas principales de las Cordilleras Béticas. *Estudios Geológicos*, **39**, 157–165.

SANZ DE GALDEANO, C. & ALFARO, P. 2004. Tectonic significance of the present relief of the Betic Cordillera. *Geomorphology*, **63**(3–4), 175–190.

SCOTNEY, P., BURGESS, R. & RUTTER, E. H. 2000. $^{40}Ar/^{39}Ar$ age of the Cabo de Gata volcanic series and displacements on the Carboneras fault zone, SE Spain. *Journal of the Geological Society, London*, **157**, 1003–1008.

SILVA, P. G., GOY, J. L., SOMOZA, L., ZAZO, C. & BARDAJÍ, T. 1993. Landscape response to strike-slip faulting linked to collisional settings: Quaternary

tectonics and basin formation in the Eastern Betics, southeastern Spain. *Tectonophysics*, **224**, 289–303.

STAPEL, G., MOEYS, R. & BIERMANN, C. 1996. Neogene evolution of the Sorbas basin (SE Spain) determined by palaeostress analysis. *Tectonophysics*, **255**, 291–305.

TELFORD, W. M., GELDART, L. P. & SHERIFF, R. E. 1990. *Applied Geophysics*. Cambridge University Press, Cambridge.

TORNÉ, M. & BANDA, E. 1992. Crustal thinning from the Betic Cordillera to the Alborán Sea. *Geo-Marine Letters*, **12**, 76–81.

TURNER, S. P., PLATT, J. P., GEORGE, R. M. M., KELLEY, S. P., PEARSON, D. G. & NOWELL, G. M. 1999. Magmatism associated with orogenic collapse of the Betic–Alboran Domain, SE Spain. *Journal of Petrology*, **40**(6), 1011–1036.

VAN DE POEL, H. M. 1991. Messinian stratigraphy of the Níjar Basin (S.E. Spain) and the origin of its gypsum-ghost limestones. *Geologie en Mijnbouw*, **70**(3), 215–234.

VÖLK, H. R. & RONDEEL, H. E. 1964. Zur Gliederung des Jungtertiars in Bechen von Vera, Südost Spanien. *Geologie en Mijnbouw*, **43**, 310–315.

WEIJERMARS, R. 1987. The Palomares brittle ductile shear zone of Southern Spain. *Journal of Structural Geology*, **9**, 139–157.

WEIJERMARS, R., ROEP, TH. B., VAN DEN EECKHOUT, B., POSTMA, G. & KLEVERLAAN, K. 1985. Uplift history of a Betic fold nappe inferred from Neogene–Quaternary sedimentation and tectonics (in the Sierra Alhamilla and Almería, Sorbas and Tabernas basins of the Betic Cordilleras, SE Spain). *Geologie en Mijnbouw*, **64**, 397–411.

The Upper Cretaceous in the Tagus Basin (Central Spain): sequential analysis based on oil-well data and outcrop correlation

MANUEL SEGURA[1], TERESA POLO[2], JOSÉ F. GARCÍA-HIDALGO[1], JAVIER GIL[1], BEATRIZ CARENAS[3] & ÁLVARO GARCÍA[4]

[1]*Departamento de Geología, Universidad de Alcalá, 28871 Alcalá de Henares, Spain (e-mail: manuel.segura@uah.es)*

[2]*Geolog SpA, Via Carlo Porta 21, 20098 San Giuliano Milanese, Milano, Italy*

[3]*Departamento Química Agrícola, Geología y Geoquímica, Universidad Autónoma, 28049 Madrid, Spain*

[4]*Departamento Estratigrafía, Universidad Complutense, 28040 Madrid, Spain*

Abstract: The logs from six oil wells drilled between 1960 and 1980 in the Upper Cretaceous succession of the Tagus Basin were analysed and correlated with surface outcrops, to estimate sedimentary environments and to detect cyclicity in sedimentation. Log interpretation has been carefully checked with outcrop data, because high peaks in gamma-ray logs, usually considered to represent open marine facies, may correspond either to open marine or to muddy coastal deposits. The former correspond to the maximum flooding surfaces of depositional sequences, whereas the latter correspond to sequence boundaries. Three second-order depositional megasequences have been recognized (MS-2, MS-3 and MS-4). The basal megasequence onlaps older rocks, grading upwards from continental to marine deposits. The megasequence MS-3 shows a basal marly transgressive interval and a thick carbonate pile at the top, grading to the SE to sabkha environments. The top megasequence is hardly recognized in surface outcrops, but in well logs it is a thick evaporite–claystone unit of mainly sabkha environments that grade westwards to coastal deposits. Sedimentation of megasequences MS-3 and MS-4 extended farther west than previously considered, covering areas considered as part of the exposed Hesperian Massif. These were areas of marine and coastal sedimentation where organic matter accumulation could be potentially high, and can be considered potential areas for oil or gas exploration.

The objective of this paper is to contribute to the establishment of a sequence-stratigraphic framework for Upper Cretaceous sedimentary successions in central Spain based on oil-well data and outcrop sections in the Tagus Basin (central Spain) (Fig. 1).

The Cretaceous rocks that crop out in the Iberian Ranges and northern Tagus Basin are composed of siliciclastic and carbonate sediments, and record sedimentation from late Albian to Santonian times. During Tertiary compression, the tectonic inversion of the Iberian Basin produced the Iberian Ranges. The Iberian Basin was a rift system that originated during Triassic times as a consequence of the Pangaea break-up.

During Cretaceous times, the Iberian Basin underwent a complex evolution as a part of the Iberian microplate in relation to the European and African plates (Martín-Chivelet *et al.* 2002). Continental, coastal and shallow marine Late Cretaceous sediments of the Iberian Basin were related to marine transgressions that penetrated into the basin along a narrow and shallow seaway that linked the northern (Atlantic) and eastern (Tethyan) continental margins of the Iberian microplate (García *et al.* 1993; Segura *et al.* 1993), separating two emerged areas, the Hesperian and Ebro Massifs (Fig. 2). These marine transgressions were due to the worldwide eustatic sea-level rise that took place from late Albian to Santonian times (García *et al.* 2004). During this period, this seaway extended and moved its depocentre westwards, onlapping the Hesperian Massif; and its sediments are at present located below the Duero and Tagus Tertiary basins.

The Tagus Basin is an intracontinental Tertiary basin formed by the Alpine orogeny. It is bordered on the NW, NE and south by mountain ranges (the Central System, the Iberian Ranges, and the Toledo Mountains, respectively; (Fig. 1). This study aims to contribute to a better understanding of the Late Cretaceous sedimentation in the western margin of the Iberian Basin through an analysis of oil-well data in the Tagus Basin (Fig. 1). These subsurface data are of primary importance because the Mesozoic sediments in the area investigated are

From: MORATTI, G. & CHALOUAN, A. (eds) 2006. *Tectonics of the Western Mediterranean and North Africa.* Geological Society, London, Special Publications, **262**, 231–244.
0305-8719/06/$15.00

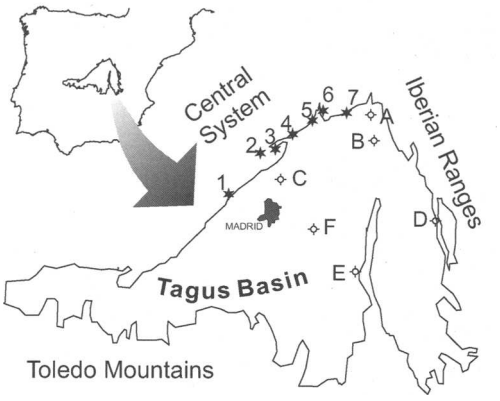

Fig. 1. Study area (Tagus Basin) showing the location of studied wells (circles) and outcrop sections (stars) along the northern border of the basin. Wells: A, Baides; B, Sta. Bárbara; C, El Pradillo; D, Torralba; E, Tribaldos; F, Tielmes. Sections shown in Figure 3: 1, Valdemorillo; 2, Soto del Real; 3, Pedrezuela; 4, Patones; 5, Valdesotos; 6, Muriel; 7, Alcorlo.

buried deep below a thick Tertiary cover, and because the stratigraphic data are limited to outcrops along the Tagus Basin borders.

Oil-well data provide an appropriate control for sedimentary facies and depositional sequences because both major types of facies and sequences show characteristic gamma-ray log signatures. A hierarchy of depositional sequences was recognized based on cycle stacking and the log patterns. These sequences allowed regional correlations across various depositional environments. The basin-wide correlation revealed a detailed stratigraphic architecture as shown by sedimentary discontinuities, variations in stratigraphical thickness, and lateral and vertical facies relationships. A further regional control for outcrop data is, thus, available. In particular, these wells provide additional information on the uppermost Cretaceous deposits that crop out only sparsely in the basin borders.

Methods

The dataset used in this study consists of the logs and master-logs of six oil wells: Baides, El Pradillo, Santa Bárbara, Tielmes, Tribaldos and Torralba (Fig. 1). These wells were drilled between 1960 and 1980, and no core sections were available. More than 15 stratigraphic sections have also been studied along the northern Tagus Basin (Figs 1 and 2).

The Baides well (A in Fig. 1; Fig. 3) was drilled in 1983 by Shell España NW. Its master-log, gamma-ray (GR), and sonic logs were studied. The El Pradillo and Santa Bárbara wells (B and C in Fig. 1; Fig. 4) were drilled by Shell España in 1980 and 1981, respectively, and the Tribaldos and Torralba wells (D and E in Fig. 1; Fig. 5) were drilled by Amospain in 1974 and 1974–1975, respectively. Master-logs, and GR and resistivity logs were available for these four wells. The Tielmes well (F in Fig. 1) was drilled by Adaro in 1965; only its master-log is available. This well was considered because of its importance for north–south correlations, owing to its location between northwestern (El Pradillo) and southeastern (Tribaldos) wells (Fig. 1). The GR log was mainly used for a detailed interpretation of the sedimentary stacking pattern. This is because it has better vertical definition and is poorly affected by other factors, such as fluid presence, compaction, etc. The sonic and resistivity logs were also used to assess the relative importance of changes in the GR log.

The analysis and interpretation of the available well datasets was carried out in successive steps: (1) the identification of several well-known stratigraphic units, based on master-log analysis; (2) the definition of the main stratigraphic succession, based on the log analysis; (3) the establishment of well–outcrop correlations based on depositional and stratigraphic constraints.

The outcrop data were obtained from vertical measured sections along the northern Tagus Basin (southern Central System), from Valdemorillo (SW) to Alcorlo (NE) (Figs 1 and 3). Stratigraphic sections were selected on the basis of accessibility and continuity of exposure. Individual beds were lithologically logged according to colour, grain size, sedimentary and biogenic structures, geometry and fossils. Attention was paid to the recognition of major, regionally extensive and local bounding surfaces using the sequence-stratigraphic framework of Van Wagoner *et al.* (1990). The working method consisted of: (1) analysing bedding patterns and facies; (2) defining different orders of depositional sequences, their hierarchy and stacking pattern; (3) correlating the sequences between the sections; (4) correlating the field sections with oil-well data. The high-resolution correlation has to be consistent between the sections and wells in order to trace timelines. The hierarchical sequence stacking pattern is formed by medium- and large-scale depositional parasequence sets, sequences and megasequences: medium-scale (fourth-order) parasequence sets are the building blocks and compose large-scale third-order sequences (e.g. Van Wagoner *et al.* 1990; Strasser *et al.* 1999), which in turn form second-order megasequences. The SW–NE correlation line (Fig. 3) provided a 2D control for thickness and lithofacies changes and allowed for correlation between the Baides and the other wells (Figs 4–6).

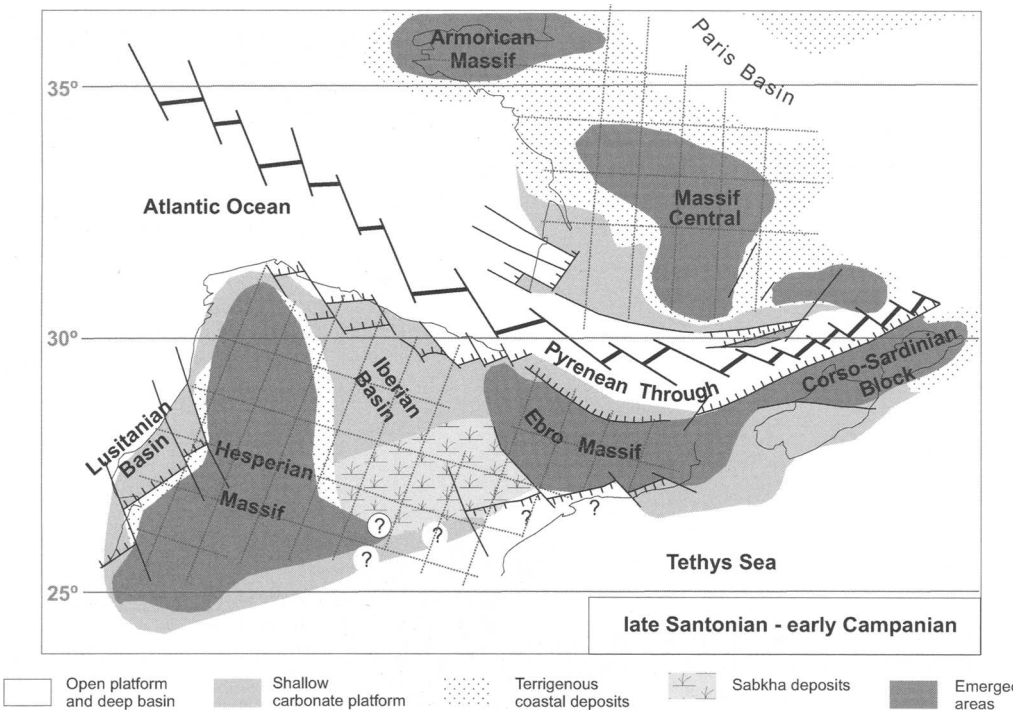

Fig. 2. Palaeogeography of the Iberian Basin during sequence S3.4 (late Santonian to early Campanian), showing the location of the Iberian Basin, a marine seaway connecting the Atlantic and Tethyan domains. Based on Dercourt *et al.* (2000), Floquet & Hennuy (2001) and Segura *et al.* (2004). The base of this sequence is the datum plane for cross-sections of Figures 3–6.

Surface data allow a more precise interpretation of the well data, especially in the case of clay sediments, which can be interpreted as shallow lagoon mudstones or as deeper offshore mudstones, when they are related to sequence boundaries or to maximum flooding surfaces, respectively.

Geological framework

Evidence from sedimentary basins around the Iberian microplate suggests that the Late Cretaceous was a time of rising sea levels. Eustatic sea-level changes (of low and high frequency) produced within these basins facies of both deepening- and shallowing-upward sequences (from second to fifth order) that spread along the entire Iberian Basin (Fig. 2). The second-order eustatic cycles exerted, on a broad scale, a major force on sedimentation through their influence on mean water depth and basin geometry.

Second-order cycles are recorded as transgressive–regressive (T–R) long-term megasequences composed of alluvial–coastal siliciclastic deposits grading to marine carbonates and marls, and finally to restricted muddy coastal and sabkha deposits (with common intercalations of stromatolites, evaporites and tidalites). Megasequences are composed of third-order depositional sequences, which consist of lowstand, transgressive and highstand systems tracts. The sea-level falls related to the sequence boundaries were associated with the deposition of prograding alluvial–shoreface siliciclastic deposits that represent a basinward shift in the coastal belts (lowstand wedges). The onset of the transgression reworked lowstand coastal deposits to form retrogradational coastal wedges that onlapped older sediments, whereas offshore marly sedimentation records transgression basinwards. The maximum flooding surface is marked by the change from retrogradational to progradational in the coastal wedges. Carbonate and sabkha sedimentation characterize highstand deposits. These can be capped by forced regressive siliciclastic wedges, by tidal deposits, or by emersion features such as karst processes, palaeosoil development, vadose cements on subtidal deposits, etc., suggesting a fall in the relative sea level and the sequence boundary.

Sea-level falls and rises in the relative sea level were the primary control for the genesis of

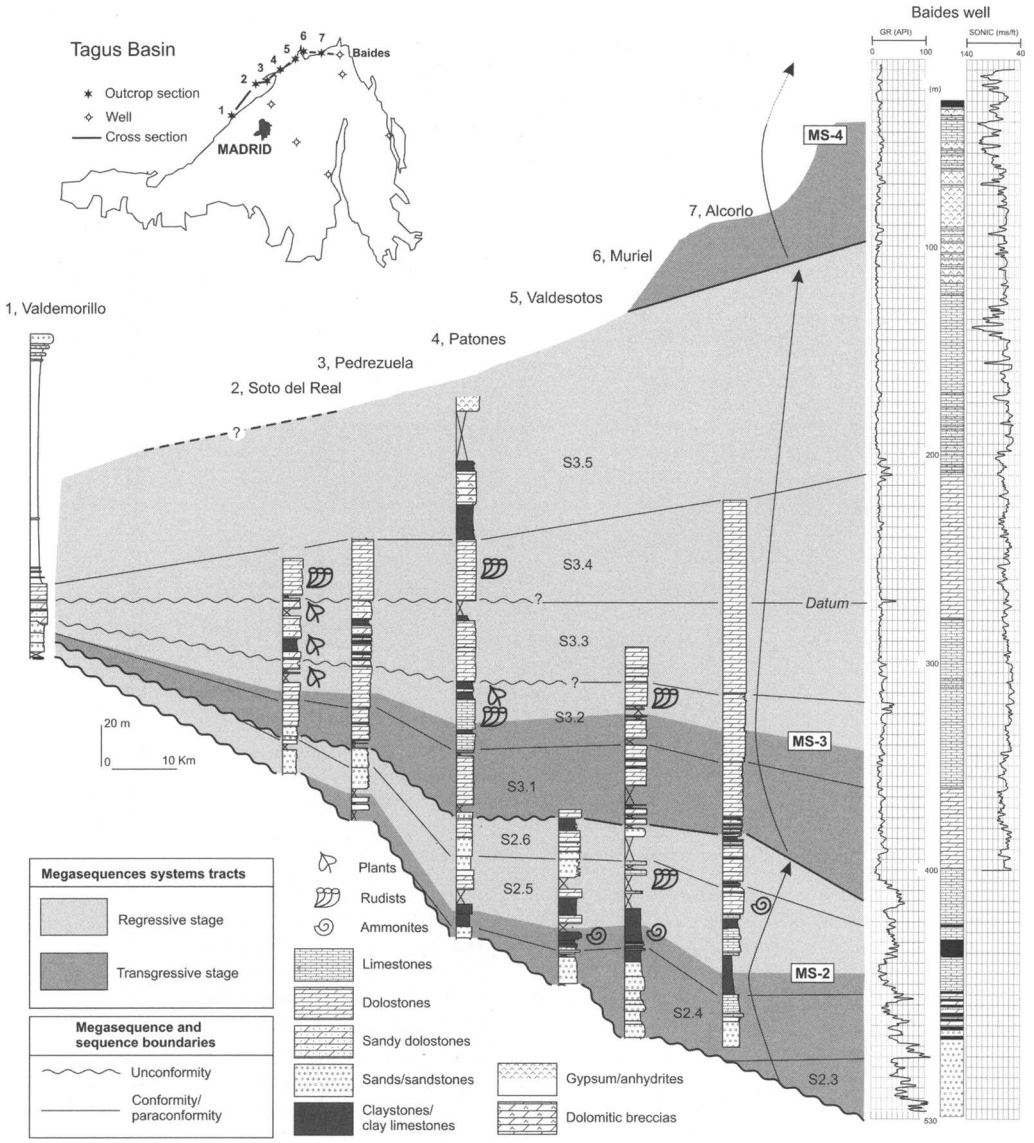

Fig. 3. Stratigraphic cross-section along the northern Tagus Basin and correlation with Baides well (inset shows location of the cross-section in the Tagus Basin; see Fig. 1 for location of sections and well). Three second-order transgressive–regressive megasequences (MS-2 to MS-4), and nine third-order depositional sequences (S2.3 to S3.5) have been distinguished. Dark and light grey represent the transgressive and regressive stages of the megasequences, respectively. Gamma-ray (GR, left) and sonic logs (right), and master-log (centre) are shown for Baides well. Datum plane is S3.4 basal boundary.

megasequence and sequence boundaries (Segura *et al.* 2002). Sequence boundaries are inferred from the presence of landward erosion (updip unconformities; Fig. 3), and parasequence stratal geometries with coastal onlap and toplap patterns, which confirm their significance as sequence boundaries. Major shifts in the facies belts (mainly basinwards in relation to sea-level falls) also support the location of these boundaries (García *et al.* 1996).

Biostratigraphic data are scarce, except for some intervals (Fig. 3), and correlations are mainly based on the sequential arrangement of lithofacies

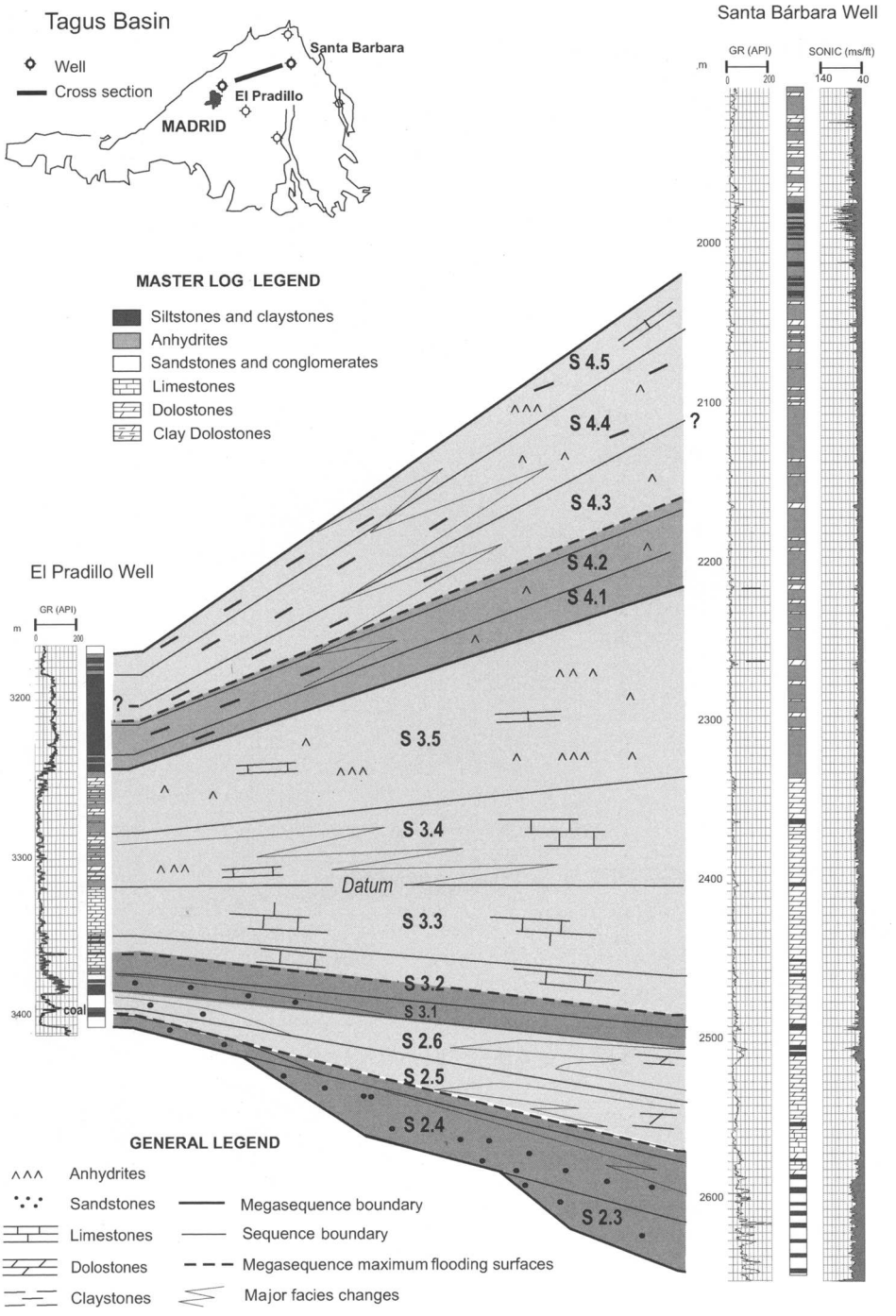

Fig. 4. Correlation of El Pradillo and Santa Bárbara wells along the northern Tagus Basin (inset shows location of the cross-section in the Tagus Basin; see also Fig. 1). GR log and master-log are shown for the El Pradillo well; GR and sonic logs and the master-log are shown for the Santa Bárbara well. Master-log and general legend for Figures 4–6 are also shown. Datum plane is S3.4 basal boundary.

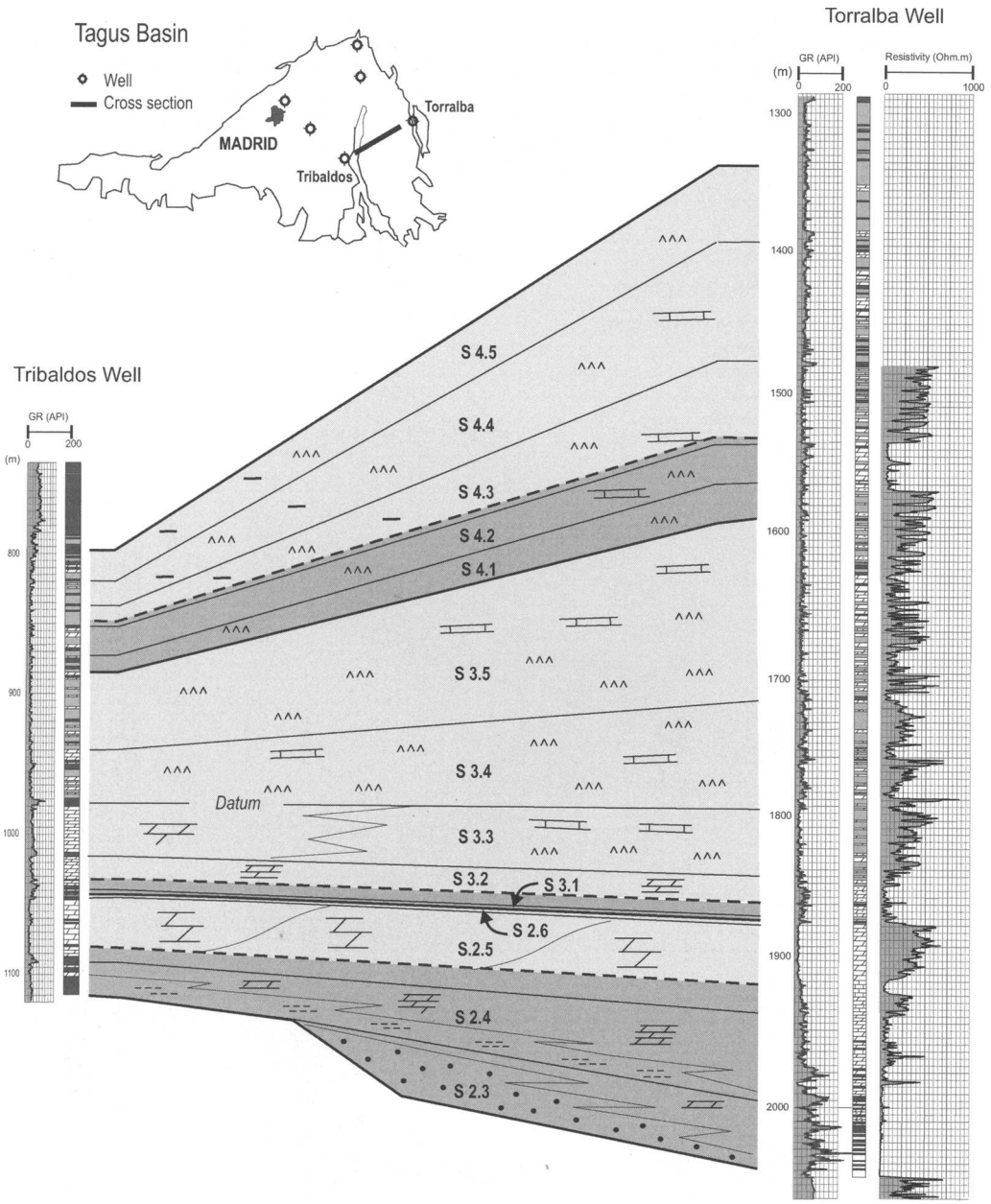

Fig. 5. Correlation of the Tribaldos and Torralba wells along the southern Tagus Basin (inset shows location of the cross-section in the Tagus Basin; see also Fig. 1). GR and resistivity logs and the master-log are shown. Legend as in Figure 4. Datum plane is S3.4 basal boundary.

(systems tracts) and bounding surfaces (sequence and parasequence boundaries, transgressive surfaces, maximum flooding surfaces, etc.). Sequence and parasequence boundaries can be traced along the Iberian Basin, calling for the use of fossil data to constrain sequence ages. Several fossil groups have been used for chronostratigraphical purposes, including ammonites, benthic Foraminifera and rudists (Segura & Wiedmann 1982; Segura *et al.* 1993; Gil *et al.* 2004).

Megasequences were described in wells based on the interpretation of both master-logs and electrical logs (Figs 3–6). The megasequence and sequence boundaries were mainly identified based on the GR logs. The log shape of a megasequence mainly shows a bell-shaped symmetrical signature. The base of the megasequence is characterized by maximum GR values (caused by a higher clay content), followed by a slow decrease in these values, whereas the top is characterized by a rapid increase in GR values. The presence in outcrops of both shallower and deeper fine-grained facies, however, has to be considered, to provide a correct log interpretation of these boundaries. Thus, in the basal siliciclastic sediments, the presence of coastal marls and claystones in the

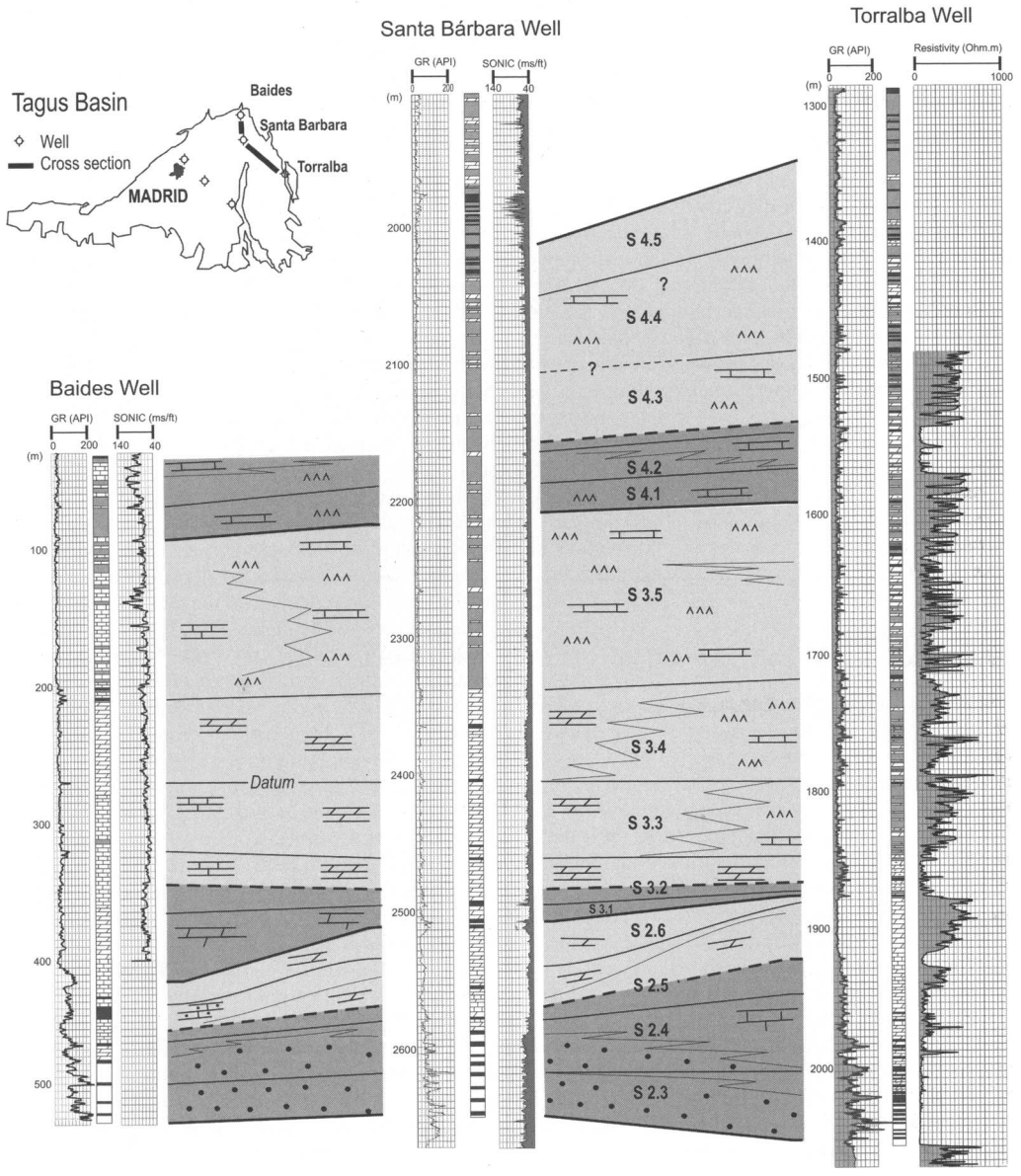

Fig. 6. Correlation of the Baides, Santa Bárbara and Torralba wells along the northeastern Tagus Basin (inset shows location of the cross-section in the Tagus Basin; see also Fig. 1). Legend as in Figure 4. Datum plane is S3.4 basal boundary.

outcrop sections suggests that an increase in GR values (which is usually interpreted as corresponding to fining-upward trends ending with deeper marine sediments) should really be interpreted as corresponding to these shallower fine-grained sediments, which are usually related to megasequence and sequence boundaries in outcrops.

The record of the carbonate units is composed of an alternation of, from base to top: outer-shelf marls, inner-shelf carbonates, and coastal marls with palaeosoils. In this facies, an increase in GR values is interpreted as originating from the presence of shallower (top coastal marls) and deeper (basal outer-shelf marls) claystone or marl beds, which are usually interpreted as representing the sequence boundary. Finally, the GR logs for the carbonate and evaporite units (mainly composed of anhydrite and limestones) are blocky, and only the higher, positive peaks in GR values are interpreted as sequence boundaries. Anhydrite deposits (flat GR values) are interpreted as shallower, sabkha deposits, whereas limestones are interpreted as shallow marine, but deeper, sediments. In any case, the log trend in these sediments is very difficult to interpret.

The above considerations show the complexity of making a sequential or genetic interpretation of the GR logs in shallow platform and coastal deposits, as the argillaceous beds (high peaks in the GR log) may be interpreted as both open marine (deeper) sediments and coastal (shallower) sediments. To make a correct interpretation of a well log, it is therefore necessary to consider the correlation of this section with those of the nearest outcrops.

Sequential analysis and correlation

In this study, depositional sequences recognized in outcrop studies and their stacking were employed for the correlation between wells. Depositional sequences are the framework of stratigraphic succession (Fig. 3). They are recognizable over all depositional outcrop sections and, thus, form ideal correlation units. For well correlation, both megasequences and sequences were used. With these correlation methods, it was possible to correlate outcrops and wells in slightly different palaeogeographical positions (coastal and shallow shelf).

Key sequence-stratigraphic surfaces have been defined through the correlation of log-based events whose significance has been established in outcrop sections. Primary control is provided by the Baides well, which provides an important link to the outcrops of the northern Tagus Basin (Fig. 3). Three second-order megasequences (MS-2 to MS-4) and at least nine third-order depositional sequences have been delimited. A basal megasequence (MS-1) of mid- to late Albian age is recognized only in the eastern Iberian Ranges, and is not studied here. These megasequences correspond to Upper Cretaceous sediments, as indicated by both the reports of the wells and their correlation with data from outcrops, in which ammonites and rudists have been found and dated (Gil *et al.* 2002).

Megasequence MS-2

The megasequence MS-2 ranges from 50 m in the west (El Pradillo well, Fig. 4) to 175 m in the east (Torralba well, Fig. 5). The megasequence wedges out farther west, and in the Valdemorillo section is about 10 m thick (Fig. 3). The megasequence MS-2 is composed of four third-order sequences showing a basal onlap on the Palaeozoic–Triassic basement (Figs 3 and 4). The thickness decrease of MS-2 is partially due to the absence of the lower third-order sequences caused by basal onlap (Figs 3 and 4). Thus, to the NE, MS-2 is composed of sequences S2.3 to S2.6 (Baides and Santa Bárbara wells; Figs 3 and 4), whereas westwards it is composed of only sequences S2.5 and S2.6 with a reduced thickness (El Pradillo well; Fig. 4). Sequences S2.3 and S2.4 were also absent westwards from the Pedrezuela section (Fig. 3). Sequence S2.6 also pinches out farther south for sedimentary reasons (see below) (Tribaldos and Torralba wells; Figs 5 and 6). The landward thickness decrease in sequences S2.5 and S2.6 causes a further decrease in thickness of the entire megasequence MS-2. This added decrease was caused by the landward reduction in the number of internal parasequences in sequences S2.5 and S2.6. This reduction was caused by both basal sequence onlap and toplap (erosion) related to the MS-2–MS-3 boundary (updip unconformity), which can be seen in the Valdemorillo section (Fig. 3).

From previous studies on outcrop sections (García *et al.* 1993; Segura *et al.* 1993), the two basal sequences (S2.3 and S2.4) were related to Tethyan transgressions, whereas the two overlying sequences (S2.5 and S2.6) were related to Atlantic transgressions. In the more basinal wells (Torralba, Figs 5 and 6), MS-2 is composed of a basal alternation of sandstones and claystones that grade upwards to dolostones and marls. The upper dolomitic and marly units grade landwards (westwards) to dolomitic sandstones, sandstones and claystones, reflecting a facies transition from platform (carbonate) to shoreface (siliciclastic) settings (Fig. 4), as can also be seen in the outcrop data (Fig. 3).

The basal sequences (S2.3 and S2.4) are described in the master-logs as a basal alternation of sandstones and claystones and dolomitic tops with minor marl–claystone intercalations (Fig. 6). Generally, GR logs showed upward-decreasing

values for both sequences (e.g. Baides well, Fig. 3). Sequence S2.3, however, locally shows first an increase and then a final decrease in GR values, with its maximum levels located at the middle of the sequence (Torralba well, Fig. 5).

These sequences are interpreted as transgressive–regressive sequences. Basal, transgressive deposits are composed of coarse-grained shoreface sediments in northwards coastal areas (e.g. Baides well, Fig. 6) and offshore fine-grained sediments basinwards (southwards; Torralba well, Fig. 6). This southward location of offshore facies also supports the Tethyan origin of these sequences. Highstand sediments are composed of coarse-grained, shoreface sediments in the north, as suggested by the upward decrease in GR values (Baides and Santa Bárbara wells; Fig. 6), and tidal dolomitic facies in the south (Torralba well, Fig. 6). Minor higher peaks within sequences S2.3 and S2.4 (Fig. 6) are considered to be related to the presence of fourth-order parasequence sets. Locally, the presence of low values at the base of S2.3 in the GR log suggests the existence of a basal sandy lowstand wedge in the southeastern-most areas (Torralba well, Fig. 6). This wedge was deposited in relation to a relative sea-level fall at the MS-1–MS-2 boundary.

The MS-2 top sequences (sequences S2.5 and S2.6) both wedge out westwards (Fig. 4) and southwards (Fig. 6), the latter in opposition to underlying sequences, which also supports their Atlantic origin. Thus, sequence S2.5 had a reduced thickness, being partially eroded by the overlying sequence S3.1 at the Valdemorillo section (Fig. 3), whereas sequence S2.6 was probably not deposited here and is not clearly identified in the Tribaldos and Torralba wells either, probably being located in the regressive sediments deposited in relation to the MS-2–MS-3 boundary (Figs 5 and 6).

Sequences S2.5 and S2.6 are mainly composed of dolostones and limestones with minor claystone–marl intercalations. The S2.5–S2.6 boundary is located in outcrops in a very characteristic marly interval, located within a thick, carbonate package. In those wells located in platform areas it is difficult to locate that boundary (Baides and Santa Bárbara wells, Figs 3 and 4) primarily because master-logs do not show such thin marly intervals, and also because the sequence S2.5 is composed of fourth-order parasequence sets, which are also bounded by thin marly beds. In GR logs, all of these marly boundaries are shown by higher peaks of increasing clay content. Locally, as in the Torralba well (Fig. 5), this claystone–marl interval is also clearly identified in the resistivity log because its low values suggest more conductive sediments (claystones). Based on outcrop correlations, the topmost GR peak (marly interval) in log correlations may represent such a boundary (Figs 4–6). In contrast, in the El Pradillo well and in the western outcrops, sequence S2.5 is composed of sandstones and claystones with a coal bed in the middle of the sequence (Fig. 4).

Sequence S2.5 starts with transgressive, hemipelagic marls with ammonites of Atlantic origin (Segura *et al.* 1993), which represent the maximum flooding sediments of the megasequence MS-2. This marly interval was clearly identified in the Torralba, Baides and Tribaldos wells (Figs 5 and 6), although in the Tribaldos well it is apparently located higher in the succession (Fig. 5). It is more difficult to identify, however, in the Santa Bárbara well (Fig. 4). The claystone–marl interval grades upwards to shallow-marine carbonates, and both facies grade landwards (westwards) to the coastal shoreface or barrier sandy sediments, which alternate with lagoonal or littoral claystones (Fig. 4). These facies show an overall shallowing-upward trend. The presence of a coal bed in the El Pradillo well, identified both in the well's lithological description and in the corresponding low peak in the GR log and located between two claystone beds, supports the interpretation of a landward transition to coastal environments, where coal beds are usually developed.

Further sequential interpretation based on outcrop data clearly suggests that sequence S2.5 is composed of minor-order parasequence sets, as can also be seen in outcrops (Gil *et al.* 2001; García-Hidalgo *et al.* 2003), and is further suggested by the well GR logs (Santa Bárbara and Torralba wells, Figs 4 and 5).

Sequence S2.6 is primarily a carbonate unit in the Baides and Santa Bárbara wells (Figs 3 and 4) and in eastward outcrop sections (Alcorlo; Fig. 3), where it is composed of limestones and dolostones with minor marly intercalations. In outcrops, these carbonates grade westwards to lagoonal green marls and siliciclastic shoreface sediments. Locally, within lagoonal sediments, minor stromatolites and palaeosoil intercalations are also present (e.g. the Patones and Valdesotos sections, Fig. 3). This sequence is usually interpreted as the top, regressive sediment for the entire megasequence (García-Hidalgo *et al.* 1997), showing a northward progradational trend, and not being deposited southward (or deposited there with only a very minor thickness) because of the lack of accommodation space owing to the relative sea-level fall at the top of the megasequence MS-2 (Tribaldos and Torralba wells, Figs 5 and 6).

The MS-2–MS-3 boundary is marked by a sudden increase in GR values (Polo *et al.* 2003; El Pradillo well, Fig. 4). This boundary is marked further eastwards by an upward increase in clay content separating two homogeneous intervals

with lower clay contents (Santa Bárbara and Torralba wells, Figs 4 and 5). There are, however, similarities in the GR-log trend (Fig. 6), which allow for correlation between wells. This is because of the higher clay content in the carbonate facies (higher values in the GR log), which suggests an eastward presence of deeper sediments at the base of the overlying megasequence MS-3. These deeper sediments were transgressive, flooding sediments. In outcrop sections, however, these sediments overlie a very discontinuous sandy level, which is currently interpreted as incised fluvial deposits related to a lowstand wedge in the northern Iberian ranges (Gil 2002). The presence of this lowstand wedge clearly indicates the presence of that boundary. The sequence boundary and the transgressive surface of the overlying sequence coincide in the study area.

Megasequence MS-3

Megasequence MS-3 ranges from 130 m in the west (El Pradillo well, Fig. 4) to about 270 m in the east (Torralba and Santa Bárbara wells, Fig. 6). It is composed of a thin basal sandy or marly unit grading upwards to dolostones and limestones, and then to dolostones with anhydrite intercalations at the top. Facies are very persistent laterally, with the only changes in the lateral facies being caused by the increase in anhydrite intercalations (Figs 5 and 6). In field sections, it is a transgressive–regressive megasequence with a short transgressive episode at the base and a large regressive episode at the top (García-Hidalgo *et al.* 2001).

Lithology and thickness agree closely with surface data; thus MS-3 thickness ranges from about 300 m in eastern sections (Alcorlo, Fig. 3) to about 150 m in the Valdemorillo section (Fig. 3). In the Patones area, MS-3 rests with an erosive and brecciated surface on MS-2 (Gil *et al.* 1999). A very thin, erosive, basal sandy unit (Somolinos sands) is discontinuously recorded from Patones eastwards. This is interpreted as incised channels representing a sudden basinward shift of the facies belts in response to a major relative sea-level fall at the megasequence boundary (García-Hidalgo *et al.* 2001). Somolinos sands grade upwards to limestones and dolostones with minor marly intercalations, which in turn grade upwards to dolomitic breccias probably produced by anhydrite dissolution. In the outcrops, MS-3 is composed of five third-order sequences (Gil & García 1996; García-Hidalgo *et al.* 2001), including foreshore, subtidal, coastal, inner platform, shoals and sabkha deposits (García-Hidalgo *et al.* 2001). All of these sequences are also present in well data.

In the El Pradillo well, the lower boundary of MS-3 is located at a sudden increase in GR values (Polo *et al.* 2003; Fig. 4), which rise to 170 API 5 m above the megasequence boundary. From this point, there is a rapid decrease in GR values for 10 m; however, GR values remain constant through the lower part of MS-3 (a *c.* 110 m interval). GR logs end with a generalized, homogeneous increase suggesting a correlative increase in clay content in the upper part of MS-3 (Polo *et al.* 2003; Fig. 4). This is interpreted as the regressive episode of the entire megasequence. In such a regressive context, these topmost clays are interpreted as low-energy coastal and littoral deposits. The MS-3–MS-4 boundary is also located in the Baides well in a GR peak, primarily based on correlation with nearby outcrop sections (Fig. 3). The stratigraphic succession of the master-logs for MS-3 and the small peaks detected in the GR logs are clearly correlated from the Baides to the Santa Bárbara wells and then, although less clearly, to the Torralba well (Fig. 6), to extend the sequences recognized in outcrop sections (Fig. 3) to well data (Figs 3 and 6).

Each sequence presents a characteristic log response, derived from the constituent sediments, with similar trends: a relative peak in GR values at the base of the sequence followed by a progressive lowering with constant GR values (e.g. the Santa Bárbara well, Fig. 4). The peaks at the base of sequences are related to the presence of claystone–marls at the sequence boundary representing transgressive sediments. The constant, relatively flat log represents carbonate marine deposits in relation to highstands (regressive sediments) of each sequence. Major differences from these features have been observed in the Torralba well (Fig. 5), where the common presence of anhydrite causes a more complex GR pattern. In this case, sequence recognition is based on, in addition to the GR log, the resistivity log, with the master-log for lithological descriptions.

In outcrop sections, the first sequence (S3.1) is composed of a basal siliciclastic interval (coastal facies) grading upwards to carbonate sediments. In well logs, the base of the sequence shows a rapid increase in GR values in the basal 5 m (El Pradillo and Santa Bárbara wells, Fig. 4) with a gradual decrease upwards through the rest of the sequence. This change in trend suggests a rapid transgressive stage of reduced thickness in which the clay proportion increases, followed by a highstand stage with the infilling of the accommodation space created in the previous stage. The presence of anhydrite beds (described in the master-log of the El Pradillo and Santa Bárbara wells, Fig. 4) indicates the top of the sequence, suggesting an overall shallowing trend.

The second sequence (S3.2) is composed of alternating limestones and dolostones; only in the

Torralba well (Fig. 5) are some anhydrite beds found at the top. Although the GR log is blocky, the presence of small peaks suggests an upward increase in clay content, supporting a transgressive–regressive interpretation for this sequence, as in the field sections. This trend in the GR log is similar to that of the log of the entire megasequence, but on a smaller scale (e.g. Tribaldos well, Fig. 5).

The third sequence (S3.3) is also composed of limestones and dolostones, except in the Torralba well, where it is composed of an anhydrite–dolostone alternation. The sequence is characterized by the homogeneous aspect of the GR log, with low values (about 20 API) bounded by two relatively higher peaks (about 40 API) in all the wells. This homogeneity is also recognized in the sonic log, with values decreasing slightly downward from 60 to 50 ms/foot^{-1} (Baides well, Fig. 3). In this sequence, small variations in the GR values are interpreted as minor-order parasequence sets and parasequences (fourth and fifth order), which are hardly noticeable in the sonic log.

Sequence S3.3 thins laterally with a complex pattern. At the northern outcrops, it is clearly eroded by the S3.4 sequence, with an unconformity being noted in the field sections (Valdemorillo section, Fig. 3). This probably corresponds to the intra-Santonian unconformity, an event also described in other areas of the Iberian microplate (Reicherter & Pletsch 2000).

The boundaries of the overlying two sequences (S3.4 and S3.5) are similar to those of the previous ones. The logs, especially the GR log, present very homogeneous trends, with minor peaks that are probably related to the presence of minor-order parasequences. Sequence S3.4 is mainly composed of dolostones (Baides and Santa Bárbara wells, Figs 3 and 4) and of a dolostone–anhydrite alternation (El Pradillo, Tribaldos, Tielmes and Torralba wells, Figs 4–6). The anhydrite content is higher than in underlying S3.3, but as in that sequence there is an increase to the SE in anhydrite content, reflecting a facies transition from marine to coastal sabkha environments in that direction (Fig. 2). The trend of increasing anhydrite content, which started in sequence S3.2 (Torralba well, Fig. 5), reaches its highest point in sequence S3.5, which is mainly composed of anhydrites and dolostones in all of the wells studied (Fig. 6).

In clear contrast to the wells, anhydrite deposits have not been observed in outcrop sections, where each sequence is composed of a thick carbonate package and a thin marly top interval. Only sequence S3.5 is composed of a thick dolomitic brecciated unit. Dolomitic breccias (Cuenca breccias) have been described in the southeastern Iberian Ranges as being formed by evaporite and carbonate dissolution and collapse (Meléndez 1975; Yébenes 1975). The presence of the breccias and the absence of evaporites in outcrop sections suggests a similar origin, evaporite dissolution, for this brecciated unit.

The systems tracts arrangement within third-order depositional sequences is conditioned by the long-term, second-order, sea-level curve. Thus, the basal sequence S3.1 is composed of a lowstand (located farther north), a transgressive, and a thin highstand systems tract. The overlying sequence S3.2 is composed of a transgressive and a highstand systems tract. The maximum flooding surface of this sequence is also the maximum flooding surface for the entire megasequence. In contrast, the overlying sequences (S3.3–S3.5) are mainly composed of highstand deposits. The boundaries of these sequences also reflect their location in the second-order highstand, when less accommodation space is available for sequence development, mainly towards coastal areas. Thus, S3.3 and S3.4 basal boundaries are locally erosive, coastal unconformities in some sections (Pedrezuela, S3.2, and Valdemorillo, S3.4, Fig. 3).

Megasequence MS-4

Megasequence MS-4 has a highly variable thickness as a result of the overlying unconformity; maximum thickness is about 250 m at the Torralba well (Fig. 5). This megasequence is primarily composed of claystones, carbonates and anhydrites. The overlying unit is described in the master-log of the Torralba well as the Garumnian Formation, which is considered to be of continental origin and to have a latest Cretaceous–Eocene age. The clays and sands located at the top in the El Pradillo, Santa Bárbara and Tribaldos wells probably correspond to this unit (Figs 4 and 5).

The GR logs of MS-4 show homogeneous low values probably because of the evaporite content, as in the underlying sequences (Fig. 6). Sequential interpretation of MS-4, however, is far from clear because correlative surface deposits are poorly studied and not totally understood, owing to the lack of continuous and uncovered exposures. The presence, as in MS-3, of minor peaks in the GR log, which can be interpreted as originating from an increase in the clay content, suggests the possible presence of several third-order sequences in the Santa Bárbara and Torralba wells (Figs 5 and 6). The minor peaks in the GR log are considered to originate from the presence of carbonate marine facies (according to the master-log).

This is a shallow-marine–coastal–continental megasequence in which the high clay content is interpreted as corresponding to continental facies.

In outcrops of the Patones area (Fig. 3), this megasequence correlates to a red argillaceous unit with gypsum beds at the top whose basal contact has been considered a cartographic unconformity (Portero *et al.* 1990). In the Iberian Ranges, MS-4 probably corresponds to the Villalba de la Sierra Formation, a unit composed of marls, siltstones and anhydrites with an attributed Campanian–Maastrichtian age (Segura *et al.* 2002). A unit with a similar age, but mainly composed of sandstones, claystones, gypsum and chert levels, has also been described in outcrops of the southern Duero Basin (del Olmo Sanz & Martínez-Salanova 1989), overlying Cretaceous dolostones. This latter unit has yielded vertebrate fauna and dinosaur eggs that indicate a Campanian–Maastrichtian age (Buscalioni & Sanz 1987; Buscalioni & Martínez-Salanova 1990). The stratigraphic position and lithological features of this unit are coincident with the megasequence MS-4 identified in the wells and support its Cretaceous (probably Campanian) age.

Conclusions

The Upper Cretaceous sequence of central Spain is commonly regarded as an example of an intracontinental succession. Important parts of this succession, however, are at present located below Tertiary basins and can only be studied by using old oil-exploration well data, which are, thus, essential to complement and constrain stratigraphical and sequential information from surface studies. In this study, regional stratigraphical cross-sections based on six wells and several outcrop sections were produced for the first time. Detailed logs revealed up to now unrecognized sedimentary cycles of various scales in these wells, where the GR log serves as a useful tool in identifying the vertical facies successions, cycles and cycle hierarchies.

The main points raised by this work are the following: (1) Environmental interpretation from logs must be carefully checked against outcrop data. This is because high peaks in GR logs, usually considered to indicate open marine facies, may correspond to either open marine or muddy coastal deposits. The former correspond to the maximum flooding surfaces of depositional sequences, whereas the latter correspond to sequence boundaries. (2) Latest Cretaceous sedimentation extended farther west than previously considered, covering wide areas considered up to now to be part of the exposed Hesperian Massif. These areas correspond to carbonate marine and muddy coastal deposits where organic matter accumulation could be potentially high. Such areas could, thus, be considered potential target areas for oil or gas exploration.

Three transgressive–regressive second-order megasequences have been distinguished. The basal megasequence (MS-2) has a Cenomanian–mid-Turonian age (Gil *et al.* 2004), being composed of five third-order depositional sequences. Sedimentation started with continental–coastal sands and sandstones onlapping Hercynian basement and Triassic rocks in a retrogradational pattern (S2.3 and S2.4, Figs 3 and 4). These sediments grade basinwards to shallow carbonate deposits, a transition that can be envisaged between the Tribaldos and Torralba wells (Fig. 5). A major palaeogeographical change occurred towards the end of Cenomanian time, with the tilt of the Iberian microplate in relation to the opening of the Bay of Biscay. A rapid Atlantic transgression occurred, drowning the underlying platform. Deep hemipelagic marls (the basal part of sequence S2.5, Figs 3–5) with open marine fauna (ammonites, echinoderms, pelecypods, etc.) of Atlantic affinity were deposited (Segura *et al.* 1993). This unit is considered the maximum transgressive event of the megasequence (Segura *et al.* 1993). During the subsequent regression, a thick carbonate unit developed, with at least two progradational units: the top of sequence S2.5 along the southern cross-section (Tribaldos–Torralba wells, Fig. 5), and sequence S2.6 when the main carbonate sedimentation area moved northwards towards the Baides (Fig. 3) and Santa Bárbara (Fig. 4) wells. This unit, in the Iberian Ranges, shows a rapid northward progradation with large clinoform development (Segura *et al.* 1993).

An important relative sea-level fall occurred in relation to the MS-2–MS-3 boundary. Marine sedimentation shifted farther northwards and the study area remained as a littoral, low-energy area with mainly lowstand marly sedimentation corresponding to the basal part of sequence S3.1, which appears discontinuously westwards (Fig. 3). Sequence S3.2 records a renewed Atlantic transgression, and the maximum flooding surface for the entire megasequence occurred then: open marine marls and carbonates completely covered the study area (mid- to late Coniacian). These marine facies grade southwards to littoral marl with palaeosoils, whereas to the east they grade to sabkha environments with evaporite and claystone sedimentation. Overlying this, there is the development of a very thick carbonate unit (late Coniacian to early Campanian; sequences S3.3, S3.4 and S3.5), locally with calcarenite bars and rudist bioherms grading eastwards and southeastwards to sabkha environments (Fig. 2). The coastal facies of this platform were extended farther westwards (Fig. 2), in relation to the underlying Cenomanian–Turonian platforms.

The MS-3–MS-4 boundary is related to a relative sea-level fall. The presence of an unconformity

related to this boundary is problematic, although it has been mentioned locally (Portero *et al.* 1990). MS-4 facies were very homogeneous, mainly with continental and coastal (sabkha) deposits, and marine sediments were never again deposited in the central parts of the Iberian Basin, including the study area (Figs 4 and 5). Minor, very thin carbonate intercalations occur, however, and they probably represent tidal sediments rather than open marine facies. MS-4 age is poorly constrained, but the scarce fauna indicate a probable Campanian age. Thus, during the last 10 Ma of the Cretaceous, sedimentation kept pace with subsidence to constantly maintain the same sedimentary environments, suggesting that other causes, rather than solely eustatic causes, had an effect on sedimentation.

This paper was funded by the DGI (Ministry of Education and Science) Project CGL2004-04113, 'Análisis de los ritmos deposicionales de alta frecuencia y cuantificación de la sedimentación en el Cretácico Superior de la Cordillera Ibérica'. The authors wish to thank F. Fonnesu (ENI E&P division), whose critical comments greatly improved the manuscript. We also thank C. Valero and the English translation group of the Alcalá University for assistance with the English manuscript.

References

BUSCALIONI, A. & MARTÍNEZ-SALANOVA, J. 1990. Los vertebrados fósiles del yacimiento cretácico de Armuña (Prov. Segovia, España). *Reunión de la Comisión de Tafonomía y fosilización*, 51–57.

BUSCALIONI, A. & SANZ, J. L. 1987. First report on a new crocodile from the Upper Cretaceous of Spain (Province of Segovia): a short comparative review with the Gondwana and Laurasia Upper Cretaceous crocodiles. *In*: CURRIE, P. M. & KOSTER, E. H. (eds) *Short Papers, 4th Symposium on Mesozoic Terrestrial Ecosystems, Drumheller, Alberta, Canada*. Occasional Papers of Tyrrel Museum of Paleontology, **3**, 36–41.

DEL OLMO SANZ, A. & MARTÍNEZ-SALANOVA, J. 1989. El tránsito Cretácico–terciario en la Sierra de Guadarrama y áreas próximas de las Cuencas del Duero y Tagus. *Studia Geologica Salmanticensia, Volumen Especial*, **5**, 55–69.

DERCOURT, J., GAETANI, M., VRIELYNCK, B., *ET AL.* 2000. *Atlas Peri-Tethys, Palaeogeographical Maps*. Commission for the Geological Map of the World, Paris.

FLOQUET, M. & HENNUY, J. 2001. Anatomy of resedimented carbonates in the latest Turonian–earliest Coniacian South-Provencal Basin. *Géologie Méditerranéenne*, **28**(1–2), 67–71.

GARCÍA, A., SEGURA, M., GARCÍA-HIDALGO, J. F. & CARENAS, B. 1993. Mixed siliciclastic and carbonate platform of Albian–Cenomanian age from the Iberian basin (Spain). *In*: SIMO, J. A. T., SCOTT, R. W. & MASSE, J. P (eds) *Cretaceous Carbonate platforms*. American Association of Petroleum Geologists, Memoirs, **56**, 255–269.

GARCÍA, A., SEGURA, M. & GARCÍA-HIDALGO, J. F. 1996. Sequences, cycles and hiatuses in the upper Albian–Cenomanian of the Iberian Ranges (Spain): a cyclostratigraphic approach. *Sedimentary Geology*, **103**, 175–200.

GARCÍA, A., MAS, R., SEGURA, M., *ET AL.* 2004. Segunda fase de post-rifting: Cretácico Superior. *In*: VERA, J. A. (eds) *Geología de España*. Sociedad Geológica de España–Instituto Geológico y Minero de España, Madrid, 510–522.

GARCÍA-HIDALGO, J. F., SEGURA, M. & GARCÍA, A. 1997. El Cretácico del borde septentrional de la Rama Castellana de la Cordillera Ibérica. *Revista de la Sociedad Geológica de España*, **10**, 39–53.

GARCÍA-HIDALGO, J. F., GIL, J. & SEGURA, M. 2001. Sedimentología de la sucesión carbonatada en el borde sur del Sistema Central (Madrid). *Geotemas*, **3**, 193–196.

GARCÍA-HIDALGO, J. F., GIL, J. & SEGURA, M. 2003. Sedimentología de los términos basales de la sucesión cretácica en el borde sur del Sistema Central. *Journal of Iberian Geology*, **29**, 55–71.

GIL, J. 2002. *Estratigrafía de alta resolución en el Turoniense superior–Coniaciense inferior de la Cordillera Ibérica septentrional*. PhD thesis, Universidad Complutense de Madrid.

GIL, J. & GARCÍA, A. 1996. El Cretácico del borde meridional del Sistema Central. Unidades litoestratigráficas y secuencias deposicionales. *Estudios Geológicos*, **52**(1–2), 37–49.

GIL, J., SEGURA, M. & GARCÍA-HIDALGO, J. F. 1999. Stratigraphic and sedimentological analysis of the Cretaceous at 'Barranco de las Cuevas' (Patones, Madrid): a geological interest site in the Community of Madrid. *In*: BARETTINO, D., VALLEJO, M. & GALLEGO, E. (eds) *Towards the Balanced Management and Conservation of the Geological Heritage in the New Millennium*. Sociedad Geológica de España, Madrid, 172–176.

GIL, J., DOMÍNGUEZ, C. & SEGURA, M. 2001. Mineralogía y estratigrafía de los materiales terrígenos del Cretácico superior en la sección de Arrebatacapas (Torrelaguna, Madrid). *Geogaceta*, **30**, 151–154.

GIL, J., PONS, J. M. & SEGURA, M. 2002. Redescripción de *Bournonia gardonica* (Toucas, 1907) (Radiolitidae, Bivalvia) y análisis de las facies en que aparece (Coniaciense, Sistema Central, España). *Revista Española de Paleontología*, **17**(2), 245–256.

GIL, J., CARENAS, B., SEGURA, M., GARCÍA-HIDALGO, J. F. & GARCÍA, A. 2004. Revisión y correlación de las unidades litoestratigráficas del Cretácico Superior en la región central y oriental de España. *Revista Sociedad Geológica de España*, **17**(3–4), 249–266.

MARTÍN-CHIVELET, J., Berástegui, X., ROSALES, I., *ET AL.* 2002. Cretaceous. *In*: GIBBONS, W. & MORENO, M. T. (eds) *The Geology of Spain*. Geological Society, London, 255–292.

MELÉNDEZ, F. 1975. Correlación del Cretácico de la Serranía de Cuenca con el del Sondeo de Villanueva

de los Escuderos 1 (Cuenca). *Actas I Symposio sobre el Cretácico de la Cordillera Ibérica*, 85–97.

POLO, T., SEGURA, M., CARENAS, B., GIL, J. & GARCÍA-HIDALGO, J. F. 2003. Estratigrafía del Cretácico superior en el Sondeo de 'El Pradillo-1' (Madrid). *Revista Sociedad Geológica de España*, **16**(1–2), 91–102.

PORTERO, J. M., DÍAZ MOLINA, M., GONZÁLEZ LODEIRO, F., PÉREZ GONZÁLEZ, A., GALLARDO, J., AGUILAR, M. J. & LEAL, M. C. 1990. *Memoria de la Hoja 485 (Valdepeñas de la Sierra) del Mapa Geológico de España a escala 1:50.000*, 2ª Serie, 1ª edición. Instituto Tecnológico y Geominero de España, Madrid.

REICHERTER, K. R. & PLETSCH, TK. 2000. Evidence for a synchronous circum-Iberian subsidence event and its relation to the African–Iberian plate convergence in the Late Cretaceous. *Terra Nova*, **12**, 141–147.

SEGURA, M. & WIEDMANN, J. 1982. La transgresión del Cretácico superior en el sector de Atienza–Sigüenza (Guadalajara, Cordillera Ibérica) y el significado de la fauna Ammonitífera. *Cuadernos de Geología Ibérica*, **8**, 293–307.

SEGURA, M., GARCÍA, A., GARCÍA-HIDALGO, J. F. & CARENAS, B. 1993. The Cenomanian–Turonian transgression in the Iberian Ranges (Spain): depositional sequences and the Cenomanian–Turonian boundary. *Cretaceous Research*, **14**, 519–529.

SEGURA, M., GARCÍA, A. CARENAS, B., GARCÍA-HIDALGO, J. F. & GIL, J. 2002. Upper Cretaceous of the Iberian basin. *In*: GIBBONS, W. & MORENO, M. T. (eds) *The Geology of Spain*. Geological Society, London, 288–292.

SEGURA, M., GARCÍA-HIDALGO, J. F., CARENAS, B., GIL, J. & GARCÍA, A. 2004. Evolución paleogeográfica de la Cuenca Ibérica en el Cretácico Superior. *Geogaceta*, **36**, 103–106.

STRASSER, A., PITTET, B., HILLGÄRTNER, H. & PASQUIER, J.-B. 1999. Depositional sequences in shallow carbonate-dominated sedimentary systems: concepts for a high-resolution analysis. *Sedimentary Geology*, **128**, 201–221.

VAN WAGONER, J. C., MITCHUM, R. M., CAMPION, K. M. & RHAMANIAN, V. D. 1990. *Siliciclastic Sequence Stratigraphy in Well Logs, Cores, and Outcrops*. American Association of Petroleum Geologists, Methods in Exploration Series, **7**.

YÉBENES, A. 1975. Estudio petrológico y geoquímica de las 'Carniolas del Cretácico superior' de la serranía de Cuenca. *Actas I Symposio sobre el Cretácico de la Cordillera Ibérica*, 99–111.

Miocene to present major fault linkages through the Adriatic indenter and the Austroalpine–Penninic collisional wedge (Alps of NE Italy)

M. MASSIRONI[1], D. ZAMPIERI[1,2] & A. CAPORALI[1]

[1]*Dipartimento di Geologia, Paleontologia e Geofisica, Università di Padova, Via Giotto 1, 35137 Padova, Italy (e-mail: matteo.massironi@unipd.it)*

[2]*CNR, Istituto di Geoscienze e Georisorse, Sezione di Padova, Corso Garibaldi 37, 35137 Padova, Italy*

Abstract: From the Miocene onwards, the Alpine and South Alpine domains have been closely coupled within the framework of fault kinematics and geodynamic processes related to the continuing indentation of the Adria plate against Europe. In this study, the post-Oligocene evolution of a wide sector of the North Adriatic indenter border and nearby areas is re-examined in an extensive regional context by means of structural, geochronological and seismotectonic data. The Adria northern edge roughly corresponds to the Periadriatic lineament which is characterized in the central–eastern Alps by an abrupt change of orientation from east–west to NNE–SSW at the North Giudicarie line. Several strike-slip fault linkages have developed along the northern and southern sections of this major fault since the Miocene. In the Alpine domain, fault connections facilitated tectonic unroofing of the deeper nappes (Penninic units) in the Tauern window and a westward crustal stretching of the upper nappes (Austroalpine units) in the Brenner detachment hanging wall. In the Southern Alps, several fault linkages are observed, which are related to reactivation of inherited faults by the indentation process. These processes began during the early Miocene, were fully developed in the latest Miocene–early Pliocene, and are very probably still continuing. The final result is a complex shear zone of 250 km length, that in the southern part is considered as an incipient divide between the nearly stationary westernmost part of the North Adriatic indenter and the still northward-pushing main body of the Adria plate.

The Alps are composed of a Europe-vergent collisional wedge (Alpine domain *sensu stricto*) and a south-propagating fold-and-thrust belt (South Alpine domain). The Alpine domain is the product of a complex subduction–collisional history between the lower European plate and the upper Adria (Africa) plate, whereas the Southern Alps developed during the last stages of the collision. Interpretations of seismic reflection and refraction data across the Alps indicate that a rigid wedge of Adriatic lower crust, named the North Adriatic indenter, was pushed into the Austroalpine–Penninic wedge in Neogene time (Nicolas *et al.* 1990; Fantoni *et al.* 1993; Pfiffner & Hitz 1997; Schmid *et al.* 1997; Lammerer & Weger 1998). The aim of this paper is to re-examine the strike-slip fault system extending from the North Giudicarie line to the Schio–Vicenza line in an extensive regional context, partly corresponding to the boundary of the North Adriatic indenter in the Italian Alps. This revision is based on structural, geochronological, geophysical and seismological data provided by decades of detailed studies in the Alps. The relationships between the tectonic evolution of the Southern Alps and the Austroalpine–Penninic collisional wedge during the last stages of the Alpine orogenesis are closely examined, as well as their interactions with the accreting Apennine orogen. In addition, particular emphasis is placed on the role of the inherited Mesozoic structures in creating tectonic linkages between major strike-slip faults in the boundary zone of the Adriatic indenter.

The Alpine orogenic wedge and the South Alpine fold-and-thrust belt

The Alpine orogenic belt originated from the Cretaceous–present convergence between the Adriatic upper plate and the subducting European lower plate, including the Mesozoic Tethyan ocean (e.g. Dewey *et al.* 1989; Kurz *et al.* 1998; Dal Piaz *et al.* 2003). It is composed of a Europe-vergent collisional wedge (Alpine domain *sensu stricto*) and a south-propagating fold-and-thrust belt (South Alpine domain) separated by a major fault system called the Periadriatic lineament (Fig. 1).

The collisional wedge of the eastern Alps is composed of the Adria-derived Austroalpine continental basement and cover system, and the Penninic unit of the Tauern window, which includes the ophiolite-bearing Glockner nappe and the underlying Europe-derived continental basement (Central

From: MORATTI, G. & CHALOUAN, A. (eds) 2006. *Tectonics of the Western Mediterranean and North Africa*. Geological Society, London, Special Publications, **262**, 245–258.
0305-8719/06/$15.00

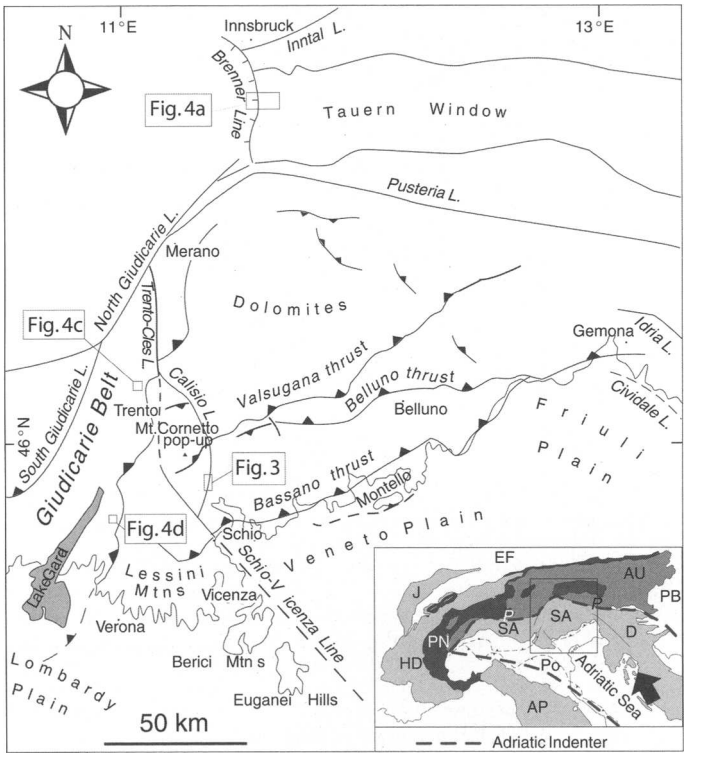

Fig. 1. Structural map of central–eastern Southern Alps. Inset: northern part of Adriatic indenter and main units. EF, European Foreland; J, Jura; HD, Helvetic–Dauphinois; PN, Penninic; AU, Austroalpine; SA, Southern Alps; Po, Po Plain; AP, Apennines; D, Dinarides; PB, Pannonian Basin; P, Periadriatic lineament.

Gneiss) and cover units (Fig. 2). During the subduction–collisional wedge development, the Periadriatic lineament was the active tectonic boundary between the Alpine exhuming wedge and the South Alpine rigid lithosphere, of which the frontal part (Austroalpine) was involved in the collisional wedge. The nappe stack was affected by subduction-related eclogite- to blueschist-facies metamorphism (scattered relics) of Eocene age (Penninic zone, Zimmermann *et al.* 1994) and a pervasive Barrovian (amphibolite- to greenschist-facies) overprint of Oligocene age (Tauern crystallization of Sander 1912; Christensen *et al.* 1994). In Oligocene time, during the continuing Adria–Europe convergence, rapid uplift took place together with magmatism along or near the Periadriatic lineament (von Blackenburg & Davies 1995; Dal Piaz 1999; Rosenberg 2004). Only the post-Oligocene evolution of the Alpine domain is of paramount importance for our purpose. From this time onward, the rigid Southern Alpine lithosphere indented the inner sector of the orogenic wedge, causing the rapid tectonic extrusion and cooling of the Penninic nappes previously softened by the Barrovian metamorphism. Consequently, the continuing north–south shortening caused the vertical exhumation of the Penninic units at the Tauern window (facilitated by erosion), tectonic unroofing along the Brenner detachment, and orogen-parallel escape of the Brenner footwall toward the opening Pannonian basin (Selverstone 1988; Ratschbacher *et al.* 1991*a*,*b*; Frisch *et al.* 2000). In the mean time, the upper part of the indenter, detached from the underlying lithosphere, was involved in the antithetic South Alpine fold-and-thrust belt propagating towards the Po Plain. From the Miocene onward, the tectonic histories of the Alpine collisional nappe stack and the Southern Alps may be considered together because both are concurrently deformed under the same regional stress field.

The Southern Alps and the Austroalpine domain preserve the original Mesozoic northwestern passive margin of the Adria plate (e.g. Bertotti *et al.* 1993). During the first stages of the Alpine orogeny (Late Cretaceous–Early Paleocene), the central and western Southern Alps constituted the slightly deformed hinterland of the Europe-vergent Austroalpine–Penninic collisional wedge.

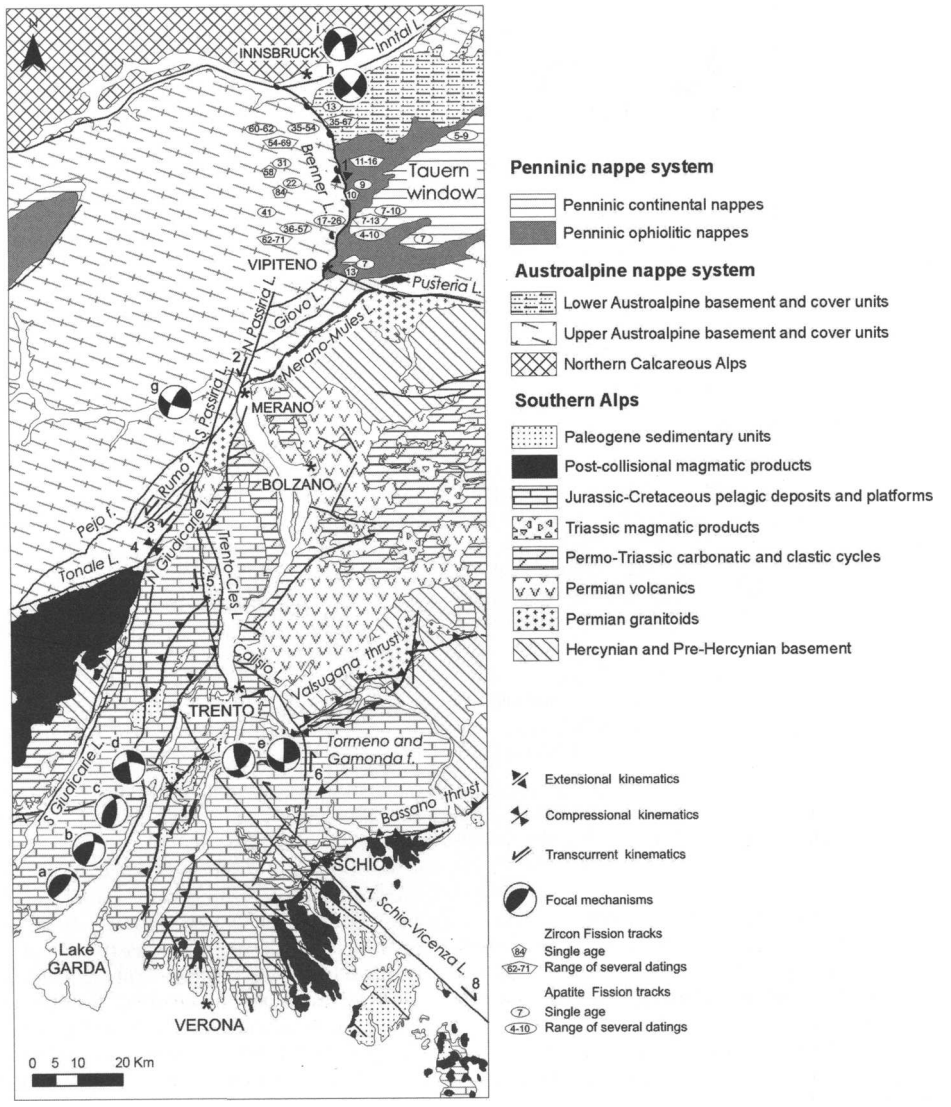

Fig. 2. Geological map of Innsbruck–Verona transect, showing Neogene fault kinematics and focal mechanisms. Fission-track dating shows the Early Miocene onset of the Brenner detachment (from Grundman & Morteani 1985; Fügenschuh *et al.* 1997, 2000). Fault kinematics: 1, Early Miocene to Pliocene (at least until 3 Ma) Brenner detachment kinematics (Behrmann 1988; Selverstone 1988, 1993; Fügenschuh *et al.* 1997; Bistacchi *et al.* 2003); 2, Mid-Miocene (*c.* 17 Ma) to Pliocene Passiria fault kinematics (Müller *et al.* 2001; Spiess *et al.* 2001; Viola *et al.* 2001); 3, Mid-Miocene to Pliocene kinematics of fault at North Giudicarie hanging wall (Fellin *et al.* 2002); 4, Mid-Miocene (*c.* 13 Ma) to Pliocene kinematics of North Giudicarie line and faults near its hanging wall (Prosser 2000; Fellin *et al.* 2002; Viola *et al.* 2004); 5, Mid-Miocene (*c.* 13 Ma) to Pliocene Trento–Cles system kinematics (Prosser 2000; Viola *et al.* 2004); 6, Mid-Miocene (*c.* 13 Ma) to Pliocene kinematics of Tormeno–Gamonda fault arrays (Zampieri *et al.* 2003); 7, Messinian (*c.* 8 Ma) to Pliocene Schio–Vicenza fault kinematics (Castellarin & Cantelli 2000; Zampieri *et al.* 2003); 8, Presumed Mid-Miocene Schio–Vicenza fault kinematics. Focal mechanisms: a, 2004.11.24, 45°54′N, 10°83′E, h = 18 km, Mi = 5.2, Salò (www.ingv.it/seismoglo/RCMT/); b, 1975.01.11, 45°39′N, 10°36′E, h = 12 km, M = 4, Gardone (Slejko *et al.* 1987); c, 1986.04.15, 45°46′N, 10°44′E, h = 15 km, M = 3.2, Tremosine (Slejko *et al.* 1987); d, 1976.12.13, 45°55′N, 10°50′E, h = 2 km, M = 4.5, Riva (Slejko *et al.* 1987); e, 1968.06.22, 45°48′N, 11°13′E, h = 24 km, M = 4.5 Pasubio (Slejko *et al.* 1987); f, 1968.06.22, 45°45′N, 11°14′E, h = 23 km, M = 4.1 Pasubio (Slejko *et al.* 1987); g, 2001.07.17, 46°39′N, 11°08′E, h = 1.6 km, M = 5.1 Merano (Pondrelli *et al.* 2004; Caporali *et al.* 2005); h, 1982.05.01, 47°17′N, 47°16′E, h = 7 km, M = 3.8 Innsbruck (Slejko *et al.* 1987); i, 1965.07.08, 47°18′N, 11°24′E, h = 5 km, M = 3.3 Mittenwald (Slejko *et al.* 1987).

In detail, pre-Mid-Eocene south-vergent structures cut by the Adamello intrusion are recorded only in the central sector of the Southern Alps (Brack 1981). In the Eocene–Early Oligocene phase, the easternmost sector was deformed by Dinaric SW-vergent thrusts. Later, from the Miocene onward (Neoalpine phase), the whole of the Southern Alps was shortened as a south-vergent fold-and-thrust belt, which developed as a retro-wedge (Doglioni & Bosellini 1987; Castellarin & Cantelli 2000).

The Southern Alps are subdivided into two main sectors by the NNE–SSW-trending Giudicarie belt (Fig. 1). The western sector exposes a complete crustal section, from the classic Ivrea lower crust to the post-Variscan Permian–Mesozoic cover. The eastern sector exposes low-grade basement and Permo-Mesozoic cover sequences, well represented in the Dolomites (Bigi *et al.* 1990). To the east, the Southern Alps are bounded by NW-trending Dinaric Palaeogene thrust fronts (Idria and Cividale lines), reactivated during the Neoalpine phase as dextral strike-slip faults (Fig. 1). The main tectonic features of the eastern Southern Alps are the Neogene south-vergent thrusts, i.e. the Valsugana (Serravallian–Tortonian), Belluno (Tortonian–Messinian?) and Bassano (Messinian–Pliocene) thrusts (Venzo 1941; Castellarin *et al.* 1992; Selli 1998) and, to the west, the NW-trending Schio–Vicenza and north-trending Trento–Cles strike-slip faults (Figs 1 and 2).

Many pre-Alpine extensional structures have been recognized from the analysis of syntectonic sediments (e.g. Castellarin 1972; Bertotti *et al.* 1993) and structures that crop out (e.g. Doglioni 1992; Zampieri 1995*b*). These normal faults, trending north–south to NNE–SSW, are derived from multiple tectonic phases, i.e. the early Permian and Mid-Triassic tectonomagmatic events (Cassinis & Perotti 1993; Dal Piaz & Martin 1998), Jurassic extension of the passive margin of the Apulian microplate (Bertotti *et al.* 1993), and Palaeogene rifting coupled with magmatism (Zampieri 1995*a*). The major map-view undulations of the Neogene SSE-vergent thrusts have been explained by inversion of these inherited normal faults (Doglioni 1992). The Giudicarie belt itself is the main example of a transpressive fault zone controlled by pre-existing Jurassic normal faults (Castellarin *et al.* 1993; Prosser 1998, and references therein).

The Giudicarie boundary of the Adriatic indenter and related fault systems in the South Alpine and Alpine domains

The western edge of the corner of the Adriatic indenter is marked by the North Giudicarie fault and a complex network of faults with dominant transcurrent kinematics, at a high angle to the east–west general trend of the chain (Figs 1 and 2). This crustal-scale shear zone includes the major strike-slip faults of the Southern Alps and the main faults of the Alpine domain *sensu stricto* involved in differential exhumation of nappes during the last stage of Alpine orogenesis.

The Schio–Vicenza line and its tectonic linkage with the Trento–Cles system

Within the Southern Alps fold-and-thrust belt, the Lombardian and Veneto–Friuli sectors and related forelands (i.e. the Po and Veneto–Friuli Plains) are separated by the Euganeo–Berico–Lessinian wedge, which is a morphological and structural divide. This high ('Adige embayment' of Laubscher 1996) is bounded to the east by the NW-trending Schio–Vicenza line and to the west by the frontal sector of the Giudicarie belt. The Schio–Vicenza fault probably originated as a Palaeogene extensional structure on the Dinaric foreland bulge (Doglioni & Bosellini 1987). South of Schio this fault shows a southward-decreasing top down-to-the-east throw connected to the development of the eastern Southern Alps foredeep (Finetti 1972; Pellegrini 1988). Many researchers have suggested that the post-Tortonian kinematics of the Schio–Vicenza line was sinistral (Semenza 1974; Zanferrari *et al.* 1982; De Vecchi *et al.* 1986; Castellarin & Cantelli 2000; Zampieri *et al.* 2003). On the other side of the Adige embayment, the Giudicarie belt is composed of a series of late Miocene ESE-vergent thrust sheets and NNE–SSW to north–south strike-slip faults, involving a large area between the Trento–Cles strike-slip systems and the South Giudicarie line (Fig. 2). All these structures are totally or partly the result of strike-slip reactivation on inherited Permian–Mesozoic normal faults (e.g. Picotti *et al.* 1995; Prosser 1998).

It is well established that faults are commonly composed of numerous discrete segments overlapping in en echelon geometry. Their mechanical linkage occurred by ductile strain structures (soft linkage), which may evolve into breaking faults connecting the initial segments (hard linkage) (e.g. Peacock & Sanderson 1991). In the area between Schio and Trento (Fig. 2), the processes of strike-slip reactivation and linkage of various fault segments are clearcut. A north–south-trending fault zone connects the Schio–Vicenza line with the Trento–Cles line via the Calisio line. These fault segments formed during earlier extensional events (Permian for the Calisio fault; Jurassic for the others), but they also were reactivated as normal faults in the Palaeogene. Finally, they were reactivated as sinistral strike-slip faults in the Neogene, when the eastern Southern Alps shortened (Zampieri *et al.* 2003). Pre-existing structures are an important mechanical anisotropy, which may be responsible for strain partitioning into strike-slip

and dip-slip displacements along different structures (e.g. Tikoff & Teyssier 1994). Consequently, the inherited normal faults, oblique to the direction of shortening, played a key role in adsorbing the strike-slip component of the transpression. In the stepovers between fault segments, restraining and releasing structures developed at various scales.

At the kilometre scale, the most impressive evidence of soft linkage between fault segments is observed at the right step between the two conjugate Gamonda and Tormeno faults (Figs 2 and 3). In the overlap zone, Jurassic to Early Cretaceous sediments, filling a narrow graben, were shortened in a direction nearly parallel to the strike of the normal faults. The shortening has been accommodated by the development of an array of east- to ENE-trending folds associated with thrusts and reverse faults (Fig. 3).

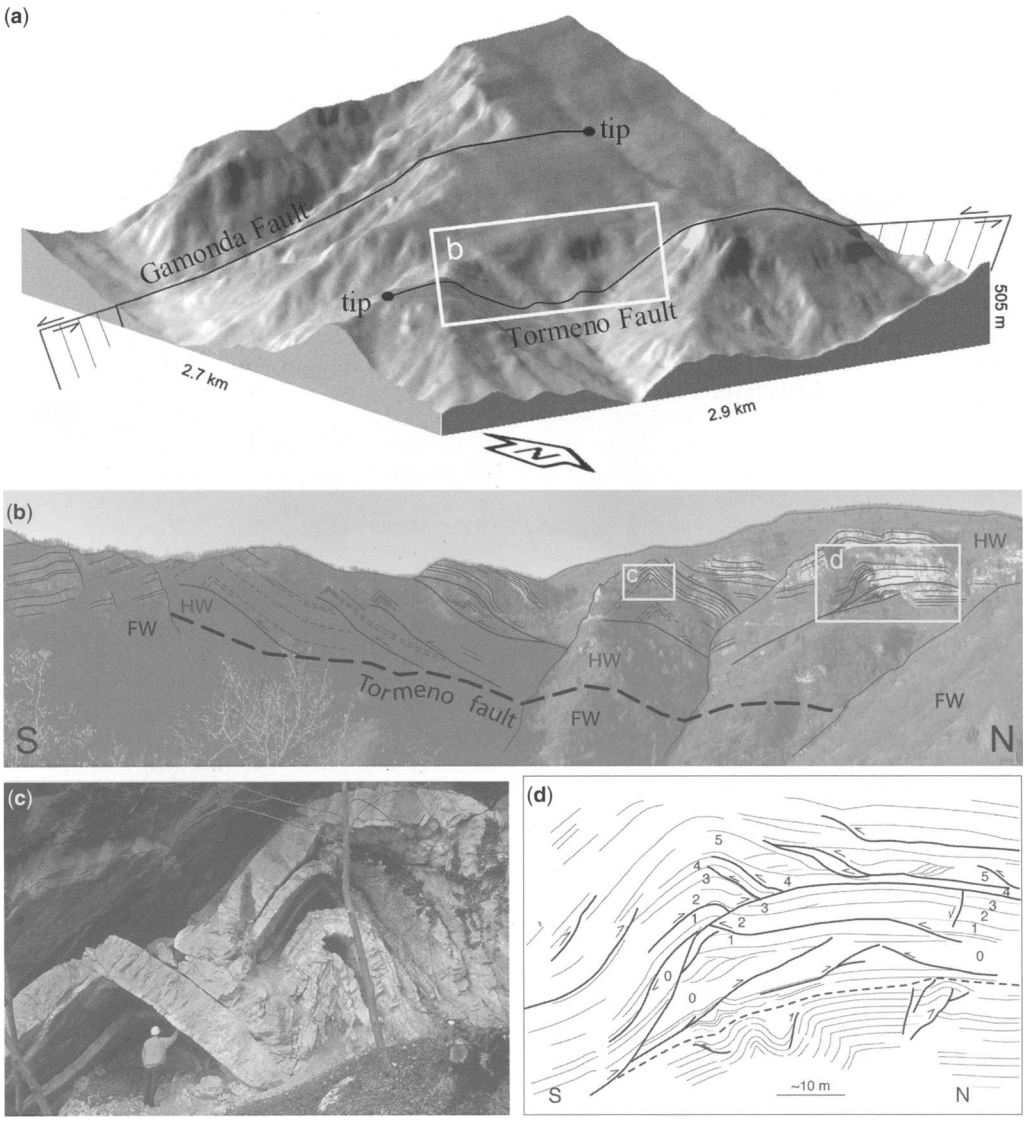

Fig. 3. Contractional stepover between Tormeno and Gamonda faults (location of the stepover structure is shown in Fig. 1). (**a**) Digital terrain model (DTM) perspective view looking NW. (**b**) Detail of fold-and-thrust structures inside stepover area (looking W). HW, hanging wall of the west-dipping Tormeno fault; FW, footwall of the west-dipping Tormeno fault. (**c**) Core of a major anticline (axis trending east–west), showing space accommodation structures (location shown in (b)). (**d**) Line drawing of contractional structures in core of the major box fold (location shown in (b)) (after Zampieri *et al.* 2003).

At a regional scale, the Schio–Vicenza line may be directly connected with the north-trending Trento–Cles line along the Adige valley, as suggested by Semenza (1974). If this hypothesis is correct, then the Trento–Cles–Schio–Vicenza fault system is a regional structure displaying a prominent right bend (Figs 1 and 2). Alternatively, the linkage between the Trento–Cles and the Schio–Vicenza strike-slip faults has been accomplished through the development of a restraining stepover limited to the east by the Calisio–Tormeno–Gamonda fault array (Monte Cornetto di Folgaria pop-up) (Zampieri *et al.* 2003) (Figs 1 and 2).

The North Giudicarie line and the related footwall and hanging-wall fault systems

The North Giudicarie fault is the moderately (45°) WNW-dipping tectonic boundary between the Austroalpine nappe-stack and the Southern Alps (low-grade pre-Alpine basement, Permian–Mesozoic sedimentary cover and scattered Oligocene intrusions). The North Giudicarie line had two distinct northern sections (Fig. 2) of different ages: (1) the NE-trending Merano–Mules fault, which is the kinematic linkage with the east–west Pusteria line, still the tectonic boundary between the Austroalpine nappe stack and the Southern Alps (Oligocene; Müller *et al.* 2001); (2) the NNE-trending Passiria fault, dissecting the Austroalpine units and connecting the Giudicarie line to the Brenner detachment through the NE-trending Giovo line (Miocene to present, Viola *et al.* 2001; Caporali *et al.* 2005). Several Alpine faults, dismembering the high-grade pre-Alpine basement of the Austroalpine nappes, are present in the hanging wall of the North Giudicarie fault and show the same average trend (e.g. the Pejo and Rumo faults). In the North Giudicarie footwall, a major north–south-trending fault system (the Trento–Cles fault system) is present. All these faults, together with some minor ones, constitute the North Giudicarie system, which underwent three main post-nappe deformational phases. The first was Late Cretaceous–Early Paleocene extension, recorded only in some faults (Pejo and Rumo mylonitic horizons) (Martin *et al.* 1991, 1998; Müller *et al.* 2001; Viola *et al.* 2003). The second involved Oligocene dextral activity along the North Giudicarie and Merano Mules faults, and is well constrained by radiometric ages on mylonites, pseodotachylytes and cross-cutting relationships with the Oligocene intrusive rocks (Prosser 1998; Müller *et al.* 2001). Only since the Early Miocene, during the third deformational phase, has the North Giudicarie system kinematics been closely related to the Southern Alpine strike-slip systems on one side and to the Brenner detachment on the other. In this period, NNW compression reactivated the North Giudicarie fault as an ESE-vergent thrust (Martin *et al.* 1991), and the sinistral strike-slip component was accommodated in its footwall by the inherited Mesozoic Trento–Cles fault system (Figs 2 and 4c,d) (Prosser 1998; Viola *et al.* 2004). An Early Miocene (21–17 Ma) nucleation and sinistral strike-slip kinematics has been demonstrated for the Passiria fault by fission-track dating and by the 20 km displacement of the older Giovo deformation belt and minor Oligocene intrusive bodies (Müller *et al.* 2001; Spiess *et al.* 2001; Viola *et al.* 2001). Similarly, the north to NNE faults in the North Giudicarie hanging wall also underwent sinistral kinematics in the same period, as demonstrated by ductile to brittle kinematic indicators (Fellin *et al.* 2002). Therefore, during the Miocene, the connection between the Giudicarie and Brenner faults was accomplished through the Passiria and Giovo faults (Fig. 2).

The Brenner low-angle detachment and tectonic exhumation in the Tauern window

At the mountain-belt scale, detachment activity at the Brenner line is due to the tectonic unroofing and eastward escape of the Tauern window units toward the extensional Pannonian basin (Fig. 1) (Ratschbacher *et al.* 1991*a*,*b*). Therefore, understanding the Brenner fault kinematics is of paramount importance in constraining the onset of differential tectonic denudation in the Eastern Alps and the activity of Alpine *sensu stricto* and South Alpine faults.

The Brenner west-dipping low-angle detachment (Fig. 4a and b) is the western tectonic boundary of the Tauern window and brings the Austrolpine basement and cover nappes (hanging wall), characterized by Cretaceous Alpine metamorphism, into contact with deeper Penninic units of the window (footwall), which record a dominant greenschist- to amphibolite-facies Alpine metamorphic imprint of Oligocene age. Its extensional activity is therefore consistent with a considerable gap in radiometric age: mica ages in the Austroalpine hanging wall go back to the Late Cretaceous (Frank *et al.* 1987, and references therein), whereas Oligocene to Miocene Rb/Sr ages in phengite and garnet are recorded inside the Tauern window (Frank *et al.* 1987; von Blackenburg *et al.* 1989; Christensen *et al.* 1994). Similarly, the Late Cretaceous–Early Miocene zircon and apatite fission-track ages in the Austroalpine nappe contrast with the Mid- to Late Miocene ages at the Brenner detachment footwall (Fig. 2) (Grundman & Morteani 1985; Fügenschuh *et al.* 1997, 2000). In addition, numerous ductile to brittle kinematic

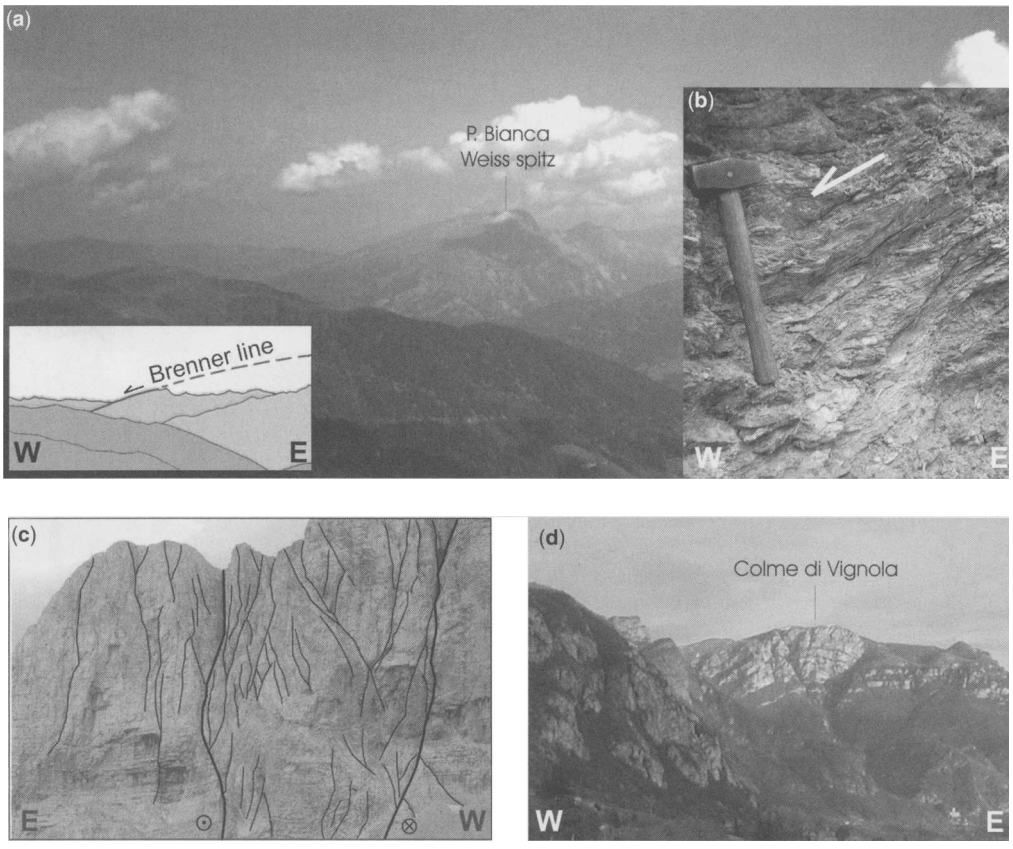

Fig. 4. Fault examples from Brenner area to Adige valley (locations shown in Fig. 1). (**a**) Panoramic view of Brenner detachment area (looking north). (**b**) Brenner detachment SC′ structures in the Penninic calcschists showing top-to-the-west movement. (**c**) NNE-trending strike-slip fault zone in Jurassic carbonates of Doss di Dalum (Brenta group, South Giudicarie system). Cliff face is *c.* 300 m high. (**d**) Panoramic view of Colme di Vignola positive flower structure (a few kilometres south of Ala) related to a NNE strike-slip fault of the Giudicarie Belt.

indicators constrain the top-to-the-west sense of shear of the Brenner detachment (Fig. 4b) (Behrmann 1988; Selverstone 1988, 1993; Fügenschuh *et al.* 2000; Bistacchi *et al.* 2003). All these data indicate that denudation of the Tauern window along the Brenner low-angle detachment began in the Early Miocene (Behrmann 1988; Selverstone 1988, 1993; von Blackenburg *et al.* 1989). The onset of lateral escape is further constrained by the dextral strike-slip deformations along the Pustertal fault system, which are coeval with or postdate the Late Oligocene intrusive bodies (Mancktelow *et al.* 2001). Nevertheless, in the light of the amount of displacement and regional tectonic influence, some workers believe that this process became important only after the Mid-Miocene (von Blackenburg *et al.* 1989; Fügenschuh *et al.* 1997; Frisch *et al.* 2000).

Present tectonic activity from the Brenner detachment to the Schio–Vicenza system

The South Alpine front between Schio and Gemona (Fig. 1) is the site of active thrusting related to the Neogene collisional convergence between Adria and Europe. The northeastern part of the Adriatic plate moved approximately toward the NNW, bordered to the NE by NW-trending dextral strike-slip faults (Idria and Cividale lines) and to the SW by the NW-trending sinistral Schio–Vicenza line (Figs 1 and 2).

In the eastern Alps the present regional velocity and strain fields, derived from global positioning system (GPS) data, *in situ* stress measurements (borehole break-outs) and seismotectonic data, indicate the maintenance of a compression running

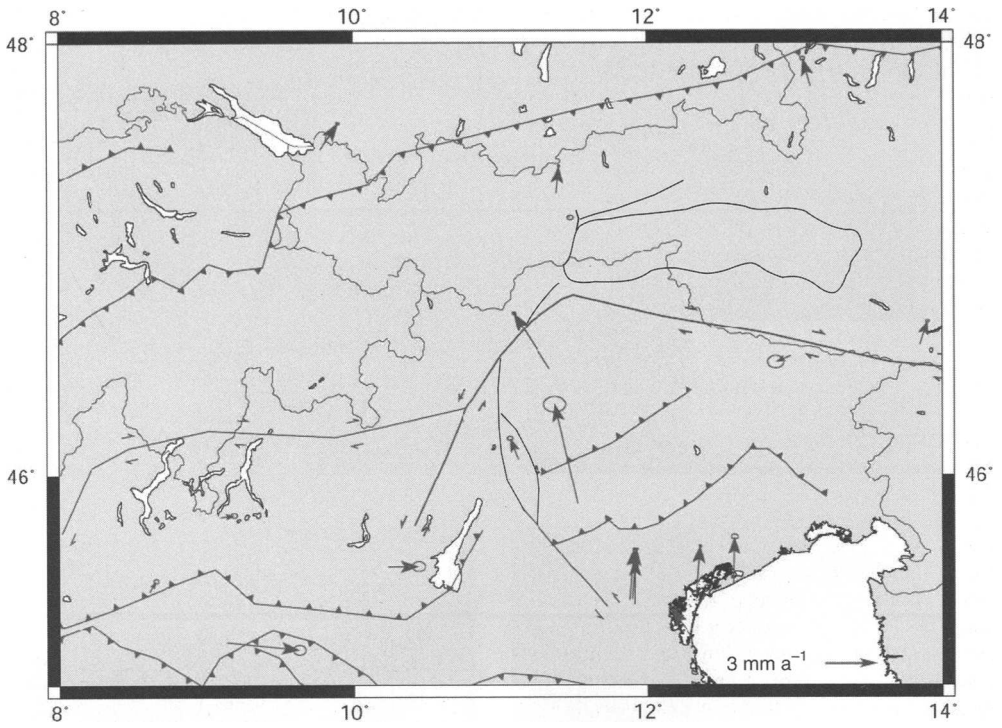

Fig. 5. Horizontal velocities of permanent GPS stations computed in ITRF2000 reference system (Altamimi *et al.* 2002), as interpreted by Caporali *et al.* (2003, 2005). Error ellipses are 1σ. Velocities are defined with respect to values predicted by Nuvel 1 A NNR (De Mets *et al.* 1994) Eulerian pole for Eurasia and, in this sense, are relative to a rigid Eurasian plate.

approximately NW–SE to NNW–SSE as in the Miocene (Müller *et al.* 1992; Zoback 1992; Bressan *et al.* 1998; Caporali *et al.* 2002, 2003; Oldow *et al.* 2002; Pondrelli *et al.* 2002, 2004; Battaglia *et al.* 2004) (http://www.ingv.it/seismoglo/RCMT/). The velocities reported by Caporali *et al.* (2002) have been improved with additional data up to November 2004 and are shown in Figure 5 with respect to a stable Eurasian plate. The velocities of permanent GPS stations east of the Schio–Vicenza fault and near the Adriatic Sea coastline, i.e. within the eastern sector of the North Adriatic indenter, are directed northwards. The velocities of the permanent stations north of the Pusteria line, i.e. within the stable Eurasian plate, are much lower. This decrease in horizontal velocity north of the Pusteria line is clear evidence of continuing compressional strain in the Friuli area, and sinistral shear strain along the Giudicarie and Schio–Vicenza fault systems. The eastward pattern of a few permanent GPS stations between longitudes of 8°E and 10.5°E in Figure 5 needs further investigation, as it may indicate a new scenario for the present-day tectonic flow in the Po Plain. This structural setting is consistent with the concept of an active northward indentation of the Adria plate against Europe (Renner & Slejko 1994; Regenauer-Lieb & Petit 1997; Bressan *et al.* 1998), whereas its westernmost part is nearly stationary (Oldow *et al.* 2002; Battaglia *et al.* 2004) or migrating eastward (Fig. 5).

According to the historical catalogue of the Istituto Nazionale di Geofisica e Vulcanologia (Valensise & Pantosti 2001; http://80.117.141.2/cft/ and http://emidius.mi.ingv.it/CPTI/), an earthquake of estimated magnitude 4.9 was recorded near Vipiteno in 1924. Based on the historical data of Schorn (1902), Lenhardt (2002) reported large earthquakes (up to M *c.* 7) in the Innsbruck area, related to the active Inntal line (Fig. 2, Reiter *et al.* 2002). Toward the Giudicarie system, the seismicity tends to be mostly at instrumental level except for the 2001 Merano earthquake (M = 4.8), and becomes stronger further south, between Verona and Vicenza (e.g. Verona 1117, M *c.* 6.4; Vicenza 1303, M *c.* 5; Lake Garda 2004, M = 5.5). Here it is associated with north–south strike-slip splays of the Giudicarie line, thrusts of the Giudicarie belt and the Schio–Vicenza

strike-slip system (Slejko *et al.* 1989; Valensise & Pantosti 2001; (http://80.117.141.2/cft/ and http://www.ingv.it/seismoglo/RCMT/). The Schio–Vicenza line itself has been classified as a potential source for earthquakes exceeding M 5.5 (Valensise & Pantosti 2001; Galadini *et al.* 2002).

From the kinematic viewpoint, focal mechanisms along the Inntal line show clear sinistral kinematics, indicating the continuing eastward lateral escape of the Tauern window block (Slejko *et al.* 1987, 1989), whereas in the Southern Alps all focal mechanisms point to regional NNW–SSE compression and more complex fault kinematics (both compressional and strike-slip) (Slejko *et al.* 1987, 1989; Pondrelli *et al.* 2004; http://www.ingv.it/seismoglo/RCMT) (Fig. 2). In addition, the recent event at Merano (M = 4.8, 17 July 2001) fits the sinistral strike-slip activity along the Passiria line (Pondrelli *et al.* 2004; Caporali *et al.* 2005), clearly indicating the northward indentation of the Adria plate into the Eurasian plate (Renner & Slejko 1994; Regenauer-Lieb & Petit 1997; Bressan *et al.* 1998). Hence, it is conceivable that the seismicity follows fault arrays connecting the Inn valley at Innsbruck to the Adige valley across the Brenner Pass, continuing south along the Passiria–Giudicarie system through Vipiteno and Merano, and to the Schio–Vicenza system.

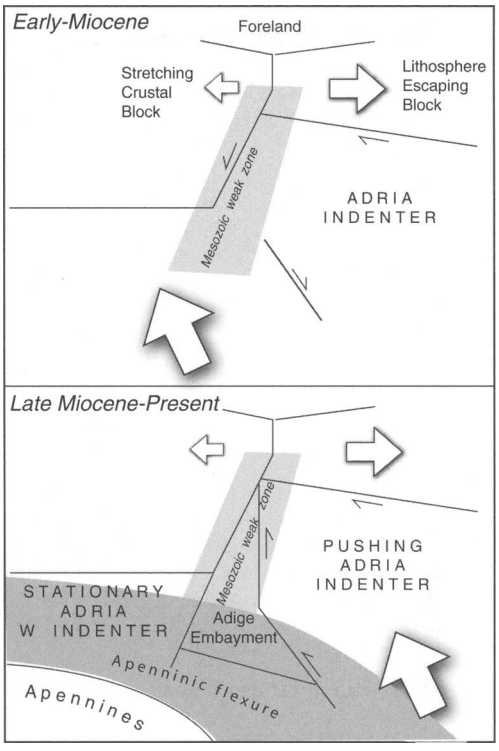

Fig. 6. Geodynamic sketch of evolution of the northern Adriatic indenter.

Discussion

Tectonic linkage from the Brenner detachment to the Schio–Vicenza system

As previously emphasized, the North Giudicarie system is closely related to the post-nappe evolution of the orogenic wedge, whereas the block bounded by the South Giudicarie and Schio–Vicenza–Trento–Cles fault systems ('Adige embayment' of Laubscher 1996) as a whole separates the Veneto–Friuli from the Lombardian Southern Alps.

During the Serravallian–Tortonian NNW–SSE contraction, the Giudicarie belt acted as an oblique ramp for the south-vergent Lombardian thrusts (Trevisan 1938; Castellarin *et al.* 1986; Picotti *et al.* 1995). Therefore, the deformation was partitioned inside the belt into sinistral north–south-trending strike-slip faults and several SSE-vergent thrusts. This kinematics completely fits the coeval strike-slip activity of the North Giudicarie–Passiria and Trento–Cles lines, which are in turn connected to the Brenner extensional activity. In fact, on the basis of the attitude and kinematics of the North Giudicarie–Passiria fault system, it is very probable that, from the Mid-Miocene onward, the lateral extrusion of the Penninic nappe stack in the Tauern window toward the Pannonian basin has also been coupled with a shallower westward crustal stretching of the Brenner fault hanging wall, both developing under the same regional stress pattern (NNW–SSE compression) (Fig. 6). This hypothesis is strongly supported by the coeval nucleation of the Brenner detachment and the onset of the sinistral kinematics along the Giudicarie–Passiria fault array. In addition, it is very unlikely that during the lateral escape of the Penninic units of the Tauern window toward the east, the hanging wall of the Brenner detachment has remained static, as it should has been affected by a westward movement related to tectonic unroofing process. In this framework, the deformation along the North Giudicarie–Passiria faults has been kinematically transferred to the Lombardian frontal thrusts through the Giudicarie belt. Furthermore, the 30 km of shortening in the Giudicarie belt and the eastern side of the Lombardian thrusts during the Mid–Late Miocene (balanced cross-sections by Picotti *et al.* 1995) reflects comparable deformation further north in the same period, as proven by recent studies on the Giudicarie–Passiria and Trento–Cles systems (Prosser 1998; Viola *et. al.* 2001). Therefore, the

North Giudicarie–Passiria system represents the SE boundary of a great estward crustal stretching block at the Brenner detachment hanging wall. At the same time, given its NW–SE trend, the Schio–Vicenza line probably acted as a right-lateral strike-slip fault (Fig. 6).

From the Messinian onward, the northern sector of the Schio–Vicenza fault inverted its kinematics and acted as a sinistral transfer fault, connecting the Bassano and Montello frontal thrusts (Fig. 1) with the Giudicarie transpressional belt, where post-Tortonian out-of-sequence reactivation occurred (Semenza 1974; Zanferrari *et al.* 1982; Picotti *et al.* 1995; Castellarin & Cantelli 2000). Therefore, from the latest Miocene onward there was kinematic linkage between the Schio–Vicenza and Trento–Cles lines and this complex fault system became a major crustal shear zone bounding to the west the Veneto–Friuli block, which is moving toward the NW to NNW (Fig. 6). This model approaches the conclusion of Boccaletti *et al.* (2005), who interpreted this shear zone as a lithospheric structure separating the Adria plate into two blocks in the context of the post-Pliocene Apennine evolution.

The Adige embayment high

The triangle between the southern sectors of Giudicarie belt and the Schio–Vicenza line includes the Lessini and Berici Mountains and the Euganean Hills (Fig. 1). This structural high, called the 'Adige embayment' by Laubscher (1996), was only slightly affected by the Neogene Alpine compression (Cantelli & Castellarin 1994). Consequently, the Palaeogene intracontinental rifting and related magmatism are well preserved (Zampieri 1995*a*, 2000). The high structural position of this embayment separates the central and eastern Southern Alps (and their foreland basins). It may be interpreted as a flexural outer rise of the Apennine foredeep basin, controlled by subsurface loads acting on the Adriatic subducted slab (Royden *et al.* 1987) or by a thicker crust (or lithosphere) with minor eastward rollback (Doglioni 1993). The Late Miocene–Pliocene uplift of the Adige embayment partly prevented the contemporaneous development of south-propagating frontal thrusts in this sector. Therefore, the prominent extensional evidence in the southern part of the Schio–Vicenza line, revealed by morphostructural (Pellegrini 1988) and geological (Zanferrari *et al.* 1982) analysis and seismic profiles (Finetti 1972), may be interpreted as the concurrent effect of subsidence caused by the load of the South Alpine thrust sheets and of uplift of the hinge zone of the Apennine flexure (Fig. 6).

A steady-state fault kinematics from the Miocene to the present

According to Dewey *et al.* (1989) and Mazzoli & Helman (1994), Africa and Europe changed their convergence direction from NNW to NW during the Messinian. Nevertheless, the relations between Africa and Adria are still a matter of debate and the change in Africa–Europe convergence direction through time does not necessarily imply an equivalent change in Adria–Europe motion. According to the kinematic data collected by Platt *et al.* (1989) in the Alpine orogenic wedge, Adria–Europe convergence remained roughly NW-directed from the Late Cretaceous to the present. In contrast, some workers have highlighted an overall change in regional compression from NNW to NW along the Giudicarie belt in the latest Miocene and have related it directly to the equivalent variation of Africa–Europe convergence at the Miocene–Pliocene transition (the 'Adria phase' of Castellarin & Cantelli 2000). Actually, the seismotectonic and GPS data agree with the Miocene fault kinematics and NW to NNW convergence between the northeastern part of the Adria plate and Europe, suggesting that no major changes happened from the Miocene to the present. In addition, Bressan *et al.* (1998) showed how the present deformation inside the Friuli area may be partitioned according to 'a cone in cone' model, which accounts for the NNW–SSE compression along the reactivated south-vergent frontal thrusts, the dextral transpression reactivating the Dinaric structures to the east, and the NW–SE compression recorded in the central and western sector of the Veneto–Friuli South Alpine belt. In this view the palaeostress changes recorded during the Messinian along the Giudicarie belt could be explained by local stress reorientation unrelated to Africa–Europe relative movements. Therefore, in our opinion, from the Miocene to the present the Alpine collisional wedge and South Alpine fold-and-thrust belt underwent the same tectonic process driven by NW migration of Adria towards Europe; faults should have kept the same overall kinematics through time, except for changes caused by the onset of linkages (e.g. inversion of Schio–Vicenza kinematics from dextral to sinistral in the Late Miocene).

Conclusions

From Miocene time, the Alpine collisional wedge and South Alpine fold-and-thrust belt have been welded together, and the fault kinematics in the two domains has been closely linked. In particular, several linkage systems between the major faults developed, mainly in the South Alpine domains, as a result of strike-slip reactivation of inherited

normal faults. From the Early Miocene onward, the Brenner detachment was connected through the Giovo and Passiria faults to the North Giudicarie line, and its splays in the South Alpine domain are represented by the Trento–Cles system. In turn, during the Late Miocene (Messinian), the linkage between the latter fault system and the Schio–Vicenza fault was completed, via the Permian Calisio line and several Mesozoic north–south fault segments (e.g. Gamonda and Tormeno faults; Fig. 6). As a whole, these complex fault systems may be viewed as a single sinistral transcurrent shear zone 250 km long and 25 km wide. The southern sector of this crustal structure may be considered as an incipient separation zone between the westernmost part of the Adriatic indenter, almost completely involved in the lithospheric flexure of the Apennine subduction (Lombardian sector), and the main body of the Adriatic plate. The northeastern portion of the Adria plate (Friuli area) was less influenced by the lithospheric flexure, the hinge zone of which probably corresponds to the rising Adige embayment. To the south (Adriatic Sea sector) the space available for the flexure of the Adriatic lithosphere is wider, as the central Apennine and Dinaric fronts are more distant than those of the northern Apennines and Southern Alps. Consequently, a sharp discontinuity (the Schio–Vicenza line) has developed between the Friuli and Lombardian sectors, whereas a wider deformation zone can be envisaged further south in the Adriatic offshore (the Middle Adriatic Ridge of Argnani *et al.* 1993). This conclusion is supported by GPS velocity fields, GPS-derived strain rates and focal mechanisms, which show continuous active migration of the Adriatic plate toward Europe, whereas its westernmost part remains nearly stationary. From the Miocene onward, the Alpine collisional nappe stack has been involved in the concurrent processes of northward propagation of this separation zone of the Adria plate and the westward stretching of the Brenner fault hanging wall related to the tectonic unroofing of the Tauern window.

This work was supported by MIUR (Cofin 2002, no. 2002043912_002 to D.Z.) and CNR (Istituto di Geoscienze e Georisorse, Sezione di Padova). The paper has benefited from the recommendations made by G. V. Dal Piaz and the comments of the reviewers G. Prosser and M. Lukesch. We thank F. De Giusti for drawing the base of Figure 2, S. Castelli for helping in electronic assemblage of the composite figures, and G. Walton and P. Ferretti for the revision of the English text.

References

ALTAMIMI, Z., SILLARD, P. & BOUCHER, C. 2002. ITRF2000: a new release of the International Terrestrial Reference Frame for earth science applications. *Journal of Geophysical Research*, **107**(B10), 2214, DOI: 10.1029/2001JB000561.

ARGNANI, A., FAVALLI, P., FRUGONI, F., *ET AL.* 1993. Foreland deformational pattern in the Southern Adriatic Sea. *Annali di Geofisica*, **36**, 212–224.

BATTAGLIA, M., MURRAY, M. H., SERPELLONI, E. & BÜRGMANN, R. 2004. The Adriatic region: an independent microplate within the Africa–Eurasia collision zone. *Geophysical Research Letters*, **31**, L09605, DOI: 10.1029/2004GL019723.

BEHRMANN, J. H. 1988. Crustal-scale extension in a convergent orogen: the Sterzing–Steinach mylonite zone in the Eastern Alps. *Geodinamica Acta*, **2**, 63–73.

BERTOTTI, G., PICOTTI, V., BERNOULLI, D. & CASTELLARIN, A. 1993. From rifting to drifting: tectonic evolution in the South-Alpine upper crust from the Triassic to the Early Cretaceous. *Sedimentary Geology*, **86**, 53–76.

BIGI, G., COSENTINO, D., PAROTTO, M., SARTORI, R. & SCANDONE, P. 1990. Structural model of Italy. Sheet no. 1. *In*: CASTELLARIN, A., COLI, M., DAL PIAZ, G. V., SARTORI, R., SCANDONE, P. & VAI, G. B. (eds) *Progetto Finalizzato Geodinamica*. CNR, Rome.

BISTACCHI, A., DAL PIAZ, G. V., DAL PIAZ, G., MARTINOTTI, G., MASSIRONI, M., MONOPOLI, B. & SCHIAVO, A. 2003. Carta geologica e note illustrative del transetto val di Vizze–Fortezza (Alpi Orientali). *Memorie di Scienze Geologiche*, **55**, 169–188.

BOCCALETTI, M., CALAMITA, F. & VIANDANTE, M. G. 2005. La Neo-Catena litosferica appenninica nata a partire dal Pliocene inferiore come espressione della convergenza Africa–Europa. *Bollettino della Società Geologica Italiana*, **124**, 87–105.

BRACK, P. 1981. Structures in the southwestern border of the Adamello intrusion (Alpi Bresciane, Italy). *Schweitzeásche Mineralogische und Petrographische Mitteilungen*, **61**, 37–50.

BRESSAN, G., SNIDARCIG, A. & VENTURINI, C. 1998. Present state of tectonic stress of the Friuli area (Eastern Southern Alps). *Tectonophysics*, **292**, 211–227.

CANTELLI, L. & CASTELLARIN, A. 1994. Analisi e inquadramento strutturale del sistema Schio–Vicenza. *Atti Ticinensi di Scienze della Terra, Serie Speciale*, **1**, 231–245.

CAPORALI, A., MARTIN, S. & MASSIRONI, M. 2002. The present day strain rate field in Italy and surrounding countries as inferred from geodetic data. *Bollettino di Geofisica Teorica ed Applicata*, **43**(1–2), 3–21.

CAPORALI, A., MARTIN, S. & MASSIRONI, M. 2003. Average strain rate in the Italian crust inferred from a permanent GPS network—II. Strain rate versus seismicity and structural geology. *Geophysical Journal International*, **155**, 254–268.

CAPORALI, A., BRAITENBERG, C. & MASSIRONI, M. 2005. Geodetic and hydrological aspects of the Merano earthquake of July 17, 2001. *Journal of Geodynamics*, **39**, 317–336.

CASSINIS, G. & PEROTTI, C. R. 1993. Interazione strutturale permiana tra la Linea delle Giudicarie ed i bacini di Collio, Tione e Tregiovo (Sudalpino

centrale, N Italia). *Bollettino della Società Geologica Italiana*, **112**, 1021–1036.

CASTELLARIN, A. 1972. Evoluzione paleotettonica sinsedimentaria del limite tra Piattaforma veneta e Bacino lombardo a nord di Riva del Garda. *Giornale di Geologia*, **38**, 11–212.

CASTELLARIN, A. & CANTELLI, L. 2000. Neo-Alpine evolution of the Southern Eastern Alps. *Journal of Geodynamics*, **30**, 251–274.

CASTELLARIN, A., FESCE, A. M., PICOTTI, V., *ET AL.* 1986. Structural and kinematics analysis of the Giudicarie deformation belt. Implications for compressional tectonics of Southern Alps. *Mineralogica et Petrographica Acta*, **30**, 286–310.

CASTELLARIN, A., CANTELLI, L., FESCE, A. M., *ET AL.* 1992. Alpine compressional tectonics in the Southern Alps. Relationships with the N Apennines. *Annales Tectonicae*, **6**, 62–94.

CASTELLARIN, A., PICCIONI, S., PROSSER, G., SANGUINETTI, E., SARTORI, R. & SELLI, L. 1993. Mesozoic continental rifting and Neogene inversion along south Giudicarie line (Northwestern Brenta Dolomites). *Memorie della Società Geologica Italiana*, **49**, 125–144.

CHRISTENSEN, J. N., SELVERSTONE, J., ROSENFELD, J. L. & DE PAOLO, D. J. 1994. Correlation by Rb–Sr geochronology of garnet growth histories from different structural levels within the Tauern window, Eastern Alps. *Contributions to Mineralogy and Petrology*, **118**, 1–12.

DAL PIAZ, G. V. 1999. The Austroalpine–Piemonte nappe stack and the puzzle of alpine Tethys. *Memorie di Scienze Geologiche*, **51**, 155–176.

DAL PIAZ, G. V. & MARTIN, S. 1998. Evoluzione litosferica e magmatismo nel dominio austro-sudalpino dall'orogenesi varisica al rifting mesozoico. *Memorie di Scienze Geologiche*, **53**, 43–62.

DAL PIAZ, G., BISTACCHI, A. & MASSIRONI, M. 2003. Geological outline of the Alps. *Episodes*, **26**, 175–180.

DE METS, C., GORDON, R. G., ARGUS, D. F. & STEIN, S. 1994. Effect of recent revisions to the geomagnetic reversal time scale on estimates of current plate motions. *Geophysical Research Letters*, **21**, 2191–2194.

DE VECCHI, G. P., DI LALLO, E. & SEDEA, R. 1986. Note illustrative della Carta geologica dell'area di Valli del Pasubio–Posina–Laghi, alla scala 1 : 20.000. *Memorie di Scienze Geologiche*, **38**, 187–205.

DEWEY, J. F., HELMAN, M. L., TURCO, E., HUTTON, D. H. W. & KNOTT, S. D. 1989. Kinematics of the Western Mediterranean. *In*: COWARD, M. P., DIETRICH, D. & PARK, R. G. (eds) *Alpine Tectonics*. Geological Society of London, Special Publications, **45**, 265–284.

DOGLIONI, C. 1992. Relationships between Mesozoic extensional tectonics, stratigraphy and Alpine inversion in the Southern Alps. *Eclogae Geologicae Helvetiae*, **85**, 105–126.

DOGLIONI, C. 1993. Some remarks on the origin of foredeeps. *Tectonophysics*, **228**, 1–20.

DOGLIONI, C. & BOSELLINI, A. 1987. Eoalpine and mesoalpine tectonics in the Southern Alps. *Geologcische Rundschau*, **76**, 735–754.

FANTONI, E., PELLINI, S., PERDICENI, S. & SCARASCIA, S. 1993. Alpi Orientali: una sezione crostale dall'avampaese europeo all'avampaese adriatico. *Studi Geologici Camerti, CROP 1-1A Special Volume*, 27–34.

FELLIN, M. G., MARTIN, S. & MASSIRONI, M. 2002. Polyphase Tertiary kinematics and Quaternary fault reactivation in the central-eastern Alps (Western Trentino). *Journal of Geodynamics*, **34**, 31–46.

FINETTI, I. 1972. Le condizioni geologiche della regione di Venezia alla luce di recenti indagini sismiche. *Bollettino di Geofisica Teorica ed Applicata*, **14**, 275–290.

FRANK, W., KRALIK, M., SCHARBERT, S. & THÖNI, M. 1987. Geochronological data from the Eastern Alps. *In*: FLÜGEL, H. W. & FAUPL, P. (eds) *Geodynamics of the Eastern Alps. Deuticke, Vienna*, 272–281.

FRISCH, W., DUNKL, I. & KUHLEMANN, J. 2000. Post-collisional orogen-parallel large-scale extension in the Eastern Alps. *Tectonophysics*, **327**, 239–265.

FÜGENSCHUH, B., SEWARD, D. & MANCKTELOW, N. 1997. Exhumation in a convergent orogen: the western Tauern window. *Terra Nova*, **9**, 213–217.

FÜGENSCHUH, B., MANCKTELOW, N. S. & SEWARD, D. 2000. Cretaceous to Neogene cooling and exhumation history of the Oetztal–Stubai basement complex, Eastern Alps: a structural and fission track study. *Tectonics*, **19**, 905–918.

GALADINI, F., POLI, E. & ZANFERRARI, A. 2002. Sorgenti sismogenetiche responsabili di terremoti distruttivi nell'Italia nord-orientale. 21° *Convegno Nazionale Gruppo Nazionale di Geofisica della Terra Solida, Abstract Volume*, 27–30.

GRUNDMAN, G. & MORTEANI, G. 1985. The young uplift and thermal history of the central Eastern Alps (Austria/Italy). Evidence from apatite fission track ages. *Jahrbuch der Geologischen Bundesanstalt*, **128**, 197–216.

KURZ, W., NEUBAUER, F., GENSER, J. & DACHS, E. 1998. Alpine geodynamic evolution of passive and active continental margin sequences in the Tauern Window (Eastern Alps, Austria, Italy); a review. *Geologische Rundschau*, **87**, 225–242.

LAMMERER, B. & WEGER, M. 1998. Footwall uplift in an orogenic wedge: the Tauern Window in the Eastern Alps of Europe. *Tectonophysics*, **285**, 213–230.

LAUBSCHER, H. P. 1996. Shallow and deep rotations in the Miocene Alps. *Tectonics*, **15**, 1022–1035.

LENHARDT, W. A. 2002. Seismicity in Tyrol in relation to the TRANSALP transect. *Memorie di Scienze Geologiche*, **54**, 49–52.

MANCKTELOW, N., STÖCKLI, D. F., GROLLIMUND, B., *ET AL.* 2001. The DAV and Periadriatic fault system in the Eastern Alps south of the Tauern window. *International Journal of Earth Science*, **90**, 593–622.

MARTIN, S., PROSSER, G. & SANTINI, L. 1991. Alpine deformation along the Periadriatic lineament in the

Italian Eastern Alps. *Annales Tectonicae*, **5**(2), 118–140.

MARTIN, S., GODARD, G., PROSSER, G., SCHIAVO, A., BERNOUILLI, D. & RANALLI, G. 1998. Evolution of the deep crust at the junction Austalpine/Southalpine: the Tanale nappe. *Memorie di Scienze Geologiche*, **50**, 1–50.

MAZZOLI, S. & HELMAN, M. 1994. Neogene patterns of relative plate motion for Africa–Europe: some implications for recent Central Mediterranean tectonics. *Geologische Rundschau*, **83**, 464–468.

MÜLLER, B., ZOBACK, M. L., FUCHS, K., *ET AL.* 1992. Regional patterns of tectonics stress in Europe. *Journal Geophysical Research*, **97**, 11783–11803.

MÜLLER, W., PROSSER, G., MANCKTELOW, N., VILLA, I. M., KELLEY, P. S., VIOLA, G. & OBERLI, F. 2001. Geochronological constraints on the evolution of the Periadriatic Fault System (Alps). *International Journal of Earth Sciences (Geologische Rundschau)*, **90**(3), 623–653.

NICOLAS, A., HIRN, A., NICOLICH, R., POLINO, R. & Ecors-Crop working group 1990. Lithospheric wedging in the western Alps inferred from the Ecors-Crop traverse. *Geology*, **18**, 587–590.

OLDOW, J. S., FERRANTI, L., LEWIS, D. S., *ET AL.* 2002. Active fragmentation of the Adria, the north African promontory, central Mediterranean orogen. *Geology*, **30**, 779–782.

PEACOCK, D. C. P. & SANDERSON, D. J. 1991. Displacement, segment linkage and relay ramps in normal fault zones. *Journal of Structural Geology*, **13**, 721–733.

PELLEGRINI, G. B. 1988. Aspetti morfologici ed evidenze neotettoniche della linea Schio–Vicenza. *Supplementi di Geografia Fisica Diname dinamica Quaternaria*, **1**, 69–82.

PFIFFNER, O. A. & HITZ, L. 1997. Geologic interpretation of the seismic profiles of the eastern traverse (lines E1–E3, E7–E9); Eastern Swiss Alps. *In*: PFIFFNER, O. A., LEHNER, P., HEITZMAN, P., MUELLER, S. & STECK, A. (eds) *Results of NRP 20; Deep Structure of the Swiss Alps*. Birkhäuser, Basel, 73–100.

PICOTTI, V., PROSSER, G. & CASTELLARIN, A. 1995. Structures and kinematics of the Giudicarie–Val Trompia fold and thrust belt (Central Southern Alps, Northern Italy). *Memorie di Scienze Geologiche*, **47**, 95–109.

PLATT, J. P., BEHRMANN, J. H., CUNNINGHAM, P. C., *ET AL.* 1989. Kinematics of the Alpine arc and the motion history of Adria. *Nature*, **337**, 158–161.

PONDRELLI, S., MORELLI, A., EKSTRÖM, G., MAZZA, S., BOSCHI, E. & DZIEWONSKI, A. M. 2002. European–Mediterranean regional centroid-moment tensors: 1997–2000. *Physics of the Earth and Planetary Interiors*, **130**, 71–101.

PONDRELLI, S., MORELLI, A. & EKSTRÖM, G. 2004. European–Mediterranean regional centroid moment tensor catalog: solutions for years 2001 and 2002. *Physics of the Earth and Planetary Interiors*, **145**, 127–147.

PROSSER, G. 1998. Strike-slip movements and thrusting along a transpressive fault zone: the North Giudicarie line (Insubric line, northern Italy). *Tectonics*, **17**, 921–937.

PROSSER, G. 2000. The development of the North Giudicarie fault zone (Insubric line, Northern Italy). *Journal of Geodynamics*, **30**, 229–250.

RATSCHBACHER, L., MERLE, O., DAVY, O. & COBBOLD, P. 1991*a*. Lateral extrusion in the Eastern Alps, Part 1: Boundary conditions and experiments scaled for gravity. *Tectonics*, **10**, 245–256.

RATSCHBACHER, L. W., FRISCH, H., LINZER, G. & MERLE, O. 1991*b*. Lateral extrusion in the Eastern Alps, Part 2: Structural analysis. *Tectonics*, **10**, 257–271.

REGENAUER-LIEB, K. & PETIT, J. P. 1997. Cutting of the European continental lithosphere; plasticity theory applied to the present Alpine collision. *Journal of Geophysical Research*, **102**, 7731–7746.

REITER, F., ORTNER, H. & BRANDNER, R. 2002. Seismically active Inntal fault zone: inverted European rift structures control upper plate deformation. *Memorie di Scienze Geologiche*, **54**, 233–234.

RENNER, G. & SLEJKO, D. 1994. Some comments on the seismicity of the Adriatic region. *Bollettino di Geofisica Teorica ed Applicata*, **36**, 141–144.

ROSENBERG, C. L. 2004. Shear zones and magma ascent: a model based on a review of a Tertiary magmatism in the Alps. *Tectonics*, **23**, TC3002, DOI: 10.1029/2003TC001526.

ROYDEN, L., PATACCA, E. & SCANDONE, P. 1987. Segmentation and configuration of subducted lithosphere in Italy: an important control on thrust-belt and foredeep-basin evolution. *Geology*, **15**, 714–717.

SANDER, B. 1912. Über einige Gesteinsgruppen des Tauernwestendes. *Jahrbuch der Geologischen Reichsanstalt*, **62**(2), 219–287.

SCHMID, S. M., PFIFFNER, O. A., SCHÖNBORN, G., FROITZHEIM, N. & KISSLING, E. 1997. Integrated cross-section and tectonic evolution of the Alps along the eastern traverse. *In*: PFIFFNER, O. A., LEHNER, P., HEITZMAN, P., MUELLER, S. & STECK, A. (eds) *Deep Structure of the Swiss Alps*. Birkhäuser, Basel, 289–304.

SCHORN, J. 1902. *Die Erdbeben von Tirol und Voralberg*. Zeitschrift des Ferdinandeums, III Folge, 46 Heft.

SELLI, L. 1998. Il lineamento della Valsugana fra Trento e Cima d'Asta: cinematica neogenica ed eredità strutturali permo-mesozoiche nel quadro evolutivo del Sudalpino orientale (NE-Italia). *Memorie della Società Geologica Italiana*, **53**, 503–541.

SELVERSTONE, J. 1988. Evidence for east–west crustal extension in the eastern Alps: implications for the unroofing history of the Tauern window. *Tectonics*, **7**, 87–105.

SELVERSTONE, J. 1993. Micro- to macroscale interactions between deformational and metamorphic processes, Tauern Window, Eastern Alps. *Schweizerische Mineralogische und Petrographische Mitteilungen*, **73**, 229–239.

SEMENZA, E. 1974. La fase Giudicariese nel quadro di una nuova ipotesi sull'orogenesi alpina nell'area italo-dinarica. *Memorie della Società Geologica Italiana*, **13**, 187–226.

SLEJKO, D., CARULLI, G. B., CARRARO, F., *ET AL.* 1987. *Modello sismotettonico dell'Italia nord-orientale.* CNR, *Gruppo Nazionale Difesa Terremoti, rendiconto* **1**, 1–82.

SLEJKO, D., CARULLI, G. B., NICOLICH, R., *ET AL.* 1989. Seismotectonics of the Eastern Southern Alps: a review. *Bollettino di Geofisica Teorica ed Applicata*, **31**(122), 109–136.

SPIESS, R., MARINI, M., FRANK, W., MARCOLONGO, B. & CAVAZZINI, G. 2001. The kinematics of the southern Passeier fault: radiometric and petrographic constraints. *Schweizerische Mineralogische und Petrographische Mitteilungen*, **81**, 197–212.

TIKOFF, B. & TEYSSIER, C. 1994. Strain modeling of displacement-field partitioning in transpressional orogens. *Journal of Structural Geology*, **16**, 1575–1588.

TREVISAN, L. 1938. Il fascio di fratture tra l'Adige a la Linea delle Giudicarie e i suoi rapporti col massiccio intrusivo dell'Adamello. *Studi Trentini di Scienze Naturale*, **19**, 177–187.

VALENSISE, G. & PANTOSTI, D. 2001. *Database of potential sources for earthquakes larger than M 5.5 in Italy.* Istituto Nazionale di Geofisica e Vulcanologia, CD-rom, Version 2.0.

VENZO, S. 1941. Studio geotettonico del trentino meridionale–orientale tra Borgo Valsugana e il M. Coppolo. *Memorie della Istituto Geologica Reale Università di Padova*, **14**, 1–86.

VIOLA, G., MANCKTELOW, N. & SEWARD, D. 2001. Late Oligocene–Neogene evolution of Europe–Adria collision: new structural and geochronological evidence from the Giudicarie fault system (Italian Eastern Alps). *Tectonics*, **20**, 999–1020.

VIOLA, G., MANCKTELOW, N., SEWARD, D., MEIER, A. & MARTIN, S. 2003. The Pejo fault system: an example of multiple tectonic activity in the Italian Eastern Alps. *Geological Society of America Bulletin*, **115**, 515–532.

VIOLA, G., ODONNE, F. & MANCKTELOW, N. S. 2004. Analogue modelling of reverse fault reactivation in strike-slip and transpressive regimes: application to the Giudicarie fault system, Italian Eastern Alps. *Journal of Structural Geology*, **36**, 401–408.

VON BLANCKENBURG, F., VILLA, I. M., BAUR, H., MORTEANI, G. & STEIGER, R. H. 1989. Time calibration of a *P–T*-path from the western Tauern window, Eastern Alps: the problem of closure temperature. *Contributions to Mineralogy and Petrology*, **101**, 1–11.

VON BLACKENBURG, F. & DAVIES, J. H. 1995. Slab breakoff: a model for syncollisional magmatism and tectonics in the Alps. *Tectonics*, **14**, 120–131.

ZAMPIERI, D. 1995*a*. Tertiary extension in the southern Trento Platform, Southern Alps, Italy. *Tectonics*, **14**, 645–657.

ZAMPIERI, D. 1995*b*. L'anticlinale di roll-over liassica dei Sogli Bianchi nel Monte Pasubio (Vicenza). *Atti Ticinensi di Scienze della Terra (serie speciale)*, **3**, 3–9.

ZAMPIERI, D. 2000. Segmentation and linkage of the Lessini Mountains normal faults, Southern Alps, Italy. *Tectonophysics*, **319**, 19–31.

ZAMPIERI, D., MASSIRONI, M., SEDEA, R. & SPARACINO, V. 2003. Strike-slip contractional stepovers in the Southern Alps (northeastern Italy). *Eclogae Geologicale Helvetiae*, **96**, 115–123.

ZANFERRARI, A., BOLLETTINARI, G., CAROBENE, L., *ET AL.* 1982. Evoluzione neotettonica dell'Italia nord-orientale. *Memorie di Scienze Geologiche*, **35**, 355–376.

ZIMMERMANN, R., HAMMERSCHMIDT, K. & FRANZ, G. 1994. Eocene high pressure metamorphism in the Pennine units of the Tauern window (Eastern Alps). Evidence from ^{40}Ar–^{39}Ar dating and petrological investigations. *Contributions to Mineralogy and Petrology*, **117**, 175–186.

ZOBACK, M. L. 1992. First and second order patterns of stress in the lithosphere: the World Stress Map Project. *Journal of Geophysical Research*, **97**, 11,703–11,728.

Palaeogeography of the Upper Cretaceous–Eocene carbonate turbidites of the Northern Apennines from provenance studies

ANDREA ARGNANI[1], DANIELA FONTANA[2], CRISTINA STEFANI[3] & GIAN G. ZUFFA[4]

[1]*ISMAR–CNR, Sezione di Bologna, Via Gobetti 101, 40129 Bologna, Italy (e-mail: andrea.argnani@ismar.cnr.it)*

[2]*Dipartimento di Scienze della Terra, Università di Modena–Reggio Emilia, Largo S. Eufemia 19, 41100 Modena, Italy*

[3]*Dipartimento di Geologia, Paleontologia e Geofisica, Università di Padova, Via Giotto 1, 35137 Padova, Italy*

[4]*Dipartimento di Scienze della Terra e Geologico-Ambientali, Università di Bologna, Via Zamboni 67, 40127 Bologna, Italy*

Abstract: The Upper Cretaceous Helminthoid Flysch (HF) of the Northern Apennines consists of thick and regionally widespread deep-water carbonate turbidite successions, deposited during the initial stages of Alpine collision. The HF spans the time from Turonian to Early Eocene and is mainly composed of intrabasinal carbonate ooze mixed with clay; siliciclastic terrigenous beds are also present, but they are a volumetrically minor component of the successions. Petrographic and sedimentological signatures indicate that the HF was deposited in distinct basins located below the carbonate compensation depth. Bulk composition and heavy minerals of terrigenous beds indicate provenance from different crustal levels of the European and Adria plates. The petrographic and palaeobathymetric characteristics of these turbidites indicate the coexistence of an active-margin tectonic setting, a palaeogeographical position suitable for carbonate ooze production and storage, and limited supply of terrigenous detritus into the basin. Palaeotectonic reconstructions and stratigraphic data suggest that Adria represented a vast repository of penecontemporaneous carbonate mud; the presumably intense seismic activity related to the pre-collisional Alpine orogeny promoted large-scale failures of shelf and/or slope biogenic muddy sediments, resulting in the deposition of a large volume of carbonate turbidites. Only occasionally, turbidity currents probably linked to exceptional fluvial floods generated pure terrigenous beds with different petrographic signatures for each HF succession.

The oceanic crust of the Tethyan domain and its overlying sediments have been extensively involved in the long-lasting subduction processes that ultimately led to the Eocene continental collision in the Alps (Coward & Dietrich 1989). Large volumes of carbonate turbidites, known in the Apennines as Helminthoid Flysch (HF), were deposited within deep-sea trenches and on the remnant ocean basin floor (Abbate & Sagri 1970; Argnani *et al.* 2004) during the period preceding collision between Africa and Europe (Dewey *et al.* 1973, 1989). Sedimentary successions comparable with the HF crop out in a fairly continuous belt along the Alpine system, from the Northern Apennines to the Eastern Alps (Fig. 1a; Rowan, 1990) and span the time from Turonian to Early Eocene.

Within orogenic regions, large volumes of siliciclastic turbidites typically record the emersion and erosion of primordial mountain belts as a result of the initial stages of collision. Pelagic–hemipelagic sediments, deposited at low sedimentation rates, usually underlie the siliciclastic turbidites within deep-water basins, characterizing the pre-orogenic sedimentary successions (e.g. Pettijohn 1957, Chapter 13). The thick and regionally widespread Helminthoid Flysch turbidite successions of the Alps and Northern Apennines represent, to some extent, an exception to this commonly encountered evolution.

The HF of the Northern Apennines is mainly composed of intrabasinal carbonate ooze mixed with clay (Scholle 1971; Fontana *et al.* 1994). Siliciclastic terrigenous beds are also present, but they represent a volumetrically minor component in the majority of the successions. The petrographic and sedimentological features of the HF suggest that these successions were deposited in distinct basins located below the carbonate compensation depth (CCD; Scholle 1971; Hesse & Butt 1976) that probably corresponded to confined sectors of ocean floor bounded by transform fault walls (Fontana *et al.* 1994).

From: MORATTI, G. & CHALOUAN, A. (eds) 2006. *Tectonics of the Western Mediterranean and North Africa.* Geological Society, London, Special Publications, **262**, 259–275.
0305-8719/06/$15.00

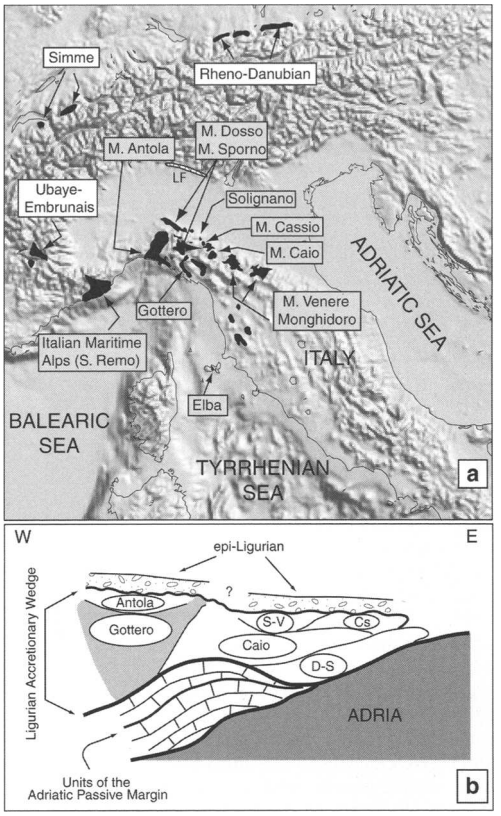

Fig. 1. (**a**) Main outcrops of the Helminthoid Flysch in the Alps and Northern Apennines. The names of the Helminthoid Flysch units considered in this paper are shown within grey boxes. The outcrop of Lombardian Flysch (LF) is also indicated. (**b**) Simplified sketch of the stack of units within the Northern Apennines showing the relative position of the flysch units described in the text (modified from Abbate *et al.* 1994). The Internal Ligurian units are shown in light grey, whereas the External Ligurian are shown in white. S-V, Solignano–M. Venere; Cs, Cassio; D-S, M. Dosso–M. Sporno.

In places the HF successions include dismembered and physically isolated remnants of oceanic rock associations. These oceanic rocks (Ligurian unit) are located in the topmost position of the Apennine chain as a result of the long history of deformation and subsequent uplift that affected the Northern Apennine chain (Fig. 1b; Abbate & Sagri 1970; Rodgers 1997). Palaeocurrent data show a remarkably dispersed pattern of transport directions (Rowan 1990, and references therein). This dispersion of palaeocurrents might reflect different provenance of bed types in the various studies (Rowan 1990, and references therein), but it may often be the product of tectonic block rotations experienced by these units during emplacement of the Ligurian Nappe. Therefore, on the basis of palaeocurrents only, it is not possible to infer the source areas of the diverse sedimentary components of the HF successions. In spite of these uncertainties, however, a number of compositional features, such as the occurrence of hemipelagic beds devoid of carbonate, and the petrographic and sedimentological attributes of turbidite beds, place some constraints on the Late Cretaceous–Eocene palaeogeography for this sector of the Apennine Tethys.

This paper aims to: (1) compile stratigraphic, sedimentological and compositional characteristics of the HF cropping out in the Northern Apennines to provide a more detailed palaeogeographical reconstruction of the Apennine sector of the Alpine Tethys for the Late Cretaceous to Eocene period; (2) show that the occurrence of the peculiar carbonate turbidites can be related to the concomitant occurrence of an active-margin tectonic setting and a palaeogeography suitable for nannoplankton production and storage.

The Helminthoid Flysch: sedimentological and compositional characteristics

The HF consists of several distinct lithostratigraphic units cropping out in the Apennine mountain belt from Liguria to Tuscany. The HF successions generally consist of an alternation of pure carbonate, pure siliciclastic and mixed (siliciclastic–carbonate) turbidite beds and of hemipelagic claystones (Fig. 2); the proportion of these different types of beds varies remarkably within

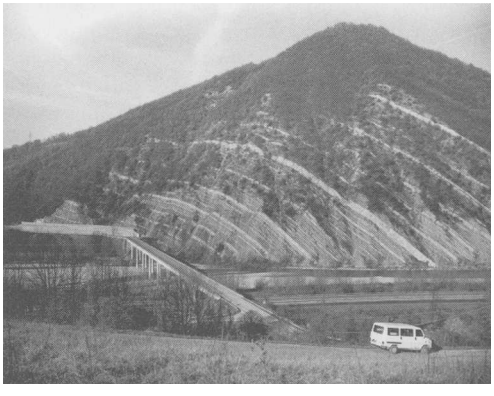

Fig. 2. The Helminthoid Flysch exposed in a superb outcrop in the Northern Apennines (M. Solignano Flysch, type locality). The thick carbonate turbidite beds (light beds) stand out within the dominantly siliciclastic part of the succession. The view is to the north.

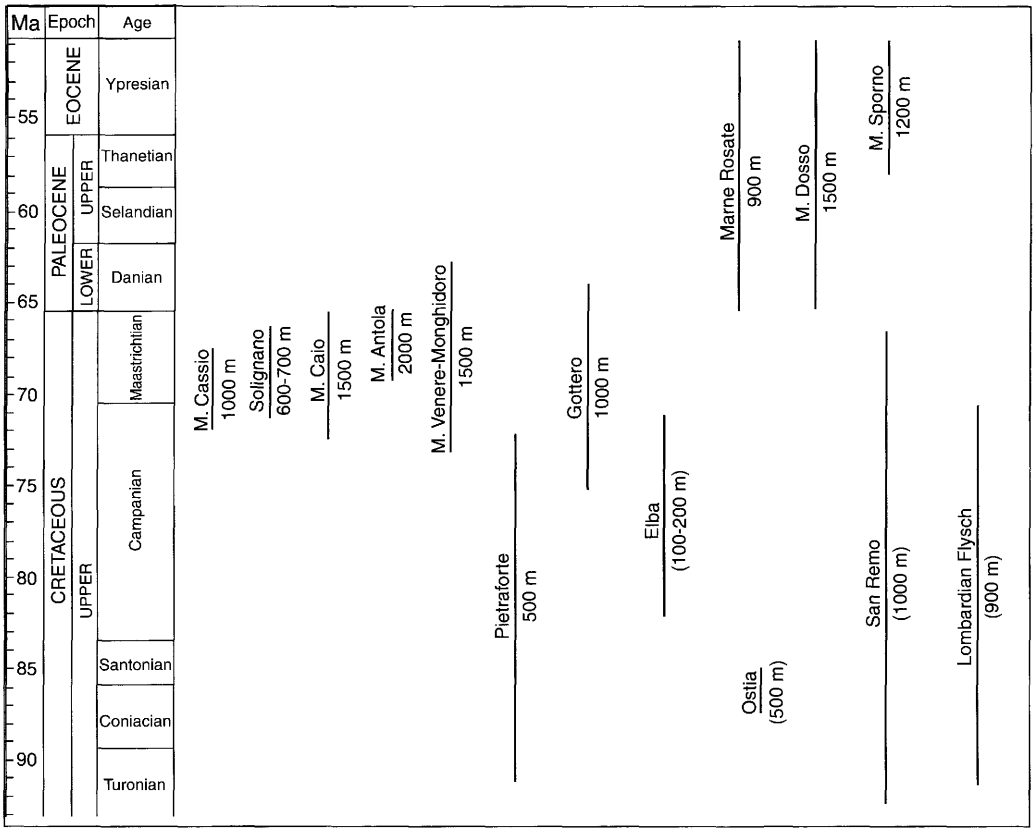

Fig. 3. Chronostratigraphy of flysch units dealt with in this paper, with ages taken from various sources (Rio *et al.* 1983; Rio 1987; Rio & Villa 1987; Bersezio & Fornaciari 1989; Cobianchi *et al.* 1991; Fontana 1991; Abbate *et al.* 1994; Pandolfi 1996). Chronostratigraphic scale is slightly modified from International Commission on Stratigraphy (2004). The maximum thickness of flysch units is also indicated, in parentheses when poorly constrained.

each stratigraphic unit. The HF sedimentation style dominated this sector of the Tethys Ocean for a long time span (Fig. 3), from Turonian (S. Remo) to Campanian–Maastrichtian time (M. Cassio, Solignano, M. Venere, Gottero, M. Antola, M. Caio, Elba), and also during the Early Palaeogene (M. Sporno, M. Dosso and Marne Rosate units) (Tables 1 and 2).

This study is based on a detailed bed by bed, high-resolution stratigraphy of significant portions of five of the major HF successions (M. Cassio, M. Caio, M. Antola, Solignano and M. Venere-Monghidoro) at the type localities (Fontana *et al.* 1994; Fontana & Stefani 2003; Argnani *et al.* 2004).

Bulk composition

The composition of 14 turbidite units, ranging in age from Turonian to Eocene, has been taken into account, with the aim of reconstructing the palaeogeographical picture. Moreover, the Lombardian turbidite successions have also been considered because of some compositional affinities with the Apennine units. Petrographic data have been plotted for comparison (Fig. 4a) where a uniform point counting approach was applied by previous investigators; in the remainder of cases, the data have been reported only in Tables 1 and 2.

In general, bulk composition and aphanitic lithic fragments indicate a dominant provenance from a continental basement exposing granites and low- to medium-grade metamorphic rocks. Clasts of dolostone and pelagic limestone often indicate the presence of a sedimentary cover (e.g. M. Cassio and Pietraforte successions; Elter *et al.* 1966), whereas shallow-water coeval bioclasts with cavities filled by glaucony (e.g. M. Cassio succession) indicate a coeval active carbonate platform system adjacent to the turbidite basin. In some instances (e.g. M. Caio succession) laterally discontinuous

Table 1. *Chronostratigraphic and petrographic data for Upper Cretaceous units*

Upper Cretaceous Helminthoid units	Composition of the terrigenous arenite framework	Rock classification	Fine-grained lithic fragments	Heavy minerals
Pietraforte	QFL + CE	Litharenite	Ls: DOLOSTONE,	ZTR–GARNET
(Late Turonian–Maastrichtian)	38–3–59		LIMESTONE, chert	picotite
			Lm: low-grade	pyroxene
			Lv: acidic	
Elba	QFL + CE	Arkose	Lm: LOW-GRADE	ZTR–GARNET
(Campanian–Maastrichtian)	55–41–4		Lv: acidic	monazite–xenotime
			Ls: shale	
Gottero	QFL + CE	Arkose	Lm: low-grade	ZTR–GARNET
(Late Campanian–Early Paleocene)	50–33–17		Lv: acidic	EPIDOTE sphene
M. Venere	QFL + CE	Arkose to lithic arkose	Lm: LOW–MIDDLE-GRADE	GARNET–ZTR STAUROLITE CHLORITOID
(Campanian–Maastrichtian)	58–29–13		Lv: ACIDIC	
			Ls: dolostone, limestone, shale	monazite–xenotime
Monghidoro	QFL + CE	Arkose to lithic arkose	Lm: LOW–MIDDLE-GRADE	GARNET–ZTR STAUROLITE CHLORITOID
(Maastrichtian–Danian)	53–37–10		Lv: ACIDIC	
			Ls: dolostone, limestone, shale	monazite–xenotime
M. Caio (petrofacies 1–3)	QFL + CE	Lithic arkose	Ls: DOLOSTONE	GARNET–ztr
(Campanian–Maastrichtian)	60–21–19		limestone; Lm: low-grade	
	QFL + CE	Arkose	Lm: LOW-GRADE	ZTR–GARNET
	48–45–7			monazite–xenotime
	QFL + CE	Litharenite	SERPENTINITE	PICOTITE
	16–24–60		SHALE, lime stone	ztr–garnet
M. Cassio	QFL + CE	Arkose	Ls: LIMESTONE,	GARNET–ZTR
(Campanian–Maastrichtian)	62–21–17	to lithic arkose	DOLOSTONE, shale	STAUROLITE
			Lm: low-grade	monazite–xenotime
Solignano	QFL + CE	Arkose	Lm: LOW-GRADE	GARNET–ZTR
(Campanian–Maastrichtian)	52–32–16	to lithic arkose	Lv: ACIDIC	STAUROLITE
			Ls: dolostone	CHLORITOID
				monazite–xenotime
M. Antola	QFL + CE	Arkose	Lm: LOW-GRADE	ZTR
(Campanian–Maastrichtian)	58–37–5		Lv: ACIDIC	MONAZITE XENOTIME garnet
S. Remo	QFL + CE	Lithic arkose	Lv: acidic	ZTR–garnet
(Cenomanian–Maastrichtian)	55–25–20	to felds pathic	Lm: low-grade	epidote–sphene
			Ls: chert	
Ostia	QFL + CE	Litharenite	Ls: LIMESTONE,	ZTR–PICOTITE
(Coniacian–Santonian)	60–4–36		DOLOSTONE, CHERT	sphene–epidote
Lombardian Flysch	QFL + CE	Litharenite	Lm: low-grade	ZTR–GARNET
(Turonian–Campanian)	55–20–25	to lithic	Ls: LIMESTONE,	STAUROLITE
	26–3–71	arkose	DOLOSTONE, chert	chromite

Q, quartz; F, feldspars; L + CE, total fine-grained lithic fragments plus carbonate rock fragments. Lm, metamorphic lithic fragments; Lv, volcanic lithic fragments; Ls, sedimentary lithic fragments. Capital letters indicate abundant and/or characteristic components. Compositional data from Mezzadri (1964), Gazzi (1965), Valloni & Zuffa (1984), Bersezio & Fornaciari (1989), Lana (1990), Bernoulli & Winkler (1990), Fontana *et al.* (1990, 1994, 1998), Fontana (1991), Zacchino (1994), Montalti (1995), Pandolfi (1996), and Daniele & Plesi (2000). Classification of arenite framework after Zuffa (1980, 1987).

Table 2. *Chronostratigraphic and petrographic data for Palaeogene units*

Palaeogene Helminthoid units	Composition of the terrigenous arenite framework	Rock classification	Fine-grained lithic fragments	Heavy minerals
Marne Rosate (Paleocene–Eocene)	QFL + CE 86–6–8	Quartzarenite	Lm: low-grade serpentinite Lv: acidic Ls: dolostone	ZTR–GARNET STAUROLITE picotite
M. Dosso (Paleocene–Eocene)	QFL + CE 68–9–23	Litharenite	Ls: CHERT–dolostone Lm: LOW-GRADE	ZTR–GARNET STAUROLITE chloritoid picotite
M. Sporno (Paleocene–Eocene)	QFL + CE 79–9–12	Quartzarenite	Lm: low-grade Lv: acidic Ls: dolostone	ZTR–GARNET STAUROLITE picotite

Q, quartz; F, feldspars; L + CE, total fine-grained lithic fragments plus carbonate rock fragments. Lm, metamorphic lithic fragments; Lv, volcanic lithic fragments; Ls, sedimentary lithic fragments. Capital letters indicate abundant and/or characteristic components. Compositional data from Mezzadri (1964), Gazzi (1965), Valloni & Zuffa (1984), Bersezio & Fornaciari (1989), Lana (1990), Bernoulli & Winkler (1990), Fontana *et al.* (1990, 1994, 1998), Fontana (1991), Zacchino (1994), Montalti (1995), Pandolfi (1996), and Daniele & Plesi (2000). Classification of arenite framework after Zuffa (1980, 1987).

rudite to arenite beds with dominant serpentinite grains and Lower Cretaceous lime–mudstone clasts with calpionellids point to intrabasinal sources composed of oceanic fracture-zone rock assemblages.

Among the Cretaceous units, the terrigenous components of pure siliciclastic and mixed beds show variable compositions from arkose, to lithic arkose, to litharenite (Table 1 and Fig. 4a). The arenites of siliciclastic beds of M. Antola, M. Venere, Monghidoro, and partially of the M. Caio (M. Caio 2; Fig. 4a) formations are composed of purely siliciclastic grains with an arkosic to subarkosic composition; lithic types are low- to medium-grade metamorphic rocks and minor acidic volcanic rocks. Arenites of the M. Cassio, Solignano, and part of M. Caio (M. Caio 1; Fig. 4a) units are more lithic in composition and share as a distinctive characteristic the presence of carbonate rock fragments in the terrigenous lithic assemblage, associated with subordinate low-grade metamorphic and volcanic rocks. The arenitic component of the basal interval of the M. Cassio mixed megabeds also contains significant amounts of coeval bioclasts. The M. Caio unit shows also a third type of siliciclastic bed made up of serpentinite and calpionellid limestone rock fragments (M. Caio 3; Fig. 4a). The M. Gottero and S. Remo units are arkosic and lithic–arkosic to feldspathic in composition, respectively (Vanossi 1965; Pandolfi 1996).

The arenites of the Elba flysch are arkosic in composition and are characterized by large amounts of low-grade metamorphic rock fragments and subordinately by acidic volcanic rock fragments and shale clasts (Aiello *et al.* 1977; Montalti 1995). The Pietraforte Formation has a litharenitic composition, with abundant dolostone and limestone grains and subordinate low-grade metamorphic and acidic volcanic rock fragments (Fontana 1991). A similar composition has been documented for the older Ostia sandstones (Mezzadri 1964; Valloni & Zuffa 1984).

Among the Palaeogene units, the terrigenous arenitic beds of the Marne Rosate and M. Sporno units are quartzarenitic in composition and characterized by low-grade metamorphic rock fragments, acidic volcanic rocks and dolostones (Fontana *et al.* 1998). The M. Dosso beds are litharenitic, but characterized by abundant quartz grains (more than 50%) and a lithic association with chert and low-grade metamorphic rocks (Lana 1990).

Finally, the Cretaceous turbidite successions cropping out in the Lombardian Southern Alps are litharenite to lithic arkose, and include high amounts of terrigenous carbonate rock fragments and subordinate chert and low-grade metamorphic rock fragments (Bersezio & Fornaciari 1989; Bernoulli & Winkler 1990).

Heavy mineral association and provenance

The stable and ultrastable fractions of heavy mineral associations have proven to be useful for characterizing the terrigenous sources; in general, the heavy minerals do not show dissolution features.

Most of the investigated units share as a common characteristic medium to high amounts of zircon, tourmaline and rutile (ZTR, Table 1; Fig. 4b), with petrofacies 1 and 3 in the M. Caio succession being a remarkable exception (Fig. 4b). Moreover, the heavy mineral associations of the M. Cassio, M. Venere, Solignano, Monghidoro, M. Dosso

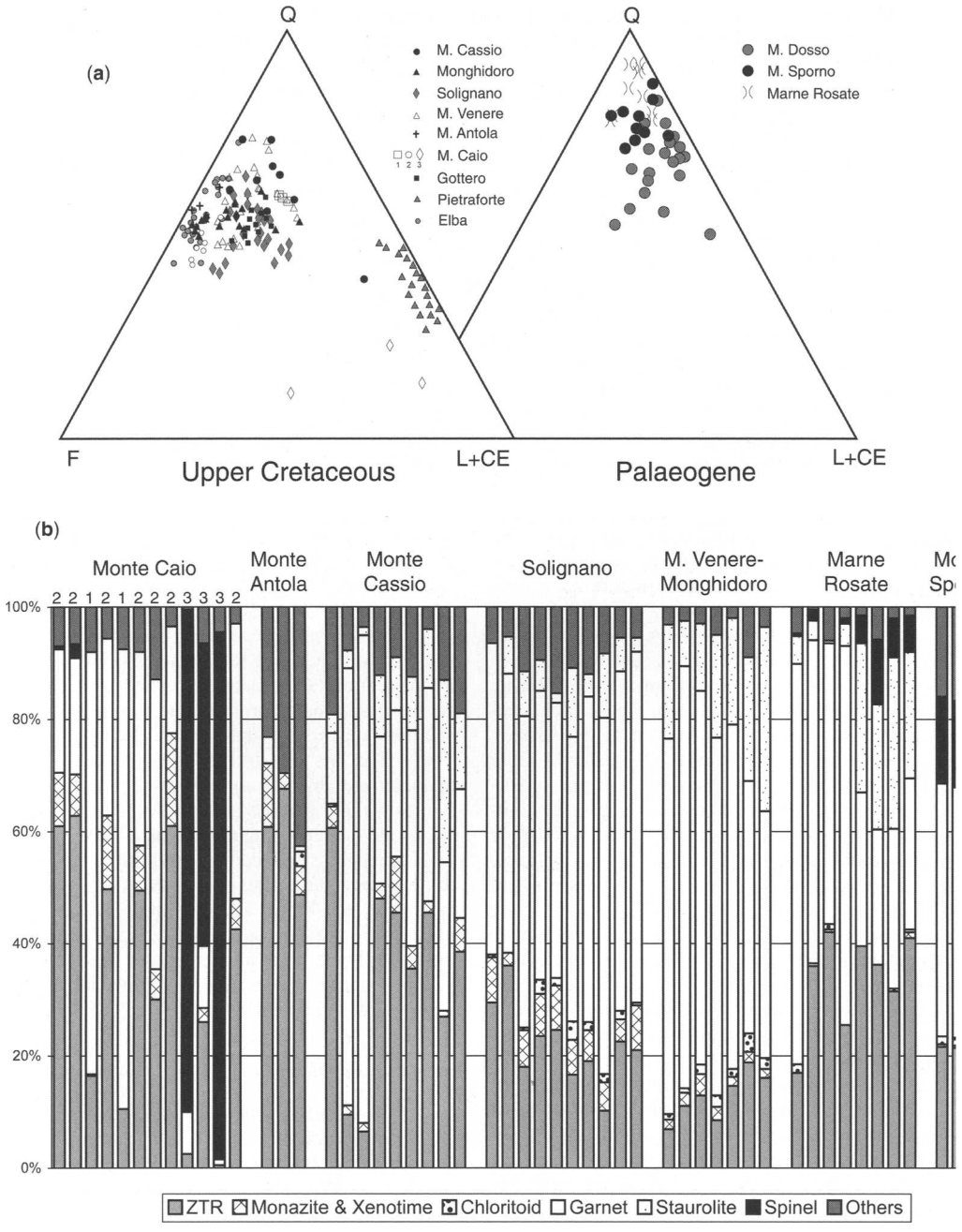

Fig. 4. Petrography of Helminthoid Flysch units. (**a**) Q, F, L + CE triangular diagrams distinguishing between Upper Cretaceous (left) and Palaeogene (right) units. Q, total quartz; F, feldspar; L + CE, non-carbonate fine-grained lithic fragments + terrigenous carbonate lithic fragments. (**b**) Heavy mineral distribution. The class 'Others' is dominated by anatase and brookite; a small percentage of epidote and zoisite is present in Monte Caio, Monte Antola and Monte Cassio, whereas sphene occurs in Solignano, Marne Rosate and M. Sporno. Numbers 1, 2 and 3 under M. Caio heading indicate the petrofacies M. Caio 1, M. Caio 2 and M. Caio 3, respectively. Spinel is mainly picotite.

and M. Sporno units contain staurolite, garnet and in some cases chloritoid. Noteworthy amounts (generally less than 10–15%) of monazite and xenotime are present in the M. Antola, M. Caio, Solignano, M. Cassio and Monghidoro units.

Data on heavy mineral associations allow us to outline diverse provenances from granitic rocks (monazite plus xenotime), metamorphic rocks of various rank (garnet, staurolite and chloritoid) and ophiolitic rocks (picotite). High values of the ultrastable group ZTR, together with abundant sedimentary lithic fragments in the framework of some units such as Pietraforte and Ostia, suggest an extensive recycling from older arenitic successions. On the other hand, the occurrence of large amounts of picotite in the M. Caio 3 succession, very abundant in the ophiolitic clastic beds together with penecontemporaneously deformed clasts of calpionellid limestone, confirms the presence of oceanic rock associations (i.e. serpentinized mantle peridotite) acting as intrabasinal sources.

In particular, the occurrence of staurolite, characteristic of medium- to high-grade metamorphic rocks, is considered indicative of denudation of the deep levels of the Adriatic crust, which are currently widely exposed in the Alps (Frey *et al.* 1999). Staurolite is abundant in some Cretaceous flysch units of the Lombardy basin (Bernoulli & Winkler 1990), where palaeocurrents suggest an eastern provenance (Bernoulli & Winkler 1990; Bersezio & Fornaciari 1994). The heavy mineral associations of the Lombardian successions are characterized by abundant ZTR, garnets and staurolite. Moreover, one of the Lombardian units (Varesotto Flysch) is also characterized by high amounts of chromite (Bernoulli & Winkler 1990). The source area of these heavy mineral associations was probably in the pre-Gosau orogen of the Eastern Alps, where both oceanic basement and deep continental basement of Adriatic affinity were exposed since the beginning of the Late Cretaceous (Winkler 1996; Neubauer *et al.* 2000).

Previous studies of the HF successions also considered the presence of staurolite and chloritoid as indicative of a provenance from the deep crustal levels of the basement of the Austroalpine or Southern Alps, i.e. from Adria (Elter *et al.* 1966; Sassi *et al.* 1978; Bernoulli & Winkler 1990; Neubauer *et al.* 1999). The fact that the European source rocks did not supply staurolite is confirmed by the absence of this mineral in the proximal turbidites of the M. Gottero and Elba successions (Nielsen & Abbate 1984; Zacchino 1994), which were deposited close to the Corsica–Sardinia block. In fact, for the sedimentary successions considered in this study, the areas surrounding the Corsica–Sardinia block represent the main European provenance.

The occurrence of monazite and xenotime is compatible with a European provenance where only shallower granitic crustal levels were exposed.

In the Palaeogene flysch units (M. Sporno, Marne Rosate, and M. Dosso), staurolite occurs together with picotite, suggesting a contribution from sediments recycled from older successions that were already exhumed in the Western Alps. Such recycling is also supported by the occurrence of garnet and abundant quartz together with a high ZTR content.

Interpretation

Provenance of the clastic detritus

In our palaeogeographical reconstructions the provenance from deep crustal rocks is related to the occurrence of a major fracture zone located along the Adria margin. It has been inferred that this fracture zone became a transform boundary during subsequent convergence (Argnani 2002); an event that would have further enhanced its original relief. In this interpretation, therefore, the deep crustal signal recorded in the petrography of some of the Upper Cretaceous sedimentary successions can be related to a localized source within the Adria region.

The other region that appears to supply lower crustal material during the Late Cretaceous is located further to the east along the Adria margin, in the current Eastern Alps, where the pre-Gosau Cretaceous orogeny had been completed and the orogen was undergoing erosion. The dismantling of the Cretaceous orogen of the Eastern Alps shed lower crustal material towards the west, feeding, besides the Rheno-Danubian Flysch, also the Lombardian Flysch, where rock fragments and heavy minerals from both lower continental crust and oceanic basement occur together (Bernoulli & Winkler 1990; Faupl & Wagreich 1992; Bersezio & Fornaciari 1994). It seems therefore that the Late Cretaceous exposure of lower crust was limited to specific tectonic settings.

Following a different approach, an asymmetric rift model has been recently applied to account for the evolution of the Mesozoic sedimentary successions that are currently piled up in the northern Apennines (Marroni *et al.* 2001). Within this scheme Adria would represent the footwall plate of a lithospheric-scale rift. The inferred exposure of lower continental crust along the footwall plate is assumed to supply the sediments that were deposited close to the Adria margin (Bracciali *et al.* 2003).

The current magma-poor passive continental margins are characterized by the occurrence of an

array of fault blocks tilted towards the continent and resting on a subhorizontal detachment (Whitmarsh *et al.* 2001). Although this structural arrangement has been used to support an asymmetric rifting model (Froitzheim & Manatschal 1996; Manatschal & Bernoulli 1999), the outcome of recent numerical modelling shows that the geometry observed at magma-poor passive margins can be better reproduced without adopting lithospheric-scale asymmetric rifting (Nagel & Buck 2004). Moreover, the asymmetric rift model predicts a footwall and a hanging-wall plate displaying remarkedly different fault geometry, which would extensively expose deep crustal rocks of the footwall plate at the distal continental margin. At the Galicia distal margin, however, the exposed continental crust is mainly made up of upper crustal rocks (Whitmarsh *et al.* 2001) and the same applies to the Alps where only limited lower crustal rocks are exposed (Muentener & Herman 2001).

To sum up, the occurrence of heavy minerals and rock fragments that are typical of the lower crust within some of the HF sediments is perhaps better accounted for by localized source areas, rather than by a widespread, cylindrical exposure all along the Adria passive margin. The origin of the localized exposure of lower crustal rocks can be explained within the regional tectonic setting proposed here.

Trigger mechanisms of turbidity currents

An intriguing question concerning the HF successions examined here and their sedimentary features is that of the trigger mechanisms of the turbidity currents. Possible mechanisms that we discuss include high-magnitude earthquakes and the tsunamis generated by them (see Heezen & Ewing 1952; Mutti *et al.* 1984; Pickering *et al.* 1991), destabilization of gas hydrates, and exceptional fluvial floods (see Mutti *et al.* 1996). This last process could be relevant for the transport of purely extrabasinal siliciclastic sediments.

An important constraint for the mechanisms of sediment remobilization comes from mixed megabeds, which are the thickest beds in the succession, suggesting a close correlation between the magnitude of the triggering event and the capacity to activate, during the same event, multiple sources, terrigenous and intrabasinal. The coexistence of terrigenous siliciclastic fine sands and clay, sand-sized shallow-water benthic fauna, pelagic Foraminifera, fine sponge spicules and coccolith micrite in mixed beds constrains the source areas in continental margin shelves and slopes.

Large-scale sediment failures affecting continental margins and slopes, possibly characterized by multiple linked slumps over a large area (Pearce & Jarvis 1992), and/or the 'concurrence of tributary turbidity currents' (Rupke 1976), are processes that can account for the origin and composition of the HF beds. These processes can be triggered by events such as earthquakes, tsunamis, exceptional fluvial floods, and destabilization of gas hydrates. It should be emphasized, however, that earthquakes probably represent the main factor promoting submarine landslides (Hampton *et al.* 1996).

Pure terrigenous sand beds can possibly be related to exceptional fluvial floods that enter the basin as hyperpycnal flows and are turned into turbidity flows (Mutti *et al.* 1996).

In principle, terrigenous turbidites of small volume can subsequently engulf much larger volumes of slope carbonate muds (e.g. Fukushima *et al.* 1985). However, the limited extent of land area and the probably subdued relief of Adria suggest that the contribution of exceptional floods was probably rather limited.

Gas hydrate dissociation can also cause the mobilization and downslope transport of enormous quantities of mud (McIver 1982; Paull *et al.* 1996; Henriet & Mienert 1998; Nisbet & Piper 1998). However, the role of gas hydrate in destabilizing sediments is hard to establish (Buffet 2000). Moreover, it is difficult to assess what triggered hydrate dissociation, particularly for events occurring in the Cretaceous–Palaeogene. At present, we cannot rule out gas hydrate dissociation as a triggering mechanism to mobilize carbonate muds along the Adria continental slope; a major role, however, seems unlikely.

Tsunamis are capable of sweeping large portions of the continental shelf, possibly mobilizing vast amounts of unconsolidated sediments (Bryant 2001), which may flow downslope as turbidity currents. For tsunamis that occurred in the past the best tracers are marine sediments and biogenic remains that were laid down on continental deposits of coastal areas by anomalously large waves (Bryant 2001). For the time interval we are interested in, i.e. the Late Cretaceous–Palaeogene, this kind of evidence is extremely difficult to come by. Instrumental monitoring carried out during the last century indicates that the majority of large-scale tsunamis originate from large earthquakes displacing the sea floor (Bryant 2001). Submarine landslides can also cause large tsunamis, but because of the lower energy involved compared with earthquakes (Ruff 2003), their effects should cover a relatively limited region, rather than affecting basins as a whole. On the other hand, large volcanic eruptions can produce huge tsunamis that affect wide regions, with the 1883 Krakatoa explosion as a chief example (Holmes 1944, pp. 470–473). Such a triggering event, however, should deliver abundant volcaniclastic sediments into the basin; this petrographic tracer has not been found within the HF successions. Therefore, to sum up, tsunamis

could possibly have contributed to trigger the HF turbidites, but in such an event they can be seen as the ultimate result of earthquakes. The ground shaking caused by earthquakes is thus the triggering mechanism that seems to satisfy both the sedimentological and compositional features of the HF turbidites and the regional tectonic setting.

Plate coupling in subduction zones and magnitude of earthquakes

During Africa–Europe convergence, the consumption of the oceanic domain and the progressive involvement of continental lithosphere in the subduction process led to increased coupling between the converging plates. This increased plate coupling, in turn, favoured the occurrence of large and frequent earthquakes (e.g. Ruff & Kanamori 1983). A similar increase in plate coupling can occur when continental slivers or allochthons enter the subduction zone. This process, which we call onset of collision, heralded the continental collision *sensu stricto* that led to the formation of the Alps. The occurrence of continental allochthons within the Alpine Tethys is now widely accepted (e.g. Dal Piaz 1999); the extent and distribution of these continental slivers, however, is difficult to constrain, and the same applies to the precise timing of their subduction. According to the most recent reviews of geochronological data (e.g. Gebauer 1999), the subduction of continental slivers or allochthons located within the Alpine Tethys certainly occurred in the Early Paleocene (Danian), with the involvement of the Sesia–Lanzo unit. An independent indication of the timing of the onset of collision comes from the intra-plate compressional deformation of Western and Central Europe. In this respect, the extensive inversion tectonics affecting the NW European basins since the Late Cretaceous (Ziegler 1990) can be taken as evidence of an increasing coupling of the Alpine orogen with its foreland. Within this tectonically active setting the amply available carbonate muds deposited along the Adriatic and European slopes above the CCD could be remobilized in several ways, together with terrigenous sediment, ultimately being deposited within the basin as thick turbidite beds. The observation that the thickest turbidite strata are mixed beds suggests that the triggering events of the largest magnitude can simultaneously mobilize sediments from diverse parts of the continental slopes and shelves.

In conclusion, it is inferred that the presumably intense seismic activity related to the pre-collisional Alpine orogeny promoted large-scale failures of shelf or slope biogenic muddy sediments, resulting in the deposition of large volumes of predominantly carbonate turbidites. Only occasionally, terrigenous turbidite currents probably linked to exceptional fluvial floods generated pure terrigenous beds with different petrographic signatures.

Palaeogeographical reconstructions

Two kinematic reconstructions have been produced (Fig. 5; Argnani 2002), taking into account the

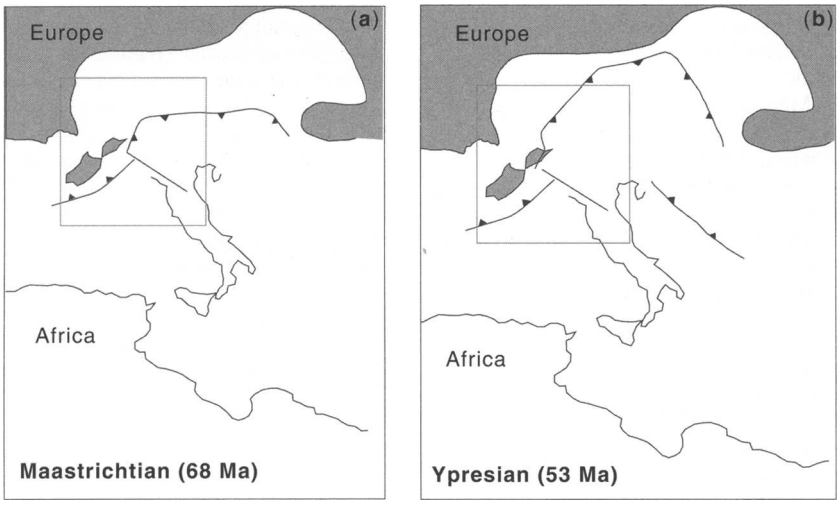

Fig. 5. Plate kinematic reconstructions of the central Mediterranean. (**a**) Maastrichtian (magnetic anomaly 31); (**b**) Ypresian (magnetic anomaly 24). The present coastline of Italy is outlined for reference, to help locate the Adria promontory. (See text for further discussion.) The square frames enclose the areas that are shown enlarged in Figure 6.

position of Africa with respect to Europe, as derived from the magnetic anomalies in the Atlantic Ocean (Dewey *et al.* 1989). The two time intervals that are represented are the Maastrichtian, with reference to magnetic anomaly 31 (68 Ma), and the Ypresian, with reference to magnetic anomaly 24 (53 Ma). In these reconstructions Adria has been considered as a promontory of the African plate, according to recent reviews of palaeomagnetic data (Channell 1996; Muttoni *et al.* 2001) that show similar palaeopoles for Adria and Africa throughout the Mesozoic. In fact, although an independent Adria plate has been required in recent reconstructions to account for the Mesozoic arrangement of plates in the Eastern Alps (e.g. Neugebauer *et al.* 2001), it has been shown that this assumption is not a necessity (Wortmann *et al.* 2001). Besides taking Adria as a promontory, the major difference with respect to most of the previous recostructions (e.g. Dercourt *et al.* 1993) consists in the polarity of subduction, which is assumed to change along the plate boundary, from a southward Alpine subduction to a northward Apennine subduction (Fig. 5; Argnani 2002).

The two time intervals that have been represented here, Maastrichtian and Ypresian, are relevant to the HF palaeogeography (Fig. 6), although from Campanian to Rupelian time the relative position of Africa with respect to Europe undergoes only minor changes, with a limited north–south convergence. The main change concerns the size of the orogen, which grows substantially from Maastrichtian to Ypresian, including the emplacement of the Alpine units of Corsica (Fig. 5). As better shown in the palaeogeographical reconstruction (Fig. 6), during the Maastrichtian to Ypresian time interval the Antola (and San Remo) and Gottero flysch units were accreted to the Alpine subduction prism. In the subsequent evolution, because of the northward motion of Adria, the Apennine subduction replaced the Alpine subduction to the east of Corsica (Argnani 2002), leading to the involvement of the Antola and Internal Ligurian units (Gottero included) within the growing Apennine edifice (Fig. 1b).

Stratigraphical, sedimentological and compositional data put some constraints on the location of the Late Cretaceous–Eocene Helminthoid Flysch within the proposed palaeogeographical frame (Fig. 6).

The sediment supplied into the HF basins was derived from multiple sources of detritus, which include the following: (1) major intrabasinal sources from outer shelf or slope areas and pelagic plateaux, which supplied coeval biogenic carbonate sediment (phytoplankton and zooplankton), mainly fine-grained; (2) minor intrabasinal sources, possibly transform ridges, which supplied the ophiolitic-derived materials in the M. Caio unit; (3) minor intrabasinal shelf areas, where intrabasinal allochems, glaucony and terrigenous detritus were assembled; resedimentation of these components formed the hybrid arenite (Zuffa 1980) that represents the basal intervals of the M. Cassio mixed beds (Zuffa *et al.* 2003); (4) minor siliciclastic terrigenous sources from hinterland rock units (crystalline basement plus minor sedimentary cover).

Estimates of the amount of sediments supplied to the basin from the various sources indicate that in the M. Cassio and M. Antola successions intrabasinal areas provided 60–70% of the sediment. Terrigenous siliciclastic sources contributed approximately 20–30% of the sediment in the M. Caio and M. Antola, 50% and 70% in the M. Venere and Solignano, respectively, and 35% in the M. Cassio successions (Fontana & Stefani 2003). Ophiolitic sources supplied less than 5% of the detritus in the M. Caio succession.

The large amount of penecontemporaneous carbonate mud that is present in the HF is the first evidence to be accounted for. Palaeotectonic reconstructions and stratigraphic data suggest that during the Late Cretaceous Adria represented a vast repository of penecontemporaneous carbonate mud (e.g. Vai 1992). Its position, isolated and remote from the African and European mainlands, favoured the accumulation of intrabasinal sediments, particularly carbonates. Shallow-water carbonate platforms and pelagic basins occurred along the African continental margin (Channell *et al.* 1979; Zappaterra 1994). The Apulian and the Dinaric platforms, with the intervening Umbria–Marche pelagic basin, were the main features of the Adriatic promontory in Late Cretaceous time (Zappaterra 1994), bounding the southeastern side of the closing Tethyan ocean. Within this setting, Adria appears as an extensive carbonate domain prone to major production and storage of carbonate sediments (Bernoulli 2001). Besides the palaeogeographical setting of the central Mediterranean, global factors also contributed to the availability of carbonate sediments. The relatively high sea level that characterized the Late Cretaceous (Haq *et al.* 1988) broadened the extent of shallow seas and, together with a warmer climate, favoured by the position of the continents and oceans (van Andel 1994), probably led to an increased nannoplankton production at a global scale. In addition to penecontemporaneous carbonates, the sources of the minor extra- and intra-basinal terrigenous sediments can be accounted for within the proposed palaeogeographical reconstructions.

Kinematic reconstructions indicate that the Alpine Tethys Ocean opened at a rather slow rate of a few centimetres a year (Dewey *et al.* 1973, 1989). In such a slow-spreading setting, fracture

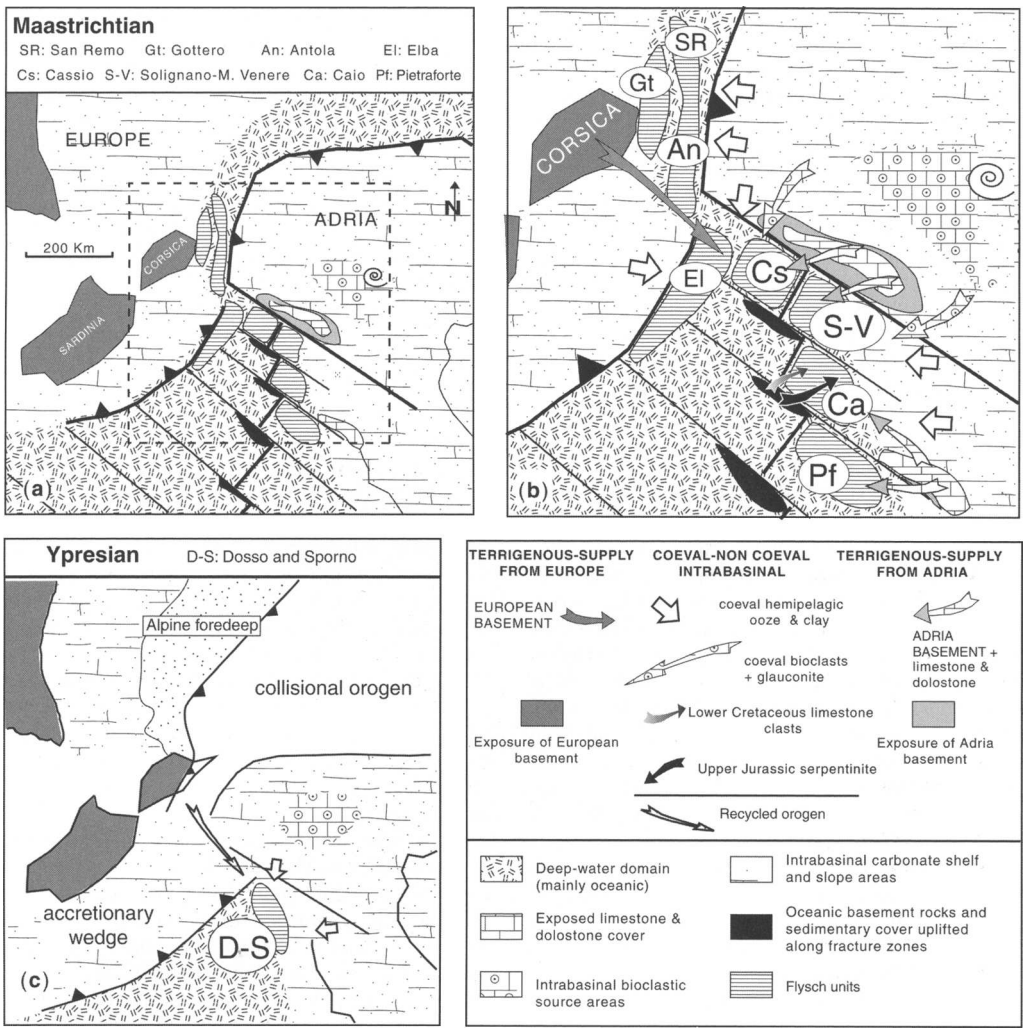

Fig. 6. Palaeogeographical reconstructions of the region encompassing the Northern Apennines and Western Alps. The location of Helminthoid Flysch units and sediment dispersal patterns in the Northern Apennine Tethys are also indicated. (**a**) Maastrichtian palaeogeography with suggested locations of the Helminthoid units. The dashed rectangle indicates the area shown enlarged in (b). (**b**) Enlarged view of the central area of (a) with abbreviation of name and provenance for each turbidite unit; key for abbreviations is shown in (a). (**c**) Ypresian palaeogeography with location of the M. Dosso and M. Sporno units. The extent of the Alpine foredeep basin is from Kempf & Pfiffner (2004). It should be noted that the mid-ocean ridge and fracture zone pattern depicted in (a) and (b) represents a fossil system, as spreading was no longer active during Maastrichtian time.

zones are expected to be abundant (Macdonald & Fox 1990; Phipps Morgan & Parmentier 1995), exposing oceanic mantle and crustal rocks and the related sedimentary cover (Auzende *et al.* 1994). Moreover, deeper crustal levels are probably exposed where fracture zones intersect the continental margin (Fig. 6a; Clift & Lorenzo 1999). As the passive continental margin begins to approach the subduction zone, during convergence, fracture zones are also likely to be reactivated. Therefore, it seems that the exposure of crustal rocks along fracture zones can account for at least some of the terrigenous detritus that characterizes the HF, particularly the clastic sediments from the Adria domain (Fontana *et al.* 1994).

The extrabasinal siliciclastic materials entering the basin represent only small amounts of sediments when compared with the dominant intrabasinal

carbonates. In some instances beds made up of pure extrabasinal material occur within the HF successions. These siliciclastic sediments indicate a limited availability of sediment sources outside the basin, and reflect an adjacent land area of limited extent and of subdued relief. In fact, it is only later, when the collision progressed (in Oligo-Miocene time), and the relief of the Alpine mountain chain developed, that abundant siliciclastic sediments filled the foredeep basins of the Alps and Apennines (Gandolfi *et al.* 1983; Homewood *et al.* 1986; Ricci Lucchi 1986).

The Ypresian palaeogeographical reconstruction (Fig. 6c) shows a well-developed Alpine collisional orogen, with a foredeep basin located on the European foreland (Kempf & Pfiffner 2004). The Apennine subduction, on the other hand, is characterized by a broad accretionary wedge (see also Gasinski *et al.* 1997), which, at this stage, included the sediments of several of the flysch units represented in the Maastrichtian palaeogeographical reconstruction. The Dosso and Sporno HF units represent the final stage of deep-water sedimentation below the CCD across the passive Adriatic continental margin. The clastic turbidite sediments belonging to the Canetolo, Macigno, and Marnoso-arenacea units (Ricci Lucchi 1986; Boccaletti *et al.* 1990; Argnani & Ricci Lucchi 2001), which were deposited from mid-Eocene to Miocene time, record the progressive encroachment of the accretionary wedge onto the Adriatic continental margin (e.g. Argnani 2002, and references therein).

The traces of mid-ocean ridge and fracture zones are not represented in the Ypresian palaeogeographical reconstruction because at that time the topography of the residual oceanic floor was probably mantled by sediments.

Palaeotectonic setting

Structural and tectonic data are also useful to help constrain the location of HF and other flysch units; particularly the Antola and Gottero flysch units within the Maastrichtian palaeogeography. The HF units are currently part of the northern Apennine tectonic stack (Fig. 1b), and their emplacement seems mainly a result of east-verging thrust faults originated within an accretionary prism (e.g. Costa & Frati 1995). However, the deformation and structuring of the Internal Ligurian units, to which the Gottero unit belongs, can be related to underplating of oceanic crust and sediment cover along an east-dipping subduction zone (Marroni & Pandolfi 1996), supporting an initial Alpine vergence. Moreover, structural data indicate that the Antola unit was emplaced onto the underlying units (e.g. Gottero unit) with a top-to-the-west shear (Alpine vergence) during the Eocene (Marroni *et al.* 1999); only subsequently were the Antola sediments folded with vergence to the east (Apennine vergence). The above-mentioned lines of evidence support a location of the Antola and Gottero flysch units in front of the advancing Alpine subduction zone during the Maastrichtian (Fig. 6a and b), with the Gottero flysch closer to the Corsica terrigenous source areas. A similar relative position of the Antola and Gottero flysch units was presented by Abbate & Sagri (1984) and Vescovi *et al.* (1999), although the former envisaged a west-dipping subduction, whereas the latter workers considered that the subduction zone dips to the east. Both contributions, however, shared the view that the Antola and Gottero (Abbate & Sagri 1984) or Antola and Cassio (Vescovi *et al.* 1999) flysch were deposited within a forearc setting. The depositional characteristics of the HF (Fontana *et al.* 1994; Argnani *et al.* 2004) and the stratigraphic relationships with their immediate substrate (Abbate & Sagri 1970; Marroni *et al.* 1992), however, do not support a forearc depositional setting. The most relevant morphological feature in the Maastrichtian reconstruction is the steep scarp located along the continental part of the major fracture zone (Fig. 6a and b). Along this feature, which has been interpreted as separating the Alpine and Apennine subduction zones having opposite polarity (Argnani 2002), the Adriatic basement and sedimentary cover were probably exposed, allowing for the particular petrographic composition of the M. Cassio and Solignano–M. Venere HF. Moreover, the steep gradient of the slope and the closeness of the source areas can better explain the occurrence of the Salti del Diavolo conglomerates, which occur stratigraphically below the M. Cassio flysch. These conglomerates have proximal sedimentological features and contain clasts of sedimentary rocks ranging in age from Permian to Late Cretaceous (Vescovi *et al.* 1999) and of Variscan granites (Sames 1967).

The Maastrichtian palaeogeographical reconstruction presented here (Fig. 6a and b) partly modifies an earlier attempt that we recently proposed (Argnani *et al.* 2004). Although the tectonic framework and the guiding principles are the same, we have here included more flysch units and we have taken into account more critically the structural data, considering all individual flysch units in the entire Apennine edifice. The main difference concerns the relative position of the Cassio, Caio and Solignano–Monte Venere units, which now better fit their observed order in the Apennine tectonic stack (Fig. 1b). In particular, the outcrops of lower crust representing the source of staurolite are now located along the main fracture zone (Fig. 6a and b). The M. Caio basin, which was

previously located closer to the European margin because of its lack of staurolite, has now been located next to the margin of Adria, but far from the main fracture zone; this location is more consistent with the east-verging stack of Apennine units in which the M. Caio unit occupies a lower position (Fig. 1b).

Conclusions

Large volumes of intrabasinal sediments (coeval shelf or slope carbonate mud), often mixed with minor extrabasinal siliciclastic sands (mixed beds), were resedimented in confined sectors of the oceanic floor, below the CCD, during the Late Cretaceous subduction of the Alpine Tethys. Intrabasinal and minor extrabasinal source areas also contributed to the sedimentation of pure terrigenous and pure carbonate intrabasinal turbidite beds, which are intercalated with mixed beds, where terrigenous and carbonate constituents coexist. In spite of their moderate recurrence frequency, mixed beds dominate the total thickness.

Heavy minerals and the bulk composition of the terrigenous component indicate two main source areas: (1) the European continental margin, and (2) the Adria continental margin. The European source area supplied the Gottero and Elba basins, whereas Adria and its basement supplied the M. Cassio, Solignano and M. Venere basins. In addition, the occurrence of rare laterally discontinuous ophiolitic-derived material in the M. Caio unit indicates source rocks located in an intra-oceanic position.

The sediment sources and the depositional areas of the HF successions have been located within palaeogeographical reconstructions that take into account the relative plate position between Africa and Europe during the Maastrichtian and Ypresian, unlike previous attempts that lack such as approach (e.g. Gardin *et al.* 1994). During the Late Cretaceous the closure of the Tethyan oceanic domain was progressively accomplished, leading to the Eocene continental collision. Sediments eroded from the Alpine orogen (synorogenic sediments *sensu stricto*) appeared only late in the stratigraphic record, but the wide Adria margin provided abundant penecontemporaneous carbonate sediments to be remobilized. In this setting the deposition of large volumes of intrabasinal sediments has been promoted by large-scale sediment failures, triggered by earthquakes during the Late Cretaceous incipient collision, perhaps with a contribution from tsunamis. These mechanisms caused mobilization and downslope transport of enormous quantities of sediment stored on shelves and slopes through multiple interlinked slumping over large areas. Exceptional fluvial floods may have been responsible for the deposition of beds with a pure terrigenous sand framework.

The HF of the Northern Apennines illustrates how the favourable coincidence of a tectonically active setting (incipient Alpine collision) and enhanced carbonate production and storage (Adria carbonate domain) has promoted the widespread occurrence of thick pre-orogenic carbonate turbidites.

We gratefully acknowledge G. Daniele and G. Plesi, who helpfully contributed with several discussions and suggestions. The thorough and extremely constructive reviews of R. Hesse and W. Winkler greatly improved the quality of the manuscript. D. Rio kindly helped us with adjusting the Cretaceous chronostratigraphy. We acknowledge financial support from Ministero dell' Istruzione Universita' e Ricerca.

References

ABBATE, E. & SAGRI, M. 1970. The eugeosynclinal sequences. *Sedimentary Geology*, **4** (Special Issue), 251–340.

ABBATE, E. & SAGRI, M. 1984. Le unità torbiditiche cretacee dell'Appennino Settentrionale ed i margini continentali della Tetide. *Memorie della Società Geologica Italiana*, **24**, 115–126.

ABBATE, E., PRINCIPI, G., SAGRI, M., *ET AL.* 1994. *Appennino Ligure-Emiliano*. Guide Geologiche Regionali, Società Geologica Italiana, Milan. BE-MA.

AIELLO, E., BRUNI, P. & SAGRI, M. 1977. Depositi canalizzati nei flysch cretacei dell'Isola d'Elba. *Bollettino della Società Geologica Italiana*, **96**, 297–239.

ARGNANI, A. 2002. The northern Apennines and the kinematics of Africa–Europe convergence. *Bollettino della Società Geologica Italiana, Special Volume*, **1**, 47–60.

ARGNANI, A. & RICCI LUCCHI, F. 2001. Tertiary siliciclastic turbidite systems of the northern Apennines. *In*: VAI, G. B. & MARTINI, I. P. (eds) *Anatomy of an Orogen: the Apennines and Adjacent Mediterranean Basins*. Kluwer, Dordrecht, 327–350.

ARGNANI, A., FONTANA, D., STEFANI, C. & ZUFFA, G. G. 2004. Late Cretaceous carbonate turbidites of the Northern Apennines: shaking Adria at the onset of Alpine collision. *Journal of Geology*, **112**, 251–259.

AUZENDE, J.-M., CANNAT, M., GENTRE, P., *ET AL.* 1994. Observation of sections of oceanic crust and mantle cropping out on the southern wall of Kane FZ. *Terra Nova*, **6**, 143–148.

BERNOULLI, D. 2001. Mesozoic–Tertiary carbonate platforms, slopes and basins of the external Apennines and Sicily. *In*: VAI, G. B. & MARTINI, P. (eds) *Anatomy of an Orogen: the Apennines and Adjacent Mediterranean Basins*. Kluwer, Dordrecht, 307–326.

BERNOULLI, D. & WINKLER, W. 1990. Heavy mineral assemblages from Upper Cretaceous South- and Austroalpine flysch sequences (Northern Italy and Southern Switzerland): source terranes and

palaeotectonic implications. *Eclogae Geologicae Helvetiae*, **83**, 287–310.

BERSEZIO, R. & FORNACIARI, M. 1989. Cretaceous sequences in the Lombardy basin: stratigraphic outline between the lakes of Lecco and Iseo. *Memorie della Società Geologica Italiana*, **40**, 187–197.

BERSEZIO, R. & FORNACIARI, M. 1994. Syntectonic Upper Cretaceous deep-water sequences of the Lombardy Basin (Southern Alps, Northern Italy). *Eclogae Geologicae Helvetiae*, **87**, 833–862.

BOCCALETTI, M., CIARANFI, N., COSENTINO, D., *ET AL.* 1990. Palinspastic restoration and paleogeographic reconstruction of the peri-Tyrrhenian area during the Neogene. *Palaeogeography, Palaeoclimatology, Palaeoecology*, **77**, 41–50.

BRACCIALI, L., MARRONI, M., PANDOLFI, L. & ROCCHI, S. 2003. Petrography and geochemistry of western Tethys Mesozoic sedimentary covers (Alpine Corsica and Northern Apennines); a valuable tool in constraining sediment provenance and margin configuration. *Ofioliti*, **28**, 69.

BRYANT, E. 2001. *Tsunamis, The Underrated Hazard*. Cambridge University Press, Cambridge.

BUFFET, B. A. 2000. Clathrate hydrates. *Annual Review of Earth and Planetary Sciences*, **28**, 477–507.

CHANNELL, J. E. T. 1996. Palaeomagnetism and palaeogeography of Adria. *In*: MORRIS, A. & TARLING, D. H. (eds) *Palaeomagnetism and Tectonics of the Mediterranean Region*. Geological Society, London, Special Publications, **105**, 119–132.

CHANNELL, J. E. T., D'ARGENIO, B. & HORVATH, F. 1979. Adria, the African promontory in Mesozoic Mediterranean paleogeography. *Earth-Science Reviews*, **15**, 213–292.

CLIFT, P. D. & LORENZO, J. M. 1999. Flexural unloading and uplift along the Cote d'Ivoire–Ghana transform margin, equatorial Atlantic. *Journal of Geophysical Research*, **104**(B11), 25257–25274.

COBIANCHI, M., DI GIULIO, A., GALBIATI, B. & MOSNA, S. 1991. Il 'Complesso di Base' del Flysch di San Remo nell'area di San Bartolomeo, Liguria occidentale (Nota preliminare). *Atti Ticinensi*, **34**, 145–154.

COSTA, E. & FRATI, G. 1995. Evoluzione strutturale delle Liguridi esterne tra la media Val Ceno e la Val d'Arda (Appennino settentrionale, province di Parma e Piacenza). *Studi Geologici Camerti, Special Volume*, **1995**(1), 325–336.

COWARD, M. & DIETRICH, D. 1989. Alpine tectonics—an overview. *In*: COWARD, M., DIETRICH, D. & PARK, R. (eds) *Alpine Tectonics*. Geological Society, London, Special Publications, **45**, 1–29.

DAL PIAZ, G. V. 1999. The Austroalpine–Piedmont nappe stack and the puzzle of Alpine Tethys. *Memorie di Scienze Geologiche*, **51**(1), 155–176.

DANIELE, G. & PLESI, G. 2000. The Ligurian Helminthoid flysch units of the Emilian Apennines: stratigraphic and petrographic features, paleogeographic restoration and structural evolution. *Geodinamica Acta*, **13**, 1–21.

DERCOURT, J., RICOU, L. E. & VRIELYNCK, B. (eds) 1993. *Atlas Tethys Paleoenvironment Map*. Gauthiers-Villars, Paris.

DEWEY, J. F., PITMAN, W. C., III, RYAN, W. B. F. & BONNIN, J. 1973. Plate tectonics and the evolution of the Alpine systems. *Geological Society of America Bulletin*, **84**, 137–180.

DEWEY, J. F., HELMAN, M. L., TURCO, E., HUTTON, D. H. W. & KNOTT, S. D. 1989. Kinematics of the western Mediterranean. *In*: COWARD, M. P., DIETRICH, D. & PARK, R. G. (eds) *Alpine Tectonics*. Geological Society, London, Special Publications, **45**, 265–283.

ELTER, G., ELTER, P. STURANI, P. & WEIDMANN, M. 1966. Sur la prolongation du domaine ligure de l'Apennin dans le Montferrat et les Alpes et sur l'origine de la nappe de la Simme s.l. de Prealpes romandes et chablaisienne. *Archives des Sciences, Genève*, **19**, 279–377.

FAUPL, P. & WAGREICH, M. 1992. Cretaceous flysch and pelagic sequences of the Eastern Alps: correlations, heavy minerals, and palaeogeographic implications. *Cretaceous Research*, **13**, 378–403.

FONTANA, D. 1991. Detrital carbonate grains as provenance indicators in the Upper Cretaceous Pietraforte Formation (northern Apennines). *Sedimentology*, **38**, 1085–1095.

FONTANA, D. & STEFANI, C. 2003. Extrabasinal and intrabasinal sources in siliciclastic–carbonate turbidite systems of the northern Apennines. *In*: VALLONI, R. & BASU, A. (eds) *Quantitative Provenance Studies in Italy*. Memorie Descrittive della Carta Geologica d'Italia, **61**, 41–48.

FONTANA, D., STEFANI, C., ZUFFA, G. G. & TATEO, F. 1990. Il Flysch di Solignano nel quadro dei Flysch a Elmintoidi (Maastrichtiano inferiore, Appennino settentrionale). *Giornale di Geologia*, **52**, 99–120.

FONTANA, D., SPADAFORA, E., STEFANI, C., STOCCHI, S., TATEO, F., VILLA, G. & ZUFFA, G. G. 1994. The Upper Cretaceous Helminthoid Flysch of the Northern Apennines: provenance and sedimentation. *Memorie della Società Geologica Italiana*, **48**, 237–250.

FONTANA, D., FAGGIANO, G. & MARASTONI, M. 1998. Sedimentation pattern and composition of Tertiary Ligurian Flysch of the northern Apennines: the Monte Sporno and Marne rosate di Tizzano formations. *Memorie di Scienze Geologiche*, **50**, 165–176.

FREY, M., DESMONS, J. & NEUBAUER, F. 1999. The new metamorphic map of the Alps. *Schweizerische Mineralogische und Petrographische Mitteilungen*, **79**, 1–4.

FROITZHEIM, N. & MANATSCHAL, G. 1996. Kinematics of Jurassic rifting, mantle exhumation, and passive-margin formation in the Austroalpine and Penninic nappes (eastern Switzerland). *Geological Society of America Bulletin*, **108**, 1120–1133.

FUKUSHIMA, Y., PARKER, G. & PANTIN, H. M. 1985. Prediction of ignitive turbidity currents in Scripps submarine canyon. *Marine Geology*, **67**, 55–81.

GANDOLFI, G., PAGANELLI, L. & ZUFFA, G. G. 1983. Petrology and dispersal pattern in the Marnoso-

Arenacea Formation (Miocene, Northern Apennines). *Journal of Sedimentary Petrology*, **53**, 493–507.

GARDIN, S., MARINO, M., MONECHI, S. & PRINCIPI, G. 1994. Biostratigraphy and sedimentology of Cretaceous Ligurid Flysch: palaeogeographical implication. *Memorie della Società Geologica Italiana*, **48**, 219–235.

GASINSKI, A., SLACZKA, A. & WINKLER, W. 1997. Tectono-sedimentary evolution of the upper Prealpine nappe (Switzerland and France); nappe formation by Late Cretaceous–Paleogene accretion. *Geodinamica Acta*, **10**, 137–157.

GAZZI, P. 1965. I minerali pesanti nei flysch arenacei del M. Ramaceto e M. Molinatico (Appennino settentrionale). *Mineralogica Petrografica Acta*, **11**, 197–212.

GEBAUER, D. 1999. Alpine geochronology of the Central and Western Alps: new constraints for a complex geodynamic evolution. *Schweizerische Mineralogische und Petrographische Mitteilungen*, **79**, 191–208.

HAMPTON, M. A., LEE, H. J. & LOCAT, J. 1996. Submarine landslides. *Reviews in Geophysics*, **34**, 33–59.

HAQ, B. U., HARDENBOL, J. & VAIL, P. R. 1988. Mesozoic and Cenozoic chronostratigraphy and cycles of sea-level changes. *In*: WILGUS, C. K., HASTINGS, B. S., KENDALL, C. G. ST. C., POSAMENTIER, H. W., ROSS, C. A. & VAN WAGONER, J. C. (eds) *Sea-Level Changes—an Integrated Approach*. Society of Economic Paleontologists and Mineralogists, Special Publications, **42**, 71–108.

HEEZEN, B. C. & EWING, M. 1952. Turbidite currents and submarine slumps, and the 1929 Grand Bank earthquake. *American Journal of Science*, **250**, 849–873.

HENRIET, J.-P. & MIENERT, J. 1998. Gas hydrates; the Gent debates; outlook on research horizons and strategies. *In*: HENRIET, J.-P. & MIENERT, J. (eds) *Gas Hydrates*. Geological Society, London, Special Publications, **137**, 1–8.

HESSE, R. & BUTT, A. 1976. Paleobathymetry of Cretaceous turbidite basins of the East Alps relative to the calcite compensation level. *Journal of Geology*, **84**, 505–533.

HOLMES, A. 1944. *Principles of Physical Geology*. Nelson, London.

HOMEWOOD, P., ALLEN, P. A. & WILLIAMS, G. D. 1986. Dynamics of the Molasse Basin of western Switzerland. *In*: ALLEN, P. & HOMEWOOD, P. (eds) *Foreland Basins*. International Association of Sedimentologists, Special Publications, **8**, 199–217.

INTERNATIONAL COMMISSION ON STRATIGRAPHY 2004. International Stratigraphic Chart. www.stratigraphy.org/chus.pdf.

KEMPF, O. & PFIFFNER, A. 2004. Early Tertiary evolution of the North Alpine Foreland basin of the Swiss Alps and adjoining areas. *Basin Research*, **16**, 549–567.

LANA, C. 1990. *La successione di M. Dosso, Appennino parmense (Paleocene–Eocene medio)*. Degree in Geological Sciences thesis, Università degli Studi di Bologna.

MACDONALD, K. C. & FOX, P. J. 1990. The mid-ocean ridge. *Scientific American*, **262**, 72–79.

MANATSCHAL, G. & BERNOULLI, D. 1999. Architecture and tectonic evolution of nonvolcanic margins: present-day Galicia and ancient Adria. *Tectonics*, **18**, 1099–1119.

MARRONI, M. & PANDOLFI, L. 1996. The deformation history of an accreted ophiolite sequence: the Internal Liguride units (Northern Apennines, Italy). *Geodinamica Acta*, **9**, 13–29.

MARRONI, M., MONECHI, S., PERILLI, N., PRINCIPI, G. & TREVES, B. 1992. Late Cretaceous flysch deposits of the Northern Apennines, Italy: age of inception of orogenesis-controlled sedimentation. *Cretaceous Research*, **13**, 487–504.

MARRONI, M., MOLLI, G., PANDOLFI, L. & TAINI, A. 1999. Foliated cataclasites at the base of the Antola unit (Italy): structural features and geological implications. *Comptes Rendus de l'Académie des Sciences*, **329**, 135–141.

MARRONI, M., MOLLI, G., OTTRIA, G. & PANDOLFI, L. 2001. Tectono-sedimentary evolution of the External Liguride units (Northern Apennines, Italy): insights in the pre-collisional history of a fossil ocean–continent transition zone. *Geodinamica Acta*, **14**, 307–320.

MCIVER, R. D. 1982. Role of naturally occurring gas hydrates in sediment transport. *AAPG Bulletin*, **66**, 789–792.

MEZZADRI, G. 1964. Petrografia delle 'Arenarie di Ostia'. *Rendiconti Società Mineralogica Italiana*, **20**, 193–220.

MONTALTI, A. 1995. *Il Flysch dell'Elba: composizione principale e sedimentologia*. Degree in Geological Sciences thesis, Università degli Studi di Bologna.

MUENTENER, O. & HERMAN, J. 2001. The role of lower crust and continental mantle during formation of non-volcanic passive margins: evidence from the Alps. *In*: WILSON, R. C. L., WHITMARSH, R. B., TAYLOR, B. & FROITZHEIM, N. (eds) *Non-volcanic Rifting of Continental Margins*. Geological Society, London, Special Publications, **187**, 267–288.

MUTTI, E., RICCI LUCCHI, F., SEGURET, M. & ZANZUCCHI, G. 1984. Seismoturbidites; a new group of resedimented deposits. *Marine Geology*, **55**, 103–116.

MUTTI, E., DAVOLI, G., TINTERRI, R. & ZAVALA, C. 1996. The importance of fluvio-deltaic systems dominated by catastrophic flooding in tectonically active basins. *Memorie di Scienze Geologiche*, **48**, 233–291.

MUTTONI, G., GARZANTI, E., ALFONSI, L., CIRILLI, S. & GERMANI, D. 2001. Motion of Africa and Adria since the Permian: paleomagnetic and paleoclimatic constraints from northern Libya. *Earth and Planetary Science Letters*, **192**, 159–174.

NAGEL, T. J. & BUCK, W. R. 2004. Symmetric alternative to asymmetric rifting models. *Geology*, **32**, 937–940.

NEUBAUER, F., HOINKES, G., SASSI, F. P., HANDLER, R., HÖCK, V., KOLLER, F. & FRANK, W. 1999. Pre-Alpine metamorphism of the Eastern Alps. *Schweizerische Mineralogische und Petrographische Mitteilungen*, **79**, 41–62.

NEUBAUER, F., GENSER, J. & HANDLER, R. 2000. The Eastern Alps: result of a two-stage collision process. *Mitteilungen der Oesterreichischen Geologischen Gesellschaft*, **92**, 117–134.

NEUGEBAUER, J., GREINER, B. & APPEL, E. 2001. Kinematics of the Alpine–West Carpathian orogen and palaeogeographic implications. *Journal of the Geological Society, London*, **158**, 97–110.

NIELSEN, H. T. & ABBATE, E. 1984. Submarine-fan facies associations of the Upper Cretaceous and Paleocene Gottero Sandstone, Ligurian Apennines, Italy. *Geo-Marine Letters*, **3**, 193–197.

NISBET, E. & PIPER, D. J. W. 1998. Giant submarine landslides. *Nature*, **392**, 329–330.

PANDOLFI, L. 1996. Le arenarie del M. Gottero nella sezione di punta Mesco (Campaniano sup.–Paleocene inf., Appennino settentrionale): analisi stratigrafica e petrografica della parte prossimale di un sistema torbiditico. *Atti Società Toscana Scienze Naturali, Memorie, A*, **103**, 197–208.

PAULL, C. K, BUELOW, W. J., USSLER, W., III & BOROWSKI, W. S. 1996. Increased continental-margin slumping frequency during sea-level lowstands above gas hydrate-bearing sediments. *Geology*, **24**, 143–146.

PEARCE, T. H. & JARVIS, I. 1992. Composition and provenance of turbidite sands, late Quaternary, Madeira abyssal plain. *Marine Geology*, **109**, 21–51.

PETTIJOHN, F. J. 1957. *Sedimentary Rocks*, 2nd ed. Harper & Row, New York.

PHIPPS MORGAN, J. & PARMENTIER, E. M. 1995. Crenulated seafloor: evidence for spreading-rate dependent structure of mantle upwelling and melting beneath a mid-oceanic spreading center. *Earth and Planetary Science Letters*, **129**, 73–84.

PICKERING, K. T., SOH, W. & TAIRA, A. 1991. Scale of tsunami-generated sedimentary structures in deep water. *Journal of the Geological Society, London*, **148**, 211–214.

RICCI LUCCHI, F. 1986. The Oligocene to Recent foreland basins of the Northern Apennines. *In*: ALLEN, P. & HOMEWOOD, P. (eds) *Foreland Basins*. International Association of Sedimentologists, Special Publications, **8**, 165–185.

RIO, D. 1987. Età ed osservazioni litostratigrafiche sul flysch di tipo 'alberese' dell'Appennino parmense. *In*: *Riassunti del Convegno 'La geologia del Versante Padano dell'Appennino settentrionale'*. STEM Mucchi Ed., Modena.

RIO, D. & VILLA, G. 1987. On the age of the 'Salti del Diavolo' conglomerates and of the M. Cassio flysch 'basal complex' (Northern Apennines, Parma province). *Giornale di Geologia*, **49**, 63–73.

RIO, D., VILLA, G. & CANTADORI, M. 1983. Nannofossil dating of the Helminthoid Flysch Units in the Northern Apennines. *Giornale di Geologia*, **45**, 57–86.

RODGERS, J. 1997. Exotic nappes in external parts of orogenic belts. *American Journal of Science*, **297**, 174–219.

ROWAN, M. G. 1990. The Upper Cretaceous Helminthoid Flysch of the Northern Apennines and Maritime Alps: correlation and provenance. *Ofioliti*, **15**, 305–326.

RUFF, L. J. 2003. Some aspects of energy balance and tsunami generation by earthquakes and landslides. *Pure and Applied Geophysics*, **160**, 2155–2176.

RUFF, L. & KANAMORI, H. 1983. Seismic coupling and uncoupling at subduction zones. *Tectonophysics*, **99**, 99–117.

RUPKE, N. A. 1976. Large-scale slumping in a flysch basin, southwestern Pyrenees. *Journal of the Geological Society, London*, **132**, 121–130.

SAMES, C. W. 1967. Sui conglomerati medio-cretacei della geosinclinale emiliana e la loro importanza per la paleogeografia. *Bollettino della Società Geologica Italiana*, **86**, 49–59.

SASSI, F. P., BORSI, S., DEL MORO, A., ZANFERRARI, A. & ZIRPOLI, G. 1978. Contributions to the geodynamic interpretations in the Eastern Alps. *In*: CLOSS, H., ROEDER, D. & SCHMIDT, K. (eds) *Alps, Apennines, Hellenides*. Schweitzerbart, Stuttgart, 154–160.

SCHOLLE, P. A. 1971. Sedimentology of fine-grained deep-water carbonate turbidites. Monte Antola Flysch (Upper Cretaceous). Northern Apennines, Italy. *Geological Society of America Bulletin*, **82**, 629–658.

VAI, G. B. 1992. Il segmento calabro-peloritano dell'orogene ercinico. Disaggregazione palinspastica. *Bollettino della Società Geologica Italiana*, **111**, 109–129.

VALLONI, R. & ZUFFA, G. G. 1984. Provenance changes for arenaceous formations of the northern Apennines, Italy. *Geological Society of America Bulletin*, **95**, 1035–1039.

VAN ANDEL, T. H. 1994. *New Views on an Old Planet, a History of Global Change*. Cambridge University Press, New York.

VANOSSI, M., 1965. Studio sedimentologico del Flysch ad Elmintoidi della valle Argentina (Liguria occidentale). *Atti dell' Istituto Geologico della Università di Pavia*, **16**, 36–71.

VESCOVI, P., FORNACIARI, E., RIO, D. & VALLONI, R. 1999. The Basal Complex of the Helminthoid Monte Cassio Flysch: a key to the Eoalpine tectonics of the northern Apennines. *Rivista Italiana Paleontologia e Stratigrafia*, **105**, 101–128.

WHITMARSH, R. B., MANATSCHAL, G. & MINSHULL, T. A. 2001. Evolution of magma-poor continental margins from rifting to seafloor spreading. *Nature*, **413**, 150–154.

WINKLER, W. 1996. The tectono-metamorphic evolution of the Cretaceous northern Adriatic margin as recorded by sedimentary series (western part of the Eastern Alps). *Eclogae Geologicae Helvetiae*, **89**, 527–551.

WORTMANN, U., WEISSERT, H., FUNK, H. & HAUCK, J. 2001. Alpine plate kinematics revisited: the Adria Problem. *Tectonics*, **20**, 134–147.

ZACCHINO, G. W. M. 1994. *Il Flysch dell'Elba: sedimentologia e minerali pesanti*. Degree in Geological Sciences thesis, University of Bologna.

ZAPPATERRA, E. 1994. Source-rock distribution model of the Periadriatic region. *AAPG Bulletin*, **78**, 333–354.

ZIEGLER, P. A. 1990. *Geological Atlas of Western and Central Europe*. Shell International Petroleum Maatschappij, The Hague.

ZUFFA, G. G. 1980. Hybrid arenites. their composition and classification. *Journal of Sedimentary Petrology*, **50**, 21–29.

ZUFFA, G. G. 1987. Unravelling hinterland and offshore palaeogeography from deep-water arenites. *In*: LEGGETT, J. K. & ZUFFA, G. G. (eds) *Marine Clastic Sedimentology*. Graham & Trotman, London, 39–61.

ZUFFA, G. G., FONTANA, D., MORLOTTI, E., PREMOLI SILVA, I., SIGHINOLFI, G. P., STEFANI, C. & FONTANI, L. 2003. Anatomy of carbonate turbidite mega-beds (M. Cassio Formation, Upper Cretaceous, northern Apennine, Italy). *In*: VALLONI, R. & BASU, A. (eds) *Quantitative Provenance Studies in Italy*. Memorie Descrittive della Carta Geologica d'Italia, **61**, 129–144.

The Argille Varicolori unit in Lucania (Italy): a record of tectonic offscraping and gravity sliding in the Mesozoic–Tertiary Lagonegro Basin, southern Apennines

L. MATTIONI[1,2], E. TONDI[3], P. SHINER[4], P. RENDA[5], S. VITALE[6] & G. CELLO[3]

[1]*Institut Français du Pétrole, 4 Av. de Bois Preau, 92852 Rueil Malmaison, France*

[2]*Present address: Beicip Franlab, Rueil Malmaison, France (e-mail: luca.mattioni@beicip.fr)*

[3]*Dipartimento di Scienze della Terra, Università di Camerino, Via Gentile III da Varano, 62032 Camerino, Italy*

[4]*Shell Italia E&P, Via Due Macelli 66, 00187 Rome, Italy*

[5]*Università di Palermo, Dipartimento di Geologia e Geodesia, Palermo 90133, Italy*

[6]*Dipartimento di Scienze della Terra, Università 'Federico II' di Napoli, Largo S. Marcellino 10, 80138 Napoli, Italy*

Abstract: Detailed geological mapping and new stratigraphic and structural data collected in the Lucania area of the southern Apennines allowed us to assess the deformation history of Il Monte–Corleto Perticara zone, in the High Agri Valley (Lucanian Apennines, southern Italy) where red and green shales (known as Argille Varicolori or Argille scagliose) crop out. Our observations suggest that: (1) 'chaotic' facies within the Argille Varicolori may be attributed to a broken formation generated by overthrusting of Apenninic Platform units onto already deformed Lagonegro basin strata; (2) gravity sliding phenomena at the thrust front enhanced the development of debris flow and the emplacement of olistostromes at distances of up to tens of kilometres from the leading edge of the Apenninic Platform thrust; (3) the above processes probably ended in mid-Miocene time, as suggested by observed structural and stratigraphic relationships among accreted terranes and synorogenic deposits. The evolutionary model envisaged here could also be relevant in other active convergent zones, where seismic and drilling data are sparse, and in subaerial fossil margins where broken formations occur.

Mélanges and broken formations (tectonic mélanges with no exotic blocks; Cowan 1985) are a common constituent of many convergent margins and also occur in other tectonic settings such as foreland basins and strike-slip zones (Byrne 1984; Cowan 1985; Needham 1995; Harris *et al.* 1998). Because of their chaotic nature, it is often difficult to understand their internal geometry and genesis, and to reconstruct their evolutionary history (Needham 1995). Furthermore, the study of mélanges in active settings is particularly problematic because seismic images do not allow us to discriminate between mesoscale structures of different type and age. For this reason, convergent margins, even fossil ones, should be investigated in detail to unravel their progressive deformation history and to assess the different mechanisms of emplacement of offscraped and accreted sediments (e.g. Vannucchi & Bettelli 2002).

In this paper, we focus on a sector of the southern Apennines of peninsular Italy where extremely tectonized varicoloured shaly sequences are extensively exposed. These terranes are known in the geological literature as Argille Varicolori or Argille scagliose unit (Ogniben 1969, and references therein); however, in spite of their abundance, the interpretation of the relationships among the Argille Varicolori unit and other tectonostratigraphic units making up the southern Apennines has often been problematic. Because of this, various hypotheses have been put forward for the palaeogeographical attribution and the evolutionary history of these terranes (see, e.g. Mostardini & Merlini 1986; Casero *et al.* 1988; Pescatore *et al.* 1988; Carbone *et al.* 1991; Monaco & Tortorici 1995; Gallicchio *et al.* 1996; Monaco *et al.* 1998; Pescatore *et al.* 1999; Lentini *et al.* 2002). In this study, we approach the problem by focusing on the geostructural characteristics of the varicoloured shaly successions exposed in Il Monte–Corleto Perticara zone, which is a key area where the geological, biostratigraphic and tectonic properties of the Argille Varicolori unit have been assessed.

From: MORATTI, G. & CHALOUAN, A. (eds) 2006. *Tectonics of the Western Mediterranean and North Africa.* Geological Society, London, Special Publications, **262**, 277–288.
0305-8719/06/$15.00

Geological setting

The Lucanian Apennines are part of the southern Apennine fold-and-thrust belt of mainland Italy, which, in turn, is a major tectonic element of the Africa-verging mountain system of the central Mediterranean (Fig. 1). This segment of the Apenninic chain was formed as a consequence of the convergent motion between the African and European plates since the Late Cretaceous (Dewey *et al.* 1989). In the first stages of accretion, the tectonic wedge involved the Cretaceous to Palaeogene sedimentary cover and the underlying basement of the Neotethyan domain (Cello *et al.* 1990; Monaco *et al.* 1998; Cello & Mazzoli 1999, and references therein). The tectonic units derived from these accretionary stages (e.g. the ophiolite-bearing Liguride units; Cello *et al.* 1991, 1996) were subsequently emplaced onto the Afro-Adriatic continental margin and then involved in the contractional deformation that affected the Mesozoic domains of the southern sectors of the continental margin from Miocene time.

The understanding of the original Mesozoic palaeogeography of the southern Apennines represents a key tool in any attempt to reconstruct the structure and geodynamic evolution of this sector of the peri-Mediterranean area. Simple models (Ogniben 1969; Mostardini & Merlini 1986; Cello & Mazzoli, 1999, and references therein) that suggest the presence of a unique Meso-Cenozoic pelagic basin (the Lagonegro basin) interposed between two shallow-water carbonate platforms (known as the Apenninic, or Internal, and Apulian Platforms) are opposed to other, more complex, palaeotectonic restorations in which the pre-orogenic palaeogeography of the Afro-Adriatic continental margin is formed by a series of carbonate platforms alternating with deep basins (e.g. D'Argenio *et al.* 1975; Sgrosso 1988). Furthermore, Marsella *et al.* (1995) reviewed the palaeogeographical and structural position of the Lagonegro basin and proposed that it may be placed west of the Campania–Lucania platform, hence joining the Neotethyan ocean. This interpretation, however, is not in agreement with the data of Pescatore *et al.* (1999), which seem to corroborate the idea of a pre-orogenic position of the Lagonegro basin between two carbonate platforms. The present-day setting of the Lucanian Apennines is shown in Figure 2. As may be seen, the deepest tectonostratigraphic units consist of Mesozoic–Tertiary shallow-water carbonates stratigraphically overlain by upper Messinian and Pliocene terrigenous marine deposits (see also Mostardini & Merlini 1986). The carbonate rocks are part of the so-called 'buried Apulian belt' (Cello *et al.* 1989) and represent the reservoir for major oil-fields located in the area (e.g. Shiner *et al.* 2004, and references therein). Available subsurface data show that above these units there occurs a mélange zone of several hundreds of metres thickness including overpressured sediments of Miocene–Early Pliocene age (Mazzoli *et al.* 2001).

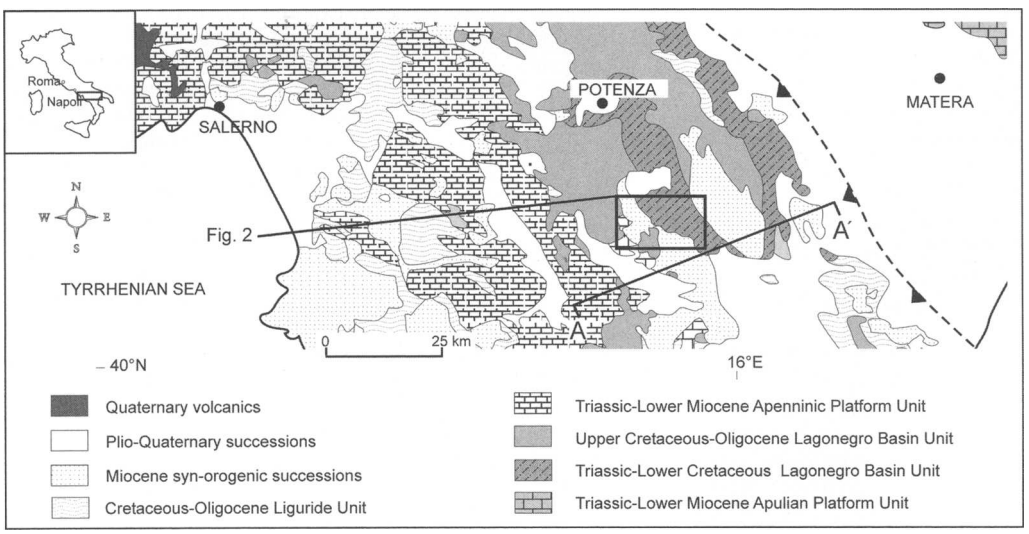

Fig. 1. Geological sketch map of the southern Apennines. A–A′, trace of the regional cross-section shown in Figure 2. Box shows location of the study area (Fig. 3).

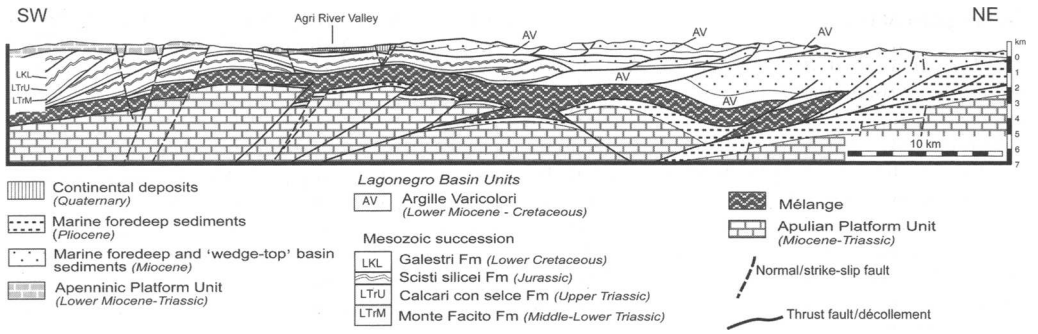

Fig. 2. Detail of geological section across the southern Apennines in the Lucania region, modified after Mazzoli *et al.* (2000).

As a whole, this deepest part of the Lucanian chain is separated from the upper portion of the thrust belt by a major décollement, which carries, in its hanging wall, allochthonous units derived from the deformation of the Triassic to Palaeogene shallow-water carbonate platform and pelagic basin successions (Apenninic Platform and Lagonegro basin, respectively), as well as the stratigraphically overlying Neogene foredeep and thrust-top basin deposits (e.g. Mostardini & Merlini, 1986; Cello *et al.* 1989, 2000; Mazzoli *et al.* 2001). Within the allochthon, a major thrust separates the Apenninic Platform units from the underlying Lagonegro basin units. It is noteworthy that the main structures involving the Mesozoic Lagonegro basin unit are characterized by roughly north–south-trending buckle folds bounded on their eastern and western sides by (either emergent or blind) thrusts and backthrusts (Cello *et al.* 2000; Mazzoli *et al.* 2001). These 'pop-up' and associated 'pop-down' structures are cut by the major thrust surface located at the base of the Apenninic Platform unit. In our opinion, this observation has fundamental implications for defining the evolutionary model of the area, and therefore it will be discussed in detail in the following sections.

The Argille Varicolori unit is exposed in the frontal zones of the southern Apennines and is mainly composed of Upper Cretaceous–Oligocene red and green shales, often extremely sheared. The various successions cropping out in the Lucanian Apennines are sometimes collectively termed the 'Sicilide complex' (Ogniben 1969), and are associated with similar units (terranes of 'Sicilide affinity' of Bonardi *et al.* 1988) included in the so-called 'Liguride complex' that crop out in the most internal sector of the southern Apennines (i.e. north of the Cilento peninsula). The strong convergence in lithology and age among these terranes has led to the proliferation of different interpretations concerning the palaeogeographical attribution and structural history of the Argille Varicolori unit. As a consequence, some palaeotectonic models suggest an internal origin (i.e. west of the Internal Platform) for the varicoloured shaly successions of the 'Sicilide complex' (Lentini 1979; Carbone *et al.* 1991; Lentini *et al.* 2002, and references therein; see also Cinque *et al.* 1993; Monaco *et al.* 1998), whereas other palaeogeographical reconstructions place these units in a more external position and suggest that they are part of the uppermost portion of the Lagonegro basin succession (Mostardini & Merlini 1986; Casero *et al.* 1988; Pescatore *et al.* 1988, 1999; Piedilato *et al.* 2000). In particular, based on the stratigraphic relationships between the varicoloured shales and the coeval deposits attributed to the uppermost part of the Lagonegro basin succession (i.e. the 'Flysch Rosso' or Monte Malomo Fm; Scandone 1967), Pescatore *et al.* (1988) suggested that the varicoloured shales exposed in the Lucanian Apennines should be placed in a palaeogeographical position occupying the central and deeper parts of the Lagonegro basin. This same conclusion was independently reached by Mostardini *et al.* (1988), who performed geochemical and mineralogical analyses on cuttings from several deep wells drilled for hydrocarbon exploration. A clear affinity between varicoloured shales and underlying Lagonegro basin sediments in the area of the present study is also shown by clay mineralogy data (Aldega *et al.* 2003). Further evidence supporting the hypothesis of an 'external' origin for the Argille Varicolori unit has been provided by Mostardini & Merlini (1986) and Casero *et al.* (1988). Based on the interpretation of a large amount of subsurface data, those workers considered the Upper Cretaceous to Oligocene varicoloured shales as the detached uppermost part of the Lagonegro basin succession; they also suggested that the detachment of the Cretaceous–Oligocene section from its Mesozoic substratum occurred during the early phases of contraction and basin inversion.

New geological data

The study area is characterized by large exposures of deformed Lagonegro successions (Fig. 3) of Late Triassic to Early Cretaceous age. Based on stratigraphic and structural analysis, the Lagonegro basin terranes cropping out in the study area have been included in the so-called Caldarosa unit (Mattioni 2001; Mazzoli *et al.* 2001). This unit is characterized by a Mesozoic succession showing peculiar lithostratigraphic properties (mainly in terms of facies and thickness) with respect to nearby Lagonegro basin successions. Within the study area, the most ancient rocks of the Lagonegro basin unit consist of grey calcilutites with bands and nodules of chert (Calcari con Selce Formation, Upper Triassic; Scandone 1967) grading upwards into a succession of radiolarian cherts and siliceous argillites (Scisti silicei Formation, Jurassic; Scandone 1967). The latter are stratigraphically overlain by siliceous marls and shales (Galestri Formation, Lower Cretaceous; Scandone 1967).

Detailed field mapping at a scale of 1:10 000 allowed us to distinguish two facies within the Argille Varicolori unit exposed in Il Monte–Corleto Perticara zone. They were recognized on the basis of their lithological characteristics and their internal deformation and structural position. We distinguished and mapped 'chaotic' facies, which are characterized by extremely tectonized rocks retaining little or no internal coherence, and 'well-bedded' facies, which are well organized and display a coherent stratigraphy. The two facies occupy different stratigraphic positions within the Argille Varicolori unit. The 'well-bedded' facies generally overlie the Lower Cretaceous Galestri Fm of the Mesozoic Lagonegro basin successions. The contact between the two units can be observed south of M. Tangia (Lentini *et al.* 2002; Fig. 3) and in several other places in the surrounding areas; it is also clearly seen on available seismic lines.

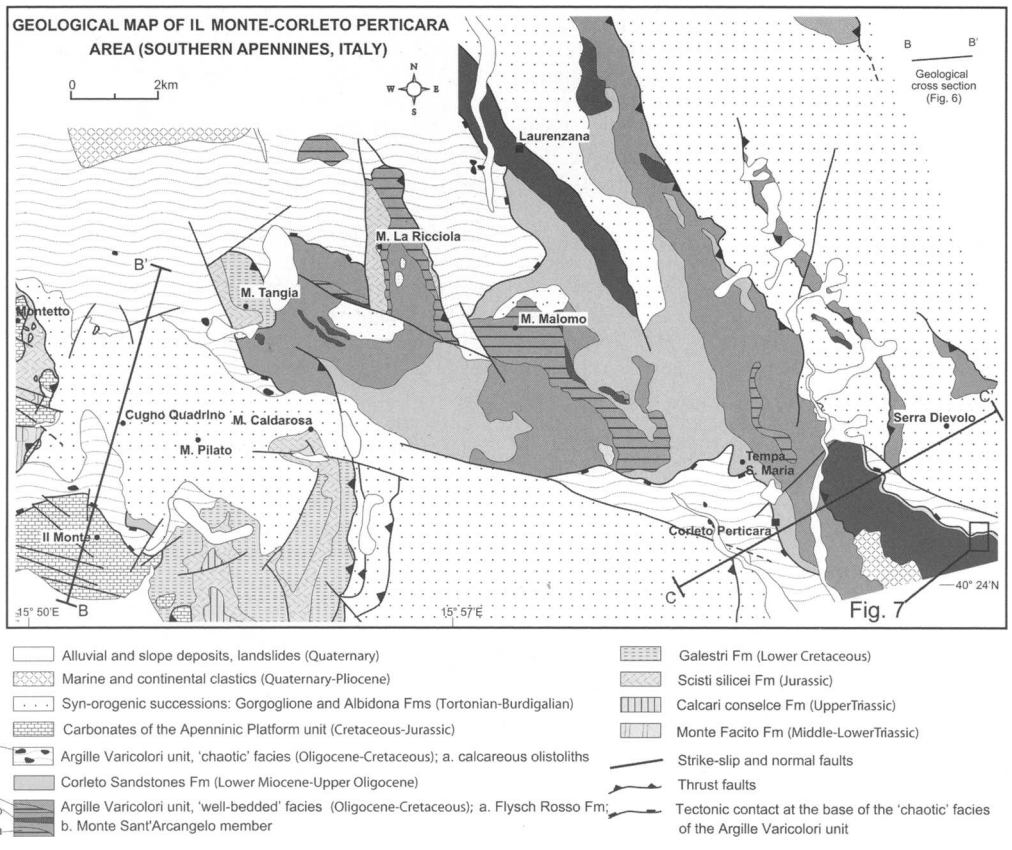

Fig. 3. Geological map of the study area. Location of the geological cross-sections of Figure 6 and of the stratigraphic log of Figure 7 is also shown.

Within the study area we did not detect any indication that the above contact is tectonic in nature; hence, following Pescatore *et al.* (1988, 1999), we suggest that it is a stratigraphic contact and that the 'well-bedded' facies of the Argille Varicolori unit can be interpreted as the Upper Cretaceous to Oligocene part of the Lagonegro basin succession. From a lithological point of view, the 'well-bedded' facies consists of red, green and brown shales and marls (including centimetre-thick grey marly limestone beds), with local intercalations of red shales and marls with interbedded calcirudites, calcarenites, calcilutites, marly limestones and bedded cherts (similar to portions of the so-called Flysch Rosso) as well as the so-called Monte Sant'-Arcangelo member (Lentini *et al.* 2002). The latter comprises centimetre-thick whitish marly limestones alternating with grey, green and red shales containing greyish calcarenites and calcareous conglomerates with subordinate graded sandstones and siltstones.

The main structures affecting this portion of the Argille Varicolori unit are roughly north–south-trending folds ranging in size from a few metres to several tens of metres. These features may be seen at M. Malomo, where the succession is exposed in a broad north–south-trending anticline. The fabrics associated with these major structures include a discontinuously developed slaty cleavage in the shaly lithologies, and both spaced pressure solution cleavage and extension fractures in the more competent units. Extension fractures consist mainly of tension gashes associated with bedding-parallel shear on fold limbs (related to flexural slip folding; Ramsay 1967) as well as radial fractures in the outer arc of fold hinge zones (related to a component of tangential–longitudinal strain; Ramsay 1967). These features all suggest that folds originated by buckling (e.g. Ramsay 1981). A dispersed bedding pattern is generally observed around major fold structures, which, however, maintain a general subcylindrical geometry (Fig. 4). In the study area, the overall thickness of the 'well-bedded' facies reaches a maximum value of about 750 m.

Unconformably overlying these successions, synorogenic siliciclastic deposits belonging to the Corleto Sandstones Fm occur (Fig. 3). These consist of up to 300 m thick turbidites of both siliciclastic (quartzo-feldspathic) and (subordinate) carbonate composition. Biostratigraphic analyses of samples collected in the Corleto Perticara area suggest a Late Oligocene–Early Miocene (Aquitanian) age for this formation.

The 'chaotic' facies of the Argille Varicolori unit systematically occurs on top of the Corleto Sandstones Fm (Fig. 3). The 'chaotic' facies consists of a mélange of pervasively deformed rocks showing a block-in-matrix fabric (Cowan 1985). The matrix is mainly represented by highly tectonized red and green shales with disrupted bedding within which competent blocks and fragments of various sizes and shapes occur. The latter consist of dismembered chert, limestone and rare sandstone beds, as well as blocks of whitish marly limestones, greyish calcarenites (locally containing *Nummulites* and *Lepidocyclina*) and calcareous microconglomerates alternating with grey, green and red shales (Fig. 5a and b). The 'chaotic' facies also includes very large blocks (up to tens of metres in size) of shallow-water limestones (refer to the geological

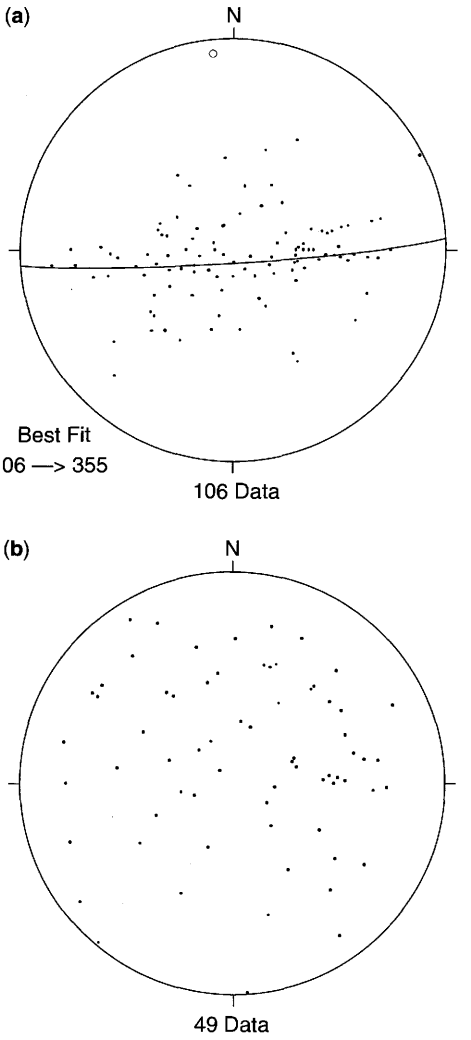

Fig. 4. Orientation data (lower-hemisphere, equal-area projection) of bedding in the Argille Varicolori unit. (**a**) Poles to bedding relative to the 'well-bedded' facies. (**b**) Poles to bedding relative to the 'chaotic' facies.

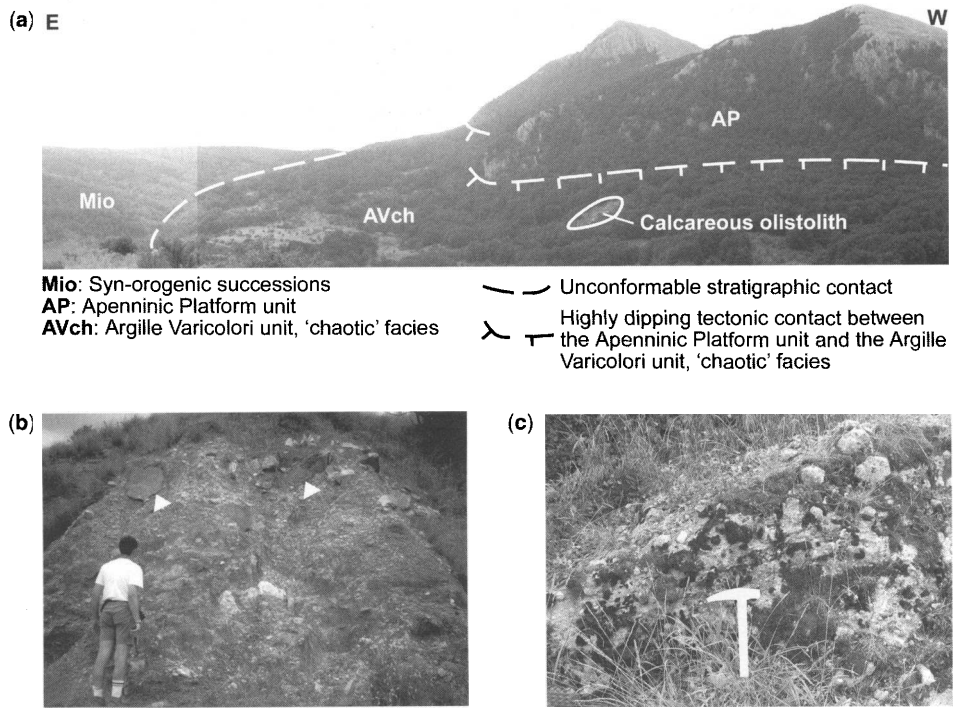

Fig. 5. (**a**) View of the contact (dashed line) between the 'chaotic' facies of the Argille Varicolori unit (AVch) and the carbonate rocks of the Apenninic Platform unit. The contact is marked by a very steep, NW–SE-trending surface (see text for explanation). (**b**) The 'chaotic' facies of the Argille Varicolori unit in the study area. Arrows indicate coherent blocks included within a red and green highly tectonized shaly matrix. (**c**) Detail of debris flow within the 'chaotic' facies of the Argille Varicolori unit.

map of Fig. 3), locally containing rudists. Biostratigraphic data from rock samples cut from these blocks indicate a general Late Cretaceous age (A. Mancinelli, pers. comm.). The contact between the 'chaotic' facies of the Argille Varicolori unit and the carbonates of the Apenninic Platform unit, as shown in Figure 5c and in cross-section B–B′ of Figure 6, is of tectonic origin. It consists of a NW–SE-oriented, NE-dipping steep surface where extremely tectonized red shales are crushed against carbonate rocks of the Apennine Platform unit. This contact is part of the leading edge of a regional thrust extending from Montetto to the NW (see Fig. 3) to San Martino d'Agri to the SE, a few kilometres outside the study area (see Carbone *et al.* 1991), and can be observed at Il Monte area (Fig. 5c) where the strongly recrystallized rudstones of Late Cretaceous age are involved in a hanging-wall anticline (Cello *et al.* 2002). Along the contact, several blocks of carbonate rocks, ranging in size from a few decimetres to tens of metres, are included within the 'chaotic' facies of the Argille Varicolori unit; these have been interpreted as olistoliths derived from carbonates of the nearby Apenninic Platform unit.

The thickness of the 'chaotic' facies is difficult to assess; however, stratimetric considerations suggest an average thickness of 350–400 m. Furthermore, from the map of Figure 3, one may observe that the 'chaotic' facies extends in outcrop regularly from the contact with the leading edge of the Apenninic Platform unit (i.e. at Il Monte) to the Laurenzana and Corleto Perticara areas.

The relationships between the 'well-bedded' and 'chaotic' facies of the Argille Varicolori unit can be observed at several locations within the study area; east of the village of Corleto Perticara, for example, a SW-vergent overturned anticline involving the Monte Sant'Arcangelo member (belonging to the 'well-bedded' facies) is bounded to the SW by a back-thrust (see the cross-section C–C′ of Fig. 6). Field observations indicate that along the gently NE-dipping normal limb, the marly limestones of the Monte Sant'Arcangelo member are involved in parasitic folds, of several metres wavelength, and are stratigraphically overlain by

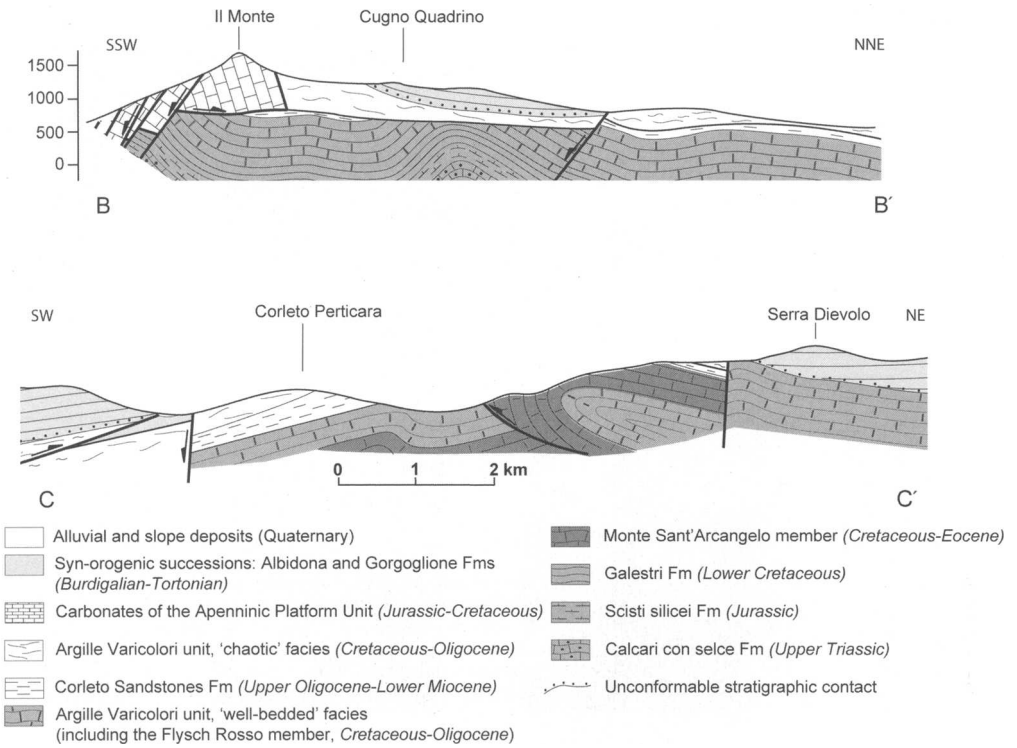

Fig. 6. Geological sections across the study area; locations are shown in Figure 3.

the arenaceous–pelitic turbidite beds of the Corleto Sandstones Formation, which, in turn, are overlain by the 'chaotic' facies (Fig. 7). A further example occurs near the village of Corleto Perticara, where red and green marls (including centimetre-thick grey marly limestone beds) belonging to the 'well-bedded' facies of the Argille Varicolori unit are stratigraphically overlain by quartzo-feldspathic sandstones and pelitic levels belonging to the Corleto Sandstones Fm. The latter, in turn, are overlain by 'chaotic' facies, the contact being well exposed at Tempa S. Maria (Fig. 3).

Both the 'well-bedded' and 'chaotic' facies of the Argille Varicolori unit are sometimes unconformably overlain by the Langhian–lower Tortonian Gorgoglione Fm (Pescatore 1988) (Figs 3 and 6). This consists of turbiditic, arenaceous (of litho-arenitic and arkosic composition) and pelitic beds, which are thought to represent the terrigenous evolution of the Burdigalian–Langhian Albidona Fm (Pescatore 1988; Fig. 3). In detail, the stratigraphic contact above is well exposed at Serra Dievolo (Fig. 3), where the Gorgoglione Fm rests unconformably on red, green and brown shales, and marls belonging to the 'well-bedded' facies of the Argille Varicolori unit. North of Il Monte (Fig. 3), highly tectonized red and green shales including several blocks of carbonate rocks are overlain by arenaceous and pelitic strata of the Gorgoglione Fm.

To the NE of the village of Corleto Perticara, several roughly NW–SE-trending thrusts and backthrusts cut through rocks belonging to both the 'chaotic' and 'well-bedded' facies. These structures superimpose the latter onto the Gorgoglione Formation, hence producing inversion of the original stratigraphic relationships. Furthermore, the activation of these younger features introduces a systematic dispersion in the bedding attitude of the Mesozoic–Oligocene Lagonegro terranes, as it can be observed from the stereographic projections of Figure 4b.

Following this late thrusting episode, the study area was affected by strike-slip tectonics; this event is well documented by the occurrence of a regional roughly WNW–ESE-trending sinistral fault known as the Scuorciabuoi Fault (Bonini & Sani 2000, and references therein).

Discussion and conclusions

The Argille Varicolori unit cropping out at Il Monte–Corleto Perticara area was investigated in

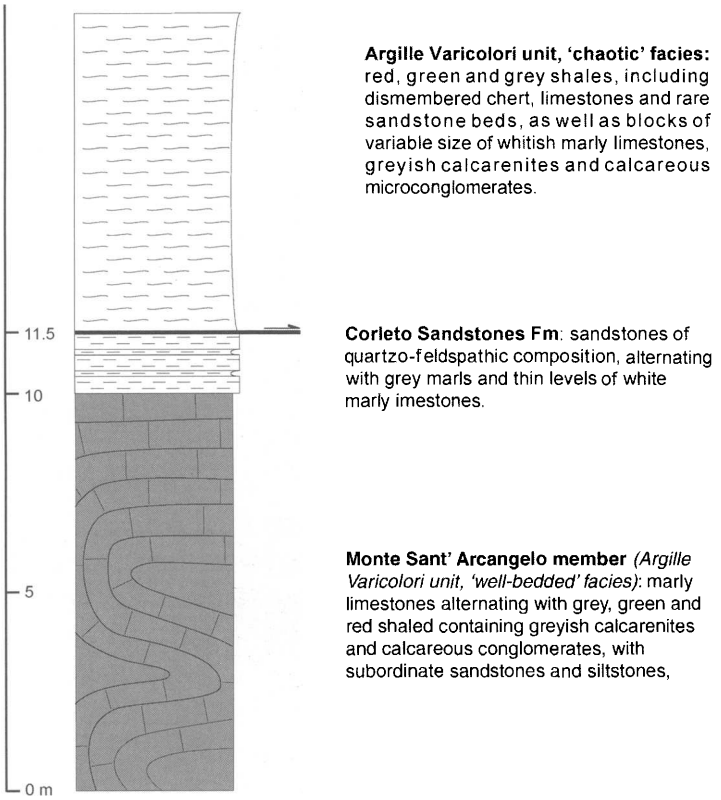

Fig. 7. Stratigraphic log showing the relationships between 'well-bedded' and 'chaotic' facies of the Argille Varicolori unit and the Upper Oligocene–Lower Miocene Corleto Sandstones Fm at Fosso Cupo. Location of the log is shown in Figure 3.

detail to assess its stratigraphic characteristics and structural position. The results of our analysis show that the Argille Varicolori unit includes two rock facies. The first facies consists of a 'well-bedded' succession (including the Monte Sant'Arcangelo member, as well as intercalations similar to the so-called 'Flysch Rosso'), which lies stratigraphically over Mesozoic Lagonegro basin strata, whereas the second facies is characterized by a chaotic succession resting in tectonic contact above the Corleto Sandstones Fm (Upper Oligocene–Aquitanian). The timing of emplacement of the 'chaotic' facies is clearly constrained by the position of the underlying Corleto Sandstones Fm, and hence an Early Miocene age for their emplacement is suggested.

The 'well-bedded' facies of the Argille Varicolori unit are involved in a series of roughly north–south-trending buckle folds ranging in size from a few metres to several tens of metres (Cello *et al.* 2000; Mazzoli *et al.* 2001). These folds show trends and structural fabrics that are similar to those affecting the Triassic–Lower Cretaceous section of the Lagonegro basin succession (Mazzoli *et al.* 2001). This suggests that these features developed during an early deformation phase that affected the Lagonegro basin succession.

The 'chaotic' facies consists of a broken formation of mixed tectonic and sedimentary origin. Compositional data from different portions of this 'chaotic' body reflect the lithological variations existing within the underlying 'well-bedded' facies, whereas the nature and age of the largest blocks of shallow-water limestones embedded within the chaotic matrix suggest that one can rule out the possibility that they represent outliers of the Apenninic Platform thrust sheet; rather, they can be best interpreted as olistoliths deposited in the Argille Varicolori basin from the nearby carbonates of the Apenninic Platform unit.

The possible steps in the deformation history of the study area are depicted schematically in Figure 8. During late Oligocene–Early Miocene times, the Lagonegro successions underwent early

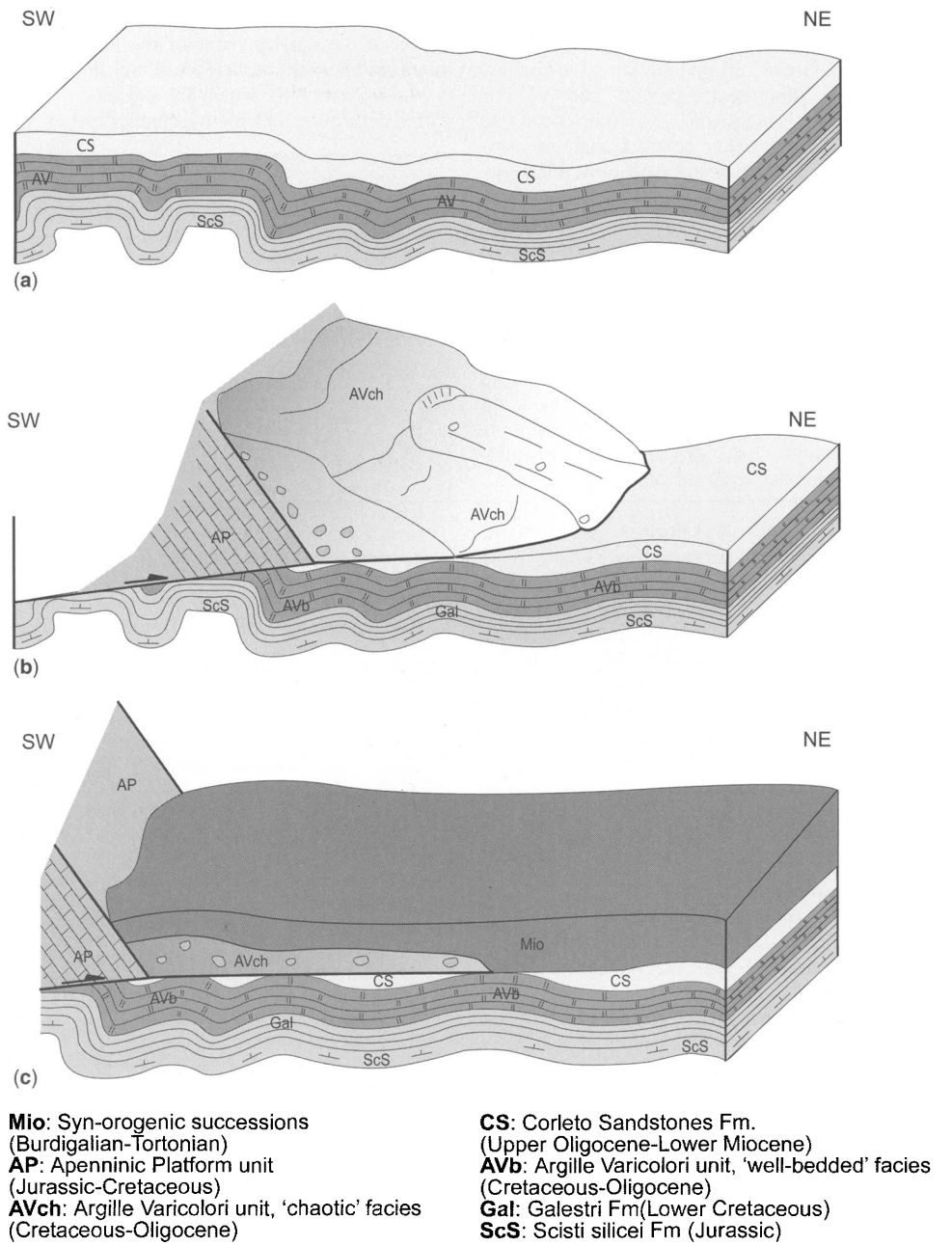

Fig. 8. Schematic reconstruction of the Late Oligocene–Mid-Miocene evolution of the study area. (**a**) During Late Oligocene times, the area was affected by the development of a series of north–south-trending folds involving the Mesozoic to Oligocene Lagonegro basin succession. (**b**) The emplacement of the Apenninic Platform unit onto the Lagonegro unit produced extensive offscraping of Lagonegro strata and the development of a tectonic mélange in the frontal zone of the leading edge of the Apenninic Platform thrust sheet. (**c**) The accretion of the tectonic mélange was accompanied by gravity sliding phenomena responsible for the activation of large debris flows and the emplacement of olistostromes at great distances from the leading edge of the Apenninic Platform thrust sheet. The deposition of the synorogenic successions of Miocene age (Albidona and Gorgoglione Formations) finally seals both the tectonic mélange and the carbonates of the Apenninic Platform unit, as well as the Lagonegro Basin unit, by means of a regional unconformable contact.

contraction and were deformed mostly by roughly north–south-trending buckle folds (Mazzoli *et al.* 2001; Fig. 8a). Gravity sliding affecting the Cretaceous–Tertiary, dominantly pelitic, part of the Lagonegro basin successions started to occur at this stage. Following this contractional episode, the thrust emplacement of the Apenninic Platform unit over Lagonegro basin units occurred. Relative chronological constraints for this thrusting episode are given by consistent observations indicating that the main thrust surface clearly truncates pre-existing folds within the underlying Lagonegro basin unit. This is emphasized by the occurrence of tectonic contacts cutting across different stratigraphic levels of the Lagonegro basin succession, and by the presence of a tectonic wedge made of offscraped material, resulting from the disruption of the Lagonegro terranes, and of olistoliths derived from gravity-induced sliding phenomena (Fig. 8b).

During the accretionary process, the tectonic wedge was probably characterized by a water–mud mixture with low values of internal cohesion and great internal instability. This may have enhanced the development of further gravity sliding phenomena, the activation of large debris flows, and the emplacement of olistostromes at great distances from the leading edge of the Apenninic Platform thrust. The emplacement of the 'chaotic' facies probably ended in mid-Miocene time, as suggested by the observation that they underlie the terrigenous deposits of the Gorgoglione Fm (Fig. 8c).

Further deformation, leading to variable degrees of modification, distortion and truncation of the main structural features described above, was associated with: (i) the development of late ('out-of-sequence') thrusts and back-thrusts, and (ii) the activation of the WNW–ESE-trending Scuorciabuoi Fault.

In conclusion, we suggest that:

(1) The 'chaotic' facies of the Argille Varicolori unit represents a mixed sedimentary and tectonic mélange derived from the detachment, disruption and redeposition of material belonging to the underlying, already deformed, Upper Cretaceous–Oligocene Lagonegro basin successions.

(2) The development of the 'chaotic' facies within the Argille Varicolori unit occurred in the frontal zones of the leading edge of the Apenninic Platform thrust. According to this interpretation, the Apenninic Platform unit acted as a moving bulldozer during its tectonic emplacement.

(3) The basal décollement developed within the mainly shaly and marly Cretaceous–Oligocene portion of the Lagonegro basin succession, which represents the most incompetent part of the Mesozoic–Palaeogene Lagonegro multilayer.

(4) A major controlling factor that may have enhanced the emplacement of the 'chaotic' facies might have been the occurrence of high fluid pressures (Cello & Nur 1988), which are expected to develop within deforming undercompacted sediments.

The authors are indebted to S. Mazzoli for the constructive discussions during the preparation of the manuscript, and to T. Pescatore and C. Sanz de Galdeano for valuable comments and suggestions during the review process.

References

ALDEGA, L., CORRADO, S., GIAMPAOLO, C. & MAZZOLI, S. 2003. Primi dati sulle ricerche mineralogiche della frazione pelitica della successione lagonegrese della Rupe del Corvo (Val d'Agri, Basilicata). *Studi Geologici Camerti*, **1**, 7–14.

BONARDI, G., D'ARGENIO, B. & PERRONE, V. 1988. Carta geologica dell'Appennino meridionale. Scala 1:250 000. *SELCA Firenze, 74° Congresso Società Geologica Italiana, Sorrento 13–17 Settembre*.

BONINI, M. & SANI, F. 2000. Pliocene–Quaternary transpressional evolution of the Anzi–Calvello and Northern S. Arcangelo basins (Basilicata, Southern Apennines, Italy) as a consequence of deep-seated fault reactivation. *Marine and Petroleum Geology*, **17**, 909–927.

BYRNE, T. 1984. Early deformation in melange terranes of the Ghost Formation, Kodiak Islands, Alaska. *In*: RAYMOND, L. A. (ed.) mélanges: *Their Nature, Origin and Significance*. Geological Society of American, Special Papers, **198**, 21–51.

CARBONE, S., CATALANO, S., LAZZARI, S., LENTINI, F. & MONACO, C. 1991. Presentazione della carta geologica del Bacino del Fiume Agri (Basilicata). *Memorie della Società Geologica Italiana*, **47**, 129–143.

CASERO, P., ROURE, F., ENDIGNOUX, L., MORETTI, I., MULLER, C., SAGE, L. & VIALLY, R. 1988. Neogene geodynamic evolution of the Southern Apennines. *Memorie della Società Geologica Italiana*, **41**, 109–120.

CELLO, G. & MAZZOLI, S. 1999. Apennine tectonics in Southern Italy: a review. *Journal of Geodynamics*, **27**, 191–211.

CELLO, G. & NUR, A. 1988. Emplacement of foreland thrust systems. *Tectonics*, **7**, 261–271.

CELLO, G., MARTINI, N., PALTRINIERI, W. & TORTORICI, L. 1989. Structural styles in the frontal zones of the Southern Apennines, Italy: an example from the Molise district. *Tectonics*, **15**, 187–200.

CELLO, G., LENTINI, F. & TORTORICI, L. 1990. La struttura del settore calabro–lucano e suo significato nel quadro dell'evoluzione tettonica del sistema a thrust sudappenninico. *Studi Geologici Camerti, Volume Speciale*, 27–34.

CELLO, G., DE FRANCESCO, A. M. & MORTEN, L. 1991. The tectonic significance of the Diamante–Terranova unit in the Alpine evolution of the

northern sector of the Calabrian Arc. *Bollettino della Società Geologica Italiana*, **110**, 685–694.

CELLO, G., INVERNIZZI, C. & MAZZOLI, S. 1996. Structural signature of tectonic processes in the Calabrian Arc (southern Italy): evidence from the oceanic-derived Diamante–Terranova unit. *Tectonics*, **15**(1), 187–200.

CELLO, G., GAMBINI, R., MATTIONI, L., MAZZOLI, S., READ, A., TONDI, E. & ZUCCONI, V. 2000. Geological analysis of the High Agri Valley (Lucania Apennines, Southern Italy). *Memorie della Società Geologica Italiana*, **55**, 149–155.

CELLO, G., COCCIA, B., MANCINELLI, A., MATTIONI, L., MAZZOLI, S., SHINER, P. & TONDI, E. 2002. Architettura pre-orogenica della piattaforma carbonatica appenninica nell'alta Val d'Agri (Lucania, Italia meridionale). *Studi Geologici Camerti*, **2**, 45–52.

CINQUE, A., PATACCA, E., SCANDONE, P. & TOZZI, M. 1993. Quaternary kinematic evolution of the Southern Apennines. Relationships between surface geological features and deep lithospheric structures. *Annali di Geofisica*, **36**, 249–260.

COWAN, D. S. 1985. Structural styles in Mesozoic and Cenozoic mélanges in the western Cordillera of North America. *Geological Society of America Bulletin*, **96**, 451–462.

D'ARGENIO, B., PESCATORE, T. & SCANDONE, P. 1975. Structural pattern of the Campania–Lucania Apennines. *Quaderni Ricerca di Scienze*, **90**, 313–327.

DEWEY, J. F., HELMAN, M. L., TURCO, E., HUTTON, D. H. W. & KNOTT, S. D. 1989. Kinematics of western Mediterranean. *In*: COWARD., M. P., DIETRICH, D. & PARK, R. G. (eds) *Alpine Tectonics*. Geological Society, London, Special Publications, **45**, 265–283.

GALLICCHIO, S., MARCUCCI, M., PIERI, P., PREMOLI-SILVA, I., SABATO, L. & SALVINI, G. 1996. Stratigraphical data from a Cretaceous claystones sequence of the 'Argille Varicolori' in the Southern Apennines (Basilicata, Italy). *Palaeopelagos*, **6**, 261–272.

HARRIS, R. A., SAWYER, R. K. & AUDLEY-CHARLES, M. G. 1998. Collisional mélange development: geologic associations of active mélange-forming processes with exhumed mélange facies in the western Banda orogen, Indonesia. *Tectonics*, **17**, 458–479.

LENTINI, F. 1979. Le Unità Sicilidi della Val d'Agri (Appennino lucano). *Geologica Romana*, **18**, 215–224.

LENTINI, F., CARBONE, S., DI STEFANO, A. & GUARNIERI, P. 2002. Stratigraphical and structural constraints in the Lucanian Apennines (southern Italy): tools for reconstructing the geological evolution. *Journal of Geodynamics*, **34**, 141–158.

MARSELLA, E., BALLY, A. W., D'ARGENIO, B., CIPPITELLI, G. & PAPPONE, G. 1995. The paleogeographic position of the Lagonegro domain, Southern Apennines. Tectonophysics, **252**, 307–330.

MATTIONI, L. 2001. *Definizione dell'assetto geologico-strutturale dell'Appennino lucano ed implicazioni sull'evoluzione tettonica della catena sud-appenninica*. Ph.D. thesis, University of Camerino.

MAZZOLI, S., CORRADO, S., DE DONATIS, M., *ET AL.* 2000. Time and space variability of 'thin-skinned' and 'thick-skinned' thrust tectonics in the Apennines (Italy). *Rendiconti Accademia dei Lincei*, **9**(11), 5–39.

MAZZOLI, S., BARKHAM, S., CELLO, G., GAMBINI, R., MATTIONI, L., SHINER, P. & TONDI, E. 2001. Reconstruction of the continental margin architecture deformed in the contraction of the Lagonegro Basin, Southern Apennines, Italy. *Journal of the Geological Society, London*, **158**, 309–319.

MONACO, C. & TORTORICI, L. 1995. Tectonic role of ophiolite-bearing terranes in the development of the Southern Apennines orogenic belt. *Terra Nova*, **7**, 153–160.

MONACO, C., TORTORICI, L. & PALTRINIERI, W. 1998. Structural evolution of the Lucanian Apennines. *Journal of Structural Geology*, **20**, 617–638.

MOSTARDINI, F. & MERLINI, S. 1986. Appennino centro-meridionale. Sezioni geologiche e proposta di modello strutturale. *Memorie della Società Geologica Italiana*, **35**, 177–202.

MOSTARDINI, F., BRIGNOLI, G. & RIVA, A. 1988. Appennino meridionale: caratteristiche geochimiche e mineralogiche delle Argille Varicolori incontrate da alcuni sondaggi. *Memorie della Società Geologica Italiana*, **41**, 265–284.

NEEDHAM, D. T. 1995. Mechanisms of mélange formation: examples from SW Japan and Southern Scotland. *Journal of Structural Geology*, **17**, 971–985.

OGNIBEN, L. 1969. Schema introduttivo alla geologia del confine Calabro–Lucano. *Memorie della Società Geologica Italiana*, **8**, 453–763.

PESCATORE, T. 1988. La sedimentazione miocenica nell'Appennino campano–lucano. *Memorie della Società Geologica Italiana*, **41**, 37–46.

PESCATORE, T., RENDA, P. & TRAMUTOLI, M. 1988. I rapporti tra le Unità Lagonegresi e le Unità Sicilidi nella media valle del Basento, Lucania (Appennino meridionale). *Memorie della Società Geologica Italiana*, **41**, 353–361.

PESCATORE, T., RENDA, P., SCHIATTARELLA, M. & TRAMUTOLI, M. 1999. Stratigraphic and structural relationships between Meso-Cenozoic Lagonegro basin and coeval carbonate platforms in southern Apennines, Italy. *Tectonophysics*, **315**, 269–286.

PIEDILATO, S., PROSSER, G., PARENTE, M. & DOGLIONI, C. 2000. Stratigraphy and structural evolution of Lagonegro units from the Southern Apennines (Basilicata, Italy). *Memorie della Società Geologica Italiana*, **55**, 141–147.

RAMSAY, J. G. 1967. *Folding and Fracturing of Rocks*. McGraw–Hill, New York.

RAMSAY, J. G. 1981. Tectonics of the Helvetic Nappes. *In*: MCCLAY, K. R. & PRICE, N. J. (eds) *Thrust and Nappe Tectonics*. Geological Society, London, Special Publications, **9**, 293–309.

SCANDONE, P. 1967. Studi di geologia lucana: la serie calcareo-silico-marnosa e i suoi rapporti con l'Appennino calcareo. *Bollettino Società Naturalisti Napoli*, **76**, 1–175.

SGROSSO, I. 1988. Nuovi elementi per un più articolato modello paleogeografico nell' Appennino centro meridionale. *Memorie della Società Geologica Italiana*, **41**, 225–242.

SHINER, P., BECCACINI, A. & MAZZOLI, S. 2004. Thin-skinned versus thick-skinned structural models for Apulian carbonate reservoirs: constraints from the Val D'Agri Fields. *In*: NEEDHAM, T. & BUTLER R. W. H. (eds) *Oil and Gas in Compressional Belts. Marine and Petroleum Geology*, **21**(7), 805–827.

VANNUCCHI, P. & BETTELLI, G. 2002. Mechanisms of subduction accretion as implied from the broken formations in the Apennines, Italy. *Geology*, **30**, 835–838.

Tectonosedimentary evolution of the Plio-Pleistocene Sant'Arcangelo Basin (Southern Apennines, Italy)

M. BENVENUTI[1], M. BONINI[2], G. MORATTI[2] & F. SANI[1]

[1]*Dipartimento di Scienze della Terra, Università degli Studi di Firenze, Via G. La Pira 4, 50121 Firenze, Italy (e-mail: marcob@geo.unifi.it)*

[2]*CNR–Istituto di Geoscienze e Georisorse, Via G. La Pira 4, 50121 Firenze, Italy*

Abstract: This paper describes a new tectonosedimentary model for the evolution of the Plio-Quaternary Sant'Arcangelo Basin, located in the Southern Apennines of Italy. To this purpose, we carried out a new field survey of the basin fill, closely integrating stratigraphy, facies analysis, and structural and tectonic analyses. The geological map at 1:50 000 scale of the whole basin is the first result of this work. We present a new stratigraphic framework for the Sant'Arcangelo Basin succession, which has been subdivided into five major stratigraphic groups, classified as synthems, following the recognition of major basin-wide unconformities. The synthems include smaller-scale stratigraphic units, which are classified as depositional sequences or sub-synthems. These sub-units are composed of different lithofacies assemblages recording cyclic activation of fluvial, deltaic, shallow marine and lacustrine environments throughout the evolution of the basin. Integration of facies analysis and tectonic data led to the definition of a series of palaeogeographical sketches, encompassing the Piacenzian and late Pleistocene, which mark the main steps in the evolution of the Sant'Arcangelo Basin. Basin-scale hinterland-verging thrust faults and folds controlled the development of sub-basins and the progressive isolation of the Sant'Arcangelo Basin from the Ionian foredeep. The new model presented here defines the Sant'Arcangelo Basin as a triangular-shaped basin, bounded by oppositely verging thrusts. The hinterland-verging Valsinni thrust anticline limited its eastern margin and exerted a major control on the basin evolution.

The Mid-Pliocene–Pleistocene Sant'Arcangelo Basin (SAB, *c.* 1300 km^2) is located in the Southern Apennines of mainland Italy (Fig. 1). The SAB is one of the largest basins of the Apennines, and its occurrence at the rear of the leading edge of the chain implies a complex stratigraphic and tectonic control; this also makes the basin a key area for unravelling the regional deformation history of this sector of the Southern Apennines during Plio-Pleistocene times.

For the above reasons, we carried out a new detailed field mapping of the whole basin area, to integrate the available information (i.e. Carta Geologica d'Italia 1968, 1970, at 1:100 000 scale, Sheet 200 *Tricarico* and Sheet 211 *S. Arcangelo*). Because of the dynamic context in which the basin developed, our approach focused on the close integration of stratigraphy, facies, and structural and tectonic analyses. The stratigraphic approach was devoted to the distinction of unconformity bounded stratigraphic units, lithofacies analysis and sedimentary succession interpretation. At the same time we also identified the major active structures both at the basin margins and within the basin, which may have controlled the deposition and geometry of the whole basin. Although this approach may constitute a powerful tool to unravel evolutionary stages of the chain, the cultural separation between stratigraphic and structural researchers has prevented fully integrated studies. In this sense the map (see inside back cover of the volume) may also demonstrate the reliability and the advantages of this integration.

The Sant'Arcangelo basin is relevant also because it is part of a sector of the Southern Apennines where some of the most important onshore oil-fields of Europe occur (Costa Molina, Monte Alpi, Cerro Falcone; Mostardini & Merlini 1986; Sella *et al.* 1988; D'Andrea *et al.* 1993; Lentini *et al.* 1996; Pieri 2001; Casero 2004). The oil-fields are located in the chain to the west of the SAB, and exploit oil from the buried Apulian carbonates below the Apennines thrust pile (Cello *et al.* 1989; Pieri 2001; Casero 2004). To the east of the basin minor gas-fields exploiting the Pliocene foredeep sediments are located at the leading edge of the chain (Casero 2004).

This paper proposes a new scenario for the basin's development and, as shown in the map, indicates the major structures active during sedimentation, providing new useful insights for oil exploration.

Structural framework

The Southern Apennines fold-and-thrust belt has been developing since the late Palaeogene through

From: MORATTI, G. & CHALOUAN, A. (eds) 2006. *Tectonics of the Western Mediterranean and North Africa.* Geological Society, London, Special Publications, **262**, 289–322.
0305-8719/06/$15.00

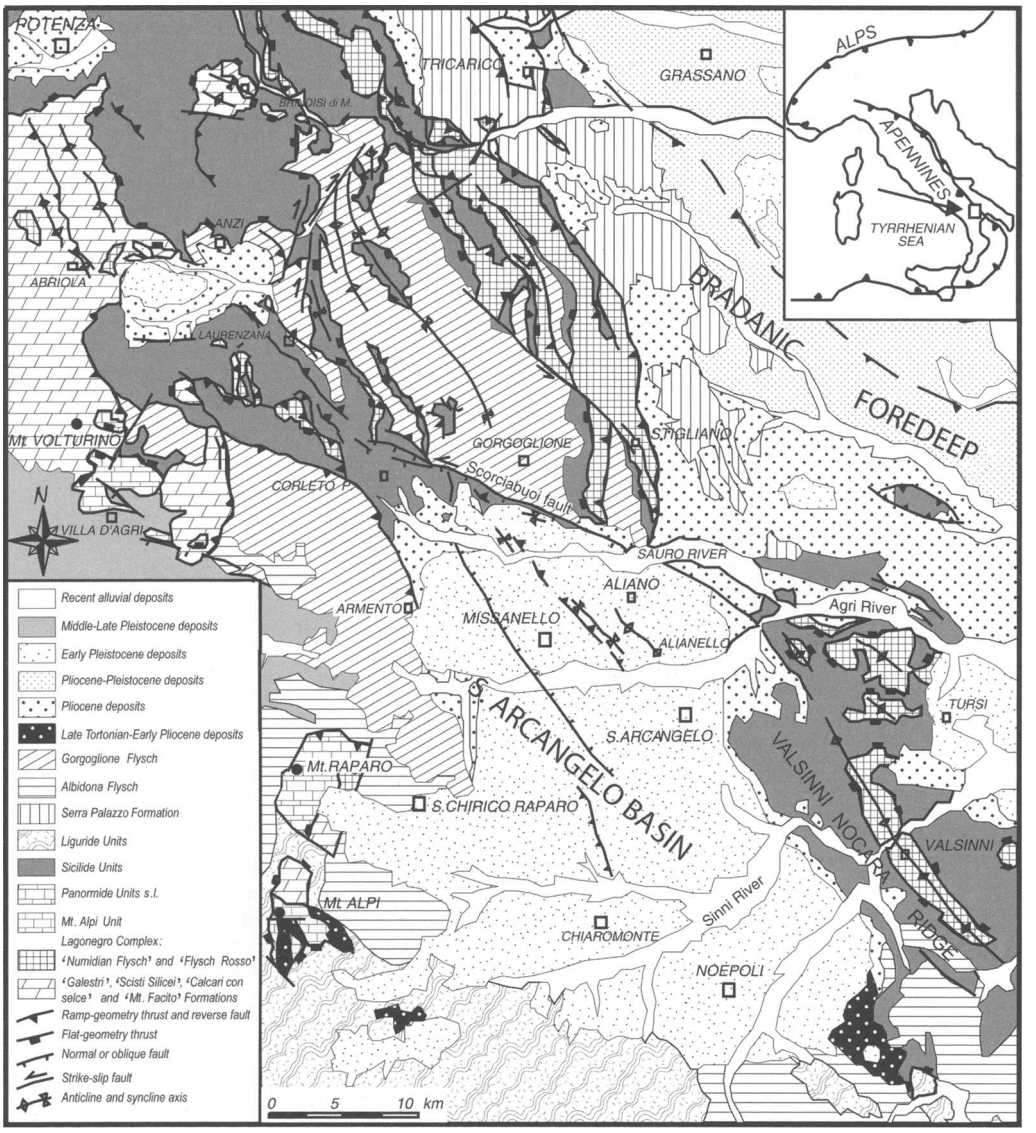

Fig. 1. Schematic geological–structural map of the Sant'Arcangelo Basin and adjoining areas of the Southern Apennines.

several tectonic phases in a geodynamic framework dominated by the subduction of the Ionian lithosphere beneath the Adriatic Plate (Malinverno & Ryan 1986; Royden *et al.* 1987; Patacca *et al.* 1990; Doglioni *et al.* 1994; Finetti *et al.* 1996; Cello & Mazzoli 1998).

Along the subduction margin, a stack of east-verging tectonic units forming an accretionary wedge made of Meso-Cenozoic sediments (Knott 1987) has been referred to different domains, ranging between basinal (Lagonegro) and shallow-water platform. These domains thrust onto the Apulian foreland to the east (Scandone 1967, 1975; Ogniben 1969*a*; D'Argenio *et al.* 1973, 1975; Pescatore & Slaczka 1984; Mostardini & Merlini 1986; Casero *et al.* 1988; Roure *et al.* 1991; Hippolyte *et al.* 1994*a*; Cello *et al.* 2000; Mazzoli *et al.* 2001). The Lagonegro basin is generally believed to have developed between two shallow-water carbonate platforms, the Apulian Platform to the east and the Panormide (or Western) Platform to the west (Mostardini &

Merlini 1986) although its original position is still debated (see discussion by Marsella *et al.* 1995). The Panormide Platform units thrust onto the Lagonegro units, and both are tectonically superimposed onto the Apulian units. Another important tectonic unit is the 'Sicilide Complex' (Ogniben 1969*a*), exposed throughout the Southern Apennines and recording most of the tectonic phases of the thrust belt (Lentini 1979; Cello *et al.* 1990; Carbone *et al.* 1991; Mattioni *et al.* 2006). In the southern sectors of the study area, different tectonic units belonging to the Liguride Complex (Ogniben 1969*a*) crop out. They are interpreted as the remnant of an accretionary wedge tied to the subduction of the Tethys oceanic crust (Knott 1987). These units are both metamorphic (Frido Unit) and non-metamorphic (Calabro Lucano Flysch and Saraceno and Albidona Formations) and experienced a complex structural history (Monaco *et al.* 1995).

The Southern Apennines fold-and-thrust belt developed at the same time as the Tyrrhenian basin opening, which is mostly related to back-arc extension (Boccaletti & Guazzone 1974; Scandone 1975, 1979; Malinverno & Ryan 1986; Royden *et al.* 1987; Ben Avraham *et al.* 1990; Boccaletti *et al.* 1990; Patacca *et al.* 1990; Roure *et al.* 1991; Hippolyte *et al.* 1995). The normal faults affecting the internal side of the fold-and-thrust belt are commonly tied to this extensional regime, which strictly followed the progressive eastward migration of the compressive front toward the Apulian foreland. Thrust-top basins, associated with the thrust system migrating toward the Apulian foreland, progressively developed from Miocene time (Casnedi *et al.* 1982; Pescatore 1988; Boccaletti *et al.* 1990; Patacca *et al.* 1990; Roure *et al.* 1991; Cello & Mazzoli 1998). Sedimentation continued at the leading edge of the chain in the Bradanic foredeep. The Plio-Pleistocene marine thrust-top basins in the internal domain of the accreted tectonic wedge include the Ofanto, Potenza, Anzi-Calvello and Sant'Arcangelo basins (Vezzani 1967*a*; Patacca *et al.* 1990; Hippolyte *et al.* 1994*a*; Pieri *et al.* 1994; Patacca & Scandone 2001). From Early Pliocene time the Apulian Platform was involved in thrusting and gave rise to a duplex geometry constituting the buried Apulian Belt (Cello *et al.* 1989, 1990; Lentini *et al.* 1990, 2002; Roure *et al.* 1991; Catalano *et al.* 1993). This mode of accretion, at depth, transferred part of the deformation to the overlying Apennine chain, causing the development of out-of-sequence thrusting and the generation of syntectonic piggyback basins (Roure *et al.* 1991).

According to most workers, the latest Mid- to Late Pleistocene tectonic phases of the Southern Apennines result from strike-slip movements related to the SE shift of the Calabrian arc (Catalano *et al.* 1993, 2004; Monaco *et al.* 1998, 2001; Menardi Noguera & Rea 2000; Van Dijk *et al.* 2000; Cello *et al.* 2003). This causes an oblique convergence that is also accommodated by relevant block rotations (Sagnotti 1992; Scheepers *et al.* 1993; Mattei *et al.* 2004).

Previous interpretations of the Sant'Arcangelo Basin

Recently, several studies have investigated the Plio-Pleistocene Sant'Arcangelo Basin. At present, this basin is limited to the east by the Valsinni–Nocara ridge, and its northern border is affected by the Scorciabuoi Fault (Fig. 1). Both the stratigraphy of the basin sequence and the origin of the basin itself have been analysed and different interpretations have been proposed (Vezzani 1967*a*; Lentini 1979; Caldara *et al.* 1988; Casero *et al.* 1988; Turco *et al.* 1990; Catalano *et al.* 1993; Hippolyte *et al.* 1994*a*,*b*, 1995; Pieri *et al.* 1994; Zavala & Mutti 1996; Zavala 2000; Giannandrea & Loiacono 2003).

A first synthesis of the SAB evolution was given by Vezzani (1967*a*). On the basis of the available deep wells for hydrocarbon research, Vezzani considered the upper Pliocene–Pleistocene succession of the basin as continuous with that of the external foredeep basin (Bradanic trough). The lowermost Lower to Middle Pliocene portion was instead considered semi-autochthonous, because in several wells it was found to rest on a pile of Apenninic thrust sheets (Vezzani 1967*a*).

More recently, the SAB has been interpreted as a thrust-top basin in a dominantly eastward thrust propagation (Caldara *et al.* 1988; Casero *et al.* 1988; Hippolyte *et al.* 1991, 1994*a*; Roure *et al.* 1991; Pieri *et al.* 1994; Monaco *et al.* 1998, 2001; Patacca & Scandone 2001; Calabrò *et al.* 2002; Catalano *et al.* 2004).

An alternative hypothesis was proposed by Turco *et al.* (1990), who interpreted the SAB, as well as other adjoining basins, as a pull-apart basin connected to roughly NW–SE-trending sinistral strike-slip fault systems in the frame of the recent evolution of the entire Southern Apennines. The role of strike-slip tectonics in controlling basin deformation in Pleistocene times (i.e. after basin formation) has been also highlighted by other researchers, who interpreted the strike-slip faulting in relation to the latest evolutionary phases affecting the whole chain (Catalano *et al.* 1993, 2004; Monaco *et al.* 1998, 2001).

In a different model, Cippitelli (1997) and Merlini & Cippitelli (2001) related the uplift of the Valsinni–Nocara (or Rotondella) ridge to a

basic magmatic intrusion or a mantle bulge. Calabrò *et al.* (2002), instead, highlighted the important role of back-thrusting in lifting this ridge.

The sedimentary succession deposited within the SAB unconformably oversteps a substratum composed of the most important units constituting the Southern Apennines (Fig. 1). On the basis of fieldwork or interpretation of seismic lines different estimations were proposed for the maximum thickness of the SAB sedimentary fill, between 3000 and 5000 m (Vezzani 1967*a*; Mostardini & Merlini 1986; Casero *et al.* 1988; Hippolyte *et al.* 1994*a*; Pieri *et al.* 1996; Van Dijk *et al.* 2000; Merlini & Cippitelli 2001; Patacca & Scandone 2001; Calabrò *et al.* 2002; Catalano *et al.* 2004). The direction of migration of the SAB depocentre is also still debated: either NE (Caldara *et al.* 1988; Pieri *et al.* 1994) or SW (Hippolyte *et al.* 1994*a*; Patacca & Scandone 2001; Calabrò *et al.* 2002) directions have been proposed.

The stratigraphic setting from previous studies

Major developments in the stratigraphic subdivision of the Plio-Pleistocene SAB succession were significantly stimulated by geological mapping (Table 1). In the 1960s the work on the second edition of the Geological Map of Italy, at a scale of 1:100 000, gave new impetus to the stratigraphic analysis of this basin. In particular, Vezzani (1966*a*,*b*, 1967*a*,*b*) proposed a detailed lithostratigraphic subdivision of the deposits, recognizing for the first time a cyclothemic organization of the succession. The 'clays' and 'sands' established in the early geological maps (Crema *et al.* 1908) were subdivided into lithostratigraphically different shallow marine and coastal deposits. Furthermore, different gravelly units, not indicated before but magnificently exposed in the basin, were included in the new schemes and maps. Biostratigraphic calibration of marine units allowed a better chronological assessment of the SAB succession. Vezzani's results were largely included in the second edition of sheet 211, *S. Arcangelo* (Carta Geologica d'Italia 1970; see also Ogniben 1969*b*).

Vezzani's stratigraphy depicts two major transgressive–regressive sedimentary cycles, the first in Early to Mid-Pliocene time (i.e. the Caliandro cycle in Table 1) and the second in Late Pliocene to Early Pleistocene time. The succession is then characterized by fully terrestrial deposits indicating isolation of the basin from marine influence since the Mid-Pleistocene time. In its overall significance this conceptual scheme is still a valid reference for interpreting the sedimentary dynamics of the SAB. Nevertheless, successive stratigraphic revisions introduced further details in terms of different stratigraphic subdivisions including deposits not recognized before. The most significant stratigraphic schemes developed by various workers in recent decades are summarized and compared in Table 1. Major differences among these schemes and Vezzani's stratigraphy are indicated by: (1) increased reference to the cyclothemic architecture of the Plio-Quaternary succession, expressed by cyclic lithological and facies changes as well as by prominent unconformities, and illustrated by informal terms such as 'cycle' (Carbone *et al.* 1991; Pieri *et al.* 1994), 'group' (Zavala 2000; Carbone *et al.* 2005) or 'sequence' (Pieri *et al.* 1996), or by formal terms such as 'synthem' (Patacca & Scandone 2001; see also Giannandrea & Loiacono 2003 for the southern SAB) and 'allogroup' (Zavala & Mutti 1996); (2) attempts to better understand the depositional characters of the newly established units based on facies analysis (Pieri *et al.* 1994; Zavala & Mutti 1996; Zavala 2000; Patacca & Scandone 2001); (3) the recognition of thick fluvio-lacustrine deposits in the northern SAB (Pieri *et al.* 1994; Zavala & Mutti 1996; Zavala 2000; Patacca & Scandone 2001; Carbone *et al.* 2005) that were missed in previous studies.

Following the chronostratigraphic calibration by Lentini and Vezzani (Lentini 1967, 1968, 1969*a*,*b*; Vezzani 1966, 1967*a*,*b*, 1968) significant revision of the biostratigraphy of the marine deposits was carried out in the last 10 years (Figs 2 and 3). Consistent data were provided by Marino (1994, 1996) for the northern SAB and by Di Stefano *et al.* (2002) for the southern SAB to calibrate the age of two shelfal muddy units marking the major marine incursions in the SAB. The 'marly clay' of the Caliandro Cycle (Pieri *et al.* 1994) and the 'blue marly clay' of the Caliandro Group (Carbone *et al.* 2005) date back to the Piacenzian–Gelasian (Figs 2 and 3). The 'silty clay' of the Agri and Sauro cycles (Pieri *et al.* 1994) and the 'grey–blue marly clay' of the S. Arcangelo Group (Carbone *et al.* 2005) are referred to the Gelasian–early Pleistocene (Figs 2 and 3). A similar calibration has been provided, for the same marine mudstones (Table 1), by Patacca & Scandone (2001) and Guerrera & Coccioni (1984), the latter referring specifically to biostratigraphic dating of mudstones and intervening siliceous deposits exposed on the eastern margin of the basin (Figs 2 and 3).

The chronological calibration of the Quaternary terrestrial deposits is more problematic, with the exception of the fluvio-lacustrine deposits first documented by Caldara *et al.* (1988) in the northern SAB. These deposits contain tephra layers and vertebrate remains that allow some chronological considerations. A tephra in the upper part of the lacustrine deposits yielded a K/Ar age of

Table 1. *Comparison between selected stratigraphic schemes proposed for the Plio-Pleistocene succession of the SAB*

Vezzani, (1966, 1967a, 1967b)	Italian Geologic Map, scale 1:100,000 sheet 211 " S. Arcangelo" (1970)	Carbone et al. (1991)	Pieri et al. (1994)	Zavala & Mutti (1996); Zavala (2000)	Carbone et al. 2005	Patacca & Scandone (2001)
Serra Corneta Conglomerate and Sand	Serra Corneta Conglomerate and Sand	Serra Corneta Conglomerate and Sand	Serra Corneta Conglomerate and Sand		Serra Corneta Conglomerate and Sand	Serra Corneta Conglomerate
Castronuovo Conglomerate	Castronuovo Conglomerate	*Upper Pliocene-Pleistocene cycle*: Castronuovo Conglomerate	*S. Lorenzo (fluv.-lac.) cycle*: " upper conglom." "lacustrine clay" "lower congl, — *Sauro cycle (marine)*: "congl. and sand" "sand" "silty clay"	Profico Group: Fluvio-lacustrine gravel, sand and mud	Guardia Perticara Group: Guardia Perticara conglomerate and sand / S. Lorenzo lacustrine deposits	Castronuovo Conglomerate / S. Lorenzo Clays
Aliano Sand	Aliano Sand	Aliano Sand	*Agri cycle*: "conglomerate and sand" / "sand" / "silty clay"	T2 weathered alluvial gravel	S. Arcangelo Group: Castronuovo Conglomerate / Aliano Sand	Sinni Synthem (Fan-delta deposits)
"blue marly clay"	"blue-grey marly clay"	"blue-grey marly clay"		Tursi Group: T1 Fluvio-deltaic gravel and sand		Sarmento Synthem Lagoonal and prodelta mudstones Fan-delta deposits
S. Giorgio Lucano Sand	S. Giorgio Lucano Sand	S. Giorgio Lucano Sand		A2 Fluvio-lacustrine gravel, sand and clay	Grey-blue marly clay and S. Giorgio Lucano Sand	S. Arcangelo sandstones
				Aliano Group: A1 Fluvio-deltaic gravel and sand and shelfal clay		Shelf mudstones
Caliandro cycle: "upper conglomerate" / "yellow sand" / "blue marly clay" / "basal conglomerate"	"blue-green marly clay" / "yellowish sand" "brackish marly clay" / "basal conglomerate"	*Mid-Upper Pliocene cycle*: "sandy matrix conglom." / "grey-yellow sand" / "marly clay" / "conglomerate and sand"	*Caliandro cycle*: "sand and conglomerate" / "marly clay" / "conglomerate and sand"	Caliandro Group: C2 brackish clay / C1 delta-front sand shelf clay delta-front sand alluvial gravel	Caliandro Group: Grey-Yellow Sand / Blue Marly Clay / White Diatomaceous Clay / Conglomerate, Sand and Calcarenites / Brackish Clay	Prograding fan-delta front deposits and shallow marine sandstones / P_{1-2} Lagoonal, prodelta and shelf mudstones / Diatomitic clays / Fan-delta front deposits and marine bars

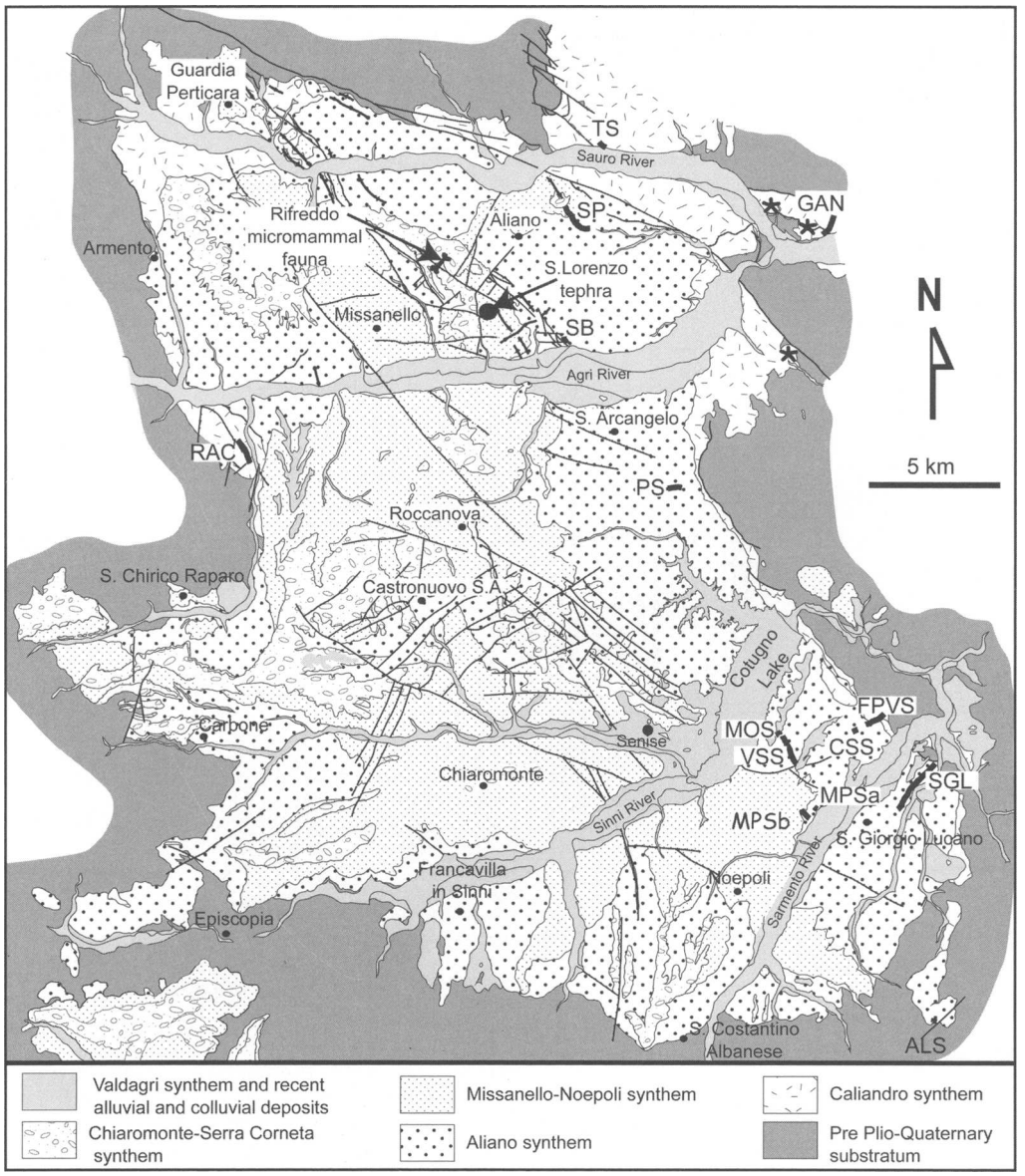

Fig. 2. Simplified geological map of the Sant'Arcangelo Basin showing the location of the biostratigraphic sections. Sources of dating: Rifreddo micromammal fauna (Masini *et al.* 2005); S. Lorenzo tephra (Caggianelli *et al.* 1992); RAC, TS and SGL biostratigraphic sections (Marino 1994); SP, SB, PS biostratigraphic sections (Marino 1996); FPVS, CSS, MOS, VSS, MPSa, MPSb, ALS biostratigraphic sections (Di Stefano *et al.* 2002); CAN biostratigraphic section (Guerrera & Coccioni 1984); biostratigraphic samples on diatomaceous mud (lithofacies Ce) are indicated by asterisks (this paper).

1.1 ± 0.3 Ma (Caggianelli *et al.* 1992) whereas a micromammal fauna sampled on strata above the dated tephra biochronologically points to an early mid-Pleistocene age (Masini *et al.* 2005; Sabato *et al.* 2005; Figs 2 and 3). Recent magnetostratigraphic analyses on this lacustrine succession (Sabato *et al.* 2005) apparently confirm the time span including the latest early and the earliest mid-Pleistocene.

This published dataset is integrated and discussed later within the stratigraphic framework proposed in this paper.

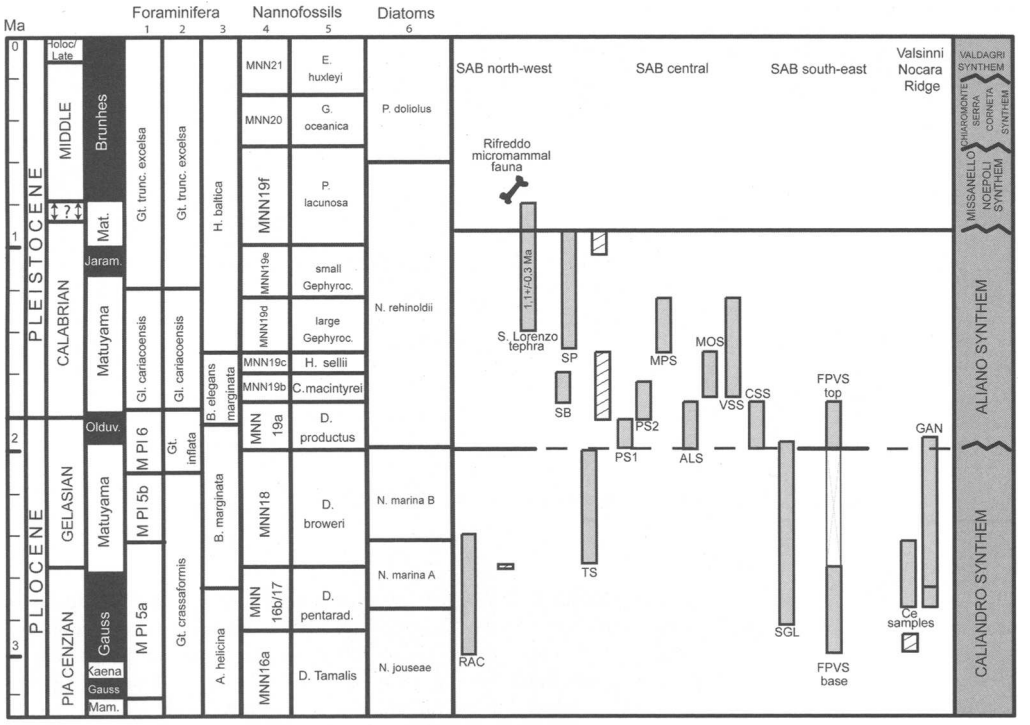

Fig. 3. Chrono- and biostratigraphic calibration of the units defined in this study based on biostratigraphic dataset available in the literature and on biostratigraphic analysis performed in this study on lithofacies Ce. Location and sources of data are given in Figure 2 with the exception of data from Patacca & Scandone (2001) (hatched bars). Biostratigraphic scale sources: 1, Cita (1975 emended); 2, Colalongo & Sartori (1979); 3, Colalongo *et al.* (1982); 4, Martini (1971); 5, Rio *et al.* (1990); 6, Barron (1985) and Baldauf & Iwai (1995).

A New Stratigraphic Framework for the Sant'Arcangelo Basin

Methods of stratigraphic subdivision

The final aim of this study, largely based on field mapping, is to exploit the surface geology to define a new tectonosedimentary model for the Plio-Quaternary basin evolution. The map at 1:50 000 scale of the whole basin is therefore a fundamental document to illustrate the model presented.

Lithofacies analysis and correlation of unconformities have been selected as the primary criteria for stratigraphic subdivision and geological mapping. A similar approach is widely adopted in the modern stratigraphic analysis and 'interpretative' stratigraphies (i.e. Exxon sequence stratigraphy, genetic stratigraphy, transgressive–regressive sequence stratigraphy, etc.), or bounding surfaces-based stratigraphies (allostratigraphy: North American Commission on Stratigraphic Nomenclature 1983; unconformity-bounded stratigraphic units: Salvador 1994), provide suitable tools to subdivide the SAB Plio-Quaternary succession (Fig. 4).

Unconformable surfaces of different rank may be recognized within the SAB succession, making possible the adoption of both synthems and depositional sequences for stratigraphic subdivisions.

Major unconformities mark: (1) subaerial truncation of older deformed strata; (2) stratigraphic hiatuses, which in a few cases (see Fig. 3) may be resolved through biostratigraphic analysis; (3) significant depositional changes expressed by the lithofacies stacking pattern. On the basis of these features, the SAB succession is subdivided into five synthems (Salvador 1994) although some specification is needed for the two older Caliandro and Aliano synthems. The Caliandro basal and the Aliano upper bounding unconformities can be traced basinwide whereas the bounding surface of the two units shows physical change along the depositional dip. An angular unconformity separates the two units at the basin margins, and biostratigraphic data from the SE margin of the basin (FPVS section, Figs 2 and 3) indicate a significant

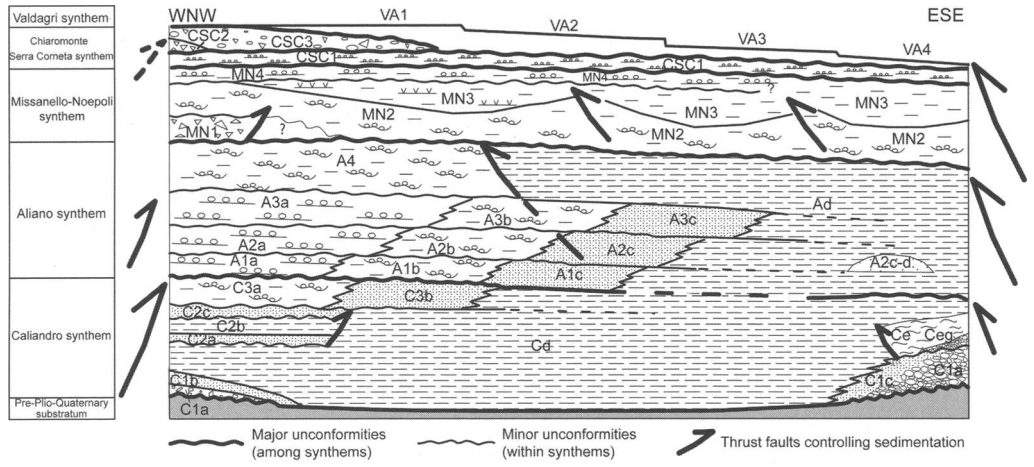

Fig. 4. Tectonostratigraphic scheme showing the relations between the units defined in this study (not to scale).

hiatus between the two units related to the erosion of the Caliandro deposits. Biostratigraphic data (Figs 2 and 3) indicate that in the central and southeastern portions of the basin the transition between the Caliandro and Aliano deposits is gradual, thus their bounding surface is stratigraphically concordant. Mixed diagnostic characters of the bounding surfaces make these units hybrid with respect to the synthem and the depositional sequence. Nevertheless, the use of synthems for classifying and mapping these units is chosen because of the discordant stratigraphic contact invariably observed at the basin margins.

Minor unconformities allow us to subdivide the five synthems into sub-units, again taking into account the physical character of the bounding surfaces alternatively expressed by: (1) low-rank angular unconformities that are traced over the entire area of exposure of specific lithofacies coinciding with the whole basin or structurally separated portions of the basin; in these cases the sub-units are classified as sub-synthems (Fig. 4); (2) low-rank angular unconformities that can be traced along the depositional dip into correlative concordant surfaces; in this case the sub-units are classified as depositional sequences including different lithofacies associations indicating progressive progradation (e.g sequences C3 and A1–3) or backstepping (e.g. sequence C1) of fluvio-deltaic systems in the basin (Fig. 4).

Following Mutti & Sgavetti (1987) the depositional sequences established within the Caliandro and Aliano synthems may be referred to as the 'tectonic' type, that is, packages of strata formed under variable sediment supply in which accommodation changes result mostly from tectonic deformation. When long-term sediment supply keeps pace with the tectonic subsidence creating accommodation, these types of depositional sequence display a typical overall coarsening-upward progradational trend made up of smaller-scale fining-upward units. A similar lithofacies stacking pattern will be discussed in the following sections as one of the lines of evidence of a dominant syntectonic control on the SAB sedimentary dynamics.

Description of the mapped units

Caliandro synthem (Piacenzian–Gelasian)

This includes deposits resting unconformably on the pre-Pliocene substratum and separated from the Aliano synthem by an angular unconformity at the basin margins passing into a conformable contact basinward (map and Fig. 4). Low-rank unconformities recognized along the basin margins allow a further subdivision into three smaller-scale unconformity-bounded units, C1–C3 (map and Fig. 4).

The deposits included in this synthem are muds, sands and subordinate gravels reaching a maximum thickness of about 1000 m.

Biostratigraphic data from previous studies (Marino 1994; Patacca & Scandone 2001; Di Stefano *et al.* 2002) allow us to confidently refer this synthem to the Piacenzian–Gelasian (Figs 2 and 3).

Terrestrial or shallow marine deposits. Depositional sequence C1 is formed by three main lithofacies assemblages, which from base to top are (Fig. 5) as follows.

Fig. 5. Panoramic view of the basal Caliandro synthem at the western SAB margin, along the Agri River valley. White lines indicate major unconformities.

C1a. Gravels resting on the substratum units along the western and eastern margins of the basin. They are polymodal, well-rounded to sub-angular, clast-supported, locally rich in silty–clayey matrix (e.g. on the western margin along the Agri River valley; see map). These deposits are massive to poorly bedded and their thickness does not exceed 20 m.

C1b. Sands mostly exposed along the western and northern margins of the basin (map and Fig. 4). They are yellowish, medium- to fine-grained, rich in bioclasts (pectinids, ostreids, etc.) and generally arranged in metre-thick, internally massive, beds.

C1c. Sands, silts and diatomaceous clays exposed along the eastern margin (map 1 and Fig. 4). The sands are yellowish, medium- to fine-grained in massive or normal graded decimetre- to metre-thick beds. The clays are dark to pale grey and generally massive, locally characterized by intervening whitish diatomaceous silt.

Sub-synthem C2 is represented by three vertically stacked lithofacies associations, exposed exclusively along the western margin, and bounded at the base and top by angular unconformities. From base to top the lithofacies associations are as follows.

C2a. Sands cropping out in the Agri River valley (Fig. 5) and as an isolated outcrop north of Armento village (map). In the Agri River valley sands are coarse- to medium-grained in decimetre to metre-thick massive, normal graded beds. In the north Armento outcrop sands are coarser, and also contain small pebbles; they are arranged in decimetre- to metre-thick trough or hummocky cross-stratified (HCS) beds.

C2b. Massive muds resting abruptly on lithofacies C2a. These deposits are dark grey as a result of the occurrence of dispersed organic matter and contain scattered mollusc remains mostly represented by *Cerastoderma* sp.

C2c. Sands exposed locally on the western margin along the right flank of the Agri River valley (map). They are coarse- to medium-grained in decimetre- to metre-thick beds characterized by trough cross-lamination.

Depositional sequence C3 consists of two lithofacies associations (C3a, C3b) resting on older deposits at an angular unconformity that changes to sharp and gradual contacts toward the east (Fig. 4).

C3a. Gravels, sands and silty clays exposed mainly on the western margin along the Agri and Armento valleys (map). Gravelly and sandy beds define a fining-upward trend. Gravels are polymodal, clast-supported, arranged in metre-thick lenticular beds erosively resting on the silty clays. Sands are coarse- to medium-grained, and are massive or normal graded. Silty clays are greyish–whitish and generally massive.

C3b. Sands cropping out on the western margin along the Agri and Sauro River valleys (map). They are medium- to fine-grained in decimetre to metre-thick beds, and are massive or cross-laminated. Scattered clay chips, pebbles and mollusc fragments are occasionally present at the base of beds.

Shelfal terrigenous and siliceous deposits. Cd. Massive silty clays and marls characterized by a dispersed macrofossil content represented by marine molluscs scattered or concentrated in thin shell beds.

Ce. This lithofacies consists of massive and subordinately planar laminated whitish diatomaceous silts exposed locally in a few locations on the northeastern margin of the basin (map). Gravels Ce_g, locally (e.g. Monticchio area, confluence of the Sauro and Agri rivers) underlying the Ce deposits, are poorly bedded, polymodal, moderately to well rounded, clast-supported with abundant interstitial sandy–silty matrix.

With respect to previous studies, these deposits are differently regarded in both (1) lithostratigraphic and (2) biostratigraphic terms.

(1) Lithofacies Ce corresponds to deposits previously ascribed to the Piacenzian–Gelasian 'Caliandro' (Guerrera & Coccioni 1984; Patacca & Scandone 2001; Carbone *et al.* 2005) and to 'Lower Pliocene' (Ogniben 1969*b*; Carbone *et al.* 1991) successions. In those studies diatomaceous deposits have been considered conformably stacked within marine mudstones. Guerrera & Coccioni (1984), for instance, reported an apparently concordant succession including diatomaceous muds exposed in two outcrops (Fiumarella and Gannano sections) along the Agri River valley. In contrast, our survey indicates that Ce rests unconformably over a pre-Pliocene substratum as well as over the lowermost portion of the Caliandro synthem, whereas the contacts with overlying deposits are invariably tectonized. In the Gannano outcrop (Fig. 6a and b), two west-verging thrust faults affect a succession including the pre-Pliocene substratum, lithofacies C1a, Cd and Ce. The easternmost fault, superimposing Cd onto Ce, lies on a covered portion of the section reported by Guerrera & Coccioni (1984), thus disproving the stratigraphic continuity claimed for this succession.

(2) Siliceous deposits are characterized by an open marine microfauna including diatoms, sponges and radiolarians (Guerrera & Coccioni 1984) not used before for biostratigraphic calibration. Dating of these deposits was based on Foraminifera assemblages suggesting a reference to the 'Middle' Pliocene (Guerrera & Coccioni 1984; Figs 2 and 3). Patacca & Scandone (2001), integrating Foraminifera and nannoplankton assemblages in the mudstones to the base and to the top of these deposits (Figs 2 and 3), placed the diatomaceous mud within the middle portion of the Piacenzian (2.99–2.83 Ma interval). Three samples of diatomaceous mud, collected in this study (Fig. 2), yielded a rich marine diatom assemblage dominated by *Thalassithrix–Thalassionema nitzschioides* forms including also *Azpeitia nodulifer* and large Coscinodiscaceae. The co-occurrence

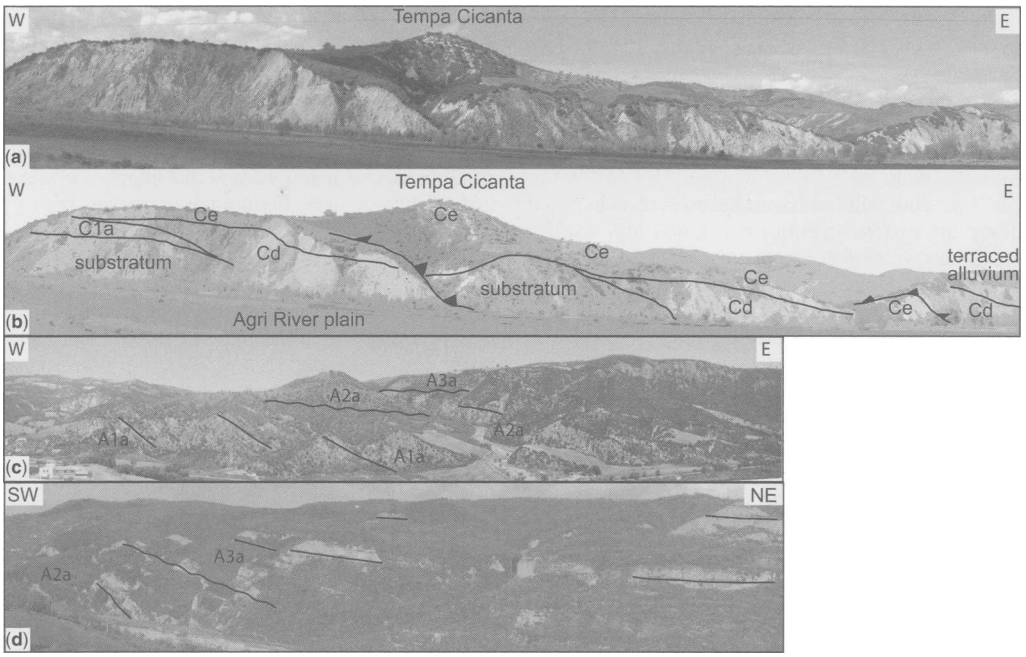

Fig. 6. (**a**) Panoramic view of the Tempa Cicanta–Gannano outcrop and (**b**) interpretative line drawing showing stratigraphic and structural relations between Ce and older deposits. (**c**) and (**d**) show basinward fanning and wedging of Upper Pliocene–Lower Pleistocene unconformity-bounded stratigraphic units (A1–A3) along the western Sant'Arcangelo Basin margin. (c) Agri River section; (d) Sarmento River section.

of *Thalassiosira oestruptii*, *Th. convexa* var. *aspinosa* and *Nitzschia reinholdii* constrains these deposits between the *T. convexa* subzone C and the *N. marina* subzone A. The lack of *N. fossilis* and of *N. jouseae* excludes respectively the *Th. convexa* subzone C and the *N. jouseae* zone, limiting the deposition of Ce to the *N. marina* subzone A, that is, between 2.77 and 2.41 Ma (Fig. 3). Finally, based on the co-occurrence of *G. crassaformis* and *A. helicina* (Gannano section, Guerrera & Coccioni 1984; GAN in Figs 2 and 3) the deposition of Ce is more precisely bracketed between 2.77 and 2.63 Ma, hence slightly later in Caliandro time with respect to the calibration of Patacca & Scandone (2001).

Aliano synthem (Gelasian–lower Pleistocene)

This synthem, widely exposed in the basin, rests partially unconformably on the Caliandro synthem and is separated from the overlying Missanello–Noepoli synthem by a basin-wide unconformity (map and Fig. 4). Low-rank unconformities recognized within the Aliano synthem along the basin margins allow a further subdivision into four smaller-scale unconformity-bounded units, A1–A4. This synthem is composed of gravelly, sandy and muddy deposits up to about 1500 m thick. Biostratigraphic data from previous studies (Marino 1996; Patacca & Scandone 2001; Di Stefano *et al.* 2002) allow us to confidently refer this synthem to the late Gelasian–early Pleistocene (Figs 2 and 3).

Terrestrial or shallow marine deposits. A stratigraphically complex clastic wedge, developed mostly from the western margin to the central SAB (map), includes sub-units A1–A4, which are described as follows.

Depositional sequences A1–A3. Because of lithological and sedimentological similarities these sub-units are described together. West to east transitions from angular unconformities to sharp and gradual stratigraphic contacts characterize the lateral–vertical relations among these sub-units throughout the basin. Intervening deposits are grouped into recurring gravelly, sandy and pelitic lithofacies associations, which depict a genetic linkage among coeval depositional systems (see below). These sequences are composed of three recurring lithofacies associations.

A1–A3a (Fig. 6c and d). Gravels and subordinate sands in decimetre- to metre-thick beds arranged in tabular bedsets 10–15 m thick, amalgamated, or separated by thin (1–2 m thick) sandy silty beds. Gravels, brownish and subordinately reddish (A1a) in colour, are polymodal, clast-supported with abundant interstitial sandy–silty matrix, and imbricated showing a palaeoflow from the western margin. Beds are commonly amalgamated with basal low-relief erosive surfaces, internally massive or with low-angle planar cross-lamination. Sands, occurring as residual lenses within the gravelly beds, are coarse- to medium-grained, and are massive or horizontally laminated.

A1–A3b (Fig. 7a). Gravels, sands and silty clays that express lateral (toward the east) and vertical transition from lithofacies A1 to A3a. Gravelly and sandy beds define a fining-upward trend. Gravels are polymodal, clast-supported and arranged in metre-thick lenticular beds erosively resting on the floodplain silty clays. Sands are coarse- to medium-grained and massive or normal graded. Silty clays are greyish–whitish–reddish (A1b) and generally massive.

A1–A3c (Fig. 7b). Sands and clayey silts mostly exposed in the central sector of the basin (map). Sands are coarse- to fine-grained in decimetre- to metre-thick beds arranged in 10–15 m thick tabular bedsets. Sands are massive, and are locally horizontally and cross-laminated. A2c is typically characterized by shallow marine molluscs (*Glycimeris*, pectinids, ostreids) dispersed or concentrated in thin shell beds and pockets of articulated specimens. Locally clay chips occur at the base or within the beds. Clayey silts occur on top of sandy bedsets defining a fining-upward stacking pattern. These deposits are generally massive and increase in thickness toward the east. At S. Giorgio Lucano the upper portion of a sandy body referred to as an A2 delta front fed from the SSW is characterized by different lithofacies (A2d) (map and Fig. 4). These consist of coarse- to medium-grained sands characterized by trough cross-lamination and low-angle laminations in decimetre-to metre-thick beds with erosive base and subordinate intervening greyish sandy silts containing a marine molluscan fauna.

Sub-synthem A4. This is made of gravels, sands and silty clays (Fig. 8a) exposed in the WSW portion of the basin (map). Gravels and sands are arranged in decimetre- to metre-thick beds stacked within bedsets up to 15 m thick. Gravels range in size from cobble to pebble, are characterized by a clast-supported framework with abundant sandy–silty interstitial matrix, and occasional clast imbrication indicates palaeoflows from the WSW. Gravelly beds are massive or crudely normal graded and rest on silty clays at high-relief erosive surfaces. Sands occur as small lenses within gravels or locally form bedsets up to 15 m thick. Silty clays are greyish, arranged in bedsets up to 30 m thick in the easternmost outcrops (i.e. around Francavilla in Sinni village; see map), generally massive locally and containing organic-rich sediments, terrestrial molluscs and rare volcaniclastic beds.

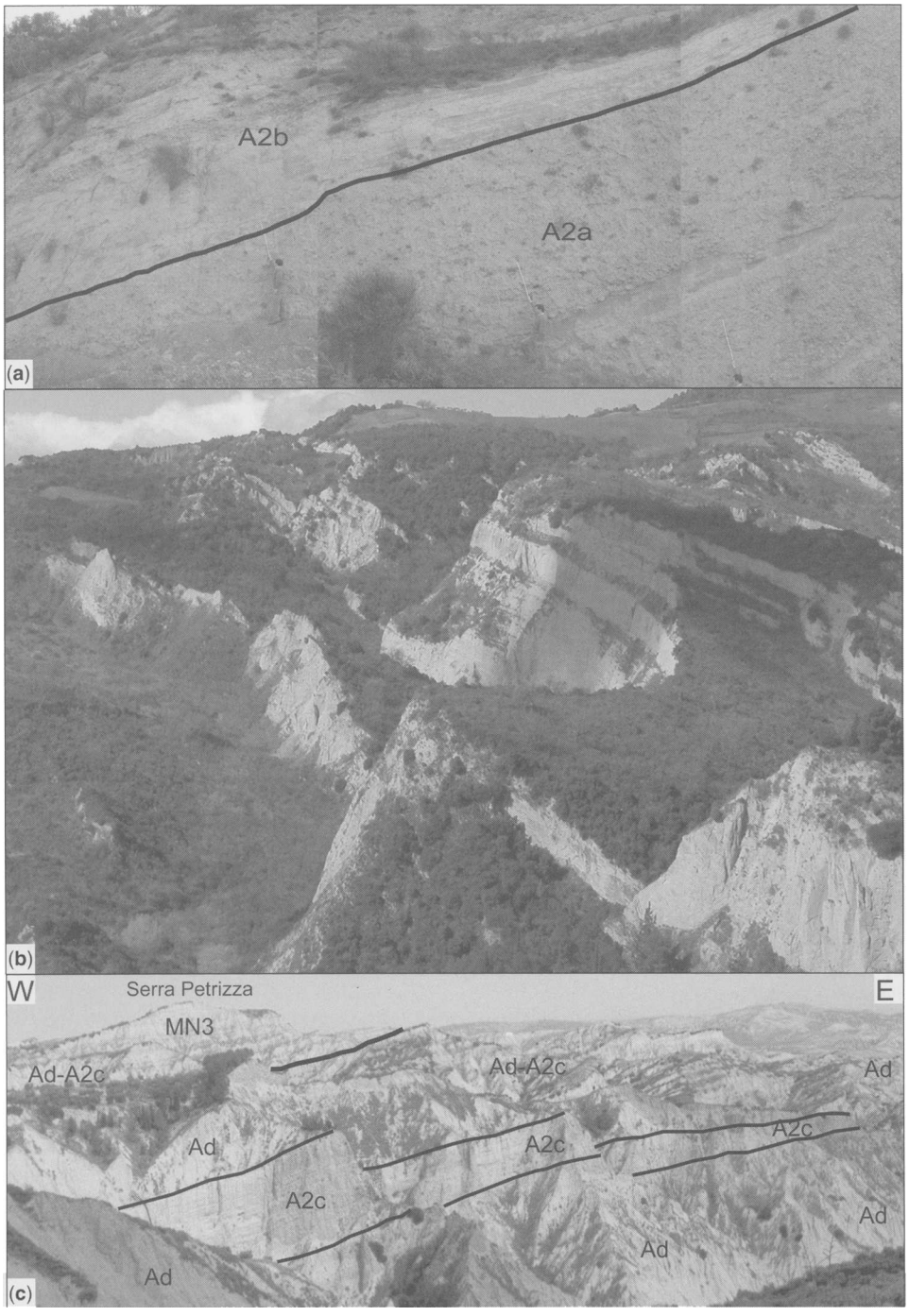

Fig. 7. (**a**) Vertical transition between lithofacies A2a and A2b, southern side of the Sauro River valley. Person for scale. (**b**) Panoramic view of lithofacies A2c, around Aliano village. The thick stacked sandy bedsets indicate a proximal delta front. (**c**) Panoramic view looking east from Aliano village; Serra Petrizza is in the background. In the foreground the pinching-out of A2c strata embedded within Ad muds marks the depositional transition between the delta front and the prodelta–shelf environments.

Fig. 8. (**a**) Panoramic view of sub-synthem A4 near Carbone village showing alternation of gravelly and muddy bedset; outcrop is about 30 m high. (**b**) Panoramic view of sub-synthem MN2 along the Serrapotamo River valley. Alternation of gravelly and muddy bedsets is the characteristic feature of this unit, indicating the rhythmic activation of gravel-bed river channel and muddy floodplain. The outcrop is about 20 m high. (**c**) CSC1 trough cross-bedded gravels and subordinate sands cropping out at Serra Petrizza. Hammer for scale.

Shelfal deposits. Ad. Silty clays (Fig. 7c), extensively exposed in the central–eastern sector of the basin (map), massive with dispersed marine molluscs, mostly bivalves (venerids). In the southern sector of the basin along the Sarmento River (map) the uppermost strata contain a brackish molluscan fauna marked by the dominance of *Cerastoderma*.

Missanello–Noepoli synthem (uppermost lower–lowermost middle Pleistocene)

The deposits included in this synthem are subdivided into four main sub-units (MN1–MN4) basing on the occurrence of low-rank unconformities within the synthem. Chronological calibration to the latest early–earliest mid-Pleistocene is constrained by the early Pleistocene age of the Aliano synthem and by the early mid-Pleistocene age of the micromammal fauna (Masini *et al.* 2005; Sabato *et al.* 2005) sampled in sub-unit MN3.

The four sub-units and the constituting lithofacies associations are, from base to top, as follows.

Sub-synthem MN1. This sub-unit crops out locally in the Racanello Creek valley west of S. Chirico Raparo (map and Fig. 4). It consists of angular to sub-angular gravels, ranging in size from boulder to pebble, rich in a clayey–silty matrix. Clasts are predominantly derived from the Albidona Flysch (Af) and subordinately from the Apenninic Platform (Ap) lithologies. These deposits are crudely bedded massive or normal graded, up to 200 m thick.

Sub-synthem MN2. Gravels in bedsets up to 20 m thick alternating with yellowish sandy–clayey silts (Fig. 8b) resting on MN1 as well as on older synthems at high-relief erosional surfaces (map and Fig. 4). Gravelly bedsets consist of decimetre- to metre-thick amalgamated beds of polymodal clast-supported cobble–pebble-sized gravels with abundant sandy–silty interstitial matrix. These deposits are massive to crudely normal graded. Sandy–clayey silts are generally massive.

Sub-synthem MN3. Greyish–whitish silty clays dominant on fluvio-deltaic sands and gravels that onlap the previous lithofacies association (Fig. 9a). Fine-grained sediments, forming bedsets up to 20 m thick, are generally massive, in places horizontally laminated (Fig. 9b). Decimetre- to metre-thick

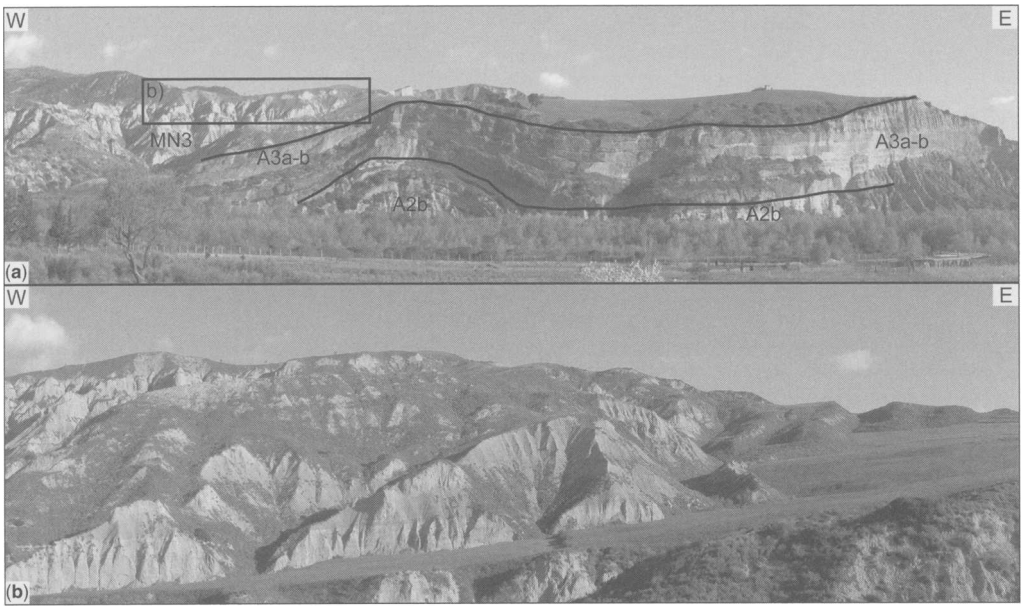

Fig. 9. (**a**) Panoramic view of a west-verging anticline magnificently exposed along the Agri River valley. Stratigraphic relations between Aliano and Missanello–Noepoli synthems are indicated. (**b**) Typical outcrop of lithofacies MN3 (see inset in (a) for location).

volcaniclastic and organic-rich beds are locally present (Rifreddo–S. Lorenzo creeks; see map). Vertebrate, mostly micromammal, remains, terrestrial–palustrine molluscs and root traces are locally present (Masini *et al.* 2005; Sabato *et al.* 2005). Coarse- to medium-grained sands occur in decimetre- to metre-thick tabular beds arranged in bedsets up to 20 m thick. Sands are massive to planar or trough cross-laminated. Pebble-sized gravelly beds are locally interbedded with sands.

Sub-synthem MN4. Gravels and sands in tabular metre-thick beds alternating with floodplain sandy–clayey silts in bedsets up to 15 m thick. Gravels are clast-supported with abundant sandy matrix. Planar cross-stratification is locally present.

Chiaromonte–Serra Corneta synthem (middle Pleistocene)

This synthem, about 100 m thick, rests unconformably on the Missanello–Noepoli synthem and is bounded at the top by an erosional surface and locally by remains of a reddish palaeosol. The reference to the middle Pleistocene is constrained by the age of the underlying Missanello–Noepoli synthem. Three sub-synthems have been identified, from base to top, as follows.

Sub-synthem CSC1. Gravel and subordinate sands in tabular decimetre- to metre-thick beds locally with planar or trough cross-lamination (Fig. 8c). Gravels are clast-supported, moderately to well imbricated. Total thickness is about 50–60 m.

Sub-synthem CSC2. Breccia of angular and subangular boulder- to pebble-size cemented gravel. This unit is exposed locally in the Racanello Creek valley at the base of Mount Raparo (map). Clasts are mostly of limestones and dolostones of the Apenninic Platform unit (Ap). Thickness does not exceed 15 m.

Sub-synthem CSC3. Deeply weathered angular to subrounded gravel and sandy silt in centimetre- to metre-thick lenticular beds. Total thickness does not exceed 30 m.

Valdagri synthem (uppermost middle–upper Pleistocene)

This synthem is made of terraced alluvial gravels and sands developed throughout the progressive incision of the drainage systems within the older SAB deposits to the present hydrography. It is composed of four sub-synthems (VA1 the oldest, VA4 the youngest; map and Fig. 4) attesting to the development of alluvial plains followed by incision caused by the progressive lowering of base level. The thickness of each sub-synthem varies from 1 to 10 m.

Tectonosedimentary Evolution

Stage 1: Caliandro synthem palaeogeography and tectonics

Deposits included in the Caliandro synthem record four major sub-stages (1a–1d) of depositional dynamics strictly related to the active deformation of the basin margin and schematically represented in Figure 10a–d.

Sub-stage 1a. The distribution of lithofacies associations in the lower part of the Caliandro synthem indicates a significant physiographic differentiation between the western and northern margins and the eastern and southeastern margins (Fig. 10a). Basal coarse-grained alluvial deposits (lithofacies C1a), characterized by relatively better textural organization, point to alluvial depositional systems, specifically short rivers dominated by hyperconcentrated flood-flows (Benvenuti & Martini 2002; Benvenuti 2003), which drained the early SAB margins. The texturally disorganized gravels, locally exposed along the western margin, indicate deposition from subaerial debris flows at the base of slopes (see Zavala & Mutti 1996; Zavala 2000). Later, different depositional systems developed on the western and eastern margins in response to relative sea-level rise. Lithofacies C1b is referred to deltaic and shoreface environments in which the dominant processes

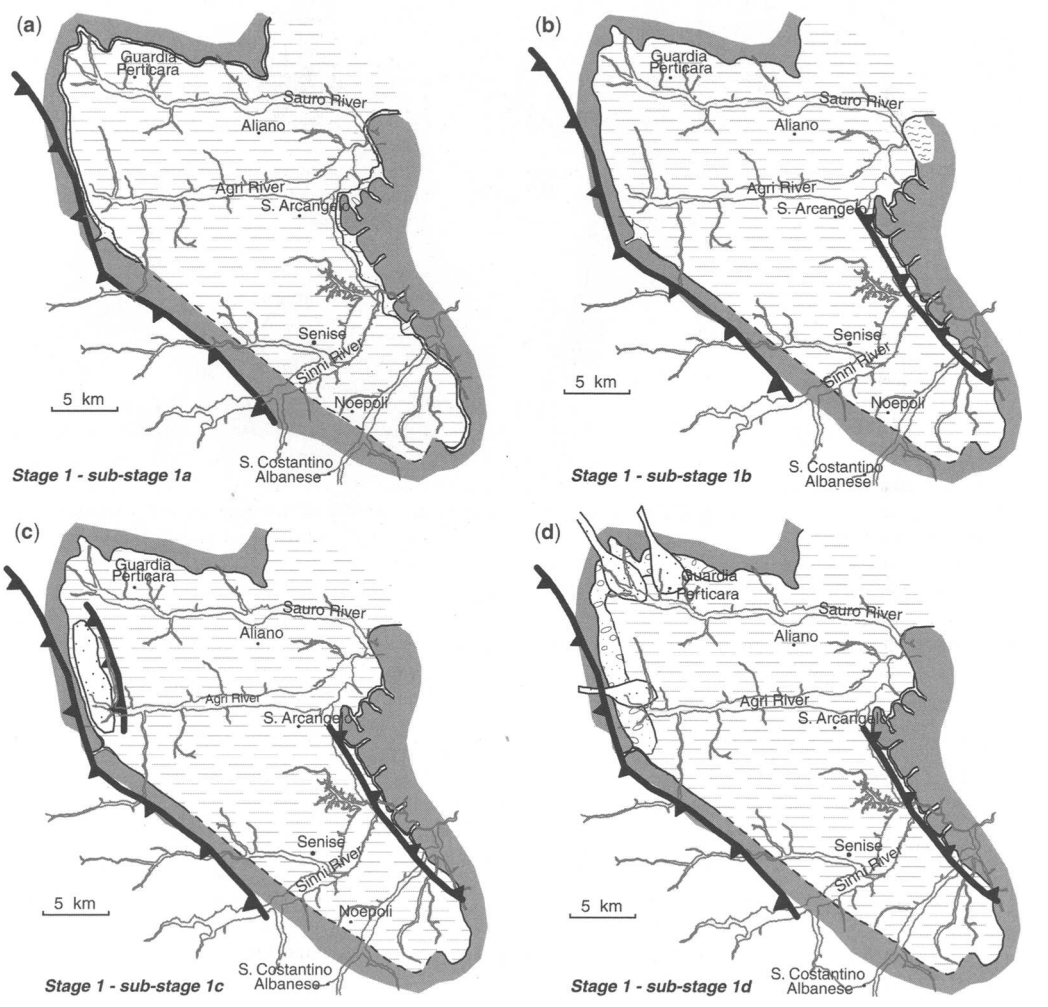

Fig. 10. Palaeogeographical sketches showing the development of the SAB (see text for details). Active thrusts during each sub-stage are indicated (see text for details).

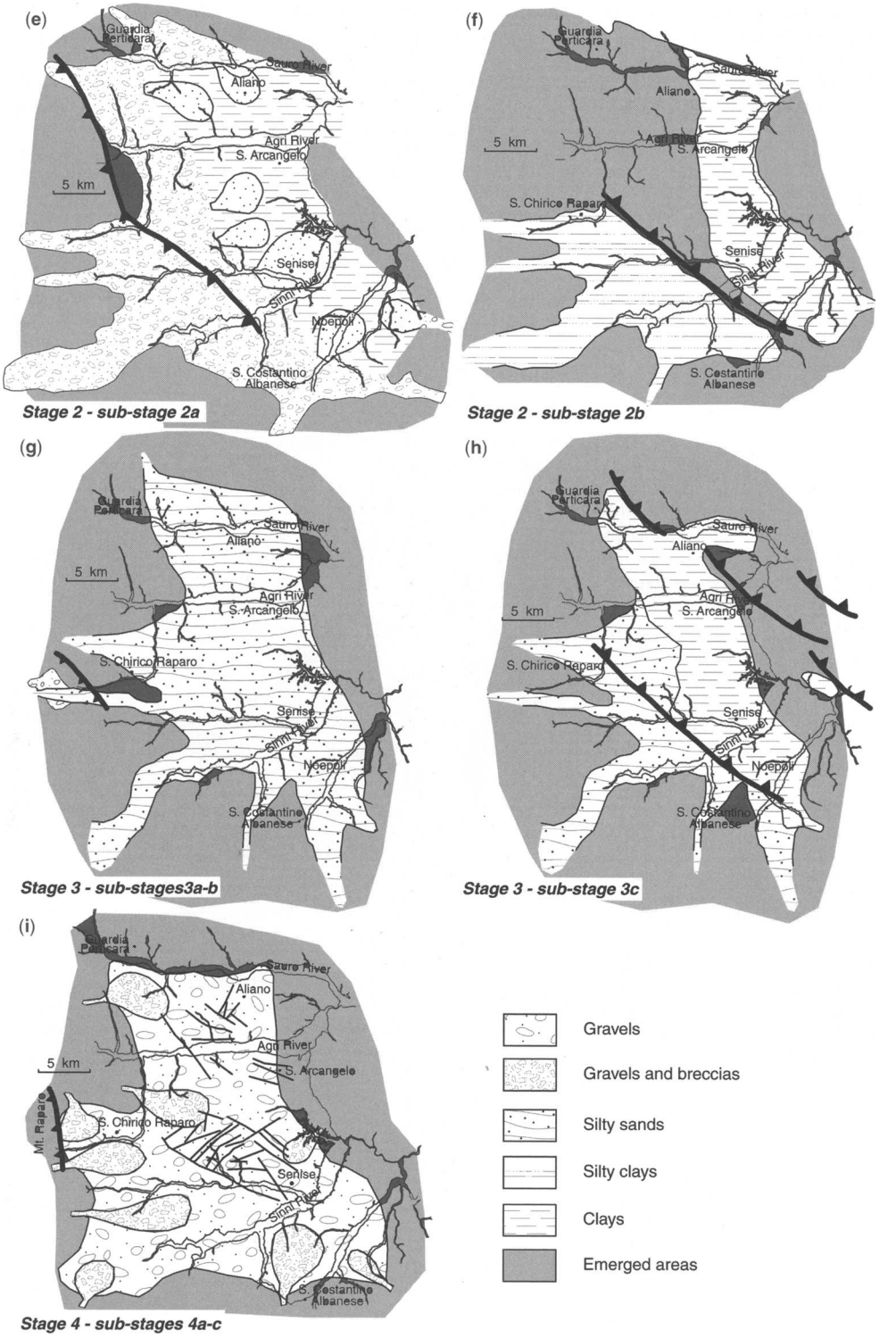

Fig. 10. (*Continued*)

were related to river flood-derived hyperpycnal flows, longshore currents and bioturbation caused by the invertebrate benthic fauna.

Lithofacies C1c, occurring along the eastern margin, is interpreted to record delta plains dominated by deposition of sands from traction currents, settling of fine material and accumulation of organic matter. From a general perspective, the development of relatively wide delta plains facing the Caliandro sea points to a slow subsidence in comparison with the western margin, which was instead characterized by a narrow shoreline system suggesting higher subsidence rates. Active growth of east-verging compressive structures along the western margin is also proven by wedging of strata within lithofacies C1a, C1b and Cd on outcrops exposed on the right side of the Agri River valley (Fig. 5).

Sub-stage 1b. The transgressive trend indicated by the transition from C1a to C1b–c culminated with a widespread marine flooding of the marginal areas and development of prodelta–inner shelf environments (Fig. 10b) recorded by lithofacies Cd. These settings were characterized by deposition from the dilute tails of hyperpycnal flows and sediment settling. Sediments were greatly affected by bioturbation caused by the invertebrate fauna thriving on the bottom.

The peculiar deposit Ce points to an open and deep (see Guerrera & Coccioni 1984) marine setting in the area connecting the SAB to the Ionian foredeep (Fig. 10b), characterized by biogenic deposition in a time of high productivity of siliceous organisms.

At the same time the observed unconformable contacts with the underlying deposits indicate that Ce deposition also followed an early deformation of the eastern basin margin. We suggest therefore that during the early–mid-Piacenzian (pre 2.77 Ma) the eastern margin underwent a first significant uplift pulse related to the incipient activity of west-verging thrust faults along the Valsinni–Nocara ridge (Fig. 10b). Besides their limited occurrence, Ce_g gravels may account for a rejuvenation of relief created by this deformative pulse. These deposits are ascribed to a short river draining the Gannano–Monticchio area and characterized by hyperconcentrated flood-flows.

Sub-stage 1c. Active tectonism along the western margin interfering with deposition is documented by deposits of sub-synthem C2. The three vertically stacked lithofacies associations C2a–b–c record the growth of an east-verging thrust fault generating a small satellite basin, which becomes progressively isolated from the open sea (Fig. 10c). Lithofacies C2a is referred to as a delta front prograding in the Caliandro sea during the early growth of the thrust fault. This environment was dominated by fluvial flood-driven hyperpycnal flows responsible for the massive settling of sands. HCS beds may have resulted from sediment reworking by storm currents or alternatively from tractional–oscillatory hyperpycnal flows (Mutti *et al.* 1996). Lithofacies C2b is referred to as a confined brackish-water body developed between the Agri and Armento rivers during the growth of the east-verging thrust with consequent progressive separation from the sea. It was an area dominated by quiet settling of fine-grained deposits and bioturbation. Finally, lithofacies C2c points to the overfilling of the small satellite basin. It is interpreted to record shallow fluvial channels filled by the downcurrent migration of sinuous-crested dunes.

Sub-stage 1d. The final deposition of the Caliandro synthem occurred in fluvio-deltaic systems widely developed on the western–northwestern margin of the SAB (Fig. 10d). Lithofacies C3a is interpreted to record an alluvial plain; gravelly and sandy beds point to fluvial channels characterized by hyperconcentrated flood-flows as indicated by textural features and lack of tractional structures, whereas mudstones were deposited in a fluvial floodplain mostly through sediment settling. Lithofacies C3b is related to delta fronts dominated by hyperpycnal flows possibly generated by river floods (Mutti *et al.* 1996).

During or immediately after this period a significant change in the basin's deformation took place, as west-verging thrust faults within the basin also took part in the basin deformation and evolution.

Tectonic remarks

The SAB activation marks a significant phase in the structural development of the Southern Apennines during the latest Zanclean–earliest Piacenzian. Core data from the Ionian foredeep (Balduzzi *et al.* 1982) indicate that the Southern Apennines chain–foredeep system underwent a significant northeastward tectonic transport during the Early Pliocene. Correlation of core data across the Valsinni–Nocara ridge (Fig. 1) demonstrates that Liguride and Sicilide units were thrust onto Lower Pliocene shelf deposits resting unconformably on the Apulian Platform units. The Lower Pliocene deposits thus represent an older foreland basin. In this perspective, the early SAB developed initially as a satellite basin, possibly a piggyback basin (*sensu* Ori & Friend 1984), partially connected to the Ionian foredeep. The present distribution of the deposits included within the Caliandro synthem provides some indication of the early basin geometry. Deposition during this stage certainly occurred throughout the northern and

eastern SAB margins, whereas along the western margin the deposition is documented up to the present Nocito River valley. Here the lithofacies C1b onlaps the folded Gorgoglione Flysch, documenting a possible narrowing toward the south of the SAB (map). Seismic images in the central portion of the SAB show onlaps of the reflectors in the lower basin fill (reasonably belonging to the Caliandro synthem) onto a buried structural high around Castronuovo S. Andrea village (Patacca & Scandone 2001) (see also cross-section 2 in the map).

Since its activation, the SAB was affected by syn-depositional deformation at both margins. Thrust activity along the western SAB margin is clearly documented in this stage, by: (1) the NE-directed overthrusting of the substratum (Gorgoglione flysch) onto the Caliandro deposits (lithofacies Cd; Carbone *et al.* 1991; Pieri *et al.* 1994; map and Fig. 11a); (2) the thrust-related deformation in the lithofacies C3a along the Armento River (Monaco *et al.* 2001; map and Fig. 11b); (3) the development in the Nocito area of a minor satellite sub-basin, the site of deposition and deformation of sub-synthem C2a-c (map).

The dominant eastward propagation of thrust faults was matched by the activation of west-verging thrusts along the western margin of the Valsinni–Nocara ridge. This event is documented by (1) the angular truncations between lithofacies Cd and Ad observed along this margin, and (2) the deposition, on the same margin, of siliceous sediments Ce into sub-basins controlled and lifted by back-thrust faults associated with the Valsinni–Nocara ridge (Map). The western structural vergence of the Valsinni–Nocara ridge and eastern SAB margin associated with back-thrusting (Calabrò *et al.* 2002) is also indicated by the bedding attitude of the Caliandro synthem deposits. These are often severely dislocated, reaching a sub-vertical (or locally overturned) attitude along the eastern SAB margin (unit Cd; see map).

Stage 2: Aliano synthem palaeogeography and tectonics

The end of Caliandro synthem sedimentation coincided with a period of strong tectonic activity of the SAB margins that uplifted and tilted the onlapping Caliandro deposits. At the beginning of the Aliano synthem deposition, therefore, fluvial erosion affected the western margin with the development of west–east- trending deep river valleys downcutting within the Caliandro synthem to the north (Figs 10e,f and 12) and to the pre-Pliocene substratum to the south. Major valleys developed (1) north of Sauro river, (2) between the Sauro and Agri rivers, (3) in the Racanello Creek area, (4) in the Serrapotamo Creek area, and (5) along the present Sinni and (6) Sarmento rivers (map). With the exception of the palaeo-river between the current Sauro and Agri river valleys, the other entry points for fluvial clastic input to the basin coincide more or less with the present hydrography, thus indicating a persistent, transverse, drainage of the Southern Apennines since the late Pliocene. These fluvial systems fed sandy deltas facing the offshore portion of the SAB (Fig. 10e). In general, fluvio-deltaic systems tracts are represented by the recurring gravelly–sandy lithofacies association within depositional sequences A1–3. Small-scale angular unconformities and continuous rejuvenation indicated by the lithofacies architecture within each sub-unit are interpreted as the result of a syndepositional tectonic control.

On the eastern margin, instead, there is no evidence of significant fluvial rejuvenation and the shelfal Ad lithofacies onlap directly the pre-Pliocene substratum, without intervening coarse-grained deposits. This setting possibly reflects the west-verging morphostructural asymmetry of the Valsinni–Nocara ridge. Well-developed drainage occurred on the relatively gentler eastern side, as documented by fluvio-deltaic gravels and sands in the Tursi area (Fig. 1) coeval with the Aliano synthem (see Patacca & Scandone 2001), but not on the steeper western flank. Preliminary work has also shown the existence of progressive unconformities in the Tursi sands, gently dipping eastwards (10–20°), consistent with the syndepositional uplift of the hanging wall of the west-verging Valsinni thrust anticline (Fig. 11d).

Two main sub-stages mark the basin development during this period.

Sub-stage 2a. Gravelly, gravelly–muddy and sandy lithofacies associations characterizing sequences A1–3 can be traced from the western margin to the central portion of the basin, indicating genetic links between different depositional systems (Fig. 10e).

Textural and bedding features of lithofacies associations A1–3a, together with the high relief of the primary bounding unconformities, suggest deposition within fluvial valleys dominated by a discontinuous regime of discharge and abundant sediment supply. These fluvial systems were in many parts similar to the present 'fiumare', which are the typical seasonal, high-gradient, river systems of the Southern Apennines. These rivers were possibly characterized by a network of shallow and wide channels feeding gravelly lobes in a plain largely inactive between major flood events. Textural features and sedimentary structures suggest that sediment transport occurred in shallow,

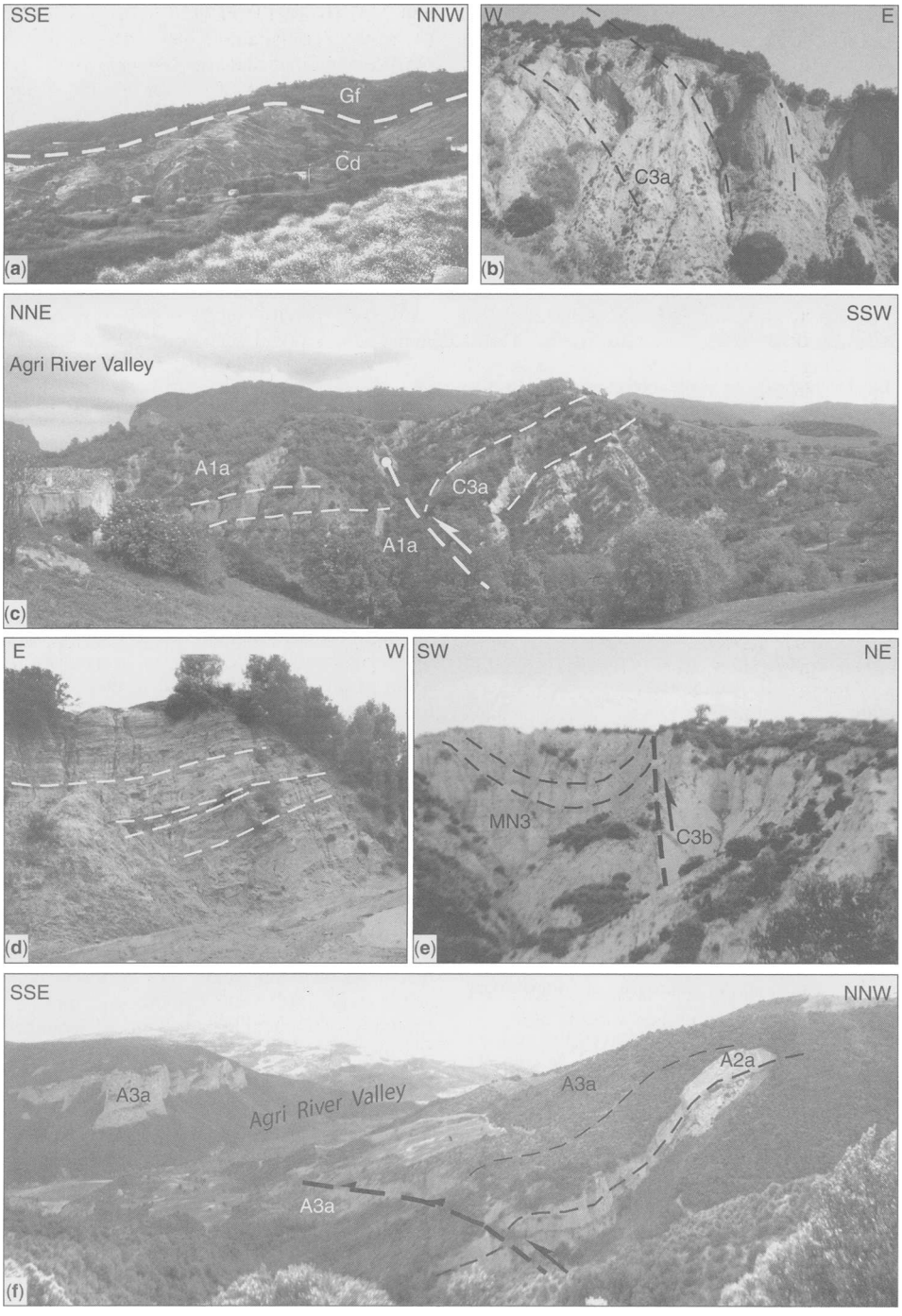

Fig. 11. Examples of thrust-related deformation in the Sant'Arcangelo Basin. (**a**) Overthrusting of the Gorgoglione Flysch (Gf) onto the Caliandro deposits (Cd; north of Armento village). (**b**) Thrust-related folding in the Unit C3a (south of Armento village). (**c**) NE-verging blind thrust superimposing Unit C3a onto Unit A1a (near the confluence between Agri and Nocito rivers; Masseria Pantolino in the foreground). (**d**) Progressive unconformities within the Tursi sands (Tursi village area). (**e**) Back-thrust superimposing the marine sands of Unit C3b onto the continental deposits of Unit MN3 (Sauro River area). (**f**) Late SE-verging thrust fold affecting Units A2a and A3a.

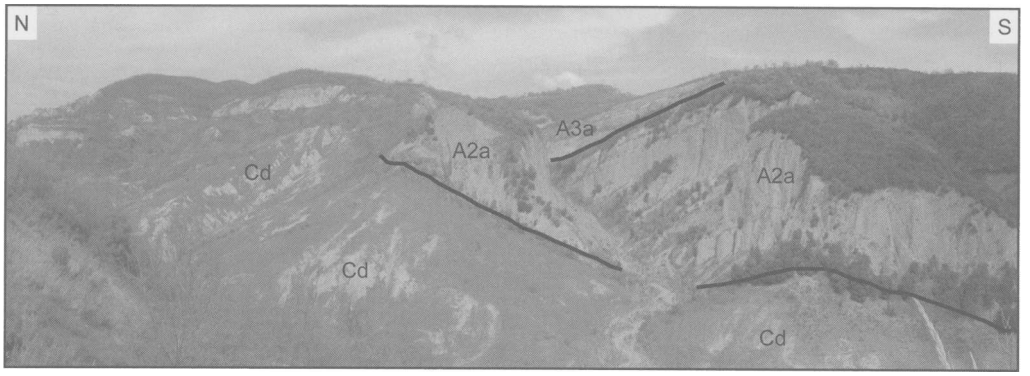

Fig. 12. The high-relief erosive contact between the Aliano and Caliandro synthems outlining the southern flank of a wide palaeovalley, developed in early Aliano time and exposed along the present Armento River valley.

poorly confined, highly concentrated flood-flows. Critical to supercritical flow regime is suggested by horizontal and low-angle inclined bedding. This depositional setting is in agreement with the hypothesis of catastrophic flood-dominated river systems of Mutti *et al.* (1996) and Zavala & Mutti (1996) for the gravelly–sandy lithofacies forming their Aliano and Tursi group deposits (Table 1) approximately corresponding to the Aliano synthem.

Lithofacies A1–3a are vertically and laterally replaced by lithofacies A1–3b, which reflect depositional conditions of a fluvial plain dominated by variable sediment supply, recorded by the development of fining-upward facies successions. Gravels and sands testify to filling of wide and shallow channels followed by the establishment of a low-energy floodplain dominated by the settlement of fine-grained sediments (Fig. 10e). This architecture suggests a response to a relative base-level rise and energy decrease of distributary systems.

Delta fronts, in the distal portion of the systems tracts, are indicated by lithofacies A1–3c (Fig. 4). The predominantly sandy deposits (map) were delivered by the fiumara-like river systems to delta fronts during a progressive rise of sea level. These delta fronts were dominated by resedimentation of sands carried in high-density subaqueous flows, that is, hyperpycnal flows, triggered by river floods (see Mutti *et al.* 1996; Zavala & Mutti 1996; Mulder *et al.* 2003). Occasional mollusc content in sands of lithofacies A1–3c records a mechanical reworking of benthic palaeocommunities by coeval flood-derived hyperpycnal currents. This implies that lower shorefaces, not preserved along the depositional profile, were catastrophically eroded by hyperpycnal flows and redeposited at the delta fronts. A1–3c bedsets show cyclic fining-upward trends (Fig. 13), from sands to sandy silts, indicating a transition from proximal to distal delta fronts. In the distal location, that is, towards the east, delta front deposits display a lateral fining and wedging out within the prodelta–shelf Ad lithofacies (Fig. 7c).

Each sequence is composite, that is, made of several elementary depositional sequences (EDS, *sensu* Mutti *et al.* 1994), and formed through the following phases (Fig. 13).

(1) Rivers transverse to the western margin and deeply entrenched within older deformed deposits accumulated gravels within high-energy alluvial plains and delivered sands to the delta systems through high-magnitude floods.

(2) High-frequency relative fluctuations of sea level and sediment supply resulted in repeated transitions respectively from gravelly-dominated to mud-dominated alluvial plains and from proximal to distal delta fronts. The resulting deposits are stacked into basic cyclothemic units corresponding to elementary depositional sequences.

(3) Major deactivation of the fluvio-deltaic systems recorded by relatively thick Ad lithofacies interbedded within A1–A3c deposits reflects a sudden transgression and a relative maximum highstand of sea level.

Following Embry (2002), the stratigraphic architecture of each composite sequence may be also described adopting the concepts of transgressive–regressive sequence stratigraphy. Erosional unconformity related to fluvial rejuvenation (see point (1) above) would be a maximum regressive surface, whereas the regressive (i.e. the fluvio-deltaic gravelly–sandy wedge) and the transgressive (i.e the prodelta–shelf muds) systems tracts would represent the T–R depositional sequences (see point (3) above).

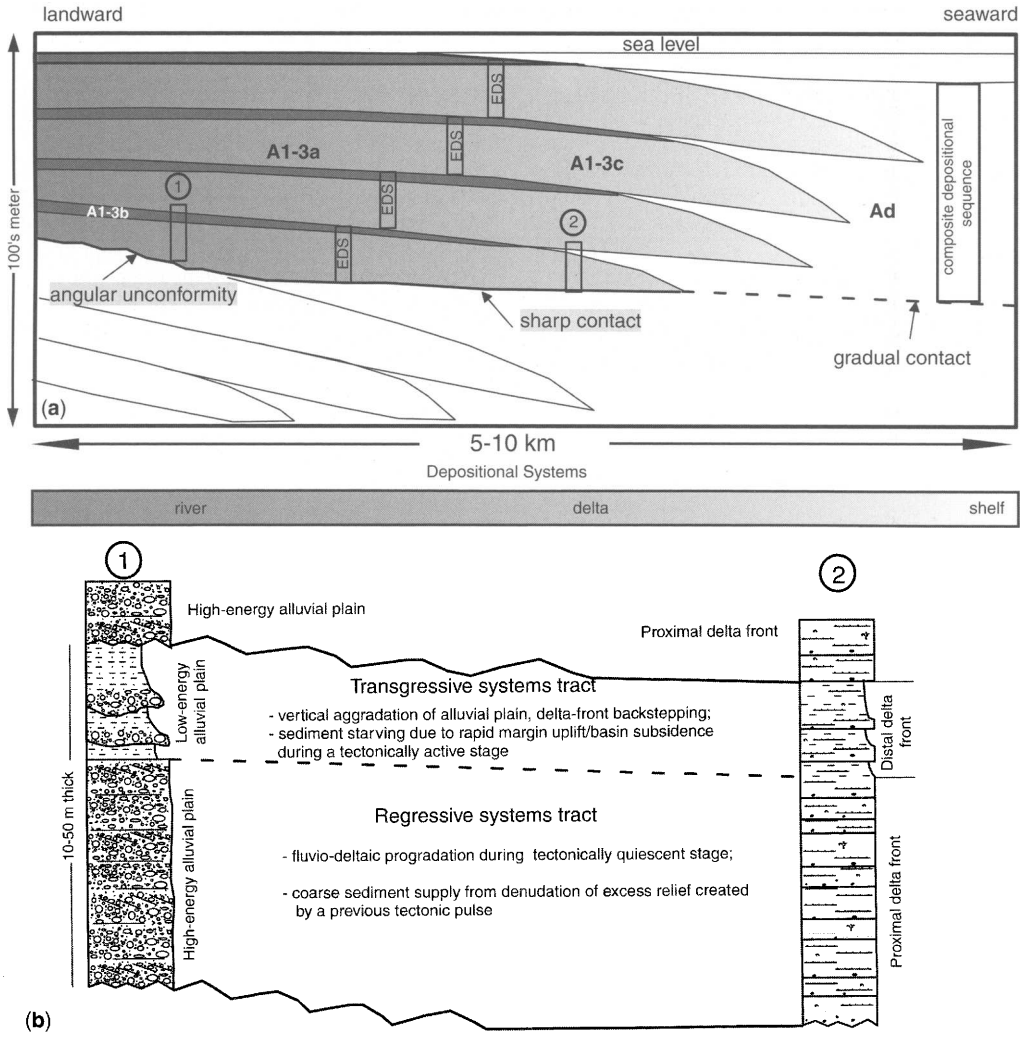

Fig. 13. (**a**) Conceptual scheme for the development of A1–3 depositional sequences. EDS, elementary depositional sequences. (**b**) Ideal correlation between the fluvial and deltaic systems tract in each EDS.

In other terms, the stratigraphic architecture of each Aliano sequence records an overall progradation of fluvio-deltaic systems punctuated by abrupt deactivations of coarse-grained supply to alluvial plains and deltas. The filling was ended by a major deactivation of the alluvial and coastal areas, causing the coarse-sediment starving of the shelf. The vertical and lateral facies stacking pattern suggests that changes of sediment supply and accommodation were jointly controlled by the uplifting and eastward-migrating sediment source, that is, the inner front of the Southern Apennines, and the rapidly subsiding SAB. Over a longer period, the A1–A3 wedge thus represents volumes of eroded Southern Apennines thrust belt accommodated in a subsiding thrust-top basin. Over a shorter period, the A1–3 sequences record high-frequency fluctuations of sediment supply and space accommodation. In terms of facies architecture, each EDS reflects an inverse correlation between coarse-grained sediment supply and creation of accommodation. During tectonically active stages rapid mountain uplift is not immediately followed by relief denudation; accommodation created by the associated basin subsidence is thus partially filled by fine-grained deposits. A

transgressive systems tract develops in this stage. During tectonically quiescent stages relief denudation provides enough sediment to fluvio-deltaic systems that prograde in the basin. A regressive systems tract is related to this stage.

This out-of-phase sedimentation pattern has been widely discussed and recognized to be a common feature in the sediment fill of basins developed in tectonically active regions (Blair & Bilodeau 1988; Paola *et al.* 1992). The basic concept of this hypothesis, coarse-grained transport and deposition during quiescent phases and fine-grained transport and deposition during tectonically active phases, appears in many parts similar to the uplift–denudation cycle invoked by Mutti *et al.* (1996) to explain the cyclothemic stratigraphy of basins developed in orogenic belts.

Sub-stage 2b. As mentioned above, west-verging reverse faults affected the central portion of the SAB, deforming the fluvial deposits of sequences A1–3 (Fig. 10f). Progressive growth of the associated relief determined the development of a satellite sub-basin within the SAB, as indicated by the deformation geometry and areal distribution of A4 deposits (Fig. 10f). Seismic images support the existence of this sub-basin (Fig. 14a and b).

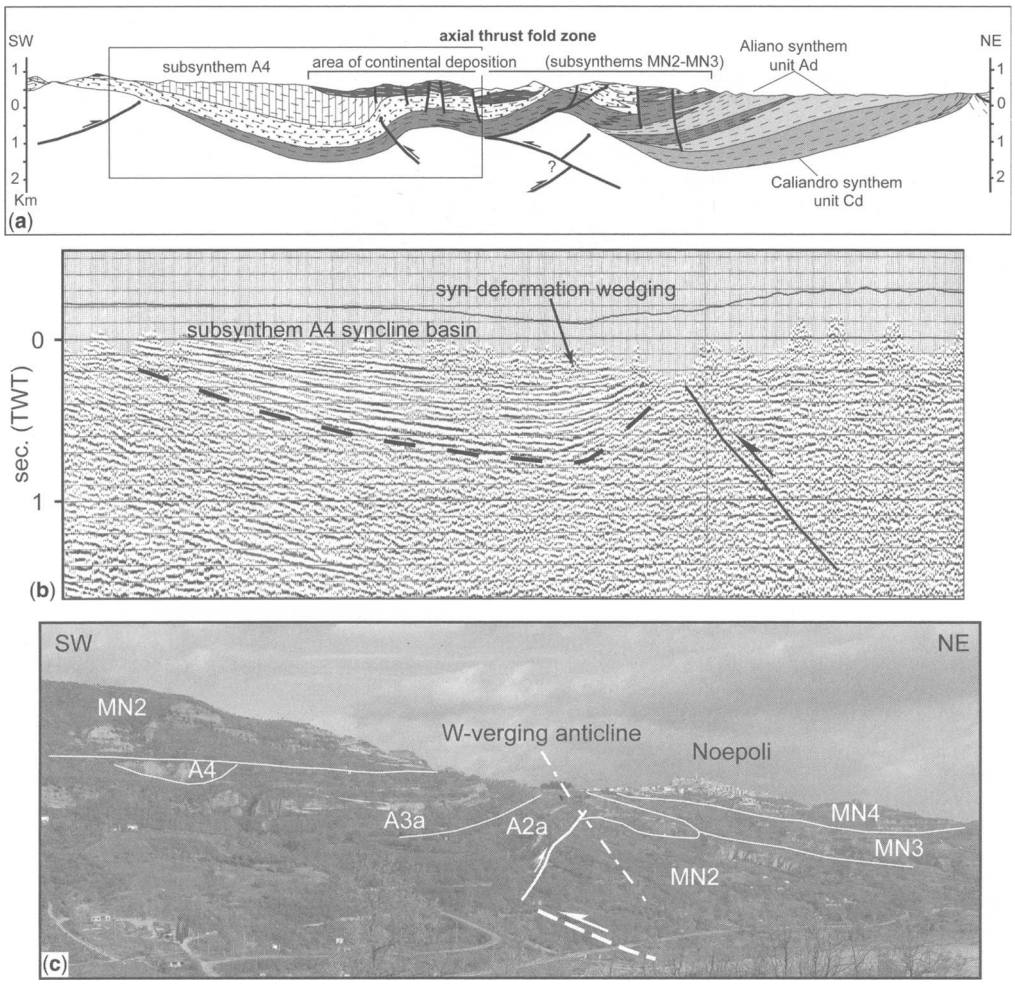

Fig. 14. (**a**) Geological cross-section (simplified from section C–C′ of the map) based on field surface data and seismic line interpretation. (**b**) Detail of a seismic line (approximately corresponding to the box in (a) showing the asymmetric syncline basin of sub-synthem A4 associated with back-thrust. Dashed line is the base of the sub-synthem A4 deposits. (**c**) West-verging blind thrust anticline affecting units A2a–A3a and sub-synthem A4 (Noepoli village in the background).

The A4 deposits represent an alluvial plain confined between the inner Apenninic front to the west and the S. Chirico Raparo–Noepoli alignments to the east (Fig. 10f). The A4 sub-synthem is characterized by a cyclothemic facies development indicating rhythmic fluctuation between alluvial gravelly channels and a muddy floodplain. This low-energy setting was characterized by waterlogging and locally by the development of ponds, such as around Francavilla in Sinni. As for the A1–3 sequences, this stratigraphic pattern is interpreted as the response to high-frequency uplift–denudation cycles (*sensu* Mutti *et al.* 1996). Active chain uplift–basin subsidence determined coarse sediment starving and fine-grained deposits filling the available accommodation space, whereas quiescent uplift–subsidence resulted in erosion of excess relief and distribution of coarse-grained supply to the alluvial plains. The occurrence of a satellite sub-basin implies that the residual Aliano sea was in large part starved of sediment supply from the western margin. Furthermore, the uppermost Ad strata indicate that the Aliano sea was becoming brackish toward the south, as proven by *Cerastoderma* remains around S. Giorgio Lucano; restricted conditions were prevalent to the north (Fig. 10f). In the Serra Petrizza section (SP in Figs 2 and 3; Fig. 15), Marino (1996) reported a micropalaeontological content decreasing upsection in abundance, variety and preservation; the scanty nannofossils suggest that the maximum extension for marine conditions occurred during the latest early Pleistocene age (zone MN19f). The restricted marine–brackish conditions in the late Aliano sea (corresponding to the Sauro Cycle of Pieri *et al.* 1994; Table 1) thus are interpreted as evidence for a progressive isolation of the SAB from the Ionian foredeep, in response to the tectonic growth of the Valsinni–Nocara ridge driven by continuing west-verging thrust fault activity (Fig. 10f). The transition between microfossiliferous and barren deposits at Serra Petrizza (Marino 1996; Figs 2 and 3) marks the unconformable stratigraphic contact between the Aliano and Missanello–Noepoli synthems. The same contact is recognized to the south in the transition observed between the *Cerastoderma*-bearing Ad and the lithofacies MN3 around S. Giorgio Lucano. Subsynthem A4 is unconformably capped by Missanello–Noepoli synthem deposits, specifically MN1 sub-synthem around S. Chirico Raparo and MN2 sub-synthem on most of the A4 exposure area (map).

A coexistence of terrestrial and marine subbasins within the SAB in the late early Pleistocene has been proposed by other workers (Pieri *et al.* 1994, 1996; Sabato 1997, 2000; Sabato *et al.*

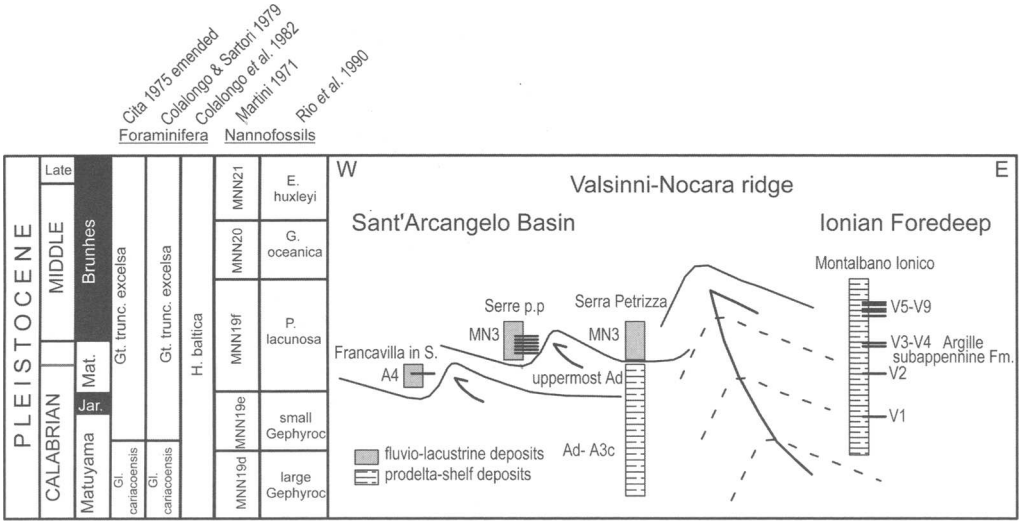

Fig. 15. Correlation among stratigraphic sections in the SAB and the Montalbano Ionico area (Ionian foredeep). Bold lines in the sections represent major tephra layers (V1–V9 tephra codes of Ciaranfi *et al.* 1996, 2001). Arrows indicate the activation of west-verging thrust faults in the SAB and along the Valsinni–Nocara ridge. The progressive tectonic uplift of this ridge is indicated by dotted lines. Data, excluding the Francavilla in Sinni section, are from Sabato *et al.* (2005; Serre section *pro parte*), Marino (1996; Serra Petrizza section) and Ciaranfi *et al.* (1996, 2001; Montalbano Ionico section).

2005). According to this proposal, a lacustrine sub-basin in the northern SAB, recorded by the 'S. Lorenzo cycle', was separated by a structural high from the adjacent sea, where the 'Sauro cycle' deposits were accumulating, between the latest early–earliest mid-Pleistocene. The biostratigraphic conclusions of Marino (1996) on the Serra Petrizza section (Figs 2 and 3) apparently established a chronological correlation between the Sauro marine deposits and the K/Ar age of a tephra interbedded within the S. Lorenzo lacustrine deposits calibrated at 1.1 ± 0.3 Ma (Caggianelli *et al.* 1992). Recent integrated data are considered to support this conclusion (Sabato *et al.* 2005), although magnetostratigraphic data place the dated tephra in a reverse interval younger than 1.1 Ma (uppermost Matuyama).

A wider correlation of stratigraphic sections in the SAB and adjacent Ionian foredeep can help in defining a palaeogeographical transect at the early–mid-Pleistocene transition (Fig. 15). Specifically, three sections in the SAB are compared with the Montalbano Ionico section located in the Ionian foredeep, about 20 km east of the SAB (Ciaranfi *et al.* 1996, 2001). Such a comparison takes advantage of the occurrence of tephra layers in the different areas indicating the following.

(1) The latest early Pleistocene portion of the Montalbano section is biostratigraphically coeval with the marine portion, i.e uppermost Ad lithofacies, of the Serra Petrizza section, suggesting shelf deposition in the contiguous Ionian foredeep and SAB.

(2) Scattered tephra layers (V1–2) are present within the lower part of the Montalbano section similarly to isolated tephra within A4 observed around Francavilla in Sinni (see Celentano 2001); a tentative correlation between the A4 tephra and the V2 tephra at Montalbano is proposed.

(3) A correlation between A4, the uppermost Ad and the mid-portion of the shelfal deposits at Montalbano Ionico is reasonable and provides a reliable reconstruction of the SAB at the early–mid-Pleistocene transition.

(4) Closely spaced tephra occur within the upper, middle Pleistocene, portion of the Montalbano section as well as within lithofacies MN3 in the SAB. Here tephra are within reverse magnetized sediments referred to as the upper portion (post-Jaramillo) of the Matuyama chron (Albianelli *et al.* 2004; Sabato *et al.* 2005) similarly to the V3–V4 tephra in the Montalbano section (Ciaranfi *et al.* 1996, 2001). Regional explosive volcanism seems to have affected a wide area at the front of the Southern Apennines at the early–mid-Pleistocene transition. A suitable source of volcanogenic sediment (see also Ciaranfi *et al.* 1996, 2001) can be envisaged in Vulture, a potassic alkaline volcano located about 100 km NW of the SAB, whose earliest activity is indeed referred to the early–mid-Pleistocene transition (La Volpe & Principe 1989).

In conclusion, these lines of evidence support a palaeogeographical transect linking sub-basins in the SAB, recorded by sub-synthem A4 and the uppermost Ad lithofacies, and the Ionian foredeep, that is, the lower portion of the Montalbano Ionico section.

Tectonic remarks

Syndepositional thrust-related uplift and progressive tilting of the western SAB margin is consistent with the geometric relations between the various sedimentary units of the Lower Pleistocene Aliano sequences A1–A3 exposed on this margin. These units are bounded by progressive unconformities (e.g. Riba 1976) depicting a characteristic fanning of growth strata away from the western basin margin (Fig. 6c and d). This setting was documented also for the underlying Caliandro synthem (lithofacies Cd) in the Agri River area (Casciello *et al.* 2002).

Although the thrust near Armento is locally emergent and the substratum overrides the Caliandro deposits (see Fig. 11a), it is likely that a large part of Early Pleistocene deformation was accommodated by blind thrusting. Such contrasting margin styles point to a decrease of, or a variation in the modes of, thrust activity with time. This geometry could be due to Early Pleistocene blind thrusting or to a deepening of the thrust detachment. East-verging thrust-tip folding is well expressed in the Nocito–Agri confluence area (map), where lithofacies C3a and A1a are involved in such a deformation style (Fig. 11c).

It is worth noting that the deformation of the western SAB margin, and that internal to the SAB infill, have been referred to various phases associated with out-of-sequence thrusting (Patacca & Scandone 2001; Calabrò *et al.* 2002). Some workers have instead hypothesized that sedimentation on this margin was controlled by normal faulting related to a negative flower structure (Merlini & Cippitelli 2001). Fieldwork has not detected any indication of significant normal faulting controlling sedimentation on this margin (map). In any case, we cannot exclude that second-order basinward-dipping normal faults might have also developed to accommodate deformation during superficial and laterally poorly confined thrust-related uplift (e.g. Bonini *et al.* 2000). The deposition of the Aliano synthem was progressively controlled by the growth of back-thrust folds identified in the axial zone of the SAB. These structures form a deformation belt that can be traced in a

NNW–SSE direction across the whole basin, from Guardia Perticara in the north to Noepoli in the south (map and cross-sections). Spectacular expressions are visible along the Sauro, Agri and Sarmento River valleys, where an asymmetric (i.e. with steeper western limbs) anticline and syncline affect lithofacies associations A2a and A3a, respectively (Figs 9a and 14c). Such axial back-thrusts exhibit different structural styles: they are currently emergent thrusts north of the Agri River (Bonini & Sani 2000*a*,*b*), whereas they are blind southwards, as also supported by the interpretation of commercial seismic lines (Fig. 14a and b, and cross-sections in the map). Sub-synthem A4 shows a clear syndepositional wedging at the margin of an asymmetric sub-basin (Fig. 10f) confined at the front of the most internal back-thrust (Fig. 14a and b; map).

Notably, this system of hinterland-verging thrust folds was superimposed onto early east-verging thrust folds that controlled or delimited the deposition of the Caliandro synthem (lithofacies Cd; see above). The timing of inversion of structural polarity on this axial belt can be referred to the deposition of sequences A2 and A3, which show a consistent (west-verging) syndepositional asymmetry of growth strata (Fig. 14c and map). Lateral heteropies and progradation of deltaic systems A2 and A3 are still apparently controlled by the syndepositional growth of the axial fault system, above which these deposits are markedly thinned (see cross-section 2 in the map). Sedimentary wedging in the muddy lithofacies Ad is consistent with this picture.

Stage 3: Missanello–Noepoli synthem palaeogeography and tectonics

The deposits grouped in this synthem mark a significant depositional and palaeogeographical change in the basin. The abrupt transition from coastal and shallow marine to fully terrestrial environments points to an increasing isolation of the SAB from the Ionian foredeep. This evolution was the consequence of a continued west-verging growth of the thrust faults observed along the Valsinni–Nocara ridge.

The narrow sea connection that fed the late residual Aliano sea was thus finally closed at the beginning of this stage (Fig. 10 g and h). Four sub-stages in the tectono-depositional development of the SAB are recognized.

Sub-stage 3a. The early Missanello–Noepoli time was apparently characterized by the denudation of the excess relief created along the western margin during the basin contraction that occurred in the previous stage. Clastic deposits produced by denudation were locally trapped in small depocentres such as in the limited area between S. Chirico Raparo and the Mount Raparo footslopes (map and Fig. 10g). Gravels of subsynthem MN1 document the deposition from debris flows subordinately reworked by floodwater along the western slope of an anticline involving the pre-Plio- or Quaternary substratum. Gentle tilting of MN1 beds defines an open syncline pointing to some activity of marginal structures in this area (Fig. 10g).

Sub-stage 3b. In contrast to the localized MN1 deposition, a major denudation of the western margin is documented by the huge volume of gravels within the MN2 sub-synthem. Stratigraphic contacts with older units clearly indicate that MN2 gravels and sandy silts fill palaeovalleys that drained the western and southern SAB margins (Fig. 10g). In the southwestern margin these valleys, which are deeply cut into older SAB deposits as can be observed in the outcrops along the middle reach of the Sarmento River, coincide more or less with the present-day drainage pattern. Toward the north a large palaeovalley is documented along the Nocito River valley, whereas to the NW other MN2 fluvial entry points are recognized north of the Armento River and around Guardia Perticara. The palaeovalley fills, well exposed in most of the basin, document both downcurrent and vertical transitions between lithofacies associations. Thinning and fining of gravelly–sandy lithofacies toward the east record the grain-size variation expected along the river profile. The vertical transition between gravelly channel belts and sandy silty floodplain indicates the rhythmic activation and deactivation of the various depositional elements characterizing a wide alluvial plain. As in the Aliano synthem, uplift–denudation cycles may explain the cyclothemic organization of the MN2 subsynthem.

Sub-stage 3c. The transition between the MN2 floodplains and the low-energy environments of lithofacies MN3 testifies to the rapid increase of accommodation space in a basin still strongly affected by the activity of west-verging thrust faults. The sub-basins developed in the present Agri and Sauro River valleys (Aliano and Guardia Perticara sub-basins; Fig. 10h) were characterized by palustrine–shallow lacustrine deposition, whereas a muddy flood basin was forming in the central–southern portion of the SAB. Onlap of MN3 on MN2 strata clearly documents the syntectonic nature of the MN3 deposition. As in the older sediments, in this lithofacies the alternation of sandy

delta lobe–alluvial bar and muddy lacustrine–floodbasin deposits records uplift–denudation cycles. Lacustrine–palustrine deposits have been described in detail in previous studies (Sabato 1997, 2000; Sabato *et al.* 2005) in terms of facies and the palaeoecology of fossil assemblages including vertebrates, freshwater molluscs and ostracodes, and pollen remains. These deposits are therefore referred to a small freshwater lake bordered by fan deltas. The pollen record indicates that this environment was characterized by high-frequency fluctuations between arid and humid climates (Albianelli *et al.* 2004; Sabato *et al.* 2005).

The occurrence of 'lacustrine' deposits in the northern portion of the SAB has been widely documented (e.g. Caldara *et al.* 1988; Pieri *et al.* 1994, 1996; Zavala & Mutti 1996; Sabato 1997, 2000; Zavala 2000; Patacca & Scandone 2001; Sabato *et al.* 2005; Carbone *et al.* 2005). In this study, the alluvial–palustrine–lacustrine MN3 deposits coincide only in part with the S. Lorenzo Cycle of Pieri *et al.* (1994, 1996) and with the Profico Group and Aliano 2 of Zavala & Mutti (1996) and Zavala (2000). Similarly to the present study, Zavala & Mutti (1996) and Zavala (2000) recognized more fluvio-lacustrine deposits between the Sauro and Agri River valleys than those reported by other researchers, but suggested that lacustrine conditions occurred twice (i.e. in their Aliano and Profico times). However, according to our study this setting is only apparent, as a NE-dipping reverse fault doubles the MN3 deposits along the M. Ginisgalli–Acqua Finera alignment (map, cross-section B–B′). Alluvial–palustrine–lacustrine systems, therefore, would have occupied the northern portion as well as the central–southern SAB only once, during the end of early–early mid-Pleistocene time (Fig. 10h).

The 'S. Lorenzo lake' (Pieri *et al.* 1994; Sabato 1997, 2000), thus, was not facing the sea, as proven by the occurrence of MN3 deposits in the Serra Petrizza area, and in the central–southern SAB, well above the presumed limit of the 'S. Lorenzo lake'. Limited lacustrine–palustrine depocentres existed in a fully terrestrial basin definitely isolated from the Ionian foredeep (Fig. 10h).

Sub-stage 3d. The end of this stage was marked by renewed deposition in a wide alluvial plain covering most of the SAB and documented by lithofacies MN4. In this stage, gravelly channel fill and muddy floodplain sediment represent the end-members of the uplift–denudation cycles. These deposits overfilled the various depocentres developed in the previous stages, indicating therefore a decreasing rate of basin deformation, a trend that will characterize the next stage.

Tectonic remarks

The deposition of the continental deposits appears to have been largely controlled by the axial back-thrust fold zone. Syndepositional growth of back-thrusts is demonstrated by the consistent growth strata geometries north of the Agri River (Bonini & Sani 2000*a*; Casciello *et al.* 2000; Fig. 9a) and along the Sarmento River (Fig. 14c). The culmination of these thrust folds is characteristically affected by several normal faults with weak vertical offset, perhaps representing the collapse of the fold crest area, which presumably took place after the deposition of the Missanello–Noepoli synthem (map). North of the Agri River, the back-thrust faults emerge at the surface, and their activity probably dismembered the area of Early–Mid-Pleistocene continental deposition into second-order sub-basins (Fig. 11e and cross sections A–A′ and B–B′ in the map). Minor east-verging thrust faults (such as that SE of Roccanova; see map) are interpreted as second-order structures of thrust triangle zones accommodating the shortening above the crest of back-folds (cross-sections C–C′ and D–D′ in the map).

Stage 4: Chiaromonte–Serra Corneta synthem palaeogeography and tectonics

This stage represents the final aggradation in the SAB that occurred in fully alluvial conditions. The relatively small amount (about 100 m thickness) of coarse-grained material recorded in the basin during the development of this synthem suggests a reduction of accommodation space. Three sub-stages can be recognized in the tectonosedimentary evolution of this stage (Fig. 10i).

Sub-stage 4a. A wide braidplain developed in the SAB at the beginning of this stage and is documented by lithofacies CSC1 (Fig. 10i). The fluvial style, characterized by laterally mobile shallow channel belts, points to reduced accommodation space in the basin, which did not allow a significant vertical aggradation of fluvial deposits and the development of low-energy floodplain areas. Stratigraphic expansion of muddy lithofacies indicative of a floodplain marked the development of MN2 and MN4 lithofacies assemblages in times of higher subsidence rate in the basin.

Sub-stage 4b. The sedimentary evidence of this sub-stage is locally represented by lithofacies CSC2, a thin breccia that testifies to a significant tectonic event that affected a limited portion of the western margin of the SAB. This breccia formed by the rapid unroofing of Mount Raparo

presumably in response to a pulse in the activity of the east-verging Armento–Raparo thrust fault (*sensu* Monaco *et al.* 2001) (Fig. 10i).

Sub-stage 4c. The final deposition during this stage was characterized by development of alluvial fans along the western basin margin (Fig. 10i). The poorly reworked clasts in the deposits of lithofacies CSC3 suggest erosion of excess relief formed in the previous sub-stage, short transport and rapid deposition of the eroded material. These deposits are deeply weathered, with the occurrence of reddish buried or relict soils (Amato & Dimase 1997), which document a complex geomorphological evolution after the deposition of this unit. Truncated and buried alfisols with petrocalcic horizons document original weathering in seasonal and contrasted climatic conditions as well as successive erosion and deposition on the surfaces on top of these deposits with development of further palaeosols.

Tectonic remarks

The deposits of this synthem record a relatively recent deformation event consisting of NE-trending thrust-fold axes superimposed on the former NW–NNW-trending structures (Piccardi *et al.* 2000) (Fig. 11f). This superimposition is also present in the Alianello area, where the NNW-striking continental S. Lorenzo syncline basin is deformed by NE-trending gentle folds (map). The chronological attribution of this folding event is, however, not well constrained, as it could be referred either to (1) the earliest Mid-Pleistocene (i.e. just after the end of continental deposition of the Missanello–Noepoli synthem), or (2) the development of the locally dense network of NW-trending shallow normal faults displacing the deposits of the Chiaromonte–Serra Corneta synthem (Fig. 10i). In the hypothesis that these normal faults developed in response to a late gravitational instability and tectonic collapse of the structural highs that developed during the previous stages, it follows that compression within the basin ceased around the earliest Mid-Pleistocene.

Stage 5: Valdagri synthem palaeogeography and tectonics

This is the last and most recent stage of basin development, indicating that, possibly since the latest mid-Pleistocene, the SAB was definitively part of the uplifting chain. The succession of four major fluvial terraces (see also Amato & Dimase 1997) attests to a rapid vertical incision of the basin fill as a consequence of overall uplift, punctuated by limited aggradation of successive alluvial plains.

Some workers have proposed that the area was affected during the Mid- to Late Pleistocene by NW-trending sinistral strike-slip faulting that dissected the previous thrust–fold belt structures (such as the Valsinni anticline) giving rise to a very complex structural pattern (Catalano *et al.* 1993; Monaco *et al.* 1998, 2001; Bonini & Sani 2000*a*). This scenario does not contrast with our findings, as this phase is hypothesized to postdate basin development (e.g. Catalano *et al.* 2004). Similarly, the so-called Scorciabuoi Fault (Lentini 1979; Fig. 1) could have developed first as a back-thrust. This possibility is suggested by the recognition of consistent SW-verging back-folds affecting the deposits of lithofacies A3a at the northeastern margin of the SAB (Masseria Gagliardo area in the map; Bonini & Sani 2000*a*,*b*). This fault zone was later reactivated as an oblique-slip or extensional fault, as indicated by its recent morphological features (Bonini & Sani 2000*a*; Salviulo *et al.* 2005). A two-phase activity for the Scorciabuoi Fault (sinistral transpression followed by extension) was also proposed by Pieri *et al.* (1997).

Discussion and conclusion

Tectonics appears to have dominantly controlled accommodation space and sediment supply in the SAB, raising the question of the role of the eustatic control. The Caliandro and Aliano synthems encompass a critical period of the late Neogene, when, starting from 2.6–2.4 Ma, the Arctic ice sheet was developing and determining the initiation of glacial–interglacial cycles in the northern hemisphere, and thus glacio-eustatic fluctuations that controlled accommodation space in the world's oceans and seas. In Figure 16, the Caliandro synthem chronostratigraphy is compared with oxygen isotopic curves of the eastern equatorial Atlantic and Mediterranean Sea and with the global chart of relative sea-level fluctuations. It can be observed that three third-order depositional sequences (TB 3.6, 3.7 and 3.8) are defined on a global scale and that several fourth- and fifth-order sequences may have formed, as suggested by the fluctuation of oxygen isotopic ratio. Nevertheless, it can be noted that: (1) the sub-units C1 and overlying lithofacies Cd, defining a transgressive trend, cross chronologically the boundary between sequences TB 3.6 and 3.7; (2) despite the deposition of lithofacies Cd, biostratigraphically calibrated in the Nocito River valley (Marino 1994, section RAC in Figs 2 and 3), C1 coincides with the trangressive portion of sequence TB 3.7, and sub-unit C2 developed out-of-sequence as a result of the growth of a compressive structure along the western margin; (3) only sub-unit C3 could have been in part controlled by eustacy

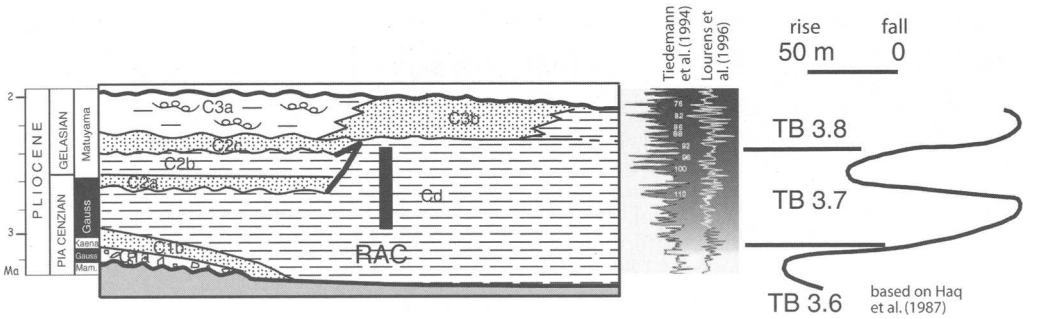

Fig. 16. Comparison of Caliandro stratigraphy (western SAB), global third-order sequences (after Haq *et al.* 1987) and astronomical cyclicity recorded from the Atlantic (Tiedemann *et al.* 1994) and Mediterranean (Lourens *et al.* 1996) basins. RAC, Racanello biostratigraphic section (Marino 1994; see Fig. 2).

as indicated by the possibly coeval sequence TB 3.8.

The hypothesis of a tectonic control on accommodation space and sediment production (by rejuvenating the relief) acting at rates comparable with those of the glacio-eustatic and climatic cycles seems to be supported also by the tectono-sedimentary events punctuating the transition from the early to the mid-Pleistocene. In a very short time span (of the order of 0.2 Ma, Fig. 15), the development of A4 and MN3 sub-basins and the progressive isolation of the SAB from the Ionian foredeep were controlled by the activity of west-verging thrust faults. Sedimentation rates higher than 0.5 m ka^{-1} estimated for the deposition of MN3 (Albianelli *et al.* 2004) indicate the fast tectonic subsidence and the huge sediment supply characterizing the SAB in this period.

The predominant role of tectonics in controlling the basin fill is generally agreed, as demonstrated by various complementary structural models, most of which have been referred to a semi-allochthonous basin since the pioneer work by Vezzani (1967*a*). The studies that have discussed in detail the tectono-depositional basin evolution (Pieri *et al.* 1994, 1996; Zavala 2000; Patacca & Scandone 2001) linked the development of depositional systems to a compressional setting dominated by east-verging thrust faults controlling the establishment of a piggyback or thrust-top basin.

Data collected in this study suggest a further model for the evolution of the SAB. This is strongly supported by the depositional and structural features magnificently exposed throughout the basin. In this new picture, the SAB is thought to have been deformed by oppositely verging thrust folds and such a progressive deformation controlled cyclical changes of sediment supply and accommodation space. Specifically, the western margin was characterized by east-verging thrust faults that controlled pulsating mountain uplift. This tectonic activity influenced sediment production and supply to the fluvio-deltaic systems developed throughout the deposition of the Caliandro, Aliano and Missanello–Noepoli synthems. Thrust loading in the inner sectors of the Southern Apennines may have caused the subsidence accommodating the Caliandro and in part also the Aliano synthems. In overall conceptual terms, the conclusion of this study fits reasonably well the hypotheses of previous workers.

The original contribution of the present study is the observation that syndepositional effects of back-thrusting developed not only along the Valsinni–Nocara ridge, as previously documented (e.g. Sant'Arcangelo back-thrust; Calabrò *et al.* 2002), but also in the axial SAB (for back-thrusts documented in the northern SAB, see also Hippolyte *et al.* 1994*a*; Bonini & Sani 2000*a*; Casciello *et al.* 2000). In terms of progressive control on deposition these structures determined: (1) a physiographic asymmetry in the Valsinni–Nocara ridge characterized by steep and gentle slopes on the western and eastern flanks, respectively, with significant implications for drainage pattern and sediment dispersal to the SAB; (2) the formation of small sub-basins in the Valsinni–Nocara ridge filled with siliceous deposits (i.e. lithofacies Ce) in mid-Caliandro time; (3) the progressive development of depocentres in the western-axial SAB since the deposition of the A2 sequence, later filled by fully terrestrial deposits of the A4 sub-synthem as a consequence of the emergence of the back-thrust; (4) the final isolation of the SAB from the sea caused by the continual activity and surfacing of back-thrusts at the western Valsinni–Nocara ridge margin in Missanello–Noepoli time. Here, back-thrusts created small subsiding depocentres favouring lacustrine conditions that are locally documented by sub-synthem MN3.

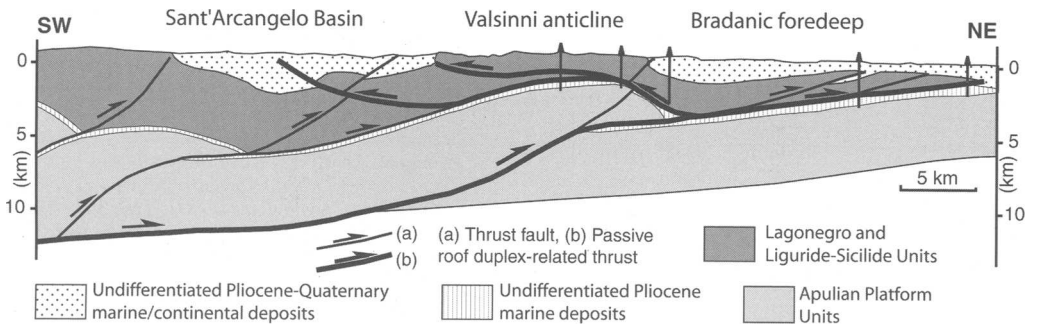

Fig. 17. Geological regional cross-section (modified from Hippolyte *et al.* 1994*a*) showing the structural–evolutionary passive-roof duplex model proposed in this study for the Sant'Arcangelo Basin. In this model, the back-thrusts affecting the SAB are coeval and genetically linked to the underlying main forethrust in the Apulian Platform. (Note the displacement of early forethrusts by the late back-thrusts). Bold lines indicate the main structures composing the passive roof duplex.

The recognition of such basin-scale hinterland-verging thrust faults and folds raises the question of their tectonic significance. Back-thrusts have been previously interpreted as second-order structures that accommodated the eastward translation of the Valsinni thrust anticline (composed of Sicilide and Flysch units) over a structural high in the underlying Apulian Platform formed by pre-existing normal faults (Calabrò *et al.* 2002). An alternative hypothesis is that back-thrusts could represent passive-roof thrusts of passive-roof duplex structures (*sensu* Banks & Warburton 1986). In this hypothesis, the hinterland-verging Valsinni anticline could be detached (via the roof-thrust) along the rheological contact given by the Sicilide Units–Apulian Platform interface, which is marked by the intervening Pliocene clays (Fig. 17). Below this surface, the Apulian Platform is affected by east-directed thrusting, as imaged in seismic lines (Calabrò *et al.* 2002).

We propose a passive-roof duplex model considering the following: (1) thrust triangle zones have been also evidenced both northward of the Valsinni–Nocara ridge (Bentivenga *et al.* 2005) and to the SSE, along-strike from the SAB, by seismic line interpretation (offshore the Gulf of Taranto; Pieri *et al.* 1997; Doglioni *et al.* 1999); (2) this structural setting is a typical feature of orogenic belts worldwide (e.g. Price 1986; Banks & Warburton 1986; Vann *et al.* 1986; Couzens-Schultz *et al.* 2003). In this scenario, some back-thrusts that have been documented with great continuity along the external frontal area to the NNE of the SAB and related to either deep-seated strike-slip faulting (Bonini & Sani 2000*a*) or associated with thrust folds (Calabrò *et al.* 2002; Piedilato & Prosser 2005) could be instead referred to the proposed passive-roof duplex model. In this interpretation, the SAB would represent a triangular basin (or full ramp basin according to the definition of Cobbold *et al.* 1993) bounded at the margins by oppositely verging structures of the same rank. Our hypothesis is schematically shown in Figure 17. It is worth noting that the chronology of the deformation inferred for the axial deformation belt (i.e. a first fore-thrust folding followed by back-thrust folding) is strikingly similar to that recognized by Doglioni *et al.* (1999) in the Ionian Sea and by Bentivenga *et al.* (2005) in the Southern Apennines frontal area.

Regarding the kinematics of the passive-roof duplex, one may expect that this structure could be characterized by some significant oblique-slip component of displacement given the importance of this kinematics during the Mid–Late Pleistocene. However, the available data collected on the Alianello thrust fold belonging to this system evidence a roughly ENE direction of shortening that is sub-orthogonal to this structure (Hippolyte *et al.* 1994*a*,*b*). Similar results are suggested by preliminary data collected in the Serra Petrizza area. These data seem to give further support to the hypothesis that the major components of strike-slip faulting started during Mid–Late Pleistocene times, thus during, or after, the last phases of the basin evolution.

Finally, the above discussion of the evolutionary model of the SAB obviously affects also the migration of the basin's depocentre through time, which has been generally referred to as a westward propagation (Hippolyte *et al.* 1994*a*; Calabrò *et al.* 2002). We still highlight the importance of the westward sense of propagation: for instance, the west-directed jump from the deposition area of lithofacies Cd and Ad to the depocentre of sub-synthem A4 is well exemplified in cross-section C-C′ (see map). However, the migration pattern of the basin's depocentre resulting from

tectonosedimentary evolution proposed in this study is more complex, with the occurrence of both forward and backward propagations. The latter have been previously recognized by Patacca & Scandone (2001) in relation to the syndepositional activity of 'competing' east-verging thrust faults bounding both the western and eastern SAB margins. In our model, such an evolution is instead strongly dependent upon the mutual interplay between the east- and west-verging thrust faults. In particular, the above-mentioned westward shift of basin depocentre manifested by subsynthem A4 was followed by an eastward migration of continental deposition (map). Continental deposition was indeed controlled by back-thrusts located to the east of the depocentre of sub-synthem A4 (Alianello area; see the map and cross-sections A–A′, B–B′, and C–C′).

M. C. Bonci, Genoa University, is acknowledged for her valuable collaboration in performing the biostratigraphic analysis of siliceous sediments. The authors are indebted to G. Cello, P. Dattilo and F. Ethridge for their critical reviews and constructive comments, which helped to improve this paper.

References

ALBIANELLI, A., BERTINI, A., LOMBARDI, C., MORETTI, M., NAPOLEONE, G. & SABATO, L. 2004. Magnetic, palynologic and sedimentary cyclicities in the lacustrine deposits of the S. Arcangelo basin (Southern Apennines) during the Jaramillo to Brunhes chrons. *32nd International Geological Congress, Florence, August 2004, Abstract Volume (Part 1)*, 389.

AMATO, A. & DIMASE, A. C. 1997. Caratteristiche paleoambientali ed evoluzione geomorfologica dei plateaux della media valle del Fiume Agri (Basilicata). *Il Quaternario*, **10**, 213–230.

BALDAUF, J. G. & IWAI, M. 1995. Neogene diatom biostratigraphy for the eastern equatorial Pacific Ocean, Leg 138. *In*: PISIAS, N. G., MAYER, L. A., JANECEK, T. R., PALMER-JULSON, A. & VAN ANDEL, T. H. (eds) *Proceedings of the Ocean Drilling Program, Scientific Results, 138*, Ocean Drilling Program, College Station, TX, 105–128.

BALDUZZI, A., CASNEDI, R., CRESCENTI, U., MOSTARDINI, F. & TONNA, M. 1982. Il Plio-Pleistocene del sottosuolo del Bacino Lucano (Avanfossa Appenninica). *Geologica Romana*, **21**, 89–111.

BANKS, C. J. & WARBURTON, J. 1986. 'Passive-roof' duplex geometry in the frontal structures of the Kirthar and Sulaiman mountain belts, Pakistan *Journal of Structural Geology*, **8**, 229–237.

BARRON, J. A. 1985. Miocene to Holocene planktic diatoms. *In*: BOLLI, H. M., SAUNDERS, J. B. & PERCH-NIELSEN, K. (eds) *Plankton Stratigraphy*. Cambridge University Press, Cambridge, 763–809.

BEN AVRAHAM, Z., BOCCALETTI, M., CELLO, G., GRASSO, M., LENTINI, F., TORELLI, L. & TORTORICI, L. 1990. Principali domini strutturali originatisi dalla collisione neogenico-quaternaria nel Mediterraneo centrale. *Memorie della Società Geologica Italiana*, **40**, 453–462.

BENTIVENGA, M., FORESI, L. M., PRESTERA, A., PROSSER, G. & SABIA, M. 2005. Structural setting at the front of a thrust and fold belt: the Craco area (Southern Apennines, Italy). *Bollettino della Società Geologica Italiana*, **124**, 367–376.

BENVENUTI, M. 2003. Facies analysis and tectonic significance of lacustrine fan–deltaic successions in the Pliocene–Pleistocene Mugello Basin, Central Italy. *Sedimentary Geology*, **157**, 197–234.

BENVENUTI, M. & MARTINI, I. P. 2002. Analysis of terrestrial hyperconcentrated flows and their deposits. *In*: MARTIN, I. P., BAKER, V. & GARZON, R. G. (eds). *Floods and Megaflood Processes and Deposits; Recent and Ancient Examples.* International Association of Sedimentologists, Special Publications, **32**, 167–193.

BLAIR, T. C. & BILODEAU, W. L. 1988. Development of tectonic cyclothems in rift, pull-apart, and foreland basins: sedimentary response to episodic tectonism. *Geology*, **16**, 517–520.

BOCCALETTI, M. & GUAZZONE, G. 1974. Remnant arcs and marginal basins in the Cainozoic development of the Mediterranean. *Nature*, **252**, 18–21.

BOCCALETTI, M., CIARANFI, N., COSENTINO, D., *ET AL.* 1990. Palinspastic restoration and paleogeographic reconstruction of the peri-Tyrrhenian area during the Neogene. *Palaeogeography, Palaeoclimatology, Palaeoecology*, **77**, 41–50.

BONINI, M. & SANI, F. 2000*a*. Pliocene–Quaternary transpressional evolution of the Anzi–Calvello and Northern S. Arcangelo basins (Basilicata, Southern Apennines, Italy) as a consequence of deep-seated fault reactivation. *Marine and Petroleum Geology*, **17**, 909–927.

BONINI, M. & SANI, F. 2000*b*. Thrusting, strike-slip faulting and syntectonic deposition in the Potenza–Guardia Perticara Area (Basilicata, Southern Apennines, Italy). (With geological map at scale 1:50 000.) *Memorie della Società Geologica Italiana*, **55**, 123–132.

BONINI, M., SOKOUTIS, D., MULUGETA, G. & KATRIVANOS, E. 2000. Modelling hanging wall accommodation above rigid thrust ramps. *Journal of Structural Geology*, **22**, 1165–1179.

CAGGIANELLI, A., DELLINO, P. & SABATO, L. 1992. Depositi lacustri infrapleistocenici con intercalazioni vulcanoclastiche (Bacino di Sant'Arcangelo, Basilicata). *Il Quaternario*, **5**, 123–132.

CALABRÒ, R. A., FELTRE, L. & PEROTTI, C. R. 2002. Structural features of the S. Arcangelo piggyback Basin (Southern Apennines—Italy) from seismic data and analogue modelling. *Bollettino della Società Geologica Italiana, Volume Speciale* **1**, 333–341.

CALDARA, M., LOIACONO, F., MORLOTTI, E., PIERI, P. & SABATO, L. 1988. I depositi plio-pleistocenici della parte nord del bacino di S. Arcangelo (Appennino Lucano): caratteri geologici e paleoambientali. *Memorie della Società Geologica Italiana*, **41**, 391–410.

CARBONE, S., CATALANO, S., LAZZARI, S., LENTINI, F. & MONACO, C. 1991. Presentazione della carta geologica del bacino del fiume Agri (Basilicata). *Memorie della Società Geologica Italiana*, **47**, 129–143.

CARBONE, S., DI STEFANO, A. & LENTINI, F. 2005. *Note Illustrative della Carta Geologica d'Italia alla scala 1: 50,000, Foglio 506, Sant'Arcangelo*. APAT, Rome.

CARTA GEOLOGICA D'ITALIA 1968. *Sheet No. 200—Tricarico. Scale 1 : 100 000*. Poligrafica & Cartevalori, Ercolano (Napoli).

CARTA GEOLOGICA D'ITALIA 1970. *Sheet No. 211—S. Arcangelo. Scale 1 : 100 000*. Poligrafica & Cartevalori, Ercolano (Napoli).

CASCIELLO, E., CESARANO, M., FERRANTI, L., OLDOW, J. S. & PAPPONE, G. 2000. *Geological map of the northern part of the S. Arcangelo basin between Alianello and Roccanuova (Southern Apennines)*. SystemCart, S.r.l., Roma.

CASCIELLO, E., PAPPONE, G. & ZUPPETTA, A. 2002. Plio-Pleistocene tectonic evolution of the western margin of the S. Arcangelo basin (Southern Apennines). *Bollettino della Società Geologica Italiana, Volume Speciale* **1**, 343–352.

CASERO, P. 2004. Structural setting of petroleum exploration plays in Italy. *Special Volume of the Italian Geological Society for the 32nd International Geological Congress, Florence 2004*, 189–199.

CASERO, P., ROURE, F., ENDIGNOUX, L., MORETTI, I., MULLER, C., SAGE, L. & VIALLY, R. 1988. Neogene geodynamic evolution of the Southern Apennines. *Memorie della Società Geologica Italiana*, **41**, 109–120.

CASNEDI, R., CRESCENTI, U. & TONNA, M. 1982. Evoluzione dell'avanfossa adriatica meridionale nel Plio-Pleistocene, sulla base di dati di sottosuolo. *Memorie della Società Geologica Italiana*, **24**, 243–260.

CATALANO, S., MONACO, C., TORTORICI, L. & TANSI, C. 1993. Pleistocene strike-slip tectonics in the Lucanian Apennine (Southern Italy). *Tectonics*, **12**, 656–665.

CATALANO, S., MONACO, C., TORTORICI, L., PALTRINIERI, W. & STEEL, N. 2004. Neogene–Quaternary evolution of the Southern Apennines. *Tectonics*, **23**, DOI: TC 200310.1029/2003TC001512.

CELENTANO, A. L. 2001. *Evoluzione sedimentaria del Bacino di Sant'Arcangelo, parte meridionale (Appennino Meridionale)*. PhD thesis, Università di Bari.

CELLO, G. & MAZZOLI, S. 1998. Apennine tectonics in Southern Italy: a review. *Journal of Geodynamics*, **27**, 191–211.

CELLO, G., TORTORICI, L., MARTINI, N. & PALTRINIERI, W. 1989. Structural styles in the frontal zones of the southern Apennines, Italy: an example from the Molise district. *Tectonics*, **8**, 753–768.

CELLO, G., LENTINI, F. & TORTORICI, L. 1990. La struttura del settore calabro-lucano e suo significato nel quadro dell'evoluzione tettonica del sistema a thrust sudappenninico. *Studi Geologici Camerti, Volume Speciale*, 27–34.

CELLO, G., GAMBINI, R., MATTIONI, L., MAZZOLI, S., READ, A., TONDI, E. & ZUCCONI, V. 2000. Geological analysis of the High Agri Valley (Lucania Apennines, Southern Italy). *Memorie della Società Geologica Italiana*, **55**, 149–155.

CELLO, G., TONDI, E., MICARELLI, L. & MATTIONI, L. 2003. Active tectonics and earthquake sources in the epicentral area of the 1857 Basilicata earthquake (Southern Italy). *Journal of Geodynamics*, **36**, 37–50.

CIARANFI, N., MARINO, M., SABATO, L., D'ALESSANDRO, A. & DE ROSA, R. 1996. Studio geologico stratigrafico di una successione infra e mesopleistocenica nella parte sudoccidentale della Fossa Bradanica (Montalbano Ionico, Basilicata). *Bollettino della Società Geologica Italiana*, **115**, 379–391.

CIARANFI, N., D'ALESSANDRO, A., GIRONE, A., MAIORANO, P., MARINO, M., SOLDANI, D. & STEFANELLI, S. 2001. Pleistocene sections in the Montalbano Jonico area and the potential GSSP for Early–Middle Pleistocene in the Lucania Basin (Southern Italy). *Memorie di Scienze Geologiche*, **53**, 67–83.

CIPPITELLI, G. 1997. Interpretazione di un profilo sismico nel Bacino di S. Arcangelo-Lucania. *1° Congresso FIST (Federazione Italiana di Scienze della Terra), Bellaria, 5–9 October 1997, Abstracts*, **2**, 163–164.

CITA, M. B. 1975. The Miocene/Pliocene boundary, history and definition. *Micropaleontology, Special Publication*, **1**, 1–30.

COBBOLD, E. R., DAVY, E., GAPAIS, D., *ET AL.* 1993. Sedimentary basins and crustal thickening. *Sedimentary Geology*, **86**, 77–89.

COLALONGO, M. L. & SARTORI, S. 1979. Schema biostratigrafico per il Pliocene e il basso Pleistocene in Italia. *Contributi alla Carta Neotettonica Italiana, Pubblicazione*, **251**, 645–654.

COLALONGO, M. L., DONDI, L., D'ONOFRIO, S. & IACCARINO, S. 1982. Schema biostratigrafico a Foraminiferi per il Pliocene e il basso Pleistocene nell'Appennino settentrionale e nella Pianura padana. *In*: CREMONINI, G. & RICCI LUCCHI, F. (eds) *Guida alla geologia del margine appenninico-padano*. Società Geologica Italiana, Bologna, 121–122.

COUZENS-SCHULTZ, B. A., VENDEVILLE, B. C. & WILTSCHKO, D. V. 2003. Duplex style and triangle zone formation: insights from physical modeling. *Journal of Structural Geology*, **25**, 1623–1644.

CREMA, C., CORTESE, E., BALDACCI, L. & VIOLA, C. 1908. *Carta Geologica d'Italia 1:100 000, 1st edn—Sheet 211, S. Arcangelo*.

D'ANDREA, S., PASI, R., BERTOZZI, G. & DATTILO, P. 1993. Geological model, advanced methods help unlock oil in Italy's Apennines. *Oil and Gas Journal*, **23**, 53–57.

D'ARGENIO, B., PESCATORE, T. & SCANDONE, P. 1973. Schema geologico dell'Appennino meridionale (Campania e Lucania). *Atti Accademia Nazionale dei Lincei*, **183**, 49–72.

D'ARGENIO, B., PESCATORE, T. & SCANDONE, P. 1975. Structural pattern of the Campania–Lucania Apennines. *Quaderni di Ricerca Scientifica*, **90**, 313–327.

DI STEFANO, A., VINCI, G. & ROMEO, M. 2002. The Plio-Pleistocene deposits at the southeastern border of the Sant'Arcangelo basin (Southern Apennines): structural setting and biostratigraphical data. *Bollettino della Società Geologica Italiana, Volume Speciale,* **1**, 527–537.

DOGLIONI, C., MONGELLI, F. & PIERI, P. 1994. The Puglia uplift (SE Italy): an anomaly in the foreland of the Apenninic subduction due to buckling of a thick continental lithosphere. *Tectonics*, **13**, 1309–1321.

DOGLIONI, C., MERLINI, S. & CANTARELLA, G. 1999. Foredeep geometries at the front of the Apennines in the Ionian Sea (central Mediterranean). *Earth and Planetary Science Letters*, **168**, 243–254.

EMBRY, A. F. 2002. Transgressive–Regressive (T–R) Sequence Stratigraphy. *In*: ARMENTROUT, J. (ed.) *Sequence Stratigraphic Models for Exploration and Production: Evolving Methodology, Emerging Models, and Application Histories. Proceedings of the 22nd Annual GCSSEPM Bob F. Perkins Research Conference 2002*, 151–172.

FINETTI, I., LENTINI, F., CARBONE, S., CATALANO, S. & DEL BEN, A. 1996. Il sistema Appennino Meridionale–Arco Calabro–Sicilia nel Mediterraneo Centrale: studio geologico–geofisico. *Bollettino della Società Geologica Italiana*, **115**, 529–559.

GIANNANDREA, P. & LOIACONO, F. 2003. Le successioni alluvionali e lacustri quaternarie affioranti nella media valle del fiume Sinni (Appennino Meridionale, Basilicata). *Il Quaternario*, **16**(2), 257–267.

GUERRERA, F. & COCCIONI, R. 1984. Caratteristiche sedimentologiche e micropalentologiche di successioni 'tripolacee' plioceniche dell'Appennino Lucano. *Bollettino della Società Geologica Italiana*, **103**, 205–223.

HAQ, B. U., HARDENBOL, J. & VAIL, P. R. 1987. Chronology of fluctuating sea levels since the Triassic (250 million years ago to Present). *Science*, **235**, 1156–1167.

HIPPOLYTE, J. C., ANGELIER, J., ROURE, F. & MULLER, C. 1991. Géometrie et mécanisme de formation d'un bassin 'piggyback': le bassin de Sant'-Arcangelo (Italie méridionale). *Comptes Rendues de l'Académie des Sciences*, **312**(2), 1373–1378.

HIPPOLYTE, J. C., ANGELIER, J., ROURE, F. & CASERO, P. 1994*a*. Piggyback basin development and thrust belt evolution: structural and paleostress analyses of Plio-Quaternary basins in the Southern Apennines. *Journal of Structural Geology*, **16**, 159–173.

HIPPOLYTE, J. C., ANGELIER, J. & ROURE, F. 1994*b*. A major geodynamic change revealed by Quaternary stress patterns in the Southern Apennines (Italy). *Tectonophysics*, **230**, 199–210.

HIPPOLYTE, J. C., ANGELIER, J. & BARRIER, E. 1995. Compressional and extensional tectonics in an arc system: example of the Southern Apennines. *Journal of Structural Geology*, **17**, 1725–1740.

KNOTT, S. 1987. The Liguride Complex of Southern Italy—a Cretaceous to Paleogene accretionary wedge. *Tectonophysics*, **142**, 217–226.

LA VOLPE, L. & PRINCIPE, C. 1989. Stratigrafia e storia evolutiva del M. Vulture, revisione ed aggiornamenti. *Bollettino del Gruppo Nazionale di Vulcanologia*, **5**, 889–903.

LENTINI, F. 1967. Le successioni stratigrafiche plio-pleistoceniche sui due lati della dorsale Nocara–Colobraro (Matera). *Atti dell'Accademia Gioenia di Scienze Naturali in Catania, Serie VI*, **18**, 181–206.

LENTINI, F. 1968. Stratigrafia micropaleontologica dei terreni plio-pleistocenici di S. Arcangelo (Potenza). *Atti dell'Accademia Gioenia di Scienze Naturali in Catania, Serie VI*, **19**(Supplemento di Scienze Geologiche), 255–344.

LENTINI, F. 1969*a*. Facies e stratigrafia dei depositi pliocenici affioranti tra il F. Agri e la zona di Craco (MT). *Atti dell'Accademia Gioenia di Scienze Naturali in Catania, Serie VI*, **19**(Supplemento di Scienze Geologiche), 529–556.

LENTINI, F. 1969*b*. Sezioni stratigrafiche plioceniche nella Val d'Agri presso Gannano (MT). *Atti dell'Accademia Gioenia di Scienze Naturali in Catania, Serie VI*, **20**(Supplemento di Scienze Geologiche), 19–79.

LENTINI, F. 1979. Le Unità Sicilidi della val d'Agri (Appennino Lucano). *Geologica Romana*, **18**, 215–224.

LENTINI, F., CARBONE, S., CATALANO, S. & MONACO, C. 1990. Tettonica a thrust neogenica nella catena appenninico-maghrebide: esempi dalla Lucania e dalla Sicilia. *Studi Geologici Camerti, Volume Speciale*, 19–26.

LENTINI, F., CATALANO, S. & CARBONE, S. 1996. The External Thrust System in southern Italy: a target for petroleum exploration. *Petroleum Geoscience*, **2**, 333–242.

LENTINI, F., CARBONE, S., DI STEFANO, A. & GUARNIERI, P. 2002. Stratigraphical and structural constraints in the Lucanian Apennines (southern Italy): tools for reconstructing the geological evolution. *Journal of Geodynamics*, **34**, 141–158.

LOURENS, L. J., ANTONARAKOU, A., HILGEN, F. J., VAN HOOF, A. A. M., VERGNAUD-GRAZZINI, C. & ZACHARIASSE, W. J. 1996. Evaluation of the Plio-Pleistocene astronomical timescale. *Paleoceanography*, **11**, 391.

MALINVERNO, A. & RYAN, W. B. F. 1986. Extension in the Tyrrhenian Sea and shortening in the Apennines as a result of arc migration driven by sinking of the lithosphere. *Tectonics*, **5**, 227–246.

MARINO, M. 1994. Biostratigrafia integrata a nannofossili calcarei e foraminiferi planctonici di alcune successioni terrigene pliocenico-superiori del Bacino di Sant'Arcangelo (Appennino Meridionale). *Bollettino della Società Geologica Italiana*, **113**, 329–354.

MARINO, M. 1996. Calcareous nannofossil and Foraminifera biostratigraphy of Pleistocene terrigenous sediments from southern Italy. *Rivista Italiana di Paleontologia e Stratigrafia*, **102**(1), 119–130.

MARSELLA, E., BALLY, A. W., CIPPITELLI, G., D'ARGENIO, B. & PAPPONE, G. 1995. Tectonic history of the Lagonegro Domain and Southern Apennine thrust belt evolution. *Tectonophysics*, **252**, 307–330.

MARTINI, E. 1971. Standard Tertiary and Quaternary calcareous nannoplankton zonation. *In*: FARINACCI, A. (ed.) *Proceedings 2nd International Conference on Planktonic Microfossils, Rome*. Edizione Tecnoscienze, Roma, **2**, 739–785.

MASINI, F., GIANNINI, T., ABBAZZI, L., FANFANI, F., DELFINO, M., MAUL, L. M. & TORRE, D. 2005. A latest Biharian small vertebrate fauna from the lacustrine succession of San Lorenzo (Sant'Arcangelo Basin, Basilicata, Italy). *Quaternary International*, **131**, 79–93.

MATTEI, M., PETROCELLI, V., LACAVA, D. & SCHIATTARELLA, M. 2004. Geodynamic implications of Pleistocene ultrarapid vertical-axis rotations in the Southern Apennines, Italy. *Geology*, **32**(9), 789–792.

MATTIONI, L., TONDI, E., SHINER, P., RENDA, P., VITALE, S. & CELLO, G. 2006. The Argille Varicolori unit in Lucania (Italy): a record of tectonic offscraping and gravity sliding in the Mesozoic–Tertiary Lagonegro Basin, southern Apennines. *In*: MORATTI, G. & CHALOUAN, A. (eds) *Tectonics of the Western Mediterranean and North Africa*. Geological Society, London, Special Publications, **262**, 277–288.

MAZZOLI, S., BARKHAM, S., CELLO, G., GAMBINI, R., MATTIONI, L., SHINER, P. & TONDI, E. 2001. Reconstruction of the continental margin architecture deformed in the contraction of the Lagonegro Basin, Southern Apennines, Italy. *Journal of the Geological Society, London*, **158**, 309–319.

MENARDI NOGUERA, A. & REA, G. 2000. Deep structure of the Campanian–Lucanian Arc (Southern Apennine, Italy). *Tectonophysics*, **324**, 239–265.

MERLINI, S. & CIPPITELLI, G. 2001. Structural styles inferred by seismic profiles. *In*: VAI, G. B. & MARTINI, I. P. (eds) *Anatomy of an Orogen: the Apennines and Adjacent Mediterranean Basins*. Kluwer, Dordrecht, 441–454.

MONACO, C., TORTORICI, L., MORTEN, L., CRITELLI, S. & TANZI, C. 1995. Geologia del versante nord-orientale del Massiccio del Pollino (confine calabro-lucano): nota illustrativa sintetica della Carta Geologica alla scala 1:50.000. *Bollettino della Società Geologica Italiana*, **114**, 277–291.

MONACO, C., TORTORICI, L. & PALTRINIERI, W. 1998. Structural evolution of the Lucanian Apennines, southern Italy. *Journal of Structural Geology*, **20**, 617–638.

MONACO, C., TORTORICI, L., CATALANO, S., PALTRINIERI, W. & STEEL, N. 2001. The role of Pleistocene strike-slip tectonics in the Neogene–Quaternary evolution of the Southern Apennine orogenic belt: implications for oil trap development. *Journal of Petroleum Geology*, **24**, 339–359.

MOSTARDINI, F. & MERLINI, S. 1986. Appennino centro-meridionale, sezioni geologiche e proposta di modello strutturale. *Memorie della Società Geologica Italiana*, **35**, 177–202.

MULDER, T. J., SYVITSKI, P. M., MIGEON, S., FAUGÈRES. J.-C. & SAVOYE, B. 2003. Marine hyperpycnal flows: initiation, behavior and related deposits. A review. *Marine and Petroleum Geology*, **20**, 861–882.

MUTTI, E. & SGAVETTI, M. 1987. Sequence stratigraphy of the Upper Cretaceous Aren strata in the Orcau–Aren region, south–central Pyrenees, Spain: distinction between eustatically and tectonically controlled depositional sequences. *Annali Università di Ferrara, Sezione Scienze della Terra*, **1**, 1–22.

MUTTI, E., DAVOLI, G., MORA, S. & SGAVETTI, M. (eds) 1994. *The eastern sector of the south–central folded Pyrenean foreland: criteria for stratigraphic analysis and excursion notes. 2nd International Conference on High-Resolution Sequence Stratigraphy, Guidebook*. Istituto di Geologia, Università di Parma.

MUTTI, E., DAVOLI, G., TINTERRI, R. & ZAVALA, C. 1996. The importance of ancient fluvio-deltaic systems dominated by catastrophic flooding in tectonically active basins. *Memorie di Scienze Geologiche, Padova*, **48**, 233–291.

NORTH AMERICAN COMMISSION ON STRATIGRAPHIC NOMENCLATURE. 1983. North American Stratigraphic Code. *AAPG Bulletin*, **67**, 841–875.

OGNIBEN, L. 1969*a*. Schema introduttivo alla geologia del confine calabro-lucano. *Memorie della Società Geologica Italiana*, **8**, 453–763.

OGNIBEN, L. 1969*b*. *Note illustrative della Carta Geologica d'Italia, Foglio 211, S. Arcangelo*. Poligrafica e Cartevalori, Ercolano (Napoli).

ORI, G. G. & FRIEND, P. F. 1984. Sedimentary basins formed and carried piggyback on active thrust sheets. *Geology*, **12**, 475–478.

PAOLA, C., HELLERT, P. L. & ANGEVINE, C. L. 1992. The large-scale dynamics of grain-size variation in alluvial basins, 1: Theory. *Basin Research*, **4**, 73–90.

PATACCA, E. & SCANDONE, P. 2001. Late thrust propagation and sedimentary response in the thrust-belt–foredeep system of the Southern Apennines (Pliocene–Pleistocene). *In*: VAI, G. B. & MARTINI, I. P. (eds) *Anatomy of an Orogen: the Apennines and Adjacent Mediterranean Basins*. Kluwer, Dordrecht, 401–440.

PATACCA, E., SARTORI, R. & SCANDONE, P. 1990. Tyrrhenian basin and Apenninic arcs: kinematic relations since Late Tortonian times. *Memorie della Società Geologica Italiana*, **45**, 425–451.

PESCATORE, T. 1988. La sedimentazione miocenica nell' Appennino campano-lucano. *Memorie della Società Geologica Italiana*, **41**, 37–46.

PESCATORE, T. & SLACZKA, A. 1984. Evolution models of two flysch basins: the Northern Carpathians and the Southern Apennines. *Tectonophysics*, **106**, 49–70.

PICCARDI, L., MORATTI, G., SANI, F., BONINI, M. & BOCCALETTI, M. 2000. Quaternary deformations and stress field changes in the Apennines (Italy). *31st International Geological Congress, Rio de Janeiro, Brazil, August 6–17 2000, Abstracts Volume* (CD-ROM), Session 20–3.

PIEDILATO, S. & PROSSER, G. 2005. Thrust sequences and evolution of the external sector of a fold and thrust belt: an example from the Southern Apennines (Italy). *Journal of Geodynamics*, **39**, 386–402.

PIERI, M. 2001. Italian petroleum geology. *In*: VAI, G. B. & MARTINI, I. P. (eds) *Anatomy of an Orogen: the Apennines and Adjacent Mediterranean Basins*. Kluwer, Dordrecht, 533–550.

PIERI, P., SABATO, L., LOIACONO, F. & MARINO, M. 1994. Il bacino di piggyback di Sant'Arcangelo: evoluzione tettonico-sedimentaria. *Bollettino della Società Geologica Italiana*, **113**, 465–481.

PIERI, P., SABATO, L. & MARINO, M. 1996. The Plio-Pleistocene piggyback Sant'Arcangelo Basin: tectonic and sedimentary evolution. *Notes et Mémoires du Service Géologique du Maroc*, **387**, 195–208.

PIERI, P., VITALE, G., BENEDUCE, P., *ET AL.* 1997. Tettonica quaternaria nell'area Bradanico–Ionica. *Il Quaternario*, **10**, 535–642.

PRICE, R. A. 1986. The southeastern Canadian Cordillera: thrust faulting, tectonic wedging and delamination of the lithosphere. *Journal of Structural Geology*, **8**, 239–254.

RIBA, O. 1976. Syntectonic unconformities of the Alto Caderner, Spanish Pyrenees: a genetic interpretation. *Sedimentary Geology*, **15**, 213–233.

RIO, D., RAFFI, I. & VILLA, G. 1990. Pliocene–Pleistocene nannofossil distribution patterns in the Western Mediterranean. *In*: KASTENS, K. A., MASCLE, J., *ET AL.* (eds) *Proceeding of the Ocean Drilling Program, Scientific Results, 107*, Ocean Drilling Program, College Station, TX, 513–533.

ROURE, F., CASERO, P. & VIALLY, R. 1991. Growth processes and mélange formation in the southern Apennines accretionary wedge. *Earth and Planetary Science Letters*, **102**, 395–412.

ROYDEN, L., PATACCA, E. & SCANDONE, P. 1987. Segmentation and configuration of subducted lithosphere in Italy: an important control on thrust belt and foredeep basin evolution. *Geology*, **15**, 714–717.

SABATO, L. 1997. Sedimentary and tectonic evolution of a lower–middle Pleistocene lacustrine system in the Sant'Arcangelo piggyback basin (Southern Italy). *Geologica Romana*, **33**, 137–145.

SABATO, L. 2000. A lower-middle Pleistocene lacustrine system in late evolutionary stages of the Sant'Arcangelo Basin (southern Italy). *In*: GIERLOWSKI-KORDESCH, E. H. & KELTS, K. R. (eds) *Lake Basins through Space and Time*. American Association of Petroleum Geologists, Studies in Geology, **46**, 543–551.

SABATO, L., BERTINI, A., MASINI, F., ALBIANELLI, A., NAPOLEONE, G. & PIERI, P. 2005. The lower and middle Pleistocene geological record of the San Lorenzo lacustrine succession in the Sant'Arcangelo Basin (Southern Apennines, Italy). *Quaternary International*, **131**, 59–69.

SAGNOTTI, L. 1992. Paleomagnetic evidence for a Pleistocene counterclockwise rotation of the Sant'Arcangelo Basin, Southern Italy. *Geophysical Research Letters*, **19**(2), 135–138.

SALVADOR, A. (ed.) 1994. *International Stratigraphic Guide*, 2nd edn. International Subcommission on Stratigraphic Classification. International Union of Geological Sciences Trondheim and Geological Society of America, Boulder, Co.

SALVIULO, L., PISCITELLI, S., LOPERTE, A. & CAPUTO, R. 2005. Late Quaternary activity of the Scorciabuoi Fault, Southern Italy. *Rendiconti della Società Geologica Italiana, Nuova Serie*, **1**, 152–153.

SCANDONE, P. 1967. Studi di geologia lucana: la serie calcareo-silica-marnosa ed i suoi rapporti con l'Appennino calcareo. *Bollettino della Società Naturalistica di Napoli*, **76**, 1–175.

SCANDONE, P. 1975. The preorogenic history of the Lagonegro Basin (Southern Apennines). *In*: SQUYRES, C. H. (ed.) *Geology of Italy*. Earth Sciences Society of the Libyan Republic, Tripoli, 305–328.

SCANDONE, P. 1979. Origin of the Tyrrhenian Sea and Calabrian Arc. *Bollettino della Società Geologica Italiana*, **98**, 27–34.

SCHEEPERS, P. J. J., LANGEREIS, C. G. & HILGEN, F. J. 1993. Counter-clockwise rotations in the southern Apennines during the Pleistocene: paleomagnetic evidence from the Matera area. *Tectonophysics*, **225**, 379–410.

SELLA, M., TURCI, C. & RIVA, A. 1988. Sintesi geopetrolifera della Fossa Bradanica (Avanfossa della catena appenninica meridionale). *Memorie della Società Geologica Italiana*, **41**, 87–107.

TIEDEMANN, R., SARNTHEIN, M. & SHACKLETON, N. J. 1994. Astronomic timescale for the Pliocene Atlantic delta ^{18}O and dust flux records of Ocean Drilling Program Site 659. *Paleoceanography*, **9**(4), 619–638.

TURCO, E., MARESCA, R. & CAPPADONA, P. 1990. La tettonica plio-pleistocenica del confine calabro-lucano: modello cinematico. *Memorie della Società Geologica Italiana*, **45**, 519–529.

VAN DIJK, J. P., BELLO, M., TOSCANO, C., BERSANI, A. & NARDON, S. 2000. Tectonic model and three-dimensional fracture network analysis of Monte Alpi (southern Apennines). *Tectonophysics*, **324**, 203–237.

VANN, I. R., GRAHAM, R. H. & HAYWARD, A. B. 1986. The structure of mountain fronts. *Journal of Structural Geology*, **8**, 215–227.

VEZZANI, L. 1966*a*. La sezione stratigrafica di Caliandro nel Pliocene medio-inferiore della Val d'Agri (Lucania), parte 1. *Rivista Italiana di Paleontologia e Stratigrafia*, **72**, 191–229.

VEZZANI, L. 1966*b*. La sezione stratigrafica di Caliandro nel Pliocene medio-inferiore della Val d'Agri (Lucania). *Rivista Italiana di Paleontologia e Stratigrafia*, **72**(1), 191–229; **72**(2), 461–488.

VEZZANI, L. 1967*a*. Il bacino plio-pleistocenico di S. Arcangelo (Lucania). *Atti dell'Accademia Gioenia di Scienze Naturali, Serie VI*, **18**, 207–228.

VEZZANI, L. 1967*b*. La sezione stratigrafica di Castronuovo S. Andrea (Potenza). *Rivista Italiana di Paleontologia e Stratigrafia, Memorie*, **13**, 11–59

VEZZANI, L. 1968. Geologia della tavoletta 'Castronuovo di S. Andrea' (Prov. Di Potenza Foglio 211 IV SE). *Atti dell'Accademia Gioenia di Scienze Naturali, Serie.VI*, **19**, 9–108.

ZAVALA, C. 2000. Stratigraphy and sedimentary history of the Plio-Pleistocene Sant'Arcangelo Basin, Southern Apennines, Italy. *Rivista Italiana di Paleontologia e Stratigrafia*, **106**(3), 399–416.

ZAVALA, C. & MUTTI, E. 1996. Stratigraphy of the Plio-PLEISTOCENE, S. Arcangelo basin, Basilicata, Italy. *Atti Riunione Gruppo Informale di Sedimentologia del CNR, Riunione Annuale Catania, 10–14 October 1996*, 279–282.

Chronology of the Middle–Upper Pliocene succession in the Strongoli area: constraints on the geological evolution of the Crotone Basin (Southern Italy)

L. CAPRARO, C. CONSOLARO, E. FORNACIARI, F. MASSARI & D. RIO

Dipartimento di Geologia, Paleontologia e Geofisica, Università di Padova, Via Giotto 1, 35137 Padova, Italy (e-mail: chiara.consolaro@unipd.it)

Abstract: The aim of this study is to reconstruct the evolution of the Strongoli area, a critical sector of the Crotone Basin (Calabria, Southern Italy), where a thick Middle–Upper Pliocene marine succession is present. The Strongoli succession shows prominent changes in the sedimentary environment that are partly forced by tectonics. Major tectonostratigraphic events have been recognized that might correlate with spreading pulses in the back-arc Tyrrhenian Sea. In particular, we demonstrate that a dramatic basinal collapse at *c.* 2.3 Ma correlates with the so-called 'Calabrian transgression' *Auctorum* and is close in age to the oceanization of the Marsili Basin.

The Strongoli area, located at the northeastern border of the late Neogene Crotone Basin, was indicated by *Roda* (1964) as a critical sector for reconstructing the tectonostratigraphic evolution of the region. The aim of this paper is to reconstruct the major geological features of the Middle–Late Pliocene succession of the Strongoli area (Figs 1 and 2). In particular, our main targets are: (1) to constrain in time and stress the regional importance of a basinal collapse event that correlates with the 'Calabrian transgression' *Auctorum* (Early Pleistocene according to Ogniben 1955); (2) to provide age control for a widespread Mid-Pliocene tectonostratigraphic event, poorly constrained so far, which corresponds to the beginning of the third sedimentary cycle of Roda (1964; Fig. 3); (3) to verify the response of the forearc stratigraphy to the dynamics of the Tyrrhenian back-arc, which can provide important clues for reconstructing the dynamics of plate interactions.

Geological and stratigraphical setting of the Crotone Basin

The Crotone forearc basin is located in the Ionian Calabria (Fig. 1), where one of the thickest and best-exposed Late Miocene to Pleistocene marine sedimentary succession of the recently uplifted Southern Italy is present. The Crotone Basin was regarded by Van Dijk (1992) as an oblique, thin-skinned strike-slip basin, created by a pull-apart between the Petilia–Rizzuto and Rossano–San Nicola NW-trending shear zones (Fig. 2) and probably detached at a depth of a few kilometres.

The stratigraphy of the Crotone Basin as established by Roda (1964) in the 1960s is still generally valid. Roda subdivided the succession into three tectonostratigraphic sequences (Fig. 3). The first sequence develops from the opening of the basin (Mid-Miocene) to intra-Messinian times, the second from late Messinian to Early Pliocene times, and the third from Mid-Pliocene to Mid-Pleistocene times. This subdivision is based on major unconformities corresponding to main reorganization events within the Crotone Basin.

Later, Van Dijk and coworkers (Van Dijk 1991, 1994; Van Dijk & Okkes 1991; Van Dijk & Scheepers 1995) proposed a model in which relationships are analysed between oceanization episodes in the Tyrrhenian Sea, active southeastward arc migration, and opening of basins in the forearc area. A long-lasting tensional regime, characterized by three major phases of subsidence and basin opening in late Tortonian, Early Pliocene and Late Pliocene times, would have been punctuated by short-lived phases of compressional deformation in the Mid-Pliocene and Mid-Pleistocene as a result of plate convergence and the end of the rollback process.

The Strongoli area: previous studies

The most prominent feature of the geological landscape of the Strongoli area is represented by a sandstone body >80 m thick and 6 km wide upon which the village of Strongoli is built (Fig. 4), extending eastwards towards the Ionian coast (Fig. 5). This sandstone body is bracketed between two mainly pelitic units that have been named and interpreted differently by Ogniben (1955) and Roda (1964), as shown in Figure 6.

Ogniben (1955) interpreted the 'Strongoli Sandstone' (hereafter SS) as the regressive unit of a Pliocene transgressive–regressive cycle, in which the underlying 'Timpa Biso Marly Clay' (TBMC)

From: MORATTI, G. & CHALOUAN, A. (eds) 2006. *Tectonics of the Western Mediterranean and North Africa.* Geological Society, London, Special Publications, **262**, 323–336.
0305-8719/06/$15.00

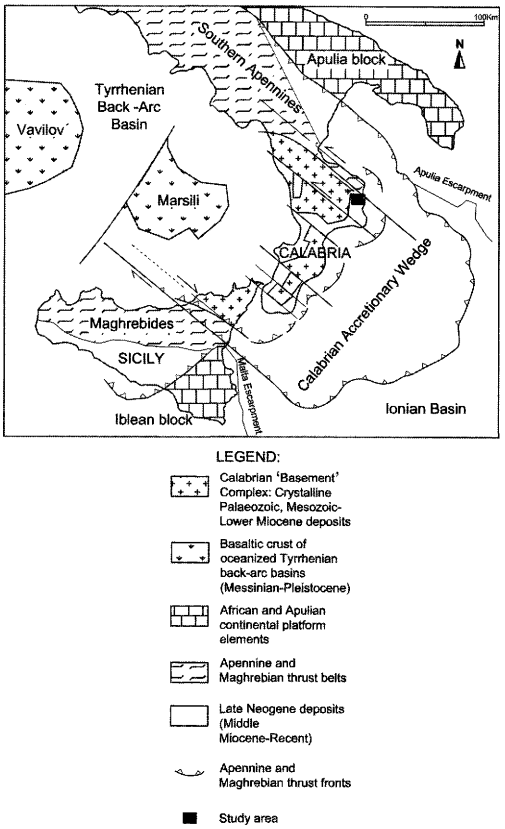

Fig. 1. Outlines of the main geological units and structural elements of southern Italy and surrounding basins (adapted from Van Dijk 1994).

would represent a transgressive portion. Likewise, the overlying 'Gigliolo Clay' (GC) would record the transgressive stage of a younger sedimentary cycle, also known as the 'Calabrian transgression' *Auctorum* (i.e. Gignoux 1913; Ruggeri & Selli 1948; Selli 1949; Ogniben 1955).

In contrast, Roda (1964) considered the TBMC and GC of Ogniben (1955) simply as component members of the Middle Pliocene–Lower Pleistocene 'Cutro Marly Clay' (CMC), whereas he regarded the SS as the record of a local sedimentary episode within the CMC with no major eustatic significance (Fig. 6). In Roda's interpretation, the offshore CMC would gradually onlap shallow-water and lagoonal units that are present in the most marginal part of the Crotone Basin (i.e. the Scandale sandstone and the Spartizzo marly clay, respectively) beginning from the base of the third tectonostratigraphic cycle (Figs 3 and 6).

In this paper, we will follow the formational terminology of Ogniben (1955) because it is more appropriate for presenting our data and more in keeping with our interpretation of the geological evolution of the Crotone Basin.

However, we could not resolve firmly the puzzling relationship between the TBMC and the underlying Murgie sandstone body (Fig. 4a), which extends west of the study area (Fig. 5). This unit was considered by Ogniben (1955) and Roda (1964) as mainly belonging to the Scandale Formation, in substantial stratigraphic continuity with the TBMC and thus belonging to the third cycle of Roda (1964). In contrast, Zecchin *et al.* (2004) correlated the Murgie body with the second cycle of Roda (1964).

Material and methods

We collected a total of about 100 samples from two sections (namely, the 'Ecce Homo' and 'Strongoli' sections) and from intervening tracts (spot samples). The integration of facies analysis with the study of foraminiferal assemblages was aimed at reconstructing the depositional environment with special reference to the formation of Mediterranean sapropel-like layers. Pollen and stable oxygen isotope studies on selected intervals provided critical information on the climatic evolution and cyclicity. The latter data, integrated with calcareous plankton biostratigraphy, allow a firm and highly resolved chronological framework for the investigated succession. The adopted time framework is reported in Figure 7, which includes the chronostratigraphic scale, geomagnetic polarity time scale (GPTS; Cande & Kent 1992, 1995), Mediterranean calcareous nannofossil biozonation (Rio *et al.* 1990), major planktonic foraminiferal bioevents (after Lourens *et al.* 1996, 2004), reference oxygen isotope curve of benthic Foraminifera from Ocean Drilling Program (ODP) Sites 846 (Shackleton *et al.* 1995*a*,*b*) and 677 (Shackleton *et al.* 1990), and Mediterranean sapropel layers with the i-cycle code (after Lourens *et al.* 1996; Kroon *et al.* 1998). Chronology was derived using the astronomical tuning of Lourens *et al.* (1996, 2004).

Here we report the most significant data collected in the Strongoli area. Calcareous nannofossil biostratigraphy has been established for about 100 samples. Calcareous nannofossil taxonomy and zonation are after Rio *et al.* (1990). Nannofossil quantitative data were collected counting the marker species of *Discoaster* within a total of 20–50 discoasterids; for rarer occurrences, three vertical traverses were analysed. Planktonic and benthic Foraminifera were studied in about 80 samples, 65 of which have been analysed with quantitative methods (at least 300 planktonic and 300 benthic specimens were identified and counted) from the >125 μm fraction

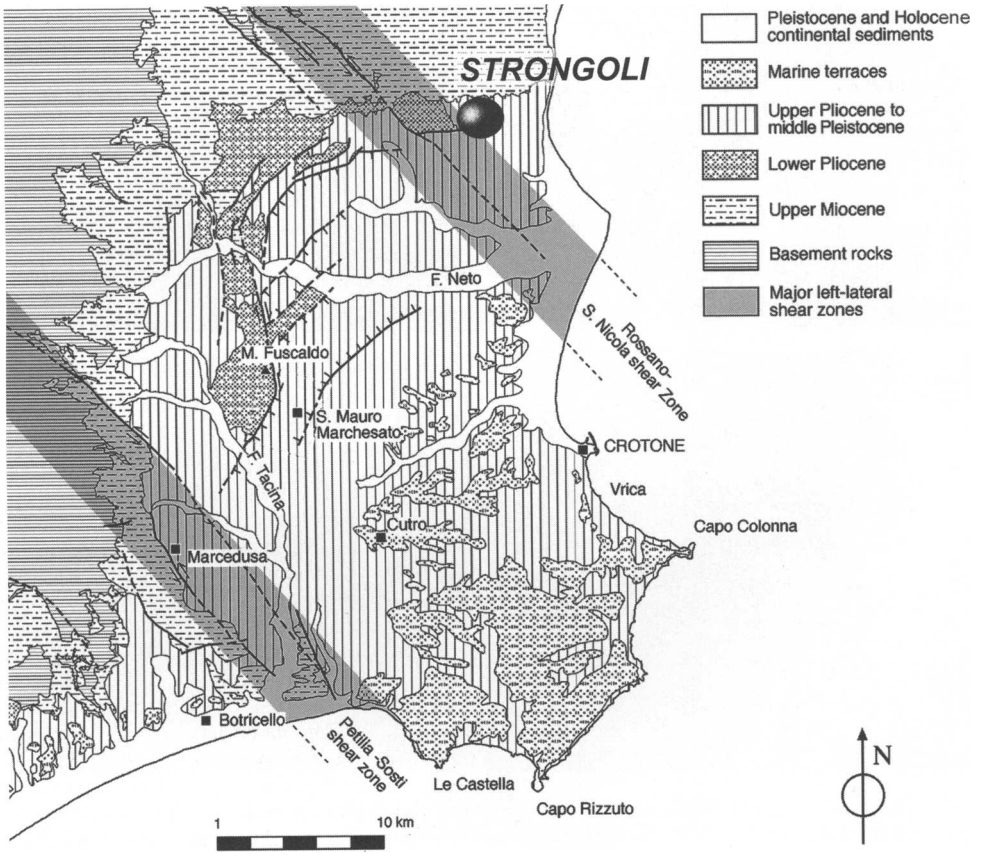

Fig. 2. Simplified geological sketch of the Crotone Basin (modified from Massari *et al.* 2002) and location of study area. Evolution of the Crotone Basin was controlled by two NW-trending crustal shear zones (the Rossano–S. Nicola and Petilia–Sosti Zones).

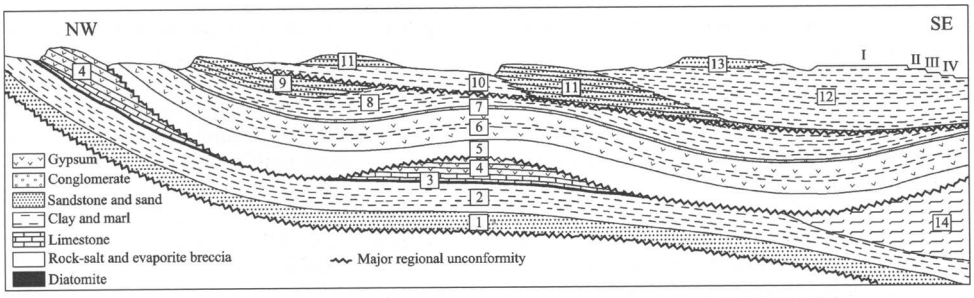

MIDDLE MIOCENE - MESSINIAN CYCLE	MESSINIAN - LOWER PLIOCENE CYCLE	MIDDLE PLIOCENE - PLEISTOCENE CYCLE	MARINE TERRACES (Gliozzi, 1987)
1 S. Nicola Formation	5 Detrital Saline Formation	10 Spartizzo Marly Clay	I Cutro
2 Ponda Marly Clay	6 Upper Evaporite Formation	11 Scandale Sandstone	II S. Leonardo - Campolongo
3 Tripoli Formation	7 Carvane Conglomerate	12 Cutro Marly Clay	III Le Castella - Capo Rizzuto
4 Lower Evaporite Formation	8 Cavalieri Clayey Marl	13 S. Mauro Sandstone	IV Capo Colonna
14 Allochthonous mass	9 Zinga Sandstone		

Fig. 3. Large-scale stratigraphy of the Crotone Basin as outlined by Roda (1964; slightly modified). This paper is focused on the third tectonostratigraphic cycle, particularly on the lower part of the Cutro Marly Clay Unit.

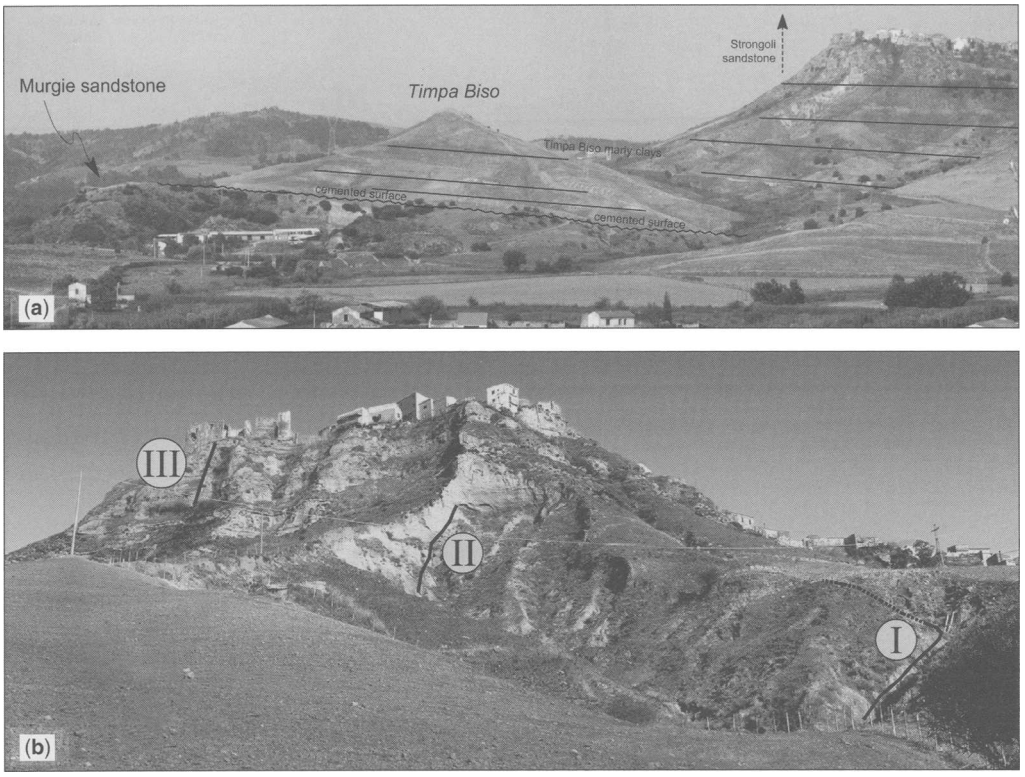

Fig. 4. (**a**) Panoramic view of the Timpa Biso–Strongoli area. Three units can be distinguished: the Murgie sandstone, the Timpa Biso Marly Clay (TBMC) and the Strongoli Sandstone (SS). (**b**) Measured segments of the upward-coarsening Strongoli section. Segments I and II belong to the TBMC; segment III crosses the SS.

of the split residues. Non-quantitative analyses only have been performed on spot samples, for which the relative distribution of foraminifer species is reported in terms of abundant, common or rare occurrence. The complete census dataset is available online as a Supplementary Publication at http://www.geolsoc.org.uk/SUP18250. A hard copy can be obtained from the Society Library. Standard techniques of preparation and microscope analysis have been used. Taxonomy of foraminiferal species is after Kennett & Srinivasan (1983) and Loeblich & Tappan (1988), and palaeoecology is after Sen Gupta (1999, and references therein). Planktonic foraminiferal quantitative data (measured sections only) are presented here in terms of the relative abundance fluctuations of marker species *Globorotalia bononiensis* and *Globorotalia crassaformis* sx (see Fig. 9). By means of the relative distribution of selected planktonic foraminiferal species, a sea surface temperature (SST) proxy model was also reconstructed (Lourens *et al.* 1996), which allows the recognition of cool and warm intervals (Fig. 9). Benthic foraminifers (measured sections only) have been used to construct the benthic foraminifera oxygen index (BFOI) curve, which is largely based on the model proposed by Kaiho (1994; Fig. 9). The planktonic foraminiferal distribution reported by Lourens *et al.* (1996) and Sprovieri *et al.* (1998) has been used as reference (particularly for the correlations of sapropel-like layers). Stable oxygen isotope analyses of 55 samples have been carried out on the planktonic foraminiferal species *Globigerinoides ruber* and the benthic foraminiferal species *Cibicidoides dutemplei*, *Uvigerina peregrina* and *Uvigerina bononiensis*. Analyses were performed by an automatic Finnigan MAT 252 mass spectrometer at the Department of Geology and Geochemistry of Stockholm University. Data are reported in δ notation with respect to the VPDB standard reference; measure precision is about $\pm 0.1‰$. For pollen analysis, we have processed 57 samples. From each sample, 10 g of sediment were treated according to standard acid–alkali procedures followed by heavy liquid separation ($ZnCl_2$ at $d = 2.004$) and ultrasound treatment. A minimum of 120 pollen grains was counted in each sample excluding *Pinus*.

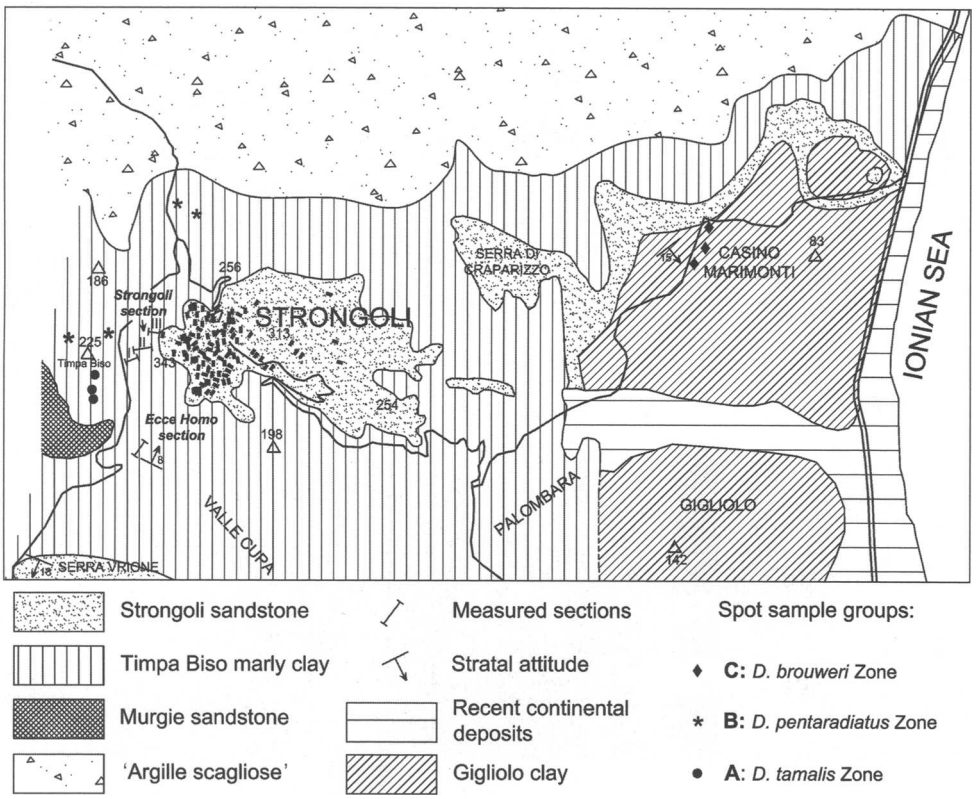

Fig. 5. Simplified geological map of the Strongoli area (modified from Ogniben 1955). Measured sections and principal spot samples are reported.

Ogniben (1955)	**Roda** (1964)
Gigliolo clay	Cutro marly clay
Strongoli sandstone	
Timpa Biso marly clay	
Scandale sandstone	Scandale
Spartizzo marly clay	Spartizzo

Fig. 6. Simplified comparison between the informal terminology proposed by Ogniben (1955) and that of Roda (1964) for subdividing the stratigraphy of the Strongoli area.

Fern and fungal spores and dinoflagellate cysts were not included in the pollen sum.

The Strongoli stratigraphic succession

In the Strongoli area, part of the stratigraphic succession is poorly exposed (Fig. 4). A continuous succession could not be reconstructed, apart from two well-exposed sections (the Ecce Homo and Strongoli sections), which have been sampled in detail (Figs 4a and 9). In contrast, intervening tracts have been spot sampled only (Fig. 5). Although distances between the measured sections might prevent a firm correlation, we reconstructed a composite representative log of the succession by splicing together four major segments (Fig. 8).

The local substrate of the Timpa Biso Marly Clay

The lower part of the TBMC crops out only along the southern flank of the Timpa Biso hill (Figs 4a and 5).

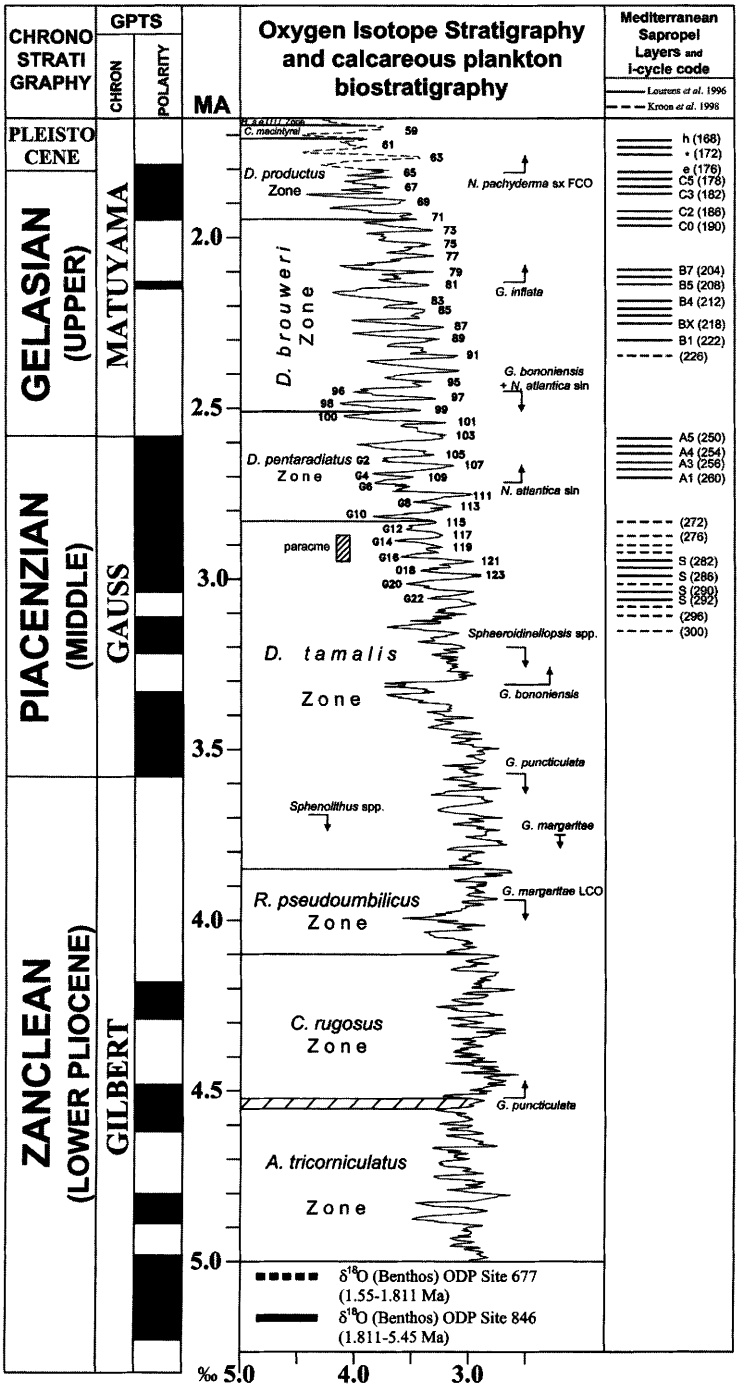

Fig. 7. Adopted time framework. Chronostratigraphic and geomagnetic polarity time scale (GPTS) are after Lourens *et al.* (1996, 2004). Oxygen isotope stratigraphy is after Shackleton *et al.* (1990, 1995*a*,*b*). Calcareous plankton biostratigraphy is after Rio *et al.* (1990), Sprovieri *et al.* (1994, 1998) and Lourens *et al.* (1996, 2004). Mediterranean sapropel layers are after Lourens *et al.* (1996) and Kroon *et al.* (1998). FCO, first common occurrence; LCO, last common occurrence.

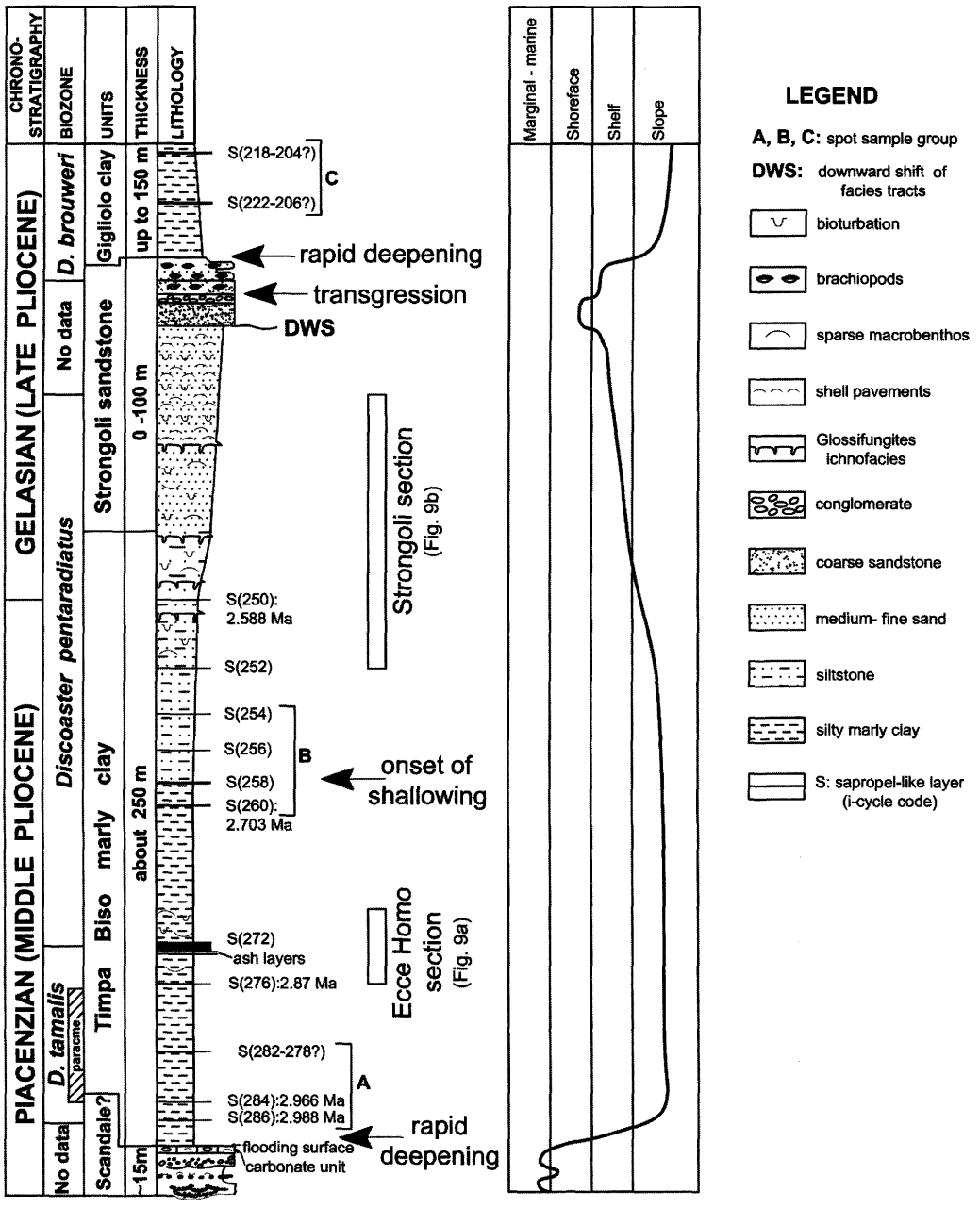

Fig. 8. Simplified log of the Strongoli succession according to the adopted chronological framework. Major stratigraphic events and inferred palaeobathymetry are indicated.

Here, below the TBMC, a sandy–pebbly unit consisting of a number of transgressive–regressive, marginal-marine cycles is present that might correlate with the Spartizzo–Scandale complex (Fig. 8). This unit is discontinuously capped by shallow-marine, highly fossiliferous and tightly cemented sandy and pebbly limestones with *Isognomon* and large pectinids. Immediately above, a thin lag of bored pebbles

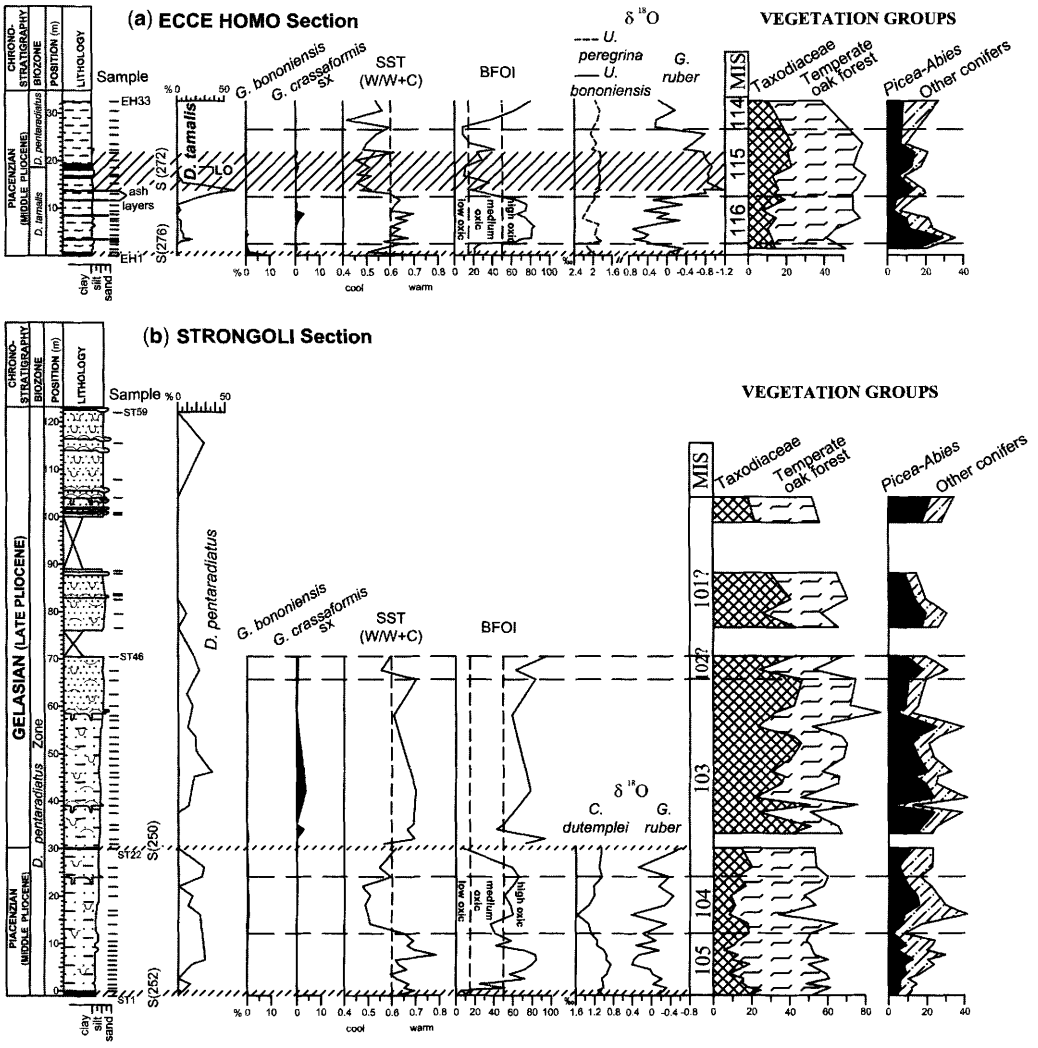

Fig. 9. Palaeoclimatic and biostratigraphic data from the Ecce Homo (**a**) and Strongoli (**b**) sections. Left: stratigraphic log of the sections and distribution of marker nannofossil species in terms of percentage of the total discoasterids assemblage. Middle: data based on foraminiferal assemblages. Distribution of planktonic Foraminifera marker species *Globorotalia bononiensis* and *Globorotalia crassaformis* sx in terms of percentage of the total assemblage. SST, proxy curve of sea surface temperature, i.e. a ratio between 'Warm' (W) and 'Cold' (C) planktonic Foraminifera species: W/(W + C). 'Warm' species are *Globigerinoides* ex gr. *ruber*, *G. obliquus*, *G. sacculifer* gr., *Zeaglobigerina* spp., *Orbulina universa* and *Globorotalia crassaformis*. 'Cold' species are *Globigerina falconensis*, *G. quinqueloba*, *G. glutinata*, *Neogloboquadrina* spp. sx and *Globorotalia scitula* (after Lourens *et al.* 1996). BFOI, Benthic foraminifer oxygen index, i.e. the ratio between 'Oxic' (O) and 'Dysoxic' (D) benthic foraminiferal species: ((O/(O + D)) × 100 (after Kaiho 1994). 'Oxic' species are *Cibicides* spp., *Cibicidoides* spp. *Globocassidulina* spp. *Pyrgo* spp. and *Quinqueloculina* spp. 'Dysoxic' species are *Bolivina* spp., *Bulimina exilis*, *Chilostomella oolina*, *Fursenkoina schrembersiana*, *Globobulimina* spp., *Stainforthia complanata*, *Stilostomella* spp., *Uvigerina bononiesis* and *U. cylindrical*. Dashed bars indicate low-oxygen intervals. Oxygen isotope data are given in δ notation with respect to the VPDB standard. MIS, correlative Marine Isotope Stages as deduced from oxygen isotope, microfaunal and pollen data. Right: selected vegetation groups with high ecological significance. Relative percentages of pollen taxa are calculated without *Pinus*. Taxodiaceae (*Taxodium* + *Sciadopitys* + *Nyssa*) and temperate forest elements (*Quercus* + other mesothermic broad-leaved trees) are indicative of a warm and humid climate; *Picea* + *Abies* + other conifers (*Tsuga* + *Cedrus*) indicate cool to cold climatic conditions with high precipitation rates.

and cobbles is present, which can be extensively traced laterally in the field as a marker horizon (Figs 4a and 8).

The Timpa Biso Marly Clay: deepening stage

The abrupt transition from the carbonate unit to the overlying outer-shelf and upper slope hemipelagic mudstones (TBMC) suggests a rapid deepening (Fig. 8). The base of the TBMC is not exposed, being generally hidden below a grass cover. The lower part of the TBMC mainly consists of silty marly clay and marly silt with sparse sandy beds, two ashbeds and a number of laminated sapropel-like layers (Figs 8 and 9). The latter usually indicate a palaeodepth in excess of 300 m (as suggested by Rohling & Gieskes 1989).

We spot sampled the lowermost outcrops of the TBMC on the southern side of the Timpa Biso hill (group A, Fig. 5). These samples belong to the *Discoaster tamalis* Zone, the paracme interval of which (extending from Marine Isotope Stage (MIS) 121 to MIS 117, according to Sprovieri *et al.* 1994, 1998) was clearly recognized (Fig. 8). In this sampling area, three sapropel-like laminated layers have been detected in the field (corresponding to samples TB/02/10, TB/02/16-17 and TB/02/23 as coded in the Supplementary Publication 18250 tables; see p. 000). In these layers, siliceous remains are abundant and benthic foraminiferal assemblages are dominated by low-oxygen tolerant genera such as *Bolivina*, *Bulimina* and *Uvigerina* (Sen Gupta 1999, and references therein). Based on their stratigraphic position with respect to the peculiar distribution pattern of *D. tamalis* (before the paracme, Fig. 8) the presence of *Globorotalia bononiensis* and the presence or absence datum of *Globorotalia crassaformis* dx (see Supplementary Publication tables), two of these sapropel-like layers can be confidently correlated with the Mediterranean sapropels i-cycle 286 (2.988 Ma) and i-cycle 284 (about 2.966 Ma). Minor constraints are available for the third sapropel-like layer (Fig. 8), which occurs within the *D. tamalis* paracme interval and thus might correlate with Mediterranean sapropel i-cycle 282 (2.943 Ma), i-cycle 280 (2.921 Ma) or i-cycle 278 (2.900 Ma). The Last Occurrence (LO) of *D. tamalis* (2.83 Ma) has been detected in the middle part of the Ecce Homo section, which belongs to the *Discoaster pentaradiatus* Zone (2.83–2.51 Ma) in its upper part (Fig. 9a). In this section, oxygen isotope analyses, as well as quantitative analyses of the foraminiferal and pollen contents, have been performed (Fig. 9a). Based on the oxygen isotope ratio, two glacial–interglacial cycles have been recognized. Both interglacials are characterized by low-oxygen conditions (dashed bars in Fig. 9a) and very light $\delta^{18}O$ planktonic values (Fig. 9a). Interestingly, the SST curve shows low values during these intervals, mainly because of a frequency drop in the oligotrophic, warmth-demanding planktonic species *Globigerinoides* ex gr. *ruber* and *Zeaglobigerina* spp. (Hemleben *et al.* 1989; Pujol & Vergnaud-Grazzini 1995). Together, these data suggest that $\delta^{18}O$ interglacials in the Ecce Homo section were characterized by eutrophic conditions possibly favoured by increases in freshwater runoff. The lower low-oxygen episode occurs just above the paracme of *D. tamalis*. As *G. bononiensis* is rather abundant (about 10% of the total assemblage; Fig. 9a), this interval might correlate with the Mediterranean sapropel i-cycle 276 (*c.* 2.87 Ma). The LO of *D. tamalis*, which is correlative with interglacial MIS 115/G11 (Fig. 7), has been confidently detected within the upper sapropel-like interval (Fig. 9a). It follows that the latter corresponds to the Mediterranean sapropel i-cycle 272 (2.828 Ma) and, consequently, correlation of glacial intervals below and above with MIS 116/G12 and 114/G10, respectively, is straightforward (Fig. 9a).

Two further laminated sapropel-like layers have been recognized in the spot samples collected between the Ecce Homo and Strongoli sections (group B in Fig. 5, TB/02/5 and ST/03/1-3 as coded in the Supplementary Publication tables), which belong to the *Discoaster pentaradiatus* Zone (Fig. 8). Both these layers are characterized by abundant *G. bononiensis*; however, one is dominated by 'cold' and 'eutrophic' planktonic species, whereas the other is dominated by 'warm' species (see Supplementary Publication tables). These planktonic assemblages closely resemble those reported by Lourens *et al.* (1996) for the Mediterranean sapropels i-cycle 260 (2.703 Ma) and i-cycle 258 (2.679 Ma), respectively.

The shallowing stage: transition from Timpa Biso Marly Clay to Strongoli Sandstone

A shallowing trend begins some tens of metres below the Strongoli section and develops in this section, as clearly indicated by coarsening from clayey silt to fine to medium, highly fossiliferous sand (Fig. 8). Below the Strongoli section, spot samples belonging to the *Discoaster pentaradiatus* Zone have been collected (group B, Fig. 5; KR/03/143 and KR/03/142 in the Supplementary Publication tables), in which benthic foraminiferal assemblages suggest the occurrence of two distinct low-oxygen intervals. The lower one (KR/03/143) is characterized by a planktonic assemblage similar to that described by Lourens *et al.* (1996) for the Mediterranean sapropel i-cycle 256 (*c.* 2.658 Ma), whereas the upper (KR/03/142) is faunistically similar to the Mediterranean sapropel i-cycle 254 (2.632 Ma; Lourens *et al.* 1996).

From the base up to *c.* 83 m, the Strongoli section (Fig. 9b) is composed of silts and fine sands that are thoroughly bioturbated with sparse macrobenthic assemblages dominated by *Turritella*, pectinids, scaphopods, ahermatypic corals and annelids. Four firmground horizons draped by *Neopycnodonte* clumps and marked by *Glossifungites* ichnofacies at 24, 39, 58.5 and 104 m may record minor flooding events. Starting from about 83 m, the dominant sedimentation pattern consists of cyclic alternation of bioturbated fine sands and highly fossiliferous fine to medium sands and sandstones with common pavements and layers of transported shells forming sedimentological concentrations with convex-up and locally nested valves (Fig. 9b). In the upper Strongoli section and above, sediments are either (1) not cemented or poorly cemented, or (2) cemented into some protruding sandstone layers as a result of selective erosion (Figs 8 and 9b). Common plant remains and sedimentological features suggest a direct or lateral link with a prograding, wave- and storm-influenced delta system developing from a prodelta to a delta-front setting.

In the upper part of the Strongoli Sandstone Unit, a sharp transition to fossiliferous coarse shoreface sandstone and fine-grained conglomerate layers that sparsely crop out may indicate a downward shift of the facies tracts (DWS in Fig. 8).

The entire Strongoli section (about 120 m) belongs to the *Discoaster pentaradiatus* Zone (Fig. 9b). In the lower part of the section (0–30 m), oxygen isotopes and both foraminiferal and pollen assemblages document a full glacial interval bracketed by two interglacials (Fig. 9b), in the midst of which two low-oxygen episodes have been recognized (see the BFOI in Fig. 9b). These low-oxygen episodes (which are located at the base of the section and at 30 m level, respectively) can be confidently correlated with the Mediterranean sapropels i-cycle 252 (2.611 Ma) and 250 (2.588 Ma; Figs 8 and 9b). Therefore, it follows that the lower part of the Strongoli section (0–30 m) corresponds to the MIS 105–MIS 103 interval (Figs 7 and 9b). Above, from 30 to 104 m level, foraminiferal assemblages (where available) indicate persisting warm climatic conditions (see the SST curve in Fig. 9b), as also confirmed by a pollen assemblage dominated by warmth-demanding Taxodiaceae (Fig. 9b). Thus, the interval from 30 to 104 m level may correlate with the long MIS 103–101 interglacial complex, during which no severe glacial occurs (Figs 7 and 9b). In fact, we did not detect pollen evidence of the prominent MIS 100–96 glacial complex, which is well documented in Northern Italy as a time of severe glacial conditions (e.g. Marecchia section: Rio *et al.* 1997), although it is not well known from Southern Italy.

Pollen and microfaunal analyses are not feasible in the upper portion of the Strongoli Sandstone because of the unsuitable facies. However, recognition of the interglacial MIS 103–101 complex (Fig. 9b) suggests that the upper part of the SS encompasses at least the glacial MIS 100. Thus, we speculate that the downward shift recognized close to the top of the SS may have been chiefly controlled by glacioeustasy (Fig. 8).

The Gigliolo Clay transgression and abrupt deepening

At the top of the SS, a distinct transgressive sheet is present that consists of highly fossiliferous sandstone and pebbly sandstone separated by a silty layer (Fig. 8). This interval, which is some 5 m thick, is overall very rich in brachiopods with subordinate echinoids, pectinids, ahermatypic corals and bryozoans, which are commonly bored and encrusted. The fossiliferous interval grades very rapidly into deep-water silts and marly clays with sapropel-like layers (namely, the Gigliolo Clay, GC; Fig. 8). The transition is rapid but without discontinuity, thus suggesting that the Strongoli area underwent a dramatic tectonic collapse after SS times. Spot samples have been collected from an exposure of the GC in the eastern part of the Strongoli area (group C, Fig. 5). Nannofossil assemblages indicate that the basal portion of the GC (0–20 m) belongs to the *Discoaster brouweri* Zone (Fig. 8). Moreover, the absence of foraminiferal marker species *Globorotalia bononiensis*, *Globorotalia inflata* and *Neogloboquadrina atlantica* provides evidence that sedimentation of the GC began after the LO of *G. bononiensis* and *N. atlantica* (2.41 Ma) and before the FO of *G. inflata* (2.09 Ma). Based on this biostratigraphic evidence, the sapropel-like layers recognized in the basal GC (KR/03/155–153 and KR/03/144 in the Supplementary Publication tables) are correlatable with the Mediterranean sapropels of cluster B, between 2.3 and 2.1 Ma (Figs 7 and 8).

Discussion

Onset of Roda's (1964) third tectonostratigraphic sequence

According to Roda's interpretation, in the Strongoli area the base of the CMC (that is, the base of the TBMC of Ogniben 1955) would be time equivalent to the base of the marginal marine–continental units laterally developing west of the study area (i.e. the Spartizzo–Scandale complex). The base of these units would also correlate with the beginning of the third tectonostratigraphic cycle of Roda (1964). Here, for the first time, we provide firm evidence that the onset of Roda's (1964) third cycle is

older than 3 Ma because, in the Strongoli area, the basal CMC (i.e. the TBMC) belongs to the upper *D. tamalis* Zone. In this area, the beginning of the third tectonostratigraphic cycle of Roda (1964) is documented by marginal–continental sediments (the Spartizzo–Scandale complex). Deposition of the deep marine CMC began later in the area, after an unresolved time interval corresponding to the deposition of both the sandy and limestone units (which we consider here as part of the Scandale sandstone) that are present below the TBMC (Figs 4a and 8). According to a very rough evaluation, the time elapsed might be very significant. Thus, evidence is provided that in the Strongoli area, the base of the CMC (i.e. the TBMC) is correlative neither with the base of the Spartizzo–Scandale complex, nor strictly with the beginning of Roda's (1964) third tectonostratigraphic cycle.

The interaction of glacioeustasy–tectonics–sediment supply

Our data suggest that a large part of the regression associated with the deposition of the SS is not primarily controlled by glacioeustasy. In fact, it is proposed that (1) most of the shallowing trend from the TBMC to the SS takes place under warm and humid climatic conditions (i.e. fully interglacial; Fig. 9b) that are usually correlative with high sea level, and (2) the total thickness of the regressive portion of the TBMC (some 100 m; Fig. 8) is not large enough to explain a simple terrigenous infill of the former accommodation space (of the order of 200–300 m) without invoking a strong synsedimentary uplift. It follows that the regressive evolution of the TBMC–SS complex was probably largely shaped by tectonics. Likewise, the rapid deepening corresponding to the base of the TBMC can be explained only in terms of accelerated subsidence. Nevertheless, we speculate that the downward shift recognized in the upper SS may reflect a major glacioeustatic event (i.e. the glacial MIS 100). In this case, we would confirm that glacioeustasy may still be readable also in active tectonic settings such as that of the Crotone Basin (i.e. Rio *et al.* 1996; Massari *et al.* 2002) although tectonics and sedimentary supply are still dominant in shaping the large-scale architecture of the stratigraphic record.

The rapid deepening events at the onset of the GC deposition

Above the SS, the GC unit records a dramatic deepening of the Strongoli area in the *Discoaster brouweri* Zone, between 2.3 and 2.1 Ma. In the interpretation of Ogniben (1955), the beginning of the GC deposition is correlative with the so-called 'Calabrian transgression' *Auctorum* (e.g. Gignoux 1913; Ruggeri & Selli 1948; Selli 1949). Apparently, this event is not just local in scope because, beginning from Late Pliocene–Early Pleistocene times, a thick succession of deep-marine sediments is widespread over the entire Crotone Basin. Here, we provide tight chronological framing that this regional event began in Late Pliocene times, and thus, the so-called 'Calabrian transgression' is not Pleistocene in age (at least in the Crotone Basin area), as suggested by previous studies (e.g. Gignoux 1913; Ruggeri & Selli 1948; Selli 1949; Ogniben 1955). Moreover, we demonstrate that the so-called 'Calabrian transgression' occurs mainly in response to the tectonic collapse of the entire Crotone Basin rather than because of glacioeustasy.

The regional geological framework

Van Dijk (1991, 1992, 1994) and Van Dijk *et al.* (1998) subdivided the tectonostratigraphic development of the Crotone Basin into four stages: (1) a Serravallian–early Messinian stage of progressive enlargement of the basin, closed by a major intra-Messinian transpressional tectonic event; (2) a mid-Messinian–Early Pliocene stage characterized by intense faulting overprinted by the Messinian salinity crisis, and closed by a major Mid-Pliocene compressional phase responsible for basin closure; (3) a Late Pliocene–Early Pleistocene stage, characterized by pulsating onlap, and later interpreted (Van Dijk & Scheepers 1995) to be closed by a regional Mid-Pleistocene contraction phase accompanied by oroclinal-type rotations, transpressions and basin inversions; (4) a Mid-Pleistocene–Recent stage, characterized by strong vertical movements. Stress analyses revealed a pattern of overall tension, with three major phases of subsidence and basin opening in late Tortonian, Early Pliocene and Late Pliocene times, interrupted by short periods of compressional deformation in the Mid-Pliocene and Mid-Pleistocene. The extensional stages would correlate with long episodes of rollback, translation of the Calabrian lithosphere to the SE, attributed to gravitational displacement and spreading in the Tyrrhenian back-arc area. Phases of cessation of spreading in the back-arc basin would have coincided with interruption of slab migration. This would have resulted in short pulses of regional compression caused by the movement of the African Plate relative to the European Plate, which generated a component of NE-directed translation of the Calabrian block (Van Dijk 1992).

Focusing specifically on the Pliocene evolution, a strongly extensional–transtensional regime and high subsidence rate dominated in the Crotone Basin from the late Messinian and especially during the Early Pliocene. This regime is recorded by

spectacular listric normal growth faults in the Lower Pliocene succession (Van Dijk 1991; Moretti 1993; Zecchin *et al.* 2004). As already noted, a contractional phase possibly at the end of the Early Pliocene can be documented throughout the Crotone Basin (Roda 1964; Van Dijk 1991, 1994; Zecchin *et al.* 2004). Transpressional and compressional effects can be recognized throughout the basin and are recorded in its northern part by a major erosional and angular unconformity corresponding to the base of Roda's (1964) third tectonostratigraphic cycle.

This contraction phase should coincide with a major phase of shortening, where upper Messinian and Lower Pliocene deposits of both internal and external chain domains were incorporated in the thrust belt and unconformably covered by sediments of the *Globorotalia puncticulata* Zone of Sprovieri (1992) (Patacca *et al.* 1990; Sartori 1990). In the Crotone Basin, data collected so far are not sufficient to firmly constrain this event in time. However, we speculate that the base of the third tectonostratigraphic cycle of Roda (1964) might fully, or at least partly, represent the regional response of the Calabrian forearc to the *G. puncticulata* event. Unfortunately, as stated above, in the Strongoli area the base of the third cycle of Roda (1964) is documented by shallow-water sediments that are not amenable to biochronological studies. Further investigations are needed on the Mid-Pliocene offshore sediments of the Crotone Basin, where the base of Roda's third cycle is likely to be represented by an uninterrupted stack of deep-marine clays belonging to the CMC.

A second, rapid acceleration of subsidence occurred during Late Pliocene times (the GC event). According to Ogniben (1955), this event corresponds to the so-called 'Calabrian transgression' reported by various workers as a supra-regional event recognized in several localities of the Italian peninsula (Gignoux 1913; Ruggeri & Selli 1948; Selli 1949). This event is well documented in the northeastern marginal part of the Crotone Basin, where deep-marine sediments abruptly were overlain on a shallow-marine substrate. Collapse was then followed by continuing high subsidence rates throughout the latest Pliocene and Early Pleistocene, as shown by the exceptionally thick dominantly hemipelagic succession of this age in the Crotone Basin.

The connections with back-arc events in the Tyrrhenian Sea

As currently known, the migration of the Calabrian arc was characterized most of the time by an upper plate velocity slower than the rollback velocity, so that extension in the upper plate and opening of back-arc basins kept pace with the trench retreat (Malinverno & Ryan 1986). The geodynamic frame leading to rapid retrograde motion of a subducting plate and concurrent opening of a back-arc basin is typically that of a subduction zone that has become narrow in the along-trench direction after a process of slab break-off (Dvorkin *et al.* 1993; Gvirtzman & Nur 1999, 2001; Faccenna *et al.* 2001*a*,*b*, 2004).

Rollback velocity was much greater in the southern Tyrrhenian Basin (5–6 cm a^{-1} according to Faccenna *et al.* 2004; 6–10 cm a^{-1} according to Rosenbaum & Lister 2004), than in the northern Tyrrhenian Basin, where it did not exceed 2 cm a^{-1}, because in the southern area the subducting lithosphere (the Ionian downgoing slab) remained oceanic until the present day, whereas in the northern area rollback slackened as a result of buoyancy of the subducting continental lithosphere (Dercourt *et al.* 1986; Malinverno & Ryan 1986; Patacca *et al.* 1990; Royden 1993; Rosenbaum & Lister 2004). Several researchers (e.g. Patacca *et al.* 1990; Rosenbaum & Lister 2004, and references therein) have argued that differential rates of extension between the northern and southern Tyrrhenian Sea may have been accommodated by the activation of two major crustal shear zones allowing the rapid southeastward migration of the Calabrian block. Slab tear led to the formation of a narrow subducting slab beneath the Ionian Sea whose width is estimated at *c.* 200 km. Lateral mantle flow around the slab flanks was accompanied by their large-scale rotation, leading to oroclinal bending of the arc (Faccenna *et al.* 2004; Rosenbaum & Lister 2004).

Oceanization in the southern Tyrrhenian Basin took place through discrete jumps with southeastward polarity. Rifting and spreading episodes first generated the Vavilov Basin, then the Marsili Basin. Kastens *et al.* (1988) concluded that formation of basaltic crust in the Vavilov Basin may have began during the late Miocene, and the process was certainly widespread by the Early Pliocene. Biostratigraphic data for the oldest cored sediments overlying the basaltic basement of Marsili Basin have been obtained from ODP site 650 (Kastens *et al.* 1987). The position of the drill site was chosen in a location (near the western rim of the basin) ensuring that the basement age is probably the oldest in the basin (Kastens *et al.* 1987). The cored nannofossil ooze has been attributed to the terminal part of the *Discoaster brouweri* Zone because of the presence of the zonal marker species associated with *G. inflata* (i.e. between 2.1 and 1.95 Ma, according to the new chronology of Lourens *et al.* 1996). This is a minimum age for the opening of the Marsili Basin, as it may be assumed that the spreading event initiated and developed somewhat before the age of the overlying sediments.

Conclusions

Data presented in this paper provide a new chronological control on the geological evolution of a

marginal although critical sector of the Crotone Basin. For the first time, a good chronology is available both for establishing a minimum age for the third tectonostratigraphic cycle of Roda (1964) and for constraining the age of the so-called 'Calabrian transgression' *Auctorum*. This chronology also provides time controls that are regional and supraregional in scope when compared with the overall evolution of the Calabrian back-arc (i.e. the Tyrrhenian Basin; Fig. 1). Our data suggest that the Gigliolo Clay collapse event in the forearc Crotone Basin is very close in time to the rifting associated with the oceanization of the Marsili Basin, which resulted in a strong acceleration in the regional subsidence. Thus, it is tempting to infer that this event in the Tyrrhenian Basin correlates with the beginning of the deposition of the exceptionally thick Late Pliocene and Early Pleistocene succession of deep-marine sediments that are exposed in the Crotone Basin (i.e. the Cutro Marly Clay *pro parte*).

This research has been funded by the University of Padova (Progetto Giovani Ricercatori 2003) to L. Capraro and by MIUR (PRIN 2001) to F. Massari. We thank J. Backman, P. Torssander and K. Hajnal for help in isotope analysis. Thanks go to R. Sprovieri and C. Turner for their constructive reviews.

References

CANDE, S. C. & KENT, D. V. 1992. A new geomagnetic polarity time scale for the Late Cretaceous and Cenozoic. *Journal of Geophysical Research*, **97**, 13917–13951.

CANDE, S. C. & KENT, D. V. 1995. Revised calibration of the geomagnetic polarity time scale for the Late Cretaceous and Cenozoic. *Journal of Geophysical Research*, **100**, 6093–6095.

DERCOURT, J., ZONENSHAIN, L. P., RICOU, L.-E., *ET AL.* 1986. Geological evolution of the Tethys belt from the Atlantic to the Pamirs since the Lias. *Tectonophysics*, **123**, 241–315.

DVORKIN, J., NUR, A., MAVKO, G. & BEN-AVRAHAM, Z. 1993. Narrow subducting slabs and the origin of backarc basins. *Tectonophysics*, **227**, 63–79.

FACCENNA, C., BECKER, T. W., LUCENTE, F. P., JOLIVET, L. & ROSSETTI, F. 2001*a*. History of subduction and back-arc extension in the Central Mediterranean. *Geophysical Journal International*, **145**, 809–820.

FACCENNA, C., FUNICIELLO, F., GIARDINI, D. & LUCENTE, F. P. 2001*b*. Episodic back-arc extension during restricted mantle convection in the Central Mediterranean. *Earth and Planetary Science Letters*, **187**, 105–116.

FACCENNA, C., PIROMALLO, C., CRESPO-BLANC, A., JOLIVET, L. & ROSSETTI, F. 2004. Lateral slab deformation and the origin of the western Mediterranean arcs. *Tectonics*, **23**, TC1012, doi:10.1029/2002TC001488.

GIGNOUX, M. 1913. *Les formations marines pliocènes et quaternaires de l'Italie du Sud et de la Sicilie*. Annales de l'Université de Lyon, Nouvelle Série 1, **36**.

GLIOZZI, E. 1987. I terrazzi del Pleistocene superiore della penisola di Crotone (Calabria). *Geologica Romana*, **26**, 17–79.

GVIRTZMAN, Z. & NUR, A. 1999. Plate detachment, asthenosphere upwelling, and topography across subduction zones. *Geology*, **27**, 563–566.

GVIRZTMAN, Z. & NUR, A. 2001. Residual topography, lithospheric structure and sunken slabs in the central Mediterranean. *Earth and Planetary Science Letters*, **187**, 117–130.

HEMLEBEN, C, SPINDLER, M. & ANDERSON, O. R. 1989. *Modern Planktonic Foraminifera*. Springer, Berlin.

KAIHO, K. 1994. Benthic foraminiferal dissolved-oxygen index and dissolved-oxygen levels in the modern ocean. *Geology*, **22**, 719–722.

KASTENS, K. A., MASCLE, J., AUROUX, C., *ET AL.* 1987. Site 650: Marsili Basin. *In*: *Proceedings of the Ocean Drilling Program, Initial Reports*, 107, Ocean Drilling Program, College Station, TX, 129–170.

KASTENS, K. A., MASCLE, J., AUROUX, C., *ET AL.* 1988. ODP Leg 107 in the Tyrrhenian Sea: insights into passive margin and back-arc basin evolution. *Geological Society of America Bulletin*, **100**, 1140–1156.

KENNETT, J. P. & SRINIVASAN, M. S. 1983. *Neogene Planktonic Foraminifera. A Phylogenetic Atlas*. Hutchinson & Ross, Stroudsburg, PA.

KROON, D., ALEXANDER, I., LITTLE, M., LOURENS, L. J., MATTHEWSON, A., ROBERTSON, A. H. F. & SAKAMOTO, T. 1998. Oxygen isotope and sapropel stratigraphy in the Eastern Mediterranean during the last 3.2 million years. *In*: ROBERTSON, A. H. F., EMEIS, K.-C., RICHTER, C. & CAMERLENGHI, A. (eds) *Proceedings of the Ocean Drilling Program, Scientific Results, 160*, Ocean Drilling Program, College Station, TX, 181–189.

LOEBLICH, A. R. & TAPPAN, H. 1988. *Foraminiferal Genera and their Classification*. Van Nostrand Reinhold, New York.

LOURENS, L. J., ANTONARAKOU, A., HILGEN, F. J., VAN HOOF, A. A. M., VERGNAUD-GRAZZINI, C. & ZACHARIASSE, W. J. 1996. Evaluation of the Plio-Pleistocene astronomical timescale. *Paleoceanography*, **11**, 391–413.

LOURENS, L. J., HILGEN, F. J., LASKAR, J., SHACKLETON, N. J. & WILSON, D. 2004. The Neogene Period. *In*: GRADSTEIN, F., OGG, J. & SMITH, A (eds) *A Geologic Time Scale 2004*. Cambridge University Press, Cambridge, 409–440.

MALINVERNO, A. & RYAN, W. B. F. 1986. Extension on the Tyrrhenian Sea and shortening in the Apennines as result of arc migration driven by sinking of the lithosphere. *Tectonics*, **5**, 227–245.

MASSARI, F., RIO, D., SGAVETTI, M., *ET AL.* 2002. Interplay between tectonics and glacio-eustacy: Pleistocene succession of the Crotone basin, Calabria (southern Italy). *Geological Society of America Bulletin*, **114**, 1183–1209.

MORETTI, A. 1993. Note sull'evoluzione tettono-stratigrafica del bacino crotonese dopo la fine del Miocene. *Bollettino della Società Geologica Italiana*, **112**, 845–867.

OGNIBEN, L. 1955. Le argille scagliose del Crotonese. *Memorie e Note dell'Istituto di Geologia Applicata di Napoli*, **6**, 1–72.

PATACCA, E., SARTORI, R. & SCANDONE, P. 1990. Tyrrhenian basin and Apenninic arcs: kinematic relations since Late Tortonian times. *Memorie della Società Geologica Italiana*, **45**, 425–451.

PUJOL, C. & VERGNAUD-GRAZZINI, C. 1995. Distribution patterns of live planktic foraminifers as related to regional hydrography and productive systems on the Mediterranean Sea. *Marine Micropaleontology*, **25**, 187–217.

RIO, D., RAFFI, I. & VILLA, G., 1990. Pliocene–Pleistocene calcareous nannofossil distribution patterns in the Western Mediterranean. *In*: KASTENS, K. A., MASCLE, J., *ET AL.* (eds) *Proceedings of the Ocean Drilling Program, Scientific Results, 107*. Ocean Drilling Program, College Station, TX, 513–533.

RIO, D., CHANNELL, J. E. T., MASSARI, F., POLI, M. S., SGAVETTI, M., D'ALESSANDRO, A. & PROSSER, G. 1996. Reading Pleistocene eustasy in a tectonically active siliciclastic shelf setting (Crotone peninsula, southern Italy). *Geology*, **24**, 743–746.

RIO, D., CHANNELL, J. E. T., BERTOLDI, R., *ET AL.* 1997. Pliocene sapropels in the northern Adriatic area: chronology and paleoenvironmental significance. *Palaeogeography, Palaeoclimatology, Palaeoecology*, **135**, 1–25.

RODA, C. 1964. Distribuzione e facies dei sedimenti Neogenici del Bacino Crotonese. *Geologica Romana*, **3**, 319–366.

ROHLING, E. J. & GIESKES, W. W. C. 1989. Late Quaternary changes in Mediterranean intermediate water density and formation rate. *Paleoceanography*, **4**, 531–545.

ROSENBAUM, G. S. & LISTER, G. 2004. Neogene and Quaternary rollback evolution of the Tyrrhenian Sea, the Apennines, and the Sicilian Maghrebides. *Tectonics*, **23**, TC1013, doi: 10.1029/2003TC001518.

ROYDEN, L. H. 1993. The tectonic expression of slab pull at continental convergent boundaries. *Tectonics*, **12**, 303–325.

RUGGERI, G. & SELLI, R. 1948. Il Pliocene ed il Postpliocene dell'Emilia. *Giornale di Geologia*, **20**, 1–14.

SARTORI, R. 1990. The main results of ODP Leg 107 in the frame of Neogene to Recent geology of perityrrhenian areas. *In*: KASTENS, K. A., MASCLE, J., *ET AL.* (eds) *Proceedings of the Ocean Drilling Program, Scientific Results, 107*. Ocean Drilling Program, College Station, TX, 715–730.

SELLI, R. 1949. Le conoscenze geologiche sul quaternario gassifero del Polesine e del Ferrarese settentrionale. *Atti VI Convegno Nazionale Metano*, 515–535.

SEN GUPTA, B. K. (ed.) 1999. *Modern Foraminifera*. Kluwer, Dordrecht.

SHACKLETON, N. J., BERGER, A. & PELTIER, W. R. 1990. An alternative astronomical calibration of the lower Pleistocene timescale based on ODP site 677. *Transactions of the Royal Society of Edinburgh*, **81**, 251–261.

SHACKLETON, N. J., CROWHURST, S., HAGELBERG, T., PISIAS, N. G. & SCHNEIDER, D. A. 1995*a*. A new late Neogene time scale: application to Leg 138 sites. *In*: PISIAS, N. G., MAYER, L. A. (eds) *Proceedings of the Ocean Drilling Program, Scientific Results, 138*. Ocean Drilling Program, College Station, TX, 73–101.

SHACKLETON, N. J., HALL, M. A. & PATE, D. 1995*b*. Pliocene stable isotope stratigraphy of Site 846. *In*: PISIAS, N. G., MAYER, L. A. (eds) *Proceedings of the Ocean Drilling Program, Scientific Results, 138*. Ocean Drilling Program, College Station, TX, 337–355.

SPROVIERI, R. 1992. Mediterranean Pliocene biochronology: a high resolution record based on quantitative planktonic foraminifera distribution. *Rivista Italiana di Paleontologia e Stratigrafia*, **6**, 61–100.

SPROVIERI, R., DI STEFANO, E., RIGGI, A. & BUSALACCHI, P. 1994. La sezione intra-pliocenica di Gibil-Gabel (Caltanisetta, Sicilia centrale): un esercizio di biostratigrafia ad alta risoluzione. *Bollettino della Società Paleontologica Italiana*, **33**, 289–298.

SPROVIERI, R., DI STEFANO, E., HOWELL, M., SAKAMOTO, T., DI STEFANO, A. & MARINO, M. 1998. Integrated calcareous plankton biostratigraphy and cyclostratigraphy at Site 964. *In*: ROBERTSON, A. H. F., EMEIS, K.-C., RICHTER, C. & CAMERLENGHI, A. (eds) *Proceedings of the Ocean Drilling Program, Scientific Results, 160*. Ocean Drilling Program, College Station, TX, 155–166.

VAN DIJK, J. P. 1991. Basin dynamics and sequence stratigraphy in the Calabrian Arc (Central Mediterranean); records and pathways of the Crotone Basin. *Geologie en Mijnbouw*, **70**, 187–201.

VAN DIJK, J. 1992. *Late Neogene fore-arc basin evolution in the Calabrian Arc (central Mediterranean); tectonic sequence stratigraphy and dynamic geohistory. With special reference to the geology of Central Calabria*. Geologica Ultraiectina, **92**.

VAN DIJK, J. P. 1994. Late Neogene kinematics of intra-arc oblique shear-zone: the Petilia–Rizzuto fault zone (Calabrian Arc, Central Mediterranean). *Tectonics*, **13**, 1201–1230.

VAN DIJK, J. P. & OKKES, M. 1991. Neogene tectonostratigraphy and kinematics of Calabrian basins; implications for the geodynamics of the Central Mediterranean. *Tectonophysics*, **196**, 23–60.

VAN DIJK, J. P. & SCHEEPERS, P. J. J. 1995. Neotectonic rotations in the Calabrian Arc: implications for a Pliocene–Recent geodynamic scenario for the Central Mediterranean. *Earth-Science Reviews*, **39**, 207–246.

VAN DIJK, J. P., BARBERIS, A., CANTARELLA, G., MASSA, E. & PESCATORI, L. 1998. Central Mediterranean Messinian basin evolution: tectono-eustasy or eustato-tectonics? *Annales Tectonicae*, **12**, 7–27.

ZECCHIN, M., MASSARI, F., MELLERE, D. & PROSSER, G. 2004. Anatomy and evolution of a Mediterranean-type fault bounded basin: the Lower Pliocene of the northern Crotone Basin (Southern Italy). *Basin Research*, **16**, 117–143.

Crustal magnetism of the Southern Tyrrhenian Sea from aeromagnetic surveys

G. L. PIANGIAMORE[1,2], O. FAGGIONI[2] & M. S. BARBANO[1]

[1]*Dipartimento di Scienze Geologiche, Università di Catania, Corso Italia 55, 95129 Catania, Italy (e-mail: gpiangiamore@yahoo.it)*

[2]*Stazione di Geofisica Marina INGV-Sede di Portovenere, Villa Pezzino, Via Pezzino Basso 2, 19020 Fezzano di Portovenere (SP), Italy*

Abstract: Aeromagnetic data from the Southern Tyrrhenian Sea have been analysed, to remove the contributions of shallow and deep sources to the magnetic anomalies by applying a processing technology that increases the informative potential of the magnetic data acquired by AGIP with great accuracy, uniform distribution and high density. The aeromagnetic anomaly field has been reduced to the bottom topographic surface by the bottom reduction method. Spectral signal analysis has been carried out to separate low- and high-frequency components. The spectral reference field (SRF), obtained from the cotransformation of low frequencies, gives information about deep magnetic structures. The high-frequency components, computed from the difference between the magnetic anomaly field and the SRF, provides the spectral anomaly field (SAF). The bottom reduced magnetic anomaly field is derived by merging the high- and low-frequency bands. The resulting map provides information about geotectonic features in the Southern Tyrrhenian area and shows the effectiveness of the adopted approach over traditional procedures.

The magnetic cartography of Italy and its surrounding seas is made up of the following previous works: (1) the aeromagnetic anomaly map of Italy (AGIP & Servicio Geologico d'Italia (SGN) 1994; scale 1:1 000 000), obtained by processing the same data as used in this work; (2) the shaded relief magnetic anomaly map at sea level (Chiappini *et al.* 2000; scale 1:1 500 000); (3) the aeromagnetic anomaly map of Italy and surveyed provinces, which is the final product of data processing of the old AGIP map after some integrative surveys conducted by Eni Exploration & Production Division in 2000–2001 in collaboration with the Istituto di Geofisica Marina (Eni Exploration–Production Division & IGMar 2002; scale 1:1 500 000).

The aeromagnetic maps (AGIP & SGN 1994; Eni Exploration–Production Division & IGMar 2002) are smoothed by the effect of the data acquisition height with respect to the Chiappini *et al.* (2000) map, the data for which were acquired in marine and ground surveys. The Chiappini *et al.* map was compiled by merging the marine data of the Osservatorio Geofisico Sperimentale (OGS) of Trieste and the ground network records of the Istituto Nazionale di Geofisica e Vulcanologia (INGV), involving many researchers for several years. This long and expensive data patchwork clearly shows differences from the previous layout and a consequent enhancement in signal informative potential.

In this study the problem of smoothing, typical of aeromagnetic maps, is overcome by means of the (bottom reduction method, BTM; Faggioni *et al.* 2001), which reduces the topographic effect in a short time and shows more highly distinct geomagnetic anomalies with a considerable improvement of informative data content. The present procedure is based on a downward continuation to cancel spectral difference caused by the topographic distance between magnetic sources (seamounts and volcanic islands) and survey level so as to better characterize the anomalies.

Main volcanic and structural features

The Southern Tyrrhenian Sea represents a complex Cenozoic oceanic back-arc basin with different areas of extensional deformation as a result of lowering, spreading, subduction and magmatism (Faccenna *et al.* 2004). Its triangular shape is irregular, with the western margin larger than the eastern one. It is delimited on the western side by the Corsica–Sardinia block, on the southern side by Sicily and on the eastern side by the Italian mainland and the Calabrian Arc. The abyssal plain is floored by basaltic crust. Different dynamic processes have generated a volcanism associated with extension and another linked to subduction phenomena, so we find different magmatic volcanic sites: (1) northward the small circular oceanic basins of Magnaghi–Vavilov and Marsili are separated by a north–south trending structural discontinuity; (2) to the SE, the Aeolian Arc with its

From: MORATTI, G. & CHALOUAN, A. (eds) 2006. *Tectonics of the Western Mediterranean and North Africa.* Geological Society, London, Special Publications, **262**, 337–348.
0305-8719/06/$15.00

seven volcanic edifices forms a semicircle offshore from the continental shelf of the Calabrian Arc; (3) Ustica is in a transition zone between two domains, the Tyrrhenian Basin and the Apennine–Maghrebian Chain.

In the Southern Tyrrhenian Sea, because of the greater extension rate than in the northern part, there are more intense magmatic processes and thinned crust. Therefore oceanic crust occurs mostly in the southern sectors of the area (Malinverno & Ryan 1986). The deep-water volcanoes have developed through an incremental growth process. Vavilov and Magnaghi were formed in the Early Pliocene back-arc basin, Marsili dates back to the Mid-Pliocene (Faggioni *et al.* 1995). Aeolian volcanism and Ustica were active from the Early Pleistocene. Furthermore, geological studies and seismic reflection profiles have revealed the presence of approximately NW–SE transcurrent faults in the Southern Tyrrhenian area. The Pleistocene and present-day rise of magmas within the Tyrrhenian domain causes a very high heat flow, reaching average values of 200 mW m^{-2} and a geothermal gradient locally exceeding 100 °C km^{-1} in the Tyrrhenian Sea and its margins (Mongelli *et al.* 1989). Across the Selli Line and the Vavilov–Magnaghi basin, heat flow values are irregular and show a wider range between <100 and >200 mWm^{-2}. This is typical of young rift domains or young oceanic crust–volcanic districts subject to hydrothermal circulation (Della Vedova *et al.* 2000*a, b*). The highest values occur as minor spots within the Vavilov–Magnaghi and Marsili basin and occupy wider sectors across the Campania margin and in the Northern Sicily basin. Crustal thickness decreased from 30 km to about 10 km during middle late Miocene to Pleistocene stretching and then both intrusive and extrusive magmatism became important (Sartori *et al.* 2004).

Input data

The input data used for the bottom reduction method are the following: Southern Tyrrhenian Sea bathymetry (kindly provided by CNR of Bologna, Fig. 1); aeromagnetic data (intensity of total magnetic field F) acquired by AGIP in the late 1970s aeromagnetic surveys (Fig. 2); vertical gradient increase parameters (parameters of vertical projection for frequency bands of the anomaly field: the first parameter is for low frequency, the second for high frequency).

Aeromagnetic surveys

The analysed data come from the aeromagnetic surveys performed by AGIP over the Southern Tyrrhenian Sea in 1977. The flight pattern covers a surface area of 69 173 km^2 and is made up of 230 850 measurements with an average spacing of sampling step of 0.5 km, covering an area approximately between 38° and 41°N and 10° and 15°E.

The surveys are arranged in a grid of lines (L) oriented NE–SW and spaced 5–10 km apart, linked to transverse check tie-lines (T) oriented SE–NW and spaced at an average of 15 and 7.5 km, respectively (Fig. 3). The area has been explored by means of a caesium-vapour magnetometer (0.01 nT sensibility) and reliable flight line positioning systems at a flying height of 2590.80 m above sea level (about 8500 feet) and 1463.04 m above sea level (4800 feet). The regional gradient is 3.232 nT km^{-1} ($\Delta\varphi$) to the north and 0.726 nT km^{-1} to the east ($\Delta\lambda$).

Data processing

The aeromagnetic data have been treated as follows: (1) pre-processing to produce a new database; (2) gridding; (3) systematic error correction; (4) reduction to the International Geomagnetic Reference Field (IGRF); (5) preliminary geomagnetic anomaly map representation; (6) further elaboration of the aeromagnetic anomaly map; (7) production of a definitive version of the magnetic anomaly map 'polished' from the linear trend. All data processing was carried by means of Oasis montaj v5.0 (Geosoft) software. The geographical data were projected into a new cartographic system based on the Transverse Mercator Projection (latitude 0°, longitude 14°, east 1 50 0000 m and false north 0 m), using the WGS84 datum. Accordingly, UTM is used as the projection system for all maps produced in this study. The grid cell size is 3 km, the scale is 1:1 500 000 and illumination has an inclination of 45° and a declination of 45°.

Short-term variations of the geomagnetic field, such as magnetic storms and bays, have been removed from the airborne magnetic data, using a reference base station within the study area. The IGRF is updated every 5 years to take into account the geomagnetic field changes over time. The 1980 epoch is the nearest to the survey one (1977–1979), so the calculated IGRF 1980.0 has been removed from the magnetic relief. The residual contribution, ΔF, is the magnetic field mainly associated with magnetic minerals in crustal rocks. The magnetic anomaly is, in fact, expressed by the relation $\Delta F = F_{obs} - F_{ref}$, where F_{obs} is the observed magnetic field and F_{ref} is the magnetic field computed through the IGRF model. The computed anomaly values on the preliminary aeromagnetic anomaly map are unreliable because at the survey time the reference field was based

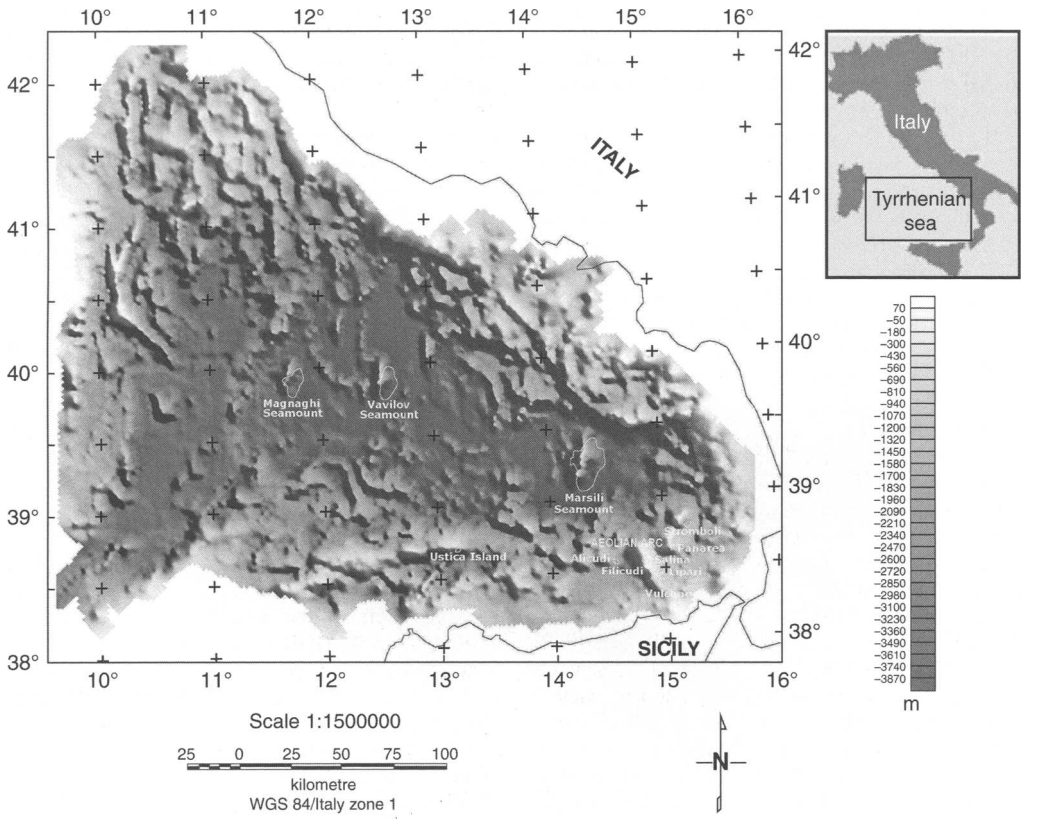

Fig. 1. Grey-scale map, in which the colour saturation from light to dark is modulated by the bathymetry values (shallow areas are the lighttest; deepest areas are the darkest). The greatest depth in the Southern Tyrrhenian Sea is about 4 km.

on a subjective surface made up of a tangle of local planes. Furthermore, the resulting anomaly map shows a shift of some tens of nanotesla with respect to the IGRF field at its composed zero level (Cassano 1984). To define and remove this difference in the reference field, the most representative geomagnetic profile in the area has been used. The procedure to remove this subjective surface contribution is as follows: a north–south-oriented profile on the reduced map has been selected (see Fig. 3 for profile location); the values extracted along the corresponding grid points have been visualized in a diagram (Fig. 4); the mean (−71 nT) between the two nearest points to the inflexion below the peak value (−62.7 and −79.7 nT) has been subtracted from the geomagnetic anomaly field values (Piangiamore 2005).

The inflexion indicates the most significant reference value to define the anomaly area and it has been assumed as a reference correction value. This procedure implies an approximation, because the compensation parameter is computed by a profile and extended to the entire area examined, but this approximation is negligible in regional studies.

Now the geomagnetic anomaly values are acceptable and the aeromagnetic anomaly map appears 'cleaned' from linear trend (Fig. 5).

A new residual aeromagnetic anomaly map in the Southern Tyrrhenian region

The reprocessed aeromagnetic anomaly map of the Southern Tyrrhenian Sea defines with precision an area that is characterized by high-frequency anomalies that can be associated with local volcanic features. Some magnetic anomalies are well isolated from the regional background and assume a strictly dipolar shape. The negative magnetic signature of the Tyrrhenian domain is caused by the high heat flow and geothermal gradient observed in this area (Mongelli *et al.* 1989), which demagnetizes crust above the 580 °C isotherm. The relative strong negative values reach −350 nT, characterizing the sea

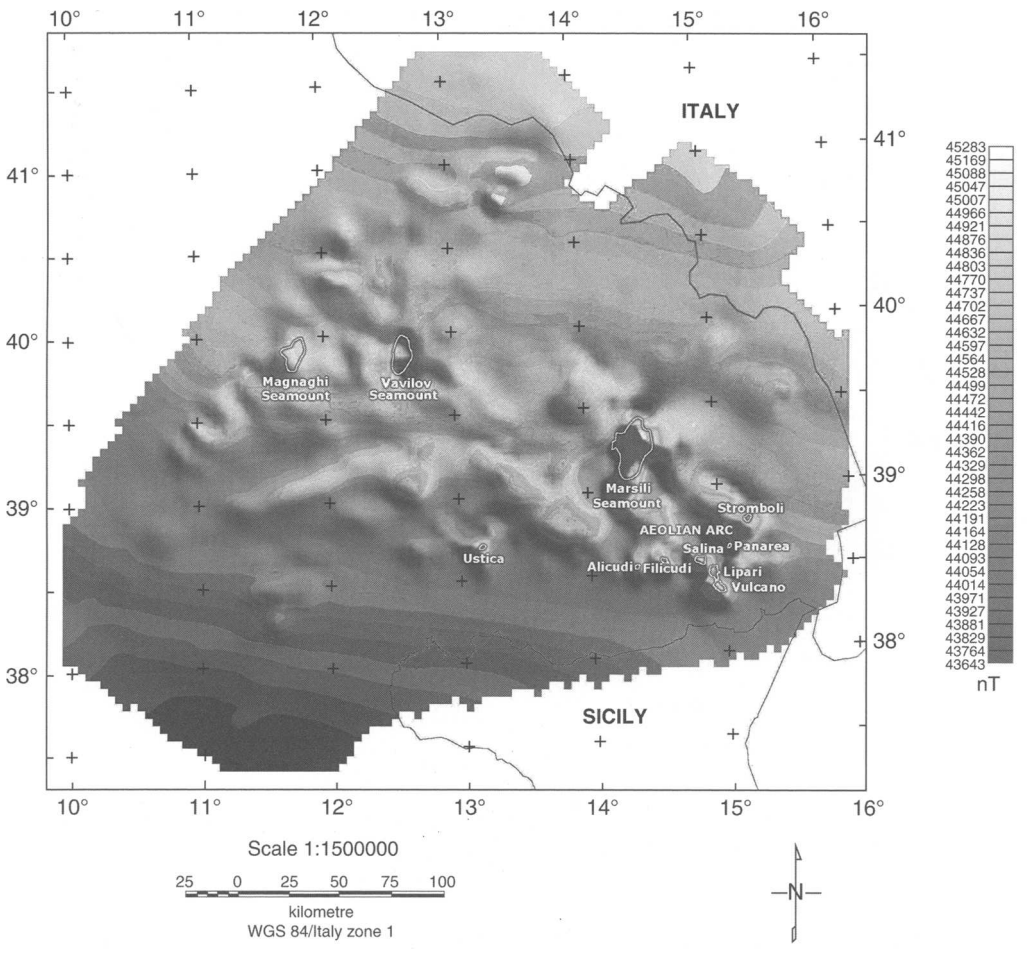

Fig. 2. Total geomagnetic field map of the Southern Tyrrhenian Sea.

bottom, whereas the magnetic values rapidly increase generally corresponding to seamounts and volcanic islands. Finally, the values decrease again to slightly negative near the Tyrrhenian margin with its large regional amplitude anomalies (up to 100 nT less than in the southwestern Tyrrhenian sector offshore). This area corresponds to the shelf and the continental margin of the northern Sicilian coast, and is due mainly to the contact between oceanic and continental crust. The seamounts match high-frequency anomaly zones. The interpretation of these magnetic features as submarine volcanic manifestations is also supported by the following evidence.

(1) Heat flow and magnetic anomalies are elevated in the Southern Tyrrhenian Sea (Della Vedova *et al.* 2000).

(2) Metal-rich sediments near the Messinian–Pliocene boundary (Robertson 1990) may have been produced by coeval hydrothermal circulation triggered by the shallow intrusions.

(3) The Moho is almost flat regionally, around a mean value of 10 km in the Magnaghi and Marsili basins where the lithospheric mantle also seems to be very thin (Panza *et al.* 2004); whereas it increases to 15 km in the Southern Tyrrhenian margin. Moreover, the very wide area with the Moho at shallow depth includes not only the inferred oceanic crust but also the lower and middle Sardinia continental margin.

Signal analysis

The magnetic signal depends on the size, shape, depth of occurrence and magnetization of the source body. Magnetic anomalies generally arise from source bodies at significantly different depth levels.

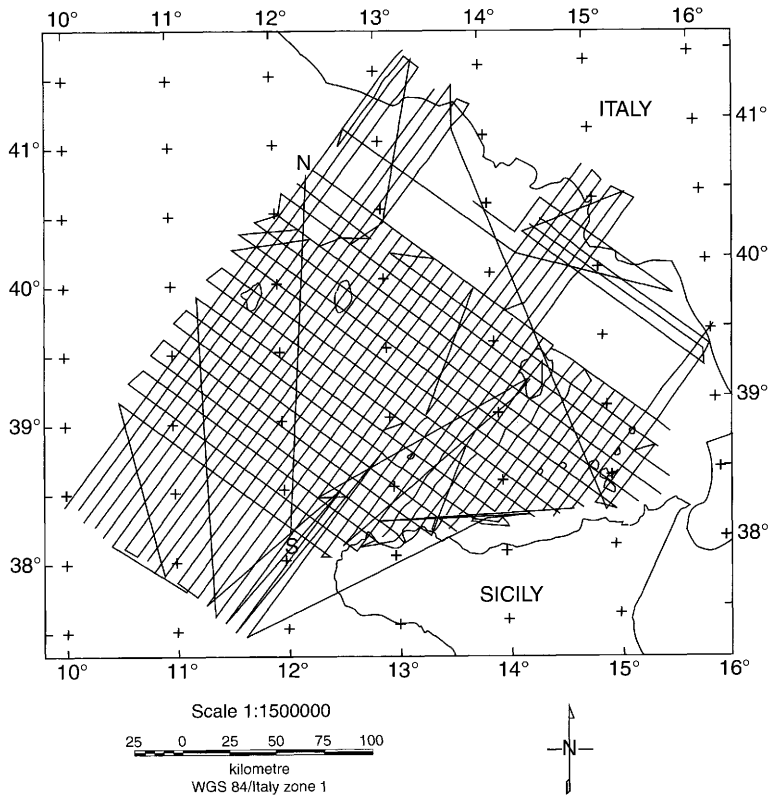

Fig. 3. Aeromagnetic track lines and north–south profile analysed in the Figure 4 and used to remove the linear trend from aeromagnetic anomaly values.

A filtering procedure is used to separate anomalies by their wavelengths as well as to enhance high-frequency (short-wavelength) residual components of the observed potential field by attenuating the dominant regional components and suppressing regular and random noise. Residual-regional anomaly separation by filtering is based on the assumption that a given geological source energy is attenuated more rapidly at high spatial frequencies (short wavelengths) than at low spatial frequencies (long wavelengths) as the source depth increases. The radially averaged power spectrum is a logarithmic plot of the Fourier transformed gridded magnetic data, representing the power

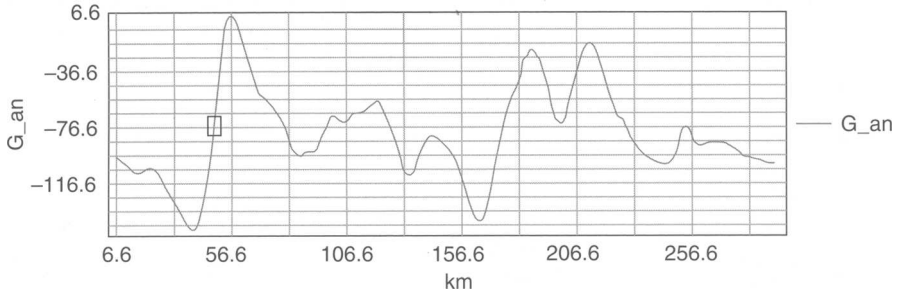

Fig. 4. North–south profile selected to correct anomaly data. The ground units in metres are represented on the x-axis, and the values extracted from the grid of anomaly data in units of nT on the y-axis.

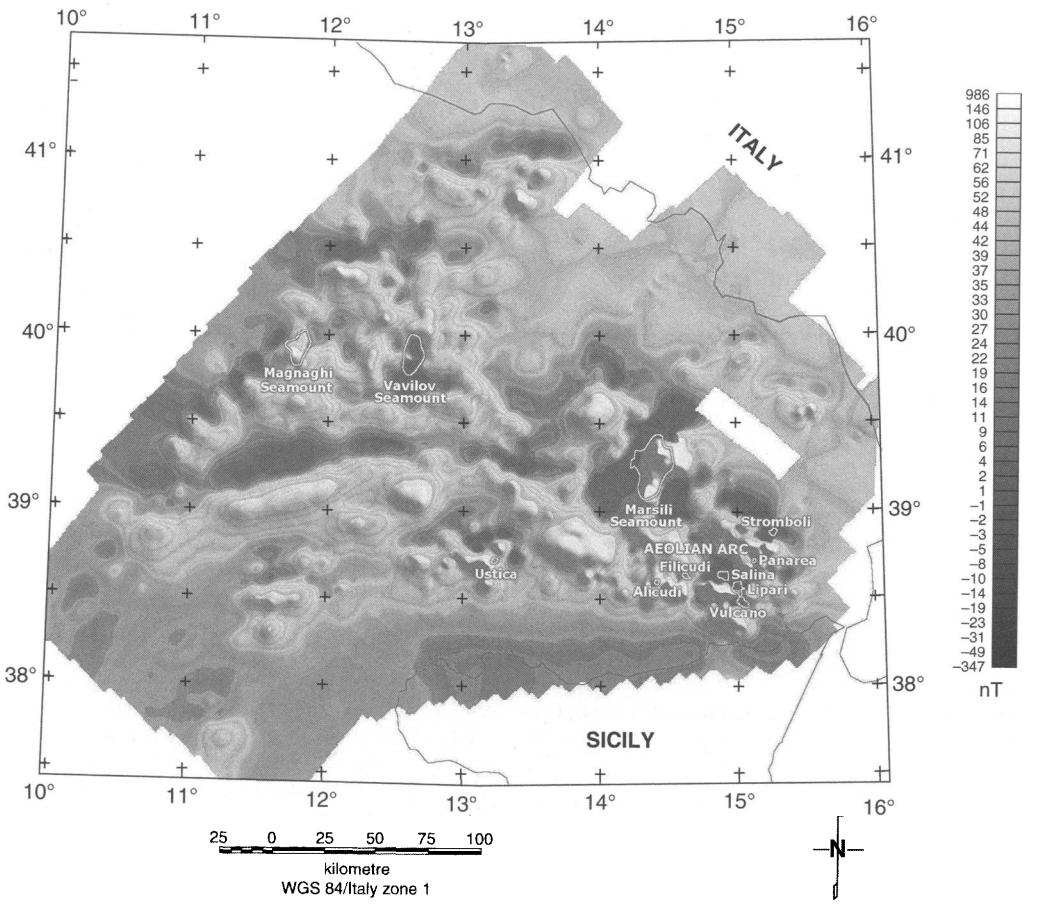

Fig. 5. The reprocessed aeromagnetic anomaly map of the Southern Tyrrhenian Sea after spurious trend removal.

logarithm, which is equal to the square of spectral amplitude. It represents the spectral energy content in all surface directions, being obtained by integrating each radial frequency component over all azimuths. The spectrum is a statistical estimate of the average frequency bands over the area.

The power spectrum exhibits a distinct slope (Fig. 6) that provides the intercept parameter for the evaluation of cut-off wavelength. It shows an amplitude decay at the wavelength λ of 90 km corresponding to a cut-off wavenumber of 0.01 cycles km^{-1}. It is assumed that the decay of the power spectrum curve may be approximated by linear slopes (gradients) associated with ensembles of magnetic sources located at different depths. Applying a 2D fast Fourier transform (FFT) filter created on this cut-off wavelength to the gridded aeromagnetic anomaly, different depth sources are separated. The low-pass filter used with 90 km cut-off wavelength value retains all wavelengths larger than 90 km and rejects all wavelengths smaller than 90 km. High-frequency (short-wavelength) components of the observed potential fields originate from relatively shallow magnetic sources, whereas low-frequency components derive from deep sources.

Spectral reference field

A low-pass filter map at a cut-off wavenumber of 0.01 cycles km^{-1} is the graphical representation of the spectral reference field (SRF) and it gives information about deep magnetic structures with long wavelength. The anomaly pattern, after low-pass filtering, tends to accentuate anomalies caused by deep sources at the expense of anomalies caused by small and shallow sources (typically volcanoes or intrusive bodies). Low-amplitude anomalies usually indicate basement block structures (e.g. uplifts, horsts). The computed

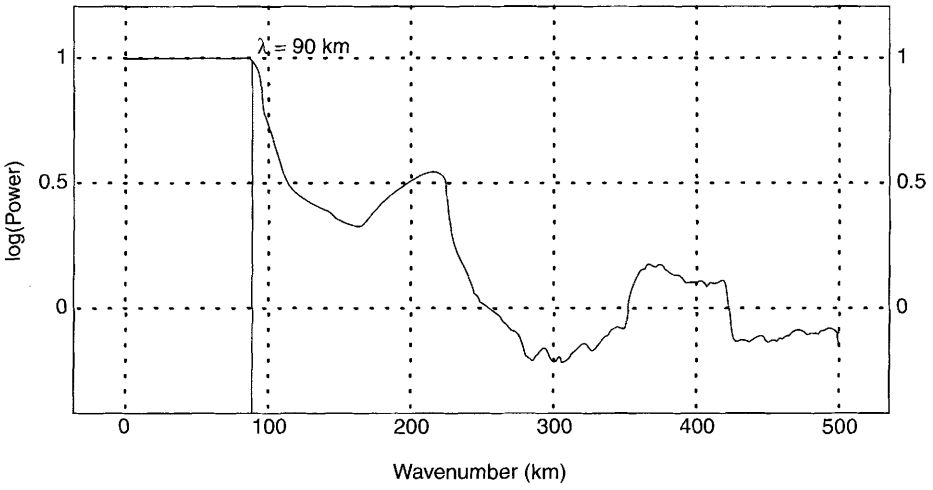

Fig. 6. Radially averaged power spectrum. The energy (power) of the observed data components is presented on a logarithmic scale. The horizontal axis represents wavenumber values in cycles per ground units (km); the cut-off wavelength $\lambda = 90$ km.

SRF map (Fig. 7) shows a minimum magnetic pattern separating the two great Southern Tyrrhenian basins (the Vavilov and Marsili basins). It is a narrow zone corresponding to a thinning continental crust called the 'Issel Bridge', which crosses Issel Seamount (Sartori 2003) (see the next map).

Spectral anomaly field

Anomaly separation is a processing method used to reveal shallow subsurface source distributions, which are often the main target of magnetic exploration. A high-frequency map has been obtained by subtracting the contribution of the SRF from the reprocessed aeromagnetic anomaly data. The result is the spectral anomaly field (SAF), which highlights shallow magnetic sources that are related to short wavelengths (Fig. 8). This map amplifies our knowledge about superficial magnetic structures, showing in detail the geomagnetic characteristics of all seamounts of the Southern Tyrrhenian area. Complex and intense short-wavelength anomalies, caused by volcanic edifices arising from crustal thinning and effusive events, are plainly evident. Magnetic anomalies clearly correspond to the emerged volcanoes (such as the Aeolian Arc and Ustica Island); some are major seamounts (Marsili, Magnaghi) and some minor ones (such as De Marchi, Flavio Gioia, Glauco, Sisifo, Aceste, Anchise, Prometeo, Enarete, Eolo and Lamentini). The Vavilov and Farfalla Seamounts and some Aeolian Arc volcanic areas show strongly negative anomalies; this is very unusual for crustal magmatic bodies, which are potentially highly magnetic (Arisi Rota & Fichera 1987). The Secchi, Sirene and Issel Seamounts magnetic anomaly are negative, too, but less than the previous seamounts. Various hypotheses can be formulated to justify the apparent incongruity of the presence of negative anomalies in an area rich in lower continental crust, oceanic crust and upper mantle, which are usually strongly magnetic: (1) demagnetization of the rocks as a result of the Curie temperature being exceeded, as this is a zone of elevated heat flow (the Moho is at about 10 km depth in the Vavilov and Marsili basins (Scrocca *et al.* 2003); (2) intense tectonization with consequent rock fracture and cataclasis favouring rock alteration and the oxidation of magnetite, eventually to other oxides (hematite, goethite); (3) hydrothermal alteration, which occurs particularly in geochemical environments with gas leaks (Etiope *et al.* 1999).

Application of the bottom reduction method (BTM) to analysis of aeromagnetic data

The intensity of the geomagnetic field is distorted by the topographic effect, especially in highly magnetic volcanic rocks. Geomagnetic anomaly field intensity strongly decreases with increasing depth. In magnetic interpretation it is referred to as the 'continuation concept', as the magnetic anomalies become broader (exhibiting lower frequency content) when the distance between the source of anomaly and magnetometer sensor increases. Moreover, the topographic compensation tends to flatten out the amplitude differences of high- and

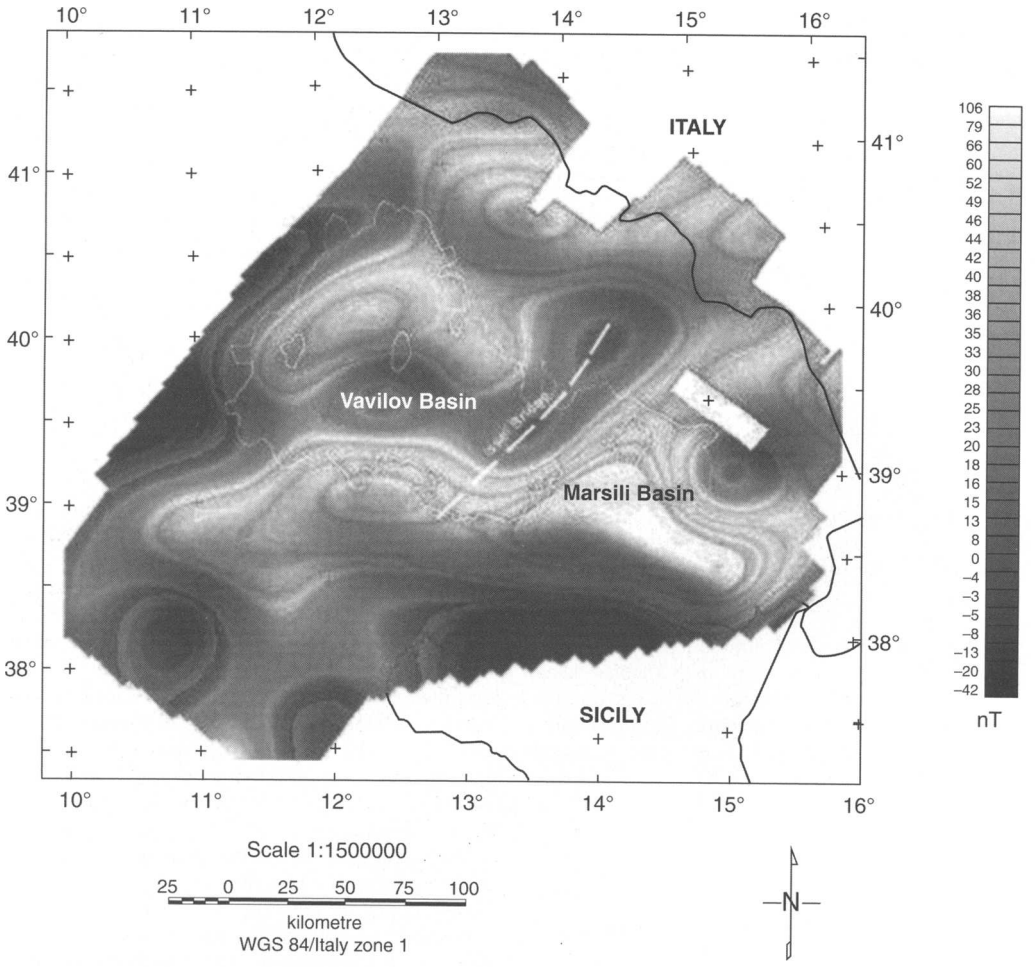

Fig. 7. Spectral reference field (SRF): low-pass component of IGRF anomaly field. The Issel Bridge is indicated by the white dashed line.

low-frequency components. The topographic reduction to the aeromagnetic anomaly field of the Southern Tyrrhenian Sea has been performed, by means of the Bottom Reduction Method (BTM) by Faggioni *et al.* (2001). This technique provides a rapid and straightforward method to process data so as to reduce the distortions of the geomagnetic anomaly field caused by the sea bottom morphology and corresponding variation of the sensor–sea bottom distance. The aim of BTM is to discriminate, in a simple and efficient way and with the highest possible definition, the high-frequency spatial anomaly field, often associated with seamounts and volcanic islands, from the low-frequency crustal structure, regardless of the depth of the sea bottom topography. The Tyrrhenian structural setting is characterized by variable bathymetry. The BTM is based on the downward continuation of the spectral high- and low-frequency bands, in accordance with their own vertical gradient. The data are projected over the topographic surface according to the following formula:

$$\Delta F^{\mathrm{L,H}}_{\mathrm{BTM}}(\varphi, \lambda) \equiv \Delta F^{\mathrm{L,H}}(\varphi, \lambda) + \frac{1}{2} d(\varphi, \lambda) K^{\mathrm{L,H}} \frac{\Delta F^{\mathrm{L,H}}(\varphi, \lambda)}{|\Delta F^{\mathrm{L,H}}_{\mathrm{max}}|}$$

where φ and λ are the geographical coordinates of array points; $\Delta F^{\mathrm{L,H}}_{c}(\varphi, \lambda)$ is the low- (high)-frequency BTM corrected intensity of geomagnetic field anomaly; $\Delta F^{\mathrm{L,H}}(\varphi, \lambda)$ is the low- (high)-frequency intensity of sea-level geomagnetic field anomaly; $d(\varphi, \lambda)$ is the bathymetric depth; $K^{\mathrm{L,H}}$ is

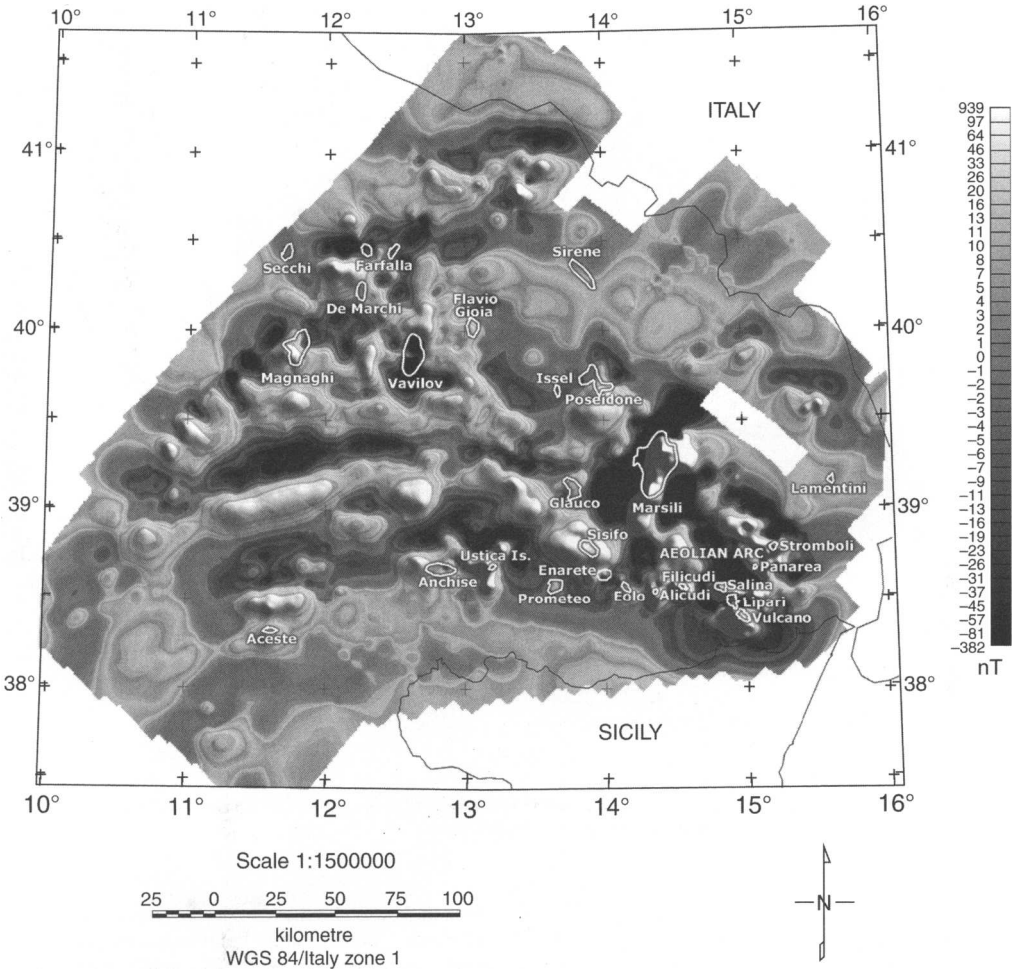

Fig. 8. Spectral anomaly field (SAF): high-pass component of the IGRF anomaly field. The Southern Tyrrhenian seamounts are indicated.

the low- (high)-frequency vertical increment coefficient; $\Delta F^{L,H}_{max}$ (φ, λ) is the low- (high)-frequency maximum intensity of the sea-level anomaly.

This metrological technique allows us to spread the magnetic data values, measured at a certain altitude over the topographic surface, varying the depth by means of low-frequency band vertical increment gradient K^L for the correction of low-frequency band anomaly field component and high-frequency band vertical increment gradient K^H for the correction of the high-frequency one. The values of K for each of the spectral bands can be computed in an empirical way. The assumption that the continuation has different behaviour according to the frequency bands is respected by using different vertical gradients for the high- and low-frequency bands. This procedure allows us to recalculate the observed potential field at the sea bottom surface beneath the plane of measurements. It enhances short-wavelength (high-frequency) components of the potential field, which are generated by relatively shallower sources. Reduction involves the following steps: (1) transform matrix of magnetic values to the frequency domain; (2) carry out spectral analysis of data and search for frequency of classification (cut frequency) to separate high (H) and low (L) bands; (3) co-transform low frequencies to obtain the spectral reference field (SRF); (4) compute the anomaly field high-frequency band to obtain the spectral anomaly field (SAF) by subtraction from the IGRF anomaly field of the SRF; (5) make a vertical projection of SRF and SAF to the sea bottom by means of the K^L (LF band vertical gradient and the K^H (HF band vertical

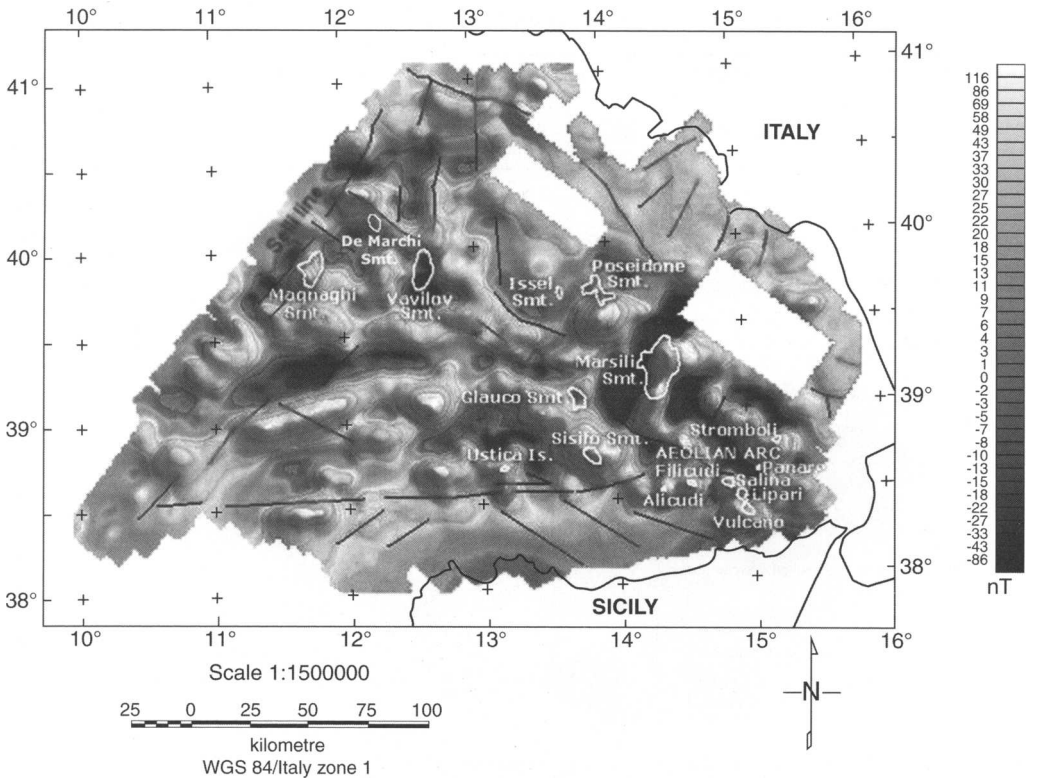

Fig. 9. BTM map of the Southern Tyrrhenian Sea: IGRF anomaly field projected to sea bottom. Tectonic lineaments redrawn from Mattei *et al.* (2004) are shown by the bold black lines.

gradient); (6) merge subsets of frequency to obtain bottom reduced magnetic anomaly field (BTM).

The definitive and 'corrected' aeromagnetic anomaly dataset is processed using an FFT. The power spectrum is analysed to delineate an appropriate cut frequency, to separate the magnetic effects of deep subsurface sources from shallow ones. To achieve an efficient merging, the low- and high-frequency components of the geomagnetic field are isolated and projected over the topographic surface by means of differentiated vertical gradients for the two bands: $K^{L} = 55\ \mathrm{nT\,km^{-1}}$ for the low-frequency band; $K^{H} = 72\ \mathrm{nT\,km^{-1}}$ for the high-frequency one. These coefficients, calculated in the central and northern Tyrrhenian Sea, are extended to the southern zone, because the differences in vertical gradients, caused by the inductive field latitude variations, are not significant at our scale of investigation (Faggioni *et al.* 1995, 2001). The style of the anomaly field is defined by shape and susceptibility of the natural crustal sources.

The BTM corrected anomaly map is then synthesized by merging the BTM corrected SAF and BTM corrected SRF. To apply the BTM formula, three database channels are necessary: geographical reference, geomagnetic anomaly intensity and depth. Thus, the magnetometric and the bathymetric databases have been linked, digitizing the line-path grid anomaly values over the topography values. At this point the data are ready to be filtered and BTM processed.

Figure 9 shows the BTM map of the Southern Tyrrhenian area. The improvement of the information potential of the geomagnetic signal is mainly due to the enhancement of the large wavelength anomalies, which are otherwise suppressed by other projection methods. The BTM procedure has emphasized some deep sources, without increasing the high-frequency noise too much. The high-frequency noise, typical of standard projection techniques, does not affect the procedure, which is more stable and shows a meaningful signal increase. This approach has allowed us to obtain a better definition of the geomagnetic signals even when applied to a large area with a strong horizontal gradient of depth and magnetic field intensity. The BTM map emphasizes geomagnetic anomalies described so far and highlights a field of relatively strong anomalies

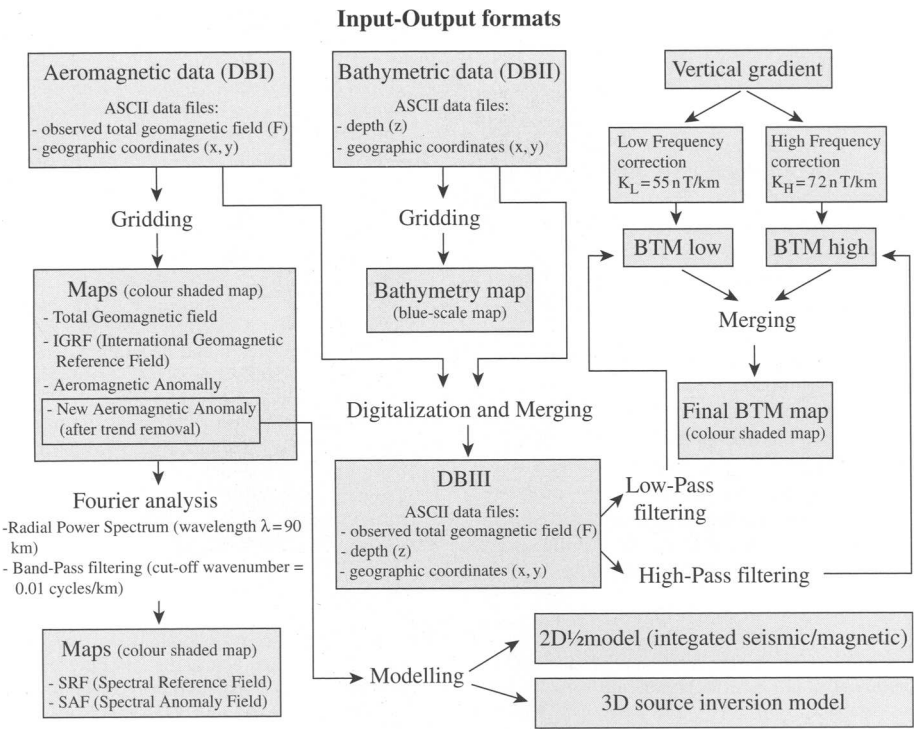

Fig. 10. Flow-chart explaining the data-processing and signal analysis steps.

confined between the Selli Line and the De Marchi Seamount. The moderate positive magnetic anomaly associated with the Campania margin and the long wavelength modest negative anomaly, trending west–east across the North Sicily Basin, shows a geomagnetic field style characterized by low intensity and low horizontal gradient, typical of continental crust geomagnetic field.

All the methods, phases of work and procedures that have been used to produce the final map layout are schematically summarized in the flow-chart shown in Figure 10.

Conclusions

The aeromagnetic anomaly map of Southern Tyrrhenian area has been reprocessed. It gives an unprecedented view of the magnetic signature of the major tectonic elements in their regional setting in comparison with the previously available compilations.

The spectral reference field (SRF) map, obtained by low-pass filtering of the reprocessed aeromagnetic anomaly data, shows the contribution of deep magnetic sources with long wavelength, without the effect of superficial anomalies, which in the Southern Tyrrhenian Sea are typically seamounts and submarine lava flow (such as Prometeo). The most important evidence in the SRF map is the minimum magnetic pattern separating the Vavilov–Magnaghi basin from Marsili one. In this area the edge of thinning continental crust called the 'Issel Bridge' is located.

The spectral anomaly field (SAF) map, obtained by subtracting the SRF contribution from the anomaly field, highlights the shallow subsurface sources. The SAF map provides a detailed picture of the geomagnetic characteristics of all the seamounts (Marsili, Vavilov, Magnaghi, Secchi, Farfalla, De Marchi, Flavio Gioia, Sirene, Issel, Poseidone, Glauco, Sisifo, Lamentini, Aceste, Anchise, Prometeo, Enarete, Eolo) and volcanic islands (the Aeolian Arc and Ustica Island) of the Southern Tyrrhenian area. Almost all volcanoes are highly magnetic, except for Vavilov and Farfalla seamounts (and other restricted volcanic areas, such as in the Aeolian Arc), which have a highly negative magnetic signature.

The sea-bed reduction of the geomagnetic anomaly field of the Southern Tyrrhenian Sea has been carried out using the bottom reduction method, which is based on downward continuation to cancel spectral differences caused by the distance

between magnetic sources (seamounts and volcanic islands) and the survey level.

A shaded relief map showing the integrated anomaly field projected over the Tyrrhenian Seabed provides a regional-scale view of the crustal magnetic anomalies of the area. There is good correlation between known structural geological features and the magnetic anomaly field. The pattern of magnetic anomalies in the Tyrrhenian Sea is similar to that of other back-arc basins worldwide, and does not show clear spreading-type lineation. The generally low magnetic field values of the Tyrrhenian Sea bottom are dominated by short-wavelength positive–negative anomaly couplets centred over volcanic or intrusive bodies. The strongest magnetic anomalies across the Marsili and Vavilov–Magnaghi basins are roughly centred on the largest seamounts of the area (Marsili and Magnaghi positive and Vavilov negative) or on subcircular or slightly elongated sea-floor elevations often related to volcanic edifices.

The BTM map derived from the AGIP survey could be used for detailed structural studies in the Tyrrhenian Sea.

We are grateful to Eni Spa Exploration & Production Division (particularly to I. Giori) for permission to use the aeromagnetic dataset, and to CNR–Ismar of Bologna (especially M. Marani) for kindly providing the Southern Tyrrhenian Sea bathymetry. The authors wish to thank A. Casas and J. W. Jones for their careful reviews and useful suggestions that improved the manuscript. The first author wishes to dedicate this paper to Giuseppe.

References

AGIP S.P.A. & SERVIZIO GEOLOGICO D'ITALIA 1994. *Aeromagnetic map of Italy at 1:1 000 000 scale.* Istituto Poligrafico e Zecca dello Stato, Rome.

ARISI ROTA, F. & FICHERA, R. 1987. Magnetic interpretation related to geo-magnetic provinces. The Italian case history. *Tectonophysics*, **38**, 179–196.

CASSANO, E. 1984. Rilievi magnetici per la ricerca mineraria. *Atti del primo convegno di geomagnetismo (INGV)*, 117–163.

CHIAPPINI, M., MELONI, A., BOSCHI, E., FAGGIONI, O., BEVERINI, N., CARMISCIANO, C. & MARSON, I. 2000. Shaded relief magnetic anomaly map of Italy and surrounding marine areas. *Annali di Geofisica*, **43**(5), 983–989.

DELLA VEDOVA, B., BELLINI, S., PELLIS, G. & SQUARCI, P. 2000*a*. Deep temperatures and surface heat-flow distribution. *In*: VAI, G. B. & MARTINI, L. P. (eds) *Anatomy of an Orogen: the Apennines and Adjacent Mediterranean Basins.* Kluwer, Dordrecht, 65–76.

DELLA VEDOVA, B., BELLINI, S., PELLIS, G. & SQUARCI, P. 2000*b*. Heat flow map of Italy and surrounding seas with the main factors influencing surface heat flow distribution. *In*: VAI, G. B. & MARTINI, L. P. (eds) *Anatomy of an Orogen: the Apennines and Adjacent Mediterranean Basins.* Kluwer, Dordrecht.

ENI EXPLORATION–PRODUCTION DIVISION & IGMAR 2002. *Aeromagnetic Anomaly Map of Italy and Surveyed Provinces.* Eni Exploration-Production Division R&D Project, Milan.

ETIOPE, G., BENEDUCE, P., CALCARA, M., FAVALI, P., FRUGONI, F., SCHIATTARELLA, M. & SMRIGLIO, G. 1999. Structural pattern and CO–CH degassing of Ustica Island, Southern Tyrrhenian basin. *Journal of Volcanology and Geothermal Research*, **88**, 291–304.

FACCENNA, C., FUNICIELLO, F., PIROMALLO, C., ROSSETTI, F., GIARDINI, D. & FUNICIELLO, R. 2004. Subduction and back-arc extension in the Tyrrhenian Sea. *Memorie Descrittive Carta Geologica d'Italia*, **44**, 165–184.

FAGGIONI, O., BEVERINI, N., CARMISCIANO, C. & GIORI, I. 2001. A metrologic method of anomaly field amplitude bottom reduction undersampled geomagnetic marine surveys. *Marine Geophysical Research*, **22**, 63–79.

FAGGIONI, O., PINNA, E., SAVELLI, C. & SCHREIDER, A. A. 1995. Geomagnetism and age study of Tyrrhenian seamounts. *International Geophysical Journal*, **123**, 915–930.

MALINVERNO, A. & RYAN, W. B. F. 1986. Extension in the Tyrrhenian Sea and shortening in the Apennines as result of arc migration driven by sinking of the lithosphere. *Tectonics*, **5**(2), 227–245.

MATTEI, M., D'AGOSTINO, N., FACCENNA, C., PIROMALLO, C. & ROSSETTI, F. 2004. Some remarks on the geodynamics of the Italian region. *Periodico di Mineralogia, Special Issue 1: A Showcase of the Italian Research in Petrology: Magmatism in Italy*, **73**, 7–27.

PANZA, G. E., PONTEVIVO, A., SARAÒ, A., AOUDIA, A. & PECCERILLO, A. 2004. Structure of the lithosphere–asthenosphere and volcanism in the Tyrrhenian Sea and surroundings. (Struttura della litosfera–astenosfera e vulcanismo nel Mar Tirreno e regioni adiacenti.) *Memorie Descrittive della Carta Geologica d'Italia*, **44**, 29–56.

PIANGIAMORE, G. L. 2005. *Geomagnetic anomaly in basin opening structures: the Tyrrhenian Sea example.* PhD thesis, University of Catania, Italy.

ROBERTSON, A. H. F. 1990. Pliocene basal dolomitic and Fe–Mn sediments from the Tyrrhenian Sea, western Mediterranean, Leg 107. *In*: KASTENS, K. A., MASCLE J., *ET AL.* (eds) *Proceedings of the Ocean Drilling Program, Scientific Results, 107.* Ocean Drilling Program, College Station, TX, 129–140.

SARTORI, R. 2003. The Tyrrhenian back-arc basin and subduction of the Ionian lithosphere. *Episodes*, **26**(3), 217–221.

SARTORI, R., TORELLI, L., ZITELLINI, N., CARRARA, G., MAGALDIA, M. & MUSSONIA, P. 2004. Crustal features along a W–E Tyrrhenian transect from Sardinia to Campania margins (Central Mediterranean). *Tectonophysics*, **383**, 171–192.

SCROCCA, D., DOGLIONI, C. & INNOCENTI, F. 2003. Contraints for an interpretation of the Italian geodynamics: a review. *Memorie Descrittive della Carta Geologica d'Italia*, **62**, 15–46.

Hinterland geology and continental margin growth: the case of the Gioia Basin (southeastern Tyrrhenian Sea)

F. GAMBERI & M. MARANI

Istituto di Scienze del Mare, Sezione Geologia Marina Bologna, CNR, Via Gobetti 101, 40129 Bologna, Italy (e-mail: fabiano.gamberi@bo.ismar.cnr.it)

Abstract: The Gioia Basin is a small trough located in the southeastern Tyrrhenian Sea between the Aeolian island arc and Sicily and Calabria. It is experiencing a post-rift margin evolution, while tectonic deformation and high rates of vertical movement are still affecting the Sicilian and Calabrian mainland. The analysis of the evolution of the post-rift depositional systems along the various sectors of the Gioia Basin margin has been carried out through the combined interpretation of multibeam bathymetry and seismic reflection data. Two seismic units have been identified and their component geomorphological elements ascertained through the analysis of seismic facies distribution. In general, the depositional architecture of the margin, the sedimentary environments and facies and related geomorphological elements that are active in the shaping of the margin appear to be mainly controlled by the physiography of the basin itself and by the geology of the hinterland that results from the structural evolution of the adjacent land areas. An evolution from a generalized slope bypass setting to a prograding offlapping slope architecture is recognized and explained as due to the transition from an out-of-grade to a graded profile progressing from the early post-rift stage to the later margin growth stage. Along the Sicilian margin, a constructional apron, mainly consisting of channel levee deposits, makes up much of the studied sedimentary package and reflects a high sediment supply related to the large size of river catchments on land. In contrast, the northeastern Sicilian basin sector is a destructional margin that flanks a region where small river drainage systems result in a low sediment supply to the basin and a continued high uplift rate promotes slope instability; as a consequence, the basin infill is here almost completely made up of mass-wasting deposits. In the Calabrian margin, a first phase of low sediment supply probably coinciding with the filling of the further inland Gioia Tauro half-graben was followed by the establishment of the Gioia–Mesima channel–canyon system that, furnishing an effective sediment flux to the margin, allows the formation of an intraslope depositional body consisting of channelized turbidite lobes.

The Western Mediterranean Sea, although characterized by a complex geology, consists, as a general rule, of rifted continental margins surrounding the deep Algero-Provencal and Tyrrhenian Basins. The different character and age of the geological processes that have shaped the region underpin the highly variable physiography, depositional architecture and sedimentary facies of the Western Mediterranean continental margins. This is particularly evident in the peri-Tyrrhenian area, which presents a highly uneven distribution of tectonics, seismicity, volcanism and rate of vertical movements through time and space. Different present-day sedimentary processes are observed along the Tyrrhenian margin at a regional scale and at the scale of the single intraslope basins that surround the deep abyssal plain of the Vavilov and Marsili Basins (Gamberi & Marani 2004).

In this paper, we unravel the evolution of the sedimentary processes that have led to the post-rift development of the margins of the Gioia Basin, one of the intraslope basins of the Tyrrhenian Sea. We then discuss the inferred depositional history, to illustrate the major importance of the geology of the adjacent land areas and of the physiography of the basin itself in controlling the growth style of the studied margin.

Geological setting

In the southeastern Tyrrhenian Sea, the Cefalù, Gioia and and Paola intraslope basins stretch across the eastern Sicilian and Calabrian margins. The basins are flanked offshore by the islands and seamounts of the active Aeolian volcanic arc, positioned southeastward of the Marsili back-arc basin (Fig. 1). The Cefalù, Gioia and Paola Basins are the result of the extensional tectonics that have led to the opening of the Marsili back-arc basin.

In particular, the Gioia Basin, located in the southeastern Tyrrhenian Sea, is a 70 km long, SW–NE-elongated trough between Sicily and Calabria to the south and east and the Aeolian island arc to the west and north (Figs 1 and 2). To the SW, the Gioia Basin is separated from the Cefalù Basin by the submerged sill of the

From: MORATTI, G. & CHALOUAN, A. (eds) 2006. *Tectonics of the Western Mediterranean and North Africa*. Geological Society, London, Special Publications, **262**, 349–363.
0305-8719/06/$15.00

Milazzo Ridge (Tramontana *et al.* 1995), which connects the Aeolian islands and the Sicilian slopes (Figs 1 and 2). The offshore extension of the Capo Vaticano Promontory and a SW–NE-trending fault scarp, which represent the barrier to the Paola Basin, form the northern boundary of the Gioia Basin.

The Gioia Basin dips and widens toward the NE, reaching, at its furthest point, a maximum depth of 1400 m and a maximum width of 70 km. In the Sicilian portion, it is composed of a slope sector, with a dip as high as 10°, followed by a base-of-slope portion with a downslope decreasing gradient reaching a value of 0.47° in the distal area. A physiography more akin to a ramp setting characterizes the Calabrian sector, with a more homogeneous dip of around 1.27° throughout.

A very narrow continental shelf, with a maximum width of 6 km in the area of Capo Rasocolmo, is present along the Sicilian margin (Fabbri *et al.* 1980). In contrast, the entire Calabrian margin, from Capo Vaticano to the northern Messina Strait, is characterized by a ramp morphology without any evident shelf-slope break (Fabbri *et al.* 1980). The proximal part of a wide submarine drainage system that drives sediment from the Aeolian, Sicilian and Calabrian slopes to the 3500 m deep Marsili back-arc basin (Gamberi & Marani 2004) is the main present-day physiographic element of the Gioia Basin. The Stromboli deep-sea axial valley (SV hereafter), in the central portion of the basin, is the main trunk of this system. Its tributaries are the Milazzo and Niceto channels from the Sicilian margin and the Gioia–Mesima channel–canyon system from the Calabrian slope. Moreover, a series of canyons and gullies in the slopes of the volcanic edifices of the Aeolian island arc connect with the SV at varying water depths. Since Late Miocene time, the Gioia basin and the adjacent land areas have been affected by major NE–SW-, north–south- and east–west-trending extensional faults related to the rifting processes that led to the opening of the Tyrrhenian Sea (Fabbri *et al.* 1980; Del Ben *et al.* 1996; Monaco *et al.* 1996; Monaco & Tortorici 2000). Whereas rifting is still active in the emerged Calabrian arc (Monaco & Tortorici 1995, 2000; Monaco *et al.* 1996; Del Ben *et al.* 1996), major extensional tectonics in the Gioia Basin has been quiescent since at least the Late Pliocene (Fabbri *et al.* 1980). However, the rifting heritage is still evident in the present-day physiography of the Gioia Basin, where intrabasinal ridges represent the edges of blocks tilted during the extensional tectonics. The Acquarone Ridge (Del Ben *et al.* 1996) separates the Sicilian from the Calabrian sector of the basin, and the Gioia Ridge, located further upslope than the limit of the available multibeam data, splits the southern portion of the Calabrian sector from the Palmi Basin (Selli 1979) (Figs 2 and 3).

Further details of the present-day physiography of the Gioia Basin will be given in the section outlining the depositional facies of the upper seismic unit of the basin infill that is intimately related to the present-day geomorphological elements.

The present-day geological setting of the Sicilian and Calabrian areas adjacent to the Gioia Basin is mainly the result of recent extensional tectonics, which exerts a profound effect on the growth style of the basin. In Sicily, differential vertical movements along NE–SW and NW–SE faults have caused the foundering of the Barcellona depression among the uplifting Naso and Castanea ridges (Fig. 2) (Catalano & Di Stefano 1997). High uplift rates of the Castanea and Naso ridges have caused the erosion of the sedimentary cover of the Calabro-Peloritanian units, and therefore, metamorphic rocks extensively crop out (Fig. 2). In contrast, a thick succession of Serravallian to Messinian mainly clastic rocks, followed by hemipelagic deposits of Early and Mid-Pliocene age and by clastic deposits of Late Pliocene

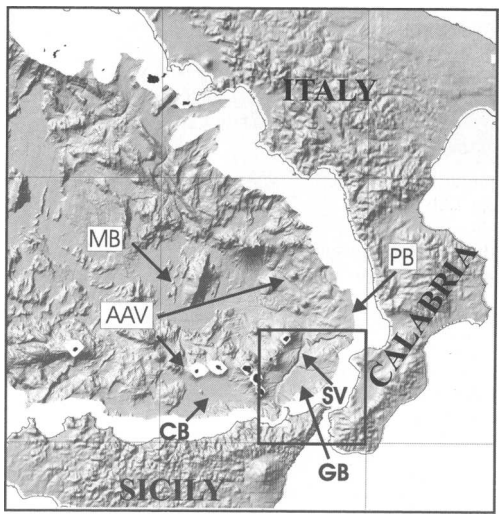

Fig. 1. Shaded relief map, from multibeam bathymetric data (grid cell size 50 m) of the southeastern Tyrrhenian Sea. The Marsili back-arc basin (MB) is located in the centre of the map and is flanked southeastward by the Aeolian island arc (AAV). The Cefalù Basin (CB), Gioia Basin (GB) and Paola Basin (PB) are intraslope basins positioned between the Sicilian and Calabrian margin and the edifices, both islands and seamounts, of the Aeolian volcanic arc. Along the axis of the Gioia Basin, the Stromboli Valley (SV) is the main trunk of a submarine sedimentary pathway that feeds a deep-sea fan in the Marsili Basin. The box corresponds to the area shown in the detailed maps of Figures 2 and 3.

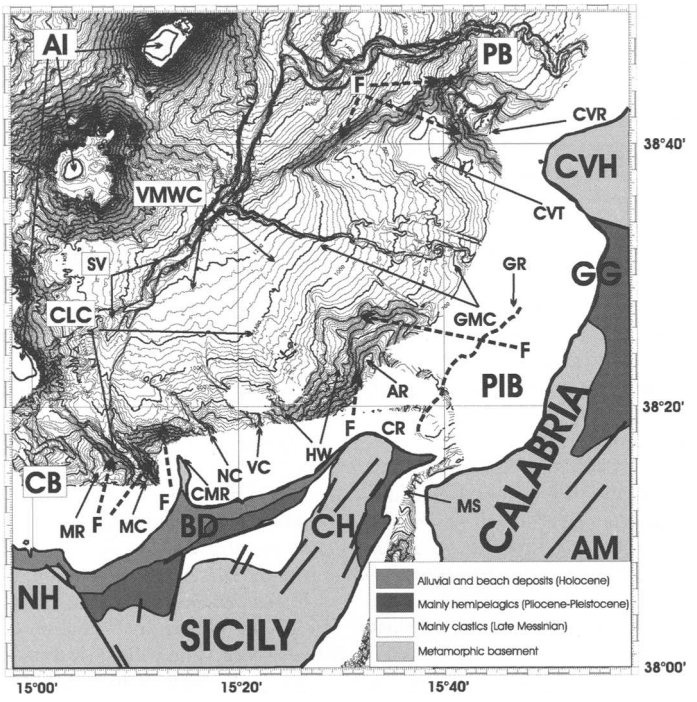

Fig. 2. Bathymetric map of the study region (contour interval 20 m, grid cell size 25 m) and schematic geology of the surrounding areas (simplified from Lentini 2000). The Milazzo Ridge (MR) and the submarine extension of the Capo Vaticano promontory (CVH), consisting of the Capo Vaticano Ridge (CVR) and of an extensional fault (F), separate the Gioia Basin respectively from the Cefalù Basin (CB) and the Paola Basin (PB). The Stromboli axial valley (SV) runs along the centre of the basin at the base of the slope of the Aeolian Islands (AI). In the southwestern Sicilian margin, a channel–levee complex (CLC), fed by the Milazzo (MC), the Niceto (NC) and the Villafranca (VC) channels, is evident. The channel course is influenced by the presence of the Capo di Milazzo Ridge (CMR). A re-entrant in the Sicilian margin (HW), west of the Acquarone Ridge (AR) corresponds to the headwall of the Villafranca mass-wasting complex (VMWC) that is responsible for the highly eneven sea floor in the distal part of the basin. The Mesima–Gioia channel–canyon system (GMC) is present in the Calabrian sector of the basin, between the Capo Vaticano Terrace (CVT) and the AR, which is offshore from Capo Rasocolmo (CR). Furthermore, the Gioia Ridge (GR), marked by the dashed bold line, separates the Gioia Basin from the Palmi intraslope basin (PIB). The slopes of the intrabasinal AR and CMR coincide with extensional faults (F) along which the foundering of the Gioia Basin depocentres has occurred. On land, two major tectonic depressions, the Barcellona (BD) and Gioia Tauro (GG) grabens, respectively in Sicily and Calabria, are filled with Late Miocene to Pleistocene mainly clastic and hemipelagic deposits. They are flanked by the Naso (NH), Castanea (CH), Aspromonte (AM) and CVH structural highs, where high uplift rates have caused the erosional unroofing and exposure of the metamorphic basement. The CH and the CVH continue offshore respectively in the AR and CVR and CVT.

and Pleistocene age, is still preserved in the Barcellona depression (Fig. 2) (Catalano & Di Stefano 1997).

In Calabria, metamorphic rocks of the Calabrian arc crop out in the areas adjacent to the Messina Strait and in the Capo Vaticano promontory (Fig. 2). Marine sediments of Late Pliocene to Mid-Pleistocene age followed by alluvial deposits crop out in the Gioia Tauro half-graben that is the result of the Calabrian arc rifting along NE–SW-trending extensional faults (Fig. 2) (Monaco & Tortorici 1995).

Dataset and methods

Multibeam (Simrad EM12) bathymetric data were acquired in 1996 and 1999 by the Institute for Marine Geology of Bologna in the Gioia Basin sectors deeper than around 500 m (Figs 2 and 3). Analogue multi-channel, unprocessed, airgun seismic lines parallel to the basin axis and spaced at around 2 km furnish a complete coverage of the areas mapped by the detailed bathymetric data; they are integrated with a lower-density grid of 30 kJ sparker single-channel seismic lines, both

parallel and transverse to the basin axis, that allow the tying of the recognized seismic horizons (Fig. 3). A well-grounded correlation of the seismic units across the SV, from the Sicilian and Calabrian side of the basin to the Aeolian one, is not possible; as a consequence, our analysis is concentrated exclusively on the sedimentary package of the Sicilian and Calabrian margin.

The lower part of the post-rift infill of the Gioia Basin is restricted to the more depressed areas and has reflectors that, onlapping the intrabasinal ridges, cannot be correlated across adjacent basin portions (Fig. 4). In contrast, two basin-wide, continuous reflectors (brown and green reflectors) allow us to split the upper, post-rift infill into two seismic units and provide the framework for interpreting the development of the Gioia Basin depositional systems (Fig. 4). Unit I is between the brown and green reflectors, and unit II is between the green reflector and the present-day sea floor (Fig. 3). The lowermost brown reflector lies above the X horizon (X in Fig. 4) that, on the basis of the result of seafloor sampling in the SV, was assigned to the late part of the Mid-Pliocene (Fabbri *et al.* 1980). Although extremely variable, the places in considerable thickness between the X horizon and the brown reflector (Fig. 4) makes an age between the Late Pliocene and the Early Pleistocene reasonable for the brown horizon, the base of the package we deal with in this study.

The analysis of the Gioia Basin depositional systems has been carried out focusing on the identification of the geomorphological elements that have contributed to the development of the margin. Five facies association components, reflecting specific sedimentary environments, have been recognized and mapped: channel fills and related levee and overbank deposits; sheet turbidites and hemipelagic drapes; slumps and mass-wasting complexes; turbidite lobes; contourite mounds.

As a first step, the present-day geomorphological elements and the sedimentary environments in the various sectors of the Gioia Basin were interpreted through the swath bathymetry and their specific seismic facies established on the seismic reflection profiles. The distribution of the recognized seismic facies was then extended back in time to the whole thickness of Units I and II, allowing us to map the evolution of the geomorphological elements and consequently of the sedimentary environments. Finally, the scheme of Galloway (1998), combining seismic unit geometry and component facies, has been used to classify the slope and base-of-slope depositional systems of the Gioia Basin.

In the following, to start with the description of the present-day geomorphological elements of the Gioia Basin we will first describe the interpretation of the sedimentary facies of Unit II, the upper unit that is closely tied to the current geomorphological elements.

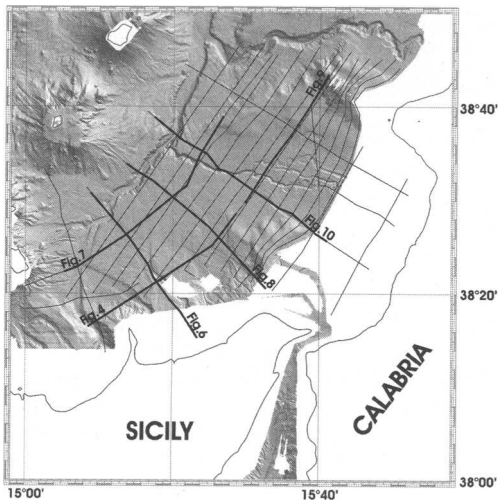

Fig. 3. Grid of available seismic lines, totalling 1000 km, on a shaded relief map of the Gioia Basin (same multibeam data and same area as in Fig. 2). The bold lines correspond to the profiles shown in this paper.

Data interpretation

Unit II

The isochron (time–thickness) map of Unit II shows a distinct depocentre in the southwestern basin sector (Fig. 5a), where the Milazzo, Niceto and Villafranca canyons evolve downslope into leveed channels (Figs 2 and 3). The Milazzo and Niceto channels join at a depth of around 1100 m in the upper reaches of the Stromboli Valley, whereas the Villafranca channel dies out at a depth of around 1100 m without joining the SV (Figs 2 and 3).

In this basin portion, a channel–levee seismic facies, with channel fill high-amplitude reflections (HARs) and convergent downlapping low-amplitude levee reflectors, characterizes Unit II. As a whole, the present-day channel–levee complex has an along-slope width of 20 km (Fig. 4). In a dip seismic line, the reflectors of the basal part of Unit II become parallel and more continuous downslope from the HARs of the Villafranca channel fill (Fig. 6); they correspond to a package of laterally discontinuous mounded reflections with sometimes bidirectional downlap terminations in the strike line of Figure 7. This is a pattern typical of turbidite lobes, indicating that, during the sedimentation of the lower part of

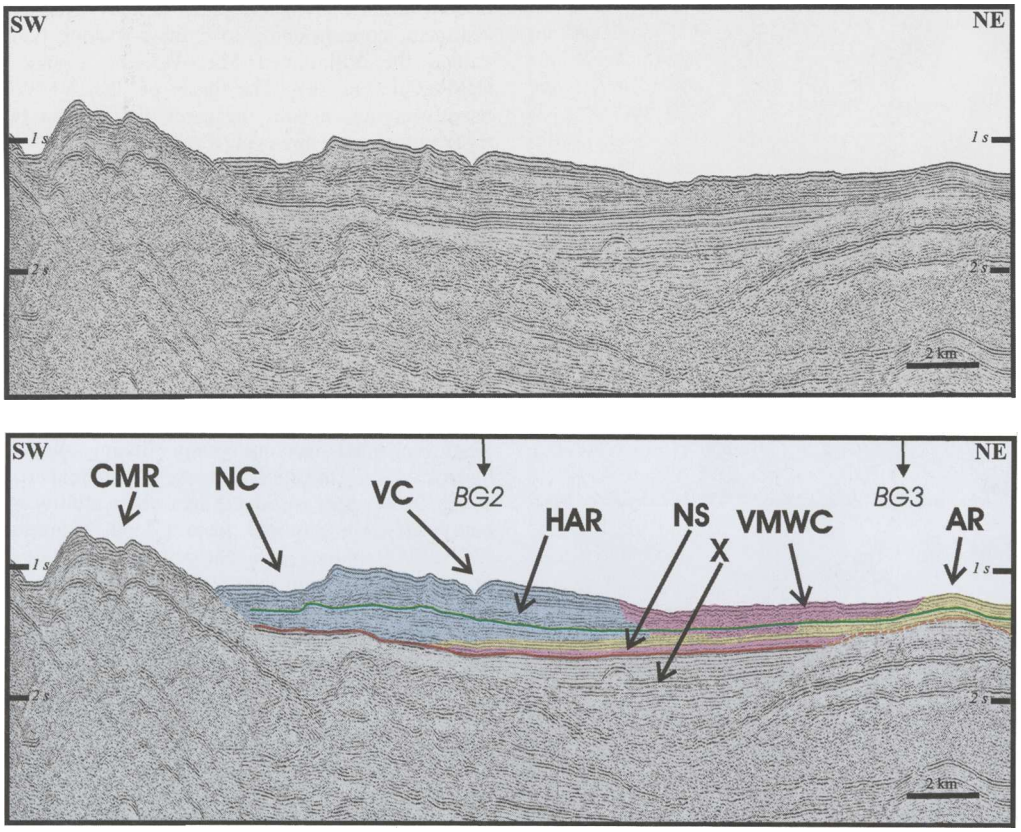

Fig. 4. Strike profile BG8 (see location in Fig. 3) over the Sicilian margin at a depth of around 1000 m (light blue, channel fills and related levee and overbank deposits; pink, slumps and mass-wasting complexes; yellow, sheet turbidites and hemipelagic drapes; light brown, turbidite lobes; green, contourite mounds); the arrows mark the crossing with the other lines presented in this paper. The multiple channel–levee complex of the southwestern Sicilian margin strands the central part of the line and progressively spreads eastward over sheet turbidites; the high-amplitude reflections (HAR) of the channel fill indicate a continuous migration of the Villafranca channel (VC) toward the west, whereas a more stable position is evident for the Niceto channel (NC). In the northeastern Sicilian margin, the lateral extent of the Villafranca mass-wasting complex (VMWC), which constitutes much of Unit II, is observable; some undeformed, horizontally layered portions are present within the otherwise transparent or chaotic deformed horizon. The transparent horizon that, although very thin, covers almost the whole margin at the base of the Unit I is the Nicotera slump (NS); it onlaps against the Capo di Milazzo Ridge (CMR) and the Acquarone Ridge (AR).

Unit II, turbidite lobes developed in the distal margin at the mouth of the leveed channels. In the same distal areas, in contrast, the upper part of Unit II is made up of continuous, low-amplitude reflectors arranged in a wedge that thins out away from the SV and has no temporal equivalent in the proximal part of the margin (Fig. 6) and downslope along the SV (Fig. 7). They can be interpreted as deposits within an overbank wedge formed by flows that run in the proximal part of the SV and are also responsible for the development of sediment waves (Gamberi & Marani 2004). It therefore appears that in the course of Unit II, in the distal western Sicilian margin, an overbank wedge developed in the eastern levee of the SV and replaced turbidite channel-mouth lobes.

In the eastern Sicilian margin, the slope can reach a gradient as high as 9°; in particular along the western side of the Acquarone Ridge, linear or circular scars are the evidence of slope degradation acting mainly through mass-wasting processes (Figs 2 and 3); in the dip seismic line of Figure 8, the areas where sediments have been removed correspond to evident evacuation surfaces in the upper slope. Further downslope, the sea floor is rough and Unit II presents either highly discontinuous hummocky or mounded reflections, or a transparent

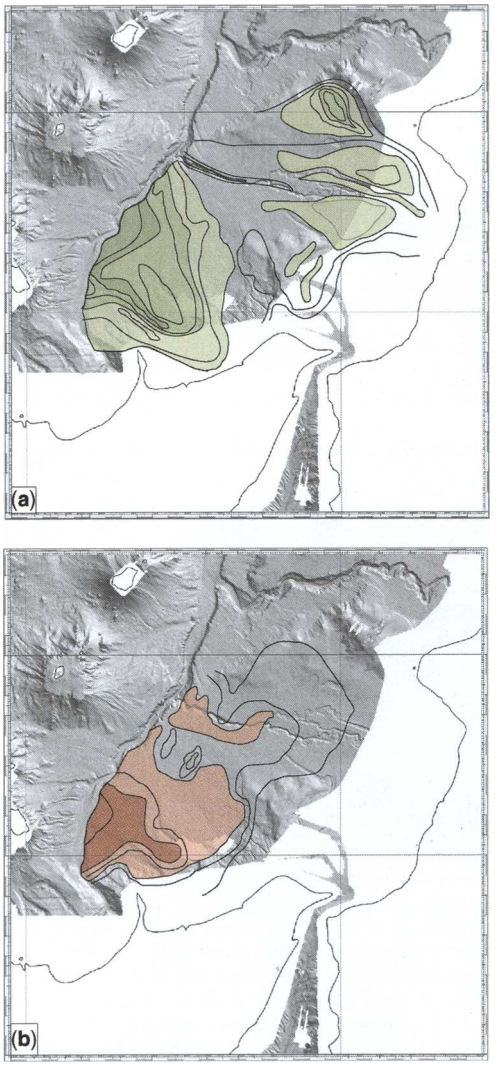

Fig. 5. Isochron maps (contour interval 50 ms) of seismic Units II (**a**) and I (**b**); the large differences in thickness of both units in the various sectors of the basin should be noted. (**a**) Unit II is arranged in three distinct depocentres coinciding respectively with the channel–levee complex of the southwestern Sicilian margin, with the intraslope turbidite lobes of the Calabrian margin and with the contourite mound in the Capo Vaticano Terrace (light green, thickness between 150 and 250 ms; medium green, thickness between 250 and 350 ms; dark green, thickness between 350 and 450 ms. (**b**) Unit I shows a pronounced difference in thickness between the southwestern Sicilian margin, where it was deposited in a channel–levee complex, and the other basin sectors, where there was a reduced depositional rate; in the Calabrian sector, the only significant accumulation corresponds to the distal, thicker portion of the Nicotera slump (light brown, thickness between 150 and 250 ms; dark brown, thickness between 250 and 350 ms).

pattern indicating a package of variably disrupted sediment, corresponding to a mass-wasting body named the Villafranca Mass-Wasting Complex (VMWC) (Fig. 8). The base of the VMWC usually coincides with the green horizon; in the easternmost area, however, it ramps upsection to a slightly higher stratigraphic level and the basal portion of Unit II is made up of subparallel reflections that probably typify the parental material of the VMWC. The VFMC has a length of around 25 km (Fig. 8) and an average lateral extent of around 9 km (Fig. 7) covering a surface of around 225 km^2; its maximum thickness is 300 ms (Fig. 5a).

In the Calabrian margin, a detailed investigation of the upper slope, not covered by our multibeam data, shows that the proximal trunk of the Gioia–Mesima channel–canyons system is mainly affected by erosional and transport processes (Colantoni *et al.* 1992). In the upper part of the area where multibeam bathymetry was acquired, from a depth of around 750 to 1000 m, the Gioia–Mesima submarine drainage network is, in contrarst, characterized by three channels with both meandering and linear segments (Fig. 2). Here, Unit II consists mainly of highly discontinuous reflectors often bounded by erosional surfaces but a pattern consisting of more continuous reflections is also observable (Figs 9 and 10). Together, the seismic facies and the present-day geomorphological elements of these areas can be taken as evidence for a depositional body developed in an intraslope setting and built through the stacking of turbidite channelized lobes and the fill of migrating channels. This 300 km^2 wide depositional area corresponds to the Unit II depocentre in the middle Calabrian slope (Fig. 5a).

At a depth of 1100 m, the channel network ends in a single canyon, which runs down the lower Calabrian slope to the axial part of the basin and joins the SV at a depth of 1600 m (Figs 2 and 3). This distal trunk of the Gioia–Mesima system has a V-shaped profile and, having mainly erosive character, cuts through a basin portion where Unit II has a reduced thickness (Fig. 5a) and parallel, continuous reflectors probably reflecting the distal deposition from the turbidity currents that build the intraslope lobes upslope (Fig. 10). In the flat sea floor of the Capo Vaticano Terrace, Unit II reflectors give rise to a thick (Fig. 5a) mounded body with progressive upslope downlap terminations that probably reflect sediment accumulation under the effects of contour currents (Fig. 9).

Unit I

An almost basin-wide horizon, with a transparent or chaotic seismic facies and a rough top, represents the basal part of Unit I. It has been interpreted as

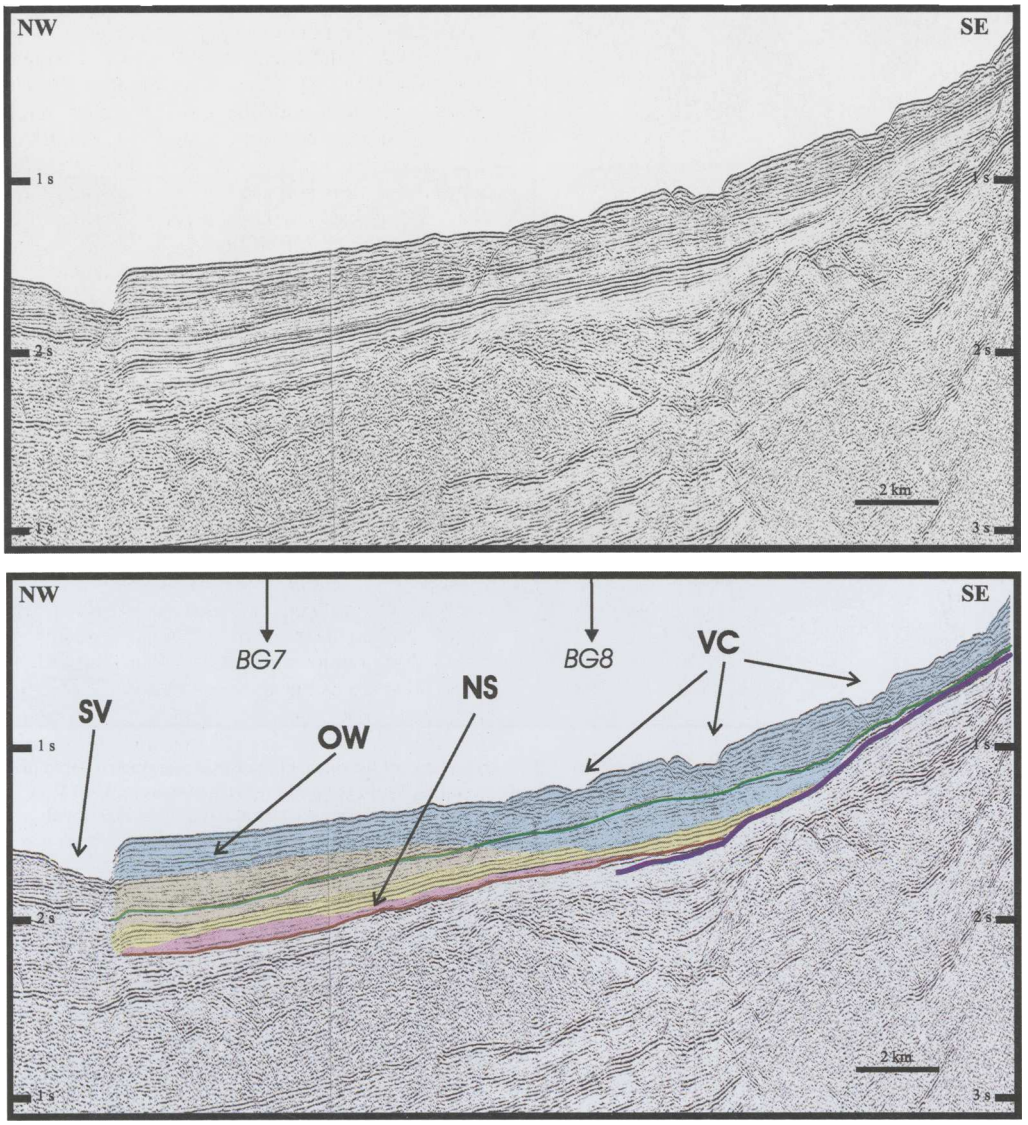

Fig. 6. Dip seismic profile (BG2) in the southwestern Sicilian margin (see location in Fig. 3; colours refer to facies as in Fig. 4). An onlap geometry prevails during Unit I deposition whereas Unit II reflectors are characterized by an offlapping architecture. The top portion of Unit I and most of Unit II are characterized by a channel–levee complex that builds over turbidite lobes in the distal margin. The Villafranca channel (VC) crossed by the line at various water depths progressively loses relief downslope. The upper part of Unit II is represented by an upslope thinning wedge of sediments (OW) flanking the Stromboli Valley (SV); it is interpreted as a levee developed on the proximal, right side of the SV. The Nicotera slump (NS) is evident in the distal margin portion at the base of Unit I.

a slump deposit and will be called hereafter the Nicotera slump (NS). In the Sicilian sector, the NS has a sheet-like form with a rather homogeneous low thickness (around 50 ms, but sometimes at the limit of seismic resolution) and shows only a gradual thinning toward the SW onlap against the Capo di Milazzo Ridge (Fig. 4). In contrast, in the Calabrian sector, to the NE of the Acquarone Ridge, the NS is a mounded body with a downslope thickness increase and reaches the intersection with the SV (Fig. 10). The NS occupies the central part of the Calabrian margin onlapping the intrabasinal

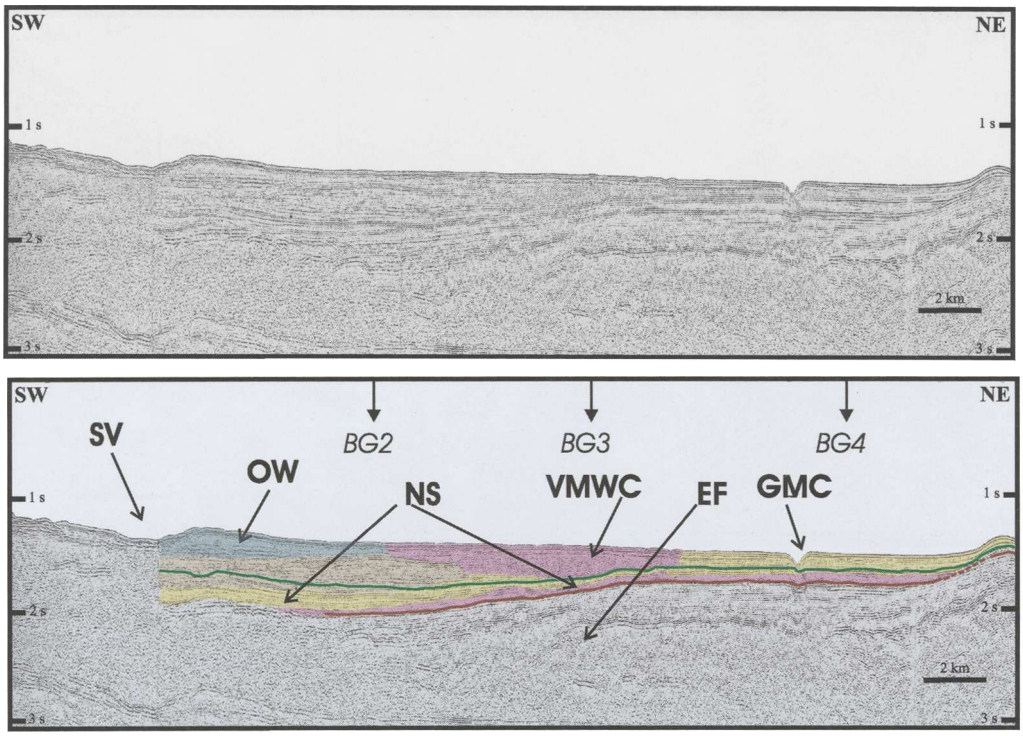

Fig. 7. Strike profile (line BG 7) furnishing a section of the whole length of the distal Gioia Basin margin at a depth of around 1100 m (see location in Fig. 3; colours refer to facies as in Fig. 4). In the eastern Sicilian margin, Unit II is characterized by a mounded body made up of discontinuous reflections, sometimes characterized by bidirectional terminations, interpreted as resulting from the stacking of turbidite lobes; in the top portion of Unit II, however, it is replaced by the same overbank wedge (OW) thinning away from the Stromboli Valley (SV) as shown in Figrue 5. The Villafranca mass-wasting complex (VMWC) is characterized by a transparent pattern; a comparison with Figure 4 highlights that the degree of disruption within the VMWC increases toward the distal portion of the chaotic body (this line). The abrupt thickness reduction of the studied interval at the crossing of an inactive extensional structure (EF) along the northern continuation of the Acquarone ridge should be noted. The thinning from the Calabrian to the Sicilian margin of the Nicotera slump (NS) at the base of Unit I is also evident. The distal part of the Gioia–Mesima channel–canyon system (GMC) is a V-shaped, mainly erosive feature.

ridges of Acquarone and Capo Vaticano Terrace. The NS has a total area of around 300 km^2 and reaches its maximum thickness of 150 ms in its middle portion at a depth of around 1220 m (Fig. 5b). The area from which the material that forms the NS was removed coincides with an erosional surface that can be tentatively followed from the western slope of the Acquarone Ridge, through the Calabrian basin sector, to the Capo Vaticano Terrace. Upslope from the NS a thin package of parallel, continuous reflections represents the base of Unit I (Fig. 10); it thickens away from the area where the NS reaches maximum thickness and mainly constitutes the filling of the embayment left by the material removed by the slump processes and of the areas where the NS is thinner. Further upslope, Unit I has a very reduced thickness (Fig. 5b) and its seismic and depositional facies cannot be ascertained. A seismic facies consisting of parallel, continuous reflections is typical of the first reflectors above the NS in the Sicilian basin sector; upward it is replaced by a channel–levee facies that progressively covers further basin portions toward the Acquarone Ridge (Fig. 4) and toward the distal margin (Fig. 6). In the upper part of Unit I, moreover, a seismic facies that can be interpreted as due to turbidite lobe deposits is developed in the most distal basin portion.

Evolution of the Gioia Basin margin depositional systems

The results of the interpretation of the multibeam and seismic data are summarized in Figure 11, which shows the distribution of the geomorphological

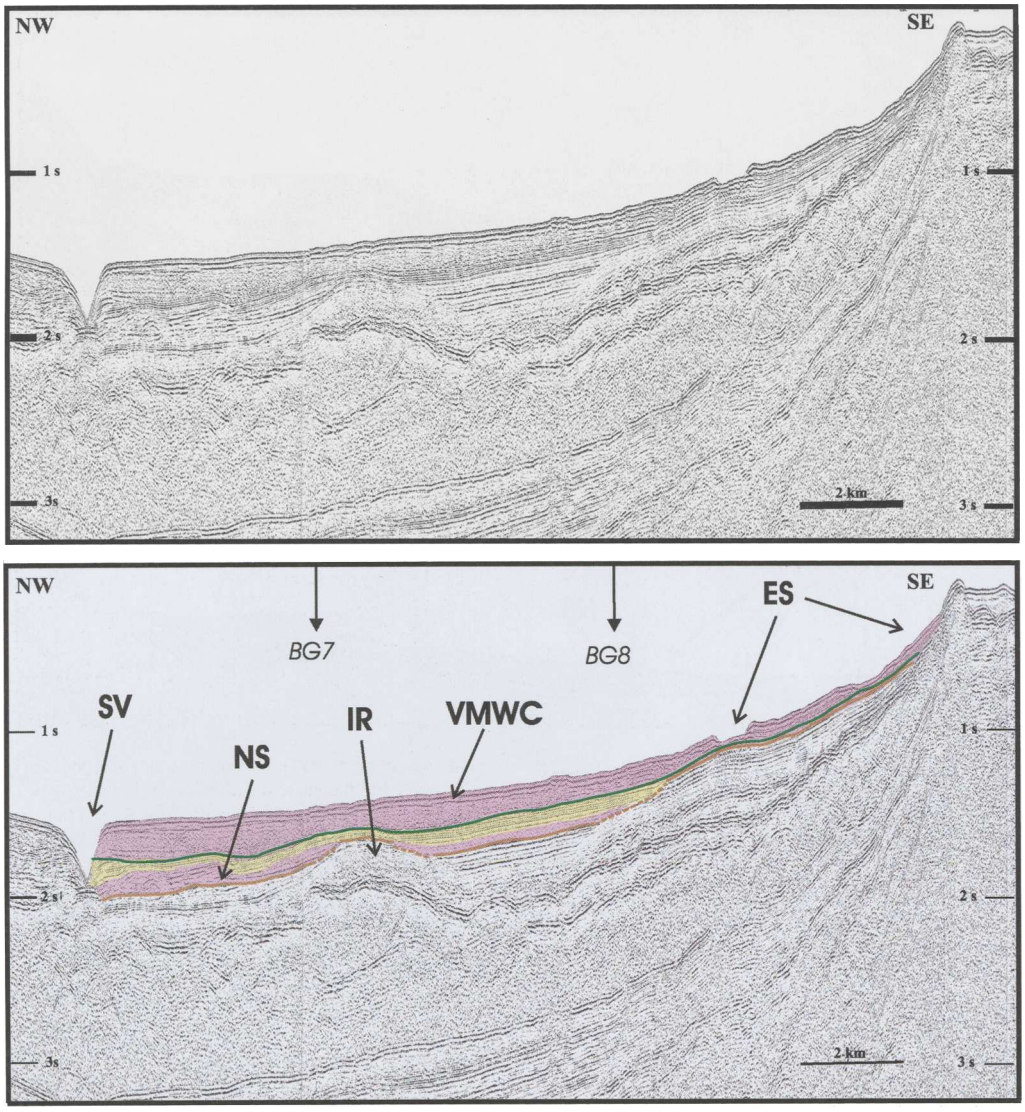

Fig. 8. Dip seismic section (line BG3) over the northeastern Sicilian margin of the Gioia Basin (see location in Fig. 3; colours refer to facies as in Fig. 4). Destructive processes dominated this basin portion up to recent times. The Nicotera slump (NS), present along most of the line, disappears only over the intrabasinal high (IR) in the centre of the profile. In the upper slope, the main headwall and smaller evacuation surfaces (ES) that have fed the Villafranca mass-wasting complex (VFMC) are present; downslope, the VMWC spans the whole margin, and reaches the Stromboli Valley (SV).

elements responsible for the deep-sea deposition during Unit II (Fig. 11a) and Unit I (Fig. 11b) in the various sectors of the Gioia Basin.

The southwestern Sicilian margin

This evolves from the Unit I onlapping constructional apron to the Unit II offlapping constructional apron (Fig. 6). Apart from the basal Nicotera slump, the Unit I apron is made up of channel–levee deposits passing downslope to channel-mouth turbidite lobes (Fig. 11b); progradation of the channel–levee deposits over turbidite lobes occurs through time both along and across the basin (Figs 4 and 6). The deposition of the Unit I apron is accompanied by erosion within canyons and slope bypass.

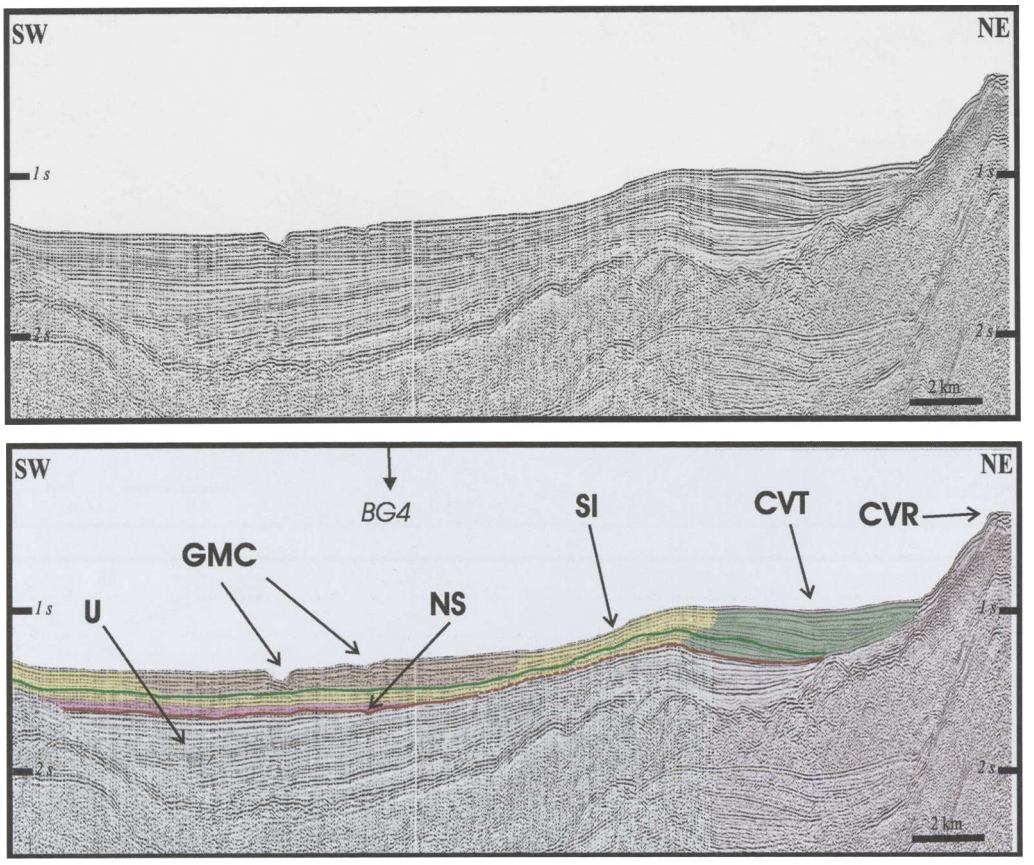

Fig. 9. Line BG 8 crossing the Calabrian margin (see location in Fig. 3; colours refer to facies as in Fig. 4). The unconformity (U) that marks the end of the extensional deformation in the Gioia Basin lies slightly deeper than the brown reflector. At the base of Unit I the Nicotera slump (NS) is evident as a transparent, thin horizon that onlaps the slope of the Capo Vaticano Terrace (CVT). The intraslope turbidite lobes of the Calabrian slope are characterized by the discontinuous reflectors of Unit II in the centre of the line where the channelized portion of the Gioia–Mesima system is crossed (GMC). Sediment instability and removal (SI) is affecting the sea floor in the CVT slope. At the base of the Capo Vaticano Ridge (CVR) most of Unit II presents features that can be related to deposition driven by contour currents.

The Unit II offlapping constructional apron is mainly made up of a multiple channel–levee complex consisting of the fill of the Milazzo, Niceto and Villafranca depositional channels and of their levee and overbank deposits (Figs 4, 6 and 11a). Whereas in the lower part of Unit II turbidite lobes were developed at the mouth of the channels, at present, the Milazzo and Niceto channels join in the upper reach of the SV, and deposition is restricted to the right levee of the SV.

The northeastern Sicilian margin

Slope bypass and erosion prevails during deposition of both Units I and II, resulting in the continuous development of an onlapping autocthonous apron (Fig. 8). The Unit I apron is mainly made up of the basal Nicotera slump followed by sheet turbidites, and by a thin hemipelagic draping over the submerged basement highs (Fig. 11b). The Unit II autocthonous apron consists of the large VMWC, which spans almost the whole basin sector and is flanked upslope by the areas where the sediments affected by instability have been removed (Fig. 11a).

The Calabrian margin

Unit I deposition occurred in an onlapping apron mainly composed of the Nicotera slump; only a very thin veneer of sheet turbidites appears to fill

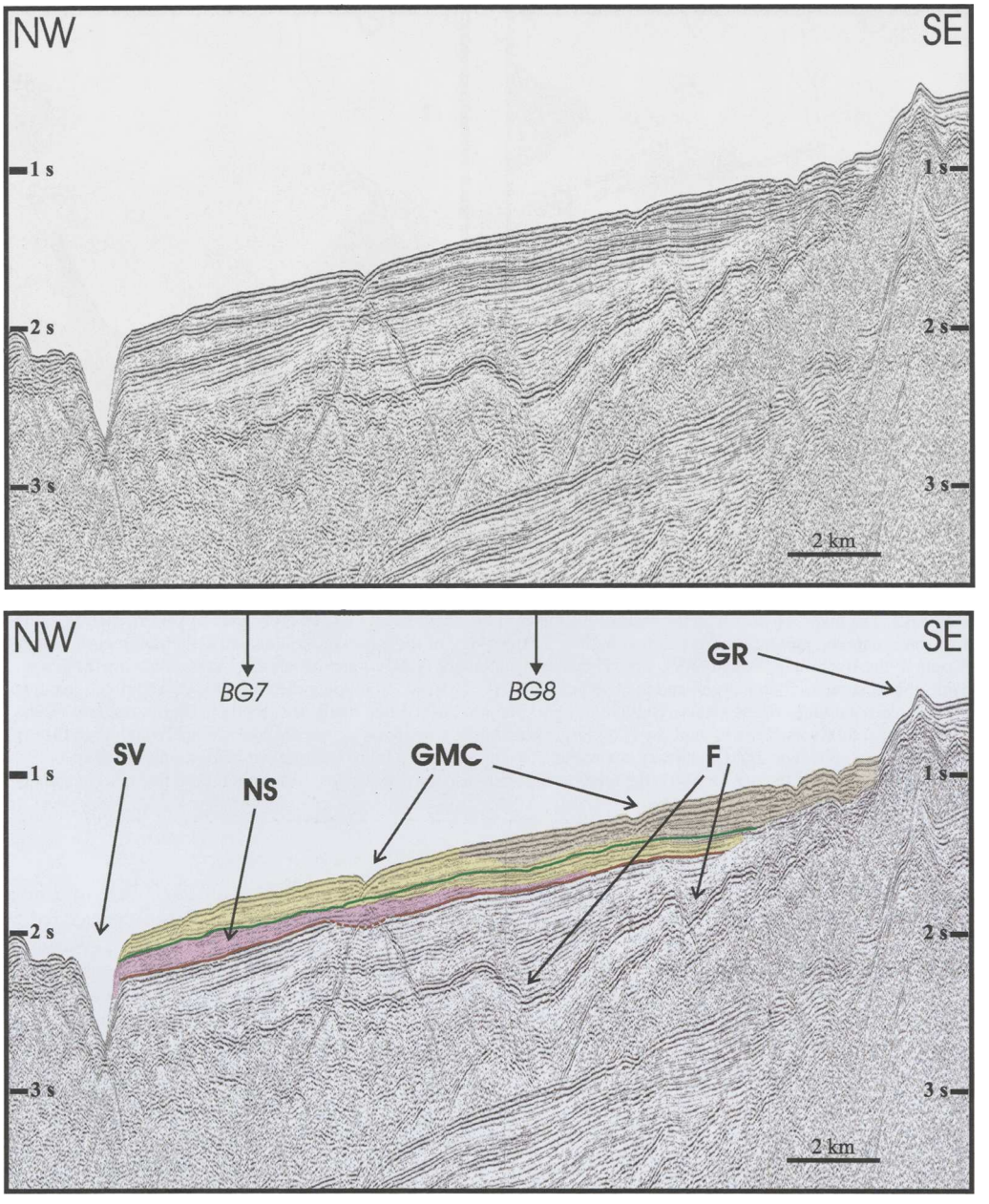

Fig. 10. Line BG 4 (see location in Fig. 3; colours refer to facies as in Fig. 4). The reflectors of both Units I and II onlap the Gioia intrabasinal ridge (GR). The Nicotera slump (NS) is a mounded package with a chaotic internal appearance that thickens downslope, reaching the Stromboli Valley (SV). The absence of any erosional feature or canyon fill within Unit I indicates that the Gioia–Mesima submarine drainage system (GMC) is a later-stage element of the Calabrian margin. The extensional faults (F), affecting the older basin infill, dip toward the east.

the space created upslope from the Nicotera slump (Fig. 11b).

The interval of Unit II deposition is still characterized by an onlapping apron terminating against the Gioia Ridge (Fig. 10) but an offlapping geometry develops in the northern portion of the Calabrian sector. In the proximal area, sheet turbidites deposited between the mainly erosive Gioia and Mesima

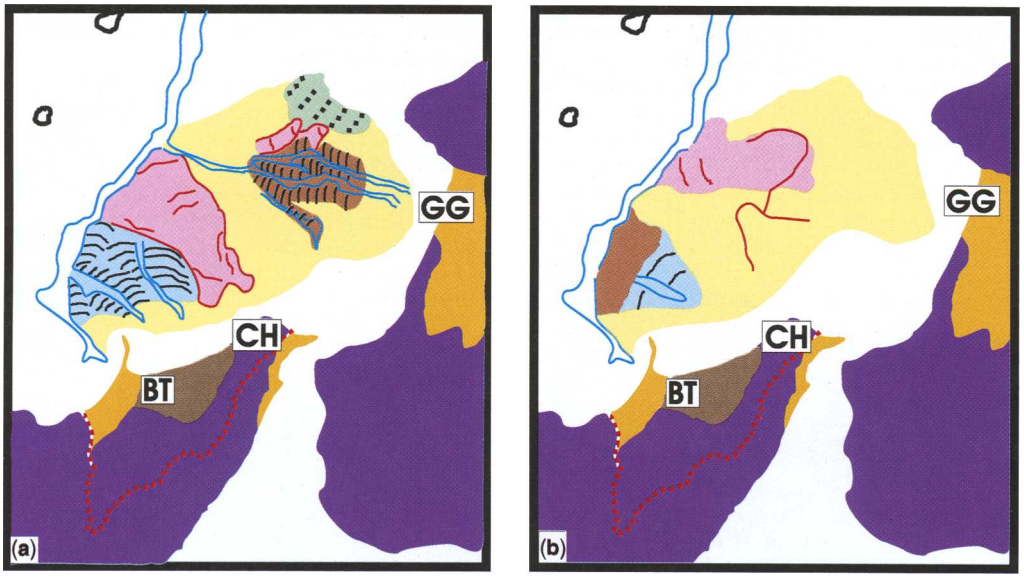

Fig. 11. Distribution of the depositional geomorphological elements and facies (colours refer to facies as in Fig. 4) along the Gioia Basin margin during Units II (**a**) and I (**b**); red continuous lines are the traces of mass wasting and slump headwalls. The maps are drawn on the basis of the facies at the top of Units I and II; in the case of Unit II, therefore, the map represents the present-day facies distribution. The geology of the adjacent Sicilian and Calabrian region is also sketched; the Barcellona trough (BT), with Pliocene–Quaternary (yellow) and Miocene clastic sediments (brown) flanks the western Sicilian margin, and the Castanea horst (CH), with outcropping metamorphic rocks (violet), extents along the coastal areas of the eastern Sicilian margin. The red dashed line marks the divide in Sicily; because on the Tyrrhenian side, rivers flows toward the NW, larger catchment size characterizes the Barcellona Trough than the Castanea horst. Pliocene and Quaternary sediments also fill the Gioia Tauro half-graben (GG) along the coast of Calabria. (See text for further details on the relationships between the depositional history of the studied margin and the geology of the surrounding land areas.)

canyons are present. The canyons evolve to depositional channels from a depth of 700 to 1000 m where an intraslope fan is present (Figs 9 and 11a). The distal basin portion is the site of sheet turbidites flanking the distal erosive trunk of the Gioia–Mesima channel–canyon system (Fig. 11a). A contourite mound is developed in the Capo Vaticano Terrace, at the base of the Capo Vaticano (Fig. 11a).

Discussion

The post-rift depositional units older than Unit I have parallel, often very faint reflectors and mainly display a draping geometry over the intrabasinal ridges that reflects sedimentation as a result of hemipelagic settling and thus indicates a reduced sediment flux to the basin. The development of Unit I and II depositional systems, consisting of geomorphological elements that record the development of effective sediment gravity flow dynamics, therefore marks an important change in the Gioia Basin sedimentary processes. During the Early Pliocene the present-day Sicilian and Calabrian landmasses were to a great extent still submerged and mainly characterized by the hemipelagic 'Trubi' deposition (Westaway 1993; Di Stefano & Lentini 1995; Monaco *et al.* 1996); hemipelagic deposition was also widespread in the Mid-Pliocene (Di Stefano & Lentini 1995). In the Late Pliocene, in response to an almost general, although differential uplift trend, much of the region started to emerge (Westaway 1993; Di Stefano & Lentini 1995; Monaco *et al.* 1996; Tortorici *et al.* 2003). As we have already argued, the age of the base of Unit I can be assumed to be between the Late Pliocene and the Early Pleistocene. We therefore relate the development of the Unit I depositional systems to the creation of sediment source areas large enough to afford an abundant sediment supply to the Gioia Basin. Moreover, the strong differential vertical movement between the basin margin and the adjacent land areas must have fostered a widespread instability of the region, which, in turn, could have triggered the mass-wasting event responsible for the basin-wide Nicotera slump, the basal horizon of Unit I.

Much of the sediment fed to the Gioia Basin during the deposition of Unit I bypassed the upper slope and formed an onlapping apron. This stratigraphic architecture, typical of out-of-grade margins (Ross *et al.* 1994; Galloway 1998) records a stage during which, probably as a heritage of the preceding rift-stage extensional tectonics, the Sicilian margin had slope gradients steeper than the depositional grade.

Within the ubiquitous scenario of slope bypass, however, a great heterogeneity of the sedimentary processes that governed the margin development is revealed by the highly varied thickness (Fig. 5b) and facies building blocks (Fig. 11b) of Unit I. Besides basin physiography, sediment supply is amongst the main factors that control facies associations in deep-water systems and is primarily influenced by the history of extensional tectonics and the resulting morphology of the emerged areas, which dominates drainage development and the distance of hinterland areas to successive sub-basins (Leeder & Jackson 1993; Gawthorpe *et al.* 1994; Ravnas & Steel 1998; Alves *et al.* 2003). Lithology of source regions is another important factor in controlling sediment yield potential and calibre to the basin (Gawthorpe *et al.* 1994; Ravnas & Steel 1998; Leeder *et al.* 2002). It is again in the geology of the adjacent emerged areas that the explanations for the observed different depositional environments can be sought. In the Sicilian mainland, the Barcellona tectonic trough flanks the southwestern portion of the Gioia Basin, whereas the Castanea horst crops out along the coast of the northeastern basin sector (Figs 2 and 11). The Barcellona depression is characterized by larger catchments than the Castanea horst and by the presence of Tertiary terrigenous rocks at variance with the metamorphic basement rocks that crop out extensively in the Castanea horst (Figs 2 and 11). Both the catchment size and the lithologies of the source regions therefore point to a present-day, relatively higher sediment yield potential and higher calibre of sediment supply to the western portion of the Gioia Basin, as is indeed confirmed by hydrological data (Amore *et al.* 1995; Brambati *et al.* 1995). As the present-day structural grain of the Sicilian mainland was, to a large extent, the result of the Late Pliocene uplift (Catalano & Cinque 1995; Del Ben *et al.* 1996), it can be assumed that a differential sediment supply to the western and eastern portion of the Sicilian Gioia Basin was already established during deposition of Unit I, thus accounting for the halving of Unit I thickness from the western to the eastern Sicilian margin (Fig. 5b). The unequal sediment supply rate also influenced facies distribution. The progradation of a channel–levee complex over basin plain sheet turbidites occurred in the well-supplied western Sicilian margin, whereas basin undersupply resulted in an autochthonous apron consisting mainly of sheet turbidites passing to hemipelagites over intrabasinal structural ridges and small-scale slumps in the eastern one (Fig. 11b).

In a similar way, the rate of sediment supply can be responsible for the character of Unit II deposition in the eastern and western Sicilian margin. A continued adequate sediment flux ultimately led to the development of an offlapping geometry along the southwestern Sicilian margin. Similar stratigraphic settings develop when sediment supply exceeds accommodation generation, allowing the progradation of the siliciclastic depositional system (Galloway 1989, 1998; Ravnas & Steel 1998; Ross *et al.* 1994). Therefore in the western Sicilian margin, Unit II deposition represents the establishment of a graded margin with a dynamic equilibrium profile. In particular, an assemblage of interfingering channel–levee, turbidite lobe deposits and SV levee and overbank deposits was responsible for the margin progradation. In contrast, in the eastern Sicilian margin, Unit II still has an onlap geometry and is characterized by the deposition of sheet turbidites successively involved in the recent downslope movement of the Villafranca mass-wasting complex. The depositional setting of the eastern Sicilian margin is therefore representative of long-lasting slope instability, which has resulted in the persistence of a destructional margin during both Units I and II. The continuing low sediment supply and the possible effect of the oversteepening of the Acquarone Ridge slope that represents the offshore extension of the uplifting Castanea horst (Catalano & Cinque 1995) can explain this depositional setting. An onlapping apron characterizes the interval of Unit I deposition also in the Calabrian sector of the Gioia Basin. As in the Sicilian margin, this stratigraphic setting can result from an out-of-grade slope, an inheritance from the rift-stage tectonics. The extremely reduced thickness of Unit I in comparison with that along the Sicilian margin (Fig. 5b) can, however, support the possibility of the role of a low sediment supply in maintaining this depositional architecture. Although the small thickness of Unit I could be interpreted to result from the larger dimension of the Calabrian margin, a low sediment supply to the basin also agrees with the absence of any submarine sediment delivery system during Unit I deposition (Fig. 11b). The Calabrian margin is flanked on land and separated from the rift hinterland by the 35 km wide, 50 km long Gioia Tauro half-graben (Monaco & Tortorici 1995, 2000), filled by at least 600 m of marine sediments of Late Pliocene to Mid-Pleistocene age, followed by alluvial deposits of Mid–Late Pleistocene age (Monaco & Tortorici 1995; Tortorici *et al.* 1995). Furthermore, in the area north of the Messina Strait, the intraslope Palmi Basin (Selli 1979) is present between the Gioia Tauro half-graben and the Gioia Basin. It could hence be

assumed that the effective trapping in the Gioia Tauro half-graben and in the Palmi Basin of most of the sediment from the rift hinterland caused a low sediment supply to the Calabrian margin during Unit I. An increase of sediment supply to the northern Calabrian margin is substantiated by the thickness of Unit II, which in some places equals that in the area of the Sicilian margin channel–levee complex (Fig. 5b). The change in the supply rate to the Calabrian margin could coincide with the establishment of sediment spilling from the Gioia Tauro half-graben following its complete filling in Mid-Pleistocene time. The mechanism of filling of successive sub-basins is in fact a typical tract of extensional settings (Ravnas & Steel 1997, 1998). The increased sediment flux, fed to the margin by the submarine Gioia–Mesima drainage network, ultimately allowed the development of an offlapping constructional apron in the northern Calabrian margin during Unit II deposition. Sediments accumulated mainly in an intraslope depositional area within channelized turbidite lobes located in the middle margin portion whereas sediment bypass prevailed further downslope, in the distal erosive trunk of the Gioia–Mesima system. A similar depositional style is frequently recognized along margins characterized by gradient variations mainly resulting from salt tectonics deformation (Satterfield & Behrens 1990). In the case of the Gioia Basin the dam effect of the NS could be the ultimate cause of the observed depositional setting.

A further effect of the basin physiography on depositional facies development arises from interaction with the path of contour currents. The development of a contourite mound in the Capo Vaticano Terrace can be in fact the result of the deflection of bottom currents by the adjacent Capo Vaticano Ridge.

Conclusions

The present study highlights the different depositional systems with distinctive sedimentary environments and processes, facies association and stratigraphic geometry that develop at the same time along the Gioia Basin margin. In addition, it emphasizes that a temporal evolution of the sedimentary dynamics along each sector of the Gioia Basin margin can be recognized.

The physiography of the margin, which is the result of the past extensional faulting in the basin, and the geology of the surrounding emerged areas, which are still affected by tectonic deformation and high rates of vertical movement, have been recognized as the major factors controlling the observed depositional evolution.

The uplift of the adjacent areas is the basic agent that, allowing for the development of large source areas, controls the switch from an almost basin-wide hemipelagic draping to the depositional systems of the studied interval that record the establishment of a high sediment flux to the Gioia Basin margins. The phase of general uplift probably led to widespread instability along the margin and promoted the movement of the basin-wide Nicotera slump body that is emplaced at the base of the studied interval.

A stage of quiescent tectonism accompanies the deposition of Units I and II. However, during the deposition of the early post-rift Unit I, the tectonic legacy is manifested in the stratigraphic architecture of the margin that, as a result of bypass on the oversteepened, out-of-grade slopes, consists of an onlapping base-of-slope sedimentary package along the whole margin. In contrast, the interval of Unit II marks the late post-rift establishment of a graded depositional profile with the development of an offlapping geometry along a large part of the margin.

The geology of the adjacent emerged areas and the physiography of the Gioia Basin itself are the main controls on the sedimentary entry points and on the course and character of the canyons and channels along the Gioia Basin margin. These two controlling parameters therefore play a major role in determining distribution, thickness and the sedimentary facies of the depositional systems along the margin. In the Sicilian margin, a channel–levee complex develops to the SW, where large catchments are present on land. In the northeastern Sicilian margin, in contrast, where rivers drain very small areas, an undersupplied margin is maintained for the whole interval studied; hence, slope destruction is the prevailing sedimentary process, as shown by an infilling consisting almost entirely of the Niceto slump and of the recent Villafranca mass-wasting complex. Finally, the presence of underfilled basins in the hinterland of the margin is a further important element that influences the Gioia margin evolution. In the Calabrian margin, in fact, the development of the Goia–Mesima canyon–channel system and of the related intraslope channelized fan is probably coincident with the complete filling of the Gioia Tauro extensional trough that previously separated the Gioia margin from the rift hinterland.

We especially thank M. Ligi for his assistance in the preparation of the bathymetric maps. A. Di Stefano and J. S. Laberg are gratefully thanked for their constructive reviews.

References

ALVES, T. M., MANUPPELLA, G., GAWTHORPE, R. L., HUNT, D. W. & MONTEIRO, J. H. 2003. The depositional evolution of diapir- and fault-bounded rift

basins: examples from the Lusitanian Basin of west Iberia. *Sedimentary Geology*, **162**, 273–303.

AMORE, C., GEREMIA, F. & RANDAZZO, G. 1995. Primi dati sulle caratteristiche tessiturali e composizionali dei sedimenti del sistema Eolie e bacini limitrofi di Cefalù e di Gioia. *In*: FARANDA, F. M. (ed.) *EUOCUMM94, Data Report*, 317–330.

BRAMBATI, A., CATANI, G., CELIO, M. & COLIZZI, E. 1995. Primi risultati delle ricerche sedimentologiche nel bacino di Gioia e sulle coste della Sicilia settentrionale tra la foce del fiuma Pollina e il Capo Peloro. *In*: FARANDA, F. M. (ed.) *EUOCUMM94, Data Report*, 303–316.

CATALANO, S. & CINQUE, A. 1995. L'evoluzione neotettonica dei Peloritani settentrionali (Sicilia nord-orientale): il contributo di una analisi geomorfologia preliminare. *Studi Geologici Camerti, Volume Speciale*, **1995**(2), 113–123.

CATALANO, S. & DI STEFANO, A. 1997. Sollevamenti e tettogenesi pleistocenica lungo il margine tirrenico dei Monti Peloritani: integrazione dei dati geomorfologici, strutturali e biostratigrafici. Il Quaternario. *Italian Journal of Quaternary Sciences*, **10**(2), 337–342.

COLANTONI, P., GENNESSEAUX, M., VANNEY, J. R., ULZEGA, A., MELEGARI, G. & TROMBETTA, A. 1992. Processi dinamici del canyon sottomarino di Gioia Tauro (Mare Tirreno). *Giornale di Geologia*, **54**(2), 199–213.

DEL BEN, A., GARGANO, C. & LENTINI, R. 1996. Ricostruzione strutturale e stratigrafica dell'area dello stretto di Messina mediante analisi comparata dei dati geologici e sismici. *Memorie della Società Geologica Italiana*, **51**, 703–717.

DI STEFANO, A. & LENTINI, R. 1995. Ricostruzione stratigrafica e significato paleotettonico dei depositi Plio-Pleistocenici del margine tirrenico tra Villafranca Tirrena e Faro (Sicilia nord-orientale). *Studi Geologici Camerti, Volume Speciale*, **1995**(2), 219–237.

FABBRI, A., GHISETTI, F. & VEZZANI, L. 1980. The Peloritani–Calabria range and the Gioia Basin in the Calabrian arc (southern Italy): relationships between land and marine data. *Geologica Romana*, **19**, 131–150.

GALLOWAY, W. E. 1989. Genetic stratigraphic sequences in basin analysis I: architecture and genesis of flooding-surface bounded depositional units. *AAPG Bulletin*, **73**, 125–142.

GALLOWAY, W. E. 1998. Siliciclastic slope and base-of-slope depositional systems: component facies, stratigraphic architecture and classification. *AAPG Bulletin*, **82**, 569–595.

GAMBERI, F. & MARANI, M. 2004. Deep Sea depositional systems of the Tyrrhenian Sea. *In*: MARANI, M., GAMBERI, F. & MONATTI, E. (eds) *From Seafloor to Deep Mantle: Architecture of the Tyrrhenian Backarc Basin*. Memorie Descrittive della Carta Geologica d'Italia, **64**.

GAWTHORPE, R. L., FRASER, A. J. & COLLIER, R. E. 1994. Sequence stratigraphy in active extensional basins: implications for the interpretation of ancient basin-fill. *Marine and Petroleum Geology*, **11**, 642–657.

LEEDER, M. R. & JACKSON, J. A. 1993. The interaction between normal faulting and drainage in active extensional basins, with example from the western United States and central Greece. *Basin Research*, **5**, 79–102.

LEEDER, M. R., COLLIER, R. E., ABDUL AZIZ, L. H., TROUT, M., FERENTINOS, G., PAPATHODOUROU, G. & LYBERIS, E. 2002. Tectono-sedimentary processes along an active marine/lacustrine half-graben margin: Alkyonides Gulf, E. Gulf of Corinth, Greece. *Basin Research*, **14**, 25–41.

LENTINI, F. 2000. *Carta geologica della Provincia di Messina, scala 1:50 000 e nota illustrativa*. SELCA, Firenze.

MONACO, C. & TORTORICI, L. 1995. Tettonica estensionale quaternaria nell'arco calabro e in Sicilia Orientale. *Studi Geologici Camerti, Volume Speciale*, **1995**(2), 351–362.

MONACO, C. & TORTORICI, L. 2000. Acting faulting in the Calabrian arc and eastern Sicily. *Journal of Geodynamics*, **29**, 407–424.

MONACO, C., TORTORICI, L., NICOLICH, R., CERNOBORI, L. & COSTA, M. 1996. From collisional to rifted basin: an example from the southern Calabrian arc (Italy). *Tectonophysics*, **266**, 233–249.

RAVNAS, R. & STEEL, R. J. 1997. Contrasting styles of Late Jurassic syn-rift turbidite sedimentation: a comparative study of the Magnus and Oseberg areas, northern North Sea. *Marine and Petroleum Geology*, **14**, 417–449.

RAVNAS, R. & STEEL, R. J. 1998. Architecture of marine rift-basin successions. *AAPG Bulletin*, **82**, 110–146.

ROSS, W. C., HALLIWELL, B. A., MAY, J. A., WATTS, D. E. & SYVITSKI, J. P. M. 1994. Slope readjustment: a new model for the development of submarine fans and aprons. *Geology*, **22**, 511–514.

SATTERFIELD, W. M. & BEHRENS, E.W. 1990. A Late Quaternary canyon/channel system, northwest Gulf of Mexico continental slope. *Marine Geology*, **92**, 51–67.

SELLI, R. 1979. Geologia e sismotettonica dello stretto di Messina. *Atti Accademia dei Lincei*, **43**, 119–154.

TORTORICI, L., MONACO, C., TANSI, C. & COCINA, O. 1995. Recent and active tectonics in the Calabrian arc (southern Italy). *Tectonophysics*, **243**, 37–55.

TORTORICI, G., BIANCA, M., DE GUIDI, G., MONACO, C. & TORTORICI, L. 2003. Fault activity and marine terracing in the Capo Vaticano area (southern Calabria) during the Middle–Late Quaternary. *Quaternary International*, **101–102**, 269–278.

TRAMONTANA, M., COLANTONI, P. & FANUCCI, F. 1995. Risultati preliminari delle indagini morfologico-sedimentologiche nell'ambito del progetto. *In*: FARANDA, F. M. (ed.) *EUOCUMM94, Data Report*, 331–338.

WESTAWAY, R. 1993. Quaternary uplift of southern Italy. *Journal of Geophysical Research*, **98**, 21741–21772.

Active faults and inferred seismic sources in the San Vito lo Capo peninsula, northwestern Sicily, Italy

E. TONDI[1], D. ZAMPIERI[2], G. GIUNTA[3], P. RENDA[3], M. ALESSANDRONI[3], M. UNTI[3], A. GIORGIANNI[3] & G. CELLO[1]

[1]*Dipartimento di Scienze della Terra, Università di Camerino, Via gentile III da Varano, 62032 Camerino (MC), Italy (e-mail: emanuele.tondi@unicam.it)*

[2]*Dipartimento di Geologia, Paleontologia e Geofisica, Università di Padova, Via Giotto 1, 35137 Padova, Italy*

[3]*Dipartimento di Geologia e Geodesia, Università di Palermo, Corso Tukory 131, 90134 Palermo, Italy*

Abstract: Two independent active faults, capable of generating medium-sized earthquakes in the San Vito lo Capo peninsula, northwestern Sicily (Italy) have been identified as a result of detailed field studies. In western Sicily, instrumental seismicity is low; in fact, except for the 1968 Belice earthquake (Ms = 5.4), historical records indicate that this area is relatively quiescent. Most of the seismicity is in the offshore sector of the Sicilian Maghrebian Chain, which is characterized by several medium- to low-magnitude events. The main shock of the 2002 Palermo seismic sequence (Mw = 5.9) represents the largest earthquake felt in the area in recent years. The deformation pattern characterizing the most recent faults mapped in northwestern Sicily includes a grid of high-angle faults consisting of major east–west-striking right-lateral and north–south-striking left-lateral features. This fault grid is related to a regional transcurrent right-lateral shear zone, here named the UEKA shear zone, bounded to the north by the Ustica–Eolie fault and to the south by the Kumeta–Alcantara fault. The UEKA shear zone accommodates the regional strain induced by the current stress field acting in the area, which, as emerges from both structural and seismological data, is characterized by a NW–SE-striking main compression.

The northern coast of Sicily and its Tyrrhenian offshore have been interpreted by various workers (e.g. Boccaletti *et al.* 1982; Malinverno & Ryan 1986; Dewey *et al.* 1989; Chironi *et al.* 2000) as a hinge zone between the Tyrrhenian basin (characterized by incipient oceanization processes) and the emerged portion of the Sicilian Maghrebian Chain. This hinge zone is interpreted as a regional east–west-striking right-lateral shear zone that developed from Pliocene time, while the structuring of the fold-and-thrust belt continued in southern Sicily (Boccaletti *et al.* 1982; Ghisetti & Vezzani 1984; Giunta *et al.* 2000).

As concerns seismicity, the Sicilian offshore is mainly characterized by medium- to low-magnitude events. The main shock of the 2002 Palermo seismic sequence (Mw = 5.9; CMT Catalog, Harvard Seismology, http://www.seismology.harvard.edu/) represents the largest earthquake felt in the area in recent years (Giunta *et al.* 2004). Onshore, in western Sicily, the 1968 Belice seismic sequence (Ms = 5.4 for the main shock; Anderson & Jackson 1987*b*) represents the strongest earthquake that has occurred in the area in historical times.

Several faults, in western Sicily, involve Pliocene and Early Pleistocene deposits; in the San Vito lo Capo peninsula, they cut through conglomerates of Tyrrhenian age and Holocene sediments, hence recording the effects of active tectonic processes in the area (Giunta *et al.* 2004). For this reason we focused our analyses in the San Vito Lo Capo peninsula, as it may be considered a key area for better understanding the tectonic processes acting in this sector of the peri-Tyrrhenian orogenic system, and to evaluate the seismic potential of northwestern Sicily.

Tectonic framework

The present-day structural setting of northern Sicily is the result of the Cenozoic collision between the North African continental margin and the Sardinia–Corsica block. The main tectonic units derived from the deformation of the northern margin of the African plate display a general southward vergence, and a structural style that is characterized by folds with a wavelength of a few kilometres and by thrusts that extend for tens of kilometres (Fig. 1;

From: MORATTI, G. & CHALOUAN, A. (eds) 2006. *Tectonics of the Western Mediterranean and North Africa.* Geological Society, London, Special Publications, **262**, 365–377.
0305-8719/06/$15.00

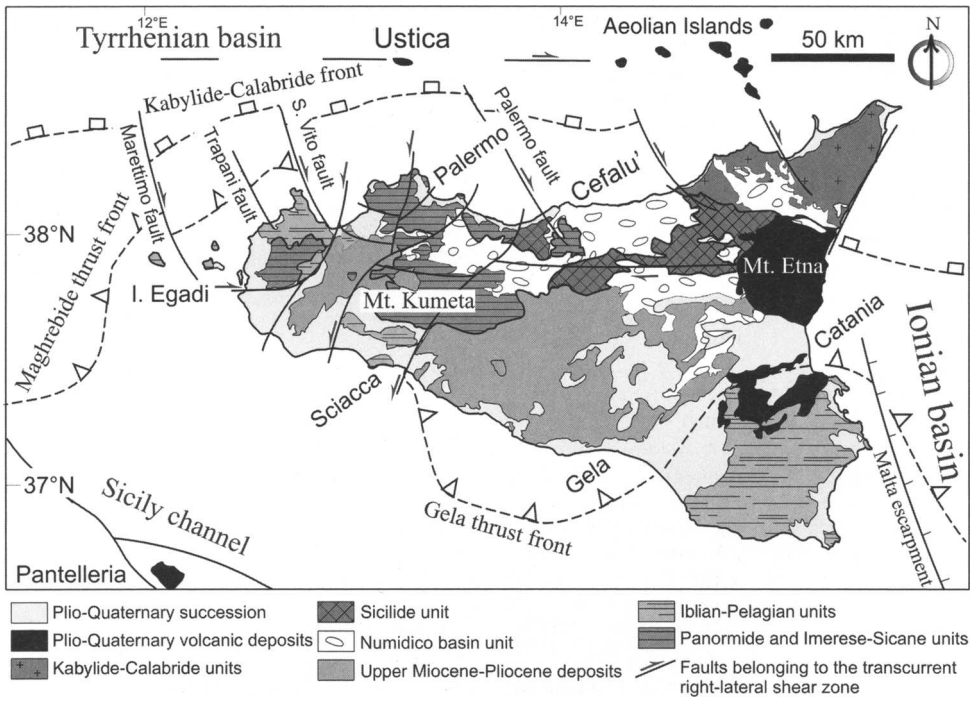

Fig. 1. Schematic geostructural map of Sicily.

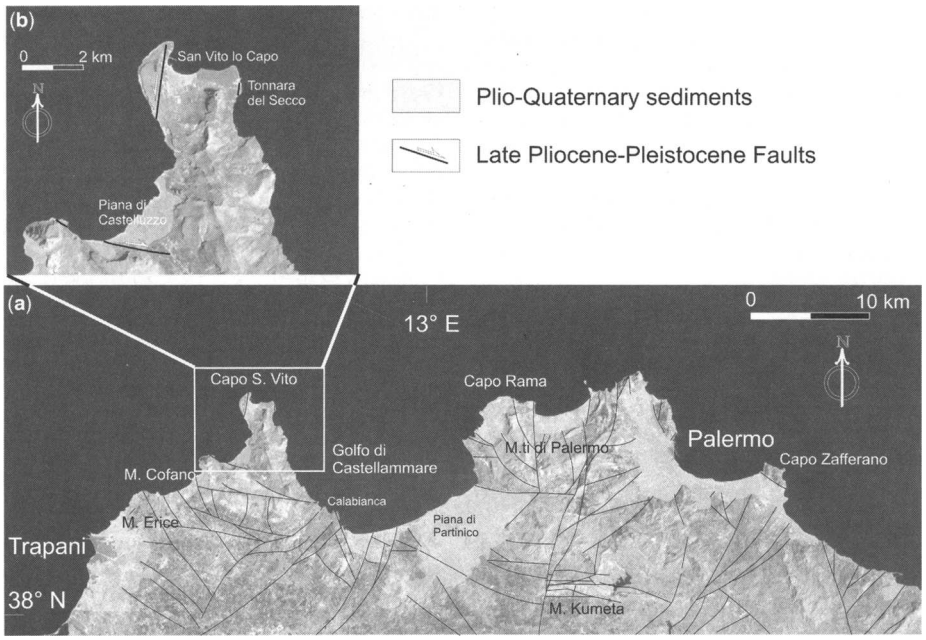

Fig. 2. (**a**) Plio-Quaternary faults of northwestern Sicily; (**b**) active fault zones in the San Vito lo Capo peninsula.

Ogniben 1960; Scandone *et al.* 1974; Catalano *et al.* 1979; Catalano & D'Argenio 1982). The main stages in the Neogene deformation history of the area include (Giunta *et al.* 2000): (1) thrust tectonic events, from the Early Miocene; (2) extensional tectonics and crustal thinning processes, from the Late Miocene; (3) strike-slip tectonic activity, often reactivating inherited structures, during the Plio-Pleistocene evolution of the northern Sicily–southern Tyrrhenian hinge zone (Boccaletti *et al.* 1982; Finetti & Del Ben 1986).

According to some workers, strike-slip tectonics, in the area separating the southern Tyrrhenian Sea from northern Sicily, started in Pliocene time, when the UEKA shear zone was first established. The latter extends offshore for more than 400 km from the island of Ustica to the Aeolian Islands (the Ustica–Eolie Line of Boccaletti *et al.* 1982), and onland, for more than 300 km, from the Trapani mountains to Mt. Etna, including the so-called Kumeta–Alcantara Line (Ghisetti & Vezzani 1984). Lower-rank structures related to the Ustica–Eolie and Kumeta–Alcantara lines comprise the NW–SE-striking faults of Marettimo, Trapani, San Vito and Palermo (Nigro *et al.* 2000; Gueguen *et al.* 2002). Taken as a whole, these structures were interpreted as a right-lateral duplex: the Southern Tyrrhenian Strike-Slip Duplex (Renda *et al.* 2000).

Related to these faults, some minor shear zones are well exposed at several localities (Fig. 2a; Giunta *et al.* 2004). Based on their geometric and kinematic characteristics, these have been grouped into three major sets: (1) an ESE-striking mainly right-lateral to transtensive fault set; (2) a north–south-striking left-lateral to transtensive fault set; (3) a NE–SW-striking set including faults with left-lateral transpressive and reverse kinematics. Some of these high-angle faults involve Pliocene and Early Pleistocene deposits; at San Vito lo Capo peninsula, in particular, two fault zones (trending roughly ESE and NNE) cut through both conglomerates, of Tyrrhenian age, and Holocene sediments (Fig. 2b).

Seismicity

The seismicity pattern recorded in the southern Tyrrhenian Sea since 1988 is shown in Figure 3a. As may be seen in Figure 3b (see also Giunta *et al.* 2004), the distribution of the hypocentres reveals the presence of two seismogenic zones. The first is located in the eastern portion of the southern Tyrrhenian Sea, where about 480 events are concentrated around a NE-dipping plane with a slope angle of 58° down to a depth of about 400 km. This distribution has been associated with the Wadati–Benioff plane of the Ionian lithospheric slab dipping beneath the Calabrian Arc (Gasparini *et al.* 1982; Anderson & Jackson 1987*a*).

The second seismogenic zone extends parallel to the northern coast of Sicily and is generally located within the upper crust. The 2002 Palermo seismic sequence is located within this belt (Fig. 3c). The hypocentral distribution of about 540 earthquakes recorded from 6 September to 15 October 2002 shows a NE–SW trend and a NW-dipping seismic belt (Fig. 3d; Giunta *et al.* 2004). The focal solutions of the main shock (Mw = 5.9) display NE–SW-striking nodal planes with compressive mechanisms (CMT Catalog, Harvard Seismology, http://www.seismology.harvard.edu/). As may be seen in Figure 3c, some 60 earthquakes cluster at about 55 km west from the main shock.

On land, in western Sicily, instrumental seismicity is very low and the 1968 Belice earthquake sequence, characterized by six main shocks with a magnitude of 5–5.4 (Anderson & Jackson 1987*b*), represents the strongest seismic event recorded in historical times (CPTI Gruppo di Lavoro 1999). There is some controversy about the seismogenic structure responsible for the 1968 Belice seismic sequence. Monaco *et al.* (1996) discussed the possibility that the seismic source might be a blind steeply north-dipping reverse fault, whereas Michetti *et al.* (1995) recognized surface faulting evidence interpreted in terms of strike-slip tectonics associated with a NW–SE-striking right-lateral fault.

Active faults in the San Vito lo Capo peninsula

The San Vito lo Capo peninsula, located at the western end of the northern coast of Sicily, extends in a roughly north–south direction into the southern Tyrrhenian Sea (see Fig. 2). This area represents the westernmost and the most external sector of the Sicilian orogenic belt, which is composed mainly of south-verging folds and thrusts. Here, deformed Mesozoic to Tertiary platform carbonates evolve upwards into deep-water marls, limestones and siliciclastic deposits. These, in turn, are unconformably overlain by terrigenous deposits of Plio-Pleistocene age that crop out widely in the coastal plain of Castelluzzo (Piana di Castelluzzo; Fig. 4). These latter deposits consist of carbonate grainstones overlain by shales and sands. Along the coast, small outcrops of Tyrrhenian conglomerates and bio-calcarenites are well exposed (see Fig. 4).

At San Vito lo Capo peninsula we analysed in detail the two main active faults shown in the map of Figure 4. The NNE-striking fault (here named the Faro fault) is exposed, for a length of about 3 km, in the Mesozoic carbonates cropping out in

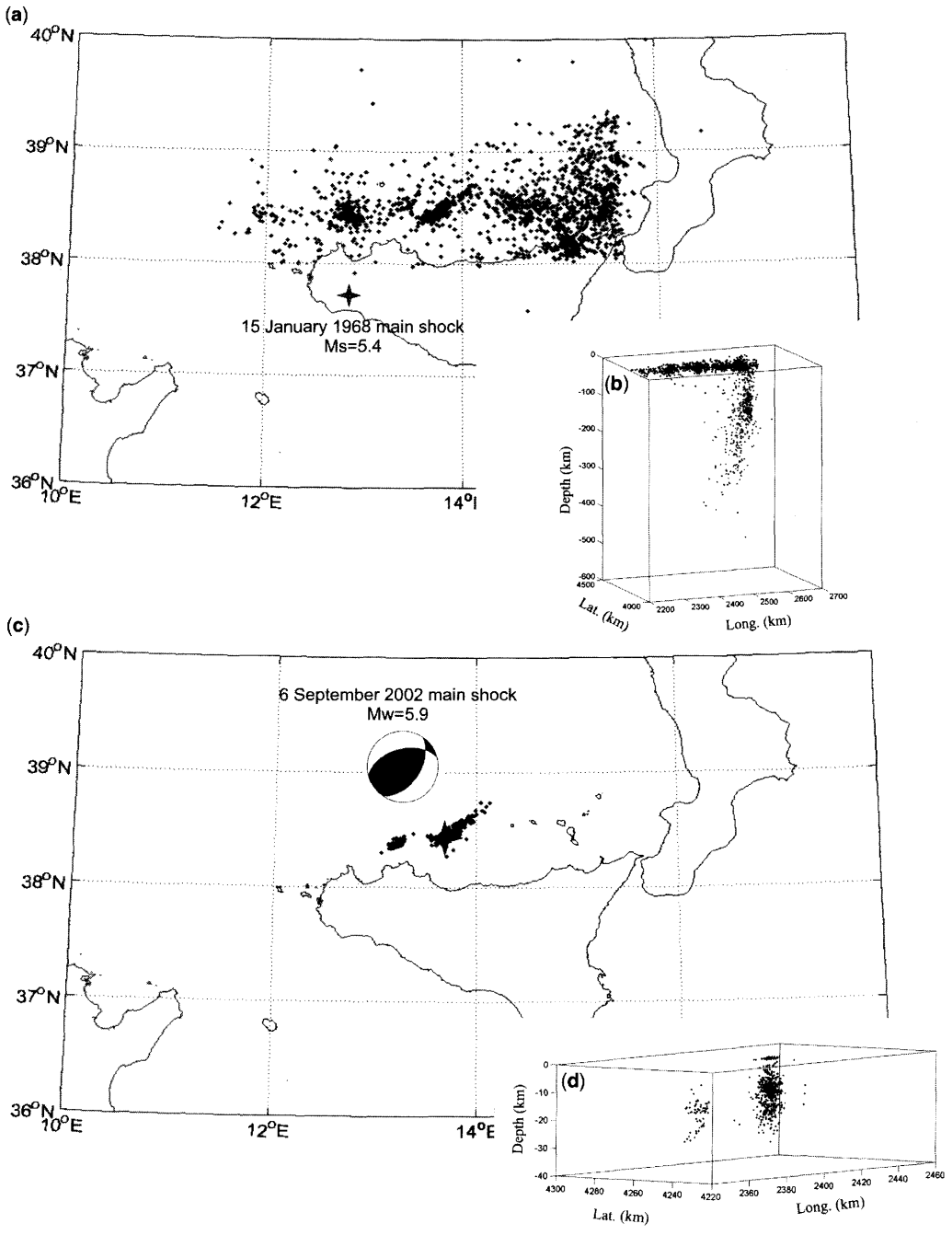

Fig. 3. Distribution of epicentres (**a**) and hypocentres (**b**) of the 2100 earthquakes occurring in the southern Tyrrhenian Sea and northern Sicily between 1988 and 15 October 2002. The epicentre location of the main shock (Ms = 5.4) of the 1968 Belice seismic sequence is also shown. (**d**) Distribution of epicentres (**c**) and hypocentres of the *c.* 540 earthquakes belonging to the Palermo seismic sequence, recorded from 6 September to 15 October 2002 (after Giunta *et al.* 2004). The epicentre and hypocentre location of the main shock (Mw = 5.9) is marked by a star.

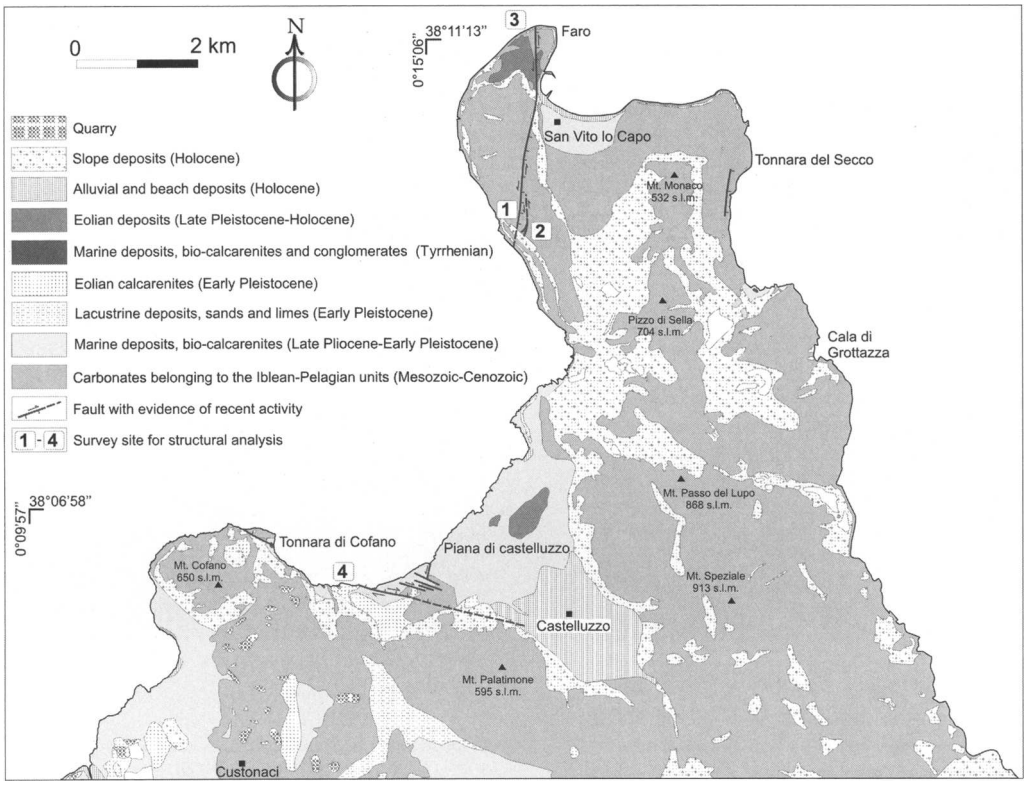

Fig. 4. Geological map of the Plio-Pleistocene deposits cropping out in the San Vito lo Capo peninsula (Abate *et al.* 1993).

the surroundings of the San Vito lo Capo village. Here, we observed striated fault surfaces showing left-lateral strike-slip kinematics, and a few morphotectonic features characterizing NE-striking lower-rank positive flower structures (Fig. 5a and d). Evidence for recent tectonic activity of the Faro fault is given by a continuous 20 m high fault scarp cutting a flat erosional surface that is interpreted to be an Early Pleistocene marine terrace (Fig. 5c; Abate *et al.* 1998). Furthermore, about 3 km north of the marine cliff shown in Figure 5a, at Faro, the fault runs across Late Pleistocene to Holocene aeolian deposits (see Fig. 4). The latter deposits are also cut by lower-rank (metre-scale) faults related to the main NNE trend (Fig. 5d).

The southern margin of the Piana di Castelluzzo is bordered by an ESE-striking fault (here named the Castelluzzo fault), which is exposed for about 2 km in Early Pleistocene marine sediments (see Fig. 4). The morphological evidence of the Castelluzzo fault is given by a fresh-looking fault scarp (about 15 m high; Fig. 6). At several localities, along the coast, we observed striated surfaces indicating prevalent right-lateral kinematics (Fig. 6b). In the fault footwall, lower-rank features (meso-faults and shear fractures) cut through Tyrrhenian conglomerates (Fig. 7).

In the Piana di Castelluzzo, Early Pleistocene bio-calcarenites cropping out along the coast are also affected by several minor faults (Fig. 8). There, we produced a detailed map (at 1:25 scale) by combining field data and image analysis of a photo mosaic composed of digital photographs taken from a helicopter. The marine flat surface is pervasively affected by individual deformation bands and zones of deformation bands with overprinted stylolites, sheared stylolites and slip surfaces (Fig. 9). Individual deformation bands are known to represent the smallest structures, caused by faulting in high-porosity, poorly cemented sandstones (Aydin & Johnson 1978; Antonellini *et al.* 1994) as well as in porous carbonate grainstones (Tondi *et al.* 2006). They consist of broken and compacted grains defining roughly planar features that record small amounts of displacement, typically from a few centimetres to <1 mm. Larger

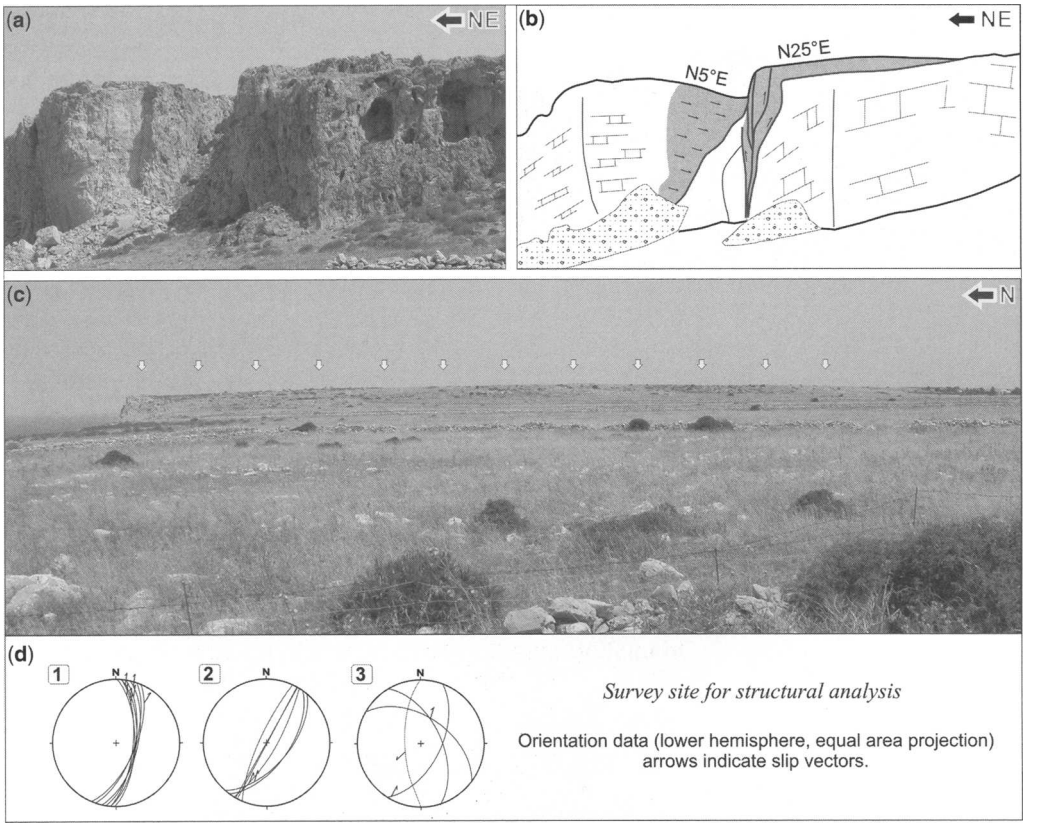

Fig. 5. (**a**) Surface evidence of active faulting associated with the NNE-striking Faro fault. (**b**) Line drawing from the digital image of the marine cliff shown in (a). (**c**) The 20 m high fault scarp, associated with the Faro fault, cutting a flat erosional surface of Early Pleistocene age. (**d**) Fault orientation and kinematic data (see Fig. 4 for locations).

amounts of displacement can be accommodated by wider zones of multiple, composite, deformation bands (Engelder 1974; Aydin & Johnson 1978; Antonellini *et al.* 1994). In the Piana di Castelluzzo, deformation bands are generally shear bands (Aydin *et al.* 2006), mostly trending ESE (Fig. 10). Sheared stylolites are associated with all sets of shear bands. The geometry of step-over zones and 'horse-tail' terminations (Figs 11 and 12) indicates a right-lateral strike-slip character for most of them (striking east–west and ESE) and left-lateral strike-slip kinematics for those (subordinate) trending NNW and north–south. The NW-striking set is often characterized by oblique-normal kinematics, whereas all sets of shear bands and related sheared stylolites show cross-cutting relationships that suggest that they sheared at the same time (see Fig. 8).

In the Piana di Castelluzzo, several mesofaults also affect the Dendropoma coastal reef platform, which is made of worm populations still growing at present in the temperate climate of northwestern Sicily (Fig. 13; Antonioli *et al.* 1999). The fault-controlled reef therefore records clear evidence of the very recent activity of these structures.

The information collected in the study area also suggests that the geometry of the stress field responsible for the overall deformation pattern observed in this sector of northwestern Sicily is characterized by a direction of maximum compression oriented roughly NW. In fact, as shown in Figure 14, the most abundant features exposed in the Piana di Castelluzzo may be interpreted as R shears related to a roughly east–west-striking fault driven by a NW-oriented compression.

As concerns chronology, our observations indicate that deformation bands are the oldest structures formed in the Piana di Castelluzzo area, from Early Pleistocene time, whereas sheared stylolites and mesofaults affecting the Dendropoma reef

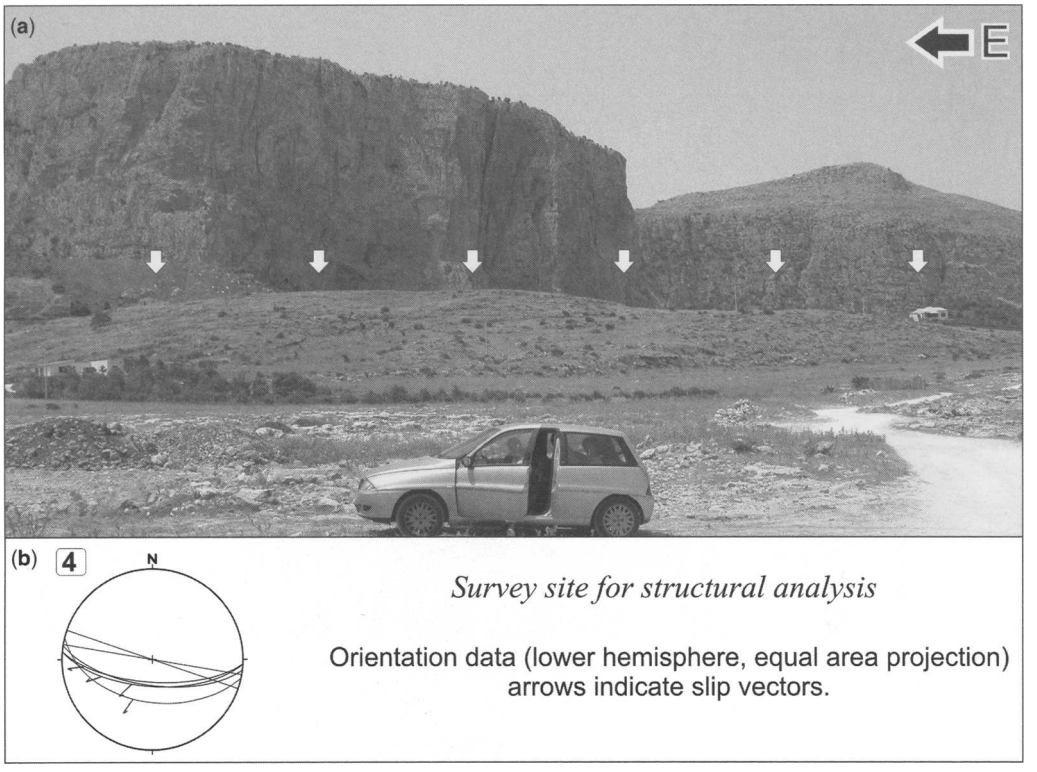

Fig. 6. (**a**) The 15 m high fault scarp in Early Pleistocene marine deposits associated with the Castelluzzo fault. (**b**) Fault orientation and kinematic data (see Fig. 4 for locations).

(characterized by distinctive slip surfaces, visible gauge, and the same kinematics of the deformation bands) developed later. This also suggests that the geometry of the stress field acting in the area has not changed from Early Pleistocene time to the present.

Discussion and conclusions

Detailed analyses of macro- and mesostructural features exposed in the San Vito lo Capo peninsula, in northwestern Sicily, show that the overall deformation pattern in the area may be interpreted in terms of strike-slip tectonics driven by a current

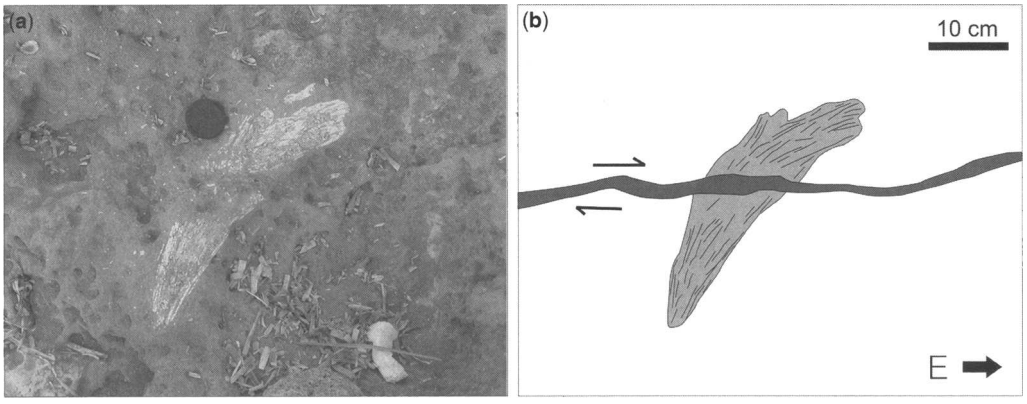

Fig. 7. Remains of macrofauna of Tyrrhenian age cut by an east-striking right-lateral shear fracture: (**a**) photograph; (**b**) schematic drawing.

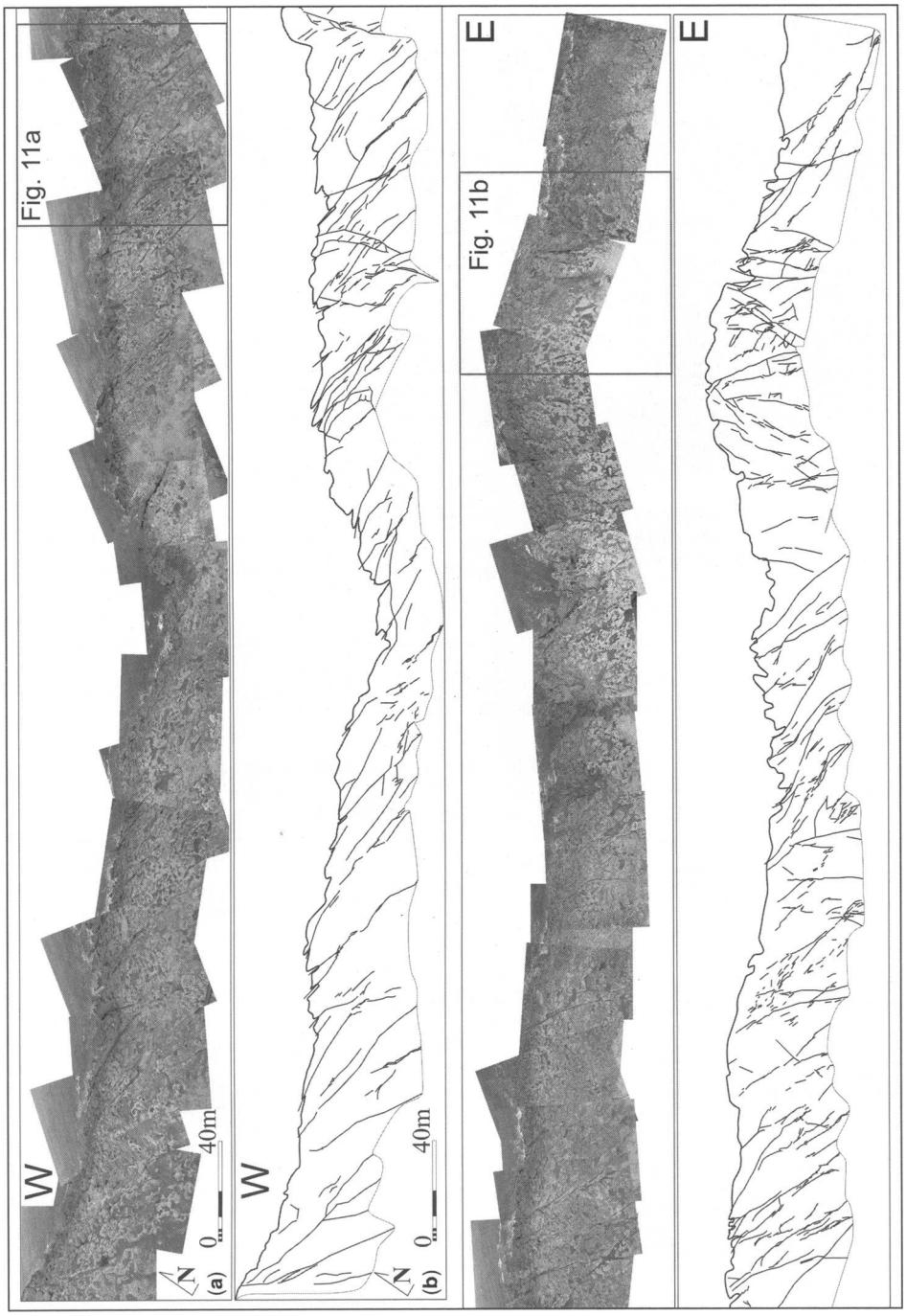

Fig. 8. Detailed map of lower-rank structures exposed in a >1 km long outcrop located along the coast of Piana di Castelluzzo. The analysed images were digitally acquired by flying at a height of about 50 m above sea level. (**a**) Photograph and (**b**) map.

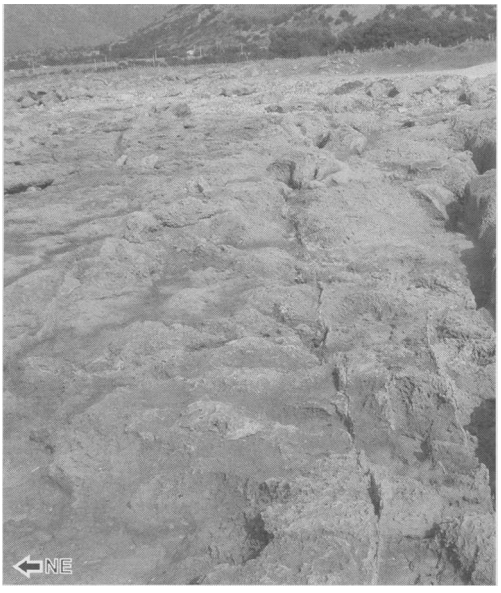

Fig. 9. East–West- and NW-striking deformation bands, in the Piana di Castelluzzo, easily recognized because of their increased resistance to weathering with respect to the host-rock.

stress field geometry characterized by a NW-oriented maximum compression. The stress field acting in the area appears to be directly controlled by the convergence between the African and European plates. The present-day Africa motion along NNW–SSE- to NW–SE-directed vectors is substantiated by geological, seismological, VLBI (very long baseline interferometry) and global positioning system data (Ward 1998; Zarraoa *et al.* 1994; Cello *et al.* 1997; Di Bucci & Mazzoli 2003; Goes *et al.* 2004; Tondi *et al.* 2005).

In the San Vito lo Capo peninsula, we identified two main active faults: the Faro and Castelluzzo faults. Both faults are marked by 15–20 m high fault scarps cutting marine deposits of Early Pleistocene age.

Integrating the values of the vertical component of motion (derived from the height of the fault scarps) and data from mesostructural analysis (which shows a mean pitch value of about 10° for the faults mapped in the area) we computed the cumulative displacement across both faults as some 90–120 m. Consequently, slip on both faults must have occurred at a rate of about 0.05 mm a^{-1} since the Pleistocene. Furthermore, the notion that empirical expressions relating fault length and displacement (Cowie & Scholz 1992; Schlische *et al.* 1996; Tondi & Cello 2003) may provide good estimates for their dimensional properties allowed us to suggest that the cumulative length of each fault is in the range of about 10 km.

Frequency Data, Gaussian

Total Data: 943

GAUSSIAN PARAMETERS					
#	%	Nor. H.	Max H.	Azimuth	sd
1	22.9	100.0	23.25	-75.0°	6.2°
2	21.3	88.6	20.60	-88.2°	6.5°
3	16.2	49.5	11.50	-60.7°	8.8°
4	26.9	36.2	8.41	-39.3°	20.0°
5	7.8	25.9	6.02	74.0°	8.1°

Min Value Fit = 0.3999954

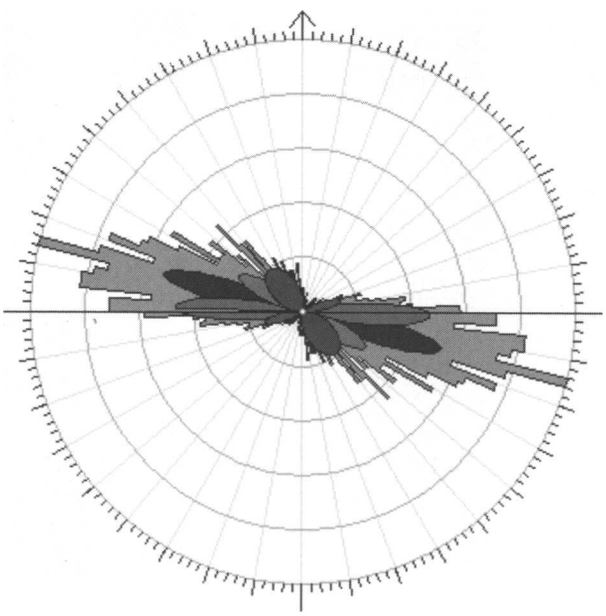

Fig. 10. Orientation data for the structures exposed in the Piana di Castelluzzo outcrop.

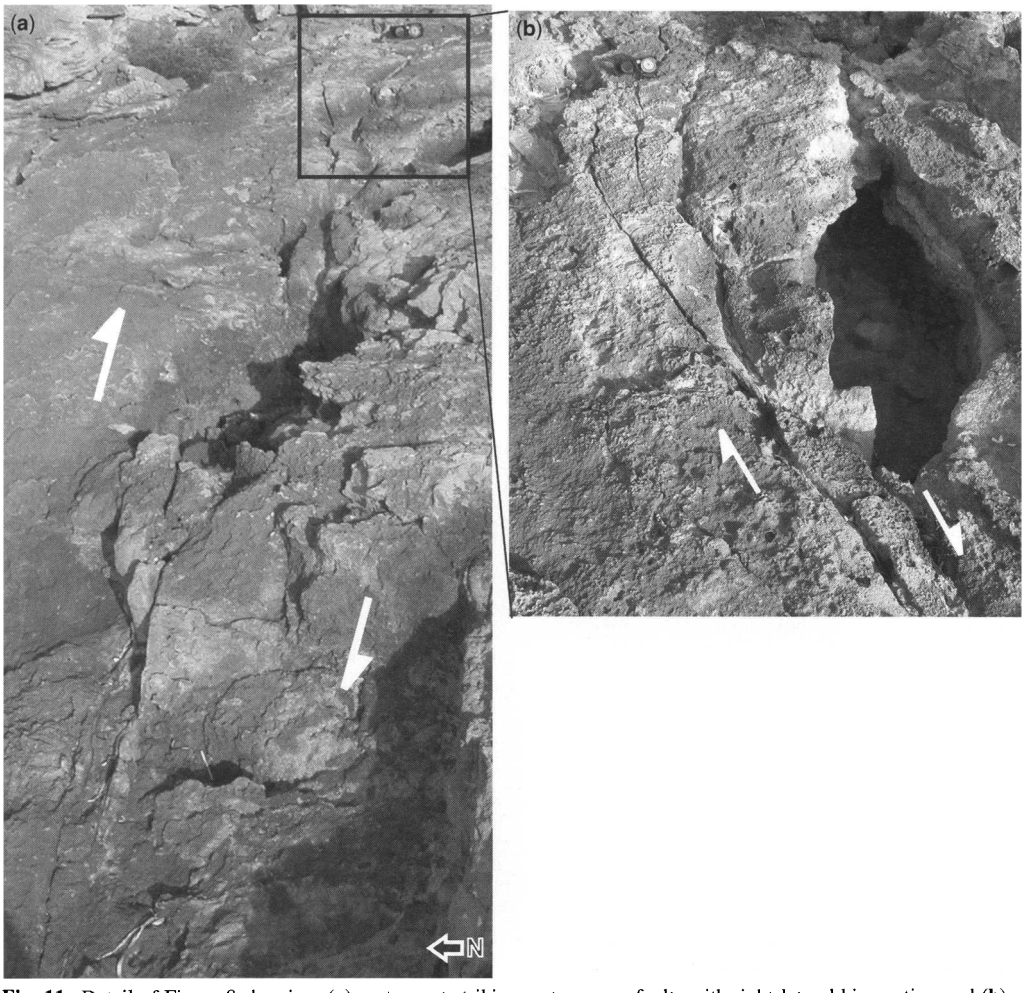

Fig. 11. Detail of Figure 8 showing: (**a**) east–west-striking mature mesofaults with right-lateral kinematics, and (**b**) NNW-striking sheared stylolites with left-lateral sense of motion.

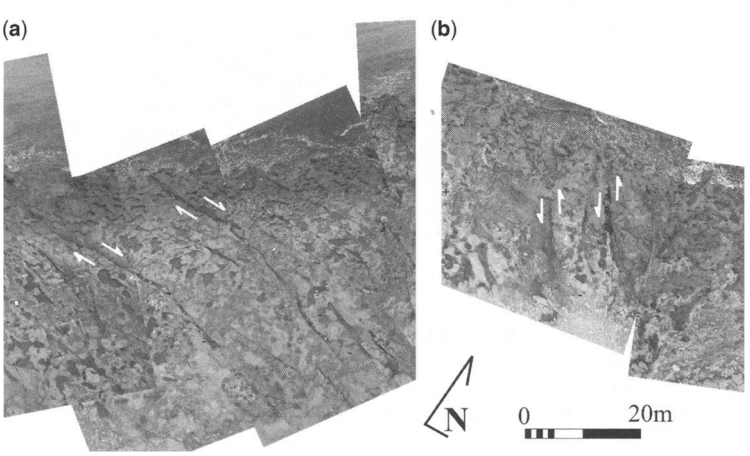

Fig. 12. (**a**) Left-stepping geometry of ESE-striking sheared stylolites; (**b**) 'horse-tail' termination showing right-lateral kinematics.

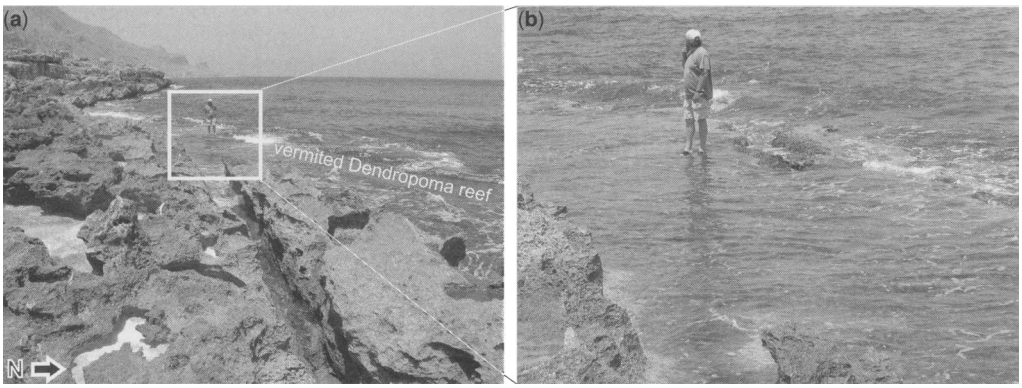

Fig. 13. (**a, b**) Fault-controlled morphology of the Dendropoma reef platform.

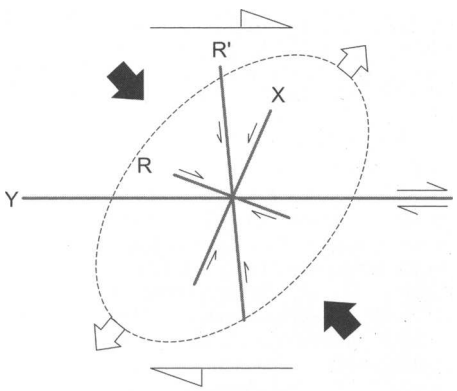

Fig. 14. Two-dimensional geometry of the stress field acting in northwestern Sicily, and structural interpretation of the structures mapped in the Piana di Castelluzzo.

Based on this estimate, we also computed the maximum expected moment magnitude for both faults from the relationship

$$\mathrm{Mo} = \mu A \delta u \qquad (1)$$

where Mo is the seismic or geological momentum, A is the fault surface area, μ is the rigidity modulus (3×10^{11} dyn cm^{-2}) and δu is the last slip increment on the fault.

We calculated A from the inferred fault length, by assuming that its width is equal to the thickness of the seismogenic layer (about 10 km; as may be averaged from the hypocentre distributions shown in Fig. 3).

From (1), it follows that the moment magnitude is (Kanamori 1977)

$$\mathrm{Mw} = (\log \mathrm{Mo}/1.5) - 10.73. \qquad (2)$$

Considering each seismogenic structure individually, and a mean coseismic displacement of the order of 0.5 m (Wells & Coppersmith 1994), we propose that the maximum expected moment magnitude for each fault is about 6.0. This result suggests therefore that, in western Sicily, as well as the Belice region, the San Vito lo Capo peninsula may also be considered as a seismic source area for medium-sized earthquakes.

This work was supported by the Universities of Camerino and Palermo (research funds to E. Tondi, G. Giunta, P. Renda and M. Unti), and by the MIUR, Cofin 2002 (research funds to G. Cello and D. Zampieri).

References

ABATE, B., DI MAGGIO, C., INCANDELA, A. & RENDA, P. 1993. *Carta Geologica dei Monti di Capo San Vito*. Dipartimento di Geologia e Geodesia dell'Università di Palermo.

ABATE, B., INCANDELA, A., NIGRO, F. & RENDA P. 1998. Plio-Pleistocene strike-slip tectonics in the Trapani Mts. (NW Sicily). *Bollettino della Società Geologica Italiana*, **117**, 555–567.

ANDERSON, H. & JACKSON, J. 1987*a*. The deep seismicity of the Tyrrhenian Sea. *Geophysical Journal of the Royal Astronomical Society*, **91**, 613–637.

ANDERSON, H. & JACKSON, J. 1987*b*. Active tectonics of the Adriatic Region. *Geophysical Journal of the Royal Astronomical Society*, **91**, 937–983.

ANTONELLINI, M. A., AYDIN, A. & POLLARD, D. D. 1994. Microstructure of deformation bands in porous sandstones at Arches National Park, Utah. *Journal of Structural Geology*, **16**, 941–959.

ANTONIOLI, F., CHEMELLO, R., IMPROTA, S. & RAGGIO, S. 1999. Dendropoma lower intertidal reef formations and their paleoclimatological significance, NW Sicily. *Marine Geology*, **161**, 155–170.

AYDIN, A. & JOHNSON, A. M. 1978. Development of faults as zones of deformation bands and as slip surfaces in sandstone. *Pure and Applied Geophysics*, **116**, 931–942.

AYDIN, A., BORJA, R. I. & EICHHUBL, P. 2006. Geological and mathematical framework for failure modes in granular rock. *Journal of Structural Geology*, **28**, 83–98.

BOCCALETTI, M., CONEDERA, C., DAINELLI, P. & GOCEV, P. 1982. The recent (Miocene–Quaternary) rhegmatic system of western Mediterranean region. A new model of ensialic geodynamic evolution in a context of plastic/rigid deformation. *Journal of Petroleum Geology*, **5**, 31–49.

CATALANO, R. & D'ARGENIO, B. 1982. Schema geologico della Sicilia. *In*: CATALANO, R. & D'ARGENIO, B. (eds) *Guida alla Geologia della Sicilia Occidentale*. Guide Geologiche Regionali, Memorie della Società Geologica Italiana, Supplemento A, **24**, 9–41.

CATALANO, R., D'ARGENIO, B., MONTANARI, L. *ET AL.* 1979. Contributo alla conoscenza della struttura della Sicilia Occidentale: Il profilo Palermo–Sciacca. *Bollettino della Società Geologica Italiana*, **19**, 485–493.

CELLO, G., MAZZOLI, S., TONDI, E. & TURCO, E. 1997. Active tectonics in the Central Apennines and possible implications for seismic hazard analysis in peninsular Italy. *Tectonophysics*, **272**, 43–68.

CHIRONI, C., DE LUCA, L., GUERRA, I., LUZIO, D., MORETTI, A., VITALE, M. & Sea Land Group 2000. Crustal structures of the Southern Tyrrhenian Sea and the Sicily Channel on the basis of the M25, M26, M28, M39 WARR profiles. *Bollettino della Società Geologica Italiana*, **119**, 189–203.

COWIE, P. A. & SCHOLZ, C. H., 1992. Displacement–length scaling relationship for faults: data synthesis and discussion. *Journal of Structural Geology*, **14**, 1149–1156.

CPTI GRUPPO DI LAVORO 1999. *Catalogo Parametrico dei Terremoti Italiani*. ING, GNDT, SGA, SSN, Bologna.

DEWEY, J. F., HELMAN, M. L., TURCO, E., HUTTON, D. H. W. & KNOTT, S. D. 1989. Kinematics of the Western Mediterranean. *In*: COWARD, M. P., DIETRICH, D. & PARK, R. G. (eds) *Alpine Tectonics. Gelogical Society, London, Special Publications*, **45**, 265–283.

DI BUCCI, D. & MAZZOLI, S. 2003. The October–November 2002 Molise seismic sequence (southern Italy): an expression of Adria intraplate deformation. *Journal of the Geological Society, London*, **160**, 503–506.

ENGELDER, T. 1974. Cataclasis and the generation of fault gouge. *Geological Society of America Bulletin*, **85**, 1515–1522.

FINETTI, I. & DEL BEN, A. 1986. Geophysical study of the Tyrrhenian opening. *Bollettino di Geofisica Teorica ed Applicata*, **28**, 75–155.

GASPARINI, C., IANNACCONE, G., SCANDONE, P. & SCARPA, R. 1982. Seismotectonics of the Calabrian Arc. *Tectonophysics*, **82**, 267–286.

GHISETTI, F. & VEZZANI, L. 1984. Thin-skinned deformation in Western Sicily. *Bollettino della Società Geologica Italiana*, **103**, 129–157.

GIUNTA, G., NIGRO, F., RENDA, P. & GIORGIANNI, A. 2000. The Sicilian–Maghrebides Tyrrhenian Margin: a neotectonic evolutionary model. *Bollettino della Società Geologica Italiana*, **119**, 553–565.

GIUNTA, G., LUZIO, D., TONDI, E. *ET AL.* 2004. The Palermo (Sicily) seismic cluster of September 2002, in the seismotectonic framework of the Tyrrhenian Sea–Sicily border area. *Annals of Geophysics*, **47**(6), 1755–1770.

GOES, S., GIARDINI, D., JENNY, S., HOLLENSTEIN, C., KAHLE, H.-G. & GEIGER, A. 2004. A recent tectonic reorganization in the south–central Mediterranean. *Earth and Planetary Science Letters*, **226**, 335–345.

GUEGUEN, E., TAVARNELLI, E., RENDA, P. & TRAMUTOLI, M. 2002. The geodynamics of the southern Tyrrhenian Sea margin as revealed by intregrated geological, geophysical and geodetic data. *Bollettino della Società Geologica Italiana, Volume Speciale* **1**, 77–85.

KANAMORI, H. 1977. The energy release in great earthquakes. *Journal of Geophysical Research*, **82**, 2981–2987.

MALINVERNO, A. & RYAN, W. B. F. 1986. Extension in the Tyrrhenian Sea and shortening in the Apennines as results of arc migration driven by sinking of the lithosphere. *Tectonics*, **5**, 227–245.

MICHETTI, A. M., BRUNAMONTE, F. & SERVA, L. 1995. Paleoseismological evidence in the epicentral area of the January 1968 earthquakes, Belice, southwestern Sicily. *In*: SERVA, L. & SLEMMONS, D. B. (eds) *Perspectives in Paleoseismology*, **6**, 127–139, Peanut Butter Publishing, Seattle.

MONACO, C., MAZZOLI, S. & TORTORICI, L. 1996. Active thrust tectonics in western Sicily (southern Italy): the 1968 Belice earthquake sequence. *Terra Nova*, **8**, 372–381.

NIGRO, F., RENDA, P. & ARISCO, G. 2000. Tettonica recente nella Sicilia nord-occidentale e nelle Isole Egadi. *Bollettino della Società Geologica Italiana*, **119**, 307–319.

OGNIBEN, L. 1960. Nota illustrativa dello schema geologico della Sicilia nord-orientale. *Rivista Mineraria Siciliana*, **64–65**, 184–212.

RENDA, P., TAVARNELLI, E., TRAMUTOLI, M. & GUEGUEN, E. 2000. Neogene deformations of Northern Sicily, and their implications for the geodynamics of the Southern Tyrrhenian Sea margin. *Memorie della Società Geologica Italiana*, **55**, 53–59.

SCANDONE, P., GIUNTA, G. & LIGUORI, V. 1974. The connection between Apulia and Sahara continental margins in the Southern Apennines and in Sicily. *Memorie della Società Geologica Italiana*, **13**, 317–323.

SCHLISCHE, R. W., YOUNG, S. S., ACKERMANN, R. V. & GUPTA, A. 1996. Geometry and scaling relations of a population of very small rift-related normal faults. *Geology*, **24**, 683–686.

TONDI, E. & CELLO, G. 2003. Spatiotemporal evolution of the central Apennines fault system (Italy). *Journal of Geodynamics*, **36**, 113–128.

TONDI, E., PICCARDI, L., CACON, S., KONTNY, B. & CELLO G. 2005. Structural and time constraints for dextral shear along the seismogenic Mattinata Fault (Gargano, southern Italy). *Journal of Geodynamics* **40**, 134–152.

TONDI, E., ANTONELLINI, M., AYDIN, A., MARCHEGIANI, L. & CELLO, G. 2006. Interaction of deformation bands and stylolites in fault development in carbonate grainstones of the Majella Mountain, Italy. *Journal of Structural Geology*, **28**, 376–391.

WARD, S. N. 1998. On the consistency of earthquake moment release and space geodetic strain rates: Europe. *Geophysical Journal International*, **135**, 1011–1018.

WELLS, D. L. & COPPERSMITH, K. J. 1994. New empirical relationships among magnitude, rupture length, rupture width, rupture area, and surface displacement. *Bulletin of Seismological Society of America*, **84**, 974–1002.

ZARRAOA, N., RIUS, A., Sardón, E. & Ryan, J. W. 1994. Relative motions in Europe studied with a geodetic VLBI network. *Geophysical Journal International*, **117**, 763–768.

Index

Page numbers in *italics* refer to Figures; page numbers in **bold** refer to Tables

From: MORATTI, G. & CHALOUAN, A. (eds) 2006. *Tectonics of the Western Mediterranean and North Africa*. Geological Society, London, Special Publications, **262**, 379–384.
0305-8719/06/$15.00

M. BENVENUTI[1], M. BONINI[2], G. MORATTI[2], F. SANI[1]

GEOLOGICAL MAP OF THE SANT' ARCANGELO BASIN (Basilicata, Italy)

Scale 1:50,000

CONSIGLIO NAZIONALE DELLE RICERCHE
Istituto di Geoscienze e Georisorse

DIPARTIMENTO DI SCIENZE DELLA TERRA
Università degli Studi di Firenze

16° 01' 00" — 16° 22' 00" — 40° 15' 00" — 40° 00' 00" — LONG. EST GREENWICH

a — Recent fluvial and alluvial gravel, sand and clays *(Holocene)*

d — Colluvial and landslide deposits composed of various lithologies related to the local substratum *(Upper Pleistocene-Holocene)*

t — Breccia of angular to subangular gravels with an abundant sandy matrix laterally and vertically passing to sandy and then massive travertines *(Middle-upper Pleistocene)*

VAn — Terraced fluvial gravel and sand mainly characterised by flat morphologies and occurring at different altitudes along the main rivers. n (1 to 4) indicates the different order of terraced surfaces *(4 the youngest , 1 the oldest)*.

CHIAROMONTE-SERRA CORNETA SYNTHEM (MIDDLE PLEISTOCENE)

CSC3 — Deeply weathered angular to subrounded gravel and sandy silt in lenticular beds cm to m thick. Total thickness does not exceeds 30 m.

CSC2 — Breccia of angular and subangular boulder- to pebble-size cemented gravel. This unit is exposed limitedly in the Racanello Creek valley at the base of Raparo Mount. Clast composition is mostly made of limestones and dolostones of Ap. Thickness does not exceeds 15 m.

CSC1 — Fluvial gravel and subordinate sands in tabular dm to m thick beds locally with planar or through-cross lamination. Gravels are clast-supported, moderately to well embricated. Total thickness is 50-60 m.

MISSANELLO-NOEPOLI SYNTHEM (UPPERMOST LOWER-LOWERMOST MIDDLE PLEISTOCENE)

MN4 — Fluvial gravels and sands in tabular m-thick beds alternated with floodplain sandy-clayey silts in bedsets up to 15 m thick. Gravels are clast-supported with abundant sandy matrix. Planar cross lamination is locally present.

MN3 — Floodplain-lacustro-palustrine greysh-whitish silty clays dominant on fluvio-deltaic sands and gravels which overlain the previous lithofacies association. Fine-grained sediments, forming bedsets up to 20 m thick, are generally massive in places horizontal laminated. Dm-m thick volcanoclastic and organic-rich beds are locally present (Rifreddo-S.Lorenzo creeks). Vertebrate, mostly micromammal, remains, terrestrial-palustrine molluscs and root traces are locally present. Coarse-medium grained sands occur in dm-m thick tabular beds arranged in bedsets up to 20 m thick. Sands are massive to planar-through cross-laminated. Pebble-sized gravelly beds are locally interbedded with sands.

MN2 — Alluvial gravels in bedsets up to 20 m thick alternated with yellowish sandy-clayey silts. Gravelly bedsets consist of dm-m thick amalgamated beds of polymodal clast-supported cobble-pebble sized gravels with abundant sandy-silty interstitial matrix. These deposits are massive to crudely normal graded. Sandy-clayey silts are generally massive.

MN1 — Matrix-rich gravels cropping out exclusively in the Racanello Creek valley west of S. Chirico Raparo. Gravels consist of boulder to pebble-sized angular to sub-angular clasts rich in clayey-silty matrix. Clast composition is predominantly derived from Af and subordinately from Ap lithologies. These deposits are crudely bedded massive or normal-graded, up to 200 m thick.

ALIANO SYNTHEM (GELASIAN-LOWER PLEISTOCENE)

A4 — Unconformable bounding contacts recognized all over the area of exposition allow to classify this sub-unit as a sub-synthem made of alluvial gravels and sands interbedded with floodplain silty clays exposed in the WSW portion of the basin. Gravels and sands are arranged in dm-m thick beds stacked within bedsets up to 15 m thick. Gravels range in size from cobble to pebble, are characterized by a clast-supported framework with abundant sandy-silty interstitial matrix, occasional clast imbrication indicates palaeoflow from WSW. Gravelly beds are massive or crudely normal graded and rest on silty clays trough high-relief erosive surfaces. Sands occur as small lenses within gravels or locally form bedsets up to 15 m thick. Silty clays are greysh arranged in bedsets up to 30 m thick in the easternmost outcrops (i.e. around Francavilla in Sinni village) generally massive locally bearing organic-rich sediments, terrestrial molluscs and rare volcaniclastic beds.

A1-A3: W-E transitions from angular unconformities to sharp and gradual stratigraphic contacts characterize the latero-vertical relations among these sub-units all over the basin. Intervening deposits are grouped into recurring gravelly, sandy and pelitic lithofacies associations which depict genetic linkage among fluvial, deltaic and shelfal systems. As a consequence these three sub-units fit the definition of composite depositional sequences.
A1-3 are composed of three recurring lithofacies associations stacked in an eastward prograding clastic wedge.

A1-3a: fluvial gravels and subordinate sands in dm-m thick beds arranged in tabular bedsets 10-15 m thick. Gravels are brownish-reddish (A1a), polymodal, clast-supported with abundant interstitial sandy-silty matrix, imbricated showing a paleoflow from the western margin. Beds are commonly amalgamated with basal low-relief erosive surfaces, internally massive or with low-angle planar cross-lamination. Sands, occuring as residual lenses within the gravelly beds, are coarse- to medium grained massive or horizontal laminated.
A1-3b: fluvial gravels and sands and floodplain silty clays which express lateral (toward E) and vertical transition from lithofacies A3a. Gravely and sandy beds define fining upward trend. Gravels are polymodal, clast-supported arranged in m thick lenticular beds erosively resting on the floodplain silty clays. Sands are coarse-medium grained massive or normal graded. Silty clays are greysh-whitish (A1b) and generally massive.
A1-3c: delta-front sands and clayey silts mostly exposed in the central sector of the basin interpreted to represent a lateral transition from lithofacies A1-3a. Sands are coarse-fine grained in dm-m thick beds arranged in 10-15 m thick tabular bedsets. Sands are massive, locally horizontal and cross-laminated. A2c is typically characterized by shallow marine molluscs (Glycimeris, Pectinid, Ostreids) dispersed or concentrated in thin shell beds and pockets of articulated specimens. Locally clay chips occur at the base or within the beds. Clayey silts occur on top of sandy bedsets defining a fining upward stacking pattern. These deposits are generally massive and increase in thickness toward E. At S.Giorgio Lucano the upper portion of a sandy body referred to as an A2 delta front fed from SSW is characterized by different lithofacies (A2d). These consist of coarse-medium sands characterized by trough-cross and low-angle laminations in dm-m thick beds with erosive base and subordinate intervening greysh sandy silts bearing a marine molluscan fauna. This portion is interpreted as a proximal delta front.
Ad: prodelta and inner shelf silty clays extensively cropping out in the central-eastern sector of the basin. Silty clays are generally massive with dispersed marine molluscs, mostly bivalves (Venerids). In the southern sector of the basin along the Sarmento River the uppermost deposits bear a brackish molluscan fauna characterized by the dominance of Cerastoderma. This lithofacies association represents the distal portions of the A1-3 fluvio-deltaic systems and the deepest basin areas.

CALIANDRO SYNTHEM (PIACENZIAN-GELASIAN)

C3: it consists of two lithofacies associations resting on older deposits through an angular unconformity making transition toward E to sharp and gradual contacts. The character of the lower bounding surface allows to classify this sub-unit as a composite depositional sequence.
C3a: fluvial gravels and sands and floodplain silty clays exposed mainly on the western margin along the Agri and Armento valleys. Gravelly and sandy beds define fining upward trend. Gravels are polymodal, clast-supported arranged in m thick lenticular beds erosively resting on the floodplain silty clays. Sands are coarse-medium grained massive or normal graded. Silty clays are greysh-whitish generally massive.
C3b: delta-front sands cropping out on the western margin along the Agri and Sauro river valleys. Sands are medium-fine grained in dm-m thick beds massive or cross-laminated. Scattered clay chips, pebbles and mollusc fragments are occasionally present at the base of beds.

C2: it is represented by three vertically stacked lithofacies associations and it is bounded at the base and to the top by angular unconformities fitting the definition of sub-synthem.
C2c: fluvial sands exposed limitedly on the western margin along the right flank of the Agri river valley. Sands are coarse-medium grained in dm-m thick beds characterized by trough-cross lamination.
C2b: brackish silty clays overlain by lithofacies C2c. Silty clays are massive, organic-rich and bear scattered molluscs mostly Cerastoderma.
C2a: deltaic sands overlain by lithofacies C2b and cropping out in the Agri river valley. An isolated outcrop is present north of Armento village. Sands are coarse-medium grained in dm-m thick massive, normal graded or cross-laminated beds.

Ce: whitish diatomaceous silts exposed exclusively on the north-eastern margin of the basin. These deposits are generally massive locally planar laminated
Ceg: alluvial gravels locally occurring at the base of Ce (Monticchio area, Sauro-Agri rivers confluence)

C1: it is formed by three main lithofacies assemblages included within a composite depositional sequence.
C1c: fluvio-deltaic sands and paralic silty and diatomaceous clays exposed along the eastern margin. Sands are yellowish, medium-fine grained in massive or normal graded dm-m thick beds. Clays are dark-pale grey generally massive, locally rich in organic matter.
C1b: deltaic and shoreface sands cropping out mostly along the western and northern margin of the basins. Sands are yellowish medium-fine grained rich in bioclasts (pectinids, ostreids, ecc.) and generally arranged in m thick massive beds.
C1a: slope and alluvial gravels resting on the substratum units along the western and eastern margins of the basin. Gravels are polymodal, well-rounded to sub-angular, clast-supported, locally rich in silty-clayey matrix (e.g. on the western margin along the Agri river valley). Thickness not exceeds 20 m.

SUBSTRATUM UNITS

P- Bradano Unit: Marine sands, clays, calcarenites, sandstones and conglomerates. Early Pliocene. Gf: Gorgoglione Flysch, Marly and silty clays alternated with sandstone layers. Late Miocene; SP: Serra Palazzo Formation: Turbidite sandstones, marls and whitish marly limestones. *Langhian-Serravallian*; Af: Albidona Flysch and Saraceno Fm: Marls and marly clays alternated with graded sandstone layers. Calciluttites and calcarenites with marls and marly clays. *Late Oligocene-Middle Miocene*; Lagonegro Unit - Nu: Numidian Flysch. Quartz -rich turbidite sandstones, alternated with shales and siltstones. *Early-Middle Miocene*; Fr: Flysch Rosso. Calcarenites and calcirudites with reddish marls and shales. *Cretaceous-Oligocene*; Lag: Galestri, Scisti Silicei, Calcari con selci Fms.: Brown-ish shales with calcarenites and thin sandstones; radiolarites and cherty shales; cherty limestones and marls. *Late Triassic-Cretaceous*; Apenninic Platform Unit - Ap: Platform limestones, dolostones and calciluttites. Middle Jurassic-Cretaceous; Frido Unit - UF: Calcschists, quartzites, slates and phyllites with marble levels and slices of metaophiolites and cristalline rocks (mainly gneiss). *Late Jurassic-Cretaceous*.; Calabro-Lucano Flysch Unit - CL: Brownish shales, sandstones and calcarenites with ophiolites blocks. *Late Jurassic-Late Oligocene*; Sicilide Complex - TT: Tufiti di Tusa. Micaceous turbidites sandstones and marls. *Late Oligocene-Early Miocene*; MSA: Monte Sant'Arcangelo Fm., Marly limestones, calcarenites, limestones and reddish marls. *Late Cretaceous-Eocene*; AVV: Argille varicolori. Varicoloured shales with many limestones and sandstones. *Cretaceous-Oligocene*.

SYMBOLS

- Stratigraphic contact
- Fault
- Normal fault (barbs on the downthrown side)
- Strike-slip fault (arrows indicate the horizontal displacement)
- Transpressional fault (triangles on the hangingwall;arrows indicate the horizontal component of displacement)
- Transtensional fault (barbs on the downthrown side; arrows indicate the horizontal component of displacement)
- Flat-geometry thrust fault (squares on the hangingwall)
- Ramp-geometry thrust fault and reverse fault (triangles on the hangingwall)
- Anticline axis
- Syncline axis
- Strike and dip of strata
- Overturned strata
- Sub-horizontal strata (<5:1
- Vertical strata
- A A' Trace of the geological cross-sections
- Palaeo sea-cliff

PECULIAR FOSSILIFEROUS LOCALITIES
- Continental molluscan fauna
- Brackish molluscan fauna (*Cerastoderma*)
- Mammal remains

ALPS — APENNINES — ADRIATIC SEA — TYRRHENIAN SEA

Topographic map by : I.G.M. (Istituto Geografico Militare autorizzazione n. 4726 in data 16-1-1998)

Field mapping performed during 2000-2005. Basin deposits from original field mapping. *Substratum* units modified from Carta Geologica d'Italia, 2ed. (scale 1:100.000), sheets 211-*Sant'Arcangelo*, and 200-*Tricarico*; Carta geologica d'Italia, 3rd ed. (scale 1:50.000), sheet 506- *Sant'Arcangelo*. Bonini and Sani (1998), Geological map of the Potenza-Guardia Perticara area.

Scale 1:50,000

TECTONIC SKETCH MAP

- Fluvial, alluvial, colluvial and landslide deposits *(Upper Pleistocene-Holocene)*
- Valdagri synthem *(middle-upper Pleistocene)*
- Chiaromonte-Serra Corneta synthem *(middle Pleistocene)*
- Missanello-Noepoli synthem *(uppermost lower-lowermost middle Pleistocene)*
- Aliano synthem *(Gelasian-lower Pleistocene)*
- Caliandro synthem *(Piacenzian-Gelasian)*
- Substratum Units

0 — 5 km

Sauro River — Agri River — Sinni River — Lago di M. Cotugno — Sarmento River — Armento — Aliano — S. Arcangelo — Roccanova — S. Chirico Raparo — Senise — Noepoli — Francavilla in Sinni — Episcopia — S. Giorgio Lucano — S. Costantino Albanese

CONCEPTUAL TECTONO-STRATIGRAPHIC SCHEME

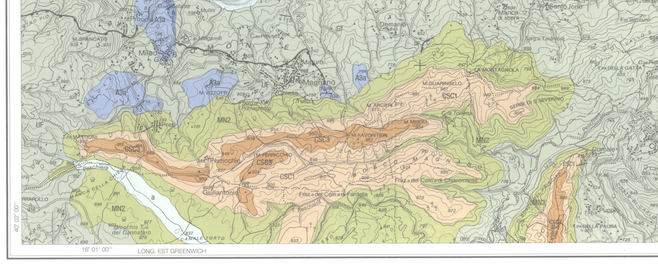

From: Benvenuti, M., Bonini, M., Moratti, G. & Sani, F. 2006. Tectono-sedimentary evolution of the Plio-Pleistocene Sant' Arcangelo Basin (Southern Apennines, Italy). *In*: Moratti, G. & Chalouan, A. (eds) *Tectonics of the Western Mediterranean and North Africa*. Geological Society, London, Special Publications, **262**. 0305-8719/06/$15.00

1- Dipartimento di Scienze della Terra, Università degli Studi di Firenze, via G.La Pira, 4 - 50121 Firenze (Italy)
2- Consiglio Nazionale delle Ricerche, Istituto di Geoscienze e Georisorse, via G.La Pira, 4 - 50121 Firenze (Italy)

Digital cartography prepared and printed: S.E.L.C.A. Via R. Giuliani, 153 - Firenze 2006

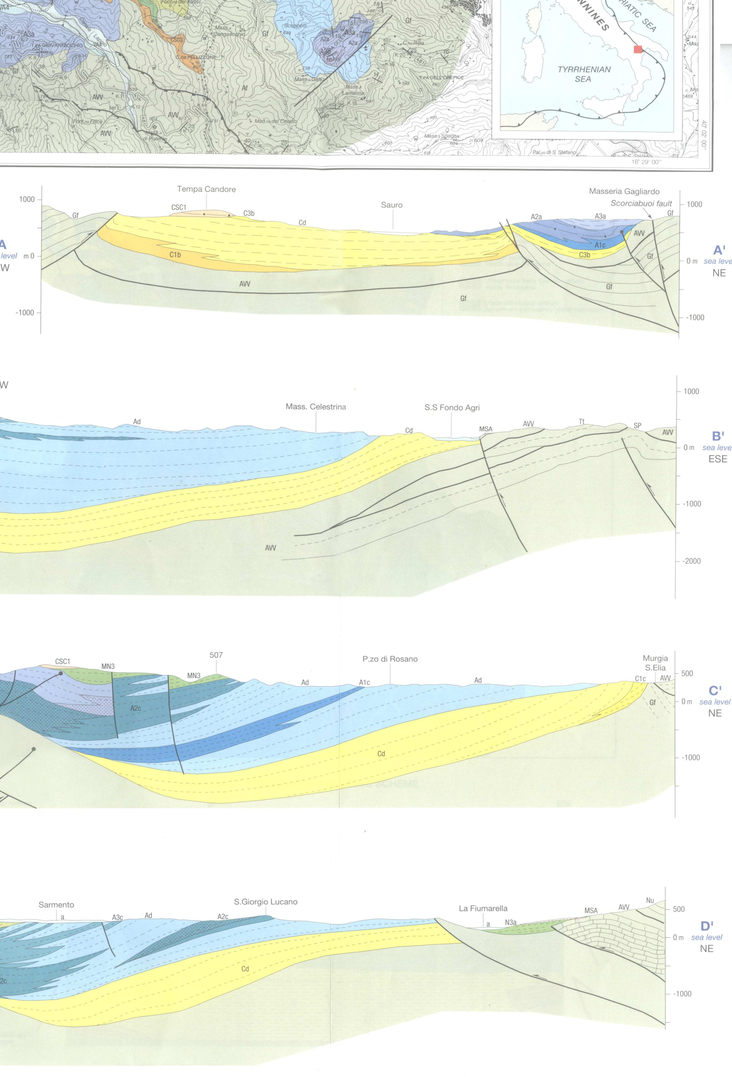

Tectonics of the Western Mediterranean and North Africa

Edited by
G. Moratti and A. Chalouan

This book provides an insight into the overall tectonic evolution of the Western Mediterranean region and North Africa. The tectonic setting of the region reflects a long-lived and complex evolution, mainly related to the Alpine Orogeny. This inheritance is expressed by an intricate pattern of arc-shaped mountain chains, the Alps, the Betic–Rif Cordilleras and the Apennine–Maghrebian belt, whose southern branches mark the present limit between the African and Eurasian plates. The volume covers the Maghrebian chains in North Africa, from Tunisia to Morocco and the Western and Central Mediterranean, from Spain to Italy from the pre-orogenic phases (Palaeozoic–Mesozoic) to the post-collisional neotectonic and Quaternary development. It includes both original research papers and syntheses dealing with the aspects of structural, sedimentary, metamorphic and marine geology.

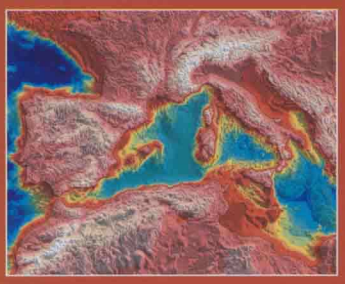

Visit our online bookshop: http://www.geolsoc.org.uk/bookshop

Geological Society web site: http://www.geolsoc.org.uk

ISBN 1-86239-202-1

Cover illustration:
Digital elevation of the Mediterranean region from ETOPO-5. Courtesy of A. Argnani, ISMAR-CNR, Bologna, Italy.